Talanta

The International Journal of Pure and Applied Analytical Chemistry

Artificial neural networks for determination of enantiomeric composition of α-phenylglycine using UV spectra of cyclodextrin host–guest complexes Comparison of feed-forward and radial basis function networks

Abbas Afkhami [a,*], Maryam Abbasi-Tarighat [a], Morteza Bahram [b]

[a] *Faculty of Chemistry, Bu-Ali Sina University, Hamadan 65174, Iran*
[b] *Department of Chemistry, Faculty of Science, Urmia University, Urmia, Iran*

Abstract

In this work feed-forward neural networks and radial basis function networks were used for the determination of enantiomeric composition of α-phenylglycine using UV spectra of cyclodextrin host–guest complexes and the data provided by two techniques were compared. Wavelet transformation (WT) and principal component analysis (PCA) were used for data compression prior to neural network construction and their efficiencies were compared. The structures of the wavelet transformation–radial basis function networks (WT–RBFNs) and wavelet transformation–feed-forward neural networks (WT–FFNNs), were simplified by using the corresponding wavelet coefficients of three mother wavelets (Mexican hat, daubechies and symlets). Dilation parameters, number of inputs, hidden nodes, learning rate, transfer functions, number of epochs and SPREAD values were optimized. Performances of the proposed methods were tested with regard to root mean square errors of prediction (RMSE%), using synthetic solutions containing a fixed concentration of β-cyclodextrin (β-CD) and fixed concentration of α-phenylglycine (α-Gly) with different enantiomeric compositions. Although satisfactory results with regard to some statistical parameters were obtained for all the investigated methods but the best results were achieved by WT–RBFNs.
© 2007 Elsevier B.V. All rights reserved.

Keywords: ANNs; Cyclodextrin; Enantiomeric ratio; α-Phenylglycine; WT

1. Introduction

Artificial neural networks (ANNs) are composed of simple elements operating in parallel. These elements are inspired by biological nervous systems. As in nature, the network function is determined largely by the connections between elements. A neural network can be trained to perform a particular function by adjusting the values of the connections (weights) between elements. Commonly neural networks are adjusted or trained, so that a particular input leads to a specific target output. The network is adjusted, based on a comparison of the output and the target, until the network output matches the target.

ANNs have now gained acceptance in numerous areas of chemistry, as illustrated by the number of applications and several reviews [1,2]. The application of ANNs for multivariate calibration with chemical data is an important source of publications in chemistry [2,3].

The multi-layer feed-forward ANNs (a layered network in which each layer only receives inputs from previous layers that is also called multi-layer perceptron, MLP) with the error back-propagation learning rule is the technique most frequently used. Radial basis function (RBF) networks on the other hand, offer interesting alternatives to MLP in the sense that they allow local training and the final models can be interpreted in terms of logical rules [4,5]. RBF networks may require more neurons than standard feed-forward back propagation networks, but often they can be designed in a fraction of the time it takes to train standard feed-forward networks. They work best when many training vectors are available [6].

Like other regression methods the ratio of the number of samples to the number of adjusted parameters (the weights in the case of ANNs) should be kept as high as possible, in order to avoid under-determination problem. The number of samples is generally limited by practical constraints, but one can partly solve the

---

* Corresponding author. Tel.: +98 811 8271541; fax: +98 811 8272404.
  E-mail address: afkhami@basu.ac.ir (A. Afkhami).

under-determination problem by reducing the number of weights in ANNs as much as possible [2]. One way for overcoming the problem is to compress input data, especially when they consist of absorbences recorded at several hundred wavelengths. In addition to reducing the size of input data, compressing allows one to eliminate irrelevant information such as noise or redundancies present in the data matrix. Successful data compression can result in increased training speed, a reduction of memory storage, better generalization ability of the model and enhanced robustness with respect to the noise in the measurements.

The most popular method for data compression in chemometrics is principal component analysis (PCA). In practice, PCs are often successfully used as inputs. Even if there is some nonlinearity in data set, all relevant information is usually contained in the first 15 PCs [2]. Alternatively, it is possible to use Fourier analysis [7], Hadamard transform [8] or wavelet analysis [9–14] to pre-process signals before ANN modeling.

Determination of enantiomers in samples of chiral compounds is of high interest. The significance of such determination stems from the fact that enantiomers may possess rather different pharmacological properties (e.g. one of them may be less active than the other, completely inactive or even toxic) [15]. Experimental discrimination of enantiomers is carried out conventionally by means of chiral auxiliary agents such as chiral shift reagents (as in NMR), chiral or non-chiral columns in LC [15–19]. Capillary electrophoresis [20] and circular dichorism [21–23] have recently become interesting alternatives to LC. But these methods use instruments that are more complicated and more expensive than a UV–Vis spectrophotometer and may not be available in all laboratories.

Recently Busch et al. [24] showed that partial least-squares (PLS-1) analysis of ordinary UV–Vis spectral data of solutions containing cyclodextrin host–guest inclusion complexes can be used for the determination of the enantiomeric purity of samples of α-phenylglycine (α-Gly). Also they showed that the formation of diastereomeric inclusion complexes would result in small changes in the near-infrared spectra of the complexes as the enantiomeric composition was varied [25]. Regression modeling of ordinary spectral data was also used for the determination of the enantiomeric composition of samples of ibuprofen and norephedrine [26].

To the best of our knowledge only one report has been published on the application of ANNs to the spectrophotometric determination of enantiomeres by Blanco et al. [27].

In the present work, FFNNs and RBFNs have been used for the determination of enantiomeric composition of α-Gly using UV spectra of cyclodextrin host–guest complexes the data provided by two techniques were compared. Wavelet transformation (WT) and PCA were used for data compressing prior to neural network construction and their efficiencies were also compared. The obtained results were also compared with those obtained previously by PLS regression [24].

1.1. Theory of wavelet transforms

A detailed description of the wavelet and WT can be found in some references [28–30]. A brief overview of this theory is presented. Wavelet is defined as a series of function $\psi a, b(t)$ derived from a mother function $\psi(t)$ by dilation and translation

$$\psi_{a,b}(\lambda) = |a|^{-1/2} \psi \left(\frac{\lambda - b}{a} \right) d_\lambda, \quad a, b \in R \text{ and } a \neq 0 \quad (1)$$

where a is the scale parameter that controls dilation and b is the shift parameter that controls the translation of wavelet. For a signal $f(\lambda)$ in wavelength domain, its CWT (continuous wavelet transform) could be described as Eq. (2)

$$W_{f(a,b)} = |a|^{-1/2} \int_{-\infty}^{+\infty} f(\lambda) \psi \left(\frac{\lambda - b}{a} \right) d\lambda \quad (2)$$

a or b is a certain constant and the CWT under a certain dilation $W_{f(a)(b)}$ or under certain translation $W_{f(b)(a)}$ can be obtained [30]. Pre-processing with CWT obtains coefficients of the spectra which can be used for calibration or regression with partial least squares (PLS) and artificial neural network or other methods [31].

Theoretically, many wavelet functions could be used to run WT, here among these, wavelet functions (Mexican Hat (mexh), daubechies4 (db4), symlets8 (sym8)) were used for signal processing. Selection of an appropriate wavelet filter may be guided by empirical rules applied to data size and signal continuity. The typical way is to visually inspect the data first, and select an appropriate wavelet filter [32].

In addition to wavelet function, dilation also has an important role to get maximum resolution and sensitivity. A proper dilation was selected using the introduced criterion by Xiaoquan et al. [33]

$$\text{fitness}(a) = \sum_{b=1}^{\text{length } f(x)} [|Wf_{(a)}(b)| - |f(b)|]^2 \quad (3)$$

fitness(a) represents the cumulated difference between the wavelet coefficients $Wf_{(a)}(b)$ and the original data at each transition. The dilation which makes the fitness(a) have the minimum value would be chosen as the best dilation.

For selection of wavelet coefficients, e.g. for a matrix of size $N*K$, the variance vector is calculated as:

$$\text{variance}_k = \frac{\sum (X_{n,k} - \bar{X}_k)^2}{N - 1} \quad (4)$$

$k = 1, 2, \ldots, K$ (column index), $n = 1, 2, \ldots, N$ (row index).

1.2. Theory of radial basis function network (RBF)

The structure of RBFNs is comprised of three node layers of input, hidden and output. The input layer serves only to distribute input to hidden layer. Each neuron of the hidden layer represents a kernel or a basis function, with equal dimensions to the input data. RB networks generally use a Gaussian function to account for the non-linearity of the hidden layer processing elements. The Gaussian function responds only to a small region of the input space where the Gaussian is centered. The successful implementation of these networks is to find suitable centers for such a Gaussian functions, which are characterized by two

parameters, i.e. center (c_i), and peak width (δ_j). The output for the jth Gaussian neuron for an input object x_i can be calculated using the following equation:

$$out_j = \phi(||x_j - c_j||) = \exp\left(\left\|\frac{x_j - c_j}{\delta_j^2}\right\|\right) \tag{5}$$

where $||x_i - c_j||$ is the calculated euclidean distance between x_i and c_j, and δ_j determines the portion of the input space where the jth RBF will have a non-significant zero response. The input value to each output node is the weighted sum of all the outputs of the hidden nodes. Finally, the response of each output node is calculated by a linear function of its input (including the bias w_{k0}), that is the output of hidden layer (out_k). The relation between the value out_k and the input variable x_i can be represented by:

$$out_k = w_{k0} + \sum_j w_{kj}\phi(||x_i - c_j||) \tag{6}$$

The weights w_{kj} are adjusted to minimize the mean square error of the net output. Two sets of parameters (the centers and the widths) in the hidden layer and a set of weights in the output layer are adjusted.

2. Experimental

2.1. Reagents

Enantiomerically pure L-(+)-α-phenylglycine (L-α-Gly) and D-(−)-α-phenylglycine (D-α-Gly) were purchased from Fluka, β-CD was purchased from Merck and used without further purification. Stock solutions of known concentrations of β-CD were prepared in doubly distilled water. A fixed concentration (7.5 mmol L^{-1}) of α-Gly, while, the enantiomeric composition of α-Gly used to prepare the solutions was varied, was prepared. So appropriate amount of them carefully weighed and diluted in 10 mL volumetric flasks with appropriate volume of β-CD till got 15 mmol L^{-1} in β-CD. The β-CD-α-Gly complexes were stabilized at pH 12 with a buffer prepared by mixing appropriate amounts of Na$_2$HPO$_4$ and Na$_3$PO$_4$. Solutions with mole fractions of D-α-Gly between 0.06–0.95, and 0.05–0.095 for L-α-Gly were prepared for training and prediction of both neural networks. Five randomly designed samples as Validation set were consequently evaluated with the constructed model. All solutions were prepared freshly daily.

2.2. Spectra and data analysis

Spectra were recorded with a Perkin-Elmer Lambda 45 UV–Vis spectrophotometer over the wavelength range 220–550 nm with 1 nm increments. Quartz cells with 1.0 cm path length were used. A pH meter (model 713 Metrohm) was used for the measurement of pH of the solutions. The autoscaled data (using the mean and standard deviation of each column) were subjected to ANNs. A short program was written in MATLAB 7.1 for performing principal component analysis and autoscal-

ing of the data and the networks calculations were performed using nnet–Toolbox for MATLAB 7.1.

3. Results and discussion

3.1. Absorption spectra

Both small and large guest molecules can form complexes with cyclodextrins because complexation is not limited to the formation of 1:1 complexes where the guest is small enough to fit in the cavity. It is well known that when a guest molecule is added to an aqueous solution of cyclodextrin to form a host–guest complex, a weak, more or less prominent tail or shoulder is observed to form on the long-wavelength side of the absorption band of the complex [24]. It is in this tail or shoulder region where the effect of enantiomeric composition of the guest molecules has the most pronounced effect on the spectrum.

Fig. 1 shows spectral data in the shoulder region for a series of aqueous solutions of calibration and prediction data sets, at optimum conditions of pH 12, fixed concentration of β-CD (15 mmol L^{-1}) and fixed concentration of α-Gly (7.5 mmol L^{-1}), while the mole fraction of two isomers varied randomly. Fig. 1 shows that the spectra obtained for different samples depend on the enantiomeric composition of the α-Gly [24].

3.2. Selection of the mother wavelet and level of decomposition

The mother wavelet and decomposition level, for best compression and smoothing of inclusion complex spectra, were chosen taking into account the degree of similarity between the original data and the one reconstructed from approximation coefficients after compression. In this paper, the appropriate wavelets chosen from many the types of wavelets are Mexican Hat (mexh), Daubechies4 (db4) and Symlet8 (sym8). WT was
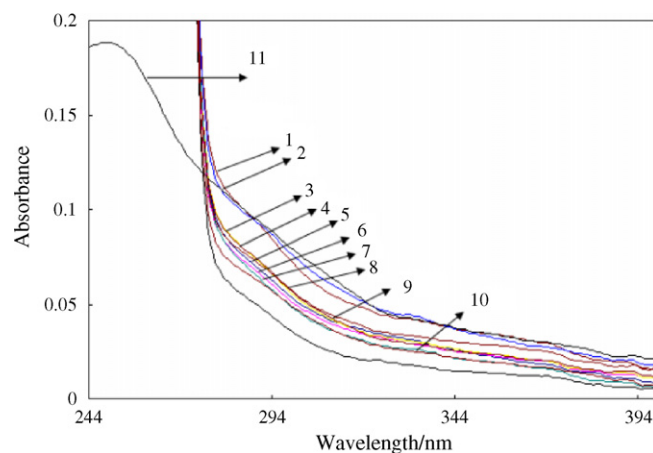
Fig. 1. Absorption spectra for the solutions for calibration set at pH 12 containing 15 mmol L^{-1} β-CD and 7.5 mmol L^{-1} α-Gly with various enantiomeric compositions (1–10). Mol fraction of D-α-Gly and L-α-Gly, respectively are: (1) 0.06,0.94; (2) 0.30,0.70; (3) 0.39,0.61; (4) 0.75, 0.25; (5) 0.82,0.18; (6) 0.95, 0.05; (7) 0.48,0.52; (8) 0.5,0.5; (9) 0.45,0.55; (10) 0.85, 0.15; (11) spectrum for 15 mmol L^{-1} β-CD.
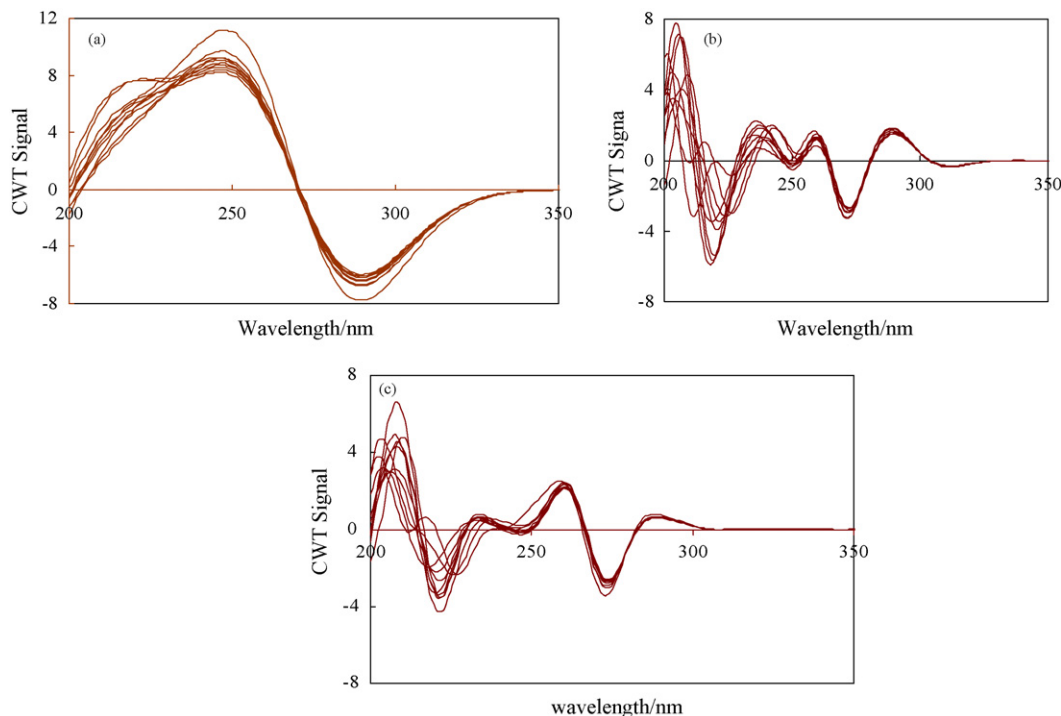
Fig. 2. The WT Coefficients spectra obtained on the calibration spectra using by (a) mexh, (b) db4 and (c) sym8.

carried out in the optimum dilations 40, 25, 25 for mexh, sym8 and db4, respectively. Fig. 2 shows the wavelet coefficients for selected mother wavelets for calibration set at optimum dilation values. Compression is achieved by eliminating the wavelet coefficients that do not hold valuable information. This is a very difficult task and the selection of how many and what wavelet coefficients will be used depends on the problem. We are interested in keeping the systematic information in the data intact, and therefore the variance vector of the data set is a reasonable answer to what coefficients to choose [34]. Therefore variance vectors were calculated by Eq. (4). With extracting the positions of the 95% variance, wavelet coefficients from the pre-processing by WT, inputs were estimated. Approximation coefficients obtained after the WT pre-processing presented in Table 1.

3.2.1. Construction of the WT–RBF network

The *exact fit* type of radial basis function networks (RBFN), from ANN Toolbox of MATLAB version 7.1, was the choice

for this part. RBF networks have two active layers, hidden layer and the output layer. In the *exact fit* RBFN the number of hidden nodes is equal to the number of nodes in the input layer. The output layer considered as a single node corresponding to the individual enantiomer. In this way, the adjustable parameters were: the number of input variable and SPREAD values. The SPREAD parameter is in relation with the spread of radial basis functions in the network. For too large or too small SPREAD values many neurons will be required to fit a fast changing or to fit smooth function. So the network may not generalize well. The original spectra were transformed with different mother wavelets (mexh, db4 and sym8). The wavelet coefficients which carried out the 95% variance were identified and used as input variables (Table 1). SPREAD values of 1–60 were investigated on optimum inputs. The SPREAD values which affected the root mean squares error of prediction (RMSE) of D-α-Gly and L-α-Gly in the synthetic samples were evaluated. The validation set was used to find the global minimum instead of local minimum to get the best value of each parameter. The optimum values of SPREAD presented in Table 1. In order to obtain accuracy of the method synthetic mixtures with different mole ratios of the D-α-Gly and L-α-Gly were analyzed using the obtained model. The results are given in Table 2. Fig. 3 shows the relation between the predicted mole fractions and known mole fractions provided using different mother wavelets by proposed methods. The figure shows that the obtained values by proposed methods are in good agreement with real values of each enatiomer.

3.2.2. Construction of the WT–FFN network

In order to choose the CWT–FFNNs that best fulfilled our purpose, different structures with supervised learning were con-

Table 1
The optimum number of wavelet coefficients and optimum SPREAD values for both isomers, after training by WT–RBFNs

Enantiomer	Filter name	Variance%	Number of wavelet coefficients	SPREAD value
D-α-Gly	mexh	95	40	20
L-α-Gly			40	20
D-α-Gly	db4	95	30	15
L-α-Gly			30	10
D-α-Gly	sym8	95	30	16
L-α-Gly			30	20

Table 2
Results obtained for the determination of enatiomeric composition of α-Gly in synthetic samples using WT–RBFNs with different mother wavelets

Sample number	Known mole fractions		Predicted by mexh		Predicted by sym8		Predicted by db4	
	D-Gly	L-Gly	D-Gly	L-Gly	D-Gly	L-Gly	D-Gly	L-Gly
1	0.800	0.200	0.800	0.203	0.805	0.213	0.799	0.200
2	0.620	0.380	0.620	0.380	0.621	0.380	0.619	0.380
3	0.700	0.300	0.711	0.302	0.713	0.302	0.699	0.300
4	0.520	0.480	0.520	0.480	0.520	0.480	0.519	0.480
5	0.200	0.790	0.201	0.795	0.206	0.793	0.200	0.800
6	0.690	0.310	0.691	0.316	0.691	0.317	0.689	0.310
7	0.380	0.620	0.380	0.620	0.380	0.620	0.384	0.612
8	0.600	0.400	0.600	0.403	0.600	0.401	0.613	0.410
RMSE%			0.414	0.338	0.565	0.592	0.524	0.452

sidered. To optimize the network architecture, the number of hidden layers was varied from one to five. The RMSE% showed a minimum at one layer for both enatiomers. Error values for number of layers more than one were very high. The number of input nodes (neurons) was selected as an optimal number of wavelet coefficients vectors. In order to determine the optimal number of hidden nodes, neural networks with different numbers of nodes were trained. Based on the data in Fig. 4, four, three and two nodes for D-α-Gly and two, three and two nodes for L-α-Gly were used as optimum number of hidden nodes by mexh, db4 and sym8, respectively. Different transfer functions in hidden and output layer such as purelin, logsig and tansig were also tested
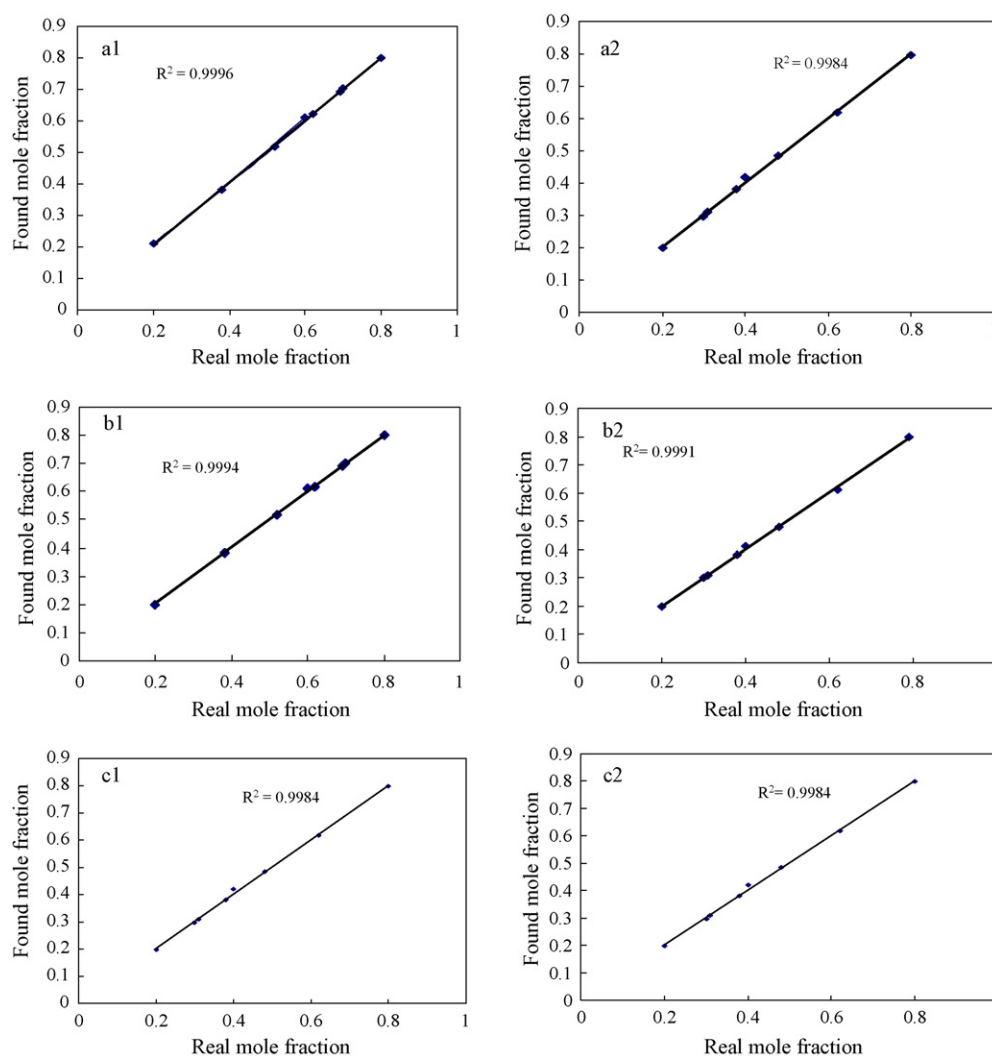
Fig. 3. Comparison of the known mole fractions versus calculated mole fractions for two considered enatiomers obtained by WT–RBFNs with different mother wavelets (a1, b1, c1) and (a2, b2, c2) for D-α-Gly and L-α-Gly by mexh, db4 and sym8, respectively.
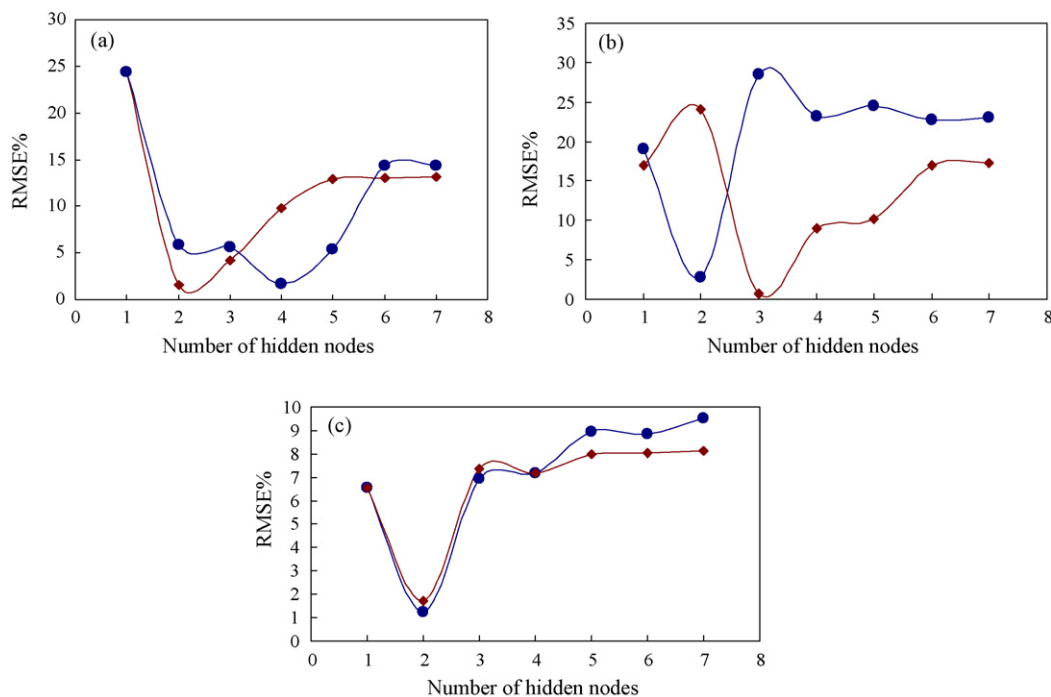
Fig. 4. Plots of RMSE% as a function of number of hidden nodes for D-α-Gly (●) and L-α-Gly (■) by (a) mexh, (b) db4 and (c) sym8 for construction of WT–FFNNs.

Table 3
Optimum parameters for WT–FFNNs by different function applied for data compressing

Parameter	mexh		sym8		db4	
	D-α-Gly	L-α-Gly	D-α-Gly	L-α-Gly	D-α-Gly	L-α-Gly
Number of wavelet coefficients	40	40	30	30	40	30
Number of hidden nodes	4	2	2	2	2	3
Number of output nodes	1	1	1	1	1	1
Number of epochs	200	200	200	200	200	200
Transfer function for hidden layer	Logsis	Logsig	Purelin	Purelin	Logsig	Logsig
Transfer function for output layer	Logsig	Logsig	Logsig	Logsig	Logsig	Logsig
Learning rate	0.1	0.1	0.1	0.1	0.1	0.1

in order to get the best modeling network. Training the network was performed with several learning rates which changed from 0.01 to 0.1. During the learning procedure of the network with the calibration set, the validation set was subsequently tested with the learned network. The most accurate networks can be seen to be those that have a relatively short training time. It was observed that continued training beyond 200 iterations for D-α-Gly and L-α-Gly causes the RMSE% to increase. The output layer considered as a single node corresponding to the individual enantiomer. The best transfer functions as well some other parameters such as number of epochs, learning rate and momentum for each enatiomer are summarized in Table 3. The results obtained in the quantification of the samples in the training and prediction sets are expressed as root mean square errors (RMSE).

$$\text{RMSE} = \sqrt{\frac{\sum_{i=1}^{n}(d_i - c_i)^2}{n}} \qquad (7)$$

where d_i is the desired output and c_i is the actual output set, n is the number of compounds in prediction set.

The RMSE values obtained for prediction samples are given in Table 4. The reasonable relative errors for each analyte indicate the accuracy of the proposed method. Tables 2 and 4 indicate that, there is a slight improvement in the estimated RMSE% values when using RBFNs instead of FFNNs. In the case of using RBFNs, the obtained results from repetition of training procedure were the same. It is due to high reproducibility of modeling that is the main advantage of RBFNs. Due to high reproducibility of modeling in each experimental condition the networks were trained only by three times repetition (Table 4).

Table 4
RMSE% values for prediction samples for determination of enatiomeric composition α-Gly in synthetic samples using WT–FFNs, PC–RBFNs and PC–FFNNs

Enantiomer	WT–FFNs			PC–RBFNs	PC–FFNNs
	mexh	db4	sym8		
D-α-Gly	0.536	0.640	0.796	0.930	1.42
L-α-Gly	0.748	0.884	0.738	0.860	1.60

Table 5
Optimized parameters used for construction of PC–FFN network

Parameter	D-α-Gly	L-α-Gly
Number of principal components	4	3
Number of hidden nodes	3	3
Number of output nodes	1	1
Number of epochs	800	800
Transfer function for hidden layer	Logsig	Logsig
Transfer function for output layer	Logsig	Logsig–Tansig[a]
Learning rate	0.01	0.01

[a] In this case using both transfer functions in output layer provides the same results.

3.3. Compressing the input data using principal component analysis

Principal component analysis was used as input data compressing prior to both types of investigated ANNs namely principal component analysis–radial basis function networks (PC–RBFNs) and principal component analysis–feed forward neural networks (PC–FFNNs).

3.3.1. Construction of the PC–RBF network

As for WT–RBFNs, the *exact fit* type of radial basis function networks (RBFNs), was the choice for this part again. Variables were compressed by PCA to identify the PCs best describing the data matrix, and the scores of such PCs were used as input variables for the PC–RBFNs model. RMSE% values were minimum at five for each enatiomer. Also SPREAD values of 1–40 were investigated and SPREAD values of 12 and 15 were found as optimum values for D-α-Gly and L-α-Gly, respectively. Table 4 presents the results obtained for prediction samples of the D-α-Gly and L-α-Gly using constructed PC–RBFNs.

3.3.2. Construction of the PC–FFN network

Feed-forward neural networks including one to eight PCs as input were trained. The lowest RMSE% values were obtained with three and four for D-α-Gly and L-α-Gly, respectively. The proper number of nodes in the hidden layer was determined by training the PC–FFNN model with a different number of nodes and then comparing the prediction errors from an independent prediction set. The plots of RMSE% as a function of number of nodes in the hidden layer showed that minimum in RMSE% occurred when three nodes were used in the hidden layer for each particular network. The optimum number of epochs for each component was also obtained. By plotting of RMSE% as a function of number of epochs it was observed that, 800 iterations for each enantiomer cause the RMSE% to be minimum. Table 5 presents optimum number of epochs, hidden layer nodes and the best transfer functions. Neural network models for individual components were made with respect to the output layer considered as a single node corresponding to the enantiomer. Table 4 shows the prediction results obtained with a model having optimized parameters.

The results obtained for both isomers in terms of RSME% are close to each other but are some better for L-α-Gly. This maybe due to magnitude of the diastereomeric spectral differ-ences observed as evident. It is clear from these results that the spectral differences that arise due to the influence of enantiomeric composition are greater for L-α-Gly.

Comparison of the results obtained by the proposed methods with those obtained by PLS method [24] shows that the proposed method provides more accurate results. The proposed procedure can be applied to the accurate and precise prediction of enantiomers.

4. Conclusions

Although inclusion complexes of two enantiomers by β-CD have lack spectral discrimination, ANNs models afford their quantitation. The proposed methods use simple spectrophotometer and do not need any separation steps. So they were recommended for determination of enantiomeric composition. The WT–ANNs or PC–ANNs model simplify the training modeling procedure of ANNs, and only the significant wavelet coefficients or PCs in the model decreases the contribution of experimental noise and other minor extraneous factors. The results showed that wavelets effectively reduce the volume of data with minimal loss of resolution and characteristics. The ability to compress data without loss of utility for analytical purposes provides direct improvements in analytical determinations.

Satisfactory precision and accuracy was obtained with all of four investigated methods, although, because of surprisingly lower RMSE% values, WT–RBFNs were the preferred methods. Totally, application of RBFNs assisted with WT data compression seems the most proper for performing the non-linear multivariate calibrations.

References

[1] D. Perez-Marin, A. Garrido-Varo, J.E. Guerrero, Talanta 72 (2007) 28.
[2] F. Despagne, D.L. Massart, Analyst 123 (1998) 157.
[3] B. Li, Y. He, Luminscence 22 (2007) 317.
[4] E.P.P.A. Derks, M.S. Sanchez Pastor, L.M.C. Buydens, Chemom. Intell. Lab. Syst. 28 (1995) 49.
[5] A. Gulbag, F. Temurtas, C. Tasaltin, Z.Z. Ozturk, Sens. Actuators B 124 (2007) 383.
[6] S. Chen, C.F.N. Cowan, P.M. Grant, IEEE Trans. Neural Networks 2 (2 (March)) (1991) 302–309.
[7] P.H. Hindle, C.R.R. Smith, J. Near Infrared Spectrosc. 4 (1996) 119.
[8] M. Dathe, M. Otto, Fresenius' J. Anal. Chem. 356 (1996) 17.
[9] M. Bos, J.A.M. Vrielink, Chemometr. Intell. Lab. Syst. 23 (1994) 115.
[10] B.K. Alsberg, D.B. Kell, J.J. Rowland, M.K. Winson, A.M. Woodward, Analyst 122 (1997) 645.
[11] C.R. Mittermayr, S.G. Nikolov, H. Hutter, M. Grasserbauer, Chemometr. Intell. Lab. Syst. 34 (1996) 187.
[12] B. Walczak, D.L. Massart, Chemometr. Intell. Lab. Syst. 38 (1997) 39.
[13] B. Walczak, B. van den Bogaert, D.L. Massart, Anal. Chem. 68 (1996) 1742.
[14] U. Depczynski, K. Molt, A. Niemöller, Chemometr. Intell. Lab. Syst. 47 (1999) 179.
[15] N.P.E. Vermeulen, J.M. Te Koppele, in: I.W. Wainer (Ed.), Drug Stereochemistry, Marcel Dekker, New York, 1993.
[16] M.G. Finn, Chirality 14 (2002) 534.
[17] M.T. Reetz, Angew. Chem. Int. Ed. 40 (2001) 284.
[18] G.R. Sullivan, Top. Stereochem. 10 (1978) 287.

[19] A.M. Krstulvic (Ed.), Chiral Separation by HPLC, Ellis Horwood, Chichester, 1989.

[20] D.K. Lioyd, D.M. Goodall, G. Scrivener, Anal. Chem. 61 (1989) 1238.

[21] J. Zukowski, Y. Tang, A. Berthod, D.W. Armstrong, Anal. Chim. Acta 258 (1992) 83.

[22] K. Nakanishi, N. Berova, R.W. Woody (Eds.), Circular Dichroism Principles Applications, VCH, New York, 1994.

[23] M. Blanco, J. Coello, H. Iturriaga, S. Maspoch, C. Pérez-Maseda, Anal. Chim. Acta 407 (2000) 233.

[24] K.W. Busch, I.M. Swamidoss, S.O. Fakayode, M.A. Busch, J. Am. Chem. Soc. 125 (2003) 1690.

[25] K.W. Busch, I.M. Swamidoss, S.O. Fakayode, M.A. Busch, Anal. Chim. Acta 525 (2004) 53.

[26] H. Suzuki, Electronic Absorption Spectra and Geometry of Organic Molecules, Academic Press, New York, 1967.

[27] M. Blanco, J. Coello, H. Iturriaga, S. Maspoch, M. Porcel, Anal. Chim. Acta 431 (2001) 115.

[28] B.K. Alsberg, A.M. Woodward, D.B. Kell, Chemometr. Intell. Lab. Syst. 37 (1997) 215.

[29] A.K. Melung, F.T. Chau, J.B. Gao, Chemometr. Intell. Lab. Syst. 43 (1998) 165.

[30] B. Walczak (Ed.), Wavelet in Chemistry, Elsevier Science Publishers B.V., 2000.

[31] L. Nie, S.G. Wu, J.W. Wang, L.Z. Zheng, X. Lin, L. Rui, Anal. Chim. Acta 450 (2001) 185.

[32] C. Cai, P.D.B. Harrington, J. Chem. Inf. Comput. Sci. 38 (1998) 1161.

[33] L. Xiaoquan, L. Hongde, X. Zhonghua, Z. Qiang, J. Chem. Inf. Comput. Sci. 44 (2004) 1228.

[34] J. Trygg, S. Wold, Chemometr. Intell. Lab. Syst. 42 (1998) 209.

Cloud point extraction of mercury with PONPE 7.5 prior to its determination in biological samples by ETAAS

Pedro R. Aranda [a,b], Raúl A. Gil [a,b], Susana Moyano [a],
Irma E. De Vito [a], Luis D. Martinez [a,b,*]

[a] *Departmento de Química Analítica, Facultad de Química, Bioquímica y Farmacia,*
Universidad Nacional de San Luis, Chacabuco y Pedernera, P.O. Box 375,
5700 San Luis, Argentina
[b] *Consejo Nacional de Investigaciones Científicas y Técnicas (CONICET),*
Rivadavia 1917, C1033 AAJ Buenos Aires, Argentina

Abstract

Cloud point extraction (CPE) has been used for the pre-concentration of mercury, after the formation of a complex with 2-(5-bromo-2-pyridylazo)-5-(diethylamino)-phenol (5-Br-PADAP), and later analysis by electrothermal atomic absorption spectrometry (ETAAS) using polyethyleneglycolmono-*p*-nonyphenylether (PONPE 7.5) as surfactant. The chemical variables affecting the separation step were optimized. Under the optimum conditions, i.e, pH 8.5, cloud point temperature 80 °C, 5-Br-PADAP = 4×10^{-5} mol L^{-1}, PONPE 7.5 = 0.2%, sample volume = 1.0 mL, an enhancement factor of 22-fold was reached. The lower limit of detection (LOD) obtained under the optimal conditions was 0.01 μg L^{-1}. The precision for 10 replicate determinations at 2.0 μg L^{-1} Hg was 4.0% relative standard deviation (R.S.D.). The calibration graph using the pre-concentration system for mercury was linear with a correlation coefficient of 0.9994 at levels near the detection limits up to at least 16 μg L^{-1}. The method was successfully applied to the determination of mercury in biological samples and in certified reference material (QC METAL LL3).
© 2007 Elsevier B.V. All rights reserved.

Keywords: Mercury; Pre-concentration; CPE–ETAAS; Microwave digestion; Human hair; Urine

1. Introduction

Mercury can be present as a trace contaminant in all environmental compartments as a result of both natural origin and anthropogenic activities, and the determination of this element is of considerable interest due to its toxicity and ability of bioaccumulation in many organisms [1]. It is well known that organomercury compounds are much more toxic than mercury in its inorganic forms. It has been found that mercury may accumulate itself in vital organs and tissue such as kidney and brain [1]. Mercury may enter in human body by inhalation of mercury vapour (mainly in the form of Hg^0), drinking water (mainly as inorganic mercury, Hg^{2+}), and/or by the consumption of fish and fish products (mainly as methyl mercury, CH$_3$Hg$^+$) in the diet. The content of mercury in hair may represent the cumulative exposure from the occupational environment and/or daily diet. The toxicological implications of the mercury contents in the environments have encouraged the development of very sensitive methods for its determination [2,3].

Because of the extremely low levels of mercury in various matrices, high sensitivity and sophistication in the analytical procedures are required for its determination, and the most commonly used ones are cold vapour generation-atomic absorption spectrometry (CV-AAS) [4–7], cold vapour generation-atomic fluorescence spectrometry (CV-AFS) [8–12], inductively coupled plasma optical emission spectrometry (ICP-OES) [13,14], inductively coupled plasma mass spectrometry (ICP-MS) [15,16] and electrothermal atomization atomic absorption spectrometry (ETAAS) [1,3,5].

---

* Corresponding author. Fax: +54 2652 430224.
E-mail address: ldm@unsl.edu.ar (L.D. Martinez).

Usually a pre-concentration step has been needed for mercury determination in several environmental samples [17]. A scheme of pre-concentration can thus be proposed mediated by surfactants (CPE, cloud point extraction) instead of liquid–liquid extraction mediated by organic solvents. CPE is an interesting alternative to conventional solvent extraction because it produces high extraction efficiencies and concentration factors and uses inexpensive, non-toxic reagents [18,19]. The cloud point extraction method is solvent-free and non-polluting [20]. Now, it has been applied to the separation of several analytes in environmental and biological samples. The surfactants that are used in CPE are mostly non-ionic surfactants, such as Triton X-100, Triton X-114, polyoxyethylene-type non-ionic surfactants (PONPE 5.0 or PONPE 7.5) [13,19,20]. CPE in connection with atomic spectrometry can be a powerful analytical technique for metal pre-concentration and determination analysis [19–22]. CPE coupled to ETAAS is an efficient alternative, particularly because the organic matrix consisting of the surfactant and residual organic substances from the digested materials can be eliminated at least in part during the gradual increase in temperature prior to the atomization of the analyte. The purpose of this study is to combine CPE with ETAAS in order to perform a sensitive mercury determination in biological samples with minimal requirements of reagents, sample consumption and time of analysis.

The mercury was extracted as Hg-2-(5-Br-2-pyridylazo)-5-diethylaminophenol [Hg(II)-(5-Br-PADAP)] complex mediated by micelles of non-ionic surfactant PONPE 7.5. Under the optimal conditions, the analyte in surfactant-rich phase was determined by ETAAS with Pd as chemical modifier. All significant variables for both the separation and determination step were studied including pH of extraction, surfactant and reagent concentration, pyrolysis and atomization temperatures, different modifiers and also the furnace aging. The developed method was applied to the determination of trace mercury in biological samples and in a certified reference material (QC METAL LL3).

2. Experimental

2.1. Reagents

All reagents were of analytical-reagent grade and the presence of the mercury was not detected within the working range. A stock mercury standard ($1000 \, \mu g \, mL^{-1}$) was prepared from mercury(II) chloride (Merck, Darmstadt, Germany) in nitric acid (Merck, Darmstadt, Germany) and made to 1000 mL with ultrapure water. A $1 \times 10^{-2} \, mol \, L^{-1}$ solution of 5-Br-PADAP (Aldrich, Milwaukee, WI, USA) was prepared by dissolution in ethanol (Merck, Darmstadt, Germany). Lower concentrations were prepared by serial dilution with ethanol. As it is not possible to obtain a real aqueous solution of the surfactant polyethyleneglycolmono-*p*-nonyphenylether (PONPE 7.5, Tokyo Kasei Industries, Chuo-Ku, Tokyo, Japan) (cloud point below room temperature) it was experimentally convenient to prepare a stock solution as follows: 20 mL of PONPE 7.5 and 40 mL of distilled ethanol, were mixed and made up to 100 mL with doubly distilled water. The buffer solution ($5 \times 10^{-2} \, mol \, L^{-1}$) was prepared dissolving sodium tetrabo-

rate (Merck, Darmstadt, Germany) and taken to 1000 mL with ultrapure water. A $NaClO_4$ (Merck, Darmstadt, Germany) solution was used in order to adjust ionic strength. Nitric acid (Fluka, Sigma–Aldrich, Seelze, Germany) used for sample pre-treatment was of ultrapure reagent grade.

A $200 \, mg \, L^{-1}$ stock palladium solution was used as a chemical modifier. This solution was prepared in 0.1% (v/v) HNO_3 from stock solution of $1000 \, mg \, L^{-1}$ Pd $(NO_3)_2$.

Solution of Pt modifier containing $200 \, mg \, L^{-1}$ of the metal was prepared by dissolution of $PtCl_4$ (from Merck) in 10% HCl.

All the solutions containing the potentially interfering ions were prepared by adding appropriate amounts of stock solutions made from Merck Titrisol or their chloride salts in $0.3 \, mol \, L^{-1}$ hydrochloric acid.

Ultrapure water (18.1 MΩ cm) was obtained from Barnstead EASY pure RF water system (IA, USA).

All solvents and reagents were of analytical-reagent grade or better, and the presence of mercury was not detected in the working range.

2.2. Instrumentation

The measurements were performed with a Shimadzu Model AA-6800 atomic absorption spectrometer (Tokyo, Japan), equipped with a deuterium background corrector, a 6500-electrothermal atomizer and an ASC-6100 autosampler. Stabilized platform (L'Vov) graphite tubes (Shimadzu, Tokyo, Japan) were used in all experiments. Mercury hollow-cathode lamp (Hamamatsu, Photonics K.K., Japan) was employed as radiation source. The temperature program for GFAAS analysis is shown in Table 1. The 253.7 nm mercury wavelength was used in the subsequent determinations. The background correction was made with deuterium lamp mode.

Microwave digestion was performed with a domestic microwave oven (Philco, Ushuaia, Argentina) operating at a maximum power of 700 W, equipped with a magnetron of 2450 MHz and milestone hermetically sealed 100 mL internal volume, 1 cm wall thickness polytetrafluoroethylene (PTFE) reactors.

2.3. Sample pre-treatment

Hair samples were obtained using the following standardized cutting and washing procedure [17]: hair samples were collected from the occipital area, by cutting strands of hair close to the scalp. The hair length ranged from 5 cm to 10 cm. The hair was

Table 1
Furnace temperature program for Hg determination

Stage	Temperature (°C)	Ramp (s)	Hold (s)	Argon gas flow (L min^{-1})
Drying	140	5	15	0.1
Pyrolysis	650	5	50	1.0
	650	–	1	0.0 (read)
Atomization	2000	–	4	0.0 (read)
Clearing	2100	–	2	1.0

first cut into approximately 0.3 cm pieces and mixed to allow a representative sub-sampling of the hair specimen. After cutting, each sample was washed four times with a 1:200 (v/v) dilution of Triton X-100. The samples were then rinsed with acetone and allowed to drain. This was followed by three rinses with ultrapure water and two rinses with acetone. The samples were then dried in an oven at $40 \pm 5\,^{\circ}\text{C}$. To carry out the digestion of the samples, 0.5 g of washed hair samples, accurately weighed, were used and placed in a microwave assisted digestion system. Then, 2 mL of concentrated nitric acid and 2 mL of hydrogen peroxide was added and the samples were digested as follows: urine samples were digested in several steps applying different microwave powers, i.e. MW power was held at 250 W (3 min), 250 W (5 min), 500 W (5 min), 500 W (5 min) and 250 W (5 min). Hair samples were digested applying a similar power–time program: 350 W (5 min), 350 W (5 min), 550 W (5 min) and 550 W (5 min). The vessels were then removed from the oven and cooled at $20\,^{\circ}\text{C}$, after they were vented and opened. A clear solution was obtained. Then, the clear solutions were heated until the remained nitric acid was eliminated. The remained acid was neutralized with sodium hydroxide and the final sample pH was adjusted with buffer solution. Finally, the solution was diluted up to 50 mL with ultrapure water. Following that procedure, losses of mercury, which can be important in an open system, were avoided. The microwave program took approximately 23 min, and the entire digestion process took a larger amount of time. However, it must be taken into account that it is possible to simultaneously treat as many samples as can be placed in the digestion system.

Urine samples in the morning were collected from voluntary patients and were digested immediately as follows: 8 mL of urine were placed in a 100-mL PTFE reactor and after that 2 mL of concentrated nitric acid and 2 mL of hydrogen peroxide were added. Then the samples were submitted to the MW-assisted digestion.

2.4. Sample preparation procedure

The pre-concentration procedure started with the addition of 0.5 mL of surfactant solution, 0.2 mL of 1×10^{-2} mol L^{-1} chelating solution, 0.2 mL of 2.5×10^{-5} mol L^{-1} metal-ion solution and 5.0 mL of buffer solution (pH 8.5). The mixture was diluted up to 50 mL with ultrapure water. The resultant solution was equilibrated at $70\,^{\circ}\text{C}$ for 10 min. The turbid solution was then cooled in an ice-bath for 10 min with the purpose of increasing the surfactant-rich phase viscosity. Then, the removal of the aqueous phase was carried out by simply inverting the tubes. Any residual water was removed using a Pasteur pipette. To reduce the viscosity of the surfactant phase prior to GFAAS analysis, 1.0 mL of methanol acidified with 0.1 mol L^{-1} HNO$_3$ was added to the extract. Finally, 20-μL aliquots of the resulting solution were directly injected into the graphite tube by means of the autosampler and submitted to the temperature program shown in Table 1. Calibration was performed against aqueous standards submitted to the same cloud point extraction procedure. A blank submitted to the same procedure described above was measured parallel to the samples and calibration solutions.

3. Results and discussion

3.1. Study of the CPE system variables

3.1.1. Effect of reagent excess

In order to determine the optimal reagent–metal-ion ratio, an experiment was carried out in which all other experimental variables, except reagent concentration, remained constant. We could verify that with a reagent:metal ratio above 10:1, best extraction was achieved. However, a reagent:metal ratio of 400 was selected in order to ensure quantitative complexation and for avoiding interference of foreign ions.

3.1.2. Effect of buffer concentration and ionic strength

Sodium tetraborate buffer agent was employed in all experiments. The system was studied within sodium tetraborate concentration range: 5×10^{-4} to 5×10^{-2} mol L^{-1} and ionic strength within the range: 0–1 mol L^{-1}, adjusted with NaClO$_4$. The best performance (higher extraction percentage, optimal stability, lower equilibration time and ease of phase separation) was achieved for a sodium tetraborate concentration of 5×10^{-3} mol L^{-1} and ionic strength 0–0.35 mol L^{-1}. For ionic strength higher than 0.4 mol L^{-1}, a quantitative phase separation was not possible.

3.1.3. Effect of pH

The effect of pH upon the complex formation of Hg-5-Br-PADAP was studied within the range of pH 5–12. The results are shown in Fig. 1. As can be seen, the complex extraction begins at pH 6 and starts to decrease at pH 9.7, showing a plateau for the range pH 7.5–9.5. Then a pH 8.5 was chosen for further experiments.

3.1.4. Surfactant concentration

The variation of the percentage of extraction (calculated as percent ratio between the mass of Hg in the extract to mass of Hg present in standard solution) upon the surfactant concentration was examined within range: $C_{\text{PONPE 7.5}} = 0.025$–1.5% (v/v). Extractions close to 100 were observed for a surfactant concentration higher than 0.07% (v/v). In order to achieve a good enrichment factor, 0.2% (v/v) was chosen as optimal.
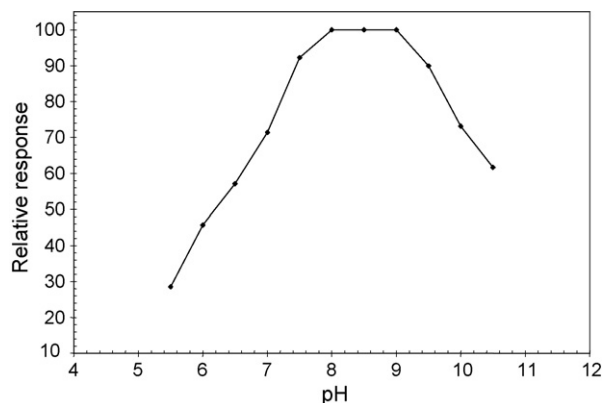

Fig. 1. Effect of the pH on the mercury analytical response.

3.2. Graphite furnace temperature programs

Study of the best condition for graphite furnace steps was carried out by optimization of hold time, temperature of pyrolysis, and temperature of atomization. For this purpose, a cloud point extraction prepared from an aqueous solution containing $2.0 \mu g L^{-1}$ of Hg was employed for all experiments. To reduce the viscosity of the surfactant phase prior to ETAAS analysis, 1.0 mL of methanol acidified with $0.1 mol L^{-1}$ HNO_3 was added to the extract. Suitable amounts of Pd were co-injected with the extract directly into the graphite furnace, to give $4 \mu g$ of Pd. Additionally, for obtaining the most suitable times and temperatures, the common way of working in ETAAS was followed.

3.2.1. The drying temperature

The drying temperature was selected at $140\,^{\circ}C$, with a hold time of 15 s, which could be sufficient to take out the solvent completely.

3.2.2. The pyrolysis temperature

The ramp time for the pyrolysis stage was carefully optimized in order to achieve a gradual elimination of the organic matrix; avoiding analyte losses during a sudden increase in the temperature.

Generally, the higher pyrolysis temperature achieved for the analysis of mercury in aqueous solutions is around $140\,^{\circ}C$ [23].

When Hg is determined in an organic matrix such as the micellar-rich phase of the CPE, the pyrolysis temperature could be as high as $550\,^{\circ}C$ when a mixture of $HNO_3 + MeOH$ was added.

The effect of Pd as chemical modifier was studied. It was observed that a considerable thermal stabilization was achieved when Pd was co-injected with the analyte. In this way, the pyrolysis temperature could be elevated at levels up to $650\,^{\circ}C$ (Fig. 2). After that, we evaluated the effect of Pt, and the results obtained indicated that this element could not be employed here as chemical modifier because of the high background generated and the poor thermal stabilization achieved. Regarding to the
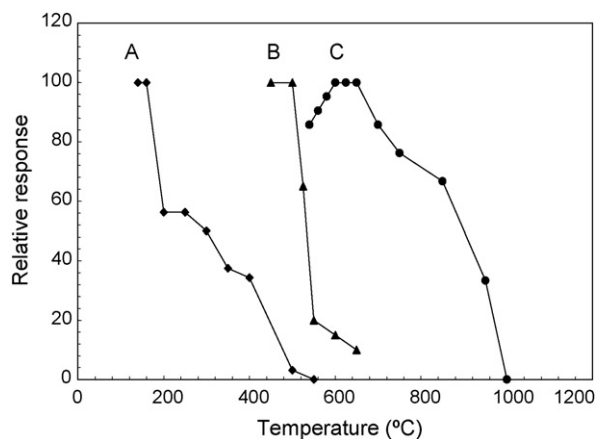
Pd effect on Hg thermal stability, it could be concluded that Pd itself enhanced the Hg stability. Fig. 2 shows that pyrolysis temperature lower than $600\,^{\circ}C$ could not be used when Pd was used because the sensitivity diminished. This was why the pyrolysis seemed to be incomplete and the background was considerable, leading an overcorrection, which generated erroneous absorbance lectures. However, the addition of methanol–nitric acid mixture was essential for efficient matrix elimination without Hg loses. This fact could be attributed to the oxidant effect of the nitric acid, which helped to the rapid oxidation of the organic matter in the pyrolysis stage.

3.2.3. The atomization and cleaning temperatures

A study of the atomization step was carried out in the range of $1200–2200\,^{\circ}C$. The optimum atomization temperature was selected at $2000\,^{\circ}C$ within the temperature interval studied. In addition, a hold time of 4 s was obtained for this step. At this temperature, no tailed peaks were observed which indicated that all mercury atoms were not adsorbed on the atomizer platform, and were fastly eliminated after the atomization [24]. Besides the obtained atomization temperatures for standards and samples were not different, and then the temperature of $2000\,^{\circ}C$ was considered for both.

A temperature of $2100\,^{\circ}C$ and a hold time of 2 s were selected for cleaning step.

The lifetime of graphite tubes, which used this temperature program, was so considerable; in fact, our studies comprised about 400 trials and no significant changes were observed in the mercury standards signal.

3.3. Interferences

The effects of representative potential interfering species were tested. Thus, Cu^{2+}, Zn^{2+}, Cd^{2+}, Ni^{2+}, Co^{2+}, Mn^{2+} and Fe^{3+} could be tolerated up to at least $2000 \mu g L^{-1}$. Commonly encountered matrix components such as alkali and alkaline earth elements generally do not form stable complexes and are not CPE extracted. The value of the reagent blank signal was not modified by the presence of the potentially interfering ions assayed. A high concentration of 5-Br-PADAP reagent was added in order to guarantee the complete chelation of the analyte even in the presence of interferents.

3.4. Analytical performance

The enhancement factor was calculated as the ratio between the slopes of a curve established using aqueous solutions submitted to the cloud point extraction procedure and a curve with aqueous standards not submitted to this procedure and we could estimate a 22-fold enrichment factor. A limit of detection of $0.01 \mu g L^{-1}$ was obtained for aqueous solutions (calculated as three times the standard deviation of the blank signal divided by the slope of the calibration plot). A LOD of $0.1 \mu g L^{-1}$ and $0.001 \mu g g^{-1}$ was obtained for urine and hair samples, respectively. The precision for 10 replicate determinations at $2.0 \mu g L^{-1}$ Hg was 4.0% relative standard deviation (R.S.D.). The calibration graph using the pre-concentration system for

Fig. 2. (A) Pyrolysis curve of Hg ($12 \mu g L^{-1}$) in aqueous solutions without modifier; (B) pyrolysis curve of Hg ($2 \mu g L^{-1}$)–CPE–MeOH–HNO_3; (C) pyrolysis curve of Hg ($2 \mu g L^{-1}$)–CPE–MeOH–HNO_3 + Pd.

Table 2
Concentrations of Hg in human urine and hair samples (95% confidence level; $n = 6$)

Sample	Base	Hg added	Hg found	Recovery (%)[a]
Hair (μg Hg g^{-1})	0.325	–	0.325	–
	0.325	0.050	0.375	100
	0.325	0.100	0.422	97
Urine (μg Hg L^{-1})	0	–	0	–
	0	0.50	0.49	98
	0	1.00	1.01	101

[a] [(found − base)/added] × 100.

mercury was linear with a correlation coefficient of 0.9994 at levels near the detection limits up to at least $10 \mu g \, L^{-1}$.

3.5. Accuracy verification

The proposed method was applied to a standard reference material, QC METAL LL3 mercury in water, with a mercury content of $6.48 \pm 0.51 \mu g \, L^{-1}$. Using the proposed method, the content of mercury determined in this CRM was $6.90 \pm 0.28 \mu g \, L^{-1}$ (95% confidence interval; $n = 6$).

4. Application to real samples

Finally, the proposed methodology was applied to human hair and urine samples. The average mercury level found in hair samples under study was $325 \, ng \, g^{-1}$. The mean mercury concentration obtained is in good agreement with those results reported by other authors. Additionally a recovery study was performed in order to evaluate any matrix interferences and/or possible analyte losses during the sample pre-treatment. For this purpose, six portions of 0.5 g of hair samples were collected. All the samples were digested following the proposed procedure. The proposed method was applied to three portions and average quantity of mercury obtained was taking as base value. Then increasing quantities of Hg were added to the other aliquots of sample and the analyte was determined by the same method. In all cases the recovery was close to 100%. In addition, the proposed methodology was applied to the determination of mercury in human urine samples and the mercury level in all cases was lower than the detection limit. A recovery study was carried out in this case, and the recoveries in all cases were close to 100. The results are shown in Table 2.

5. Conclusion

Cloud point extraction using PONPE 7.5 has shown to be an efficient, simple and versatile pre-concentration methodology to determine Hg by ETAAS in biological samples submitted to a microwave-assisted acid digestion. Phase separation can be achieved at relatively low temperatures and the extraction percentages were high, resulting in high enhancement factors and low detection limits, which are enough when a mercury determination is made in a variety of biological and environmental samples. Furthermore, although the analytical performance of the proposed methodology was similar to the method devel-

oped in our research group where we employed PONPE 5.0 as surfactant agent for CPE-coupled CV-ICP OES [13]; furthermore, the method developed here is a promising method for Hg determination which joins the advantages of the CPE with the obvious advantages of any ETAAS method, i.e. minimal reagent employment, feasibility, low cost and sensibility. Additionally, the microwave digestion makes it such a versatile method, being adequate for environmental and biological studies.

The use of chemical modifiers has shown to be necessary, which is added, allowing a maximum pyrolysis temperature of 650 °C to be used for Hg. This procedure might well be extended to other biological materials after proper acid digestion and certainly to other elements that form complexes with 5-Br-PADAP.

References

[1] A. Tessier, D. Turner, Metal speciation and bioavailability in aquatic systems, John Wiley and Sons, Chichester, UK, 1995 (Chapter 3).
[2] M.S. Hosseini, H. Hashemi-Moghaddam, Talanta 67 (2005) 555.
[3] M. Saber-Tehrani, M.H. Givianrad, H. Hashemi-Moghaddam, Talanta 71 (2007) 1319.
[4] J.C.A. Wuilloud, R.G. Wuilloud, R.A. Olsina, L.D. Martinez, J. Anal. Atom. Spectrom. 17 (2002) 389.
[5] J.L. Capelo, C.D. dos Reis, C. Maduro, A. Mota, Talanta 64 (2004) 217.
[6] J.C.A. Wuilloud, R.G. Wuilloud, J.A. Gásquez, R.A. Olsina, L.D. Martinez, Atom. Spectrosc. 22 (2001) 398.
[7] D.P. Torres, M. Antunes Vieira, A. Schwingel Ribeiro, A.J. Curtius, J. Anal. Atom. Spectrom. 20 (2005) 289.
[8] Z. Long, J. Xin, X. Hou, Spectrosc. Lett. 37 (2004) 263.
[9] T. Labatzke, G. Schlemmer, Anal. Bioanal. Chem. 378 (2004) 1075.
[10] Y.W. Chen, J. Tong, A. D'Ulivo, N. Belzile, Analyst 127 (2002) 1541.
[11] E. Bramanti, C. Lomonte, M. Onor, R. Zamboni, A. D'Ulivo, G. Raspi, Talanta 66 (2005) 762.
[12] Y. Cai, Trends Anal. Chem. 19 (2000) 62.
[13] J.C.A. Wuilloud, R.G. Wuilloud, M.F. Silva, R.A. Olsina, L.D. Martinez, Spectrochim. Acta, Part B 57 (2002) 365.
[14] E.J. dos Santos, A.B. Herrmann, M. Antunes Vieira, V.L. Azzolin Frescura, A.J. Curtius, Spectrochim. Acta, Part B 60 (2005) 659.
[15] J.C.A. Wuilloud, R.G. Wuilloud, A.P. Vonderheide, J.A. Caruso, Spectrochim. Acta, Part B 59 (2004) 755.
[16] R.J.C. Brown, M.J.T. Milton, Trends Anal. Chem. 24 (2005) 266.
[17] N. Ferrúa, S. Cerutti, J.A. Salonia, L.D. Martinez, J. Hazard. Mater. 141 (2007) 693.
[18] H. Watanabe, T. Saitoh, T. Kamidate, H. Haraguchi, Microchim. Acta 106 (1992) 83.
[19] X. Zhu, X. Zhu, B. Wang, J. Anal. Atom. Spectrom. 21 (2006) 69.
[20] M.F. Silva, E.S. Cerutti, L.D. Martinez, Microchim. Acta 155 (2006) 349.
[21] D.L.G. Borges, M.A.M. Silva da Veiga, V.L.A. Frescura, B. Welz, A.J. Curtius, J. Anal. Atom. Spectrom. 18 (2003) 501.
[22] T.A. Maranhao, D.L.G. Borges, A.J. Curtius, M.A.M. Silva da Veiga, Spectrochim. Acta, Part B 60 (2005) 667.
[23] D.J. Butcher, J. Sneddon, in: J.D. Winefordner (Ed.), A Chemical Analysis: A Series of Monographs on Analytical Chemistry and its Applications, vol. 149, John Wiley and Sons, Inc., New York, 1998, pp. 215–225.
[24] G. Schlemmer, B. Radziuk, A Laboratory Guide, Birkhaüser Verlag, Berlin, 1999, pp. 195–200.

Determination of anti-inflammatory drugs in water samples, by in situ derivatization, solid phase microextraction and gas chromatography–mass spectrometry

Lilia Araujo, Johana Wild, Noreiva Villa, Nuris Camargo,
Dalia Cubillan, Avismelsi Prieto *

*Laboratory of Analytical Chemistry and Electrochemistry, Faculty of Engineering,
University of Zulia, P.O. Box 4011-A-526, Maracaibo, Venezuela*

Abstract

A new analytical method for the determination of non-steroidal acidic anti-inflammatory drugs in water samples is described. These compounds are used as anti-inflammatory, antipyretic and analgesic drugs in human health care and in veterinary applications. Analytical procedure involves in situ derivatization of analytes to their methyl esters with dimethyl sulphate, headspace sampling using solid-phase microextraction (SPME), and gas chromatography–mass spectrometry (GC–MS). The effects of pH, ionic strength, extraction time, SPME fibre, extraction temperature as well as derivatization conditions were studied. Methyl esters were extracted with a fused-silica fibre coated with $100 \, \mu m$ polydimethylsiloxane. Response was linearly dependent on concentration in the range $0.1–10.0 \, ng \, mL^{-1}$. Detection limits were achieved at the level of $0.3–2.9 \, ng \, L^{-1}$. Derivatization-SPME/GC–MS analysis yielded good precision (R.S.D. between 7.9 and 17.2%). The method was validated by analysis of spiked matrix samples.
© 2007 Elsevier B.V. All rights reserved.

Keywords: Pharmaceutical residues; Tap water and wastewater analysis; Direct derivatization-SPME; GC–MS

1. Introduction

Pharmaceuticals products used for humans and animals have been identified as emerging environmental pollutants [1–4]. Non-steroidal acidic anti-inflammatory drugs (NSAIDs) are among the group of pharmaceutical compounds most often used to treat human and animal illnesses. These compounds are excreted unchanged or as active metabolites in high percentages and continuously discharged into domestic wastewaters. Incomplete removal during wastewaters biological treatments has caused their presence into surface waters at concentrations from $ng \, L^{-1}$ to $\mu g \, L^{-1}$ level [5–7]. The complete effects on aquatic organisms and humans are not well understood. Due to their biological activity, their determination in the environment is important [8].

Suitable methods exist for a quantitative measurement of NSAIDs in water samples, using gas chromatography–mass spectrometry (GC–MS), high performance liquid chromatography–mass spectrometry (HPLC–MS), micellar electrokinetic capillary chromatography (MEKC) and capillary electrophoresis [9–14], but in general the preconcentration step is extensive, requires large sample volumes (between 0.5 and 2.0 L), sample clean-up or the use of organic solvents. There is a need for fast and simple methods to supply this analysis.

Solid phase microextraction (SPME) is a two-step process conducive to the simultaneous extraction and preconcentration of organic compounds. Since its introduction, SPME has gained popularity as a simple, solvent-free, reliable and flexible tool for the sampling of a variety of volatile and semivolatile compounds. SPME requires less sample volume than solid phase extraction or liquid–liquid extraction. SPME is suitable for analysis of drugs residues in water. On the other hand GC analysis of acidic drugs is complicated because a derivatization step is necessary prior to analysis. Generally, prior to the determination of acidic drugs in water, the analytes are transferred to an organic matrix where

* Corresponding author. Fax: +58 261 7598736.
E-mail address: aprieto@luz.edu.ve (A. Prieto).

derivatization takes place. SPME allows the derivatization of the analytes to take place in the sample matrix, in the SPME fibre coating or in the GC injector port [15–18]. However few studies consider the option of performing the derivatization directly in the water matrix [19,20]. To date, NSAIDs have not been investigated by direct derivatization-SPME procedure. By in situ methylation, the acidic drugs are converted to less polar methyl esters, which may improve the extraction into the SPME fibre.

In this paper, a new method for analysis of six non-steroidal acidic anti-inflammatory drugs (ibuprofen, flufenamic acid, naproxen, mefenamic acid, tolfenamic acid, and meclofenamic acid) in water samples using headspace SPME/GC–MS is proposed. Analytical procedure involves in situ derivatization of acidic drugs to their methyl esters with dimethyl sulfate.

2. Experimental

2.1. Materials and reagents

All reagents were of analytical-reagent grade unless stated otherwise. Water was purified with a Nanopure system (Barnstead, USA). Ibuprofen, flufenamic acid, naproxen, mefenamic acid, tolfenamic acid and meclofenamic acid were supplied by Sigma (St. Louis, MO, USA). A stock standard solution of $1000 \, \mu g \, mL^{-1}$ of each compound was prepared in basic deionized water. Working solutions were obtained by appropriated dilutions with deionized water. The derivatization reagent dimethyl sulfate (DMS) was purchased from Riedel-de Haen. Tetrabutylammonium hydrogen sulfate (TBA-HSO$_4$) was obtained from Fluka. A manual fibre holder for SPME was purchased from Supelco (Bellefonte, PA, USA). Two types of fibre, 100 μm polydimethylsiloxane and 85 μm polyacrylate were obtained from the same manufacturer. The fibres were conditioned as recommended by the manufacturer.

2.2. Instrumentation

Chromatography analysis was performed using a 6890N series gas chromatograph equipped with a split–splitless injector for the HP-5MS fused silica capillary column (30 m × 0.25 mm i.d., 0.25 μm film thickness), and 5973 quadrupole mass selective detector (Agilent Technologies, USA). A silanized narrow-bore injector liner (0.75 mm i.d.) for the SPME injections was installed and the fiber was inserted into this injector using the splitless mode with the split closed for 3 min. The injector temperature was set at 250 °C and the transfer line temperature was 260 °C. The oven temperature was held at 50 °C for 3 min, and then heated to 250 °C at a heating rate of 30 °C min^{-1}. Temperature was held at 250 °C for 4.5 min. The carrier gas was helium (purity 99.999%) at a flow rate of 1 mL min^{-1}. The mass spectrometer detector was tuned by maximum sensitivity autotune. The following *m/z* values were acquired in the electron impact ionization mode by single ion monitoring and used for quantification of the analytes: 161–220 for ibuprofen, 263–295 for flufenamic acid, 185–244 for naproxen, 223–255 for mefenamic acid, 208–275 for tolfenamic acid and 242–309 for meclofenamic acid.

2.3. Procedure

6.0 mL of standard solution or sample was placed in a 14 mL screw-cap glass vial. Phosphate buffer solution (pH 6.0, 3.0 mol L^{-1}, 2.0 mL) and Na$_2$SO$_4$ (2.88 g) were then added and the sample was agitated with a 1.8 cm long PTFE-coated stir bar. After addition of the ion-pairing reagent (TBA-HSO$_4$, 0.1 M, 60 μL), the vial was closed. 15 μL of derivatization reagent (DMS) was then injected through the septum and the vial was immersed in a temperature-controlled oil bath. After 10 min at 70 ± 2 °C, the PDMS fibre was exposed to the headspace above the aqueous solution for 45 min. The samples were agitated with a magnetic stirring bar at 500 rpm during both derivatization and extraction. After the extraction the fibre was directly exposed to the hot injector of the GC for 3 min and the chromatogram was registered.

Aqueous standards were prepared and analyzed for calibration.

3. Results and discussion

3.1. Optimization of the microextraction with in situ derivatization

It has been reported that DMS reacts with haloacetic acids and chlorophenoxy acid herbicides in water to produce the corresponding methyl ester [21,22]. The addition of ion-pairing agents, which activate the analytes during derivatization, increases esterification yields and thus improves the sensitivity of the procedure. In this work, experiments were performed in which DMS and the ion-pair agent TBA-HSO$_4$ was added to aqueous solutions containing each of the six test compounds. After the reaction, the solution was extracted with headspace SPME and analyzed by means of GC–MS. Detectable yields of methyl esters were achieved for the analytes and identified on the basis of their mass spectra. Next, preliminary experiments were carried out to optimize the main parameters affecting both derivatization and SPME of the analytes investigated. In this study deionized water samples spiked with the appropriate amount of the standard solution was used. The more adequate fibre was found by comparing the extraction behavior on two commercial SPME fibres, 100 μm polydimethylsiloxane and 85 μm polyacrylate. Polydimethylsiloxane fibre exhibited the highest extraction performance and was chosen for the rest of experiments.

The effect of pH was investigated by changing the pH in the range 3–10. As shown in Fig. 1, no significant effect was observed in the range of 3–7. At higher pH, a decrease was observed in the response. From these results it was decided to adjust the pH of water samples to 6.0. A 0.75 M concentration of the phosphate buffer (pH 6.0) was selected to obtain an adequate buffering capacity.

The effect of temperature was monitored by extracting samples of 10 ng mL^{-1} of NSAIDs in the range of 40–80 °C. Fig. 2 shows a clear increase in the amount of analytes adsorbed when the temperature increases. However, when the temperature exceeded 70 °C, there was a decrease in the amount of
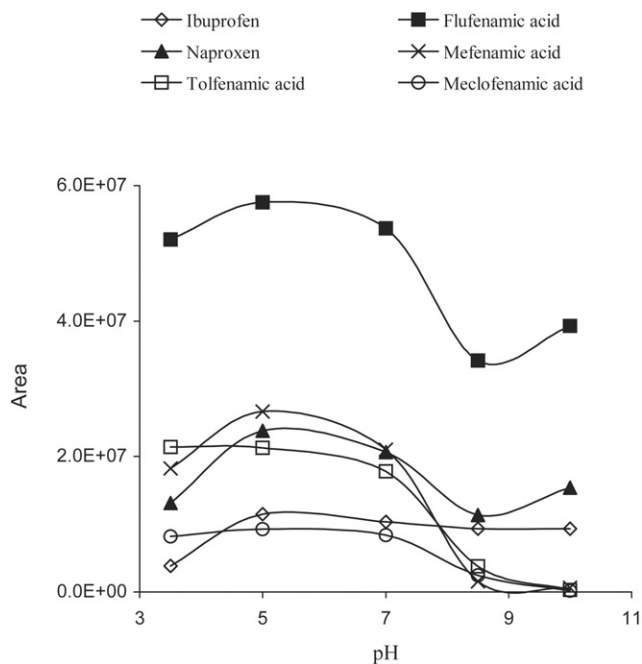
Fig. 1. Effect of sample pH for in situ methylation headspace SPME of the six NSAIDs.

NSAIDs extracted except for mefenamic acid, tolfenamic acid and meclofenamic acid. As a compromise, 70 °C was chosen as the optimum temperature for the derivatization and SPME extraction of all the methyl derivatives of NSAIDs.

In order to set an optimal volume of the derivatization reagent necessary for complete esterification of NSAIDs, a range of 5–100 µL of DMS volumes were tested at 70 °C. Increasing the volume of DMS in the range 5–60 µL improved slight the yield of methyl esters while the response decreased at higher amounts of DMS. However, 100 µm PDMS fibre was too fragile at DMS volume higher than 15 µL and it could only be used for a limited number of experiments. For this reason 15 µL was used for the rest of the experiments.
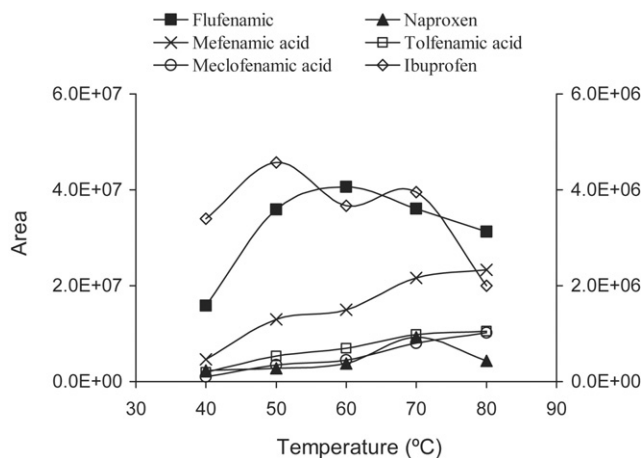
Fig. 2. Effect of temperature on the extraction of $10 \, \text{ng mL}^{-1}$ of NSAIDs with polydimetilsiloxane fibre. For ibuprofen, the scale is shown on the right. Concentration of ibuprofen is $5 \, \text{ng mL}^{-1}$ ($n = 2$).
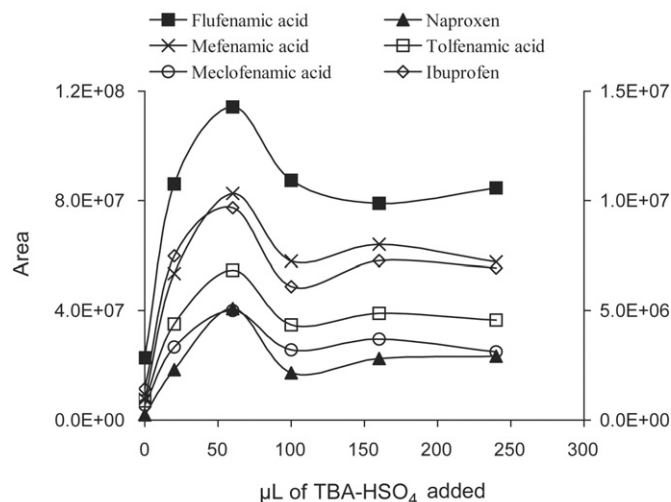
Fig. 3. Influence of amount of 0.1 M TBA-HSO$_4$ added on NSAIDs reaction yields to the corresponding methyl esters. For ibuprofen, the scale is shown on the right.

We investigated the effect of the TBA-HSO$_4$ volume on the amount of NSAIDs extracted from the sample onto the PDMS fibre. TBA-HSO$_4$ volume profile was studied by monitoring the GC area counts as a function of TBA-HSO$_4$ volume. The effect of the ion-pairing agent on the yield of the methylation is shown by the increase in the peak area obtained with the use of TBA-HSO$_4$ (Fig. 3). The addition of 60 µL of TBA-HSO$_4$ ensured the maximum response for NSAIDs methyl esters.

Extraction time profiles were studied extracting samples of $10 \, \text{ng mL}^{-1}$ of NSAIDs and monitoring the GC area counts as a function of exposure time (Fig. 4). Equilibrium was not attained even after 90 min. For quantitative analysis it is not necessary for the analytes to have reached equilibrium, but only for sufficient loading onto the fibre and reproducible extraction time [23]. An
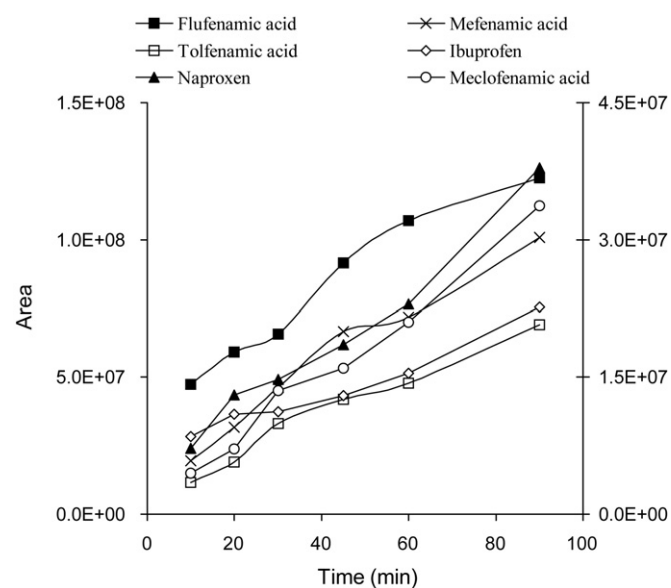
Fig. 4. Absorption time profile of $10 \, \text{ng mL}^{-1}$ of NSAIDs in deionized water with polydimetilsiloxane fibre. For naproxen, ibuprofen and meclofenamic acid, the scale is shown on the right. Concentration of ibuprofen is $5 \, \text{ng mL}^{-1}$.

Table 1
Analytical parameters

	Analytes[a]					
	IBU	FLU	NAP	MEF	TOL	MEC
Correlation coefficient	0.999	0.996	0.998	0.991	0.997	0.994
Linearity $[1-\text{R.S.D.}(b)]$ (%)	99.3	97.6	98.7	97.9	98.6	98.1
Detection limit (ng L^{-1})	0.3	0.4	2.7	1.3	1.6	2.9
Quantification limit (ng L^{-1})	1.0	1.4	9.0	4.4	5.4	9.7
Repeatability (R.S.D.,%), $n=8$ (ng mL^{-1})						
0.03	15.1	15.5	16.6	17.2	16.8	15.4
0.1	13.2	13.9	14.3	14.2	14.1	11.8
1.3	11.4	10.6	11.3	10.0	12.7	10.9
2.5	11.5	10.7	11.4	10.2	12.6	11.2
3.0	7.9	8.9	9.8	9.6	10.2	11.4

[a] IBU: ibuprofen, FLU: flufenamic acid, NAP: naproxen, MEF: mefenamic acid, TOL: tolfenamic acid, MEC: meclofenamic acid.

extraction time of 45 min was selected as a compromise between analyte response and time analysis.

The role of the ionic strength of the matrix was investigated by using sodium chloride and sodium sulfate. For many organic analytes, aqueous solubility decreases with increasing ionic strength, and thus, the partitioning from the aqueous solution to the headspace is improved. The amounts tested for a sample volume of 8 mL varied from 0 to 2.88 g of NaCl or Na$_2$SO$_4$. The results obtained show a strong increment in the signal for all analytes when the NaCl or Na$_2$SO$_4$ amount increases. Responses for the sample with 2.88 g of Na$_2$SO$_4$ added were between 2.7 and 6.2 times that for the sample with 2.88 g of NaCl. Thus, 2.88 g of Na$_2$SO$_4$ was selected to obtain an adequate salting-out effect.

In order to study the carryover effect, blanks were ran after extractions of 50 ng mL^{-1} of NSAIDs. No signals were obtained when a 3 min desorption time was chosen, which ensured a complete desorption of methyl esters.

3.2. Application and validation of the proposed method

Calibration graphs for deionized water samples treated according to the procedure described previously, monitored using SIM mode, were linear for the concentration range 0.1–10.0 ng mL^{-1}. This range agreed with environmental levels in water currently reported in the literature for these compounds [24–26]. Two replicates were used for each of six prepared standards to obtain the calibration graphs. Results for regression coefficient (r) and linearity $[1-\text{R.S.D.}(b)]$ (%) are summarised in Table 1. The precision was measured by performing 8 independent determinations. Precisions ranged from 7.9 to 17.2% R.S.D. (Table 1), which should be satisfactory for determining the NSAIDs in water matrix.

The detection limit was calculated by comparing the signal–to–noise ratio (S/N) of the lowest detectable concentration to a S/N = 3. A S/N of 10 was applied for the calculation of the quantification limit. The detection limits found were between 0.3 and 2.9 ng L^{-1} (Table 1). Detection limits are in accordance with other methods based on SPE-MEKC, SPE-derivatization–GC/MS, SPME-derivatization–GC/MS or SPE-HPLC/MS [13,16,27,28].

Optimum headspace SPME sampling conditions for deionized water were applied to the tap water and wastewater matrices.

Absolute response value was lower for the wastewater samples rather than for the deionized water. The presence of additional organic and inorganic compounds could interfere with the diffusion and volatilization of the methyl esters. Thus, it decreased the extraction performance by headspace SPME.

Table 2
Results of assays to check the accuracy of the proposed method for NSAIDs in spiked tap water and wastewater samples

Analyte	Sample	Spiked (ng mL^{-1})	Found[a] (ng mL^{-1})	% recovery[b]
Ibuprofen	Tap water	0.09	0.08 ± 0.01	88.9
		3.0	2.83 ± 0.33	94.3
	Wastewater	0.5	0.38 ± 0.05	76.0
		4.0	3.47 ± 0.48	86.8
Flufenamic acid	Tap water	0.09	0.12 ± 0.02	133.3
		3.0	2.75 ± 0.37	91.6
	Wastewater	0.5	0.57 ± 0.09	114.0
		4.0	3.46 ± 0.55	86.5
Naproxen	Tap water	0.09	0.09 ± 0.01	100.0
		3.0	3.08 ± 0.41	102.7
	Wastewater	0.5	0.48 ± 0.06	96.0
		4.0	3.69 ± 0.70	92.3
Mefenamic acid	Tap water	0.09	0.07 ± 0.01	77.8
		3.0	2.76 ± 0.40	92.0
	Wastewater	0.5	0.58 ± 0.11	116.0
		4.0	3.63 ± 0.67	90.8
Tolfenamic acid	Tap water	0.09	0.08 ± 0.02	88.9
		3.0	2.97 ± 0.39	99.0
	Wastewater	0.5	0.56 ± 0.12	112.0
		4.0	3.46 ± 0.56	86.5
Meclofenamic acid	Tap water	0.09	0.10 ± 0.02	111.1
		3.0	2.76 ± 0.32	92.0
	Wastewater	0.5	0.41 ± 0.10	82.0
		4.0	3.14 ± 0.59	78.5

[a] Average value ± standard deviation of five determinations.
[b] "% recovery" refers to the NSAIDs concentrations determined rather than the actual percent of analytes extracted by the SPME analysis.
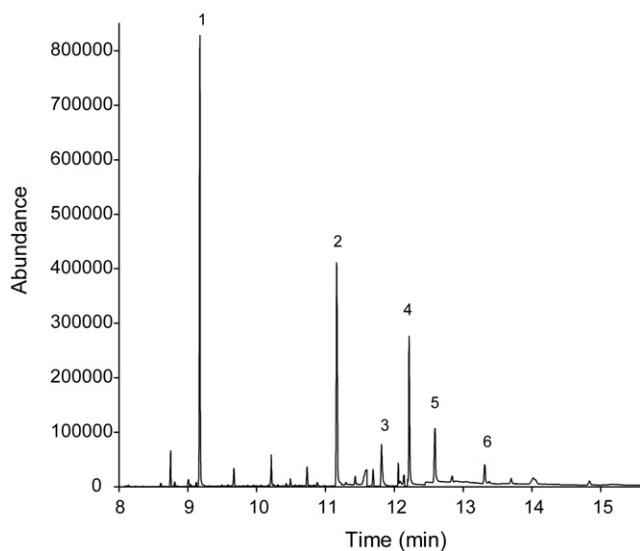
Fig. 5. Typical chromatogram obtained in SIM mode of a wastewater sample spiked with $1.0\,ng\,mL^{-1}$ of each analyte. 1: ibuprofen, 2: flufenamic acid, 3: naproxen, 4: mefenamic acid, 5: tolfenamic acid, 6: meclofenamic acid.

Samples were diluted 3:1 with buffer solution to improve the extraction yield.

We tried to find NSAIDs in tap water samples and effluent of a sewage treatment plant. We did not find NSAIDs above our detection limit. Samples were fortified with different levels of NSAIDs. External calibration was used in the evaluation of NSAIDs for tap water samples and standard addition calibration was used for wastewater samples because matrix effects were observed. Identity of these compounds was confirmed by using a peak retention times window within 1.5% and ratios of two of the most intensive and characteristic ions of the mass spectrum. Table 2 shows results of the study of recovery and a representative chromatogram of wastewater samples spiked with $1.0\,ng\,mL^{-1}$ of each analyte is depicted in Fig. 5. The recoveries were greater than 76.0% and no interfering peaks were observed for the blank samples.

Finally, three urban wastewater samples collected in Maracaibo, Venezuela were analyzed using the proposed method. Each sample was analyzed by triplicate. Ibuprofen was detected at concentrations between 0.57 and $0.89\,ng\,mL^{-1}$. These results demonstrate the usefulness of the proposed method for this application.

4. Conclusions

A simple and practical GC–MS method in combination with in situ derivatization headspace SPME for the determination of the non-steroidal acidic anti-inflammatory drugs ibuprofen, flufenamic acid, naproxen, mefenamic acid, tolfenamic acid, and meclofenamic acid in water samples is presented. Sensitive responses were obtained using $15\,\mu L$ of DMS, $60\,\mu L$ of $0.1\,M$ TBA-HSO$_4$, a $100\,\mu m$ polydimetilsiloxane fibre, $2.88\,g$

Na$_2$SO$_4$, 45 min extraction time, pH 6.0 and 70 °C in combination. Non-equilibrium conditions were adopted in order to reduce the extraction time. The application of standard addition method was effective to compensate the matrix effect observed and improved the method accuracy. In view of it simplicity and sensitivity, the proposed method is applicable for the quantification of residues of NSAIDs studied in tap water and wastewater samples.

References

[1] T. Heberer, Toxicol. Lett. 131 (2002) 5.
[2] T.A. Ternes, A. Joss, H. Siegrist, Environ. Sci. Technol. 38 (2004) 392A.
[3] E. Zuccato, S. Castiglioni, R. Fanelli, G. Reitano, R. Bagnati, C. Chiabrando, F. Pomati, C. Rossetti, D. Calamari, Environ. Sci. Pollut. Res. 13 (2006) 15.
[4] J. Debska, A. Kot-Wasik, J. Namiesnik, Crit. Rev. Anal. Chem. 34 (2004) 51.
[5] Z. Moldovan, Chemosphere 64 (2006) 1808.
[6] N. Nakada, T. Tanishima, H. Shinohara, K. Kiri, H. Takada, Water Res. 40 (2006) 3297.
[7] A. Tauxe-Wuersch, L. De Alencastro, D. Grandjean, J. Tarradellas, Water Res. 39 (2005) 1761.
[8] E. Emmanuel, G. Keck, J. Blanchard, P. Vermande, Y. Perrodin, Environ. Int. 30 (2004) 891.
[9] Z. Yu, S. Peldszus, P. Huck, J. Chromatogr. A 1148 (2007) 65.
[10] W.C. Lin, H.C. Chen, W.H. Ding, J. Chromatogr. A 1065 (2005) 279.
[11] M. Gros, M. Petrovic, D. Barceló, Talanta 70 (2006) 678.
[12] A. Macia, F. Borrull, C. Aguilar, M. Calull, Electrophoresis 25 (2004) 428.
[13] A. Macia, F. Borrull, M. Callul, C. Aguilar, J. Chromatogr. A 1117 (2006) 234.
[14] S. Weigel, R. Kallenborn, H. Huhnerfuss, J. Chromatogr. A 1023 (2004) 183.
[15] T. Henriksen, B. Svensmark, B. Lindhardt, R. Juhler, Chemosphere 44 (2001) 1531.
[16] I. Rodríguez, J. Carpinteiro, J.B. Quintana, A.M. Carro, R.A. Lorenzo, R. Cela, J. Chromatogr. A 1024 (2004) 1.
[17] M. del Olmo, A. Zafra, B. Suarez, A. Gonzalez-Casado, J. Taoufiki, J.L. Vilchez, J. Chromatogr. B 817 (2005) 167.
[18] M. Lee, R. Lee, Y. Lin, C. Chen, B. Hwang, Anal. Chem. 70 (1998) 1963.
[19] M. Llompart, M. Lourido, P. Landin, C. García-Jares, R. Cela, J. Chromatogr. A 963 (2002) 137.
[20] A. Díaz, F. Ventura, M.T. Galceran, Anal. Bioanal. Chem. 386 (2006) 293.
[21] M.I. Catalina, J. Dalluge, R. Vreuls, U. Brinkman, J. Chromatogr. A 877 (2000) 153.
[22] M.N. Sarrión, F.J. Santos, M.T. Galceran, Anal. Chem. 72 (2000) 4865.
[23] J. Ai, Anal. Chem. 68 (1997) 3260.
[24] B. Soulet, A. Tauxe, J. Tarradellas, Intern. J. Environ. Anal. Chem. 82 (2002) 659.
[25] H. Lee, T. Peart, M. Svoboda, J. Chromatogr. A 1094 (2005) 122.
[26] D. Bendz, N. Paxeus, T. Ginn, F. Loge, J. Hazard. Mater. 122 (2005) 195.
[27] S. Ollers, H. Singer, P. Fassler, S. Muller, J. Chromatogr. A 911 (2001) 225.
[28] M. La Farré, I. Ferrer, A. Ginebreda, M. Figueras, L. Olivella, L. Tirapu, M. Vilanova, D. Barceló, J. Chromatogr. A 938 (2001) 187.

pH gradient reversed-phase liquid chromatography as a fractionation tool for the separation of peptides

Tomasz Bączek [*], Łukasz Walijewski, Roman Kaliszan

Medical University of Gdańsk, Department of Biopharmaceutics and Pharmacodynamics, Hallera 107, 80-416 Gdańsk, Poland

Abstract

Recent reports from our laboratory presented a comprehensive theory and demonstrated feasibility of reversed-phase liquid chromatography (RP-LC) employing the programmed gradient of pH of the mobile phase. The aim of that work was to explore the usefulness of the pH gradient-based approach in fractionation of peptides. The experiments were performed on a series of peptides separated at various LC conditions. Retention parameters of peptides in the pH gradient and in the simultaneous pH/organic modifier gradient RP-LC were compared. The best results were obtained with eluents comprising low but constant concentrations of organic modifier while gradient of pH in the mobile phase was developed several times during each chromatographic run. The elaborated LC conditions allowed controlling the elution of peptides not only according to their hydrophobic properties, but also taking into account their electronic properties, represented by isoelectric point (pI) values. The combination of isocratic (regarding organic modifier) LC mode with recurring eluent pH gradient is proposed as an effective fractionation method of peptide mixtures. Moreover, information on hydrophobicity and pI of the peptides, obtained by that approach, might be an additional peptides database matching constraint. Hence, a new tool for analytical and bioinformatics studies of peptides fractionation is proposed.
© 2007 Elsevier B.V. All rights reserved.

Keywords: Liquid chromatography (LC); pH gradient; Peptides; Isoelectric point (pI)

1. Introduction

While two-dimensional gel electrophoresis suffers from a number of factors, it has a high resolving power and still is widely applied in the practice for the separation of proteins [1–9]. On the other hand, new high-resolution separation approaches, like two-dimensional chromatography (for example, a combination of ion exchange chromatography and reversed-phase liquid chromatography, coupled directly to mass spectrometry), are currently under intensive development and evaluation [10–14]. Despite the wide use of the methods based on the differences in isoelectric point values for just protein fractionation (like the first step in 2D gels electrophoresis) [15–18], separation of peptides with the use of reversed-phase liquid chromatography (RP-LC) based on just isoelectric point values could be a new subject of interest.

In chromatography the fundamental general equation describing analyte retention is [19]:

$$\int_0^{V_R} \frac{dV}{V_0(1 + k_a)} = 1 \tag{1}$$

where V_R is the retention volume, V_0 is the column dead volume and k_a is the instantaneous value of the retention factor, corresponding to the composition of the mobile phase at the point in the column, where actually the analyte finds itself. From Eq. (1) it seems that a flux of an infinitesimally small volume of the mobile phase, dV, through the middle of the analyte zone causes partial zone migration, dx. It can be assumed that the zone is temporarily under isocratic conditions for which a value of k_a of the analyte can be assigned. When the total volume of the mobile phase, equal to the retention volume, passes through the middle of the zone, then the sum of partial migrations equals 1. Thus, equations describing analyte retention at the mobile phase composition occurring at column inlet, k_i, have the following

---

* Corresponding author. Tel.: +48 58 3493261; fax: +48 58 3493262.
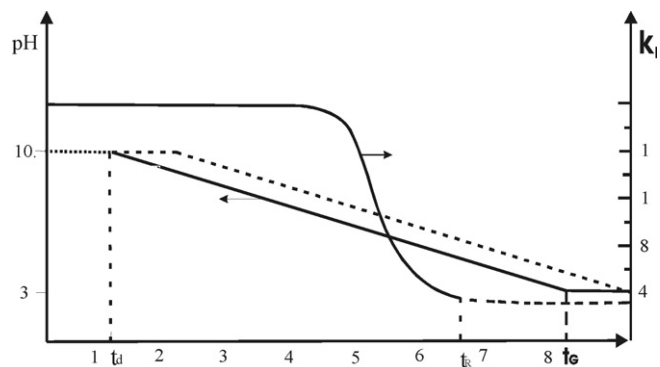 *E-mail address:* tbaczek@amg.gda.pl (T. Bączek).

Fig. 1. Changes of k_i values during a pH gradient for a hypothetical weak base of pK_a 9.

forms:

$$\int_0^{V_R} \frac{1}{V_0} \frac{dV}{k_i} = 1 \tag{2}$$

$$\int_0^{t_R} \frac{1}{t_0} \frac{dt}{k_i} = 1 \tag{3}$$

Changes of pH at column inlet lead to changes of retention factor, k_i. Changes of k_i during gradient of pH developed in the mobile phase for a hypothetical weak base of pK_a 9 are illustrated in Fig. 1.

Changes of k_i of acids and bases with pH of eluent are described by the following relationships:

$$k_i = \frac{k_{[A^-]} + k_{[HA]} 10^{pK_a - (pH_0 + at)}}{1 + 10^{pK_a - (pH_0 + at)}} \tag{4}$$

$$k_i = \frac{k_{[BH^+]} + k_{[B]} 10^{(pH_0 + at) - pK_a}}{1 + 10^{(pH_0 + at) - pK_a}} \tag{5}$$

In RP-LC with a mobile phase pH gradient (formed by mixing appropriate buffers in appropriate proportions) a linear change of pH within gradient time is programmed according to the general equation:

$$pH = pH_0 + at \tag{6}$$

where pH_0 is the initial pH and a denotes gradient steepness.

Recent reports from our laboratory [19–22] demonstrated a comprehensive theory of reversed-phase liquid chromatography employing the programmed pH gradient of the mobile phase. Also, the principles of the double gradient RP-LC, employing simultaneous gradients of organic modifier content and of pH of the mobile phase, have been provided.

The aim of presented work was to explore the usefulness of the pH gradient RP-LC approach as a new fractionation tool for the separation of peptides. Moreover, the approach was applied in analytical and bioinformatics studies of peptides fractionation behavior employing information on their isoelectric point values.

Table 1
Retention times obtained for 22 peptides chromatographed with the use of linear gradient of acetonitrile content and linear gradient of acetonitrile content combined with gradient of pH of the eluent

No.	Peptide sequence	Linear gradient 0–60% ACN (60 min)	Linear gradient 0–60% ACN/pH gradient (60 min)
1	GH	2.07	2.02
2	GM	3.35	2.98
3	DAEFRH–NH$_2$	11.48	11.68
4	DAEFGHDSG–NH$_2$	13.05	11.15
5	GL	4.28	4.80
6	DAEFGH–NH$_2$	11.50	9.65
7	AF	7.07	15.68
8	MAGASELGTGPGA–NH$_2$	16.52	18.50
9	Ac–DAEFRH–NH$_2$	18.07	11.15
10	EVRHQK	13.42	22.15
11	DAEFRHDSGY–NH$_2$	11.32	11.13
12	YL	12.98	19.37
13	Ac–DAEFRH	15.72	11.13
14	HWHTVAKETS	12.40	17.25
15	GKTKEGVLY–NH$_2$	14.38	19.45
16	EGVLY–NH$_2$	19.62	14.62
17	Ac–DAEFRHDSGY–NH$_2$	19.45	12.37
18	LHWHT	17.40	21.22
19	DAEFGHDSGF–NH$_2$	16.60	28.45
20	ETHLHWHT	16.13	21.30
21	HLHWHT	14.65	28.93
22	WF	24.60	29.55

2. Materials and methods

2.1. Chromatographic experiments

The experiments were performed on a standard LC column packed with octadecyl-bonded silica. An XTerra MS C18 column, 15.0 cm × 0.46 cm i.d., particle size 5 µm, from Waters (Millford, MA, USA) was applied.

Twenty-two structurally diverse peptides, collected in Tables 1 and 2, were chromatographed. The following peptides were purchased from Sigma–Aldrich (St. Louis, MO, USA): GH, GM, GL, AF, YL and WF. All other peptides were synthesized at the Department of Organic Chemistry, University of Gdańsk [23,24]. Peptides were encoded with the standard amino acids letter code: alanine (A), arginine (R), asparagines (N), aspartic acid (D), cysteine (C), glutamic acid (E), glutamine (Q), glycine (G), histidine (H), isoleucine (I), leucine (L), lysine (K), methionine (M), phenylalanine (F), proline (P), serine (S), threonine (T), tryptophan (W), tyrosine (Y), valine (V). Some peptides possessed amide and/or acetyl group, what was indicated in the peptide sequence as –NH$_2$ or Ac–, respectively.

Mobile phase was made of water and acetonitrile with the addition of 0.1% (v/v) of trifluoroacetic acid. Linear gradient from 0 to 60% of acetonitrile, developed within gradient time of 60 min, was applied. In isocratic experiments content of acetonitrile was fixed at 11% (v/v).

Mobile phase in pH gradient experiments comprised, as the weaker eluents, water with the addition of 0.1% (v/v) of tri-

Table 2
Retention times obtained at constant content of acetonitrile and fixed pH, and after applying gradient of pH, along with the values of structural descriptors for 22 peptides chromatographed

No.	Peptide	11% ACN	11% ACN/pH gradient	pI	log sum$_{AA}$	$c \log P$
1	GH	1.64	1.71	6.74	0.59	−1.89
2	GM	2.42	3.79	5.53	0.84	−1.90
3	DAEFRH–NH$_2$	3.38	3.42	5.32	1.35	−2.57
4	DAEFGHDSG–NH$_2$	3.75	3.87	4.02	1.44	−5.27
5	GL	3.85	3.99	5.53	1.05	−0.08
6	DAEFGH–NH$_2$	3.91	3.52	4.35	1.34	−3.23
7	AF	5.39	5.60	5.57	1.14	0.95
8	MAGASELGTGPGA–NH$_2$	5.80	6.75	4.00	1.56	−6.46
9	Ac–DAEFRH–NH$_2$	6.79	5.40	5.32	1.35	−2.41
10	EVRHQK	6.96	7.09	8.76	1.17	−3.36
11	DAEFRHDSGY–NH$_2$	7.24	6.32	4.54	1.56	−3.93
12	YL	7.63	6.57	5.53	1.26	1.86
13	Ac–DAEFRH	7.97	6.36	5.32	1.35	−1.71
14	HWHTVAKETS	8.19	8.91	6.92	1.51	−4.10
15	GKTKEGVLY–NH$_2$	12.78	17.23	8.59	1.53	−1.69
16	EGVLY–NH$_2$	13.11	7.79	4.00	1.42	0.51
17	Ac–DAEFRHDSGY–NH$_2$	22.70	7.63	4.54	1.56	−3.77
18	LHWHT	30.69	13.21	6.92	1.44	−0.30
19	DAEFGHDSGF–NH$_2$	35.50	8.07	4.02	1.59	−3.79
20	ETHLHWHT	43.90	17.96	6.26	1.52	−2.27
21	HLHWHT	45.50	27.63	7.02	1.47	−1.11
22	WF	54.92	18.15	5.53	1.37	2.41

fluoroacetic acid and water with the addition of 0.1% (v/v) of ammonia. pH gradient from pH 2.5 to 10.5 was generated in 5 min intervals in experiments involving simultaneous pH and acetonitrile content gradient.

2.2. Analysis of quantitative structure–retention relationships (QSRR)

Molecular structural descriptors of all the peptides studied were calculated by the molecular modeling program Hyper-Chem for personal computers with the extension ChemPlus (Hypercube, Gainsville, FL, USA). The software performed geometry optimization of the molecules with the use of molecular mechanics MM+ force field method.

Having retention data and the values of structural descriptors determined for a series of peptides tested, the appropriate multiple regression QSRR equations were derived with Statistica 7.1 software (StatSoft, Tulsa, OK, USA). The goodness of description of retention time by those equations was evaluated with the use of the values of significance level, p, of each term of the equations and of the whole equation, multiple correlation coefficients, R, standard error of estimate, s, and the values of the F-test of significance, F.

3. Results and discussion

At first, retention of peptides in double pH/organic modifier gradient RP-LC mode was determined (Fig. 2). The series of 22 structurally diversified peptides was chromatographed with the use of linear gradient of organic modifier and again after employing the linear gradient of organic modifier combined with gradient of pH (Table 1). As can be seen, minor differences of

Fig. 2. Schematic representation of the RP-LC conditions employing eluent pH gradient from pH 2.5 to 10.5, generated every 5 min, combined with gradient of acetonitrile content.

retention times of the peptides studied were observed (Fig. 3). However, two groups of more retained peptides, differing in elution order with regards to acetonitrile gradient itself and gradient of acetonitrile content combined with pH gradient, could be recognized.

More distinctive results were obtained in case of fixed acetonitrile content and gradient of pH (Fig. 4). The largest differences between retention times were again found for the more strongly retained peptides (Table 2). Generally, the conditions applied resulted in decrease of retention times of the most hydrophobic peptides (Fig. 5).

Next, it was demonstrated that the elaborated LC conditions affect elution of peptides not only according to their hydrophobic properties [23,24], but also according to their electronic properties, represented by isoelectric point values.

Fig. 3. Relationships between retention times of peptides chromatographed with linear gradient of acetonitrile content in the eluent and after applying linear gradient of acetonitrile content combined with gradient of pH.
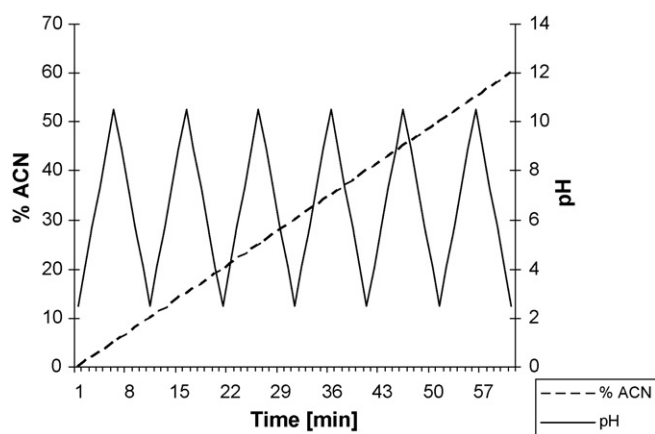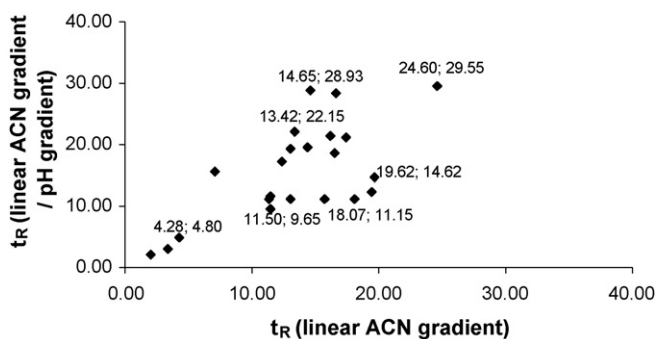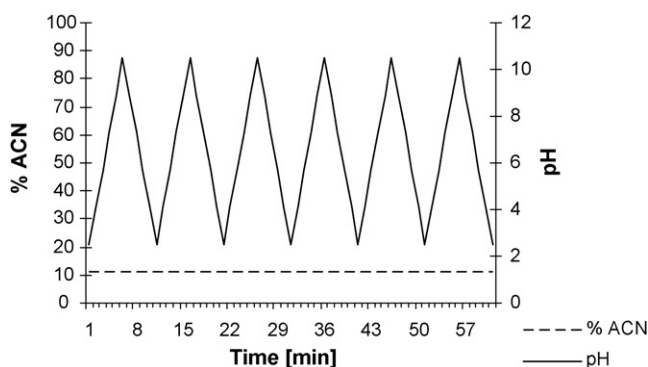

Fig. 4. Schematic representation of the RP-LC conditions employing eluent pH gradient from pH 2.5 to 10.5, generated every 5 min, with fixed content of the organic modifier.

For that, quantitative structure–retention relationships were derived describing retention time of peptides observed at constant pH and the concentration of acetonitrile in the eluent. Appropriate QSRR were also derived after applying eluent with gradient of pH. The following statistically significant QSRR models were found:
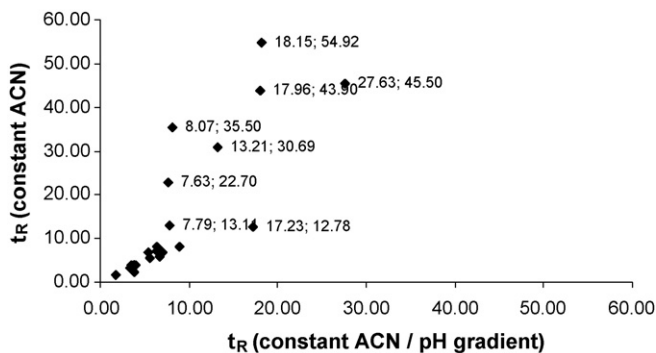

Fig. 5. Relationships between retention times of peptides chromatographed at fixed content of acetonitrile and constant pH of eluent and those obtained after applying gradient of pH in the eluent.

Table 3
Plate numbers calculated for some peptides chromatographed with the use of linear gradient of acetonitrile content and linear gradient of acetonitrile content combined with gradient of pH of the eluent

No.	Peptide sequence	Plate number (linear gradient 0–60% ACN (60 min))	Plate number (linear gradient 0–60% ACN/pH gradient (60 min))
1	DAEFRHDSG–NH$_2$	6,607	101,306
2	DAEFGHDSG–NH$_2$	10,916	77,841
3	DAEFGH–NH$_2$	5,776	77,423
4	Ac–DAEFRHDSGY–NH$_2$	10,816	6,779
5	LHWHT	7,569	62,206
6	Ac–DAEFRH–NH$_2$	7,255	88,566
7	YL	1,009	19,202
8	DAEFGHDSGF–NH$_2$	3,062	191,979
9	ETHLHWHT	6,480	37,495

- Constant content of acetonitrile and gradient of pH:

$$t_R = -14.98(\pm5.16) + 155(\pm0.49)\,\mathrm{p}I + 11.12\log\mathrm{sum}_{AA}$$
$$\underset{p=0.0100}{} \qquad \underset{p=0.0058}{}$$

$$+1.51(\pm0.31)c\log P + 0.0030(\pm0.0006)E_A^2$$
$$\underset{p=0.0002}{} \qquad \underset{p=0.0002}{}$$

$$n = 22; \quad R = 0.913; \quad F = 21.2; \quad s = 2.88;$$

$$p < 2 \times 10^{-6} \tag{7}$$

- Constant content of acetonitrile and constant pH:

$$t_R = -15.69(\pm20.09) - 0.03(\pm1.92)\,\mathrm{p}I$$
$$\underset{p=0.4457}{} \qquad \underset{p=0.9885}{}$$

$$+24.15(\pm11.30)\log\mathrm{sum}_{AA} + 4.34(\pm1.21)c\log P$$
$$\underset{p=0.0474}{} \qquad \underset{p=0.0023}{}$$

$$+0.0073(\pm0.0024)E_A^2 \quad n = 22; \quad R = 0.780;$$
$$\underset{p=0.0074}{}$$

$$F = 6.6; \quad s = 11.21; \quad p < 0.0021 \tag{8}$$

where t_R is the retention time, $\mathrm{p}I$ the isoelectric point; $\log\mathrm{sum}_{AA}$ the logarithm of the sum of gradient retention times of the amino acids forming the individual peptide; $c\log P$ the logarithm of the theoretical *n*-octanol—water partition coefficient and E_A^2 is the square of the angle energy.

In the case of Eq. (8), isoelectric point descriptor appeared to be statistically insignificant ($p \geq 0.05$), in contrary to Eq. (7) ($p = 0.0058$). Hence, the retention of peptides in RP-LC in mobile phase pH gradient mode is significantly affected by isoelectric point values of the peptides.

Finally, some issues related to peak shape and separation efficiency in RP-LC in mobile phase pH gradient mode should be considered. For that case, exemplary comparison between the chromatograms obtained for Ac–DAEFRHDSGY–NH$_2$ and LHWHT peptides eluted in acetonitrile gradient itself and gradient of acetonitrile content combined with pH gradient is demonstrated in Fig. 6. It is seen that base line in the case of gradient of acetonitrile content combined with pH gradient is more disturbed applying UV detection. However, it must be noted that the number of theoretical plates obtained for the
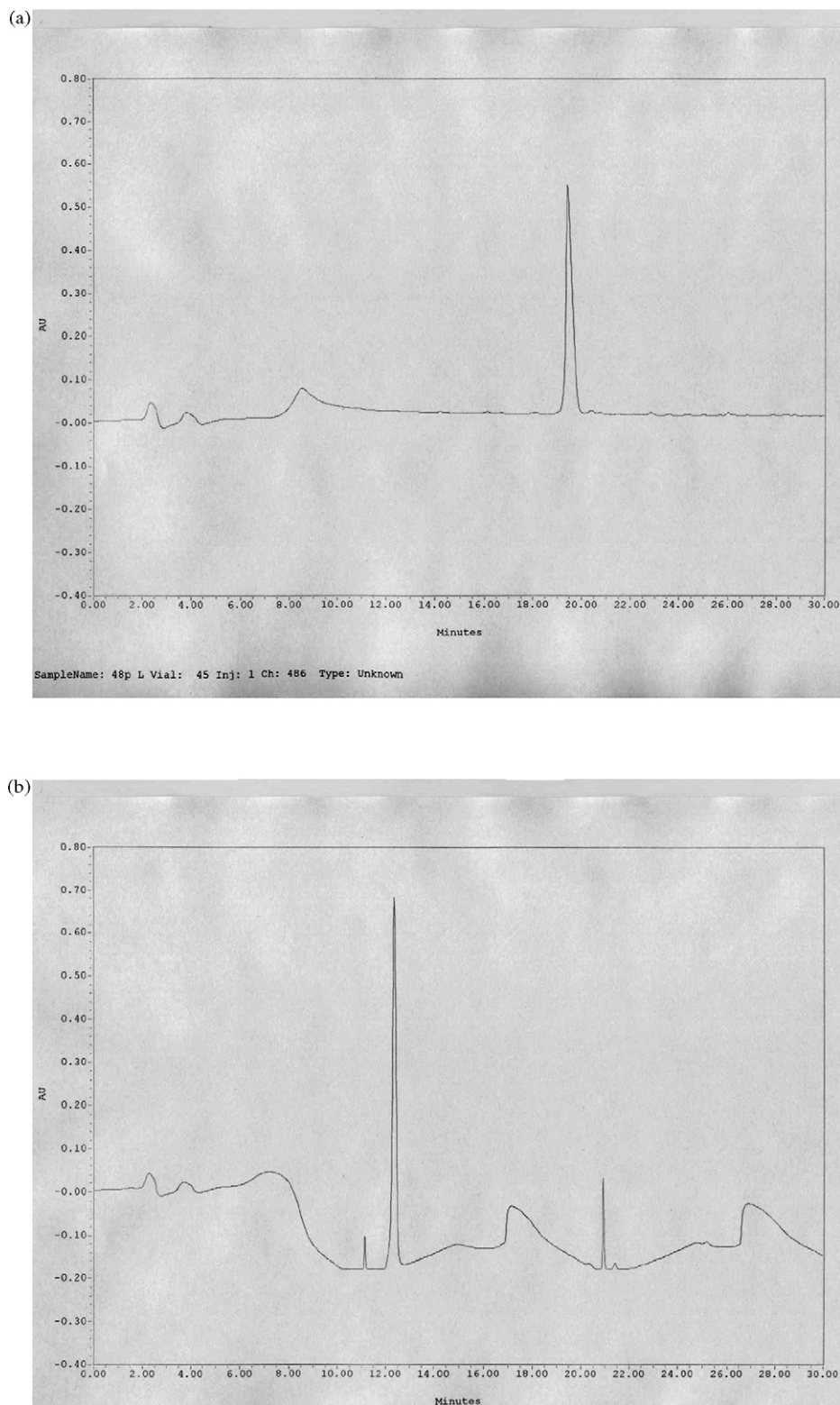
Fig. 6. Chromatograms obtained for (a) Ac–DAEFRHDSGY–NH$_2$ eluted in acetonitrile gradient itself and (b) Ac–DAEFRHDSGY–NH$_2$ eluted in gradient of acetonitrile content combined with pH gradient.

peaks in chromatograms when applying gradient of acetonitrile content combined with pH gradient is much higher in comparison elution with acetonitrile gradient itself (Table 3). Additionally, the peak shape can be analyzed visually in more details in Fig. 7, when overlapped chromatograms achieved in acetonitrile gradient itself and gradient of acetonitrile content combined with pH gradient are presented. It must be emphasized that all sharper peaks in Fig. 7 were obtained with the
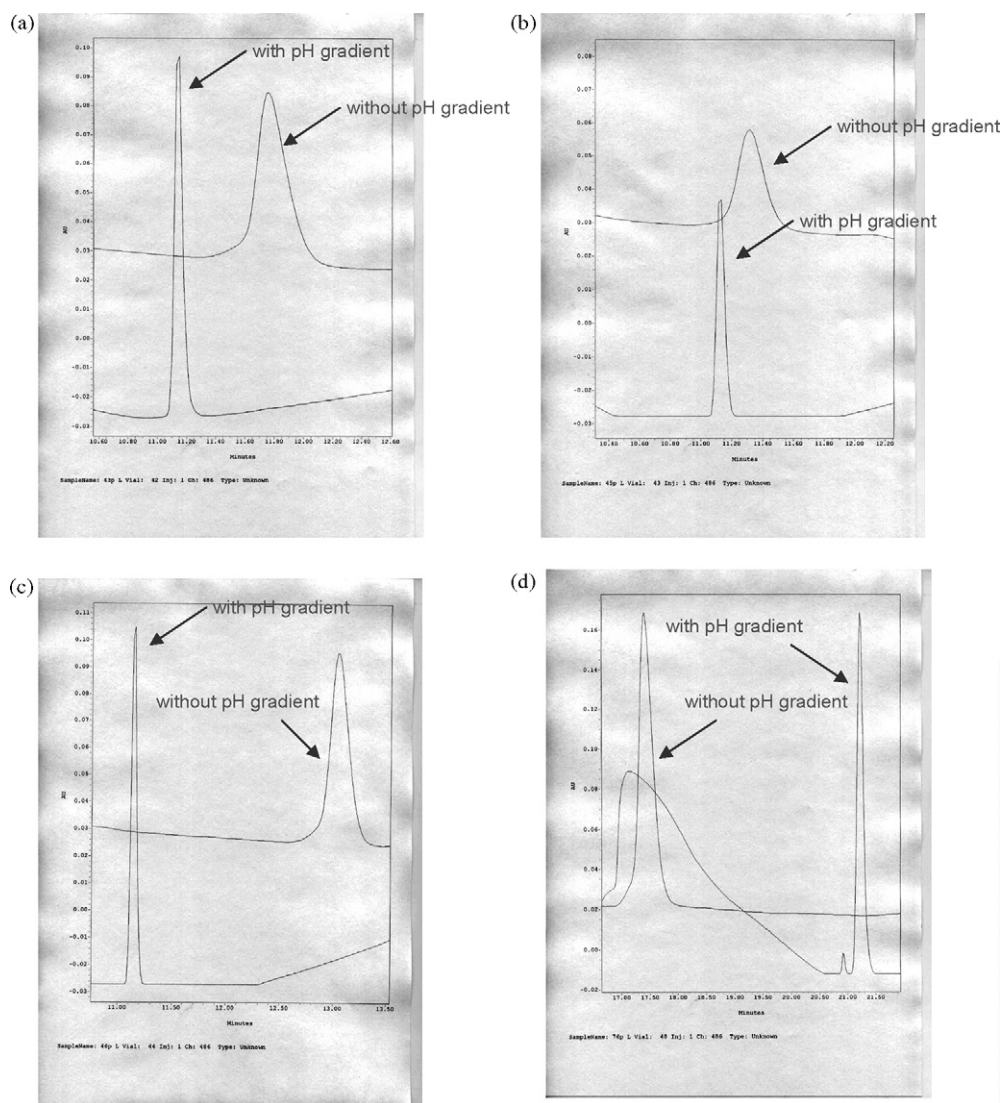
Fig. 7. Chromatograms eluted in acetonitrile gradient itself or eluted in gradient of acetonitrile content combined with pH gradient obtained for (a) DAEFGH–NH$_2$, (b) DAEFRHDSG–NH$_2$, (c) DAEFGHDSG–NH$_2$ and (d) LHWHT.

use of gradient of acetonitrile content combined with pH gradient.

4. Conclusions

The pH gradient RP-LC mode allows for separation of peptides not only according to their hydrophobic properties but also according to their isoelectric points. An application of a fixed concentration of acetonitrile with recurrent gradient of pH of the eluent is proposed as a new means of peptides fractionation.

Acknowledgements

References

[1] International Human Genome Project Consortium, Nature 409 (2001) 860–921.
[2] J.C. Venter, et al., Science 291 (2001) 1304–1351.
[3] A. Dove, Nat. Biotechnol. 17 (1999) 233–236.
[4] R. Kelner, Fresenius J. Anal. Chem. 366 (2000) 517–524.
[5] A. Pandey, M. Mann, Nature 405 (2000) 837–846.
[6] T. Rabilloud, Proteomics 2 (2002) 3–10.
[7] A. Gorg, G. Boguth, C. Obermaier, W. Weiss, Electrophoresis 19 (1998) 1516–1519.
[8] P.G. Righetti, A. Castagna, B. Herbert, F. Reymond, J.S. Rossier, Proteomics 8 (2003) 1397–1407.
[9] A. Gorg, W. Weiss, M.J. Dunn, Proteomics 4 (2004) 3665–3685.
[10] H.J. Issaq, K.C. Chan, G.M. Janini, T.P. Conrads, T.D. Veenstra, J. Chromatogr. B 817 (2005) 35–47.
[11] M.P. Washburn, D. Wolters, J.R. Yates, Nat. Biotechnol. 19 (2001) 242–247.
[12] M.T. Davis, J. Beierle, E.T. Bures, M.D. McGinley, J. Mort, J.H. Robinson, C.S. Spahr, W. Yu, R. Leuethy, S.D. Patterson, J. Chromatogr. B 752 (2001) 281–291.
[13] D.A. Wolters, M.P. Washburn, J.R. Yates, Anal. Chem. 73 (2001) 5683–5690.
[14] H. Wang, S. Hanash, J. Chromatogr. B 787 (2003) 11–18.
[15] B. Herbert, P.G. Righetti, Electrophoresis 21 (2000) 3639–3648.
[16] X. Zuo, D.W. Speicher, Proteomics 2 (2002) 58–68.

[17] A. Ros, M. Faupel, H. Mees, J. Oostrum, R. Ferrigno, F. Reymond, P. Michel, J.S. Rossier, H.H. Girault, Proteomics 2 (2002) 151–156.

[18] M. Cretich, G. Pirri, G. Carrea, M. Chiari, Electrophoresis 24 (2003) 577–581.

[19] R. Kaliszan, P. Wiczling, Anal. Bioanal. Chem. 382 (2005) 718–727.

[20] P. Wiczling, P. Kawczak, A. Nasal, R. Kaliszan, Anal. Chem. 78 (2006) 239–249.

[21] P. Wiczling, M.J. Markuszewski, R. Kaliszan, Anal. Chem. 76 (2004) 3069–3077.

[22] R. Kaliszan, P. Wiczling, M.J. Markuszewski, Anal. Chem. 74 (2004) 749–760.

[23] R. Kaliszan, T. Bączek, A. Cimochowska, P. Juszczyk, K. Wisniewska, Z. Grzonka, Proteomics 5 (2005) 409–415.

[24] T. Bączek, P. Wiczling, M. Marszałł, Y.V. Heyden, R. Kaliszan, J. Proteome Res. 4 (2005) 555–563.

A low-cost and low-tech electrochemical flow system for the evaluation of total phenolic content and antioxidant power of tea infusions

Susanna Buratti, Matteo Scampicchio *, Gabriella Giovanelli, Saverio Mannino

University of Milan, Department of Food Science and Technology, Via Celoria, 2 20133 Milan, Italy

Abstract

A disposable, small scale and low-cost electrochemical "wall-jet" flow-cell was build up together with a graphite lead mounted onto a pencil holder able to modulate the current response by the control of the surface area of the electrode. The total phenolic content of different types of tea infusions was determined and compared with the conventional Folin–Ciocolteau method. An index of antioxidant power was also proposed and data were compared with those obtained by the DPPH* assay.
© 2007 Elsevier B.V. All rights reserved.

Keywords: Pencil graphite electrode; Antioxidant power; Phenolic acids; Flow injection analysis; Tea infusion

1. Introduction

Field experiments in food analysis represent a challenge for every analytical chemist since sample preparation, set-up of the experiment and extensive time delays are often a critical factor to provide industry with useful and interpretable results. In this context, electrochemical techniques have often been considered superior than the optical based assay, thanks to higher sensitivity, negligible effect of the sample turbidity and inherent portability. The combination of electrochemical detectors with flow injection systems speed up the time of analysis and open to miniaturization and automation devices [1].

During the analysis of complex food matrices with electrochemical assays, a common drawback is the oxidation products of some compounds which deposit on the carbon electrode as a thin film, decreasing the magnitude of the analytical response; even though a cleaning step can be inserted into the analytical protocol, the renewing of the electrodes surface is awkward and it will result in a loss of reproducibility [2]. Therefore, the maintenance of the electrodes is still one of the major problems discouraging electrochemical techniques to be widespread used in analytical assays.

Phenolic compounds are commonly responsible of such passivation at solid electrodes [3]. They are characteristic components of many fruit and vegetable, and they are also the main antioxidant components of food [4]. Therefore, analysis of such substances has been of central interest in the scientific community due to their beneficial health effects [5,6].

Tea represents a major source of antioxidants since it is the most widely consumed beverage worldwide and contains large amounts of flavonoids and phenolics. In literature, many studies deal with the identification and quantification of antioxidants in tea, but emphasis has been given to organic solvent extracts isolated from dried leaves [7]; little is known about the phenolic content and the antioxidant activity of tea infusions [8].

In this paper, the development of a low-cost, low-tech flow injection system composed by an electrode based on a pencil lead (graphite) and by a modified PVC Pasteur pipette as flow cell, is proposed for the determination of phenolic content and antioxidant power of infusion (water extract) of different types of tea. Pencil graphite electrodes (PGEs) have been demonstrated to be excellent material for measurements in the field thanks to their low cost, high sensitivity, portability, easy maintenance, low background current, wide potential window, chemical inertness and suitability for various sensing and detection applications [1,9,10]. By virtue of its high electrochemical reactivity, good mechanical rigidity and ease of renewal, PGE has been applied in several different analytical fields, i.e. for the detection of

---

trace metals [11–14], DNA [9,15–17], immunoassay [18], caffeine [19], titratable acidity [20], pollutants [21], nitrate [22,23], ozone [24], some drug in pharmaceutical preparations [25] and chlorophenols in conjunction with liquid chromatography [26]. To the best of our knowledge this is the first time that an amperometric flow injection system operating with a disposable PGE was employed for the evaluation of tea antioxidant power and phenolic content. With respect to the conventional glassy carbon electrodes (CGEs), disposable PGEs significantly reduce total analysis time by by-passing the cleaning and pre-treatment process. Furthermore, PGEs have a surface area that can be modulated, therefore are able to detect also low concentration of the analyte.

2. Experimental

2.1. Samples and samples preparation

Twelve different types of tea were analysed. Japanese oolong tea in leaves, and Chinese white tea in leaves were purchased at the herbalist; the other teas were purchased from a local supermarket. They consisted of: Ceylon black tea in leaves, cherry flavoured black tea in leaves, Himalayan black tea in bags, apple flavoured Kenyan black tea, Japanese green tea in bags, green tea in bags, green tea in leaves, peach flavoured green tea in bags, Chinese red tea in bags, detheinated black tea in bags.

A standardised procedure for the preparation of tea infusions was applied: 2 g of tea (tea bags were opened and tea was weighted) were placed in 200 ml of boiling water for 4 min. After the infusion time, 50 ml of teas were filtered, allowed to cool to room temperature and then analysed. Before injection in the flow system tea samples were diluted 100 times with the carrier solution.

2.2. Apparatus

The amperometric measurements were performed with the potentiostat CHI 1010 (CH Instruments, Inc., USA). A simple "home-made" low-cost flow cell was made up by cutting the bottom of a PVC Pasteur pipette, which formed the "chamber" of the cell. A glass tube, with nominal internal diameter of 1 mm, was easily inserted into the PVC Pasteur pipette and sealed with epoxy glue. One side of the glass tube was linked to the pump (Jasco 880 PU, Tokyo, Japan) by a connecting tube in PEEK (1.5 mm o.d. × 1.0 mm i.d.), and the other side was laid into the chamber of the cell. The three-electrode system consisted of the PGE as the working electrode, the pseudoreference electrode (Ag/AgCl), and the platinum wire as auxiliary electrode. Unless otherwise indicated, all potentials are referred to the silver–silver chloride electrode (SSC). The lead rods were 0.5 mm in diameter and 6 cm in length. The pencil-lead was used as received, inserted into a commercial pencil holder and about 4 mm vertically dipped into the glass tube of the chamber giving a geometric surface area of 6.41 mm^2. The electrical connection was made on the outer side of the stainless steel tip of the pencil holder.
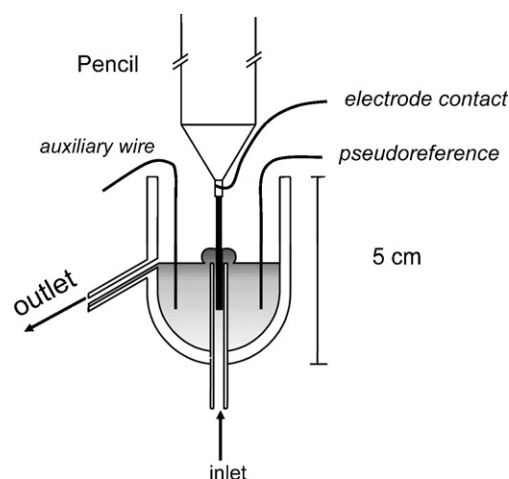
Fig. 1. Schematic configuration of the home-made flow injection cell.

The overall configuration of the flow system is shown in Fig. 1.

2.3. Operating procedure

Analyses were performed at room temperature using a carrier solution made of acetate buffer (0.1 mol l^{-1}, pH 4.0) added of 0.050 mol l^{-1} sodium chloride. A 1 ml min^{-1} flow rate and a 20 μl injection volume were employed. The flow injection (FI) experiment were performed operating in amperometric mode and the total phenols content or the antioxidant power were evaluated by measuring the current resulted from the oxidation of the electroactive compounds at the established potentials of +0.8 or +0.5 V, respectively. The antioxidant power was quantified by a calibration curve built up with trolox (6-hydroxy-2,5,7,8-tetramethylchroman-2-carboxylic acid, Sigma–Aldrich Italia) and data were expressed as mg of trolox equivalent per 100 ml of tea infusion. The total phenolic content was evaluated using a calibration curve built up with caffeic acid (Sigma–Aldrich Italia) and data were expressed as mg of caffeic acid equivalent per 100 ml of tea infusion.

2.4. DPPH* assay

The antioxidant activity was measured by the DPPH* (2,2-diphenyl-1-picrylhydrazyl) assay [27]. A 25 mg l^{-1} DPPH* methanolic solution was prepared daily and stored protected from light. One milliliter sample (properly diluted with deionised water) was added to 5 ml DPPH* solution and incubated at 40 °C for 30 min. The DPPH* discoloration reaction was followed by measuring the absorbance at 515 nm (optical path of 1 cm), against the blank (1 ml deionised water +5 ml DPPH* solution). Dose-response curves were built for each sample and the amount of antioxidant, corresponding to 50% inactivation of the DPPH* radical (I_{50}), was calculated. A calibration curve was built up with trolox and the antioxidant activity of the tea infusions was expressed as trolox equivalents (milligram of trolox per 100 ml of tea infusion). All determinations were carried out in triplicate.

2.5. Determination of total phenolic compounds

The amount of total phenolics was also determined using the Folin–Ciocalteau method [28]. Absorbance was read at 760 nm, a calibration curve was built up with caffeic acid and the results were expressed as milligram of caffeic acid equivalent per 100 ml of tea infusion.

3. Results and discussion

Initial investigation was undertaken to characterise the electrochemical properties of a range of commercial available pencil leads and to establish the best electrode surface area. Fig. 2 displays the flow injection responses for increasing concentrations of caffeic acid, obtained by using four pencil leads of different hardness (2B; HB; 2H; 5H) and applying an operating potential of +0.5 V. Since the four leads contain different amount of clay and polymers as well as graphite, they showed different amperometric signals even if all of them responded rapidly to the dynamic changes in caffeic acid concentration, showing that all of the leads are suitable for electrochemical studies. In particular, the HB pencil lead showed the best performance concerning the signal/noise ratio and was used in further studies.

The intensity of the amperometric signal was modulated by extruding the lead from the pencil holder so that the length of the graphite electrode and consequently its surface area could be increased. During a preliminary experiment, the electrode
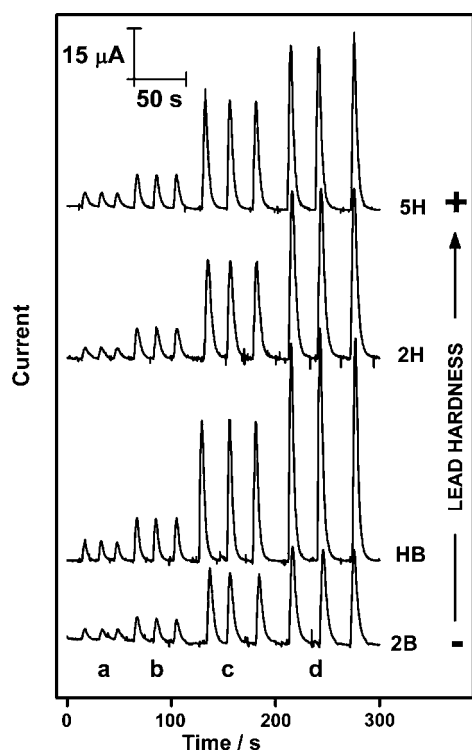

Fig. 2. Flow injection responses of caffeic acid standard solutions ((a) 5 μmol l^{-1}; (b) 15 μmol l^{-1}; (c) 50 μmol l^{-1}; (d) 70 μmol l^{-1}), obtained by using pencil leads of different hardness (2B; HB; 2H; 5H). *Operative conditions:* flow rate, 1 ml min^{-1}; carrier solution: acetate buffer (0.1 mol l^{-1}, pH 4.0), 0.050 mol l^{-1} sodium chloride; injection volume, 20 μl; working potential, +0.5 V.
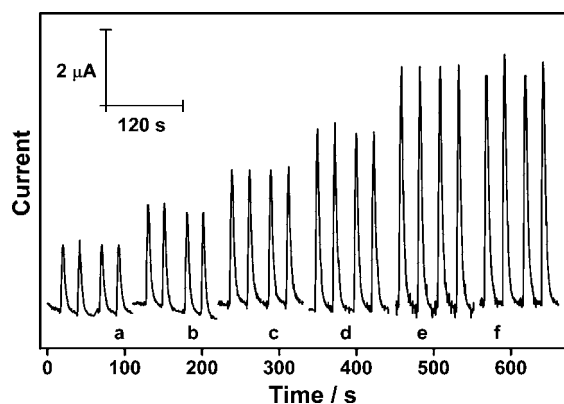

Fig. 3. Amperometric responses of caffeic acid standard solution (50 μmol l^{-1}) at different HB leads lengths ((a) 0 mm; (b) 1 mm; (c) 2 mm; (d) 3 mm; (e) 4 mm; (f) 5 mm). *Operative conditions:* flow rate, 1 ml min^{-1}; carrier solution: acetate buffer (0.1 mol l^{-1}, pH 4.0), 0.050 mol l^{-1} sodium chloride; injection volume, 20 μl; working potential, +0.5 V.

was placed in front of the flow stream, with the end of the lead positioned at the level of the stream outlet (click 0). Subsequent clicks (from 1 to 5) on the pencil holder lengthen the lead into the glass tube of the chamber from 1 to 5 mm. Fig. 3 shows the amperometric responses of a 50 μmol l^{-1} standard solutions of caffeic acid at different HB lead lengths and at an applied potential of +0.5 V. As it can be observed, the amperometric signals increased with the lead length till 4 mm, corresponding to a geometric surface area of 6.41 mm^2. A reproducible and stable signal was observed for all the lead lengths. When the lead length of 4 mm was chosen, the relative standard deviation of the current signals for ten repeated injections of 50 μmol l^{-1} caffeic acid was 3% (not shown). This length was used in all further studies.

Fig. 4 shows the hydrodynamic voltammograms of caffeic acid and trolox, used as standard in the determination of the total phenolic content and of antioxidant power of tea infusions, respectively. The hydrodynamic voltammograms were obtained by plotting the amperometric signal versus the applied potential. For trolox and caffeic acid, the potential started rising at +0.2 and +0.3 V respectively; both standards reached a plateau at about +0.6 V.

Further investigations dealt with the application of the proposed FI system to the evaluation of the total phenolic content and the antioxidant power of tea infusions. The antioxidant power of phenols is related to their redox properties, which in turn are related to their chemical structure. In our previous works [29–31], we have demonstrated that electrochemical behavior of flavonoids, phenolic acids and carotens is related to their antioxidant activity. Since the oxidation potential of a compound provides an estimate of the energy required to donate an electron, the lower the oxidation potential, the higher will be its expected antioxidant activity. The applied potential of +0.5 V has been demonstrated to be selective to discriminate those compounds having high reducing capacity, hence with effective antioxidant power. At potential greater than +0.6 V all the phenolic compounds present into the sample can be oxidized and consequently electrochemically evaluated. Based on these considerations, dif-
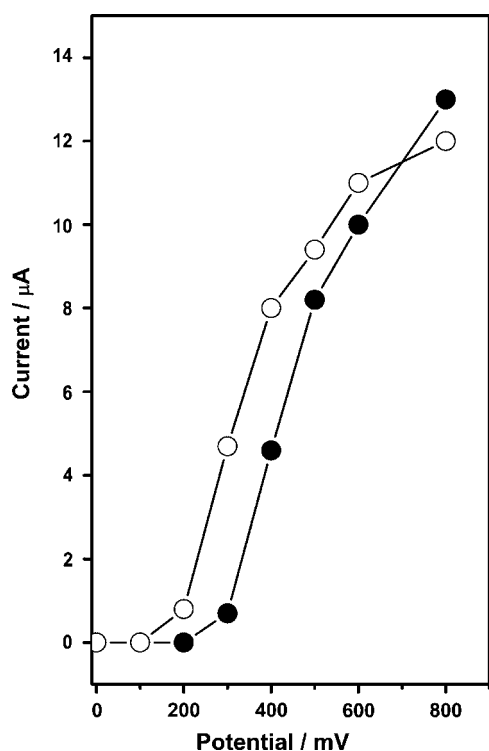
Fig. 4. Hydrodynamic voltammetric profiles of trolox (○) and caffeic acid (●). Operative conditions: standard concentrations, $50\,\mu\text{mol}\,l^{-1}$; flow rate, $1\,\text{ml}\,\text{min}^{-1}$; carrier solution: acetate buffer ($0.1\,\text{mol}\,l^{-1}$, pH 4.0), $0.050\,\text{mol}\,l^{-1}$ sodium chloride; injection volume, $20\,\mu l$.

ferent types of tea infusion were analysed with the PGE at two different potentials. A potential of +0.5 V was applied in order to evaluate the antioxidant power. The total phenolic content was evaluated applying a potential of +0.8 V. The antioxidant power was quantified using trolox as reference while total antioxidant content was expressed as caffeic acid equivalents. Quantification was based on peak height. The amperometric detection resulted in well-defined linear concentration dependence in a range between 1 and $20\,\text{mg}\,l^{-1}$ of trolox (working potential +0.5 V) and caffeic acid (working potential +0.8 V). The relative standard deviation at the concentration level of $10\,\text{mg}\,l^{-1}$ was 3.2% for trolox and 2.8% for caffeic acid ($n = 15$). In Table 1 the antioxidant power and the total phenolic content of the tea infusions are reported. As it can be seen tea infusions evaluated with the electrochemical method showed widely different antioxidant power (b) (ranging from $10.2\,\text{mg}\,100\,\text{ml}^{-1}$ to $83.5\,\text{mg}\,100\,\text{ml}^{-1}$) and phenolic content (d) (ranging from $14.1\,\text{mg}\,100\,\text{ml}^{-1}$ to $119.4\,\text{mg}\,100\,\text{ml}^{-1}$). This variability depends on the kind and extent of fermentation and drying treatment, which, in black and oolong tea, caused the oxidation and condensation of phenolics, the oxidation of carotenoids and the formation of Maillard reaction products. Furthermore, very different values of antioxidant power and phenolic content were found among teas of the same type, probably reflecting differences in quality, geographical origin, technological and storage conditions. Nevertheless, considering the ratio between the antioxidant power and total antioxidant content (b)/(d), green teas (except for Japanese green tea) showed higher values with respect to black, oolong and

Table 1
Antioxidant power and total phenolic content of tea samples (average ± s) (n = 3)

	Antioxidant power		Total phenols		EC Ratio 500/800 mV
	DPPH* Trolox eq. (mg 100 ml⁻¹) (a)	EC^a 500 mV Trolox eq. (mg 100 ml⁻¹) (b)	Folin–Ciocalteau Caffeic eq. (mg 100 ml⁻¹) (c)	EC^a 800 mV Caffeic eq. (mg 100 ml⁻¹) (d)	(b)/(d)
Ceylon black tea	20 ± 1	10 ± 0.8	21 ± 1	14 ± 1	0.72
Cherry flavoured black tea	23 ± 1	17 ± 1.8	34 ± 2	26 ± 1	0.68
Himalayan black tea	66 ± 2	84 ± 3	106 ± 3	119 ± 2	0.70
Detheinated black tea	48 ± 1	48 ± 1	84 ± 2	74 ± 1	0.65
Apple flavoured Kenian black tea	58 ± 3	58 ± 2	96 ± 3	88 ± 2	0.66
Peach flavoured green tea	36 ± 2	30 ± 1	41 ± 1	36 ± 1	0.85
Green tea in bags	59 ± 2	72 ± 3	79 ± 2	89 ± 2	0.81
Green tea in leaves	41 ± 2	45 ± 1	51 ± 1	48 ± 1	0.94
Japanese green tea	30 ± 1	48 ± 2	72 ± 2	77 ± 1	0.63
Japanese oolong tea	24 ± 1	26 ± 1	38 ± 2	33 ± 2	0.78
Chinese red tea	22 ± 1	28 ± 1	57 ± 1	45 ± 2	0.61
Chinese white tea	58 ± 2	59 ± 2	72 ± 2	81 ± 3	0.72

[a] Electrochemical method.

white teas. This result, in agreement with other studies [32,33], demonstrate that green tea, not subjected to the fermentation process, is rich of highly antioxidant phenols. The electrochemical responses were compared with the colorimetric DPPH* assay (*a*) and with the Folin–Ciocalteau assay (*c*) (Table 1). In order to correlate the methods the linear regression model was used. A good correlation was found between the proposed electrochemical method (EC 500 mV) and the DPPH* assay (*r* = 0.92) or between the electrochemical method (EC 800 mV) and the Folin–Ciocalteau assay (*r* = 0.97). The good agreement with the DPPH* assay demonstrate that the proposed method supply a measurement of the total amount of natural antioxidant (phenolic acids and flavonols), even though it is based on a different principle: the redox properties of phenolics in the electrochemical method, and the ability of phenolics to scavenge the radical in the DPPH* assay. Not surprisingly, agreement between the Folin–Ciocolteau method and the proposed method is high, since the first is a redox reaction between fosfo-molibdenum ions and the phenols and the second is a direct redox reaction between phenols and the surface of the PGE.

The proposed electrochemical method based on a flow injection system with pencil graphite electrode could be successfully employed for the direct and rapid monitoring of the antioxidant power and of the total phenolic content of tea infusions.

4. Conclusion

A renewable, low-cost and low-tech electrochemical system was developed by using a pencil graphite lead and a simple home-made flow cell, based on a modified plastic Pasteur pipette. The system is extremely inexpensive with the cost of material being a few euros and provides an attractive alternative to the high-tech carbon electrodes. The operational cost associated with the renewing the pencil lead is of few cents. Furthermore, the intrinsic ease renewably of the pencil lead is extremely useful during on-field analysis, in particular, when passivating compounds have to be evaluated.

References

[1] J. Wang, Trac-Trends Anal. Chem. 21 (2002) 226.
[2] D.E. Weisshaar, T. Kuwana, Anal. Chem. 57 (1985) 378.
[3] M. Ferreira, H. Varela, R.M. Torresi, G. Tremiliosi, Electrochim. Acta 52 (2006) 434.
[4] B. Dimitrios, Trends Food Sci. Technol. 17 (2006) 505.
[5] S.U. Lule, W.S. Xia, Food Rev. Int. 21 (2005) 367.
[6] S. Coimbra, E. Castro, P. Rocha-Pereira, I. Rebelo, S. Rocha, A. Santos-Silva, Clin. Nutr. 25 (2006) 790.
[7] Z. Pineiro, M. Palma, C.G. Barroso, J. Chromatogr. A 1026 (2004) 19.
[8] A.K. Atoui, A. Mansouri, G. Boskou, P. Kefalal, Food Chem. 89 (2005) 27.
[9] J. Wang, A.N. Kawde, Anal. Chim. Acta 431 (2001) 219.
[10] J. Wang, Talanta 56 (2002) 223.
[11] D. Demetriades, A. Economou, A. Voulgaropoulos, Anal. Chim. Acta 519 (2004) 167.
[12] A. Bund, J. Dittmann, D. Lordkipanidze, G. Schwitzgebel, Fresenius J. Anal. Chem. 356 (1996) 27.
[13] T. Kakizaki, K. Hasebe, Fresenius J. Anal. Chem. 360 (1998) 175.
[14] A.M. Bond, P.J. Mahon, J. Schiewe, V. VicenteBeckett, Anal. Chim. Acta 345 (1997) 67.
[15] J. Wang, A.N. Kawde, E. Sahlin, Analyst 125 (1999) 5.
[16] J. Wang, A.N. Kawde, A. Erdem, M. Salazar, Analyst 126 (2001) 2020.
[17] H. Karadeniz, B. Gulmez, F. Sahinci, A. Erdem, G.I. Kaya, N. Unver, B. Kivcak, M. Ozsoz, J. Pharmaceut. Biomed. 33 (2003) 295.
[18] L. Engel, W. Baumann, Fresenius J. Anal. Chem. 346 (1993) 745.
[19] S.Y. Ly, Y.S. Jung, M.H. Kim, I.K. Han, W.W. Jung, H.S. Kim, Microchim. Acta 146 (2004) 207.
[20] A. Kotani, Y. Miyaguchi, D. Harada, F. Kusu, Anal. Sci. 19 (2003) 1473.
[21] M. Ozsoz, A. Erdem, D. Ozkan, K. Kerman, T.J. Pinnavaia, Langmuir 19 (2003) 4728.
[22] T.A. Bendikov, T.C. Harmon, J. Chem. Educ. 82 (2005) 439.
[23] A. Kitajima, T. Teranishi, M. Miyake, Electrochemistry 69 (2001) 16.
[24] K. Aoki, A. Kobayasi, Bunseki Kagaku 41 (1992) 375.
[25] P. Masawat, S. Liawruangrath, Y. Vaneesorn, B. Liawruangrath, Talanta 58 (2002) 1221.
[26] J.Y. Jin, T. Hiroi, K. Sato, T. Miwa, T. Takeuchi, Anal. Sci. 18 (2002) 549.
[27] C. Sánchez-Moreno, J.A. Larrauri, F. Saura-Calixto, J. Sci. Food Agric. 79 (1999) 1301.
[28] R. Di Stefano, S. Guidoni, Vignevini 1–2 (1989) 47.
[29] S. Buratti, S. Benedetti, M.S. Cosio, Talanta 71 (2007) 1387.
[30] S. Mannino, S. Buratti, M.S. Cosio, N. Pellegrini, Analyst 124 (1999) 1115.
[31] S. Buratti, N. Pellegrini, O.V. Brenna, S. Mannino, J. Agric. Food Chem. 49 (2001) 5136.
[32] I.F.F. Benzie, Y.T. Szeto, J. Agric. Food Chem. 47 (1999) 633.
[33] Q.Y. Zhu, R.R. Holt, S.A. Lazarus, J.L. Ensunsa, J.F. Hammerstone, H.H. Schmitz, C.L. Keen, J. Agric. Food Chem. 50 (2002) 1700.

Evaluation of a carbon paste electrode modified with organofunctionalised SBA-15 nanostructured silica in the simultaneous determination of divalent lead, copper and mercury ions

Ivana Cesarino [a], Glimaldo Marino [a], Jivaldo do Rosário Matos [b], Éder Tadeu Gomes Cavalheiro [a],*

[a] *Departamento de Química e Física Molecular, Instituto de Química de São Carlos, Av Trabalhador Sãocarlense, 400, Centro, CEP 13560-970, São Carlos, São Paulo, Brazil*
[b] *Departamento de Química Fundamental, Universidade de São Paulo, Cidade Universitária Armando Salles Oliveira, São Paulo(SP), Brazil*

Abstract

The performance of a carbon paste electrode (CPE) modified with SBA-15 nanostructured silica organofunctionalised with 2-benzothiazolethiol in the simultaneous determination of Pb(II), Cu(II) and Hg(II) ions in natural water and sugar cane spirit (*cachaça*) is described. Pb(II), Cu(II) and Hg(II) were pre-concentrated on the surface of the modified electrode by complexing with 2-benzothiazolethiol and reduced at a negative potential (-0.80 V). Then the reduced products were oxidised by DPASV procedure. The fact that three stripping peaks appeared on the voltammograms at the potentials of -0.48 V (Pb^{2+}), -0.03 V (Cu^{2+}) and $+0.36$ V (Hg^{2+}) in relation to the SCE, demonstrates the possibility of simultaneous determination of Pb^{2+}, Cu^{2+} and Hg^{2+}. The best results were obtained under the following optimised conditions: 100 mV pulse amplitude, 3 min accumulation time, 25 mV s^{-1} scan rate in phosphate solution pH 3.0. Using such parameters, calibration graphs were linear in the concentration ranges of $3.00–70.0 \times 10^{-7}$ mol L^{-1} (Pb^{2+}), $8.00–100.0 \times 10^{-7}$ mol L^{-1} (Cu^{2+}) and $2.00–10.0 \times 10^{-6}$ mol L^{-1} (Hg^{2+}). Detection limits of 4.0×10^{-8} mol L^{-1} (Pb^{2+}), 2.0×10^{-7} mol L^{-1} (Cu^{2+}) and 4.0×10^{-7} mol L^{-1} (Hg^{2+}) were obtained at the signal noise ratio (SNR) of 3. The results indicate that this electrode is sensitive and effective for simultaneous determination of Pb^{2+}, Cu^{2+} and Hg^{2+} in the analysed samples.
© 2008 Published by Elsevier B.V.

Keywords: SBA-15 nanostructured silica; Carbon paste electrode; 2-Benzothiazolethiol; *Cachaça*; Well water

1. Introduction

One-dimensional uniform tubular pores, in the form of hexagonally arranged mesoporous SBA-15 silica, attracted much attention when it was first reported by Zhao et al. [1], due to their marked hydrothermal stability, amenability to synthesis in a wide range of pore sizes (4.6–30 nm), and particle morphologies as well as their potential applications in emergent areas, such as energy storage in doublelayer supercapacitors, catalytic support in fuel cell electrodes, adsorption of bulky molecules in liquid phase, improvement of selectivity and sensitivity in the preparation of electrodes for electroanalysis, etc. [2–5]. Mesoporous silica can be modified and functionalised by incorporation of organic groups in the silica structure via synthesis procedure and the immobilisation of organic substances that can be bonded to the silanol groups on the surface of mesoporous silica. A wide range of functional groups, such as thiols, amines, epoxides, imadizoles, chromophores, phenyls and alkyorganosilanes are reported to be incorporated [6–10].

Walcarius [11,12] presents extensive reviews about the preparation and application of silica modified electrodes showing their importance as electroanalytical sensors. Electrochemical sensors based on stripping voltammetry use to be a useful technique for determining aqueous heavy metal concentrations. These sensors are usually sensitive, compact, low cost and easily integrated into field-deployable units [13–15]. Stripping voltammetry for trace metal ions usually involves pre concentration of metal ions at an electrode surface, followed by quantification of

* Corresponding author. Fax: +55 16 3373 9987.
  E-mail address: cavalheiro@iqsc.usp.br (É.T.G. Cavalheiro).

the accumulated species by voltammetric methods. The carbon paste electrode (CPE) has the advantages of surface renewal and very low background currents, mainly in positive potential ranges [16]. CPE modified with functional ligands have been more widely used to pre-concentrate and quantify trace metal ions [17–22]. These ligands improve the selectivity of the determination step compared to using an unmodified CPE [23,24].

Lead, copper and mercury are cumulative toxic metals whose presence in the environment has increasing concerning. The pollution of lead and mercury is one of the most serious environmental problems because of they stability in contaminated site and complexity of mechanism in biological toxicity. Once absorbed, lead and mercury can be accumulated in the body and greatly threaten the health of human [25,26]. Copper is an essential element at trace level (i.e. catalytic action in heme synthesis) [27], but the intake of large quantities can be toxic. According to Brazilian regulations, it may be sold raw or with addition of sugar and may contain up to $5\,mg\,L^{-1}$ ($79\,\mu mol\,L^{-1}$) of copper and $200\,\mu g\,L^{-1}$ ($0.97\,\mu mol\,L^{-1}$) of lead [28]. In well water may contain up to $7.8\,\mu g\,L^{-1}$ ($0.20\,\mu mol\,L^{-1}$) of copper, $0.210\,mg\,L^{-1}$ ($1.0\,\mu mol\,L^{-1}$) of lead and $1.8\,\mu g\,L^{-1}$ ($9.0\,nmol\,L^{-1}$) of mercury [29].

In the present work, the use of organofunctionalised SBA-15 silica with 2-benzothiazolethiol in the preparation of carbon paste electrodes is described. SBA-15 silica presented the advantage of no need of surface pre-treatment before modification when compared with silica gel usually employed in such methods. The best conditions for a differential pulse anodic stripping voltammetric procedure were optimised and the electrode was applied in the simultaneous determination of Pb^{2+}, Cu^{2+} and Hg^{2+} spiked in a well water and sugar cane spirit (*cachaça*) samples. The organofunctionalised SBA-15 silica modified carbon paste electrode offers great promise for wider application as a metal ion sensor.

The main goal here is to evaluate the CPE electrode modified with organofunctionalised SBA-15 silica with 2-benzothiazolethiol in the analysis of cations. Thus, we selected Cu^{2+} and Pb^{2+} that use to be present in low levels in *cachaça* samples and Hg^{2+}, which is not supposed to be present nor in beverages nor in natural waters due to its environmental relevance.

2. Experimental

2.1. Apparatus

All the voltammetric measurements were carried out in a 20.0 mL total capacity thermostated glass cell at 25.0 °C, using a carbon paste electrode modified with SBA-15 silica organofunctionalised with 2-benzothiazolethiol (BTPSBA–MCPE) as a working, saturated calomel as reference (SCE) and platinum wire as auxiliary electrodes. High purity nitrogen (FID. 4.9 AGA) was used for deaeration of the electrolyte solution. DPASV were performed in BAS CV −50 W Voltammetric Analyzer (Bioanalytical Systems) controlled by the BAS 50 W windows control software, v. 2.3 (Bioanalytical Systems).

2.2. Reagents and solutions

All the solutions were prepared with water purified in a Millipore Milli-Q system. All the chemicals were of analytical grade and used without further purification. The supporting electrolyte used for most experiments was a $0.10\,mol\,L^{-1}$ phosphate solution pH 3.0. Stock solutions containing $1.00 \times 10^{-3}\,mol\,L^{-1}$ Pb(II), $1.00 \times 10^{-3}\,mol\,L^{-1}$ Cu(II) and $1.00 \times 10^{-3}\,mol\,L^{-1}$ Hg(II) were prepared daily by dissolving an appropriate amount of a $1000\,mg\,L^{-1}$ reference lead nitrate solution (Merck), $1000\,mg\,L^{-1}$ reference copper nitrate solution (Tec-Lab) and $1000\,mg\,L^{-1}$ reference mercury nitrate solution (Tec-Lab) in 100 mL of the $0.10\,mol\,L^{-1}$ phosphate solution pH 3.0.

The 3-(chloropropyl)-trimethoxysilane (Aldrich) and 2-benzothiazolethiol (Sigma) were used in the functionalisation of the SBA-15 silica.

A 1–2 μm particle size graphite powder (Aldrich) and mineral oil (Aldrich) were used for the preparation of the carbon pastes.

2.3. Preparation of the organofunctionalised SBA-15 silica

The SBA-15 silica was synthesised according to a previously described procedure [2]. SBA-15 silica with a large surface area ($>1500\,m^2\,g^{-1}$) and large pore volumes ($>1\,cm^3\,g^{-1}$) was used without further treatment, in a procedure described earlier [13,30]. Thus, 3.0 g of SBA-15 silica was refluxed with 2 mL of the 3-(chloropropyl)-trimethoxysilane in 40 mL of dry xylene for 24 h. The solid was filtered and washed with xylene, ethanol, acetone and ether, successively.

In the organofunctionalisation procedure, a sample of 3-chloropropyl SBA-15 silica was suspended in an *N,N'*-dimethylformamide solution containing 2-benzothiazolethiol kept under constant stirring and reflux during 24 h. The suspension was filtered and washed successively with *N,N'*-dimethylformamide, ethanol, acetone and ether. The solid was treated with hot ethanol in a Soxlet extractor during 8 h for elimination of the excess of organoalcoxisilane. Finally, the product was dried in air at 80 °C for 12 h. The organofunctionalised SBA-15 silica was characterised by IR spectroscopy and NMR in solid phase.

2.4. Preparation of the modified carbon paste electrodes

Modified carbon paste electrodes (MCPE) were prepared by mixing the graphite powder with BTPSBA. The mixture was added to 0.250 g of mineral oil and mixed in a mortar for at least 20 min to produce the final paste in order to each electrode containing 10, 15, 20 and 25% of BTPSBA, w/w. The carbon paste electrode was finally obtained by packing the paste into a plastic tube 4.5 mm i.d. (geometrical area 0.16 cm^2) and arranged with a copper wire serving as an external electric contact. Appropriate packing was achieved by pressing the electrode surface against a bond paper until a smooth surface was obtained.

2.5. Sample preparation and analysis of lead, copper and mercury in well water and sugar cane spirit (cachaça)

An exactly known amount of lead, copper and mercury were spiked to an aliquot of 10.0 mL of well water in order to reach a final concentration of 2.0×10^{-5} mol L^{-1} in Pb^{2+}, Cu^{2+} and Hg^{2+}. This sample was mixed with 10.0 mL of 0.1 mol L^{-1} phosphate solution pH 3.0.

An exactly known amount of lead and mercury were spiked to an aliquot of 10.0 mL of sugar cane spirit (Sant'Antonio), which already contained 3.97 mg L^{-1} of Cu^{2+}. To sample it was added 1.0 mL of 0.1 mol L^{-1} nitric acid. Then 1.0 mL of this mixed was diluted in 10.0 mL of 0.1 mol L^{-1} phosphate solution pH 3.0.

The Pb(II), Cu(II) and Hg(II) contents in these samples were determined by three successive additions of a standard lead(II), copper(II) and mercury(II) solutions. The optimised parameters of DPASV for simultaneous determination of lead, copper and mercury in the samples were potential interval −0.80 to +0.60 V (versus SCE); scan rate of 25 mV s^{-1}, 100 mV pulse amplitude; accumulation time 180s at −0.80 V. All measurements were performed in solutions deaerated by bubbling N$_2$ for 15 min.

2.6. Comparison method

Atomic absorption spectrometry (AAS) determinations were performed in spectrofotometry AAnalyst 100 (Perkin-Elmer), using cathode lamp, air–acetylene flame and the wavelength of 324.8 nm for copper and 283.3 nm for lead. The Pb(II) and Cu(II) contents in these samples were determined by four successive additions of a standard lead(II) and copper(II) solutions. The mercury(II) was determined by inductively coupled plasma atomic emission spectrometry (ICP-OES), using a Thermo Jarrel Ash-IRIS/AP spectrometer.

3. Results and discussions

3.1. Characterisation of the chemically modified SBA-15 silica

Fig. 1 presents the IR spectra of unmodified SBA-15 silica (curve a), 3-chloropropyl SBA-15 silica (curve b) and BTPSBA (curve c).

IR spectroscopy is employed for accompanying the functionalisation steps of SBA-15 silica. In the region of 1300–2000 cm^{-1}, it was possible to observe the most significant changes, when the spectra of SBA-15 silica is compared with the functionalised SBA-15 silica one. The infrared spectra shown in Fig. 1 confirm the presence of 2-benzothiazolethiol groups bound to the silica surface. The bands in the 1600–1700 cm^{-1} region represents the OH bending and stretching vibration of Si–OH groups and physisorbed water. The bands in the 1435–1410 cm^{-1} region correspond to the stretching vibration of CH$_2$–S group and at 1540 cm^{-1} relative to the stretching of Si–NH$_2$ groups.
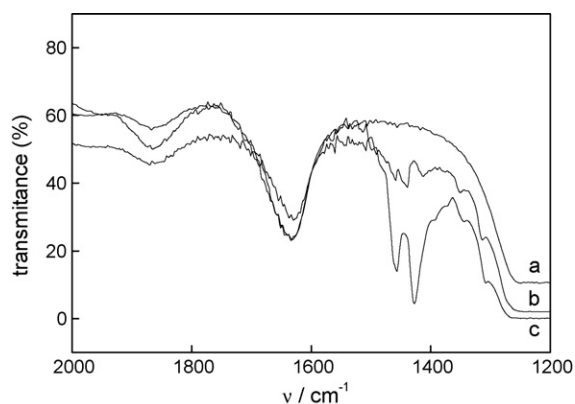
Fig. 1. IR spectra for the silica SBA-15 after each functionalisation step: (a) unmodified silica SBA-15; (b) 3-chloropropyl SBA-15 silica and (c) BTPSBA.

The NMR ^{13}C spectra of the BTPSBA (Fig. 2) shows signals at 10.7, 23.7 and 36.6 ppm, and these are assigned to the methylene groups 1, 2 and 3, respectively. Carbon atoms of the heterocycle resonate at lower fields: 65.5 and 121.5 ppm (4 and 5, respectively). So, NMR data showed that the functionalisation process occurs mainly by the bonding of the thiol group with 3-(chloropropyl)-trimethoxysilane, previously fixed on the silica matrix. This fact was proved since CH$_2$–S bonds were observed in the NMR ^{13}C spectra in solid state.

3.2. Differential pulse anodic stripping voltammetry (DPASV)

DPASV of 3.00×10^{-5} mol L^{-1} Pb(II), Cu(II) and Hg(II) each solutions in 0.1 mol L^{-1} phosphate solution pH 3.0, showed three anodic peaks at −0.48 (Pb^{2+}), −0.03 (Cu^{2+}) and +0.36 V (Hg^{2+}) versus SCE. Parameters, such as accumulation potential and time, scan rate, supporting electrolyte, pH, electrode composition that affects the voltammetric peak current were optimised as described bellow.
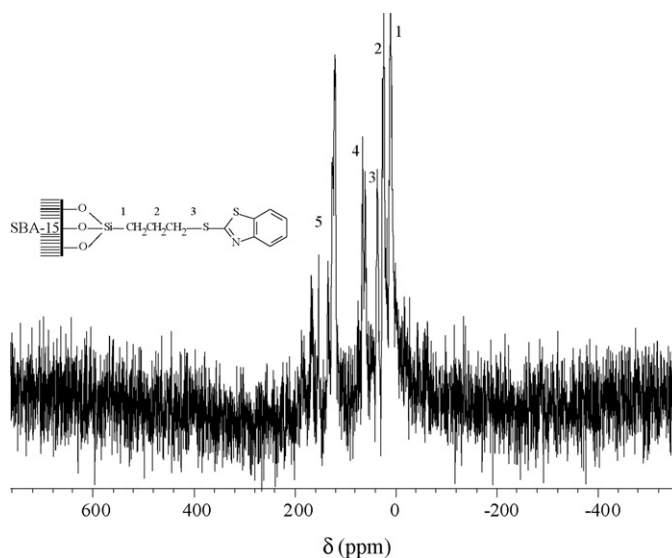
Fig. 2. ^{13}C NMR spectrum of BTPSBA in deuterated chloroform.

3.2.1. Effect of scan rate and pulse amplitude

The anodic peak currents for lead, copper and mercury in DPASV were evaluated as a function of the scan rate between 5 and 50 mV s^{-1} and pulse amplitudes from 15 to 100 mV. For this purpose pre-concentration of Pb(II), Cu(II) and Hg(II) from a 3.00×10^{-5} mol L^{-1} solutions in 0.1 mol L^{-1} phosphate solution pH 3.0 were performed for 15 s and a carbon paste composition of 15% (w/w) modified SBA-15 silica, 60% (w/w) graphite and 25% (w/w) mineral oil [13]. The scan rate of 25 mV s^{-1} was chosen because it presented higher anodic peak currents for Pb(II) and Cu(II). The scan rate of 5 mV s^{-1} presented higher anodic peak current for Hg(II), however the difference in relation the scan rate of 25 mV s^{-1} was not significative. Thus, a scan rate of 25 mV s^{-1} was employed in next experiments.

The peak current increased in higher pulse amplitude up to 100 mV.

3.2.2. Effect of accumulation potential

Accumulation potentials between -1.30 and -0.70 V were investigated, under the same conditions as above. Then Pb(0), Cu(0) and Hg(0) were oxidised by differential pulse voltammetry at 25 mV s^{-1} and pulse amplitude of 100 mV. It was observed that for an accumulation potential at -0.70 V, a decrease in the anodic peak current occurs caused by an inefficient reduction of Pb(II) to Pb(0) at the electrode surface. In -1.30 and -0.80 V interval higher anodic peak current for Pb(II) was observed in -0.80 V. Thus, -0.80 V was chosen as the accumulation potential in further studies.

3.2.3. Effect of pre-concentration time

The dependence of anodic peak currents with the pre-concentration time for 3.00×10^{-5} mol L^{-1} Pb(II), Cu(II) and Hg(II) were also investigated. The anodic peak currents increased with the increasing in the pre-concentration time between 0 and 180 s above which it became practically constant due to the surface saturation [31]. Hence, for all subsequent measurements pre-concentration time of 180 s was employed.

3.2.4. Electrode composition effect

The effect of the carbon paste composition in the voltammetric response of the electrode modified with BTPSBA was evaluated by DPASV of 3.00×10^{-5} mol L^{-1} Pb(II), Cu(II) and Hg(II) in 0.1 mol L^{-1} phosphate solution pH 3.0 in the optimised conditions described above. The anodic peak currents for Pb(II) and Cu(II) increased with the amount of organofunctionalised SBA-15 silica in the paste up to 15% (w/w). The anodic peak currents for Pb(II) and Cu(II) decreased significantly when more than 15% (modified silica, w/w) is used in the electrode preparation. For Hg(II), the anodic peak current was nearly constant until 20% and decreased when more than 20% (modified silica, w/w) is used in the electrode preparation. This probably occurs due to a decrease in the conductive area at the electrode surface. According to these results a carbon paste composition of 15% (w/w) modified SBA-15 silica, 60% (w/w) graphite and 25% (w/w) mineral oil was used in further experiments.

3.2.5. Effect of supporting electrolyte and pH

The voltammetric behaviour was examined in different supporting electrolytes as 0.10 mol L^{-1} sodium hydrogen phosphate, 0.10 mol L^{-1} sodium acetate, 0.10 mol L^{-1} potassium chloride, 0.10 mol L^{-1} potassium nitrate and 0.10 mol L^{-1} sodium perchlorate solution with pH adjusted to 2.0, 3.0, 4.0, 5.0 and 6.0. Voltammetric peaks were observed in all these electrolytes, however, in phosphate solution the anodic peak currents were higher and better defined peak shapes were observed for Pb(II) and Cu(II). For Hg(II), in acetate solution it was observed higher anodic peak current, although in this electrolyte presented lower anodic peak currents for Pb(II) and Cu(II) were observed. Thus, phosphate solution was employed in next experiments.

The effect of pH on the voltammetric response of the carbon paste electrode modified with organofunctionalised SBA-15 silica was studied in a pH range between 2.0 and 6.0 in a solution containing 3.00×10^{-5} mol L^{-1} Pb(II), Cu(II) and Hg(II) in 0.1 mol L^{-1} phosphate solution. The anodic peak current for Pb(II) increased as the pH is changed from 2.0 to 3.0, reaching a maximum at the last. In the pH range 4.0–6.0 the current decreased. For Cu(II), the anodic peak current increased in the pH range 2.0–4.0, thus the maximum anodic peak was observed at pH 4.0. For Hg(II), the anodic peak current was nearly constant as the pH is changed from 2.0 to 3.0 and decreased in the pH range 4.0–6.0. Therefore, 0.1 mol L^{-1} phosphate solution pH 3.0 was used in the further studies.

3.3. Comparison of voltammetric behaviour of Pb(II), Cu(II) and Hg(II) on carbon paste electrodes

Fig. 3 presents the differential pulse anodic stripping voltammograms obtained with unmodified carbon paste electrode, SBA-15 silica and organofunctionalised SBA-15 silica modified carbon paste electrodes in 0.10 mol L^{-1} phosphate solution
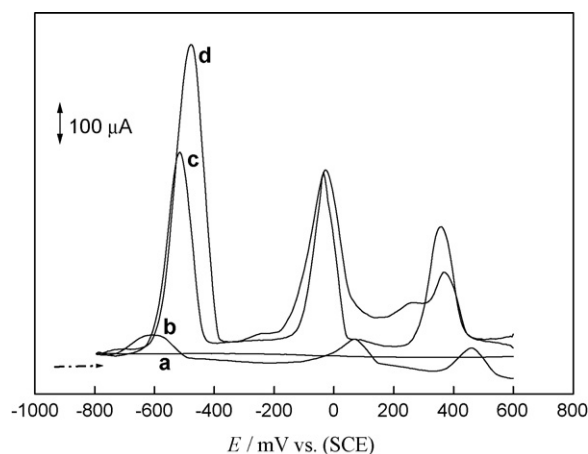
Fig. 3. Differential pulse anodic stripping voltammograms obtained at 25.0 °C, scan rate of 25 mV s^{-1} and pulse amplitude of 100 mV for (a) BTPSBA–MCPE in the presence only the 0.10 mol L^{-1} phosphate solution pH 3.0, (b) unmodified electrode in the presence of 3.00×10^{-5} mol L^{-1} Pb(II), Cu(II) and Hg(II), (c) SBA-15–MCPE in the presence of 3.00×10^{-5} mol L^{-1} Pb(II), Cu(II) and Hg(II) and (d) BTPSBA–MCPE in the presence of 3.00×10^{-5} mol L^{-1} Pb(II), Cu(II) and Hg(II). Potential interval -0.80 to $+0.60$ V (vs. SCE) and accumulation time 180 s.
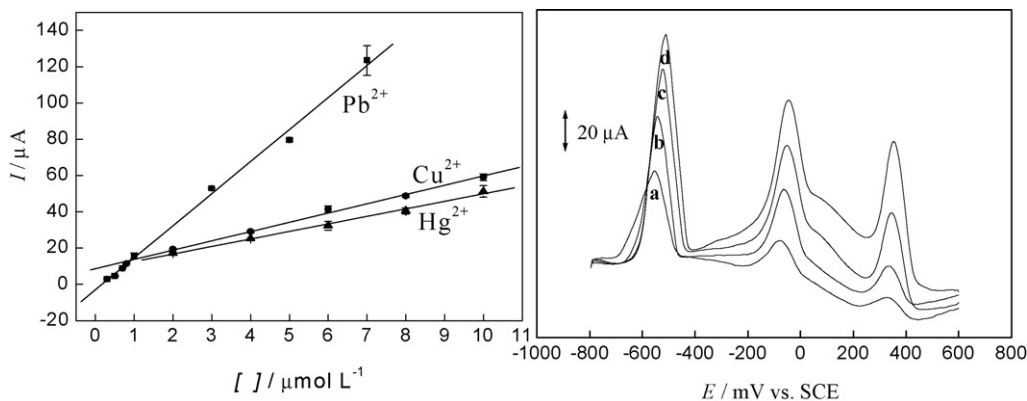
Fig. 4. Analytical curves obtained under the conditions describe in Table 1 and differential pulse anodic voltammograms for: (a) 2.00; (b) 3.00; (c) 5.00; (d) 6.00 μmol L^{-1} Pb(II), Cu(II) and Hg(II).

pH 3.0. No peaks were observed in the potential range -0.80 to $+0.60$ V (versus SCE) in the phosphate solution at the BTPSBA–MCPE (curve a) in the absence of Pb(II), Cu(II) and Hg(II).

However, when the accumulation process was carried out for 180 s at -0.8 V in a solution containing 3.00×10^{-5} mol L^{-1} Pb(II), Cu(II) and Hg(II), at the unmodified carbon paste electrode (curve b), peaks appeared on the voltammograms at -0.60 V (Pb^{2+}), $+0.07$ V (Cu^{2+}) and $+0.46$ V (Hg^{2+}) versus SCE.

The same solution exhibits peaks at -0.50 V (Pb^{2+}), -0.03 V (Cu^{2+}) and $+0.38$ V (Hg^{2+}) versus SCE when the SBA-15–MCPE (curve c) is used. At the BTPSBA–MCPE (curve d) the oxidation peak appears at -0.48 V (Pb^{2+}), -0.03 V (Cu^{2+}) and $+0.36$ V (Hg^{2+}) versus SCE, with higher intensity of the anodic currents in comparison to that observed at another electrodes. The increase in anodic currents at the modified electrode demonstrates that the BTPSBA plays an important role in the accumulation process of Pb(II), Cu(II) and Hg(II) on the electrode surface with some advantages in sensitivity.

As the ligand presents stronger interaction with Pb^{2+} ions [32] the sensitivity for this cation is much higher than that observed for Cu^{2+} and Hg^{2+}.

3.4. Analytical curves, precision, detection limits and recovery in phosphate solutions

Analytical curves for Pb(II), Cu(II) and Hg(II) are presented in Fig. 4 under the set of optimum conditions resumed in Table 1. Using such parameters, analytical curves were linear in the concentration ranges of 3.00–70.0×10^{-7} mol L^{-1} (Pb^{2+}), 8.00–100.0×10^{-7} mol L^{-1} (Cu^{2+}) and 2.00–10.0×10^{-6} mol L^{-1} (Hg^{2+}). Detection limits of 4.0×10^{-8} mol L^{-1} (Pb^{2+}), 2.0×10^{-7} mol L^{-1} (Cu^{2+}) and 4.0×10^{-7} mol L^{-1} (Hg^{2+}) were obtained at the signal noise ratio (SNR) of 3 [33]. The linear regression equations are:

$$I_{\text{pa}} = -2.24 \times 10^{-6} + 17.1[\text{Pb}^{2+}]; \quad r = 0.996; \; n = 7 \quad (1)$$

$$I_{\text{pa}} = 8.30 \times 10^{-6} + 4.23[\text{Cu}^{2+}]; \quad r = 0.998; \; n = 6 \quad (2)$$

$$I_{\text{pa}} = 9.19 \times 10^{-6} + 4.92[\text{Hg}^{2+}]; \quad r = 0.999; \; n = 5 \quad (3)$$

Table 1
Optimum parameters for simultaneous determination of lead, copper and mercury using the carbon paste electrode modified with organofunctionalised SBA-15 silica with 2-benzothiazolethiol in differential pulse anodic stripping voltammetry

Parameter	Optimised value
Scan rate	25 mV s^{-1}
Pulse amplitude	100 mV
Accumulation potential	-0.8 V (vs. SCE)
Pre-concentration time	180 s
Electrode composition	15% (w/w) modified SBA-15 silica, 60% (w/w) graphite and 25% (w/w) mineral oil
Supporting electrolyte and pH	0.10 mol L^{-1} phosphate solution and pH 3.0

The present electrode can be used without resurfacing or activation between successive determinations and with a relatively low pre-concentration time, when compared with other methods.

Again is possible to observe the sensitivity for lead, copper and mercury in the decreasing order. The limits of detection are low enough to determine Cu^{2+} and Pb^{2+} under the maximum admitted by the Brazilian Law in both well water and *cachaça* samples. The LOD for mercury is higher than that allowed for natural waters.

3.5. Interferences

The influence of Zn(II), Co(II), Cd(II) and Mn(II) in the Pb(II), Cu(II) and Hg(II) anodic peak currents have been evaluated and the results are presented in Table 2. All the interferants increased the lead signal. Cd(II) at lower concentration and Zn(II) provoked an increase in copper signal. On the other hand higher cadmium amounts as well as cobalt and manganese diminished the copper signal. The mercury signal diminished in the presence of Zn(II) and Co(II) and increased in the presence of Cd(II) and Mn(II). These effects should be related with the interactions of the metal ions with the silica modifier. The changes in the behaviour of Cu^{2+} in the presence of different Cd^{2+} and Mn^{2+} concentrations, could be explained by the facilitate deposition of the analite in the presence of low concentrations of the interferant and a competition by the active sites in higher interferant amounts.

Table 2
Effect of some divalent cations in the Pb(II), Cu(II) and Hg(II) recovery of 5 μmol L^{-1} of each cation in phosphate solution, pH 3.0; under the optimised DPASV conditions

Interferant	Concentration (μmol L^{-1})	Recovery of Pb(II) (%)	Recovery of Cu(II) (%)	Recovery of Hg(II) (%)
Zn^{2+}	2.5	115.9	132.4	84.2
	5.0	218.8	156.6	72.8
	10.0	271.3	154.3	87.9
Co^{2+}	2.5	115.7	85.3	88.6
	5.0	147.0	76.5	85.0
	10.0	156.5	81.8	93.5
Cd^{2+}	2.5	146.9	113.3	127.7
	5.0	202.3	90.9	156.6
	10.0	236.5	90.5	139.3
Mn^{2+}	2.5	118.0	86.2	124.9
	5.0	158.2	77.5	128.7
	10.0	178.6	70.5	121.2

Table 3
Results for the simultaneous determination of lead, copper and mercury in water sample[a] by DPASV proposed method and AAS, ICP-OES procedure

Repetition	Pb^{2+} (μmol L^{-1})		Relative errors (%)		Cu^{2+} (μmol L^{-1})		Relative errors (%)		Hg^{2+} (μmol L^{-1})		Relative errors (%)	
	DPASV	AAS	$|E_1|$[b]	$|E_2|$[c]	DPASV	AAS	$|E_1|$[b]	$|E_2|$[c]	DPASV	ICP-OES	$|E_1|$[b]	$|E_2|$[d]
1	1.95		2.5	8.5	2.01		0.5	6.5	2.06		3.0	4.0
2	2.07	2.13	3.5	2.8	1.96	2.15	2.0	8.8	2.08	1.98	4.0	5.1
3	2.02		1.0	5.2	2.07		3.5	3.7	1.85		7.5	6.6
4	1.96		2.0	8.0	1.91		4.5	11.2	1.99		0.5	0.5
Mean $\pm$ S.D.	2.00 $\pm$ 0.06				1.99 $\pm$ 0.07				2.00 $\pm$ 0.10			

[a] Added value for lead(II), copper(II) and mercury(II): 2 μmol L^{-1}.
[b] E_1: DPASV vs. added (DPASV-added/added) $\times$ 100%.
[c] E_2: DPASV vs. AAS (DPASV–AAS/AAS) $\times$ 100%.
[d] E_2: DPASV vs. ICP-OES (DPASV–ICP-OES/ICP-OES) $\times$ 100%.

This means that all the cations evaluated interfered positive or negatively in the response of Pb^{2+}, Cu^{2+} and Hg^{2+}. However, in the matrixes analysed, well water and *cachaça* Sant′Antonio, the standard addition procedure allowed to a successful simultaneous determination of the analytes as described bellow.

3.6. Analysis of lead, copper and mercury in well water

The proposed electrode was applied for DPASV determination of Pb(II), Cu(II) and Hg(II) spiked in a well water sample.

The results obtained using the standard addition method are presented in Table 3. Recoveries between 91.5 and 104.0% of Pb(II), 97.0 and 109.0% of Cu(II) and 95.5 and 102.7% of Hg(II) from well water samples ($n = 3$) were obtained, for 0.99, 2.00, 2.99 μmol L^{-1} of Pb(II), Cu(II) and Hg(II) spiked to each sample. There were no significant differences between the calculated and added concentrations, indicating that BTPSBA–MCPE can be used for simultaneous determination of lead, copper and mercury in water samples, under the optimised conditions and using the standard addition approach.

Table 4
Results for the simultaneous determination of lead, copper and mercury in *cachaça* sample[a] by DPASV proposed method and AAS, ICP-OES procedure

Repetition	Pb^{2+} (μmol L^{-1})		Relative errors (%)		Cu^{2+} (μmol L^{-1})		Relative errors (%)	Hg^{2+} (μmol L^{-1})		Relative errors (%)	
	DPASV	AAS	$|E_1|$[b]	$|E_2|$[c]	DPASV	AAS	$|E_2|$[c]	DPASV	ICP-OES	$|E_1|$[b]	$|E_2|$[d]
1	5.3		1.9	0	59.3		5.0	5.0		3.8 2.0	
2	4.9	5.3	5.7	7.5	64.1	62.4	2.7	5.3	4.9	1.9	8.2
3	5.1		1.9	3.8	64.1		2.7	5.0		3.8 2.0	
Mean $\pm$ S.D.	5.1 $\pm$ 0.2				62.5 $\pm$ 2.8			5.1 $\pm$ 0.2			

[a] Added value for lead(II) and mercury(II): 5.2 μmol L^{-1}.
[b] E_1: DPASV vs. added (DPASV–added/added) $\times$ 100%.
[c] E_2: DPASV vs. AAS (DPASV–AAS/AAS) $\times$ 100%.
[d] E_2: DPASV vs. ICP-OES (DPASV–ICP-OES/ICP-OES) $\times$ 100%.

3.7. Analysis of lead, copper and mercury in sugar cane spirit (cachaça)

The proposed electrode was applied in the DPASV determination of lead and mercury spiked in *cachaça* sample. These cations were not present in detectable concentration in the original sample, however the Cu(II) content in the *cachaça* was previously determined by AAS as being 3.97 mg L^{-1} (62.4 μmol L^{-1}). This analysis was performed at *"Laboratório para o Desenvolvimento da Química de Aguardente"* do IQSC/USP.

The results obtained using the standard addition method are presented in Table 4. Recoveries between 94.0 and 102.4% of Pb(II), 94.5 and 102.0% of Cu(II) and 93.0 and 105.0% of Hg(II) from *cachaça* samples ($n = 3$) were obtained, for 2.00, 3.92, 5.77 μmol L^{-1} of Pb(II), Cu(II) and Hg(II) added to each sample. So, BTPSBA–MCPE can be used for simultaneous determination of lead, copper and mercury in *cachaça* samples, under the optimised conditions and using the standard addition approach.

4. Conclusion

The use of the organofunctionalised SBA-15 silica with 2-benzothiazolethiol in the preparation of modified carbon paste electrodes showed to be an interesting alternative in the simultaneous determination of lead, copper and mercury in *cachaça* and in natural water samples. The linear ranges of $3.00–70.0 \times 10^{-7}$ mol L^{-1} (Pb^{2+}), $8.00–100.0 \times 10^{-7}$ mol L^{-1} (Cu^{2+}) and $2.00–10.0 \times 10^{-6}$ mol L^{-1} (Hg^{2+}) are extended and lower detection limits inrelation to potentiometric methods were observed [34,35]. These figures are similar to those reported by other authors using stripping voltammetry [22,36]. Several procedures have been proposed for determination of lead, copper and mercury with lower detection limits, however, these procedures used long deposition times [37,38]. Even so, the considerable sensitivity and selectivity towards lead(II), copper(II) and mercury(II) can be useful for routine analysis. Long-term stability was also obtained since one single electrode was used during the all experimental work described here.

The interference of some other cations seems to be minimised by using standard addition procedures.

Acknowledgements

References

[1] D. Zhao, Q. Huo, J. Feng, B.F. Chmelka, G.D. Stucky, J. Am. Chem. Soc. 120 (1998) 6024.
[2] J.R. Matos, L.P. Mercuri, M. Kruk, M. Jaroniec, Chem. Mater. 13 (2001) 1726.
[3] A.B. Fuertes, Microporous Mesoporous Mater. 67 (2004) 273.
[4] Y. Shan, L. Gao, Mater. Chem. Phys. 89 (2005) 412.
[5] A. Walcarius, C. Delacote, S. Sayen, Electrochim, Acta 49 (2004) 3775.
[6] C.E. Fowler, S.L. Burkett, S.J. Mann, Chem. Commun. 18 (1997) 1769.
[7] M.H. Lim, C.F. Blanford, A. Stein, J. Am. Chem. Soc. 119 (1997) 4090.
[8] C.M. Bambrough, R.C. Slade, R.T. Williams, J. Mater. Chem. 8 (1998) 569.
[9] W.M. Van Rhijin, D.E. De Vos, B.F. Sels, W.D. Bossaert, P.A. Jacobs, Chem. Commun. 3 (1998) 317.
[10] M.H. Lim, A. Stein, Chem. Mater. 11 (1999) 3285.
[11] A. Walcarius, Electroanalysis 8 (1996) 971.
[12] A. Walcarius, Chem. Mater. 13 (2001) 3351.
[13] G. Marino, M.F. Bergamini, M.F.S. Teixeira, E.T.G. Cavalheiro, Talanta 59 (20031021).
[14] J. Wang, Y.H. Lin, L. Chen, Analyst 118 (1993) 277.
[15] C. Timchalk, T.S. Poet, Y.H. Lin, K.K. Weitz, R. Zhao, K.D. Thrall, Aihaj 62 (2001) 295.
[16] J. Wang, Stripping Analysis, VCH Publishers Inc., Florida, 1985.
[17] R.P. Baldwin, J.K. Christensen, L. Kryger, Anal. Chem. 58 (1986) 1790.
[18] S.V. Prabhu, R.P. Baldwin, L. Kryger, Anal. Chem. 59 (1987) 1074.
[19] T. Molina-Holgado, J.M. Pinilla-Macias, L. Hernández-Hernández, Anal. Chim. Acta 309 (1995) 117.
[20] B. Ogorevc, X.H. Cai, I. Grabec, Anal. Chim. Acta 305 (1995) 176.
[21] M.F. Mousavi, A. Rahmani, S.M. Golabi, M. Shamsipur, H. Sharghi, Talanta 55 (2001) 305.
[22] V.S. Ijeri, A.K. Srivastava, Anal. Sci. 17 (2001) 605.
[23] J. Wang, M. Bonakdar, Talanta 35 (1988) 277.
[24] S.V. Prabhu, R.P. Baldwin, L. Kryger, Electroanalysis 1 (1989) 13.
[25] M.J. Melgar, B. Miguez, M. Perez, M.A. Garcia, M.I. Fernandez, M. Vidal, J. Environ. Sci. Health, Part A: Toxic/Hazard. Subst. Environ. Eng. 32 (1997) 687.
[26] J.G. Wiener, D.P. Krabbenhoft, G.H. Heinz, A.M. Scheuhammer, in: D.J. Hoffmanm (Ed.), Handbook of Ecotoxicology, second ed., CRC Press LLC, Boca Raton, FL, 2003, p. 409.
[27] D.G. Barceloux, Clin. Toxicol. 37 (1999) 217.
[28] Ministério da Agricultura, Pecuária e Abastecimento, Complementação de Padrões de Identidade e Qualidade para Destilados Alcóolicos, Portaria no. 124, Brasília, 2005.
[29] Resolução CONAMA, Qualidade da Água, Portaria no. 357, Brasília, 2005.
[30] G. Marino, I. Cesarino, E.T.G. Cavalheiro, Acaij 2 (2006) 37.
[31] R. Inam, G. Somer, Food Chem. 69 (2000) 345.
[32] C.N. Cimerman, D. Bogin, Anal. Chim. Acta 12 (1955) 218.
[33] B.D. Ripley, M. Thompson, Analyst 112 (1987) 377.
[34] D. Jagner, E. Sahlin, B. Axelsson, Anal. Chim. Acta 278 (1993) 237.
[35] M.L. Ruberte Sanchez, K. Vytras, Analyst 113 (1988) 959.
[36] R. Agraz, M.T. Sevilla, L. Hernandez, Anal. Chim. Acta 273 (1993) 205.
[37] J. Labuda, V. Plaskon, Anal. Chim. Acta 228 (1990) 259.
[38] R.M. Takeuchi, A.L. Santos, P.M. Padilha, N.R. Stradiotto, Talanta 71 (2007) 771.

Building a novel vitronectin assay by immobilization of integrin on calixarene monolayer

Hongxia Chen [a], Minsu Lee [b], Jaebeom Lee [c], Won Gun An [c], Heung-Jin Choi [d], Sung-Hoon Kim [d], Kwangnak Koh [c,*]

[a] *College of Pharmacy, Pusan National University, Pusan 609-735, Republic of Korea*
[b] *SEED BioChips Inc., Oh-Chang, Chung-Buk 363-883, Republic of Korea*
[c] *College of Nanoscience and Nanotechnology, Pusan National University, Pusan 609-735, Republic of Korea*
[d] *College of Engineering, Kyungpook National University, Taegu 702-701, Republic of Korea*

Abstract

Membrane proteins possess significant hydrophobic domains and are likely to deplete their native activity immobilized on the solid surface relative to those occurring in a membrane environment. To investigate an efficient immobilization method, calix[4]crown-ether monolayer as an artificial protein linker system was constructed on the gold surface and characterized by Fourier transform infrared reflection absorption spectroscopy (FTIR-RAS), atomic force microscopy (AFM) and cyclic voltammetry (CV). Integrin $\alpha_v\beta_3$ was functionally immobilized onto the monolayer and the integrin–vitronectin interaction was investigated by surface plasmon resonance (SPR). It was found that calix[4]crown-ether was assembled as a monolayer on the gold surface. Orientation and accessibility of integrin $\alpha_v\beta_3$ was assessed by sensitive binding of its natural ligand, vitronectin at pg mL^{-1} level. Moreover, surface coverage of integrin layer and thickness calculated through SPR curve simulation verified that integrin layer was a monolayer in activated form. In combination with the SPR method, this calix[4]crown monolayer provided a reliable and simple experimental platform for the investigation of isolated membrane proteins under experimental conditions resembling those of their native properties.
© 2007 Elsevier B.V. All rights reserved.

Keywords: Membrane protein; Calixarene crownether; Self-assembled monolayer (SAM); Integrin; Vitronectin; Surface plasmon resonance (SPR)

1. Introduction

Investigations on various interactions of membrane receptors (MR) are of special importance not only to academic research, but also to the pharmaceutical industry since half of the best-selling drugs are targeted to a MR [1]. Integrin is one group of main MR proteins and it is known that the integrin mediates cell adhesion and continuous adaptation between cells and the surrounding major extracellular matrix (ECM) in many physiological processes including tumor cell adhesion, migration, and proliferation [2–6]. The membrane proteins readily lose their activity when they are separated from their physiological state. The investigation of native activity of immobilized membrane proteins is quite crucial for the fabrication of efficient

high-throughput biological sensing devices [7–9]. However, less optical and electrical analysis methodologies have been developed due to the requirement of delicate preparation of integrins as biological sensing receptors even though the protein chip fabrication of dexterous integrin receptor would be very efficient in the investigation of integrin related disorders.

A calixarene derivative has a unique surface chemistry, which forms a self-assembled monolayer (SAM) on the gold surface and allows tight binding of capture proteins to the crown moiety of the linker molecules. The major binding force could be attributed to the ionized amine groups of capture proteins, which bind to the crown moiety of the linker molecule via host–guest interactions [10,11]. Also, hydrophobic interactions between hydrophobic residues of a protein and methoxy groups of the calix[4]crown-ether molecule may also be involved in protein immobilization. It could preserve the random orientation of capture proteins, keep the native composition of proteins and improve the accessibility for interaction proteins [12]. Recently,

---

a novel method based on SPR, immobilization by calixarene derivative monolayers on noble metals have been utilized to control bio-molecular density and native activity of capture proteins on solid surface and to obtain better reproducibility [13]. The approaches of protein immobilization on solid surfaces have improved controlled interfacial architectures compared to that obtained with physisorption techniques. The SPR technique and careful construction of appropriate SAM are very useful methods to the development of more efficient biosensing interface.

Our research purpose here is to prepare a novel vitronectin assay by an advanced and simple optical system in order to obtain high sensitive and selective sensors. To approach the goal, we employed a SPR system with an artificial linker system in order to keep the native activity of immobilized receptor proteins. Self-assembly technique was utilized to construct a well-characterized linker layer and then, the monolayer formation process was investigated with SPR spectroscopy. The characterization of calixarene SAM was monitored by FT-infrared reflection absorption spectroscopy (FTIR-RAS), atomic force microscopy (AFM) image, and electrochemical analysis. Immobilization of integrin $\alpha_v\beta_3$ as a sample of integrin proteins on the calixarene monolayer was measured. The surface concentration of integrin $\alpha_v\beta_3$ on the monolayer was calculated by simulation of experimental SPR data. In addition, specific binding with its natural ligand vitronectin was observed to evaluate its application potential to integrin chip based on SPR.

2. Experimental details

2.1. Chemicals and reagents

ProLinker[TM], one of calix[4]arene derivatives with crown-ether moiety, was purchased from Proteogen (Seoul, Korea) and used as a linker system for the immobilization of protein (Scheme 1(a)). Vitronectin and integrin $\alpha_v\beta_3$ were purchased from Chemincon (CA, Temecula, USA). Integrin solution was prepared and used at the concentration of 0.1 mg mL^{-1} in PBS buffer solution. For studying protein interaction on ProLinker[TM] surface, vitronectin was used as a target protein against integrin and BSA was used to block the nonspecific binding. Protein solution contained 1 mM MgCl$_2$ and 0.1 mM CaCl$_2$. Octyl-β-D-glucopyranoside, PBS solution (10×), and other reagents were obtained from Sigma Chemicals (St. Louis, MO). Milli-Q

grade (18.2 mΩ cm^{-1}) water was used for the preparation of the sample and buffer solutions.

2.2. Formation and characterization of ProLinker[TM] SAM

A microscope cover glass (18 mm × 18 mm × 0.15 mm, with a refractive index of 1.515, Matsunami, Japan) with gold layer was used as a substrate for the formation of ProLinker[TM] SAM. The gold film (thickness ≈ 50 nm) was deposited on the cover glass by the sputter coating system (E5000, Polaron Co., UK) under conditions of 2.0×10^{-2} mbar and 20 mA for 135 s. The sputtered Au substrate was rinsed using distilled water, methanol and acetone, sequentially. Then, the gold chip was dried in a nitrogen stream softly and ready to use.

The calix[4]crown solution was prepared by the mixture of chloroform and methanol. Their volume ratio was 1:100 (v:v). The SAM was formed by immersion of the gold chip into the 0.1 mM calix[4]crown solution. The immobilization process was monitored by SPR spectroscopy. After immobilization, the sensor chip was rinsed with chloroform–methanol mixture solution (1:100, v:v), methanol for 15 min and then dried under N$_2$ stream. The calix[4]crown SAM was carefully characterized by FTIR-RAS, AFM and CV.

The FTIR-RAS spectra (Magma-IR TM 550, Nicolet, USA) were measured with a resolution of 2 cm^{-1}. The glazing angle was maintained at 80° and a p-polarized IR beam was utilized as the light source. AFM images (SPM-LS, Park Scientific Instruments, USA) were collected by the non-contact tapping mode. The silicon nitride cantilevers had a nominal spring constant of about 0.067 N m^{-1}. The scanning parameters were adjusted to provide clear images, revealing the effects of SAM on the deposited gold surface. CV measurements were performed on a BAS-100B electrochemical analyzer (Bioanalytical Systems Inc., USA). The three electrode system consisted of an Ag/AgCl reference electrode with a filling solution of saturated KCl, platinum coil as the auxiliary electrode and gold as a working electrode with a scan rate 50 mV s^{-1}.

2.3. Immobilization of integrin $\alpha_v\beta_3$ on the ProLinker[TM] monolayer and vitronectin binding assay

A home-made SPR system was utilized based on the traditional Kretschmann configuration, which was described on
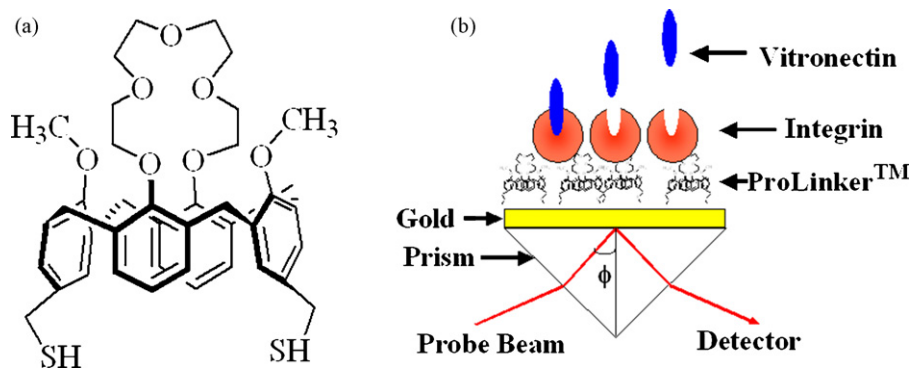
Scheme 1. Schematic diagrams of (a) molecular structure of ProLinker[TM] and (b) the sensor chip configuration.

our previous work [13,14]. The sensor chip configuration was shown in Scheme 1(b). The ProLinker^TM modified gold chip was rinsed firstly by PBS solution. Then, 0.1 mg mL^{-1} integrin $\alpha_v\beta_3$ (containing 1 mM MgCl$_2$, 0.1 mM CaCl$_2$ and 10 mM octyl-β-D-glucopyranoside) was injected into the cell and incubated for 3 h, followed by rinsing with PBS solution to remove reversible bound integrin. After immobilized with integrin, the chip was immersed with 3% BSA in PBS solution for 1 h to block the nonspecific binding sites. Finally, thirteen various vitronectin solutions in a concentration range of 1–1000 pg mL^{-1} was injected into the cell from lower one to higher one for 1 h and followed by rinsing with PBS.

2.4. Integrin surface concentration calculation

The surface concentration of immobilized protein was calculated according to a previously reported method [15]. The optical parameters that required calculating the surface concentration were determined by simulation with experimental SPR data. The surface concentration of immobilized protein on the surface was calculated by following equation:

$$\Gamma = 3d \frac{(n^2 - n_b^2)}{(n^2 + 2)(r(n_b^2 + 2) - v(n_b^2 - 1))} \tag{1}$$

where Γ and d are the surface concentration of the adsorbed molecules and the thickness of the adsorbed layer, respectively. n_b and n are the refractive index of the buffer solution and of the adsorbed layer, respectively. r and v are the specific refractivity of global protein (0.243 mL g^{-1}) and the

partial specific volume of protein deposited on the linker layer (0.729 mL g^{-1}) [16,17].

3. Results and discussion

3.1. Characterization of ProLinker^TM SAM

ProLinker^TM possessing crown-ether moiety acts as a host cavity for amine groups of protein surface. The previous reports [10,11] demonstrated that ProLinker^TM locked up protein molecules tightly and its self-assembled monolayer was a very efficient molecular linker system for immobilization of protein onto substrate surface without any loss of activity. To construct an integrin chip on solid substrate, we prepared ProLinker^TM surface onto gold-coated cover glass. In the Fig. 1(a), we confirmed the typical FTIR-RAS spectra of ProLinker^TM SAM on gold surface. In particular, v(sp^2 C–O) stretching at 1209 cm^{-1} confirmed the appearance of crown-ether group on the gold surface.

The properties of the electrode modified with ProLinker^TM SAM can be estimated by submitting the electrode to reductive desorption experiments. Fig. 1(b) shows the reductive desorption peak of ProLinker^TM SAM on the gold electrode. This peak has been attributed to the reductive desorption of thiolated compounds that are chemisorbed on the gold. Assuming that all thiolated compounds are reduced/oxidized in the CV experiments, the surface coverage can be determined from CV measurements [18]. After accounting for the surface roughness of the gold electrode, The surface coverage of calix[4]crown SAM was calculated to be
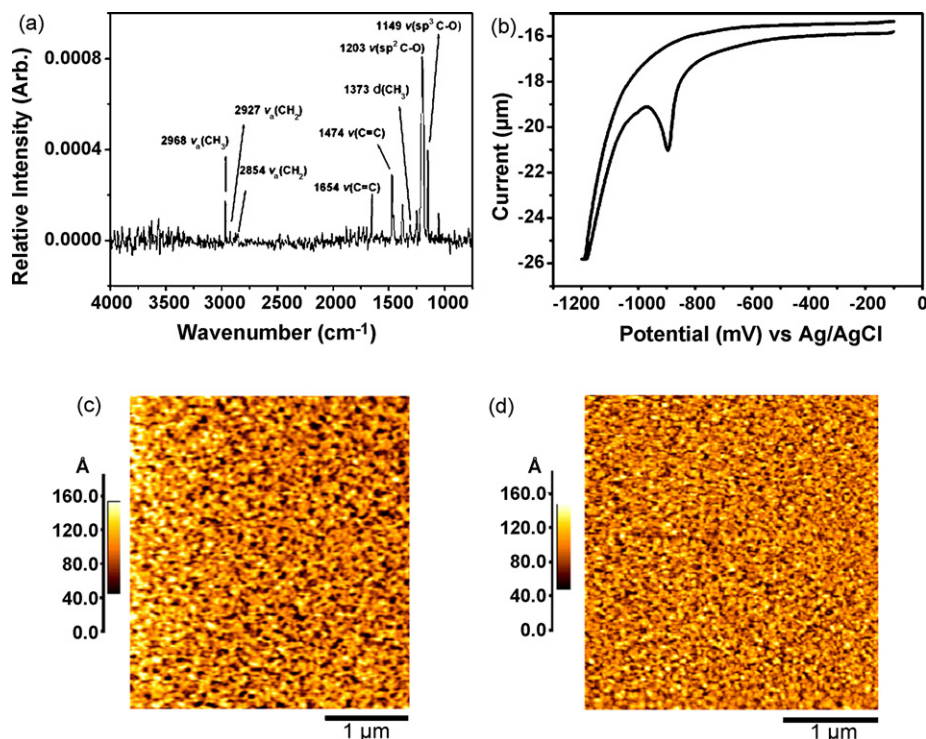

Fig. 1. Characterization of ProLinker^TM SAM: (a) FTIR-RAS spectra; (b) CV recorded for the reduction of ProLinker^TM on the gold electrode in 0.5 M KOH and AFM images of bare gold (c) and ProLinker^TM SAM (d).
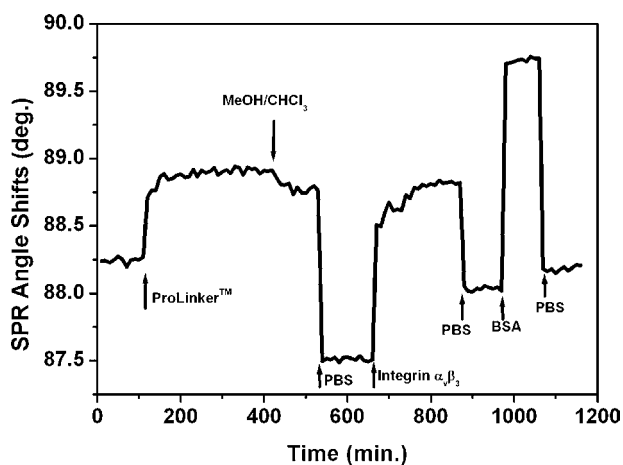
Fig. 2. The sensogram of integrin $\alpha_v\beta_3$ receptor protein chip immobilization processes.

$2.209 \times 10^{-10} \, \text{mol cm}^{-2}$, which was consistent with the theoretical monolayer value ($6.002 \times 10^{-10} \, \text{mol cm}^{-2}$) from CS Chemdraw™ (Cambridgesoft Co., USA).

The AFM images showed the surface geometry of bare gold and ProLinker™ modified gold surface (Fig. 1(c) and (d)). Bare gold surface showed relatively large size domain, whereas ProLinker™ surface had a remarkably smooth and densely uniform surface characteristics compared with bare gold surface. These increases of smoothness and uniformity on ProLinker™ modified surface were caused by the formation of self-assembled monolayer of ProLinker™ molecules. These results suggested that the self-assembled ProLinker™ monolayer can provide favorable condition for promoting detection resolution of protein molecular interaction.

Combining FTIR-RAS, AFM and CV results, it was clear that ProLinker™ was immobilized as a densely monolayer. The engineered construction of artificial protein linker on the gold surface was ready to fabricate integrin protein chip.

3.2. Immobilization of integrin $\alpha_v\beta_3$ onto ProLinker™ SAM

Immobilization of integrin $\alpha_v\beta_3$ onto ProLinker™ SAM was monitored by SPR and was depicted in Fig. 2. As the adsorbed integrin $\alpha_v\beta_3$ molecule increased on the chip surface,

SPR angle were gradually increased and saturated within 3 h. Immobilization of integrin $\alpha_v\beta_3$ resulted in shift of the SPR angle 1.3°. However, for BSA blocking, no alteration of angle shift was observed. Assuming that protein layer composed of integrin and BSA, it was shown that integrin was constructed on the ProLinker™ SAM in a dense state due to the artificial constructed linker layer.

To calculate the protein surface concentration, the optical parameters were required by simulation with experimental SPR data [19]. The optical parameters and protein surface concentration were shown in Table 1. The ProLinker™ SAM dimension of 1.19 nm was in agreement with the simple molecular 3D analysis results. Immobilization of the integrin $\alpha_v\beta_3$ produced a diffuse layer with the thickness of 17.8 nm on the ProLinker™ SAM. The integrin $\alpha_v\beta_3$ surface concentration was 416 ng cm^{-2} calculated from optical parameters according to Eq. (1). In the previous works on the structure of integrin, it was reported that integrin $\alpha_v\beta_3$ formed a prolate spheroid shape and the single molecular dimension of integrin was either 10 nm (inactivated form) or 20 nm (activated form) along major axes [20,21]. Moreover, the theoretical surface concentration was 400 ng cm^{-2} using the crystal dimensions (12 nm × 8 nm × 20 nm) [21]. Based on these results, it can be concluded that integrin $\alpha_v\beta_3$ was immobilized as a single molecular monolayer on the ProLinker™ surface in the activated form.

3.3. Vitronectin binding assay

To confirm the efficiency of integrin immobilized on ProLinker™ system, the integrin $\alpha_v\beta_3$ receptor protein chip was then incubated with various vitronectin solutions with 13 different concentrations ranging from 1.0×10^{-3} to 1.0 ng mL^{-1}. After rinsing with the PBS buffer, SPR analysis was carried out at each concentration. Fig. 3 showed the various concentration of vitronectin that was bound to the corresponding integrin chip. As the vitronectin concentration increased, the SPR angle of the integrin chip was gradually shift to the right. Detection limit of vitronectin was observed at a concentration of 1.0×10^{-2} ng mL^{-1}. These data confirmed that the integrin–vitronectin interaction occurred on the surface of the ProLinker™ SAM without any functional changes of the integrin receptor molecule. Taken together, these data suggested that the ability to make membrane protein chip on ProLinker™ sur-

Table 1
Surface concentration of the immobilized proteins and optical parameters determined by theoretical simulation, $r^2 = 0.98$

Layer	Optical parameters			Surface concentration
	n	k	d	
Au	0.280	3.6	49	
ProLinker™ SAM	1.350	0.2	1.19	$2.209 \times 10^{-10} \pm 0.23 \times 10^{-10} \, \text{mol cm}^{-2}$
Integrin	1.390	0.006	17.80	$416 \pm 5 \, \text{ng cm}^{-2}$
Vitronectin	1.391	0.012	5.20	$79 \pm 3 \, \text{ng cm}^{-2}$

Note: n, k, d denote refractive index, extinction coefficient, geometrical thickness (nm), respectively. The surface concentration data are means ± S.D. for three independent samples.
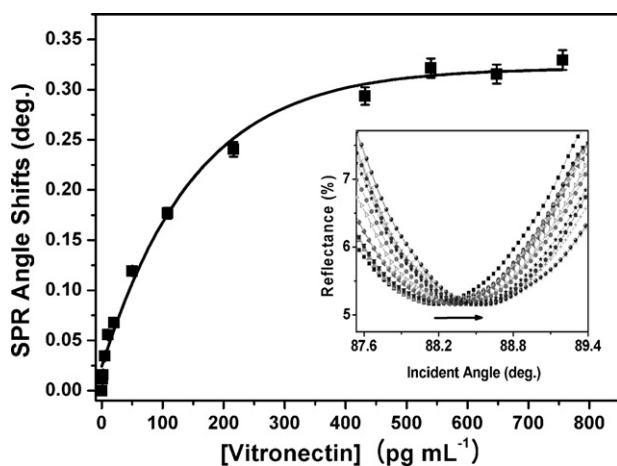
Fig. 3. Dose–response curve of integrin $\alpha_v\beta_3$ receptor protein chip represented by SPR angle shifts according to the interaction between integrin and vitronectin. Solid line indicates the result of non-linear regression ($r^2 = 0.992$). Insert is SPR angle shifts according to the interaction between integrin $\alpha_v\beta_3$ and vitronectin.

face with accurately engineered feature, size and shape should increase the capabilities of studying fundamental interactions between protein and solid surfaces.

4. Conclusions

We have generated a simple assay system for studying the interaction of integrin $\alpha_v\beta_3$ with its ligand on a calix[4]crown-ether monolayer based on SPR spectroscopy. Calix[4]crown-ether was immobilized on the gold surface and characterized by FTIR-RAS, AFM and CV. The integrin layer was immobilized on the calix[4]crown surface and found to be as a monolayer in an active form. The detection of integrin and vitronectin interaction at the very low concentration (pg mL^{-1} level) is accessible based on SPR detection system. This approach provides an efficient method for immobilization of membrane receptor proteins on the gold substrate without requiring additional modification processes for coupling capture proteins to calix[4]crown-ether monolayer.

References

[1] G.C. Terstappen, R. Angelo, Trends Pharmacol. Sci. 22 (2001) 23.
[2] R.O. Hynes, Cell 48 (1987) 549.
[3] V. Beck, H. Herold, A. Benge, B. Luber, P. Hutzler, H. Tschesche, H. Kessler, M. Schmitt, H. Geppert, U. Reuning, Int. J. Biochem. Cell Biol. 37 (2005) 590.
[4] M.A. Horton, Int. J. Biochem. Cell Biol. 29 (1997) 721.
[5] F. Carreiras, S. Cruet, C. Staedel, F. Sichel, P. Gauduchon, Gynecol. Oncol. 72 (1999) 312.
[6] R.O. Hynes, Cell 110 (2002) 673.
[7] M. Tulla, O.T. Pentikainen, T. Viitasalo, J. Kapyla, U. Impola, P. Nykvist, L. Nissinen, M.S. Johnson, J. Heino, J. Biol. Chem. 276 (2001) 48206.
[8] M.A. Cooper, J. Mol. Recog. 17 (2004) 286.
[9] E.K. Sinner, U. Reuning, F.N. Kök, B. Sacca, L. Moroder, W. Knoll, D. Oesterhelt, Anal. Biochem. 333 (2004) 216.
[10] Y. Lee, E.K. Lee, Y.W. Cho, T. Matsui, I.-C. Kang, T.-S. Kim, M.H. Han, Proteomics 3 (2003) 2289.
[11] Y. Sasakura, K. Kanda, T.Y. Suzuki, T. Matsui, S. Fukuzono, M.H. Han, T. Shimizu, Anal. Chem. 76 (2004) 6521.
[12] M. Lee, D.K. Kang, H.K. Yang, K.H. Park, S.Y. Choe, C. Kang, S.I. Chang, M.H. Han, I.C. Kang, Proteomics 6 (2006) 1094.
[13] H. Chen, M. Lee, S. Choi, J.H. Kim, H.J. Choi, S.H. Kim, J. Lee, K. Koh, Sensors 7 (2007) 1091.
[14] M. Lee, W.G. An, J.H. Kim, H.J. Choi, S.H. Kim, M.H. Han, K. Koh, Mater. Sci. Eng. C 24 (2004) 123.
[15] M. Marquart, J. Deisenhofer, R. Huber, W. Palm, J. Mol. Biol. 141 (1980) 369.
[16] J.W. Corsel, G.M. Willems, J.M.M. Kop, P.A. Cuypers, W.T. Hermens, J. Coll. Interf. Sci. 111 (1986) 544.
[17] L.S. Jung, C.T. Campbell, T.M. Chinowsky, M.N. Mar, S.S. Yee, Langmuir 14 (1998) 5636.
[18] J. Bard, L.R. Faulkner, Electrochemical Methods: Fundamentals and Application, John Wiley & Sons, New York, 2001, p. 239.
[19] Y. Hur, K. Ock, K. Kim, S. Jin, Y. Gal, J. Kim, S. Kim, K. Koh, Anal. Chim. Acta 460 (2002) 133.
[20] J. Takagi, T.A. Springer, Immunol. Rev. 186 (2002) 141.
[21] J.P. Xiong, T. Stehle, R. Zhang, A. Joachimiak, R. Dunker, D.L. Scott, A. Joachimiak, S.L. Goodman, M.A. Arnaout, Science 294 (2001) 339.

Rapid amperometric detection of coliforms based on MWNTs/Nafion composite film modified glass carbon electrode

Yuxiao Cheng, Yajun Liu, Jingjing Huang, Yuezhong Xian,
Wen Zhang, Zhonghai Zhang, Litong Jin *

Department of Chemistry, East China Normal University, Shanghai 200062, PR China

Abstract

A multi-wall carbon nanotubes (MWNTs)/Nafion modified glassy carbon electrode (GCE) was fabricated for the rapid amperometric detection of coliforms, represented by *Escherichia coli* (*E. coli*). In the bacterial solution, β-galactosidase which was used as an indicator of coliforms reacted with substrate, *p*-aminophenol-β-galactopyranoside (PAPG), and produced *p*-aminophenol (PAP). PAP was detected by MWNTs/Nafion modified GCE. Due to the cation-exchange capacity of Nafion and the electrocatalytic ability of MWNTs, the detection sensitivity of PAP was improved and the detection time of coliforms was shortened. The bacterial can be detected within 5 h ranging from 10 to 10^4 cfu/mL. The MWNTs/Nafion modified GCE was easy to be constructed and regenerated. To our best knowledge, it was the first time to use MWNTs/Nafion modified GCE to detect the concentration of coliforms.
© 2007 Published by Elsevier B.V.

Keywords: Multi-wall carbon nanotubes; Nafion; Coliforms; Amperometric detection; β-Galactosidase; *p*-Aminophenol

1. Introduction

Coliforms and *Escherichia coli* (*E. coli*) which are found in large numbers among the intestinal of humans and other warm-blooded animals spread abroad in natural environment and are commonly used as indicators of fecal contamination of aquatic systems. They may cause bloody diarrhea, hemorrhagic colitis, renal failure and meningitis [1,2]. During 1993–1997, among the reported outbreaks of foodborne illness in the United States, bacterial pathogens caused the largest percentage of outbreaks (about 75%) [3]. *Salmonella* sp., *Listeria monocytogenes* and *E. coli* accounted for the largest number of outbreaks and deaths. Conventional microbiological detection of coliforms includes plate counting, multiple-tube fermentation and membrane filter technique relying on the culture-based assays [4]. Although these methods are accurate, they have the drawbacks of long incubation time (24–48 h), lack of specificity and complex operation. Therefore, rapid and sensitive detection methods are essential for minimizing the outbreak of infection, surveillance, and sanitary supervision.

The β-galactosidase is widely used as an indicator for total coliforms. When the coliforms are induced by isopropyl-β-D-thiogalactopyranoside (IPTG), the activity of β-galactosidase is at least 100 times higher than that of non-coliforms [5]. Thus, the interference from nontarget galactosidase-positive bacteria is low and insignificant except that they are present in high concentration. A number of optical assays have been developed to detect the coliforms and *E. coli* based on the activity of β-galactosidase [6–10]. A colorimetric method was developed for the detection of coliforms in sewage using *o*-nitrophenyl-β-D-galactopyranoside as a substrate [6]. The absorbance of *o*-nitrophenol produced by the reaction of β-galactosidase and substrate was proportional to the concentration of coliforms. Mathew and Alocilja developed a chemiluminescence-based assay for the rapid detection of *E. coli* based on the reaction of β-galactosidase with a phenylgalactosidase-substituted dioxetane substrate [10]. Light emitted from the reaction was measured by a luminometer and the data correlated to the concentration of *E. coli*. Although these methods have been shown to be suitable alternatives to the classic techniques, they have disadvantages

---

of expensive reagents, long incubation time and high detection limit.

Several amperometric sensors based on various electrode materials such as indium tin oxide (ITO), glassy carbon and graphite have been applied to detect coliforms and *E. coli* [11–16]. The amperometric sensors showed favorable ability to determine the electroactive substances produced in the bacterial solution. A graphite–Teflon–tyrosinase composite electrode was fabricated to detect phenol produced by enzymatic reaction in the bacterial solution, and the detection sensitivity was improved [15]. Zhang and coworkers developed a bismuth nanofilm modified GCE in a flow injection system to detect the 4-nitrophenol concentration that is proportional to the cell numbers of *E. coli*. The amperometric sensor was able to detect as low as 1.0×10^2 cfu/mL with the detection time of ca. 3 h [16].

Carbon nanotubes (CNTs) have unique geometrical, mechanical, electronic and chemical properties [17–19]. Such properties of CNTs make them an attractive material of electroanalysis. Several studies have demonstrated that CNTs can strongly enhance the electrocatalytic activity and minimize the fouling on the surface of electrodes [20–22]. Nafion is a perfluorosulfonated cation-exchanger polymer, and it can incorporate positively charged ions and reject the anionic species [23–25]. Furthermore, Nafion has properties of exceptional chemical and thermal stability, which enable it to incorporate various electrocatalysts (such as CNTs or dyes) into the Nafion films [26,27]. In this study, a MWNTs/Nafion modified electrode was fabricated for amperometric detection of coliforms, represented by *E. coli* (BL21). The method was based on the detection of PAP that was released after the hydrolysis of the substrate *p*-aminophenyl-β-D-galactopyranoside (PAPG) by β-galactosidase. MWNTs/Nafion modified GCE not only accumulated the PAP into the Nafion film but also enhanced the transfer rate of electrons, thus evidently improving the detection sensitivity of PAP. Because of these advantages, the detection sensitivity of coliforms was increased and the detection time was shortened.

2. Experimental

2.1. Chemicals

Nafion perfluorinated ion-exchange resin (5.0 wt% solution in lower aliphatic alcohols/H$_2$O mixture), *p*-aminophenyl-β-D-galactopyranoside, polymyxin B sulfate (POL), isopropyl-β-D-thiogalactopyranoside and lysozyme (LYS) were purchased from Sigma Company (St. Louis, MO, USA). Multi-walled carbon nanotubes (purity more than 95%) with diameter between 10 and 30 nm were bought from Shenzhen Nanotech Port Co., Ltd. (Shenzhen, China). Sodium chloride, phosphate disodium, and phosphoric acid were purchased from Shanghai Chemical Reagent Company (Shanghai, China). *E. coli* (BL21) was a gift from School of Life Sciences, East China Normal University (Shanghai, China). Luria broth medium contains 1.0% of tryptone, 0.5% of sodium chloride and 0.5% of yeast extract. All solutions were prepared with doubly distilled water.

2.2. Apparatus

Electrochemical measurements were performed on a CHI 1140 electrochemical analyzer (CH Instruments, Chenhua, Shanghai, China) with a three-electrode system consisting of an Ag/AgCl/3.0 M KCl as the reference electrode, a platinum wire electrode as the auxiliary electrode and a modified or bare glassy carbon electrode (GCE) as the working electrode.

2.3. Preparation of the Nafion and MWNTs/Nafion modified GCE

Before use, the MWNTs was purified to remove graphitic nanoparticles, amorphous carbon, and catalyst impurities, and then functionalized with carboxylic acid groups according to the literature [28]. A 1.0 wt% Nafion solution was prepared by diluting the 5.0 wt% Nafion solution with ethanol. 5.0 mg MWNTs were added to 10 mL 1.0 wt% Nafion solution, and then ultrasonicated for 3 h to form a homogeneous MWNTs/Nafion solution.

The GCE was first mechanically polished with alumina paste (0.3 μm), and rinsed with doubly distilled water, and then further cleaned ultrasonically in 1.0 M HNO$_3$, 1.0 M NaOH, acetone and doubly distilled water successively. MWNTs/Nafion modified GCE was prepared by dropping 9.0 μL suspension of above-mentioned MWNTs/Nafion, and allowed to evaporate ethanol at room temperature in the air. The Nafion film modified GCE was fabricated with the same procedure described previously, but without MWNTs.

2.4. Bacteria cultivation

E. coli (BL21) cultures were grown overnight in LB medium at 37 °C with aeration by shaking, which allowed the growing stationary phase to be reached. For optimization of the detection conditions, the stationary phase *E. coli* cultures were diluted to 2.0×10^4 and 2.0×10^5 in 50 mL LB medium containing 0.5 mM IPTG, and incubated for 3 h with aeration. The activity of β-galactosidase was detected under different conditions after permeabilization.

For the detection of *E. coli*, the bacterial cultures were diluted to concentrations of $10–10^4$ cfu/mL in 1.0 L of sterile water. The solution was filtered through 0.45 μm filter papers which were placed into flasks containing 50 mL LB medium. Then IPTG was added to the flasks to a final concentration of 0.5 mM. The cultures were incubated at 37 °C with aeration and withdrawn at 0.5 h intervals for the detection of galactosidase activity.

2.5. Amperometric detection of E. coli

Prior to detection, the bacterial solution, which was supplied with POL (10 μg/ml) and LYS (25 μg/ml), was vigorously shaked for 25 min at 30 °C, and then phosphate buffer solution (pH 6.0) was added.

The bacterial solution was put into electrochemical cell which was placed in a thermostatic bath to keep the temperature at 45 °C. The bacterial solution was stirred at a constant rate and

amperometric *i–t* curve was recorded at +250 mV. While background current was stable, PAPG solution was added into the electrochemical cell to a final concentration of 2.0 mM. The concentration of PAP increased because of the hydrolysis of PAPG by β-D-galactosidase. After 10 min enzymatic reaction, the current response was recorded again.

2.6. Plate count method

E. coli cultures grown at 37 °C overnight in LB medium were serially diluted (10-fold steps) 10^7 times with LB medium, and 100 μL diluted solutions of *E. coli* were plated on LB agar plates. After incubation at 37 °C for 24 h, *E. coli* colonies on plates were counted to determine the number of colony-forming units per milliliter. Glass apparatus, LB medium and doubly distilled water, which were used in this section, were sterilized at 121 °C for 20 min.

3. Results and discussion

3.1. Electrochemical behaviors of PAP

The electrochemical behaviors of PAP on bare GCE, Nafion coated GCE and MWNTs/Nafion modified GCE were investigated by cyclic voltammetry (CV) with scanning potential from −0.30 to +0.60 V. The reaction of PAP on the electrode can be described as follows (Scheme 1).

As seen from Fig. 1, 1.0×10^{-4} mol/L PAP in pH 6.0 phosphate buffer solution, a pair of redox peak was observed at GCE. While the surface of GCE was coated with 9 μL 1.0% Nafion film, the peak current increased obviously. The concentration of
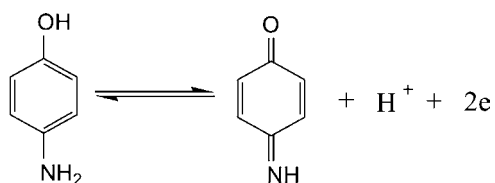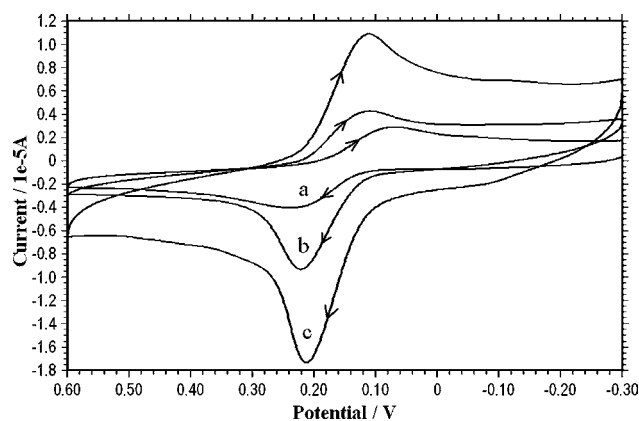
PAP on the surface of electrode was increased due to the electrostatic attraction of the cationic form of PAP ($pK_b = 8.74$) with Nafion ion-exchange resin at pH 6.0, thus the peak current was enhanced. Moreover, the peak current at the GCE modified with MWNTs/Nafion was further increased, and the oxidation peak potential shifted from +0.236 V at bare GCE to +0.213 V at MWNT/Nafion modified GCE. The results indicated the electrocatalytic activity of MWNTs toward PAP. The controlled experiments demonstrated that the MWNTs/Nafion film had the ability to accumulate and electrocatalyze PAP.

3.2. Effect of the amount of MWNTs/Nafion suspension on GCE surface

The effect of the amount of MWNTs/Nafion suspension modified onto the GCE was investigated by differential pulse voltammetry (DPV). The oxidation peak current of PAP (5.0×10^{-5} mol/L) increased as the volume of MWNTs/Nafion suspension increased from 0 to 9.0 μL, then reached an approximate plateau from 9.0 to 15.0 μL. It ascribed to that the active sites for accumulation of PAP increased with the increment of the amount of MWNTs/Nafion. However, the peak current decreased when the volume exceeded 15.0 μL because that the mass transport and charge transfer rate may decrease when the MWNTs/Nafion film was too thick. Thus, the optimized amount of MWNTs/Nafion was chosen as 9.0 μL.

3.3. Electrochemical detection of E. coli with MWNTs/Nafion modified GCE

E. coli cultures were incubated for 3 h in LB medium supplied with 0.5 mM IPTG to achieve the induction of β-D-galactosidase [5]. Before the activity of galactosidase was detected, a permeabilizaion step was carried out by vigorously shaking the bacterial with POL (10 μg/mL) and LYS (25 μg/mL) [6,29], which could disrupt the outer and cytoplasmic membranes of bacterial culture and release galactosidase into the solution [30]. Fig. 2 shows the amperometric response of 2.0×10^4 cfu/mL,

Scheme 1. Reaction equation of PAP on the electrode.

Fig. 1. Cyclic voltammograms of 1.0×10^{-4} mol/L PAP in 0.02 mol/L, pH 6.0 phosphate buffer solution with scan rate of 100 mV/s at: GCE (a); Nafion modified GCE (b); MWNTs/Nafion modified GCE (c).

Fig. 2. Current responses of blank growth medium (a), 2.0×10^4 cfu/mL (b), and 2.0×10^5 cfu/mL (c) of *E. coli* detected by MWNTs/Nafion modified GCE with applying potential of +250 mV at pH 6.0 and 45 °C. *E. coli* cultures were incubated for 3 h with IPTG and permeabilized with POL and LYS.
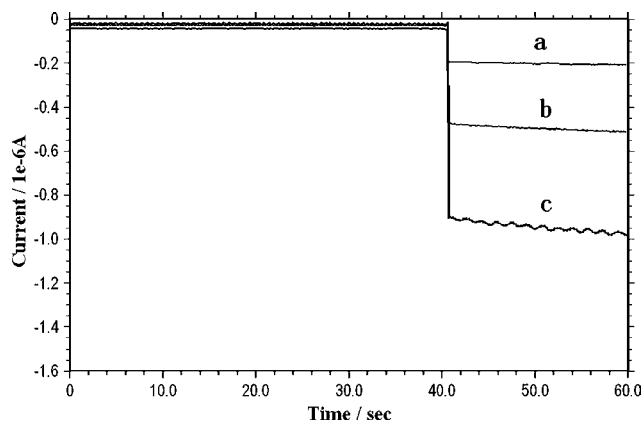
Fig. 3. Current responses of 2.0×10^5 cfu/mL *E. coli* at GCE (a), Nafion modified GCE (b) and MWNTs/Nafion modified GCE (c). Other conditions were the same as Fig. 2.

2.0×10^5 cfu/mL of *E. coli* and the blank growth medium. The concentration of PAP in the bacterial solution was increased as the hydrolysis of PAPG by galactosidase. After 10 min reaction, the current was recorded and the change of current was related to the quantity of enzyme that was directly related to the concentration of *E. coli* in the sample solution.

Bacterial cultures were measured by GCE, Nafion coated GCE and MWNTs/Nafion modified GCE, respectively. From Fig. 3, the current response was enhanced at Nafion modified G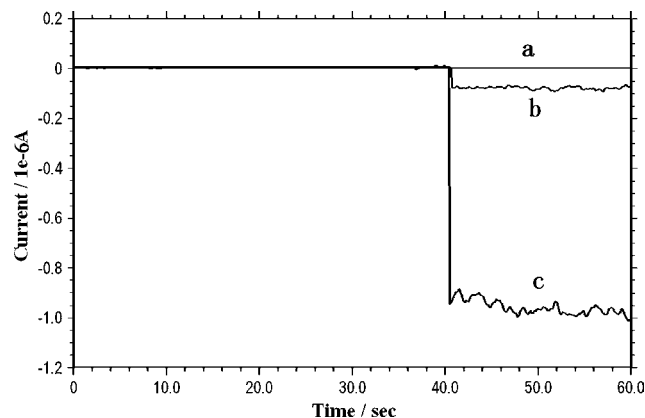CE (about three times than that at GCE) because Nafion has high cation-exchange capacity for PAP produced by enzymatic reaction. Otherwise, the current response was further increased (about six times than that on GCE) by MWNTs/Nafion modified GCE due to the ability of MWNTs to promote electron transfer rate. The results showed that MWNTs/Nafion modified GCE could greatly improve the detection sensitivity when it is used to measure the concentration of *E. coli*.

3.4. The optimization of pH and temperature

The activity of galactosidase may be affected by the pH value and temperature. Thus, the influence of pH value and temperature on the detection of bacteria was investigated. After the *E. coli* cultures were incubated and permeabilized, 4.0 mL of bacterial solution was withdrawn from the flask, and placed into the electrochemical cell. A serial of 1.0 mL, 0.1 mol/L phosphate buffer solution of different pH value was added to adjust the pH of the bacterial solution. Fig. 4 showed the maximum of current response was obtained while the bacteria were detected at pH value of 6.0. When they were detected in the pH value lower than 6.0 or higher than 7.0 the current response decreased. The results may be due to the decrease of the activity of β-D-galactosidase [32] in acidic and alkaline solution. In addition, there were more PAP ($pK_b = 8.74$) of cationic form at pH 6.0 than in neuter or alkaline solution so that the concentration of PAP accumulated to the Nafion film was augmented and the detection sensitivity was improved. On the other hand, bacterial were detected at 25, 35, 45 and 55 °C respectively to examine the temperature dependence of β-D-galactosidase. The results indicated that
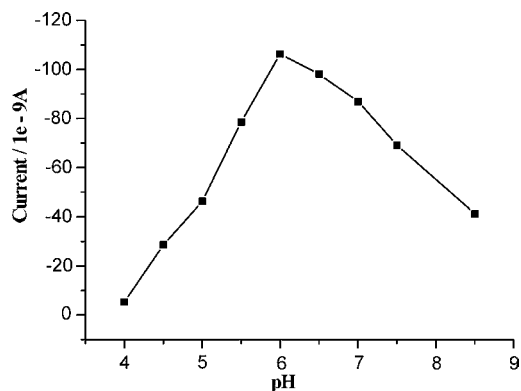
Fig. 4. Influence of pH value on the detection of 2.0×10^4 cfu/mL of *E. coli* at MWNTs/Nafion modified GCE. Other conditions were the same as Fig. 2.

the activity of β-D-galactosidase increased with the increase of detection temperature, and reached a maximal value at 45 °C. It might be unstable when the temperature was higher than 45 °C. [5]. Hence, pH 6.0 and 45 °C was selected for the further work.

3.5. Detection of E. coli

Under the optimized conditions, different bacterial concentrations were assayed by MWNTs/Nafion modified GCE after different periods of incubation. As can be observed from Fig. 5, the bacteria could be detected within 5 h ranging from 10 to 10^4 cfu/mL, with the detection limit of 10 cfu/mL, and the current response was increased with the increment of the incubation time. Furthermore, when the concentration of bacteria was increased, the incubation time needed decreased simultaneously. In this work, the sensitivity of the detection was improved by MWNTs/Nafion modified electrode due to the accumulation of PAP by Nafion film and the electrocatalysis of MWNT to PAP. So, the incubation time was shortened. 10 cfu/mL of bacterial cannot been detected by GCE until after 6 h enrichment, and the detection time was 1 h longer than that with MWNTs/Nafion modified GCE. The results obtained in this work were superior to other relevant reported amperometric methods for the detection of *E. coli* [12,16,29]. Fiksdal and his coworkers developed
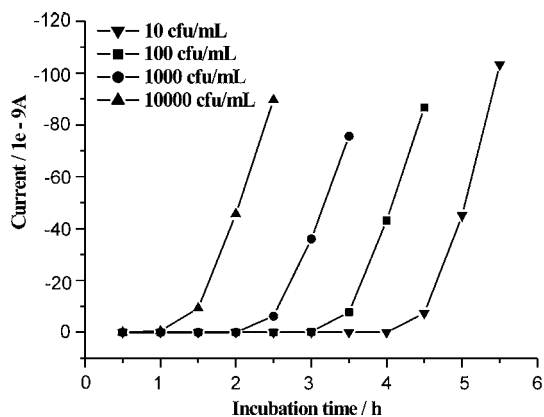
Fig. 5. Current responses of 10, 1.0×10^2, 1.0×10^3 and 1.0×10^4 cfu/mL of *E. coli* after different incubation periods. The *E. coli* cultures were in 1.0 L sterilized water and steps of filtration, incubation and permeabilization were carried out.

an amperrametric method combined with flow inject analysis for detecting *E. coli* in water [12]. It needed more than 5 h enrichment to detect 4.5×10^2 cfu/mL. The method did not have any permeabilization step which could improve the sensitivity of several orders of magnitude according to literature [31]. Although the graphite–Teflon–tyrosinase composite electrode mentioned above can detect 10 cfu/mL of *E. coli* after 5 h enrichment [15], the fabrication of enzyme electrode was complicated and the preservation of the electrode was rigorous.

The repeatability of MWNTs/Nafion modified electrode was investigated with an initial concentration of 2.0×10^4 cfu/mL of *E. coli*, which was incubated with IPTG for 3 h. The relative standard deviation (RSD, $n = 7$) of the current responses was about 4.60%. Five MWNTs/Nafion modified electrodes were prepared for the investigation of electrode-to-electrode reproducibility under the same conditions, and the RSD was less than 6.00%. After the detection, the MWNTs/Nafion modified electrode was dipped in 2.0 mol/L NaCl for 10 min, and the activity sites of Nafion film could be regenerated easily.

3.6. Detection of E. coli in river water

The MWNTs/Nafion modified GCE was applied to detect the sample which was collected from river water in Shanghai. A liter of the river water was filtered by 0.45 μm pore sized filter paper. Then, the filter paper was placed into flask containing 50 mL LB medium and 0.5 mM IPTG. After 3.5 h incubation, the bacterial sample was detected by the amperometric method introduced above. The result indicated that the concentration of coliforms in the river water was 100 cfu/mL, which was consistent to the result obtained by plate count method (113 cfu/mL).

4. Conclusions

A MWNTs/Nafion modified GCE was fabricated, and was applied to detect the concentration of coliforms. Due to the improvement of detection ability to PAP, the detection sensitivity of the bacteria was improved by MWNTs/Nafion modified GCE. Under the optimized experiment conditions, bacterial solution of 10 cfu/mL coliforms could be detected after 4.5 h enrichment. The method was rapid and could be exploited for controlling the bacterial contamination in water environment or food industry.

References

[1] J.H. Thomas, N.J. Ronkainen-Matsuno, S. Farrell, H.B. Halsall, W.R. Heineman, Microchem. J. 74 (2003) 267.
[2] S.F. Altekruse, M.L. Cohen, D.L. Sherdlow, Emerg. Infect. Dis. 3 (1997) 285.
[3] S.J. Olsen, L.C. MacKinnon, J.S. Goulding, N.H. Bean, L. Slutsker, Surveillance for foodborne-disease outbreaks-United States 1993–1997, MMWR CDC Surveillance Summaries 49 (No. SS-1) (2000) 1-64.
[4] L. Clesceri, A. Greenberg, A. Eaton, Standard Methods of the Examination of water and Wastewater, 20th ed., American Public Health Association, American Water Works Association and Water Environment Federation, Washington, DC, 1998.
[5] I. Tryland, L. Fiksdal, Appl. Environ. Microbiol. 64 (1998) 1018.
[6] S.C. Apte, C.M. Davies, S.M. Peterson, Water Res. 29 (1995) 1803.
[7] S.O. Van Poucke, H.J. Nelis, Appl. Environ. Microbiol. 61 (1995) 4505.
[8] S.O. Van Poucke, H.J. Nelis, J. Microbiol. Methods 42 (2000) 233.
[9] K. Geissler, M. Manafi, I. Amoros, L. Alonso, J. Appl. Microbiol. 889 (2000) 280.
[10] F.P. Mathew, D. Alagesan, E.C. Alocilja, Luminescence 19 (2004) 193.
[11] C. Ruan, H. Wang, Y. Li, Trans. ASAE 45 (2002) 249.
[12] F. Pérez, I. Tryland, M. Mascini, L. Fiksdal, Anal. Chim. Acta 427 (2001) 149.
[13] A.G. Gehring, J.D. Brewster, P.L. Irwin, S. Tu, L.J. Van Houten, J. Electroanal. Chem. 469 (1999) 27.
[14] H. Tang, W. Zhang, P. Geng, Q. Wang, L. Jin, Z. Wu, M. Lou, Anal. Chim. Acta 562 (2006) 190.
[15] B. Serra, M.D. Morales, J. Zhang, A.J. Reviejo, E.H. Hall, J.M. Pingarron, Anal. Chem. 77 (2005) 8115.
[16] H. Tang, W. Zhang, P. Geng, Q. Wang, L. Jin, Z. Wu, Electrochem. Commun. 9 (2007) 833.
[17] C.N. Rao, B.C. Satishkumar, A. Govindaraj, M. Nath, ChemPhysChem 2 (2001) 79.
[18] R.H. Baughman, A. Zakhidov, W.A. De Heer, Science 297 (2002) 787.
[19] P.M. Ayayan, Chem. Rev. 99 (1999) 1787.
[20] J. Wang, M. Musameh, Y. Lin, J. Am. Chem. Soc. 125 (2003) 2408.
[21] M. Musameh, J. Wang, A. Merkoci, Y. Lin, Electrochem. Commun. 4 (2002) 743.
[22] J. Wang, M. Li, Z. Shi, N. Li, Z. Gu, Anal. Chem. 74 (2002) 1993.
[23] W.J. Vining, T.J. Meyer, J. Electroanal. Chem. 237 (1987) 191.
[24] Ti.H. Lu, I.W. Sun, Talanta 53 (2000) 443.
[25] L.S. Rocha, H.M. Carapuca, Bioelectrochemistry 69 (2006) 258.
[26] V. Ganesan, S. Abraham John, R. Ramaraj, J. Electroanal. Chem. 502 (2001) 167.
[27] S. Shahrokhian, H.R. Zare-Mehrjardi, Electrochim. Acta 52 (2007) 6310.
[28] X. Tan, M. Li, P. Cai, L. Luo, X. Zou, Anal. Biochem. 337 (2005) 111.
[29] A.S. Mittelmann, E.Z. Ron, J. Rishpon, Anal. Chem. 74 (2002) 903.
[30] M. Teuber, Arch. Mikrobiol. 73 (1970) 61.
[31] V.K. Jain, I.T. Magrath, Anal. Biochem. 199 (1991) 119.
[32] R. Guven, K. Guven, A. Poli, B. Nicolaus, Enzyme Microb. Tech. 40 (2007) 1570.

ELSEVIER

Simultaneous derivatization and extraction of anilines in waste water with dispersive liquid–liquid microextraction followed by gas chromatography–mass spectrometric detection

Jing-Shan Chiang, Shang-Da Huang *

Department of Chemistry, National Tsing Hua University, Hsinchu 30043, Taiwan

Abstract

The one-step derivatization and extraction technique for the determination of anilines in river water by dispersive liquid–liquid microextraction (DLLME) is presented. In this method the anilines are extracted by DLLME and derivatized with pentafluorobenzaldehyde (PFBAY) in aqueous solution simultaneously. In this derivatization/extraction method, 0.5 ml acetone (disperser solvent) containing 10 μl chlorobenzene (extraction solvent) and 30 g/l pentafluorobenzaldehyde (PFBAY) dissolved in methanol was rapidly injected by syringe into 5 ml aqueous sample (pH 4.6). Within 20 min the analytes extracted and derivatized were almost finished. After centrifugation, 2 μl sedimented phase containing enriched analytes was determined by GC–MS. The effects of extraction and disperser solvent type and their volume, pH value of sample solution, derivatization and extraction time, derivatization and extraction temperature were investigated. Linearity in this developed method was ranging from 0.25 to 70 μg/l, and the correlation coefficients (R^2) were between 0.9955 and 0.9989, and reasonable reproducibility ranging from 5.8 to 11.8% ($n = 5$). Method detection limits (MDLs) ranged from 0.04 to 0.09 μg/l ($n = 5$).
© 2007 Elsevier B.V. All rights reserved.

Keywords: Anilines; Dispersive liquid–liquid microextraction; Gas chromatography–mass spectrometry

1. Introduction

Aromatic amines, such as aniline and its substituted derivatives, are generally dangerous because of their toxicity and carcinogenicity [1,2] or else they can be converted into toxic *N*-nitroso compounds through reactions with nitrosylating agents in the environment [3]. These contaminants may be released as chemical residues of dyestuffs, cosmetics, medicines and rubber manufacture [3,4] and also as by-products of energy technologies such as coal-conversion waste processing [1]. Chlorinated anilines such as *p*-chloroaniline and 3,4-dichloroaniline were also found as degradation products and intermediates of various phenylurea and phenylcarbamate pesticides [1,3]. In view of the importance of these compounds, a rapid and sensitive method of analysis is needed to detect them in the environment.

Several methods have been developed for the determination of anilines in environmental samples. Gas chromatography (GC) is a classical method [5,6], and presently GC–mass spectrometry (MS) is often used [5,6]. For non-volatile aniline compounds high-performance liquid chromatography (HPLC) may be used with fluorescence detection after derivatization [7,8], or with amperometric detection [9,10]. Some sample preparation techniques have been reported for the pretreatment of anilines in aqueous samples based on solid-phase extraction (SPE) [11]. In the past years, solid-phase microextraction (SPME) [12–14] has emerged as a versatile solvent-free alternative to SPE procedures. In recent years, a novel technique termed liquid-phase microextraction (LPME) [15] has been developed. However a fast simple preconcentration and microextraction method, DLLME has been presented in 2006 for determination of polycyclic aromatic hydrocarbons (PAHs), organophosphorus pesticides (OPPs) and chlorobenzenes (CBs) in water samples [16–19] and for the first time, simultaneous DLLME and derivatization combined with gas chromatography-electroncapture detection (GC-ECD) were studied for the analysis of 19 chlorophenols (CPs) in water samples [20]. In this method,

* Corresponding author at: Department of Chemistry, National Tsing Hua University, 101 Kung Fu Road, Section 2, Hsinchu 30043, Taiwan.
Tel.: +886 3 5721194; fax: +886 3 5736979.
E-mail address: sdhuang@mx.nthu.edu.tw (S.-D. Huang).

the appropriate mixture of extraction solvent and disperser solvent are injected into the aqueous sample (5 ml) by syringe, rapidly. Therefore, cloudy solution is formed. In fact, it is consisted of fine particles of extraction solvent which is dispersed entirely into aqueous phase. After centrifuging, the fine particles of extraction solvent are sedimented in the bottom of the conical test tube. The advantages of DLLME method are simplicity of operation, rapidity, low-cost, high-recovery, and enrichment factor.

In the present work, simultaneous DLLME and derivatization have been carried out in one-step for the analysis of anilines in water samples at the sub-ppb level and various parameters affecting the extraction efficiency were also investigated in this study.

2. Experimental

2.1. Chemicals and sample preparation

All chemicals used in this study were reagent grade, aniline and 4-chloroaniline were obtained (purity > 99%) from Fluka (Buchs, Switzerland), 3-chloro-2-methylaniline and 3,5-dichloroaniline were purchased (purity ≧ 98%) from Sigma–Aldrich (Portugal). Derivatization reagent pentafluorobenzaldehyde (PFBAY) was purchased from Alfa-Aesar (Ward Hill, MA, USA), chlorobenzene (J.T. Baker, Mallinckrodt, Baker), tetrachloroethylene (J.T. Baker, Mallinckrodt, Baker), tetrachlorocarbon (Showa Chemicals, Tokyo, Japan), acetone (Echo, Maioli, Taiwan), acetonitrile (J.T. Baker, Mallinckrodt, Baker), and methanol (Echo, Maioli, Taiwan) were also used for this study.

The stock solutions were prepared by adding approximately 3 mg of analytes into vials and diluted to 10 ml with methanol. The stock solutions were kept storage at 4 °C. Before extraction, stock solutions were diluted with blank stream water to aqueous standard of 33 μg/l (aniline), 57 μg/l (4-chloroaniline), 62 μg/l (3-chloro-2-methylaniline), and 48 μg/l (3,5-dichloroaniline) for the optimization experiments. A waste water from Tou Cian stream (Hsinchu, Taiwan) served as the environmental sample.

2.2. Instrumentation

Analysis was carried-out using a gas chromatograph Agilent (Wilmington, Delaware, USA) 6850 with split/splitless injector operated at 250 °C in pulse splitless mode (1 min), mass detector Agilent (Wilmington, Delaware, USA) 5978B. A 30 m HP-5MS (J&W Scientific, Folsom, CA, USA) fused silica capillary column (0.25 mm I.D., 0.25 μm film thickness) was used for separation. The column oven was initially held at 70 °C, raised to 295 °C at 15 °C/min, held at 295 °C for 1 min. The carrier gas was helium (purity 99.9995%); it was further purified by passage through a superior helium gas purifier Agilent (Wilmington, DE, USA) model RMSH-2. A Sorvall 5C Plus Centrifuge (Global Medical, Ramsey, MN, USA) was used.

All of the 10 ml screw cap conical bottomed glass test tubes (extraction vessel) were manufactured by Ching Fa glass factory (Hsingchu, Taiwan).

Deionized water was prepared using a Milli-Q (Millipore, MA, USA) purification system.

2.3. DLLME procedure

In the simultaneous DLLME and derivatization, an aliquot of 5 ml of a blank stream solution containing 33 μg/l (aniline), 57 μg/l (4-chloroaniline), 62 μg/l (3-chloro-2-methylaniline), and 48 μg/l (3,5-dichloroaniline) was placed in a 10 ml screw cap conical bottomed glass test tube. An aliquot of 0.5 ml of acetone (disperser solvent) containing 8.75 μl chlorobenzene (extraction solvent) and 10 μl methanol containing PFBAY (30 g/l, derivatization reagent) was injected rapidly into the aqueous solution with a 1 ml syringe (gastight, Hamilton, Reno, NV, USA) and a 10 μl syringe (gastight, Hamilton, Reno, NV, USA), then the mentioned mixture was kept in a water bath (30 °C). Dispersed fine droplets of chlorobenzene form a cloudy solution. In this step, anilines and PFBAY were extracted into the fine droplet of chlorobenzene rapidly and derivatized in the chlorobenzene, in 20 min. After centrifugation for 2 min at 6000 rpm, fine droplets of extraction solvent were sedimented at the bottom of the conical test tube. The volume of the sedimented phase was determined to approximately 2 ± 0.2 μl. The sedimented phase (2 μl) was injected into GC for separation and analysis.

3. Results and discussion

3.1. Optimization of DLLME

3.1.1. Method evaluation

For evaluating the pretreatment procedure, the sensitivities of two experiments were compared. In the first experiment, derivatization reagent was added to aqueous sample containing anilines to proceed derivative reaction for 20 min, then 0.5 ml acetone including 8.75 μl chlorobenzene was injected into above aqueous sample and then the centrifugation was proceeded in 2 min. In the second experiment, simultaneous DLLME and derivatization, 0.5 ml acetone including 8.75 μl chlorobenzene and derivatization reagent were injected into aqueous sample spiked with anilines, and then centrifugation was proceeded after 20 min. As shown in Fig. 1, better sensitivity was obtained, except for 3,5-dichloroaniline with similar sensitivity, with simultaneous DLLME and derivatization. It was inferred that difference of sensitivity of anilines between experiment 1 and 2 should be affected by the solubility of anilines in water (Table 1) [23–26]. Therefore simultaneous derivatization and extraction was decided to be the pretreatment procedure.

Table 1
Water solubility of anilines

Analyte	Water solubility (g/l)
Aniline	34 [23]
4-Chloroaniline	3 [24]
3-Chloro-2-methylaniline	4.5 [25]
3,5-Dichloroaniline	0.6 [26]
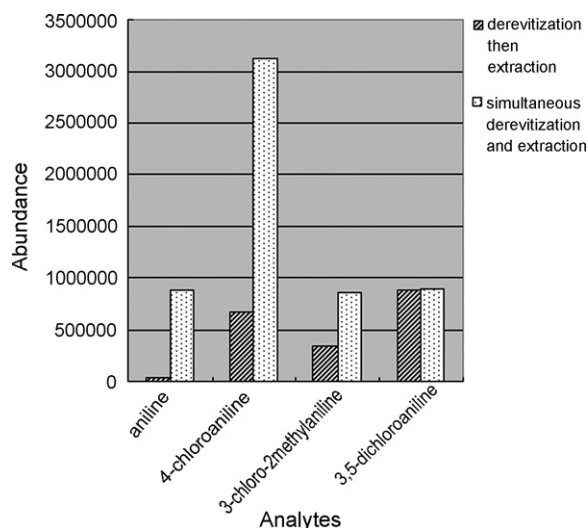
Fig. 1. Method evaluation.

3.1.2. Selection of extraction solvent

In DLLME method, some characteristics of extraction solvent such as low solubility in water, extraction capability of interested compounds, good chromatographic behavior and higher density than water must be achieved. Thus there are extra limitations on the selection of extraction solvent in DLLME method. Most of the halogenated solvents own above properties.

To obtain the better extraction efficiency, chlorobenzene, tetrachloroethylene, and tetrachlorocarbon were tested as extraction solvents. A 5 ml of aqueous sample containing the target compounds were extracted using the procedure described above.

As shown in Fig. 2, the extraction efficiency of aniline and 4-chloroaniline extracted with tetrachlorocarbon were higher than other solvents but from the view of average sensitivity for these four analytes, chlorobenzene was selected as the extraction solvent.
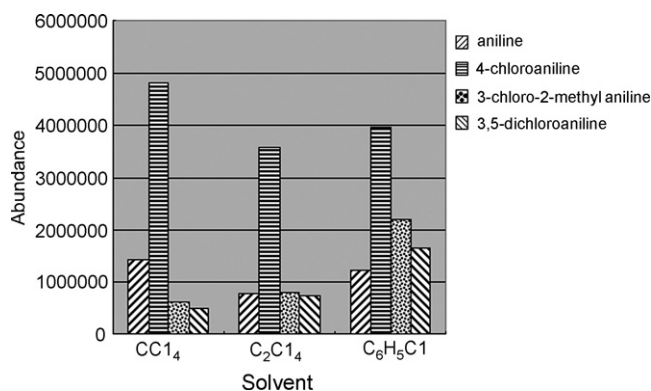
Fig. 2. Effect of extraction solvent on the sensitivity. Extraction conditions: water sample volume, 5 ml; disperser, solvent (acetone) volume, 1 ml; extraction solvent, 8 μl tetrachloroethylene; 13.5 μl carbon tetrachloride and 13 μl chlorobenzene; 30 °C; concentration of anilines, 33 μg/l aniline, 57 μg/l 4-chloroaniline, 62 μg/l 3-chloro-2-methylaniline, and 48 μg/l 3,5-dichloroaniline; 30 min.
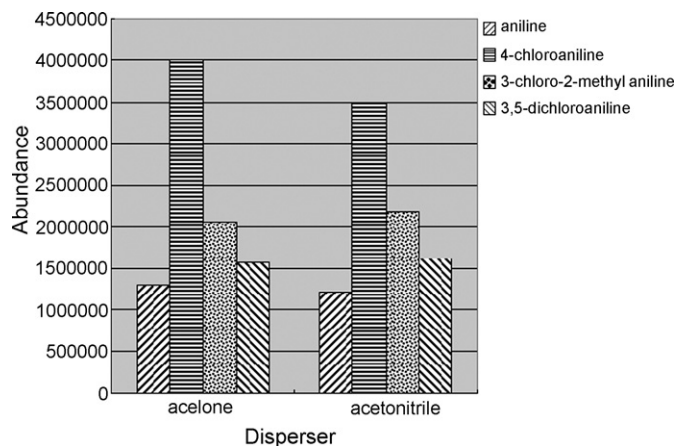
Fig. 3. Effect of dispersive solvent on the sensitivity. Extraction conditions: as with Fig. 2; volume of chlorobenzene, 13 μl.

3.1.3. Selection of dispersing solvent

Disperser solvent should be miscible in water; also it should dissolve the extraction solvent. Thus acetone and acetonitrile were selected as disperser solvents to investigate the effect of these solvents on the performance of DLLME.

When acetone and acetonitrile were tested as disperser solvents containing chlorobenzene to inject into aqueous sample, as shown in the following result (Fig. 3), extraction efficiency of acetone was similar to acetonitrile but acetone was less toxic, referred with LC_{50}, than acetonitrile [21,22]. Consequently, the acetone was selected as disperser solvent because of less toxicity and cheaper.

3.1.4. Amount of dispersing solvent

For investigating the effect of volume of disperser solvent on extraction efficiency, various volumes of acetone (0.5, 1, 1.5 ml) containing (10, 13, 16.5 μl) chlorobenzene were performed, respectively. Increasing the volume of chlorobenzene by increasing the volume of acetone is required to obtain the constant volume of the sedimented phase (3 ± 0.2 μl). As shown in Fig. 4, the optimized sensitivity was achieved when 0.5 ml acetone and 10 μl of chlorobenzene were used.
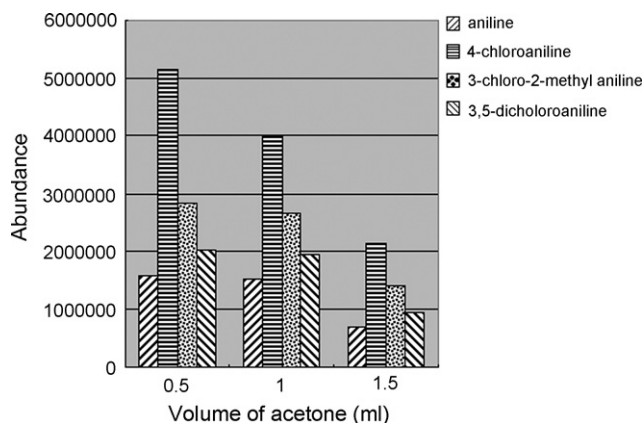
Fig. 4. Effect of amount of dispersive solvent on the sensitivity. Extraction conditions: as with Fig. 3; solvent (acetone) volume, 1 ml.

3.1.5. Amount of extraction solvent

Increasing extraction solvent would increase extracted amount of analytes, however the concentration of analytes in the sedimented phase were also diluted. For enhancing sensitivity, 2 μl of sedimented phase was injected to GC–MS. Over 2 μl of injection would cause peak broaden. Here 8.75 and 10 μl of extraction solvent was used to study for obtaining the effect of 2 and 3 μl of sedimented phase on extraction efficiency. There is no considerable change on the extraction efficiency of these anilines between 8.75 and 10 μl of extraction solvent. Consequently, 8.75 μl chlorobenzene was selected.

3.1.6. Adjustment of pH value in sample solution

In this work, the matrices in the river water would influence derivatization and extraction efficiency. Here, different pH values (4, 4.6, 5, 7.8) in sample solution were adjusted to investigate the derivatization and extraction efficiency. The lower sensitivity of stream water (pH 7.8) was observed. Higher sensitivity was acquired as lowering pH value, however sensitivity descended below pH 4.6. As shown in Fig. 5, the better derivatization and extraction efficiency would be obtained at pH 4.6.

3.1.7. Effect of extraction and derivatization temperature on extraction efficiency

In simultaneous extraction and derivatization with DLLME, raising temperature would cause different derivatization performance and solubility of analytes in aqueous. Here, various extraction and derivatization temperatures were investigated to obtain the better extraction efficiency. As shown in Fig. 6, the sensitivity decreased by increasing extraction and derivatization temperature from 30 to 60 °C. Thus 30 °C was used for further study.

3.1.8. Effect of extraction and derivatization time on extraction efficiency

In simultaneous extraction and derivatization with DLLME, dispersed fine droplets of chlorobenzene form a cloudy solution and the surface area between extraction solvent and aqueous

Fig. 6. Effect of extraction and derivatization temperature on the sensitivity. (▲) 3-Chloro-2-methyl aniline; (×) 3,5-dichloroaniline; (■) 4-chloroaniline; (♦) aniline. Extraction conditions: as with Fig. 5; pH of water sample, 4.6.

phase (water sample) is very large. Transition of anilines and PFBAY from aqueous phase (water sample) to extraction solvent is fast enough to let a quick achieve of the equilibrium state. Thereby, most of the required time was for derivatization of anilines with PFBAY.

Various experiments were performed in the range of 0–50 min to obtain the better extraction efficiency. As shown in Fig. 7, there is no considerable change on the sensitivity of these anilines after 20 min and 20 min was selected for extraction and derivatization time.

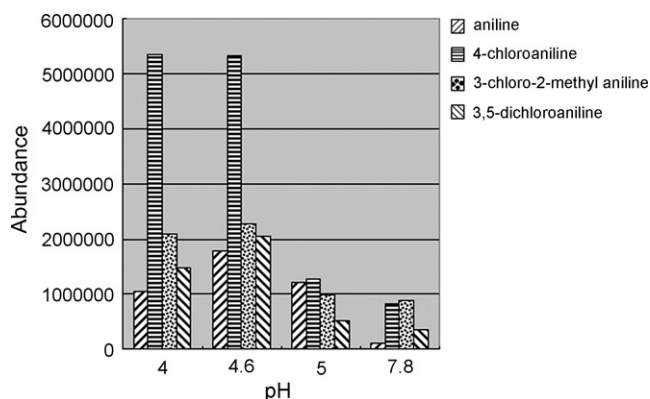Fig. 5. Effect of pH on the sensitivity. Extraction conditions: as with Fig. 4; solvent (acetone) volume, 0.5 ml.
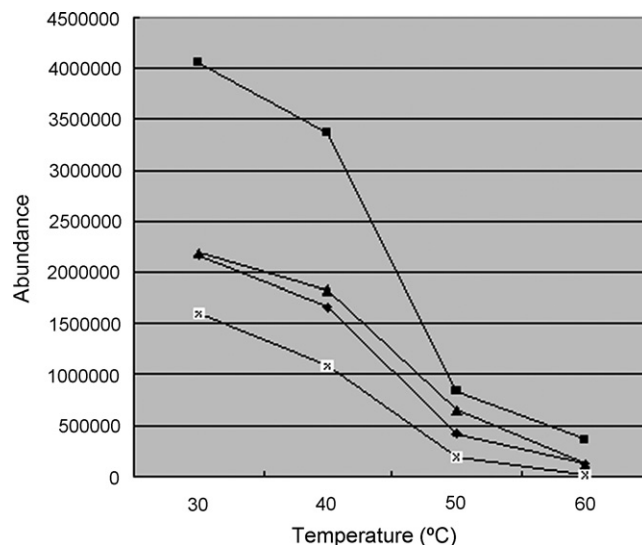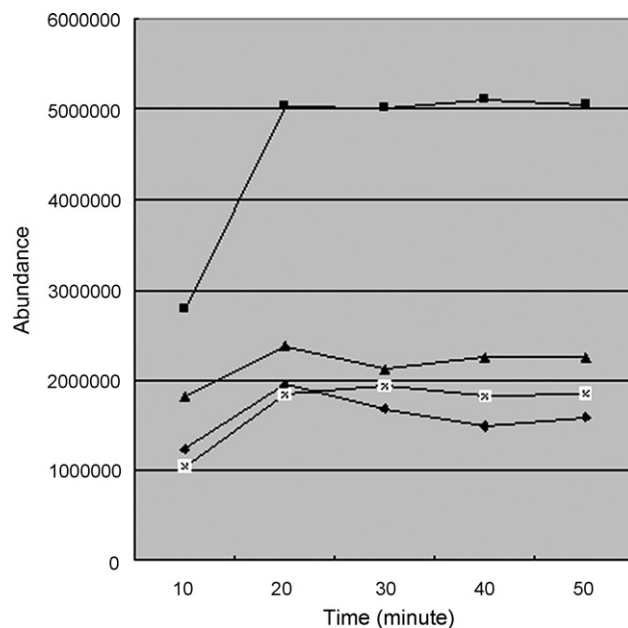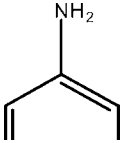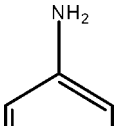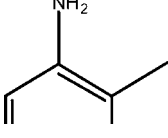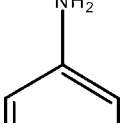

Fig. 7. Effect of extraction and derivatization time on the sensitivity. (▲) 3-Chloro-2-methyl aniline; (×) 3,5-dichloroaniline; (■) 4-chloroaniline; (♦) aniline. Extraction conditions: as with Fig. 6; extraction and derivatization temperature, 30 °C.

Table 2
Ions of analytes

Analytes	Structure	Molecular mass	Qualified ions	Quantity ions
Aniline	NH₂	271.1	271.1, 77.0, 104.0	271.0
4-Chloroaniline	NH₂	305.0	305.0, 110.0, 138.0	305.0
3-Chloro-2-methylaniline	NH₂	319.0	319.0, 117.1, 152.0	319.0
3,5-Dichloroaniline	NH₂	339.0	339.0, 145.0, 172.0	339.0

3.2. Evaluation of method performance

The characteristics of analytes were listed in Table 2. Enrichment factors, which were defined as formula 1, achieved by the DLLME procedure were 212–645-fold. The linearity of the DLLME for blank water samples of anilines detected by GC–MS was investigated with spiked concentrations of analytes ranging from 0.25 to 70 µg/l; and method detection limits (MDLs), which were calculated as three times the standard deviation of five replicated runs of spiked samples at lowest concentration of calibration curve, were in the range 0.04–0.09 µg/l. Correlation coefficients, (R^2) values, were between 0.9955 and 0.9985. Linear equation was used to calculate R^2 for GC–MS. The range of the relative standard deviations is 5.8–11.8% (Table 3):

$$\text{enrichment factor} = \frac{V_s C_s}{V_{aq} C_0} \tag{1}$$

where C_s is the concentration of analytes in sediment phase after extraction, V_s the volume of sediment phase for injecting to GC, V_{aq} the volume of sample solution and C_0 is the initial concentration of analytes in aqueous sample before extraction.

3.3. Analysis of stream water sample

The optimum condition for each factor may be inter-related. The conditions we finally selected may not be the optimum. However, we have checked back and forth the conditions from time to time. For instance, the data shown in Fig. 1 should be run at the beginning of the experiment. We have re-run the experiment using the selected conditions we found at the final stage. In Fig. 2, the selectivity for the less sensitive analytes, 3-chloro-2-methylaniline and 3,5-dichloroaniline, was much better as using chlorobenzene for extraction solvent, it therefore may not absolutely required to check it once again. For Fig. 3, the extraction

Table 3
Summary of the performance of the developed methods[a]

Analyte	Linear range (µg/l)	R^2	R.S.D. (%)[b]	MDL (µg/l)[c]	Enrichment factor[d]	Relative recovery[e]
Aniline	0.25–70	0.9989	10.6	0.08	449	69
4-Chloroaniline	0.25–70	0.9982	8.1	0.04	645	77
3-Chloro-2-methyl aniline	0.5–70	0.9955	5.8	0.09	214	94
3,5-Dichloro aniline	0.5–70	0.9985	11.8	0.09	212	88

[a] The selected conditions were listed as follows: (1) disperser solvent, acetone; (2) extraction solvent, chlorobenzene; (3) amount of disperser solvent, 0.5 ml; (4) amount of extraction solvent, 8.75 µl; (5) pH value of sample solution, 4.6; (6) derivatization and extraction temperature, 30 °C; (7) derivatization and extraction time, 20 min.

[b] Repeatability was investigated at concentration: 0.25 µg/l of aniline and 4-chloroaniline; 0.5 µg/l of 3-chloro-2-methyl aniline and 3,5-dichloro aniline.

[c] MDLs are calculated as three times the standard deviation of seven replicated runs of spiked sample. Concentraction: 0.25 µg/l of aniline and 4-chloroaniline; 0.5 µg/l of 3-chloro-2-methyl aniline and 3,5-dichloro aniline.

[d] Enrichment factor was determined at concentration 10 µg of anilines/l.

[e] Relative recovery was determined at concentration: 2.5 µg/l of aniline and 4-chloroaniline; 5 µg/l of 3-chloro-2-methyl aniline and 3,5-dichloro aniline.

Fig. 8. Chromatogram of (A) real stream sample and (B) blank stream sample spiked with 33 μg/l aniline, 57 μg/l 4-chloroaniline, 62 μg/l 3-chloro-2-methylaniline, and 48 μg/l 3,5-dichloroaniline. Extraction conditions: as with Fig. 7; extraction and derivatization time, 30 min.

efficiencies were similar using acetone or acetonitrile. Acetone was selected as disperser solvent because of less toxic and cheaper (Refs. [21,22]). Similar situation can be found from the date shown in other figures.

Stream waste water sample was filtered through a filter paper before analysis. The aqueous samples were extracted with DLLME under the selected conditions. The selected conditions were listed as below: (1) disperser solvent, acetone; (2) extraction solvent, chlorobenzene; (3) amount of disperser solvent, 0.5 ml; (4) amount of extraction solvent, 8.75 μl; (5) pH value of sample solution, 4.6; (6) derivatization and extraction temperature, 30 °C; (7) derivatization and extraction time, 20 min. No anilines were detected in the stream water samples (Tou Cian stream) neighbor to the dye factory tested. The relative recoveries defined as the peak area ratio between blank stream water and the tested stream water sample, which was free of the analytes, spiked at the same concentration (2.5, 2.5, 5, 5 μg/l) was found to be 69–94% (Table 3). No analytes were detected in the stream waste water sample (Fig. 8).

4. Conclusion

This work indicates that a selective trace enrichment of carcinogenic anilines from river water samples can be achieved by a DLLME method. The newly developed microextraction technique has distinct advantages over conventional methods with respect to extraction time and volume of solvents required, and low detection limits are readily achieved. This proposed sample preparation procedure is much simpler than the conventional LLE, SPE, and SPME.

Acknowledgement

References

[1] S. Laha, R.G. Luthy, Environ. Sci. Technol. 24 (1990) 363.
[2] M. Dalene, G. Skarping, J. Chromatogr. 331 (1985) 321.
[3] H. Kataoka, J. Chromatogr. A 733 (1996) 19.
[4] L.M. Games, R.A. Hites, Anal. Chem. 49 (1977) 1433.
[5] A.T. James, A.J.P. Martin, Br. Med. Bull. 10 (1954) 170.
[6] L. Fishbein, Chromatography of Environmental Hazards, vol. II, Elsevier, Amsterdam, 1979 (chapter 23).
[7] R.B. Geerdink, J. Chromatogr. 445 (1988) 273.
[8] D. Djozan, M.A. Faraj-Zadeh, Chromatographia 41 (1995) 568.
[9] R. Boussenadji, P. Dufek, M. Porthault, LC–GC 11 (1993) 450.
[10] S. Hatrik, J. Lehotay, J. Tekel, J. High Resolut. Chromatogr. 17 (1994) 756.
[11] J. Patsias, E. Papadopoulou-Mourkidou, J. Chromatogr. A 904 (2000) 171.
[12] L. Müller, E. Fattore, E. Benfenati, J. Chromatogr. A 791 (1997) 221.
[13] C.-T. Yan, T.-S. Shih, J.-F. Jen, Talanta 64 (2004) 650.
[14] H. Berrada, G. Font, J.C. Moltó, J. Chromatogr. A 1042 (2004) 9.
[15] Y. He, H.K. Lee, Anal. Chem. 69 (1997) 4634.
[16] M. Rezaee, Y. Assadi, M.R. Milani Hosseini, E. Aghaee, F. Ahmadi, S. Berijani, J. Chromatogr. A 1116 (2006) 1.
[17] S. Berijani, Y. Assadi, M. Anbia, M.R. Milani Hosseini, E. Aghaee, J. Chromatogr. A 1123 (2006) 1.
[18] R. Rahnama Kozani, Y. Assadi, F. Shemirani, M.R. Milani Hosseini, M.R. Jamali, Chromatographia 66 (2007) 81.
[19] N. Fattahi, Y. Assadi, M.R. Milani Hosseini, E. Zeini Jahromi, J. Chromatogr. A 1157 (2007) 23.
[20] R. Rahnama Kozani, Y. Assadi, F. Shemirani, M.R. Milani Hosseini, M.R. Jamali, Talanta 72 (2007) 387.
[21] http://rais.ornl.gov/tox/profiles/acetone.shtml.
[22] http://www.lakes-environmental.com/toxic/ACETONITRILE.HTML.
[23] http://www.inchem.org/documents/icsc/icsc/eics0011.htm.
[24] http://www.chemyq.com/xz/xz9/85178ffxpl.htm.
[25] https://fscimage.fishersci.com/msds/04639.htm.
[26] http://www.chemyq.com/xz/xz9/86273yksgf.htm.

Validation of a fluorimetric assay for 4-aminophenol in paracetamol formulations

B. Dejaegher [a], M.S. Bloomfield [b], J. Smeyers-Verbeke [a], Y. Vander Heyden [a],*

[a] *Analytical Chemistry and Pharmaceutical Technology, Pharmaceutical Institute, Vrije Universiteit Brussel (VUB), Laarbeeklaan 103, 1090 Brussels, Belgium*
[b] *GlaxoSmithkline (GSK) Consumer Healthcare, St Georges Avenue, Weybridge, Surrey KT13 0DE, United Kingdom*

Abstract

4-Aminophenol (4-AP) is the primary degradation product of paracetamol (PARA). According to the European Pharmacopoeia, 50 ppm 4-AP/PARA is the specification limit of 4-aminophenol in paracetamol drug substance. For drug products, often higher specification limits, such as 1000 ppm 4-AP/PARA are applied. This paper describes a fluorimetric method to quantify the low amount of this degradant (50 ppm) in a pharmaceutical preparation, i.e. in paracetamol tablets. The fluorimetric method was validated and the linearity, precision, trueness, range, limit of detection and limit of quantification were determined. They were found acceptable to assay the low amounts of 4-aminophenol in paracetamol tablets.
© 2007 Elsevier B.V. All rights reserved.

Keywords: 4-Aminophenol; Fluorimetry; Method validation

1. Introduction

Paracetamol, acetaminophen or *N*-acetyl-*p*-aminophenol is a commonly used analgesic and antipyretic drug, present in different pharmaceutical formulations, such as tablets, soluble powders, syrups and suppositories. It is administered to both children and adults [1,2]. The primary degradation product of paracetamol (PARA) is 4-aminophenol (4-AP) or 1-hydroxy-4-aminobenzene. It is formed during the synthesis of paracetamol or during the storage of the pharmaceutical preparations [3–5]. For paracetamol drug substance, this degradant is limited to a low specification limit, i.e. 50 ppm or 0.005% (w/w) 4-AP/PARA. For drug products containing paracetamol, often less tight limits are applied, such as 1000 ppm or 0.1% (w/w) 4-AP/PARA [6].

Different methods to assay 4-aminophenol in paracetamol drug substance, drug products and/or biological fluids have been described. Derivative ultra-violet (UV) spectroscopy was used in [3,7,8]. Other spectrophotometric methods such as colorimetry [5,9] and fluorimetry [7] also have been reported. Several high-performance liquid chromatographic (HPLC) methods with spectrophotometric (HPLC–UV) [4,8,10,11] or electrochemical (HPLC–ED, amperometric [12] or voltammetric [13]) detection have been applied. Capillary electrophoretic (CE) methods have been described, with spectrophotometric (CE–UV) [14] or electrochemical detection (CE–ED) [15,16]. In [6], a flow injection analysis (FIA) method with colorimetric detection (FIA–vis) was developed to determine 4-AP in paracetamol tablets. Some of the above methods [5,6,9] require a derivatisation.

After development, analytical assay methods are validated to ensure their quality or suitability [17]. For pharmaceuticals, detailed guidelines of the ICH (International Conference on Harmonisation of Technical Requirements for the Registration of Pharmaceuticals for Human Use) [18], the ISO (International Organization for Standardization) [19–21], or the AOAC (Association of Official Analytical Chemists) [22] exist, describing the requirements to validate analytical methods. The linearity, precision, trueness, specificity, detection and quantification limits, and/or the range of the method are then evaluated, depending on the type of analytical procedure [18]. For quantitative testing of

* Corresponding author. Tel.: +32 2 477 47 34; fax: +32 2 477 47 35.
E-mail address: yvanvdh@vub.ac.be (Y. Vander Heyden).

impurities, such as the 4-AP quantity in paracetamol tablets, all above-mentioned criteria need to be examined. It is also advised to consider performing a robustness test.

In Ref. [7], it is suggested that 4-AP might be determined by fluorimetry without interference from paracetamol. It was also described that the fluorimetric method is less sensitive than a colorimetric, such as the reaction of sodium nitroprusside with 4-AP, forming an indophenol-derivative, which is described as limit test for 4-AP in the European Pharmacopoeia [23] and which is used as derivatisation reaction in the FIA–vis method of Ref. [6]. However, the fluorimetric method was not fully validated.

In this study, it was tried to determine the quantity of 4-AP fluorimetrically in paracetamol tablets containing 500 mg paracetamol, with the aim to obtain detection (LOD) and quantification (LOQ) limits that are below the lowest specification limit of 50 ppm 4-AP/PARA. Since in Ref. [6], 10 paracetamol tablets were dissolved in 100 mL solvent, 50 ppm 4-AP/PARA corresponds to 0.25 mg/100 mL 4-AP. The fluorimetric method was validated. The linearity was visually assessed, as well as by performing a test for the significance of the quadratic coefficient [17,24]. The correlation and quality coefficients were calculated for informative purposes [17,24,25]. A precision study was performed, from which the repeatability and the time-different intermediate precisions were estimated [17,26]. The trueness was evaluated and the predictability of the method was verified from a small prediction set [17]. The LOD and LOQ of the fluorimetric method were determined [17] and compared with those from derivative UV spectrophotometric [8], HPLC–UV [4,8,11], HPLC–ED [12,13], CE–UV [14], CE–ED [15,16], and FIA–vis [6] methods for the determination of 4-AP in drug substance (DS), drug products (DP) and/or biological fluids (BF). Then, the range, which is the 4-AP concentration interval where the method exhibits a suitable level of linearity, precision and trueness, can be determined [18]. Finally, the 4-AP quantity was determined in 500 mg paracetamol tablets and it was also tried to transfer the method to the 4-AP determination in some other paracetamol-containing pharmaceutical formulations.

2. Theory

2.1. Linearity, limit of detection and limit of quantification

To assess the linearity of the method, the calibration line was plotted, and a test for the significance of the quadratic coefficient in a second-order model was performed [17,24]. Another possibility, not executed here, is performing a lack-of-fit (LOF) test [17]. The correlation coefficient r and the quality coefficient QC are also given. When assuming a constant absolute standard deviation, the quality coefficient QC can be computed with Eq. (1) [17,24,25]

$$QC = 100 \sqrt{\frac{\sum (y_i - \hat{y}_i/\bar{y})^2}{n-1}} \tag{1}$$

where y_i and $\hat{y}_i$ are the measured and predicted responses, respectively, $\bar{y}$ the average of the measured responses, and n the

number of calibration standards, including the blank. The QC is a quality criterion and a measure for the percentage deviations of the predicted concentrations from the true. It describes how adequately the data fits the straight-line model. A QC below 5% was found acceptable for atomic absorption spectrometry measurements [24,25].

An approach to verify linearity, is to fit a second-order polynomial model, $y = b_0 + b_1 x + b_2 x^2$, to the data and to test the significance of the quadratic coefficient b_2 [17,24] by means of the 95% two-sided confidence interval for β_2 or by means of a two-sided t-test (Eq. (2))

$$|t| = \left| \frac{b_2}{s_{b_2}} \right| \leftrightarrow t_{\text{tab}(\alpha, df = n-3)} \tag{2}$$

where s_{b_2} is the standard deviation of b_2. The absolute t-value is compared with a tabulated t-value at significance level α, usually $\alpha = 0.05$, and $n - 3$ degrees of freedom, with n equal to the number of measurements, including the blank. When $|t| \geq t_{\text{tab}}$, b_2 is significantly different from zero and the straight-line model is considered inadequate. On the other hand, when $|t| < t_{\text{tab}}$, b_2 is not significantly different from zero and the linear model is considered to fit the data correctly.

The limit of detection (LOD) and the limit of quantification (LOQ) can be determined as follows according to IUPAC [17] (Eqs. (3)–(6)).

$$L_d = \mu_{bl} + k'_d \sigma_{bl} \quad \text{with} \quad k'_d = k_c + k_d \tag{3}$$

$$X_d = \frac{L_d - \mu_{bl}}{b_1} = k'_d \frac{\sigma_{bl}}{b_1} \tag{4}$$

$$L_q = \mu_{bl} + k_q \sigma_{bl} \tag{5}$$

$$X_q = \frac{L_q - \mu_{bl}}{b_1} = k_q \frac{\sigma_{bl}}{b_1} \tag{6}$$

L_d and X_d are the limits of detection, expressed as response/signal and as concentration, respectively. L_q and X_q are the limits of quantification, expressed as response/signal and as concentration, respectively. μ_{bl} and σ_{bl} are the mean response and the standard deviation of the blank, and b_1 is the slope of the calibration line. μ_{bl} is estimated by its experimentally obtained value, $\bar{y}_{bl}$, and σ_{bl} by the pooled standard deviation of the lower standards, s_p. The multiplication factors k_c, k_d, k'_d, and k_q are constants and their values determine the risk one is willing to take of making a wrong decision. In order to obtain $\alpha = \beta = 5\%$, $k_c = k_d = 1.645$, and $k'_d = 3.29$. With $k_q = 10$, one expects at the quantification limit a precision, expressed as relative error, of 10% [17]. It needs to be noted that Eqs. (4) and (6) are only valid when a linear relationship occurs between the response and the concentration. When a quadratic relationship would be found, the concentration should be determined by solving the quadratic equation.

2.2. Precision

To evaluate the method precision according to [17], estimations of the repeatability and the time-different intermediate precision can be derived from the experimental set-up used, i.e.

two replicates of three concentrations, measured under repeatability conditions, during 6 days. With the measured response and the suitable calibration equation, the concentration in each solution is calculated. The repeatability or within-days variance, s_r^2, and the time-different intermediate precision, $s_{I(t)}^2$, can be estimated at each concentration level from an ANOVA table and Eq. (7) [26]

$$s_{I(t)}^2 = s_r^2 + s_{between}^2 \qquad (7)$$

where $s_{between}^2$ represents the between-days variance.

2.3. Trueness

To verify the trueness of the method, a prediction set is measured, for which the true concentration of each solution ($x_{i,true}$) is known. The concentration of each solution is predicted from the model ($\hat{x}_{i,pred}$). Both the straight-line and the second-order polynomial model were considered (see Section 4.2.3). Consequently, for each solution of the prediction set, the %recovery ($\hat{x}_{pred}/x_{true} \times 100$) is calculated.

Finally, the average %recovery and the root mean square error of prediction (RMSEP) are determined (Eq. (8)) [17]

$$RMSEP = \sqrt{\frac{\sum (x_{i,true} - \hat{x}_{i,pred})^2}{n}} \qquad (8)$$

$x_{i,true}$ and $\hat{x}_{i,pred}$ are the true and the predicted concentrations, respectively, and n the number of observations.

3. Experimental

An LS-3B fluorescence-spectrometer (Perkin-Elmer, Beaconsfield, United Kingdom) was used. Responses were determined in two solvents: 0.05% acetic acid and methanol/H$_2$O (1:1, V:V). Solvents were prepared by mixing the necessary amounts of acetic acid (Merck, Darmstadt, Germany) and methanol (BDH, Poole, UK) with H$_2$O. The excitation wavelengths in these solvents were 278 and 300 nm, and the emission wavelengths 372 and 370 nm, respectively.

3.1. Preliminary experiments: determination of 4-aminophenol in solvent

A calibration line of 4-aminophenol (Sigma–Aldrich, Steinheim, Germany) in each of the two solvents was constructed. The concentrations of the standards in 0.05% acetic acid were 0.1, 0.2, 0.25, 0.3, 0.4, 0.5, 1.0, 2.0, 3.0, 4.0, 5.0, and 6.0 mg/100 mL, and in methanol/H$_2$O 0.1, 0.2, 0.25, 0.3, 0.4, 0.5, 0.6, 0.7, 0.8, 0.9, 1.0, and 2.0 mg/100 mL. A blank was also measured for each calibration line. The fluorescence at the maximal excitation and emission wavelengths was measured six times in each solvent. This allowed determining the linearity, the limit of detection (LOD) and the limit of quantification (LOQ) of the method in the solvents. The calibration line was plotted and linearity was assessed by means of a test for the significance of b_2 (Eq. (2)). For informative purposes, the correlation coefficient, r, and the quality coefficient, QC (Eq. (1)), also were calculated.

3.2. Determination of 4-aminophenol in tablet matrix

Calibration lines of 4-AP were prepared and measured in a solution, simulating paracetamol tablets, using both solvents. Since in the FIA–vis assay 10 paracetamol tablets were dissolved in 100 mL [6], here an excipients mixture (gift from GlaxoSmithKline, Dartford, UK) corresponding to the quantity of one tablet was added per 10 mL solution. Then the necessary volume of stock solution was added to the excipients to obtain 4-AP concentrations of 0.1, 0.2, 0.3, 0.4, 0.5, 0.6, 0.7, 0.8, 0.9, and 1.0 mg/100 mL. A blank solution, containing only excipients, was also prepared. All solutions were prepared as the paracetamol tablet samples, i.e. they were sonicated during 15 min and centrifuged (20 min at 3000 rpm). In each of the two solvents, the supernatant was used for analysis and measured six times at the maximal excitation and emission wavelengths. The blank supernatant was measured 12 times. This allowed determining the linearity, limit of detection (LOD) and limit of quantification (LOQ) of the method in tablet matrix. To assess linearity, a test of the significance of b_2 (Eq. (2)) was performed. For informative purposes, the correlation and the quality coefficients again were calculated.

Since the calibration line was only considered linear up to 0.5 mg/100 mL (see Section 4), the precision and trueness were evaluated in the concentration interval 0.1–0.5 mg/100 mL.

The precision was determined at concentrations situated towards the minimum, middle and maximum of the linear range, i.e. 0.10, 0.25 and 0.50 mg/100 mL. Each sample solution was measured twice on 6 days. Daily new samples were prepared in tablet matrix using methanol/H$_2$O as solvent. Also a calibration line was prepared in tablet matrix. The concentrations of the calibration standards were 0.1, 0.3, and 0.5 mg/100 mL. A blank solution, containing only excipients, was also prepared. All calibration solutions were measured twice at the maximal excitation and emission wavelengths.

To evaluate the trueness, a calibration line and a prediction set were prepared in tablet matrix using methanol/H$_2$O as solvent and were measured on the same day. For the calibration line also a blank solution, containing only excipients, was prepared. The 4-AP concentrations in the mixtures of both sets were 0.10, 0.15, 0.20, 0.25, 0.30, 0.35, 0.40, 0.45, and 0.50 mg/100 mL. The solutions were each measured three times ($n = 3$) at the maximal excitation and emission wavelengths. The concentrations in the solutions of the prediction set were predicted from both the straight-line and the second-order polynomial model, their %recovery was calculated, and finally, the average %recovery and the root mean square error of prediction (RMSEP) were determined (Eq. (8)) [17]. This allows comparing the trueness from both models.

3.3. Determination of 4-aminophenol in paracetamol formulations

A sample solution was prepared by dissolving 10 paracetamol tablets (gift from GlaxoSmithKline), containing 500 mg paracetamol per tablet, in 100 mL solvent (methanol/H$_2$O). The solution was sonicated during 15 min and centrifuged 20 min at

3000 rpm to obtain a clear supernatant, which was measured six times at the maximal excitation and emission wavelengths. A calibration line was also prepared in tablet matrix. Besides the blank, standards with concentrations of 0.1, 0.2, 0.25, 0.3, 0.4 and 0.5 mg/100 mL were used.

Since no fluorimetric response was obtained when measuring tablets (see Section 4.3), it was verified whether a known added amount of 4-AP could be found in spiked tablets. Therefore, additionally, two sample solutions were prepared, a first spiked with 0.25 mg/100 mL 4-AP, i.e. corresponding to the 50 ppm limit, and a second with only 0.10 mg/100 mL 4-AP. These two sample solutions were sonicated during 15 min and centrifuged 20 min at 3000 rpm, and the supernatant was measured six times at the maximal wavelengths.

It was also tried to transfer the method for the assay of 4-AP in paracetamol tablets with a blue coating and a soluble paracetamol-containing powder. Both were gifts from Glaxo-SmithKline.

4. Results and discussion

4.1. Preliminary experiments: determination of 4-aminophenol in solvent

The average fluorimetric responses (F) for all standards prepared in 0.05% acetic acid are given in Table 1. A quadratic model seemed to fit the data best. In the restricted concentration range 0.1–0.5 mg/100 mL, a straight-line model was found to fit the data. A test for the significance of the b_2 coefficient confirmed this. The second-order polynomial model fitted to the data was $y = 0.0061 + 11.24x + 0.9804x^2$, and $|t| = |0.9804/1.621| = 0.6048 < t_{tab(0.05, df=4)} = 2.776$, indicating that in the restricted range the quadratic model did not fit the data better. Therefore, the calibration line ($F = 11.74$ $C_{4\text{-}AP}$ (mg/100 mL) $- 0.0310$) was considered linear up to 0.5 mg/100 mL with $r = 0.9989$ and QC = 3.2%.

Since the average response and standard deviation s of the blank were both 0.00, the standard deviations of the lower standards were used to estimate LOD and LOQ. Since the s values for concentrations 0.2–0.5 mg/100 mL (standards 3–7) were simi-

Table 1
Average response ($n = 6$) of the 4-AP calibration line in 0.05% acetic acid

Standard	Concentration (mg/100 mL)	Average response	s	%RSD
1 = Blank	0.00	0.00	0.00	0.00
2	0.10	1.20	0.00	0.00
3	0.20	2.25	0.05	2.43
4	0.25	2.73	0.12	4.43
5	0.30	3.58	0.04	1.14
6	0.40	4.73	0.08	1.72
7	0.50	5.83	0.05	0.89
8	1.00	8.87	0.12	1.37
9	2.00	15.22	0.19	1.28
10	3.00	20.67	0.37	1.78
11	4.00	23.37	0.31	1.32
12	5.00	25.07	0.21	0.82
13	6.00	25.33	0.85	3.35

Table 2
Average response ($n = 6$) of the 4-AP calibration line in methanol/H$_2$O (1:1, V:V)

Standard	Concentration (mg/100 mL)	Average response	s	%RSD
1 = Blank	0.00	0.10	0.00	0.00
2	0.10	11.12	0.15	1.32
3	0.20	21.92	0.26	1.17
4	0.25	27.27	0.16	0.60
5	0.30	30.17	0.14	0.45
6	0.40	37.42	0.71	1.90
7	0.50	47.03	0.34	0.73
8	0.60	55.43	0.49	0.89
9	0.70	61.60	0.68	1.10
10	0.80	67.78	0.45	0.67
11	0.90	74.97	0.73	0.98
12	1.00	77.20	0.91	1.18
13	2.00	97.17	2.53	2.61

lar, their pooled s ($s_p = 0.08$) was used. The LOD and LOQ were then estimated as 0.021 and 0.064 mg/100 mL, respectively. The LOQ corresponds to 13 ppm in the paracetamol tablets or 26% of the 50 ppm specification limit.

The average results for the standards prepared in methanol/H$_2$O (1:1, V:V) are given in Table 2. Again a quadratic fit seemed most appropriate, while in the restricted concentration range 0.1–0.5 mg/100 mL, a test for the significance of b_2 was performed. The second-order polynomial model was given by $y = 0.2728 + 114.1x - 45.64x^2$, and $|t| = |-45.64/15.70| = 2.907 \geq t_{tab(0.05, df=4)} = 2.776$, indicating that the quadratic model still fits better than the straight-line. Since the test is only borderline significant ($p = 0.044$) and since in this range, the deviation from linearity is small, the straight-line model was anyway considered to describe the data sufficiently well. Thus, the straight-line model ($F = 91.04$ $C_{4\text{-}AP}$ (mg/100 mL) $+ 2.015$) was used up to 0.5 mg/100 mL with $r = 0.9952$ and QC = 6.2%.

When comparing Tables 1 and 2, it is observed that the signal is much higher in methanol/H$_2$O. The LOD and LOQ were determined according to IUPAC ($k_c = k_d = 1.645$, $k_{d'} = 3.29$, $\alpha = \beta = 5\%$, $k_q = 10$). The mean response of the blank was 0.10. Since the standard deviation of the blank was 0.00, again the standard deviations of the lower standards were used. When using the pooled s of standards 2 till 5 (0.1–0.3 mg/100 mL, $s_p = 0.18$), LOD and LOQ were estimated as 0.0066 and 0.020 mg/100 mL, respectively. The latter LOQ corresponds to 4.0 ppm in the paracetamol tablets or 8.0% of the 50 ppm specification limit.

4.2. Determination of 4-aminophenol in tablet matrix

4.2.1. Linearity, limit of detection and limit of quantification

The average fluorimetric responses for the standards prepared in tablet matrix using 0.05% acetic acid as solvent are given in Table 3. It is evident that no calibration is possible.

Comparing Tables 1 and 3, it is observed that in the latter the fluorescence is lost. Possible explanations are adsorption of 4-

Table 3
Average response ($n = 12$ for the blank, otherwise $n = 6$) of the 4-AP calibration line in tablet matrix using either 0.05% acetic acid or methanol/H$_2$O (1:1, V:V)

Standard	Concentration (mg/100 mL)	0.05% acetic acid			Methanol/H$_2$O (1:1, V:V)		
		Average response	s	%RSD	Average response	s	%RSD
1 = Blank	0.0	0.050	0.0012	2.29	0.294	0.0076	2.60
2	0.1	0.050	0.0013	2.71	9.000	0.0899	1.00
3	0.2	0.055	0.0010	1.78	17.79	0.1381	0.78
4	0.3	0.069	0.0012	1.69	25.34	0.3254	1.28
5	0.4	0.066	0.0012	1.88	32.82	0.3300	1.01
6	0.5	0.075	0.0022	2.88	40.95	0.3404	0.83
7	0.6	0.086	0.0035	4.07	46.82	0.5317	1.14
8	0.7	0.106	0.0012	1.09	49.68	0.3903	0.79
9	0.8	0.119	0.0040	3.32	55.58	0.3941	0.71
10	0.9	0.125	0.0029	2.29	59.87	0.4503	0.75
11	1.0	0.115	0.0048	4.23	64.61	1.0517	1.63

AP to the excipients, occurrence of quenching and/or inner filter effects [27]. It does not seem to make sense to further evaluate the method in this solvent.

The average results for the standards prepared in tablet matrix using methanol/H$_2$O as solvent are also given in Table 3. A quadratic model seemed to fit the data best. However, in the restricted concentration range 0.1–0.5 mg/100 mL, a straight-line model also fitted the data sufficiently well, which was confirmed by the test of the significance of b_2. The second-order polynomial model fitted to the data is $y = 0.3849 + 88.27x - 14.64x^2$, and since $|t| = |-14.64/6.082| = 2.408 < t_{tab(0.05, df=3)} = 3.182$, b_2 was not considered significantly different from zero at $\alpha = 0.05$. Therefore, it was decided to use the straight-line model, and to further evaluate whether the LOD, LOQ, precision and trueness were acceptable. The calibration line ($F = 80.97$ C$_{4-AP}$ (mg/100 mL) $+ 0.8691$) was considered linear up to 0.50 mg/100 mL with $r = 0.9995$ and QC $= 2.3\%$.

Comparing Tables 2 and 3, the response is found lower when measuring in tablet matrix. However, statistically the slopes of these two lines having a different residual variance [28] were considered borderline non-significant ($t_{cal} = 2.395 < t_{tab} = 2.591$). Possible explanations for the lower response when measuring in tablet matrix are occurrence of

quenching and/or inner filter effects [27]. Adsorption of 4-AP to the excipients seems less evident since a linear relation is found up to 0.50 mg/100 mL. To take matrix interferences into account, a calibration line with matrix-matched standards should thus be used.

The LOD and LOQ were determined according to IUPAC ($k_c = k_d = 1.645$, $k_{d'} = 3.29$, $\alpha = \beta = 5\%$, $k_q = 10$). When using the pooled s of standards 1 till 3 (blank–0.2 mg/100 mL, $s_p = 0.08$), LOD and LOQ are estimated as 0.0033 and 0.010 mg/100 mL, respectively. This LOQ corresponds to 2.0 ppm in the paracetamol tablets or 4.0% of the 50 ppm 4-AP specification limit. Compared to other analytical methods described in [4,6,8,11–16] (Table 4), lower or similar LOD and/or LOQ values are obtained with the HPLC–UV [8], HPLC–ED [12], CE–UV [14] and FIA–vis [6] methods. However, the fluorimetric method is not a separation method, while the HPLC or CE methods are. Measurements and occasional method transfer are therefore faster and easier with the former. Above all, it is a spectroscopic method that does not require derivatisation, in contrast to the FIA–vis method. In conclusion, the LOD and LOQ values obtained for the fluorimetric method are found acceptable to assay the 4-aminophenol impurity in paracetamol tablets. However, it needs to be mentioned that it is often not clear how the LOD and LOQ reported in Table 4 were obtained, and usually

Table 4
Limit of detection (LOD) and limit of quantification (LOQ) of different analytical methods for 4-aminophenol in drug substance (DS), drug product (DP) and/or biological fluids (BF); (–) not reported

| Method	Derivatisation	DS, DP and/or BF	LOD (mg/100 mL)	LOQ (mg/100 mL)	Reference
First derivative UV spectroscopy	No	DS/DP	0.0046	–	[8]
Second derivative UV spectroscopy	No	DS/DP	0.0041	–	[8]
HPLC–UV	No	DS/DP	0.01	0.03	[4]
HPLC–UV	No	DS/DP	0.0025	–	[8]
HPLC–UV	No	DS/DP	0.005	0.0145	[11]
HPLC–ED	No	DS	0.0001	0.00035	[12]
HPLC–ED	No	DP	0.0004	–	[12]
HPLC–ED	No	DS/BF (urine)	0.005	–	[13]
CE–UV	No	DS/DP	0.00112	0.00373	[14]
CE–ED	No	DS	0.012	–	[15]
CE–ED	No	DS/DP	0.054	–	[16]
FIA–vis	Yes	DP	–	0.001	[6]
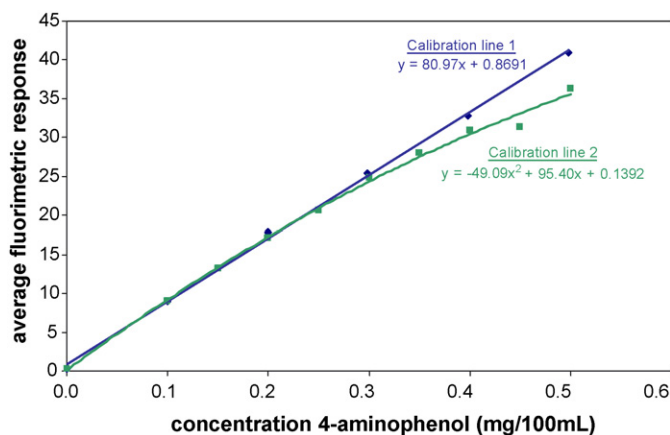
Fig. 1. Comparison of calibration line 1 (♦) and calibration line 2 (■). For calibration line 1, the straight-line model fits the data, while for calibration line 2, a second-order polynomial model is required.

the applied values of the multiplication factors are not mentioned. Therefore, one needs anyway to be careful in comparing the LOD and LOQ values of the different methods.

4.2.2. Precision

For each precision sample, the fluorimetric response (F) was normalized (Eq. (9)) before the concentration was calculated

$$F_{weighted} = \frac{F \times \text{theoretical weight}}{\text{experimental weight}} \tag{9}$$

For the 0.10 mg/100 mL sample, the repeatability, expressed as standard deviation, is 3.06×10^{-5}, and the time-different intermediate precision 5.93×10^{-5}. For the 0.25 mg/100 mL sample, they are 5.35×10^{-5} and 1.45×10^{-4}, respectively, and for the 0.50 mg/100 mL sample, 6.37×10^{-5} and 9.21×10^{-5}, respectively. When using the pooled standard deviation, the repeatability is 5.12×10^{-5} and the time-different intermediate precision 1.05×10^{-4}. In conclusion, both the repeatability and the time-different intermediate precisions were found acceptable in the examined 4-AP concentration range.

4.2.3. Trueness: predictability of the method

The above calibration lines 1 (Section 4.2.1) and 2 (prepared for determining the trueness) are compared (Fig. 1). Calibration line 2 deviates more from linearity, which is confirmed by the test for significance of b_2. For this line 2, the straight-line model is $y = 2.243 + 70.15x$ and the second-order model $y = 0.1392 + 95.40x - 49.09x^2$. Since $|t| = |-49.09/11.19| = 4.387 \geq t_{tab(0.05, df=7)} = 2.365$, the quadratic model fits better. Both models were used to evaluate the trueness of the method. Possibly, the difference in linearity is inherent to the fluorimetric technique, which is sensitive to day-to-day temperature changes. However, a temperature control during the measurements is not possible, since the laboratory, where the fluorimetric equipment is located, is not thermostatted.

Table 5 shows the average fluorimetric responses ($n = 3$) of the prediction set in tablet matrix using methanol/H$_2$O as solvent. The responses for both the calibration line and the prediction set

Table 5
Average response ($n = 3$) for the standards of the prediction set in tablet matrix using methanol/H$_2$O (1:1, V:V)

Standard	Concentration x_{true} (mg/100 mL)	Average response	s	%RSD	Straight-line model $y = 2.243 + 70.15x$			Second-order polynomial model $y = 0.1392 + 95.40x - 49.09x^2$		
					$\hat{x}_{pred}$ (mg/100 mL)	$|x_{true} - \hat{x}_{pred}|$ (mg/100 mL)	% recovery	$\hat{x}_{pred}$ (mg/100 mL)	$|x_{true} - \hat{x}_{pred}|$ (mg/100 mL)	% recovery
1 = Blank	0.00	0.299	0.01	2.87						
2	0.10	9.091	0.05	0.52	0.0976	0.0024	97.62	0.0989	0.0011	98.87
3	0.15	13.25	0.12	0.89	0.1569	0.0069	104.59	0.1488	0.0012	99.21
4	0.20	17.07	0.16	0.92	0.2113	0.0113	105.64	0.1975	0.0025	98.75
5	0.25	20.79	0.14	0.69	0.2644	0.0144	105.77	0.2482	0.0018	99.28
6	0.30	24.86	0.37	1.48	0.3223	0.0223	107.44	0.3079	0.0079	102.62
7	0.35	28.74	0.09	0.33	0.3777	0.0277	107.92	0.3704	0.0204	105.84
8	0.40	31.21	0.06	0.20	0.4128	0.0128	103.21	0.4137	0.0137	103.43
9[a]	0.45	31.12	0.75	2.41	0.4117	0.0383	91.49	0.4122	0.0378	91.61
10	0.50	36.42	0.17	0.47	0.4871	0.0129	97.43	0.5187	0.0187	103.75

The true and predicted concentrations, their differences, and the %recovery of the standards in the prediction set are also given. The trueness was evaluated for both the straight-line and the second-order models.

[a] Possible outlier.

(Table 5) were rather similar to those of the calibration line measured in tablet matrix (Table 3), but lower than those measured in solvent (Table 2).

The concentrations are predicted from both models (Table 5). The bias of standard 9 (possible outlier) is the highest. The prediction from the second-order model is somewhat better than that from the straight-line. For the latter model, the average %recovery was 102.35% (range 91.49%–107.92%) and the RMSEP 0.01959 mg/100 mL. For the second-order model, they are 100.37% (range 91.61%–105.84%) and 0.01652 mg/100 mL, respectively. The RMSEP's are compared to the specification limit of 50 ppm 4-AP/PARA, i.e. 0.25 mg/100 mL. The RMSEP's of 0.01959 mg/100 mL for the straight-line model and of 0.01652 mg/100 mL for the second-order model correspond to 7.8 and 6.6% of that limit. When discarding standard 9, the range of %recovery is 97.43–107.92% for the straight-line model and 98.75–105.84% for the second-order model. Thus, in conclusion, the prediction was found best for the second-order polynomial model in the examined range of 4-AP concentrations.

4.3. Determination of 4-aminophenol in white 500 mg paracetamol tablets

The results of the sample solution, without supplementary spiked 4-AP, were about the same as that of the blank of Table 3. Therefore, sample solutions spiked with 0.25 or 0.10 mg/100 mL 4-AP were prepared. From the difference in responses before and after spiking, the added concentrations were predicted. When adding 0.250 mg/100 mL 4-AP, the predicted concentration was 0.255 ± 0.002 mg/100 mL 4-AP ($n = 6$), and when adding 0.100 mg/100 mL 4-AP, it was 0.105 ± 0.001 mg/100 mL ($n = 6$). Thus, the added concentrations are correctly predicted, which implies that the 4-AP quantity in the paracetamol tablets is too low to be assayed.

4.4. Determination of 4-aminophenol in other paracetamol-containing drug formulations

4.4.1. Paracetamol tablets with a blue coating

It was also tried to assay the 4-aminophenol content in 500 mg paracetamol tablets with a blue coating, containing a blue dye that disturbs the FIA–vis assay [6]. Therefore a transfer to the fluorimetric method was evaluated. Since the blue dye might also disturb the fluorimetric determination, its excitation and emission spectra were measured. However, even for high dye concentrations, no emission was observed. Moreover, the dye has a negligible fluorimetric response ($F < 0.050$) at the excitation and emission wavelengths of 4-AP in methanol/water.

Although the blue dye concentration in the coating is constant, its concentration in solution after sonication and centrifugation is variable. A possible explanation could be that a part of the dye is present as a soluble dye absorbed onto a substrate of silica, aluminium oxide or some other type of inorganic material, and in the different samples, it does not desorbs equally from the substrate. The dye concentration in solution was determined by measuring 10 solutions, each from one blue tablet coating per 10.0 mL (after sonication and centrifugation), and a

blue dye calibration line. The dye concentration in the solutions varied between 0.7 and 1.1 mg/100 mL. Therefore, to simulate the assay of 4-AP in a sample prepared from 10 tablets dissolved in 100 mL solvent, three calibration lines and corresponding prediction sets were prepared and measured in tablet matrices containing 0.7, 0.9 and 1.1 mg/100 mL blue dye, respectively. Besides a blank, 4-AP standards with concentrations of 0.1, 0.2, 0.3, 0.4 and 0.5 mg/100 mL were prepared. The concentrations of the prediction solutions were 0.10, 0.15, 0.20, 0.25, 0.30, 0.35, 0.40, 0.45 and 0.50 mg/100 mL. After sonication (15 min) and centrifugation (20 min at 3000 rpm), the supernatant was measured at least four times at the maximal excitation and emission wavelengths of 4-AP.

For the calibration and prediction solutions containing 0.7 mg/100 mL blue dye, the average %recovery was 98.13% (range 92.19%–105.83%) and the RMSEP 0.01440 mg/100 mL. For those with 0.9 mg/100 mL blue dye, the average %recovery was 114.11% (range 106.29%–119.11%) and the RMSEP 0.04315 mg/100 mL. These are worse results than those with 0.7 and 1.1 mg/100 mL blue dye, because the calibration line and the prediction set with 0.9 mg/100 mL blue dye were measured on different days. For the solutions with 1.1 mg/100 mL blue dye, the average %recovery was 96.83% (range 90.83–104.75%) and the RMSEP 0.02418 mg/100 mL. In conclusion, the prediction is bad.

The average response for solutions with the same 4-AP concentration was seen to decrease when the blue dye concentration increases. Since different blue paracetamol tablets provide different amounts of dye, which is affecting the response, a problem occurs. For each dye concentration, i.e. for each tablet, a different 4-AP calibration line would be required, which is unfeasible.

The above problems are illustrated when the 4-AP concentrations of all prediction samples, regardless the blue dye concentration, are predicted from one calibration line, e.g. that with 0.9 mg/100 mL. Bad average %recovery and RMSEP were obtained, i.e. 118.66% and 0.06456 mg/100 mL, respectively. Similarly, all samples were once estimated from the calibration lines with 0.7 or 1.1 mg/100 mL blue dye, resulting in an average %recovery of 88.47% and 104.00%, respectively, and a RMSEP of 0.04950 and 0.03126 mg/100 mL, respectively. Both RMSEP are lower than when using the calibration line of 0.9 mg/100 mL, but still the prediction is bad. Thus, a separation method seems to be required for this type of samples.

4.4.2. Soluble powder containing paracetamol

It was also tried to determine the 4-AP quantity in a soluble powder, containing 750.0 mg paracetamol, 10.0 mg pseudoephedrine hydrochloride, 60.0 mg ascorbic acid, 4.18 g excipients and a yellow dye. Since all (active) ingredients showed a negligible fluorimetric response ($F < 0.050$) at the excitation and emission wavelengths of 4-AP in methanol/H_2O, a calibration line in powder matrix was prepared. This powder matrix contained all excipients and all active substances, except paracetamol. After sonication (15 min) and centrifugation (20 min at 3000 rpm) of the calibration standards, the supernatants were measured five times. Contrary to the white 500 mg paracetamol tablets, where 4-AP could be determined,

almost no fluorimetric signal was measured in the powder matrix with methanol/H$_2$O as solvent. A possible explanation for the problems occurring is the large difference in the amount of excipients between the tablets and the powder. In the tablets 500 mg paracetamol is present and the amount of excipients is about 100 mg (total = 600 mg). In the soluble powder 750 mg paracetamol, 10 mg pseudoephedrine hydrochloride, and 60 mg ascorbic acid are present and the amount of excipients is about 4.18 g (total = 5 g). Much more excipients are present in the powder. Above all, more excipients will dissolve, since it is a soluble powder, and therefore, more quenching or a higher inner filter effect [27] may occur. This could explain why the fluorescence was lost.

It was tried to dissolve less excipients by reducing the sonication time, but a minimum of 10 min is needed to dissolve 4-AP [6]. Fluorescence also then was lost. Thus, also here a separation method seems to be required.

5. Conclusions

A fluorimetric method to assay 4-aminophenol in paracetamol tablets was validated. Although a quadratic model seemed most appropriate to describe the data, it was found that in a restricted concentration range up to 0.50 mg/100 mL 4-AP a linear model could as well be applied.

The fluorimetric response in methanol/H$_2$O was higher than in 0.05% acetic acid. When acetic acid was used, no calibration was possible. For the linear model, the LOD, LOQ, and precision estimates were acceptable. The limits of detection (LOD) and quantification (LOQ) were found to be lowest when using methanol/H$_2$O as solvent. Then the LOD and LOQ were 0.0033 and 0.010 mg/100 mL (∼2.0 ppm 4-AP/PARA), respectively, which is acceptable since the 4-AP quantity that needs to be quantified is 0.25 mg/100 mL, corresponding to 50 ppm 4-AP/PARA when 10 tablets are dissolved in 100 mL solvent. The precision of the method was acceptable since both the repeatability and the time-different intermediate precision were good in the concentration range considered. From the pooled standard deviations, they were estimated as 5.12×10^{-5} and 1.05×10^{-4}, respectively. Concerning the trueness, the average %recovery and the RMSEP were 102.35% and 0.01959 mg/100 mL, when using the straight-line model. However, the prediction from the quadratic model was found to be somewhat better: the average %recovery and the RMSEP were 100.37% and 0.01652 mg/100 mL. All trueness values were considered acceptable.

This method could possibly be transferred to assay other paracetamol-containing pharmaceutical formulations, provided that the tablet, syrup, ..., i.e. the matrix, has a constant composition (does not contain disturbing and variable dye concentrations, for instance), and that the amount of dissolved excipients is not too high, since otherwise fluorescence might be lost.

Acknowledgement

References

[1] L.F. Prescott, Am. J. Ther. 7 (2000) 143–147.
[2] B. Ward, J.M. Alexander-Williams, Acute Pain 2 (1999) 139–149.
[3] A. Yesilada, H. Erdogan, M. Ertan, Anal. Lett. 24 (1991) 129–138.
[4] L. Monser, F. Darghouth, J. Pharm. Biomed. Anal. 27 (2002) 851–860.
[5] F.A. Mohamed, M.A. Abdallah, S.M. Shammat, Talanta 44 (1997) 61–68.
[6] M.S. Bloomfield, Talanta 580 (2002) 1301–1310.
[7] G. Milch, É. Szabó, J. Pharm. Biomed. Anal. 9 (1991) 1107–1113.
[8] I.I. Hewala, Anal. Lett. 27 (1994) 561–582.
[9] M.A. Korany, D. Heber, J. Schnekenburger, Talanta 29 (1982) 332–334.
[10] A. Garcia, F.J. Rupérez, A. Marín, A. de la Maza, C. Barbas, J. Chromatogr. B 785 (2003) 237–243.
[11] R. Nageswara Rao, A. Narasaraju, Anal. Sci. 22 (2006) 287–292.
[12] E. Wyszecka-Kaszuba, M. Warowna-Grzeskiewics, Z. Fijalek, J. Pharm. Biomed. Anal. 32 (2003) 1081–1086.
[13] Z. Liu, J. Li, S. Dong, E. Wang, Anal. Chem. 68 (1996) 2432–2436.
[14] T. Perez-Ruiz, C. Martinez-Lozano, V. Tomas, R. Galera, J. Pharm. Biomed. Anal. 38 (2005) 87–93.
[15] G. Chen, J. Ye, H. Bao, P. Yang, J. Pharm. Biomed. Anal. 29 (2002) 843–850.
[16] F.Y. He, A.L. Liu, X.H. Xia, Anal. Bioanal. Chem. 379 (2004) 1062–1067.
[17] D.L. Massart, B.G.M. Vandeginste, L.M.C. Buydens, S. De Jong, P.J. Lewi, J. Smeyers-Verbeke, Handbook of Chemometrics and Qualimetrics: Part A, Elsevier, Amsterdam, 1997, pp. 179–186, 221–223, 282, 379–440.
[18] Guidelines prepared within the International Conference on Harmonisation of Technical Requirements for the Registration of Pharmaceuticals for Human Use (ICH), 2005, 1–13, http://www.ich.org/.
[19] International Organization for Standardization (ISO), Statistical Methods for Quality Control, vol. 2, 4th ed., ISO, 1994 (E), 5725–2.
[20] International Organization for Standardization (ISO), Statistical Methods for Quality Control, vol. 2, 4th ed., ISO, 1994 (E), 5725–3.
[21] International Organization for Standardization (ISO), Statistical Methods for Quality Control, vol. 2, 4th ed., ISO, 1994 (E), 5725–4.
[22] W.J. Youden, E.H. Steiner, Statistical Manual of the Association of Official Analytical Chemists, The Association of Official Analytical Chemists ed., Arlington, 1975.
[23] European Pharmacopoeia, 4th ed., Council of Europe, Strasbourg, France, 2002.
[24] P. Vankeerberghen, J. Smeyers-Verbeke, D.L. Massart, J. Anal. At. Spectrom. 11 (1996) 149–158.
[25] P. Vankeerberghen, J. Smeyers-Verbeke, Chemom. Intell. Lab. Syst. 15 (1992) 195–202.
[26] G.E.P. Box, W.G. Hunter, J.S. Hunter, An Introduction to Design, Data Analysis and Model Building, J. Wiley, New York, 1978.
[27] IUPAC Compendium of Chemical Terminology, Electronic version, http://goldbook.iupac.org/.
[28] D.L. Massart, J. Smeyers-Verbeke, F.X. Rius, Trends Anal. Chem. 8 (1989) 49–51.

ELSEVIER

Effect of oxidation of activated carbon on its enrichment efficiency of metal ions: Comparison with oxidized and non-oxidized multi-walled carbon nanotubes

Amjad H. El-Sheikh *

Department of Chemistry, Faculty of Science, Hashemite University, P.O. Box 150459, Al-Zarqa (13115), Jordan

Abstract

The effect of oxidation of activated carbon (AC) with various oxidizing agents (nitric acid, hydrogen peroxide, ammonium persulfate) on preconcentration of metal ions (Cr^{3+}, Mn^{2+}, Pb^{2+}, Cu^{2+}, Cd^{2+} and Zn^{2+}) from environmental waters prior to their flame atomic absorption spectroscopic analysis was investigated. The highest recoveries and adsorption capacities towards metal ions were achieved when using nitric acid-oxidized AC (sorbent AC-NA) as preconcentrating sorbent at pH 9. A preconcentration procedure was optimized using AC-NA as sorbent, which was then compared with non-oxidized AC in terms of analytical performance of the preconcentration method. Higher sensitivity, lower detection limits and wider linear ranges were achieved when AC-NA was used. The analytical performance of the method using AC-NA as preconcentrating sorbent was also compared with nitric acid-oxidized multi-walled carbon nanotubes (sorbent MWCNT-NA) and non-oxidized multi-walled carbon nanotubes (sorbent MWCNT). The analytical performance of the preconcentration method using AC-NA was close to MWCNT-NA, but AC-NA was better than non-oxidized MWCNT. Application of the optimized preconcentration method (using AC-NA sorbent) to environmental waters (tap water, reservoir water, stream water) gave spike recoveries of the metals in the range 63–104%.
© 2007 Elsevier B.V. All rights reserved.

Keywords: Activated carbon; Multi-walled carbon nanotubes; Solid phase extraction; Preconcentration; Water samples; Atomic absorption spectrometry

1. Introduction

Monitoring environmental pollutants at ultra-trace level needs an effective sample preconcentration step. Solid phase extraction (SPE) is the most common technique used for preconcentration of analytes in environmental waters. In SPE procedure, the choice of appropriate adsorbent is a critical factor to obtain full recovery and high enrichment factor. Many sorbents have been used for preconcentration of pollutants, such as activated carbon (AC), multi-walled carbon nanotubes (MWCNT), etc. Sometimes it is useful to consider the cost of sorbent, in addition to its analytical performance. AC is a relatively cheap sorbent, while MWCNT is a relatively expensive one.

AC is an excellent-common sorbent consisting of graphite sheets randomly substituted with hetero-atoms (mainly oxygen)

[1]. The surface properties of AC may improve or hinder its ability to adsorb certain species. Reports have explored the role of surface chemistry, oxygen content and textural properties of ACs on its adsorption properties [2–6]. Characteristics of AC depend on the precursor and the activation technique employed in the manufacturing process of AC [6]. These characteristics may be altered by treatment of AC with certain oxidizing agents, such as nitric acid, ammonium persulfate, hydrogen peroxide, etc. By this treatment, it is possible to alter the textural properties of the AC and to generate acidic oxides (carboxylic, phenolic, lactonic) and/or basic groups (pyrone-like groups) on the surface of AC.

Authors have previously used AC for enrichment of metals from environmental samples prior to their analysis. Jankowski et al. [7] reported the preconcentration of cadmium, copper, chromium, iron, manganese, lead and zinc ions from water samples by adsorption on AC at pH 8–8.5 coupled with continuous powder introduction microwave induced plasma atomic emission spectroscopic analysis. Yusof et al. [8,9] reported the determination of some toxic metals from water samples after

---

* Tel.: +962 5 3903333; fax: +962 5 382 6613.
E-mail addresses: amjadelsheikh3@yahoo.com, elsheikh@hu.edu.jo.

preconcentration on modified AC (Zr/AC) and non-modified AC coupled with neutron activation analysis. They found that Zr/AC was capable of adsorbing As^{5+}, Se^{6+}, Cr^{6+} and Hg^{2+} ions at any pH, while AC was capable of adsorbing As^{3+}, Se^{4+}, Cr^{3+} and Hg^+ ions at high pH values. Yaman et al. [10–12] reported the use of AC for speciation of copper, nickel and lead from soil samples. Yaman and Avci [13] reported the determination of beryllium in solid samples after preconcentration on AC at various pH values. Beinrohr et al. [14] reported on-line preconcentration of Cr^{3+} on AC from water samples at pH 7, while total chromium was determined after reduction of chromate into Cr^{3+}. Gil et al. [15,16] reported on-line preconcentration and speciation of Cr^{6+} and Cr^{3+} from water samples by sorption on conical mini-column packed with AC at pH 5. Sommer et al. [17] reported speciation of mercury by trapping on AC surface then desorption followed by gas chromatographic analysis. Granados et al. [18] reported preconcentration of radioactive Co^{60} on AC. Adsorption of cadmium on AC was also reported by LeyvaRamos et al. [19], in which maximum adsorption occurred at pH 8. Preconcentration of Se^{4+} from agricultural and natural water samples by precipitation on AC surface was reported by Berotino et al. [20], van der Hock et al. [21] and Castilla et al. [22]. Babel and Kurniawan [23] reported the use of AC modified with oxidizing agents (HNO_3 and H_2SO_4) for removal of Cr^{6+} from synthetic wastewater. It was evident that nitric acid treated-AC showed better Cr^{6+} removal than as-received AC in terms of adsorption rate and adsorption capacity. Zhang et al. [24] studied the role of physical and chemical properties of AC on lead speciation.

Multi-walled carbon nanotubes (MWCNT), which is an expensive sorbent, were previously used for preconcentration of metal ions, such as rare earth elements [25], copper [26,27], silver [28] and cadmium [27,29]. Munoz et al. [30] reported the speciation of organo-metallic compounds of lead, mercury and tin in environmental samples using MWCNT. Some researchers have tried to improve the properties of the MWCNT via oxidation with nitric acid. For example, Zhang et al. [31] reported that diameter of the single-walled carbon nanotubes may be enlarged by nitric acid treatment. Liang et al. [32] applied nitric acid-oxidized MWCNT to concentrate cadmium, manganese and nickel ions. Hennrich et al. [33] reported the modification of adsorption properties of single-walled carbon nanotubes via nitric acid exposure. Chakraborty et al. [34] found that treatment of the carbon nanotubes with nitric acid/sulfuric acid mixture then baking at 1000 °C increased its surface area.

Although some works (such as those of Babel and Kurniawan [23] and Zhang et al. [24]) have reported the use of oxidized AC for adsorption (removal) of heavy metals from aqueous medium, however, to the best of our knowledge, it seems that nobody has studied the effect of oxidation of AC on its preconcentration performance towards metal ions from water samples. Additionally none of the researchers who conducted research on preconcentration of metal ions have compared the enrichment efficiency of oxidized AC with that of MWCNT.

In this work, the effect of oxidation of AC with various oxidizing agents (nitric acid, hydrogen peroxide, ammonium persulfate) on preconcentration of metals from environmental waters was reported. Metal ions selected were Cr^{3+}, Mn^{2+}, Pb^{2+}, Cu^{2+}, Cd^{2+} and Zn^{2+}. Comparison between the analytical performance achieved by using oxidized AC and non-oxidized AC as preconcentrating sorbents for metal ions from water was reported for the first time in this work. Additionally the analytical performance of the oxidized AC was also compared with non-oxidized and nitric acid-oxidized MWCNT as preconcentrating sorbents for metal ions.

2. Experimental

2.1. Standard solutions and reagents

Standard stock solutions (1000 μg mL^{-1}), of individual metals, were purchased from the following suppliers: Cd^{2+} and Cr^{3+} standard solutions from Aldrich; Pb^{2+} standard solution from BDH; Cu^{2+} standard solutions from Scharlau, Zn^{2+} and Mn^{2+} standard solutions from Panreac. Working standard solutions were prepared by appropriate dilution of the stock standard solutions. All the reagents used were of analytical grade or better. Doubly distilled water was used throughout the work. The following buffers were used to control the pH of water samples: hydrochloric acid–glycine (pH 1–3), sodium acetate–acetic acid (pH 3–6), disodium hydrogen phosphate–sodium dihydrogen phosphate (pH 6–8), and ammonium chloride–ammonia (pH 8–10).

Activated carbon (AC) was purchased from Sigma (untreated granular activated charcoal, 20–60 mesh, product number C3014). Multi-walled carbon nanotube (MWCNT) was purchased from Shenzhen Nanotechport Co. Ltd., Shenzhen, China. MWCNT was of 5–15 μm length and 10–30 nm external diameter. Before use, MWCNT was dried at 80 °C for 2 h.

2.2. Oxidation of sorbents

AC was oxidized with various reagents to study the effect of oxidation of AC on its on enrichment efficiency towards the targeted metal ions. Details of oxidation conditions are shown in Table 1. Oxidized sorbents were thoroughly washed with doubly distilled water and then dried. The produced sorbents were labelled AC-NA, AC-HP and AC-APS, which refers to AC sorbents oxidized with nitric acid, hydrogen peroxide and ammonium persulfate, respectively. AC refers to non-oxidized AC.

MWCNT was oxidized with nitric acid in a procedure similar to that of AC-NA, which is shown in Table 1. The produced sorbent was labeled MWCNT-NA. Sorbent MWCNT refers to non-oxidized MWCNT.

2.3. Characterization of ACs

Characterization of the oxidized ACs and the non-oxidized AC involved determination of methylene blue relative surface area; determination of iodine numbers; and determination of surface oxides by Boehm titrations. Methylene blue (MB)-relative surface area [35,36] was estimated by introducing 25 mL of aqueous solutions of 10, 20, 30, 40, 50, 60, 70, 90, 110 mg L^{-1} methylene blue separately into 50 mL conical flasks each con-

Table 1
Preparation conditions and characteristics of the oxidized ACs and non-oxidized AC with appropriate labelling of the sorbents

Adsorbent abbreviation	Oxidation conditions	MB relative surface area ($m^2 g^{-1}$)	Iodine number ($mg\,g^{-1}$)	Boehm titrations				
				a	b	c	d	e
AC	–	303	200	1.46	0	0	0	0
AC-NA	100 mL of conc. HNO_3, 25 °C, 24 h	240	140	0.121	2.164	0.613	0.563	0.988
AC-APS	100 mL of a saturated solution of $(NH_4)S_2O_8$ in 1 M H_2SO_4, 25 °C, 18 h	205	120	0.135	2.151	0.625	0.288	1.238
AC-HP	Mixture of 50 mL H_2O_2 and 50 mL 1 M H_2SO_4, 50 °C, 1 h	265	170	0	2.051	0.838	0.438	0.775

Note—(a) total basic group ($mmol\,g^{-1}$), (b) total acidic group ($mmol\,g^{-1}$), (c) phenolic groups ($mmol\,g^{-1}$), (d) lactonic groups ($mmol\,g^{-1}$), (e) carboxylic groups ($mmol\,g^{-1}$).

taining 25 mg of the adsorbent. The tubes were tightly stoppered and left for one week in the dark, with shaking from time to time. The remaining concentrations were analyzed spectrometrically at 614 nm. Langmuir adsorption isotherms were plotted to find the monolayer capacity through which MB-relative surface areas were estimated [35,36]. The determination of surface oxides was described by Boehm [37]. Iodine numbers were estimated according to procedure described by *ASTM* [38].

2.4. Apparatus

An Analyst 300 Perkin-Elmer atomic absorption spectrometer was used for the quantitative determination of all metals under the following conditions: optical path was 10 mm; slit width was 0.7 nm for all metals except for Mn it was 0.2 nm; wavelength was 279.5 nm for Mn, 357.9 nm for Cr, 217.0 nm for Pb, 228.8 nm for Cd, 324.8 nm for Cu, 213.9 nm for Zn; lamp current was 30 mA for Mn lamp, 25 mA for Cr lamp, 10 mA for Pb lamp, 4 mA for Cd lamp, 15 mA for Cu lamp, 15 mA for Zn lamp. Instrumental conditions for electro-thermal atomic absorption spectrometric (ET AAS) method were similar to those described by Sweileh [39].

A Cary 100 Bio UV–vis spectrophotometer was used for determination of the remaining concentrations of methylene blue. A visiprep-12-port vacuum manifold (from Supelco) connected to a vacuum pump (KNF NEUBERGER D-7800, Germany) was used to control the flow rate in the preconcentration procedure of metals.

2.5. Cartridge preparation

Cartridge was prepared by placing a specific mass of the sorbent in an empty 6 mL polypropylene SPE-tube "filtration tube" (from Supelco). Polyethylene frits "from Supelco" were used to hold the adsorbent packing in the cartridge. Cartridge was preconditioned by washing with 6 ml of 1.0 M HNO_3, then with 12 ml of doubly distilled water, then with 12 ml of the desired buffer solution, ahead of the preconcentration procedure.

2.6. General preconcentration procedure

The desired mass of the sorbent was packed into the SPE-cartridge and preconditioned as described in Section 2.5. Water sample (spiked with the desired concentration of metal ions and adjusted to the desired pH value) was then passed through the cartridge. The flow rate was maintained at 6 mL min^{-1}. Subsequently, metals retained on the cartridge were eluted with the desired volume and concentration of nitric acid solution.

2.7. Determination of adsorption capacity of the sorbents

Adsorption capacity of the sorbents was estimated in separate experiments at optimum pH by passing 50 mL of 10 μg mL^{-1} of each metal ion solution (separately) into a 0.200 g of the sorbent packed in the cartridge and preconditioned as described above. The adsorbed metal was eluted with 10 mL of 1.0 M HNO_3 to ensure full elution.

2.8. Environmental water samples

Three types of environmental waters were used for evaluation of the proposed SPE method; tap water, reservoir water and stream water. Tap water samples were collected after flowing for 10 min from various water taps in our school at various days, and then pooled and used to generate a composite tap water sample. Reservoir water composite sample was generated by collecting various samples from local household reservoirs, which are known to store water for several weeks. Stream water composite sample was generated by collecting various samples from Al-Zarqa stream from various positions at various days. Before use, all the environmental water samples were filtered through 0.45 μm micropore membranes and stored in polyethylene bottles at 4 °C.

2.9. Application of the proposed method on real water samples

The optimum SPE procedure was applied first on un-spiked real water samples and then on real water samples spiked with the target metal ions. To ensure reproducibility of the results, SPE procedures were applied in five replicates ($n = 5$), after which each extract was analyzed for metal ions as separate sample.

3. Results and discussion

3.1. Characterization of the oxidized and non-oxidized ACs

The oxidized and non-oxidized ACs were characterized in our laboratory by relative surface area estimation by Methylene blue adsorption method, iodine number and Boehm titrations. The results are shown in Table 1. From Boehm titrations, it is noted that nitric acid oxidation produced maximum number of oxygen-containing groups in each category as classified by Boehm [37]. Hydrogen peroxide treatment significantly reduced the number of basic groups but enhanced number of acidic surface oxides. Ammonium persulfate treatment resulted in the generation of the greatest number of strongly acidic carboxylic groups.

From Table 1, it is noted that Methylene blue (MB) adsorption is less favored on oxidized activated carbon sorbents relative to non-oxidized activated carbon. It was reported by Krupa and Canon [40] that MB adsorption occurs mainly within large micropores and mesopores. The decrease in MB relative surface area is probably due to more carboxyl groups on the surface and thus forming water clusters, which blocks micropore openings [4] and hinders the passage of MB molecules inside micropores. Additionally El-Sheikh et al. [41] reported that nitric acid treatment decreases the surface area and pore volume of the AC. A similar trend was also observed in the results of iodine number (Table 1).

3.2. Adsorption capacity of the oxidized and non-oxidized ACs

Adsorption capacity of the oxidized and non-oxidized ACs towards metal ions was estimated as described in Section 2.7. The results are presented in Table 2. It is noted that the lowest adsorption capacity of AC was found towards Mn^{2+} and Zn^{2+}. Oxidation of AC with various oxidizing agents generally increased the adsorption capacity towards all metal ions, but the highest increase was observed with AC-NA. This explains the highest recoveries achieved in the preconcentration process using AC-NA as the preconcentrating sorbent (see later Section 3.3.2).

3.3. Optimization of the preconcentration procedure using AC as sorbent

Optimization of preconcentration procedure is an important process to get appropriate enrichment efficiency and full recovery. The effect of oxidation of AC with various oxidizing agents was the main factor investigated in this work. Other variables that were investigated included: pH of water sample, concentration and volume of eluting solvent, mass of adsorbent and breakthrough volume.

3.3.1. Effect of pH of water sample

It is believed that pH of the solution affects the structure of adsorbent surface and the structure of adsorbate present in the aqueous solution. For example, at basic pH medium, metals are precipitated as their hydroxides while functional groups on adsorbent surface (carboxyl, phenolic, lactonic) exist in the deprotonated form. On the other hand, at acidic pH medium, free metal ions exist in solution while surface functional groups present in the protonated form. Thus the mechanism of metal uptake may vary at various pH values.

A series of experiments was performed to investigate the influence of sample pH over the range from pH 1 to 10. The three oxidized sorbents (AC-NA, AC-HP, AC-APS) and the non-oxidized AC were tested for preconcentration of the metal ions in aqueous solutions at various pH values. Variations of the percentage recovery of metal ions with changing the pH of water sample using various sorbents are shown in Figs. 1–4. It is generally noted that the highest recoveries were achieved at pH 9 for almost all metal ions with all the oxidized and the non-oxidized AC sorbents. Moderate recovery was sometimes achieved at pH 5 for some metals, such as for Pb^{2+} using AC-APS sorbent (Fig. 3). The high recovery achieved for metal ions at pH 9 is probably due to precipitation of their hydroxides at this pH value, and thus metal hydroxides are captured inside the micropores of AC or stick to the surface of AC. On the other hand, at pH 5 metal ions uptake is probably due to direct binding of the metal ions with the acidic surface groups that are present on the activated carbon surface. However, recoveries achieved at pH 5 were not satisfactory and thus pH 9 was selected as the optimum pH of aqueous solution in the preconcentration process.

Table 2
Adsorption capacity ($mg\,g^{-1}$) of oxidized and non-oxidized AC towards metal ions at pH 9

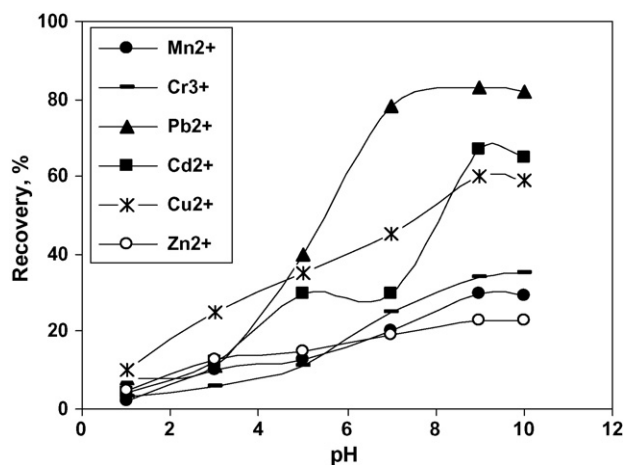|	Mn^{2+}	Cr^{3+}	Pb^{2+}	Cd^{2+}	Cu^{2+}	Zn^{2+}
AC	0.095	0.117	0.336	0.280	0.225	0.076
AC-NA	0.248	0.178	0.555	0.392	0.366	0.270
AC-APS	0.221	0.102	0.186	0.121	0.107	0.255
AC-HP	0.228	0.195	0.505	0.352	0.304	0.262

Fig. 1. Effect of pH of the water sample on % recovery of the metal ions using non-oxidized AC sorbent: 25 mL water sample spiked with $0.30\,\mu g\,mL^{-1}$ metal (each), 0.200 g sorbent, elution with 10 mL of $0.50\,M\,HNO_3$.

Fig. 2. Effect of pH of the water sample on % recovery of the metal ions using AC-NA sorbent: 25 mL water sample spiked with $0.30 \mu g \, mL^{-1}$ metal (each), 0.200 g sorbent, elution with 10 mL of 0.50 M HNO_3.
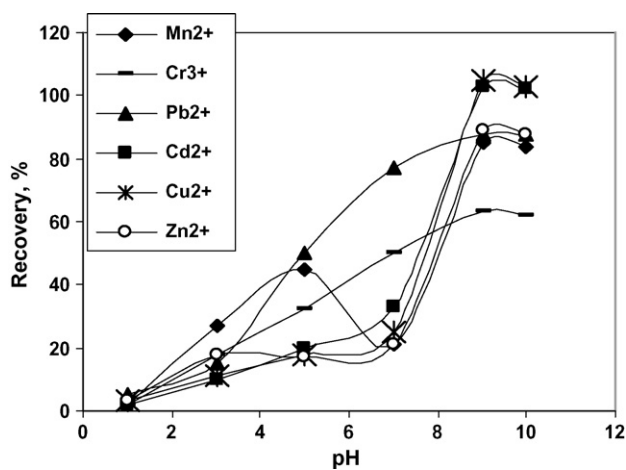

Fig. 4. Effect of pH of the water sample on % recovery of the metal ions using AC-HP sorbent: 25 mL water sample spiked with $0.30 \mu g \, mL^{-1}$ metal (each), 0.200 g sorbent, elution with 10 mL of 0.50 M HNO_3.

3.3.2. Effect of adsorbent oxidation

The preconcentration efficiency of the oxidized AC was compared with the non-oxidized AC sorbent at pH 9. The non-oxidized AC sorbent (Fig. 1) did not give satisfactory percentage recovery for all metal ions at pH 9, i.e. percentage recoveries are 80% for Pb^{2+}, 22% for Zn^{2+}, 58% for Cu^{2+}, 30% for Cr^{3+}, 68% for Cd^{2+} and 28% for Mn^{2+}.

It is noted that using AC-NA sorbent has generally improved the recovery at pH 9 for all metal ions relative to the non-oxidized AC (Fig. 2). Thus at pH 9, the recovery increased for Mn^{2+} from 28% to 85%; for Cd^{2+} the recovery increased from 68% to 100%; for Cr^{3+} the recovery increased from 30% to 60%; for Cu^{2+} the recovery increased from 58% to 102%; for Zn^{2+} the recovery increased from 22% to 85%; while the recovery of Pb^{2+} was almost unchanged.

Treatment of AC with ammonium persulfate gave unexpected results (Fig. 3). It is noted that recoveries of Zn^{2+} and Mn^{2+} increased four times (Fig. 3) relative to the non-oxidized AC

(Fig. 1); but unfortunately recoveries of Pb^{2+}, Cd^{2+}, Cu^{2+} and Cr^{3+} significantly decreased relative to the non-oxidized AC sorbent.

Treatment of AC with hydrogen peroxide gave recovery range 65–85% for metal ions at pH 9 (Fig. 4). These recoveries (Fig. 4) are generally higher than recoveries obtained with non-oxidized AC (Fig. 1), but they are generally lower than those obtained with AC-NA sorbent (except for Cr^{3+}) (Fig. 2).

Two postulates may be proposed to explain the highest recoveries achieved with AC-NA. The first postulate is that oxidation increases the oxygen content and thus increases the hydrophilicity of the surface (see Section 3.1 above), which in turn promotes the formation of water clusters on the activated carbon surface. This may facilitate the uptake process of metal hydroxides at pH 9, in which metal uptake is probably due to H-bonding of the metal hydroxides to the hydrophilic surface of AC. Thus metal hydroxides stick to the hydrophilic surface of AC. The second postulate is that nitric acid treatment may alter the porosity of the surface in a manner that makes it more capable of capturing precipitated metal hydroxides. El-Sheikh et al. [41] reported that nitric acid treatment decreases the surface area and pore volume of the AC. Thus a decrease in the diameter of the pore openings occurred. This may support the retaining process of the precipitated metal hydroxides inside the pores of AC.

Due to the highest recoveries achieved with AC-NA sorbent at pH 9, this sorbent was selected for subsequent optimization of the preconcentration SPE procedure of metal ions at pH 9.

3.3.3. Optimization of other parameters

Nitric acid was used as the eluting solvent in this work. The optimum concentration of nitric acid is 1.0 M HNO_3, while 10 mL of this eluting solvent is the optimum volume to elute maximum amount of the adsorbed metal ions. The optimum mass of AC-NA is 0.400 g, while the breakthrough volume is 400 mL.
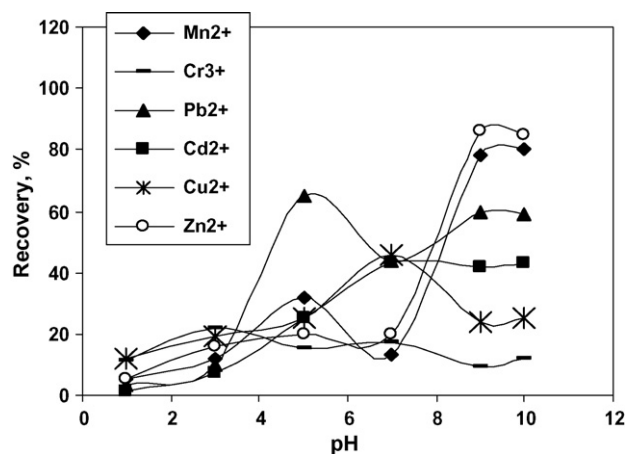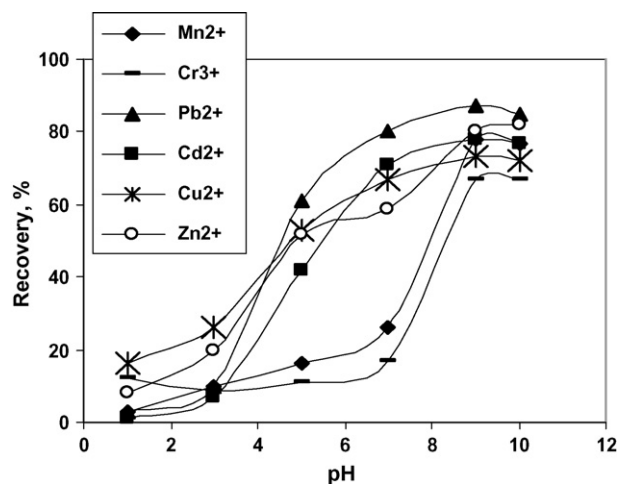

Fig. 3. Effect of pH of the water sample on % recovery of the metal ions using AC-APS sorbent: 25 mL water sample spiked with $0.30 \mu g \, mL^{-1}$ metal (each), 0.200 g sorbent, elution with 10 mL of 0.50 M HNO_3.

3.3.4. The optimum preconcentration method

Based on the above discussion, the following optimized method is proposed for preconcentration of the metal ions using AC-NA as sorbent:

400 mL aqueous solution (containing the metal ions simultaneously) at pH 9 is passed through a 0.400 g of AC-NA packed inside the cartridge and preconditioned as described in Section 2.5. The retained metals are eluted with 10 mL of 1.0 M HNO_3 solution and then directly analyzed by the flame atomic absorption spectroscopy (FAAS) under the conditions stated in Section 2.4.

3.3.5. Effect of coexisting ions

The effect of coexisting ions on preconcentration of metal ions using AC-NA as sorbent at pH 9 was investigated by adding the following amounts of interfering ions (separately) to water samples containing 0.30 μg mL^{-1} of each metal ion: 1000 μg mL^{-1} Na^+, 1000 μg mL^{-1} K^+, 50 μg mL^{-1} Al^{3+}, 500 μg mL^{-1} SO_4^{2-}, 500 μg mL^{-1} Ca^{2+}, 500 μg mL^{-1} Mg^{2+}, 200 μg mL^{-1} HCO_3^-, 10 μg mL^{-1} Fe^{3+}. Water samples were then treated according to the optimum SPE procedure (see Section 3.3.4). Results are not given, but they indicated that the % recovery of all metals remained above 90%, even in the presence of the assigned concentrations of coexisting ions.

3.4. Comparing the enrichment efficiency of AC–NA with non-oxidized AC

For the purpose of comparing the enrichment efficiency of sorbent AC-NA with that of non-oxidized AC, the optimum preconcentration method (described in Section 3.3.4) was applied by using either AC-NA or the non-oxidized AC. The two sorbents will be compared in terms of linear range, detection limit and sensitivity of the preconcentration methods. For that purpose, 400 mL of doubly distilled water samples were spiked with various concentrations of the metal ions: 20, 50, 100, 150, 200, 250 and 300 ng mL^{-1} and then enriched (using either AC-NA or non-oxidized AC) according to the optimized preconcentration method. Preconcentration experiments were performed in five replicates ($n = 5$) and the five extracts were analyzed as separate samples.

Precision was estimated as percent relative standard deviations (%RSD, $n = 5$). Linear ranges for the metal ions were estimated based on the value of the R-squared for the calibration curve. Sensitivity of the method (m) for each metal ion was estimated as the slope of the calibration curve. The detection limit for each metal ion was estimated as three times the standard deviation of the blank signal. The analytical parameters of the method using both sorbents (AC-NA and AC) are presented in Table 3.

Table 3
Analytical performance of the proposed SPE method using AC-NA, AC, MWCNT-NA and MWCNT towards the targeted metal ions

	Linear range (ng mL^{-1})	R^2	Detection limit (ng L^{-1})	%RSD range ($n = 5$)	Slope	Intercept
Sorbent: AC-NA						
Mn^{2+}	20–300	0.9997	54	1.1–2.9	0.980	0.930
Cr^{3+}	20–300	0.9939	88	1.1–3.5	0.845	0.793
Pb^{2+}	20–300	0.9990	193	1.5–3.8	0.185	0.753
Cd^{2+}	20–300	0.9998	42	1.5–3.9	1.720	0.680
Cu^{2+}	20–300	0.9997	84	1.7–4.5	0.680	0.450
Zn^{2+}	20–300	0.9832	33	1.1–3.1	4.189	0.516
Sorbent: AC						
Mn^{2+}	20–100	0.9999	113	0.8–3.6	0.325	1.612
Cr^{3+}	–	–	–	–	–	–
Pb^{2+}	20–100	0.9999	187	1.1–4.2	0.195	0.022
Cd^{2+}	20–100	0.9911	465	0.9–3.3	0.450	5.628
Cu^{2+}	20–100	0.9414	226	1.3–4.2	0.419	8.242
Zn^{2+}	20–100	0.9345	302	1.6–3.6	2.923	61.08
Sorbent: MWCNT-NA						
Mn^{2+}	20–150	0.9978	38	0.9–3.4	0.865	0.425
Cr^{3+}	20–300	0.9990	37	1.1–3.9	0.901	0.339
Pb^{2+}	20–300	0.9999	214	1.2–4.0	0.181	0.683
Cd^{2+}	20–150	0.9973	24	1.3–3.1	1.402	0.161
Cu^{2+}	20–300	0.9998	46	1.5–4.0	0.722	0.321
Zn^{2+}	20–200	0.9936	9	1.3–3.5	4.179	0.365
Sorbent: MWCNT						
Mn^{2+}	–	–	–	–	–	–
Cr^{3+}	20–100	0.9324	310	1.3–3.6	0.116	0.339
Pb^{2+}	20–100	0.9985	378	1.5–4.1	0.170	0.683
Cd^{2+}	20–100	0.9997	116	0.9–3.4	0.258	0.060
Cu^{2+}	20–100	0.9978	47	1.1–3.8	0.557	0.323
Zn^{2+}	20–150	0.9925	9	1.0–3.9	3.895	0.367

Table 4
Concentration of metal ions (μg L^{-1} $\pm \sigma$, $n = 5$) in the unspiked environmental waters and their spike recoveries ($n = 5$) using AC-NA according to the optimized SPE procedure

		Tap water	Reservoir water	Stream water
Mn^{2+}	Found concentration (ng mL^{-1}) in unspiked water sample.	ND[a]	ND[a]	77.2 ± 3.1[b]
	Spike recovery range, %[c]	85–95	97–100	85–100
Cr^{3+}	Found concentration (ng mL^{-1}) in unspiked water sample.	ND[a]	ND[a]	20.1 ± 1.6[b]
	Spike recovery range, %[c]	90–100	88–100	98–102
Pb^{2+}	Found concentration (ng mL^{-1}) in unspiked water sample.	ND[a]	ND[a]	22.7 ± 2.6[b]
	Spike recovery range, %[c]	63–100	77–100	95–100
Cd^{2+}	Found concentration (ng mL^{-1}) in unspiked water sample.	ND[a]	ND[a]	26.3 ± 2.4[b]
	Spike recovery range, %[c]	98–104	97–103	97–101
Cu^{2+}	Found concentration (ng mL^{-1}) in unspiked water sample.	ND[a]	ND[a]	52.6 ± 3.2[b]
	Spike recovery range, %.[c]	63–100	98–102	97–102
Zn^{2+}	Found concentration (ng mL^{-1}) in unspiked water sample.	ND[a]	ND[a]	63.7 ± 2.9[b]
	Spike recovery range, %[c]	79–101	85–99	73–100

[a] ND: not detected.
[b] Uncertainty is the standard deviation for five replicate runs.
[c] Added concentrations: 20, 50, 100, 150, 200, 250 and 300 ng mL^{-1}.

From Table 3, it was clear that the main difference between the two sorbents was in the linear range, in which AC-NA sorbent had wider linear range of the method for all the metal ions. This is probably due to higher adsorption capacity of AC-NA (see Table 2). It was also noted that sensitivity of the method was higher when AC-NA was used and thus lower detection limits were achieved with AC-NA (Table 3). The relative standard deviations %RSD, ($n = 5$) was always less than 4.5%.

3.5. Comparing the enrichment efficiency of AC–NA with MWCNT

For the purpose of comparison, MWCNT-NA and non-oxidized MWCNT were used separately for preconcentration of metal ions. Optimization of the preconcentration parameters gave similar procedure to that described in Section 3.3.4, except that 0.200 g of MWCNT-NA or MWCNT was optimum instead of 0.400 g. 400 mL of doubly distilled water samples were spiked with various concentrations of the metal ions: 20, 50, 100, 150, 200, 250 and 300 ng mL^{-1} and then enriched (using either MWCNT-NA or non-oxidized MWCNT) according to the optimized preconcentration method described above in this section. Preconcentration experiments were performed in five replicates ($n = 5$) and the five extracts were analyzed as separate samples. The analytical parameters of the method using MWCNT-NA and non-oxidized MWCNT are presented in Table 3. These were compared with the analytical performance achieved with AC-NA.

It was noted that the sensitivities towards metal ions achieved with AC-NA and MWCNT-NA were close to each other, while the linear ranges were generally wider when AC-NA was used.

When non-oxidized MWCNT was used for preconcentration of metal ions, it was noted that the sensitivities towards metal ions achieved were noticeably smaller than those achieved with AC-NA. Additionally the linear ranges with non-oxidized

MWCNT sorbent were noticeably narrower than AC-NA sorbent.

3.6. Analytical application

Environmental water samples (tap water, reservoir water and stream water) were used to validate the proposed preconcentration method of metal ions using AC-NA as sorbent (see Section

Table 5
Concentrations of metals (μg L^{-1} $\pm \sigma$, $n = 5$) in un-spiked and spiked tap waters using the optimum preconcentration method (using AC-NA as sorbent) and independent method (ET AAS)

Element	Added	Found	
		Optimum SPE method (using AC-NA)	ET AAS
Mn^{2+}	0	ND[a]	ND[a]
	20	19.0 ± 1.3	20.1 ± 1.2
	50	46.5 ± 1.9	49.8 ± 2.1
Cr^{3+}	0	ND[a]	ND[a]
	20	20.0 ± 1.1	20.1 ± 0.9
	50	49.0 ± 1.9	48.4 ± 1.7
Pb^{2+}	0	ND[a]	ND[a]
	20	20.0 ± 1.1	20.2 ± 0.9
	50	45.5 ± 2.2	48.9 ± 1.8
Cd^{2+}	0	ND[a]	ND[a]
	20	20.5 ± 1.3	20.3 ± 1.0
	50	49.0 ± 1.8	49.1 ± 2.1
Cu^{2+}	0	ND[a]	ND[a]
	20	20.0 ± 0.9	20.1 ± 1.1
	50	45.5 ± 2.1	48.1 ± 2.3
Zn^{2+}	0	ND[a]	ND[a]
	20	20.2 ± 1.3	20.2 ± 0.9
	50	48.5 ± 2.3	49.4 ± 1.9

[a] ND: not detected.

3.3.4). Some metal ions were found in the unspiked real waters according to the proposed procedure, as shown in Table 4. Environmental waters were then spiked with the metal ions at various concentrations according to the linear ranges shown in Table 3. Spike recoveries of the target metal ions in real water samples are shown in Table 4. The spike recovery range of all metal ions was 63–104%. The results indicate that the proposed method is satisfactory and can be used for the analysis of the targeted metals.

In order to establish the validity of the proposed method, un-spiked and spiked tap water samples were analyzed twice, first by the optimum preconcentration method (using AC-NA as preconcentrating sorbent), second, by electro-thermal atomic absorption spectroscopy (ET AAS). The results are given in Table 5, from which it is clear that the results of the two methods are comparable to each other.

4. Conclusion

Oxidation of AC with various oxidizing agents produces sorbents of different enrichment efficiencies, although significant amount of acidic oxides is generated by the three oxidation schemes. Nitric acid treatment of activated carbon increases the enrichment efficiency of metal ions relative to the non-oxidized AC, AC-HP and AC-APS sorbents. This may be attributed to the fact that nitric acid treatment increases the hydrophilicity of the AC surface. Thus the precipitated metal hydroxides at pH 9 stick to AC-NA surface probably by hydrogen bonding between metal hydroxides and the acidic oxides on the surface. Treatment of AC with hydrogen peroxide increases the enrichment efficiency relative to non-oxidized AC, but it is lower than that achieved with AC-NA sorbent. On the other hand, ammonium persulfate treatment of AC do not improve the recovery of metal ions at pH 9.

Comparing the enrichment efficiency of AC with AC-NA reveals that the main difference between the two sorbents was in the limit of linearity, in which AC-NA gives wider linear ranges due to higher adsorption capacity of AC-NA towards all metal ions. AC-NA also gives higher method sensitivity and thus lower detection limits than non-oxidized AC.

Comparing the enrichment efficiency of AC-NA with non-oxidized MWCNT and MWCNT-NA indicates that the analytical performance of AC-NA is close to MWCNT-NA, but the analytical performance of AC-NA is much better than non-oxidized MWCNT.

Application of the optimum (proposed) method using AC-NA as preconcentrating sorbent on real environmental waters and comparison with independent method indicates that the proposed method can be recommended for preconcentration of metal ions from aqueous medium.

Acknowledgements

References

[1] R. Bansal, J. Donnet, F. Stoeckli, Active Carbon, Marcel Dekker, New York, 1988.
[2] E. Diamadopoulos, P. Samaras, G. Sakellaropoulos, Water Sci. Technol. 25 (1992) 153.
[3] C. Ania, J. Parra, J. Pis, Fuel Process. Technol. 79 (2002) 265.
[4] C. Ania, J. Parra, J. Pis, Fuel Process. Technol. 77–78 (2002) 337.
[5] C. Leng, N. Pinto, Carbon 35 (1997) 1375.
[6] R. Vidic, C. Tessmer, L. Uranowski, Carbon 35 (1997) 1349.
[7] K. Jankowski, J. Yao, K. Kasiura, A. Jackowska, A. Sieradzka, Spectrochim. Acta B 60 (2005) 369.
[8] A.M. Yusof, M.M. Rahman, A.K.H. Wood, J. Radioanal, Nucl. Ch. 271 (2007) 191.
[9] A.M. Yusof, M.M. Rahman, A.K.H. Wood, J. Radioanal. Nucl. Ch. 259 (2004) 479.
[10] M. Yaman, Commun. Soil Sci. Plan. 31 (2000) 3205.
[11] M. Yaman, B. Environ. Contam. Tox. 65 (2000) 545.
[12] M. Yaman, Y. Dilgin, S. Gucer, Anal. Chim. Acta 410 (2000) 119.
[13] M. Yaman, H. Avci, Anal. Sci. 22 (2006) 721.
[14] E. Beinrohr, A. Manova, J. Dzurov, Fresenius' J. Anal. Chem. 355 (1996) 528.
[15] R.A. Gil, S. Cerutti, J.A. Gasquez, R.A. Olsina, L.D. Martinez, Talanta 68 (2006) 1065.
[16] R.A. Gil, S. Cerutti, J.A. Gasquez, R.A. Olsina, L.D. Martinez, Spectrochim. Acta B 60 (2005) 531.
[17] J. Sommar, X.B. Feng, O. Lindqvist, Appl. Organomet. Chem. 13 (1999) 441.
[18] F. Granados, V. Bertin, S. Bulbulian, M. Solache-Rios, Appl. adiat. Isotopes 64 (2006) 291.
[19] R. LeyvaRamos, J.R. RangelMendez, J. MendozaBarron, L. FuentesRubio, R.M. GuerreroCoronado, Water Sci. Technol. 35 (1997) 205.
[20] F.A. Bertolino, A.A.J. Torriero, E. Salinas, R. Olsina, L.D. Martinez, J. Raba, Anal. Chim. Acta 572 (2006) 32.
[21] E.E. vanderHoek, J.T. vanElteren, R.N.J. Comans, Int. J. Environ. An. Ch. 63 (1996) 67.
[22] M.I. Castilla, Y. Cortazar, J.V.L. Cosin, Agrochimica 39 (1995) 233.
[23] S. Babel, T.A. Kurniawan, Chemosphere 54 (2004) 951.
[24] K. Zhang, W.H. Cheung, M. Valix, Chemosphere 60 (2005) 1129.
[25] P. Liang, Y. Liu, L. Guo, Spectrochim. Acta Part B 60 (2005) 125.
[26] P. Liang, Q. Ding, F. Song, J. Sep. Sci. 28 (2005) 2339.
[27] H.D. Liang, D.M. Han, Anal. Lett. 39 (2006) 2285.
[28] Q. Ding, P. Liang, F. Song, A.M. Xiang, Sep. Sci. Tech. 41 (2006) 2723.
[29] C.R.T. Tarley, A.F. Barbosa, M.G. Segatelli, E.C. Figueiredo, P.O. Luccas, J. Anal. Atom. Spectrom. 21 (2006) 1305.
[30] J. Munoz, M. Gallego, M. Valcarcel, Anal. Chem. 77 (2005) 5389.
[31] M. Zhang, M. Yudasaka, S. Iijima, J. Phys. Chem. B 108 (2004) 149.
[32] P. Liang, Y. Liu, L. Guo, J. Zeng, H. Lu, J. Anal. Atom. Spectrom. 19 (2004) 1489.
[33] F. Hennrich, R. Wellmann, S. Malik, S. Lebedkin, M.M. Kappes, Phys. Chem. Chem. Phys. 5 (2003) 178.
[34] S. Chakraborty, J. Chattopadhyay, H.Q. Peng, Z.Y. Chen, A. Mukherjee, R.S. Arvidson, R.H. Hauge, W.E. Billups, J. Phys. Chem. B 110 (2006) 24812.
[35] S. Gregg, K. Sing, Adsorption, Surface Area and Porosity, Academic Press Inc., London, 1967.
[36] A.H. El-Sheikh, A.P. Newman, H. Al-Daffaee, S. Phull, N. Cresswell, J. Anal. Appl. Pyrol. 71 (2004) 151.
[37] H.P. Boehm, Carbon 40 (2002) 145.
[38] R.F. Allen, N.C. Baldini, P.E. Donofrio, E.L. Gutman, E. Keefe, J.G. Kramer, C.M. Leinweber, V.A. Mayer, Annual Book of ASTM Standards, volume 15.01. Refractories, Carbon and Graphite Products, Activated Carbon, American Society for Testing and Materials, Easton, 1996.
[39] J. Sweileh, Anal. Bioanal Chem. 375 (2003) 450.
[40] N. Krupa, N. Canon, J. Amer. Water Works Assoc. 88 (1996) 94.
[41] A.H. El-Sheikh, A.P. Newman, H. Al-Daffaee, S. Phull, D. Lynch, Adsorpt. Sci. Technol. 22 (2004) 451.

Comparing the precision of selenium isotope ratio measurements using collision cell and sector field inductively coupled plasma mass spectrometry

Nagmeddin Elwaer *, Holger Hintelmann

Chemistry Department, Trent University, 1600 West Bank Drive, Peterborough, Ontario K9J 7B8, Canada

Abstract

The performance of two different types of inductively coupled plasma mass spectrometry (ICP-MS) instruments for resolving spectral overlaps on Se isotopes was compared by means of selenium isotopic ratio measurements. Examined were a quadrupole-based, hexapole collisions cell CC-ICP-MS and a double-focusing sector field SF-ICP-MS. Due to the importance of precise and accurate isotope ratio determination in environmental, clinical and nutritional studies, a thorough investigation of the critical instrumental parameters of each technique was performed. A hydride generation system was coupled with SF-ICP-MS to maintain high signal-to-noise ratios (S/N) at high mass resolution. However, $^{80}Se^+$ was not completely separated from the argon dimer $^{40}Ar_2{}^+$ at $m/z = 80$, even in high-resolution mode. The same hydride generation system was coupled to a collision cell instrument and it was found that argon dimers are significantly reduced using a mixture of H_2 and He gas with the cell. A lower mass bias of 2.5% per amu was determined for measured Se isotopes using the SF-ICP-MS instrument compared 3.6% observed for the CC-ICP-MS instrument. Under optimized conditions, the precision for Se isotope ratio measurements of both instruments was evaluated and compared measuring NIST-3149 Se standard solution. On average, the uncertainty determined by repeated measurements over the span of three individual measuring sessions in a period of 3 weeks ranged from 0.06% to 0.15% and 0.09% to 0.30% R.S.D. for the various isotope ratios using the CC-ICP-MS and SF-ICP-MS instrument, respectively. The detection limits (3σ) for total Se were determined by measuring ^{82}Se and found to be 1.7 and 4.0 ng L^{-1} for the CC-ICP-MS and SF-ICP-MS, respectively.

1. Introduction

Interest in the determination of selenium isotope ratios in environmental and biological samples using ICP-MS has steadily increased with the development of systems capable of more precise measurements. Despite the fact that selenium has six stable isotopes, its determination in environmental samples by ICP-MS is seriously hampered by spectral interferences [1–5]. Major sources of interference are argon based molecular ions matching the m/z of Se isotopes as illustrated in Table 1 [6–10]. With its relatively low ionization efficiency in the argon plasma (31%) and the abundance of Ar related ions in the spectral region between $m/z = 74$ and $m/z = 82$, accurate and precise

determination of Se isotope ratios is still a challenging task using ICP-MS techniques. These factors, coupled with the relatively low concentrations of Se present in certain matrices of interest (e.g. environmental samples) have significantly reduced the application of ICP-MS methods for isotope ratio applications such as ID-MS for the measurement of Se.

Recently, new generations of ICP-MS instruments have been introduced to overcome the aforementioned spectral interferences encountered with Se isotopic ratio measurements. The most conventional approach to separate spectral interferences is to use a sector field mass spectrometer, with the ability to separate many isotopes from their overlaps such as $^{38}Ar^{40}Ar$ and $^{38}Ar^{40}Ca$ from ^{78}Se and $^{40}Ar^{16}O$ from ^{56}Fe, when operated at high-resolution setting [11–12].

The SF-ICP-MS instrument also provides low signal background, high-ion transmission and consequently better detection limits compared to quadrupole ICP-MS [13]. Another bene-

* Corresponding author. Tel.: +1 705 670 5662.
  E-mail address: nagmeddinelwaer@trentu.ca (N. Elwaer).

Table 1
Potential interferences in the determination of Se by ICP-MS

Isotope	Abundance (%)	Potentially interfering species	Required resolution $m/\Delta m$
$^{74}Se^+$	0.89	$^{36}Ar^{38}Ar^+$	9476
$^{76}Se^+$	9.37	$^{38}Ar^{38}Ar^+$	12145
		$^{40}Ar^{36}Ar^+$	7083
		$^{40}Ar\,^{35}Cl^1H^+$	3825
$^{77}Se^+$	7.63	$^{38}Ar_2H^+$	3167
		$^{40}Ar^{37}Cl^+$	9190
		$^{76}SeH^+$	10797
$^{78}Se^+$	23.77	$^{40}Ar\,^{38}Ar^+$	9975
		$^{40}Ar\,^{36}ArH_2^+$	2755
		$^{40}Ar\,^{37}Cl^1H^+$	4142
		$^{77}SeH^+$	7471
$^{80}Se^+$	49.61	$^{40}Ar\,^{40}Ar^+$	9699
		$^{40}Ar\,^{38}Ar^1H_2^+$	3297
$^{82}Se^+$	8.73	$^{40}Ar_2H_2^+$	3456

fit of using sector field SF-ICP-MS instruments is that flat top peaks can be achieved in low-resolution mode, which is extremely useful in high precision isotope ratio measurements at low concentrations of Se [14]. Due to its simplicity, sector field instruments have gained large popularity for isotopic ratio measurements.

Another approach takes advantage of ion–molecule reactions, to analyze isotopes with overlapping spectra. Collision and reaction cell technologies have proven to be very effective in dealing with molecular interferences [15–17]. These techniques rely on elimination or displacement of the interference by ion–molecule reactions employing different types of gases and/or by application of kinetic energy discrimination. Such reactions allow the analysis of ions with overlaps by either reacting with the interfering ion itself, and removing the overlap from its interfering mass or by reacting with the analyte of interest and moving it to another mass, where it can be analyzed. For Se, which suffers from the presence of argide molecular interferences, the development of a hexapole collision cell [18] allowing the removal of these interferences opened new possibilities for the study of this element. However, while the argon overlaps on Se isotopes can be resolved effectively with collision cell technology using reactive gases such as hydrogen and methane, this technique can be plagued by the formation of Se hydride, which introduces new interferences on adjacent Se isotopes, e.g. ^{77}SeH on ^{78}Se.

Since the precision of isotope ratio measurements improves significantly with high-ion count rates, a hydride generation sample introduction system is employed with both instruments, significantly enhancing the transfer yield of analyte to the ICP-MS. This step not only maximizes signal intensities, but also eliminates matrix interferences. Both are particularly important for precise Se isotope ratio measurements, because of the low ionization potential of Se in the argon plasma (30%) and low natural abundances of four of the six stable selenium isotopes (^{74}Se, ^{76}Se, ^{77}Se and ^{82}Se are >10%). Hydride generation itself suffers from potential challenges including transition metals affecting the efficiency of the hydride formation, interferences from other hydride forming elements and the importance of introducing Se

in the proper oxidation state. The effect of these parameters for the presented method are described in detail [19].

The application of the above mentioned ICP-MS techniques in resolving spectral interferences on selected Se isotopes to improve the sensitivity and detection limits has been studied extensively. However, these techniques have not been investigated for multiple isotope ratio determination of Se. To date, to the best of our knowledge no comparison study has been conducted to determine which of these two techniques is more suitable for accurate and precise measurements of multiple Se isotope ratios. We do not know for certain, which technique better capable of resolving spectral and matrix overlaps on multiple Se isotopes simultaneously. This study compares the potential of two ICP-MS instruments, a double-focusing sector field SF-ICP-MS and a quadrupole-based, hexapole collision cell CC-ICP-MS, to accurately and precisely determine Se isotope ratios.

2. Materials and methods

2.1. Reagent and solutions

Unless stated otherwise, all acids used in this study were trace reagent grade purchased from Fisher and were used without any further purification. Se standard solutions were prepared from 10.11 ± 0.02 mg g^{-1} (NIST SRM 3149) Se stock solution was obtained from National Institute of Standard and Technology (NIST) (Gaithersburg, MD, USA). All Se standards were prepared daily in 4 M HCl using trace metal grade hydrochloric acids obtained from Fisher Scientific (Ottawa, ON, Canada). Sodium borohydride (MERCK) solution at (0.16 M) was prepared daily and stabilized in (0.13 M) NaOH. High-purity deionized water (18 M∧.cm) produced with Milli-Q Plus water purification system (Millipore, Bedford, MA, USA) was used for the dilution and preparation of the samples, standards and reagents throughout this work. All glassware and Teflon© (PTFE) materials were cleaned with 10% analytical reagent grade nitric acid and Milli-Q water before use.

2.2. Instrumentation

Two types of mass spectrometers were used in the present study—a hexapole collision cell CC-ICP-MS (Platform ICP, Micromass Ltd., Manchester, UK) equipped with a quadrupole mass analyzer and unique ion transfer system, and a double-focusing sector field SF-ICP-MS (Element2, Finnigan MAT, Bremen, Germany) equipped with electric and magnetic scanning analyzers, which are configured in a reverse near Johnson geometry for high-resolution measurements. Detailed description of these instruments can be found elsewhere [20–22]. Briefly, the two instruments have almost identical sample introduction systems consisting of Ni sampler and skimmer cones (1.1 and 0.8 mm orifice diameters, respectively), demountable Fassel torch (1.5 mm internal diameter) equipped with capacitive decoupling system, also known as guard electrode or plasma shield. Each instrument was interfaced with LI2 cold-vapor generation system as illustrated in Fig. 1A detailed description of
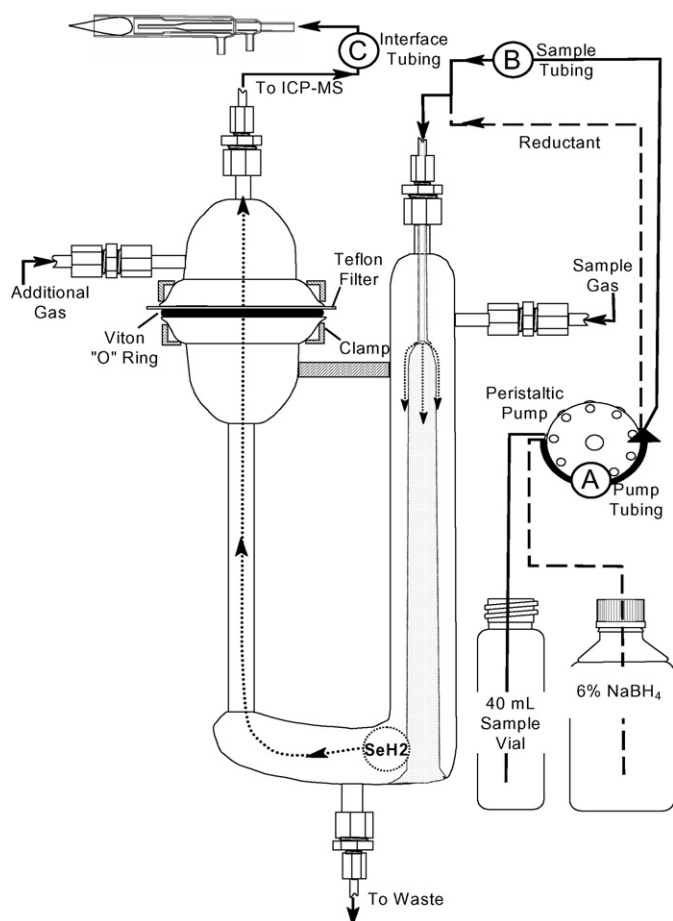
Fig. 1. Schematic diagram of the cold-vapor (LI2) hydride generation sample introduction system used for isotopic ratio measurements of Se with the ICP-MS instruments.

the LI2 cold-vapor generation apparatus used in this study has been given elsewhere [23]. The instrumental parameters, including torch positioning, rf-power, cooling, auxiliary and nebulizer gas flow rates of each ICP-MS were initially optimized for maximum signal-to-noise ratio (S/N) and highest precision of the ^{78}Se/^{82}Se isotope ratio.

2.2.1. CC-ICP-MS measurements

Prior to Se isotopic ratio measurements, the influence of H_2 and He gas flow rates (adjustable by individual mass flow controllers), hexapole bias and spectral interferences on the (S/N) ratio of Se isotopes was investigated. Using a 100 ng mL^{-1} Se standard solution and a reagent blank prepared in 4 M HCl solution, the data for each experiment was acquired in triplicate, monitoring all six Se isotopes at $m/z = 74$, 76, 77, 78, 80 and 82, plus Ge at $m/z = 73$, As at $m/z = 75$ and Kr at $m/z = 83$. Once instrumental parameters were optimized, the isotopic composition of Se was determined using the operating conditions and sample introduction parameters illustrated in Table 2. Before calculating isotope ratios, the background signal of a blank solution was subtracted from Se isotope signals and mathematical corrections were applied to correct for hydride formation (SeH$^+$) at $m/z = 77$ and 78.

2.2.2. SF-ICP-MS measurements

Prior to isotopic ratio measurements, the instrument was carefully mass calibrated using a 1 ng mL^{-1} mixed standard. After argon gas flow rates and ion lens settings were optimized, the instrument was tuned for maximum sensitivity at $m/z = 74$, 78 and 82 using a 10 ng/mL^{-1} Se standard. To determine the effect of high mass resolution for resolving spectral overlaps on, the data for a 10 ng mL^{-1} Se standard solution was acquired in medium (MR, $R_p = 4000$) and high (HR, $R_p = 10,000$) resolution mode. Using both analog and pulse counting in medium resolution, the data for the same standard solution (10 ng mL^{-1}) was determined using both B-scan (magnetic) and E-scan (electric) to determine the best scanning strategy for obtaining the highest precision. Mathematical corrections were applied to correct for background and hydride formation (SeH$^+$) at $m/z = 77$ and 78 prior to calculating isotope ratios.

3. Results and discussion

3.1. Optimization of the CC-ICP-MS experimental conditions

3.1.1. Effect of the hydrogen collision gas flow rate on the Se signal

The effect of the H_2 flow rate on eliminating ArAr+ ions from Se spectra at $m/z = 76$, 78 and 80 was investigated and is shown in Fig. 2. As can be seen, the best results are obtained at gas flow rates of 2.5 mL min^{-1}, which increases the (S/N) ratio at $m/z = 76$, 78 and 80 by a factor of 1.4, 1.5 and 100, respectively. Increasing the H_2 gas flow rate to ~5 mL min^{-1} resulted in 35 and 20% decreases of the (S/N) ratio at $m/z = 78$ and 80, respectively.

The gradual decrease of (S/N) ratio with increasing collision gas flow rates may be due either to formation of ^{40}Ar^{36}ArH$_2$$^+$ and ^{40}Ar^{38}ArH$_2$$^+$ at $m/z = 78$ and 80, respectively or to scattering of Se ions by the H_2 gas at high flow rate. The (S/N) ratio at $m/z = 76$ increased by 23% when increasing the H_2 gas flow rate from 2.5 to 5 mL min.$^{-1}$ The cause of the increase in the S/N

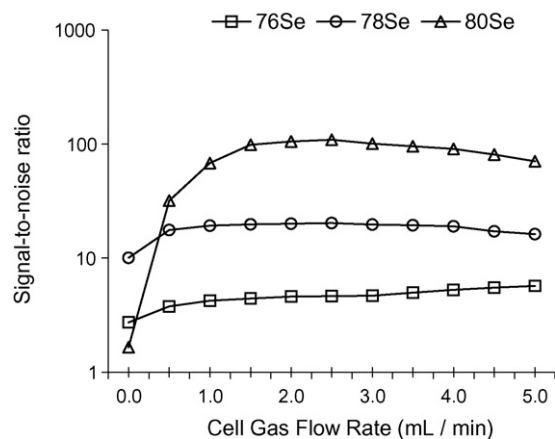Fig. 2. Effect of H_2 gas flow on the Se signal to noise ratio at $m/z = 76$, 78 and 80 using 1.5 mL min^{-1} He flow rate, −1.0 V hexapole bias potential, 400 V hexapole exit lens voltage and 450 V multiplier voltage settings.

Table 2
Optimized operating conditions and experimental settings of CC-ICP-MS and SF-ICP-MS

ICP-MS type sample introduction technique	CC-ICP-MS LI2	SF-ICP-MS LI2
Sample/skimmer cone	Nickel	Nickel
Torch		
RF–power[a]	1350	1375
X, Y, Z torch position[a]	Daily	Daily
Guard electrode (GE)	On	On
Gases flow rates		
Plasma gas flow rate (L min^{-1})[a]	14.75	14.50
Auxiliary gas flow rate (L min^{-1})[a]	1.15	0.80
Nebulizer gas flow rate (L min^{-1})[a]	0.90	0.91
He gas flow rate (mL min^{-1})	4.0	
H$_2$ gas flow rate (mL min^{-1})	2.5	
Analyzer parameters		
Hexapole exit lens (V)	400	
Hexapole bias voltage (V)	−2	
Multipler voltage	475	
Acquisition parameters		
Mass resolution ($m/\Delta m$)	300	4000
Runs/passes	–	2 × 50
Number of repeats	10	–
Mode	Peak hopping	Peak hopping
Dwell time (s)	0.20	
Total analysis time (min)	5.0	6.6
Cold-vapor hydride generation (LI2)		
NaBH$_4$ flow rate (mL min^{-1})	0.90	0.85
Sample uptake (mL min^{-1})	1.05	1.15
NaBH4 concentration (%)	0.6	0.6
HCl concentration (M)	4	4

[a] Parameter is optimized daily for maximum signal-to-noise ratio (S/N).

ratio at higher H$_2$ gas flow rate is not obvious. However, one of the possibilities is that probably due to the formation of AsH$^+$ ions at high H$_2$ gas flow rate in the presence of a trace amounts of As in the standard solution. Therefore, the H$_2$ gas flow rate was kept at 2.5 mL min^{-1} for Se isotope ratio measurements in future experiments.

3.1.2. Effect of the helium collision gas flow rate on the Se signal

He gas with a purity of 99.999% was introduced into the collision cell while keeping the reaction gas H$_2$ constant at 2.5 mL min.$^{-1}$. An increase of He gas flow rate from 0 to 4 mL min^{-1} increased the S/N ratio by a factor of 2 for all measured Se isotopes (results not shown). As the reaction cell is pressurized with He gas, the (S/N) ratio of Se initially increased due to collision focusing, attained a maximum at a flow rate of 4.0 mL min^{-1}, and then decreased by a factor of 3 at 10 mL min^{-1} He gas flow rates. The increase in sensitivity is due to the loss of kinetic energy of Se ions, which enabled better focusing of these ions into the quadrupole and transmission to the detector. The drastic loss of Se signals at higher flow rate is most likely due to the scattering of Se ions by the large volume of gas present in the cell. Therefore, to obtain high sensitivity and avoid any mass bias occurring during Se isotope ratio mea-

surements a blend of He and H$_2$ gases at 2.5 and 4.0 mL min^{-1} gas flow rates were chosen, respectively and used for future experiments.

3.1.3. Mass bias

While reducing ion kinetic energies by He gas may improve the sensitivity for Se ions, it is also well known that the collision gas pressure can alter the mass discrimination in the collision cell. Depending on the mass of the analyte ion and the collision gas flow rate used, ions are scattered at high-collision gas flow rates, which results in an appreciable change in the ion trajectories. Light isotopes are preferentially scattered compared to heavier isotopes, which leads to inaccurate and variable isotope ratio data [24–26]. Therefore, the effect of a pressurized collision cell on the mass bias was investigated. The influence of the He gas flow rate on instrument mass bias per mass unit (MD) for the measured ^{78}Se/^{82}Se isotope ratio is calculated according to the following equation:

$$MD\,(\%) = \frac{(f_{MD} - 1) \times 100}{\Delta m} \qquad (1)$$

with $f_{MD} = r/R$, r and R being the true and measured ^{78}Se/^{82}Se isotope ratios, respectively. Due to the lack of a certified reference material for Se isotopes, the measured isotope ratio was compared to IUPAC ^{78}Se/^{82}Se isotope ratio values [27]. Without any He gas in the cell and the hexapole bias potential set to zero, the instrument mass bias for ^{78}Se/^{82}Se isotope ratio was 2.4% per atomic mass unit (amu) (results not shown). This value increased linearly to 4.5%, when increasing the He gas flow rate to 10 mL min^{-1}. An increasing mass bias at higher collision gas flow rates is explained by more effective scattering of the lighter ^{78}Se caused by repeated collision with He gas, or the occurrence of a more pronounced space charge effect within the rf-hexapole.

3.1.4. Effect of hexapole bias on Ar$_2$$^+$ signal

The hexapole bias can influence the residence time of ions in the cell, which ultimately affects the efficiency of gas phase reactions. To investigate the effect of the hexapole bias potential on polyatomic Ar$_2$$^+$ ions, the intensity of ^{40}Ar$_2$$^+$ was measured as a function of H$_2$ gas flow rates with and without hexapole bias voltage. A 4 M HCl blank solution prepared with Milli-q water and trace reagent HCl was used as a sample. At 0 mL min^{-1} of H$_2$ gas, the intensities of ^{40}Ar$_2$$^+$ ions at $m/z = 80$ were almost identical (∼1.0E + 07 cps), with and without applied hexapole bias voltage (results not shown). The ^{40}Ar$_2$$^+$ ion intensities were reduced by approximately 3–4 orders of magnitude, when the H$_2$ gas flow rate increased to 2.0 mL min^{-1} and the hexapole bias voltage was set to 0 and −1.8, respectively.

The decrease in ^{40}Ar$_2$$^+$ ions intensities is most likely due to the collision-induced reaction of Ar$_2$$^+$ ions with H$_2$ gas and the loss of kinetics energy of the ions caused by the collision with H$_2$ inside the cell. The discrepancy observed with the two hexapole mass bias voltage settings, is due to the large energy loss of the polyatomic Ar$_2$$^+$ ions as result of an increased number of collisions with the H$_2$ gas, when a hexapole mass bias voltage is applied to the cell. Therefore, a hexapole bias potential value

of -2 V was used to minimize the Ar_2^+ ion interference on Se isotopes in future experiments.

3.2. Optimization of the SF-ICP-MS experimental conditions

The SF-ICP-MS instrument was carefully mass calibrated using a $1\,ng\,mL^{-1}$ mixed standard solution and the following instrumental parameters influencing the isotopic ratio determination were carefully optimized.

3.2.1. Lens voltage

The electrostatic lenses in SF-ICP-MS instrument are optimized to keep the ions focused in a compact "ion beam" as they pass through the vacuum system into the detector. Proper optimization of the applied lense voltage can also prevent unwanted photons and neutral particles from reaching the detector, hence, improving analyte signal by reducing background noise. However, improper ion lens voltage settings can affect the transmission of lighter isotopes into the detector, introducing a mass bias, which might affect the precision and the accuracy of isotopic ratio measurement. Therefore, to asses the effect of ion lens voltage on Se signal in SF-ICP-MS instrument, the settings of focus voltage, Y-defection voltage and X-deflection voltage were investigated individually by varying each voltage while aspirating a $100\,ng\,mL^{-1}$ Se standard solution using the hydride generation system for sample introduction. The signal intensity in cps of the measured Se isotopes obtained at each voltage interval of focus voltage, Y-deflection voltage and X-deflection voltage was plotted as a function of voltage settings and is shown in Fig. 3A–C, respectively.

As the ions travel towards the detector the signal for Se ions increased with increasing focus voltage (Fig. 3A). The maximum signal intensity of all six ions was found at -900 V focus voltage. Then the signal intensity decreased rapidly to almost background level at -500 V. Similarly, the signal for Se increased significantly by increasing the Y-deflection voltage from -10 to -2 V and X-deflection voltage from -12 to -5 V, after which the signal reached maximum strengths at approximately -2 V and -5 V (Fig. 3B and C) for Y-deflection voltage and X-deflection voltage, respectively. Further increase resulted in a significant decrease of Se signal. Therefore, to obtain maximum sensitivity, values of -900, -2 and -5 V were adopted for focus, Y- deflection and X-deflection voltage, respectively.

3.2.2. Mass resolution

Mass resolution is defined as the ability to separate adjacent peaks in the mass spectrum to the extent that the magnitude of the valley between the two peaks does not exceed 10% of the mean magnitude of the height of the peaks [28]. It is calculated by the term $m/\Delta m$, where m is the mean mass of the peak and Δm is the mass difference between two peaks. There are some spectral polyatomic ions interferences such as argon dimers with the same m/z as each of the six Se isotopes that can not be separated chemically and may require high mass resolution to be resolved.
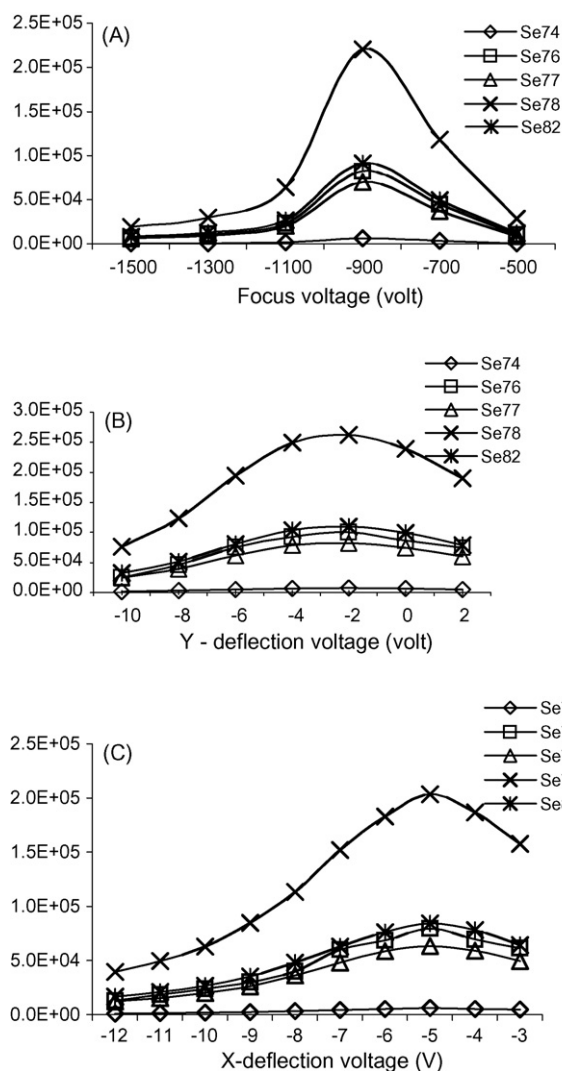
Fig. 3. Dependence of Se isotope signals on focus voltage (A), Y-deflection voltage (B) and X-deflection voltage in Element2 SF-ICP-MS.

Table 1 illustrates some of these interferences and the resolution required to resolve the overlaps on Se isotopes.

On the SF-ICP-MS Element2, three settings are available; low resolution (LR: $m/\Delta m = 300$), medium resolution (MR: $m/\Delta m = 4000$) and high resolution (HR: $m/\Delta m = 10,000$). Using the high mass resolution capability it is possible to overcome some of these interferences. However, eliminating or reducing these interferences by mean of high mass resolution has a significant impact on the sensitivity of the measurement. For example, scanning a $10\,ng\,mL^{-1}$ Se standard solution at three different mass resolution modes (LR, MR and HR) resulted in significant reduction of the sensitivity. A loss of approximately 89.7% and 99.6% of the ^{76}Se signal was observed when switching mass resolution from low to medium and from low to high resolution, respectively.

In this study, due to the limited resolving power (max. $R_p = 10,000$) of the SF-ICP-MS, some of the mentioned interferences were not baseline separated from Se isotopes. Fig. 4 shows the collected spectra measured at m/z 76, 78 and 80 from a $10\,ng\,mL^{-1}$ Se standard solution using medium and high resolu-

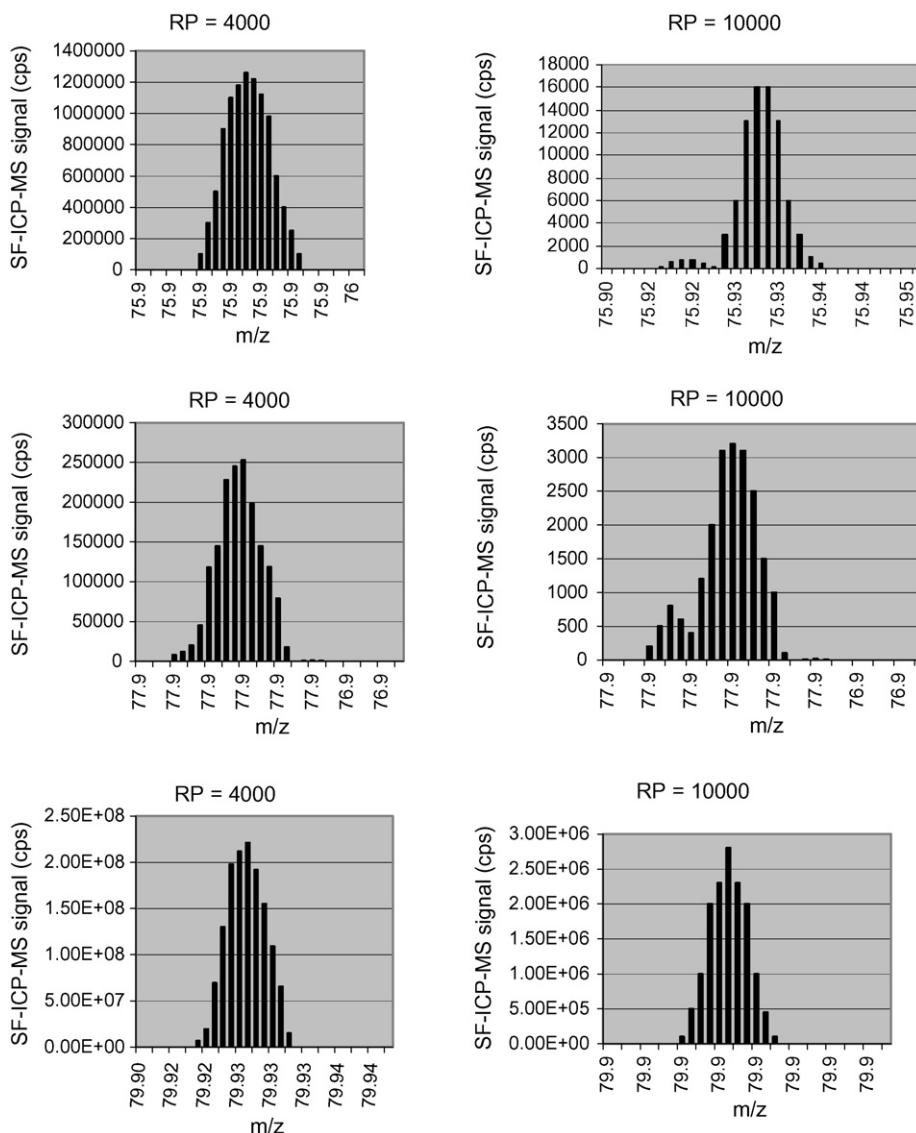Fig. 4. Medium and high-resolution spectra of Se isotopes at m/z 76, 78 and 80 using a SF-ICP-MS Elements2 instrument.

tion. At medium mass resolution, the peaks of the ^{76}Se, ^{78}Se and ^{80}Se isotopes are indistinguishable from the respective ArAr$^+$ background ions. However, at high resolution, two distinctive peaks are observed at $m/z = 76$ and 78. The peaks on the low mass side are the Se isotopes, while the second peak is from the ArAr$^+$ background dimer.

The ^{78}Se$^+$ peak appears at $m/z = 77.920$, while the ^{40}Ar^{38}Ar$^+$ peak is at $m/z = 77.926$. Similarly, the ^{76}Se$^+$ peak appears at $m/z = 75.924$, while the ^{38}Ar^{38}Ar$^+$ peak is at $m/z = 75.931$. At $m/z = 80$, the background signal is very large, with >2 million counts even at high resolution and the ^{80}Se signal is completely covered by the ^{40}Ar$_2$$^+$ background, supporting the findings by Vanhaecke and Moens [29]. For $m/z = 74$ and 77, the spectra (not shown) show two distinct peaks at high mass resolution, whereas at $m/z = 82$, the ^{40}Ar$_2$H$_2$$^+$ background lies directly over the ^{82}Se signal, and could not be resolved even when using high mass resolution. Although complete separation of ArAr$^+$ background from all major Se isotopes at $m/z = 76$, 78 and 80 was not possible

using increased mass resolution, applying medium resolution helped in reducing and eliminating some matrix interferences (Table 1). Thus, to avoid additional loss of sensitivity using high mass resolution, it was decided to apply medium resolution in subsequent experiments.

3.2.3. Scanning mode

The SF-ICP-MS instrument is able to scan ions using an electrostatic sector analyzer (ESA, E-scanning) or a magnetic sector analyzer (MSA, B-scanning). For maximum isotope ratio precision, it is desirable to spend as much time of the measurement cycle as possible on the analyte isotopes. Therefore, to determine the best scanning mode for measuring precise Se isotope ratios, the two scanning modes were evaluated experimentally with medium resolution. The results are summarized in Table 3.

Without correcting for instrument mass bias, the best isotope ratio precision was achieved by E-scanning Se isotopes at $m/z = 74$, 76, 77, 78, 80 and 82. Obtained precision ranged

Table 3
Effect of scanning mode on Se isotopic ratio measurements using SF-ICP-MS

Scanning mode	$^{78}Se/^{74}Se$	$^{78}Se/^{76}Se$	$^{78}Se/^{77}Se$	$^{78}Se/^{82}Se$
	$^{78}Se/^{74}Se$ R.S.D. (%)	$^{78}Se/^{76}Se$ R.S.D. (%)	$^{78}Se/^{77}Se$ R.S.D. (%)	$^{78}Se/^{82}Se$ R.S.D. (%)
E-scanning	29.3320 0.35	2.6536 0.21	3.1508 0.16	2.4636 0.12
B-scanning	29.0961 0.50	2.6566 0.39	3.1961 0.23	2.4522 0.19

Scans were performed with 10 ng mL^{-1} Se standard solution in LR ($n = 5$).

from 0.12% to 0.21% and from 0.19% to 0.39% for $^{78}Se/^{76}Se$, $^{78}Se/^{77}Se$ and $^{78}Se/^{82}Se$ using E-scanning and B-scanning, respectively. Higher relative standard deviations of 0.35% and 0.50% were observed for the $^{78}Se/^{74}Se$ ratio, which was attributed to the low abundance of ^{74}Se, resulting in poorer counting statistics. The lower precision attained with B-scanning is explained by the longer settling time required for the magnet to stabilize compared to E-scanning. In magnetic scanning, the scanning is performed in small jumps depending on the number of points chosen per peak width, each jump requiring 1000 μs of settling time. E-scanning requires no settling time after changing the voltage and therefore, more time per cycle is available to measure the analyte ions. Hence, E-scanning was chosen for isotope ratio measurements.

3.2.4. Selenium hydride formation

In spite of the advanced technologies used to resolve spectral interferences by either increasing the mass resolution in SF-ICP-MS or employing ion–molecular reactions with CC-ICP-MS, problems with interferences in Se determinations still remain. The most obvious interference, which complicated the analysis of Se isotopes in addition to the Ar_2^+ dimers, is SeH^+ formation caused either from the use of H_2 gas in the collision cell or the use of cold-vapor LI2 hydride generation sample introduction system. These interferences can have a significant impact on the accuracy and precision of measured isotope ratios [30–31]. Therefore, the impact of these interferences on the measured Se signals at $m/z = 77$ and 78 was investigated using both ICP-MS techniques. After each instrument optimization, a 100 ng mL^{-1} Se standard solutions was repeatedly ($n = 3$) measured on each ICP-MS instrument using the cold-vapor LI2 hydride generation system as sample introduction method.

Monitoring the intensities at $m/z = 82$ and 83, the magnitude of the SeH^+ formation at $m/z = 77$ and 78 was calculated by measuring the $^{82}SeH^+/^{82}Se^+$ ratio. The $^{76}SeH^+$ and $^{77}SeH^+$ interference on ^{77}Se and ^{78}Se signals was corrected according to:

$$^{77}Se = {}^{77}I - \left(\frac{^{82}SeH^+}{^{82}Se^+}\right)(^{76}Se) \tag{2}$$

and

$$^{78}Se = {}^{78}I - \left(\frac{^{82}SeH^+}{^{82}Se^+}\right)(^{77}Se) \tag{3}$$

Since the ratio of $^{82}SeH^+/^{82}Se^+$ can vary depending on the daily experimental conditions [15], measurements were conducted on multiple days to estimate the average SeH^+ formation. Table 4 compares the two ICP-MS techniques with respect to

their SeH^+ formation. As can be seen from the data shown, the ratio of $^{82}SeH^+/^{82}Se^+$ varied depending on the instrument in use. The highest of $^{82}SeH^+/^{82}Se^+$ values ranging from 5.0 to 5.9% were observed using the CC-ICP-MS instrument. These values are lower than the value reported in previous studies by Boulyga et al. [30] and Sloth et al. [17,32], using a hexapole collision cell and a dynamic reaction cell with hydrogen, respectively, and approximately 50% higher than what was reported by Reyes et al. [30] using an octapole reaction system with hydrogen gas. The higher values reported in our measurements are most likely caused by the LI2 hydride generation sample introduction system. The sector field SF-ICP-MS instruments produced an average $^{82}SeH^+/^{82}Se^+$ ratio of 3.4%. This value is approximately 34% lower than what was observed in the collision cell. This apparent difference in the magnitude of Se hydride formation between CC-ICP-MS and SF-ICP-MS can be attributed to the use of H_2 as reaction cell gas in the CC-ICP-MS instrument.

Another complication that can arise from using the hydride generation as a sample introduction system is the formation of $^{75}AsH^+$, $^{79}BrH^+$ and $^{81}BrH^+$ that can cause an interference with Se ions at $m/z = 76$, 80 and 82, respectively. To quantify the formation of such interferences a number of As and Br (1–1000 ng mL^{-1}) standard solutions were analyzed using the cold-vapor LI2 hydride generation system with both CC-ICP-MS and SF-ICP-MS instruments. Regardless of the concentration of Br in the standard solutions no significant Br^+ and BrH^+ signals were observed at $m/z = 79$, 80, 81 and 82 during the analyses in both ICP-MS instruments. The absence of this interference is probably related to the lack of BrH^+ formation under the alkaline hydride generation conditions used and the removal of Br from the matrix using a hydride generation technique for sample introduction.

No signal at $m/z = 76$ was observed for $^{75}AsH^+$ on the SF-ICP-MS instrument. Using the CC-ICP-MS instrument the $^{75}AsH^+$ signals was only apparent at As concentrations >750 ng mL^{-1}. Therefore, no correction was necessary for AsH^+ during Se isotope ratio analysis measuring the SRM NIST 3149 Se standard solution. However, measuring isotope ratios of Se

Table 4
Comparison of CC-ICP-MS and SF-ICP-MS regarding their SeH^+ forming potential using the cold-vapor LI2 hydride generation introduction system ($n = 3$)

ICP-MS	CC-ICP-MS $^{82}SeH^+/^{82}Se$	SF-ICP-MS $^{82}SeH^+/^{82}Se$
Day 1	5.01 ± 0.32	3.34 ± 0.20
Day 2	5.13 ± 0.24	3.05 ± 0.19
Day 3	5.89 ± 0.25	3.94 ± 0.23
Average	5.34 ± 0.48	3.44 ± 0.45

Table 5
Mass fractionation factor (f_{MD}) and mass discrimination (MD) per mass unit for Se isotopes ratio measurements using CC-ICP-MS and SF-ICP-MS instruments

Isotope ratio	CC-ICP-MS		SF-ICP-MS	
	f_{MD}	MD (%)	f_{MD}	MD (%)
$^{74}Se/^{78}Se$	1.161	4.02	1.118	2.92
$^{76}Se/^{78}Se$	1.067	3.63	1.049	2.43
$^{77}Se/^{78}Se$	1.035	3.47	1.022	2.22
$^{78}Se/^{80}Se$	1.066	3.30	1.060	3.01
$^{78}Se/^{82}Se$	1.149	3.72	1.092	2.31

A LI2 hydride generation system was used for Se standard solution introduction into the plasma.

in samples with high arsenic concentration of >500 ng mL^{-1} a chemical separation of this element is required prior to analysis with the CC-ICP-MS technique. We also tested for krypton interferences. Nevertheless, the background at $m/z = 78$, 80, 82 and 83 was measured in blank solutions and was subtracted from sample signals prior to isotope ratio calculations to avoid any potential Kr interferences.

3.2.5. Mass bias

The magnitude of the mass bias depends strongly on the ICP-MS instrument in use [31] but is independent of the particular Se isotope ratio measured with the same instrument. Different processes contribute to this deviation. Space charge effects in the skimmer cone region are often responsible for differential ion transmission in ICP-MS and are discussed in detail elsewhere [33–35]. The total mass bias in a mass spectrometer can be calculated experimentally from the mass discrimination factor f_{MD} as shown in Eq. (1).

The mass discrimination factor and the mass discrimination per mass unit for Se isotopes were determined for each ICP-MS instrument under optimized instrumental conditions and are shown in Table 5. To keep the total ion current in the ion beam constant, the Se concentration was always kept the same at 100 ng mL^{-1} with each instrument. Due to the lack of isotope certified materials for Se, the representative isotopic composition given by International Union of Pure and Applied Chemistry (IUPAC) [36] was used for calculating the f_{MD} values.

The magnitude of mass discrimination reported in this study is comparable to those reported for Se isotope ratio measurements using other quadrupole ICP-MS instruments [17,30,37,38]. Similar mass bias factors have been reported for Se by ICP-MS [17,30,38]. In all cases the f_{MD} values are >1, indicating that the lighter isotopes are much more discriminated

than heavier isotopes. In the CC-ICP-MS and SF-ICP-MS instruments, these values were found to vary between (1.066–1.161) and (1.022–1.118), respectively, depending on the daily instrumental working conditions. The values for both instruments varied within days and between days, but always with values >1, which suggests that space charge effect is the major source of mass discrimination in both instruments. The results also show that the mass discrimination (MD) per mass unit in percent was higher for the CC-ICP-MS ($3.63 \pm 0.27\%$) compared to the SF-ICP-MS ($2.58 \pm 0.36\%$). This apparent discrepancy in the MD between the two instruments is most likely due to differences in the ion optics and the extraction potential applied in each instrument. SF-ICP-MS uses much higher ion energy and extraction lens potentials (6000 and 4200 V), respectively. Such high potentials have been reported [37] to reduce the magnitude of matrix effects in the region between the skimmer cone and the mass analyzer, hence, reducing the space charge effect.

3.3. Selenium isotope ratio precision: collision cell versus high resolution

To quantify the accuracy and precision of the developed methods, the isotope ratios of $^{78}Se/^{74}Se$, $^{78}Se/^{76}Se$, $^{78}Se/^{77}Se$, $^{78}Se/^{80}Se$ and $^{78}Se/^{82}Se$ were measured under optimized instrument conditions at 100 ng mL^{-1} of Se introduced by means of the cold-vapor LI2 hydride generation system. The mass bias and SeH$^+$ formation corrected Se isotope ratios are compared with tabulated values from IUPAC in Table 6. The reported uncertainty was determined by repeated measurement ($n = 9$) of a NIST SRM 3149 Se standard during three individual measuring sessions over a period of 3 weeks.

Considerably better precision (0.060%–0.16% R.S.D.) was achieved using the CC-ICP-MS compared to the SF-ICP-MS (0.10%–0.30% R.S.D.) for all measured Se ratios. The measured $^{78}Se/^{74}Se$ and $^{78}Se/^{80}Se$ ratios showed the highest standard deviations in both instruments. The lower precision for $^{78}Se/^{74}Se$ was most likely due to the low counting statistics for ^{74}Se. The relatively high relative standard deviation for $^{78}Se/^{80}Se$ compared to the other measured Se ratios is attributed to the incomplete removal of the $^{40}Ar_2^+$ ion the H$_2$ gas in the collision cell and limited resolving power of the SF-ICP-MS instruments for these two ions.

Also compared in this study are the method limits of detection (LOD) of each instrument. Using a repeated measurement ($n = 7$) of 4 M HCl solution in a single session the LODs (3σ) for both instruments were evaluated by measuring ^{82}Se

Table 6
Comparison of measured isotope ratio of selenium in 100 ng mL^{-1} SRM NIST 3149 Se standard solution using SF-ICP-MS in medium resolution and CC-ICP-MS

ICP instrument isotope ratio	No. of runs	CC-ICP-MS		SF-ICP-MS IUPAC		IUPAC values
		Measured ratio	R.S.D. (%)	Measured ratio	R.S.D. (%)	
78Se/74Se	$n = 9$	26.7912	0.11	26.5376	0.25	26.7057
78Se/76Se	$n = 9$	2.5304	0.097	2.5881	0.18	2.5363
78Se/77Se	$n = 9$	3.1107	0.090	3.1861	0.14	3.1131
78Se/80Se	$n = 9$	0.4747	0.16	0.4692	0.30	0.4791
78Se/82Se	$n = 9$	2.7695	0.06	2.6917	0.09	2.7206

using the optimized method conditions and found to be 1.67 and 4.03 ng L^{-1} for CC-ICP-MS and SF-ICP-MS, respectively. These LODs are in the range of what have been reported by others [31,39,40] using similar ICP-MS instruments with different sample introduction systems. The relatively high LOD obtained for SF-ICP-MS compared to the CC-ICP-MS is explained by the loss of sensitivity using medium resolution (MR = 4000). It is important to recognize that the optimized instrument parameters used to determine the LODs do not necessarily correspond to the parameters providing maximum net intensity, but were rather chosen to provide optimal isotope ratio precision. For example, in the CC-ICP-MS the H$_2$ and He gases flow rates were optimized for argon interference removal rather than for the best sensitivity. Similarly, the SF-ICP-MS settings were optimized for precise isotope ratio measurement, which not necessarily corresponds to the highest signal intensity for a selected single isotope.

Overall, the superiority of CC-ICP-MS over the SF-ICP-MS instrument in precision for Se isotope ratio measurements can be attributed to the removal of most of ArAr$^+$ dimers by reaction with H$_2$ and the improvement in ion transmission efficiency due to reduction of the ion energy spread with collision of the ion beam with He gas in cell. A factor, which might have contributed to the poorer precision of the SF-ICP-MS instrument is low counting statistics achieved for the low abundant isotopes in medium resolution. In addition, measurements in medium resolution lack flat-top peaks, which dramatically improves the isotope ratio precision in low mass resolution.

4. Conclusions

Isotope ratios precision varies with the type of plasma source mass spectrometer; it is helpful to know the "normal" range of the standard deviation that can be achieved under good operating conditions. In this study, the collision cell ICP-MS technique proved to be more effective in removing argon dimer interferences on measured Se isotopes and provided a better precision compared to the sector filed ICP-MS technique. While the SF-ICP-MS instrument was not entirely successful in separating ArAr$^+$ ion interferences on the most abundant Se isotopes, using medium resolution mode was useful in eliminating some of the ArArH$^+$ ion interferences listed in Table 1. In general, isotope ratio values measured using both ICP-MS techniques are in a good agreement with tabulated values from IUPAC. The accuracy and precision of Se isotope ratios measured in 100 ng mL^{-1} SRM NIST 3149 Se standard solution seemed to be satisfactory, taking into account the relatively low concentration. One should note that the precision achieved with both the SF-ICP-MS and the CC-ICP-MS instruments would not be possible with conventional Q-ICP-MS.

The obtained precision might be sufficient for monitoring Se isotope ratios in tracer and isotope dilution experiments, or for applications, where there are few spectral interferences and extreme sensitivity is not needed. However, one should note that the precision achieved in this study is not sufficient for highly precise measurement of Se isotope ratios with the purpose of studying the natural fractionation of Se isotopes. For such stud-

ies, other techniques like MC-ICP-MS and TIMS are required. Moreover, even though the potentially interfering argon dimers on the Se isotopes at m/z = 76, 78 and 80 were almost quantitatively eliminated with the CC-ICP-MS technique by the use of a He/H$_2$ gas mixture, the inherent mass fractionation caused by using a reaction gas in the collision cell can be a limiting factor using this technique.

References

[1] T.M. Johnson, M.J. Herbel, T.D. Bullen, P.T. Zawislanski, Geochimica et cosmochimica. Acta 63 (18) (1999) 2775.
[2] T.M. Johnson, T.D. Bullen, P. Zawislanski, Environ. Sci. Technol. 34 (2000) 2075.
[3] A.S. Ellis, T.M. Johnson, T.D. Bullen, M.J. Herbel, Chem. Geol. 195 (2003) 119.
[4] R.S. Oremland, J. Stolz, in: D.R. Lovely (Ed.), Environ Metal–microbe Interact, ASM Press, 2000, pp. 199–224.
[5] M.J. Herbel, T.M. Johnson, R.S. Oremland, T.D. Bullen, Geochim. Cosmochim. Acta 64 (2000) 3701.
[6] L.R. Hinojosa, J.M. Marchante Gayon, J.I. Garcia Alonso, A. Sanz-Medel, J. Anal. At. Spectrom. 18 (2003) 11.
[7] J. Goossens, F. Vanhaecke, L. Moens, R. Dams, Anal. Chim. Acta 283 (1993) 137.
[8] L.S. Zhang, S.M. Combs, J. Anal. At. Spectrom. 11 (1996) 1049.
[9] S.H. Tan, G. Horlick, Appl. Spectrosc. 4 (1983) 445.
[10] F.H. Konad, M.H. Yang, J. Anal. At. Spectrom. 11 (1996) 413.
[11] N.S. Belshaw, X.K. Zhu, Y. Guo, R.K. O'Nions, Int. J. Mass Spectrom. 197 (2000) 191.
[12] A.D. Anbar, Earth Planetary Sci. Lett. 217 (2004) 223–236.
[13] N. Jakubowski, L. Moens, F. Vahaecke, Spectrochim. Acta B 53 (1998) 1739.
[14] F. Vanhaecke, L. Moens, P.D. Taylor, Anal. Chem. 68 (1996) 567.
[15] E.H. Larsen, J. Sloth, M. Hansen, S. Moesgaard, J. Anal. At. Spectrom. 18 (2003) 310.
[16] J.J. Sloth, E.H. Larsen, S.H. Bugel, S. Moesgaard, J. Anal. At. Spectrom. 18 (2003) 317.
[17] J.J. Sloth, E.H. Larsen, J. Anal. At. Spectrom. 15 (2000) 669.
[18] P. Turner, T. Merrent, J. Speakman, C. Haines, Royal Society of Chemistry, Chambridge, 28 (1997) 312.
[19] N. Elwaer, H. Hintelmann, Anal. Bioanal. Chem. 389 (2007) 1889.
[20] S. Weyer, J.B. Schwieters, Int. J. Mass Spectrom. 226 (2003) 355.
[21] N. Jakubowski, L. Moens, V. Vahaecke, Spectrochim. Acta B 53 (1998) 1739.
[22] V.N. Epov, V. Taylor, D. Lariviere, R.D. Evans, R.J. Cornett, J. Radioanalyt. Nucl. Chem. 258 (3) (2003) 473.
[23] D. Foucher, H. Hintelmann, Anal. Bioanal. Chem. 348 (2006) 1470.
[24] S.F. Boulyga, H.J. Dietze, J.S. Becker, Mikrochem. Acta 137 (2001) 39.
[25] J.T. Rowan, R.S. Houk, Appl. Spectrosc. 43 (1989) 976.
[26] G.C. Eiden, C.J. Barinaga, D.W. Koppenaal, J. Anal. At. Spectrom. 11 (1994) 317.
[27] K.J.R. Rosman, P.D.P. Taalor, J. Anal. At. Spectrom. 14 (1999) 5.
[28] R.N. Taylor, T. Warnecke, J.A. Milton, I.W. Croudace, P.E. Warwick, R.N. Nesbitt, J. Anal. At. Spectrom. 16 (2001) 279.
[29] F. Vanhaecke, L. Moens, Anal. Bioanal. Chem. 378 (2) (2004) 232.
[30] S.F. Boulyga, J.S. Becker, J. Fresen. Anal. Chem. 370 (2001) 618.
[31] L.H. Reyes, J.M. Gayon, J.I. Alonso, A.S. Medel, J. Anal. At. Spectrom. 18 (2003) 11.

[32] T.F.D. Mason, D.J. Weiss, M. Horstwood, R.R. Parish, S.S. Russell, E. Mullane, B.J. Coles, J. Anal. At. Spectrom. 19 (2004) 218.

[33] G.P Russ III., J.M. Bazan, Spectrochim. Acta 42B (1987) 49.

[34] H.P. Longerich, B.J. Fryer, D.F. Strong, Spectrochim. Acta 42B (1987) 39.

[35] H. Andren, I. Rodushkin, A. Stenberg, D. Malinovsky, D.C. Baxter, J. Anal. At. Spectrom. 19 (2004) 1217.

[36] IUPAC Commission on Atomic Weights and Isotopic Abundances, Pure Appl. Chem., 69 (1997) 2384.

[37] T.W. Burgoyne, G.M. Hieftje, R.A. Hites, Anal. Chem. 69 (1997) 485.

[38] K.G. Heumann, S.M. Gallus, G. Radlinger, J. Vogl, J. Anal. At. Spectrom. 19 (1998) 1001.

[39] K.S.K. Danadurai, Y.L. Hsu, S.J. Jiang, J. Anal. At. Spectrom. 17 (2002) 552.

[40] D. Wallschlager, R. Roehl, J. Anal. At. Spectrom. 16 (2001) 922.

In-line application of electric field in capillary separation systems: Joule heating, pH and conductivity

Björn O. Eriksson [a], Inger Lill Skuland [a,1], Nicola D. Marlin [a],
Magnus B.O. Andersson [b], Lars G. Blomberg [a,*]

[a] *Department of Chemistry, Karlstad University, SE-651 88 Karlstad, Sweden*
[b] *Early Development, Pharmaceutical and Analytical Research & Development, AstraZeneca, SE-151 85 Södertälje, Sweden*

Abstract

This study concerns the technique electric field-assisted capillary liquid chromatography. In this technique, an electric field is applied over the separation capillary in order to provide an additional selectivity. In this technique, the electric field is applied *in-line* in the separation capillary and here the electric current is the factor limiting the magnitude of applied electric field. The influence of Joule heating and other factors on the current in such systems has been investigated.

The temperature in the capillary was first measured within a standard CE set-up, as function of effect per unit of length. Then the same cooling system was applied to an in-line set-up, to replicate the conditions between the two systems, and thus the temperature. Thus Joule heating effects could then be calculated within the in-line system. It was found that for systems applying an electric field in line, the direct influence from Joule heating was only relatively small.

The pH in the capillary was measured in the in-line set-up using cresol red/TRIS solutions as pH probe. Significant changes in pH were observed and the results suggested that electrolysis of water is the dominant electrode reaction in the in-line system. In summary, the observed conductivity change in in-line systems was found to be mainly due to the pH change by hydrolysis of water, but primarily not due the temperature change in the capillary column.

© 2007 Elsevier B.V. All rights reserved.

Keywords: Conductivity changes; In-line voltage application; Joule heating; pH changes; Electric field-assisted capillary liquid chromatography

1. Introduction

Separations that are performed within packed capillaries under an applied electric field are usually achieved with either end of the capillary column being immersed into a reservoir. There are several reasons for this but the most obvious being its simplicity. Buffer reservoirs make it easy to apply a voltage across the capillary, to switch the run buffer, inject sample and automate the separation system. Most commercial CE instruments utilize reservoirs, and are also often employed for CEC separations. However, it is sometimes impractical to use this type of set-up and in such cases the voltage has to be applied in-line as opposed to using reservoirs [1]. Commonly, this is necessary when an external pressure is applied to the inlet of the column to obtain a pressurized flow [2–31].

The main driving force behind combining an in-line applied electric field with a pressurized flow is that the system does not then depend upon the generation of an EOF for transporting the mobile phase through the column, and that the separation can then be optimized by the mobile phase flow rate and electrophoretic migration separately [2–5,8–11,13,15,19,27]. The magnitude or polarity of the electric field can thus be altered to achieve a good separation without entirely changing the transport of the mobile phase. The removal of the dependency on the EOF also means that any pH or buffer composition can be used, that would otherwise not have generated an EOF [6,17]. The application of pressure has also frequently been used for in-line CEC methods in order to suppress bubble formation

---

* Corresponding author. Tel.: +46 54 7001530; fax: +46 54 7002040.
  E-mail address: lars.blomberg@kau.se (L.G. Blomberg).
¹ On leave from: Department of Chemistry, University of Oslo, P.O.B. 1033 Blindern, N-0315 Oslo, Norway.

[2,9,14,16,17,28], to give a more stable and reliable flow [9,14,19] or to obtain higher flow rates and reduced separation times [6]. The use of HPLC pumps with in-line application of a voltage, as opposed to reservoirs, also simplifies the use of solvent gradients in CEC [13,17,18,20,22–24,26,28,29].

It has been shown previously by our group that in-line application of an electric field generates increased conductivity [21,30,1]. The use of high electric field strengths is highly desirable for electrically assisted capillary separation systems. However, the maximum field strengths that may be applied are limited due to the high currents generated. Therefore investigation into the increased conductivity when using in-line systems is of great importance in order to be able to maximize the electric fields that can be applied over the column.

It is well known that in any capillary separation system with an applied electric field, such as CE, CEC and electric field-assisted liquid chromatography (EFLC), the conductivity of the running buffer/mobile phase will increase with higher applied voltages. This is due to Joule heating effects, and these effects have been thoroughly studied in recent years [32–47]. We have earlier suggested [21,30,1] that the conductivity changes observed within an in-line system cannot be due to Joule heating alone. The most apparent reason is perhaps that the conductivity changes shown within an in-line system are often dependent upon the direction of the current. Even though these conductivity changes cannot be explained by Joule heating alone, the high currents often experienced within in-line systems will always give rise to Joule heating which inevitably will result in a positive feedback, also called autothermal effect [32], leading to increasing conductivity. This paper details two main aims of research. Firstly it was necessary to find a suitable method to separate the influence of Joule heating on the conductivity, from other sources of conductivity changes observed within in-line separation systems. For this reason, we have used the theory that within a standard CE set-up the only source of conductivity changes is arising from Joule heating. CE experiments were therefore performed in order to estimate the conductivity change at a given power per unit of length, P/L (W m^{-1}). The pressure driven in-line experiments were then performed using the same capillary and the same instrument, while applying the same cooling to mimic the standard CE system. The conductivity changes observed within the CE experiments could then be subtracted from the data generated with the in-line experiments, thereby resulting in only non-Joule heating generated conductivity changes being observable at given P/L.

The second aim was to generate a method for estimating the potential pH changes in an in-line system. Within in-line systems, when OH$^-$ and H$_3$O$^+$ ions are created at the electrode surface, they cannot be diluted into a relatively large volume (as with reservoir systems) but instead they must enter the column. Changes in pH can therefore be difficult to prevent in such separation techniques with an applied electric field, because the most logical solution to the problem (increasing the buffer concentration) shall give rise to problems with increased current (and potentially an even larger change of pH). The potential pH change is important for many separations in itself, but it is also of interest because it can give information about the role of

the electrolysis of water for the conductivity changes within the in-line systems, which until now has still not been clear.

Throughout this study the general method for estimating the pH within the capillary was to use a pH indicator solution and measure the absorption changes with a DAD detector. We used cresol red/TRIS solution as a pH indicator because of the unique property of having two pH-dependent wavelength regions with opposite pH responses. This property allowed us to measure pH as a function of the difference in absorbance between these two wavelength regions, rather than measuring a single wavelength, which allowed the method to be less sensitive to drift and noise affecting the entire spectrum. The temperature dependence of the pH indicator was also examined in this study. This was possible as the temperature could be estimated from the standard CE experiments and assumed to be similar in both the CE and the in-line experiments at given P/L. Therefore the temperature effect could thus be subtracted before determining the pH. The mean temperature within the CE capillary was calculated using the change in conductivity at given P/L using the standard CE experiments and a method first described by Burgi et al. [37]. The conductivity (κ) can be calculated from the voltage (V), current (I) and the cross section area (A) and length (L) of the column:

$$\kappa = \frac{IL}{VA} \tag{1}$$

It should be noted that this equation is applicable for a homogeneous, stationary liquid medium. As in the CE process, the buffer solution is in motion and variation in ionic concentration and species concentration are present in the capillary. The conductivity depends on the velocity of the conducting ions, which depends upon the viscosity of the solution, and in turn depends upon the temperature. If the rate at which the viscosity and thereby the conductivity increases with temperature (the thermal coefficient of electrical conductivity (γ)) is known, then the mean temperature (T_{Mean}) in the solution can be calculated using the following equation:

$$T_{Mean} = T_0 + \frac{\kappa_T/\kappa_0 - 1}{\gamma} \tag{2}$$

T_0 is the original temperature of the solution and κ_T and κ_0 are the conductivities at elevated temperature and at original temperature, respectively. Burgi et al. [37] determined κ_0 by means of applying a low voltage (5 kV), recording the current and calculating the conductivity under the assumption that the Joule heating could be neglected at the low voltage. Kok [47] improved the method by using a κ as function P/L plot and extrapolate it to $P/L = 0$ to determine κ_0. Evenhuis et al. [42] recently improved the method further by utilizing conductance (G) instead of conductivity. G is used by the authors as the inverse of resistance (R):

$$G = \frac{1}{R} = \frac{I}{V} \tag{3}$$

As for Eq. (1), Eq. (3) is applicable for a homogeneous, stationary liquid medium.

However, in this work κ is used rather than G because we consider the change in conductivity an important topic in it self. For temperature measurements only, the use of G is more convenient and we also suggest plotting G against P rather than P/L. When the same capillary and experimental set-up is used no information about the capillary dimensions is then required for temperature calculations.

In Refs. [37,42] $\gamma = 0.0205\,°C^{-1}$ was used, but it was pointed out by Evenhuis et al. [42] that, because of the rather small effect of the stoichiometry of the solution [48], the use of $\gamma = 0.02\,°C^{-1}$ could be an acceptable approximation in most cases. We have here used $\gamma = 0.02\,°C^{-1}$. In our experiments the temperature was set to $20\,°C$ giving the expression used here for temperature determination:

$$T_{Mean} = 20\,°C + \frac{\kappa_T/\kappa_0 - 1}{0.02} \tag{4}$$

2. Experimental

An HP^{3D} CE instrument (Agilent, Waldbronn, Germany) was used in this study due to its ability to measure absorbance, voltage, current and temperature within the CE cassette simultaneously. This was crucial for our experiments. Furthermore the HP^{3D} DAD detector was required to allow different wavelengths to be measured simultaneously. Most importantly though, this instrument allowed the cooling mechanism of the capillary to be similar for both the CE experiments and the pressure driven experiments with in-line application of a voltage (referred to as the "in-line experiments" from here on).

The same batch of cresol red/TRIS solution was used throughout all experiments. Hundred milligrams per liter cresol red (Aldrich, Steinheim, Germany) was prepared from 10 mM TRIS (Aldrich, Steinheim, Germany) buffer, pH 7.5. The TRIS buffer was adjusted to the desired pH with 25% HCl. The pH of the final solution was recorded immediately prior to all experiments, and was found to be pH 7.7. Fused silica capillaries, 50 μm i.d., were from Polymicro Technologies, Phoenix, AZ, USA. Before use, the capillaries were rinsed with buffer solution.

In the CE experiments the only raw data of interest was the current at different voltages. Each CE run started with 5 min of rinsing under low pressure (50 mbar) followed by 2 min of applied voltage. The voltage and current were recorded and P/L and κ were calculated for further calculations. For the in-line experiments each run was initiated by pumping the solution through the capillary at 2 μL min^{-1}. Once a stable baseline was achieved, the voltage was applied until a steady baseline was obtained again (2–5 min). After this the change in ΔAbs was recorded.

A syringe pump (Isco 100DM, Lincoln, NE, USA) was used together with the CE instrument for the in-line experiments. An HP^{3D} CE together with a solvent delivery system has also previously been used by Apfel et al. [15] and Hennessy et al. [29].

For the in-line experiments a CE cassette normally used for CE-MS was utilized. The CE-MS cassette which is commonly used to get flow out of the CE for detection was here instead
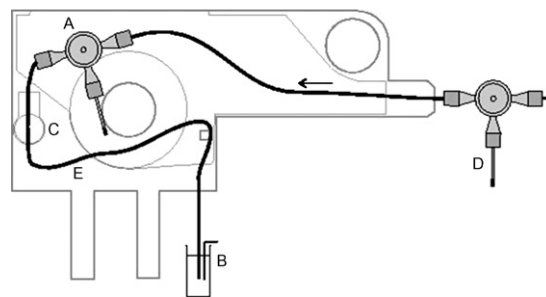

Fig. 1. Set-up of the in-line experiments using a CE-MS cassette. The inlet vial of the CE instrument was used as outlet vial for in-line work as the CE instrument can only apply voltage to the inlet vial. A Pt wire inside the PEEK, poly(etherether ketone), tee was used as inlet electrode and was connected to the electrode normally used as outlet electrode in the CE instrument. The outlet electrode of the CE instrument was used, rather than a ground outside the instrument, because it enabled current measurements by the instrument. A = inlet electrode (grounded); B = outlet electrode, in vial (high voltage); C = detector window; D = split for purge; E = capillary used to measure conductivity; the arrow indicates the direction of the pressurized flow.

used to pump liquid into the capillary (Fig. 1). Some practical considerations regarding this are given below.

The most practical and safe method was to apply a voltage to the outlet vial of the CE instrument and ground the inlet in-line electrode. However, within the CE instrument used here, the voltage is usually applied to the inlet vial. As a consequence the capillary had to pass the detection at the outlet side of the cassette, then make a turn and end in the vial normally used as inlet (Fig. 1). For practical reasons it would have been easiest to place the in-line inlet electrode outside the CE instrument just prior to the flow entering the cassette, however the length of the capillary would, with such a set-up, be at least 50 cm and with the available 30 kV high voltage supply, only a maximum electric field of 0.6 kV cm^{-1} could have been applied. By instead placing the inlet electrode inside the CE cassette as close to the detector as possible we could use a capillary as short as 25 cm. In order to put the inlet electrode inside the cassette some minor alterations to the cassette were required. As it was essential for the study to use the same capillary in both the CE and the in-line set-up, a 25 cm capillary would have been too short for the CE set-up and therefore a 32 cm, 50 μm i.d. capillary was finally used in both the CE and the in-line set-up.

Further, it was found that due to the design of the CE instrument, the in-line inlet electrode had to be grounded at the electrode normally used as the outlet electrode in the CE instrument. This was to enable the proper measurement of the electric current by the instrument. In all set-ups using a CE cassette, as in these experiments, there are areas of the capillary that are cooled with forced air flow inside the cassette and other areas, inside the detection section and outside the cassette, that has no forced cooling. We estimated that in the CE experiments ∼12 cm and in the in-line experiments ∼14 cm of the total 32 cm capillary was cooled by forced air, which we considered acceptable for comparisons.

Unlike in the CE experiments, during the in-line experiments the difference in absorbance of the cresol red/TRIS solution between 430 and 573 nm (ΔAbs) was recorded, as well as the

voltage and the current. During these experiments, as well as throughout both pH and temperature calibrations, it was ensured that the ΔAbs was measured relative to a fixed starting point.

The ΔAbs of cresol red is both pH and temperature sensitive; therefore calibration of both was essential. For the pH calibration, a plug of the standard pumping solution was injected, containing different concentrations of added OH^- or H_3O^+ ions. The solutions containing added OH^- or H_3O^+ ions were prepared by the addition of measured volumes of NaOH (1 M) or HCl (1 M) to a 50 mL volume of the original pumping solution. Throughout the calibrations, the same flow rate (2 μL min^{-1}) as used for the in-line experiments was applied, and the sample plug was injected for ~2 min using a large (~50 μL) loop. The change in ΔAbs between the original pumping solution and the plug with added base or acid was then recorded.

The temperature calibration was conducted by means of changing the temperature inside the cassette while monitoring the change in ΔAbs between 20 °C and the new set temperature. To ensure that the pumping liquid entering the column was already at the desired cassette temperature, an extra length of capillary (30 cm) was inserted into the CE-MS cassette and connected prior to the inlet electrode to act as a preheating device.

3. Results and discussion

3.1. Joule heating

As outlined above, the conductivity changes arising from Joule heating were separated from other sources of conductivity changes. This was done by comparing the conductivity changes obtained within a standard CE set-up with those generated in an in-line system with an analogous cooling system. While equivalent cooling was applied to the pressure driven in-line system, the temperature can still be expected to be slightly lower, due to the increased flow of cooler liquid that is being pumped into the column. Therefore, the mean temperature of the standard CE capillary should be considered as a maximum temperature of the in-line experiments. However, it shall be shown through our results, that the small difference

does not give rise to any significant importance in the overall results.

In Fig. 2A conductivity is plotted as a function of effect per unit length, with either positive or negative polarity applied to the outlet electrode in an in-line system as well as in a CE system. The evident conclusion arising from Fig. 2A is that the conductivity changes observed with the in-line experiments are much greater than those observed in the standard CE experiments. Also, it can be observed that the conductivity in the standard CE experiments is virtually independent upon the direction of the current, while using the in-line set-up the conductivity was strongly dependent upon the current direction.

This result was not unexpected considering our previous research [21,30,1]. It has previously been proposed that the polarity dependence of the conductivity results from the use of buffers that contain two ions with differing electrophoretic mobilities, as has been applied here with slower TRIS ions and more rapid chloride ions being present.

However, Joule heating alone should affect the conductivity equally, independently of the current direction. This supports the assumption that the conductivity changes observed in CE are primarily arising from Joule heating, while it cannot be the only source of conductivity change within an in-line set-up.

It is clear from Fig. 2A that Joule heating has a minor influence upon the conductivity change within the in-line system. It is also evident that the conductivity method (as a function of effect per unit length) commonly used to determine the temperature within CE capillaries, is not suitable for use with an in-line set-up.

In Fig. 2A and B it can be seen that when applying a positive voltage to the capillary outlet, the conductivity decreases with increasing *P/L* (or *E*). Through our experience, conductivity changes do, in general, differ depending upon the polarity, however, a decrease in conductivity at increasing field strengths is rarely observed. A decrease in conductivity is normally only observed when a fast ion has an electrophoretic mobility downstream, while a slow ion has an electrophoretic mobility upstream, as in this case.

The conductivity as a function of power per length unit, using standard CE methods, has been linearly plotted in earlier work
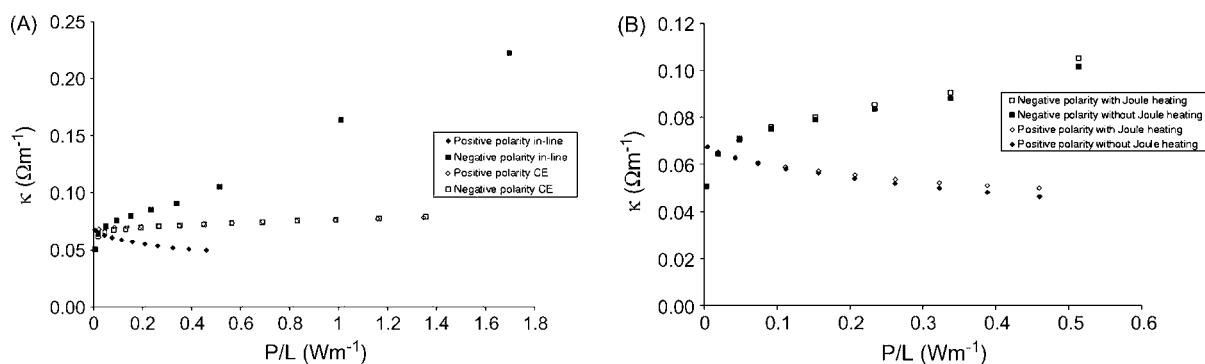
Fig. 2. (A) Conductivity as a function of W m^{-1} in standard CE and in the in-line set-up, with positive or negative voltage applied to the outlet electrode. The same 32 cm, 50 μm i.d. silica capillary, reference solutions (cresol red/TRIS solution, as described in Section 2) and flow rate = 2 μL min^{-1} were used throughout all experiments. (B) Conductivity as a function of W m^{-1} with voltage applied in-line. Open markers show the original data, while filled markers show the data where the contribution of Joule heating to conductivity change has been subtracted.

[37,42,47]. With respect to these previous studies we found good linearity for a large portion of the *P/L* range, as shown in Fig. 2A. However, at the lowest *P/L* regions ($<0.03\,W\,m^{-1}$) the conductivity dropped dramatically. This was even more apparent for the experiments with a negative voltage applied to the outlet electrode. The lack of linearity at low *P/L* values has, to the best of our knowledge, not been previously reported. These results support the choice of using a plot method rather than a single measurement at low voltage, in order to determine the conductivity at the temperatures unaffected by Joule heating (κ_0).

Using the linear region at *P/L* ($W\,m^{-1}$) >0.3, a κ_0 value of $0.0693\,S\,m^{-1}$ could be determined as the intercept. κ_0 was used below to determine the temperature in the capillary at a given *P/L*. Furthermore, κ_0 was also used to generate a plot for the conductivity changes within the in-line set-up, with and without the effects of Joule heating (Fig. 2B). The difference between κ_0 and the given κ value in the CE experiments was then subtracted from the κ values of the in-line experiments.

Using the CE data presented in Fig. 2A and the κ_0 value, the mean temperature as function of *P/L* could thus be calculated using Eq. (4). Linear regression gave the following empirical relationship between temperature and *P/L*:

$$T_{mean} = 5.1\frac{P}{L} + 20 \tag{5}$$

3.2. pH changes

3.2.1. Calibrations

The detection window was created 8 cm from the inlet electrode, and the absorption variation was recorded upon the application of an electric field to the in-line set-up. Calibration for the correlation of $\triangle Abs$ to the added concentration of OH^- and H_3O^+ ions was performed, allowing the estimation as to the change in OH^- and H_3O^+ concentration within the capillary, resulting from electrode reactions.

Cresol red's UV response is however not only pH sensitive, but also temperature sensitive, and cresol red/TRIS solutions have previously been used as temperature probes in multi-cuvettes [49]. Due to the increased temperatures, arising from Joule heating, within the in-line experiments, the $\triangle Abs$ as a function of temperature rise had to be subtracted from the exper-imental result to allow the data to show only the UV response arising from the OH^- and H_3O^+ ions formed in the electrode reactions. A plot of $\triangle Abs$ as a function of temperature followed a linear relationship.

The temperature at given *P/L* was already calculated from the standard CE experiments, and as mentioned previously the CE and in-line experiments were performed using the same capillary cooling system. However, the temperature measurements derived from conductivity for the standard CE experiments, are average temperatures. The correct temperature to employ when compensating for temperature effects on $\triangle Abs$ is actually the local temperature found in the detection window. The temperature found locally in the detection window may differ from the average temperature, due to the fact that the CE instrument does not cool this section, and the added effect from the removal of the polyimide coating. It can be observed from the results below that temperature differences within the in-line experiments were not significant, and therefore it was believed that the average temperature difference and that found in the detection window were relatively comparable.

Synergy effects, from the combination of pH and temperature, upon the absorption of cresol red may be expected, and therefore calibration of added OH^- and H_3O^+ concentrations with respect to $\triangle Abs$ was performed at 20, 25 and 30 °C (Fig. 3). The $\triangle$ absorption was measured using the absorption of a large injected plug of reference solution with controlled added OH^- or H_3O^+ concentrations, relative to the unmodified reference solution. In these experiments a six-port injector valve was mounted between the pump and the split prior to the CE cassette. The calibration was primarily performed using $\triangle Abs$ as a function of added OH^- or H_3O^+ concentration, rather than as a function of pH. This was because we wanted to relate to ions formed at the electrode surface.

Some synergy effects were observed upon the addition of an acid (Fig. 3). A lower response was observed upon the large addition of H_3O^+ ions at high temperatures, while the response on the addition of OH^- was virtually equal for all three temperatures (Fig. 3B).

Due to these synergy effects, consideration was given to the generation of a multivariate calibration with $\triangle Abs$ as a function of added OH^- or H_3O^+ concentration, and as a function of temperature. However, it was found from the in-line experiments
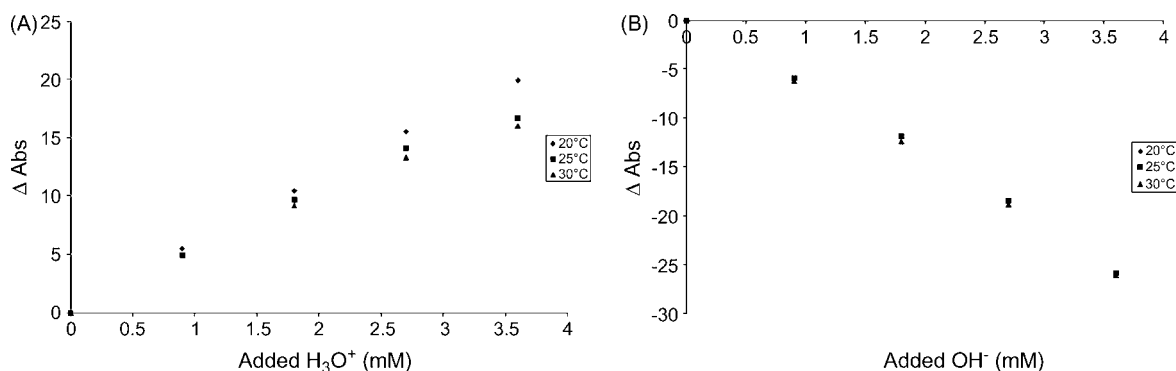
Fig. 3. (A) Calibration of $\triangle Abs$ (430 and 573 nm) as a function of added H_3O^+ to the reference solution. Capillary, reference solution, flow rate as in Fig. 2A. (B) Calibration of $\triangle Abs$ (430 and 573 nm) as a function of added OH^- to the reference solution. Capillary, reference solution, flow rate as in Fig. 2A.

that the temperature increase was relatively low and therefore the data from 20 °C was used for calibration. It will also be shown in Section 3.2.2 that this simplification has no significant impact on the conclusions drawn from the study.

3.2.2. Changes in OH^- and H_3O^+ concentrations

During the in-line experiments, the increase in concentration of either OH^- or H_3O^+ ions resulting from electrode reactions was estimated using the ΔAbs values. These concentrations were then plotted as function of current as shown in Fig. 4. The direct influence from Joule heating to the ΔAbs was subtracted prior to calculation, using the temperatures generated from the standard CE experiments described above. The calibration curve at 20 °C (Fig. 3) was employed for both the OH^- and H_3O^+ calibrations, with the highest temperature observed during the in-line experiments being 21.8 °C. Within Fig. 4A, the grey markers represent experiments under temperatures between 22.7 and 28.8 °C; these data were excluded from this study. The data points were however, primarily excluded as the calibration was performed only up to 3.6 mM. At larger added concentrations of HCl the pH was found to drop dramatically due to the decreasing buffer capacity of the TRIS buffer, and subsequently the ΔAbs values no longer followed the same trend. Therefore the concentrations obtained from the grey data points shown, can only be known to be above 3.6 mM.

A theoretical maximum plot line was added to Fig. 4A and B. This was done to demonstrate how the concentration within the capillary would change if, at the given current, each electron would form an OH^- and an H_3O^+ ion from water at the electrodes, which then would be diluted into the given flow. However, in both Fig. 4A and B the experimental data is above the theoretical maximum. This result is believed to illustrate that the dominant electrode reaction products are OH^- or H_3O^+ ions. The larger experimental values than the theoretic are believed to be a result of inhomogeneous distribution of the concentration changes along the capillary. Previous results [30] suggest that the concentration changes are larger in the beginning of the

capillary, where the detection window is placed in the present experiments.

This result indicates that the virtually exclusive electrode reaction in the system is water forming OH^- or H_3O^+ ions according to

$$2H_2O + 2e^- \rightarrow H_2 + 2OH^-, \qquad 2H_2O \rightarrow O_2 + 4H^+ + 4e^-$$
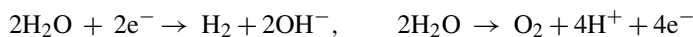
The difference in conductivity between the standard CE and the in-line set-up appears to be a consequence of the presence of more formed OH^- and H_3O^+ ions within the in-line set up. When using an in-line system, the formed ions cannot be diluted in a relatively large volume as when using a standard CE set-up, with buffer vials. Within the in-line set-up the formed ions will instead increase the ion strength of the mobile phase inside the capillary, which shall result in an increased conductivity. The increase in concentration of OH^- or H_3O^+ ions must however also result in the formation of an equivalent quantity of oppositely charge ions. For example a 3 mM increase in H_3O^+ ions, which according to Fig. 4A is formed at $\sim$10 μA, must be accompanied by a 3 mM increase in negative buffer ions, otherwise the column would not be electro-neutral. This increase in concentration of oppositely charged ions, arising from the buffer, is essential for the formation of OH^- and H_3O^+ ions, and the increase in buffer ion concentration therefore ultimately determines the change in conductivity within in-line set-up systems.

We have earlier demonstrated [30] that if the only two processes present within an in-line set-up were the pressure driven flow and the electrophoretic velocity of the buffer ions, then there would be (at electric fields in the range of 1 kV m^{-1} and above) a large increase in the number of ions moving upstream under their own electrophoretic velocity. In such a simplified system, the increase was shown to be greatest at the inlet of the electric field and close to the capillary wall, as a result of the parabolic flow profile. The ions with an electrophoretic velocity downstream would however generate an increase in concentration after the outlet. This would not have any influence on the conductivity due to the increase in ion concentration being outside the electric field.
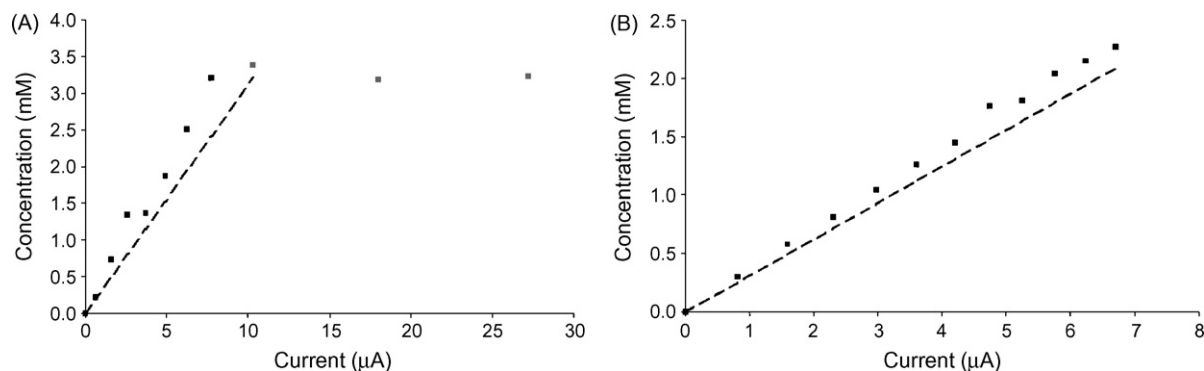
Fig. 4. (A) Added H_3O^+ concentration 8 cm from the inlet electrode as a function of current when applying negative voltage at the outlet electrode. The dashed line illustrates the theoretical maximum concentration of formed H_3O^+ ions calculated from the current and the volume flow. The concentration change illustrates apparent addition of H_3O^+ ions rather than added free H_3O^+ ions in the solution because of the buffer capacity of the solution. (B) Added OH^- concentration observed 8 cm from the inlet electrode as a function of current, upon application of a negative voltage at the outlet electrode. The dashed line illustrates the theoretical maximum concentration of formed OH^- ions calculated from the current and the volume flow. The concentration change illustrates apparent addition of OH^- ions rather than added free OH^- ions in the solution because of the buffer capacity of the solution.

Through most of our previous work on conductivity changes within in-line systems, a non-buffering salt solution has been employed. We have found [21] that there has been no major difference in the conductivity change when using buffering or non-buffering systems, and this has also been observed in this study. When OH^- or H_3O^+ ions are formed at the electrodes, within a buffering solution the ions can pass their charge on to the buffer. The buffer ions always display far lower mobilities than OH^- or H_3O^+ ions, meaning that if the buffer transports the charge, then the current would be lower than if transported by the faster moving OH^- or H_3O^+ ions. The mobility of the ion transporting the charge is however, not the major factor for conductivity changes within in-line systems. The major factor is instead, the fact that an in-line system allows the increase in concentrations of OH^- or H_3O^+ ions, and buffer ions. The capacity of the buffer in the mobile phase therefore has an influence upon the conductivity within an in-line system, however, this influence is of secondary importance.

3.2.3. Changes in pH

During the calibration shown in Fig. 3, the pH for each solution was directly measured, making it possible to calculate and then plot the pH as function of current within the in-line experiments (Fig. 5). The pH of the original solution was slightly lower than the pK_a of TRIS, and therefore the pH decreased further (as function of current) using positive as opposed to negative polarity. Under the assumption that OH^- or H_3O^+ ions are formed during almost all electrode reactions, as suggested by the results in Fig. 4, the change in pH of a solution lacking buffering capacity would theoretically be ~2.5 and ~11.5 at either end of the column, with a current of only 10 μA.

Fig. 5 may show the apparent pH change in the in-line system, but may not give the pH change of the whole system affecting conductivity. When the applied current is high, the radial distribution of pH is inevitable because of the parabolic flow profile. The pH of the sample solution near the wall should be very low or very high due to hydrolysis, depending on the measurement position relative to the electrodes. Thus the observed pH change in Fig. 5 may be underestimated because the axial photometric signal is volume-weighted.

Further, we suggest that as well as a pH variation from the inlet to the outlet being formed within the capillary, the buffer ions may be accumulated close to the capillary wall where the flow velocity is low [30]. Thereby, radial pH variations within the separation column may occur, which could have negative effects upon the separation. Therefore, a high buffer capacity seems of great importance when using in-line application of electric fields in capillary separations. Using buffers in high concentrations will, of course, result in higher currents and the formation of more OH^- or H_3O^+ ions. On the basis of our experience we believe that this can be a difficult problem to solve in some cases. Often solutions with higher concentration than ~10 mM cannot be employed when electric fields higher than 1 kV cm^{-1} are applied due to high currents generated. With such low buffer concentrations, the pH differences along and perhaps also across the column, could be a problem.

If the characteristic increase in conductivity using in-line systems can be avoided or minimized, this would facilitate the elimination of many of the common problems associated with in-line systems. Through the precise control of operating parameters or perhaps employing buffer reservoirs or flow splitting [1] at the inlet electrode, the increase in conductivity can often be minimized and therefore the performance of the system improved.

4. Conclusions

The most important conclusion is that the observed conductivity change in in-line systems is mainly due to the pH change by electrolysis of water, but not due to the temperature change in the capillary column.

Acknowledgements

References

[1] B.O. Eriksson, M.B.O. Andersson, L.G. Blomberg, J. Chromatogr. A 1119 (2006) 170.
[2] T. Tsuda, Anal. Chem. 59 (1987) 521.
[3] T. Tsuda, Anal. Chem. 60 (1988) 1677.
[4] E.R. Verheij, U.R. Tjaden, W.M.A. Niessen, J. van der Greef, J. Chromatogr. 554 (1991) 339.
[5] T. Tsuda, LC–GC Int. 5 (1992) 26.
[6] M. Hugener, A.P. Tinke, W.M.A. Niessen, U.R. Tjaden, J. van der Greef, J. Chromatogr. 647 (1993) 375.
[7] S. Kitagawa, T. Tsuda, J. Microcol. Sep. 6 (1994) 91.
[8] T. Eimer, K.K. Unger, J. van der Greef, Trends Anal. Chem. 15 (1996) 463.
[9] J.T. Wu, P. Huang, M.X. Li, D.M. Lubman, Anal. Chem. 69 (1997) 2908.
[10] S. Kitagawa, A. Tsuji, H. Watanabe, M. Nakashima, T. Tsuda, J. Microcol. Sep. 9 (1997) 347.
[11] C. Chaiyasut, S. Kitagawa, H. Wada, T. Tsuda, Anal. Sci. 16 (2000) 413–416.
[12] Y. Zhang, W. Shi, L. Zhang, H. Zou, J. Chromatogr. A 802 (1998) 59.
[13] B. Behnke, J.W. Metzger, Electrophoresis 20 (1999) 80.
[14] P. Huang, X. Jin, Y. Chen, J.R. Srinivasan, D.M. Lubman, Anal. Chem. 71 (1999) 1786.
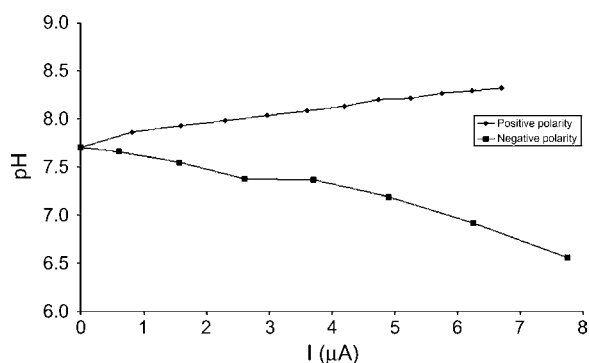

Fig. 5. pH as a function of current at positive and negative polarities in the in-line experiments. Capillary, reference solution, flow rate as in Fig. 2A.

[15] A. Apffel, H. Yin, W.S. Hancock, D. McManigill, J. Frenz, S.L. Wu, J. Chromatogr. A 832 (1999) 149.

[16] S. Nagaraj, H.T. Karnes, Biomed. Chromatogr. 14 (2000) 234.

[17] Q.H. Ru, J. Yao, G.A. Luo, Y.X. Zhang, C. Yan, J. Chromatogr. A 894 (2000) 337.

[18] T. Adam, K.K. Unger, J. Chromatogr. A 894 (2000) 241.

[19] M.B.O. Andersson, L.G. Blomberg, J. Sep. Sci. 24 (2001) 304.

[20] M. Stahl, A. Jakob, A. Von Brocke, G. Nicholson, E. Bayer, Electrophoresis 23 (2002) 2949.

[21] B.O. Eriksson, M.B.O. Andersson, L.G. Blomberg, J. Chromatogr. A 1010 (2003) 17.

[22] K. Zhang, Z. Jiang, C. Yao, Z. Zhang, Q. Wang, R. Gao, C. Yan, J. Chromatogr. A 987 (2003) 453.

[23] C. Yao, R. Gao, C. Yan, J. Sep. Sci. 26 (2003) 37.

[24] K. Zhang, R. Gao, Z. Jiang, C. Yao, Z. Zhang, Q. Wang, C. Yan, J. Sep. Sci. 26 (2003) 1389.

[25] E. Rapp, A. Jakob, A.B. Schefer, E. Bayer, K. Albert, Anal. Bioanal. Chem. 376 (2003) 1053.

[26] R. Nakashima, S. Kitagawa, T. Yoshida, T. Tsuda, J. Chromatogr. A 1044 (2004) 305.

[27] C. Yao, S. Tang, R. Gao, C. Jiang, C. Yan, J. Sep. Sci. 27 (2004) 1109.

[28] Z. Liang, J. Duan, L. Zhang, W. Zhang, Y. Zhang, C. Yan, Anal. Chem. 76 (2004) 6935.

[29] T.P. Hennessy, M. Quaglia, O. Kornysova, B.A. Grimes, D. Lubda, K.K. Unger, J. Chromatogr. B 817 (2005) 127.

[30] B.O. Eriksson, M. Dahl, M.B.O. Andersson, L.G. Blomberg, Electrophoresis 25 (2004) 3092.

[31] S. Kitagawa, H. Watanabe, T. Tsuda, Electrophoresis 20 (1999) 9.

[32] W.A. Gobie, C.F. Ivory, J. Chromatogr. 516 (1990) 191.

[33] N.J. Petersen, R.P.H. Nikolajsen, K.B. Mogensen, J.P. Kutter, Electrophoresis 25 (2004) 253.

[34] G.Y. Tang, C. Yang, C.J. Chai, H.Q. Gong, Langmuir 19 (2004) 10975.

[35] G.Y. Tang, C. Yang, C.J. Chai, H.Q. Gong, Anal. Chim. Acta 507 (2004) 27.

[36] S.P. Porras, E. Marziali, B. Gas, E. Kenndler, Electrophoresis 24 (2003) 1553.

[37] D.S. Burgi, K. Salomon, R.-L. Chien, J. Liquid Chromatogr. 14 (1991) 847.

[38] J.H. Knox, K.A. McCormack, Chromatographia 38 (1994) 207.

[39] J.H. Knox, K.A. McCormack, Chromatographia 38 (1994) 215.

[40] J.R. Veraart, C. Gooijer, H. Lingeman, Chromatographia 44 (1997) 129.

[41] T. Nishikawa, H. Kambara, Electrophoresis 17 (1996) 1115.

[42] C.J. Evenhuis, R.M. Guijt, M. Macka, P.J. Marriott, P.R. Haddad, Electrophoresis 26 (2005) 4333.

[43] C.J. Evenhuis, R.M. Guijt, M. Macka, P.J. Marriott, P.R. Haddad, Anal. Chem. 78 (2006) 2684.

[44] M.S. Bello, M. Chiari, M. Nesi, P.G. Righetti, M. Saracci, J. Chromatogr. 625 (1992) 323.

[45] M.S. Bello, P.G. Righetti, J. Chromatogr. 606 (1992) 103.

[46] A.S. Rathore, J. Chromatogr. A 1037 (2004) 431.

[47] W. Kok, Chromatographia 51 (Suppl.) (2000) 24.

[48] T. Isano, J. Chem. Eng. Data 29 (1984) 45.

[49] K. Schilling, G.A. Cumme, E. Hoffmann-Blume, H. Hoppe, A. Horn, Clin. Chem. 39 (1993) 251.

Differential amperometric determination of hydrogen peroxide in honeys using flow-injection analysis with enzymatic reactor

Rômulo Augusto de Abreu Franchini, Maria Auxiliadora Costa Matos,
Rosana Colombara, Renato Camargo Matos *

*NUPIS (Núcleo de Pesquisa em Instrumentação e Separações Analíticas), Departamento de Química, Instituto de Ciências Exatas,
Universidade Federal de Juiz de Fora, 36036-330 Juiz de Fora, MG, Brazil*

Abstract

Hydrogen peroxide (H_2O_2) present in honey was rapidly determined by the differential amperometric method in association with flow-injection analysis (FIA) and a tubular reactor containing immobilized enzymes. A gold electrode modified by electrochemical deposition of platinum was employed as working electrode. Hydrogen peroxide was quantified in 14 samples of Brazilian commercial honeys using amperometric differential measurements at +0.60 V vs. $Ag/AgCl_{(sat)}$. For the enzymatic consumption of H_2O_2, a tubular reactor containing immobilized peroxidase was constructed using an immobilization of enzymes on Amberlite IRA-743 resin. The linear dynamic range in H_2O_2 extends from 1 to 100×10^{-6} mol L^{-1}, at pH 7.0. At flow rate of 2.0 mL min^{-1} and injecting 150 μL sample volumes, the sampling frequency of the 90 determinations per hour is afforded. This method is based on three steps involving the flow-injection of: (1) the sample spiked with a standard solution, (2) the pure sample and (3) the enzymatically treated sample with peroxidase immobilized. The reproducibility of the current peaks for hydrogen peroxide in 10^{-5} mol L^{-1} range concentration showed a relative standard deviation (R.S.D.) better than 1%. The detection limit of this method is 2.9×10^{-7} mol L^{-1}. The honey samples analyses were compared with the parallel spectrophotometric determination, and showed an excellent correlation between the methods.
© 2007 Elsevier B.V. All rights reserved.

Keywords: Amperometry; Honey; Hydrogen peroxide; Peroxidase immobilized

1. Introduction

Honey contains a complex matrix of components, which presents a considerable analytical challenge. It is a liquid (or semiliquid) product made up of about 80% solids. It is produced by bees from the nectar of plants, as well as from honeydew. Bees and plants are the primary sources of components such as: carbohydrates (fructose, glucose, maltose and sucrose with traces of many other sugars depending on the floral origin), water, traces of organic acids, enzymes, aminoacids, pigment, and other components like pollen and wax which arise during honey maturation [1]. The chemical analysis of honey has three main purposes: (1) to determine the geographical and botanical origin, (2) verification of adulteration and (3) identification of pharmacological active compounds. The first and second points assist with cer-

tification of quality of the product which is commonly used as a food product; and the third area allows the examination of content for the use of honey in medicinal purposes.

Hydrogen peroxide is a product of many biological reactions catalyzed by several oxidase enzymes. All honeys contain peroxide, which imbues them with antibacterial properties. It has been shown that the antibacterial activity of honey occurs due to hydrogen peroxide generation [2–5]. Therefore, the determination of hydrogen peroxide is important in the characterization and selection of honey samples for its use as an antimicrobial agent. Hydrogen peroxide is generated by the enzyme glucose oxidase when honey is diluted and maximum levels of hydrogen peroxide encountered in the diluted honeys are in the range of 1–2 mmol L^{-1} [6]. Dilution is needed to decrease the acidity of the medium and for adjusting the pH for proper action of glucose oxidase. Weston [5] stated that the level of hydrogen peroxide in honey is essentially determined by the amount of catalase, which originates from flower pollen, and glucose oxidase, which originates from the hypopharyngeal glands of

---

* Corresponding author. Fax: +55 32 3229 3314.
  E-mail address: renato.matos@ufjf.edu.br (R.C. Matos).

bees. Manzoori et al. [7] have proposed the spectrofluorometric determination of hydrogen peroxide in several honey samples using crude extract of kohlrabi (*Brassica oleracea gongylodes*), which is a rich source of peroxidase. Franchini et al. [8] have described a versatile method for spectrophotometric determination of micromolar hydrogen peroxide in commercial Brazilian honey samples using a peroxidase immobilized on resin and the determination of trace metals using capillary zone electrophoresis without any treatment of honey samples.

Electrochemical determinations of hydrogen peroxide are generally performed by oxidation on a platinum electrode [9]. Depending upon the pH of the solution, a very high positive potential must be applied for the oxidation of hydrogen peroxide. The typical applied potentials are in the range of +0.7 to +0.9 V vs. SCE [10]. As a result, many substances can interfere with the measurements. The use of biosensors with immobilized enzymes such as peroxidase and catalase has been extensively investigated for hydrogen peroxide analysis, based on spectrophotometry [8,11], fluorometry [7,12], chemiluminescence [13,14] and electrochemical [15] techniques.

Strategies have been investigated to adapt quantification methods to the range of sample concentrations with low cost. In the analytical methods using enzymes, the reduction in cost of the determination is generally associated with reduced enzyme consumption. Recently, various ion-exchange resins have gained considerable attention not only for separation purposes but also as carriers of catalytic active substances. Considerable thought has been paid to their application for immobilization of enzymes [11,14,16–19]. The resins should meet several requirements. Their porous structure must be strong enough to withstand the enhanced pressure usually applied in forced flow bioreactors. Furthermore, the membrane material must be chemically and physically resistant. These requirements can be met by various aromatic and aliphatic polyamides. Therefore, resin prepared from these polymers is a suitable substrate for the immobilization of enzymes [20]. The covalent binding of the enzyme to the polymer matrix is one of the most prospective methods for immobilization.

In the present work, we describe a versatile method for differential amperometric determination of hydrogen peroxide in honey, using a gold microelectrode modified by electrodeposition of platinum, combined with an on-line tubular reactor containing peroxidase immobilized on resin (Amberlite IRA-743) without any treatment of samples. The concentration of the hydrogen peroxide in each sample was calculated based on the difference between the current measurement before and after the enzymatic treatment.

2. Experimental

2.1. Enzymes immobilization

The procedure adopted to immobilize the peroxidase enzyme was quick and very simple [15]. Amberlite IRA-173 resin was selected as support, because it has active amine groups in its chemical structure. The enzyme immobilization process begins with the addition of 100 μL of glutaraldehyde 0.1% to 250 mg of resin, and this mixture was stirred for 5 min. Subsequently, 200 units of enzymes were introduced into the mixture and stirred for an additional 10 min. In the next step, the resin was transferred to a length of tygon tubing (2.5 mm of i.d. and 25 mm long) with one of its extremities closed with a thin layer of glass wool to assemble the reactor. At this point, the other extremity of the tubing was then closed with glass wool. To adapt the enzymatic reactor to a FIA (flow-injection analysis) system, the tubing (0.8 mm of i.d) was attached at in each of its extremities with the aid of a small piece of silicone tubing (1.3 mm i.d. and 5 mm long). Finally, the reactor was washed with 10 mmol L^{-1} phosphate buffer solution (pH 7.0) to remove the excess of peroxidase.

2.2. Reagents and chemicals

All solutions used were of analytical grade. Hydrogen peroxide, mono- and di-hydrogen phosphates were obtained from Merck (Darmstadt, Germany). Solutions were prepared by dissolving the solids in distilled water that was also treated with a nanopure system. Commercial peroxidase (EC 1.11.1.7–115 U mg^{-1}) was obtained from Sigma (St. Louis, MO, USA). The Amberlite IRA-743 ion-exchange resin and glutaraldehyde were obtained from Aldrich (Milwaukee, WI, USA). Diluted solutions of hydrogen peroxide were prepared daily using deionized water.

2.3. Sample collection

This work was carried out on 14 samples in Brazil. The samples were stored in the dark at room temperature prior to analysis. For determination of hydrogen peroxide, 1 g of honey was dissolved in 10 mL of purified water and injected in the flow-injection system. Each sample was injected in triplicate.

2.4. Electrodes and instrumentation

The electrochemical cell comprised a platinum-modified gold electrode (3.0 mm diameter). Modification was done by electrochemical deposition of Pt (K$_2$PtCl$_6$ 2×10^{-3} mol L^{-1}, pH 4.8, at -1.00 V for 15 min). Microscopic observation of the electrodes after electrodeposition showed uniform platinum deposit, with a very rough surface. Electrodes so modified were stable for at least 1 week under intense use. The reference electrode was a miniaturized Ag/AgCl$_{(sat)}$ electrode constructed in our laboratory [21] and a stainless steel tube (1.2 mm i.d.) was used as auxiliary electrode.

In this work, a double channel flow system was employed. The solutions were propelled by pressurization, utilizing an aquarium air pump to avoid the undesirable pulsation observed when peristaltic pumps are employed [22]. Control of the flow rate was done by adaptation of the aquarium valve outlet with a pinched tygon tube inserted in the line. Teflon tubing of 0.5 mm i.d. was used throughout the flow system. The flow system used during the development of this work consisted of two lines, in first the sample was added in the detection system, in the second the sample was inserted in the line that

contain the enzymatic reactor before of the detection system. A potentiostat (μ-AUTOLAB) operating in the amperometric mode was employed for FIA measurement. Temperature control was achieved using a THERMOMIX 18 BU B thermostatic bath Braun Biotech. International. The system contains an aquarium air pump, a pinch valve, sampling loop, a tubular reactor (Ø = 0.25 cm and 2.5 cm of length) with peroxidase chemically immobilized in Amberlite IRA-743 resin, an electrochemical cell and the potentiostat.

2.5. Procedure

For amperometric detection of hydrogen peroxide, +0.60 V was found the most favorable potential to be applied to the gold electrode modified with platinum. The differential determination of this analyte requires at last three measurements, one involving the sample containing a standard addition in the channel without the reactor, a second containing just the sample in the channel without the reactor, and the third measurement involves a sample passes through the enzyme reactor. In the first case a signal, corresponding to hydrogen peroxide standard, hydrogen peroxide of the sample and plus the interfering components is registered. In the second case, the signal corresponds to the sample without hydrogen peroxide standard. In the third case, the signal corresponds to the sample without H_2O_2 (i.e., only to the interfering species). The calculated difference is compared with a H_2O_2 standard.

3. Results and discussion

Preliminary tests employing platinum-modified electrodes showed a very interesting behavior in the presence of hydrogen peroxide. The current enhancement was remarkable and in addition a decrease in the oxidation potential of hydrogen peroxide occurs when the electrodes are modified. Part of the increase in current can probably be attributed to the increase in the effective area of the electrodes. Observations with a microscope showed the formation of a very porous surface after platinum deposition.

3.1. Immobilized peroxidase and optimization of the flow system

To examine the efficiency of the tubular reactor containing immobilized peroxidase in a resin, experiments involving consecutive injections of hydrogen peroxide solution were performed. Responses of a gold electrode modified by electrodeposition of platinum for injections of 150 μL of hydrogen peroxide 1×10^{-5} mol L^{-1} for a channel without enzyme and with immobilized peroxidase were obtained. For a channel without enzyme a current of 0.17 μA was measured, while for the reactors with immobilized peroxidase currents of 0 μA was found. The reactor with immobilized peroxidase was effective, once it was able to eliminate completely the H_2O_2, a fundamental condition for applications in differential measurements.

The influence of parameters such as flow rate and sample volume was studied. Fig. 1A shows the amperometric
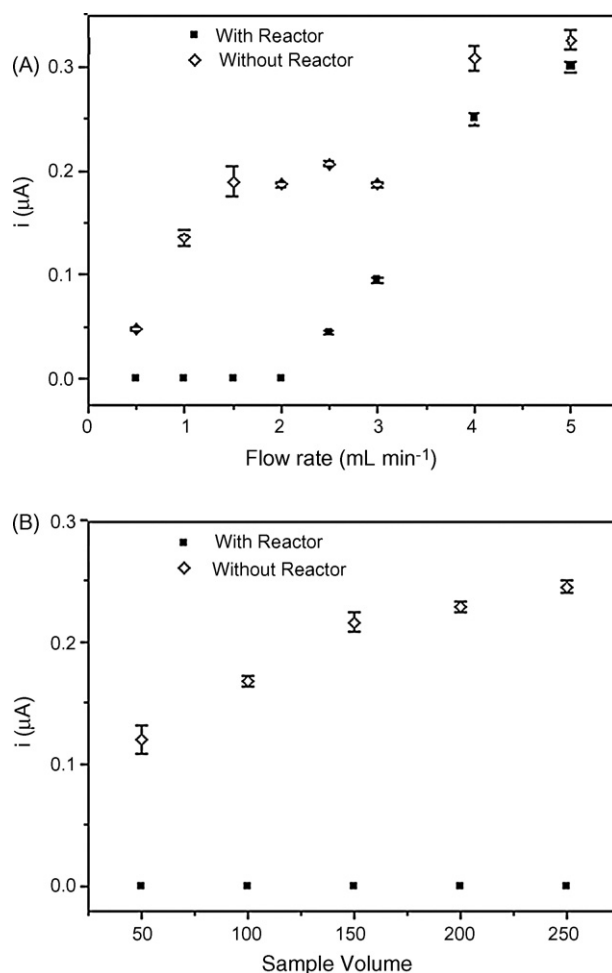

Fig. 1. Repetitive injections of hydrogen peroxide 1×10^{-5} mol L^{-1} to find the most suitable working conditions. (A) Flow rate from 0.5 to 5.0 mL min^{-1} and (B) samples volume injected from 50 to 250 μL. Measurements made with a gold electrode modified by electrodeposition of platinum. Applied potential, +600 mV vs. Ag/AgCl$_{(sat)}$.

responses of a gold electrode modified with platinum for injections of 150 μL of hydrogen peroxide 1×10^{-5} mol L^{-1}, as a function of the flow rate, varied from 0.5 to 5.0 mL min^{-1} with and without reactor. The signal remains virtually constant when the flow rate is changed from 1.5 to 3.0 mL min^{-1}. For high flow rates, the peroxidase immobilized in the tubular reactor was unable to eliminate completely the hydrogen peroxide. The elimination reaction rate has to decrease when the flow rate decreases. A flow rate of 2.0 mL min^{-1} was chosen as the most favorable, since it combines good reproducibility, high throughput (90 samples h^{-1}), lower consumption of carrier solution and complete elimination of the hydrogen peroxide.

Fig. 1B shows the influence of the sample volume on the analytical signal which was also evaluated. Loops with internal volumes varying from 50 to 250 μL were tested. When the volume of the sample is increased, the amperometric signal grew but the analysis time also increased, once the cell wash-out process also requires a longer time. The volume of 150 μL was selected as the working volume in the following experiments.
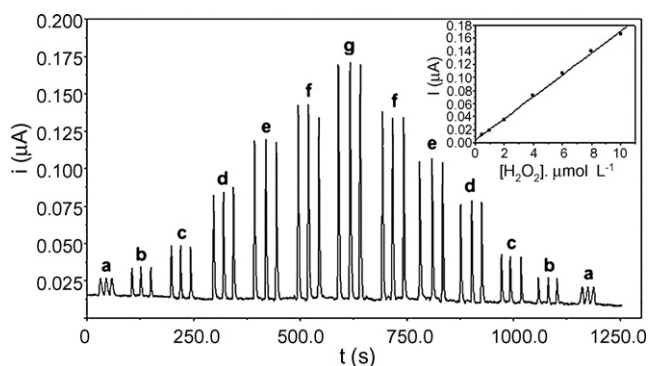
Fig. 2. FIA-amperometric measurements involving injections of 150 μL solution containing $1-10 \times 10^{-6}$ mol L^{-1} of hydrogen peroxide. The inset shows the respective calibration plot. Conditions: sample volume, 150 μL; flow rate, 2.0 mL min^{-1}; applied potential, +600 mV vs. Ag/AgCl$_{(sat)}$.

For all the volumes studied the peroxidase immobilized in the tubular reactor completely eliminated the hydrogen peroxide in the samples when used flow rate of 2.0 mL min^{-1}.

An important characteristic observed for the immobilized enzyme was a storage stability of at last 2 week under intense use with hydrogen peroxide standard. After this period, a decrease on the order of 30–45% of the enzyme activity was observed. When applied in the determination of hydrogen peroxide in honey, the enzymatic reactor showed a loss in the enzyme activity after 50 injections, requiring construction of a new reactor. When not in use, the reactors were stored in a freezer at $-20\,^{\circ}$C [8].

3.2. Calibration plot

Fig. 2 shows the amperometric response of the modified gold electrode for successive injections of 150 μL of hydrogen peroxide from (a) 1 μmol L^{-1} to (e) 10 μmol L^{-1}. The proportionality between the amperometric current and the hydrogen peroxide concentrations was confirmed from the calibration plot shown in the inset (i (μA) $= 3.77 \times 10^{-3} + 1.67 \times 10^{-2}$[H$_2O_2$](μmol L^{-1}); correlation coefficient, 0.999). Notice the very favorable signal-to-noise ratio, demonstrated by the very stable base line obtained for these low micromolar concentrations. The detection limit for the conditions adopted in present study was found as 2.9×10^{-7} mol L^{-1} (3 times the standard deviation of the blank) [23].

3.3. Determination of hydrogen peroxide in honey by flow-injection analysis

The samples to be analyzed were mixed on-line with buffer solution, used as the carrier solution. Fig. 3(A–C) shows three sequences of hydrogen peroxide analysis for three samples. Each group of three peaks corresponds to 150 μL injections of the honey sample containing (I) a standard addition (2×10^{-6} mol L^{-1} of the standard hydrogen peroxide), (II) the sample without treatment, and (III) the sample after enzymatic treatment with peroxidase immobilized. The standard addition

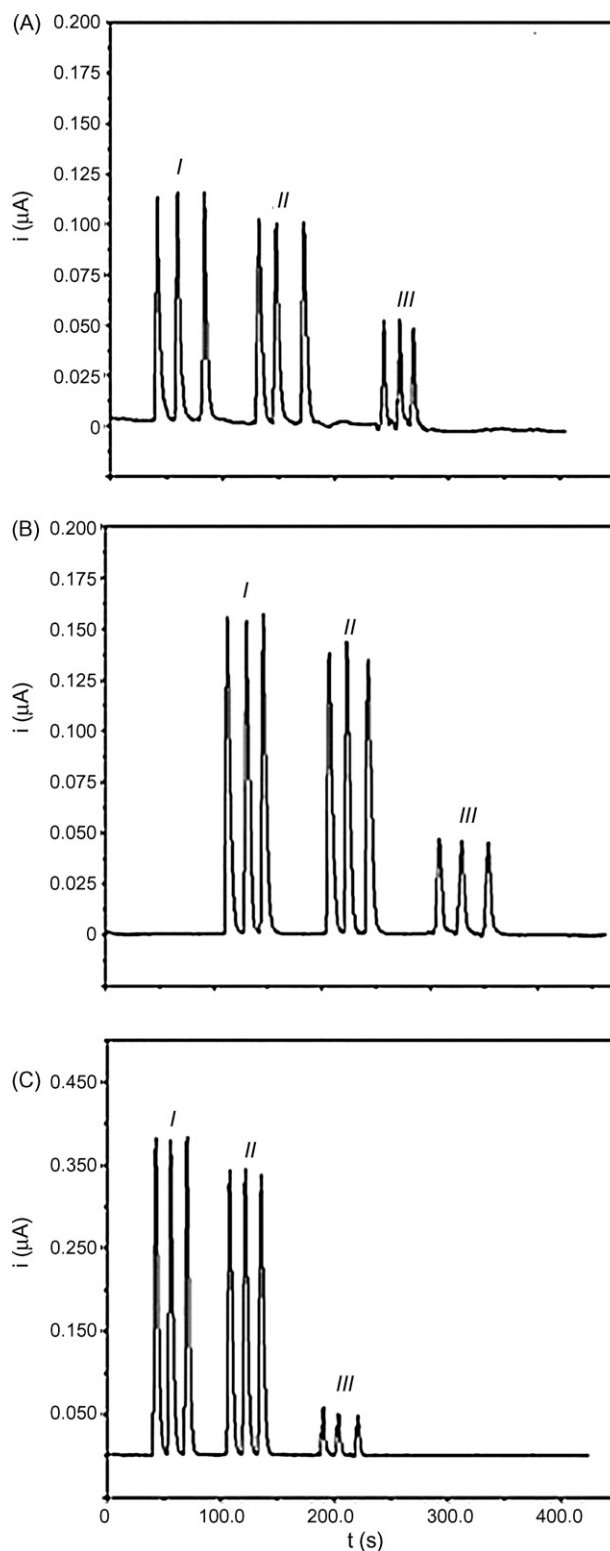Fig. 3. Differential FIA-amperometric measurements of hydrogen peroxide in three different samples of honey: (A) sample 3; (B) sample 4; and (C) sample 7. The triplicate injection correspond to: (I) 150 μL of sample $+2 \times 10^{-6}$ mol L^{-1} of the standard hydrogen peroxide solution, (II) 150 μL of the sample and (III) 150 μL of the sample after enzymatic treatment with peroxidase immobilized. Other conditions as in Fig. 2.

Table 1
Results obtained in analysis of hydrogen peroxide (mg kg^{-1}) in honey samples

Number of sample	Geographical origin	H$_2$O$_2$ (mg kg^{-1}) (amperometry)	H$_2$O$_2$ (mg kg^{-1}) (spectrophotometry)
1	Viçosa	150 ± 3	155 ± 2
2	Teresópolis	139 ± 3	135 ± 4
3	Teresópolis	56 ± 2	71 ± 6
4	Teresópolis	130 ± 3	131 ± 6
5	Teresópolis	30 ± 1	28 ± 1
6	Teresópolis	8 ± 0	9 ± 0
7	Teresópolis	205 ± 2	214 ± 4
8	Espírito Santo	157 ± 3	158 ± 5
9	Belo Horizonte	140 ± 2	139 ± 3
10	Tabuleiro	148 ± 4	142 ± 4
11	Coronel Pacheco	47 ± 1	62 ± 3
12	Coronel Pacheco	80 ± 2	91 ± 3
13	Volta Redonda	155 ± 4	147 ± 6
14	Juiz de Fora	37 ± 0	47 ± 1
Mean	–	103	109
V_{min}	–	8	9
V_{max}	–	205	214

method was carried out with the peaks (I) and (II) after subtracting of the height of the peak (III).

Table 1 and Fig. 4 compare the results of the analyses performed by amperometry developed in this work and using the spectrophotometric detection [8] for 14 different samples (in triplicates). Comparing the amperometry with gold/platinum electrode and spectrophotometry gives a slope and intercept very close to unity and zero, respectively. The confidence interval for the slope and intercept are (0.95 ± 0.03) and (8.14 ± 4.04) mg kg^{-1}, respectively, for a 95% confidence level. Taking into account these results, no significant differences between the three methods were observed, which strongly indicates the absence of systematic errors.

4. Conclusions

This work demonstrated the potentiality of the amperometric method using gold electrodes modified with platinum coupled with flow-injection analysis techniques, for the detection of hydrogen peroxide in honey using peroxidase immobilized in a tubular reactor. The very high sensitivity provided by amperometry, combined with the low volume of the flow cell, allows us to work with small sample volumes and at low concentrations. The association of amperometric detection with flow-injection analysis and the possibility of avoiding cumbersome processes such as separation, extraction and filtration substantially increase the speed of analysis. These advantages offer a very favorable way for the rapid analysis of hydrogen peroxide in honey samples (throughput of 90-samples h^{-1}).
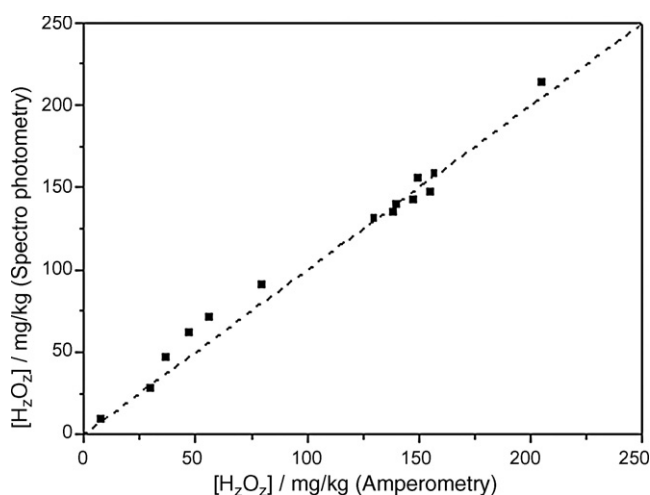
Fig. 4. Comparison of the results obtained by differential amperometric analysis for 10 different samples of rainwater using a gold microelectrode modified by the deposition of platinum and (A) differential amperometric analysis using a mercury microelectrode and (B) spectrophotometric methods for the analysis of hydrogen peroxide.

References

[1] R.F. Torres, J.L.P. Bernal, M.A.B. López, M.C. Mochón, J.C.J. Sánchez, A.G. Pérez, Talanta 65 (2005) 686.
[2] K.L. Allen, P.C. Molan, G.M. Reid, J. Pharm. Pharmacol. 43 (1991) 817.
[3] P.C. Molan, K.M. Russell, J. Apic. Res. 27 (1988) 62.
[4] M.J. Snow, M. Manley-Harris, Food Chem. 84 (2004) 145.
[5] R.J. Weston, Food Chem. 71 (2000) 235.
[6] L.M. Bang, C. Buntting, P. Molan, J. Altern. Complement. Med. 9 (2) (2003) 267.
[7] J.L. Manzoori, M. Amjadi, M. Orooji, Anal. Sci. 22 (2006) 1201.
[8] R.A.A. Franchini, C.F. de Souza, R. Colombara, M.A.C. Matos, R.C. Matos, J. Agric. Food Chem. 55 (17) (2007) 6885.

[9] J.E. Harrar, Anal. Chem. 35 (1963) 893.

[10] G.G. Guibault, G.L. Lubrano, Anal. Chim. Acta 64 (1973) 439.

[11] R.C. Matos, E.O. Coelho, C.F. de Souza, F.A. Guedes, M.A.C. Matos, Talanta 69 (2006) 1208.

[12] F. Schubert, F. Wang, H. Rinnerberg, Mikrochim. Acta 121 (1995) 237.

[13] R.W. Marshall, T.D. Gibson, Anal. Chim. Acta 266 (1992) 309.

[14] U. Spohn, F. Preuschoff, G. Blankenstein, D. Janasek, M.R. Kula, A. Hacker, Anal. Chim. Acta 303 (1995) 109.

[15] R.C. Matos, J.J. Pedrotti, L. Angnes, Anal. Chim. Acta 441 (2001) 73.

[16] A.C.A. Oliveira, V.C. Assis, M.A.C. Matos, R.C. Matos, Anal. Chim. Acta 535 (2005) 213.

[17] R.W. Marshall, T.D. Gibson, Anal. Chim. Acta 226 (1992) 309.

[18] P.D. Wentzell, S.J. Vanslyke, K.P. Bateman, Anal. Chim. Acta 246 (1991) 43.

[19] H. Hwang, P.K. Dasgupta, Mikrochim. Acta 3 (1985) 77.

[20] B.A. Watkins, D.D. Parrish, M. Trainer, R.B. Norton, J.E. Yee, J. Geophys. Res. 100 (1995) 22831.

[21] J.J. Pedrotti, L. Angnes, I.G.R. Gutz, Electroanalysis 8 (1996) 673.

[22] R.C. Matos, I.G.R. Gutz, L. Angnes, R.S. Fontenele, J.J. Pedrotti, Quim. Nova 24 (2001) 795.

[23] J.C. Miller, J.N. Miller, Statistics for Analytical Chemistry, Harwood, Chichester, 1992.

Spectrophotometric determination of hydrazine

Mary George [a], K.S. Nagaraja [a,*], N. Balasubramanian [b]

[a] *Department of Chemistry, Loyola Institute of Frontier Energy (LIFE), Loyola College, Chennai 600034, India*
[b] *Department of Chemistry, Indian Institute of Technology, Chennai 600036, India*

Abstract

Hydrazine is determined spectrophotometrically by forming the derivative 2,4-dinitrophenylhydrazine from 2,4-dinitrochlorobenzene. The formed dinitro derivative undergoes condensation reaction to form the hydrazone with *p*-dimethylaminobenzaldehyde (*p*-DAB). The resulting yellow colored product is stable in acidic medium and has a maximum absorption at 458 nm. The colour system obeys Beer's law in the range 0–7 μg of hydrazine in an overall volume of 25 mL. The molar absorptivity is calculated to be 8.1×10^4 L mol^{-1} cm^{-1} with a correlation coefficient of 0.998. The relative standard deviation is 1.7% ($n = 10$) at 6 μg of hydrazine. Interferences due to foreign ions have been studied and the method has been applied for the determination of hydrazine in boiler feed water.
© 2007 Elsevier B.V. All rights reserved.

Keywords: Hydrazine; 2,4-Dinitrophenylhydrazine; Spectrophotometry

1. Introduction

Hydrazine derivatives have found application as drugs, antioxidants, photographic developers, insecticides and blowing agents for plastics. It is used as a reducing agent and as analytical reagent for sugars and carbonyl compounds.

Besides being reactive and explosive, hydrazine is highly toxic. It may cause skin irritation and systemic poisoning [1]. Hydrazine is a suspected carcinogen [2] and the threshold limit value for workroom air is 0.1 ppm in the USA [3]. Because of these considerable toxicological effects and its industrial significance, the determination of hydrazine at microlevels is of interest.

Several methods have been described in the literature for the determination of hydrazine in trace amounts using different analytical techniques such as voltammetry [4], coulometry [5], gas chromatography [6], spectrofluorimetry [7], spectrophotometry [8,9] and titrimetry [10]. Many methods have been suggested for the determination of hydrazine based on its basic character or reducing property [11,12] Spectrophotometric methods are more useful for the determination of hydrazine at low concentration levels [13,14].

A kinetic spectrophotometric method has been reported [15] based on hydrazine inhibition effect on the reaction between bromate and hydrochloric acid. The method is based on the bleaching of methyl orange by the reaction products. A sensitive spectrophotometric method was reported based on the reduction of hydrazine to ammonium sulphate with Zn/H_2SO_4 reductor column. The formed ammonium sulphate is determined based on Berthelot reaction forming indophenol dye [16].

In this paper we present a highly sensitive method for the determination of hydrazine by the synthesis of 2,4-dinitrophenylhydrazine in situ. Hydrazine reacts with 2,4-dinitrochlorobenzene in the presence of sodium acetate under boiling condition to form 2,4-dinitrophenylhydrazine [17]. The formed product undergoes condensation reaction to form the hydrazone with *p*-dimethylaminobenzaldehyde. The formed yellow colored hydrazone is highly stable in acidic condition and has maximum absorption at 458 nm.

The present method is very sensitive for the determination of hydrazine in trace amounts. It is compared with the well known method based on the condensation of hydrazine with *p*-dimethylaminobenzaldehyde [18] and it is observed to have a higher sensitivity. The developed method has been applied successfully to the determination of hydrazine in boiler feed water.

* Corresponding author.
E-mail address: ksnagi@vsnl.net (K.S. Nagaraja).

2. Experimental

2.1. Apparatus

All absorbance measurements were made using Elico SL 177 Scanning Spectrophotometer with 1 cm matched glass cells.

2.2. Reagents

All chemicals used were analytical grade reagents. Oxygen free water was used for the preparation of solutions. This was prepared according to ASTM specification by boiling distilled water and then cooling it under a nitrogen atmosphere to keep it free of dissolved oxygen [19]. A stock solution of hydrazine (1000 μg mL^{-1}) was prepared by dissolving 0.4066 g of hydrazinium sulphate in water and diluting to the mark with water in a 100 mL volumetric flask. A suitable aliquot of the stock solution was further diluted to give a 2 μg mL^{-1} solution of hydrazine. A stock solution of sodium acetate (0.6%) was prepared by dissolving 600 mg of sodium acetate in water and diluting to 100 mL. It was further diluted to obtain a solution (0.06%). A stock solution of 2,4-dinitrochlorobenzene (0.1%) was prepared by dissolving 100 mg of 2,4-dinitrochlorobenzene in methanol and diluting to 100 mL with methanol. A suitable aliquot of the stock solution was further diluted to obtain 0.014% solution. (2,4-Dinitrochlorobenzene must be handled cautiously. It is a skin irritant. Any contact with skin should be washed with methylated spirit immediately.) A solution of *p*-dimethylaminobenzaldehyde (*p*-DAB) 1% was prepared by dissolving 1 g of *p*-dimethylaminobenzaldehyde with 100 mL of methanol water mixture in the ratio 1:3. Hydrochloric acid (2 M) was prepared by adding 182 mL of concentrated hydrochloric acid to 250 mL of water and diluting to 1 L. Diethylene glycol solution was prepared by diluting 25 mL diethylene glycol to 100 mL with distilled water to get 25% solution. Hydroxylamine solution (600 μg mL^{-1}) was prepared by dissolving 0.1264 g of hydroxyl ammonium chloride in 100 mL of distilled water.

2.3. Preparation of calibration graph

To a series of 50 mL glass beakers, 10 mL of sample containing 0–7 μg of hydrazine 2 mL of 0.06% sodium acetate, 2 mL of 0.014% 2,4-dinitrochlorobenzene, 3 mL of 25% diethylene glycol, 7 mL of methanol were added. The solutions were mixed well and heated on a hot plate till the volume is reduced to one half of the initial volume. To the hot solution 2 mL of 1% *p*-dimethylaminobenzaldehyde was added and mixed well. The contents were cooled to room temperature and transferred to 25 mL calibrated flasks. The beakers were washed with 2 M hydrochloric acid and transferred to the calibrated flasks and finally diluted to the mark with 2 M hydrochloric acid. The absorbances of the solutions were measured at 458 nm against a reagent blank to construct a calibration graph.

2.3.1. Determination of hydrazine in boiler feed water

A sample volume of 10 mL containing not more than 7 μg of hydrazine was subjected to analysis by following the procedure described under calibration graph.

3. Results and discussion

2,4-Dinitrophenylhydrazine serves as an excellent reagent for the characterization of carbonyl compounds. The formed hydrazone is colored, often more crystalline and less prone to oxidation and cyclisation.

The present investigation is based on the synthesis of 2,4-dinitrophenylhydrazine in situ by the reaction of hydrazine with 2,4-dinitrochlorobenzene in the presence of sodium acetate and diethylene glycol or triethylene glycol [17]. The reaction was carried by heating the contents on a hot plate till the volume is reduced to one half of the initial volume. The formed product undergoes condensation reaction with *p*-dimethylaminobenzaldehyde in acidic condition to form a yellow colored hydrazone (Fig. 1) which has an absorption maximum at 458 nm (Fig. 2) in acidic condition.
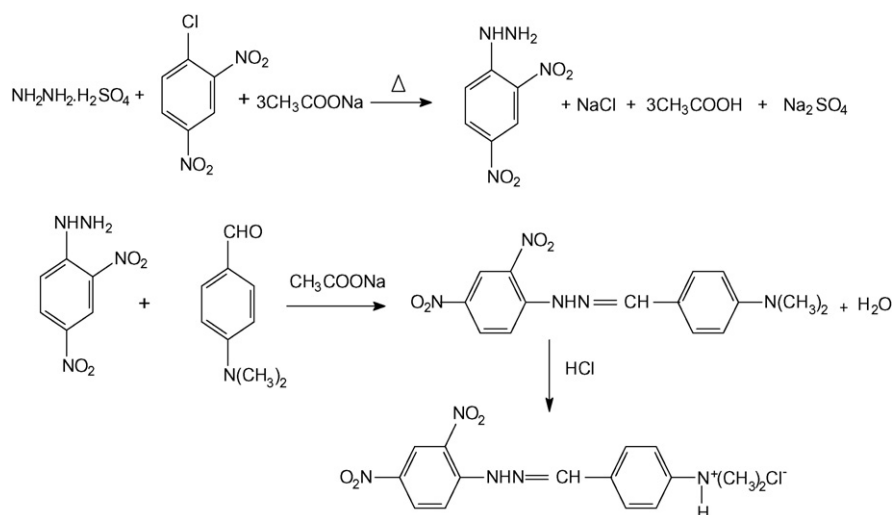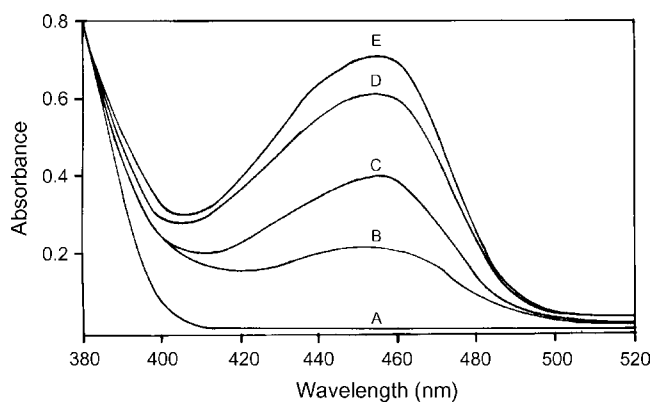

Fig. 1. Reaction scheme.

Fig. 2. Absorption spectra (A) blank; (B) 2 µg NH_2NH_2; (C) 4 µg NH_2NH_2; (D) 6 µg NH_2NH_2; (E) 7 µg NH_2NH_2 (all measurements made against water).

Experimental conditions were optimized for the synthesis of 2,4-dintrophenylhydrazine from 2,4-dinitrochlorobenzene using hydrazine in the presence of 3 mL of 25% diethylene glycol followed by condensation with *p*-dimethylaminobenzaldehyde.

It was established that the formation of 2,4-dinitrophenylhydrazine is slow at room temperature and heating the contents on a hot plate till the volume is reduced to half the initial volume is recommended. The absorbance value of the formed hydrazone was found to decrease slowly after 30 min in the sodium acetate medium. Changing the medium to acidic condition by the addition of 2 M HCl after the condensation of *p*-dimethylaminobenzaldehyde, stabilized the colour for a longer period.

The amount of 2,4-dinitrochlorobenzene required for reaction with hydrazine to form 2,4-dinitrophenylhydrazine was studied. The study indicated that a minimum of 0.008% of the reagent was sufficient for the formation of the product. Addition up to 0.02% 2,4-dinitrochlorobenzene showed no change in the formation of 2,4-dinitrophenylhydrazine for a given concentration of hydrazine. Hence 2 mL of 0.014% of 2,4-dinitrochlorobenzene is recommended as optimum concentration.

Effect of variation of sodium acetate required for the reaction between hydrazine and 2,4-dinitrochlorobenzene was studied. The results indicated that a minimum of 1 mL of 0.06% sodium acetate was sufficient. Further addition up to 3 mL of 0.06% of sodium acetate showed no change in the formation of 2,4-dinitrophenylhydrazine. Hence 2 mL of 0.06% sodium acetate is recommended for further investigations.

The amount of *p*-dimethylaminobenzaldehyde (*p*-DAB) required for the condensation reaction was studied. It was found that a minimum of 1 mL of a 1% *p*-dimethylaminobenzaldehyde (*p*-DAB) solution was required for formation of the yellow colored hydrazone. Addition up to 4 mL of 1% *p*-dimethylaminobenzaldehyde (*p*-DAB) caused no change in the absorbance value for a given concentration of hydrazine. Hence 2 mL of a 1% *p*-dimethylaminobenzaldehyde (*p*-DAB) solution is recommended.

Effect of acidity on the stability of the hydrazone colour was studied. The results indicated that a minimum of 0.8 M of HCl is sufficient for stable colour and the absorbance remained constant in the presence of excess acid. Hence 2 M hydrochloric acid is recommended for diluting the sample to 25 mL.

Effect of variation of diethylene glycol required for the reaction between hydrazine and 2,4-dinitrochlorobenzene was studied. The results indicated that a minimum of 2 mL of 25% diethylene glycol solution was sufficient. Further addition up to 4 mL of 25% diethylene glycol solution showed no change in the formation of 2,4-dinitrophenylhydrazine. Hence 3 mL of 25% diethylene glycol solution is recommended.

Under these conditions the system obeys Beer's law in the concentration range 0–7 µg of hydrazine in a sample volume of 10 mL with a detection limit of 0.21 µg. The molar absorptivity of the system was found to be 8.1×10^4 L mol^{-1} cm^{-1} and the hydrazone colour remained stable up to 3 days in acidic condition. A calibration graph was obtained with a positive slope and the equation being $Y = 0.099X$ where Y is the absorbance and X (µg) is the concentration of hydrazine. The correlation coefficient was 0.998 and the relative standard deviation was 1.7% ($n = 10$) for 6 µg of hydrazine.

3.1. Effect of interferences

The interfering effect of anions and cations, which may co-exist with hydrazine were studied. Any deviation in the absorbance of ±0.01 to that obtained in the absence of other interfering ions in hydrazine determination was taken as a sign of interference. Varying concentration of interfering species was introduced along with 6 µg of hydrazine and the absorbance values were compared to that in the absence of interference. Tolerance limit of various ions studied in hydrazine determination are summarized in Table 1.

Hydroxylamine is an interferent in most of the methods for hydrazine determination. In the proposed method hydroxylamine is tolerated up to 600 µg. Reaction between formaldehyde and hydroxylamine is very fast to form the oxime

Table 1

Effect of some interfering species in the hydrazine determination ($NH_2NH_2 = 6$ µg)

Species	Amount tolerated (µg)
Phosphate, oxalate, citrate, tartrate, borate, chloride	1000
Ba(II), Pb(II), Mg(II), Co(II), Cd(II), Bi(III), Ni(II), Li(I), Mn(II), Sr(II), Cr(III)	1000
NO_2^{-} [a]	100
Ammonia	200
Hydroxylamine	600
HCHO[b]	360
Fe(II)	500
Fe(III)[b]	240
Glucose, acetone[b]	100

[a] Treated with 1 mL of 0.5% sulphamic acid.
[b] Treated with 1 mL of 600 ppm hydroxylamine prior to heating the sample on the hot plate.

Table 2
Determination of residual hydrazine in boiler feed water

Samples[a]	Added NH_2NH_2 (μg)	Amount of NH_2NH_2 (μg) in diluted samples by proposed method (ppm)[b]	Recovery of added hydrazine (%)	Amount of NH_2NH_2 (μg) in diluted samples by p-DAB method (ppm)[b]	Paired t-test[c] calculated value $t = \bar{d}\sqrt{n}/S_d$
	–	1.50	–	1.52	$t = 0.0066\sqrt{3}/0.0294 = 0.3888$
	2.0	3.52	100.95	–	
	–	1.53	–	1.48	
Sample 1	3.0	4.51	99.23	–	
	–	1.48	–	1.57	
	4.0	5.49	100.25	–	
		1.50[d] (150 ± 0.044)[b]		1.52[d] (152 ± 0.045)[b]	
Sample 2	–	1.96	–	1.93	$t = 0.0233\sqrt{3}/0.0630 = 0.6406$
	2.0	3.94	99.00	–	
	–	2.00	–	2.02	
	3.0	5.02	100.66	–	
	–	1.92	–	2.00	
	4.0	5.91	99.75	–	
		1.96[d] (196 ± 0.040)[b]		1.98[d] (198 ± 0.041)[b]	
	–	1.80	–	1.80	$t = 0.0233\sqrt{3}/0.0435 = 0.9277$
	2.0	3.77	98.00	–	
	–	1.77	–	1.73	
Sample 3	3.0	4.76	99.66	–	
	–	1.81	–	1.78	
	4.0	5.82	100.25	–	
		1.79[d] (179 ± 0.021)[b]		1.77[d] (177 ± 0.036)[b]	

[a] Water samples were withdrawn at the entry point of the boiler on different days.

[b] Hydrazine content in the sample (ppm). One milliliter of sample diluted to 100 mL before analysis. One milliliter of the diluted sample was used for hydrazine determination by both methods.

[c] The tabulated value of $t_{95,2}$ is 4.303. The calculated value is less than the tabulated value and hence there is no significant difference between these methods.

[d] Average of three determinations in the diluted sample.

[20], compared to the reaction between hydrazine and formaldehyde. Hence the interference of formaldehyde is tolerated up to 360 μg by the addition of 1 mL of 600 μg hydroxylamine, prior to heating the sample on the hot plate. Acetone and glucose were tolerated up to 100 and 120 μg, respectively, by the addition of 1 mL of 600 μg hydroxylamine by forming the oximes. Fe^{2+} shows no interference up to 500 μg. The interference of Fe^{3+} is removed by reducing it to Fe^{2+} by the addition of 1 mL of 600 μg hydroxylamine [21]. Fe^{3+} is tolerated up to 240 μg. Nitrite is tolerated up to 100 μg in the presence of 0.5% sulphamic acid. NH_3 is tolerated up to 200 μg.

4. Application

Hydrazine is normally added in small amounts to boiler feed water. Hydrazine is oxidized by dissolved oxygen to nitrogen and prevents the corrosion of boilers.

The application of the proposed method is evaluated with feed water samples taken from high-pressure steam generating boilers to determine the hydrazine concentration. Boiler feed water samples were collected on different days and analyzed. One milliliter of sample was diluted to 100 mL. One milliliter of diluted sample was subjected to analysis. Known amounts of hydrazine were added and their recovery was established (Table 2). Added hydrazine showed recovery greater than 98%. The results obtained using the proposed method was validated by comparison with the *p*-dimethylaminobenzaldehyde (*p*-DAB) method [18] having a molar absorptivity of 3.6×10^4 L mol^{-1} cm^{-1}. A calibration graph for *p*-DAB method was prepared using 0–10 μg of hydrazine in 10 mL of sample volume. Diluted boiler feed water sample (10 mL) was taken in a 25 mL calibrated flask. To this, 10 mL of *p*-dimethylaminobenzaldehyde solution was added and made up to the mark with 1 M hydrochloric acid. The absorbance was measured at 458 nm against the reagent blank. Based on paired *t*-test there is no significant difference between these methods. The results of the proposed method compare well with *p*-DAB method (Table 2).

5. Conclusions

The proposed method for the determination of hydrazine is sensitive and reliable. Although the method require heating on a hot plate for the synthesis of 2,4-dinitrophenylhydrazine followed by the condensation reaction, the method is more sensitive compared to existing spectrophotometric methods.

The 'ε' (L mol^{-1} cm^{-1}) values of spectrophotometric methods based on condensation of hydrazine with vanillin [8], verataldehyde [9] and *p*-DAB [18] are 5.25×10^4, 6.72×10^4 and 3.6×10^4, respectively. The 'ε' value for indophenol method [16] is 1.8×10^4 L mol^{-1} cm^{-1}. The molar absorptivity of the developed method is found to be 8.1×10^4 L mol^{-1} cm^{-1}. The detection limit of hydrazine for the proposed method is 0.21 μg. The proposed method is used for the determination of hydrazine in boiler feed water.

Acknowledgements

References

[1] N.I. Sax, Dangerous Properties of Industrial Materials, 4th ed., van Nostrand-Reinhold, New York, 1980, p. 814.
[2] H.W. Schiessl, Encyclopedia of Chemical Technology, vol. 12K, Othmer Wiley, New York, 1980, p. 734.
[3] ASTM, Annual Book of ASTM Standards 11.01, American Society for Testing Materials, Easton, MD, 1989, D 1385-88, p. 383.
[4] J. Wang, Z. Taha, Talanta 35 (1988) 965.
[5] A.G. Fogg, A.Y. Chamsi, A.A. Barros, J.O. Cabral, Analyst 109 (1984) 901.
[6] Y.Y. Liu, I. Schmeltz, D. Hoffmann, Anal. Chem. 46 (1974) 885.
[7] M. Roth, J. Rieder, Anal. Chim. Acta 27 (1962) 20.
[8] S. Amlathe, V.K. Gupta, Microchem. J. 42 (1990) 331.
[9] R. Kaveeshwar, V.K. Gupta, Fresenius' J. Anal. Chem. 344 (1992) 114.
[10] K.K. Verma, A. Srivastava, J. Ahmed, S. Bose, Talanta 26 (1979) 469.
[11] A. Afkhami, A.R. Zarei, Talanta 62 (2004) 559.
[12] S. Dadfarmia, K. Dehghan, Bull. Korean Chem. Soc. 25 (2004) 213.
[13] A.A. Ensafi, B. Naderi, Microchem. J. 56 (1997) 269.
[14] A.A. Ensafi, B. Rezaei, Talanta 47 (1998) 645.
[15] A. Afkhami, A. Afshar-E-Asl, Anal. Chim. Acta 419 (2000) 101.
[16] B. Deepa, N. Balasubramanian, K.S. Nagaraja, Asian J. Chem. 17 (2005) 1140.
[17] B.S. Furniss, A.J. Hannaford, V. Rogers, P.W.G. Smith, A.R. Tatchell, Vogel's Textbook of Practical Organic Chemistry, 4th ed., ELBS Publication, London, 1984, p. 729.
[18] W.D. Basson, J.F. Van Staden, Analyst 103 (1978) 998.
[19] ASTM standards, Part 23 Water, "Atmospheric Analysis", American Society for Testing and Materials, Philadelphia, 1973, p. 318.
[20] M. Ferriol, J. Gazet, Anal. Chim. Acta 174 (1985) 365.
[21] F. Dias, A.S. Olojola, B. Jaselkis, Talanta 26 (1979) 47.

Parameters affecting the determination of mercury by anodic stripping voltammetry using a gold electrode

Agnese Giacomino, Ornella Abollino *, Mery Malandrino, Edoardo Mentasti

Department of Analytical Chemistry, University of Torino, Via Giuria 5, 10125 Torino, Italy

Abstract

The electrochemical determination of aqueous Hg(II) by anodic stripping voltammetry (ASV) at a solid gold electrode is described. The aim of this work is to optimise all factors that can influence this determination. Potential wave forms (linear sweep, differential pulse, square wave), potential scan parameters, deposition time, deposition potential and surface cleaning procedures were examined for their effect on the mercury peak shape and intensity. Five supporting electrolytes were tested. The best responses were obtained with square wave potential wave form and diluted HCl as supporting electrolyte. Electrochemical and mechanical surface cleaning, aimed at removing the amount of mercury deposited onto the gold surface, were necessary for obtaining a good performance of the electrode. Response linearity, repeatability, accuracy and detection limit were also evaluated.
© 2007 Elsevier B.V. All rights reserved.

Keywords: Mercury; Anodic stripping voltammetry; Gold electrode; Supporting electrolyte; Wave form

1. Introduction

The determination of metals at trace and ultratrace levels is an important issue in environmental and clinical sciences, owing to their potential toxicity at concentrations above certain threshold limits. Much attention is devoted to mercury, which is particularly harmful even at low concentrations: strict legislation limits are imposed in many countries for its concentration in all environmental compartments, e.g. waters, soils and organisms [1].

The analytical techniques preferred for mercury quantification are cold vapour atomic absorption spectrometry (CV-AAS) [2], cold vapour atomic fluorescence spectrometry (CV-AFS) [3], inductively coupled plasma mass spectrometry (ICP-MS) [4] and, for relatively high concentrations, inductively coupled plasma atomic emission spectrometry (ICP-AES) [5]. Several chromatographic techniques coupled with spectrometric methods have also been used for mercury speciation [6,7]. Among these, CV-AFS procedure is the preferred detection method due to its sensitivity. All these techniques require expensive and

sophisticated instrumentation and/or the use of specific instruments (which cannot be applied to the determination of other analytes), in combination with complicated sample preparation processes [8]. Stripping electrochemical methods represent an interesting alternative for mercury determination owing to their sensitivity, versatility and low costs. The recommendation of the US Environmental Protection Agency (EPA) for the adoption of stripping analysis for the quantification of heavy metals as mercury [9] is a very representative example of this application. Electroanalytical techniques for the detection of aqueous mercury, either alone or in conjunction with such emerging technologies as piezoelectric sensors, were utilized for the development of sensors capable of remote quantification of mercury in the environment [10]. A number of papers were devoted to the determination of mercury by anodic stripping voltammetry (ASV) at different solid electrodes [e.g. 11,12]. Gold was found to be the best electrode material for the determination of mercury by ASV, with conventional [13], film- [14,15] and micro-[16,17] electrodes. Also stripping chronopotentiometry at a gold wire microelectrode was adopted for trace measurements of mercury [18]. One reason for the use of gold is its high affinity for mercury, which enhances the preconcentration effect.

The main disadvantage of gold electrodes is the well known phenomenon of structural changes of their surface, caused by

* Corresponding author. Fax: +39 011 6707615.
  E-mail address: ornella.abollino@unito.it (O. Abollino).

amalgam formation, and the time-consuming cleaning treatments that are needed to achieve reproducibility [19].

Many parameters influence the analytical signal of mercury and we did not find in literature a paper reporting a complete study of their effect on the determination of mercury with gold electrodes. Moreover, the information about the optimal working conditions and the electrode performance is heterogeneous and sometimes discordant. For these reasons, in the present study, the use of a solid Au electrode for Hg(II) determination by ASV was investigated in terms of the parameters that normally can influence the analytical response. The shapes and intensities of the mercury peak in five supporting electrolytes were compared. The effects of different potential wave forms, namely linear scan (LS), differential pulse (DP) and square wave (SW), scan parameters (amplitude, frequency, step potential, interval time, modulation time, modulation amplitude) and of deposition time and potential were examined. The linearity, repeatability, detection limit and accuracy of the method were determined. The possible interference of As(V), Bi(III), Cd(II), Co(II), Cr(III), Cu(II), Fe(II), Mn(II), Ni(II), Pb(II) and Se(IV) was evaluated and compared with some data in literature [1,14,19].

The findings of this study can be useful for analysts in order to evaluate the real potentialities of the gold electrode and to choose the best conditions for the determination of mercury by ASV.

2. Experimental

2.1. Apparatus and reagents

Voltammetric analyses were performed with a PGSTAT 10 potentiostat (Eco Chemie, Utrecht, The Netherlands) coupled to a 663 VA Metrohm (Herisau, Switzerland) stand, equipped with a rotating solid gold electrode as working electrode, a Ag/AgCl reference electrode and a glassy carbon counter electrode. The analyzer was interfaced to a personal computer. High purity water (HPW) obtained from a Milli-Q (Millipore, Bedford, MA, USA) apparatus was used throughout. Analytical grade reagents were used. In particular a 1000 mg/l standard solution of mercury was prepared from $HgCl_2$ in 0.012 M HCl. More diluted Hg(II) standard solutions were prepared from the concentrated standard in the desired supporting electrolytes. HNO_3 and HCl were obtained by sub-boiling distillation in a quartz still.

2.2. Procedures

Ten-millilitre test solutions of supporting electrolyte were delivered into the voltammetric cell.

After 120 s of deposition a voltammetric scan was performed. Initially, the scan parameters were: (i) for SWV: frequency 100 Hz, step potential 0.002 V, amplitude 0.02 V; (ii) for DPV: modulation amplitude 0.05 V, modulation time 0.05 ms, interval time 0.3 ms, step potential 0.002 V; (iii) for LSV: step potential 0.002 V, interval time 0.30 s. Initial and final potentials were 0 V and 0.80 V, respectively.

For the values of the scan parameters after optimization, refer to Section 3.3.

After recording the voltammogram of the blank, aliquots of Hg(II) were added and the corresponding signals were recorded.

A cell containing 50 µg/l of Hg(II) was utilized to investigate the effects of the different parameters on the signal of mercury.

The detection limit was estimated as three times the standard deviation of the blank signal.

All experiments were performed in triplicate.

3. Results and discussion

The voltammetric behaviour of Hg(II) was investigated in different supporting electrolytes and in different conditions of analysis.

3.1. Preliminary considerations

A brand-new gold electrode displays an ill-defined anodic stripping voltammogram for mercury. In order to overcome this drawback the electrode was dipped into a solution composed by 10 mM HNO_3 and 10 mM NaCl and activated by applying a potential of 0.90 V for 60 s between the working electrode and the reference electrode. The activation procedure applied is identical to that used by Bonfil et al. [19]. This simple 1-min electrochemical pre-treatment was found to be of utmost importance [20], as can be seen by comparing the anodic stripping voltammograms of 50 µg/l of mercury in HCl before and after activation (Fig. 1).

The measurement of an analytical signal for Hg(II) on a gold surface is somewhat hindered by the baseline (background current) behaviour. This problem results from the nature of the deposit on the electrode, i.e. the amount of mercury deposited and/or the type of interaction between gold and mercury [16]. A possible origin of the high background, when working with HCl as supporting electrolyte, is the formation of calomel onto the electrode surface [16,21]. The definition of a proper baseline is difficult. Good results in terms of accuracy and repeatability were obtained considering a horizontal baseline from the right base of the peak.
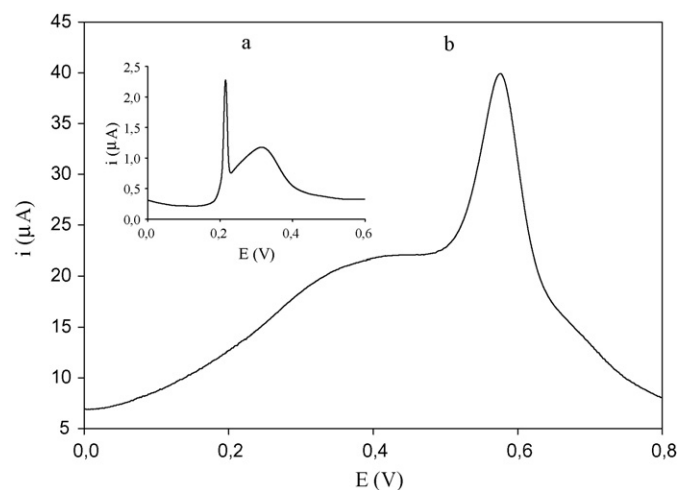

Fig. 1. Anodic stripping voltammograms of 50 µg/l of Hg(II) in HCl using SW (a) before and (b) after activation of the electrode.

This determination does not require to purge the solutions with nitrogen. This finding is in agreement with the work of other researchers [22,23], while others suggest a purge time of 300 s before each measurement [24]. We found that the signal does not vary before and after purging.

3.2. Effect of supporting electrolyte and potential wave form

Five supporting electrolytes were tested, namely 70 mM HNO_3, 50 mM $HClO_4$, 60 mM HCl [22], 5 mM HNO_3/5 mM NaCl [19] and 40 mM $HClO_4$/0.6 mM NaCl/0.2 mM EDTA [24]. Each of the five considered electrolytes was tested working in LSV, DPV and SWV. After recording the voltammogram of the blank, the test solutions were spiked with two additions of Hg(II) standard solution (50 µg/l). Table 1 shows the heights and the potentials of the peaks obtained for 50 µg/l Hg(II) for each supporting electrolyte and scan mode. As an example, Fig. 2 reports the voltammograms obtained with the same electrolyte (HCl) using different potential wave forms, and Fig. 3 shows the effect of the supporting electrolyte composition using SW scan mode.

With HCl the shape of the baseline was good, especially for SW and DP, and the peak was well-defined and regular. In the presence of HNO_3 and $HClO_4$ baseline and peak shape were somewhat irregular, and the peak did not increase after the second standard addition working in DPV. $HClO_4$ is used as supporting electrolyte in the determination of Hg(II) with other techniques: gold micro- [16] or film- [14] electrodes. Using $HClO_4$/NaCl/EDTA the baseline was almost regular with DP and SW scans and the peak shape was well-defined. The mix-

Table 1
Peak potentials (E_p) and intensities (i_p) obtained for a 50 µg/l Hg(II) solution with different supporting electrolytes and scan modes

Electrolyte	Scan mode	i_p (µA)	(V)
HCl	LS	0.13	0.54
	DP	0.80	0.51
	SW	19.0	0.58
HNO_3	LS	n.d.	n.d.
	DP	1.45	0.66
	SW	6.63	0.73
$HClO_4$	LS	n.d.	n.d.
	DP	1.48	0.66
	SW	5.14	0.73
$HClO_4$/NaCl/EDTA	LS	0.19	0.62
	DP	0.76	0.60
	SW	16.2	0.69
HNO_3/NaCl	LS	0.00	n.d.
	DP	0.78	0.55
	SW	16.3	0.67

n.d. = not detectable.

ture HNO_3/NaCl gave the worst results among the electrolytes tested, for all the investigated techniques: the baseline was very ill-shaped, and the peak height did not increase after the second addition of mercury.

Among the three utilized techniques, DPV and SWV are the most popular because they allow to enhance the analytical signal by removing the non-Faradic current. Also in these experiments DP and SW wave forms permitted to obtain better signals than LSV. In particular, a peak for mercury with LS was observed
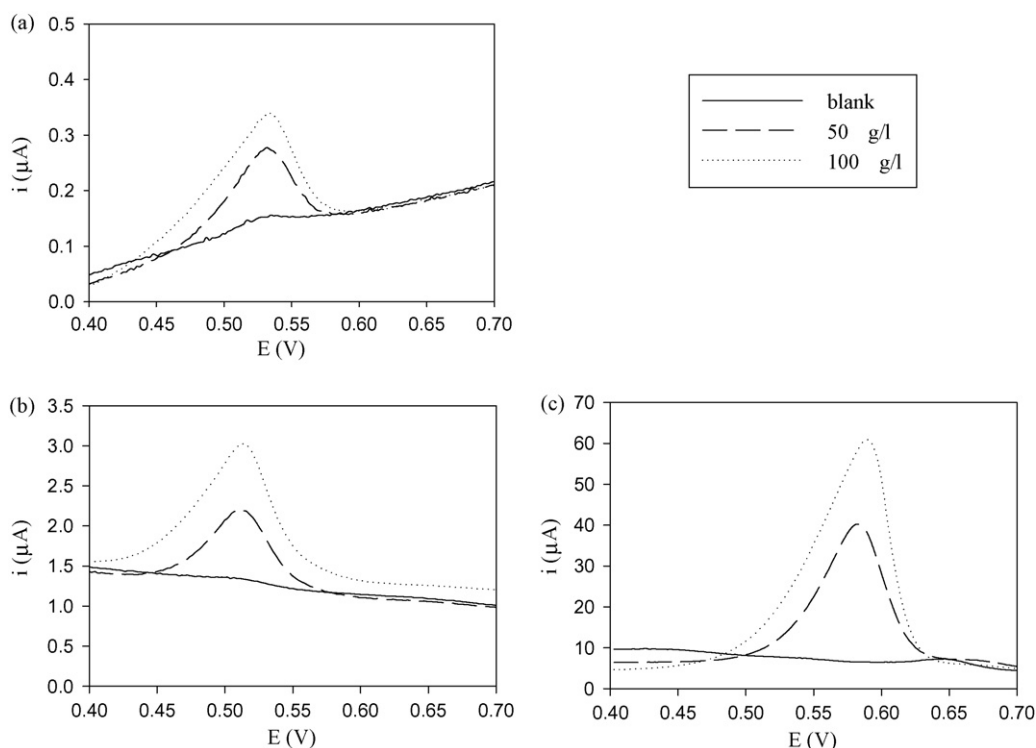

Fig. 2. Voltammograms recorded using using HCl as electrolyte and (a) LSV; (b) DPV; and (c) SWV: blank, 50 µg/l and 100 µg/l of Hg(II).
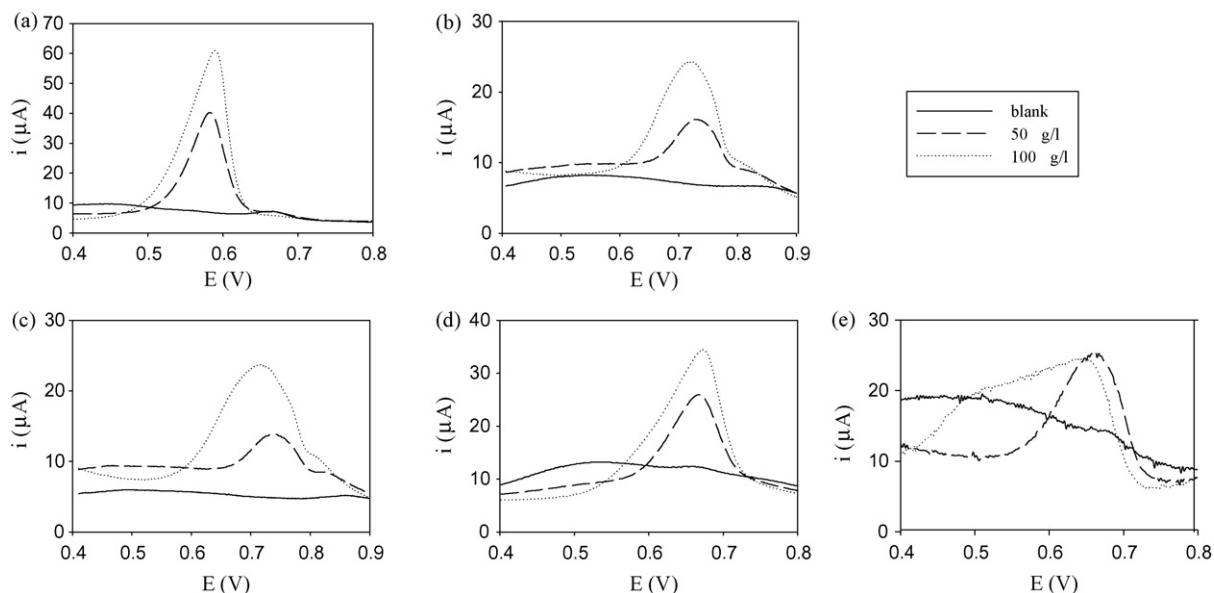
Fig. 3. Voltammograms recorded using SW as potential wave form and (a) HCl; (b) HNO$_3$; (c) HClO$_4$; (d) HClO$_4$/NaCl/EDTA; (e) HNO$_3$/NaCl as electrolyte: blank, 50 μg/l and 100 μg/l of Hg(II).

only in HCl and HClO$_4$/NaCl/EDTA, and the sensitivities were very low. This behaviour is not in agreement with the studies of Jayaratna [22], who concluded that this scan mode was a good choice, but confirmed the findings of many other researchers that used DPV [e.g. 25] or SWV [e.g. 19].

The peak potentials vary in the order HCl < HNO$_3$/NaCl < HClO$_4$/NaCl/EDTA < HNO$_3$ = HClO$_4$ for both DP and SW modes. In particular, the stripping peak with HCl appears at a much more negative potential than those observed using the other electrolytes. This is in agreement with the results obtained by Okçu et al. with the gold film electrode: they used perchloric acid as supporting electrolyte, but they found that the addition of HCl was necessary to shift the stripping peak of mercury to less positive potentials, in order to reduce the background current, and to increase the sensitivity [14]. Probably the formation of mercury chlorocomplexes favours the oxidation of mercury, which therefore occurs at less positive potentials. This shift is found at a lesser extent also in the case of the mixtures HNO$_3$/NaCl and HClO$_4$/NaCl/EDTA.

The peak heights increase in the order: HNO$_3$/NaCl < HClO$_4$/NaCl/EDTA < HCl < HNO$_3$ < HClO$_4$ with DPV, and in the order: HClO$_4$ < HNO$_3$ < HClO$_4$/NaCl/EDTA < HNO$_3$/NaCl < HCl with SWV. The reasons of the different order of sensitivity is not clear. It is possible that the reversibility of the redox reaction of mercury, which enhances sensitivity in SW, increases in complexing electrolytes.

We decided to continue our work with HCl and with the mixture HClO$_4$/NaCl/EDTA using both DP and SW, because the best results, in terms of peak shape and linearity, were obtained in these conditions.

3.3. Effect of wave form parameters

The effect of the different potential scan parameters on the mercury (50 μg/l) peak height and potential was inves-

tigated with the two supporting electrolytes selected. The results are shown in Figs. 4 and 5 for DP and SW, respectively.

Working in DP mode, with the increase of the step potential, the signal slightly shifted to more positive potentials, and its height increased with scan rate. An increase of interval time had the opposite effect on the mercury peak owing to a decrease in scan rate. An increase of the modulation amplitude caused an increment of the signal intensities, probably due to the larger difference between the currents before and after the application of the pulse, as measured in DP, and their shift to less positive potentials, whereas the variation of the modulation time had the opposite effect, likely because of the decrease of the Faradic current for long pulses.

The results obtained using SW showed that when frequency and step potential were increased, the signal increased and shifted to slightly more positive potentials, in agreement with the increase in scan rate. The peak height increased with wave amplitude, as discussed above for modulation amplitude, and shifted to more negative potentials.

Therefore, the trends observed for the mercury peak following the variation of scan parameters are in agreement with theoretical predictions [26,27].

Optimal values for the parameters were found to be: (i) for DP, step potential 0.004 V, interval time 0.075 s, modulation amplitude 0.075 V, modulation time 0.0125 s with HCl, and 0.004 V, 0.075 s, 0.050 V, 0.0125 s, respectively with HClO$_4$/NaCl/EDTA; (ii) for SW, step potential 0.004 V, frequency 150 Hz, amplitude 0.03 V with HCl, and 0.004 V, 150 Hz, 0.04 V, respectively with HClO$_4$/NaCl/EDTA.

The peak shape remained almost unchanged when the scan parameters were varied. The signals found in HCl were narrower and higher than the ones obtained using HClO$_4$/NaCl/EDTA for
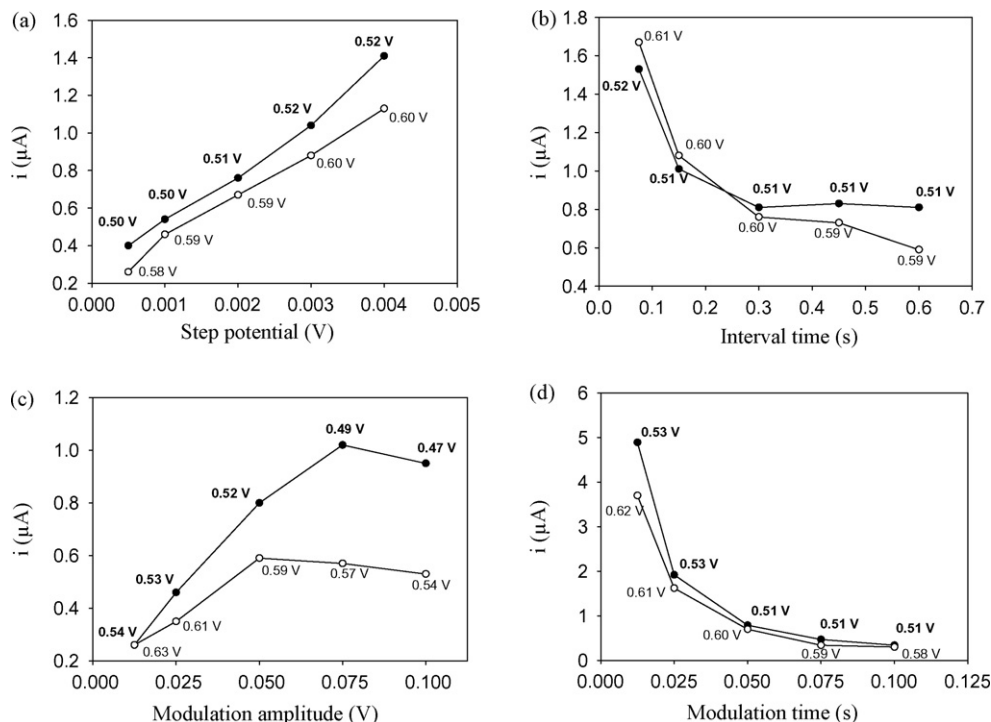
Fig. 4. The effect of (a) step potential; (b) interval time; (c) modulation amplitude; (d) modulation time on the mercury (50 µg/l) peak height. The corresponding peak potentials are reported in each plot. Wave form: DP. Supporting electrolyte: (●) HCl and (○) HClO$_4$/NaCl/EDTA.

both scan modes. The highest peaks were obtained with SW, which is also the most rapid technique. As a consequence of the results obtained we continued our experiments using HCl as supporting electrolyte and SW with the optimized parameters as scanning mode.

3.4. Effect of deposition time and deposition potential

The effect of deposition potential (with 120 s of deposition) and deposition time (at 0 V) on the signal of 50 µg/l of Hg(II) was evaluated and the results are reported in Fig. 6.
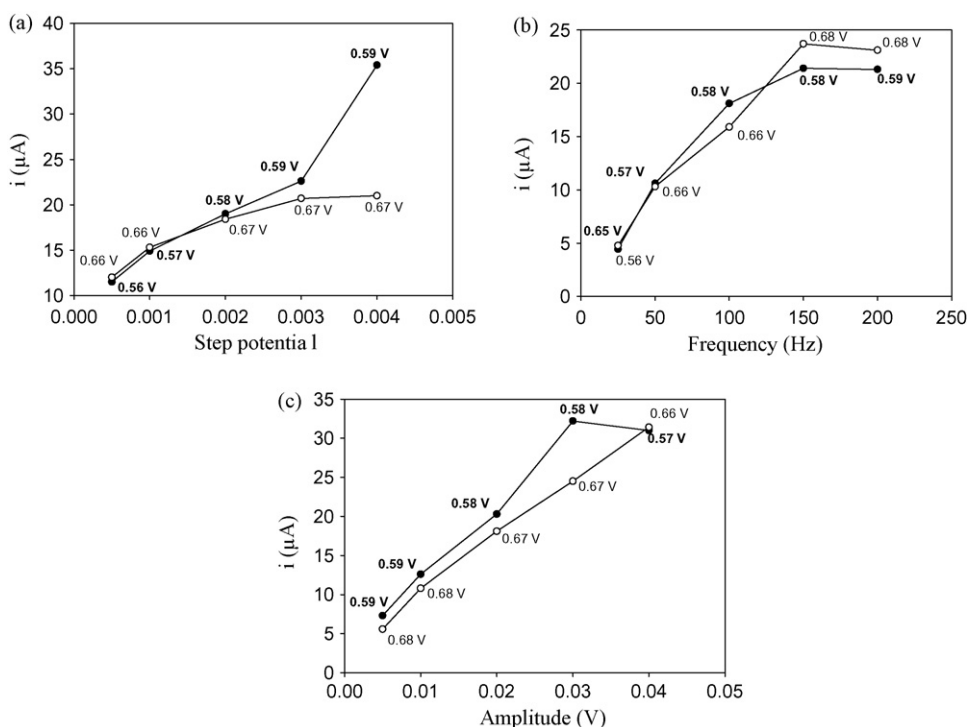

Fig. 5. The effect of (a) step potential; (b) frequency; (c) amplitude on the mercury (50 µg/l) peak height. The corresponding peak potentials are reported in each plot. Wave form: SW. Supporting electrolyte: (●) HCl and (○) HClO$_4$/NaCl/EDTA.

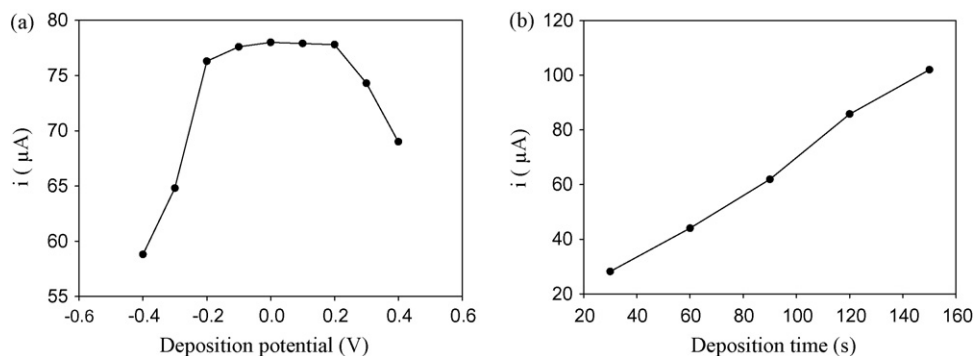Fig. 6. The effect of (a) deposition potential and (b) deposition time on the mercury (50 μg/l) peak height ($E_p = 0.58$ V). Wave form: SW. Supporting electrolyte: HCl.

The highest signal with the best baseline shape was obtained with a deposition potential of 0 V. Other researchers worked with 0.1 [28], 0.2 [14], 0.3 [22] or 0.37 [24] V as deposition potentials, but using different supporting electrolytes. Using HCl, at deposition potentials more positive than 0 V the background is more relevant. Bonfil, working with 10 mM NaCl/10 mM HNO$_3$, observed that the repeatability and the magnitude of the analytical signal were independent of the deposition potential in the range +0.55 to −0.4 V [19].

The amount of mercury deposited onto a gold surface should be carefully controlled to avoid saturation and to maintain linearity with increased loading. The greater solubility of mercury in gold compared to other metals could result in non-linear performance. Therefore, we investigated the effect of the deposition time on the peak currents. As expected, the height of mercury peak increased with increasing deposition time (Fig. 6b). However, with deposition times longer than 120 s the electrochemical cleaning procedure was not sufficient to remove all deposited mercury, causing a worsening in the repeatability of the subsequent analyses.

Taking into account the results obtained, a deposition potential of 0 V and a deposition time of 120 s were adopted.

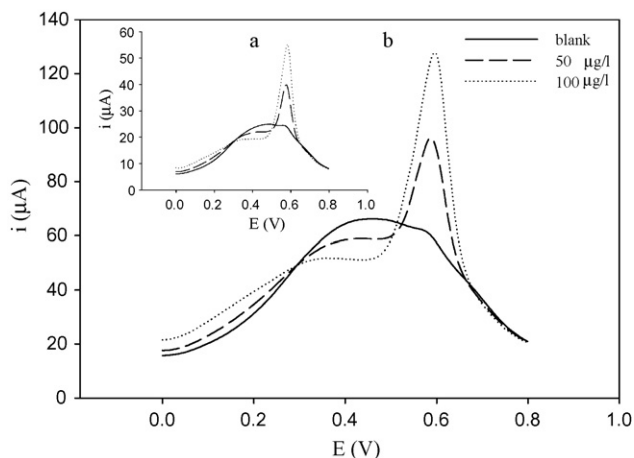The effect of the optimisation of all parameters is well shown in Fig. 7.

Fig. 7. Comparison between the determination of Hg(II) with (a) default and (b) optimized parameters using HCl and SW.

3.5. Repeatability, linearity, detection limit and accuracy

The performance of the analytical method was evaluated using HCl as supporting electrolyte and the SW wave form, in the following conditions: frequency 150 Hz; step potential 0.004 V, amplitude 0.03 V, deposition potential 0 V, deposition time 120 s.

The repeatability was evaluated with 10 replicates on 10 different cells containing 50 μg/l of mercury. The relative standard deviation was 4.40%. This value can be considered satisfactory, taking into account the relatively low concentration level involved.

The linearity of the analytical response was investigated. Initially, successive additions of 50 μg/l of Hg(II) were made, but the peak height increased linearly with concentration only up 100 μg/l; therefore, we studied in more detail the increment of the signals in the range 0–100 μg/l (with standard additions of 25 μg/l) and in lower ranges, namely 0–25 μg/l and 0–5 μg/l (with standard additions of 5 μg/l and 1 μg/l, respectively). Table 2 shows the equations of the calibration curves, R^2 values, and average sensitivities obtained.

We examined both (i) all data in the considered ranges (named a, b, c in the table) and (ii) sub-sets of the same data (named a1, a2, etc.).

The value of R^2 increases, within each range, as the number of considered data decreases (e.g. in the order a < a1 < a2): this trend is due to the more relevant increase of the peak height after the first additions, within each range, in comparison with the last ones; in fact the data in Table 2 show that the average sensitivity decreases with the successive additions of mercury (e.g., in the order a2 > a1 > a). However, the intensities for 5 μg/l were the same both after adding five 1-μg/l spikes and one 5-μg/l spike. According to previous studies [10], mercury is deposited onto the gold electrode and does not diffuse deeply into the gold, at least in the timescale of the experiment: therefore, at low concentrations the lower competition for electrode surface ensures a more efficient deposition and a higher sensitivity. Also the loss of linearity at concentrations higher than 100 μg/l is presumably due to a partial saturation with mercury of the electrode surface. This change in sensitivity must be taken into account when analyzing real samples and indicates that it is convenient to perform the calibration with standard

Table 2
The equations of the calibration curves, R^2 values and the corresponding sensitivities obtained in different concentration ranges: (a) 0–100 µg/l (additions of 25 µg/l); (b) 0–25 µg/l (additions of 5 µg/l); (c) 0–5 µg/l (additions of 1 µg/l)

Data set	Concentration range (µg/l)	Equation of the calibration curve[a]	R^2	Average sensitivity (µA/µg l^{-1})
a	0–100	$y = 9 \times 10^{-7} \times + 3 \times 10^{-5}$	0.9868	1.03
a1	25–100		0.9981	0.90
a2	50–100		0.9987	0.85
b	0–25	$y = 1 \times 10^{-6} \times + 2 \times 10^{-5}$	0.9999	1.45
b1	5–25		0.9999	1.44
b2	15–25		0.9999	1.43
c	0–5	$y = 3 \times 10^{-6} \times + 1 \times 10^{-5}$	0.9978	2.96
c1	1–5		0.9991	2.78
c2	2–5		0.9999	2.67

R^2 values and sensitivities are also reported for sub-sets of the same data (a1; a2; b1; b2; c1; c2).

[a] Equations are referred to data sets a, b, c.

solutions having concentrations close to the ones present in the samples.

It can be presumed that at lower deposition times the dynamic linear range will be extended.

The limit of detection was estimated as LOD = $3\sigma_B$/slope of the calibration curve for the range 1–5 µg/l and was found to be 0.40 µg/l. Other papers in literature report lower detection limits than this, but the deposition times are generally very long; for example, Wu et al. found a detection limit of 22 ng/l using a deposition time of 40 min [23].

The accuracy of the procedure was tested by analysing a solution containing a known concentration (50 µg/l) of Hg(II). The concentration found was 49 ± 2 µg/l and the relative error was −2%. Therefore, the accuracy of the method can be considered good.

3.6. Interferences

The interference of several metal ions (As(V), Bi(III), Cd(II), Co(II), Cr(III), Cu(II), Fe(II), Mn(II), Ni(II), Pb(II), and Se(IV)) on the mercury stripping signal was investigated. The voltammogram of a solution with 25 µg/l of Hg(II) was recorded in the presence of each element (added into the polarographic vessel in 1:1, 1:10, 1:100 concentration ratios with respect to Hg(II)). As other researchers [1,14,19] found, no interference was observed after the addition of 250 µg/l of each element. Moreover, the linearity of the calibration curve of mercury was maintained also in the presence of 2.5 mg/l of the other ions in solution.

The only peak which appeared in the considered range of potential, at less positive potentials than the one of Hg(II), was caused by copper, but it did not interfere with the determination of mercury.

3.7. Cleaning procedure of the electrode surface

The importance of electrode cleaning in order to maintain linearity is well known, but the opinions found in literature about the frequency and the procedure of this step are not in good agreement. Some papers indicate a decrease in the signal of mercury in the absence of cleaning [22,29], whereas other researchers found that the electrochemical characteris-

tics of the electrode were not affected by repeated depositions and dissolutions of mercury, and stated that no pre-treatment of the gold surface between experiments was required in order to achieve good reproducibility [19,30]. Watson et al. underline the importance of a cleaning step after each determination, defining this stripping determination as composed by a three-step cycle: preconcentration (deposition), measurement (stripping) and regeneration (cleaning) [10].

The results obtained in the present study showed that the determination of Hg(II) at a gold electrode was always hindered by the incomplete removal of previously deposited mercury. To eliminate this drawback, a good cleaning procedure was essential. Electrochemical and mechanical surface cleaning, as well as the control of the amount of mercury deposited onto the gold surface, were necessary for maintaining good reproducibility and linearity.

An electrochemical cleaning procedure was adopted: a positive potential (1.3 V) was applied for 30 s to remove the deposited mercury after each determination (consisting of the recording of three voltammograms: blank and two additions). During this step the polarographic vessel was filled with 20 ml of the mixture HClO$_4$/NaCl/EDTA [24]: in fact, this electrolyte was more efficient to clean the electrode than the other four electrolytes used in this work. Probably the presence of EDTA favours the removal of mercury from the electrode.

Moreover, after about 100 determinations a mechanical polishing with alumina was necessary to obtain a good repeatability and a homogeneous background.

No difference in terms of cleaning requirement was observed among the use of the five supporting electrolytes tested in this study. This finding is in agreement with the results obtained by Jagner and Josefson [31], whereas Jayaratna chose to work with HClO$_4$ instead of HCl also because he noted that HCl required longer cleaning times than HNO$_3$ or HClO$_4$ [16].

Some problems of repeatability began after 5 months of intensive use. In order to check if this drawback was due to a damaged electrode surface, a SEM analysis was performed. The images obtained revealed that the surface of the gold electrode presented holes and scratches, caused by the repeated cleaning treatments with aluminum oxide: this was confirmed by a microanalysis of the holes, that showed only the presence of Al in these points.

In order to avoid, or at least reduce, this drawback, now another procedure for the mechanical cleaning is being adopted: alumina is suspended in water before being transferred onto the cloth. In this way, it forms a smoother layer and the electrode lifetime is extended.

4. Conclusions

The results obtained showed the efficiency of the gold electrode for the determination of low concentrations of Hg(II) by anodic stripping voltammetry. The reproducibility, sensitivity and accuracy are good, provided the proper instrumental parameters and supporting electrolyte are used.

We also demonstrated that the determination of Hg(II) at a gold electrode is negatively affected by the incomplete removal of previously deposited mercury. To eliminate this drawback, an electrochemical and a mechanical cleaning procedure are essential.

References

[1] M.A. Augelli, R.A.A. Munoz, E.M. Richter, A.J. Gouveia, L. Angnes, Electroanalysis 17 (2005) 755.
[2] S.C. Hight, J. Cheng, Food Chem. 91 (2005) 557.
[3] M. Roulet, M. Lucotte, J.R.D. Guimarães, I. Rheault, Sci. Total Environ. 261 (2000) 43.
[4] P. Ugo, S. Zamperi, L.M. Moretto, D. Paolucci, Anal. Chim. Acta 434 (2001) 191.
[5] A.C. Barbarosa, G.A. East, Ecol. Trace Element Res. 60 (1997) 153.
[6] C. Sarzanini, G. Sacchero, M. Aceto, O. Abollino, E. Mentasti, Anal. Chim. Acta 284 (1994) 661.
[7] Y.F. Li, C.T. Chen, B. Li, Q. Wang, J. Wang, Y. Gao, Y. Zaho, Z. Chai, J. Anal. Atom. Spectrom. 22 (2007) 925.
[8] C.C. Huang, H.T. Chan, Anal. Chem. 78 (2006) 8332.
[9] EPA, Mercury in aqueous samples and extracts by anodic stripping voltammetry (ASV), Method 7472, http://www.epa.gov/mercury/information.htm#-tech_docs.
[10] C.M. Watson, D.J. Dwyer, J.C. Andle, A.E. Bruce, M.R.M. Bruce, Anal. Chem. 71 (1999) 3181.
[11] N.Y. Stojko, K.Z. Brainina, C. Faller, G. Henze, Anal. Chim. Acta 371 (1998) 145.
[12] S. Meyer, F. Scholtz, R. Trittler, Fresenius J. Anal. Chem. 356 (1996) 247.
[13] S.S. Ermakov, A.V. Borzhitskaya, L.N. Moskvin, J. Anal. Chem. 56 (2001) 542.
[14] F. Okçu, F.N. Ertaş, I. Gökçel, H. Tural, Turk J. Chem. 29 (2005) 355.
[15] M.A. Augelli, R.A.A. Munoz, E.M. Richter, M.I. Cantagallo, L. Angnes, Food Chem. 101 (2007) 579.
[16] A. Widmann, C.M.G. van den Berg, Electroanalysis 17 (2005) 825.
[17] P. Salaun, C.M.G. van den Berg, Anal. Chem. 78 (2006) 5052.
[18] J. Wang, P. Grüdler, G.U. Fleghsig, M. Janinski, J. Lu, J. Wang, Z. Zhao, B. Tian, Anal. Chim. Acta 396 (1999) 33.
[19] Y. Bonfil, M. Brand, E. Kirowa-Eisner, Anal. Chim. Acta 424 (2000) 65.
[20] R.D. Riso, M. Waeles, P. Monbet, C.J. Chaumery, Anal. Chim. Acta 416 (2000) 97.
[21] O. Ordeig, C.E. Banks, J. del Campo, F.X. Muñoz, R.G. Compton, Electroanalysis 18 (2006) 573.
[22] H.G. Jayaratna, Curr. Sep. 16 (1997) 93.
[23] Q. Wu, S.C. Apte, G.E. Batley, K.C. Bowles, Anal. Chim. Acta 350 (1997) 129.
[24] Metrohm, Mercury in waste water, VA Application Note No. V-89.
[25] Metrohm, Stripping voltammetry analysis of mercury, Application Bulletin No 96/4 e.
[26] F.G. Thomas, G. Henze, Introduction to Voltammetric Analysis, Theory and Practise, CSIRO Publishing, Collingwood, Australia, 2001.
[27] J. Wang, Analytical Electrochemistry, Wiley-VCH, Hoboken, NJ, 2006.
[28] I. Gustavsson, J. Electroanal. Chem. 214 (1986) 31.
[29] T.S. Hsi, J.S. Tsai, J. Chin. Chem. Soc. 41 (1994) 315.
[30] J. Inukai, S. Sugita, K. Itaya, J. Electroanal. Chem. 403 (1996) 168.
[31] D. Jagner, M. Josefson, Anal. Chim. Acta 141 (1982) 147.

Effect of graphite and metallic impurities of C$_{60}$ fullerene on determination of salbutamol in biological fluids

Rajendra N. Goyal [a],*, Davinder Kaur [b], Sudhanshu P. Singh [a], Ashish K. Pandey [a]

[a] *Department of Chemistry, Indian Institute of Technology Roorkee, Roorkee 247667, India*
[b] *Department of Physics and Centre of Nanotechnology, Indian Institute of Technology Roorkee, Roorkee 247667, India*

Abstract

A new method for the determination of salbutamol has been developed using fullerene C$_{60}$-modified glassy carbon electrode and validated using GC–MS. The presence of graphite and metallic impurities in C$_{60}$ are found to diminish the peak. The oxidation of salbutamol was observed in a single well-defined, diffusion-controlled process using square wave voltammetry. The peak potential of oxidation peak was dependent on pH and determination was carried out at physiological pH 7.4. The peak current versus concentration plot was linear in the range 100–2000 ng/ml of salbutamol. The detection limit was found to be 40 ng/ml. The determination of salbutamol was carried out in human blood and urine samples and common interferents such as dopamine, ascorbic acid and uric acid do not interfere. The method proved to be specific, rapid, and accurate and can be easily applied for detecting cases of doping. A cross-validation of the observed results with GC–MS indicated a good agreement.
© 2007 Elsevier B.V. All rights reserved.

Keywords: Salbutamol; Fullerene; Blood plasma; Urine; Doping; Square wave voltammetry

1. Introduction

A significant increase in doping cases has been observed in last few decades due to the tremendous pressure developed on sportspersons by expectations of their supporters. Use of doping agents by athletes to improve their performance in sports is unfair as well as contrary to the ethics of sports. β-2-Agonists have been abused by the athletes to such an extent that International Olympic Committee (IOC) and World Anti Doping Agency (WADA) have made it mandatory for every athlete to prove medical necessity and seek the permission to use this class of drug for medicinal purposes [1]. Salbutamol {2-(hydroxymethyl)-4-[1-hydroxy-2-(tert-butylamino)ethyl] phenol} is a sympathomimetic amine drug with β-2 adrenergic activity and is clinically used for curing asthma [2]. It works by relaxing the muscles and air passages in the lungs so that airflow becomes easier and improves breathing. Detailed guidelines for the recognition, prophylaxis, and management of asthma and exercise-induced asthma have been recently

published [3]. It has also been demonstrated that prolonged administration of salbutamol in oral form resulted in an increase in quadriceps femoris and hamstring muscle group strength [4]. Hence, determination of salbutamol turns out to be of utmost importance and several procedures have been developed to quantify salbutamol.
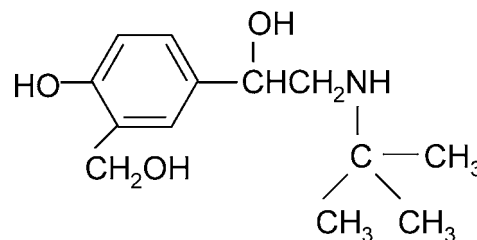
Salbutamol

A method based on on-line solid-phase extraction and sequential injection analysis for determination of salbutamol in standard solutions, human serum and urine has been reported in literature [5]. Extraction followed by analysis using liquid

---

* Corresponding author. Tel.: +91 1332 285794; fax: +91 1332 273560.
E-mail address: rngcyfcy@iitr.ernet.in (R.N. Goyal).

chromatography and gas chromatography has also been used for analysis of salbutamol [6]. Spectrophotometric techniques [7,8], GC–MS [9], HPLC with UV-detection [10] and capillary electrophoresis [11] have also been explored for the determination of salbutamol in pharmaceutical formulations. However, all these techniques are time consuming, require sample pretreatment procedure and also the instrumentation required is expensive. Electrochemical techniques, on the other hand, are less expensive, simple and rapid. These techniques do not require preliminary separation step and the formulation matrix can be used directly for quantification of electroactive substances [12]. Literature survey revealed that determination of salbutamol using electrochemical methods has attracted little attention. The oxidation of salbutamol at a glassy carbon electrode has been reported using differential pulse voltammetry [13]. However, studies are carried out at pH 5.0, which probably provides little useful information about biological systems and the oxidation occurred in adsorption-controlled process. Nafion-mediated carbon paste electrode has also been used for determination of salbutamol [14] and a detection limit of 2.5×10^{-8} M has been suggested using cyclic voltammetry. Recently salbutamol has also been determined using flow injection system [15]. In all these reports diffusion-controlled process was noticed at higher concentrations whereas at low concentrations, that is close to detection limit, adsorption complications were observed. Almost all the reported papers simply present a method for determination and recovery in tablets and no attempt has been made so far to determine salbutamol in biological samples such as blood or urine.

In recent years application of modified electrodes has been found to enhance the sensitivity of electrochemical determinations. Hence, fullerene-modified and nanogold-modified electrodes have been widely used for the determination of large number of organic compounds and biomolecules [16,17]. Fullerene-modified electrodes have an additional advantage of long stability and wide potential window. However, very recently [18] the catalytic property of fullerenes is ascribed to graphite impurities present in it. In this paper a comparison of voltammetric behavior of salbutamol at glassy carbon electrodes modified with pure fullerene and fullerene having graphite or Fe(III) has been described and it is concluded that the catalytic property is due to fullerene itself and graphite or metallic impurities do not cause electrocatalytsis. The determination of salbutamol has been carried out with emphasis on quantification of drug in biological and pharmaceutical samples. A comparison of observed results with gas chromatography–mass spectrometry (GC–MS) clearly indicate that the results are in good agreement.

2. Experimental

2.1. Chemicals and apparatus

C_{60} fullerene of purity (>99.5%) was purchased from Bucky USA, Houston, TX, USA. Graphite powder (purity 99.99%) was obtained from Aldrich, USA. Salbutamol sulphate in powdered form was obtained as a gift sample from Vamsi Labs Ltd., Maharashtra, India. Salbutamol containing tablets and syrup of different companies were purchased from the local market. All other chemicals used were of analytical grade and were purchased from Merck. Double distilled water was used to prepare the solutions.

The voltammetric experiments were carried out using Bioanalytical System (BAS, West Lafayette, IN, USA) CV-50W voltammetric analyzer. The determination of Fe(III) in fullerene C_{60} was carried out using Perkin Elmer A Analyst 800 atomic absorption spectrophotometer. The voltammetric cell used was a single compartment glass cell containing fullerene-modified glassy carbon electrode (3 mm diameter) as working electrode, a platinum wire as counter electrode and Ag/AgCl (3 M NaCl) as reference electrode (model BAS MF-2052 RB-5B). All potentials are reported with respect to Ag/AgCl electrode at an ambient temperature of $30 \pm 2 \,^{\circ}$C.

GC-mass spectral studies (EI: 70 eV) were carried out using Perkin-Elmer clarus 500 GC–mass spectrometer. The initial temperature of the column was kept at 60 $^{\circ}$C and the temperature was programmed up to 280 $^{\circ}$C at a rate of 10 $^{\circ}$C/min. The final temperature was maintained for 1 min. The temperature of the injector was 250 $^{\circ}$C. Helium was used as the carrier gas at a flow rate of 1 ml/min.

2.2. Preparation of C_{60}-modified electrode and FE-SEM characterization

Fullerene-modified glassy carbon electrode was prepared using method as described in literature [19]. Briefly, glassy carbon electrode was cleaned by polishing it with alumina and zinc oxide (Aldrich) on micro-cloth pads (BAS, USA). The electrode was then soaked in 0.2 M H_3PO_4 solution and washed with jet of distilled water. A mirror-like finish was obtained. Fullerene solution (150 µM) was prepared by dissolving 1.08 mg of C_{60} in 10 ml dichloromethane solution. To prepare C_{60} with graphite/Fe(III) impurities, 0.1 mg of ultrapure graphite or 0.01 mg of ferric nitrate were also added in 10 ml of dichloromethane. Glassy carbon electrode (GCE) surface was then modified by adsorbing a fixed amount of C_{60} solution followed by fast drying of the solution using hair dryer. Then, the electrode surface was pre-treated in 1 M KOH in potential range 0 to -1.5 mV at the scan rate of 10 mV/s. Such a treatment caused partial reduction of fullerene layers to form conductive films. The partially reduced fullerene has been found to exhibit electrocatalytic activity, which leads to lowering of peak potential and enhancement of peak current in voltammetry [20]. Finally electrode was transferred to another cell containing 50 mM phosphate buffer solution of pH 7.4 and successive cyclic potentials were applied between 550 to -50 mV for 20 min at a sweep rate of 20 mV/s. The electrode so prepared was characterized by recording FE-SEM using Quanta 200 FE-SEM instrument. A typical FE-SEM image of the fullerene-modified electrode clearly showed deposition of C_{60} at the surface of glassy carbon as shown in Fig. 1.

To refresh the electrode surface after each determination, electrode was kept at -200 mV in phosphate buffer solution of pH 7.4 for 60 s. Electrode was stored in air under dry conditions when not in use.
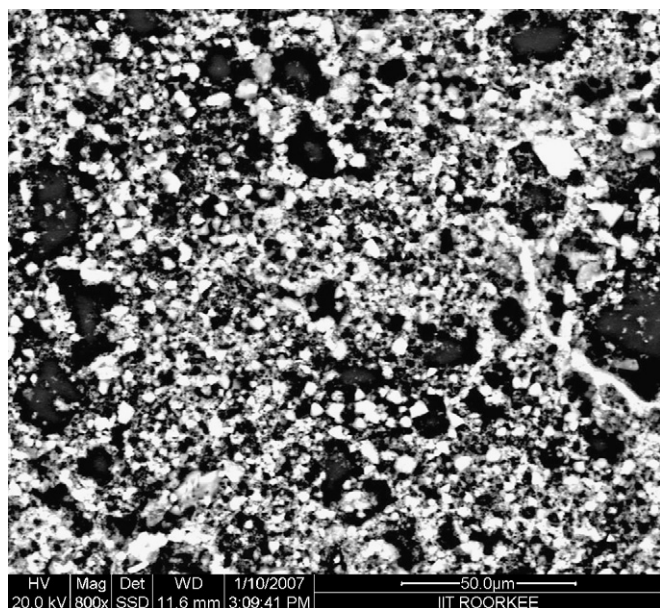
Fig. 1. A typical FE-SEM image of fullerene C_{60} (purity > 99.5%)-modified glassy carbon electrode.

2.3. Procedure

The stock solution of salbutamol (2 mM) was prepared in double distilled water. Required amount of the stock solution was added to 2.0 ml phosphate buffer and the total volume was made 4.0 ml with double distilled water. Osteryoung squarewave voltammograms were then recorded employing fullerene-modified glassy carbon electrode as working electrode. The optimized parameters used for OSWV were: initial E: 0 mV, final E: 1200 mV, square wave frequency (f): 15 Hz, square wave amplitude (E_{sw}): 25 mV, step E: 4 mV.

Blood samples of patients undergoing treatment with salbutamol were obtained from the Institute hospital. Normally blood samples and urine samples were collected after 3 h of taking tablet (8 mg). Urine samples were also collected from the patients who used salbutamol for inhalation. In such cases urine samples were collected after 3 h of using salbutamol as inhalation. The blood, with EDTA as anticoagulant, was ultra-centrifuged at a speed of 1000 rpm for 5 min and the supernatant blood plasma was used to determine salbutamol concentration. Urine samples were diluted 10 times and blood plasma samples 2 times with phosphate buffer of pH 7.4 prior to use for analysis.

3. Results and discussion

3.1. Voltammetric oxidation of salbutamol

Initial studies on oxidation of salbutamol were carried out at fullerene (>99.5% pure)-modified glassy carbon electrode using linear sweep voltammetry. A broad bump was noticed in the entire pH range of 3.0–10.0. As electrocatalytic oxidation may also occur due to differing capacitative effects likely to occur in differential pulse voltammetry, it was considered desirable to
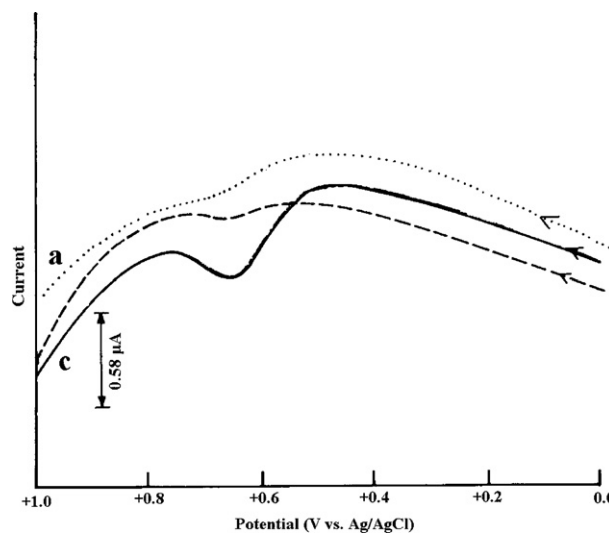
Fig. 2. A comparison of linear sweep voltammograms of 0.2 mM salbutamol at bare glassy carbon (a), at graphite-modified glassy carbon (b) at C_{60}-modified glassy carbon electrode and (c) at pH 7.4.

compare the linear sweep voltammograms (LSVs) of salbutamol at C_{60} with graphite powder-modified electrode. Hence, LSV curves were recorded for 0.2 mM salbutamol solution at three electrodes (bare GCE, C_{60}-modified GCE and graphite powder-modified GCE). It is observed that at the bare electrode no peak is observed, while at the graphite powder-modified GCE; an ill-defined voltammetric peak is seen as shown in Fig. 2. However, at the C_{60}-modified GCE, the peak becomes well-defined with an increase in peak current response and appeared at less positive potential ($E_p \sim 640$ mV). The LSVs at different scan rates were also recorded in 0.6 μM salbutamol solution at C_{60}-modified GCE and it was noticed that the peak current varied linearly with increase in $\sqrt{v}$ in the range of 20–500 mV s^{-1}. Such a dependence of ip on sweep rate confirmed the faradaic nature of the electrode reaction.

Similarly differential pulse voltammetry was carried out at different electrodes and the pulse voltammograms exhibited a well-defined peak as shown in Fig. 3. Square wave voltammetry was then used, which is more sensitive with regard to peak current sensitivity. The oxidation of salbutamol occurred in a well-defined peak (I_a) in the entire pH range. The peak current of salbutamol oxidation peak was practically independent of pH
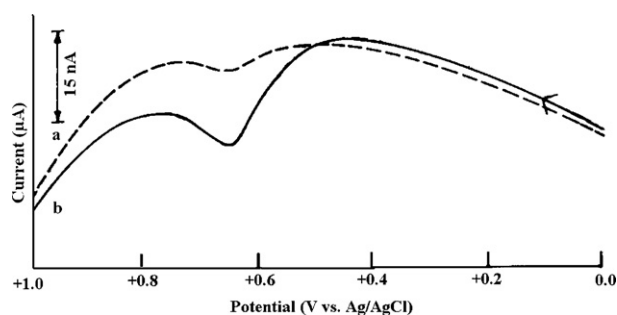

Fig. 3. A comparison of differential pulse voltammograms (a, b) of 0.6 μM salbutamol at bare glassy carbon and C_{60} (>99.5%)-modified glassy carbon electrodes at pH 7.4.
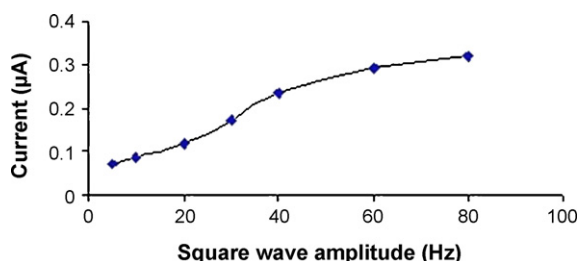
Fig. 4. Observed effect of square wave amplitude on peak current of salbutamol at pH 7.4.

whereas, the peak potential of peak I_a was dependent on pH and shifted to less positive potential with increase in pH. The plot of E_p versus pH was linear and the dependence of E_p on pH can be expressed by the relation:

$$E_p = [1.154 - 0.059 \text{pH}] \text{vs.Ag/AgCl}$$

having a correlation coefficient ~ 0.980. The $dE_p/d\,\text{pH}$ value of ~ 59 mV/pH clearly indicates that the equal number of protons and electrons are taking part in the electrode reaction.

The effect of scan frequency on peak current was studied in the OSWV frequency range of 5–80 Hz. A plot between peak current and square root of scan frequency was found to be linear in the observed frequency range. The linear relation between ip and $\sqrt{f}$ can be represented by the following equation:

$$\text{ip} = 0.0618\sqrt{f} + 0.0335$$

having a correlation coefficient as 0.965. The values of peak current function (ip/$v^{1/2}$) were found to remain practically constant with increase in scan frequency. Such a behavior indicates that the nature of electrode reaction is diffusion controlled [21]. At frequencies higher than 80 Hz, oxidation peak I_a merged with the background current and the peak disappeared.

The effect of square wave pulse amplitude on peak current was studied in the amplitude range of 5–80 mV. It was found that the peak current (ip) sharply increased up to pulse amplitude 40 mV and then tends to level off at higher amplitude (Fig. 4). The variation of peak current with step E values (ΔE) has also been monitored. The peak current was found to increase linearly with increasing step E in the range of 4–24 mV. The linear dependence of ip on step E can be presented by the following equation:

$$\text{ip} = 0.0426\,\Delta E + 0.2809$$

with correlation coefficient as 0.996.

3.2. Effect of graphite and metallic impurity

In a recent communication [18], it has been reported that catalytic effect of fullerenes during oxidation of cysteine is due to the graphite impurities present in it. To determine whether such an effect is also observed for oxidation of salbutamol, a systematic study is planned. For this purpose fullerene (>99.5% purity) was analyzed for Fe(III) using atomic absorption spectrometry. As analysis indicated presence of 0.18% Fe(III), it was considered worthwhile to study effect of graphite as well as Fe(III)
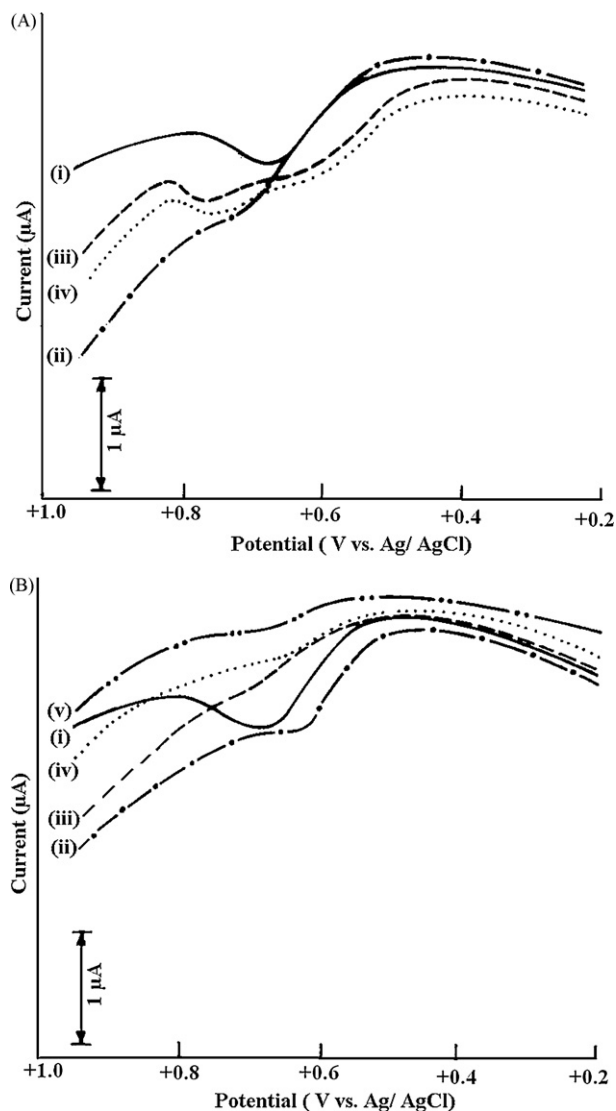
Fig. 5. (A) Effect of Fe(III) on oxidation peak of 0.2 mM salbutamol at pH 7.4. Curves were recorded at bare glassy carbon (i), C_{60}-modified electrode having Fe(III) 15 μl (ii), 30 μl (iii), and 60 μl (iv). (B) Effect of graphite impurities on oxidation peak of 0.2 mM salbutamol at pH 7.4. Curves were recorded at bare glassy carbon (i), C_{60}-modified electrode having graphite added nil (ii), 15 μl (iii), 30 μl (iv), and 60 μl (v).

impurities on oxidation of salbutamol. For this purpose oxidation of salbutamol was studied at bare glassy carbon electrodes as well as modified with fullerene C_{60} having different amounts of metallic or graphite impurities followed by partial reduction of fullerenes in KOH solution. A comparison of square wave voltammograms observed at glassy carbon electrodes modified with different amounts of graphite or ferric nitrate are presented in Fig. 5. Fig. 5B presents a comparison of square wave voltammograms of salbutamol observed at bare glassy carbon- and graphite-modified electrodes. It is observed that at bare glassy carbon salbutamol exhibits an oxidation peak at 634 mV. At C_{60}-modified electrode the peak potential of salbutamol remains same, however, the peak current increased significantly (Fig. 5, curve (ii)). With increasing graphite impurity the peak of salbutamol diminished as shown in Fig. 5B.
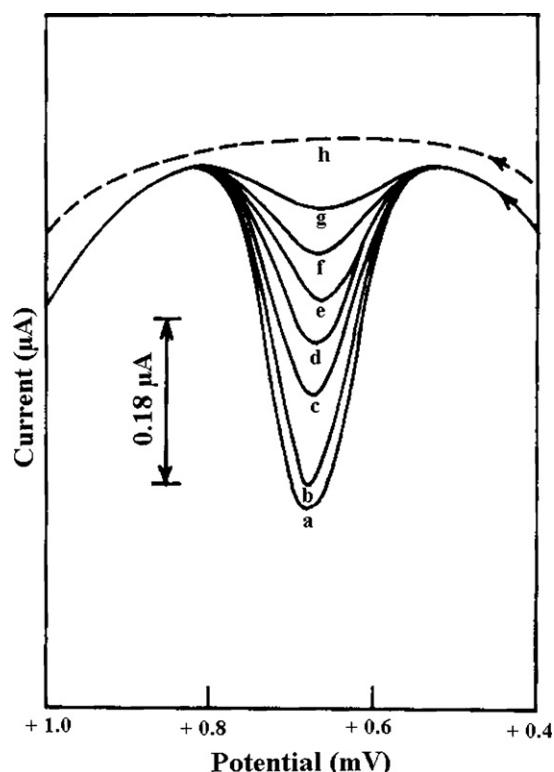
Fig. 6. Effect of increasing concentration of salbutamol on voltammetric peak current at pH 7.4. Curves are recorded at (a) 2000 ng/ml, (b) 1250 ng/ml, (c) 1000 ng/ml, (d) 800 ng/ml, (e) 500 ng/ml, (f) 250 ng/ml and (g) 200 ng/ml. The background is represented by curve h.

As fullerenes have also been reported to possess trace impurity of metals [22], the effect of fullerene having different amounts of Fe(III) was investigated. It was noticed that with 15 μl of C_{60} solution doped with Fe(III), the E_p of salbutamol oxidation peak shifted to more negative potential (curve (iii)) whereas at higher concentrations the peak splitted into two as shown in Fig. 5A. The peak current also decreased with increase in concentration of graphite or Fe(III). Thus, it is concluded that oxidation of salbutamol is catalyzed by fullerenes and not by graphite or metallic impurities.

3.3. Concentration study

The voltammetric method has been optimized for determination of salbutamol in pharmaceutical preparations and biological fluids by recording Osteryoung square wave voltammograms of salbutamol at different concentrations at fullerene-modified glassy carbon electrode. It was found that the peak current of oxidation peak systematically increased with increase in concentration of salbutamol as shown in Fig. 6. A calibration plot observed between ip (after subtracting background current) and salbutamol concentration was linear in the concentration range 100–2000 ng/ml of salbutamol. The linear relation between peak current (ip) and concentration (C) of salbutamol can be expressed by following relation:

$$ip\,(\mu A) = 0.0002\,C$$

where C is the concentration of salbutamol in ng/ml. The correlation coefficient for the expression was 0.995 and the sensitivity of the proposed method was $0.0002\,\mu A\,(ng/ml)^{-1}$. The detection limit for salbutamol was calculated to be 40 ng/ml in phosphate buffer solution of pH 7.4. At a concentration level of 200 ng/ml salbutamol, the peak current signals were obtained with a relative standard deviation of 2.9% for $n = 6$.

3.4. Salbutamol in pharmaceutical tablets and biological samples

Salbutamol containing tablets and syrup were examined for their salbutamol content using fullerene-modified GCE. Tablets were crushed, dissolved in double distilled water and solutions were subsequently diluted to the extent that salbutamol concentration falls in the range of calibration plot. Salbutamol syrup was also diluted with double distilled water before recording OSWV. Voltammograms were then recorded under identical conditions. The concentration of salbutamol determined in different pharmaceutical preparations is compared with labeled concentration of salbutamol and listed in Table 1. It was found that the results are in good agreement with the values printed on labels.

To detect the cases of doping, urine is considered as the most preferred biological specimen [22]. Hence, attempts were made to determine salbutamol in urine samples of the patients undergoing treatment with this drug. The urine samples collected from the patients having taken tablet showed presence of salbutamol as shown in Table 2. On the other hand urine sample of the patient taking salbutamol by inhalation did not show presence of salbutamol. One of the reason for non-observance of salbutamol in case of inhalation is that only 10% of inhaled amount is retained and hence only traces are passed to urine as reported in literatures [23,24]. Diluted urine samples were then also spiked with salbutamol solution and Osteryoung square wave voltammograms were recorded. The results obtained for salbutamol concentration determined in urine sample are summarized in Table 2.

Table 1

A comparison of observed and labeled salbutamol concentration in tablets/syrup of different pharmaceutical companies

Tablet (syrup) name/company	Labeled concentration (ng/ml)	Observed concentration[a] (ng/ml)	Error (%)
Asthalin (Cipla Ltd., Daman)	2000	1900	−5.0
Asthalin Syrup (Cipla Ltd., Kolhapur)	2000	1890	−5.5
Salbetol (FDC Ltd., Salcete, Goa)	1000	1029	+2.9
Theo-Asthalin (Cipla Ltd., Dabhal, Daman)	500	494	−1.2

[a] The R.S.D. for $n = 3$ was always less than ±2.9%.

Table 2
Salbutamol determined in blood and urine samples of asthma patients with the help of fullerene-modified glassy carbon electrode

Sample	Amount spiked (ng/ml)	Amount detected[a] by		Error (%)	
		Proposed method	GC–MS	Proposed method	GC–MS
Blood plasma 1	–	353.9	–	–	–
	250.0	604.5	–	+0.09	–
	375.0	727.9	765.0	−0.14	+4.90
Blood plasma 2	–	375.2	–	–	–
	125.0	501.4	504.5	+0.24	+0.80
	250.0	659.3	–	+5.40	–
Urine 1 (after inhalation)	–	–	–	–	–
	520.0	540.0	–	+3.80	–
	550.0	570.0	–	+3.60	–
Urine (after oral dose)	–	268.9	–	–	–
	250.0	512.0	–	−1.32	–
	500.0	788.2	–	+2.50	–

[a] ng/ml, the R.S.D. for $n = 3$ was always less than ±3.5%.

A typical square wave voltammogram observed for blood plasma sample is shown in Fig. 7. It was found that a broad peak around 380 mV is observed in addition to salbutamol peak at 675 mV. The broad peak at 380 mV is due to uric acid as observed in authentic uric acid as well as reported earlier [25]. In both the blood samples the presence of salbutamol was found and its amount was further confirmed by spiking the samples. The results of voltammetric determination of salbutamol were also cross-validated by comparison with GC/MS analysis. For this purpose various concentrations of salbutamol were also analyzed using GC/MS and a well-defined peak was obtained at Rt ∼ 18.35 min. The peak area under the peak was determined and the calibration curve was obtained by plotting the peak area ratio of the analyte peaks relative to that of the internal standard. The resulting curve so obtained was linear. The diluted blood serum or urine sample was then analyzed after filtering with 5μ Whatman filter paper. A 2.0 μl serum or urine was injected in GC/MS and the area under the peak was determined.

The GC/MS chromatogram observed for blood plasma collected after 3 h of oral medication of salbutamol showed well-defined peaks at retention time ∼17.20, 18.01, 18.52, 20.54, 22.50 min as shown in Fig. 8. The peak at Rt ∼ 18.36 min was due to salbutamol and no attempt was made to characterize other peaks of chromatogram. Using calibration curve, the concentration of salbutamol was determined. A comparison of the salbutamol values obtained by GC/MS and proposed method clearly indicate that the results obtained by the two methods are in good agreement as presented in Table 2. The results presented in Table 2 clearly indicate that salbutamol can be easily determined in blood and urine using the proposed method. Thus, it is believed that the method can be effectively used in case of doping by athletes.

3.5. Effect of excipients

The effect of common excipients usually found in the salbutamol tablets or syrups was investigated by observing the effect on peak potential and peak current. The common excipients usually found in the pharmaceutical tablets and formulations are starch, sodium chloride, lactose, sucrose and benzyl alcohol. The tablet salbetol had sodium chloride and sucrose in traces (actual amount not mentioned on label). Hence, it was considered desirable to elucidate the effect of these common excipients on the peak current of salbutamol. The effect of the excipients was examined by recording voltammograms of 1000 ng/ml salbuta-
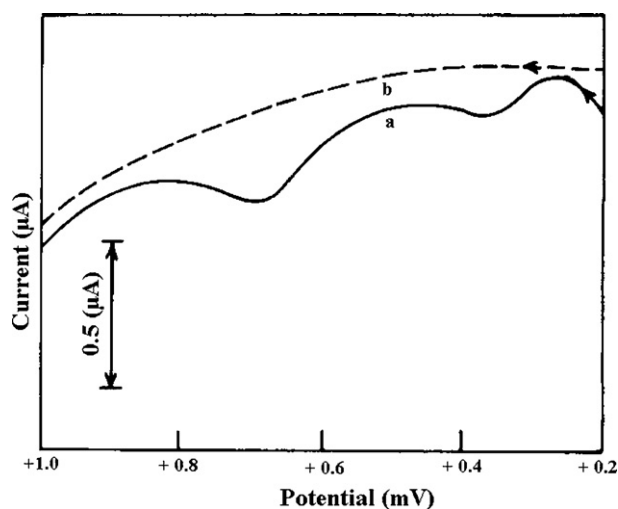

Fig. 7. A typical square wave voltammogram (—) observed for blood plasma sample-2 at pH 7.4 at fullerene-modified (>98% purity) glassy carbon electrode. The background at pH 7.4 is shown by curve (- - -).
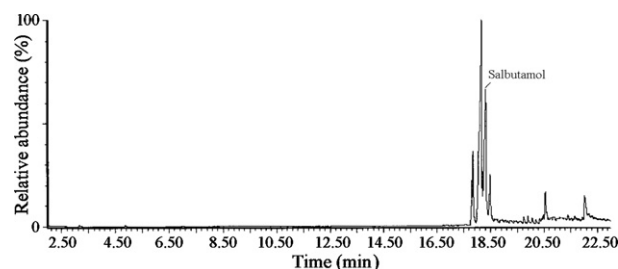

Fig. 8. Typical GC–MS observed for blood plasma (sample 1).

mol in the presence of different excipients in the concentration range of 1000 ng to 10 μg/ml. The study showed that none of the excipients used affected the peak current by greater than ±2%. Thus, it is concluded that the procedure is applicable to determine salbutamol in pharmaceutical formulations directly.

3.6. Oxidation mechanism

The most probable site of oxidation in salbutamol is phenolic hydroxyl group. Thus 1e, 1H$^+$ oxidation of this hydroxyl group would lead to a free radical at oxygen. The free radical can resonate to adjacent carbon atom and combination of two such species will lead to C–C-linked dimer as has been reported in literatures [26,27].

4. Conclusions

A square wave voltammetric method has been described to determine salbutamol using fullerene-modified glassy carbon electrode. It was observed that fullerenes-modified glassy carbon electrode catalyses the oxidation of salbutamol and enhances the peak current values. The bia-amperometric oxidation of salbutamol is reported in literature [28] and two peaks are observed corresponding to hydroxyl group and amino group in differential pulse voltammetry in sodium acetate–acetic acid buffer. Some other workers suggested the second peak due to strong adsorption of the product [14,27]. However, the main advantage in present studies is that only one diffusion-controlled peak corresponding to oxidation of phenolic group is observed. Thus, determination is based on electrode reaction free from adsorption. In contrast to earlier studies [18], where catalytic action in case of cystine is assigned to graphite impurities present in fullerenes, it is observed on the basis of comparison of voltammograms using glassy carbon electrodes modified with C$_{60}$ fullerenes having different amounts of graphite or Fe(III) that catalysis is due to fullerenes and not due to graphite or Fe(III) impurities. The surface of the modified electrode has been characterized by using field emission scanning electron microscope. A linear calibration plot was obtained for salbutamol in the concentration range of 100–2000 ng/ml. Since the threshold level of salbutamol (1000 ng/ml), which renders an athlete to be doped, falls in this concentration range, the procedure described is highly beneficial for first line detection of doped cases. A comparison of detection limit of salbutamol determined by present method with reported ones [14,27] clearly indicate that the present method can detect salbutamol even below the previously reported detection limits. The main advantage of the present method is that the electrode reaction is free from adsorption complications. Determination of salbutamol content in various pharmaceutical preparations using proposed method was found to be satisfactory as the amount determined matches with their labeled quantity. The application of the proposed method for determination of salbutamol in urine and blood samples has also been demonstrated and a comparison of observed result with GC–MS indicates that the method is sensitive and the results are comparable.

References

[1] A. Pichon, N. Venisse, F.E. Krupka, M.C. Perault-Pochat, A. Denjean, Int. J. Sports Med. 27 (2006) 187.
[2] J.E.F. Reynolds, The Extra Pharmacopoeia, 30th ed., The Pharmaceutical Press, London, 1993, p. 1255.
[3] M.G. Miller, J.M. Weiler, R. Baker, J. Collins, G. D'Alonzo, J. Athl. Train. 40 (2005) 224.
[4] L. Martineau, M.A. Horan, N.J. Rothwell, R.A. Little, Clin. Sci. 83 (1992) 615.
[5] J. Huclova, D. Satinsky, H. Sklenarova, R. Karlicek, Anal. Bioanal. Chem. 376 (2003) 448.
[6] M.I. Saleh, Y.M. Koh, S.C. Tan, A.L. Aishah, Analyst 125 (2000) 1569.
[7] I.H.I. Habib, M.E.M. Hassouna, G.A. Zaki, Farmaco 60 (2005) 249.
[8] N. El-Enany, F. Belal, M. Rizk, Chem. Anal. 49 (2004) 587 (Warsaw, Poland).
[9] C. Gabiola, M.A. Garcia-Calonge, M.P. Portillo, J.A. Martinez, A.S. De Barrio, J. Microcolumn. Sep. 8 (1996) 361.
[10] V.B. Sutariya, R.C. Mashru, M.G. Sankalia, J.M. Sankalia, Ars Pharmaceutica 47 (2006) 185.
[11] Y. Shi, Y. Huang, J. Duan, H. Chen, G. Chen, J. Chromatogr. A 1125 (2006) 124.
[12] C.A. Lindino, L.O.S. Bulhões, Talanta 72 (2007) 1746.
[13] K.A. Sagar, M.R. Smyth, R. Munden, J. Pharm. Biomed. Anal. 11 (1993) 533.
[14] D. Boyd, J.R. Barreira Rodriguez, A.J.M. Ordieres, P.T. Blanco, M.R. Smyth, Analyst 119 (1994) 1979.
[15] M.R. Ganjali, P. Norouzi, M. Ghorbani, A. Sepehri, Talanta 66 (2005) 1225.
[16] R.N. Goyal, S.P. Singh, J. Nanosci. Nanotechnol. 6 (2006) 3699.
[17] R.N. Goyal, M. Oyama, S.P. Singh, Electroanalysis 19 (2007) 575.
[18] R.T. Kachoosangi, C.E. Banks, R.G. Compton, Anal. Chim. Acta 566 (2006) 1.
[19] W.T. Tan, A.M. Bond, S.W. Ngooi, E.B. Lim, J.K. Goh, Anal. Chim. Acta 491 (2003) 181.
[20] A. Szucs, A. Loix, J.B. Nagy, L. Lamberts, J. Electroanal. Chem. 397 (1995) 191.
[21] R.H. Wopschall, I. Shain, Anal. Chem. 39 (1967) 1514.
[22] A.V. Talyzin, A. Dzwilewski, J. Nanosci. Nanotechnol. 7 (2007) 1151.
[23] N.C. Durham, in: J.M. Rosenberg, A. Davis, R.J. Fuentes (Eds.), Athletic Drug Reference 94, Clean Data Inc., 1994, p. 109.
[24] B.J. Lipworth, D.J. Clark, Br. J. Clin. Pharmacol. 42 (1996) 257.
[25] R.N. Goyal, V.K. Gupta, M. Oyama, N. Bachheti, Electroanalysis 17 (2005) 2217.
[26] C. Karuwan, T. Mantim, P. Chaisuwan, P. Wilairat, K. Grudpan, P. Jittangprasert, Y. Einaga, O. Chailapakul, L. Suntornsuk, O. Anurukvorakun, D. Nacapricha, Sensors 6 (2006) 1837.
[27] R.N. Goyal, M. Oyama, S.P. Singh, J. Electroanal. Chem. 611 (2007) 140.
[28] M.S.M. Quintino, L. Angnes, Talanta 62 (2004) 231.

Evaluation of feed-forward back propagation and radial basis function neural networks in simultaneous kinetic spectrophotometric determination of nitroaniline isomers

Masoumeh Hasani *, Fereshteh Emami

Faculty of Chemistry, Bu-Ali Sina University, Hamedan 65174, Iran

Abstract

Mixtures of 2-, 3-, and 4-nitroanilines, are simultaneously analyzed with spectrophotometry, based on their different kinetic properties. These nitroanilines react differentially with 1,2-naphtoquinone-4-sulphonate (NQS) at pH 7 in micellar medium to produce colored product. The differential kinetic spectra were monitored and recorded at 500 nm, and the data obtained from the experiments were processed by chemometric approaches, such as back-propagation neural networks (BPNNs), radial basis function neural networks (RBFNNs), and partial least squares (PLS). Experimental conditions were optimized and training the network was performed using principal components (PCs) of the original data. A set of synthetic mixtures of nitroanilines was evaluated and the results obtained by the application of these chemometric approaches were discussed and compared. The analytical performance of the models was characterized by relative standard errors. It was found that the artificial neural networks model affords relatively better results than PLS. The proposed method was applied to the determination of considered nitroanilines in water samples.
© 2007 Elsevier B.V. All rights reserved.

Keywords: Nitroanilines; Artificial neural network; Ternary mixtures; Kinetic; Simultaneous determination; 1,2-Naphthoquinone-4-sulphonate; Partial least squares

1. Introduction

Nitroanilines are commonly encountered organic contaminants in environmental systems which are found in wastewater discharges from industries where they are either manufactured or used as intermediates such as in the synthesis of dyes, antioxidants, pharmaceuticals, in gum inhibitors, poultry medicines, and as corrosion inhibitor. They have been listed as a priority pollutant by many countries due to their toxicity, potential carcinogenic and mutagenic effects.

Due to their solubility in water, anilines can readily permeate through soil and contaminate ground water. They have been found to be harmful to aquatic organisms and may cause long-term damage to the environment [1,2]. They can be taken up by humans via the skin, the respiratory tract and the gastrointestinal tract, and may lead to anoxia, jaundice or anemia. The presence of a nitro group in the aromatic ring enhances the stability to resist chemical and biological oxidation degradation, while the anaerobic degradation produces nitroso and hydroxylamines compounds which are known as carcinogenic [3,4]. Because of their toxicity, bioaccumulation and vast scale distribution in the ecological environment, their separation and determination have become one of the important studies of environmental analysis.

Several methods including high-performance liquid chromatography (HPLC) [5–7], gas chromatography (GC) [8,9], solid phase microextraction [10], thin layer chromatography [11], colorimetry [12], room temperature phosphorescence (RTP) [13] and polarography [14] have been employed to analyze these compounds. In general only the GC and LC approaches have sufficient sensitivity and selectivity for nitroanilines in complex environmental media. However, these multistep procedures are time consuming and they may introduce significant errors caused by adsorption losses, contamination or even decomposition of the sample. Thus, simple analytical methods should be investigated for environmental monitoring of these compounds.

One of the main drawbacks of the application of spectrophotometric methods in the simultaneous determination of aniline

---

derivatives is the high degree of spectra overlapping of these constituents. Nowadays combination of chemometrics methods with the computer-controlled instruments to monitor the absorption spectra creates a powerful method in multicomponent analysis avoiding preliminary separation step [15].

Kinetic spectrophotometric methods are becoming of great interest in chemical analysis. The application of these methods offered some specific advantages such as improved selectivity. The differential kinetic methodology is an efficient way to simultaneously analyze several analytes [16], and a great improvement has been made by using the chemometric procedures [17,18], Kalman filter [19] and classical least squares (CLS) [20–22]. Partial least squares (PLS) [23–25], and artificial neural networks (ANN) [26–29] which do not require prior knowledge of reaction order or reaction rate constant of the involved analytical systems have found increasing applications for multicomponent kinetic determination. The advantages of the ANN approach to the multivariate calibration of data are well known. Firstly, the network architecture can be easily programmed, secondly, the correlation between spectral features and structural categories need not be known in advance, that is, the neural networks can learn by example without any a priori assumption on the behavior of the data. This leads to the ability to process input data containing some degree of uncertainty. These methods make it possible to eliminate or reduce the effects of the analyte–analyte interaction, the synergistic effect (non-additivity of reaction rates), the multistep process and any other unknown nonlinearity.

Among neural networks, the most popular is the multilayer feed-forward networks (FFNNs) with a back-propagation learning algorithm. Recently radial basis function networks (RBFNs) as potential alternative approach has been described [30,31]. This offers some advantages such as robustness to noisy data, compared with FFNN. The theory for RBFN and application to chemical problems are found in the literature [32,33].

Surfactant micelles are organized molecular assemblies, which have great utility in many applications of analytical chemistry [34–36]. Many advantages including sensitivity and improved selectivity in analysis can be achieved by the use of micellar system. They offer a relatively large microscopic nonpolar environment for solute partition. This effect can increase the solubility of solutes in the micellar surfactant solution in comparison with water solution. This is due to the amphiphilic character of the micellar surface, which provides both electrostatic and hydrophobic sites of interaction with solutes in aqueous solutions. They also have substantial catalytic effect on many reactions. Surfactants usually affect spectral parameters. The intensity of the absorption bands can be increased and shifts in the absorption maxima of reagents and complexes are observed [37,38].

1,2-Naphtoquinone-4-sulphonate (NQS) is commonly used for spectrophotometric determination of aliphatic amines [39–41]. It is a general spectrophotometric reagent for both primary and secondary amine groups. However, to the best of our knowledge, the use of sodium 1,2-naphtoquinone-4-sulphonate as a chemical derivative chromogenic reagent for the determination of nitroanilines by a condensation reaction has not been reported so far.

In this paper, a differential reaction rate method for the simultaneous analysis of ternary mixtures of nitroaniline isomers, 2-, 3-, and 4-nitroanilines, with the aid of chemometric approaches, back-propagation neural networks (BPNNs), radial basis function neural networks (RBFNNs), and partial least squares (PLS) has been developed. The method is based on the kinetics of the individual nitroanilines with NQS. The measured kinetic data was processed by the chemometric methods to develop calibration models, and the method was then validated with the use of a set of synthetic samples containing mixtures of the nitroanilines; thereafter, it was applied to several water samples to demonstrate general applicability .

2. Experimental

2.1. Apparatus and software

UV–visible absorbance digitized spectra were collected on a Perkin-Elmer Lambda 45 spectrophotometer, using a 1 cm quartz cell within the wavelength range 450–600 nm. Absorbance measurements as a function of time, at a fixed wavelength were made with a Shimadzu UV-265 spectrophotometer. The apparatus was equipped with a temperature controlled cell holder. Both sample and blank compartment were kept at constant temperature by a Shimadzu CPS-260 thermostat. The pH measurements were performed on a Metrohm 744 pH-meter using a combined glass electrode.

2.2. Solutions and reagents

All chemicals were analytical reagents grade and used without further purification. All solutions were prepared with triply distilled water. Stock solutions (1.23×10^{-3} M) of 2-, 3-, and 4-nitroaniline (Merck) were prepared by dissolving the appropriate amount of each compound in water. A 1.84×10^{-2} M stock solution of 1,2-naphtoquinone-4-sulphonate was prepared by dissolving 24 mg of the sodium salt (Merck) in water in a 5-ml volumetric flask. This solution was prepared fresh for each experiment and was stored in the dark at room temperature. Working solutions were prepared by dilution as required. The 0.05 M tris hydroxymethyl amino methane (tris) buffer (pH 7) was prepared by dissolving 1.2 g of the chemical (Merck) in about 150 ml of water, adjusting the pH to 7 with hydrochloric acid and diluting to 200 ml with distilled water. The solution of surfactant Triton X-100 (Merck) was prepared by dissolving 0.232 g of the reagent in 50 ml volumetric flask with triply distilled water. All chemicals used in the interference study were from Merck and used as received.

2.3. Data processing

Data were processed on Pentium IV computer. Softwares of BPNNs and RBFNNs were employed with the use of the Neural Network Toolbox, Matlab 7.0. Other chemometric programs including principal component analysis (PCA) and PLS were also written in MATLAB 7.0 on Windows. The data for training

BPNNs and RBFNNs were the scores obtained by the PCA of kinetic data.

2.4. Procedures

Aliquots of either one of the nitroaniline isomer solution or a mixture of these compounds (so that their final concentrations would be in the range of 4–41 µg ml^{-1}), 2 ml tris buffer 0.05 M (pH 7), 0.3 ml Triton X-100 7.2×10^{-3} M, were transferred into a 5 ml volumetric flask. Then 0.5 ml of NQS solution 1.84×10^{-2} M was added. This solution was diluted to volume with water and mixed well. After mixing, 3 ml of the reaction was immediately transferred to a spectrophotometric cell which was kept at a constant temperature of 35 °C. The absorbance was recorded as a function of time for 30 min at 500 nm against reagent blank treated similarly. The zero time was taken as the moment the last drop of the sample solution was diluted to the mark with water. The signal ΔA ($\Delta A_{total} - \Delta A_{blank}$) between 1 and 30 min was considered as analytical signal. The same procedure and experimental conditions were used in interference study in the presence of interfering substances. The kinetic data obtained from experiments were processed by BPNNs, RBFNNs and PLS calibration models.

3. Results and discussion

In the present work, the reactions of nitroaniline isomers with NQS reagent were investigated. These reactions yielded colored products with similar and overlapped spectra. The formation of these colored products was utilized in the development of a kinetic spectrophotometric method for the simultaneous determination of 2-, 3-, and 4-nitroanilines. Spectra of the colored product and the corresponding reagent blank were measured in the range of 450–600 nm at a reaction time of 30 min according to the previously described experimental procedure (Fig. 1). The spectral shapes resulting from the three reactions of the nitroanilines are very similar, which complicates the analysis of the spectral output from their mixtures. It is impossible to determine the three compounds simultaneously by conventional methodology. The spectra of nitroaniline isomers in reaction with NQS are time dependent. Sample spectra for 4-nitroaniline in the presence of other reagents at optimum conditions is shown in Fig. 2.
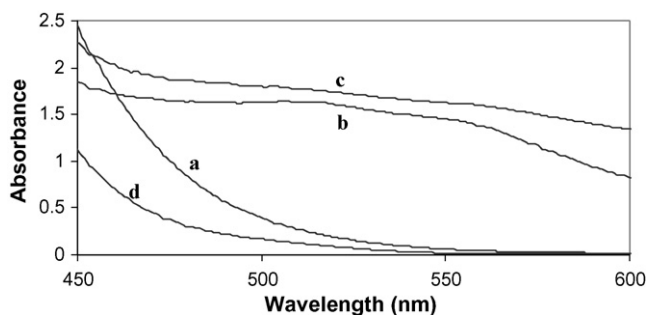

Fig. 1. The absorbance spectra of (a) 2-nitroaniline; (b) 3-nitroaniline; (c) 4-nitroaniline, 7.38×10^{-4} M in the presence of 1.22×10^{-3} M NQS and 4.8×10^{-4} M Triton X-100 at pH 7 at 35 °C; and (d) reagent blank.
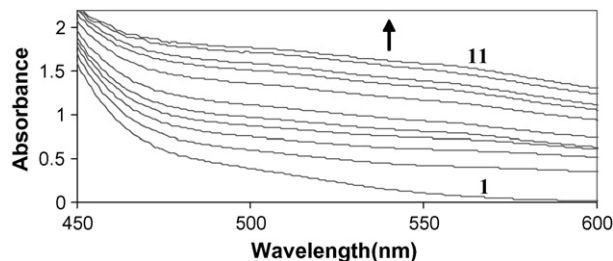
Fig. 2. The absorbance spectra of a mixture of 4-nitroaniline (7.38×10^{-4} M) and NQS (1.22×10^{-3} M) at the optimum experimental conditions. time interval (1) 3 min; (2) 6 min; (3) 9 min; (4) 12 min; (5) 15 min; (6) 21 min; (7) 33 min; (8) 42 min; (9) 45 min; (10) 50 min; and (11) 60 min.

As seen, the absorption at 500 nm increases with elapse of time. Preliminary investigations showed that the reaction rates for the three nitroanilines with NQS are different. Thus the differential kinetic rates should be useful for resolving the spectra from the nitroaniline mixtures with the use of chemometric methods. In the chemometric methods used, generally a set of calibration samples with known compositions is first prepared and the kinetic measurements are carried out, after which, the mathematical models are established by processing the measured kinetic data. Subsequently, the mathematical models are used for the prediction of unknown samples under the same experimental conditions.

3.1. Influence of variables

The overall process is influenced by factors such as pH of the buffer, concentration of NQS, concentration of Triton X-100 and temperature which affect the absorbance of the colored product. So, the various experimental parameters affecting the development of the reaction were carefully studied and optimized.

3.1.1. Effect of micelle

The influence of various kinds of surfactants on the determination of nitroanilines was studied. This study was carried out by addition of different micellar solutions of anionic (sodium dodecyl sulphate, SDS), cationic (cetyl trimethylammonium bromide, CTAB and cetylpyridinium chloride, CPC), and nonionic (Triton X-100, TX-100 and Triton X-114, TX-114) surfactants to the nitroaniline-NQS systems with fixed concentration of nitroaniline isomers (1.23×10^{-4} M) and NQS (1.23×10^{-3} M). The maximum enhancement in the absorbance of the nitroaniline isomers-NQS was occurred in presence of Triton X-100. Therefore, Triton X-100 was selected as a micellar medium in the proposed procedure. Studies for optimization of micelle concentration on the reaction revealed that the optimum concentration in the final assay solution was 4.8×10^{-4} M. ΔA ($\Delta A_{total} - \Delta A_{blank}$) signals were found to be maximum at 4.8×10^{-4} M of Triton X-100 (2 CMC) (Fig. 3).

3.1.2. Influence of pH

The influence of pH on the absorbance of the reaction of individual nitroailine isomers with NQS was studied in order to establish the experimental conditions resulting in the greatest

Fig. 3. Effect of Triton X-100 concentration on the ΔA signals of (a) 2-nitroaniline; (b) 3-nitroaniline; and (c) 4-nitroaniline 1.23×10^{-4} M in the studied reaction.

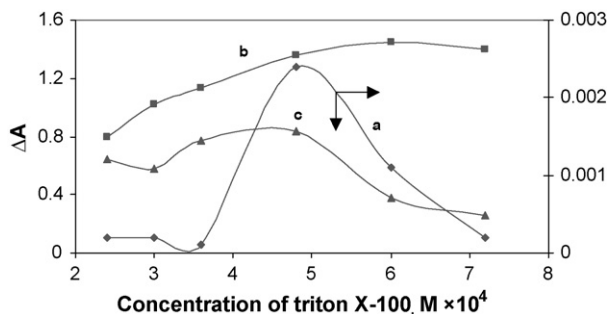Fig. 5. Effect of temperature on the ΔA signals of (a) 2-nitroaniline; (b) 3-nitroaniline; and (c) 4-nitroaniline 1.23×10^{-4} M in the studied reaction.

possible discrimination between the kinetic behavior of nitroaniline isomers and greatest value of signal. For this purpose, changes in absorbance at different pHs at 500 nm over 30 min following the initiation of the reaction were monitored and ΔA ($\Delta A_{total} - \Delta A_{blank}$) signal is plotted against pH (Fig. 4). It was found that under high acidity condition (not shown in Fig. 4); it is difficult for nitroaniline to react with NQS. The possible reason may be that in acidic medium the amino group of nitroaniline isomers is protonated and turns into protonated amine salt. So it loses nucleophilic capacity for 4-sodium sulphunate of NQS and the condensation reaction cannot take place easily. But the absorbance of the solution increases with growth of pH. It may be that protonated amine salt of nitroanilines turns into amino group again when the acidity of the solution becomes low. At pH 7 the ΔA ($\Delta A_{total} - \Delta A_{blank}$) signal reaches its maximum; in other words, the degree of the condensation reaction is also maximal. At higher pH the ΔA signal decreases again, presumably due to the increase of hydroxide ion holds back the condensation reaction between nitroanilines and NQS. Consequently, the absorbance of the solution is reduced. In order to keep the high sensibility for determination of nitroanilines, pH 7 was selected for the optimal experimental conditions.

3.1.3. Temperature

Keeping pH at 7 and micelle concentration at 4.8×10^{-4} M, the influence of temperature on the absorbance of the solution was studied in the range of 10–55 °C. The changes in absorbance at 500 nm in the time interval of 1–30 min at different temperatures were monitored for each nitroaniline individu-

ally. It was found that the ΔA signal for 2-, and 4-nitroaniline increases up to 35 °C and after that level off or slightly increase. For 3-nitroaniline the ΔA signal decreases with increasing the temperature up to 35 °C and remained approximately constant (Fig. 5). In order to make the determination of nitroanilines more sensitive the 35 °C was chosen as the optimum temperature. So, this temperature was selected to be used in further experiments.

3.1.4. Effect of NQS concentration

The amount of NQS has to be in reasonable excess to maintain a pseudo-first order reaction. In order to find the optimal concentration of NQS, the effect of its concentration on the reaction of each nitroaniline was studied by carrying out the reaction at 35 °C using preselected pH 7 and Triton X-100 concentration, and varying concentration of NQS in the range of 6.15×10^{-4} to 2.46×10^{-3} M. The concentration of NQS affects the spectral sensitivity and kinetic behavior of all three compounds. It was also noted that the blank increased with increasing amount of NQS, and the reasonable ΔA were obtained when the concentration of NQS in the final assay solution was 1.84×10^{-3} M (Fig. 6).

3.2. Synergistic effect

Application of ANNs in multivariate calibrations was proposed when a significant nonlinearities is observed in the data. The nonlinearity due to synergistic effect, which is the main factor to the error of the kinetic analysis, has attracted much attention, and some work has been done for solving this problem in nonlinear systems with the aid of chemometrics [42].
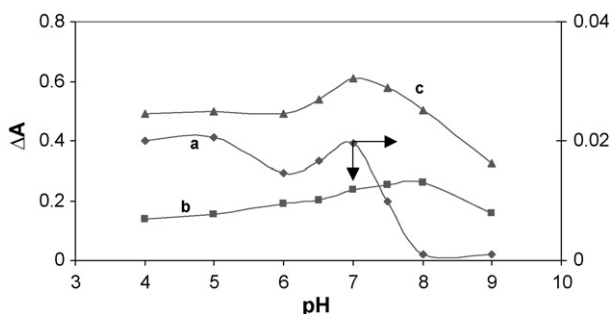

Fig. 4. Effect of pH on the ΔA signals of (a) 2-nitroaniline; (b) 3-nitroaniline; and (c) 4-nitroaniline 1.23×10^{-4} M in the studied reaction.

Fig. 6. Effect of NQS concentration on the ΔA signals of (a) 2-nitroaniline; (b) 3-nitroaniline; and (c) 4-nitroaniline 1.23×10^{-4} M in the studied reaction.

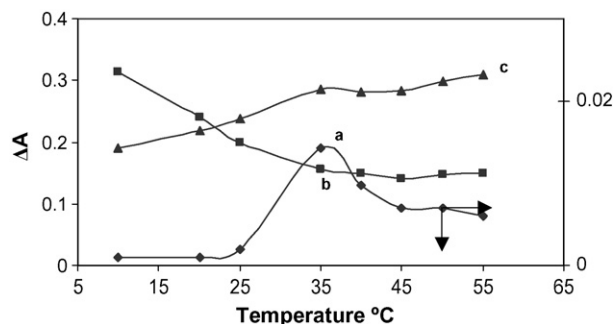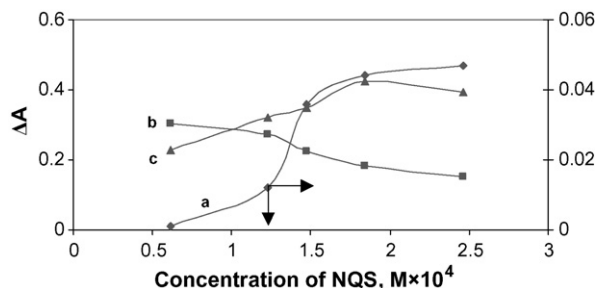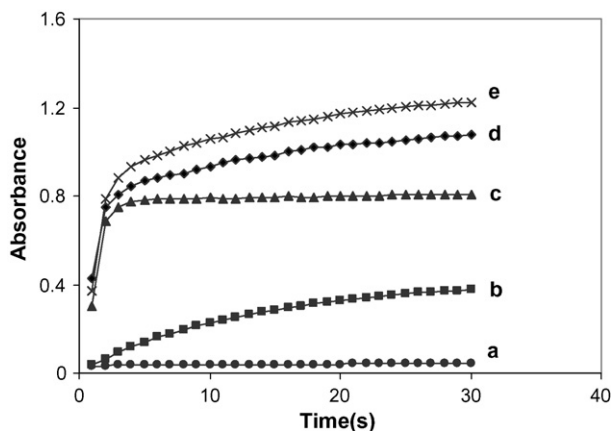Fig. 7. Synergistic effects: (a) 2-nitroaniline; (b) 4-nitroaniline; (c) 3-nitroaniline (1.23×10^{-4} M); (d) mixture of 1.23×10^{-4} M of 2-, 3-, and 4-nitronilines (experimental); and (e) mixture of 1.23×10^{-4} M of 2-, 3-, and 4-nitronilines (expected). Other experimental parameters are those selected as optimum, $\lambda = 500$ nm.

As Fig. 7 shows the kinetic curve of NQS after reaction with the ternary mixture of the nitroanilines (curve d) has a lower overall intensity than the one computed from the sum of the kinetic curve of NQS after reaction with the individual amino acid components (curve e). Thus there is a factor(s), which is not accounted for by the simple Beer's and absorbance additivity laws and ANN models can be used for such nonlinear systems to resolve mixtures.

3.3. Kinetic study of reaction between nitroaniline isomers and NQS

Amino group of nitroanilines display nucleophilicity due to the fact that its lone pair of electron of nitrogen can attack the electron deficiency center. The 4-C of sodium 1,2-naphtoquinone-4-sulphonate becomes an electron deficiency center because three 4–C=C bond conjugates with 2–C=O. So, nitroanilines can react with NQS in a condensation reaction [43]. According to the literature [43], the reaction equation is as Scheme 1.

Fig. 7(curves a–c) shows the kinetic runs of 2-, 3-, and 4-nitroaniline in presence of an excess amount of NQS at pH 7 in
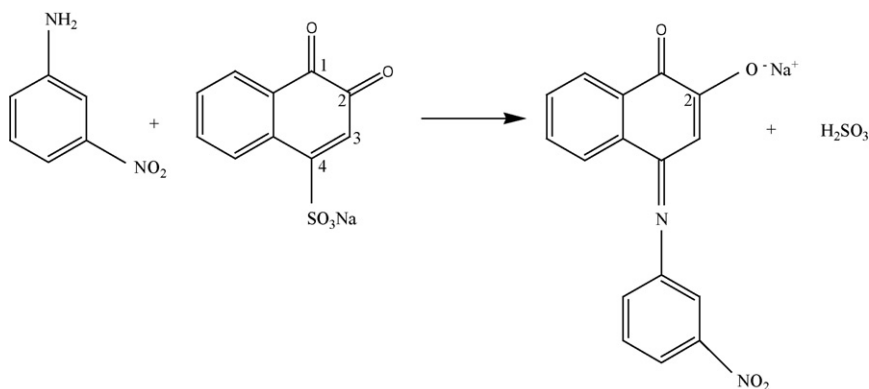
micellar medium at 35 °C. As seen, 3-nitroaniline isomer (curve c) has a comparatively higher absorbance, which indicates this reaction has a higher rate than those involving the other two isomers. This observed difference in the kinetic behavior of the nitroanilines may be understood by considering some of the possible structures of the nitroaniline molecules and the nature of the products formed. Two parameters of strick hindrance of NO_2 and resonance effect of NH_2 groups affect the rate of the reaction. In 2-, and 4-nitroanilines, the electron pair of the nitrogen atom in NH_2 group is partly shared with the ring and it is less available in the reaction. The tendency (through resonance) for the –NH_2 group to release electrons to the aromatic ring makes the amine less nucleophile. Moreover, the strick hindrance in 2-nitroaniline is very high. These two factors cause the reaction rate of 2-nitroaniline has the least value. In 3-nitroaniline the strick hindrance is relatively low, at the same time due to absence of resonance effect of NH_2 group the rate of the reaction is the maximum among the three isomers. According to the pseudo-first order reaction model, the rate constant for each nitroaniline can be calculated by fitting the kinetic data obtained from several known single component samples into equation $A_t = A_\infty + (A_0 - A_\infty)\exp(-kt)$ by a suitable regression method (A_0, A_∞ and A_t are the measured absorbances at initial, infinite and time t, respectively). The observed rate constant for each system was evaluated by fitting the corresponding absorbance–time data to the above equation using a nonlinear least squares curve fitting program KINFIT [44]. The program is based on the iterative adjustment of calculated to observed absorbance values by using either the Wentworth matrix [45] technique or the Powel procedure [46]. The adjustable parameters are k and A_∞. Estimates of the three rate constants (min^{-1}) for the reaction of NQS with desired analytes are $(2.62 \pm 0.25) \times 10^{-2}$, (1.13 ± 0.03), $(6.03 \pm 0.19) \times 10^{-2}$ for 2-, 3-, and 4-nitroaniline, respectively.

3.4. Individual calibration of single nitroaniline components

A set of solution samples with different analyte concentrations was prepared for each of the three nitroanilines and the kinetic measurements were carried out under optimum condition according to the experimental procedure described in Section 2.4. Fig. 8 shows the individual calibration plots obtained for
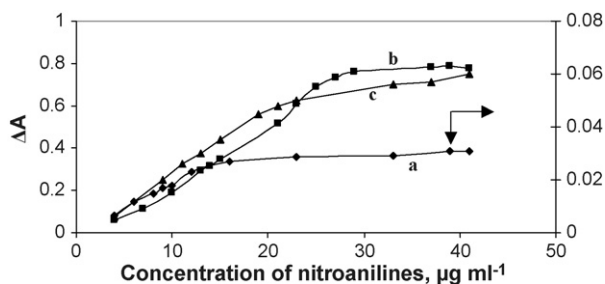

Scheme 1.

Fig. 8. Individual calibration graphs for (a) 2-nitroaniline; (b) 3-nitroaniline; and (c) 4-nitroaniline under optimum conditions at 30 min.

kinetic runs of these three amino acids in which the difference in absorbance ΔA (=$\Delta A_{\text{total}} - \Delta A_{\text{blank}}$) between 1 and 30 min is plotted against concentration of nitroanilines.

3.5. Quantitative analysis using back-propagation neural networks

Among neural networks, the most popular is the multilayer feed-forward net with the back-propagation learning algorithm. Its basic theory and application to chemical problems can be found in the literature [47,48]. At the first step of this study, the BPNNs were used for the quantitative determination of nitroaniline isomer mixtures. The neural network performs a nonlinear iterative fit of data. The structure of the network was comprised of three node layers: an input layer, a hidden layer and an output layer. The nodes in the input layer transfer the input data to all nodes in the hidden layer. These nodes calculate a weighted sum of the inputs that is subsequently subjected to a nonlinear transformation function. The output of the network is a weighted sum of the output of the hidden layer and it is the calculated concentration. During the training process (i.e. calibration) the weights are iteratively calculated in order to minimize the sum of squared difference between the known concentrations and the calculated concentrations. The iteration would be finished when the error of prediction reached a minimum. The kinetic data obtained from experiments were processed by ANN with error back-propagation as training scheme and generalized delta rule for weighting.

The first step in simultaneous determination of coexisting species, by using a multivariate calibration method, involves designing standard composition of calibration set to provide the best prediction. In order to select the mixtures that provide more information using a few experimental trials from calibration set, 17 standard ternary mixtures of nitroaniline isomers were prepared for the training (calibration) set. Another eight synthetic mixtures were used for verification of the calibrations (prediction or test set). The calibration set was used for construction and optimization of ANN model. The prediction set was employed as an independent test set to evaluate the predictive ability of the model. Table 1 shows the composition of the calibration and prediction samples. The predictive ability of each model for each nitroanilines was described in terms of relative standard error for estimation of concentration in the prediction set (RSEP%). Both calibration and prediction concentration sets

were randomly selected. In this way the correlation between concentrations of species was avoided because collinear components in the training set data tend to cause overfitting in the model. The concentration ranges for 2-, 3-, and 4-nitroanilines were 4–23, 4–20, and 4–13 μg ml^{-1}, respectively. The both sets were subjected to the kinetic measurements according to the procedure in Section 2.4. The kinetic data were recorded at 500 nm, and sampled every 1 min between 0 and 30 min.

3.5.1. Reducing the number of data

The number of elements of input vectors is one of the factors which determine the number of weights that should be adjusted in the training process. Decreasing the data volume before using ANNs for nonlinear multivariate calibration was suggested as a preprocessing step in many of the previous studies [49,50]. So before building the ANN models, the original kinetic data for the nitroaniline mixtures were subjected to principal component analysis and decomposed to PC scores which are then submitted as input data for the input layer of ANN. Reducing the number of input data without loosing information decreases the effect of chance in getting accurate adjustment of weights. Also, when the PCA data reduction procedure is applied prior to the construction of the nonlinear ANN model, its dimensional effect is to increase the numerical stability of the model construction process and reduce the amount of colinearity between variables [51]. The optimum numbers of scores for each analyte is determined based on the prediction ability of constructed network for a set of independent sample.

3.5.2. Network optimization

The BPNNs methodology has several empirically determined parameters. These include: when to stop training (i.e. the number of epochs or the convergence criterion), the number of hidden units, the learning rate and momentum terms. In this study, all parameters for the network models were tested and then chosen for inclusion in the analytical model corresponds to the minimum value of the relative standard error (RSE%). The RSE for a single component in mixtures can be formulated as

$$\text{RSE}\,(\%) = 100 \times \left[\frac{\sum_{j=1}^{N} (_j\hat{C} - C_j)^2}{\sum_{j=1}^{N} (C_j)^2} \right]^{1/2}$$

and designated as %RSEC, and %RSEP for the calibration, and prediction sets, respectively.

PC-ANN architectures were constructed by using different number of PCs with one bias node for the input layer and the number of PCs to be included in the PC-ANN model was investigated. The %RSEP for each analyte reached a minimum at 4, 2, and 4 PCs for 2-, 3-, and 4-nitroaniline, respectively (Table 2). In order to determine the optimum number of hidden nodes, a series of different topologies was used, in which the number of nodes was varied from 1 to 15. Each topology was repeated five times to avoid random correlation due to the random initialization of the weights. According to its generalization ability on the test set, the RSEP% of the test set of each topology was calculated. It was found that the lowest RSEP% value obtained

Table 1
Composition of calibration, and prediction samples in ternary mixtures of nitroaniline isomers (concentration in $\mu g\,ml^{-1}$)

Sample	Calibration set			Validation set		
	2-Nitroaniline	3-Nitroaniline	4-Nitroaniline	2-Nitroaniline	3-Nitroaniline	4-Nitroaniline
1	4.1	4.1	9.2	4.1	8.2	9.2
2	11.2	17.0	12.9	11.2	17.0	9.2
3	11.2	20.0	9.2	11.2	20.0	6.1
4	19.0	4.1	12.9	19.0	4.1	8.2
5	19.0	8.2	9.9	5.1	9.2	9.9
6	23.1	17.0	12.9	11.2	12.9	8.2
7	5.1	5.1	6.1	11.2	17.0	12.9
8	5.1	9.2	8.2	20.0	17.0	9.9
9	11.2	12.9	12.9			
10	11.2	17.0	9.9			
11	17.0	5.1	8.2			
12	20.0	12.9	6.1			
13	4.1	4.1	12.9			
14	19.0	8.2	4.1			
15	23.0	20.0	12.9			
16	17.0	5.1	12.9			
17	17.0	9.2	6.1			

when the number of hidden units was 7, 6 and 6 for 2-, 3-, and 4-nitroanilines, respectively. All other parameters of ANN with back-propagation learning algorithm including number of iterations, momentum, learning rate and transfer functions were optimized using minimum RSEP% values of the test set during the training process. The construction of optimized ANN model is summarized in Table 2. Different characteristics of ANN models for three analytes do not permit to use a single ANN model with three output nodes as a suitable model for simultaneous analysis of three analytes. So, neural network models for individual components were made with respect to output layer considered as a single node corresponding to the analyte. The results obtained for prediction samples are given in Table 3.

3.6. Quantitative analysis using radial basis function neural networks

At the second step of the study, the RBFNNs used for the quantitative analysis of nitroaniline isomer mixtures. RBFNN is a type of neural network used to solve several problems such as modeling and classification. The RBFNN consists of three layers: input layer, hidden layer and output layer. The input layer

Table 2
Optimized parameters used for construction of BPANN models

Parameters	Compound		
	2-Nitroaniline	3-Nitroaniline	4-Nitroaniline
Input nodes	4	2	4
Output nodes	1	1	1
Hidden nodes	7	6	6
Number of iterations	9	16	11
Momentum	0.0007	0.0014	0.0014
Learning rate	0.2	0.2	0.2
Hidden layer transfer function	Tansig	Logsig	Logsig
Output layer transfer function	Linear	Linear	Linear
PCs	4	2	4

does not process the information. It only distributes the input vectors to the hidden layer. The hidden layer of RBFNN consists of a number of RBF units. Each neuron on the hidden layer employs a radial basis function as nonlinear transfer function to operate on the input data. The output neurons calculate a linear combination of the basis function.

3.6.1. Establishing RBF neural network

In this section, attempt was made to select the best parameters for establishing neural network for each analyte separately. In this way separate networks were trained for 2-, 3-, and 4-nitroanilines. Relative standard error percent estimated for the prediction of analytes concentrations in the verification set was the criteria for illustration of the performance of the trained networks as calibration models. When RBF neural networks are used basically two parameters must be optimized and defined: the number of neurons on the hidden layer and the width of the radial basis function (spread). The larger the spread, the flatter and smoother will be the Gaussian function approximation. If the spread is too large, each neuron responds essentially the same and due to the large overlap of the input regions, the network cannot be designed well. If the spread is too small then many neurons are needed to obtain a smooth function, and the network may not generalize well. The optimal values of the parameters are chosen to provide minimum training and test set error.

The RBFNN employed in the study utilized the newrb function implemented in Matlab. The function newrb iteratively creates a radial basis network by adding one neuron at a time. Neurons are added to the network until the minimum error for prediction has been reached. The number of radial basis functions (the hidden layer units) greatly influences the performance of a RBFNN. If the number is too low, the network may not calculate a proper estimation of the data. On the other hand, if too many hidden layer units are used, the network tends to overfit the training data.

Table 3
%RSE and %recovery values for prediction samples in the determination of nitroaniline isomers in ternary mixtures with different chemometric models

Method	%RSEP			%RSET[a]	%Recovery[b]		
	2-Nitroaniline	3-Nitroaniline	4-Nitroaniline		2-Nitroaniline	3-Nitroaniline	4-Nitroaniline
RBFNN	5.7	6.7	5.2	6.1	102	96	102
BPNN	7.8	6.3	6.5	6.8	92	98	103
PLS	20.0	6.2	6.7	12.7	118	99	104

[a] $\mathrm{RSE}_T = [(\sum_{i=1}^{n}\sum_{j=1}^{m}(C_{ij(\mathrm{found})} - C_{ij(\mathrm{added})})^2)/(\sum_{i=1}^{n}\sum_{j=1}^{m}(C_{ij(\mathrm{added})})^2)]^{0.5}$.

[b] Recovery (%) $= 100 \times ((\sum_{i}(C_{i(\mathrm{found})}/C_{i(\mathrm{added})}))/n)$, where n is the number of samples.

Input variables for this part were PCs from application PCA on kinetic data. In this way, PCs values of 1–8, spread values of 1–25 and number of hidden nodes of 1–10 were investigated. For each PC, spread and number of hidden nodes changed simultaneously. RSE% for the prediction of each nitroaniline isomers (in the verification samples) was calculated for each case. The three-dimensional graph of RSEP% versus number of hidden node and spread for each nitroaniline is plotted in Fig. 9. We selected the spread and number of hidden nodes at which the RSEP% has minimum value. The number of epochs is also optimized in order to obtain minimum RSEP% error which has to be selected by the user taking into account overfitting and overtraining situations. The construction of optimized RBFNN model is given in Table 4. In the case of using RBFNNs, the obtained results from repetition of training procedure for each condition were the same. It was due to high reproducibility of modeling that is a main advantage for RBFFNS.

When all the adjustable parameters of the neural network had been optimized, this neural network showed a high ability of generalization. The %RSEP values calculated from the concentration values of the mixtures predicted by the optimized RBFNN are also listed in Table 3.

3.7. Modeling with PLS

In addition to ANN, the concentration of mixtures of nitroaniniline isomers was estimated by processing the kinetic data from the test samples by applying the calibration model including partial least squares. PLS was selected as a standard multivariate calibration method for comparing and evaluating the results of ANN. PLS method involves a calibration step in which the relation between signal and component concentrations

is estimated from a set of reference samples, and a prediction step in which the results of the calibration are used to estimate the component concentration in an unknown sample spectrum. Herein, we implemented the PLS-1 version that is optimized
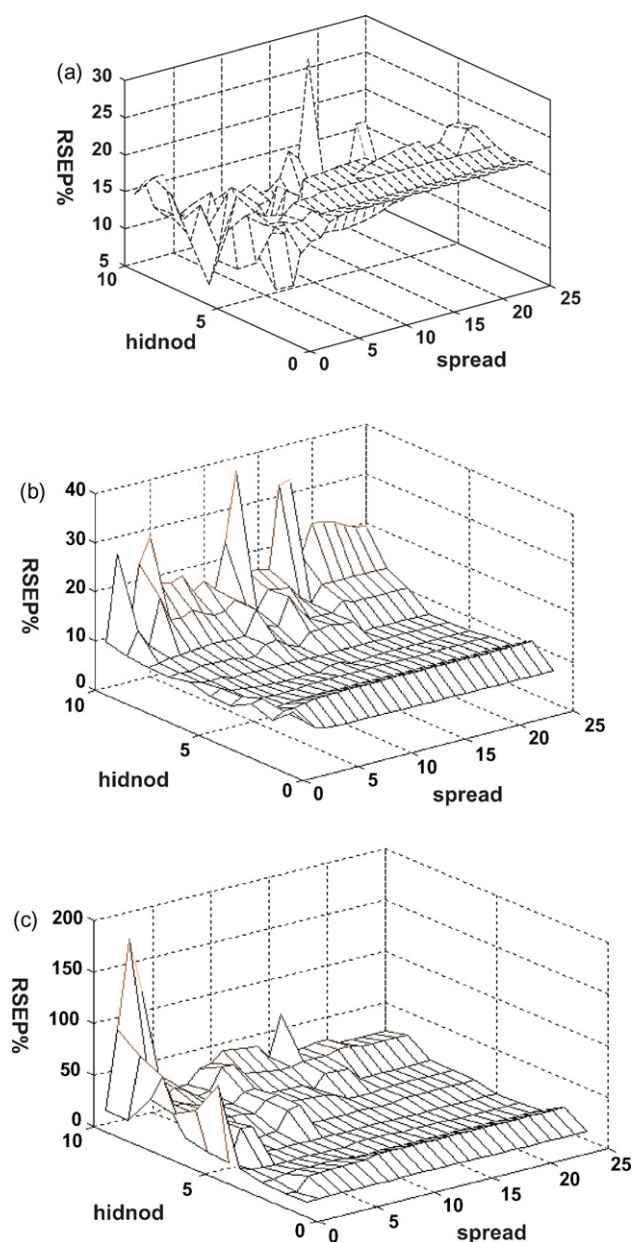
Fig. 9. Plots of %RSEP as a function of number of nodes in the hidden layer and spread for (a) 2-nitroaniline; (b) 3-nitroaniline; and (c) 4-nitroaniline.

Table 4
Optimized parameters used for construction of RBFANN models

Parameters	Compound		
	2-Nitroaniline	3-Nitroaniline	4-Nitroaniline
Spread	6	19	2
Number of PCs	4	2	4
Hidden nodes	9	7	5
Number of iterations	9	7	5
Output nodes	1	1	1
Hidden layer transfer Function	Gaussian	Gaussian	Gaussian
Output layer transfer function	Linear	Linear	Linear

Table 5
Effect of potential chemical interferents on the determination 2-, 3-, and 4-nitroaniline by the proposed method

Compound	Maximum tolerance ($\mu g \, ml^{-1}$)
Cl^-, NO_3^-, S^{2-a}, SO_3^{2-a}, Ag^+, pb^{2+}, K^+, Na^+, Zn^{2+}, Mg^{2+}, Ca^{2+}, Ni^{2+}, lactose, fructose, glucose	5000
CH_3COO^-, Ba^{2+}	4000
Phenol, hydroquinone	3000
4-Methoxyphenol	2000
Sr^{2+}, Rb^{2+}, MoO_4^{2-}	1000
SO_4^{2-}	400
Starch	200
IO_4^-, IO_3^-, Fe^{2+}, Fe^{3+}, Co^{+3}, Hg^{2+}, 3-chlorophenol, catechol	100
NH_4^+	27
Triptophane, hydroxy proline, cystein, arginin, serine, leucine, glycine, phenyl-alanin, methionin, glutamine, lysine, proline, sucarose, 1-naphtol	5

Concentration of 2-, 3-, and 4-nitroaniline was 5, 4 and 4 $\mu g \, ml^{-1}$, respectively.
[a] In the presence of NaCl.

for the determination of a single analyte of interest (each of the three nitroanilines in turn). The optimum number of factors to be used within the PLS-1 algorithm is an important parameter to achieve better performance in prediction. This allows one to model the system with the optimum amount of information, avoiding overfitting. The selection of the optimum number of factors was estimated by cross-validation, leaving out one sample at a time. The predicted concentration of the analytes in each sample was then compared with the known concentration of them in the respective sample and the prediction error sum-of-square (PRESS) was calculated. This parameter was calculated each time adding a new factor to the model. A plot of the PRESS against the number of factors for each individual component indicates a minimum value for optimal number of factors. The obtained PLS factors for 2-, 3-, and 4-nitroaniline were 6, 5 and 3, respectively. The results from application of

the PLS method for prediction samples are also included in Table 3.

3.8. Interference

Various possible interfering substances were tested under the same experimental conditions for interference in the kinetic measurements. A species was considered as interference when its presence produced a variation in the absorbance of the sample greater 5%. Table 5 summarizes the maximum tolerance of these compounds by the proposed analytical procedure. The kinetics of condensation reaction of compounds such as amino acids is not very different to nitroanilines and the high concentration of these compounds alter the kinetics of the reactions by causing an increase in absorption at 500 nm due to reaction with NQS.

3.9. Application

Three water samples, tap water, river water and well water, obtained from different places in Hamedan, Iran were sampled for analysis. Each sample was treated as described in Section 2.4. The measured data of these water samples were analyzed with the use of the same of BPNN, RBFNN and PLS calibration model (each sample was analyzed in triplicate), and the results (Table 6) showed that the efficiency of the procedure was satisfactory.

4. Conclusion

Three nitroanilines that are considered dangerous pollutants could be directly and simultaneously determined in water samples by resorting spectrophotometric measurements and chemomertric modeling. The method is based on the difference in the reaction rate of nitroanilines with NQS in micellar medium. As the spectra of the reaction products of individual analytes with NQS overlapped heavily, and there was some nonlinearity in the measured data of analyte mixtures, various chemometrics calibration models were applied, e.g. PLS, PC-BPNNs, PC-RBFNNs, to facilitate simultaneous prediction of the analytes. The prediction of nitroaniline concentrations was

Table 6
Simultaneous determination of nitroaniline isomers (concentration in $\mu g \, ml^{-1}$) in water samples ($n = 3$)

Sample	Method	Spiked			Found			%Recovery		
		2-Nitro	3-Nitro	4-Nitro	2-Nitro	3-Nitro	4-Nitro	2-Nitro	3-Nitro	4-Nitro
Tap water	RBFNN	4.0	5.0	6.0	3.6	4.9	5.8	90.0	98.0	97.0
	BPNN	4.0	5.0	6.0	3.7	5.2	5.8	92.5	105.0	97.0
	PLS	4.0	5.0	6.0	3.3	5.5	5.0	82.5	110.0	84.0
River water	RBFNN	5.1	4.8	6.1	5.0	4.8	6.2	98.5	100.0	102.0
	BPNN	5.1	4.8	6.1	4.9	5.1	5.8	97.0	107.5	95.0
	PLS	5.1	4.8	6.1	5.9	5.7	5.5	115.0	118.0	90.0
Well water	RBFNN	5.1	6.1	4.1	4.6	6.6	4.1	90.0	109.0	100.0
	BPNN	5.1	6.1	4.1	4.2	6.7	4.8	84.0	110.0	118.0
	PLS	5.1	6.1	4.1	5.0	3.8	3.0	99.0	62.0	73.5

No detectable nitroanilines before spiking.

facilitated by the use of a random design to build a calibration data set, which was then applied for the building of calibration models with three chemometrics methods for the testing of a validation data set constructed from synthetic solutions of the three isomers. Investigation of these models and prediction measurements from synthetic mixtures of the analytes showed that PC-RBFNNs, was the most effective calibration method on the basis of the RSET% criteria. In this work, the nonlinear behavior of the analytes' responses is clear and it appears that in such cases, the RBFNN procedure reflects the well-known ability of ANN models to accommodate nonlinear data rather better than the essentially linear PLS models. The RBFNNS greatly reduce the training time and make related analyses much easier. This modeling shows a powerful potential for the considered system without the prior knowledge of the kinetic rate constant and reaction order.

Appendix A. Overview of back-propagation and radial basis function neural networks

A.1. Back-propagation neural network architecture

Back-propagation neural network is a three-layered feed-forward architecture. The three layers are input layer, hidden layer and output layer. Functioning of back propagation proceeds in three stages, namely learning or training, testing or inferences and validation. Fig. A.1 shows the l–m–n (l, input neurons; m, hidden neurons; and n, output neurons) architecture of a back-propagation neural network model. Input layer receives information from the external sources and passes this information to the network for processing. Hidden layer receives information from the input layer, and does all the information processing, and output layer receives processed information from the network, and sends the results out to an external receptor. The input signals are modified by interconnection weight, known as weight factor w_{ji}, which represents the interconnection of ith node of the first layer to jth node of the second layer. The sum of modified signals (total activation) is then modified by a sigmoid transfer function (f). Similarly, outputs signal of hidden layer are modified by interconnection weight (w_{kj}) of kth node of output layer to jth node of hidden layer. The sum of the modified signal is then modified by sigmoid transfer (f) function
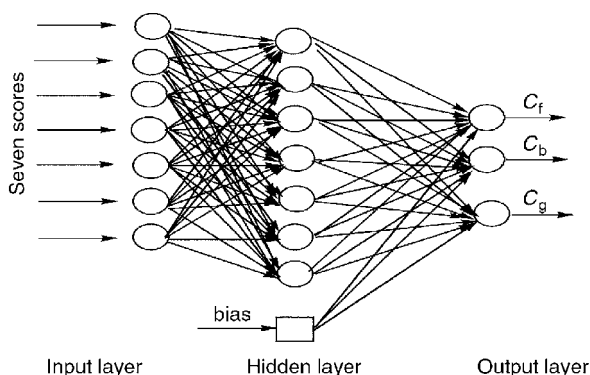
and output is collected at output layer. Let $I_p = (I_{p1}, I_{p2}, \ldots I_{pl})$, $p = 1, 2, \ldots, N$ be the pth pattern among N input patterns. Where W_{ji} and W_{kj} are connection weights between ith input neuron to jth hidden neuron, and jth hidden neuron to kth output neuron, respectively.

Output from a neuron in the input layer is

$$O_{pi} = I_{pi}, \quad i = 1, 2, \ldots, l \tag{A.1}$$

Output from a neuron in the hidden layer is

$$O_{pj} = f(\text{NET}_{pj}) = f\left(\sum_{i=0}^{l} W_{ji} O_{pi}\right), \quad j = 1, 2, \cdots, m \tag{A.2}$$

Output from a neuron in the output layer is

$$O_{pk} = f(\text{NET}_{pk}) = f\left(\sum_{j=0}^{m} W_{kj} O_{pj}\right), \quad k = 1, 2 \ldots n \tag{A.3}$$

where $f(\,)$ is the transfer function.

Batch mode type of supervised learning has been used in the present case, where, interconnection weights are adjusted using delta rule algorithm after sending the entire training sample to the network. During training, the predicted output is compared with the desired output, and error is calculated. If the error is more than a prescribed limiting value, it is back propagated from output to input, and weights are further modified till the error or number of iterations is within a prescribed limit. Weight change at any time t, is given by

$$\Delta W(t) = -\eta \frac{\partial E_p(t)}{\partial W} + \alpha \times \Delta W(t-1) \tag{A.4}$$

η is the learning rate, i.e. $0 < \eta < 1$. α is the momentum coefficient, i.e. $0 < \alpha < 1$.

A.2. Architecture of radial basis function network

Basically radial basis function network is composed of large number of simple and highly interconnected artificial neurons and can be organized into several layers, i.e. input layer, hidden layer, and output layer as shown in Fig. A.2. An input pattern enters the input layer and is subjected to direct transfer function

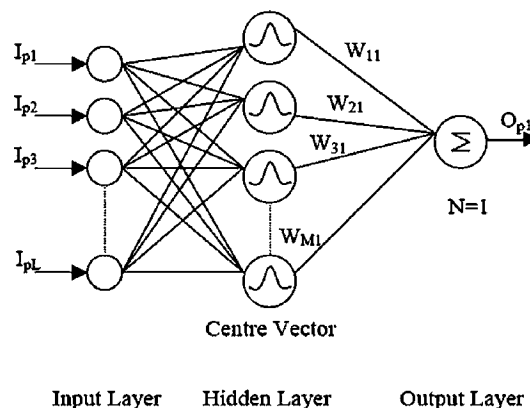Fig. A.1. The typical architecture of a back-propagation neural network model.

Fig. A.2. Radial basis function network architecture containing one hidden layer with j neurons and the output layer with k neurons.

and output from input layer is same as input pattern. Number of nodes in the input layer is equal to the dimension of input vector L. Output from input layer with element I_i ($i = 1$ to L) is I_i. The hidden layer does all the important process and these nodes satisfy a unique property being radially symmetry. Being radially symmetry it must have the following:

(a) *A centre vector* v_j in the input space, made up of cluster centre with element v_{ji} ($j = 1$ to M). '$M \leq P$' where M is the number of centre vectors and P is number of training patterns. The vector typically is stored as weight factors from input layer to hidden layer.

(b) *A distance measure* to determine how far an input pattern with element I_i is from cluster centre v_{ji}. We have used Euclidean distance norm for this purpose:

$$\text{Euclidean distance } \text{ed}_j = \left\| I - v_j \right\| = \sqrt{\sum_{i=1}^{L}(I_i - v_{ji})^2}$$
(A.5)

(c) A transfer function, which transfers Euclidean distance to give output for each node. In our case we used the Gaussian function for this purpose:

$$\text{output}_j = \exp\left(\frac{\text{ed}_j^2}{\sigma^2}\right)$$
(A.6)

where σ is the spread parameter determined from

$$\sigma = \frac{\max(\text{ed})}{\sqrt{M}}$$
(A.7)

And max(ed) is maximum Euclidean distance between selected centers and M is the number of centers.

There are weight factor w_{kj} ($k = 1$ to N, $j = 1$ to M) between kth nodes of output layer and jth nodes of hidden layer. 'N' is the dimension of output vector. Output from output layer transferred through a transfer function like log sigmoid or tan sigmoid.

Output from the output layer is given by

$$\text{output}_k = f\left(\sum_{k=1}^{N} w_{kj} \times \text{output}_j\right)$$
(A.8)

References

[1] K.T. Chung, S.C. Chen, Y.Y. Zhu, Environ. Toxicol. Chem. 16 (1997) 1366.
[2] N.I. Sax, Dangerous Properties of Industrial Materials, Van Nortrand Reinhold Company Inc., New York, 1984.
[3] M.A. Oturan, J. Peiroten, P. Chartrin, A.J. Acher, Environ. Sci. Technol. 34 (2000) 3474.
[4] A. Saupe, Chemosphere 39 (1999) 2325.
[5] L.F. Yao, H.B. He, Y.Q. Feng, S.L. Da, Talanta 64 (2004) 244.
[6] S.P. Wang, H.J. Chen, J. Chromatogr. A 979 (2002) 439.
[7] T.V. Reddy, B.E. Wiechman, E.L. Lin, L.W. Chang, M.K. Smith, F.B. Daniel, G. Reddy, J. Chromatoger. A 655 (1993) 331.
[8] P.J. Marriott, R.M. Kinghorn, R. Ong, P. Morrison, P. Haglund, M. Harju, J. High Resolut. Chromatogr. 23 (2000) 253.
[9] E. Krasuska, W. Celler, J. Chromatogr. A 147 (1978) 470.
[10] S.D. Huang, C.P. Cheng, Y.H. Sung, Anal. Chim. Acta 343 (1997) 101.
[11] R.S. Dhillon, J. Singh, V.K. Gautam, B.R. Chhabra, J. Chromatogr. A 435 (1988) 256.
[12] K.K. Verma, D. Gupta, Anal. Chim. Acta 199 (1987) 233.
[13] J.J. Donkerbrock, A.C. Veltkamp, C. Gooijer, N.H. Velthorst, R.W. Frei, Anal. Chem. 55 (1983) 1886.
[14] B.S. Grabaric, Z. Grabaric, M. Esteban, E. Casassas, J. Electroanal. Chem. 420 (1997) 227.
[15] J. Ghasemi, A. Niazi, Talanta 65 (2005) 1168–1173.
[16] D. Perez-Bendito, Analyst 115 (1990) 689.
[17] S.R. Crouch, Anal. Chim. Acta 283 (1990) 453.
[18] M. Otto, Analyst 115 (1990) 685.
[19] P.D. Wentzell, M.I. Karayannis, S.R. Crouch, Anal. Chim. Acta 224 (1989) 263.
[20] D.M. Haaland, R.G. Easterling, Appl. Spectrosc. 34 (1980) 539.
[21] D.M. Haaland, R.G. Easterling, Appl. Spectrosc. 36 (1982) 665.
[22] D.M. Haaland, R.G. Easterling, D.A. Vopicka, Appl. Spectrosc. 39 (1985) 73.
[23] W. Lindberg, J.A. Persson, S. Wold, Anal. Chem. 55 (1983) 643.
[24] M. Otto, W. Wegscheider, Anal. Chem. 57 (1985) 63.
[25] P. Geladi, B.R. Kowalski, Anal. Chim. Acta 185 (1986) 1.
[26] A. Safavi, H. Abdollahi, M.R. Hormozi Nezhad, Talanta 59 (2003) 515.
[27] M. Hasani, L. Yaghoubi, H. Abdollahi, Anal. Biochem. 367 (2007) 74.
[28] M. Hasani, M. Moloudi, F. Emami, Anal. Biochem. 370 (2007) 68.
[29] Y. Ni, Y. Wang, Microchem. J. 86 (2007) 216.
[30] Y. Dou, H. Mi, L. Zhao, Y. Ren, Y. Ren, Spectrochim. Acta A 65 (2006) 79.
[31] Y. Akhlaghi, M. Kompany-Zareh, Anal. Chim. Acta 537 (2005) 331.
[32] B. Walczak, D.L. Massart, Anal. Chim. Acta 331 (1996) 177.
[33] A. Pulido, I. Ruisanchez, F.X. Ruis, Anal. Chim. Acta 388 (1999) 273.
[34] E. Pelizzetti, E. Pramauro, Anal. Chim. Acta 169 (1985) 1.
[35] J. Szymanowski, J. Radioanal. Nucl. Chem. 246 (2000) 635.
[36] C.D. Stalikas, Trends Anal. Chem. 21 (2002) 343.
[37] J. Rosendorfova, L. Cermakova, Talanta 27 (1980) 705.
[38] V. Kuban, I. Jancarova, J. Hedbavny, M. Vrchlabsley, Collect. Czech. Chem. Commun. 54 (1989) 70.
[39] H. Koizumi, Y. Suzuki, Anal. Sci. 4 (1988) 537.
[40] M.C. Gutierrez, A. Gomez-Hens, D. Perez-Bendito, J. Pharm. Biomed. Anal. 7 (1989) 413.
[41] Y. Nakahara, A. Ishigami, Y. Takeda, J. Chromatogr. A 489 (1989) 371.
[42] M. Blanco, J. Coello, H. Iturriaga, S. Maspoch, M. Redon, Analyst 121 (1996) 395.
[43] P. Nagaraja, K.C. Srinivasa Murthy, H.S. Yathirajan, Talanta 43 (1996) 1075.
[44] J.L. Dye, V.A. Nicely, J. Chem. Educ. 48 (1971) 443.
[45] W.E. Wentworth, J. Chem. Educ. 42 (96) (1965) 162.
[46] M.J.D. Powel, Comput. J. 7 (1964) 155.
[47] J. Zupan, J. Gasteiger, Anal. Chim. Acta 248 (1991) 1.
[48] J. Zupan, J. Gasteiger, Neural Network for Chemists, An Introduction, VCH, Weinheim, 1993.
[49] F. Despangne, D.L. Massart, Analyst 123 (1998) 157R.
[50] P.J. Gemperline, Chemom. Intel. Lab. Syst. 15 (1992) 115.
[51] S. Sekulic, M.B. Seasholtz, Z. Wang, B.R. Kowalski, S.E. Lee, B.R. Holt, Anal. Chem. 65 (1993) 835A.

Simultaneous determination of silicon and phosphorus in soil and plants by reversed-phase ion-pair chromatography

Shengjie Hou [a,b], Mingyu Ding [a,*], Jiang Zhu [b]

[a] *Key Lab of Bioorganic Phosphorus Chemistry & Chemical Biology, Ministry of Education,*
Department of Chemistry, Tsinghua University, Beijing 100084, China
[b] *College of Resources & Environment, Anhui Agricultural University, Hefei 230036, China*

Abstract

A reversed-phase ion-pair high-performance liquid chromatographic method, using tetrabutylammonium bromide (TBABr) as ion-pair reagent, has been developed for the simultaneous analysis of silicon (Si) and phosphorus (P) as heteropoly acids in soil and plant samples. The effect of the concentrations of ion-pair reagent, acetate buffer and organic modifier as well as the pH of buffer on separation was made clear. The reaction conditions and stability of heteropoly acids were investigated. Furthermore, the phenomenon occurred in the optimized process was also further researched. The separation was performed on a reversed-phase C_{18} column within 11 min with 40:60 (v/v) 0.1 M acetate buffer (pH 3.9)–acetonitrile (ACN) containing 0.8 mM TBABr as a mobile phase. The linear ranges of the peak area calibration curves for Si and P were 0.08–50 mg/L and 0.40–50 mg/L, respectively. The detection limits calculated at S/N = 3 were 0.0057 mg/L and 0.0280 mg/L for Si and P, respectively. The method was successfully applied to the analysis of soluble and total contents of Si and P in soil and plant samples.
© 2007 Published by Elsevier B.V.

Keywords: Silicon; Phosphorus; Heteropoly acid; Soil and plant analysis; Ion-pair chromatography

1. Introduction

Silicon (Si) and phosphorus (P) are very important for animals and plants [1,2]. Si and P are essential trace elements and necessary in bone formation and other metabolic processes for human [3,4]. The main source of Si and P for human is diet [5]. Plant food is a source of biophilic Si and P [3,4], but most of Si and P in plants are unavailable for human body due to their low solubility [6]. In soil, though the total contents of Si and P are large, only a very small part of them can be utilized by plant [7]. Plant-available P and Si are mainly composed of soluble phosphate ions and silicate ions [8].

The analysis of Si and P, especially in soluble Si and P, in soil and plant samples is very significant in the fields of plant nutrition and soil. Several methods including spectrophotometry [3,9,10], atomic absorption spectrometry [6], ion chromatography [1,11,12] and ion-pair high-performance liquid chromatography (IP-HPLC) [13] had been reported for the determination of Si and P. There were also studies on the determination of Si and P by a combination of ion chromatography and inductivity coupled plasma mass spectrometry [14,15].

The spectrophotometric determination, the most common method for the analysis of Si and P in agriculture, is based on the reaction between silicate or phosphate and an excess of ammonium molybdate reagent to give a yellow heteropoly acid complex, which is reduced subsequently to the heteropoly blue compound by ascorbic acid. However, the colorimetric determination of phosphate or silicate encounters mutual interference. The interference of phosphate on silicate is usually reduced by the addition of oxalic acid to preferentially decompose molybdophosphoric acid (MPA) [16]. The common anion-exchange chromatography is difficult to elute silicate and phosphate simultaneously with an isocratic elution and detect them without pre-column derivation because their ionization degrees distinguish greatly in deionized water. Furthermore, other anions in plant and soil samples might interfere with them. Ikedo [12] determined phosphate and silicate ions in leaching process waters and ceramics glaze raw materials of natural origin by

* Corresponding author. Tel.: +86 10 62797087; fax: +86 10 62782485/1106.
E-mail address: dingmy@mail.tsinghua.edu.cn (M. Ding).

ion-exclusion chromatography coupled with UV-detection after post-column derivation, but this kind of method needs a special post-column reactor. In addition, the retention of phosphoric acid is usually very weak on ion-exclusion column. Tikhomirova [13] reported IP-HPLC to determine Si and P as molybdic heteropoly acids with a preconcentration operation. However, in their paper, without the complicated preconcentration, Si and P could not be quantified exactly. It is also not advisable that standard solutions of heteropoly acids were diluted with deionized water, which led to the decomposition of heteropoly acids. In addition, detailed research about the forming conditions of heteropoly acids and separating conditions of IP-HPLC of Si and P are lack.

In this research, a reversed-phase IP-HPLC for the determination of Si and P as yellow heteropoly acids has been developed. The effect of the concentration of ion-pair reagent, buffer salt and organic modifier as well as the pH of buffer on separation was optimized. The forming conditions and stability of heteropoly acids were investigated. The method developed had good peak shape and high sensitivity. The method eliminated the mutual interference of Si and P when compared with spectrophotometric determination. The interference caused by ammonium molybdate was avoided too. Furthermore, the method saved the trouble of preconcentration. The method was successfully applied to the analysis of soluble and total contents of Si and P in soil and plant samples. An accurate and sensitive method was offered for simultaneous determination of Si and P in agriculture, food and biology.

2. Experimental

2.1. Apparatus and chromatographic conditions

Chromatographic analysis was carried out with an Agilent 1100 HPLC consisting of a G1311A quaternary pump, a G1379A degasser and a G1314A UV detector. The separation column was HiQ Sil C_{18} column (250 mm × 4.6 mm i.d., 5 μm). Samples were injected using a six-port injection valve with a loop volume of 20 μL. Data acquisition was accomplished using a HP ChemStation.

An isocratic elution was performed, using a mobile phase of 40:60 (v/v) 0.1 M acetate buffer (pH 3.9)–acetonitrile (ACN) containing 0.8 mM tetrabutylammonium bromide (TBABr) at a flow rate of 1 mL/min. The detection wavelength was 310 nm.

2.2. Reagents and solutions

All solutions were prepared from analytical reagent-grade chemicals in deionized water. The stock solutions of Si and P were 1 g/L which were prepared by dissolving sodium metasilicate nonahydrate ($Na_2SiO_3 \cdot 9H_2O$) and potassium dihydrogen orthophosphate (KH_2PO_4), respectively in deionized water. The working solutions were prepared by the dilution of the stock solutions. A mixed solution of molybdosilicic acid (MSA) and MPA was obtained by a reaction of a certain amount of $Na_2SiO_3 \cdot 9H_2O$ and KH_2PO_4 with an excess of ammonium molybdate ((NH_4)$_6$$Mo_7$$O_{24} \cdot 4H_2O$) in required acidity which was adjusted by 0.5 M sulfuric acid (H_2SO_4). Plant samples

were classified into dry ones and fresh ones. The dry ones were rice, grain and maize. The fresh ones were cole and capsicum. All these plant samples were taken from the supermarket in Tsinghua University. The soil sample was taken from the campus of Tsinghua University.

2.3. Preparation of soil and plant samples for soluble silicon and phosphorus extraction

In order to determine soluble Si and P, an amount of 1 g of ground and dried sample or 5 g of fresh plant sample was weighed in a jar, and then 50 mL of water was added. The extraction was carried out with deionized water in an ultrasonic processor for 30 min. After that time, the sample was cooled and filtered. The sample was diluted and then adjusted to pH 1.1. At last, the solution of heteropoly acids was formed by adding at least 0.56 mM ammonium molybdate per 1 mg/L Si and 1 mg/L P. The solution was passed through a 0.45 μm Millipore filter before injection.

2.4. Preparation of soil and plant samples for total silicon and phosphorus extraction

An amount of 0.5 g of ground and dried sample or 2 g of fresh plant sample was weighed into a flask, and then 5 mL of concentrated H_2SO_4 was added. The flask was heated moderately until the sample was carbonized completely. After cooling for a while, 10 drops of hydrogen peroxide (H_2O_2) were added and then went on to heat, which were repeated until the solution was clear for plant and offwhite for soil. After that time, the sample was topped up with deionized water to a 50-mL calibrated flask. The sample was diluted and then adjusted to pH 1.1. At last, the solution of heteropoly acids was formed by adding at least 0.56 mM ammonium molybdate per 1 mg/L Si and 1 mg/L P. The solution was passed through a 0.45 μm Millipore filter before injection.

3. Results and discussion

3.1. Optimization of chromatographic conditions

A detailed study was performed on the effect of the concentration of TBABr, acetate buffer and ACN as well as the pH of acetate buffer in the mobile phase on separation. These parameters were optimized using a univariate strategy.

3.1.1. Effect of ion-pair reagent

In IP-HPLC, the sorption of ion-pair reagent on the column offers dynamic ion-exchange site to retain analytes. For a better separation of MSA and MPA, three ion-pair reagents, tetramethylammonium bromide (TMABr), cetyltrimethylammonium bromide CTMABr and TBABr, were examined for improving the separation of MSA and MPA. The results showed that TMABr was difficult to separate MSA from ammonium molybdate and the use of CTMABr could extend the retention times of MSA and MPA. It was found that TBABr was the most suitable ion-pair reagent. The effect of TBABr concentration

was studied in the range of 0.2–1.2 mM. An increase in the retention times of MPA and MSA occurred with increasing concentration of TBABr, particularly for MPA. When the concentration of TBABr was 0.6 mM, double peaks were observed for MPA, but when TBABr was 0.2 mM or 0.4 mM, only the first one occurred. Furthermore, with the increase of TBABr from 0.6 mM to 0.8 mM, the first peak disappeared with the second peak heightened. The above phenomena might be attributed to insufficient counter-ions in mobile phase, thus stable MPA ion-pair molecules and their unstable portion coexisted when 0.6 mM TBABr was added. Good separation was achieved when more than 0.8 mM of TBABr was added in mobile phase, so we chose 0.8 mM TBABr in this study.

3.1.2. Effect of buffer pH

Several acetate buffers at pH values ranging between 3.5 and 5.1 were used to investigate the effect of buffer acidity. Retention of MSA and MPA slightly decreased as pH values were increased. The result showed that higher pH values promote further decomposition of heteropoly acids [17], which might cause less heteropoly anions to combine with counter-ions, so both MSA and MPA tended to elute with increasing pH. At the same time, the detection sensitivity of MSA and MPA decreased for higher pH values. As a compromise between retention time and detection sensitivity, the pH of buffer was controlled at 3.9.

3.1.3. Effect of organic modifier

The formed neutral ion-pairs will adsorb onto the surface of a reversed-phase column firmly owing to the large size of the ion-pair. Therefore, an organic modifier is often added to the eluent to compete with stationary phase for ion-pairs to control the elution rate. ACN was selected as the organic modifier. With the increasing concentration of ACN, the elution of MPA was quickened remarkably when compared with MSA. When the concentration of ACN was higher than 70%, MSA and MPA were coeluted. Sixty percent of ACN provided a good resolution.

3.1.4. Effect of buffer concentration

Eluent strength of mobile phase is related to buffer concentration. Acetate buffer of higher concentration tended to elute MSA and MPA more quickly. In the studied range of 0.01–0.2 mM, 0.1 mM buffer was suitable, so we used it in this study.

3.2. Optimization of the forming conditions of heteropoly acids

The formation conditions of MSA and MPA were also optimized using a univariate strategy. The key parameters optimized were the concentrations of ammonium molybdate and H_2SO_4. All of these studies for MSA and MPA were performed with a standard solution containing 10 mg/L Si and 10 mg/L P in a 25-mL calibrated flask. The effect of ammonium molybdate concentration on the formation of heteropoly acids was studied in the range of 0.56–11.2 mM (Fig. 1). The amount of ammonium molybdate was insufficient to form heteropoly acids in the range of 0.56–5.6 mM. The variation of the peak height was not obvious in the range of 5.6–11.2 mM, but the peak of ammonium
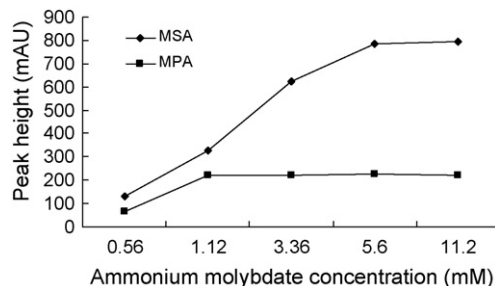

Fig. 1. Effect of ammonium molybdate concentration in the forming process of MSA and MPA. Forming conditions: 10 mg/L Si, 10 mg/L P and 0.56–11.2 mM ammonium molybdate at pH 1.1 in a 25-mL calibrated flask.

molybdate appeared at about 2.5 min and its height increased gradually with the increase of the concentration of ammonium molybdate in the range of 5.6–11.2 mM, which might interfere with the peak of MSA. These results showed that 5.6 mM was the optimum concentration for ammonium molybdate. In theory, ammonium molybdate should be added at least 0.56 mM per 1mg/L Si and 1 mg/L P, but the contents of Si and P in samples were uncertained, so excessive ammonium molybdate was added according to the rough calculation of the contents of Si and P in samples. Fig. 2 shows the effect of different pH on the peak heights of MSA and MPA. The peak heights of MSA and MPA remained constant up to pH 1.1 and then decreased in the pH range of 1.1–4.6. However, with the increasing acidity in the pH range of 0.7–0.4, there was another peak appearing at about 4 min for MPA and its peak height increased gradually; this might be because MPA had been changed in the composition or structure and combined with counter-ions to give different MPA ion-pair molecules. The peak of MPA at pH 4.6 was absent because more acidity was required for the formation of MPA than MSA. The similar phenomenon occurred in the formation of MSA and MPA of different concentrations. Considering the above factors, pH 1.1 was used for the subsequent experiments.

3.3. Stability of heteropoly acids

The stability of MSA and MPA mixture obtained by the optimized conditions was investigated at room temperature within 51 h. As can be seen from Fig. 3, the peak height of MPA attained
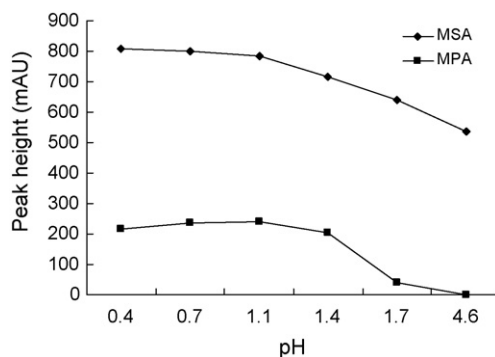

Fig. 2. Effect of pH in the forming process of MSA and MPA. Forming conditions: 10 mg/L Si, 10 mg/L P and 5.6 mM ammonium molybdate at pH 0.4–4.6 in a 25-mL calibrated flask.
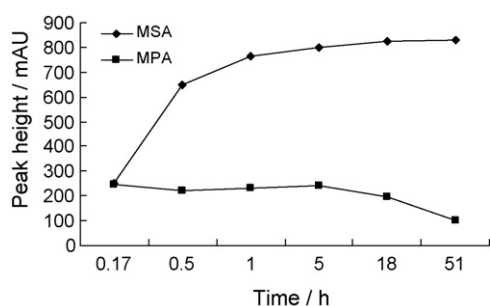
Fig. 3. Stability of MSA and MPA under the optimized conditions. Forming conditions: 10 mg/L Si, 10 mg/L P and 5.6 mM ammonium molybdate at pH 1.1 in a 25-mL calibrated flask.

gradually to the maximum within 1 h and then remained stable up to 5 h. After 18 h, the peak height of MPA decreased obviously because of the decomposition of MPA. However, MSA seemed to be more stable than MPA under the optimized conditions, so all experiments were performed within 1–5 h.

3.4. Method evaluation

The HPLC system was calibrated by injecting five standard solutions of different concentrations with three repetitions at each concentration. These standard solutions were prepared as follows: a heteropoly acid solution containing 50 mg/L Si and 50 mg/L P was prepared under the optimized conditions; the linearity was obtained by diluting the solution with 0.04 M H_2SO_4 (pH 1.1). In the study, an attempt to dilute the solution with deionized water was unsuccessful, because the decomposition of heteropoly acids led to narrower linear ranges of Si and P in water than that in 0.04 M H_2SO_4. The calibration curves of Si and P were obtained by plotting the peak areas against their concentrations. The regression lines, linear ranges, correlation coefficients and detection limits (S/N = 3) for Si and P are listed in Table 1.
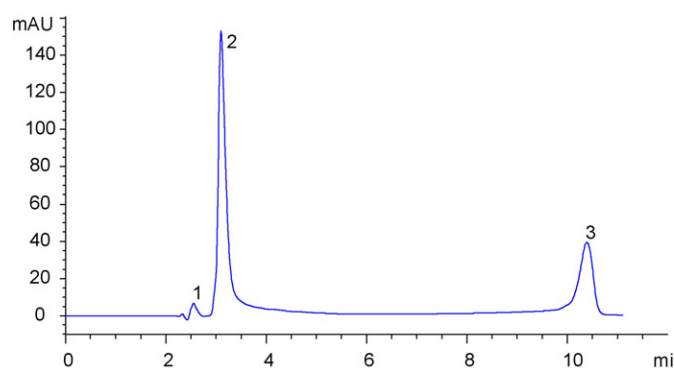

Fig. 4. Chromatogram of MSA and MPA standard containing 2 mg/L of Si and 2 mg/L P, respectively. Chromatographic conditions: column, HiQ Sil C_{18}; eluent, 60% (v/v) of ACN, 40% of 0.1 mM acetate buffer (pH 3.9), 0.8 mM TBABr; flow rate, 1.0 mL/min; detection wavelength, 310 nm. Peak: 1 = molybdate ammonium, 2 = MSA and 3 = MPA.

The precision of the present method was determined by five repeated chromatographic injections of a standard solution. The relative standard deviations (R.S.D.s) of retention times, peak areas and half peak widths were all under 5% for MSA and MPA (Table 1). The recoveries of Si and P in rice and soil samples were determined by adding standard at two different levels of 2 mg/L and 4 mg/L into samples before extraction. The recoveries were ranged from 91.6% to 110.3% (Table 2). The chromatogram of MSA and MPA standard containing 2 mg/L Si and 2 mg/L P is shown in Fig. 4.

3.5. Quantitative analysis of plant and soil samples

The method developed in this study was successfully applied to analyze Si and P in plant and soil samples. The chromatograms of the rice and soil sample are shown respectively in Figs. 5 and 6 as examples. The analytical results of soluble and total contents of Si and P in different soil and plant samples are summarized in Table 3. The reproducibilities of retention times and half peak

Table 1
Regression lines and other quantitive data for Si and P

Analyte	Regression line	Correlation coefficient	Linear range (mg/L)	Detection limit (mg/L)	R.S.D. (%, $n = 5$)		
					Retention time	Peak area	Half peak width
Si	$Y = 805.1x − 99.957$	0.9998	0.08–50	0.0057	0.70	4.65	2.47
P	$Y = 566.6x − 29.699$	0.9992	0.40–50	0.0280	0.66	3.11	2.35

Table 2
Recoveries of Si and P in rice and soil samples ($n = 3$)

Species	Analyte	Original (mg/L)	Added (mg/L)	Found ± S.D. (mg/L)	Recovery (%)
Rice	Si	2.76	2	4.45 ± 0.18	93.5
			4	7.46 ± 0.24	110.3
	P	4.48	2	6.43 ± 0.20	99.2
			4	7.77 ± 0.13	91.6
Soil	Si	5.5	2	7.38 ± 0.29	98.4
			4	9.87 ± 0.34	103.9
	P	2.26	2	4.02 ± 0.20	94.4
			4	5.92 ± 0.16	94.6

Table 3
Analytical results of soluble and total contents of Si and P in soil and plant samples ($n = 3$)

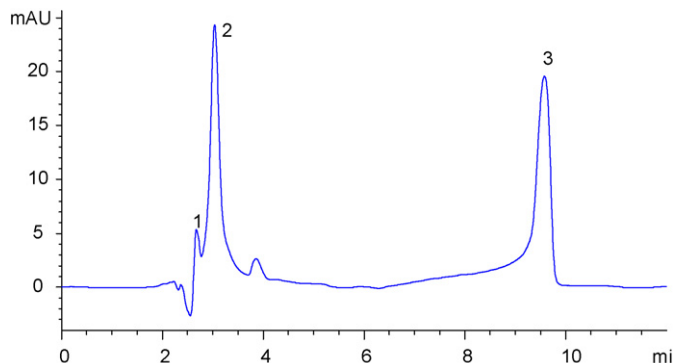| Species	Mean ± S.D.			
	Soluble Si (mg/g)	Total Si (mg/g)	Soluble P (mg/g)	Total P (mg/g)
Rice (dry)	0.138 ± 0.006	0.831 ± 0.025	0.224 ± 0.010	2.821 ± 0.102
Grain (dry)	0.119 ± 0.008	0.612 ± 0.029	0.589 ± 0.031	2.960 ± 0.089
Maize (dry)	0.120 ± 0.005	1.288 ± 0.036	0.349 ± 0.016	3.855 ± 0.093
Cole (fresh)	0.101 ± 0.005	0.318 ± 0.017	0.126 ± 0.004	0.330 ± 0.015
Capsicum (fresh)	0.085 ± 0.004	0.157 ± 0.007	0.407 ± 0.020	0.800 ± 0.044
Soil (dry)	0.275 ± 0.011	1.188 ± 0.041	0.113 ± 0.005	1.813 ± 0.051

Fig. 5. Chromatogram of MSA and MPA in rice sample. Chromatographic conditions and peak remark were the same as Fig. 4.
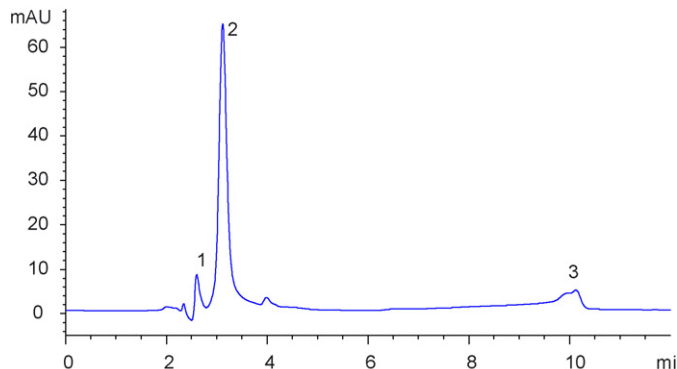

Fig. 6. Chromatogram of MSA and MPA in soil sample. Chromatographic conditions and peak remark were the same as Fig. 4.

widths of Si and P in rice and soil samples were investigated by three repeated determinations. The R.S.D.s of retention times and half peak widths in rice sample were 2.46% and 5.07% for Si and 2.24% and 2.13% for P, respectively. The R.S.D.s of retention times and half peak widths in soil sample were 3.02% and 3.05% for Si and 4.8% and 2.11% for P, respectively.

4. Conclusions

A method for the determination of Si and P as heteropoly acids in plant and soil samples by reversed-phase IP-HPLC has been described, which showed good sensitivity and separation. The method was successfully applied to the analysis of soluble and total contents of Si and P in soil and plant samples. The present method can be adopted as a routine analytical method for the determination of Si and P in the field of agriculture.

References

[1] H.B. Li, F. Chen, J. Chromatogr. A 874 (2000) 143.
[2] P.K. Sarkar, E. Morrison, U. Tinggi, S.M. Somerset, G.S. Craven, J. Sci. Food Agric. 78 (1998) 498.
[3] M.P. Kolesnikov, V.K. Gins, Appl. Biochem. Microbiol. 37 (2001) 524.
[4] H. Zhang, J. Shen, J. Henan Univ. Chin. Med. 21 (2006) 75.
[5] R. Jugdaohsingh, S.H. Anderson, K.L. Tucker, H. Elliott, D. Kiel, R.P. Thompson, J.J. Powell, Am. J. Clin. Nutr. 75 (2002) 887.
[6] W. Dejneka, J. Łukasiak, Food Control 14 (2003) 193.
[7] J. Katznelson, Oecologia (Berl.) 26 (1977) 325.
[8] P. Demaria, R. Flisch, E. Frossard, S. Sinaj, J. Plant Nutr. Soil Sci. 168 (2005) 89.
[9] A.V. Medvetskii, T.I. Tikhomirova, G.I. Tsizin, S.G. Dmitrienko, Y.A. Zolotov, J. Anal. Chem. 58 (2003) 841.
[10] M.A. Raggi, C. Sabbioni, R. Mandrioli, Q. Zini, G. Varani, J. Pharm. Biomed. Anal. 20 (1999) 335.
[11] T. Fujiwara, K. Kurahashi, T. Kumamaru, H. Sakai, Appl. Organomet. Chem. 10 (1996) 675.
[12] M. Ikedo, M. Mori, K. Kurachi, W.Z. Hu, K. Tanaka, Anal. Sci. 22 (2006) 117.
[13] T.I. Tikhomirova, O.V. Krokhin, D.B. Dubovik, A.V. Ivanov, O.A. Shpigun, J. Anal. Chem. 57 (2002) 18.
[14] E. Engstrom, I. Rodushkin, D.C. Baxter, B. Öhlander, Anal. Chem. 78 (2006) 257.
[15] A. Hioki, J.W.H. Lam, J.W. McLaren, Anal. Chem. 69 (1997) 21.
[16] M. Yaqoob, A. Nabi, P.J. Worsfold, Anal. Chim. Acta 519 (2004) 137.
[17] A. Jiirgensen, J.B. Moffat, Catal. Lett. 34 (1995) 237.

Determination of steroid sex hormones in urine matrix by stir bar sorptive extraction based on monolithic material and liquid chromatography with diode array detection

Xiaojia Huang [a,*], Dongxing Yuan [a], Benli Huang [b]

[a] *State Key Laboratory of Marine Environmental Science, Environmental Science Research Center, Xiamen University, Xiamen 361005, China*
[b] *Department of Chemistry & The MOE Key Laboratory of Analytical Sciences, Xiamen University, Xiamen 361005, China*

Abstract

A simple, rapid and sensitive method for simultaneous determination of six steroid sex hormones in urine matrix was developed by the combination of stir bar sorptive extraction (SBSE) with high performance liquid chromatography (HPLC) and diode array detection (DAD). A poly (methacrylic acid stearyl ester–ethylene dimethacrylate) was synthesized and selected as SBSE extraction medium. To achieve the optimum extraction performance, several parameters, including agitation speed, desorption solvent, extraction and desorption time, pH value, inorganic salt and organic solvent content of the sample matrix were investigated. Under the optimized experimental conditions, low detection limits (S/N = 3) and quantification limits (S/N = 10) of the proposed method for the target compounds were achieved within the range of 0.062–0.38 and 0.20–1.20 ng/mL, respectively from spiked urine, respectively. The calibration curves of six steroid sex hormones showed good linearity ranging from 1.0 to 200 ng/mL with linear coefficient R^2 values above 0.990. Good method reproducibilities presented as intra- and inter-day precisions were also found with the R.S.D.s less than 9.2 and 10.0%, respectively. Finally, the proposed method was successfully applied to the determination of the target compounds in a urine sample from a pregnant woman.
© 2007 Elsevier B.V. All rights reserved.

Keywords: Stir bar sorptive extraction; Monolithic material; HPLC/DAD; Endocrine disrupters; Steroid sex hormones; Urine matrix

1. Introduction

Steroid sex hormones (SSHs) are referred to those regulating the differentiation and development of male and female reproductive organs, secondary sex characteristics and behaviour patterns. There are important biological messengers [1]. The effects of steroid sex hormones are receiving a growing attention from scientific community, regulatory agencies and the public at large, as there is a continuous widespread of anthropogenic substances into the environment. The main sources of those chemicals are from domestic effluents, mainly due to the widespread use of birth-control pills and other analogous drugs used for the treatment of hormonal disorders or cancers. Other major sources of SSHs are the livestock wastes as well as growth

regulators in aquaculture [2]. It is reported that steroid sex hormones can cause human and animal endocrine disorders even at very low level (ng/L range) [3,4]. On the other hand, toxicological and pharmacological levels evaluated by biomedical research rely deeply on the monitoring on a restricted number of hormones in biological fluids, e.g. urine. These procedures allow a more accurate medical interpretation and a rapid access to metabolic pathway information in both human and animal body. Therefore, developing a simple, rapid and sensitive method to monitor steroid sex hormones in environment is important for human.

In the last years, several analytical strategies have been proposed to monitor hormones in water and biomedical matrices, based on either biological assays [5–7] or chromatographic techniques [8–14]. Among chromatographic techniques, HPLC is widely accepted as an advantageous technique for monitoring steroid hormones because HPLC is more rugged and versatile without a derivatization step. In order to low the detection limits, sample pretreatment based on the method, such as solid

* Corresponding author at: P.O. Box 1009, Xiamen University, Xiamen 361005, China. Tel.: +86 592 2183661.
E-mail address: hxj@xmu.edu.cn (X. Huang).

phase extraction, solid phase micro-extraction (SPME) [3,14] or SBSE [13] is usually need before HPLC analyse. Almeida and Nogueira [13] have used stir bar sorptive extraction and liquid desorption followed by high performance liquid chromatography with diode array detection (SBSE–LD–HPLC/DAD) to simultaneously detected several SSHs in water and urine matrices. Acceptable results were obtained but long time should be spent in the extraction step.

SBSE is an extraction technique that was developed by Baltussen et al. [15] in 1999 based on the same principles as those of SPME. The SBSE has been widely used for enrichment and sensitive determination of priority organic micro-pollutants in water samples, as well as in other matrices [16–20]. Polydimethylsiloxane (PDMS) is typical coating material in the commercial stir bars and the amount of PDMS is 25–125 μL, which is substantially higher than that on a SPME fiber with a maximum volume of 0.5 μL. The phase ratio of SBSE is about 50–250 times lower than SPME, resulting in much higher recoveries, especially for volatile compounds with higher octanol–water partition coefficients ($K_{o/w}$) [21,22]. We have used methacrylic acid octyl ester as monomer to copolymerize with ethylene dimethacrylate (EDMA) and used the copolymer as SBSE extraction medium [23,24]. The new stir bar can extract apolar analytes effectively and polar compounds also can be extracted. In this research, a novel stir bar based on monolithic material (SBSEM), which was obtained by in-situ copolymerization of methacrylic acid stearyl ester and EDMA in the presence of a porogen solvent containing 1-propanol and 1,4-butanediol, was prepared. Then, a methodology combining the stir bar sorptive extraction and liquid desorption, followed by high performance liquid chromatography with diode array detection for the analysis of traces of steroid sex hormones in urine matrix was developed. The method developed in our research is more rapid and lower LOD in the determination of SSHs than previous research [13].

2. Experimental

2.1. Chemicals

Methacrylic acid stearyl ester (MASE) (99%), ethylene dimethacrylate (97%) and 3-(trimethoxysilyl)-propyl methacrylate (γ-MAPS) (95%) were supplied by TCI (Tokyo Kasei Kogyo Co., Japan); azobisisobutyronitrile (AIBN) (97%, recrystallized before use), 1-propanol (97%) and 1,4-butanediol (98%) (distilled before use) were purchased from Shanghai Chemical Co. (China); HPLC-grade acetonitrile (ACN) and methanol were purchased from Tedia Company (Fairfield, USA); Water used throughout the study was purified using a Milli-Q water purification system (Millipore, USA). Progesterone (PG) (98.0%) and diethylstilbestrol (DES) (99.5%) were supplied from Sigma–Aldrich (Steinheim, Germany); testosterone (TS) (>98%), methyltestosterone (MTS) (99.0%), testosterone propionate (PTS) (>98%) and nandrolone phenylpropionate (PNT) (>98%) were supplied by Jiubang Chemical Co. Ltd. (Shanghai, China); the mobile phases as well as the samples were degassed before use.

Stock standard solutions of individual SSH (100 μg/L) were used to prepare the working and calibration standard mixtures in MeOH at the desired concentration, stored refrigerated at 4 °C and renewed monthly. For real urine sample assays, 20 mL of urine was diluted to 50 mL with Mill-Q water.

2.2. Equipments and materials

HPLC analyses were carried out on a LC chromatographic system (Shimadzu, Japan) equipped with a binary pump (LC-20AB) and a diode array detector (SPD-M20A) and LC solution workstation and CBM-20A controller. Sample injection was carried out using a RE3725i manual sample injector with a 20 μL loop (Rheodyne, Cotati, CA, USA); all experiments were performed at room temperature.

The pore size distribution of the polymer was measured on mercury intrusion porosimeter (Porous Materials Inc., Ithaca, NY). Before measurement, the bulk polymer was cut into small pieces, Soxhlet-extracted with methanol for 12 h, vacuum-dried for 6 h at 70 °C. The morphology of stir bar was examined by a Model XL30 scanning electron microscopy (SEM) instrument (Philips, Eindhoven, The Netherlands).

2.3. Preparation of SBSEM

The procedure of preparation of glass bar, pretreatment and chemical modifications of the glass bar was described previously [23,24]. The monolithic material was prepared by an in-situ polymerization. First, a mixture consisting of 160 mg MASE, 160 mg EDMA, 336 mg 1-propanol, 144 mg 1,4-butanediol, 8 mg AIBN was mixed ultrasonically into a homogenous solution, then the solution was purged with nitrogen for 3 min. Subsequently, the solution was poured into a flat bottom borosilicate glass tube with 5.0 mm inner diameter. The stir bar that has been pretreated was vertically immersed into the reactant mixture, care should be taken to avoid the bar contact with glass wall. The tube was sealed with septa and kept at 60 °C for 24 h. After the polymerization, capillary tubing cutter was used to crack off the glass. Firm, integrated and polished monoliths could be obtained. The monolithic material on the bar was then Soxhlet-extracted with methanol for 24 h to remove the residue monomers, porogen, uncross-linked polymers and initiator. Finally, the stir bar was vacuum-dried for 6 h at 70 °C to obtain the final SBSEM (20 mm in length and 1.5 mm monoliths thickness).

2.4. Extraction and desorption mode

Stirring extraction and stirring liquid desorption modes were used. The samples were stirred at room temperature. After reaching extraction equilibrium, the SBSEM was removed and immersed in 5 mL methanol, stirred for a certain time to release the extracted analytes. Then the stir bar was removed by means of a magnetic rod, while the stripping solvent was evaporated to dryness under a gently stream of nitrogen. The dried residue was redissolved in 0.5 mL methanol for HPLC/DAD analysis.

2.5. Chromatographic conditions

All separation was performed on a Shim-pack VP ODS column (5 μm particle size, 250 mm × 2.0 mm i.d.). The mobile phase consisted of a mixture of 75% (v/v) ACN aqueous solution. The detector wavelength was set at 240 nm; the flow rate was 0.6 mL/min and the injection volume was 20 μL.

3. Results and discussion

3.1. Characterization of poly (MASE–EDMA) monolithic material

The morphology of the poly (MASE–EDMA) monolithic material was examined by SEM, and a typical microphotograph is displayed in Fig. 1. The interconnected skeletons and interconnected textural pore of the monolithic material can be clearly observed.
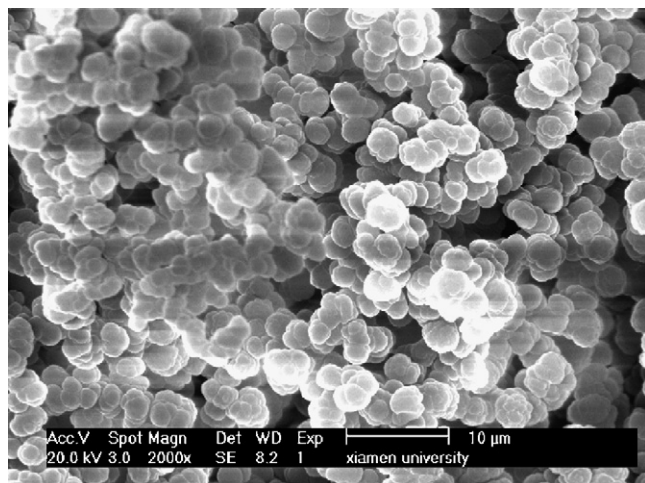

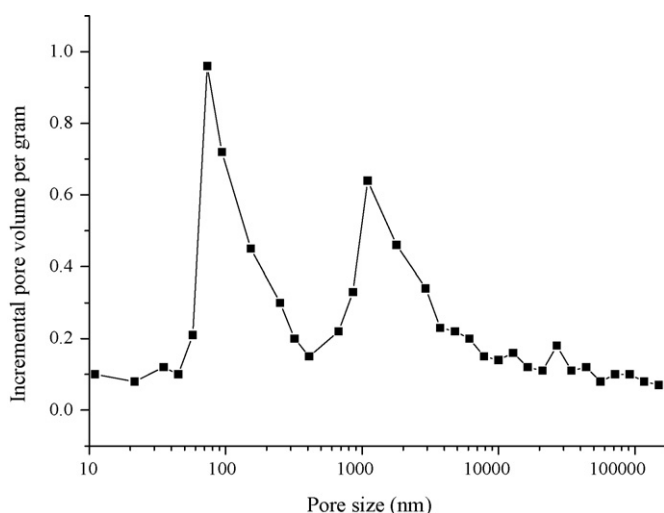Fig. 1. Scanning electron microphotograph of the poly (MASE–EDMA) monolithic material.

Fig. 2. Pore size distribution profile of the poly (MASE–EDMA) monolithic material.

Fig. 2 showed the pore size distribution plot. It was found that there were two types pore size existing in the monolithic material. One was large pore with the size about 1100 nm, and the other was mesopore with the size about 73.4 nm. The existence of large pore ensures the monolithic material possess very good permeability. While the mesopore ensures the material possess surface area. The total surface area was 4.25 m^2/g for the material calculated from Brunauer–Emmett–Teller (BET) plot. Experiment demonstrated that the material possessed high extraction capacity.

3.2. Optimization of SBSEM operating conditions

In order to optimize the SBSEM operating conditions for SSHs analysis, systematic studies were carried out in blank urine samples spiked at the 40 μg/L level. Several parameters that could influence the SBSEM extraction efficiency were investigated by coupling SBSEM to HPLC-DAD. According to literature [15], the agitation speed may effect on the SBSE efficiency significatively. However, assays performed at 600, 750 and 1000 rpm demonstrated that the differences observed were negligible. Consequently, a 600 rpm agitation speed was used in our research. The effect of different desorption solvent included methanol, ACN and mixture of methanol and ACN, on the desorption efficiency also was performed. The result shown that effect of the different solvent was also negligible. Therefore, methanol was chosen as desorption solvent considering methanol is more cheap and less poisonous than ACN. Others' important parameters included extraction and desorption time, pH value, inorganic salt concentration and organic phase content of the sample solution, which might play an important role in SBSEM efficiencies were studied in detail.

3.2.1. The effect of extraction and desorption time

The extraction time profiles of six SSHs were monitored by varying the extraction time from 0.5 to 2.0 h. Fig. 3 shows the extraction profile obtained for all SSHs studied, from which it can be observed that all SSHs reach adsorption equilibrium after 1.0 h. In the Almeida and Nogueira [13] work which used
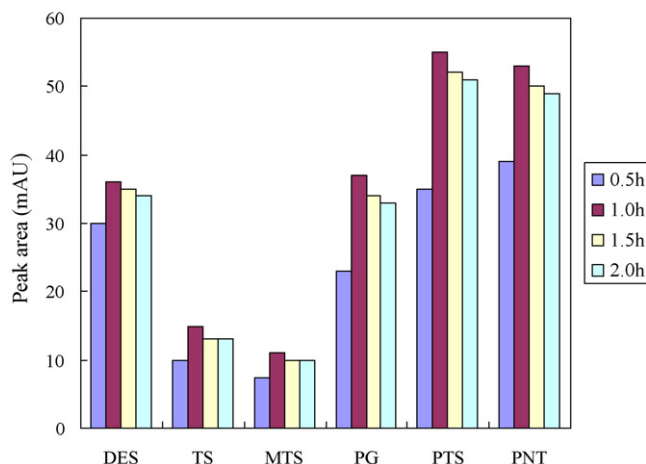

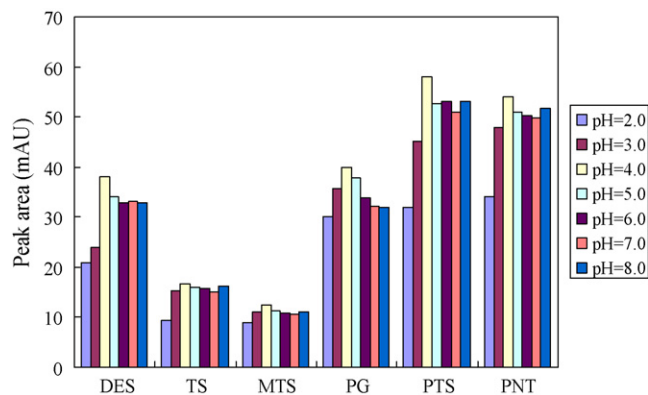Fig. 3. The effect of extraction time on extraction efficiency.

Fig. 4. The effect of pH of the sample matrix on extraction efficiency. The sample pH values of were adjusted by 0.1 mol/L HCl and 0.1 mol/L NaOH.

Fig. 5. The effect of NaCl addition on extraction efficiency.

SBSE with PDMS coating to analyze SSHs in water, the time to reach extractive equilibrium for progesterone and other SSHs was found to be 4 and 2 h, respectively. The fast equilibrium for SBSEM may be explained that by the faster mass transfer process of monolithic material than PDMS coating. Thus, the time for SBSEM operation could be shorter than that SBSE with PDMS coating. The effect of liquid desorption time on result was also studied. It was found that the desorption efficiency reached max after 1.5 h.

Consequently, 1.0 and 1.5 h were adopted for the extraction and desorption, respectively, in the following research.

3.2.2. The effect of pH value

The effect of sample pH on the extraction efficiency was investigated in the range from 2.0 to 8.0. As shown in Fig. 4, the extraction efficiency increased drastically from pH 2.0 to 4.0, and decreased slowly from pH 4.0 to 6.0. There was no obviously change when pH was higher than 6.0. The reason of the above changes may be explained that steroids are ionisable compounds, changing the pH of the aqueous matrix might have strong effect on their extraction yield [13,25]. All the six SSHs obtained highest extraction efficiency at pH 4.0. Therefore, setting the pH value of matrix at 4.0 was recommended for analyzing SSHs in urine matrix with SBSEM.

3.2.3. The effect of ionic strength

Ionic strength of matrix was adjusted by addition of NaCl from 0 to 50 mmol/L. The effect of ionic strength on the extraction efficiency was shown in Fig. 5. The results indicated that increasing the ionic strength in the matrix disadvantaged the extraction of SSHs. This observation can be explained that the molecules of NaCl also enter the inner of monolithic materials during the process of extraction. Methanol was used as desorption solvent in the desorption step, and the solubility of NaCl in methanol significantly lower than in water. Therefore, some pore of monoliths were blocked by crystal NaCl during desorption step which leaded some adsorptive SSHs cannot be released from monoliths. In order to avoid the crystal NaCl blocks, damages the monolithic coating, the SBSEM should be dipped in solvent of water and methanol (v/v, 80/20) to dissolve residual NaCl in the monoliths after each experiment. According
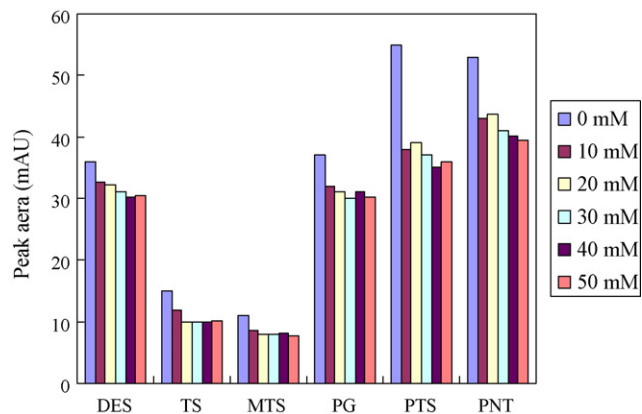
the above results, no additional salt was used in the further research.

3.2.4. The effect of organic effect

Sample solutions spiked with SSHs containing different levels of methanol were extracted under the same conditions to compare extraction efficiency. As shown in Fig. 6, extraction efficiencies decreased when the content of methanol in sample solutions increased. The reason may be that an organic modifier increases the solubility of SSHs in aqueous media, thus reduce the affinity of the target compounds for the monolithic materials of the stir bar. Consequently, further experiments were performed in the absence of MeOH in the aqueous matrix.

In a word, the optimized parameters for extraction of SSHs from urine matrix with SBSEM are the followings: agitation speed of 600 rpm; extraction and desorption time of 1.5 and 1.0 h, respectively; the pH value of matrix 4.0; no addition of salt and organic modifier.

3.3. Validation of the SBSE–LD–HPLC/DAD method

Six steroid sex hormones spiked at 40 ppb level were analyzed by SBSEM–LD–HPLC–DAD method under the above-optimized conditions. The typical chromatogram is showed in Fig. 7. Due to the high extraction capacity of SBSEM, great

Fig. 6. The effect of methanol content in sample solutions on extraction efficiency.

Table 1
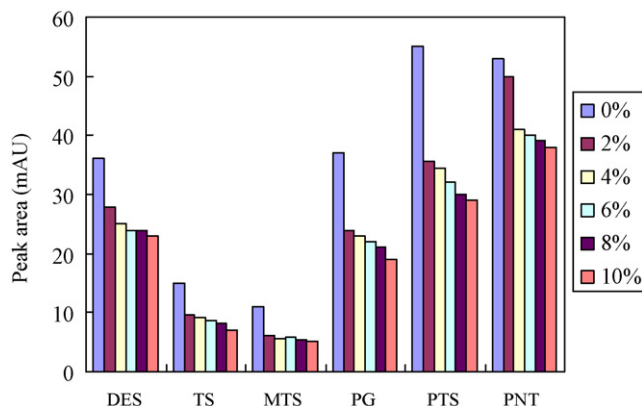Linear dynamic range, correlation coefficients, LODs and LOQs, average recoveries, inter-day and intra-day precisions achieved for the six steroid hormones (10 µg/L)

Hormones	Linear range (µg/L)	R^2	LOD[a] (µg/L)	LOQ[b] (µg/L)	Recovery[c] (%±R.S.D., $n=3$)	Inter-assay[c] variability (R.S.D.%, $n=3$)	Intra-assay variability (R.S.D.%, $n=3$)
DES	1.0–200.0	0.9987	0.062	0.20	48.0 ± 5.6	6.0	5.6
TS	4.0–200.0	0.9912	0.18	0.58	21.2 ± 9.2	10.0	9.2
MTS	4.0–200.0	0.9906	0.38	1.20	27.5 ± 8.9	9.1	8.9
PG	1.0–200.0	0.9976	0.12	0.41	49.5 ± 4.8	4.2	4.8
PTS	1.0–200.0	0.9992	0.12	0.41	80.0 ± 4.2	4.4	4.2
PNT	1.0–200.0	0.9984	0.18	0.58	81.8 ± 5.2	5.0	5.2

[a] S/N = 3.
[b] S/N = 10.
[c] Assays at 40 ng/mL level.

enhancement of the peak height can be obtained, which indicates that a lower detection limit could be achieved by SBSEM. The proposed method showed 48-, 21-, 27-, 49-, 76- and 81-fold higher sensitivity for DES, TS, MTS, PG, PTS and PNT, respectively, than the direct sample injection method (20 µL injection).

The blank urine samples were spiked with six SSHs and taken for analysis to evaluate the developed method. The data of linear dynamic range, correlation coefficients, LODs, LOQs, average recoveries and reproducibility for the six-hormones under the optimized experimental conditions were listed in Table 1. It can be seen from the data that the SBSEM–LD–HPLC/DAD methodology presents a good performance. The linear dynamic
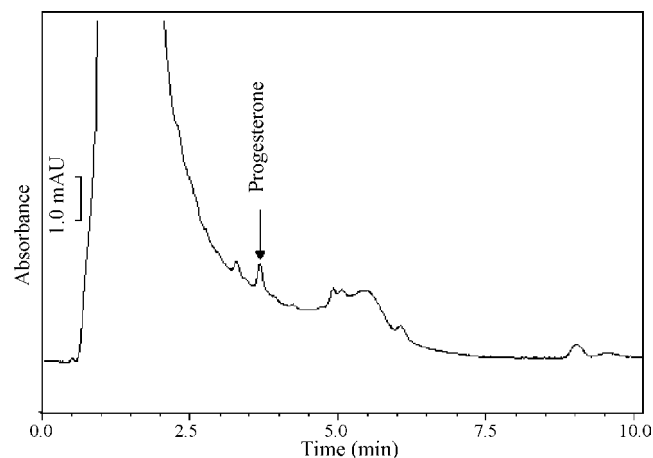

Fig. 8. Chromatogram of a urine sample from a pregnant woman (30 weeks) obtained by SBSEM–LD–HPLC/DAD.

range of a 50 mL sample was 1.0–200 µg/L with good linearity ($R^2 > 0.99$). The LOD and LOQ were determined at a concentration at which signal-to-noise ratios were equal to 3 and 10, and those were in the range of 0.062–0.38 and 0.2–1.20 µg/L, respectively. The LOD and LOQ were low enough to analyze trace hormones residuals in urine matrix. The recoveries of six SSHs ranged from 21.2% (TS) to 81.8% (PNT). The precision of the proposed method was evaluated using within and between-day repeatability calculated as R.S.D. on three replicates, and the variations were between 4.2% (PG) and 10.0% (TS). The data in Table 1 well indicate the SBSEM–LD–HPLC–DAD method may be used to effectively analyze hormones in urine matrix or other aqueous matrix, such as water.

Finally, a urine sample from a 30 weeks pregnant woman was analyzed by the present methodology. Fig. 8 depicts an overall profile of the corresponding chromatogram obtained by SBSE–LD–HPLC/DAD, under optimized experimental conditions. Although the urine matrix presented some complexity, traces of progesterone (2.54 µg/L) could be clearly detected, as well as other metabolites.

4. Conclusions

In this work, a new SBSE based on a poly (methacrylic acid stearyl ester–ethylene dimethacrylate) was synthesized.
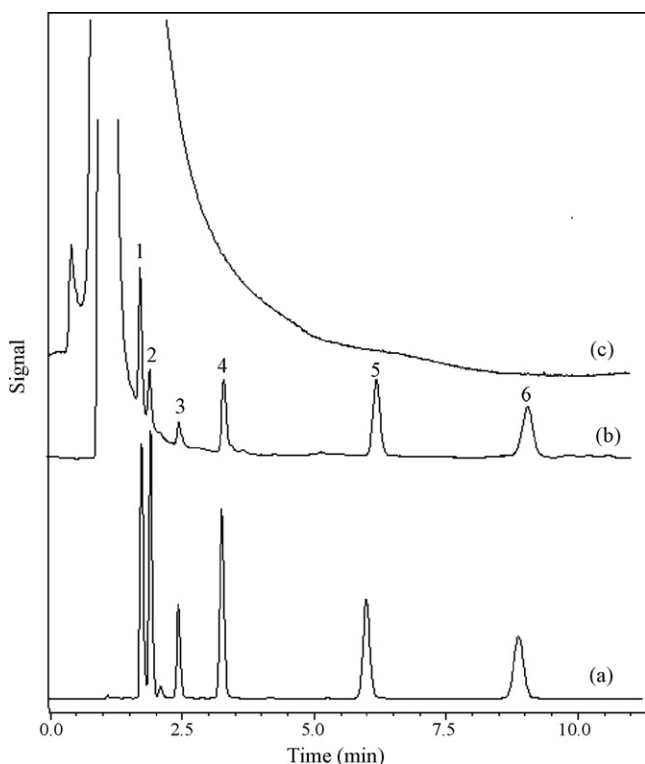

Fig. 7. HPLC chromatograms of six SSHs. (a) standard sample with each SSH at 10 µg/mL, (b) spiked urine sample with each SSH at 40 ng/mL and treated with SBSEM, (c) direct injection of spiked urine sample with each SSH at 40 ng/mL. Peaks: 1, diethylstilbestrol; 2, testosterone; 3, methyltestosterone; 4, progesterone; 5, testosterone propionate; 6, nandrolone phenylpropionate.

The combination of stir bar sorptive extraction and liquid desorption followed by high performance liquid chromatography with diode array detection was successfully applied to the determination of six steroid sex hormones in urine matrix, at the trace level. In comparison to the existing extraction methods for SSHs determination, the proposed method was simple, rapid, and precise. Therefore, it will be useful and practical in the screening and determination of SSHs in biological and environmental samples, such as urine and water.

Acknowledgements

References

[1] L. Guillette, D.A. Crain, Environmental Endocrine Disrupters: An Evolutionary Perspective, Taylor & Francis, USA, 2000.
[2] G.G. Ying, R.S. Kookana, Y.J. Ru, Environ. Int. 28 (2002) 545.
[3] M.J. Lopez de Alda, D. Barcelo, J. Chromatogr. A 911 (2001) 203.
[4] C. Desbrow, E.J. Routledge, G.C. Brighty, J.P. Sumpter, M. Waldock, Environ. Sci. Technol. 32 (1998) 1549.
[5] S.A. Snyder, T.L. Keith, D.A. Verbrugge, E.M. Snyder, T.S. Gross, K. Kannan, J.P. Giesy, Environ. Sci. Technol. 33 (1999) 2814.
[6] V.J. Kramer, S. Miles-Richardson, S.L. Pierens, J.P. Giesy, Aquat. Toxicol. 40 (1998) 335.
[7] M. Seifert, G. Brenner-Weiß, S. Haindl, M. Nusser, U. Obst, B. Hock, Fresenius J. Anal. Chem. 363 (1999) 767.
[8] V. Ingrand, G. Herry, J. Beausse, M. de Roubin, J. Chromatogr. A 1020 (2003) 99.
[9] S.A. Hewitt, M. Kearney, J.W. Currie, P.B. Young, D.G. Kennedy, Anal. Chim. Acta 473 (2002) 99.
[10] S. Nakamura, T. Hwee Sian, S. Daishima, J. Chromatogr. A 919 (2001) 275.
[11] J.B. Quintana, J. Carpinteiro, I. Rodrıguez, R.A. Lorenzo, A.M. Carro, R. Cela, J. Chromatogr. A 1024 (2004) 177.
[12] B. Tienport, F. David, K. Desmet, P. Sandra, Anal. Bioanal. Chem. 373 (2002) 46.
[13] C. Almeida, J.M.F. Nogueira, J. Pharm. Biomed. Anal. 41 (2006) 1303.
[14] M.J. Lopez de Alda, D. Barcelıo, Fresenius J. Anal. Chem. 371 (2001) 437.
[15] E. Baltussen, P. Sandra, F. David, C. Cramers, J. Microcolumn Sep. 11 (1999) 737.
[16] S. Nakamura, S. Daishima, Anal. Bioanal. Chem. 382 (2005) 99.
[17] C. Huertas, J. Morillo, J. Usero, I. Gracia-Manarillo, Talanta 72 (2007) 1149.
[18] A. Stopforth, A. Tredoux, A. Crouch, P. Van Helden, P. Sandra, J. Chromatogr. A 1071 (2005) 135.
[19] E.D. Guerrero, R.N. Marin, R.C. Mejias, C.G. Barroso, J. Chromatogr. A 1104 (2006) 47.
[20] M. Kawaguchi, Y. Ishii, N. Sakui, N. Okanouchi, R. Ito, K. Saito, H. Nakazawa, Anal. Chim. Acta 539 (2005) 83.
[21] M. Kawaguchi, R. Ito, K. Saito, H. Nakazawa, J. Pharm. Biomed. Anal. 40 (2006) 500.
[22] F. David, B. Tienpont, P. Sandra, LC–GC N. Am. 21 (2003) 108.
[23] X.J. Huang, D.X. Yuan, Chinese Patent, Appl. CN 200610122341.1 (2006).
[24] X.J. Huang, D.X. Yuan, J. Chromatogr. A 1154 (2007) 152.
[25] K. Kureckova, B. Maralıkova, K. Ventura, J. Chromatogr. B 770 (2002) 83.

Non-covalent anionic porphyrin functionalized multi-walled carbon nanotubes as an optical probe for specific DNA detection

Cheng Zhi Huang [a,*], Qie Gen Liao [b], Yuan Fang Li [b]

[a] *College of Pharmaceutical Sciences, CQKL-LRTA, Southwest University, Chongqing 400715, China*
[b] *College of Chemistry and Chemical Engineering, CQKL-LRTA, Southwest University, Chongqing 400715, China*

Abstract

With water-soluble anionic tetra (*p*-carboxyphenyl) porphyrin (TCPP) to solubilize multi-walled carbon nanotubes (MCNTs), we obtained a suspension that could be stable more than 1 week. With this TCPP/MCNTs suspension, we propose a spectrofluorometric method of DNA hybridization in this contribution. Our basic finding for this work is that the fluorescence from a dye-tagged single stranded DNA (ssDNA), which was directly added to the TCPP/MCNTs suspension, gets quenched, and the fluorescence could be remained if the dye-tagged single stranded DNA is first to be hybridized with its complementary target DNA to form a double stranded DNA (dsDNA) hybrid and added into the TCPP/MCNTs suspension. Mechanism investigations showed that the reason for the former is due to the adsorption of ssDNA on the surfaces of MCNTs, and that for the latter is due to the strong electrostatic repulsion force between the negative charge TCPP/MCNTs complexes and dsDNA. Thus, target DNA in a DNA sample and single-base mismatch in DNA sequences could be easily detected.
© 2007 Elsevier B.V. All rights reserved.

Keywords: Multi-walled carbon nanotubes (MCNTs); Tetra (*p*-carboxyphenyl) porphyrin (TCPP); DNA hybridization

1. Introduction

Individually dispersed carbon nanotubes (CNTs) are excellent candidates for optical sensors [1]. However, polydispersity and poor solubility in both aqueous and non-aqueous medium impose a considerable challenge for their applications. To effectively be utilized as building blocks for nanotechnology, CNTs have been covalently and non-covalently functionalized in order to make them soluble in aqueous or organic solutions [2–7]. It has reported that the non-covalent binding of zinc protoporphyrin IX (ZnPP) or *meso*-hexadecyloxyphenyl-substituted porphyrin to CNTs could render CNTs soluble in DMF or DMSO through π–π interaction [8,9]. Recent similar discoveries had showed that *meso*-(tetrakis-4-sulfonatophenyl) porphine (TPPS$_4$) and 5,15-bis (3,5-di–*tert*- butylphenyl) porphyrin non-covalently make CNTs soluble in aqueous medium [10,11]. Functionalization of CNTs with porphyrins could supply the nanotubes with unique intrinsic properties of porphyrins, such

as luminescence, photovoltaic properties, and biocompatibility. It has reported that single-stranded DNA (ssDNA) could non-covalently interact with CNTs [12–14] owing to the π-stacking interaction between bases in DNA and the sidewalls of CNTs, while that double stranded DNA (dsDNA) is hardly adsorbed on the surface of CNTs owing to the screening effect of the negatively charged phosphate backbones of dsDNA on their bases, which blocks the π-stacking interaction of the bases with CNTs [15–17]. The different adsorption properties of ssDNA and dsDNA on the CNTs have been applied to the detection of specific DNA sequences with the near-infrared band-gap fluorescence of nanotubes or network field-effect transistors (NFETs) [18,19]. These methods, however, either suffer from slow response or require surface-immobilized probes.

Considering the different adsorption properties of ssDNA and dsDNA on the surface of CNTs and unique intrinsic properties of porphyrins, we propose a detection method of specific DNA in this work with non-covalent anionic porphyrin functionalized multi-walled carbon nanotubes (MCNTs) suspension as an optical probe. We found that tetra (*p*-carboxyphenyl) porphyrin (TCPP) could well disperse multi-walled carbon nanotubes (MCNTs), forming stable TCPP/MCNTs suspension

---

in the neutral medium. If a fluorescent dye-tagged ssDNA was added into the TCPP/MCNTs suspension, the fluorescence emission of the dye-tagged DNA was quenched, while the dsDNA, a hybrid formerly formed from the dye-tagged ssDNA with its complementary target ssDNA, was added into the TCPP/MCNTs suspension, the fluorescence emission of the tagged dye remained. With that, we proposed a method of DNA hybridization and single base-mismatched detection in this contribution.

2. Materials and methods

2.1. Apparatus

The fluorescence spectra were obtained by using a Hitachi F-4500 fluorescence spectrophotometer (Tokyo, Japan), while the absorption spectra were obtained by using a Hitachi UV-3010 UV–visible spectrophotometer (Tokyo, Japan) with water as a reference. The SEM images of dispersed carbon nanotubes were obtained by using a S-4800 scanning electron microscope (Tokyo, Japan). A pHS-3D digital pH meter (Leici, Shanghai, China) was used to adjust the pH-values of the solutions, and a MVS-1 vortex mixer (Beide Scientific Instrumental Ltd., Beijing, China) was used to blend the mixture.

2.2. Materials

DNA oligonucleotides were synthesized and purified by SBS Genetech Co. (Beijing, China). The sequences of the oligonucleotides used in this work are as follows: (1) FAM-5′-GTGAGGCATTGCCCC-3′ (probe DNA, p-DNA); (2) 5′-GGGGCAATGCCT CAC-3′ (complementary target DNA, ct-DNA); (3) 5′-GGGGCAA*A*GCCTCAC -3′ (mismatched DNA, m-DNA). Concentration of ssDNA was determined by measuring the absorbance at 260 nm. The tetra (*p*-carboxyphenyl) porphyrin (TCPP) was purchased from Sigma (Jiehua Chemical Co. Ltd., Chengdu, China). Na_2HPO_4–KH_2PO_4 buffer (pH 7.4) was employed for acidity control. All other reagents were of analytical-reagent, and double distilled water (18.2 MΩ) was used throughout.

MCNTs (Organic Chemical Co., Ltd., Chengdu, China) were purified according to literature protocols [20,21]. Typically, 50 mg of MCNTs were refluxed in 50 mL of 2 M HNO_3 for 2 days. Precipitate of MCNTs as a solid was allowed to proceed overnight, and the clear solution above the suspension was then removed. About 15 mL of suspension was separated by filtration membrane. 2.76×10^{-5} M TCPP and the purified MCNTs mixed to form TCPP/MCNTs complexes for about 8 h in an ultrasonic bath, and the complexes were ultrasonicated for 30 min before used.

2.3. Methods

As for hybridized detection, into a 1.5 ml eppendorf cup was added 30 μl of 0.75 μM probe ssDNA, 30 μl of 0.75 μM ctDNA, 40 μl of phosphate buffer with pH 7.4. The mixture was diluted to 170 μl. After mixed thoroughly, and incubated for about

5–10 min at 37 °C, 30 μl TCPP/MCNTs solution was added into the samples and stood at room temperature for 5.0 min to form complexes. Fluorescence measurements were made with F-4500 spectrofluorometer by keeping the excitation and emission slit widths of 10.0 nm, and the working PMT voltage of 700 V.

3. Results and discussion

3.1. Interaction of TCPP and MCNTs

A freshly prepared solution of TCPP dissolved in pure water in neutral medium exits in a free base form and displayed a deep magenta-colored transparent solution. After 8 h ultrasonication together with MCNTs, however, the TCPP/MCNTs mixture became a black-colored suspension (Fig. 1). The SEM images of TCPP/MCNTs mixture showed that MCNTs in the suspension got well dispersed (Fig. 2). It was found that this suspension could be stable more than 1 week.

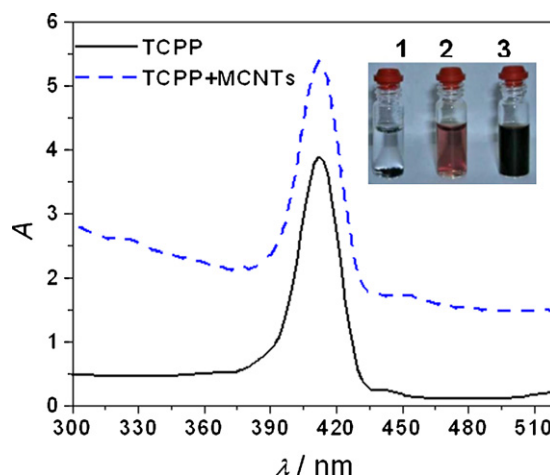In order to investigate the interaction between TCPP and MCNTs, we measured the absorption and fluorescence emission

Fig. 1. Absorption spectra of TCPP solution (solid) and TCPP/MCNTs suspension (dashed). c_{TCPP}, 3.86×10^{-6} M; c_{MCNTs}, 0.066 mg ml^{-1}; pH 7.4. The inserted photographs show MCNTs in water (1), TCPP aqueous solution (2), and TCPP/MCNTs suspension (3).
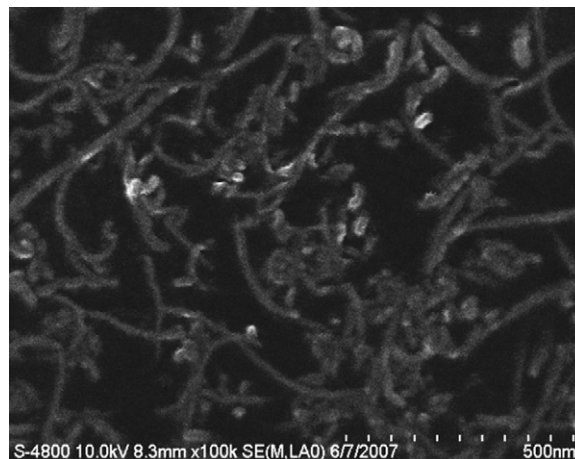

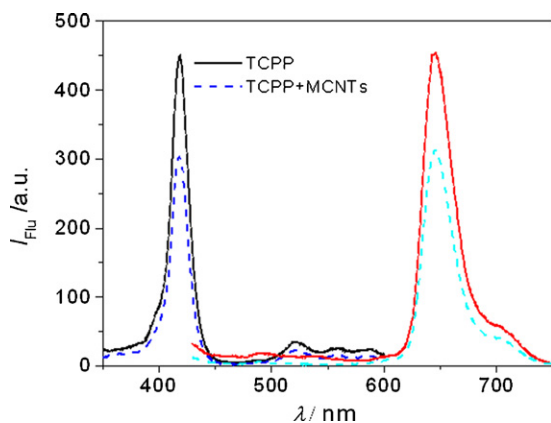Fig. 2. SEM image of TCPP/MCNTs suspension.

Fig. 3. Fluorescence excitation (left) and emission spectra (right) of TCPP solution (solid line) and TCPP/MCNTs suspension (dashed line). c_{TCPP}, 3.86×10^{-6} M; c_{MCNTs}, 0.066 mg ml^{-1}; pH 7.4. λ_{ex}, 418 nm, λ_{em}, 646 nm, 700 V.

feature of both TCPP and TCPP/MCNTs suspensions. It was found that the Soret absorption band characterized at 414 nm of TCPP in the neutral medium was not perturbed even if TCPP experienced 8 h ultrosonication with MCNTs together (Fig. 1), while the fluorescence emission at 646 nm of the TCPP when excited at 418 nm (Fig. 3) was quenched by MCNTs. The fluorescence quenching possibly results from the inner-filter effect of MCNTs since they have strong and broad absorption band throughout the range from 200 to 900 nm [22].

3.2. Fluorescence of dye-tagged ssDNA and dsDNA in TCPP/MCNTs suspension

It was found that the fluorescence emission of FAM characterized at 520 nm excited at 485 nm was very weak if a fluorescent FAM-tagged ssDNA solution was added into TCPP/MCNTs suspension (Curve 3 in Fig. 4). However, if a dsDNA hybrid solution, formed from the fluorescent FAM-tagged DNA with its complementary DNA sequence, was added, the fluorescence emission of dye-tagged dsDNA got strong (Curve 1 in
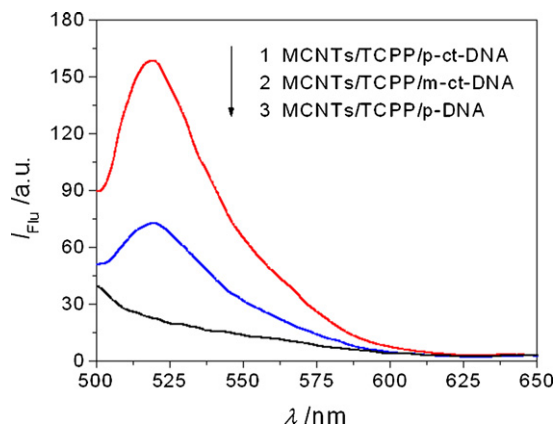
Fig. 4). It was also found that the TCPP/MCNTs suspension was highly specific in discriminating against complementary DNA sequences and single-base mismatches. The addition of a single-base mismatched dsDNA could have about 46% enhanced fluorescence emission compared with the fluorescence intensity of perfectly matched targets (Curve 2 in Fig. 4).

In the neutral medium, TCPP/MCNTs suspensions are negative-charged on the surface owing to the carboxyl group and could restrain adsorption of dsDNA due to electrostatic repulsion forces. This negative-charged environment, however, could not exert any effect on the adsorption of ssDNA for the adsorption depended on the π-stacking interaction between the exposed bases and the MCNTs. In addition, the hydrophobic aromatic fluorescein group of FAM-tagged ssDNA could also bind to the sidewalls of CNTs via π-stacking [23], and it was found about 90% of the fluorescence of MCNTs-bound tagged fluorescein could be quenched compared to free fluorescein-tagged DNA owing to the interactions between fluorescein and MCNTs. Similar fluorescence quenching phenomenon could found in reference between CNT and pyrene due to energy transfer [24,25]. Therefore, we suppose that TCPP as a medium might induce effective energy transfer from dye to MCNTs when the TCPP/MCNTs were used as nano-probes for hybridization detection of DNA in Fig. 4.

3.3. Effects of bivalent cationic ions on DNA hybridization

The ring structure of porphyrin enriches π-electron and could make MCNTs non-covalently functionalized through π–π interaction, and its substituted groups such as carboxyl are well hydrophilic. Therefore, TCPP/MCNTs suspension could be stable. When bivalent cationic ions such as Mg^{2+} and Ca^{2+} were added to the TCPP/MCNTs suspension, the negative charges of the TCPP/MCNTs would be partly neutralized and their hydrophilicity would be reduced, resulting in precipitate (Fig. 5). Compared with Mg^{2+}, the neutralization of Ca^{2+}

Fig. 4. Fluorescence emissions demonstrating detection of specific DNA sequences and single-base mismatches using TCPP/MWNTs suspension as optical probes. Concentrations: c_{MCNTs}, 0.02 mg ml^{-1}; c_{TCPP}, 4.14×10^{-7} M; c_{p-DNA}, 1.1×10^{-7} M; c_{ct-DNA}, 1.1×10^{-7} M; c_{m-DNA}, 1.1×10^{-7} M; pH 7.4; λ_{ex}, 485 nm.
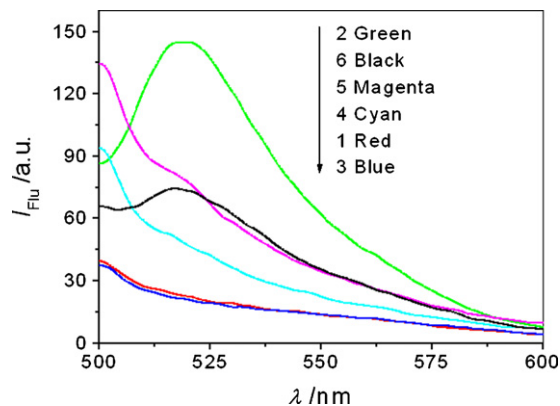
Fig. 5. Effects of bivalent cationic ions on DNA hybridization in the presence of MCNTs probes. Curves: (1) MCNTs/TCPP + ssDNA; (2) MCNTs/TCPP + dsDNA; (3) MCNTs/TCPP + ssDNA + MgCl$_2$; (4) MCNTs/TCPP + ssDNA + CaCl$_2$; (5) MCNTs/TCPP + dsDNA + CaCl$_2$; (6) MCNTs/TCPP + dsDNA + MgCl$_2$. Concentrations: c_{MCNTs}, 0.02 mg ml^{-1}; c_{TCPP}, 4.14×10^{-7} M; c_{p-DNA}, 1.1×10^{-7} M; c_{ct-DNA}, 1.1×10^{-7} M; c_{Mg2+}, 5.0 mM; c_{Ca2+}, 5.0 mM; Na$_2$HPO$_4$–KH$_2$PO$_4$ buffer (pH 7.4, 10 mM, 250 mM NaCl). λ_{ex}, 485 nm.
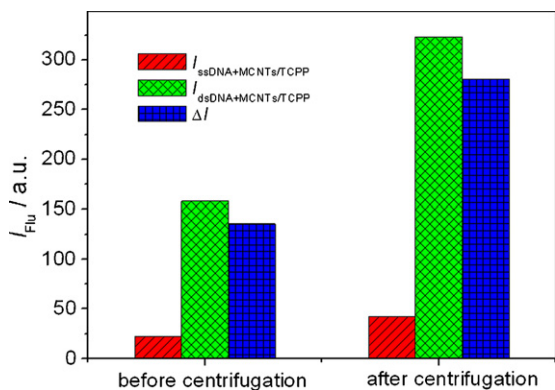
Fig. 6. Effects of centrifugation on DNA hybridization in the presence of MCNTs probes. Concentrations: c_{MCNTs}, 0.02 mg ml^{-1}; c_{TCPP}, 4.14 × 10^{-7} M; c_{p-DNA}, 1.1 × 10^{-7} M; c_{c-DNA}, 1.1 × 10^{-7} M; Na$_2$HPO$_4$–KH$_2$PO$_4$ buffer (pH 7.4, 10 mM, 250 mM NaCl). λ_{ex}, 485 nm, λ_{em}, 520 nm.

marked stronger, and the precipitate could be observed at 5 mM Ca^{2+}. Thus, we could find that fluorescence recovery of dsDNA reduced due to decrease of electrostatic repulsion forces. On the contrary, fluorescence quenching of ssDNA did not get affected, for ssDNA depended on π-stacking but not related to charges. It should be noted that the addition of Ca^{2+} resulted in high background fluorescence due to appearance of precipitate. These results conform the different adsorption properties of ssDNA and dsDNA on the CNTs in the presence of TCPP.

3.4. Effects of centrifugation on DNA hybridization

Since the ssDNA could be adsorbed strongly on the surface of CNTs and the absorption could markedly increase suspended forces, thus, DNA-CNTs complexes were hardly centrifugalized. However, the dsDNA could hardly be adsorbed strongly on the surface of CNTs, and the centrifugation, 10 min at 3000 rmp for instance, could give rise to marked CNTs precipitate containing dsDNA. The appearance of precipitate could decrease the inner-filter effect of CNTs on the fluorescence of dye-tagged DNA. Fig. 6 showed that fluorescence recovery of ssDNA and dsDNA got increased after centrifugation. The fluorescence recovery degree of dsDNA was obviously stronger than that of ssDNA, further conforming the different adsorption properties of ssDNA and dsDNA on the CNTs in the presence of TCPP.

4. Conclusion

By combining the different adsorption properties of ssDNA and dsDNA on the surface of CNTs and unique intrinsic properties of porphyrins, we propose a method of specific DNA detection with TCPP functionalized MCNTs as an optical probe since TCPP could well disperse MCNTs, forming a stable TCPP/MCNTs suspension with negative charges in the neutral medium. This optical probe could be used for the detections of DNA hybridization and single base-mismatched recognition. Absorption and fluorescence measurements of the water-soluble TCPP/MCNTs complexes indicate that the free base form is primarily responsible for rendering the nanotubes soluble in water.

Water-soluble TCPP/MCNTs could be applied to detect DNA sequence. Effects of bivalent cationic ions and centrifugalization could conform the different adsorption properties of ssDNA and dsDNA on the CNTs.

Acknowledgements

References

[1] P.W. Barone, S. Baik, D.A. Heller, M.S. Strano, Nat. Mater. 4 (2005) 86–92.
[2] V. Krstic, G.S. Duesberg, J. Muster, M. Burghard, S. Roth, Chem. Mater. 10 (1998) 2338–2340.
[3] N. Nakashima, N.H. Kobae, T. Sagara, H. Murakami, Chem. Phys. Chem. 3 (2002) 456–458.
[4] M.J. O'Connell, P. Boul, L.M. Ericson, C. Huffman, Y. Wang, E. Haroz, C. Kuper, J. Tour, K.D. Ausman, R.E. Smalley, Chem. Phys. Lett. 342 (2001) 265–271.
[5] A. Star, J.F. Stoddart, D. Steuerman, M. Diehl, A. Boukai, E.W. Wong, S.X. Yang, S.-W. Chung, H. Choi, J.R. Heath, Angew. Chem. Int. Ed. 40 (2001) 1721–1725.
[6] J. Chen, H. Liu, W.A. Weimer, M.D. Halls, D.H. Waldeck, G.C. Walker, J. Am. Chem. Soc. 124 (2002) 9034–9035.
[7] D.W. Steuerman, A. Star, R. Narizzano, H. Choi, R.S. Ries, C. Nicolini, J.F. Stoddart, J.R. Heath, J. Phys. Chem. B 106 (2002) 3124–3130.
[8] H. Murakami, T. Nomura, N. Nakashima, Chem. Phys. Lett. 378 (2003) 481–485.
[9] H. Li, B. Zhou, Y. Lin, L. Gu, W. Wang, K.A.S. Fernando, S. Kumar, L.F. Allard, Y.-P. Sun, J. Am. Chem. Soc. 126 (2004) 1014–1015.
[10] T. Hasobe, S. Fukuzumi, P.V. Kamat, J. Am. Chem. Soc. 127 (2005) 11884–11885.
[11] J. Chen, C.P. Collier, J. Phys. Chem. B 109 (2005) 7605–7609.
[12] M. Zheng, A. Jagota, E.D. Semke, B.A. Diner, R.S. McLean, S.R. Lustig, R.E. Richardson, N.G. Tassi, Nat. Mater. 2 (2003) 338–342.
[13] M. Zheng, A. Jagota, M.S. Strano, A.P. Santos, P. Barone, S.G. Chou, B.A. Diner, M.S. Dresselhaus, R.S. McLean, G.B. Onoa, G.G. Samsonidze, E.D. Semke, M. Usrey, D.J. Walls, Science 302 (2003) 1545–1548.
[14] M.S. Strano, M. Zheng, A. Jagota, G.B. Onoa, D.A. Heller, P.W. Barone, M.L. Usrey, Nano Lett. 4 (2004) 543–550.
[15] H.X. Li, L.J. Rothberg, Proc. Natl. Acad. Sci. U.S.A. 101 (2004) 14036–14039.
[16] H.X. Li, L.J. Rothberg, Anal. Chem. 76 (2004) 5414–5417.
[17] H. Li, J. Huang, J. Lv, H. An, X. Zhang, Z. Zhang, C. Fan, J. Hu, Angew. Chem. Int. Ed. 44 (2005) 5100–5103.
[18] E.S. Jeng, A.E. Moll, A.C. Boy, J.B. Gastala, M.S. Strano, Nano Lett. 6 (2006) 371–375.
[19] A. Star, E. Tu, J. Niemann, J.P. Gabriel, C.S. Joiner, C. Valcke, Proc. Natl. Acad. Sci. U.S.A. 103 (2006) 921–926.
[20] Y. Lin, A.M. Rao, B. Sadanadan, E.A. Kenik, Y.P. Sun, J. Phys. Chem. B. 106 (2002) 1294–1298.
[21] P. He, M. Bayachou, Langmuir 21 (2005) 6086–6092.
[22] I.W. Chiang, B.E. Brinson, A.Y. Huang, P.A. Willis, M.J. Bronikowski, J.L. Margrave, R.E. Smalley, R.H. Hauge, J. Phys. Chem. B 105 (2001) 8297–8301.
[23] N. Nakayama-Ratchford, S. Bangsaruntip, X. Sun, K. Welsher, H. Dai, J. Am. Chem. Soc. 129 (2007) 2448–2449.
[24] Y. Tomonari, H. Murakami, N. Nakashima, Chem. Eur. J. 12 (2006) 4027–4034.
[25] H. Paloniemi, T. Aaritalo, T. Laiho, H. Liuke, N. Kocharova, K. Haapakka, F. Terzi, R. Seeber, J. Lukkari, J. Phys. Chem. B 109 (2005) 8634–8642.

Molecularly imprinted polymers microsphere prepared by precipitation polymerization for hydroquinone recognition

Xianwen Kan, Qun Zhao, Zhong Zhang, Zhilin Wang [*], Jun-Jie Zhu [*]

State Key Laboratory of Coordination Chemistry, MOE Key Lab of Analytical Chemistry for Life Science, School of Chemistry and Chemical Engineering, Nanjing University, Nanjing 210093, PR China

Abstract

A one-step precipitation polymerization synthesis was adopted for the preparation of molecularly imprinted polymers (MIPs) by using hydroquinone as a template molecule. The transmission electron microscopy (TEM) exhibited that the polymers were uniform spheres with the diameter of about 700 nm. The results of adsorption experiments showed that the microspherical imprinted polymers possessed fast adsorption dynamics. Compared to the structurally similar compounds, catechol and resorcinol, the MIPs exhibited a high recognizable capacity to hydroquinone. And the electrochemical sensor fabricated by modifying the prepared MIPs microsphere on the glassy carbon electrode surface was used to detect the hydroquinone concentration. The current response was proportional to the concentration of hydroquinone in the range of 2.0×10^{-6} to 1.0×10^{-4} mol/L with the detection limit of 1.0×10^{-6} mol/L.
© 2007 Elsevier B.V. All rights reserved.

Keywords: Molecularly imprinted polymers microsphere; Precipitation polymerization; Hydroquinone; Recognition; Electrochemical detect

1. Introduction

Molecular imprinting of synthetic polymers is an approach where functional monomer and cross-linker are copolymerized in the presence of template molecule [1]. Removal of the template molecule from the obtained polymer by simple solvent extraction reveals the complementary binding sites that can recognize the template molecule from its structurally similar compounds. Owing to their mechanical and chemical stability, low cost of preparation, ease of mass production and fitting for wide range of operating conditions, molecularly imprinted polymers (MIPs) have been developed in wide fields, such as solid-phase extraction [2], chromatographic separation [3], catalysis [4] and biosensor [5].

Conventional MIPs have been prepared in the form of bulk monolith. The copolymers are then ground and sieved to obtain appropriate size particles with irregularly shape for further use [6–8]. This procedure is time-consuming and yields only moder-

ate amounts of "useful" product [9]. And the obtained copolymer particles have low capacity and poor site accessibility for the template molecules because the grinding process may be detrimental to some of the binding sites. In order to overcome above limits, recently efforts have been made to prepare MIPs with desired shape and achieve MIPs materials for wide applications [10,11]. The ideal shape of MIPs for many applications may be the microsphere with regular size and shape [12], which can be prepared by precipitation polymerization [13], emulsion polymerization [14], suspension polymerization [15] and seed polymerization [16]. Compared with the latter three methods, precipitation polymerization might be the easiest method to prepare microspherical MIPs because this procedure is easy, and there is no need to add emulsifier or suspending reagent to reaction system.

Since it was first reported by Ye et al. [17], precipitation polymerization for the preparation of spherical MIPs has been developed rapidly and applied to recognize and determine various compounds, which mostly are biomolecules, such as amino acids [18], antibiotics [19] and herbicides [20]. Likewise, a little attention has been devoted for analytes of environmental interest, such as toxic compounds. Hydroquinone, a potentially carcinogenic substance, causes severe effects on the central nervous

---

* Corresponding authors. Tel.: +86 25 83686082; fax: +86 25 83594976.
  E-mail addresses: wangzl@nju.edu.cn (Z. Wang),
jjzhu@nju.edu.cn (J.-J. Zhu).

system. Several methods have been used for the determination of hydroquinone, including gas chromatography [21], chemiluminescence [22] and flow injection analysis [23]. These methods exhibited high sensitivity, but all needed relatively expensive instrument and long time to complete the determination process.

In the present work, a simple and efficient synthesis method, precipitation polymerization, was employed to prepare the MIPs microsphere by using hydroquinone as the template molecule. Ultraviolet–visible (UV–vis) spectrophotometry was used to evaluate the adsorption kinetics, special rebinding and selective recognition capability of the MIPs. At the same time, an electrochemical sensor prepared by modifying the MIPs microsphere on the glassy carbon electrode surface was used to detect the concentration of hydroquinone.

2. Experimental

2.1. Chemicals

The cross-linker, trimethylolpropane trimethacrylate (TRIM), was purchased from Sigma. The functional monomer, methacrylic acid (MAA) was purified by distillation in vacuum to remove the polymerization inhibitor. All other reagents were of analytical grade and were used without further purification. 0.1 mol/L phosphate buffer solution (PBS) prepared in mixed solvent of doubly distilled water and methanol (9:1, v/v) at pH 7.0 was used as supporting electrolyte.

2.2. Apparatus and procedure

The morphology of MIPs microsphere was characterized by transmission electron microscopy (TEM, JEOL IEM-200CX).

Ultraviolet–visible absorption spectra of hydroquinone were recorded by a UV-2401PC spectrometer. Electrochemical measurements were performed with a CHI 660B electrochemical workstation (Shanghai Chenhua Instrument) in a glass vial containing 10 mL of electrolyte at the room temperature. Chronoamperometry experiments were carried out in a typical three-electrode system with a platinum wire used as an auxiliary electrode, a saturated calomel electrode (SCE) as a reference electrode, and the MIPs microsphere modified glassy carbon electrode as a working electrode.

2.3. Preparation of MIPs microsphere

The hydroquinone MIPs microsphere were prepared by precipitation polymerization using hydroquinone, MAA, TRIM and 2, 2′-azobisisobutyronitrile (AIBN) as template molecule, functional monomer, cross linker and initiator, respectively. The procedure of preparing the MIPs was described in Scheme 1. One millimole template molecule and 8 mmol functional monomer were dissolved in a mixed solvent of acetonitrile and toluene. The mixture was sonicated to facilitate the combination between template molecule and functional monomer. Then 10 mmol cross-linker and 50 mg initiator were added to above mixture and stirred with magnetic stirrer. The temperature was increased from room temperature to 70 °C within 2 h under N_2 gas, and then kept at 70 °C for 24 h. After polymerization process, the resulting polymers were collected by centrifugation of 9000 rpm for 10 min. Then the polymers were eluted by the mixture solvent of methanol and acetic acid (9:1, v/v) for several times to extract the template molecules until there was no hydroquinone that could be detected by UV spectrometer in the eluent. The obtained polymers were finally rinsed with ethanol for
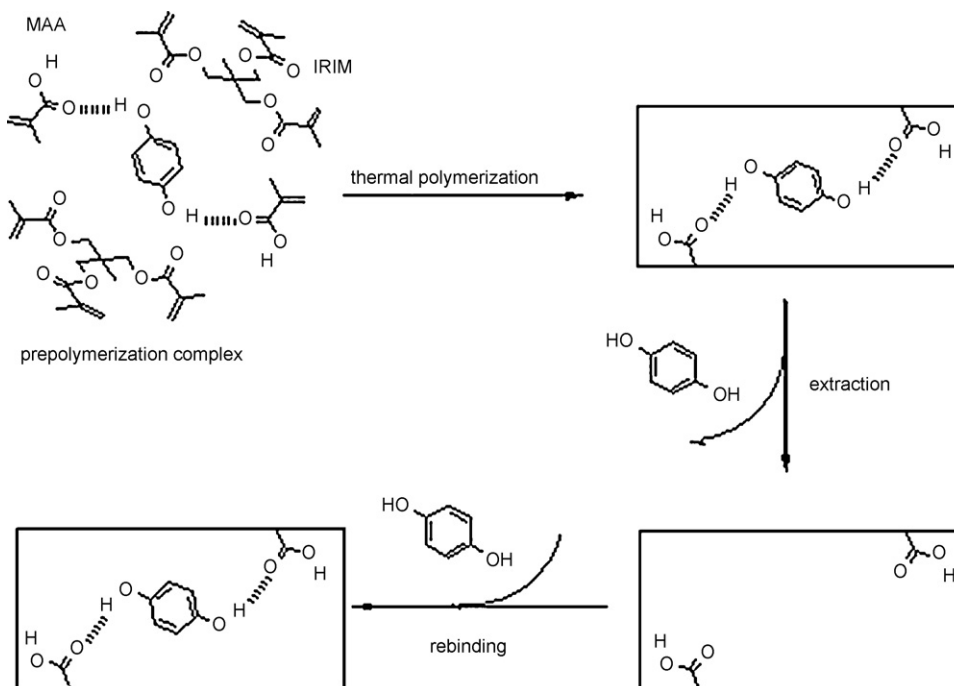
Scheme 1. Schematic illustration of the molecular imprinting procedure.

one time to remove the remaining acetic acid and then dried in the vacuum desiccators for 24 h before used. As a control, the non-molecularly imprinted polymer (NIPs) microspheres were prepared and treated in the same way, except that the template molecule was omitted from the polymerization process.

2.4. Binding experiments

Twenty milligrams microspherical MIPs or NIPs were added into 5 mL tubes, and mixed with 2.0 mL of hydroquinone–acetonitrile solutions with specific initial concentrations ranging from 0 to 5.0 mmol/L. After the samples were shaken at 25 °C for 4 h, the solution was centrifuged at 12,000 rpm for 5 min. The concentration of free hydroquinone in the supernate was measured by UV spectrophotometry at 289 nm. The amount of hydroquinone bound to the MIPs was calculated by subtracting the amount of free hydroquinone from the amount of hydroquinone initially added. Meanwhile, the adsorption dynamics of the MIPs was performed by measured the free hydroquinone concentration in the supernate at the different adsorption time intervals. The selectivity of the MIPs was investigated using catechol and resorcinol as the structurally related compounds.

2.5. Electrochemical detection of hydroquinone

Twenty milligrams MIPs were dispersed in 1 mL methanol with ultrasonic for 20 min. Then 10 µL of the suspension of MIPs was dropped on the clean glassy carbon electrode surface and dry at room temperature. Then 10 µL of 1% (v/v) agarose aqueous solution was overlapped on the above electrode surface till the accomplishment of gelling process of agarose. The prepared MIPs modified electrode was used as the work electrode to detect the concentration of hydroquinone by chronoamperometry.

3. Results and discussion

3.1. Preparation of MIPs microsphere

In the precipitation polymerization, the polymer was synthesized in the present of a larger amount of solution than that used in the traditional polymerization. The growing polymer chains do not overlap or coalesce but continue to grow individually by capturing newly formed oligomers and monomers in this diluted reaction system, and then separate from the solution with microspherical morphologies [24]. Molecular imprinting using a covalent approach was reported to be more efficient than the non-covalent approach. Nevertheless, imprinting using a non-covalent approach presents the advantage that guest binding and release are very fast [25]. Therefore, the present imprinted polymers were synthesized using a non-covalent approach.

MIPs microsphere was prepared using MAA as a functional monomer, TRIM as a cross-linker in a large volume mixed solvent of acetonitrile and toluene in presence of hydroquinone
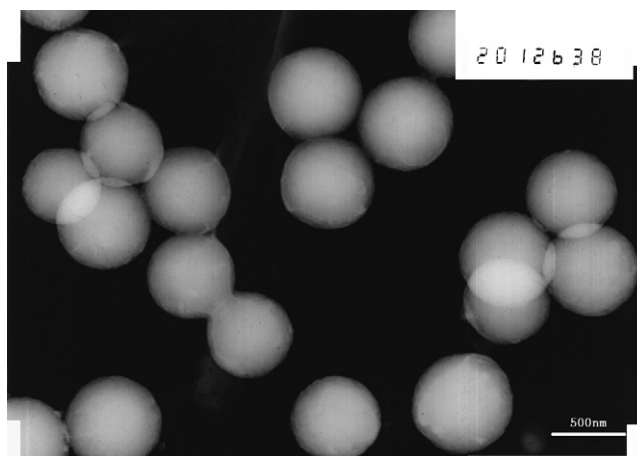
Fig. 1. TEM image of MIPs microsphere.

via thermal polymerization. Generally speaking, the most commonly used functional monomer is MAA, which can form hydrogen bond with template molecule prior to polymerization. The resulting specific and positioned interactions would contribute to the MIP's selectivity. As a cross-linker, TRIM, with three allyl groups, can much more favorably form the porous structure of polymers than ethylene glycol dimethacrylate (EMDA) with two allyl groups. And it has been shown that imprinted polymers prepared using this trifunctional cross-linker had higher load capacity [26]. In addition, both of MAA and TRIM are much more hydrophilic than vinylpyridine or divinylbenzene, which make the poly (MAA-co-TRIM) can be used in aqueous solution for the further detection of hydroquinone [27]. A mixture solvent of acetonitrile and toluene (11:1, v/v) was chosen as reactive medium and porogen to minimize the interference of a polar solvent like acetone with hydrogen bonding, as well as to increase the porosity of the polymers microsphere.

The TEM image as shown in Fig. 1 indicated the resulting polymers was uniform spherical morphology with about 700 nm in diameter.
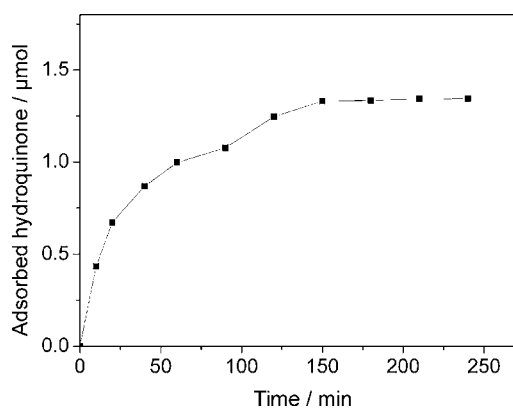
Fig. 2. Adsorption dynamics of MIPs towards hydroquinone in acetonitrile. Initial concentration of hydroquinone: 2.5 mmol/L, amount of MIPs: 20 mg, volume: 2.0 mL.
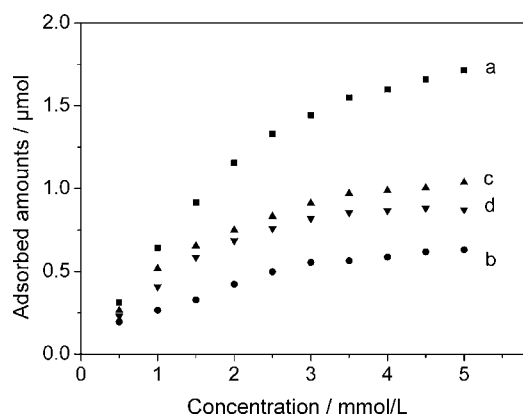
Fig. 3. Adsorption isotherms of (a) hydroquinone to MIPs, (b) hydroquinone to NIPs, (c) resorcinol to MIPs and (d) catechol to MIPs. Amount of polymers: 20 mg, volume: 2.0 mL, binding time: 4 h.

3.2. Adsorption characterizations of MIPs microsphere

3.2.1. Adsorption kinetics of MIPs microsphere

The adsorption kinetics of the MIPs for template molecule was carried out by adding 20 mg MIPs into 2 mL acetonitrile solution with template molecule concentration of 2.5 mmol/L. The curve of the adsorption dynamics was shown in Fig. 2. It can be seen that the adsorption amounts of hydroquinone increased with the increase of adsorption time. In the early 90 min, the adsorption rate increased quickly, while after 150 min, the adsorption almost reached equilibrium, which indicated that the imprinted cavities were saturated with the template molecules. At the early time, hydroquinone molecules were easy to reach the surface imprinting cavities of the MIPs microspheres and the adsorption rate increased very quickly. With the saturation of the surface imprinting cavities, hydroquinone began to diffuse towards the deep cavities, because the diffusion of hydroquinone met great resistance and led to the decrease of the adsorption rate. Compared with other spherical MIPs with the diameter about several microns or bulk MIPs prepared by traditional method, the present MIPs microspheres showed a faster binding kinetics [12,28]. This difference might be attributed to the small and uniform size of MIPs microsphere, which made the

recognition sites of MIPs be easy accessible for the template molecules.

3.2.2. Binding property and selectively of MIPs microsphere

The binding properties of MIPs were measured with initial concentrations of hydroquinone ranging from 0 to 5.0 mmol/L. Curves (a) and (b) in Fig. 3 showed the adsorption isotherms of hydroquinone on MIPs and NIPs, respectively. It is obvious that the binding amount of template molecules to MIPs were much higher than that to NIPs. The high adsorption amount of hydroquinone to MIPs might result from the shape, size, and chemical functionality in imprinted cavities produced by the hydroquinone in the polymerization process.

In addition, curves (c) and (d) in Fig. 3 showed the adsorption isotherms of resorcinol and catechol to MIPs, respectively. The binding ability of MIPs to these compounds is speculated on the same interaction, two hydrogen bonds between the phenolic hydroxyl groups linked with aromatic ring of the phenolic compound and the carboxyl groups of MAA. When comparing curves (c) and (d) with curve (a), we found that the binding amounts of resorcinol and catechol to MIPs are much lower than that of hydroquinone. With the uniform molecular weight, the chemical structures of those three compounds are almost the same except for the different replacement site of phenolic hydroxyl groups. Since the structures of these two analogs are not complementary to the imprinted cavities in the polymers produced by the hydroquinone molecular imprinting, the ability of resorcinol or catechol interaction with the binding sites was weaker than that of hydroquinone. Therefore, the selective recognition for hydroquinone of MIPs may be attributed to shape selective fitting of hydroquinone into complementary cavities created into the MIPs during the imprinting procedure.

3.3. Electrochemical detection of hydroquinone

The electrochemical determination of hydroquinone in PBS was carried out by chronoamperometry. Fig. 4A represented the amperometric response obtained on the MIPs modified elec-
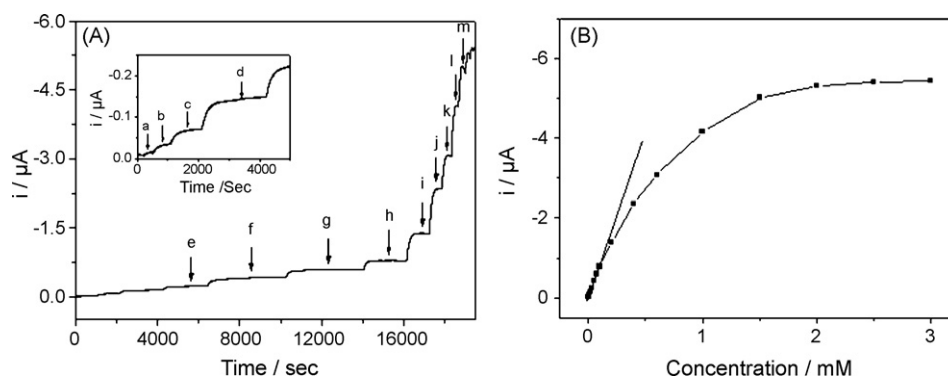
Fig. 4. (A) Typical current response curve at MIPs modified electrode on the addition of increasing concentration of hydroquinone in 0.1 M phosphate buffer pH 7.0. The electrode was polarized at 300 mV. (B) Calibration curve for hydroquinone obtained by i–t curve. Concentration of hydroquinone (a) 2.0×10^{-6} M, (b) 5.0×10^{-6} M, (c) 1.0×10^{-5} M, (d) 2.0×10^{-5} M, (e) 3.0×10^{-5} M, (f) 5.0×10^{-5} M, (g) 7.0×10^{-5} M, (h) 1.0×10^{-4} M, (i) 2.0×10^{-4} M, (j) 4.0×10^{-4} M, (k) 6.0×10^{-4} M, (l) 1.0×10^{-3} M, (m) 1.5×10^{-3} M.

trode. 0.3 V was chosen as the operating potential and aliquots of hydroquinone was injected into a stirred PBS solution. Stable response was obtained upon the repeated injection of hydroquinone into supporting electrolyte solution. Fig. 4B illustrates the corresponding plot showing a linear relationship between current response and hydroquinone concentration in the range of 2.0×10^{-6} to 1.0×10^{-4} mol/L with a correlation coefficient $r = 0.9983$. And the detection limit was found to be 1.0×10^{-6} mol/L. It was also found that the current response of the modified electrode leveled off at high concentration of hydroquinone, indicating the adsorption saturation of template molecule to the MIPs modified electrode.

4. Conclusion

MIPs composed of poly (MAA-*co*-TRIM) has been prepared by a one-step precipitation polymerization using non-covalent bond in the presence of template molecule, hydroquinone. The polymer particles showed excellent uniform microsphere and the precipitation polymerization was proved to be a feasible method for preparation spherical MIPs. Because of their small diameters, the MIPs possessed the fast adsorption kinetics, special adsorption capacity. Compared to the structurally similar compounds, catechol and resorcinol, the MIPs exhibited a high recognizable capacity to hydroquinone. An electrochemical sensor fabricated by modified MIPs on the glassy carbon electrode surface was used to detect the concentration of hydroquinone. A linear range between current response and the concentration of hydroquinone was obtained from 2.0×10^{-6} to 1.0×10^{-4} mol/L with a detection limit of 1.0×10^{-6} mol/L. And the present method may be a useful approach for the combination of MIPs microspheres and modified electrode to form a novel electrochemical sensor for detection of template molecule concentration.

References

[1] K. Haupt, K. Mosbach, Chem. Rev. 100 (2000) 2495–2504.
[2] C. Schirmer, H. Meisel, J. Chromatogr. A 1132 (2006) 325–328.
[3] Y. Xia, J.E. McGuffey, S. Bhattacharyya, B. Sellergren, E. Yilmaz, L.Q. Wang, J.T. Bernert, Anal. Chem. 77 (2005) 7639–7645.
[4] J.Q. Liu, G. Wulff, J. Am. Chem. Soc. 126 (2004) 7452–7453.
[5] S. Reo, T. Toshifumi, K. Izumi, Anal. Chem. 75 (2003) 4882–4886.
[6] S.V. Martha, S. DavidA, J. Am. Chem. Soc. 126 (2004) 7827–7833.
[7] R.Y. Hsieh, H.A. Tsai, M.J. Syu, Biomaterials 27 (2006) 2083–2089.
[8] T. Takeuchi, T. Mukawa, J. Matsui, M. Higashi, K.D. Shimizu, Anal. Chem. 73 (2001) 3869–3874.
[9] L. Ye, K. Mosbach, React. Funct. Polym. 48 (2001) 149–157.
[10] C.D. Ki, J.Y. Chang, Macromolecules 39 (2006) 3415–3419.
[11] Y. Li, X.F. Yin, F.R. Chen, H.H. Yang, Z.X. Zhuang, X.R. Wang, Macromolecules 39 (2006) 4497–4499.
[12] F. Puoci, F. Iemma, R. Muzzalupo, U.G. Spizzirri, S. Trombino, R. Cassano, N. Picci, Macromol. Biosci. 4 (2004) 22–26.
[13] G. Ciardelli, C. Borrelli, D. Silvestri, C. Cristallini, N. Barbani, P. Giusti, Biosens. Bioelectron. 21 (2006) 2329–2338.
[14] S.R. Carter, S. Rimmer, Adv. Funct. Mater. 14 (2004) 553–561.
[15] H. Kempe, M. Kempe, Macromol. Rapid Commun. 25 (2004) 315–320.
[16] G.E.M. Tovar, I. Kraeuter, C. Gruber, Top. Curr. Chem. 227 (2003) 125–144.
[17] L. Ye, P.A.G. Cormack, K. Mosbach, Anal. Commun. 36 (1999) 35–38.
[18] I. Morelli, G. Ciardelli, D. Silvestri, P. Giusti, J. Appl. Biomater. Biomech. 2 (2004) 213.
[19] O. Bruggemann, K. Haupt, L. Ye, E. Yilmaz, K. Mosbach, J. Chromatogr. A 889 (2000) 15–24.
[20] F.G. Tamayo, A. Martin-Esteban, J. Chromatogr. A 1098 (2005) 116–122.
[21] C. Sharma, S. Mahanty, S. Kumar, N.J. Rao, Talanta 44 (1997) 1911–1918.
[22] S.L. Fan, L.K. Zhang, J.M. Lin, Talanta 68 (2006) 646–652.
[23] M.E. Rueda, L.A. Sarabia, A. Herrero, M.C. Ortiz, Anal. Chim. Acta 479 (2003) 173–184.
[24] W.H. Li, H.D.H. Sẗover, J. Polym. Sci. A Polym. Chem. 36 (1998) 1543–1551.
[25] K. Haupt, Analyte 126 (2001) 747–756.
[26] M. Kempe, Anal. Chem. 68 (1996) 1948–1953.
[27] B.N. Kolarz, D. Jermakowicz-Bartkowiak, A. Trochimczuk, Eur. Polym. J. 34 (1997) 1191.
[28] P. Li, F. Rong, C.W. Yuan, Polym. Int. 52 (2003) 1799–1806.

ELSEVIER

Development of a green chromatographic method for determination of fat-soluble vitamins in food and pharmaceutical supplement

Vanessa Kienen, Willian F. Costa, Jesuí V. Visentainer, Nilson E. Souza, Cláudio C. Oliveira *

Departamento de Química, Universidade Estadual de Maringá, Avenida Colombo 5790, DQI, Maringá, PR 87020-990, Brazil

Abstract

A green chromatographic analytical method for determination of fat-soluble vitamins (A, E, D_3 and K_1) in food and pharmaceutical supplement samples is proposed. The method is based on the modification of a C18 column with a 3.00% (w/v) sodium dodecyl sulphate (SDS) aqueous solution at pH 7 ($0.02\,mol\,L^{-1}$ phosphate buffer solution) and in the usage of the same surfactant solution as mobile phase with the presence of 15.0% (v/v) butyl alcohol as an organic solvent modifier. After the separation process, the vitamins are detected at 230 nm (K_1, D_3 and E), 280 nm (A, E, D_3 and K_1) and 300 nm (K_1, D_3 and E). The chromatographic procedure yielded precise results (better than 5%) and is able to run one sample in 25 min, consuming 1.5 g of SDS, 90 mg of phosphate and 7.5 mL of butyl alcohol. When the flow rate of the mobile phase is $2\,mL\,min^{-1}$ the retention times are 4.0, 9.6, 13.0 and 22.7 min for D_3, A, E and K_1 vitamins, respectively; and all peak resolutions are higher than 2. The analytical curves present the following linear equations: area = $6290 + 34852$ (vitamin A), $R^2 = 0.9998$; area = $4092 + 36333$ (vitamin E), $R^2 = 0.9997$; area = $-794 + 30382$ (vitamin D_3) $R^2 = 0.9998$ and area = $-7175 + 82621$ (vitamin K_1), $R^2 = 0.9996$. The limits of detection and quantification for vitamins A, E, D_3 and K_1 were estimated for a test pharmaceutical vitamin supplement sample as 0.81, 1.12, 0.91 and $0.83\,mg\,L^{-1}$ and 2.43, 3.36, 2.73 and 2.49, respectively. When the proposed method was applied to food and pharmaceutical sample analysis, precise results were obtained (R.S.D. < 5% and $n = 3$) and in agreement with those obtained by using the classical chromatographic method that uses methanol and acetonitrile as mobile phase. Here, the traditional usage of toxic organic solvent as mobile phase is avoided, which permits to classify the present method as green.
© 2007 Elsevier B.V. All rights reserved.

Keywords: HPLC; Green chemistry; Fat-soluble vitamin

1. Introduction

Vitamins are organic substances present in several foods in low quantities and are indispensable to organism functions. Its systematic absence in the diet can results in deficient growing and development [1,2]. Independently of the ambient factors, normally the animals cannot synthesis vitamins by anabolic vial, and for this reason, it is necessary to include vitamins in the alimentary diet. In general, the vitamins are necessary in micro-quantities and the doses vary with the age, physiological state and person physic activity. The nutritional necessity for vitamins increase in the growing, pregnancy and lactation periods, in condition of intensive work and during the occurrence of diseases, mainly the infectious one [3]. Traditionally the vitamins

are classified in fat-soluble (A, D, E and K) and hydro soluble (C and B complex—B_1, B_2, B_3, B_5, B_6, B_8, B_9 and B_{12}).

The correlation between diet and health has led the consumers to ingest foods containing vitamins, included the fortifier ones, and more recently, the pharmaceutical supplements; but the addition of these nutrients to industrial products can be utilized as only marketing strategy, and several times, the commercial advantage has priority in damage of individual real necessity [4].

Due to the nutritional importance of the vitamins several analytical methodologies have been developed for determination of these substances in food, pharmaceutical supplements and biological fluids [5–8]. There are a lot of analytical procedures to carry out the determination of vitamins in food, pharmaceutical and physiological samples such as spectrophotometry [5], spectrophotoflurorimetry [6], voltametry [7] and chromatography [8–10]. As normally, it is necessary to determine more than one vitamin, the analytical method should be able to determine multi-

* Corresponding author. Tel.: +55 44 32613684; fax: +55 44 32614125.
E-mail address: ccoliveira@uem.br (C.C. Oliveira).

components in complex samples, which can leads to interference in the chemical analysis; thus, the chromatographic method is one of the most important one to carry out determination of vitamins as its exploitation permits to separate the analytes before the detection, which can avoid interferences.

As the chromatographic method is predominant to determine vitamins in several samples, and normally, this method cannot be considered green, including the ones to determine fat-soluble vitamins, due to the utilization of several organic solvents as mobile phase and, considering that the society claim for the development of analytical methods able to associate selectivity, sensitivity and green characteristics [11], the chemists should develop analytical methods that not use hazardous reagents and that the amount of generated chemical waste should be minimal.

In this way, the aim of the present work is to develop a green chromatographic method to determine fat-soluble vitamins (A, E, D_3 and K_1) in food and pharmaceutical supplement samples by using the HPLC associated to micelar medium [12]. The presence of the surfactant can modify the stationary phase (C18) by adsorption on its surface and, the aqueous mobile phase can present affinity by the low polar vitamins due to the presence of micelles. The strategy is exploited here to decrease the amount of toxic organic solvent, normally utilized in the chromatographic determination of fat-soluble vitamins.

2. Experimental

2.1. Reagent and solutions

The vitamins standard stock solution, $100.0 \, \text{mg L}^{-1}$, were prepared by dissolving 10 mg of each reactive (retinol acetate: vitamin A, tocopherol acetate: vitamin E, cholecalciferol: vitamin D_3 and phylloquinone: vitamin K_1) obtained from Sigma–Aldrich (St. Louis, USA) in 100 mL of methanol using dark brown volumetric flasks. These solutions were stable for at least 1 month when stored in the dark at 4 °C. Working solutions were prepared from the stock solutions by appropriate dilution with ethanol and shielded from light.

The mobile phase was prepared dissolving the adequate quantities of SDS (0.10–3.0% (w/v)) and butyl alcohol (10.0%, 12.0% and 15% (v/v)) (Sigma–Aldrich, St. Louis, USA) and up to 1000 mL with $20 \, \text{mmol L}^{-1}$ of phosphate buffer solution at pH 7 and, the solution was passed, before use, through a 0.45 μm membrane filter.

2.2. Samples

30 g of food samples (fortified milk, powdered milk and soybean oil) were weighted, grinded and transferred to a 250-mL Erlenmeyer flask, and 3 g of ascorbic acid and 65 mL of KOH–ethanol solution (prepared dissolving 50 mL of ethanol in 15 mL of KOH 60% (w/v)) were added. The samples were shaken continuously overnight at room temperature. After, the samples were transferred to a separating funnel where liquid extraction with 25-mL of hexane and shaking the funnel for 5 min was carried. This procedure was repeated two more times. The organic phases were joined and washed two times with

25 mL of water. Then, the organic phase was collected and evaporated to dryness in a vacuum rotary evaporator at 40° C and the residue was re-dissolved in 5 mL of methanol [13]. For pharmaceutical supplement 3.0 g of each sample was weighted and transferred to a 100-mL Erlenmeyer flask, and 0.5 g of ascorbic acid and 15 mL of KOH–ethanol solution were added. After this step, the samples were treated in the same way that the food samples but the hexane extraction was carried out three times with portions of 3 mL of the organic solvent. After the extraction processes, the samples were filtered through a 0.45 μm membrane filter and in the sequence were injected in the chromatographic system for analysis.

2.3. Liquid chromatography and separation conditions

Chromatographic separation was carried out using a Varian ProStar System with Star Chromatography Workstation and LC control software (Varian Analytical Instruments) comprising a ProStar 240 solvent delivery modules, a Model ProStar 410 AutoSampler with a sample loop of 50 μL, a Model ProStar 330 photodiode array detector with the Polyview 2000^{TM} program and a microsorb C18 250 mm × 4.6 mm column with particles of 5 μm equipped with a microsorb C18 10 mm × 4 mm guard column. All the experiments were conducted at 30 °C. Before analysis, the column was conditioned making the mobile phase flows through the system for 20 min at $2.0 \, \text{mL min}^{-1}$. During the chromatographic separation the mobile phase was kept isocratic, at $2.0 \, \text{mL min}^{-1}$ and the acquisition of the data were done at 230 nm (absorption of K_1, D_3 and E vitamins), 280 nm (absorption of A, E, D_3 and K_1 vitamins) and 300 nm (absorption of K_1, D_3 and E vitamins).

2.4. System optimization

For system optimization the main important parameters such as buffer concentration, surfactant concentration, organic modifier concentration, pH and mobile phase flow rate were investigated. It should be stressed that for pH optimization acetate and phosphate buffer solutions were used.

2.5. Method calibration, validation and sample analysis

For quantitative determination external calibration was used plotting peak area (y) versus injected amount of the vitamins (vitamin A: 0.0 1.0, 10.0, 20.0, 32.0, 48.0 and $60.0 \, \text{mg L}^{-1}$; vitamin D_3: 0.0, 1.0, 5.0, 15.0, 25.0, 35.0 and $40.0 \, \text{mg L}^{-1}$; vitamin E: 0.0, 1.0, 12.0, 21.0, 30.0, 48.0 and $60.0 \, \text{mg L}^{-1}$ and vitamin K_1: 0.0, 1.0, 10.0, 20.00, 29.0, 48.0 and $60.0 \, \text{mg L}^{-1}$. The calibration curves were used to determine the analyte concentrations in the samples and in the blank with and without spiking. The LODs and LOQs (n = 6) were estimated by using a signal-to-noise ratio of 3 and 9, respectively, and processing the analysis (including extraction step item 2.2) of a test pharmaceutical formulation sample containing only vegetable oil.

The method validation was carried out spiking blank matrix with vitamins at five different levels of concentration (vitamin A: 0.0, 10.0, 20.0, 30.0 and $40.0 \, \text{mg L}^{-1}$; vitamin D_3: 0.0, 2.0,

4.0, 8.0 and 11.0 mg L^{-1}; vitamin E: 0.0, 10.0, 20.0, 40.0 and 60.0 mg L^{-1} and vitamin K$_1$: 0.0, 2.0, 4.0, 8.0 and 10.0 mg L^{-1}), before carried out the 2.2 extraction procedure and, analyzing the extracts three times during 5 days.

3. Results and discussion

In the present work, initially two conditions were elected before planning all the subsequent experiments. First, as the main goal was to develop green chromatographic method, all reagents selected as mobile phase component should be as non-toxic as possible. Second, it was decided that the stationary phase should be a C18 column due to its popularity in laboratories devoted to chromatographic analysis, which can increase the applicability of the analytical method.

The vitamins A, E, D$_3$ and K$_1$ are high hydrophobic (Fig. 1) and, for this reason, present high affinity by the selected stationary phase (C18 group). Thus, to promote the elution of fat-soluble vitamins from the column, even in conventional methods exploiting reversed phase chromatography, it is necessary the usage of high concentrations of methanol and acetonitrile [14] to increase the affinity of the vitamins by the mobile phase, becoming possible to elute them from the column. In this way, the elimination of organic solvent in chromatographic methods

to determine fat-soluble vitamin using C18 as stationary phase is a very hard task. Here, to circumvent this trouble the exploitation of micelar medium was selected.

With the selected strategy, the mechanism of the separation is changed as the surfactant is absorbed by the stationary phase increasing its polarity and at the same time, the mobile phase characteristics are changed too, as the presence of the surfactant induces the micelles formation. Thus, the affinity of the fat-soluble vitamins by the stationary phase decreases whereas the solubility of the vitamins in the mobile phase increases due to the benefits of micelles formation. The association of both factors becomes possible to get the separation of fat-soluble vitamins using a C18 stationary phase and an aqueous surfactant solution as mobile phase.

As the fat-soluble vitamins do not present charge in a large pH interval, the selection of nonionic surfactant could be adequate for the present application, but experiments showed that Triton X-100 as well as other ionic surfactants as dodecylbenzenesulphonic acid (SBDS) and cetyl trimethyl ammonium bromide (CTAB) scattered and absorbs electromagnetic radiation in the UV region, where the fat-soluble vitamins should be monitored, which impair the usage of these surfactants. The anionic SDS surfactant almost did not present absorption in the UV region and because of this characteristic was selected as mobile and stationary phase modifier.

Initially, experiments were conducted using a simple SDS aqueous solution in concentrations higher than the critical micelar concentration (CMC, 0.24% (w/v)) as mobile phase, but due to the low affinity of the fat-soluble vitamins by water, only part of the analytes was eluted from the column (Fig. 2), indicating that a less polar solvent should be used to modify the mobile phase solution. In this way, the low toxic ethanol alcohol was used.

When ethanol and SDS were present in the mobile phase an improvement in the elution process was observed when compared to the SDS aqueous solution, but even for ethanol concentrations as high as 30% (v/v) not all analytes were eluted from
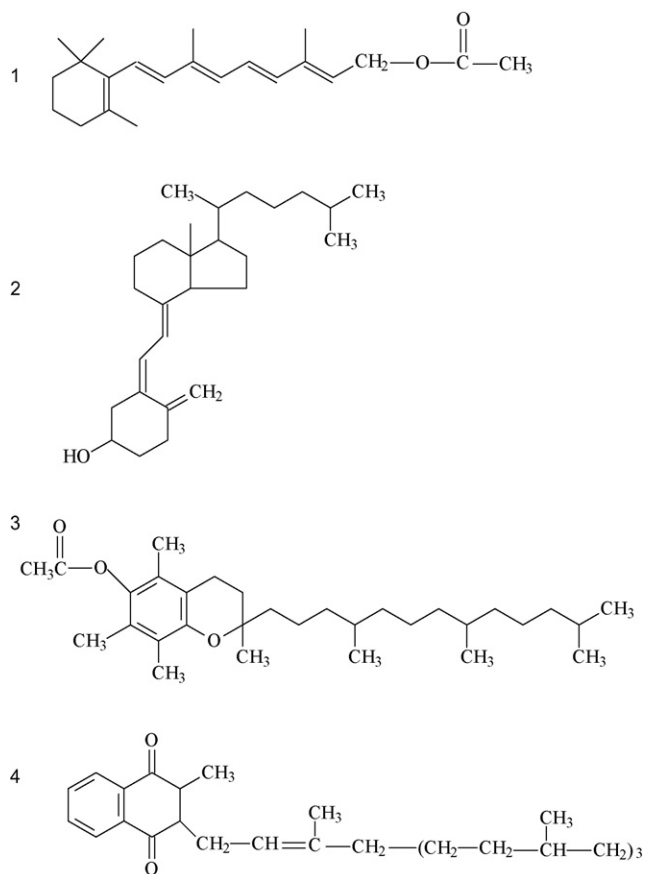
Fig. 1. Structure of the fat-soluble vitamins: (1) retinol acetate (vitamin A), (2) tocopherol acetate (vitamin E), (3) cholecalciferol (vitamin D$_3$) and (4) phylloquinone (vitamin K$_1$).
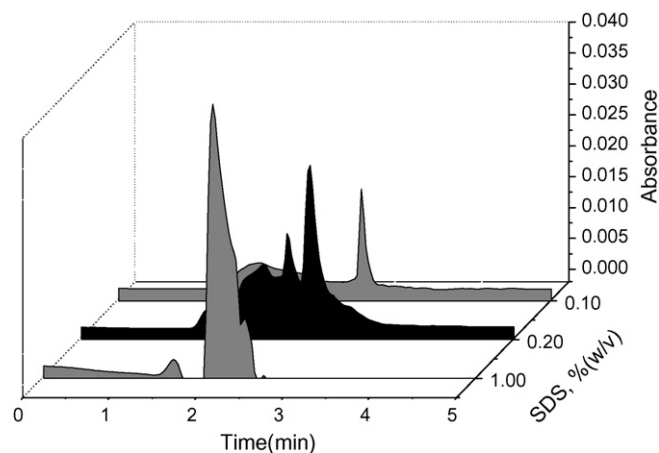
Fig. 2. Effect of the SDS in the separation of fat-soluble vitamins. Data obtained to concentrations of vitamins A, D$_3$, E and K$_1$ of 40.0, 11.0, 60.0 and 10.0 mg L^{-1}, respectively; sample volume of 20 μL, flow rate of 1.0 mL min^{-1} and aqueous mobile phase containing 0.1, 0.2 and 1.0 (w/v) of SDS.
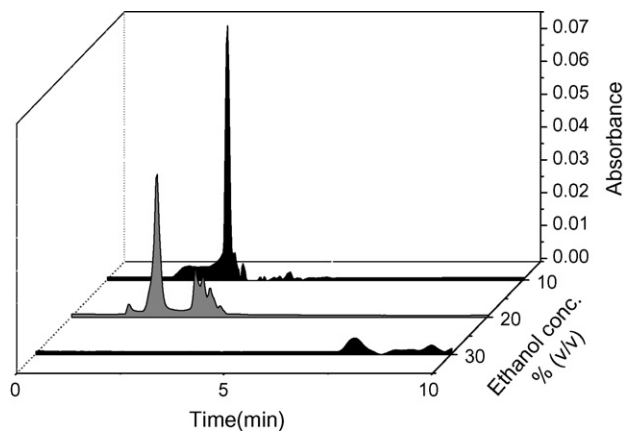
Fig. 3. Effect of the ethanol in the chromatographic separation of fat-soluble vitamins. Data obtained to concentrations of vitamins A, D_3, E and K_1 of 40.0, 11.0, 60.0 and 10.0 mg L^{-1}, respectively; sample volume of 20 μL, flow rate of 1.0 mL min^{-1}, with aqueous mobile phase containing 1.0% (w/v) of SDS and 5%, 10%, 15%, 20%, 25% and 30% (v/v) of ethanol.

the column (Fig. 3). It should be emphasised that the ethanol concentrations could not be increased due to its high viscosity that led to the high backpressure in the chromatographic system. Thus, the ethanol was substituted by the less polar *n*-butyl alcohol.

The presence of *n*-butyl alcohol was very benefic to the separation of the fat-soluble vitamins (Fig. 4) and, to mobile phase flow rate of 1.3 mL L^{-1} it was possible to elute all the analytes in 70 min. When the mobile flow rate was lower than 1.3 mL min^{-1} the vitamins retention times were very high, decreasing the analytical frequency. As by using the conventional chromatographic method it is possible to analyse vitamins A, E, D_3 and K_1 in only 25 min the green chromatographic method was optimized to improve the analytical frequency.

Butyl alcohol presents high viscosity, and for this reason, the temperature was fixed as high as possible (30 °C) to decrease the
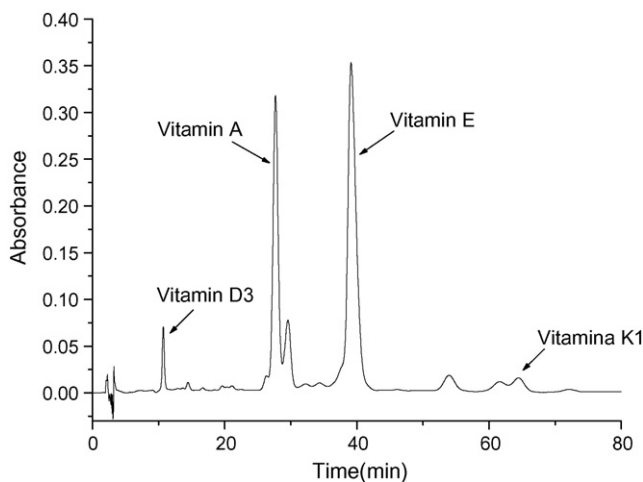
Fig. 4. Effect of the butyl alcohol in the chromatographic separation of fat-soluble vitamins. Data obtained to concentrations of vitamins A, D_3, E and K_1 of 40.0, 11.0, 60.0 and 10.0 mg L^{-1}, respectively; sample volume of 50 μL, flow rate of mobile phase of 1.3 mL min^{-1} containing 2.2% (w/v) of SDS, 0.02 mol L^{-1} of phosphate buffer at pH 7.0 and 12.0% (v/v) of butyl alcohol at the temperature of 30 °C.

Table 1
Conditions of the factorial experiment 2^3 to optimize the determination of the fat-soluble vitamins A, E, D_3 and K_1[a]

| Experiment	Butyl alcohol	SDS	Flow rate
1	−	−	−
2	+	−	−
3	−	+	−
4	+	+	−
5	−	−	+
6	+	−	+
7	−	+	+
8	+	+	+

[a] Data were obtained to 0.02 mol L^{-1} Na$_2$HPO$_4$ at pH 7. Levels: butyl alcohol (− corresponds to 10.0% (v/v) and + to 15.0% (v/v) of butyl alcohol); SDS (− corresponds to 1.50% (w/v) and + to 15.0% (w/v) of SDS) and mobile phase flow rate (− corresponds to 1.5 mL min^{-1} and + to 2.0 mL min^{-1}).

backpressure in the chromatographic system, increasing analytes diffusion between the mobile and stationary phases [12] and permitting to increase the mobile phase flow rate. It should be stressed that the temperature could not be increased as the fat-soluble vitamins are not thermally stables and because the solubility of the stationary phase support increases with the temperature.

The pH did not present influence in the separation process, mainly because the vitamins are not charged, thus the pH was fixed at 7.0 by using a 0.02 mol L^{-1} of phosphate buffer. The choice of the pH and the nature of the buffer solutions are justified in view of the possibility to obtain a neutral waste with nontoxic species. Thus the pH, temperature and sample volume (50 μL) were kept constant and, a factorial experiment 2^3 (Table 1) was carried out to optimize the mobile phase flow rate and SDS and butyl alcohol concentration in the mobile phase. It is necessary to keep in mind the relationship between butyl alcohol and SDS concentrations as the butyl alcohol presents low solubility in aqueous medium.

It was verified that the minimal butyl alcohol concentration in the mobile phase to get chromatographic resolution adequate to quantitative analysis was 15.0% (w/v). For lower butyl alcohol concentration it was observed peaks broadening which decrease the sensitivity and the chromatographic resolution as well as increase the time of analysis (Fig. 5). For higher butyl alcohol concentration it was necessary to increase the SDS concentration to get a homogenized solution due to the low solubility of the alcohol in water. In this way, the butyl alcohol concentration was selected as 15.0% (v/v) as the better compromise among sensitivity, analytical frequency and consumption of reagents.

The presence of SDS in the mobile phase was fundamental as without the surfactant the dissolution of butyl alcohol is not possible in the aqueous medium; to dissolve 15.0% (v/v) of butyl alcohol it is necessary to have at least 1.5% (w/v) of SDS. Furthermore, the surfactant changes the characteristics of the stationary phase due to its adsorption on C18 surface, increasing the polarity of the column and decreasing the affinity of the fat-soluble vitamins by this phase. At the same time, the surfactant changes the mobile phase characteristics too, forming micelles that permit to increases the solubility of the fat-soluble vitamins in the mobile phase, becoming possible the elution of

among time of analysis, chromatographic resolution and reagent consumption.

The chromatographic resolution and time of analysis were influenced by the mobile phase flow rate (Fig. 5). When the flow rate was fixed as $1.0 \, mL \, min^{-1}$ associated to low butyl alcohol and SDS concentrations it was verified that the time of analysis was superior to 90.0 min, increasing the peaks broadening and degrading the sensitivity. For mobile phase flow rate of $2.0 \, mL \, min^{-1}$ the time of analysis decreased considerably (Fig. 5) and, the chromatographic resolutions were better; for this reason, this flow rate value was considered adequate.

It should be noted that experiment 8 (Table 1) led to the better relation cust/benefits. When this condition was established it was possible to quantify the fat-soluble vitamins in 25.0 min (Fig. 5) with retention times of 4.0, 9.6, 13.0 and 22.7 min to D_3, A, E and K_1 vitamins, respectively.

Quantitative data were obtained injecting a sample volume of $50 \, \mu L$ and monitoring the vitamins at 230 nm (K_1, D_3 and E), 280 nm (A, E, D_3 and K_1) and 300 nm (K_1, D_3 and E). It should be emphasised that it is possible to do the measurements of the four vitamins at the same wavelength, 280 nm, with a lost in sensitivity to same vitamins, but this procedure is recommended to laboratories that did not have chromatographic system with photodiode array detector. The elution process is done in an isocratic mode, thus a simple HPLC can be used to carry out the chemical analysis.

The chromatographic procedure is able to run one sample in 25 min with all peak resolutions higher than two, consuming 1.5 g of SDS, 90 mg of phosphate and 7.5 mL of butyl alcohol.
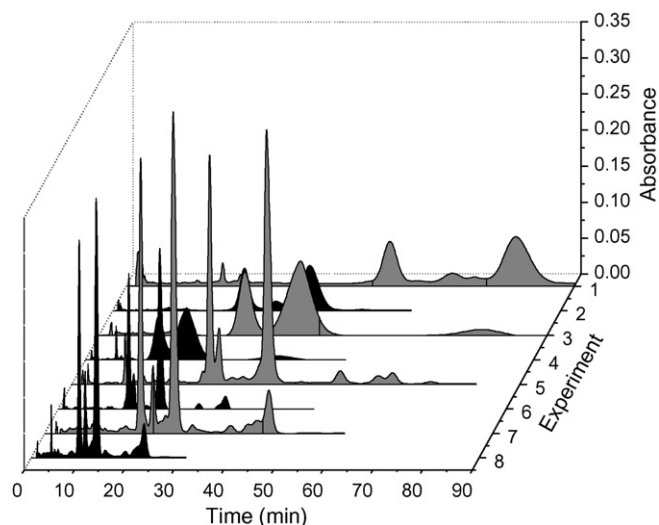

Fig. 5. Effect of the mobile flow rate, butyl alcohol and SDS concentrations in the chromatographic separation of fat-soluble vitamins. Data obtained to concentrations of vitamins A, D_3, E and K_1 of 40.0, 11.0, 60.0 and $10.0 \, mg \, L^{-1}$, respectively; sample volume of $50 \, \mu L$ and temperature of $30 \, °C$. For mobile phase composition see Table 1.

the low polar analytes without the usage of solvents as methanol and acetonitrile [9,10]. It was observed an improvement in the chromatographic resolution and in the time of analysis with the increase of SDS concentration (Fig. 5) even in situations of butyl alcohol concentration lower than 15.0% (v/v). Thus, the SDS concentration was fixed as 3.0% (w/v) as the better compromise

Table 2
Recovery test

Vitamin addition (mg L^{-1})	Day 1	Day 2	Day 3	Day 4	Day 5
Vitamin A					
0.0	0.0	0.0	0.0	0.0	0.0
10.0	9.8 ± 0.3	9.9 ± 0.3	9.6 ± 0.5	9.4 ± 0.4	9.2 ± 0.4
20.0	20.3 ± 0.4	19.7 ± 0.5	19.3 ± 0.6	19.1 ± 0.5	18.8 ± 0.7
30.0	31.5 ± 1.3	29.2 ± 0.9	29.3 ± 1.4	26.4 ± 1.6	25.7 ± 0.9
40.0	39.1 ± 1.5	38.3 ± 1.6	36.2 ± 1.3	36.0 ± 1.5	35.4 ± 1.3
Vitamin D$_3$					
0.0	0.4 ± 0.1	0.0	0.0	0.0	0.0
2.0	2.3 ± 0.1	1.9 ± 0.1	2.1 ± 0.1	1.8 ± 0.1	1.6 ± 0.1
4.0	3.8 ± 0.2	3.7 ± 0.1	3.5 ± 0.1	3.6 ± 0.1	3.6 ± 0.1
8.0	7.9 ± 0.2	8.5 ± 0.3	7.6 ± 0.3	7.4 ± 0.3	7.3 ± 0.2
11.0	9.0 ± 0.3	8.7 ± 0.2	8.7 ± 0.3	8.6 ± 0.3	8.1 ± 0.3
Vitamin E					
0.0	0.0	0.0	0.0	0.0	0.0
10.0	10.2 ± 0.4	10.0 ± 0.3	9.5 ± 0.3	9.3 ± 0.2	9.4 ± 0.4
20.0	19.6 ± 0.2	19.8 ± 0.3	18.4 ± 0.1	18.6 ± 0.3	18.7 ± 0.2
40.0	39.4 ± 0.4	39.5 ± 0.5	39.6 ± 1.0	38.8 ± 0.7	38.9 ± 0.6
60.0	62.5 ± 1.3	63.0 ± 1.2	61.7 ± 1.8	58.5 ± 1.1	54.9 ± 2.1
Vitamin K$_1$					
0.0	0.0	0.0	0.3 ± 0.1	0.0	0.0
2.0	1.8 ± 0.1	2.3 ± 0.1	2.0 ± 0.1	2.1 ± 0.1	1.7 ± 0.1
4.0	4.2 ± 0.2	3.9 ± 0.1	4.1 ± 0.1	3.9 ± 0.1	3.8 ± 0.1
8.0	8.6 ± 0.4	8.1 ± 0.3	8.4 ± 0.5	8.2 ± 0.3	8.3 ± 0.2
10.0	9.9 ± 0.4	10.3 ± 0.5	10.2 ± 0.3	9.7 ± 0.4	9.2 ± 0.4

Determination of fat-soluble vitamins in a placebo sample without and with addition of five different levels of each vitamin. Data were obtained by the proposed green chromatographic method. The results are expressed in mg L^{-1} $\pm$S.D.

Table 3
Determination of fat-soluble vitamins in food and pharmaceutical supplement samples by the proposed green chromatographic method and by the conventional one

Samples	Proposed method				Conventional method			
	A	D_3	E	K_1	A	D_3	E	K_1
Fortified milk	0.19 ± 0.01	–	0.86 ± 0.04	–	0.18 ± 0.01	–	0.78 ± 0.03	–
Powdered milk	–	–	–	–	–	–	–	–
Soybean oil	–	–	0.84 ± 0.04	–	–	–	0.88 ± 0.05	–
Pharmaceutical supplement[a]	3.4 ± 0.2	5.2 ± 0.3	3.0 ± 0.2	8.5 ± 0.4	3.5 ± 0.2	5.5 ± 0.2	2.9 ± 0.1	8.3 ± 0.4

The results are expressed in mg g^{-1} ±R.S.D.

[a] Liquid sample and the results are expressed in mg L^{-1}.
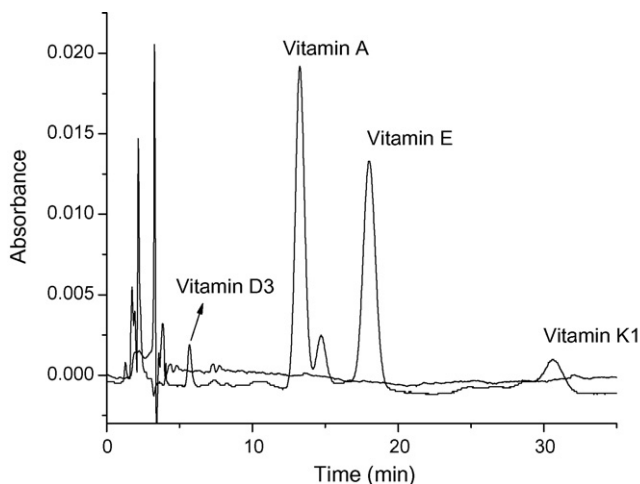

Fig. 6. Chromatogram of placebo sample without and with the addition of vitamins A, D_3, E and K_1 at concentrations of 25.0, 5.0, 15.0 and 5 mg L^{-1}, respectively. Data obtained for sample volume of 50 μL, temperature of 30 °C and mobile flow rate 2.0 mL min^{-1} containing SDS 3.0% (w/v), butyl alcohol 15.0% (v/v) and 0.02 mol L^{-1} Na$_2$HPO$_4$ at pH 7.

The analytical curves present the following linear equations: area = 6290 + 34852 (vitamin A), R^2 = 0.9998; area = 4092 + 36333 (vitamin E), R^2 = 0.9997; area = −794 + 30382 (vitamin D_3), R^2 = 0.9998 and area = −7175 + 82621 (vitamin K_1), R^2 = 0.9996 and, the limits of detection and quantification for vitamins A, E, D_3 and K_1 were estimated in a test pharmaceutical vitamin supplement sample as 0.81, 1.12, 0.91 and 0.83 mg L^{-1} and 2.43, 3.36, 2.73 and 2.49, respectively.

The proposed method was applied to a placebo sample with and without addition of vitamins and it was possible to observe that any interference in the vitamins peak occurs in the presence of the sample matrix (Fig. 6).

The accuracy of the method was always better than 5% and 8% for intra-day and inter-day, respectively (Table 2), but some vitamin degradation occurs as the inter-day results decrease systematically with the time.

When different samples were analysed by the proposed method the results (Table 3) were in agreement with those obtained by using the classical chromatographic one [15], but the proposed method is more friendly because of the lower toxicity of the mobile phase, avoiding the traditional usage of acetonitrile and methanol to determine fat-soluble vitamin, which permits to classify the present method as green.

4. Conclusion

It is possible to do the chromatographic determination of fat-soluble vitamins (A, E, D_3 and K_1) in food and pharmaceutical supplement samples using a C18 column as stationary phase and an aqueous SDS/butyl alcohol solution as mobile phase. The procedure is simple, robust, precise and present analytical frequency comparable to the conventional method.

References

[1] F.R. Rejon, G. Matin-Pena, F. Granado, J. Ruiz-Galiana, I. Blanco, B. Olmedilla, Nutrition 18 (2002) 26.
[2] W.H.J. Sebrel, R.S. Harris, The Vitamins: Chemistry, Physiology, Pathology, Methods, 2nd ed., Publishing Academic Press, 1971.
[3] R. Andreoli, P. Manini, D. Poli, E. Bergamaschi, A. Mutti, W.A. Niessen, Anal. Bioanal. Chem. 378 (2004) 987.
[4] J.A. Paixão, T.L.M. Stamford, Quím. Nova 27 (2004) 100.
[5] H. Abdollahi, L. Bagheri, Anal. Chim. Acta 514 (2004) 211.
[6] A. Alonso, M.J. Almendral, M.J. Porras, Y. Curto, J. Pharm. Biomed. Anal. 42 (2006) 171.
[7] S.G. Li, W.T. Xue, H. Zhang, Electroanalysis 18 (2006) 2337.
[8] P.F. Chatzimichalakis, V.F. Samanidou, I.N. Papadoyannis, J. Chromatogr. B 805 (2004) 289.
[9] A. Jedlicka, J. Klimes, Chem. Pap. 59 (2005) 202.
[10] H. Iwase, Anal. Chem. Acta 463 (2002) 21.
[11] E.C. Vidotti, W.F. Costa, C.C. Oliveira, Talanta 68 (2006) 516.
[12] Z. Moneni, J.H. Khorasani, J. Pharm. Biomed. Anal. 37 (2005) 383.
[13] S. Perales, M.M. Delgado, A. Alegria, R. Barbera, R. Farre, Anal. Chim. Acta 543 (2005) 58.
[14] A.G. Swiglo, E. Sikorska, J. Chromatogr. A 1048 (2004) 195.
[15] P. Moreno, V. Salvadò, J. Chromatogr. A 870 (2000) 209.

Preparation of PVA membrane for immobilization of GOD for glucose biosensor

Jitendra Kumar, S.F. D'Souza *

Nuclear Agriculture and Biotechnology Division, Bhabha Atomic Research Centre, Mumbai 400085, India

Abstract

A membrane was prepared using polyvinyl alcohol (PVA) with low and high degree of polymerization (DOP), acetone, benzoic acid (BA) and was cross-linked by UV treatment. Membrane composition was optimized on the basis of swelling index. Membrane prepared with 12% low DOP and 8% high DOP of PVA, 2% BA, dissolved in buffer containing 20% acetone and cross-linked with UV treatment exhibited lower swelling index. Fourier transform infrared (FTIR) study of the membranes showed appearance of a strong band at $\sim$2337 cm^{-1} when UV was used for cross-linking in the presence of benzoic acid. Scanning electron microscope (SEM) study revealed that membrane cross-linked with UV treatment was smoother. Glucose oxidase (GOD)–PVA membrane was associated with the dissolved oxygen (DO) probe for biosensor reading. Glucose was detected on the basis of depletion of oxygen, when immobilized GOD oxidizes glucose to gluconolactone. A wide detection range, 0.9–225 mg/dl was estimated from the linear range of calibration plot of biosensor reading. Membranes were reused for 32 reactions without significant loss of activity and stored for 30 days ($\sim$90% activity) at 4 °C. Membranes were also used with real blood samples.
© 2007 Elsevier B.V. All rights reserved.

Keywords: PVA membrane; Swelling index; FTIR study; Glucose oxidase; Dissolved oxygen; Glucose biosensor

1. Introduction

The basic requirement of a biosensor is that the biological material should bring the physico-chemical changes in close proximity of a transducer. In this direction, immobilization technology has played a major role [1–3]. Immobilization not only helps in forming the required close proximity between the biomaterial and the transducer, but also helps in stabilizing it for reuse. The biological material has been immobilized directly on the transducer or in most cases, in membranes, which can subsequently be mounted on the transducer. Biomaterials can be immobilized either through adsorption, entrapment, covalent binding, cross-linking or a combination of all these techniques [3–5]. A number of techniques have been developed in our laboratory for the immobilization of enzymes as well as cells for this purpose [3,6,7]. Generally, entrapment is considered as a suitable method for enzyme immobilization because of mild coupling procedure.

Synthetic polymer that has been extensively used for immobilization of biocatalysts in a membranous form is polyvinyl alcohol (PVA). It is a non-toxic and biocompatible synthetic polymer with good chemical and thermal stability [8]. Large numbers of hydroxyl groups in the PVA provide a biocompatible microenvironment for the enzyme [9]. However major limitation of PVA membrane is its high swelling index and dissolves readily in water when not cross-linked [10]. Swelling of the PVA membrane was reduced by cross-linking with a variety of chemical and physical methods [11,12]. In our laboratory, urease enzyme was entrapped in the composite polymer membrane of polyvinyl alcohol–polyacrylamide and cross-linked by γ-irradiation and was reused for a number of times without any significant loss of urease activity [13].

We report the preparation of a membrane containing glucose oxidase (GOD), using PVA with low and high degree of polymerization (DOP), acetone as a mixture of solvent, benzoic acid (BA) as sensitizer and cross-linked using UV treatment.

Glucose oxidase was selected for immobilization since it is a well studied and applicable in the field of biosensor [14,15]. Most of glucose biosensors are based on oxidation of glucose

---

* Corresponding author. Tel.: +91 22 25593632; fax: +91 22 25505342.
E-mail address: sfdsouza@barc.gov.in (S.F. D'Souza).

catalysed by glucose oxidase:

$$\text{D-Glucose} + O_2 \xrightarrow{\text{GOD}} H_2O_2 + \text{D-Gluconolactone}$$
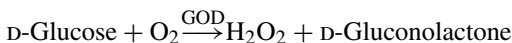
The amperometric response of consumed O_2 was monitored for glucose oxidation using oxygen-sensitive electrode [16].

Composition for preparation of membrane was optimized on the basis of the swelling index. Fourier transform infrared (FTIR) and scanning electron microscope (SEM) studies of the membranes were carried. Operational reusability as well as stability of the GOD–PVA membrane was studied. The applicability of the membrane was confirmed with real blood samples.

2. Materials and methods

2.1. Materials

Polyvinyl alcohol (degree of hydrolysis 98–99%) with DOP ∼360 and 1700–1800 were purchased from Fluka Chemie, GmbH. Benzoic acid from Merck, Mumbai, India. Glucose oxidase (E.C.1.1.3.4), type II from *Aspergillus niger* lyophilized powder (100 units/mg protein) from Sisco Research Laboratory, Mumbai. Glucose, acetone and other chemicals were obtained from standard sources. Clark dissolved oxygen (DO) electrode (probe) was purchased from M/S Century Instruments, Chandigarh, India. Blood samples and their glucose values were provided by the pathology department of BARC Hospital, Anushaktinagar, Mumbai.

2.2. Optimization of PVA membrane composition

Different compositions of PVA with low (∼360) and high (1700–1800) DOP and benzoic acid were dissolved in milliQ water containing different percentages of acetone (Table 1). The mixtures were dissolved homogenously at 70–80 °C on heat-

Table 1
Compositions of the membrane and their swelling index

Membrane compositions	Swelling index (%)
12% LDOP PVA + 8% HDOP PVA (no UV treatment)	103 ± 10.8
12% LDOP PVA + 8% HDOP PVA + UV treatment	96.7 ± 10.4
12% LDOP PVA + 8% HDOP PVA + 20% acetone as solvent (no UV treatment)	89.65 ± 9.5
12% LDOP PVA + 8% HDOP PVA + 20% acetone as solvent + UV treatment	87.8 ± 9.2
12% LDOP PVA + 8% HDOP PVA + 2% BA (no UV treatment)	70.17 ± 7.1
12% LDOP PVA + 8% HDOP PVA + 2% BA + UV treatment	33.6 ± 3.5
12% LDOP PVA + 8% HDOP PVA + 2% BA + 20% acetone as solvent + UV treatment	26.3 ± 3.1

LDOP PVA: Polyvinyl alcohol of low degree of polymerization (∼360). HDOP PVA: Polyvinyl alcohol of high degree of polymerization (∼1700–1800). BA: Benzoic acid. UV treatment: Ultra violet light (irradiation) treatment for 1 h.

ing magnetic stirrer with vigorous stirring. PVA mixture was allowed to cool to room temperature and overlaid as a thin membranous layer on the lid of a Petri plate in order to obtain required thin and uniform membranes. Membranes were air-dried for 2 h. Dried membranes were peeled off carefully and were cross-linked by exposure to UV light for 1 h.

2.3. Swelling index of the PVA membrane

Circular pieces of the membranes were cut and weighed. The pieces were then immersed in milliQ water for 24 h at room temperature to attain the equilibrium sorption. Surface adhered water drops were wiped using soft filter papers after attainment of equilibrium and weighed immediately. Weights were noted down, after and before water treatment. Swelling index (S) was calculated according to equation [10,17]:

$$S(\%) = \frac{W_s - W_d}{W_d} \times 100$$

where W_s and W_d are the weight of wet membrane at equilibrium of sorption and the weight of dry membrane respectively. Inferences were made for the quality of the membranes on the basis of swelling index.

2.4. FTIR study of the membrane

Membranes were studied by FTIR spectra and scanned in the range of 4000–400 cm^{-1} on Jasco (Model FTIR-660 plus) FTIR Spectrometer. The membranes were pressed directly onto the attenuated reflectance crystal KBr (KBr was supplied with FTIR instrument) with the sampling unit.

2.5. SEM study of the membrane

A scanning electron microscope (Model 435 VP, Leo Electron Microscopy Ltd., Cambridge, UK) was employed to observe the surface of the PVA membranes. For SEM, pieces of the membranes were mounted on stubs and were then coated with gold using a sputter coater. The SEM micrographs of the PVA membranes (before and after the UV treatment) were taken at magnifications 100, 500 and 2000×.

2.6. GOD immobilization in PVA membrane

A 10 ml homogenous mixture of 12% LDOP PVA, 8% HDOP PVA and 2% BA was prepared in 50 mM sodium phosphate buffer (pH 6.0) containing 20% acetone and 2 ml GOD (2000 units/ml) was added to the mixture and mixed homogenously. The mixture was overlaid as a thin membranous layer, air-dried, peeled off carefully and placed under UV light for cross-linking. Cross-linked GOD–PVA membranes were stored at 4 °C.

2.7. Operating condition and calibration of the DO probe

Commercial Clark-type dissolved oxygen electrode in conjunction with GOD entrapped PVA membrane was used for
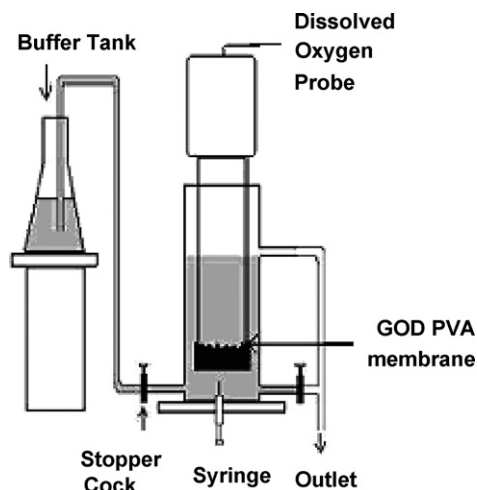
Fig. 1. Schematic diagram of association of GOD–PVA membrane with the DO probe biosensor.
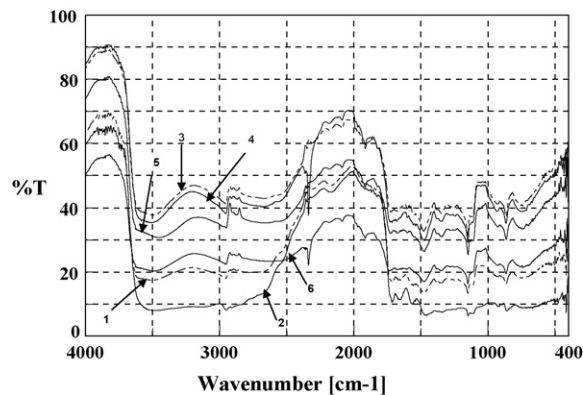

Fig. 2. FTIR spectrum studies of the membranes prepared using mixtures of the compositions given below: (1) 12% LDOP PVA + 8% HDOP PVA (no UV treatment). (2) 12% LDOP PVA + 8% HDOP PVA + UV treatment. (3) 12% LDOP PVA + 8% HDOP PVA + 2% BA (no UV treatment). (4) 12% LDOP PVA + 8% HDOP PVA + 2% BA + UV treatment. (5) 12% LDOP PVA + 8% HDOP PVA + 2% BA + 20% acetone as solvent (no UV treatment). (6) 12% LDOP PVA + 8% HDOP PVA + 2% BA + 20% acetone as solvent + UV treatment.

biosensor reading as shown in Fig. 1. The electrode was filled with 1 M potassium chloride solution. Blank readings of the probe with air and 50 mM sodium phosphate buffer (pH 6.0) were taken without the membrane being attached to the electrode. Membrane was tightly attached to the electrode using O-ring with the support of cheesecloth. The DO probe was allowed to obtain a base line corresponding to the buffer volume 20 ml in the reaction vessel. 500 μl of standard glucose solutions (concentration 0.9, 4.5, 22.5, 90, 225 and 450 mg/dl) were introduced into the reaction vessel and oxidation reaction occurred at electrode surface was observed. Oxygen was consumed from sample during oxidation of glucose and depletion of oxygen was measured using DO probe. All experiments were performed at room temperature.

3. Results and discussions

3.1. Optimization of composition for preparation of PVA membrane

Membranes were prepared using low and/or high degrees of polymerized PVA, acetone, and benzoic acid and were cross-linked by UV treatment. Membrane composition was optimized on the basis of swelling index. Swelling index was reduced after cross-linking membrane with UV treatment in presence of benzoic acid as sensitizer (Table 1) and the result is better than the earlier report [9]. This shows that the stability of the membrane was improved because of cross-linking.

Swelling properties was further reduced when the membrane was prepared using both low and high degree of polymerized PVA. From the study, it was observed that membrane prepared with solution comprising 12% LDOP PVA and 8% HDOP PVA was having lower swelling index (32.5 ± 4.1%) than the either only 20% low (53.4 ± 5.6%) or only 20% high (55.3 ± 5.5) DOP of PVA. Membrane properties, flexibility and tensile strength were improved when mixture of both, low and high DOP of PVA was used for preparation of membrane. Flexibility of the membrane increased with decrease of degree of polymerization

of the PVA and tensile strength of the membrane increased with increase of DOP of the PVA [18].

Swelling index was further reduced by using solvent with 20% acetone for preparation of membrane as shown in Table 1.

Above study indicated that the membrane comprised of 12% LDOP and 8% HDOP of PVA along with sensitizer (2% BA), dissolved in buffer containing 20% acetone and cross-linked with the UV treatment was having lowest swelling property (Table 1). This composition was used further for preparation of membrane and immobilization of enzyme for biosensor development.

3.2. FTIR study of the membranes

FTIR spectra of PVA membranes with different composition are shown in Fig. 2 and their peaks were assigned in Table 2 [19–21]. It was observed that a strong band appeared at ∼2337 cm^{-1} after UV cross-linking in the presence of benzoic acid and same band was absent when either benzoic acid or UV treatment was absent. The band appeared at ∼2337 cm^{-1} was corresponding to the free CO_2 gases entrapped inside the alkoxide polymer [20]. It was earlier reported that the UV treatment could be used for cross-linking in presence of benzoate [9], where benzoate acted as a sensitizer. The cross-linking was always accompanied by photolysis of the sensitizer and in the absence of sensitizer, no cross-linking occurred. Probable mechanism was reported in literature [22], a free radical arising from the photolysis of benzoate would abstract a tertiary hydrogen atom from the polymer chain to yield a polymeric radical, which can cross-link by combination with another such radical.

3.3. SEM study of the membranes

SEM study of the surface of PVA membranes before and after UV treatment was carried out. It was observed that surface of the membranes after UV treatment was having less ridges

Table 2
FTIR peaks assignment for PVA membranes

Wave number (cm^{-1})						Peak assignments
1	2	3	4	5	6	
~2954	~2951	~2954	~2954	~2951	~2953	Asymmetrical stretching vibration of methylene ($\nu_{as}CH_2$ and CH aliphatic)
				~2876		C–H stretching of the symmetric methyl band, $\nu s(CH_3)$
		~2337			~2337	C=O stretching of CO_2. Free CO_2 gas was permanently entrapped within polymer during cross-linking
		~1914	~1914	~1914	~1914	Vibration stretching of C=O bands due to excited state
~1715	~1715	~1723	~1716	~1729	~1729	Vibration stretching of C=O
~1472	~1456	~1479	~1473	~1473	~1472	Methylene deformation $\delta(CH_2)$
~1341	~1345	~1345	~1348	~1346	~1348	Stretching C=O and methylene deformation
~1149	~1148	~1150	~1149	~1148	~1149	Before CO_2 adsorption, a band assigned to the C–H bending mode. C–O–C asymmetric and symmetric stretching and C=O stretching vibration and C–H bending and rocking mode
~865	~860	~864	~865	~864	~864	Deformation of a anomeric C–H vibration
~748	~669	~739	~741	~740	~738	Skeletal mode of vibration of anomeric carbons

(1) 12% LDOP PVA + 8% HDOP PVA (no UV treatment). (2) 12% LDOP PVA + 8% HDOP PVA + UV treatment. (3) 12% LDOP PVA + 8% HDOP PVA + 2% BA (no UV treatment). (4) 12% LDOP PVA + 8% HDOP PVA + 2% BA + UV treatment. (5) 12% LDOP PVA + 8% HDOP PVA + 2% BA + 20% acetone as solvent (no UV treatment). (6) 12% LDOP PVA + 8% HDOP PVA + 2% BA + 20% acetone as solvent + UV treatment.
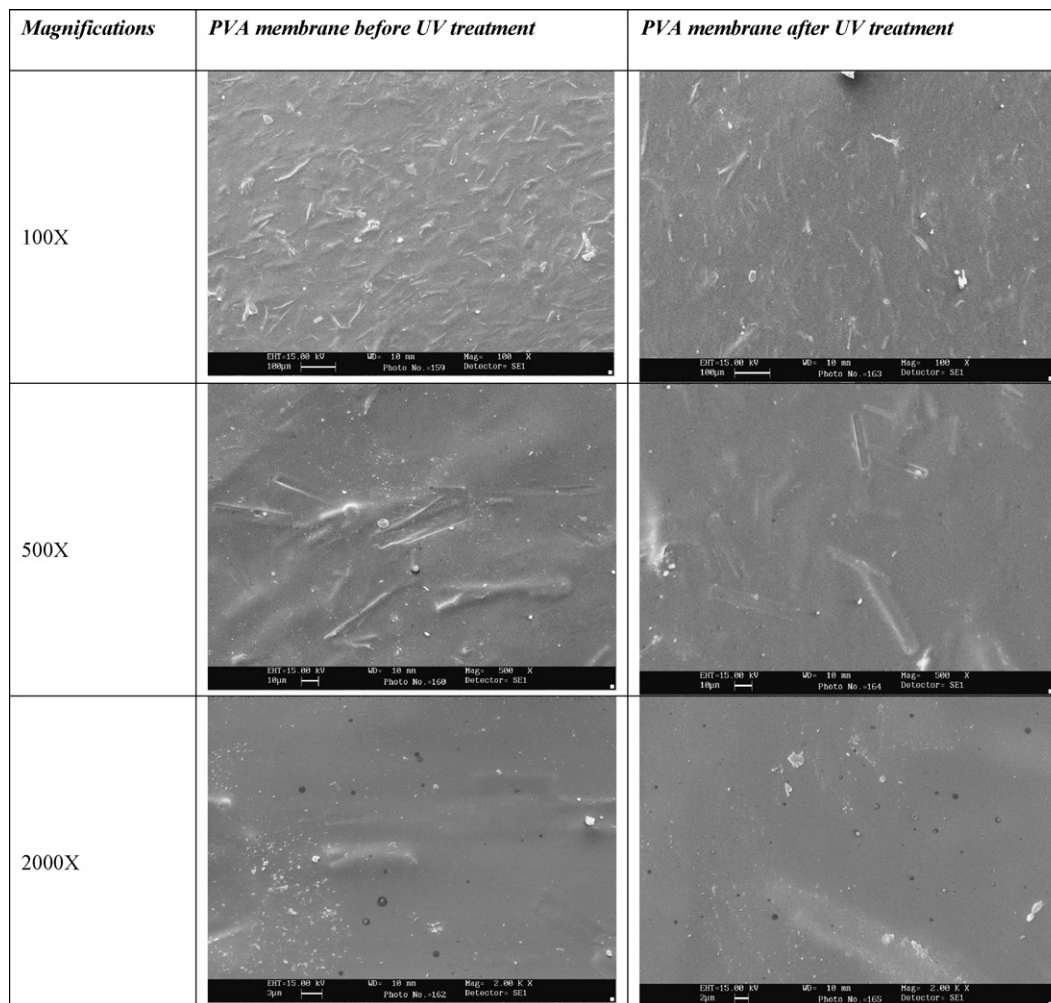

Fig. 3. SEM study of PVA membranes before and after UV treatment (magnifications: 100, 500 and 2000×).

and roughness and is smoother than the surfaces of the membrane before UV treatment (as shown in Fig. 3). The membrane with smoother surfaces has greater antifouling capability [23] for better quality and longevity.

3.4. Immobilization of GOD in PVA membrane

GOD of different concentrations was immobilized in PVA membranes and optimum activity was obtained when 2000 units/ml concentration was used. There after there was no further significant increase in activity. Hence 2000 units/ml concentration of GOD was used for further study.

Km for free and immobilized GOD was studied and was found to be 76 and 119 mM respectively. No drastic changes in Km on immobilization suggest any major alteration in its conformation.

3.5. Calibration of DO probe using GOD–PVA membranes

Calibration of DO electrode response with the standard concentration (0.9, 4.5, 22.5, 90, 225, and 450 mg/dl) of glucose was carried using GOD–PVA membrane. Linear fit ($Y = 0.1512 + 0.52X$) with a slope of 0.52 ($R^2 = 0.989$; S.D. = 1.9214) was estimated between 0.9 and 225 mg/dl of glucose.

3.6. Detection range, detection limit and response time

From the linear fit of calibration of DO electrode in response to standard concentration of glucose, the detection range of biosensor was estimated between 0.9 and 225 mg/dl. The detection ranges were comparable to the commercial glucose biosensor available in the market [15]. Standard deviation of the noise was 0.011×10^{-2} ppm, twice of this inferred the detection limit 0.6 mg/dl of the biosensor.

The enzymatic reaction using immobilized enzyme was observed for 30 min and the readings were acquired after 2 min of interval in terms of change in depletion of dissolved oxygen. It was observed that maximum dissolved oxygen was consumed in first reading than the subsequent readings therefore 2 min was considered as response time of the biosensor.

3.7. Reusability, reproducibility and stability of the GOD–PVA membrane

The reusability of the four GOD–PVA membranes in response to glucose is shown in Fig. 4. Membranes were reused for 32 reactions without significant loss of activity.

The low relative standard deviations 2.8×10^{-2} (mean = 46.2×10^{-2} ppm, when $n = 6$) in the response of immobilized enzyme for 90 mg/dl glucose demonstrated the high reproducibility of analysis. Additionally, a very low relative standard deviation 3.1×10^{-2} (mean = 46.78×10^{-2} ppm) of three different experiments carried; using the same condition further demonstrated the result.

As shown in Fig. 5 the immobilized GOD–PVA membranes were stable for 30 days of investigation with retention of
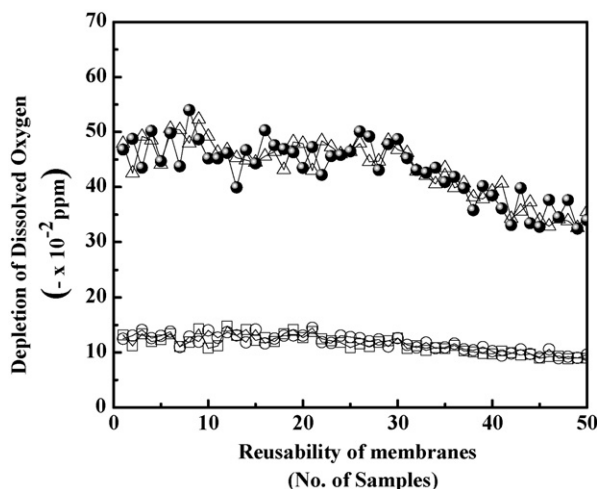
Fig. 4. Reusability of the GOD–PVA membrane (four GOD–PVA membranes were studied against glucose concentrations: (□) 22.5 mg/dl, (○) 22.5 mg/dl, (△) 90 mg/dl and (●) 90 mg/dl).
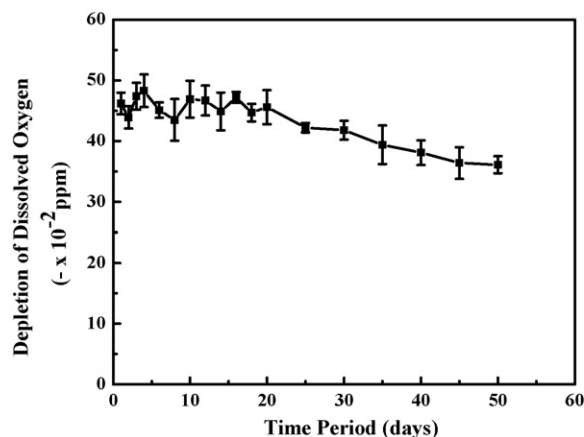

Fig. 5. Stability of the GOD–PVA membrane (a concentration of 90 mg/dl glucose was used for the study).
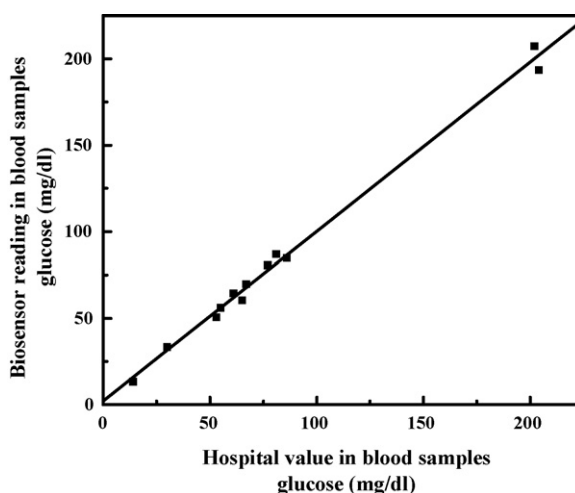

Fig. 6. Correlation of the biosensor reading (glucose mg/dl) with the BARC hospital value in blood sample. Linear fit ($Y = 2.2 + 0.979X$) and correlation ($R^2 = 0.992$).

90% activity, when stored at 4 °C and subsequently response decreased.

3.8. Detection of glucose in blood samples

Biosensor was also used to detect glucose in blood sample (from the BARC hospital). Biosensor readings were compared with the values obtained from the hospital. The correlation and straight-line fit plot between the two results was shown in Fig. 6. The straight-line fit yielded slope of 0.979 ($R^2 = 0.992$), which demonstrates the feasibility and a good correlation of the GOD–PVA membrane response with the existing analysis method. Blood consists of many other biological components, which did not interfere with the response of GOD–PVA membrane.

4. Conclusions

An alternate method to prepare the polyvinyl alcohol membrane for biosensor application using high and low DOP of PVA, acetone, benzoic acid and cross-linking by UV treatment is described. Swelling index study indicates that the membrane prepared with 12% low DOP and 8% high DOP of PVA, 2% BA, dissolved in buffer containing 20% acetone and cross-linked with the UV treatment, was having lower swelling index and suitable for immobilization. FTIR study showed appearance of strong band at ~2337 cm^{-1} when UV was used for cross-linking in the presence of the benzoic acid. SEM study revealed the smoother quality of the membrane after UV treatment. Glucose oxidase enzyme was immobilized and GOD–PVA membrane was associated with the dissolved oxygen probe for biosensor reading. A wide detection range, 0.9–225 mg/dl was estimated and membrane was reused for 32 reactions without significant loss of activity. Membranes were stored for 30 days (~90% activity) at 4 °C. Use of GOD–PVA membranes were also demonstrated with real blood samples.

References

[1] A.P.F. Turner, I. Karube, G.S. Wilson, Biosensors Fundamentals and Applications, Oxford University Press, Oxford, UK, 1987.
[2] S.F. D'Souza, Appl. Biochem. Biotechnol. 96 (2001) 225.
[3] S.F. D'Souza, Biosens. Bioelectron. 16 (2001) 337.
[4] S.F. D'Souza, Curr. Sci. 77 (1999) 69.
[5] G.F. Bickerstaff (Ed.), Methods in Biotechnology, Immobilization of Enzymes and Cells, vol. 1, Humana Press, Inc., Totowa, NJ, 1997, p. 1.
[6] J. Kumar, S.K. Jha, S.F. D'Souza, Biosens. Bioelectron. 21 (2006) 2100.
[7] S. Tembe, M. Karve, S. Inamdar, S. Haram, J. Melo, S.F. D'Souza, Anal. Biochem. 349 (2006) 72.
[8] S. Majumdar, B. Adhikari, Sens. Actuators B 114 (2006) 747.
[9] K. Imai, T. Shiomi, K. Uchida, M. Miya, Biotechnol. Bioeng. XXVIII (1986) 1721.
[10] V.S. Praptowidodo, J. Mol. Struct. 739 (2005) 207.
[11] J. Gohil, A. Bhattacharya, P. Ray, J. Polym. Res. 13 (2006) 161.
[12] C.K. Yeom, K.H. Lee, J. Membr. Sci. 109 (1996) 257.
[13] S.K. Jha, S.F. D'Souza, J. Biochem. Biophys. Met. 62 (2005) 215.
[14] D. Shan, D. Zhu, H. Xue, S. Cosnier, Biosens. Bioelectron. 22 (2007) 1612.
[15] J.D. Newman, A.P.F. Turner, Biosens. Bioelectron. 20 (2005) 2435.
[16] L.C. Clark, C. Lyons, Ann. N. Y. Acad. Sci. 102 (1962) 29.
[17] M.J. Kim, Y.I. Park, K.H. Youm, K.H. Lee, J. Appl. Polym. Sci. 91 (2004) 3225.
[18] DC Chemical Co. Ltd., http://www.dcchem.co.kr/english/product/p_petr/p_petr8.htm.
[19] R.M. Silverstein, F.X. Webster, Spectrometric Identification of Organic Compounds, sixth ed., John Wiley & Sons, Inc., New York, 1998, p. 71.
[20] G. Bucher, M. Halupka, C. Kolano, O. Schade, W. Sander, Eur. J. Org. Chem. (2001) 545.
[21] M.H. Moore, R.F. Ferrante, J.A. Nuth, Planet. Space Sci. 44 (1996) 927.
[22] T.M.R. Miranda, A.R. Goncalves, M.T.P. Amorin, Polym. Int. 50 (2001) 1068.
[23] X. Cao, J. Ma, X. Shi, Z. Ren, Appl. Surf. Sci. 253 (2006) 2003.

Biomonitoring method for the simultaneous determination of cadmium and lead in whole blood by electrothermal atomic absorption spectrometry for assessment of environmental exposure

Fábio Kummrow [a,b], Fábio F. Silva [a,c], Rúbia Kuno [a,d],
Alexandre L. Souza [c], Pedro V. Oliveira [c,*]

[a] *Cia de Tecnologia de Saneamento Ambiental-CETESB, 05459-900 São Paulo, SP, Brazil*
[b] *Departamento de Análises Clínicas e Toxicológicas, Universidade Federal de Alfenas, 37130-000 Alfenas, MG, Brazil*
[c] *Instituto de Química, Universidade de São Paulo, 05513-970, C.P. 26077 São Paulo, SP, Brazil*
[d] *Faculdade de Medicina, Universidade de São Paulo, 01246-903 São Paulo, SP, Brazil*

Abstract

The aim of this work is to propose a biomonitoring method for the simultaneous determination of Cd and Pb in whole blood by simultaneous electrothermal atomic absorption spectrometry for assessment of environmental levels. A volume of 200 μL of whole blood was diluted in 500 μL of 0.2% (w v^{-1}) Triton® X-100 + 2.0% (v v^{-1}) HNO$_3$. Trichloroacetic acid was added for protein precipitation and the supernatant analyzed. A mixture of 250 μg W + 200 μg Rh as permanent and 2.0% (w v^{-1}) NH$_4$H$_2$PO$_4$ as co-injected modifiers were used. Characteristic masses and limits of detections ($n = 20$, 3 s) for Cd and Pb were 1.26 and 33 pg and 0.026 μg L^{-1} and 0.65 μg L^{-1}, respectively. Repeatability ranged from 1.8 to 6.8% for Cd and 1.2 to 1.7% for Pb. The trueness of method was checked by the analysis of three Reference Materials: Lyphocheck® Whole Blood Metals Control level 1 and Seronorm™ Trace Elements in Whole Blood levels 1 and 2. The found concentrations presented no statistical differences at the 95% confidence level. Blood samples from 40 volunteers without occupational exposure were analyzed and the concentrations ranged from 0.13 to 0.71 μg L^{-1} (0.32 ± 0.19 μg L^{-1}) for Cd and 9.3 to 56.7 μg L^{-1} (25.1 ± 10.8 μg L^{-1}) for Pb.
© 2007 Elsevier B.V. All rights reserved.

Keywords: Atomic absorption spectrometry; Simultaneous determination; Biomonitoring; Blood; Cadmium; Lead

1. Introduction

Lead and cadmium are considered two of the most toxic elements for living organisms [1–6]. The environmental persistence of these metals in concert with their intensive use by modern society has, over the years, created a concentration in the biosphere, and continuous exposure to low levels of cadmium and lead may result in bioaccumulation and health effects, by both occupational and environmental exposition [7,8].

Human biomonitoring is a useful tool in environmental medicine to assess and evaluate the background levels of internal dose of environmental pollutants in general population, population groups and individuals through measurements of those chemicals, or their metabolites in human specimens, such as blood and urine [9].

Normal exposure levels of cadmium may be small [10,11], and the improvement of working conditions and the actions taken to minimize the environment exposure to lead, such as the phase-out of leaded gasoline and improvements in food preparations and packaging, have led to a substantial reduction of the blood lead levels in general population [12–15]. Although environment quality has improved, during the last decades in many countries air levels of cadmium and lead in the vicinity of certain industrial sources, frequently located closely to residential areas, are still increased and health concerns were raised [16–19].

The determination of lead and cadmium in biological materials poses several problems mainly due to the low concentrations of these metals, the great variation of the matrix from sample to sample and contamination. Among the instrumental techniques available, electrothermal atomic absorption spectrometry

* Corresponding author. Tel.: +55 11 3091 8516; fax: +55 11 3815 5579.
E-mail address: pvolivei@iq.usp.br (P.V. Oliveira).

(ETAAS) is still one of the most widely used for trace element determination in biological samples [20–22]. Particularly, ETAAS is a well-established technique for cadmium [19,23–27] and lead [19,23–25,27–29] determination in whole blood.

The availability of simultaneous atomic absorption spectrometry (SIMAAS) allowed the development of methods for the determination of two or more elements, improving the analytical frequency, reducing the cost related to instrument maintenance, sample and high purity reagents. The determinations of cadmium and lead by SIMAAS have been proposed in the literature for many types of samples including serum, urine and whole blood [30–34]. Otherwise, detection and quantification limits of these methods are not enough sensible for assessing environmental levels of these elements, mainly cadmium in whole blood of population who has low levels of internal doses. The objective of this work is to propose a high sensible method aiming the simultaneous determination of low levels of cadmium and lead in whole blood for environmental exposure assessment. The proposed method can be used in population surveys including those to determine reference values in biomonitoring programs.

2. Experimental

2.1. Instrumentation

All measurements were performed with an electrothermal atomic absorption spectrometer, SIMAAS-6000 (PerkinElmer Life and Analytical Sciences, Shelton, CT, USA), equipped with longitudinal Zeeman-effect background correction, Echelle optical arrangement and solid-state detector. End-capped transversal heating graphite tubes (EC-THGA) with integrated pyrolytically coated platforms were used throughout in this work. All solutions were delivered into the graphite tube by means an AS-72 autosampler (PerkinElmer Life and Analytical Sciences). Argon 99.996% ($v\,v^{-1}$) (White Martins, São Paulo, SP, Brazil) was used as the purge gas. The instrumental setting up conditions is shown in Table 1.

After proteins precipitation, the solid phase was separated from the solution using a centrifuge (Quimis®, São Paulo, SP, Brazil).

Table 1
Instrumental setting for the simultaneous determination of Cd and Pb in blood by SIMAAS-6000

Element	Pb	Cd
Wavelength (nm)	283.3	228.8
Band pass (nm)	0.7	0.7
Lamp type	EDL*	EDL
Lamp current (mA)	450	230
Calibration range ($\mu g\,L^{-1}$)	2.5–20	0.1–0.8
Signal measurements	Peak area (AA-BG)	
Calibration equation	Linear	
Read time (s)	5.0	
Standard and sample volume (μL)	12	
Modifier volume (μL)	5	
Standard and sample replicates	3	

EDL: Electrodeless discharge lamp.

2.2. Reagents

All reagents were of analytical-reagent grade unless otherwise specified. Ultra pure water with a final resistivity of $18.2\,M\Omega\,cm^{-1}$ was provided by a Milli-Q water purification system (Millipore, Bedford, MA, USA). Analytical grade HNO_3 65% ($m\,v^{-1}$) (Merck, Darmstadt, Germany) and Triton® X-100 (Fisher Scientific, NJ, USA) was used to prepare diluent solutions. Tricloroacetic acid (TCA) (Merck) was used to precipitate proteins of whole blood. The analytical reference solutions were prepared by successive dilution of $1000\,mg\,L^{-1}$ of Cd ($Cd(NO_3)_2$ in H_2O) and Pb ($Pb(NO_3)_2$ in H_2O) from Titrisol® standard solutions (Merck).

The permanent chemical modifier was thermally obtained from high purity $Na_2WO_4\cdot2H_2O$ (Merck) and $RhCl_3$ (Sigma, St. Louis, MO, USA). A solution of 2% ($m\,v^{-1}$) $NH_4H_2PO_4$ (Merck) was used as co-injected chemical modifier. All solutions were stored in decontaminated polyethylene bottles at room temperature.

2.3. Sample

Lyphocheck® Whole Blood Metals Control level 1 (Bio-Rad, Irvine, USA) and Seronorm™ Trace Elements in Whole Blood level 1 (Lot OK0336) and level 2 (Lot MR9067) from Sero AS (Billingstad, Norway) reference materials were used to check the reliability of the entire proposed method. These lyophilized materials were reconstituted with 2 mL of ultrapure water.

Whole blood samples provided from 40 adult volunteers (>18 years old) from São Paulo State Environment Agency (CETESB, São Paulo, SP, Brazil) were analyzed. The samples were collected in heparinized Vaccuntainer tubes and stored at $-22\,°C$ for about 1 week prior to the simultaneous Cd and Pb determinations.

2.4. Procedure

All glassware and Eppendorf® (Brinkmann Instruments, Westbury, NY, USA) tubes were cleaned with detergent solution, soaked in 10% ($v\,v^{-1}$) HNO_3 for 24 h, rinsed with ultra pure water, dried and stored in a closed polypropylene container. All solution and sample manipulations were conducted in a laminar flow bench (Class II, Pachane) to avoid airborne contamination.

A solution containing $0.2\,\mu g\,L^{-1}$ Cd(II) and $5\,\mu g\,L^{-1}$ Pb(II) in 0.1% ($w\,v^{-1}$) Triton® X-100 + 1.0% ($v\,v^{-1}$) HNO_3 + 6% ($w\,v^{-1}$) TCA was used to optimize the heating program. The pyrolysis and atomization temperatures were also optimized in presence of diluted blood solution. Pyrolysis and atomization temperature curves were simultaneously obtained for Cd and Pb in absence and presence of co-injected 2.0% ($w\,v^{-1}$) $NH_4H_2PO_4$. The permanent chemical modifier ($250\,\mu g$ W + $200\,\mu g$ Rh) was used in all experiments. The permanent chemical modifier was thermally deposited following the literature recommendations [35]. The pyrolysis holding time was studied considering the background absorbance intensity in presence of the diluted blood solution.

The analytical calibration solutions were prepared in the range of 0.10–0.80 $\mu g\,L^{-1}$ for Cd and 2.5–20 $\mu g\,L^{-1}$ for Pb in 0.1% (w v^{-1}) Triton® X-100 + 1.0% (v v^{-1}) HNO$_3$ + 6% (w v^{-1}) TCA.

Samples and reference materials were prepared by diluting 200 μL of whole blood with 500 μL of diluent 0.2% (w v^{-1}) Triton® X-100 + 2.0% (v v^{-1}) HNO$_3$ in Eppendorf® (Brinkmann Instruments, Westbury, NY, USA) tubes with 1.5 mL. All diluted blood samples were pumping with the micropipette several times to ensure that the pipet was completely rinsed and to allow homogenization. The blood solution was kept in a laminar flow bench during 60 min for complete red blood cells lysing. Afterwards, 300 μL of 20% (w v^{-1}) TCA solution was added to the blood solution for proteins precipitation. Subsequently, Eppendorf® tube was manually agitated before centrifugation during 5 min at 7000 rpm to enhance the separation. A volume of approximately 600 μL of supernatant was transferred to the autosampler cup (1.2 mL) for analyze. A 12 μL aliquot of reference or sample solutions and 5 μL of 2.0% (m v^{-1}) NH$_4$H$_2$PO$_4$ solution were deposited onto the integrated platform. The rinse solution was 0.1% (w v^{-1}) Triton® X-100 to perform the probe cleaning and resulting better standard deviation between the sampling. All measurements were made with at least three replicates and based on integrated absorbance.

To evaluate occlusion or co-precipitation of Cd and Pb in the precipitate a mass of approximately 50 mg of Seronorm™ Trave Elements level 2 dry precipitate were transferred to microwave vessel with a diluted oxidant mixture (1 mL HNO$_3$ + 2 mL H$_2$O$_2$ + 3 mL H$_2$O) for digestion in a closed vessel microwave oven (Microwave 3000, Anton Paar, Austria), using the following heating program (temperature, °C; ramp, min; hold, min): (140, 5, 1), (180, 8, 2) and (220, 4, 10). Cadmium and Pb were determined in the resulted solution by SIMAAS.

3. Results and discussions

3.1. Heating program optimization

Based on previous results for the simultaneous determination of Cd and Pb in whole blood by SIMAAS [33], the mixture 250 μg W + 200 μg Rh was initially elected as the permanent chemical modifier. In aqueous solution, the best pyrolysis temperatures were 400 and 500 °C for Cd and Pb, respectively, while atomization temperatures were 1700 °C for both elements (Fig. 1). For diluted blood sample (1 + 4), after proteins precipitation, the pyrolysis temperatures were 300 and 350 °C for Cd and Pd, respectively (Fig. 2).

Pyrolysis and atomization temperatures must be selected based on the most and least volatile analyte to be simultaneously determined. The most suitable temperatures for Cd and Pb determination, using W + Rh as chemical modifier, were 300 and 1700 °C for pyrolysis and atomization steps, respectively.

The spectrometer calibration was performed by using aqueous analytical reference solutions ranging from 0.10 to 0.80 $\mu g\,L^{-1}$ for Cd and 2.5 to 20 $\mu g\,L^{-1}$ for Pb in 0.1% (w v^{-1}) Triton® X-100 + 1.0% (v v^{-1}) HNO$_3$ + 6% (w v^{-1}) TCA. The same concentrations of matrix matched analytical reference
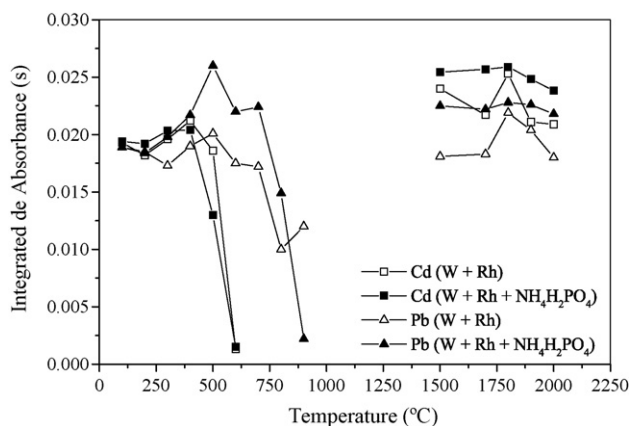
Fig. 1. Pyrolysis and atomization curves for 0.2 $\mu g\,L^{-1}$ Cd and 5.0 $\mu g\,L^{-1}$ Pb in 0.1% (w v^{-1}) Triton® X-100 + 1.0% (v v^{-1}) HNO$_3$ + 6% (w v^{-1}) TCA with two different chemical modifier: 250 μg W + 200 μg Rh and 250 μg W + 200 μg Rh + co-injected 2.0% (w v^{-1}) NH$_4$H$_2$PO$_4$.

solutions were also used for spectrometer calibration to check the influence of matrix concomitants on the Cd and Pb atomization. The analytical curves for Cd and Pb in aqueous solution and diluted blood sample are shown in Figs. 3 and 4, respectively. The comparison of the slopes (b) observed for calibration graphs obtained from aqueous solution with those in presence of diluted blood can be use to estimate the effect caused by the matrix. In absence of matrix effect, the ratio between the slopes obtained from aqueous solutions and diluted blood must be, approximately, 1, and this condition ensures the adequacy of using aqueous reference solution for instrument calibration [34]. This experiment showed more pronounced matrix effects over Cd (0.03568/0.02668 = 1.3) than Pb (0.00129/0.00133 = 0.97) atomization. This was confirmed when the reference materials were analyzed. Recoveries based on the recommended values ranged from 76 to 89% for Cd and 89 to 96% for Pb.

Due to the low boiling point (199 °C) TCA was probably removed during the drying step [36]. Consequently, the reduction in Cd and Pb thermal stability might be caused by the presence of residual organic and inorganic components of 1 + 4 diluted blood. As reported in the literature, permanent chemical

Fig. 2. Pyrolysis and atomization curves for blood (1 + 4) diluted after protein precipitation with two different chemical modifier: 250 μg W + 200 μg Rh and 250 μg W + 200 μg Rh + co-injected 2.0% (w v^{-1}) NH$_4$H$_2$PO$_4$.

to combine with any matrix concomitants, such as chloride ions. The conventional co-injection of a chemical modifier in solution form with the sample seemed to be more successful.

Taking into account the good results obtained for Pb, we decided to combine the permanent chemical modifier (W + Rh) with the co-injected $NH_4H_2PO_4$ solution.

The thermal behavior of Pb and Cd was again evaluated in presence of 2.0% (m v^{-1}) $NH_4H_2PO_4$ co-injected with analytical solutions over W–Rh permanent chemical modifier. In this condition, Cd and Pb pyrolysis temperatures were 400 and 700 °C for aqueous reference solution (Fig. 1) and 400 and 700 °C for diluted sample (Fig. 2), respectively. The atomization temperatures were 1800 and 1900 °C for aqueous and diluted blood sample, respectively. For the combined modifiers, the presence of concomitants practically did not affect the pyrolysis temperatures. Considering the compromised conditions, pyrolysis an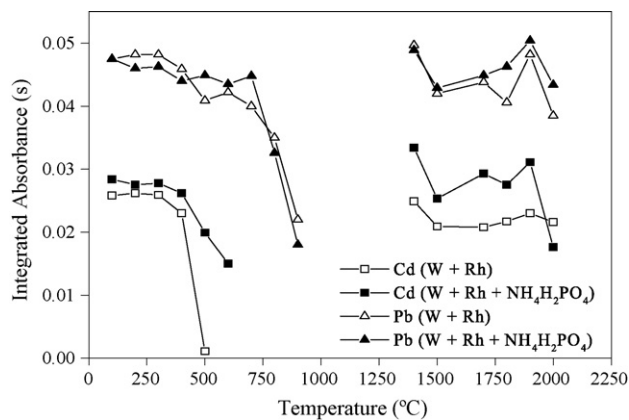d atomization temperatures for Cd and Pb were 400 and 1900 °C, respectively. The atomization temperature was established by considering the relationship between peak area and standard deviation of three replicates for the elements.

The spectrometer was again calibrated using analytical reference solutions in aqueous and matrix matched solutions to check the performance of the combined chemical modifier. The regression coefficients (r) obtained from aqueous solution and diluted blood solutions were very close to those obtained without the co-injected chemical modifier (Figs. 3 and 4). However, the slopes (b) observed for calibration graphs obtained from aqueous and in presence of diluted blood solutions were much better than those obtained in absence of co-injected modifier. The ratio between the slopes obtained from aqueous and diluted blood solutions for Cd (0.02706/0.02703 = 1.0) and Pb (0.00114/0.00120 = 0.95) showed reduction of the matrix effects, allowing instrument calibration with aqueous reference solutions.

Pyrolysis holding time was also optimized and 20 s was sufficient to ensure effectiveness of background correction. Peak shapes and background absorption were also considered when choosing the furnace conditions. Typical atomization peak for Cd and Pb are shown in Fig. 5. The heating program described in Table 2 was used for the determination of Cd and Pb in whole blood samples.

3.2. Analytical characteristics of method

Methods for simultaneous determination of Cd and Pb in whole blood have been successfully proposed using TGHA [23–29] and SIMAAS [30–34]. In many cases, whole blood was diluted 1 + 9 and directly introduced into the graphite tube for

Fig. 3. Analytical curves for Cd in aqueous and blood sample (1 + 4) using 250 μg W + 200 μg Rh and 250 μg W + 200 μg Rh + co-injected 2.0% (w v^{-1}) $NH_4H_2PO_4$ as chemical modifiers: (□) abs. = 0.35688× + 0.0004, r = 0.99961; (■) abs. = 0.27058× + 0.0014, r = 0.99812; (△) abs. = 0.26682× + 0.0059, r = 0.99447; (▲) abs. = 0.27028× + 0.0044, r = 0.99929.
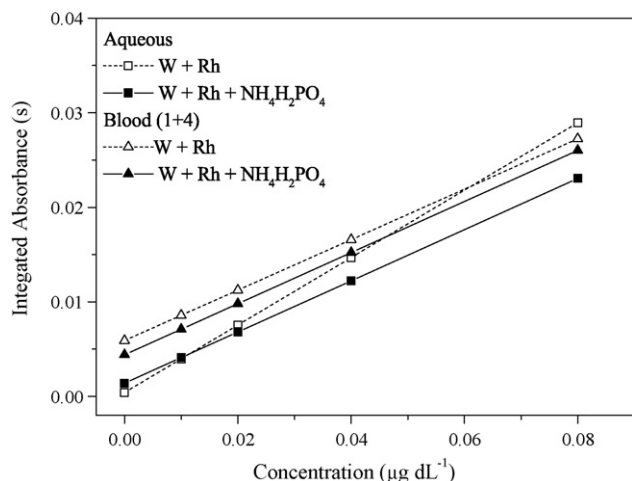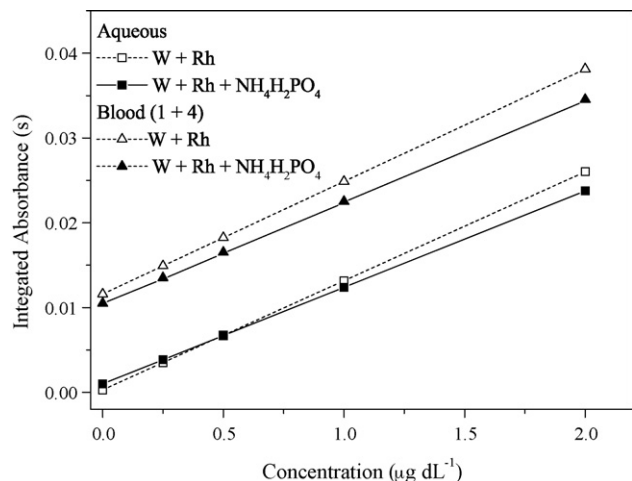

Fig. 4. Analytical curves for Pb in aqueous and blood sample (1 + 4) using 250 μg W + 200 μg Rh and 250 μg W + 200 μg Rh + co-injected 2.0% (w v^{-1}) $NH_4H_2PO_4$ as chemical modifiers: (□) abs. = 0.01286× + 0.0003, r = 0.99806; (■) abs. = 0.01138× + 0.0010, r = 0.99812; (△) abs. = 0.01327× + 0.0116, r = 0.99976; (▲) abs. = 0.01202× + 0.0105, r = 0.99949.

modifier has always led to lower pyrolysis temperature when undigested biological materials are directly analyzed [37]. The high concentration of concomitants in the solution might be restrained the interaction between Cd and Pb with the permanent chemical modifier. Thus, the analyte was more susceptible

Table 2
Transversal heating graphite atomizer program (end-capped tube with integrated platform) for the simultaneous determination of Cd and Pb in blood

Step	Temperature (°C)	Ramp (s)	Hold (s)	Ar gas flow (mL min^{-1})	Read
Drying	130	10	5	250	
Pyrolysis I	200	5	5	250	
Pyrolysis II	400	10	20	250	
Atomization	1900	0	3	–	Yes
Cleaning	2100	1	4	250	

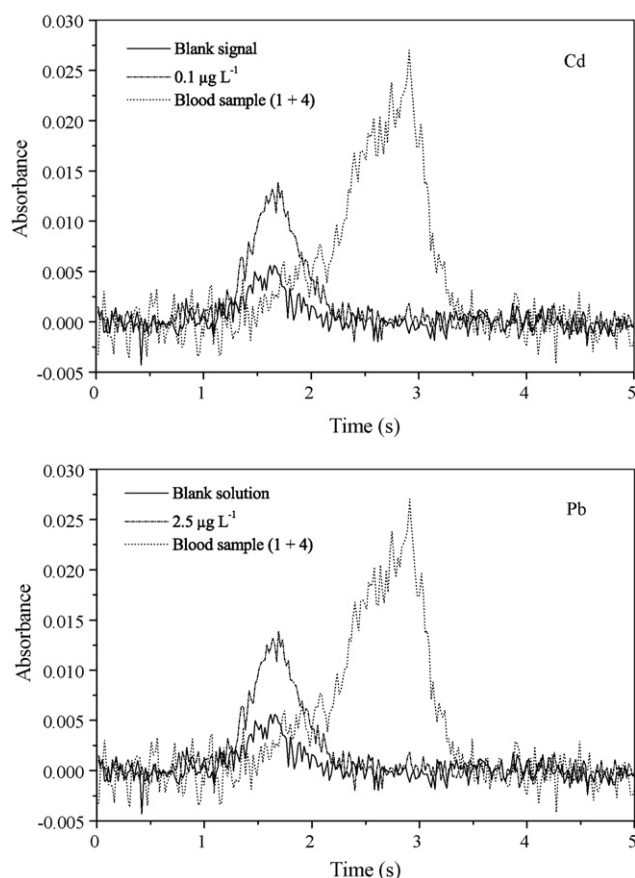Injection temperature: 100 °C; pipette speed: 50%.

Fig. 5. Analytical signals for Cd and Pb in aqueous and blood sample (1 + 4) using $250 \mu g$ W + $200 \mu g$ Rh + co-injected 2.0% (w v^{-1}) NH$_4$H$_2$PO$_4$ as chemical modifiers.

analysis and screening purposes. However, for the assessment of background levels of these elements, high sensible methods are imperative. The use of EC-THGA graphite tube is one instrumental alternative to improve the sensitivity of SIMAAS [26]. It was observed a decrease of 13 and 20% for the Cd and Pb detection limits for end-capped in comparison to the standard graphite tubes, respectively.

But, even using this strategy we certified the necessity to improve the detectability of method to achieve background levels. The alternative was reduced the dilution of blood sample. However, when aliquots of blood solutions diluted 1 + 4 were directly injected in the graphite tube, random absorbance and high background signals were observed for Cd and Pb. This can be due to high concentration of organic concomitants in the final diluted whole blood. Based on previous work [38], one alternative to diminish organic concomitants in 1 + 4 blood dilution was the protein precipitation with TCA. Concentrations of 5, 10, 15 and 20% (v v^{-1}) TCA were tested. The best TCA concentration to improve the quantitative precipitation of proteins was 20% (v v^{-1}). After precipitation, solutions were manually agitated before centrifugation for 5 min.

The determination of Cd and Pb in the precipitate showed concentrations below of the detection limits which attested there was not occlusion or co-precipitation of these elements.

It was essential to introduce Triton® X-100 prior to the TCA solution to promote complete lysis of the cells before protein precipitation. In previous investigation (1 + 9 dilution), negative errors were observed when Triton® X-100 and TCA were simultaneously introduced [38]. But in this work, probably because of the low blood dilution it was necessary to wait more time to promote complete lysis of red cells. Different times (0, 20, 40 and 60 min) were studied and 60 min showed the better recoveries for Cd and Pb when reference materials were analyzed. This step can be implemented during the spectrometer calibration avoiding analytical frequency damage.

The characteristics masses were calculated from the calibration curves and based on the integrated absorbance. The detection limits (DL) were calculated considering the variability of 20 consecutive measurements of 0.1% (w v^{-1}) Triton® X-100 + 1.0% (v v^{-1}) HNO$_3$ + 6% (w v^{-1}) TCA as the blank solution (0.0066 ± 0.0028 for Cd and 0.0057 ± 0.0026 for Pb, $n = 20$), according to $3s_{blk}/b$ (s_{blk} = standard deviation of the blank and b = calibration curve slope). Taking into account a 1 + 4 dilution factor, detection limits for the sample concentration would be 0.13 $\mu g L^{-1}$ for Cd and 3.25 $\mu g L^{-1}$ for Pb. The characteristic masses and detection limits obtained in this work and in others methods for Cd and Pb determination in whole blood by SIMAAS are shown in Table 3.

The performance of the EC-THGA was evaluated by comparing the slopes of calibration graphs in different lifetime of the graphite tube (0 up to 1060 heating cycles). The slopes (s) observed for Cd (0.03783 ± 0.003644, R.S.D. = 9.6%) and Pb (0.00155 ± 0.00021, R.S.D. = 13.5%) indicated acceptable performance, even after 1060 heating cycles. The relative standard deviations were based on the slopes obtained by using a new EC-THGA. Up to 846 heating cycles the relative standard deviations of slopes were below 10% for both elements. More than 846 heating cycles, the EC-THGA graphite tube was worn down. Consequently, we recommend working with the same EC-THGA graphite tube up to, approximately, 850 heating cycles. As related in previous work [35] and attested in this work, the improvement in the graphite lifetime can be credited to the permanent chemical modifier ($250 \mu g$ W + $200 \mu g$ Rh).

Considering the simultaneous determination of Cd and Pb, it was possible to have up to 1700 analytical results with the

Table 3

Characteristic masses and detection limits of Cd and Pb in whole blood for different methods by SIMAAS

Element	m_o (pg)	DL ($\mu g L^{-1}$)	Reference
Cd	1.26	0.026	This work
Pb	33	0.65	End-capped tube
Cd	–	0.24	31
Pb	–	1.06	–
Cd	1.6	0.03	33
Pb	35	0.8	THGA tube
Cd	1.68	0.095	34
Pb	30.3	0.86	THGA tube

Table 4
Results for the simultaneous determination of Cd and Pb in reference materials ($n = 3$)

CRM	Found value ± uncertainty		Recommended values	
	Cd ($\mu g\,L^{-1}$)	Pb ($\mu g\,L^{-1}$)	Cd ($\mu g\,L^{-1}$)	Pb ($\mu g\,L^{-1}$)
I	3.7 ± 0.1	94 ± 1	3.8 (3.0–4.5)	83 (66–100)
II	0.9 ± 0.2	36 ± 2	0.7	33
III	6.6 ± 0.1	442 ± 5	6.2 (5.4–7.2)	401 (353–443)

I, Liphochek Bio-Rad level 1; II, Seronorm^{TM} level 1 and III, Seronorm^{TM} level 2.

same atomizer, lowering costs associated with the replacement of graphite parts.

3.3. Cadmium and lead determination

The spectrometer was calibrated using aqueous reference solutions ranging from 0.10 to 0.8 $\mu g\,L^{-1}$ for Cd and from 2.5 to 20 $\mu g\,L^{-1}$ for Pb in 0.1% (w v^{-1}) Triton$^®$ X-100 + 1.0% (v v^{-1}) HNO$_3$ + 6% (w v^{-1}) TCA using instrumental conditions and the heating program listed in Tables 1 and 2, respectively. The analytical curves are depicted in Figs. 3 and 4.

The trueness of the proposed method was checked by analysis of three certified reference materials (Lyphocheck$^®$ Whole Blood Metals Control level 1 and Seronorm^{TM} Trace Elements in Whole Blood levels 1 and 2. Results are presented in Table 4. The found Cd and Pb concentrations for the reference materials are in accordance to the acceptable range at 95% of the confidence level (Student's t-test).

Cadmium and Pb concentrations in whole blood of 40 volunteers from environmental exposure are shown in Table 5. Four blood samples were spiked with 0.1 $\mu g\,L^{-1}$ of Cd and 2.5 $\mu g\,L^{-1}$ of Pb. Good recoveries were obtained, ranging from 98 to 115% for Cd and 99 to 112% for Pb, corroborating to the use of co-injected NH$_4$H$_2$PO$_4$ as chemical modifier for minimization of interferences caused by matrix constituents.

Analysis of whole blood of 40 environmental exposure volunteers ranged from 0.13 to 0.71 $\mu g\,L^{-1}$ (0.32 ± 0.19 $\mu g\,L^{-1}$) for Cd and 9.3 to 56.7 $\mu g\,L^{-1}$ (25.1 ± 10.8 $\mu g\,L^{-1}$) for Pb.

The relative standard deviations between sampling ($n = 3$) ranged from 2.0 to 21% for Cd and 1.5 to 13% for Pb. The repeatability (within-run precision) of method was assessed by analysis of CRMs (Lyphocheck$^®$ Whole Blood Metals Control level 1 and Seronorm^{TM} Trace Elements in Whole Blood level

Table 6
Blood lead levels (BLL) in adults of São Paulo city

Year of publication	Total population	Pb ($\mu g\,L^{-1}$)	Reference
1981	$n = 63$ (men)	142 ± 43	[18,39]
	$n = 37$ (women)	93 ± 39	
1985	$n = 26$	130 ± 8	[40]
1997	$n = 30$	63.0 ± 2.3	[41]
2007	$n = 40$	25.1 ± 10.8	This work

2). Six separated samples of each CRM were prepared according to the proposed method and analyzed in triplicate. The repeatabilities ranged from 1.8 to 6.8% for Cd and 1.2 to 1.7% for Pb. The reproducibility (between-day precision) of method was monitored by analysis of CRM (Lyphocheck$^®$ Whole Blood Metals Control level 1) over a 6-month period. The relative standard deviations of the results in this period of time were 10.2% for Cd and 8.8 for Pb.

In Table 6 are showed the reference values for blood lead level (BLL), in adult population of São Paulo city (Brazil) obtained in different period of times 1981, 1985, 1997 and 2007. Brazil does not have a health public regular program for measuring the BLL in the general population. Therefore, data reported in Table 6 are individual studies to determine BLL for specific interest. But, it is evident the reduction of lead concentration in whole blood with the time, claiming for high sensible methods for quantitative determination.

Recently, studies coordinated by New York City Health and Nutrition Examination Survey (NYC HANES), from United States allowed assessing the environmental exposure of Cd, Hg and Pb in blood of New York City adults. The geometric mean blood of these elements concentrations were 0.77 and 17.0 $\mu g\,L^{-1}$, respectively. The authors comment that Cd concentration is slightly higher than the 1999–2000 national estimated for adults (0.47 $\mu g\,L^{-1}$) [42].

4. Conclusions

The low dilution of blood samples (1 + 4) combined with protein precipitation with TCA can be considered as the up-to-date strategy for the simultaneous determination of Cd and Pb by SIMAAS to assess the environmental exposure. Additionally, the combination of permanent chemical modifier (250 μg W + 200 μg Rh) and co-injected 2.0% (w v^{-1}) of NH$_4$H$_2$PO$_4$ enlarged the graphite tube up to 846 heating cycles without

Table 5
Analysis and recoveries test for the simultaneous determination of Cd and Pb in whole blood volunteers

Sample	Cd ($\mu g\,L^{-1}$)	Pb ($\mu g\,L^{-1}$)	Recoveries (%)	
			Cd spike (0.10 $\mu g\,L^{-1}$)	Pb spike (2.5 $\mu g\,L^{-1}$)
1	1.23 ± 0.08	34.4 ± 0.9	104	108
2	0.61 ± 0.11	27.6 ± 1.2	115	102
3	0.72 ± 0.05	39.1 ± 3.9	107	112
4	0.78 ± 0.06	33.3 ± 1.5	98	99
Mean ± S.D.* ($n = 40$)	0.32 ± 0.19	25.1 ± 10.8	–	–

* S.D., Standard deviation.

long-term precision damage (<21% for Cd and <13% for Pb) and reduced the matrix effects, respectively.

Acknowledgements

References

[1] N.C. Papanikolaou, E.G. Hatzidaki, S. Belivanis, G.N. Tzanakakis, A.M. Tsatsakis, Med. Sci. Monitor 11 (2005) RA329.

[2] D.C. Bellinger, Pediatrics 113 (2004) 1016.

[3] M.P. Waalkes, J. Inorg. Biochem. 79 (2000) 241.

[4] S.J. Stohs, D. Bagchi, Free Rad. Biol. Med. 18 (1995) 321.

[5] E. Rojas, L.A. Herrera, L.A. Poirier, P. Ostrosky-Wegman, Mutat. Res.-Genet. Tox. Environ. Mutag. 443 (1999) 157.

[6] A.L. Mendelsohn, B.P. Dreyer, A.H. Firman, C.M. Rosen, L.A. Legano, H.A. Kruger, S.W. Lim, C.D. Courtlandt, Pediatrics 101 (1998) 1.

[7] W.I. Mortada, M.A. Sobh, M.M. El-Defrawy, S.E. Farahat, Environ. Res. 90 (2002) 104.

[8] P. Kakkar, F.N. Jaffery, Environ. Tox. Pharmacol. 19 (2005) 335.

[9] P. Boffetta, Mutat. Res.-Genet. Tox. Environ. Mutag. 608 (2006) 157.

[10] M. Wilhelm, C. Schulz, M. Schwenk, Int. J. Hyg. Environ. Health 209 (2006) 301.

[11] C.D. Palmer, M.E. Lewis Jr., C.M. Geraghty, F. Barbosa Jr., P.J. Parsons, Spectrochim. Acta Part B 61 (2006) 980.

[12] F. Barbosa Jr., J.E. Tanus-Santos, R.F. Gerlach, P.J. Parsons, Environ. Health Perspect. 113 (2005) 1669.

[13] P. Apostoli, A. Baj, P. Bavazzano, A. Ganzi, G. Neri, A. Ronchi, L. Soleo, L. Di Lorenzo, P. Spinelli, T. Valente, C. Minoia, Sci. Total Environ. 287 (2002) 1.

[14] M. Cerna, V. Spevackova, M. Cejchanova, B. Benes, P. Rossner, D. Ocadilikova, J. Smid, Sci. Total Environ. 204 (1997) 263.

[15] E. Bárány, I.A. Bergdahl, L.E. Bratteby, T. Lundh, G. Samuelson, A. Shütz, S. Skerfving, A. Oskarsson, Environ. Res. 89 (2002) 72.

[16] M. Wilhelm, G. Eberwein, J. Hölzer, J. Begerow, D. Sugiri, D. Gladtke, U. Ranft, J. Trace Elem. Med. Biol. 19 (2005) 83.

[17] M. Castelli, B. Rossi, F. Corsetti, A. Mantovani, G. Spera, C. Lubrano, L. Silvestroni, M. Patriarca, F. Chlodo, A. Menditto, Microchem. J. 79 (2005) 349.

[18] M.M.B. Paoliello, E.M. De Capitani, Environ. Res. 103 (2007) 288.

[19] H.I. Afridi, T.G. Kazi, M.K. Jamali, G.H. Kazi, M.B. Arain, N. Jalbani, G.Q. Shar, R.A. Sarfaraz, Toxicol. Ind. Health 22 (2006) 381.

[20] A.C. Davis, P. Wu, X.F. Zhang, X.D. Hou, B.T. Jones, Appl. Spectros. Rev. 41 (2006) 35.

[21] M. Rose, M. Knaggs, L. Owen, M. Baxter, J. Anal. At. Spectrom. 16 (2001) 1101.

[22] D.L. Tsalev, J. Anal. At. Spectrom. 9 (1993) 405.

[23] H.I. Afridi, T.G. Kazi, M.B. Arain, M.K. Jamali, G.H. Kazi, N. Jalbani, J. AOAC Int. 90 (2007) 470.

[24] A. Viitak, A.B. Volynsky, Talanta 70 (2006) 890.

[25] E.J. Daftsis, G.A. Zachariadis, Talanta 71 (2007) 722.

[26] M. Stoeppler, K. Brandt, Fresenius J. Anal. Chem. 300 (1980) 372.

[27] N. Campilo, P. Viñas, I. Lópes-García, M. Hernándz-Córdoba, Anal. Chim. Acta 390 (1999) 207.

[28] P.J. Parsons, W. Slavin, Spectrochim. Acta Part B 48 (1993) 925.

[29] C.R. dos Santos, R.S. Rodrigues, C.S. Silva, E.S. Nascimento, J. Radioanal. Nucl. Chem. 269 (2006) 481.

[30] M.A. White, A. Panayi, At. Spectros. 19 (1998) 89.

[31] A. Deval, J. Sneddon, Microchem. J. 52 (1995) 96.

[32] A. Viksna, E.S. Lindgren, Anal. Chim. Acta 353 (1997) 307.

[33] P.R.M. Correia, P.V. Oliveira, At. Spectrosc. 24 (2004) 222.

[34] P.R.M. Correia, P.V. Oliveira, J.A.G. Neto, J.A. Nóbrega, J. Anal. At. Spectrom. 19 (2004) 917.

[35] E.C. Lima, F.J. Krug, K.W. Jackson, Spectrochim. Acta Part B 53 (1998) 1791.

[36] R.C. West (Ed.), Handbook of Chemistry and Physics, 66th ed., CRC Press, Boca Raton, FL, 1985.

[37] Y. Zhou, R.A. Zanão, F. Barbosa Jr., P.J. Parsons, F.J. Krug, Spectrochim. Acta Part B 57 (2002) 1291.

[38] F.J. Krug, M.M. Silva, P.V. Oliveira, J.A. Nóbrega, Spectrochim. Acta Part B 50 (1995) 1469.

[39] N.A.G.G. Fernícola, F.A. Azevedo, Rev. Saúde Publ. 15 (1981) 272.

[40] H.P. Monteiro, D.S.P. Abdalla, A.S. Arcuri, E.J.H. Bechara, Clin. Chem. 31 (1985) 1673.

[41] C.A. Costa, G.C. Trivelato, A.M.P. Pinto, E.J.H. Bechara, Chin. Chem. 43 (1997) 1196.

[42] W. Mckelvey, R.C. Gwynn, N. Jeffery, D. Kass, L.E. Thrope, R.K. Garg, C.D. Palmer, P.J. Parsons, Environ. Health Perspect. 115 (2007) 1435.

Comparison of four extraction methods for the analysis of 24 pesticides in soil samples with gas chromatography–mass spectrometry and liquid chromatography–ion trap–mass spectrometry

C. Lesueur [a,b], M. Gartner [a], A. Mentler [c], M. Fuerhacker [b,*]

[a] *Gartner & LVA GmbH, Blaasstrasse 29, 1190 Vienna, Austria*
[b] *BOKU-University of Natural Resources and Applied Life Sciences,*
Institute of Sanitary Engineering and Water Pollution Control,
Muthgasse 18, 1190 Vienna, Austria
[c] *BOKU-University of Natural Resources and Applied Life Sciences,*
Institute of Soil Research, Peter Jordanstrasse 82,
1190 Vienna, Austria

Abstract

With a view to analyse multiresidues of pesticides in soil samples, a new ultrasonic solvent extraction (USE) was compared to the European Norm DIN 12393 for foodstuff (extraction with acetone, partitioning with ethylacetate/cyclohexane and clean-up with gel permeation chromatography (GPC)), the QuECheRS method and a pressurised liquid extraction (PLE) method. Pesticides were analysed with both GC-MS and HPLC-MS/MS. The reference materials were the EUROSOIL 7 and its subsoil SO26 as well as a sea sand. All the substances were observed to be linear in the range of 4–800 ng g^{-1} for the European Norm DIN 12393, 7–1400 ng g^{-1} for the USE method and 20–4000 ng g^{-1} for the QueCheRS and the PLE methods. Limits of detection (LOD) and limits of quantification (LOQ) were with HPLC between 0.006 and 0.23 ng g^{-1} and between 0.022 and 0.77 ng g^{-1}, respectively, with the exception of diuron (LOD up to 11.8 ng g^{-1}; LOQ up to 39.2 ng g^{-1}). With GC they ranged from 3.0 to 87.5 ng g^{-1} and from 10 to 292 ng g^{-1}, respectively. All substances could be recovered with USE as well as with the QuECheRS method; the European Norm DIN 12393 could not recover carbendazim and metamitron; the PLE carbendazim, metamitron and monolinuron. For the remaining substances, recoveries at a 500 ng g^{-1} fortification level ranged from 10.9 to 96.3% with the USE. In comparison, the QuECheRS method was the most efficient extraction method with recoveries from 27.3 to 120.9%. It was followed by the European Norm DIN 12393 with recoveries between 6.8 and 108.1% and the PLE with recoveries from 12.2 to 153.2%. Recoveries were higher from the EUROSOIL 7 than from the SO 26. The repeatability expressed in term of standard deviation was below 20% for all substances and all materials.
© 2007 Elsevier B.V. All rights reserved.

Keywords: Pesticides; Soil; Gas chromatography; Liquid chromatography; Mass spectrometry

1. Introduction

The increasing worldwide need for food demands a higher agricultural productivity, which can only be achieved by an extensive use of pesticides. Unfortunately pesticides contami-

nate the environment through intensive or inappropriate use [1]. Although organochlorine insecticides like DDT and its metabolites, lindane, aldrin or dieldrin for instance have been banned years ago in many countries based on their mutagenic, carcinogenic and endrocrine disrupting properties, they still can be found in environmental samples due to their persistence and lipophilic properties [2–6]. Organophosphorus insectices (like chlorpyrifos, chlorpyrifos-methyl or chlorfenvinphos) and triazine herbicides (like atrazine, simazine, metribuzine) are the

---

* Corresponding author. Tel.: +43 1 36006 5821; fax: +43 1 36899 49.
E-mail address: maria.fuerhacker@boku.ac.at (M. Fuerhacker).

most commonly used pesticides around the world; they and their metabolites are detected in the environment although several members of these classes have been banned for years [4–6]. Among the different groups of pesticides, herbicides are more likely to pollute soils. In 1997, Barceló and Hennion [7] published valuable data about herbicides use: herbicides have been extensively used in the world for over 40 years representing 45% of the total market value in 1993 with more than 80% of herbicide use localised in North America, Western Europe and East Asia; 22% of the total herbicides are also used for non-agricultural purposes. Phenylurea and urea herbicides (e.g. linuron, diuron or metamitron) are in a sense emerging herbicides in recent years, but are already considered in EU list of priority substances containing some endocrine disruptors [8] and monitored in environmental samples [9]. Therefore, the monitoring of trace levels of pesticides in environmental samples is imperative because of their widespread use in agriculture but the sample preparation methods for the monitoring of multiresidues of pesticides in soil are scarce. The reason is the wide range of physico-chemical properties of the pesticides of interest that implies a comprehensive extraction and furthermore an expensive equipment such as GC-MS and HPLC-MS [10].

Ideally, a sample preparation should be rapid, simple, cheap, environmentally friendly and provide clean extracts. Traditionally pesticide analyses in soils were prepared by the time- and solvent-consuming Soxhlet extraction [11], which is more and more replaced by more environmentally friendly procedures including ultrasonic solvent extraction (USE) [2,4,9,12–17], pressurised liquid extraction (PLE) [3,18–22], shake-flask extraction [23–25], microwave assisted extraction (MAE) [26–28] or supercritical fluid extraction (SFE) [28] followed in some cases by a clean-up step with solid-phase extraction (SPE) [8,21,23,24,27] or solid-phase microextraction (SPME) [13,14,26].

Liquid–solid extractions (LSE) have the disadvantage of being time-, solvent-consuming and tedious. The new strategies are more environmentally friendly with advantages like rapidity, automation, selectivity and low consumption of solvents but lack sensitivity and selectivity [10]. Among them the ultrasonic extraction of contaminants from solid samples is becoming more and more favoured. USE and MAE are reported to improve the extraction efficiency but due to their limited selectivity and simultaneous co-extraction of soil and sediment components together with the target analytes, they often require a further clean-up step [4,23]. Usually, USE is operated with ultrasonic baths [2,4,9,13,15–17]. In the last years, a norm using a horn-type device equipped with a titanium tip was published for the extraction of nonvolatile and semivolatile organic compounds from solids such as soils, sludges, and wastes [29]. Recently, a more efficient system using a cylindrical ultrasonic probe for the sonication of soil samples was developed, described and applied to the dispersion of soil [12,14]. PLE and SFE are sample-volume restricted; in addition the recoveries of polar and/or thermolabile pesticides can be critical [4].

In addition to the techniques devoted to pesticide analysis in soil, some other procedures can be adopted from the analysis of pesticide multiresidues in foodstuff. To that purpose two main methods have been employed in the past and recent years: the European Norm DIN 12393 method [30,31] is applied in many laboratories as reference methods for the analysis of apolar and middle polar pesticides in non-fatty food samples and the QuECheRS multimethod has been developed recently and implemented in numerous laboratories for the analysis of apolar, middle polar and polar pesticides in non-fatty food samples [32–34]. Although until now these reference methods for foodstuff are rarely used for the extraction of soil samples, it is interesting to state whether these methods could be applied to soil analysis.

The goal of this study was the application of a new ultrasonic system, based on an ultrasonic cylindrical probe, for the extraction of pesticides from soil samples and to compare its efficiency to different extraction methods such as a PLE or methods conventionally applied to food analysis, i.e. the Norm method DIN 12393 and the QuECheRS method, a recent but well-known and quick method, for the determination of apolar, middle polar and polar pesticides with gas chromatography (GC) coupled to single quadrupole mass selective detector (MS) and high-performance liquid chromatography (HPLC) combined to ion trap (IT) mass spectrometry.

2. Material and methods

2.1. Reagents and chemicals

Pesticide standards were purchased either from Dr. Ehrenstorfer or from Sigma–Aldrich with the highest available purity.

Magnesium sulfate anhydrous, sodium chloride and sodium citrate dihydrate were purchased from J.T.Baker, di-sodium hydrogen citrate sesquihydrate was provided from Fluka and Bondesil-PSA (Primary Secondary Amine) 40 μm was from Varian.

Ultra-residue reagent acetone, ultra-residue reagent ethylacetate, ultra-residue reagent acetonitrile, HPLC-MS grade methanol, ultra HPLC-MS grade water and HPLC-MS grade formic acid were purchased from J.T.Baker.

Individual stock solutions were prepared dissolving 10 mg of standard in 10 ml acetonitrile and further diluted with acetonitrile to 10 μg ml^{-1}. Multicompound stock standard solutions were prepared dissolving 10 mg of each standard in 1000 ml acetonitrile reaching 10 μg ml^{-1} and further diluted with acetonitrile to achieve concentrations of 5, 2, 0.5, 0.2 and 0.05 μg ml^{-1}. The solution used to spike the samples was prepared dissolving 10 mg of each standard in 100 ml acetone reaching 100 μg ml^{-1} and further diluting 10 ml of this multicompound solution in 2000 ml petroleum ether to reach a 0.5 μg ml^{-1} concentration. The single and multicompound standards were stored at 4 °C in the dark.

2.2. Pesticide selection

24 pesticides reported as soil pollutants in the literature [2–7,9] were selected. Preliminary experiments were carried out to find the best chromatographic technique for the few substances that can be analysed with GC and LC like atrazine and its

Table 1
Physico-chemical properties (MW: molecular weight, solubility in water, K_{OW}: octanol/water coefficient, K_{OC}: organic carbon sorption constant) of the selected pesticides

Substance	Pesticide class	MW (g mol^{-1})	Water solubility (mg l^{-1})	log K_{OW}	K_{OC} (cm^3 g^{-1})
Atrazine	Triazine herbicide	215.10	35	2.7	100
Carbendazim	Carbamate fungicide	191.07	8	1.48	400
Chlorfenvinphos	Organophosphorus insecticide	357.97	145	3.8	680
Chloroxuron	Phenylurea herbicide	290.08	3.7	3.4	2,820
Chlorpyrifos	Organophosphorus insecticide	348.93	1.4	4.7	6,925
Chlorpyrifos-methyl	Organophosphorus insecticide	320.89	2.6	4.24	4,645
Deltamethrin	Pyrethroid insecticide	502.97	0.0002	4.60	460,000
Desethylatrazine	Metabolite of atrazine	187.63	n.a.	n.a.	n.a.
Desisopropylatrazine	Metabolite of atrazine	176.61	n.a.	n.a.	n.a.
Dieldrin	Organochlorine insecticide	377.87	0.14	3.7	12,000
Diuron	Phenylurea herbicide	232.02	35.6	2.87	1067
Flufenoxuron	Phenylurea herbicide	488.04	0.0043	4.01	3,200
Isoproturon	Phenylurea herbicide	206.14	70.2	2.5	139
Lindane	Organochlorine insecticide	287.86	8.52	3.69	1,100
Linuron	Phenylurea herbicide	248.01	63.8	3.0	620
Metamitron	Triazinone herbicide	202.09	1700	0.83	242
Methabenzthiazuron	Urea herbicide	221.06	60	2.64	527
Metobromuron	Phenylurea herbicide	258.0	330	2.41	197
Metoxuron	Phenylurea herbicide	228.07	678	1.6	120
Monolinuron	Phenylurea herbicide	214.05	735	2.2	200
Pencycuron	Phenylurea herbicide	328.13	0.3	4.68	6,207
Simazine	Triazine herbicide	201.08	5	2.3	130
Trifluralin	Dinitroaniline herbicide	335.11	0.221	5.27	8,765
Vinclozoline	Dicarboximide fungicide	285.0	3.4	3.01	100

n.a.: not available.

derivates, simazine or flufenoxuron for instances. On the ground of their peak shape/response and LOD/LOQ, this resulted in the analyses of 12 GC-amenable and 12 LC-amenable herbicides (dinitroaniline, phenylurea, urea, triazine and triazinone) and other fungicides/insecticides (carbamate, dicarboximide, organochlorine, organophosphorus and pyrethroid). Table 1 presents some of their physico-chemical properties [35].

2.3. Soil selection and preparation

The soils used in this study were the European reference material EUROSOIL 7 and its subsoil SOIL SO26 from the European Commission Environment Institute, Joint Research Center, ISPRA as well as a sea sand, purified by acid and calcinated, from Merck. The soils have been selected since they represent 24% of the arable land in Austria. The main physico-chemical properties of the 2 soils are given in Table 2 [36].

600 g of each solid material was contaminated with 600 ml of the 0.5 μg ml^{-1} multicompound standard solution, air-dried at room temperature for 7 days to obtain "aged soil" samples [10].

Table 2
Physico-chemical properties of the soils

Parameter	EUROSOIL 7	SO26	Sea sand
pH (CaCl$_2$)	4.4	4.6	5.5
Organic matter	11.52	1.81	0
Sand (w/w%)	46.0	64.3	100
Slit (w/w%)	35.2	31.1	0
Clay (w/w%)	18.8	4.6	0
CaCO$_3$	0.15	0.13	0

After the bulk of the solvent was evaporated, the materials were finally dried overnight at 30 °C. Sensitivity, recovery and precision of the methods were tested as assigned for foodstuff by the SANCO European Guideline [37] at a 500 ng g^{-1} soil fortification level for 7 replicates. The linearity of the methods was tested for 5 standards in acetonitrile in the range 0.010–2 μg ml^{-1} (i.e. 4–800 to 20–2000 ng g^{-1} depending on the extraction method). LOD and LOQ were assessed for the target ion (GC) and most important fragmentation ion (HPLC) as the lowest concentration that yielded to a signal to noise ratio of 3 and 10, respectively.

2.4. Soil sample extraction

Four extraction methods were assessed and compared in this study: (i) a new ultrasonic extraction method; (ii) a pressurised liquid extraction; (iii) the European Norm DIN 12393 [30] as multiresidue method for the gas chromatographic determination of pesticide residues in non-fatty foodstuff; (iv) the QuECheRS method [32] for the analysis of pesticide multiresidue in non-fatty foodstuff. The solvent composition and ratio used for PLE and USE were the same as in the QuECheRS method in order to compare the results.

2.4.1. Ultrasonic solvent extraction (USE)

USE experiments were carried out with 20 g of sample extracted with 60 ml of a water/acetonitrile (1:2, v/v) solution in a 200 ml glass beaker. The device design and set-up used in this study is given in details elsewhere [12,14]. The samples were homogenised with a small magnetic stirring bar during the ultrasonic extraction with a Sonoplus HD 2200 from Ban-

delin equipped with a cylindrical probe US 70 T with a diameter of 12.7 mm. The sonication took place for 2 min at 20 kHz; the vibration amplitude was 35 μm; the energy value was 7.8 J ml^{-1} and the insertion depth 10 mm. A second set-up with a vibration amplitude of 60 μm and an energy value of 13.6 J ml^{-1} was investigated to test the influence of these parameters on the extraction of the pesticides. The extract was filtered through 0.45 μm and 1.8 ml aliquot was evaporated under a gentle stream of nitrogen and collected in 400 μl acetonitrile/acetone (1:1, v/v) for the soil samples and 700 μl acetonitrile/acetone (1:1, v/v) for the sea sand samples, respectively. Triphenylphosphate (TPP) was used as internal standard and spiked before the extraction to reach a concentration of 0.5 μg ml^{-1} in the final extract.

The first main difference between the system used in this study [12,14] and the system recommended by the US EPA method 3550C [29], is the definition of the input energy that is to be at least 300 W in the US EPA method 3550C. The application as defined inhere (insertion depth, vibration amplitude and energy value) reflects the real input energy received by the samples since the vibration amplitude, i.e. the energy has been calibrated, and is measured and controlled through stain gauges of a feedback system of the ultrasound amplifier [12,14]. This owns the particularity of delivering a constant vibration amplitude (lower than 0.01%).

The second difference is the recommended use of a pulse mode in the US EPA method 3550C for low concentrations to be extracted. This is not necessary with our cylindrical probe since its geometry guaranties a strong circular laminar flow that is enhanced through the use of a magnetic stirring device.

The extraction took place only once, and not three times as recommended by the US EPA method 3550C, due to the relatively high fortification concentration of 500 ng g^{-1}.

2.4.2. Pressurised liquid extraction (PLE)

For the PLE experiments, 5 g of sample was mixed with 1 g silica gel and introduced in a 10 ml steel column. The accelerated solvent extractor was an ASE 100 from Dionex. In preliminary experiments the best set-up for the extraction with water/acetonitrile (1:2, v/v) was found to be 110 bar and 140 °C during 20 min with 3 PLE cycles. The collected extract (ca. 40 ml) was evaporated as far as it could, i.e. almost to dryness with rotary evaporator at 40 °C, further dissolved in 10 ml acetonitrile/acetone (1:1, v/v), filtrated through 0.45 μm and 1.5 ml were filled in 2 autosampler vials for GC-MS and HPLC-MS analysis. TPP was used as internal standard and spiked before extraction to reach a concentration of 0.5 μg ml^{-1} in the final extract.

2.4.3. European Norm DIN 12393

Although traditionally applied to foodstuff, this method [30] was used here for the extraction of soil samples. This conventional method consists of an extraction step of 25 g of the sample with 50 ml water and 100 ml acetone (1:2, v/v) followed by partitioning with ca. 100 ml ethylacetate/cyclohexane (1:1, v/v). After evaporation to dryness with rotary evaporator at 40 °C, the samples were collected in 10 ml ethylacetate/cyclohexane (1:1, v/v), filtered through 0.45 μm and 1.5 ml of the extract

were cleaned-up by gel permeation chromatography (GPC). The extracts were consequently evaporated almost to dryness with rotary evaporator at 40 °C and diluted to 1.5 ml acetonitrile/acetone (1:1, v/v) prior to analysis with GC-MS and HPLC-MS. Aldrin, which is forbidden to use since over 20 years, was used as internal standard spiked at the partitioning step.

2.4.4. QuECheRS method

The QuECheRS method described by Anastassiades [32] is based on the extraction of 10 g of sample with 20 ml acetonitrile followed by a salting-out step with 4 g MgSO$_4$, 1 g NaCl, 1 g sodium citrate dihydrate and 0.5 g di-sodium hydrogen citrate sesquihydrate. The clean-up step of the samples was carried out with 150 mg Bondesil-PSA and 950 mg MgSO$_4$ before filtration of the sample through 0.45 μm filter and transfer of 1.5 ml of the extract into 2 autosampler vials for GC-MS and HPLC-MS analysis. TPP was used as internal standard and spiked before extraction to reach a concentration of 0.5 μg ml^{-1} in the final extract.

2.5. Apparatus and analytical conditions

2.5.1. GC-MS

The GC-MS analyses were performed on a Hewlett-Packard (Agilent Technologies, Waldbronn, Germany) GC-MS Model 6890N Series gas chromatography coupled to a 5973N mass selective detector. A HP 5 MS (30 m × 0.25 mm i.d.) (Agilent Technologies, Waldbronn, Germany) fused silica capillary column with a 0.25 μm film thickness was used with helium as carrier gas at a constant pressure daily adjusted (chlorpyriphos-methyl RT relocked to 16.596 min). One microliter of the sample was injected in the splitless mode at 280 °C with a splitless time before opening the injector valve of 2 min. The GC oven was operated with the following temperature program: initial temperature 70 °C held for 2 min, ramped at 25 °C/min to 150 °C not held, followed by a ramp of 3 °C/min to 200 °C not held, followed by another ramp of 8 °C/min to 280 °C held for 10 min and finally ramped to 320 °C at 15 °C/min held for 2.47 min. The total run time was 47 min, the interface was kept at 320 °C, the ion source at 250 °C, the quadrupole at 150 °C and the mass spectra were obtained at an electron energy of 70 eV. The analyses were operated in simultaneous full scan/SIM mode method presented elsewhere [19,23]. The target ions and qualifiers used for quantification are presented in Table 3. The Agilent Chemstation Software G1701DA version D.02.00.237 was used for data analysis.

2.5.2. HPLC-MS/MS

The high-performance liquid chromatography system was an Agilent Technologies HP-1100 Series (Agilent Technologies, Waldbronn). Chromatographic separation was achieved using a Zorbax SB-C18 analytical column 2.1 × 150 mm, 3.5 μm particle size from Agilent Technologies at a flow rate of 300 μl min^{-1}. The mobile phases consisted of A: H$_2$O–MeOH, 90%–9.95% (v/v) with 0.05% HCOOH and B: H$_2$O–MeOH, 9.95%–90% (v/v) with 0.05% HCOOH. The gradient was 100% A at 0 min, 100% A at 1 min, 0% A at 10 min, 0% A at 17 min,

Table 3
Target ions and qualifier ions for the GC-MS

Substance	R.T. (min)	Target ion (m/z)	Qualifier ion (m/z)	Qualifier ion (m/z)	Qualifier ion (m/z)
Atrazine	13.5	200	215	173	202
Chlorfenvinphos	21.6	267	269	323	325
Chlorpyrifos	19.2	314	197	97	258
Chlorpyrifos-methyl	16.6	286	288	323	290
Deltamethrin	36.2	181	253	251	255
Desethylatrazine	11.7	172	187	174	145
Desisopropylatrazine	11.5	158	173	145	175
Dieldrin	23.8	279	277	237	345
Lindane	13.6	219	254	181	
Simazine	13.3	186	201	173	158
Trifluraline	11.5	306	264	290	307
Vinclozoline	16.8	285	198	189	241

100% A at 20 min. The post time was 2 min with 100% A and the stop time 22 min. The HPLC was controlled with the Agilent Technologies Chemstation for LC 3D System Software.

The HPLC system was interfaced to an Agilent Technologies mass spectrometer LC/MSD trap XCT Plus (Agilent Technologies, Waldbronn) equipped with an electrospray ionisation (ESI) interface operated in positive mode and controlled with the Agilent Technologies LC/MSD trap software 5.3. The nebulizer gaz (nitrogen) pressure was 40 psi, the drying gas flow rate was 8 ml/min and the drying gas temperature was 325 °C. The capillary voltage was −4500 V, the endplate offset was fixed at −500 V. The ion trap was operated in the ion charge control (ICC) mode with a target ion count of 150 000 and a maximum accumulation time of 50 ms. The quantification was done in the selected reaction monitoring (SRM) mode with a fragmentation voltage of the $[M + H]^+$ ion set at 0.6 V. The precursor and fragmentation ions selected for quantification are presented in Table 4.

3. Results and discussion

3.1. Optimization of the method

Figs. 1–3 present the recoveries achieved for the 3 soil materials with the 4 extraction methods. In preliminary tests with USE, the influence of the energy value was tested at 2 levels (7.8 and 13.6 J ml^{-1}) and concluded to be insignificant since the

experiments produced comparable results (not shown). USE was further carried out with the parameters given in Section 2.4.1.

For all the methods and samples, the recovery of the internal standard was between 90 and 100%. First of all, it can be noticed that only the QuECheRS and the USE methods allowed the recovery of all the substances. Carbendazim and metamitron were recovered neither with the European Norm DIN 12393 nor with PLE as well as additionally monolinuron were unable to be extracted with PLE. When considering their soil sorption coefficient (K_{OC}), carbendazim, metamitron and monolinuron were not expected to present any problem as to their extraction from the materials since they present K_{OC} between 200 and 400 cm^3 g^{-1}. Nevertheless, they own the lowest octanol–water partition coefficient (K_{OW}) of all the selected substances between 0.8 and 2.2 implying a possibly high repartition in the water phase and as a consequence low concentration in the analysed organic phase. Overall the substances often reported for their strong binding to soil [10] like lindane, trifluralin, dieldrin or deltamethrin for instances (i.e. those with the highest K_{OC}) were always recovered.

3.2. Validation of the method

3.2.1. Linearity of the calibration curve, LOD and LOQ

The linearity, plotted as MS response area vs. concentration, as well as the achieved LOD and LOQ with GC-MS and HPLC-MS, estimated for the target ion and the parent ion, respectively,

Table 4
Target ions and qualifier ions for the HPLC-MS/MS

Substance	R.T. (min)	Precursor ion (m/z)	Fragmentation ion (m/z)	Fragmentation ion (m/z)
Carbendazim	6.2	191.9	159.9	
Chloroxuron	11.5	291.1	163.9	
Diuron	10.7	232.9	232.9	72.3
Flufenoxuron	13.2	489.1	158.1	141.1
Isoproturon	10.6	207.1	207.1	72.1
Linuron	11.1	248.9	182.0	160.0
Metamitron	8.3	202.9	202.9	
Methabenzthiazuron	10.6	221.9	164.9	
Metobromuron	10.5	258.9	147.9	
Metoxuron	9.1	228.9	228.9	
Monolinuron	10.2	214.9	214.8	
Pencycuron	12.3	329.1	329.1	

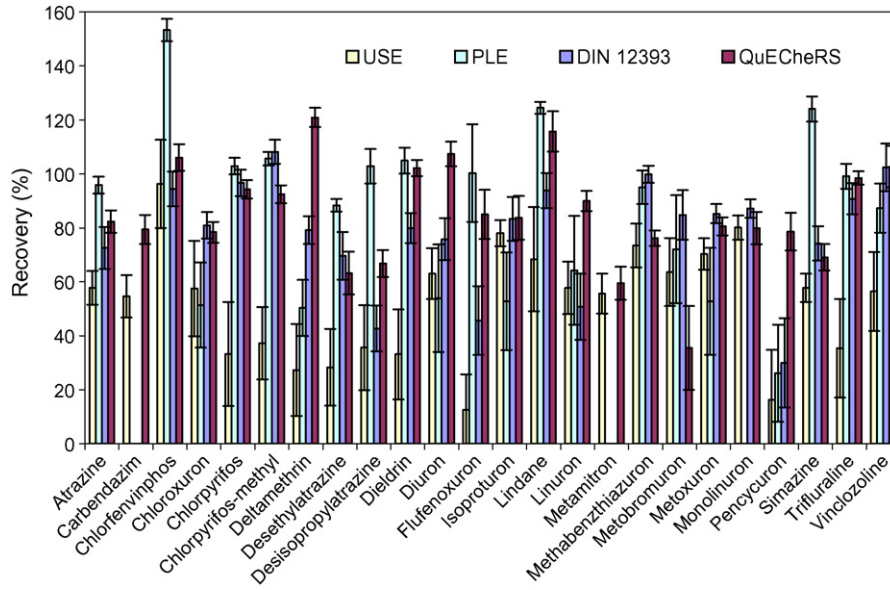Fig. 1. Recovery (%) of the pesticides at 500 ng g^{-1} from EUROSOIL 7 ($n = 7$) with error bars representing the standard deviation.
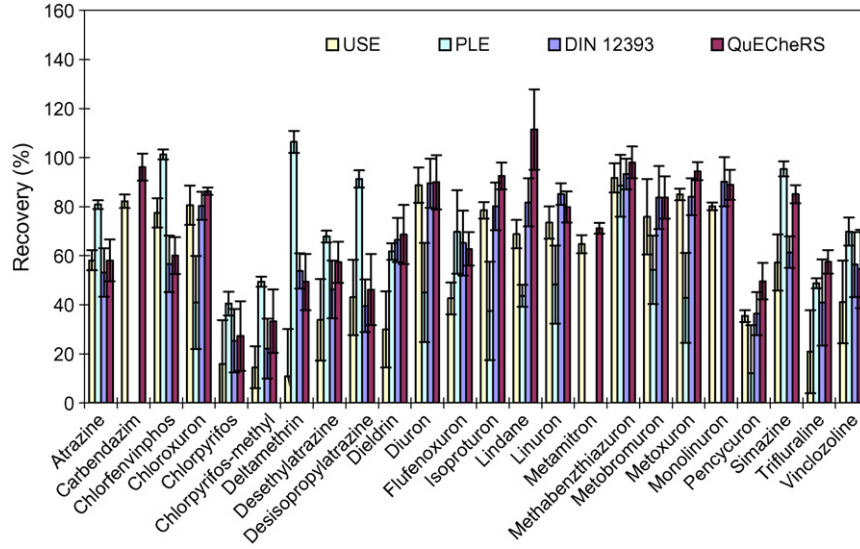

Fig. 2. Recovery (%) of the pesticides at 500 ng g^{-1} from SO 26 ($n = 7$) with error bars representing the standard deviation.
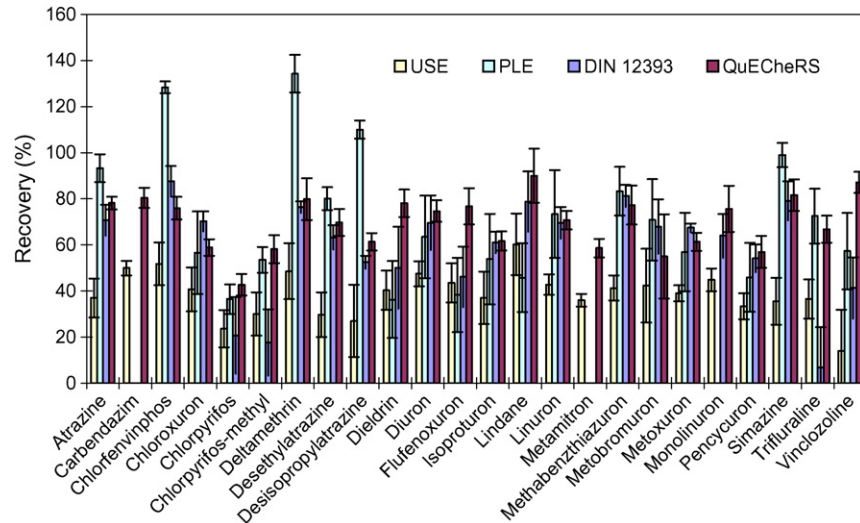

Fig. 3. Recovery (%) of the pesticides at 500 ng g^{-1} from sea sand ($n = 7$) with error bars representing the standard deviation.

Table 5
Linearity, LOD and LOQ of the selected pesticides with GC-MS and HPLC-MS/MS

Substances	Linearity	QuECheRS		DIN 12393		PLE		USE	
	R^2	LOD (ng g^{-1})	LOQ (ng g^{-1})	LOD (ng g^{-1})	LOQ (ng g^{-1})	LOD (ng g^{-1})	LOQ (ng g^{-1})	LOD (ng g^{-1})	LOQ (ng g^{-1})
Atrazine	0.9952	13	43	5	17	4	12	7	23
Desethylatrazine	0.9996	13	43	5	17	4	12	7	23
Desisopropylatrazine	0.9959	11	38	5	15	3	10	6	20
Carbendazim	0.9995	0.02	0.08	0.01	0.03	0.006	0.02	0.01	0.04
Chlorfenvinphos	0.9970	22	73	8.7	29	6	19	12	39
Chloroxuron	0.9996	0.10	0.33	0.04	0.13	0.03	0.09	0.05	0.17
Chlorpyrifos	0.9937	24	79	10	32	6	21	13	42
Chlorpyrifos-methyl	0.9946	37	125	15	50	10	33	20	67
Deltamethrin	0.9962	14	47	6	20	3.8	13	8	25
Dieldrin	0.9990	88	292	35	117	23	78	47	156
Diuron	0.9956	12	39	5	16	3	11	6	21
Flufenoxuron	0.9969	0.23	0.77	0.09	0.30	0.06	0.21	0.12	0.41
Isoproturon	0.9990	0.17	0.56	0.07	0.20	0.04	0.15	0.09	0.30
Lindane	0.9962	13	42	5	17	3	11	7	22
Linuron	0.9992	0.09	0.30	0.04	0.12	0.02	0.08	0.05	0.16
Metamitron	0.9992	0.05	0.16	0.02	0.07	0.01	0.04	0.03	0.09
Methabenzthiazuron	0.9986	0.17	0.58	0.07	0.23	0.05	0.16	0.09	0.31
Metobromuron	0.9994	0.12	0.42	0.05	0.17	0.03	0.11	0.07	0.22
Metoxuron	0.9999	0.08	0.26	0.03	0.10	0.02	0.07	0.04	0.14
Monolinuron	0.9988	0.10	0.35	0.04	0.14	0.03	0.09	0.06	0.19
Pencycuron	0.9952	0.09	0.30	0.04	0.12	0.02	0.08	0.05	0.16
Simazine	0.9928	14	48	6	19	4	13	8	25
Trifluraline	0.9965	20	65	8	26	5	17	10	35
Vinclozoline	0.9949	20	68	8	27	5	18	11	36

as the lowest concentration injected that yielded to a S/N ratio of 3 (LOD) and 10 (LOQ), for the selected substances, are presented in Table 5.

All the substances presented a linear behaviour with GC-MS and LC-MS/MS analysis in the standard concentration range of 0.010–2 µg ml^{-1} corresponding to a soil concentration range of 4–800 ng g^{-1} for the European Norm DIN 12393, 7–1400 ng g^{-1} for the USE method and 20–4000 ng g^{-1} for the QueCheRS and the PLE methods. The lowest LOD/LOQ were achieved with the European Norm DIN 12393 and the highest with the QueCheRS and the PLE methods. With the present methods the LC-amenable substances presented LOD and LOQ in the low ng g^{-1} range between 0.006 ng g^{-1} (carbendazim) and 0.23 ng g^{-1} (flufenoxuron) and from 0.022 to 0.77 ng g^{-1}, respectively, except for diuron with LOD from 3.1 to 11.8 ng g^{-1} and LOQ from 10.5 to 39.2 ng g^{-1}. Unlikely, GC-amenable analytes and in particular chlorpyrifos-methyl and dieldrin presented higher LOD and LOQ in the range 3.0 ng g^{-1} (desisopropylatrazine) to 87.5 ng g^{-1} (dieldrin) and 10 to 292 ng g^{-1}, respectively. Similar LOD and LOQ were reported in the literature [2,4,9,10,13,15–17]. Figs. 4 and 5 also shows a GC-MS chromatogram of a 0.060 µg ml^{-1} standard and a LC-MS/MS chromatogram of a 0.010 µg ml^{-1} standard, respectively.

3.2.2. Recovery and precision

When considering only the substances that were recovered from the materials, the lowest recoveries were obtained with the USE (between 10.9 and 96.3% with a median recovery of

57.0% for the 3 materials). On the contrary the highest recoveries were obtained with the QuECheRS method (between 27.3 and 120.9% with a median recovery of 72.7% for the 3 materials). The remaining method produced similar results: European Norm DIN 12393 (between 6.8 and 108.1% with a median recovery of 65.7% for 3 materials) and PLE (between 12.2 and 153.2% with a median recovery of 63.5% for 3 materials). The QuECheRS method was the method with the highest rate of substances (around 50%) in the 3 matrices satisfying the 70–110% recovery range.

The repeatability was similar and acceptable below 20% for all the methods: USE (S.D. between 1.5 and 19.3% with a median repeatability of 8.5%); PLE (S.D. between 1.8 and 20.2% with a median repeatability of 6.4%); QuECheRS method (S.D. between 1.5 and 18.3% with a median repeatability of 5.4%) and European Norm DIN 12393 (S.D. between 1.9 and 17.8% with a median repeatability of 7.7%). Nevertheless, it was slightly higher for the USE and the PLE.

It is known that organochlorine pesticides have a high affinity to organic humic substances of soil matrices (high K_{OW}) with which they develop chemical bonds [10,38,39]. Since the bond energy between two atoms is higher than the Van der Wals energy, which is related to surface processes, or than ion exchange energy, the energy produced by the ultrasonic dispersion (40 W) is too weak to break down the created C–C bonds (348 kJ mol^{-1}) between organo-mineral complexes [14]. This is valid for chlorpyriphos, chlorpyriphos-methyl, deltamethrin and dieldrin. As far as lindane is concerned, it owns the highest water solubility and the lowest soil sorption coefficient, which
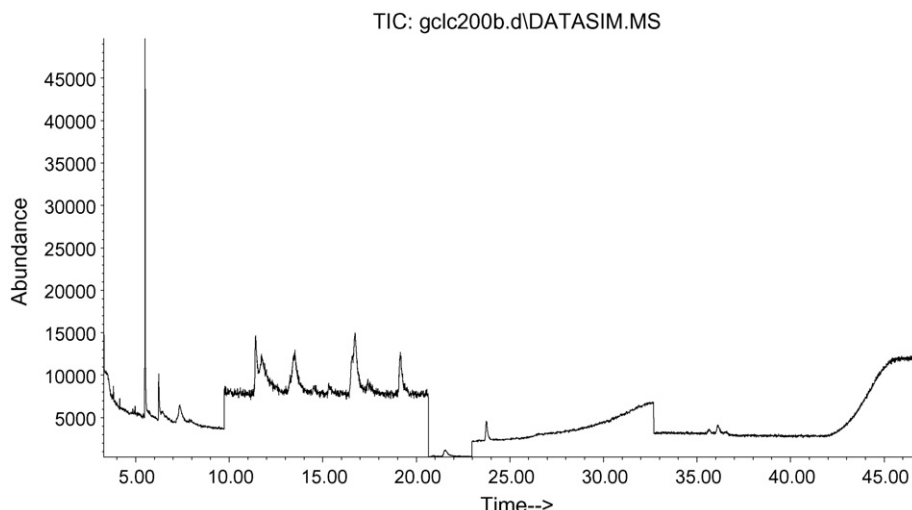
Fig. 4. SIM mode GC-MS chromatogram of a 0.060 µg ml^{-1} standard corresponding to 25 ng g^{-1} sample with the European Norm DIN 12393, 40 ng g^{-1} with USE and 120 ng g^{-1} with the QuEChERS and PLE methods.

can explain the better recovery than with the other organochlorine pesticides [40]. The secondary and tertiary amine pesticides (phenylureas, triazines and their metabolites) tend to adsorb on the soils' inter-crystalline layers of clay minerals [41] that cannot be reached with ultrasonic vibration and makes this extraction less efficient with these substances [14].

Higher recoveries were achieved with the EUROSOIL 7 than with the SO 26 and in any case than with the sea sand whatever the extraction method. Since the adsorption of pesticides increases with the organic matter content [9,38,39], pesticides should adsorb better to the EUROSOIL 7 than to its subsoil SO 26 and consequently be possibly harder to desorb from the materials. The recoveries obtained with the sea sand were in contradiction with the expected results since the material was not expected to retain the substances. An explanation could be that the samples were dried overnight at 30 °C and analytes can build bonds to soil aggregates and solid matter that do not take place with sea sand.

Especially for chlorpyrifos and chlorpyrifos-methyl far better recoveries were obtained for the EUROSOIL 7 than for the SO 26 with all extraction methods. Since recoveries as high as 150% (chlorfenvinphos, deltamethrin, lindane and simazine) were obtained with PLE, a clean-up step is strongly recommended. An explanation for these recoveries higher than 100% could be the interference of the matrix also known as "matrix induced chromatographic response enhancement" effect as detailed by Molins et al. [42] and Mol et al. [43]. Trifluralin, chlorpyriphos and chlorpyriphos-methyl presented extreme low recoveries from sea sand with the European Norm DIN 12393 although this method has been demonstrated to be effective for these analytes but for other matrices. The adsorption of ionisable substances like atrazine and its metabolites is reported to increase with decreasing pH [10,38,39], which explains the rather low recoveries of atrazine, desethylatrazine and desisopropylatrazine with less acidic extraction methods.
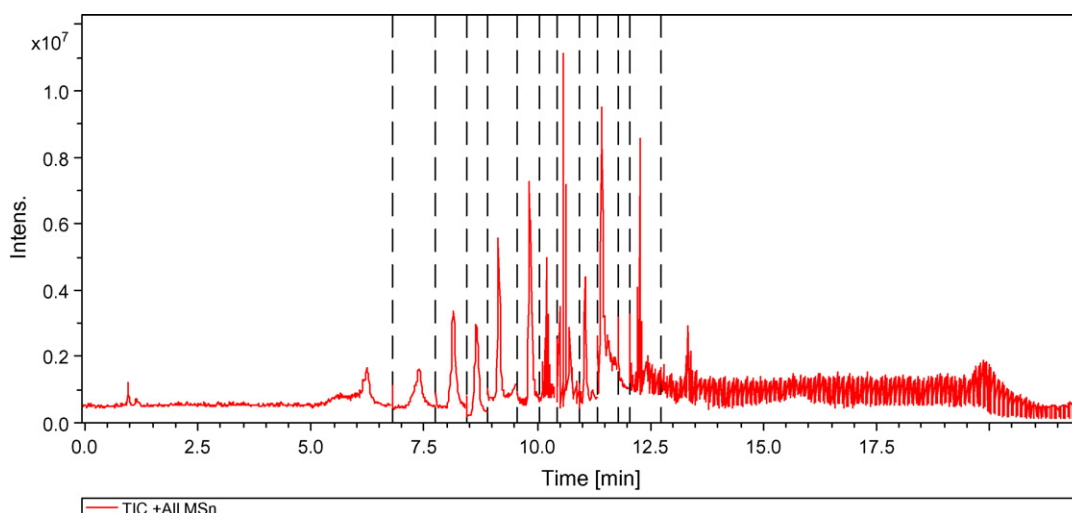

Fig. 5. LC-MS/MS chromatogram of a 0.010 µg ml^{-1} standard corresponding to 0.4 ng g^{-1} with the European Norm DIN 12393, 0.7 ng g^{-1} with USE and 2 ng g^{-1} with the QuEChERS and PLE methods.

The European Norm DIN 12393 has been developed for the analysis of GC-amenable substances and is known to be low efficient in the recovery of polar pesticides like phenylureas or carbamates. Lambropoulou et al. [13] noticed that water, acetone, acetonitrile and methanol showed similar results for the extraction of vinclozoline but that acetone was significantly more efficient in the case of dicloran. Tor et al. [2] recognized acetone, a more polar solvent, as best solvent for the break-up and disintegration of aggregates leading to a better contact between particles and solvent and an improvement of the extraction especially in the case of organochlorine pesticides. By studying the USE of tetramethrin and chlorpropham, Babić et al. [16] noticed that acetonitrile was the only solvent out of 7 that was not able to recover these substances, whereas Gonçalves and Alpendurada [4] recommend acetonitrile for the extraction of organochlorine pesticides from soil samples. Nevertheless most of the studies approve the use of water:solvent mixture since better recoveries are reported [22]. The use of acetone might favor the extraction of analytes from soil matrices but together with that of co-eluents inherent to the materials. This results in less clean extracts leading to the drawbacks of higher LOD and LOQ and the need for a clean-up step, which is always critical in the case of multiresidue methods.

4. Conclusions

The lowest LOD for the analysis of the selected pesticides from soil samples were achieved with the European Norm DIN 12393 and the highest with the QueCheRS and the PLE methods. The LODs achieved with LC-MS/MS were much lower than those achieved with GC-MS, namely in the low $ng\,g^{-1}$ range between $0.006\,ng\,g^{-1}$ (carbendazim) and $0.23\,ng\,g^{-1}$ (flufenoxuron) for the LC-MS/MS against values in the range $3.0\,ng\,g^{-1}$ (desisopropylatrazine) to $87.5\,ng\,g^{-1}$ (dieldrin) for the GC-MS. The investigation of a new ultrasonic extraction method for analysis of 24 herbicides and insecticides showed that this new USE was successful to recover all the selected substances with a good repeatability (S.D. between 1.5 and 19.3% with a median repeatability of 8.5%) in comparison with the European Norm DIN 12393 that could recover neither carbendazim nor metamitron and the PLE that could not recover carbendazim, metamitron and monolinuron at a $500\,ng\,g^{-1}$ fortification level. Nevertheless, the QuECheRS method presented the highest recoveries (median recovery of 72.7%) followed by the European Norm DIN 12393 (median recovery of 65.7%) and the PLE (median recovery of 63.5%) whereas the USE showed the lowest recovery (median recovery of 57.0%) of the four selected methods at a $500\,ng\,g^{-1}$ fortification level. Especially the pesticides with a water solubility lower than $5\,mg\,l^{-1}$ could not be extracted properly. The QuECheRS method was the most adapted method with around 50% of the substances with recoveries in the recommended range of 70–110%. Some substances presented recoveries as high as 150% with PLE implying the need for a cleaning step. The ultrasonic energy seems to be too low to extract the substances that either create bonds with humic substances or adsorb on the inter-crystalline layers of clay minerals. The European

Norm DIN 12393 and the PLE were proven to be not adapted for the extraction of polar pesticides. The EUROSOIL 7 presented the highest recoveries and the sea sand the lowest. For some substances (chlorpyrifos and chlorpyrifos-methyl for instances) the recoveries with the EUROSOIL 7 were much higher than with the SO 26. Atrazine, desethylatrazine and desisopropylatrazine presented low recoveries with almost all the methods.

This new USE method is accurate as monitoring method for the extraction of the selected pesticides from soil but cannot be implemented as currently applied as quantification method due to its low recovery for chorpyrifos, chlorpyrifos-methyl, deltamethrin, desethylatrazine, desisopropylatrazine, dieldrin, flufenoxuron, pencycuron and trifluraline. The QuECheRS method seems so far to be the most adapted method for these analyses. Nevertheless, another solvent like acetone for instances should be investigated with USE to increase the recoveries.

References

[1] Commission of the European Communities, Directive 91/414/EEC, Directorate General for Agriculture, DG VI B II-1, Brussels, Belgium, 1991.

[2] A. Tor, M. Emin Aydin, S. Özcan, Anal. Chim. Acta 559 (2006) 173.

[3] E. Concha-Graña, M.I. Turnes-Carou, S. Muniategui-Lorenzo, P. López-Mahía, D. Prada-Rodríguez, E. Fernández-Fernández, Chemosphere 64 (2006) 588.

[4] C. Gonçalves, M.F. Alpendurada, Talanta 65 (2005) 1179.

[5] G.H. Ludvigsen, O. Lode, in the 4th European Conference on Pesticides and Related Organics Micropollutants in the Environment, Almeria, Spain, 2006.

[6] J. Kreuger, S. Adielsson, in the 4th European Conference on Pesticides and Related Organics Micropollutants in the Environment, Almeria, Spain, 2006.

[7] D. Barceló, M.C. Hennion, Introduction, in Trace determination of Pesticides and their Degradation Products in Water, Elsevier, Amsterdam, NL, 1997.

[8] Commission of the European Communities, Directive 2000/60/EC, EU Water Framework Directive, Brussels, Belgium, 2000.

[9] A. Belmonte Vega, A. Garrido Frenich, J.L. Martinez Vidal, Anal. Chim. Acta 538 (2005) 117.

[10] V. Andreu, Y. Picó, TrAC 23 (2004) 772.

[11] US EPA method 3540C, US Government Printing Office, Washington, USA, 1996, available at: http://www.epa.gov/sw-846/pdfs/3540c.pdf.

[12] A. Mentler, H. Mayer, P. Strauß, W.E.H. Blum, Int. Agrophys. 18 (2004) 39.

[13] D. Lambropoulou, T.A. Albanis, Anal. Chim. Acta 514 (2004) 125.

[14] H. Mayer, A. Mentler, M. Papakyriacou, N. Rampazzo, Y. Marxer, W.E.H. Blum, Int. Agrophys. 16 (2002) 53.

[15] A. Bouaid, L. Ramos, M.J. Gonzalez, P. Fernández, C. Cámara, J. Chromatogr. A 939 (2001) 13.

[16] S. Babić, M. Petrović, M. Kaštelan-Macan, J. Chromatogr. A 823 (1998) 3.

[17] P. Popp, P. Keil, M. Möder, A. Paschke, U. Thuss, J. Chromatogr. A 774 (1997) 203.

[18] T. Dagnac, S. Bristeau, R. Jeannot, C. Mouvet, N. Baran, J. Chromatogr. A 1067 (2005) 225.

[19] J.L. Luque-García, M.D. Luque de Castro, J. Chromatogr. A 959 (2002) 25.

[20] T. Henriksen, B. Svensmark, R.K. Juhler, J. Chromatogr. A 957 (2002) 79.

[21] S. Marchese, D. Perret, A. Gentitli, R. Curini, A. Marino, Rapid Commun. Mass Spectrom. 15 (2001) 393.

[22] Y. Zhu, K. Yanagihara, F. Guo, Q.X. Li, J. Agric. Food Chem. 48 (2000) 4097.

[23] H. Dabrowska, L. Dabrowski, M. Biziuk, J. Gaca, J. Namieśnik, J. Chromatogr. A 1003 (2003) 29.

[24] O. Pozo, E. Pitarch, J.V. Sancho, F. Hernández, J. Chromatogr. A 923 (2001) 75.

[25] E. Börjesson, L. Torstensson, J. Chromatogr. A 886 (2000) 207.

[26] G. Shen, H.K. Lee, J. Chromatogr. A 985 (2003) 167.

[27] E.N. Papadakis, E. Papadopoulou-Mourkidou, J. Chromatogr. A 962 (2002) 9.

[28] L. Sun, H.K. Lee, J. Chromatogr. A 1014 (2003) 165.

[29] US EPA method 3550C, US Government Printing Office, Washington, USA, 2000, available at: http://www.epa.gov/sw-846/pdfs/3550c.pdf.

[30] DIN EN 12393 (1998).

[31] H.-J. Stan, J. Chromatogr. A 892 (2000) 347.

[32] M. Anastassiades, S. Lehotay, J. AOAC Int. 86 (2003) 412.

[33] C. Díez, W.A. Traag, P. Zommer, P. Marinero, J. Atienza, J. Chromatogr. A 1131 (2006) 11.

[34] C. Lesueur, M. Gartner, A. Mentler, M. Fuerhacker, Int. J. Environ. Anal. Chem. 87 (2007) 1013.

[35] Footprint Pesticide Properties Database, available at: http://www.herts.ac.uk/aeru/footprint/en.

[36] Ch. Weissteiner, A. Brandstetter, A. Mentler, H. Unterfrauner, W.W. Wenzel, W.H.E. Blum, in: B.M. Gawlik, H. Muntau (Eds.), EUROSOILS II, Laboratory Reference Materials for Soil-related studies, Office for Official Publications of the European Communities, 1999, pp. 57–68.

[37] Commission of the European Communities, Directive SANCO/10232/2006, Directorate of General Health and Consumer Protection, Brussels, Belgium, 2006.

[38] H.-P. Blume, Handbuch des Bodenschutzes, second ed., Ecomed, Landsberg, 1992.

[39] G. Rippen, Handbuch der Umweltchemikalien (Loseblattwerk), Ecomed, Landsberg, 1987.

[40] F. Scheffer, P. Schachtschabel, Lehrbuch des Bodenkunde, 15th ed., Spektrum Akademischer Verlag GmbH, Heidelberg, Berlin, 2002, pp. 398–399.

[41] F. Scheffer, P. Schachtschabel, Lehrbuch des Bodenkunde, 15th ed., Spektrum Akademischer Verlag GmbH, Heidelberg, Berlin, 2002, pp. 16– 17.

[42] C. Molins, E.A. Hogendoorn, H.A.G. Heusinkveld, A.C. van Beuzekom, P. van Zoonen, R.A. Baumann, Chromatographia 48 (1998) 450.

[43] H.G.J. Mol, M. Althuizen, H.-G. Janssen, C.A. Cramers, U.A.Th. Brinkman, J. High Resolut. Chromatogr. 19 (1996) 69.

Determination of chloride, chlorate and perchlorate by PDMS microchip electrophoresis with indirect amperometric detection

Xin-Ai Li [a,b], Dong-Mei Zhou [b], Jing-Juan Xu [a,*], Hong-Yuan Chen [a]

[a] *Key Lab of Analytical Chemistry for Life Sciences (MOE), School of Chemistry and Chemical Engineering, Nanjing University, Nanjing 210093, China*
[b] *State Key Laboratory of Soil and Sustainable Agriculture, Institute of Soil Science, Chinese Academy of Sciences, Nanjing 210008, China*

Abstract

In this work, chloride, chlorate and perchlorate are fast separated on PDMS microchip and detected via in-channel indirect amperometric detection mode. With PDMS/PDMS microchip treated by oxygen plasma, anions chloride (Cl^-), chlorate (ClO_3^-), and perchlorate (ClO_4^-) are separated within 35 s. Some parameters including buffer salt concentration, buffer pH, separation voltage and detection potential are investigated in detail. The separation conditions using 15 mM (pH 6.12) of 2-(*N*-morpholino)ethanesulfonic acid (MES) + L-histidine (L-His) as running buffer, −2000 V as separation voltage and 0.7 V as detection potential are optimized. Under this condition, the detection limits of Cl^-, ClO_3^-, and ClO_4^- are 1.9, 3.6, and 2.8 μM, respectively.
© 2007 Elsevier B.V. All rights reserved.

1. Introduction

Chlorine has extensive application in many fields. For example, it can be used for sterilization and disinfection of waters and wastes, and applied as a bleaching agent in the textile and paper industry. However, in these processes various anions such as chloride, chlorate and perchlorate are formed. These anions are considered to be dangerous to public health even at low levels. For instance, perchlorate is known to affect the production of thyroid hormones, which are considered critical to brain development. Chlorate is considered in the World Health Organization guidelines for drinking water quality, its provisional guideline value is 0.7 mg/L [1]. In addition, perchlorate has been added to the U.S. Environmental Protection Agency's Drinking Water Contaminant Candidate List (CCL) [2–4]. And chlorate is also "listed for regulation" by the U.S. EPA [5].

Ion chromatography is a common method for the detection of chloride, chlorate, and perchlorate. Biesaga et al. [6] have investigated the separation of some anions including the

three ions with indirect UV detection using 1 mM phthalate of pH 4.0 as eluents solutions. Stahl [6,7] and Poovey et al. [8] have respectively reported a single-column ion chromatographic determination of several chlorine-containing species in different eluents with conductivity detection. A microwave sample preconcentration technique is introduced to this method by Liu et al. [9] for the simultaneous determination of perchlorate, chlorate and chlorite in drinking water. Perchlorate can also be detected by electrospray ionization mass spectrometry [10,11]. However, the instruments are very expensive and their operation are discommodious. For many years, capillary electrophoresis has been developed as an alternative method with a lot of advantages, such as limited consumption of sample, short analysis time, high-separation efficiency. And it has been applied to the determination of chlorine-containing anions [6,14–17].

In the CE determination of chlorine-containing anions, indirect ultraviolet–vis absorption spectrometry is the most popular detection mode, but it suffers from the lack of sensitivity when miniaturized for the use in micro-CE [12,13]. Jones and Jandik [6,14,15] have shown the possibility of CE separation of 36 different anions using chromate electrolyte with indirect UV detection, including several chlorine-containing anions. Wu et al. [16] and Pirogov [17] both applied this method to determine

---

chlorine-containing anions and several other anions, and they respectively used 0.4 mM cetyltrimethylammonium bromide (CTAB) and 0.05% 2,4-ionenes as capillary modifiers. In addition, electrochemical detection is an alternative method because of its excellent sensitivity compared with optical detection when miniaturized in CE [18–20]. It includes three electrochemical detection techniques, i.e., amperometric, potentiometric, and conductometric detection techniques. However, these techniques generally suffer from interferences due to the presence of the CE separation voltage which drives fluids to flow.

In our previous work, we established a new in-channel indirect amperometric detection mode for microchip CE, in which the negative effect of separation electric field has been transformed into a new universal approach [21]. This detection method has been successfully used to detect alkali metal ions, heavy metal ions, some inorganic anions and native amino acid, as well as EOF rates [21–25]. The aim of the present work is to establish a simple, cheap and fast micro-CE–EC system for the analysis of these chlorine-containing anions.

2. Experimental

2.1. Materials

Sylgard 184 (PDMS) was purchased from Dow Corning (Midland, MI, USA). Histidine (His) and 2-(N-morpholino) ethanesulfonic acid (MES) were purchased from Sigma (St. Louis, MO, USA). $LiClO_4$, $NaCl$, $NaClO_3$, and CH_3COOH with analytical grade were purchased from Shanghai Chemical Reagents Factory (Shanghai, China). The electrolyte solutions were prepared from stock solutions of 40 mM 2-(N-morpholino)ethanesulfonic acid (MES) and 40 mM L-histidine (L-His). The pH of all electrolytes was adjusted with 10% (v/v) acetic acid (Shanghai, China). Stock solutions (10 mM) of Cl^-, ClO_3^- and ClO_4^- were prepared from their salts and then stored in a refrigerator. Solution of chlorate was prepared once a week, whereas solutions of chloride and perchlorate were prepared once a month. Before use, the analytes were diluted with corresponding running buffer solutions. In addition, all solutions were degassed in an ultrasonic bath for 5 min and passed through a 0.22 μm cellulose acetate filter (Xinya Purification Factory, Shanghai, China). Hypodermic needles were used to introduce the buffer and solutions into the microchip reservoirs. All other chemicals were of reagent grade and doubly distilled water was used throughout.

2.2. Instrumentation

The integrated CE–EC PDMS microsystem was similar to that described previously [23,25]. It comprised a home-made negative HV power provided an adjustable voltage range between 0 and −5000 V. Parameters including sampling voltage, sampling time, separation voltage, and separation time could be set up and automatically switched via a RS232 communication port of PC through a home-made computer program. The current in the microchannel could be monitored graphically in real time.

The simple-cross single-separation channel PDMS microchip was made based on a master composed of a positive relief structure of GaAs made in No. 55 Electronic Institute (Nanjing, China) by using standard microphotolithographic technology and reaction ion etching. The chip had a 40-mm long separation channel (from injection cross to the channel outlet) and a 5-mm long injection channel (between the sample reservoir and injection cross). The channels had a maximum depth of 18 μm and a width of 50 μm. Before use, the PDMS layer with microchannel and the PDMS flat should be ultrasonically cleaned subsequently with acetone, methanol and water for 20 min each and were then dried under infrared lamp. Then they were sealed together directly or after oxygen plasma (PDG-32G, Harrick Plasma, USA) treatment to form a requisite PDMS microchip.

A plexiglass holder that integrated a precisely three-dimensional system (Shanghai Lian Yi Instrument Factory of Optical Fibre and Laser, China) was for emplacing the PDMS microchip. A clip of optical fiber that can be fastened in the three-dimensional system, was used to closely clip the carbon fiber micro-cylinder electrode. Platinum wires, inserted into the individual reservoirs on the holder, served as contacts to the HV power supply.

A computer-controlled potentiostat-function generator system Model CHI-660A from CH Instruments, Shanghai, China, was used in all the electrochemical tests. The working microelectrodes were single carbon fiber cylinders with diameter of 8 μm. All the microelectrodes were home-made, according to the method reported in the literatures [18,26]. First, a glass capillary with an inner diameter of 0.5 mm was pulled to form a fine tip. And then a single carbon fiber with diameter of 8 μm was carefully mounted into the tip and fixed with epoxy. A copper wire was connected with the carbon fiber through carbon powder on the other end of capillary and then fastened on the capillary with epoxy. Before use, the tip of the protruded carbon fiber was cut with a clean scalpel to form a 1 mm cylinder electrode under a microscope.

2.3. Procedure

In all electrochemical tests, a three-electrode configuration was used. The reference, the auxiliary, and the working electrode were an Ag/AgCl reference, a Pt wire, and a single carbon fiber cylinder microelectrode, respectively. After the microchip was held on a plexiglass holder, a working electrode was inserted into the electrode hole on the platform and then pegged on the 3D system. The working electrode was treated at +1.5 V for 200 s and then −1.0 V for 200 s in 15 mM MES + His (pH 6.12) buffer before use and once the baseline current obviously changed. The electropherograms were recorded at a fixed detection potential with the end of the working electrode located in the separation channel for about 20 μm from the exit. Then the running buffer reservoir was filled with the buffer and the sample reservoir with the sample mixture diluted by the buffer. The injections were performed by applying a desired potential for 5 s to the sample reservoir with the detection reservoir grounded while all other reservoirs floating. Separations were

performed by switching the HV contacts and applying the corresponding separation voltages to the running buffer reservoir with the detection reservoir grounded and all other reservoirs floating. All experiments were performed at room temperature.

3. Results and discussion

3.1. Effect of the oxygen plasma treatment

PDMS was the most widely used polymer for fabricating microchip in the last few years because of its well-known good properties such as easy fabrication using a replica molding process, high-chemical resistance, optical transparency, nontoxicity and good elasticity. However, its application in microfluidics has been limited due to its hydrophobic nature. Using oxygen plasma to treat the PDMS microchip is an effective approach to create hydrophilic surfaces and to irreversibly bind the PDMS microchip together. The surface of PDMS microchip changed to silicon hydroxy after oxygen plasma treatment. EOF is a useful parameter to investigate surface modification. Fig. 1 shows the relationship between EOF and pH (in acidic condition) on the oxygen plasma treated chip (OP-chip) and native PDMS chip in 15 mM MES + L-His buffer. The pH greatly influenced the EOF of OP-chip and native PDMS microchip. The EOF of OP-chip increased with the increase of pH as a whole and suppressed by about two times compared with that of native PDMS chip. This phenomenon is different from our previous results in 10 mM borate buffer [27]. In that work, the EOF of OP-chip enhanced doubly than that of native PDMS chip. This difference may be due to the different running buffer used.

As we know, MES is an ampholytic surfactant which is commonly used as biological buffer in capillary electrophoresis. This surfactant has both apolar and polar parts. It is expected that its hydrophobic parts compete with analytes for hydrophobic sites on PDMS surface, while its hydrophilic part stretches out of the surface and changes the surface charge density. In order to eliminate the adsorption or absorption of analytes in the PDMS separation channel, the surfactant MES was used to dynamically
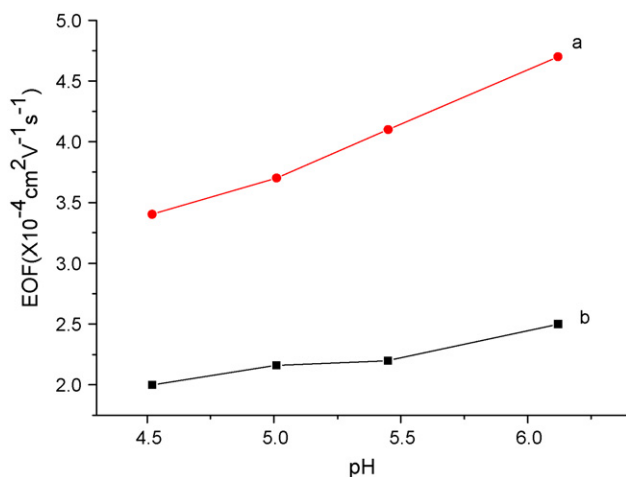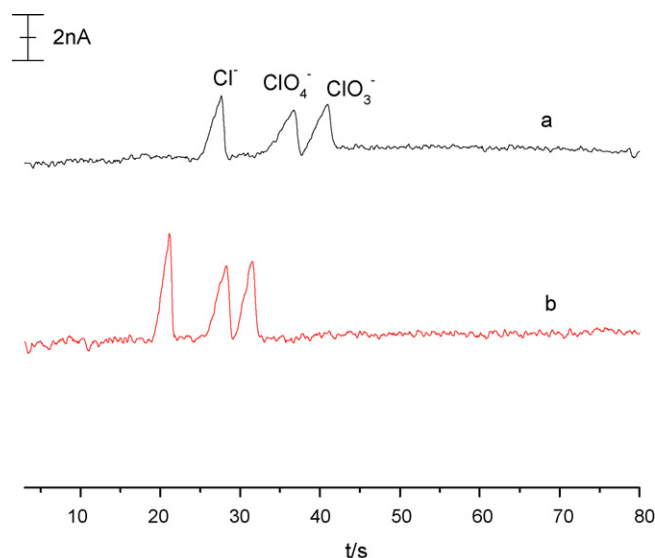

Fig. 2. Electropherograms of 0.5 mM chloride, chlorate and perchlorate anions with (a) native microchip and (b) microchip after oxygen plasma treatment. Experimental parameters: running buffer solution, 15 mM MES + L-His, pH 6.12; sampling voltage, 800 V; sampling time, 5 s; separation voltage, −1800 V; detection potential, 0.6 V.

modify the PDMS surface in NaOH solution in our previous work [28]. Regulating the surfactant's proportion can control the EOF. The EOF is decreased with increased MES concentration in the running buffer. When the microchip was treated by the oxygen plasma, the interaction between MES and the PDMS was not only the hydrophobic interaction, but also the hydrogen bond due to the increased silicon hydroxyl groups. Thus the EOF decreased in OP-chip.

Fig. 2 shows the electropherograms of 0.5 mM chloride, chlorate and perchlorate anions in native microchip and OP-chip in negative separation electric field. The migration time of anions apparently decreased after oxygen plasma treatment, which also indicated that the electro-osmotic flow decreased by the treatment due to the opposite EOF and electrophoretic flow. In addition, the peak height increased in OP-chip with the half-peak width decreased, indicating that the oxygen plasma treatment is in favour of the enhancement of signal-to-noise ratio. The sequence of migration of the three anions were in accord with the mobility of appropriate acid given in by Hirokawa et al. [29] (79.1×10^5, 69.8×10^5 and 67.0×10^5 cm^2 V^{-1} s^{-1} for hydrochloric, perchloric and chloric acid, respectively).

3.2. Effect of the buffer pH

The choice of buffer pH was an important factor for the separation of analytes. Microchip capillary electrophoresis was the same as traditional capillary electrophoresis, in which the separation medium pH influenced the ξ potential of the interior of capillary, EOF rate, the migration time and separation efficiency of analytes, even the speciation of analytes. Fig. 3 shows that the resolution of chlorate and perchlorate were gradually diminished by the decrease of solution pH. It may be due to the decreased EOF and the similar mobility of ClO_4^- and ClO_3^-. While, it

Fig. 1. Influence of the MES + L-His (15 mM) buffer pH on EOF. (a) Native microchip and (b) microchip after oxygen plasma treatment.
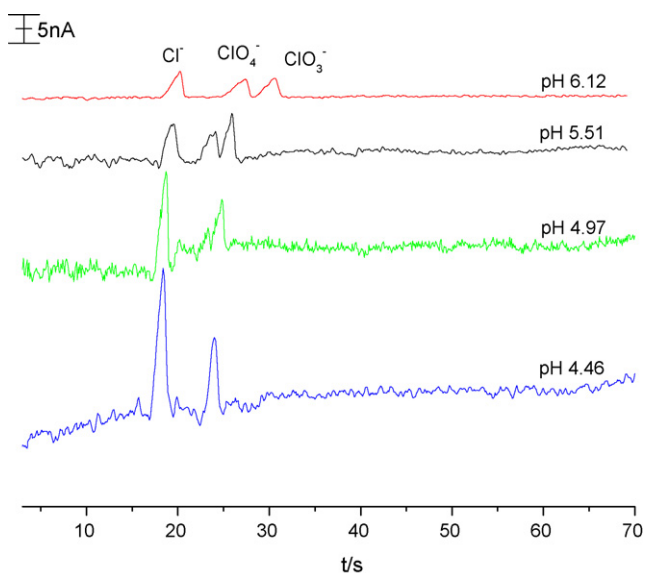
Fig. 3. Electropherograms of 0.5 mM chloride, chlorate and perchlorate anions in different pH buffers. Other experimental parameters same as in Fig. 2.

could be observed that the peak height clearly increased. Since the signal is resulted from the difference of coupling degree of CE voltage to the oxidation potential of carbon fibre itself under a negative separation electric field, the separation current is an essential factor to influence the detection signal. With the decrease of buffer pH from 6.12 to 4.46, the separation current increased from 2.4 to 4.2 μA, indicating the enhancement of the coupling degree. Fig. 4 shows the linear scanning voltammo-grams of a carbon fiber electrode in the separation channel with the presence and absence of negative separation voltages in different pH buffers at a scan rate of 20 mV/s. In the absence of separation electric field, the linear scanning voltammograms of the carbon fiber electrode have no obvious change in different pH buffers. When −1800 V separation voltage was applied, the oxidation current greatly increased with the buffer pH decrease, which also approved that the coupling degree increased with the decrease of buffer pH. Thus the signal increased with the
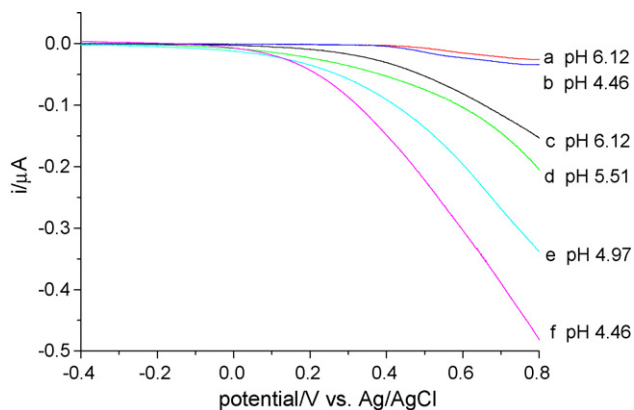

Fig. 4. Linear scanning voltammograms of a carbon fiber electrode in the separa-tion channel with the absence (a and b) and presence (c–f) of negative separation voltage (−1800 V) in different pH buffer at a scan rate of 20 mV/s. Experimental parameters: running buffer solution, 15 mM MES + His.
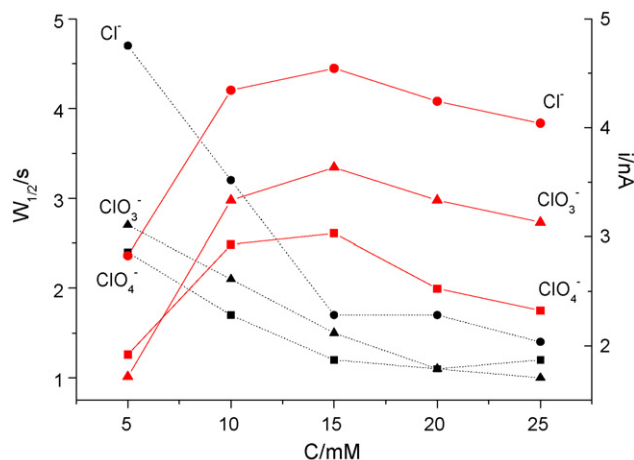

Fig. 5. The effects of the buffer concentration on the half-peak widths (dot) and the peak heights (line). Other experimental parameters same as in Fig. 2.

decrease of the buffer pH. However, the baseline become more and more unsteady with the buffer pH changed from 6.12 to 4.46. Synthetically considering these factors of separation efficiency and detection sensitivity, pH 6.12 was chosen for the following experiments.

3.3. Effect of the buffer salt concentration

The difference of conductivity between the sample plug and the running buffer is also an essential factor to influence the detection signal. Thus we investigated the effect of the buffer salt concentration (from 5 to 25 mM) on the separation and detection (shown in Fig. 5). It was observed that the peak height increased when the buffer salt concentration changed from 5 to 15 mM and then decreased with the further increase of the buffer salt concentration. There may be two reasons. On one hand, higher concentration of the running buffer could bring electrostacking for the carrier electrolytes with a low-mobility co-ion, which causes relatively higher concentration of the sample plug and then a relatively high signal. On the other hand, higher concen-tration of the running buffer will result in higher ion strength and joule heat, which decrease the difference of conductivity between the buffer salt and the sample plug and then result in a low signal. Meanwhile, the half-peak width of the anions decreased with increasing of the running buffer concentration because of the peak dispersion in low buffer concentrations. Thus 15 mM MES + His buffer solution was selected.

3.4. Effect of the separation voltage

Fig. 6 exhibits the effect of the separation voltages on the half-peak width and peak height of 0.5 mM Cl^-, ClO_3^- and ClO_4^-. The half-peak widths decrease and the peak heights increase with the increase of separation voltage. The migration time of the three anions decreased with the increase of sepa-ration voltage. It was due to the EOF and electrophoretic flow in the opposite direction, in which the rate of electrophoretic flow increased rapidly compared with the increase of EOF with the increase of separation electric field. When separation
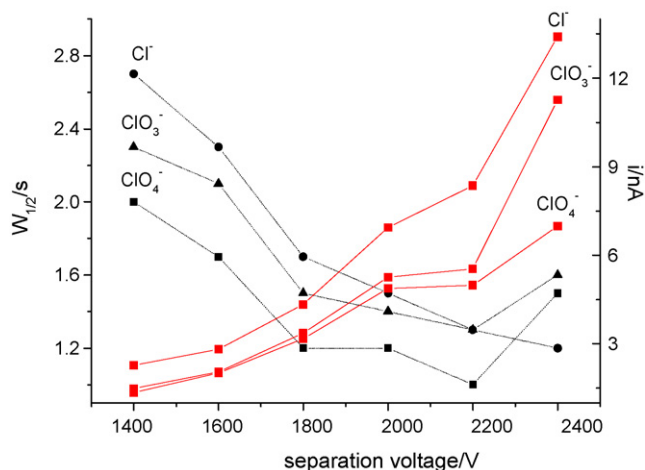
Fig. 6. The effects of the separation voltage on the half-peak widths (dot) and the peak heights (line). Other experimental parameters same as in Fig. 2.

voltage was more negative than −2000 V, the baseline become more and more unsteady and resolutions of ClO_3^- and ClO_4^- gradually decreased. Furthermore, higher separation potential would produce air bubble and consequently resulted in clogging of the channel. Thus, the separation voltage of −2000 V was a good choice for the detection of these chlorine-containing anions.

3.5. Effect of detection potential

The influence of the detection potential applied to the carbon fiber electrode was also important to the determination of analytes with electrochemical detection. Fig. 7 shows the influence of detection potential on the signal. The current response increased obvious with the increase of detection potential while the baseline becomes unsteady because of a large noise in higher potential. By increasing the detection potential, the peak became broadly and the resolution of analytes decreased. A better detection potential for the analysis was 0.7 V.
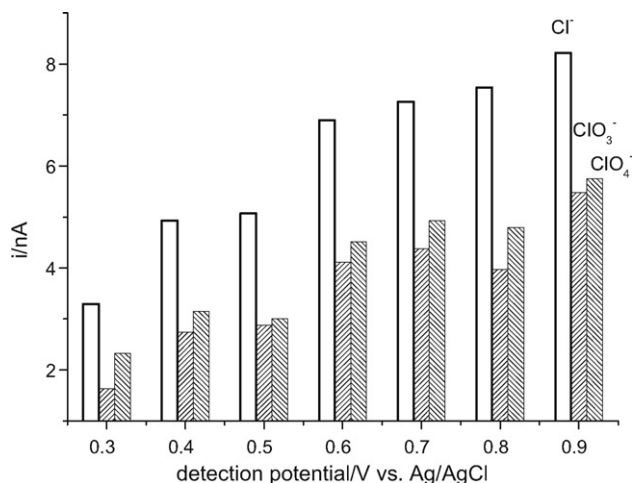

Fig. 7. The relationship between the peak heights and the detection potentials. Other experimental parameters same as in Fig. 2.
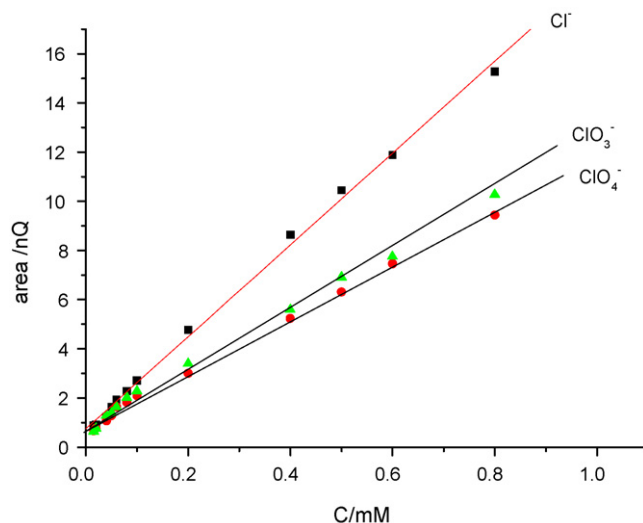

Fig. 8. The linear relationship between the detection signal of the three anions and different concentrations. Experimental parameters: running buffer solution, 15 mM MES + L-His, pH 6.12; sampling voltage, 800 V; sampling time, 5 s; separation voltage, −2000 V; detection potential, 0.7 V.

3.6. Linear range and detection limit

The in-channel indirect amperometric detection could successfully used for the determination of several chlorine-containing anions. According to the above studies, optimized conditions of −2000 V separation voltage, 0.7 V detection potential, 15 mM (pH 6.12) running buffer of MES + L-His were selected. Under the conditions, linear ranges of peak area from 15.0 to 0.8 mM were obtained for Cl^-, ClO_3^-, and ClO_4^-, and correlation coefficients were 0.9987, 0.9984 and 0.9970, respectively (Fig. 8). The detection limits for Cl^-, ClO_3^-, and ClO_4^- were estimated to be 1.9, 3.6, and 2.8 μM (S/N = 3), respectively. Furthermore, the microchip indirect amperometric detection system showed a good reproducibility and stability. The R.S.D. (%) of migration time (n = 6) for run-to-run, day-to-day and chip-to-chip are 0.8, 1.2, 1.2 for Cl^-, 1.2, 1.7, 1.2 for ClO_3^-, 0.9, 1.2, 0.9 for ClO_4^-, respectively.

4. Concluding remarks

In conclusion, three chlorine-containing anions have been successfully separated and detected with a simple indirect amperometric detection mode in a PDMS microchip by oxygen plasma treatment. Experimental results showed that the separation efficiency and detection sensitivity can be controlled by many factors such as buffer pH, concentration, separation voltage and detection potential, etc. Such a micro-CE–EC system provides a simple and fast analysis platform for non-electroactive ions and may have wide applications.

Acknowledgements

References

[1] Chlorite and chlorate in drinking water, http://www.who.int/water_sanitation_health/dwq/chemicals/chloritechlorate/en/.

[2] L.M. Matthew, T.U. Edward, A.K. Catherine, Anal. Chem. 72 (2000) 25.

[3] Health Advisories for Drinking Water Contaminants, Office of Water Health Advisories, U.S. Environmental Protection Agency, Washington, DC, 1998.

[4] Environmental Protection Agency Status Report on Development of Regulation for Disinfectants and Disinfection By-products, U.S. Environmental Protection Agency, Washington, DC, 1991.

[5] Fed. Regist. 63 (1998) 10274.

[6] M. Biesaga, M. Kwiatkowska, M. Trojanowicz, J. Chromatogr. A 777 (1997) 375.

[7] R. Stahl, Chromatography 37 (1993) 300.

[8] H.G. Poovey, R.J. Rando, J. Liq. Chromatogr. 18 (1995) 261.

[9] Y.J. Liu, S.F. Mou, B. Du, A.W. Lin, Chin. J. Chromatogr. 20 (2002) 129.

[10] M.L. Magnuson, E.T. Urbansky, C.A. Kelty, Anal. Chem. 72 (2000) 25.

[11] C.J. Koester, H.R. Beller, R.U. Halden, Environ. Sci. Technol. 34 (2000) 1862.

[12] C.J. Evenhuis, R.M. Guijt, M. Macka, P.R. Haddad, Electrophoresis 25 (2004) 3602.

[13] C. Vogt, G.L. Klunder, Fresen. J. Anal. Chem. 370 (2001) 316.

[14] W.R. Jones, P. Jandik, J. Chromatogr. 546 (1991) 445.

[15] W.R. Jones, P. Jandik, J. Chromatogr. 608 (1992) 385.

[16] M.J. Wu, H.X. Ren, Chin. J. Anal. Chem. 24 (1996) 1178.

[17] A.V. Pirogov, A.V. Yur'ev, O.A. Shpigun, J. Anal. Chem. 58 (2003) 781.

[18] I. Poels, L.J. Nagels, Anal. Chim. Acta 385 (1999) 417.

[19] J. Wang, Talanta 56 (2002) 223.

[20] J. Wang, Electrophoresis 17 (2005) 1133.

[21] J.J. Xu, N. Bao, X.H. Xia, Y. Peng, H.Y. Chen, Anal. Chem. 76 (2004) 6902.

[22] J.J. Xu, Y. Peng, N. Bao, X.H. Xia, H.Y. Chen, Electrophoresis 26 (2005) 3615.

[23] J.J. Xu, Y. Peng, N. Bao, X.H. Xia, H.Y. Chen, J. Chromatogr. A 1095 (2005) 193.

[24] N. Bao, J.J. Xu, Q. Zhang, J.L. Hang, H.Y. Chen, J. Chromatogr. A 1099 (2005) 203.

[25] X.A. Li, D.M. Zhou, J.J. Xu, H.Y. Chen, Talanta 71 (2007) 1130.

[26] P. Kubáň, P. Kubáň, V. Kubáň, Electrophoresis 23 (2002) 3725.

[27] Y. Xiao, X.D. Yu, K. Wang, J.J. Xu, J. Huang, H.Y. Chen, Talanta 71 (2007) 2048.

[28] Y.H. Dou, N. Bao, J.J. Xu, H.Y. Chen, Electrophoresis 23 (2002) 3558.

[29] T. Hirokawa, M. Nishimo, N. Aoki, Y. Kiso, Y. Sawamoto, T. Yagi, J. Akiyama, J. Chromatogr. 271 (1983) D1.

Flow-injection chemiluminescence determination of polyphenols using luminol–NaIO$_4$–gold nanoparticles system

Shifeng Li, Xiangzi Li, Jing Xu, Xianwen Wei *

*College of Chemistry and Materials Science, Anhui Key Laboratory of Functional Molecular Solids,
Anhui Normal University, Wuhu 241000, PR China*

Abstract

It was found that gold nanoparticles with different sizes could enhance the chemiluminescence (CL) of the luminol–NaIO$_4$ system in alkaline solution. The most intensive CL signals were obtained with gold nanoparticles in diameter of 4 nm and the CL intensity increased linearly with the concentration of gold nanoparticles. The studies of UV–vis spectra, CL spectra, effects of concentrations of luminol and periodate solution were carried out to explore the CL enhancement mechanism. Catechol, hydroquinone and resorcinol were found to inhibit the CL signals of the luminol–NaIO$_4$ reaction catalyzed by gold nanoparticles, which made it applicable for the determination of these polyphenols. Under the selected experimental conditions, the detection limits (3σ) were in the range of 2.1×10^{-9} to 1.0×10^{-10} g ml^{-1}, the relative standard deviation (R.S.D., $n = 11$) were in the range of 1.7–2.9%. The method has been successfully applied to the determination of catechol in tap water and synthesized samples with satisfactory results.
© 2008 Published by Elsevier B.V.

Keywords: Chemiluminescence; Gold nanoparticles; Luminol; Polyphenol

1. Introduction

Polyphenols are biologically and environmentally important compounds. Some of them are found in plants, wines, water, etc., which have important physiological functions and some pharmacological activities; and some of them are used in cosmetics, tanning, components of insecticides, herbicides, synthetic fibers, pharmaceutical industry and developing photographs. On the other hand, they are the environmental pollutants [1]. Therefore, the development of a highly sensitive and selective method for the determination of polyphenols in food testing, biological studies, toxicity analysis and environmental monitoring is of great importance. The methods for determination of polyphenols are mainly based on spectrophotometry [2–6], fluorescence [7–10], electroanalytical method [11] and high-performance liquid chromatography (HPLC) [12–18]. These methods have their respective advantages, also exist some different shortcomings,

such as insufficient sensitivity, high commercial price, time-consuming procedure or not being suitable for automatic and continuous analysis.

Flow-injection chemiluminescence (CL) method is known to be a useful analytical technique because of its low detection limit, wide linear dynamic range, relatively low cost instrumentation [19–27]. Recently using nanoparticles, especially metal nanoparticles, as catalysts for the chemiluminescence system has attracted considerable interest [28–30]. Cui and co-workers [28] have found that gold nanoparticles with a size regime from 6 to 99 nm could enhance the CL from the luminol–H$_2$O$_2$ system, and that the enhancement was supposed to originate from the catalysis of gold nanoparticles. We extended this method to the luminol–NaIO$_4$ system and found that gold nanoparticles of different sizes in the range of 4–16 nm could enhance the chemiluminescence from luminol–NaIO$_4$ system in alkaline media. Catechol, hydroquinone and resorcinol were observed to inhibit the CL signal of the luminol–NaIO$_4$–gold nanoparticles, which made it applicable for the determination of such compounds in the tap water with satisfactory results.

* Corresponding author. Tel.: +86 553 3937138; fax: +86 553 3869303.
E-mail address: sfli@mail.ahnu.eu.cn (X. Wei).

2. Experimental

2.1. Reagents and materials

All chemicals and reagents were of analytical grade and used without further purification; and the deionized and triple-distilled water was used throughout.

A 2.5×10^{-2} mol l^{-1} stock solution of luminol (3-aminophthalhydrazide) was prepared by dissolving luminol (Fluka) in 0.1 mol l^{-1} sodium hydroxide solution without purification. Working solutions of luminol were prepared by diluting the stock solution. Periodate stock solution 1.0×10^{-2} mol l^{-1} was prepared by dissolving 0.2139 g NaIO$_4$ (Shanghai Chemical Reagent Plant, China) in 0.01 mol l^{-1} sodium hydroxide solution, and stored in a brown bottle to avoid photochemical decomposition. HAuCl$_4$·4H$_2$O (48%, w/w) was obtained from Sinopharm Group Chemical Reagent Co. Ltd. (Shanghai, China). A 4.0 g l^{-1} HAuCl$_4$ stock solution was prepared by dissolving 1 g of HAuCl$_4$ in 250 ml of triple-distilled water and stored at 4 °C. A 1% (w/w) trisodium citrate (Na$_3$C$_6$O$_7$) solution and 0.075% sodium hydroborate (NaBH$_4$)–1% (w/w) trisodium citrate (Na$_3$C$_6$O$_7$) solution were prepared by dissolving trisodium citrate, hydroborate (Shanghai, China) solids in triple-distilled water. The stock solutions of 1.0×10^{-4} g ml^{-1} polyphenols were all stored in a refrigerator at 0–4 °C to avoid long exposure to light and air before use.

2.2. Synthesis of gold nanoparticles

Colloidal gold nanoparticles with 4 and 6.0 nm in diameters were synthesized by the hydroborate reduction method according to the literature [31]. For the synthesis of 6.0 nm gold colloids, 100 ml of HAuCl$_4$ (10^{-2}%, w/w) solution were mixed with 0.40 ml of 1% trisodium citrate and 0.15 ml of 0.075% NaBH$_4$–1% trisodium citrate solution whilst stirring vigorously at room temperature. The mixed solution was stirred for 30 min and then stored at 4 °C. Similar procedures were adopted for the synthesis of 4.0 nm gold colloids, except that the volumes of trisodium citrate solution and NaBH$_4$–trisodium citrate solution were 1.0 ml.

Colloidal solution of 16 nm diameter gold nanoparticles were synthesized by the citrate reduction method according to the ref. [32]. A 50 ml portion of HAuCl$_4$ (10^{-2}%, w/w) solution was heated to boiling. While stirring vigorously, 1 ml of 1% trisodium citrate was added rapidly. The solution was maintained at the boiling point for 15 min, during which time a color change from gray to blue to purple was observed before a wine-red color was reached. The heating source was removed, and the colloid was kept at room temperature for 15 min and then stored at 4 °C. The average diameter of the synthesized gold particles was measured by transmission electron microscope (TEM).

2.3. Apparatus

The CL measurements were conducted on a model IFFM-E flow-injection CL analysis system (Xi'an, China). A pHS-3B meter (Leici, Shanghai) was used for pH measurement. The CL spectra of this system was recorded with a Hitachi FL-4500 spectrofluorometer (Tokyo, Japan) combined with a flow-injection system, whose excitation light source being turned off. Fluorescence spectra, UV–visible spectra were measured on the model FL-4500 spectrofluorometer (Tokyo) and a model U-4100 UV–vis spectrophotometer (Hitachi), respectively. TEM images were taken using an H-800 transmission electron microscope (Hitachi), with an accelerating voltage of 200 kV.

2.4. Procedures

A diagram shown in Fig. 1 illustrates the flow-injection chemiluminescence detection system employed in this work. The solutions of luminol, NaIO$_4$ and carrier water were pumped into the flow cell by the peristaltic pump at the rate of 3.0 ml min^{-1}, respectively. The gold colloid solution was injected by a valve injector with a sample loop of 100 μl. The light output from the CL reaction was detected and amplified by the PMT and luminometer. The signal was imported to the computer for data acquisition. The net CL intensity $\Delta I = I_s - I_0$ was used for the quantitative determination, where I_s and I_0 were the CL intensity of sample and blank solutions, respectively.

3. Results and discussion

3.1. CL kinetic characteristics

The kinetic prorate of the reaction plays an important role in the design of CL flow system. It was found that the present
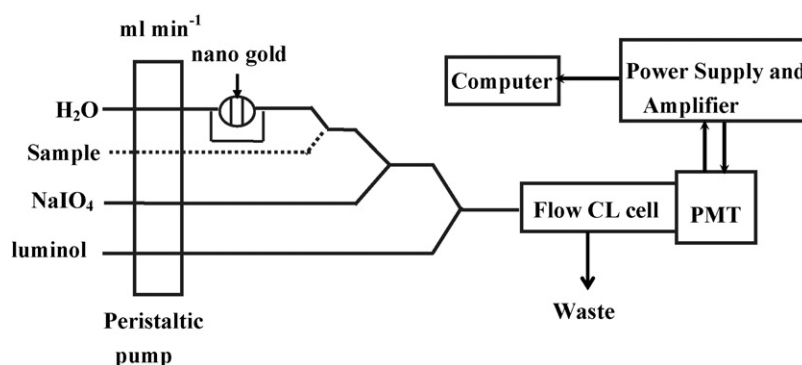

Fig. 1. A diagram of the flow-injection chemiluminescence detection system.
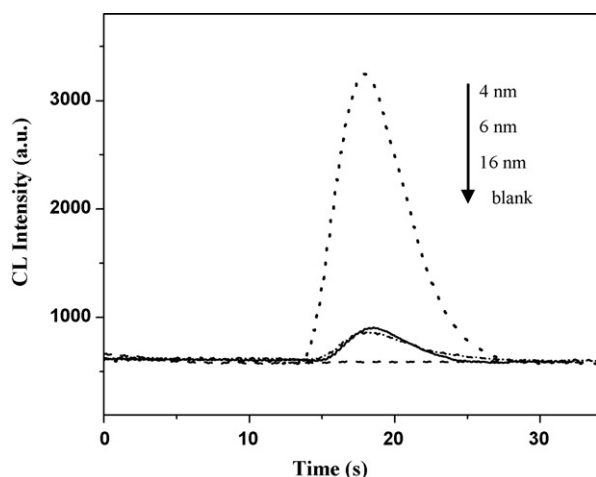
Fig. 2. Kinetic characteristics of the luminol–NaIO$_4$–gold colloids CL system. Luminol solution: 1.0×10^{-4} mol l^{-1}, pH 12.7; NaIO$_4$ solution: 5.0×10^{-4} mol l^{-1}, 0.03 mol l^{-1} NaOH; gold colloids: 2.5×10^{-6} g ml^{-1}; blank: luminol–NaIO$_4$ CL system.

reaction goes fast, only 3 s was needed for the maximum peak to appear, and it took 8 s for the signal to decline to the basement. The effects of gold colloids on the luminol–NaIO$_4$ chemiluminescent system were investigated. As shown in Fig. 2, the CL signal was enhanced by the 4–16 nm diameter gold nanoparticles, and the most intensive CL signal was obtained with the gold nanoparticles in diameter of ca. 4 nm.

3.2. Effect of pH of luminol solution

It is well known that the CL of the luminol–NaIO$_4$ system occurs in alkaline mediums. Various buffer solutions (NaH$_2$PO$_4$–Na$_2$HPO$_4$, NaHCO$_3$, Na$_2$CO$_3$, NaHCO$_3$–Na$_2$CO$_3$, NaOH–Na$_2$HPO$_4$, NaOH–Na$_2$CO$_3$, NaOH) at 0.02 mol l^{-1} were examined and the strongest CL signal was obtained in NaOH medium. The pH of the luminol solution influenced on the increased CL reaction was investigated over the range of 11.0–13.5. When the pH of luminol solution was lower than pH 12.7, both the CL intensity (S) and the noise (N) increased dramatically. Therefore, the ratio of the peak height of CL signal to noise (S/N) was used for the optimization of the concentration of NaOH in luminol solution. The relative CL intensity reached the maximum and the highest ratio of S/N was obtained when pH of 12.7.

3.3. Effect of luminol concentration

The effect of the concentration of luminol on the increased CL intensity was examined in the range of 7.5×10^{-4} to 1.0×10^{-5} mol l^{-1}. The results showed that the CL intensity increases with the increase of luminol concentration, however, the CL intensity of the blank become very strong when the concentration of luminol was higher than 1.0×10^{-4} mol l^{-1} and led to poor reproducibility. Considering the CL intensity and the consumption of the reagents, the concentration of luminol solution was adjusted to 1.0×10^{-4} mol l^{-1} for consequent research work.

3.4. Effect of media and concentration of NaIO$_4$

The effect of NaOH concentration on the increased CL reaction was examined from 0.02 to 0.15 mol l^{-1}. The maximum CL signal was obtained when 0.03 mol l^{-1} NaOH was used. Lower or higher concentration of NaOH caused a decrease of the CL signal. Therefore, 0.03 mol l^{-1} NaOH was employed for further studies.

The effect of NaIO$_4$ concentration in the range 7.5×10^{-5} to 1.0×10^{-3} mol l^{-1} on the CL intensity has been examined. It was found that the relative CL intensity increased then got a maximum by increasing NaIO$_4$ concentration up to 5.0×10^{-4} mol l^{-1}. With lower concentrations of NaIO$_4$, net CL intensity was weak. With higher concentrations of NaIO$_4$, net CL intensity decreased dramatically. Therefore, 5.0×10^{-4} mol l^{-1} NaIO$_4$ was chosen as the optimum concentration for further experiments.

3.5. Effect of flow rate

The effect of flow rate on the CL reaction was also examined. The relative CL intensity continued to increase with increasing the flow rate from 1.0 to 3.5 ml min^{-1}, probably because the reaction was very fast. But a high flow rate might lead to the irreproducibility and excess consume of the reagents. Finally, 3.0 ml min^{-1} of flow rate was chosen by considering the sensitivity, reagents consumption and reproducibility.

3.6. Mechanism discussion

In order to explore the possible mechanism, the UV–visible absorption spectra were recorded. As shown in Fig. 3, it can be seen that 4 nm gold colloids had a maximum absorption peak at around 506 nm, and the luminol–NaIO$_4$ system had two absorption peaks at 300 and 346 nm. Nevertheless, the light absorption of the mixed system was approximately equal to the sum of the light absorption of the two individual systems, which implied
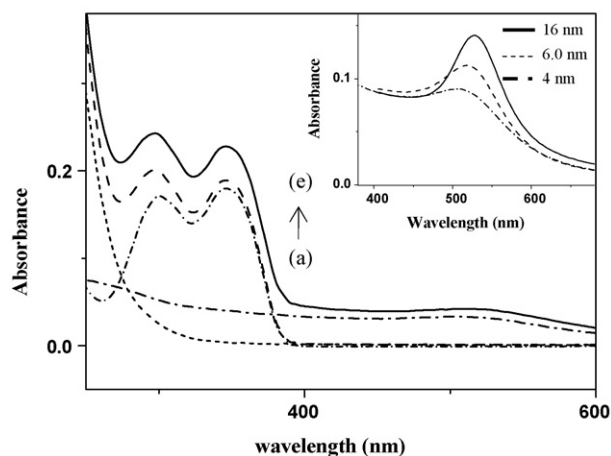

Fig. 3. UV–visible absorption spectra of (a) NaIO$_4$; (b) gold colloids (4 nm); (c) luminol; (d) luminol–NaIO$_4$; (e) luminol–NaIO$_4$–gold colloids CL system. (Inset) UV–visible absorption for gold colloids with different sizes.

that no change was taken between the species after the reaction. Therefore, the enhancement of CL signals may have originated from the catalytic effects of gold nanoparticles [28]. In this case, the gold nanoparticles still remain after the CL reaction. It is well known that the rate of heterogeneous catalysis increases with the available active surface area of the catalyst. Therefore, a higher number of particles of smaller size would be present in a given mass of catalyst material, leading to a higher rate of catalytic reaction. The active surface areas of the gold nanoparticles decreased with increasing particle size, and the catalytic efficiency of the gold nanoparticles decreased accordingly.

Thus, the CL emission spectrum of the system was obtained using the modified FL-4500 spectrofluorimeter, with the light source taken off, combined with a flow-injection system. The luminol-based CL reaction is a well-known method for the detection of reactive oxygen species, such as O_2^-, $^1O_2$ and H_2O_2, because these species react quickly with luminol in alkaline solution to emit light, as the hydroperoxide intermediate of luminol decomposes into aminophthalate [33–35]. The results (Fig. 4) showed that the maximum wavelengths of CL emission enhanced by gold nanoparticles were 425 nm. It is well known that 3-aminophthalate (3-APA[*]) is the luminophor of the system of luminol-periodate, and the maximum emission of CL reaction is at 425 nm. So the CL emitter in the both CL reactions between luminol and periodate with and without gold nanoparticles is the same species, which is the oxidation product of luminol.

It has been reported that superoxide radical ions ($O_2^{\bullet-}$) can be obtained by reaction of periodate with oxygen in alkaline solution [36]. Because the reaction of luminol with periodate in alkaline solution in the absence of a catalyst underwent
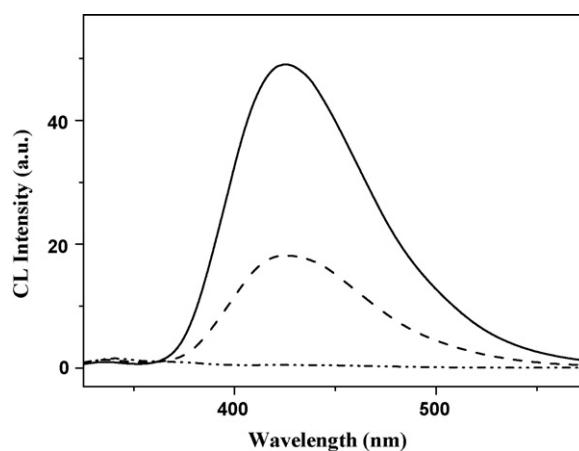
Fig. 4. CL spectra for luminol–NaIO$_4$–gold colloids CL system: (–·–·–) NaIO$_4$; (– – –) luminol–NaIO$_4$; (—) luminol–NaIO$_4$–gold colloids. Luminol solution: 1.0×10^{-4} mol l^{-1}, pH 12.7; gold colloids: 2.5×10^{-6} g ml^{-1}; NaIO$_4$ solution: 5.0×10^{-4} mol l^{-1}, 0.03 mol l^{-1} NaOH.

weak CL, it is assumed that the catalyst gold nanoparticles may interact with the reactants or the intermediates of the reaction of luminol with periodate. When gold nanoparticles were used as the catalysts, the formation of active oxygen-containing reactant intermediates such as OH$^\bullet$ and $O_2^{\bullet-}$ were frequently reported [37,38]. So in this system it can be concluded that the enhancement effect on CL by gold nanoparticles was attributed to the formation of $O_2^{\bullet-}$. The oxidation reaction of luminol was accelerated by $O_2^{\bullet-}$, thus, the CL emission enhanced. A schematic reaction process [22,23,36,39] could be shown as Scheme 1.
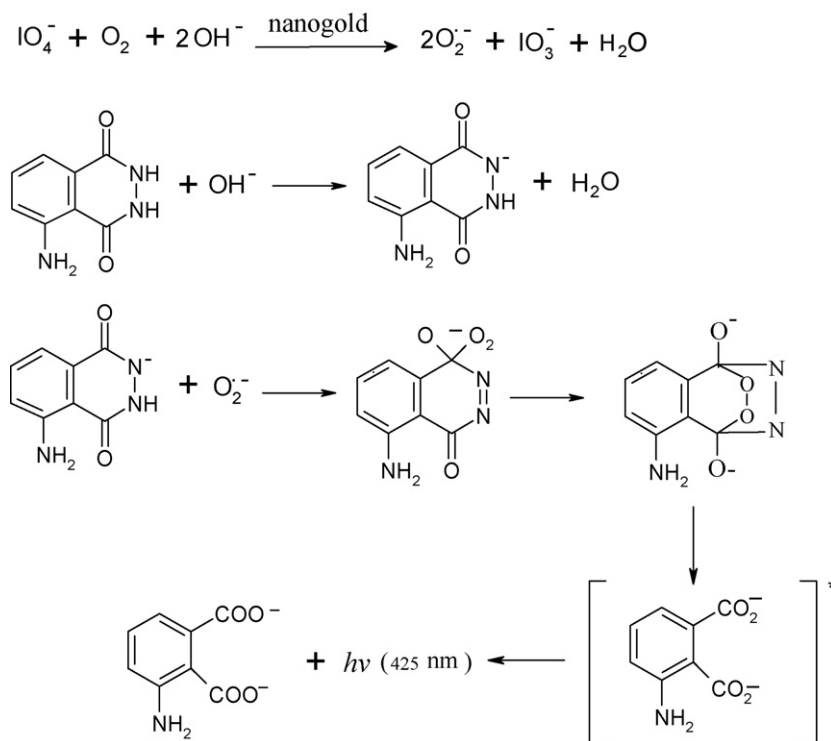
Scheme 1. Possible mechanism for the luminol–NaIO$_4$–gold colloids CL system.

Table 1
Analytical parameters of the proposed CL system for polyphenols

Polyphenols	Linear range (g ml^{-1})	Regression equation (C: g ml^{-1})	Correlation coefficient	Detection limit (g ml^{-1})	Precision ($n = 11$)	
					(g ml^{-1})	R.S.D.
Hydroquinone	8.0×10^{-9} to 1.0×10^{-6}	lg $\Delta I = 5.8690 + 0.3009$ lg C	0.9967	2.1×10^{-9}	5.0×10^{-7}	2.3
Catechol	4.0×10^{-10} to 6.0×10^{-7}	lg $\Delta I = 7.3318 + 0.4565$ lg C	0.9958	1.0×10^{-10}	1.0×10^{-7}	2.9
Resorcinol	2.0×10^{-8} to 4.0×10^{-6}	lg $\Delta I = 7.6081 + 0.7049$ lg C	0.9982	8.3×10^{-9}	5.0×10^{-7}	1.7

Table 2
Determination of catechol in tap water and synthesized samples ($n = 9$)

Sample	Initially present (g ml^{-1})	Added (g ml^{-1})	Found (g ml^{-1})	Recovery (%)	R.S.D. (%)
1	1.87×10^{-7}	1.0×10^{-7}	3.01×10^{-7}	104.9	2.7
		2.0×10^{-7}	3.96×10^{-7}	102.3	3.1
2	0	1.0×10^{-7}	9.76×10^{-8}	97.6	2.1
		3.0×10^{-7}	3.11×10^{-7}	103.7	3.8
3	1.0×10^{-7}	2.0×10^{-7}	3.06×10^{-7}	102	1.5
		4.0×10^{-7}	5.23×10^{-7}	104.6	2.9
4	2.0×10^{-7}	2.0×10^{-7}	4.05×10^{-7}	101.2	4.0
		4.0×10^{-7}	5.81×10^{-7}	96.8	1.4

3.7. Analytical applications

3.7.1. Standard curve and detection limit

The analytical potential of the inhibition effects of the polyphenols on the proposed luminol–NaIO$_4$–4 nm gold colloids CL system was explored by use of a flow-injection procedure. Under the selected optimum conditions given above, the working curves of polyphenols were established. The parameters of the regression equations for each polyphenol are shown in Table 1. Linear ranges are about two to three orders of magnitude for the detection of tested polyphenols. The detection limits at a signal-to-noise ratio of 3 (3σ) were in the range of 2.1×10^{-9} to 1.0×10^{-10} g ml^{-1} and the relative standard deviation (R.S.D., $n = 11$) were in the range of 1.7–2.9%. These results indicated that the precision is good enough for the determination of polyphenols at low concentrations.

3.7.2. Interferences

The influence of various foreign species on the determination of 1.0×10^{-7} mol l^{-1} catechol were studied. The tolerable concentration ratios with respect to 1.0×10^{-7} mol l^{-1} catechol were more than 500 for methanol, ethanol, 2-propanol, 1,2,3-propanetriol, Zn^{2+}, K^+, Na^+, Br^-, $C_2O_4^{2-}$, Cl^-, I^-, SO_4^{2-}, NO_3^-; 100 for 2,4-dinitrophenol, p-aminobenzene sulfonic acid; 50 for tartaric acid, Hg^{2+}; 20 for benzoic acid, p-hydroxyl benzoic acid, PO_4^{3-}; 5 for salicylic acid, Ca^{2+}, Mg^{2+}, Ni^{2+}; 1 for chlorogenic acid, phenol, Cu^{2+}, Pb^{2+}; 0.5 for Fe^{3+}, Cd^{2+}, Mn^{2+}, Cr^{3+}, respectively.

3.7.3. Applications

The proposed method has been utilized for the determination of catechol in tap water and in the synthesized samples with satisfactory results. The results shown in Table 2 indicated that

this new flow-injection chemiluminescence method is sensitive and accurate for the polyphenol detection.

4. Conclusions

Gold nanoparticles could enhance the chemiluminescence of the luminol–NaIO$_4$ system. The enhancement mechanism of gold nanoparticles on luminol CL was discussed. The CL from luminol–NaIO$_4$–gold nanoparticles system is strongly inhibited by the presence of catechol, hydroquinone and resorcinol. Based on this inhibition, a novel CL method with a lower detection limit and wider linear range was developed for the determination of these polyphenols.

References

[1] J.J. Dalluge, B.C. Nelson, J.B. Thomas, L.C. Sander, J. Chromatogr. A 793 (1998) 265.
[2] I. Nukatsuka, S. Nakamura, K. Watanabe, K. Ohzeki, Anal. Sci. 16 (2000) 269.
[3] K.O. Lupetti, F.R.P. Rocha, O. Fatibello-Filho, Talanta 62 (2004) 463.
[4] A. Afkhami, A.H. Khatami, J. Anal. Chem. 56 (2001) 429.
[5] Y.C. Fiamegos, C.D. Stalikas, G.A. Pilidis, M.I. Karayannis, Anal. Chim. Acta 403 (2000) 315.
[6] C.L. Kang, Y. Wang, R.B. Li, L.M. Zhou, Y.Z. Du, Microchem. J. 64 (2000) 161.

[7] D. Jie, F. Gang, D.X. Li, J.R. Liu, Chem. Anal. Meterage 11 (2002) 20 (in Chinese).

[8] M.F. Pistonesi, S.D.N. María, C.E. María, E.P. Miriam, G.L. Adriana, S. Beatriz, B. Fernández, Talanta 69 (2006) 1265.

[9] G.H. Wu, C.Y. He, R. Chen, Spectrosc. Spect. Anal. 22 (2002) 813 (in Chinese).

[10] J.T. Hu, J.H. Yang, W.Y. Ma, R.J. Han, Spectrosc. Spect. Anal. 18 (1998) 633 (in Chinese).

[11] M.J. Christophersen, Anal. Chim. Acta 323 (1996) 39.

[12] M. Careri, C. Corradini, L. Elviri, I. Nicoletti, I. Zagnoni, J. Agric. Food Chem. 51 (2003) 5226.

[13] H. Cui, J. Zhou, F. Xu, C.Z. Lai, G.H. Wan, Anal. Chim. Acta 511 (2004) 273.

[14] H. Cui, C.X. He, G.W. Zhao, J. Chromatogr. A 855 (1999) 171.

[15] K.R. Maatta, A. Kamal-Eldin, A.R. Torronen, J. Agric. Food Chem. 51 (2003) 6736.

[16] R. Sladkovsky, P. Solich, M. Urbanek, J. Chromatogr. A 1040 (2004) 179.

[17] D. Sterbova, D. Matejicek, J. Vlcek, V. Kuban, Anal. Chim. Acta 513 (2004) 435.

[18] S.H. Hakkinen, S.O. Karenlampi, I.M. Heinonen, J. Agric. Food Chem. 77 (1998) 543.

[19] R.A. Agbaria, P.B. Oldham, M. McCarroll, L.B. McGown, I.M. Warner, Anal. Chem. 74 (2002) 3952.

[20] P.E. Nicholaos, K.T. Nicholaos, G.V. Athanasios, Talanta 46 (1998) 179.

[21] R. Wirat, L. Saisunee, T. Alan, Talanta 69 (2006) 976.

[22] P. Fletcher, K.N. Andrew, A.C. Calokerinos, S. Forbes, P.J. Worsfold, Luminescence 16 (2001) 1.

[23] Y.H. Li, W.F. Niu, J.R. Lu, Talanta 71 (2007) 1124.

[24] S.F. Li, H.Q. Chen, X.W. Wei, X.J. Lu, L. Zhang, Microchim. Acta 155 (2006) 427.

[25] M. Kamil, O. Antonije, M. Pavel, V. Zbyněk, Talanta 71 (2007) 900.

[26] Z.F. Zhang, H. Cui, M.J. Shi, Phys. Chem. Chem. Phys. 8 (2006) 1017.

[27] B. Denis, P. Paolo, F. Gabriella, M. Carlo, Talanta 72 (2007) 249.

[28] Z.F. Zhang, H. Cui, C.Z. Lai, L.J. Liu, Anal. Chem. 77 (2005) 3324.

[29] Z.P. Li, Y.C. Wang, C.H. Liu, Y.K. Li, Anal. Chim. Acta 551 (2005) 85.

[30] H. Cui, Z.F. Zhang, M.J. Shi, J. Phys. Chem. B 109 (2005) 3099.

[31] K.R. Brown, A.P. Fox, M.J. Natan, J. Am. Chem. Soc. 118 (1996) 1154.

[32] A. Doron, E. Katz, I. Willner, Langmuir 11 (1995) 1313.

[33] L. Liu, C. Dahlgren, H. Elwing, H. Lundqvist, J. Immunol. Methods 192 (1996) 173.

[34] A.M.G. Campana, W.R.G. Baeyens, X.R. Zhang, E. Smet, G.V. Weken, K. Nakashima, A.C. Calokerinos, Biomed. Chromatogr. 14 (2000) 166.

[35] H.A.G. Niederlander, C. Gooijer, N.H. Velthorst, Anal. Chim. Acta 285 (1994) 143.

[36] J.M. Lin, M. Yamada, Anal. Chem. 71 (1999) 1760.

[37] R. Grisel, K.J. Weststrate, A. Gluhoi, B.E. Nieuwenhuys, Gold Bull. 35 (2002) 39.

[38] S.H. Overbury, L. Ortiz-Soto, H.G. Zhu, B. Lee, M.D. Amiridis, S. Dai, Catal. Lett. 95 (2004) 99.

[39] B.X. Li, X.Y. Zhang, C.X. Zhang, Anal. Chim. Acta 575 (2006) 212.

Online solid-phase extraction liquid chromatography–electrospray-tandem mass spectrometry analysis of buprenorphine and three metabolites in human urine

An-Chan Liu [a], Tzuen-Yeuan Lin [a], Lien-Wen Su [b], Ming-Ren Fuh [a],*

[a] *Department of Chemistry, Soochow University, 111 Shihlin, Taipei, Taiwan*
[b] *Taipei City Psychiatric Center, Department of Addiction Science, Taipei City Hospital, Taipei, Taiwan*

Abstract

An online solid-phase extraction (SPE) liquid chromatography–electrospray tandem mass spectrometry (LC–ESI-MS/MS) method for the determination of buprenorphine (Bup), norbuprenorphine (nBup), buprenorphie-3-β-D-glucuronide (Bup-3-G) and norbuprenorphie-3-β-D-glucuronide (nBup-3-G) in human urine was developed and validated. A mixed mode SPE column with both hydrophilic and lipophilic functions was used for online extraction. A C_{18} column was employed for LC separation and ESI-MS/MS was utilized for detection. Buprenorphine-D_4 (Bup-D_4) and norbuprenophine-D_3 (nBup-D_3) were used as internal standards for quantitative determination. The extraction, clean-up and analysis procedures were controlled by a fully automated six-port switch valve. Identification and quantification were based on the following transitions: m/z 468→414 for Bup, m/z 414→364 for nBup, m/z 644→468 for Bup-3-G and m/z 590→414 for nBup-3-G, respectively. Good recoveries from 93.6% to 102.2% were measured and satisfactory linear ranges for these analytical compounds were determined. Minimal ion suppression effect (∼7% response decrease) was determined. Intra-day and inter-day precision showed coefficients of variance, CV, ranged from 3.3% to 10.1% and 4.4% to 9.8%, respectively. Accuracy ranging from 97.0% to 104.0% was determined. The applicability of this newly developed method was demonstrated by analyzing human urine samples from the patients in Bup treatment program for therapeutic monitoring purpose.
© 2007 Elsevier B.V. All rights reserved.

Keywords: Buprenorphine; Urine analysis; Online solid-phase extraction; Liquid chromatography–electrospray-tandem mass spectrometry

1. Introduction

Buprenorphine (Bup) is a synthetic opioid drug for the treatment of chronic pain. Bup is more potent than morphine and has been used for the treatment of heroin addiction [1,2]. In human, Bup is *N*-dealkylated to norbuprenorphine (nBup); furthermore, both Bup and nBup undergo extensive conjugation to glucuronides, buprenorphie-3-β-D-glucuronide (Bup-3-G) and norbuprenorphie-3-β-D-glucuronide (nBup-3-G), prior to urine excretion [3,4]. The structures of these chemicals are shown in Fig. 1. It has been reported the concentration of free Bup in urine is in low nanogram ranges and the glucuronides are

the major metabolites found; in addition, extensive difference of inter-individual Bup metabolism in human was observed [5]. Therefore, accurate monitoring of Bup and its metabolites in biological fluids of patient is needed to effectively personalize the treatment program. The determination of drug and its metabolites in plasma provides the real indication of active amount of a drug; however, monitoring the concentrations of active component in urine is an useful complement to plasma measurement for therapeutic drug monitoring purpose.

Several analytical methods have been developed for the analysis of Bup and nBup in biological matrices using gas chromatography–mass spectrometry (GC–MS) [6–8], liquid chromatography (LC) with electrochemical detector [9], UV detector [10], electrospray mass spectrometry (ESI-MS) [11–13], or atmospheric pressure chemical ionization mass spectrometry (APCI-MS) [14]. However, there are only few reported methods for the quantitative determination of Bup, nBup, Bup-3-G and nBup-3-G. Two reported methods

* Corresponding author at: Department of Chemistry, Soochow University, P.O. Box 86-72, Taipei, Taiwan. Tel.: +886 2 2881 9471x6821; fax: +886 2 2881 1053.

E-mail address: msfuh@mail.scu.edu.tw (M.-R. Fuh).
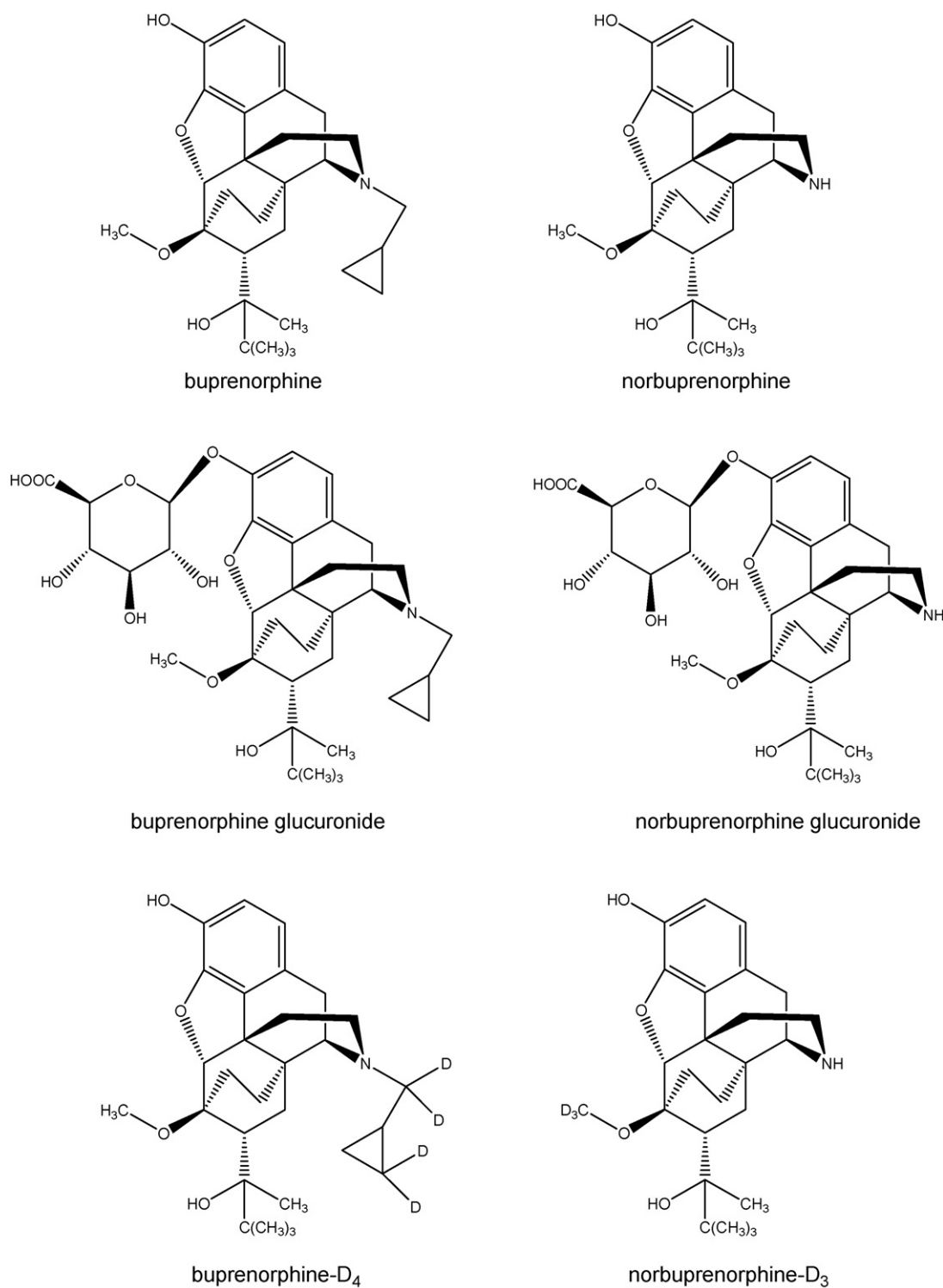
Fig. 1. Structure of analytical component.

utilized LC–ESI-tandem MS to quantify Bup, nBup and their glucuronides in plasma [15,16]. Liquid-liquid extraction combined with solid-phase extraction was employed as sample pre-treatment processes for these studies. The limit of detection of buprenophine and its metabolites were 0.1–0.3 ng/ml. In addition, LC–tandem MS method has been reported to approximate the concentrations of Bup-3-G and nBup-3-G in human urine based on the quantification of Bup and nBup before and after hydrolysis [17]. In this investigation, authors estimated the cutoff of LC-ES assay was near 1 ng/ml.

For LC–ESI-MS analysis of biological samples, ion suppression effect is frequently observed [18–20]. Solid-phase extraction (SPE) has been proven to be an effective sample pre-treatment technique to minimize ion suppression effect.

However, SPE generally requires laborious and time-consuming equilibrium, clean-up and evaporation procedures. Online SPE has been successfully applied to LC–ESI-MS analysis for the analysis of various drugs in biological fluid [21–23].

This paper describes the development and validation of an online SPE LC–ESI-MS/MS method to quantify Bup, nBup, Bup-3-G and nBup-3-G in human urine for therapeutic application. This fully automated method required little minimum sample pre-treatment and was applicable to high through-put analysis. In addition, ion suppression effect was examined and the short-term stability of analyte was evaluated. The applicability of this newly developed method to monitor the urine samples of Bup treatment patients was demonstrated. To our knowledge, this is the first study to direct quantitative measurement of Bup and three metabolites (nBup, Bup-3-G and nBup-3-G) in human urine.

2. Experimental

2.1. Chemicals and reagents

Bup, nBup, Bup-3-G, nBup-3-G, Bup-D$_4$ and nBup-D$_3$ were purchased from Cerilliant Corp. (Austin, TX, USA). HPLC-grade acetonitrile and methanol were from Milinckrodt Baker, Paris, KY, USA. Reagent-grade trifluoroacetic acid (TFA) was obtained from Riedel-de Haen AG, Germany. Purified water from a Milli-Q system from Millipore Corp. (Beford, MA, USA) was used. Drug-free urine samples collected from five healthy volunteers were used for method development and preparation of calibration standards.

2.2. Equipments

An Agilent 1100 LC system (Agilent Co., Palo Alto, CA, USA), consisting of a quaternary pump, an online degasser, an auto-sampler and a six-port switch valve was used. A Symmetry Shield RP18 column (2.1 mm × 50 mm, 3.5 μm; Waters Corp., Milford, MA, USA) was utilized for LC separation and an Oasis HLB column (2.1 mm × 20 mm, 3.5 μm) from Waters Corp. was employed for online SPE.

All mass spectrometric measurements were performed on an Agilent LC/MSD SL ion trap mass spectrometer with an electrospray ionization source operating in positive ion mode. Agilent 1100 series LC/MSD Trap software (version 4.0) was utilized for system control, data acquisition and data analysis. The spray voltage was set at −3.5 kV and compressed nitrogen gas (50 psi) was used for nebulization. Heated nitrogen (350 °C, 10 L/min) was for solvent evaporation.

The data acquisition was performed under the following conditions: normal scan speed, molecular mass scan range 100–700, ion charge control target 30,000, maximum accumulation time 300 ms and the isolation width for precursor ions was 2.

2.3. Standard and sample preparation

Individual stock solutions (100 μg/mL) of each compound were prepared in methanol and stored in a refrigerator (4 °C)
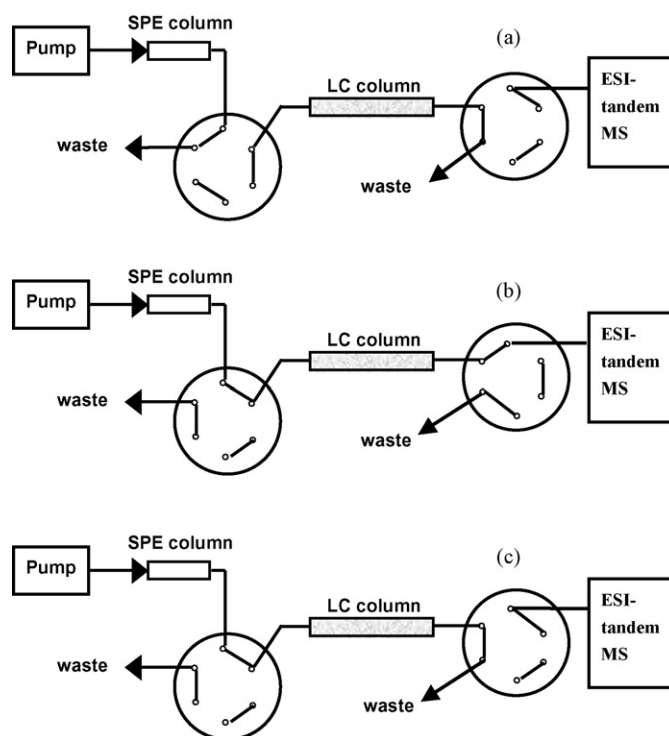
Fig. 2. Configuration of online SPE LC–ESI-tandem MS: (a) extraction, (b) analysis and (c) clean-up.

when not in use. Spiked urine standards were prepared by spiking appropriate amounts of each analytical component into drug-free urine.

Prior to online SPE LC–tandem MS analysis, each urine sample (2 mL) was diluted with 2 mL of 0.01% TFA solution with internal standards (Bup-D$_4$ and nBup-D$_3$, 5 ng/ml each) and centrifuged for 5 min at 1500 × g. A 50-μL aliquot of supernatant was used for analysis.

2.4. Online sample preparation and LC separation

The experimental setup for online SPE LC–ESI-tandem MS is shown in Fig. 2 and the time program for extraction, washing and analysis is listed in Table 1. First, the SPE extraction column was equilibrated by 0.05% TFA aqueous solution for 2 min at 1 mL/min with the system in "extraction" configuration as shown in Fig. 2a. Urine sample was introduced by an auto-sampler and transported by 0.05% TFA aqueous solution at 1 mL/min. While the endogenous components of urine were washed to waste, the analytical compounds were withheld in the SPE column. From 1.1 to 5.0 min, the extracted compounds in SPE column were further washed by methanol/water (5/95, v/v) with 0.05% TFA mixture and then by acetonitrile/water mixture as described in Table 1. At 5.1 min after sample injection, a gradient elution (at flow rate of 0.2 mL/min) was employed for chromatographic separation of the analytes. At the same time, the system was turned to "analysis" configuration as shown in Fig. 2b and the eluted components were delivered to ESI-tandem MS for determination. At 12.1 min, the system was converted to "clean-up" position as shown in Fig. 2c. The system was washed

Table 1
Time program of extraction and LC separation (see Section 2 for detail)

Time (min)	Solvent				
	A (%)[a]	B (%)[b]	C (%)[c]	D (%)[d]	Flow rate (ml/min)
0.0	100	0	0	0	1.0
1.0	100	0	0	0	1.0
1.1	0	100	0	0	1.0
4.0	0	100	0	0	1.0
4.1	0	0	70	30	1.0
5.0	0	0	70	30	1.0
5.1[e]	0	0	30	70	0.2
11.0	0	0	0	100	0.2
12.0	0	0	0	100	0.2
12.1[f]	0	0	70	30	0.4
16.0	0	0	70	30	0.4
16.1[g]	100	0	0	0	1.0
19.0	100	0	0	0	1.0

[a] 0.05% TFA aqueous solution.
[b] Methanol/water (5/95, v/v) with 0.05% TFA.
[c] Acetonitrile/water (5/95, v/v) with 0.05% TFA.
[d] Acetonitrile/water (95/5, v/v) with 0.05% TFA.
[e] At 5.1 min, the system is turned to "analysis" configuration.
[f] At 12.1 min, the system is turned to "clean-up" configuration.
[g] At 16.1 min, the system is turned to "extraction" configuration.

with acetonitrile/water (95/5, v/v) with 0.05% TFA mixture and then equilibrated by the initial mobile phase of gradient elution. At 16.1 min, the system was switched to "extraction" mode and the SPE column was re-equilibrated with 0.05% TFA aqueous solution for 3 min at flow rate of 1.0 mL/min. Afterwards, the system was ready for next injection.

2.5. Investigation of ion suppression effect

Ion suppression effect was examined by a previously reported post-column infusion setup [18]. Drug-free urine blank from five volunteers and water were injected into online SPE LC–ESI-tandem MS system while a mixture of four analytes (100 ng/mL each) in water was continuously infused in parallel at 20 μL/min through a PEEK tee-junction (Upchurch Scientific, Oak Har-

bor, WA, USA) and a syringe pump (Harvard Apparatus, South Natick, MA, USA).

3. Results and discussion

3.1. ESI-MS/MS

In order to optimize the condition for ES-MS/MS determination, 100 ng/mL standard solutions of each analyte were directly infused ESI-ion trap MS. In ESI-MS analysis, proton adduct ion was detected as base ion for all analytes and internal standards; therefore, $[M+H]^+$ of each compound was selected as the precursor ion for the subsequent ESI-MS/MS measurement. The MS/MS results and tentative assignments of MS/MS fragmented ions are summarized in Table 2. The MS/MS for Bup gives the fragment 414 (m/z) resulted from the loss of cyclopropylmethylene group of $[M+H]^+$; further cleavage of t-butyl group (–C(CH$_3$)$_3$) and methoxy group (–OCH$_3$) produces fragment 326 (m/z). For nBup, the MS/MS fragment ions are similar to those of Bup since it has comparable structure of Bup but without cyclopropylmethy group. The tetrahydropyranyl six-membered rings in both Bup-3-G and nBup-3-G can easily be cleaved to give fragments 468 (m/z) and 414 (m/z), respectively. MS/MS results for Bup-D$_4$ and nBup-D$_3$ furthermore supported the identification of fragment ions. The MS/MS fragmentation pathways of these compounds in ion trap have previously proposed [12,15]. The results of this study are similar to those of the previous investigation.

3.2. Online SPE LC–ESI-MS/MS method development

A HLB SPE column which is packed with micro-porous material consisting of both hydrophilic and lipophilic groups was employed as an extraction column. Loading, washing and separation procedures were a modification of previously reported method [21]. Diluted urine sample was introduced into system by 0.05% TFA solution. TFA was used as an ion paring reagent to form an ion pair with analytical molecule and then retained in the SPE column.

Table 2
ESI-MS/MS results

Compound	Frag. energy (V)	MS/MS product ion[a]
Bup	1.55	$[M+H]^+$ (468), $[M+H-H_2O]^+$ (450), $[M+H-C_3H_6]^+$ (426), **$[M+H-C_4H_6]^+$ (414)**, $[M+H-C_4H_6-H_2O]^+$ (396), $[M+H-C_4H_6-C(CH_3)_3-OCH_3]^+$ (326)
nBup	1.30	$[M+H]^+$ (414), $[M+H-H_2O]^+$ (396), $[M+H-CH_3OH]^+$ (382), **$[M+H-H_2O-CH_3OH]^+$ (364)**, $[M+H-H_2O-C_4H_8]^+$ (340), $[M+H-C(CH_3)_3-OCH_3]^+$ (326)
Bup-3-G	1.35	$[M+H]^+$ (644), **$[M+H-C_6H_8O_6]^+$ (468)**, $[M+H-C_6H_8O_6-C_4H_6]^+$ (414), $[M+H-C_6H_8O_6-C_4H_6-H_2O]^+$ (396)
nBup-3-G	1.00	$[M+H]^+$ (590), $[M+H-H_2O]^+$ (572), **$[M+H-C_6H_8O_6]^+$ (414)**, $[M+H-C_6H_8O_6-H_2O]^+$ (396), $[M+H-C_6H_8O_6-CH_3OH]^+$ (382), $[M+H-C_6H_8O_6-CH_3OH-H_2O]^+$ (364), $[M+H-C_6H_8O_6-C(CH_3)_3OH]^+$ (340)
Bup-D$_4$	1.55	$[M+H]^+$ (472), $[M+H-H_2O]^+$ (454), $[M+H-C_3H_4D_2]^+$ (428), **$[M+H-C_4H_3D_3]^+$ (415)**, $[M+H-C_4H_3D_3-CH_3]^+$ (400), $[M+H-C_3H_3D_2-C(CH_3)_3]^+$ (372), $[M+H-C_4H_2D_3-C(CH_3)_3-OCH_3]^+$ (328)
nBup-D$_3$	1.30	$[M+H]^+$ (417), $[M+H-H_2O]^+$ (399), $[M+H-CH_3OH]^+$ (382), $[M+H-H_2O-CH_3OH]^+$ (364), $[M+H-H_2O-C_4H_8]^+$ (343), **$[M+H-C(CH_3)_3-OCD_3]^+$ (326)**

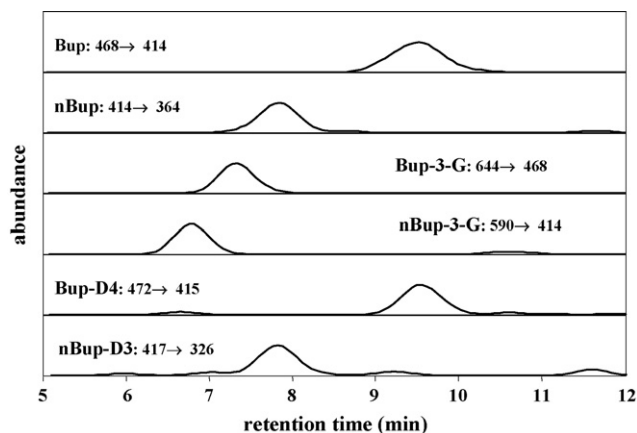[a] m/z of each ion in parenthesis; quantitative ions are in bold.

Fig. 3. Extracted ion chromatograms of a spiked human urine sample (10 ng/ml for each analyte, 5 ng/ml for each ISTD).

We examined various compositions of methanol/water (3/97, 5/95, 10/90) with 0.05% TFA mixtures as washing solutions to remove endogenous components retained on the SPE column. The results indicated that analytical compounds were easily washed out from SPE column when the methanol content is greater than 5/95. Therefore, methanol/water (5/95, v/v) with 0.05% TFA solution was selected as the washing solution. During the investigation of gradient elution, broadened eluted peaks of four analytes were observed and there was little chromatographic separation of analytical compounds when LC column coupled to SPE column. As the result, a second washing step using acetonitrile/water with 0.05%TFA was introduced to minimize the peak broadening effect.

A gradient elution was employed for LC separation. The flow rate was reduced to 0.2 mL/min to enhance the sensitivity of ESI-tandem MS. The online SPE LC–ESI-tandem MS results of a spiked human urine sample are shown in Fig. 3. The retention time for Bup, nBup, Bup-3-G and nBup-3-G was 9.5, 7.9, 7.4 and 6.8 min, respectively. There was no deuterium effect in chromatographic separation observed for the internal standards. Each analysis including post-separation clean-up and equilibrium was accomplished in less than 20 min.

3.3. Evaluation of ion suppressing effect and sample pre-treatment procedure

Ion suppression often diminishes response of ESI-MS and the sensitivity of analytical method. In order to examine the effect of ion suppression of this newly developed method, drug-free urine samples without analytes from five volunteers were examined by the apparatus described in Section 2.5. First, TFA (5 μL) was added to drug-free urine or water sample (5 ml), vortex for approximately 1 min then centrifuged for 5 min at $1500 \times g$. A 50-μL aliquot of supernatant was injected for ion suppression examination. The responses of analytical components of these drug-free urine samples were compared to TFA added water sample; there was more than 35% decrease in each analyte detected. The results indicated that considerable ion suppression was observed in TFA added urine sample. Secondly, diluted drug-free urine, as described in Section 2.3, was evalu-

Table 3
Recovery[a]

	Bup	nBup	Bup-3-G	nBup-3-G
1.0 ng/mL	98.0 ± 2.9%	95.2 ± 3.1%	97.1 ± 4.7%	100.7 ± 4.0%
5.0 ng/mL	96.6 ± 4.0%	94.7 ± 4.4%	98.4 ± 7.4%	99.7 ± 3.5%
30.0 ng/mL	93.6 ± 2.5%	99.1 ± 3.1%	102.2 ± 3.8%	94.9 ± 4.5%
75.0 ng/mL	97.6 ± 5.7%	96.0 ± 3.7%	98.6 ± 5.4%	97.7 ± 5.5%

[a] Average ± standard deviation, $n = 5$.

ated. There was less than 7% decline in response of each analyte comparing to the responses of water sample. This indicated that online SPE LC method effectively removes and separates the potential interfering components in diluted urine sample.

3.4. Extraction recovery

Spiked urine and water samples at four different concentrations (1.0, 5.0, 30.0 75.0 ng/mL) over the linear range were analyzed to evaluate the recovery of this newly developed method. The recovery was determined by the peak area of spiked urine as a fraction of the corresponding standard in water solution. The results of this study are summarized in Table 3. Good recovery ranged from 93.6% to 102.2% for all analytes at the tested concentrations. It suggested that this assay is adequate for the analyses of these compounds in urine.

3.5. Calibration and validation

Isotope internal standards, Bup-D$_4$ and nBup-D$_3$, were utilized for quantitative determination. Due to the lack of availability of the isotope standard of glucuronides, Bup-D$_4$ and nBup-D$_3$ were also used as the internal standard for Bup-3-G and nBup-3-G, respectively. A series of spiked urine solutions was used to evaluate the linearity of this newly developed assay and the results are summarized in Table 4. A $1/x$ weighting factor was applied to least squares regression of quantities of each analyte versus peak are ratio of analyte peak area to that of its internal standard.

For the analytes, except for nBup, good linearity was determined from 0.5 to 100 ng/mL. For nBup, linear range of 1–100 ng/mL was measured. Base on the signal-to-noise ratio of 3, the limit of detection for the analytes ranged from 0.2–0.5 ng/mL. Comparable detection limits of these analytes, 0.1 to 0.3 ng/ml, in human plasma have been reported previ-

Table 4
Linearity and detection limit

Compound	Calibration curve[a]	r^2	Range (ng/mL)[b]	Detection limit (ng/mL)
Bup	$Y = 0.4864X - 0.0023$	0.999	0.5–100	0.2
nBup	$Y = 0.3218X + 0.0201$	0.999	1.0–100	0.5
Bup-3-G	$Y = 0.2627X - 0.0103$	0.999	0.5–100	0.2
nBup-3-G	$Y = 0.4494X - 0.0207$	0.999	0.5–100	0.2

[a] Y: peak area ratio of standard and internal standard, X: concentration (ng/mL).
[b] Concentration of standards: Bup, Bup-3-G, nBup-3-G: 0.5, 1, 3, 5, 10, 30, 50, 75 and 100 ng/mL; nBup: 1, 3, 5, 10, 30, 50, 75 and 100 ng/mL.

Table 5
Precision and accuracy

	Intra-day ($n = 5$)			Inter-day ($n = 5$)		
	1.0 ng/mL	10.0 ng/mL	100.0 ng/mL	1.0 ng/mL	10.0 ng/mL	100.0 ng/mL
Bup						
Mean	1.04	9.89	98.94	1.02	9.96	99.44
Accuracy (%)	104.0	98.9	98.9	102.0	99.6	99.4
CV (%)[a]	8.8	4.2	4.2	9.8	6.4	7.4
nBup						
Mean	0.99	9.72	100.4	1.01	9.78	99.0
Accuracy (%)	99.0	97.2	100.4	101.2	97.8	99.0
CV (%)[a]	6.3	3.4	3.9	7.4	4.9	5.9
Bup-3-G						
Mean	0.99	9.86	99.42	0.99	10.68	101.15
Accuracy (%)	99.0	98.6	99.4	99.0	100.7	101.2
CV (%)[a]	3.3	3.4	5.1	5.7	4.4	6.8
nBup-3-G						
Mean	0.97	10.15	98.06	0.98	10.06	98.75
Accuracy (%)	97.0	101.5	98.1	98.0	100.6	98.8
CV (%)[a]	10.1	7.3	3.9	9.6	6.8	6.2

[a] CV: coefficient of variation, $n = 5$.

ously [15,16]. These reported methods utilized SPE cartridge as a sample pre-treatment and detected by LC–ESI-tandem MS. They required laborious and time-consuming sample preparation procedures. However, only minimal sample preparation was required for this newly developed method.

Precision and accuracy of the method were appraised at three concentrations (1.0, 10.0 and 100.0 ng/mL) over the linear range and the results were summarized in Table 5. The intra-day and inter-day precision showed coefficients of variance, CV, ranged from 3.3% to 10.1% and 4.4% to 9.8%, respectively. The accuracy was evaluated by [mean measured concentration/spiked concentration] × 100%. Accuracy ranging from 97.0% to 104.0% was determined.

3.6. Short-term stability study

The short-term stabilities of all four analytes under various storage conditions were examined. Fortified human urine samples (30 ng/ml of each analyte) were utilized for this study. Short-term temperature stability was evaluated by urine samples stored for 12 and 24 h at room temperature and 4 °C. The freeze–thaw stabilities of all analytes were determined after three freeze–thaw cycles of the fortified human urine samples. For all four analytes, the concentrations were within ±12% under all five storage conditions.

3.7. Analysis of urine samples from buprenorphine treatment patients

This method has been applied to the analysis of urine samples from the patients in the buprenorphine treatment program at Taipei City hospital. Extracted ion chromatograms of a patient urine sample are shown in Fig. 4. All four analytical compounds were detected in all patients' urine samples examined and the results are summarized in Table 6. For all samples studied,
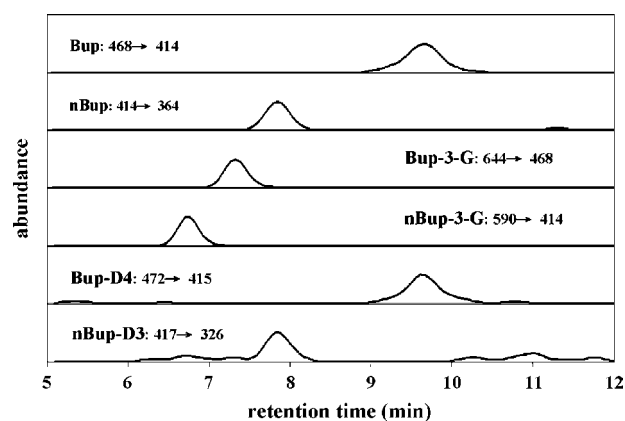
Fig. 4. Extracted ion chromatograms of a patient urine sample (sample #11) with the addition of ISTD (5 ng/ml for each ISTD).

Table 6
Bup, nBup, Bup-3-G and nBup-3-G concentration in urine collected from buprenorphine treatment patients

Sample	Bup (ng/ml)	nBup (ng/ml)	Bup-3-G (ng/ml)	nBup-3G (ng/ml)
1[a]	14.1	116.4	352.5	406.3
2[b]	29.8	136.6	213.3	858.8
3[a]	16.2	62.1	31.7	122.8
4[b]	10.2	216.7	88.7	983.9
5[a]	8.2	86.8	115.4	390.4
6[a]	14.4	150.4	31.9	212.8
7[a]	21.1	62.1	85.8	437.3
8[a]	17.5	63.2	108.2	407.6
9[a]	18.5	76.5	30.1	373.1
10[a]	30.5	120.3	107.1	372.2
11[a]	19.1	95.8	137.4	438.9

[a] Sample was diluted fivefold prior to analysis.
[b] Sample was diluted 10-fold prior to analysis.

concentration of Bup was lower than its metabolites and nBup-3-G exhibited highest concentration of the four analytical compounds. Additional examination of urine samples is needed for better understanding of urinary concentration of Bup and its metabolites of each patient and the effectiveness of treatment program.

4. Summary

This newly developed online SPE LC–ESI-tandem MS method has proven to be an efficient and sensitive method for the determination of Bup, nBup, Bup-3-G and nBup-3-G in human urine. The assay was fully automated and minimal sample preparation was required. The detection limits of this method, 0.2 to 0.5 ng/mL, are comparable to other reported studies; however, no laborious and time-consuming sample pre-treatment was needed in this assay. There was minimal ion suppression effect observed and good recovery was obtained. This method will be used to support the clinical study of continuing buprenorphine treatment program.

References

[1] D. Jansinski, J. Pevnick, J. Griffth, Arch. Gen. Pyschiatry 34 (1978) 501.
[2] C.N. Chiang, R.L. Hawks, Drug Alcohol Dependence 70 (2003) S39.
[3] E.J. Cone, C.W. Gorodetzky, D. Yousefnejad, W.F. Buchwald, R.E. Johnson, Drug Metab. Dispos. 12 (1984) 577.
[4] R.C. Baselt, R.H. Cravey, Disposition of Toxic Drugs and Chemicals in Man, 4th ed., Chemical Toxicology Institute, Foster City, CA, 1995.
[5] A. Elkader, B. Sproule, Clin. Pharmacokinet. 44 (2005) 661.
[6] S. Gopal, T.B. Tzeng, A. Cowan, Eur. J. Pharm. Biopharm. 51 (2001) 147.
[7] J. Kuhlman Jr., J. Magluilo Jr., E.J. Cone, J. Anal. Toxicol. 20 (1996) 229.
[8] D.E. Moody, J.D. Kaycock, A.C. Spanbauer, D.J. Crouch, R.L. Foltz, J.L. Josephs, J. Amass, W.K. Bickel, J. Anal. Toxicol. 21 (1997) 406.
[9] E. Schleyer, R. Lohmann, C. Rolf, A. Gralow, C.C. Kaufmann, M. Unterhalt, W. Hiddemann, J. Chromatogr. 614 (1993) 275.
[10] L. Mercolini, R. Mandrioli, M. Conti, C. Leonardi, G. Gerra, M.A. Raggi, J. Chromatogr. B 847 (2007) 95.
[11] D.E. Moody, M.H. Slawson, E.C. Strain, J.D. Laycock, R.L. Foltz, Anal. Biochem. 306 (2002) 2002.
[12] D. Favretto, G. Frison, S. Vogliardi, S.D. Ferrara, Rapid Commun. Mass Spectrom. 20 (2006) 1257.
[13] S. Pirnay, F. Herve, S. Bouchonnet, B. Perrin, F.J. Baud, I. Ricordel, J. Pharm. Biomed. Anal. 41 (2006) 1135.
[14] A. Ceccato, R. Klinkernberg, P. Hubert, B. Streel, J. Pharm. Biomed. Anal. 32 (2003) 619.
[15] A. Polettini, M.A. Huestis, J. Chromatogr. B 754 (2001) 447.
[16] C.M. Murphy, M.A. Huestis, J. Mass Spectrom. 40 (2005) 70.
[17] R. Kronstrand, T.G. Selden, M. Josefsson, J. Anal. Toxicol. 27 (2003) 464.
[18] R. King, R. Bonfiglio, C. Fernandez-Metzler, C. Miller-Stein, T. Olah, J. Am. Soc. Mass Spectrom. 11 (2000) 942.
[19] D.L. Buhrman, P.I. Price, P.J. Rudewicz, J. Am. Soc. Mass Spectrom. 7 (1996) 1099.
[20] H. Mei, Y. Hsieh, C. Nardo, X. Xu, S. Wang, K. Ng, W.A. Korfmacher, Rapid Commun. Mass Spectrom. 17 (2003) 97.
[21] M.R. Fuh, S.W. Lin, L.L. Chen, T.Y. Lin, Talanta 72 (2007) 1329.
[22] T.Y. Wu, M.R. Fuh, Rapid Commun. Mass Spectrom. 19 (2005) 775.
[23] C. Mallet, Z. Lu, J. Mazzeo, U. Neue, Rapid Commun. Mass Spectrom. 16 (2002) 805.

Ion-selective electrodes for anionic surfactants using a cyclam derivative as ionophore

Josefa Lizondo-Sabater, Ramón Martínez-Máñez *, Felix Sancenón,
Mª Jesús Seguí, Juan Soto *,[1]

*Instituto de Química Molecular Aplicada, Departamento de Química, Universidad Politécnica de Valencia,
Camino de Vera s/n, 46022 Valencia, Spain*

Abstract

The cyclam derivative 1,4,8,11-tetra(*n*-octyl)-1,4,8,11-tetraazacyclotetradecane (L) has been used as carrier for the preparation of PVC-based membrane ion-selective electrodes for anionic surfactants. Different membranes were prepared using L as ionophore, tetra-*n*-octylammonium bromide (TOAB) as cationic additive and dibutyl phthalate (DBP) or *o*-nitrophenyl octyl ether (NPOE) as plasticizers. The final used electrode contained a membrane of the following composition: 56% DBP, 3.4% ionophore, 3.8% TOAB and 36.8% PVC. This electrode displays a Nernstian slope of -60.0 ± 0.9 mV/decade in a 2.0×10^{-3} to 7.9×10^{-6} mol dm^{-3} concentration range and a limit of detection of 4.0×10^{-6} mol dm^{-3}. The electrode can be used for 144 days without showing significant changes in the value of slope or working range. The electrode shows a selective response to dodecyl sulfate (DS$^-$) and a poor response to common inorganic cations and anions. The selective sequence found was DS$^- >$ ClO$_4^- >$ HCO$_3^- >$ SCN$^- >$ NO$_3^- \approx$ CH$_3$COO$^- \approx$ I$^- >$ Cl$^- >$ Br$^- >$ IO$_3^- \approx$ NO$_2^- \approx$ SO$_3^{2-} >$ HPO$_4^{2-} >$ C$_2$O$_4^{2-} >$ SO$_4^{2-}$, i.e. basically following the Hoffmeister series except for the hydrophilic anion bicarbonate. Most of the potentiometric coefficients determined are relatively low indicating that common anions would not interfere in the DS$^-$ determination. A complete study of the response of the electrode to a family of surfactant was also carried out. The electrode showed a clear anionic response to DS$^-$ and to Na-LAS and a much poorer response to other anionic surfactants and to non-ionic surfactants. Also the electrode shows certain non-linear cationic response in the presence of cationic and zwitterionic surfactants. The electrode was used for the determination of anionic surfactants in several mixtures, and the results obtained were compared to those found using a commercially available sensor.
© 2007 Elsevier B.V. All rights reserved.

Keywords: Ion-selective electrodes; Anionic surfactants; Cyclam; Polyamines; Ionophores

1. Introduction

Surfactants are one of the most common pollutants of both natural and technogenic waters. Surfactants contain two parts: a hydrophilic polar head, that determines its application and a lipophilic part consisting on hydrocarbonated chains usually with a (CH$_2$)$_n$ motif. Depending on the charge of the hydrophilic group the surfactants have been traditionally divided into four types; i.e. anionic, cationic, zwitterionic and non-ionic. Ionic

surfactants are produced in large amounts and are widely used for industrial and domestic purposes, household cleaning products, cosmetic formulations, biochemistry research laboratories, agricultural and horticultural chemicals. Due to their anthropogenic origin and extensive use, it is quite usual to find those anions in environments such as lakes and rivers where they can cause serious environmental problems mainly due to foam formation and because they act as transfer system of other pollutants (petroleum products, oils, pesticides and organochlorine compounds). Additionally, although most anionic surfactants in use today are biodegradable and non-toxic to humans [1], several authors have reported impair in respiratory function in fish caused by damage to the gill epithelium at concentrations of surfactants as low as 3 ppm [2]. Apart from the efforts developed in the study of degradation processes of this family of compounds to reduce their

* Corresponding authors. Tel.: +34 963877343; fax: +34 963879349.
E-mail addresses: rmaez@qim.upv.es
(R. Martínez-Máñez), juansoto@qim.upv.es (J. Soto).
[1] Tel.: +34 963877343; fax: +34 963879349.

environmental impact, another important aspect is the design of new and improved methods for their determination. Thus, environmental protection services have shown considerable interest in developing rapid methods for the determination of trace amounts of anionic surfactants. A number of methodologies for the determination of these environmentally important anions have been reported such as titrimetry [3], spectrophotometry[4], spectrofluorimetry [5], chromatography [6] and optical sensing [7]. However, some of these well-known methods require tedious procedures and they are not generally suitable for *in situ* or *at-site* quantitative determinations. As an alternative we have reported recently a novel organic solvent-free approach for the colorimetric determination of anionic surfactants in water based on supramolecular concepts [8]. Another option to these classical methods is the use of ion-selective electrodes [9,10]. However, these still show certain problem mainly related with reproducibility and signal stability. Most of the reported ISE for anionic surfactants use simple quaternary ammonium salts as ionophores. The main trouble in the use of this class of receptors is that they can only display electrostatic interactions and there are in the literature relatively few examples studying the potential use of advanced hosts as ionophores; i.e. able to multiple electrostatic and hydrogen bonding interactions. In this line, we have recently reported the design and use of the aza-oxa macrocycles 7,13-bis(*n*-octyl)-1,4,10 trioxa-7,13-diazacyclopentadecane and 7-methyl-7,13-bis(*n*-octyl)-1,4,10-trioxa-13-aza-7-azonia-cyclopentadecane as an alternative active carriers to simple quaternary ammonium salt for the selective detection of anionic surfactants. Two recent reviews have been published covering the topic of surfactant ISEs [11,12]. Following our general interest in anion sensing [13], anion-selective electrodes [14] and in particular ISEs for the detection of anionic surfactants [15,16] we report herein the use of a cyclam derivative (1,4,8,11-tetra(*n*-octyl)-1,4,8,11-tetraazacyclotetradecane) as carrier in the development of PVC-based membrane ion-selective electrodes for anionic surfactants.

2. Experimental

2.1. Apparatus

The potentiometric measurements were performed with a pH-meter (GLP22 Crison pH/mV meter). A Crison 52–40 double junction Ag/AgCl reference electrode-containing 0.1 M NaCl solution in the outer compartment was used. The internal reference electrode was a Hg/Hg_2Cl_2 electrode (XR100 Radiometer Copenhagen). A Metrohm 6.0507.120 ionic surfactant electrode was used as commercially available electrode. Potentiometric titrations were conducted with the help of an automatic burette and a titriprocessor using a $25.0 \pm 0.1\,^{\circ}C$ water-thermostated vessel and an automatic burette.

2.2. Reagents and solutions

Poly(vinyl chloride) of high molecular weight (PVC), 2-nitrophenyl octyl ether (NPOE), dibutyl phthalate (DBP), *N*-2-

hydroxyethyl-piperazine-*N'*-2-ethanesulfonic acid (HEPES) and tris(hydroxymethyl)aminomethane (TRIS) were purchased from Sigma–Aldrich. Tetrahydrofuran (THF), acetonitrile and tetra-*n*-octylammonium bromide (TOAB) were purchased from Merck. Acetate, chloride, bromide, sulfate, thiocynate, perchlorate, iodide, nitrate, phosphate, oxalate, carbonate, nitrite, sulfite and iodate solutions were prepared from potassium salts purchased from Scharlau. Dodecyl sodium sulfate ($CH_3(CH_2)_{11}OSO_3Na$) (NaDS) was purchased from Merck. Others anionic surfactants, hexyl sodium sulfate ($CH_3(CH_2)_5OSO_3Na$), decyl sodium sulfate ($CH_3(CH_2)_9OSO_3Na$), tetradecyl sodium sulfate ($CH_3(CH_2)_{13}OSO_3Na$), 1-decanesulfonic acid sodium salt ($CH_3(CH_2)_9SO_3Na$) and isethionic acid sodium salt ($HOCH_2CH_2SO_3Na$) were purchased from Acros Organics. Cholic acid sodium salt ($C_{24}H_{39}O_5Na$), glycodeoxycholic acid sodium salt ($C_{26}H_{42}NO_5Na$), hexadecyltrimethylamonium bromide ($CH_3(CH_2)_{15}N(CH_3)_3Br$), *t*-octylphenoxypolyethoxyethanol (Triton X-100) and myristyl sulfobetaine ($CH_3(CH_2)_{13}N^+(CH_3)_2CH_2CH_2CH_2SO_3{}^-$) surfactants were purchased from Sigma–Aldrich. Alkylbenzenesulfonate sodium (Na-LAS) was obtained from Petresa. Calcium, sodium, magnesium and ammonium solutions were prepared from chloride salts purchased from Scharlau. The reagent used for potentiometric titrations of anionic surfactants was a 0.004 mol/L TegoTrant A100 (1,3-didecyl-2-methylimidazolium chloride) solution from Metrohm. Working solutions were prepared by dilution with deionised-distilled water (Milli-Q water purification system). Experiments were performed at 25 °C in an argon atmosphere. The cyclam derivative 1,4,8,11-tetra(*n*-octyl)-1,4,8,11-tetraazacyclotetradecane (L) was synthesised following literature procedures [14c].

2.3. Membrane preparation and electrode construction

Membranes containing different composition were studied. These are shown in Table 1. The membranes A–E were prepared by dissolving 0–25.7 mg of the receptor 1,4,8,11-tetra(*n*-octyl)-1,4,8,11-tetraazacyclotetradecane (L), 0–21.0 mg TOAB, 200 mg PVC and 0–300 mg of DBP or NPOE in 5 mL of tetrahydrofuran. This solution was poured into a glass dish 5 cm in diameter. The solvent was allowed to evaporate overnight and a transparent membrane was obtained. A 6 or 7 mm diameter piece was cut out for ion-selective membranes and glued onto a PVC tube containing 0.01 M sodium dodecyl sulfate-TRIS pH 7, 0.01 M NaCl as the internal filling solution. The electrodes were conditioned by soaking overnight in a solution containing

Table 1
Composition of the membranes

Membrane	L	PVC	NPOE	DBP	TOABr
A	3.4	36.8	–	56.0	3.8
B	3.0	41.0	–	56.0	–
C	–	40.0	–	56.0	3.8
D	4.9	39.6	–	56.0	–
E	3.0	40.0	57.0	–	–
F	–	43.4	–	56.6	–

0.01 M sodium dodecyl sulfate-TRIS pH 7. When not in use, the electrode was kept immersed in the same solution.

2.4. emf measurements

The external reference electrode was a saturated calomel electrode and an electrode body ISE of Fluka ref. 45137 was used for all emf measurements. Potentiometric measurements were obtained by using the following cell assembly: external reference electrode| test solution |membrane| 0.01 M DS^-, 0.01 M TRIS, 0.01 M NaCl| Ag/AgCl. All potential measurements were carried out at pH 7 (0.01 M TRIS) on a GLP22 Crison pH/mV meter. Other buffers such as HEPES were also tested but generally worse electrode response was found. The detection limit was defined as the intersection of the extrapolated linear regions of the calibration graph. Potentiometric selectivity coefficients were determined according to the fixed interference method using 0.01 M solutions of interfering ion. Activity coefficients were calculated according to Debye-Hückel approximation. Calibration curves were constructed by plotting the potential, E, versus the logarithm of the sodium dodecyl sulfate activity at pH 7.0.

3. Results and discussion

3.1. Influence of membrane composition

Following our general interest in anion coordination chemistry and signalling, receptor L was synthesised and tested as ionophore in PVC-membrane electrodes. The use of this somewhat complex receptor is motivated by the presence in L of multiple binding sites that might result in an enhancement in selectivity and coordination ability due to both entropic and enthalpic factors. The receptor L is a tetraaza macrocycle (see Scheme 1) containing a cyclam core (cyclam = 1,4,8,11-tetraazacyclotetradecane). Cyclam and cyclam derivatives are very well-known ligands that have been extensively used as receptors for both metal cations and anions [17–19]. Cyclam behaves as a tetrabase and it has four protonation constants in water. It contains two relatively basic amines and at neutral pH is in its di-cationic form. It is specially the protonated forms of L that are expected to display both electrostatic and hydrogen bonding interactions with anionic groups such as those of anionic surfactants. Part of the work we develop herein is inspired on some previous studies by us showing the formation of strong complexes between polyazaoxacycloalkanes and dodecyl sulfate in aqueous environments [15].

L
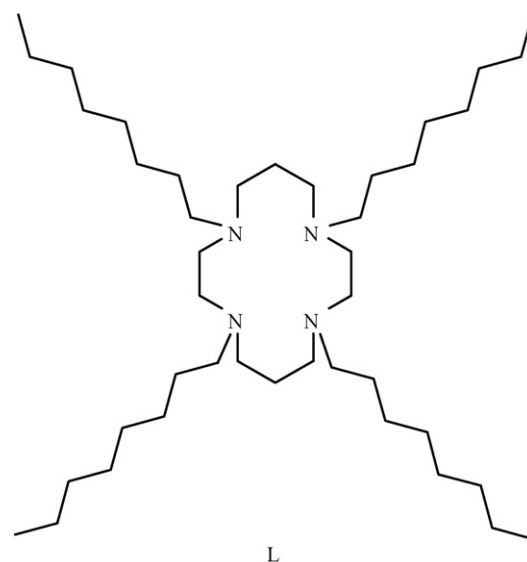
Scheme 1. Representation of ionophore L.

As it has been reported, the response of ion-selective electrodes in terms of selectivity and sensitivity depends on the ionophore but also on the final composition of the membrane ingredients, the plasticizer used and the presence of cationic or anionic additives. Therefore, in a first step several proportions of the membrane components ionophore, plasticizer, PVC and cationic additives were tested. All the membranes prepared were studied against dodecyl sulfate. Among the electrodes prepared with different membrane compositions, Table 1 shows five selected ones (electrodes A–E). Electrode A and B contain membranes with a similar composition the only difference being the presence in the later of the cationic additive tetra-*n*-octylammonium bromide (TOAB). The membrane C also contains the TOAB additive but lacks of the presence of L. Finally, the electrodes D and E represent certain studies related with the presence of a higher proportion of L in the membrane composition and a change in plasticizer (from DBP to NPOE), respectively. A comparison of the response of electrodes A–C against anions are shown in Fig. 1, whereas Table 2 shows some electrode characteristics. Electrodes A and B containing the cyclam-based carrier L show a remarkable selective Nernstian response to dodecyl sulfate (DS^-) whereas other anions gave a poorly defined response or no response at all. In contrast, electrode C that does not contain L, show a preferential response to perchlorate. By comparison of membrane A with membrane C it is also apparent that the former display a better

Table 2

Variation of potentiometric response properties with composition of various membranes based on Table 1 for DS^--selective electrodes measured in buffered solutions (TRIS pH 7)

Membrane	Slope (mV/decade)	Linear range (mol dm^{-3})	Limit of detection (mol dm^{-3})	Lifetime (days)	Response time (s)
A	−60.0	2.0×10^{-3} to 7.9×10^{-6}	4.0×10^{-6}	144	2.8 ± 1.2
B	−53.2	2.5×10^{-3} to 3.2×10^{-5}	2.0×10^{-5}	5	–
C	−59.0	3.2×10^{-3} to 4.3×10^{-6}	2.5×10^{-6}	28	–
D	−73.5	3.2×10^{-3} to 4.0×10^{-5}	1.1×10^{-5}	–	–
E	−59.5	2.5×10^{-3} to 4.0×10^{-5}	2.0×10^{-5}	25	–
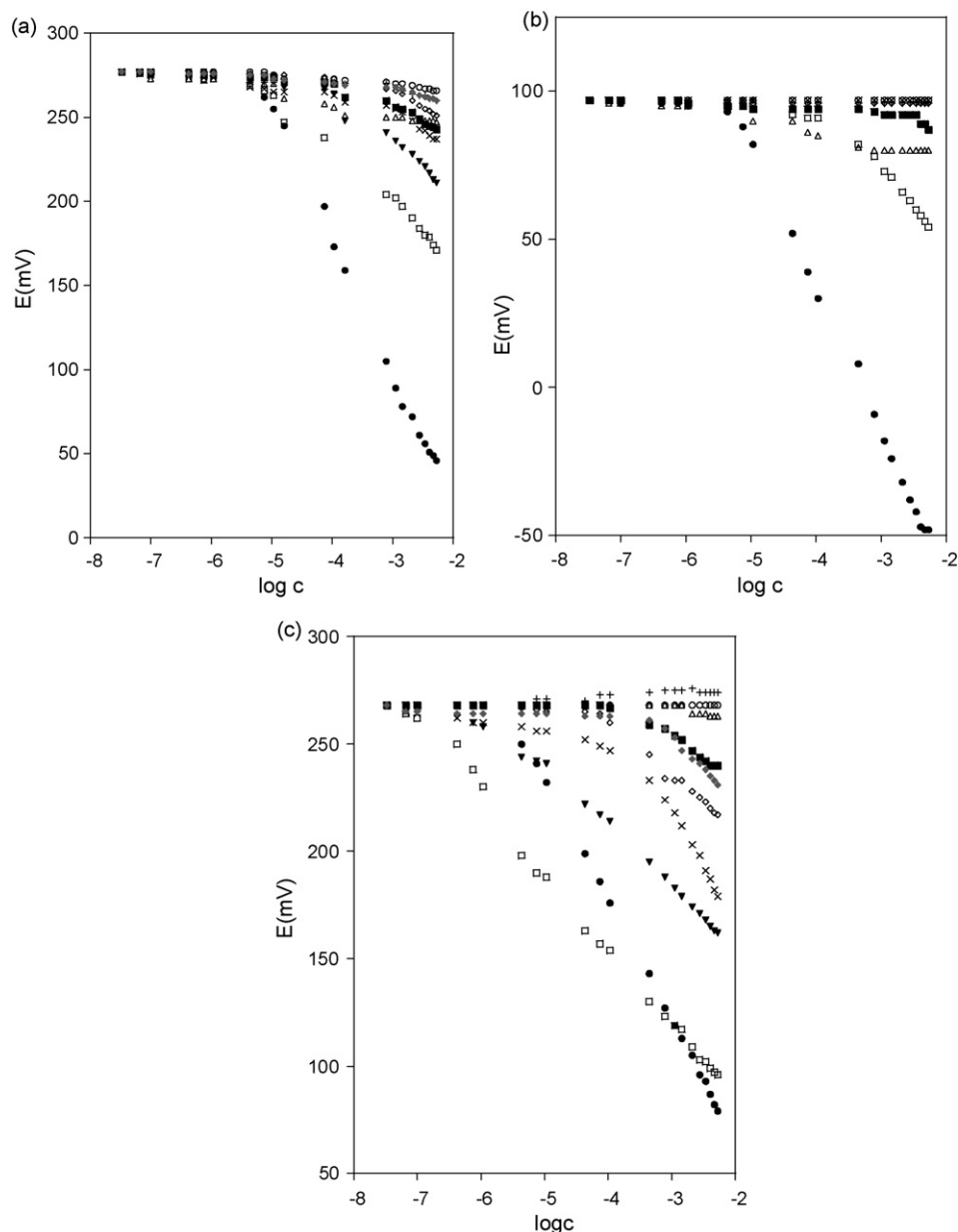
Fig. 1. Response of the PVC-based membrane electrode A (a), electrode B (b) and electrode C (c) at pH 7 in the presence of certain anions: (●) Dodecyl sulfate; (◇) NO_3^-; (□) ClO_4^-; (×) NO_2^-; (○) SO_4^{2-}; (▲) $H_2PO_4^-$/HPO_4^{2-}; (+) IO_3^-; (■) I^-; (▼) SCN^-; (♦) Cl^-.

performance in terms of selectivity (see Fig. 1) and lifetime suggesting that L displays a decisive role in the membrane response. Additionally, Table 2 shows that the best electrode in terms of slope, stability, reproducibility and lifetime was that prepared with membrane A. A comparison of the response found with membranes A and B shows that, in our case, the presence of the lipophilic cationic additive increases significantly the lifetime of the A electrode. The better performance of electrode A versus B or C in term of lifetime can be seen in Fig. 2 that shows a comparison of slope observed in their response to DS^- as a function of time (days); i.e. whereas electrode B is highly unstable and electrode C can only be used for 8 days, electrode A shows an acceptable slope (within 80% of the initial) for near 5 months. This result is in line with other reported systems that

show an enhanced response by the incorporation into the membrane of lipophilic ionic sites with a charge sign opposite to that of the primary ion [20]. At the same time, the incorporation of ionic additives lowers the electrical resistance of the membrane, which is especially important for the potential development of microelectrodes [21]. Table 3 illustrates the electrode characteristics of electrode A obtained at various time intervals. The electrode A exhibited good reproducibility in slope, linear concentration range and detection limit for 16 weeks, but slight drifts in its slope and detection limit were observed after 19 weeks. Additionally, Table 2 shows that a larger amount of ionophore (compare membrane D with membrane B) results in a poorer response towards DS^-. Changes in the plasticizer were also tested. In our case, the non-polar dibutyl phthalate

Fig. 2. Plot of the slope of electrodes A–C in the presence of DS⁻ vs. time (days).

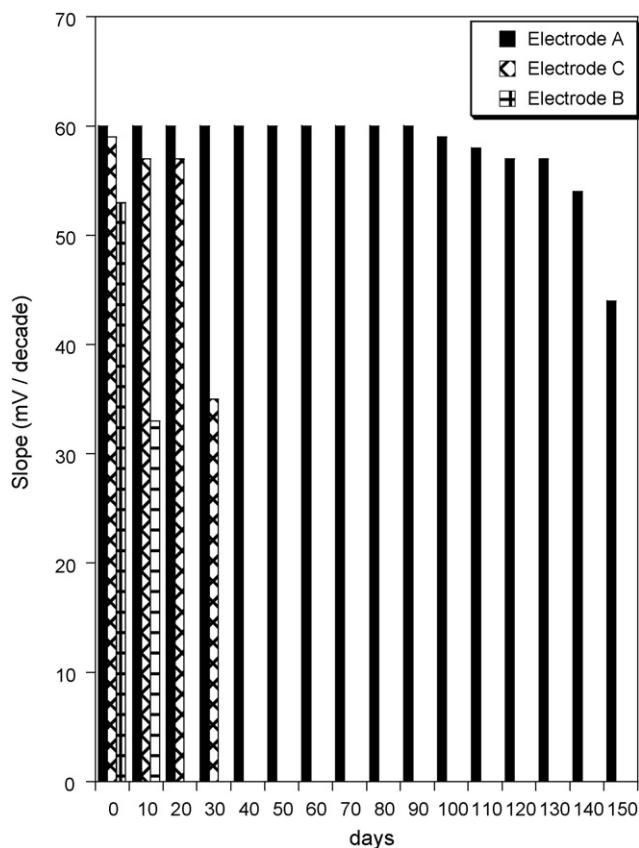DBP ($\varepsilon = 6.4$, membrane A) results in membranes showing a much better performance than when more polar plasticizers such as 2-nitrophenyl octyl ether NPOE ($\varepsilon = 14$, membrane E) were used.

Table 3
The life time study of the DS⁻-selective membrane A

Period (weeks)	Slope (mV/decade)	Linear range (M)	Detection limit (M)
1	−60.0	2.0×10^{-3} to 7.9×10^{-6}	4.0×10^{-6}
2	−60.0	2.0×10^{-3} to 7.9×10^{-6}	4.0×10^{-6}
3	−60.0	2.0×10^{-3} to 7.9×10^{-6}	4.0×10^{-6}
4	−60.0	2.0×10^{-3} to 7.9×10^{-6}	4.0×10^{-6}
5	−60.6	2.5×10^{-3} to 7.9×10^{-6}	5.0×10^{-6}
6	−60.1	1.1×10^{-3} to 1.1×10^{-5}	6.8×10^{-6}
7	−60.0	2.8×10^{-3} to 4.5×10^{-5}	5.8×10^{-6}
8	−60.1	2.2×10^{-3} to 5.0×10^{-5}	4.0×10^{-6}
9	−60.0	2.5×10^{-3} to 4.0×10^{-5}	8.9×10^{-6}
10	−60.1	1.4×10^{-3} to 7.9×10^{-6}	1.6×10^{-6}
11	−60.1	2.2×10^{-3} to 4.0×10^{-5}	5.6×10^{-6}
12	−9.2	2.6×10^{-3} to 4.2×10^{-5}	5.8×10^{-6}
13	−58.0	1.9×10^{-3} to 4.2×10^{-5}	6.2×10^{-6}
14	−57.0	2.2×10^{-3} to 4.2×10^{-5}	6.1×10^{-6}
15	−56.9	2.2×10^{-3} to 4.2×10^{-5}	6.0×10^{-6}
16	−56.0	5.2×10^{-3} to 7.9×10^{-6}	5.6×10^{-6}
19	−54.0	5.2×10^{-3} to 1.0×10^{-5}	5.9×10^{-6}
20	−54.0	4.6×10^{-3} to 1.0×10^{-5}	5.9×10^{-6}
21	−44.1	4.0×10^{-3} to 2.5×10^{-5}	1.3×10^{-5}

The receptor L was introduced in the membrane in their unprotonated form. Electrodes made with this ionophore, however, gave an anionic response (see for instance response of membrane B) suggesting that it is finally protonated in the membrane. This protonation of the cyclam derivative can be reached during the stabilization of the membrane when in contact with aqueous solutions or could also be favoured by some residual acid that usually contains PVC. Although protonation stability constants cannot be determined in the PVC membranes, the degree of protonation might be estimated by comparison with the protonation constants in aqueous media. It has been reported that ionophore L behaves as tetra-protic base in dioxane:water mixtures [14c]. The first two protonation constants ($L + H^+ = LH^+$, $LH^+ + H^+ = LH_2^{2+}$, $\log K = 10.12$ and $\log K = 7.04$, respectively) are less basic than the corresponding protonation of cyclam in water ($\log K = 11.59$ and $\log K = 10.62$). In contrast L acts as a stronger base than cyclam when the last two protonations are compared (the logarithm of the last two protonations for cyclam in water are $\log K = 1.61$ and $\log K = 2.42$) [22]. In general the protonation behaviour of L is similar to other tetra-substituted cyclam derivatives. The values of the protonation constants of L in dioxane:water mixtures suggest that a mixture of the species $[HL]^+$ and $[H_2L]^{2+}$ would most likely exist in the prepared membranes when those are left in contact with an aqueous solution at neutral pH.

3.2. Effect of pH and influence of the buffer

The influence of pH on the potential response of the electrode A was studied at a fixed concentration of DS⁻ of 1×10^{-4} mol dm⁻³ over a pH range 4–11. The pH was varied by potassium hydroxide and hydrochloric acid addition. The electrode potential is independent on the pH range 5–8.5 and the pH 7 was chosen as the pH for the following studies. At basic pH the potential decreases most likely due to a membrane response to the OH⁻ anion.

Then effect of the buffer used in the response towards DS⁻ of electrodes A and B was also studied. A better response was found to TRIS-buffered solutions of DS⁻ than when HEPES was used. Thus for instance, electrode A displays in TRIS a Nernstian slope of -60.0 ± 0.9 mV/decade over a relatively wide concentration range (2.0×10^{-3} to 7.9×10^{-6} mol dm⁻³) and a limit of detection of 4.0×10^{-6} mol dm⁻³, whereas in HEPES show significantly poorer figures with a slope of -51.0 ± 0.8 mV/decade, linear range of 5.4×10^{-3} to 7.4×10^{-5} mol dm⁻³ and a detection limit of 3.2×10^{-5} mol dm⁻³.

3.3. Response time

The response time of electrode A was evaluated by measuring the time required to achieve a steady-state potential [23,24]. A response time of 3.5 s was found as the time required for the electrode to reach a potential within ± 1 mV of the final equilibrium when the measurements were performed alternatively in 10^{-3} M and 10^{-5} M solutions of dodecyl sulfate. The standard deviation of the response time calculated from six measurements was ± 1.4 s. When the measurements were carried out alternatively

in a 10^{-3} M solution of dodecyl sulfate and deionised-distilled water, the response time of the electrode was 2.8 ± 1.2 s.

3.4. Response of the electrode to anionic surfactants

We carried our several studies with electrode A in relation to its response in the presence of surfactants. As it has been shown in Fig. 1, the electrode A displays a remarkable selective response to DS⁻, the electrode show certain response to ClO_4^- and HCO_3^- and a very poor change of the potential in the presence of the anions NO_3^-, NO_2^-, SO_4^{2-}, phosphate, IO_3^-, I⁻, SCN⁻ or Cl⁻. Although cyclam derivatives are well-known anion coordination systems, they can also act as ligand for cations coordination, therefore, a study of the response of electrode A to the usually water-present cations Na⁺, NH_4^+, Ca^{2+} and Mg^{2+} was carried out. The results are shown in Fig. 3. As it can be seen the electrode displays negligible response to these species when compared with that found for DS⁻.

In order to quantify the selective behaviour found for electrode A towards dodecyl sulfate, we have carried out studies to determine selectivity coefficients. Selectivity is one of the most important characteristics of electrodes that gives an idea of the preference of the sensor for the primary ion with respect to potentially interfering species and display the ability of distinguish this ion from a complex mixture. The potentiometric selectivity coefficients (K_{DS^-,X^-}^{pot}) of electrode A were calcu-
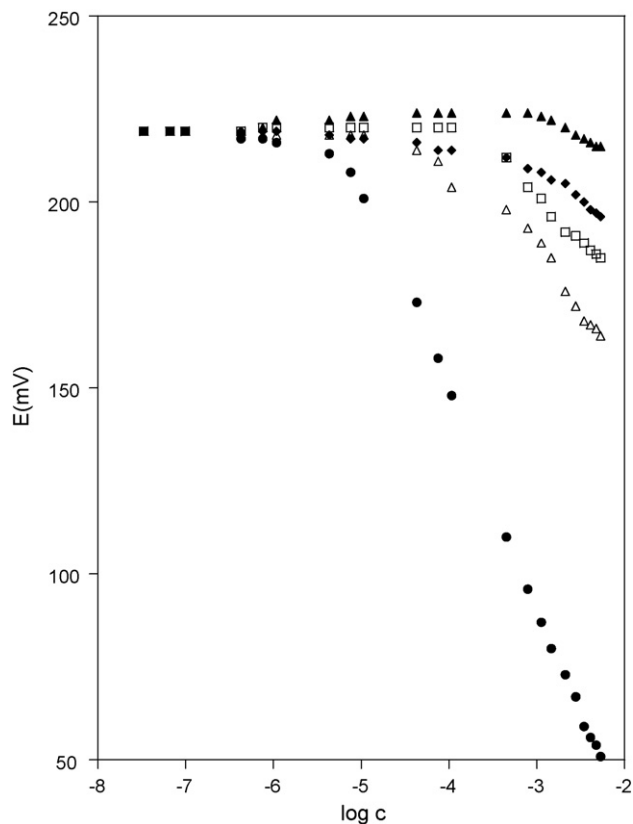

Fig. 3. Response of the PVC-based membrane electrodes A at pH 7 in the presence of DS⁻ and certain cations: (▲) Na⁺; (□) Mg^{2+}; (◆) NH_4^+; (△) Ca^{2+}; (●) Dodecyl sulfate.

Table 4
Potentiometric selective coefficients for electrode A

Interfering ion (B)	$K_{DS^-,B}^{pot}$ (−log)	Interfering ion (B)	$K_{DS^-,B}^{pot}$ (−log)
ClO_4^-	1.9	Br⁻	3.1
HCO_3^-	2.2	IO_3^-	3.2
SCN⁻	2.6	NO_2^-	3.2
NO_3^-	2.8	SO_3^{2-}	3.2
CH_3COO^-	2.8	$H_2PO_4^-/HPO_4^-$	3.4
I⁻	2.8	$C_2O_4^{2-}$	4.0
Cl⁻	3.1	SO_4^{2-}	4.3

lated by means of the fixed interference method considering dodecyl sulfate (DS⁻) as the principal anion and using concentrations of 1.0×10^{-2} mol dm⁻³ for interfering anions. K_{DS^-,X^-}^{pot} was calculated with Eq. (1) [25]:

$$K_{ij}^{pot} = \frac{a_{DS^-}}{(a_{X^-})^{z_{DS^-}/z_{X^-}}} \tag{1}$$

where a_{DS^-} is the activity of the primary ion, DS⁻, a_{X^-} the activity of the corresponding interfering ion, and z_{DS^-} and z_{X^-} are the corresponding charge of the primary ion and the interfering ion, respectively. All the measurements were carried out at pH 7.0 buffered with TRIS. The calculated selectivity coefficients are listed in Table 4. These values clearly show that A behaves as a selective electrode for the anion dodecyl sulfate (DS⁻) over other different ion tested. The selectivity sequence for A was $DS^- > ClO_4^- > HCO_3^- > SCN^- > NO_3^- \approx CH_3COO^- \approx I^- > Cl^- > Br^- > IO_3^- \approx NO_2^- \approx SO_3^{2-} > phosphate > C_2O_4^{2-} > SO_4^{2-}$. The electrode shows some deviations from the Hoffmeister series ($ClO_4^- > SCN^- > I^- > NO_3^- > Br^- > Cl^- > HCO_3^- > CH_3COO^- > SO_4^{2-} > HPO_4^{2-}$) being the most significant that found for the hydrophilic anion bicarbonate. Although this deviation is not very important in relation to the selective behaviour found for DS⁻, it can be related with certain preferential coordination of certain anions such as carbonate with the receptor L in the PVC media. As can be seen in Table 4, the logarithm of the selectivity coefficients determined for electrode A are in general lower than −2.6 (except for ClO_4^- and HCO_3^-) indicating that most of the anions would not significantly disturb the determination of dodecyl sulfate in real samples.

Another study carried out with electrode A was to determine the response of the electrode towards different surfactants. As it is well-known surfactants can be divided in anionic, cationic, non-ionic and zwitterionic. As it can be seen in Fig. 4 electrode A displays a different response to these groups of surfactants. As seen above, electrode A displays a Nernstian response to DS⁻ (an alkyl sulfate). Also a linear but sub-Nernstian outcome was found in the presence of to Na-LAS (an alkylbenzene sulfonate) in a wide concentration range. In contrast a poorer response was found for the 1-decanesulfonic acid sodium salt and no response was observed in the presence of the isethionic acid sodium salt (alkylsulfonate). Neither response was found for *t*-octylphenoxypolyethoxyethanol (a non-ionic surfactant) and cholic acid and glycodeoxycholic acid (anionic surfactants
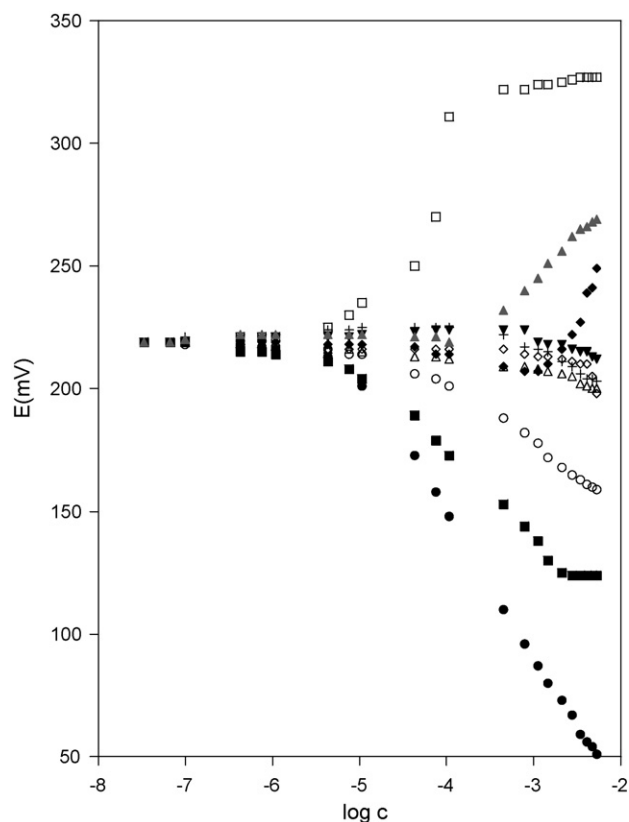
Fig. 4. Response of the PVC-based membrane electrodes A at pH 7 in the presence of certain surfactants: (●) Dodecyl sulfate; (□) Hexadecyltrimethylammoniun; (▲) *N*-tetradecyl-*N*,*N*-dimethyl-3-ammonium-1-propanesulfonate; (◆) Triton X-100; (△) 1-Decane sulfonic acid; (○) Decyl sulfate; (▼) Isethionic acid; (■) Alkylbenzenesulfonate; (+) Cholic acid; (◇) Glycodeoxycholic acid.

containing carboxylate groups). In the presence of the zwitterionic surfactant *N*,*N*,-dimethyl-3-ammonio-1-propanesulfonate a very poor no well-defined cationic response was found. Moreover, the electrode A displays a clear non-linear response in the presence of the cationic surfactant hexadecyltrimethylammonium bromide.

3.5. Analytical applications

The new electrode has been used for the determination of DS$^-$ in water by titration using electrode A in conjunction with an Ag/AgCl reference electrode and the results have been compared with those obtained for the commercially available "Ionic surfactant" electrode from Metrohm. In a typical experiment, 30 mL of the corresponding sample mixture was placed in a beaker with 2.5 mL of methanol and 5 mL of buffered water at pH 3. The electrodes were immersed in the cell and the solution was titrated using 0.004 mol dm^{-3} TegoTrant A100. Fig. 5 shows a typical sigmoidal shape of the curve obtained from the titration of DS$^-$. The titration volume was measured as the inflection point of the titration curve. Table 5 shows the results obtained for the analysis of anionic surfactants in certain prepared and natural samples by using electrode A and the Methrom electrode. An accurate determination was observed.
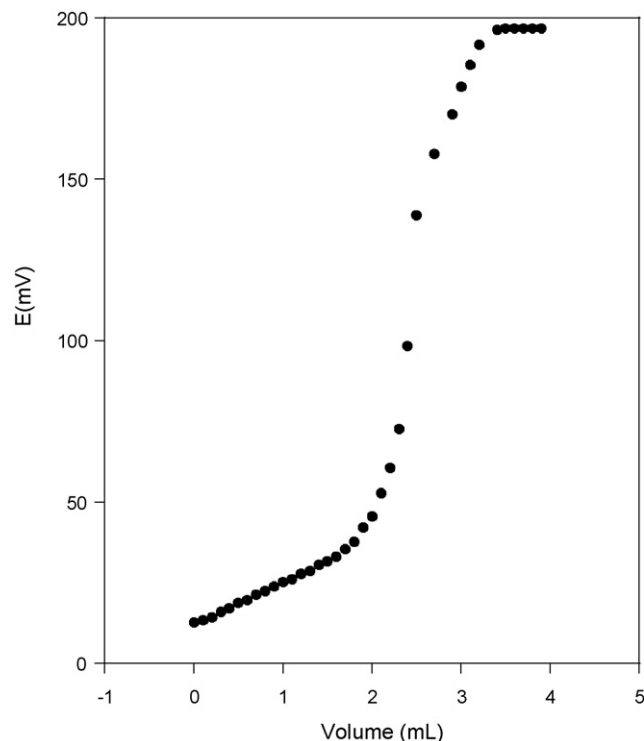
Fig. 5. Potentiometric titration curve of dodecyl sulfate ($10^{-4.5}$ M) with 0.04 M TegoTrant A100 as titrant in water.

Table 5
Analysis of the anionic surfactants concentration in water by using electrode A and a commercially available Metrohm electrode

Samples	Metrohm (mmol dm^{-3})[f]	Electrode A (mmol dm^{-3})[f]
Lab-1[a]	0.313 ± 0.001	0.322 ± 0.012
Lab-2[b]	0.032 ± 0.001	0.035 ± 0.002
Lab-3[c]	0.100 ± 0.001	0.110 ± 0.001
Lab-4[d]	0.034 ± 0.001	0.037 ± 0.001
River water-1[e]	0.002 ± 0.001	0.004 ± 0.001
River water-2[e]	0.052 ± 0.001	0.073 ± 0.007

[a] Sample Lab-1 contains 0.316 mmol dm^{-3} of DS$^-$.
[b] Sample Lab-2 contains 0.032 mmol^{-3} DS$^-$ and 0.031 mmol^{-3} CH$_3$(CH$_2$)$_5$OSO$_3$Na.
[c] Sample Lab-3 contains 0.032 mmol^{-3} DS$^-$, 0.031 mmol^{-3} CH$_3$(CH$_2$)$_5$OSO$_3$Na, 0.030 mmol^{-3} CH$_3$(CH$_2$)$_{13}$OSO$_3$Na and 0.031 mmol^{-3} CH$_3$(CH$_2$)$_9$SO$_3$Na.
[d] Sample Lab-4 contains 0.032 mmol^{-3} DS$^-$, 0.031 mmol^{-3} CH$_3$(CH$_2$)$_9$SO$_3$Na, 0.031 mmol^{-3} CH$_3$(CH$_2$)$_{13}$N$^+$(CH$_3$)$_2$CH$_2$CH$_2$CH$_2$SO$_3$$^-$, 0.031 mmol^{-3} C$_{24}H_{39}NaO_5$ and 0.032 mmol^{-3} Triton X-100.
[e] Natural samples form river water.
[f] Averaged values from three measurements.

4. Conclusions

As far as we know we have used herein for the first time the very well-known cyclam ligand as carrier in PVC membrane ion-selective electrodes for anionic surfactants. L was used as an alternative ionophore to simple quaternary ammonium salts. The electrode A contains a membrane of the following composition: 56% DBP, 3.4% ionophore, 3.8% TOABr and 36.8% PVC. This electrode displays a Nernstian slope of -60.0 ± 0.9 mV/decade over the 2.0×10^{-3} to

7.9×10^{-6} mol dm^{-3} concentration range and shows a limit of detection of 4.0×10^{-6} mol dm^{-3}. The electrode can be use to a period of 144 days without showing significant changes in the value of slope or working range. The electrode showed a clear anionic response to DS$^-$ and to Na-LAS and a much poorer response to other anionic surfactants and to non-ionic surfactants. The selective sequence found for electrode A was DS$^- >$ ClO$_4^- >$ HCO$_3^- >$ SCN$^- >$ NO$_3^- \approx$ CH$_3$COO$^- \approx$ I$^- >$ Cl$^- >$ Br$^- >$ IO$_3^- \approx$ NO$_2^- \approx$ SO$_3^{2-} >$ phosphate $>$ C$_2$O$_4^{2-} >$ SO$_4^{2-}$. Furthermore, most of the potentiometric coefficients determined are relatively low indicating that most common anions would not interfere in the DS$^-$ determination. The new electrode A has been used for the determination of DS$^-$ in water samples by titration procedures.

Acknowledgement

References

[1] R.D. Swisher, Surfactant Biodegradation, 2nd ed., Dekker, New York, 1987.

[2] M. Swedmark, B. Braaten, E. Emanuels, A. Granmo, Mar. Biol. 9 (3) (1971) 183.

[3] (a) G. Eppert, G. Liebscher, Z. Chem. 18 (1978) 188;
(b) C.J. Dowle, B.G. Cooksey, W.C. Campbell, Anal. Proc. 25 (1988) 78;
(c) L.I. Makovetskaya, I.L. Maislina, S.P. Volosovich, Seifen, Oele, Fette, Wachse 117 (1991) 565;
(d) H.W. Leuchte, H.D. Kahleyss, J. Faltermann, Fett-Wiss-Technol. 94 (1992) 64;
(e) S. Alegret, J. Alonso, J. Bartroli, J. Baro-Roma, J. Sanchez, M. del Valle, Analyst 119 (1994) 2319;
(f) K. Vytras, J. Kalous, J. Jezkova, Egypt J. Anal. Chem. 6 (1997) 107;
(g) R. Schulz, P. Bruttel, H. Reger, G. Wulk, J. Thiede, R. Unthan, C. Götz, Titrimetric Determination of Surfactants and Pharmaceuticals, Metrohm, Switzerland, 1999, p. 242.

[4] (a) H. Hellman, Fresenius J. Anal. Chem. 293 (1978) 359;
(b) S. Taguchi, K. Goto, Talanta 27 (1980) 289;
(c) F. Canete, A. Rios, M.D. Luque de Castro, M. Valcarcel, Anal. Chem. 60 (1988) 2354;
(d) H. Liu, P.K. Dasgupta, Anal. Chim. Acta 288 (1994) 237;
(e) S. Motomizu, Y.H. Gao, K. Uemura, S. Ihsibara, Analyst 119 (1994) 473.

[5] (a) S. Rubio-Barroso, M. Gomez-Rodriguez, L.M. Polo-Diez, Microchem. J. 37 (1988) 93;
(b) S. Rubio-Barroso, V. Rodríguez-Gamonal, L.M. Polo-Diez, Anal. Chim. Acta 206 (1988) 351.

[6] (a) A. Nakae, K. Tsuji, M. Yamanaka, Anal. Chem. 52 (1980) 2275;
(b) S.I. Abidi, J. Chromatogr. 200 (1980) 216;
(c) T. Saito, K. Higashi, G. Hagiwara, Z. Fresenius, Anal. Chem. 313 (1982) 21;
(d) M.Y. Ye, R.G. Walkup, K.D. Hill, J. Liq. Chromatogr. 17 (1994) 4087.

[7] Z.M. Shakhsher, W.R. Seitz, Anal. Chem. 62 (1990) 1758.

[8] C. Coll, R. Martínez-Máñez, M.D. Marcos, F. Sancenón, J. Soto, Angew. Chem. Int. Ed. 46 (2007) 1675.

[9] (a) T. Fuginaga, S. Okazaki, H. Freiser, Anal. Chem. 46 (1974) 1842;
(b) B.J. Birch, D.E. Clarke, Anal. Chim. Acta 69 (1974) 473;
(c) N. Ishibashi, T. Masadome, T. Imato, Anal. Sci. 2 (1986) 487;
(d) T. Masadome, T. Imato, N. Ishibashi, Anal. Sci. 3 (1987) 121;
(e) C.J. Dowle, B.G. Cooksey, J.M. Ottaway, W.C. Campbell, Analyst 113 (1988) 117;
(f) W. Szczepaniak, Analyst 115 (1990) 1451;
(g) T. Tominaga, D. Hachisu, M. Kamado, Langmuir 10 (1994) 4676.

[10] (a) M. Gerlache, Z. Sentürk, J.C. Viré, J.M. Kauffmann, Anal. Chim. Acta 349 (1997) 59;
(b) F.A. Chmilenko, I.V. Koroboca, L.N. Danilenko, J. Anal. Chem. 55 (2000) 1058;
(c) J. Sanchez, M. del Valle, Talanta 54 (2001) 893;
(d) B. Kovács, B. Csóka, G. Nagy, A. Ivaska, Anal. Chim. Acta 437 (2001) 67;
(e) S. Matysik, F.M. Matysik, W.D. Einicke, Sens. Actuators B 85 (2002) 104;
(f) H. Fukui, A. Kaminaga, T. Maeda, K. Hayakawa, Anal. Chim. Acta 481 (2003) 221;
(g) M. Arvand-Barmchi, M.F. Mousavi, M.A. Zanjanchi, M. Shamsipur, Microchem. J. 74 (2003) 149.

[11] M. Sak-Bosnar, Z. Grabaric, B.S. Grabaric, Biotechnology 42 (2004) 197.

[12] J. Sánchez, M. del Valle, Crit. Rev. Anal. Chem. 35 (2005) 15.

[13] (a) R. Martínez-Máñez, F. Sancenón, Chem. Rev. 103 (2003) 4419;
(b) M. Comes, G. Rodríguez-López, M.D. Marcos, R. Martínez-Máñez, F. Sancenón, J. Soto, L.A. Villaescusa, P. Amorós, D. Beltrán, Angew. Chem. Int. Ed. 44 (2005) 2918;
(c) R. Martínez-Máñez, F. Sancenón, J. Fluoresc. 15 (2005) 267;
(d) R. Martínez-Mañez, F. Sancenón, Coord. Chem. Rev. 250 (2006) 3081;
(e) A.B. Descalzo, R. Martínez-Máñez, Sancenón, K. Hoffmann, K. Rurack, Angew. Chem. Int. Ed. 45 (2006) 5924;
(f) R. Casasús, E. Aznar, M.D. Marcos, R. Martínez-Máñez, F. Sancenón, J. Soto, P. Amorós, Angew. Chem. Int. Ed. 45 (2006) 6661;
(g) C. Coll, R. Casasús, E. Aznar, M. D: Marcos, R. Martínez-Máñez, F. Sancenón, J. Soto, P. Amorós, Chem. Commun. (2007) 1957;
(h) E. Padilla-Tosta, R. Martínez-Máñez, T. Pardo, J. Soto, M.J.L. Tendero, Chem. Commun. (1997) 887.

[14] (a) M.-J. Seguí, J. Lizondo-Sabater, R. Martínez-Máñez, F. Sancenón, J. Soto, Analyst 127 (2002) 387;
(b) J. Lizondo-Sabater, R. Martínez-Máñez, F. Sancenón, M.-J. Seguí, J. Soto, Anal. Chim. Acta 459 (2002) 229;
(c) J. Lizondo-Sabater, M.-J. Seguí, J.M. Lloris, R. Martínez-Máñez, T. Pardo, F. Sancenón, J. Soto, Sens. Actuators B Chem. 101 (2004) 20;
(d) R. Martínez-Máñez, J. Soto, E. García-Breijo, L. Gil, J. Ibáñez, E. Llobet, Sens. Actuators B Chem. 104 (2005) 302;
(e) C. Coll, R.H. Labrador, R. Martínez-Máñez, J. Soto, F. Sancenón, M.-J. Seguí, E. Sánchez, Chem. Commun. (2005) 3033;
(f) M.-J. Seguí, J. Lizondo-Sabater, R. Martínez-Máñez, F. Sancenón, J. Soto, Talanta 68 (2006) 1182;
(g) M.-J. Seguí, J. Lizondo-Sabater, R. Martínez-Máñez, F. Sancenón, J. Soto, E. García-Breijo, L. Gil, Sensors 6 (2006) 480;
(h) L. Gil, E. García-Breijo, J. Ibáñez, R.H. Labrador, E. Llobet, R. Martínez-Máñez, J. Soto, Sensors 6 (2006) 697.

[15] M.-J. Seguí, J. Lizondo-Sabater, R. Martínez-Máñez, T. Pardo, F. Sancenón, J. Soto, Anal. Chim. Acta 525 (2004) 83.

[16] M.-J. Seguí, J. Lizondo-Sabater, A. Benito, R. Martínez-Máñez, T. Pardo, F. Sancenón, J. Soto, Talanta 71 (2007) 333.

[17] M.E. Padilla-Tosta, J.M. Lloris, R. Martínez-Máñez, A. Benito, J. Soto, T. Pardo, M.A. Miranda, M.D. Marcos, Eur. J. Inorg. Chem. (2000) 741;
M. Lloris, R. Martínez-Máñez, M.E. Padilla-Tosta, T. Pardo, J. Soto, P. D: Beer, J. Cadman, D.K. Smith, J. Chem. Soc., Dalton Trans. (1999) 2359.

[18] M.E. Padilla-Tosta, J.M. Lloris, R. Martínez-Máñez, T. Pardo, F. Sancenón, J. Soto, M.D. Marcos, Eur. J. Inorg. Chem. (2001) 1221;
J.M. Lloris, R. Martínez-Máñez, T. Pardo, J. Soto, M.E. Padilla-Tosta, Chem. Commun. (1998) 837.

[19] H. Plenio, C. Aberle, Y. Al Shihadeh, J.M. lloris, R. Martínez-Máñez, T. Pardo, J. Soto, Chem. Eur. J. 7 (2001) 2848;

M.J.L. Tendero, A. Benito, R. Martínez-Máñez, J. Soto, E. García-España, J.A. Ramirez, M.I. Burguete, S.V. Luis, J. Chem. Soc., Dalton Trans. (1996) 2923.

[20] E. Bakker, P. Bühlmann, E. Pretsch, Chem. Rev. 97 (1997) 3083.

[21] D. Ammann, Ion-selective Microelectrodes: Principles, Design and Application, Springer-Verlag, Berlin, 1984.

[22] A.E. Martell, R.M. Smith, R.M. Motekaitis, NIST Critical Stability Constants of Metal Complexes Database, Texas A&M University, College Station, 1993.

[23] R.P. Buck, E. Lindner, Pure Appl. Chem. 66 (12) (1994) 2527.

[24] C. Macca, Anal. Chim. Acta 512 (2004) 183.

[25] IUPAC, Pure Appl. Chem. 48 (1976) 127.

Immobilized phospholipid capillary electrophoresis for study of drug–membrane interactions and prediction of drug activity

Jie Mei [a], Jian-Rong Xu [a], Yu-Xiu Xiao [a,*], Qian-Rui Zhang [a], Yu-Qi Feng [b]

[a] *College of Pharmacy, Wuhan University, Wuhan 430072, PR China*
[b] *Department of Chemistry, Wuhan University, Wuhan 430072, PR China*

Abstract

Immobilized phospholipid capillary electrophoresis (IPCE) was developed for studying the interactions between a set of nonsteroidal anti-inflammatory drugs (NSAIDs) and membrane and predicting the biological activity of NSAIDs. Supported vesicle layers and supported phospholipid bilayers were attached to the inner surface of a capillary wall simply by rinsing with liposome solutions. The liposomes, composed of soybean phosphatidylcholine (SPC) or SPC and different proportions of cholesterol (Ch), were small unilamellar vesicles prepared by sonication. The normalized capacity factor (K_{IPCE}) was introduced into IPCE for evaluating drug–membrane interactions. Related theories and equations were derived to calculate K_{IPCE} values from apparent migration time of a solute and electroosmotic flow. The strong relationships were observed between $\log K_{IPCE}$ (SPC) values and $\log K_{lw}$ values (the partition coefficients determined in free SPC-liposome partitioning system) ($R = 0.9855$ and $P < 0.0001$) or $\log K_{ILC}$ values (the normalized capacity factors determined by immobilized POPC-liposome chromatography, POPC represents 1-palmitoyl-2-oleoyl-*sn*-glycero-3-phosphocholine) ($R = 0.9875$ and $P < 0.0001$). In addition, $\log K_{IPCE}$ (SPC/Ch 80:20%) values correlated well with the pIC_{50} (the minus logarithm of IC_{50}) values for cyclooxygenase 2 determined on intact cells ($R = 0.959$ and $P < 0.001$). These results confirmed that IPCE, K_{IPCE} value as evaluation index, can be effactually used for studying drug–membrane interactions and it has the potential to predict drug activity. Cholesterol-containing (20 mol%) liposomes may be more suitable to mimic real cell membrane.
© 2007 Elsevier B.V. All rights reserved.

Keywords: Capillary electrophoresis; Coated capillaries; Liposomes; Nonsteroidal anti-inflammatory drugs; Drug–membrane interactions

1. Introduction

Interest in liposome as model membrane for the study of interactions between membrane and drugs or biologically important molecules is rapidly increasing, since liposomal lipid bilayers are structurally similar to biomembrane [1,2]. Nowadays, there are several liposome-related methods available for studying solute–membrane interactions, such as free liposome partitioning system [3–5], immobilized artificial membrane (IAM) [6,7], immobilized liposome chromatography (ILC) [8–11] and liposome electrokinetic capillary chromatography (LECC) [12–16]. The free liposome partitioning method is a classical technique used to determine membrane partition coefficients of solutes. However, the method not only is time-consuming and tedious, but also requires large amount of samples and liposomes. In

IAM, a monolayer of phospholipid analogs is covalently bonded to silica particles at high-molecular surface density, but fails to mimic the bilayer structure of biomembrane. In ILC, liposomes are entrapped in gel beads and analysis is directly performed on liposomal membrane. Generally, the preparation of immobilized liposome chromatographic columns is tedious, time-consuming and costly.

In LECC, liposomes are used as carrier in an electrophoretic buffer solution and act as pseudostationary phase providing sites of interaction for solutes. LECC has an essential advantage that analysis time is much shorter and the consumption of phospholipids, liposomes and samples is much less. Nevertheless, the main shortcoming of LECC is the existence of an elution window that limits the dynamic range for compounds [14]. Besides, the consumption of liposomes as a free flowing pseudostationary phase is still high and LECC is unfit for direct coupling to mass spectrometry.

In recent years, liposomes have been developed as coating materials in capillary electrophoresis because this

* Corresponding author. Tel.: +86 27 68759892; fax: +86 27 68754629.
E-mail address: yuxiuxiao@yahoo.com.cn (Y.-X. Xiao).

liposome-coating technique can overcome some drawbacks of LECC. Cunliffe et al. [17] coated the inner wall of silica capillary with 1,2-dilauroyl-*sn*-phosphatidylcholine (DLPC) by rinsing the capillary repeatedly with a solution of small unilamellar vesicles prepared by sonication. In their research, phospholipid bilayers were not intentionally applied as chromatographic stationary phase rather to prevent protein adsorption. Later, Riekkola and co-workers [18–22] published a series of papers describing the methodologies to prepare a coated capillary with liposome solutions. The prepared capillaries showed the ability to separate neutral compounds (e.g. steroids and phenols) due to the difference in interactions between neutral compounds and liposomal membrane. Manetto et al. [23] prepared a liposome-modified capillary for studies of acidic drugs–liposome binding, which was expressed as free binding energy changes $[\Delta(\Delta G^\circ)]$ relatively to an arbitrarily selected standard (aspirin).

In the present study, capillary electrophoresis with a liposome-coated capillary was used to study the interactions between a set of nonsteroidal anti-inflammatory drugs (NSAIDs) and membrane and predict the biological activity of NSAIDs. When a capillary was coated with liposomes, the final form of coating in the inner wall of a capillary was supported phospholipid bilayers or supported vesicular layers or both of them depending on the conditions during the coating procedure [24]. However, analysis was directly performed on phospholipid bilayers no matter what the final form of coating was. Therefore, capillary electrophoresis with a liposome-coated capillary was shortly called for immobilized phospholipid capillary electrophoresis (IPCE) in our paper. The normalized capacity factor (K_{IPCE}) was introduced into IPCE as an index for evaluating drug–membrane interactions. Related theories and equations were derived to calculate K_{IPCE} values. The properties of IPCE for studying drug–membrane interactions were investigated by comparing K_{IPCE} with the partition coefficient (K_{lw}) in free liposome partitioning system, the ILC normalized capacity factor (K_{ILC}) and the IAM chromatographic retention factor (k_w^{IAM}). In order to further assess the capability of IPCE for predicting drug activity, the relationship between K_{IPCE} and IC$_{50}$ for cyclooxygenase 2 (COX-2) determined on intact cells was investigated. IC$_{50}$, an index of NSAIDs activity, is NSAIDs concentration required for 50% inhibition of COX-2.

2. Experimental

2.1. Materials

Cholesterol (Ch), Tris and phosphate were purchased from National Medicine Co. Ltd. (Shanghai, China). Soybean phosphatidylcholine (SPC) was prepared from commercially available soybean powder phospholipids by solvent extraction and column chromatography (purity 92.80%) [25]. A set of model drugs, NSAIDs, e.g. sulindac was from National Institute for the Control of Pharmaceutical and Biological Products (Beijing, China), oxaprozin, ibuprofen, naproxen, indomethacin and salicylic acid were provided by Tianmen Pharmaceutical Factory (Tianmen, Hubei, China), diclofenac sodium by Shashi Pharmaceutical Factory (Shashi, Hubei, China), aspirin by Hubei

Pharmaceutical Factory (Wuhan, Hubei, China), flubiprofen by Sanwei Pharmaceutical Co. Ltd. (Shanghai, China), piroxicam by Yupeng Pharmaceutical Co. Ltd. (Shanxi, China). Chloroform and methanol were of analytical grade, obtained from Shanghai Medicine Company (Shanghai, China). Ultrapure distilled water with a resistance greater than 17 MΩ was used (SG, German).

2.2. Equipments

The CE experiments were carried out with a CAPEL-105 CE system (LUMEX, Russia) which consists of a high-voltage power supply, a multi-wavelength UV–vis detector, a water cooling circulating device for temperature control of the cartridge containing capillary and 1.5 X Chrom&Spec software providing data acquisition and evaluation. Uncoated fused-silica capillaries of 50 μm i.d. and 375 μm o.d. were purchased from Yongnian Optic Fiber Plant (Hebei, China). Capillaries of 60 cm in total length and 50.5 cm to detector were used. The pH of all the buffers was measured with PHS-3C pH meter from REX Instrument Factory (Shanghai, China).

2.3. Determination of K_{IPCE} by IPCE

2.3.1. Sample and buffer preparation

The aqueous solutions of NSAIDs (0.3–0.7 mM) for injection into capillary were prepared by diluting their stock solutions in methanol with water. 1% methanol in the sample solutions was used as a marker for electroosmotic flow (EOF). All of the sample solutions were stored in the refrigerator in the dark at 4 °C. The pH of Tris buffer was adjusted to 7.4 with 1 M hydrochloric acid. The concentration of Tris was 20 mM in pH 7.4 Tris buffer.

2.3.2. Preparation and characterization of liposomes

Appropriate amount of SPC or SPC and cholesterol was dissolved in chloroform in a round-bottom flask. The round-bottom flask was placed in a rotary evaporator at 50 °C to produce a thin layer of phospholipids on the inner surface of the flask. The trace amount of solvent left was removed under vacuum for several hours. By vigorous vortex, the lipid film was hydrated in Tris buffer at 50 °C to yield a suspension of multilamellar vesicles (MLVs) with a lipid concentration of *ca*. 3 mM. Unilamellar vesicles were produced from the suspension of MLVs by KQ-100 sonication (Kunshan, Jiangsu, China) for several minutes until the solution was clear. The resulting suspension of unilamellar vesicles was filtered three times through 0.45 μm inorganic membrane from Shanghai Bandao Industrial Co. Ltd. (Shanghai, China) and the suspension obtained was directly used for injection into capillary. All liposome solutions were used on the day they were prepared. The average diameter and polydispersity of liposomes containing SPC or SPC and different proportions of cholesterol, which were analyzed by Zetasizer 3000HS (Malvern Instrument Ltd, USA) fit to raw data which had been collected at 25 °C at an angle of 90°, were 31.8 nm and 0.334 for SPC/Ch (100:0 mol%), 35.4 nm and 0.366 for SPC/Ch (80:20 mol%), 33.7 nm and 0.348 for SPC/Ch (60:40 mol%),

respectively. The size distribution of all the liposomes investigated was not broader.

2.3.3. Preparation of immobilized phospholipid capillaries

The pretreatment of a fresh capillary was as follows: under a pressure of 996–998 mbar, a 15-min rinse with 1 M HCl, a 15-min rinse with water, a 15-min rinse with 1 M NaOH, a 15-min rinse with water and in the end a 20-min rinse with Tris buffer. A coated capillary was prepared according to Ref. [18]. The capillary was rinsed for 10 min with liposome solutions. Then it was left to stand filled with the liposome solutions for 15 min. Finally, it was washed with Tris buffer for 5 min to remove the unbound liposomes. The coated capillary was conditioned for 20 min with Tris buffer prior to analysis.

2.3.4. Determination by IPCE

The experimental conditions were as follows: Tris buffer as CE buffer solution, voltage 20 kV, the temperature of capillary cassette 25 °C, UV detection at 210 nm, injection of each sample for 10 s at 30 mbar. Each sample was measured alone in order to avoid the cross-contamination resulting from competition among drugs. The coated capillaries were rinsed with liposome solutions for 1 min and CE buffer solutions for 2 min between runs. CE buffer solutions in both vials were changed after every six runs to ensure their quality. The K_{IPCE} value of per drug was the average for three runs.

2.3.5. Theory

The apparent velocity (v_{obs}) of a given solute is calculated according to the following equation:

$$v_{obs} = \frac{l}{t_{obs}} \tag{1}$$

where l is the effective length of capillary (from the injection point to the detector's window); t_{obs} is observed migration time; v_{obs} can be visualized as a vector sum of the electromigration velocity (v_E) of a solute and the velocity of EOF.

Manetto et al. [23] have derived a factor R for the change of electromigration velocity of a solute if phospholipids are present in capillary:

$$v_E^+ = R v_E^- \tag{2}$$

where v_E^+ and v_E^- are the electromigration velocities of a solute in the presence and absence of phospholipids, respectively. The value of R is also related to the capacity factor (k_{IPCE}):

$$R = \frac{1}{1 + k_{IPCE}} \tag{3}$$

To obtain a normalized retention quantity, the normalized capacity factor, K_{IPCE}, being similar to that used in ILC [9], is introduced.

$$K_{IPCE} = \frac{k_{IPCE}}{B} = \frac{(v_E^- - v_E^+)/v_E^+}{B} \tag{4}$$

where B is the amount of immobilized phospholipids in the inner of capillaries during runs. The amount of immobilized phospholipids is usually determined as being of phosphorus as described

by Bartlett [26]. However, it is difficult to determine dynamically the amount of immobilized phospholipids by Bartlett's method.

In our experiments, not only immobilized phospholipids might leak out of the coated capillary during runs, but also the coated capillary was repeatedly rinsed with liposome solutions for 1 min between runs to ensure a more stable coating (see Section 2.3.4). It was therefore difficult to accurately calculate B. Cunliffe et al. [17] and Hautala et al. [18] reported that EOF variation could be utilized as an indirect measure of the completeness of the coating of phospholipids and the evidence of leak of phospholipids out of capillary. Thus, the change of electroosmotic mobility between in phospholipid-coated capillary and in uncoated capillary can be used to indirectly express the change of immobilized phospholipid amount during CE analysis. Hence, K_{IPCE} can be also expressed as Eq. (5):

$$K_{ILCE} = \frac{(v_E^- - v_E^+)/v_E^+}{B_{max}(\mu_{eo}^- - \mu_{eo}^+)/\mu_{eo}^-} \tag{5}$$

where B_{max} is the maximal amount of immobilized phospholipids in the inner of capillaries, μ_{eo}^+ and μ_{eo}^- are the electroosmotic mobility in the presence and absence of phospholipids, respectively. B_{max} is constant under identical experiment conditions and liposome components. Provided that B_{max} is 1 nmol, K_{IPCE} can be calculated by Eq. (5) and expressed in the unit of nmol^{-1}. It is noticeable that μ_{eo}^+ can be measured in each run. Consequently, the change of the amount of immobilized phospholipids can be dynamically observed during runs.

2.4. Determination of K_{lw} in free liposome partitioning system

2.4.1. Sample and buffer preparation

The pH of phosphate buffer was adjusted to 7.4 with 1 M sodium hydroxide. The concentration of KH_2PO_4 was 20 mM in pH 7.4 phosphate buffer. Appropriate amount of NSAIDs tested in this study was dissolved in phosphate buffer by sonication, except that oxaprozin was dissolved in methanol–phosphate buffer (1:99, v/v).

2.4.2. Determination

K_{lw} values were determined in free liposome partitioning system according to literature [3]. SPC films were formed on the wall of round-bottom flask following rotary evaporation of 10 ml SPC solution (ca. 3 mM) in chloroform–methanol (2:1, v/v). The resulting dried films were dispersed in 50 ml phosphate buffer, to which one of NSAIDs (ca. 0.3 mM) had been added, by vortex mixing for 15 min. This resulted in the formation of MLVs. K_{lw} values were determined by using an equilibrium anti-dialysis technique. A dialysis bag with a cutoff of 10,000–12,000 Da (USA) was first filled with 5 ml phosphate buffer, then immersed in 50 ml of drug-loaded liposome dispersion and magnetically stirred. The concentrations of free drugs taken from the inner of the dialysis bag at predetermined equilibrium times were determined by RP-HPLC with UV detection by using calibration plots ($R > 0.999$ and $n = 5$ or 6). For NSAIDs tested, it took 6–10 h to reach the dialysis equilibrium in phosphate buffer. However,

piroxicam and aspirin were transformed or hydrolyzed during equilibrium. Thus K_{lw} values of these two drugs in free liposome partitioning system cannot be determined by the equilibrium anti-dialysis technique. Loss of NSAIDs due to adsorption to the dialysis membrane was also checked by recovery tests and was found to be within the range of experimental error (the recoveries >95%). The K_{lw} value of per drug was the average for three times.

2.4.3. Theory

According to Ref. [3], apparent partition coefficient, K'_{lw}, was calculated from the distribution results by employing Eq. (6):

$$K'_{lw} = \frac{(C_T - C_w)w_1}{C_w w_2} \tag{6}$$

where C_T is the total initial concentration of drug in 50 ml of drug-loaded liposome dispersion before equilibration, C_w the final aqueous buffer phase concentration of drug, w_1 the weight of aqueous buffer phase, and w_2 the weight of phospholipids. Ion-corrected partition coefficient, K_{lw}, was calculated by Eq. (7):

$$K_{lw} = K'_{lw}(1 + 10^{pK_a - 7.4}) \tag{7}$$

3. Results and discussion

3.1. Evaluation of the coated capillaries

The capillaries were coated with the suspension of liposomes containing SPC and different proportions of cholesterol (0, 20 and 40 mol%) by the procedure described in Section 2.3.3, respectively. Cholesterol is an important component of human cell membranes, so liposomes are closer to human cell membrane if cholesterol is added into liposomes. Commonly the content of cholesterol do not preponderate over one-third of total lipids in human cell [27]. Consequently, molar ratio of cholesterol in liposomes was just set as 20% and 40%, not being increased to higher proportion in our experiments.

The nature of coating was investigated by monitoring the EOF variation for 21 consecutive runs. The coated capillaries were rinsed with the liposome solutions for 1 min and Tris buffer for 2 min between runs in order to improve the stability of coating. When a capillary was coated with liposome dispersion, the EOF in the capillary was suppressed from $4.45 \times 10^{-8}\,\mathrm{m^2\,V^{-1}\,s^{-1}}$ in the uncoated capillary to $2.17 \times 10^{-8}\,\mathrm{m^2\,V^{-1}\,s^{-1}}$ in a pure SPC-coated capillary, suggesting that the phospholipids were successfully coated in the inner wall of capillaries. The EOF ($2.31 \times 10^{-8}\,\mathrm{m^2\,V^{-1}\,s^{-1}}$) for the 20 mol% cholesterol-containing coating was slightly faster than that for the pure SPC coating, and the EOF ($3.81 \times 10^{-8}\,\mathrm{m^2\,V^{-1}\,s^{-1}}$) for the 40 mol% cholesterol-containing coating was distinctly faster than that for the pure SPC-coated capillary, probably because the amount of phospholipids coated in the inner wall of capillaries decreased when cholesterol was added to SPC liposomes. The stability was good for the pure SPC-coated capillary, as can be seen from the small R.S.D. (6.8%) of EOF for 21 runs. Furthermore, R.S.D. of EOF for the SPC/Ch (80:20 mol%) coated capillary and the
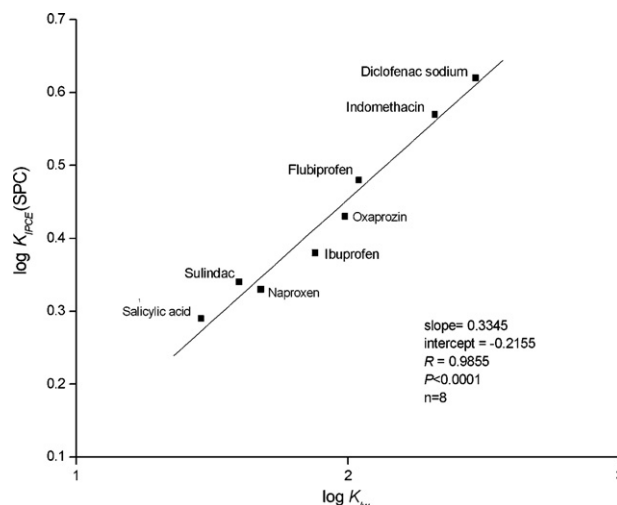

Fig. 1. Correlation between log K_{IPCE} (SPC) values and log K_{lw} values for eight NSAIDs listed in Table 1.

SPC/Ch (60:40 mol%) coated capillary was only 6.0% and 4.3%, respectively, indicating that a more stable coating was achieved when adding cholesterol. This might be explained by the fact that cholesterol can minimize the movement of the acyl chains in lipid bilayers and make lipid bilayers more rigid and gel-like [28]. These results accorded very well with the results obtained in literature [18].

3.2. Comparison between log K_{IPCE}, log K_{lw}, log K_{ILC} and log k_w^{IAM}

To evaluate a suitable IPCE mode for drug partitioning studies, we compared log K_{IPCE} values (SPC) measured by IPCE (the capillary was coated with a pure SPC liposomes) with log K_{lw} values measured in free SPC-liposome partitioning system and log K_{ILC} values measured by ILC. Some NSAIDs, which are structurally unrelated molecules, were selected as solutes. Related physico-chemical and biological data of NSAIDs were shown in Table 1. Log K_{IPCE} value and log K_{lw} value for each drug were the mean for three runs in our experiments. The obtained R.S.D.s for all log K_{IPCE} values (R.S.D. $\leq 7.51\%$) and log K_{lw} values (R.S.D. $\leq 3.02\%$) were both satisfactory. The retentions of nine NSAIDs on 1-palmitoyl-2-oleoyl-*sn*-glycero-3-phosphocholine (POPC) liposome chromatography column [9] were selected for a comparison because the head groups of POPC were of the PC type, being the same as the head groups of SPC. The linear regressions were performed with origin, Version 7.0 (OriginLab Corporation, USA).

As can be seen from Figs. 1 and 2, log K_{IPCE} (SPC) values correlated very well with log K_{lw} and log K_{ILC} values ($R > 0.98$ and $P < 0.0001$), indicating that there is a very close relationship between IPCE and free liposome partitioning system or ILC. The linear correlations between log K_{IPCE} (SPC), log K_{lw} and log K_{ILC} values were expected since both the same kind of membrane system (lipid bilayers) and phospholipids (SPC, POPC) with the same head groups were used in three methods. It was demonstrated that IPCE, K_{IPCE} as an

Table 1
K_{IPCE} values $\pm$ S.D. ($n=3$) and K_{lw} values $\pm$ S.D. ($n=3$) determined in our experiments and compilation of related physico-chemical and biological data obtained from literatures

Compounds	MW	pK_a[a]	Charge at pH 7.40	$\log K_w^{IAM}$ [b]	$\log K_{ILC}$[c]	$\log K_{lw}$	$\log K_{IPCE}$ (SPC)	$\log K_{IPCE}$ (SPC/Ch 80:20%)	$\log K_{IPCE}$ (SPC/Ch 60:40%)	IC_{50}[d]
Sulindac	356	4.26	–	1.80	1.26	1.60 ± 0.021	0.34 ± 0.011	0.40 ± 0.022	0.29 ± 0.011	112
Diclofenac sodium	318	4.50	–	2.43	2.71	2.47 ± 0.03	0.62 ± 0.019	0.70 ± 0.052	0.58 ± 0.024	1.1
Oxaprozin	293	4.19	–	–	–	1.99 ± 0.06	0.43 ± 0.017	0.60 ± 0.026	0.39 ± 0.013	–
Naproxen	230	4.84	–	1.26	1.43	1.68 ± 0.027	0.33 ± 0.009	0.52 ± 0.024	0.28 ± 0.013	5.65
Ibuprofen	206	4.41	–	1.12	1.48	1.88 ± 0.015	0.38 ± 0.013	0.40 ± 0.021	0.08 ± 0.003	72.8
Aspirin	180	3.48	–	−0.95	−0.01	–	0.14 ± 0.007	0.10 ± 0.005	0.11 ± 0.004	278
Salicylic acid	138	3.01	–	0.05	0.91	1.46 ± 0.032	0.29 ± 0.009	0.23 ± 0.015	0.24 ± 0.006	725
Indomethacin	358	3.96	–	2.39	2.57	2.32 ± 0.062	0.57 ± 0.023	0.62 ± 0.013	0.31 ± 0.011	1.68
Piroxicam	331	4.50; 3.80	–	1.85	1.60	–	0.44 ± 0.020	0.62 ± 0.016	0.33 ± 0.025	0.604
Flubiprofen	244	4.27	–	2.02	1.91	2.04 ± 0.048	0.48 ± 0.024	0.68 ± 0.023	0.44 ± 0.009	0.102

Abbreviation: MW: molecular weight; $\log k_w^{IAM}$: logarithm of IAM chromatographic retention factor extrapolated to 100% aqueous phase (eluent: mixture of acetonitrile/0.1 M sodium phosphate buffer 10:90%, v/v, pH 7.0); $\log K_{ILC}$: logarithm of normalized capacity factor by immobilized liposome chromatography; $\log K_{lw}$: logarithm of partition coefficient of a drug in free liposome partitioning system; $\log K_{IPCE}$ (SPC), $\log K_{IPCE}$ (SPC/Ch 80:20%), $\log K_{IPCE}$ (SPC/Ch 60:40%): logarithm of normalized capacity factor by immobilized SPC/Ch (100:0 mol%), (80:20 mol%), (60:40 mol%) phospholipid capillary electrophoresis, respectively, with 20 mM Tris buffer (pH 7.40); IC_{50}: NSAIDs concentration required for 50% inhibition of COX-2.

[a] Data calculated using advanced chemistry development (1994–2005 ACD/labs) Software Solaris V 467 (from SciFinder Scholar) except for diclofenac sodium obtained from Ref. [29].

[b] Data obtained from Ref. [7].

[c] Data obtained from Ref. [9].

[d] Data obtained from Ref. [30].

evaluation index, could be used to study solute–membrane interactions.

Nevertheless, a closer look at Table 1, it was found that the data of IPCE were greatly less than that of free liposome partitioning system and ILC for selected NSAIDs except for aspirin. It was most likely because the amount of phospholipids coated in the inner of capillaries was not taken into account in the calculation of K_{IPCE} values (see Eq. (5)). In addition, the difference between K_{IPCE} and K_{lw} or K_{ILC} might be related to different methodology, PC source, liposomal lamellarity and buffer system. For instance, for IPCE (SPC) and ILC (POPC) method, the fatty acyl chains of phospholipids used to prepare liposomes were different despite the same head groups of phospholipids. The fatty acid composition (mol%) of SPC was mainly C16:0,

12.1%; C18:0, 3.3%; C18:1, 9.0%; C18:2, 66.2%; C18:3, 7.7% [31]. But the fatty acyl chain of POPC was C_{16} saturated acyl chain at C-1 and C_{18} unsaturated acyl chain at C-2 [9].

IAM, where a monolayer of phospholipid analogs is covalently coupled to a silica matrix, has been also used for studying drug partitioning. The retentions of eight NSAIDs on the IAM PC.MG monolayer (an ester linkage between two C14 saturated acyl chains and the glycerol backbone of the PC ligand) were taken from literature [7]. As can be seen from Fig. 3, the $\log K_{IPCE}$ (SPC) values for eight NSAIDs only showed a moderate linear relationship with $\log k_w^{IAM}$ values although the head groups of SPC used in IPCE were the same as that of PC.MG monolayer used in IAM. Similarly, the comparison between ILC (POPC) and IAM (PC.MG monolayer) has been studied by Lundahl and co-workers, and it was found that the
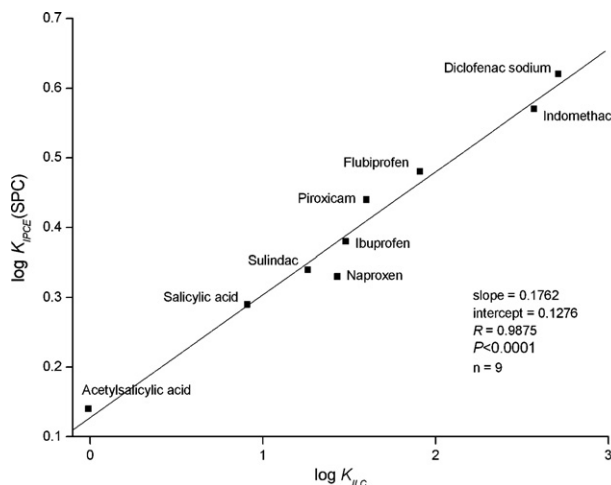

Fig. 2. Correlation between $\log K_{IPCE}$ (SPC) values and $\log K_{ILC}$ values for nine NSAIDs listed in Table 1.
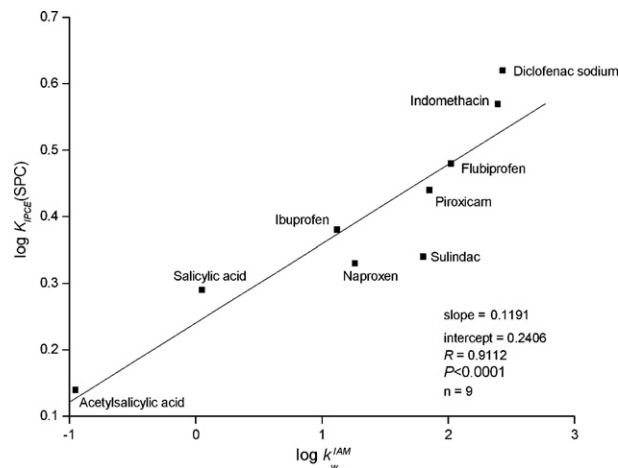

Fig. 3. Correlation between $\log K_{IPCE}$ (SPC) values and $\log k_w^{IAM}$ values for nine NSAIDs listed in Table 1.

Table 2
The correlations between pIC_{50} and $\log K_{IPCE}$ values for a series of NSAIDs

SPC/Ch (mol%)	Equations	n	R	S	P
100:0	$pIC_{50} = -3.736(\pm0.956) + 6.854(\pm2.263) \log K_{IPCE}$ (SPC)	9	0.753	0.944	<0.019
100:0	$pIC_{50} = -3.868(\pm1.637) + 7.250(\pm3.572) \log K_{IPCE}$ (SPC)	7	0.672	1.066	<0.098
80:20	$pIC_{50} = -4.629(\pm0.551) + 7.393(\pm0.982) \log K_{IPCE}$ (SPC/Ch 80:20%)	7	0.959	0.410	<0.001
60:40	$pIC_{50} = -2.463(\pm0.982) + 5.625(\pm2.773) \log K_{IPCE}$ (SPC/Ch 60:40%)	7	0.672	1.066	<0.098

In these equations, number in parentheses is the error of slope and intercept, respectively. n denotes the number of drugs, R is the correlation coefficient, S is the standard error of estimate and P is the probability.

$\log K_{ILC}$ values showed the weak relationship with the $\log k_w^{IAM}$ values ($R = 0.8899$ and $P < 0.001$) [9]. The above regressions indicated that drug partitioning into liposomal lipid bilayers was virtually different from drug partitioning into IAM monolayer. Considering that liposomal lipid bilayers are structurally similar to biomembrane, liposome model (e.g. IPCE, free liposome partitioning system, ILC) is more suitable to study drug–membrane interactions than IAM.

3.3. Prediction of drug activity

It has been demonstrated that the major anti-inflammatory mechanism of NSAIDs is the inhibition of cyclooxygenase (COX), of which two forms defined as COX-1 and COX-2 exist [30,32]. Inhibition of COX-2 generates the activity of NSAIDs; however, inhibition of COX-1 does the side-effect of NSAIDs. The penetration of cell membrane by NSAIDs has been reported to have an important relationship with the anti-inflammatory activity of NSAIDs [32]. Moreover, the results given in Section 3.2 showed that IPCE, K_{IPCE} as an evaluation index, could be used to study membrane affinity of drugs. These lead us to investigate the correlation between IC_{50} values for COX-2 determined on intact cells and K_{IPCE} values determined by our IPCE method. The IC_{50} value for COX-2 can be considered as an index of NSAIDs activity.

As shown in Table 2, for nine NSAIDs, no significant correlation was found between $\log K_{IPCE}$ (SPC) values and pIC_{50} (the minus logarithm of IC_{50}) values for COX-2. It is important to note that all other NSAIDs except aspirin and sulindac possess the structural features that allow enzyme inhibition by a common mechanism. Aspirin has its additional acetylating capacity, whereas sulindac is a prodrug that lacks the structural features for the appropriate receptor binding and/or interaction [7]. To verify the capability of $\log K_{IPCE}$ (SPC) to predict the biological activity of NSAIDs again, we excluded aspirin and sulindac. However, it was a pity that no correlation between $\log K_{IPCE}$ (SPC) values and pIC_{50} values for COX-2 was observed.

A relatively high correlation for NSAIDs except aspirin and sunlindac was observed between $\log K_{IPCE}$ (SPC/Ch 80:20%) values and pIC_{50} values for COX-2, whereas no obvious correlation was observed between $\log K_{IPCE}$ (SPC/Ch 60:40%) values and pIC_{50} values for COX-2 (see Table 2). These demonstrated that SPC/Ch (80:20 mol%) liposome model might be fit to mimic real cell membrane and IPCE has the potential to predict the biological activity of drugs.

4. Conclusions

IPCE exhibited strong relationship with free liposome partitioning system and ILC. It was indicated that IPCE, K_{IPCE} as an evaluation index, could be used as a simple model for studying drug–membrane interactions. Compared with the drug partitioning into cholesterol-containing (0 and 40 mol%) liposomes, the drug partitioning into cholesterol-containing (20 mol%) liposomes showed the best correlation with IC_{50} values for COX-2. Consequently, cholesterol-containing (20 mol%) liposome model might be more fit to mimic real cell membrane, and IPCE had the potential to predict the biological activity of drugs. However, it should be emphasized that numerous factors were involved in biological activity of drugs, although membrane affinity of drugs was an important prerequisite for biological activity of drugs. It was actually impossible for only an IPCE model to account for all factors. Better predictions on drug activity would be possible by using a few of different model systems.

Acknowledgements

References

[1] K.A. Edwards, A.J. Baeumner, Talanta 68 (2006) 1421.
[2] K.A. Edwards, A.J. Baeumner, Talanta 68 (2006) 1432.
[3] G.V. Betageri, J.A. Rogers, Int. J. Pharm. 36 (1987) 165.
[4] N. Rojo, M.J. Gómara, M.A. Busquets, M.A. Alsina, I. Haro, Talanta 60 (2003) 395.
[5] M. Munoz, N. Rojo, I. Haro, V. Girona, C. Mestres, M.A. Busquets, Talanta 60 (2003) 483.
[6] H. Liu, S. Ong, L. Glunz, C. Pidgeon, Anal. Chem. 67 (1995) 3550.
[7] F. Barbato, M.I. La Rotonda, F. Quaglia, J. Pharm. Sci. 86 (1997) 225.
[8] X.Y. Liu, Q. Yang, M. Hara, C. Nakamura, J. Miyake, Mater. Sci. Eng. C 17 (2001) 119.
[9] T. Österberg, M. Svensson, P. Lundahl, Eur. J. Pharm. Sci. 12 (2001) 427.
[10] X.-Y. Liu, Q. Yang, N. Kamo, J. Miyake, J. Chromatogr. A 913 (2001) 123.
[11] W.N. Zhang, Z.X. Hu, Y. Liu, Y.Q. Feng, S.L. Da, Talanta 67 (2005) 1023.
[12] Y.X. Zhang, R. Zhang, S. Hjertén, P. Lundahl, Electrophoresis 16 (1995) 1519.
[13] S.K. Wiedmer, J. Hautala, J.M. Holopainen, P.K.J. Kinnunen, M.-L. Riekkola, Electrophoresis 22 (2001) 1305.
[14] S.T. Burns, M.G. Khaledi, J. Pharm. Sci. 91 (2002) 1601.
[15] D. Corradini, G. Mancini, C. Bello, J. Chromatogr. A 1051 (2004) 103.

[16] S.K. Wiedmer, M.S. Jussila, J.M. Holopainen, J.-M. Alakoskela, P.K.J. Kinnunen, M.-L. Riekkola, J. Sep. Sci. 25 (2002) 427.

[17] J.M. Cunliffe, N.E. Baryla, C.A. Lucy, Anal. Chem. 74 (2002) 776.

[18] J.T. Hautala, M.V. Lindén, S.K. Wiedmer, S.J. Ryhänen, M.J. Säily, P.K.J. Kinnunen, M.-L. Riekkola, J. Chromatogr. A 1004 (2003) 81.

[19] J.T. Hautala, S.K. Wiedmer, M.-L. Riekkola, Anal. Bioanal. Chem. 378 (2004) 1769.

[20] M.V. Lindén, S.K. Wiedmer, R.M.S. Hakala, M.-L. Riekkola, J. Chromatogr. A 1051 (2004) 61.

[21] S.J.O. Varjo, J.T. Hautala, S.K. Wiedmer, M.-L. Riekkola, J. Chromatogr. A 1081 (2005) 92.

[22] S.K. Wiedmer, M. Jussila, R.M.S. Hakala, K.-H. Pystynen, M.-L. Riekkola, Electrophoresis 26 (2005) 1920.

[23] G. Manetto, M.S. Bellini, Z. Deyl, J. Chromatogr. A 990 (2003) 281.

[24] I. Reviakine, A. Brisson, Langmuir 16 (2000) 1806.

[25] Y.X. Xiao, J. Mei, X.F. He, Chinese J. Chromatogr. 24 (2006) 30.

[26] G.R. Bartlett, J. Biochem. 234 (1959) 466.

[27] Z.H. Di, in: X.Z. Wang, M.X. Ding (Eds.), Cell Biology, vol. 3, Higher Education Press, Beijing, 2002, p. 76.

[28] B.D. Ladbrooke, D. Chapman, Chem. Phys. Lipids 3 (1969) 304.

[29] P.N. Craig, in: C. Hansch, P.G. Sammes, J.B. Taylor (Eds.), Comprehensive Medicinal Chemistry, vol. 6, Pergamon Press, Oxford, 1990, pp. 237–991.

[30] J.R. Vane, R.M. Botting, Inflamm. Res. 44 (1995) 1.

[31] P. Coutteau, E.K.M. Kontara, P. Sorgeloos, Aquaculture 181 (2000) 331.

[32] J.A. Mitchell, P. Akarasereenot, C. Thiemermann, R.J. Flower, J.R. Vane, Proc. Natl. Acad. Sci. U.S.A. 90 (1993) 11693.

Rapid determination of lead in water samples by dispersive liquid–liquid microextraction coupled with electrothermal atomic absorption spectrometry

Mohammad Taghi Naseri [a,b], Mohammad Reza Milani Hosseini [a,b], Yaghoub Assadi [a,b,*], Armin Kiani [a,b]

[a] *Department of Analytical Chemistry, Faculty of Chemistry, Iran University of Science and Technology, Tehran, Iran*
[b] *Electroanalytical Chemistry Research Center, Iran University of Science and Technology, Tehran, Iran*

Abstract

The need for highly reliable methods for the determination of trace and ultratrace elements has been recognized in analytical chemistry and environmental science. A simple and powerful microextraction technique was used for the detection of the lead ultratrace amounts in water samples using the dispersive liquid–liquid microextraction (DLLME), followed by the electrothermal atomic absorption spectrometry (ET AAS). In this microextraction technique, a mixture of 0.50 mL acetone (disperser solvent), containing 35 µL carbon tetrachloride (extraction solvent) and 5 µL diethyldithiophosphoric acid (chelating agent), was rapidly injected by syringe into the 5.00 mL water sample, spiked with lead. In this process, the lead ions reacted with the chelating agent and were extracted into the fine droplets of CCl_4. After centrifugation (2 min at 5000 rpm), the fine CCl_4 droplets were sedimented at the bottom of the conical test tube (25 ± 1 µL). Then, 20 µL from the sedimented phase, containing the enriched analyte, was determined by ET AAS. The next step was the optimization of various experimental conditions, affecting DLLME, such as the type and the volume of the extraction solvent, the type and the volume of the disperser solvent, the extraction time, the salt effect, pH and the chelating agent amount. Moreover, the effect of the interfering ions on the analytes recovery was also investigated. Under the optimum conditions, the enrichment factor of 150 was obtained from only a 5.00 mL water sample. The calibration graph was linear in the range of 0.05–1 µg L^{-1} with the detection limit of 0.02 µg L^{-1}. The relative standard deviation (R.S.D.) for seven replicate measurements of 0.50 µg L^{-1} of lead was 2.5%. The relative lead recoveries in mineral, tap, well and sea water samples at the spiking level of 0.20 and 0.40 µg L^{-1} varied from 93.5 to 105.0. The characteristics of the proposed method were compared with the cloud point extraction (CPE), the liquid–liquid extraction, the solid phase extraction (SPE), the on-line solid phase extraction (SPE) and the co-precipitation, based on bibliographic data. The main DLLME advantages combined with ET AAS were simplicity of operation, rapidity, low cost, high-enrichment factor, good repeatability, low consumption of extraction solvent, requiring a low sample volume (5.00 mL).
© 2007 Elsevier B.V. All rights reserved.

Keywords: Dispersive liquid–liquid microextraction; Preconcentration; Electrothermal atomic absorption spectrometry; Lead; Water analysis

1. Introduction

The steady increase in pollution necessitates the analysis and monitoring of toxic species that could become a serious potential hazard if not controlled [1]. Lead is one of the most toxic elements, has an accumulative effect and is an environmental priority pollutant [2]. The harmful effects on the human health, caused by the lead contamination, are well-known and among them, the reduction of the enzymatic activity, the kidneys function and the neuromuscular difficulties have been reported [3]. The U.S. Environmental Protection Agency (EPA) has classified lead as a Group B2 (probable) human carcinogen [4]. Nowadays, there are legal restrictions concerning the lead release to the environment. Nevertheless, it is used as a raw material in the manufacturing industry such as automotive batteries, ceramic and ink [3]. Furthermore, lead is a leftover of some industrial processes in the production of fertilizers and pesticides. In both cases, it could be either delivered to the environment by

inadequate manufacturing process or caused by accident [4]. The environmental and health problems arise fundamentally from the use of gasoline antiknock products and paint pigments [5]. As a consequence, the World Health Organization (WHO) has established the maximum allowable limit of $10 \mu g L^{-1}$ for lead in drinking water [6]. It is, therefore, important to monitor the lead level in the environmental samples.

Currently, the most common analytical methods for the lead trace determination are the flame atomic absorption spectrometry (FAAS) [7,8], the electrothermal atomic absorption spectrometry (ET AAS) [9–11] and the inductively coupled plasma emission spectrometry (ICP) [12]. Of the three aforementioned methods, ET AAS is the most sensitive technique with a detection limit in the sub-picogram range for most metals [13]. More recently, the inductively coupled plasma-mass spectrometry (ICP-MS) [14] has produced a detection limit in the same range with ET AAS. However, the use of ICP-MS often involves a greater cost, higher sample volume requirements and increased instrumentation complexity, limiting its widespread application to routine analytical works. ET AAS is still being used because it combines a fast analysis time, a relative simplicity, a cheaper cost, low sample volume requirements and low detection limits. All of these features have been responsible for its broad utilization in the determination of trace and ultratrace elements in different samples [15].

Although the development of modern analytical instruments provides a great enhancement in analysis, in many cases the available analytical instrumentation does not demonstrate enough sensitivity for the analysis of natural samples [16]. Nevertheless, the detection of metal trace elements in aqueous samples is difficult due to various factors, particularly their low concentration and the matrix effects [2]. Preconcentration and separation techniques, such as liquid–liquid extraction [17], ion exchange [18], co-precipitation [19] and solid phase extraction (SPE) [20,21], can solve these problems, leading to a higher confidence level and an easy determination of the trace elements. Each technique has its advantages and disadvantages and should be chosen according to the analytical problem.

Solvent extraction has been one of the most extensively studied and widely applied methods in preconcentration and separation procedures for the determination of trace elements due to its simplicity, convenience, wide scope, etc. Separation and preconcentration procedures using solvent extraction generally result in a high-enrichment factor, owing to the difference between the volumes of the aqueous and organic phases. Although this procedure is operated in batch mode, it is time-consuming and produces large amounts of potentially toxic organic solvents as waste. These drawbacks could be overcome by the implementation of supplementary techniques in microextraction [22]. In view of this aspect, several novel microextraction techniques are being developed in order to reduce the analysis step, increase the sample throughput and to improve the quality and the sensitivity of the analytical methods. The cloud point extraction (CPE) [23], the homogeneous liquid–liquid extraction (HLLE) [24,25], the liquid phase microextraction (LPME) [26,27] and the solid phase microextraction (SPME) [28,29] are fairly new methods of sample preparation. They are employed in the separation and preconcentration of environmental contaminants in different matrices and can solve some of the problems, encountered with the conventional pretreatment techniques.

In previous studies, we demonstrated a novel microextraction technique, named dispersive liquid–liquid microextraction (DLLME), which was successfully used for the extraction and determination of polycyclic aromatic hydrocarbons (PAHs) [30], organophosphorus pesticides (OPPs) [31], chlorobenzenes (CBs) [32], chlorophenols [33], trihalomathans [THMs] [34], cadmium [35] and selenium [36] in water samples. In addition, other researchers developed this method for the measurement of antioxidants [37], volatile phenols [38] and triazine herbicides [39]. DLLME is a miniaturized sample pretreatment technique that uses microliter volumes of the extraction solvent. Operation simplicity, rapidity, low sample volume, low cost and high-enrichment factor are some of the DLLME advantages [40].

We now report the DLLME application, as a separation and preconcentration technique, for the rapid determination of lead ultratrace amounts in water samples using the diethyldithiophosphoric acid (DDTP) as chelating agent. Eventually, the electrothermal atomic absorption spectrometry (ET AAS) was used for detection.

2. Experimental

2.1. Reagents and solutions

All solutions were prepared with ultra pure water (Ghazi Co., Tabriz, Iran). The stock lead solution ($1000 \, mg \, L^{-1}$ as the atomic spectroscopy standard) was purchased from Merck (Darmstadt, Germany). The working standard solutions were prepared by serial dilutions of the stock solution with ultra pure water immediately prior to analysis. The chelating agent, diethyldithiophosphoric acid (DDTP) with the density of $1.17 \, kg \, L^{-1}$ was supplied from Merck. The rest of the used chemicals were carbon tetrachloride (analytical grade for determination with dithizone), chloroform (analytical grade for the determination with dithizone) and tetrachloroethylene (analytical grade) as extraction solvent, methanol (for spectroscopy), ethanol (for spectroscopy), acetone (suprasolv) and acetonitrile (HPLC grade) as disperser solvent, HCl (37%, suprapure), CH_3COONa (suprapure) and NaCl (analytical grade), NH_3 (25%, suprapure), supplied by Merck.

The NaCl solution was prepared by dissolving the appropriate NaCl amount (analytical grade, Merck) in ultra pure water and was extracted by carbon tetrachloride in the presence of DDTP for further purification.

All the glass vessels, used for the trace analysis, were kept in a 0.1% (v/v) DDTP solution for at least 24 h and, subsequently, washed twice with ultra pure water and twice with acetone before use. All of the 10 mL screw cap glass test tubes with conical bottom (extraction vessels) were maintained at 500 °C in a furnace (Carbolite, model CWF 1200, UK) for the removal of any organic and volatile inorganic compounds as well as a good sedimentation of the fine particles of the extraction solvent in the centrifugation step.

Table 1
The graphite furnace temperature program for lead determination

Step	Temperature (°C)	Ramp time (s)	Hold time (s)	Argon flow rate (mL min^{-1})
Drying	80	1	15	200
Pyrolysis	500	10	10	200
Atomization	1800	0	2	0
Cleaning	2400	0	2	1000

The mineral, tap, well and sea water samples, analyzed for the method development, were collected in PTFE containers from Northern Iran. They were stored in a dark place at 4 °C and analyzed within 24 h of collection without previous treatment or filtration. The TM-23.3 certified reference water sample was supplied from the National Water Research Institute (Ontario, Canada).

2.2. Instrumentation

An atomic absorption spectrometer, Shimadzu AA-6300 (Kyoto, Japan) with a deuterium background correction, equipped with a graphite furnace atomizer (GFA-EX7i), was used for this work. The lead hollow cathode lamp (Hamamatsu Photonics, Shizuoka, Japan) was run under the conditions recommended by the manufacturer (current: 10 mA). Also, the wavelength (283.3 nm), the slit bandwidth (0.7 nm) had conventional values. High-density graphite-coated tubes (Shimadzu) were used.

The optimized electrothermal temperature program for pyrolysis and atomization is given in Table 1. All measurements were based on the peak height. The good graphite wetting by the organic solvents promoted its penetration by the extracts, probably giving rise to the signals of the complicated shapes. To prevent this undesirable effect, the organic extracts were placed at the graphite furnace atomizer, heated at the drying temperature, preventing the sample from spreading over the atomizer surface [41].

A volume of 20 μL for all samples and calibration solution was pipetted directly into the graphite furnace 5 s after starting the drying step in all experiments. Argon (99.999%) was purchased from Air Products (UK) as sheath gas. The Centurion Scientific Centrifuge (Model 1020D, West, Sussex, UK) was used for centrifugation. The pH values were measured with a Metrohm pH-meter (Model: 691, Herisau, Switzerland), supplied with a glass-combined electrode.

2.3. Dispersive liquid–liquid microextraction procedure

The extraction of the lead ultratrace amount from an aqueous sample into a micro-volume of the organic solvent (carbon tetrachloride) was made by complexation with diethyldithiophosphoric acid (DDTP). Five millilitres of ultra pure water were placed in a 10 mL screw cap glass test tube with a conical bottom and were spiked at the lead concentration of 0.50 μg L^{-1}. 0.50 mL of acetone (disperser solvent), containing 35 μL of carbon tetrachloride (extraction solvent) and 5 μL DDTP (chelating agent), were injected rapidly into a sample solution with a

0.50 mL syringe (gastight, Hamilton, Reno, NV, USA). A cloudy solution (water, acetone and carbon tetrachloride) was formed in the test tube. In this step, the lead ions reacted with DDTP and were extracted into the fine droplets of carbon tetrachloride. The mixture was, then, centrifuged for 2 min at 5000 rpm. After this process, the dispersed fine droplets of carbon tetrachloride were sedimented at the bottom of the conical test tube (25 ± 1 μL). Twenty microlitres of this sedimented phase were removed using a micropipette (Biohit, Finland), manually injected into the electrothermal atomic absorption spectrometer and submitted to the temperature program of Table 1.

3. Results and discussion

In order to obtain a high-enrichment factor, the effect of different parameters, influencing the complex formation and the extraction conditions, were optimized. These parameters were the type and the volume of the extraction solvent, the type and the volume of the disperser solvent, pH, the chelating agent concentration, the extraction time and the ionic strength. Finally, these optimal conditions were applied to extract and detect lead in the real water samples. Eq. (1) was used for the calculation of the enrichment factor.

$$EF = \frac{C_{sed}}{C_0} \tag{1}$$

where EF, C_{sed} and C_0 are the enrichment factor, the analyte concentration in the sedimented phase and the initial analyte concentration in the aqueous sample, respectively. C_{sed} was calculated from the calibration graph obtained by the conventional LLE-ET AAS (extraction conditions: 2.0 mL from the standard water sample in the Pb concentration range of 10–100 μg L^{-1}, 0.50 mL from the aqueous solution of 1% (v/v) DDTP, 2.0 mL CCl$_4$, pH 2.5).

3.1. Pyrolysis and atomization curves

Fig. 1 depicts the curves of the pyrolysis and atomization temperature on the signal height for Pb. The pyrolysis and atomization temperatures were optimized with the standard organic extract, obtained by the conventional LLE (extraction conditions have been mentioned in Section 3). Aliquots containing 20 μL of the resulting solution were used for the ET AAS analysis. The pyrolysis temperature and atomization temperature were investigated in the range of 200–1000 °C and 600–2200 °C, respectively. The pyrolysis temperature of 500 °C and the atomization temperature of 1800 °C were used without adding any modifier, indicating that the considerable analyte stabilization
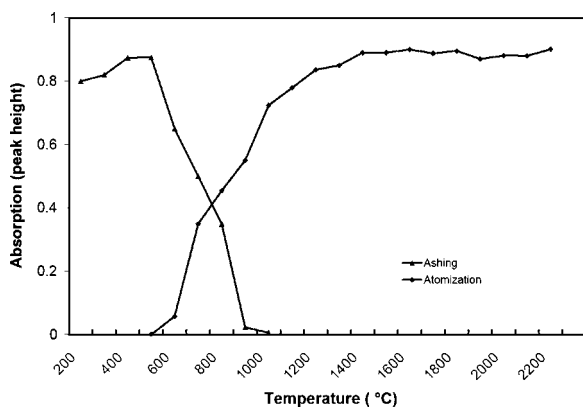
Fig. 1. Pyrolysis and atomization curves for lead. Optimum temperatures obtained by conventional LLE (extraction conditions have been mentioned in Section 3). 500 °C pyrolysis temperature, 1800 °C atomization temperature.

was provided by the DDTP phosphorus content (acting as chemical modifier) [23].

3.2. Selection of the extraction solvent

For the selection of the extraction solvent, some properties must be considered. The extraction solvent should have a higher density than water, an extraction capability of the interested compounds and a low solubility in water.

Chloroform, carbon tetrachloride and tetrachloroethylene were employed and compared in the lead extraction. A series of sample solutions were tested using 0.50 mL acetone, containing 5 μL DDTP and different volumes of the extraction solvents to achieve a 25 μL volume of the sedimented phase. The solubility of the extraction solvents in water is different. Therefore, to recover a 25 μL volume of the sedimented phase at the bottom of the test tube, it is necessary to add an excess amount to reach this solubility level. Thereby, 70, 35 and 28 μL of chloroform, carbon tetrachloride and tetrachloroethylene were used, respectively.

The resulting enrichment factors from this experiment were equal to 151.5 ± 2.3, 152.4.1 ± 4.5 and 132.7 ± 2.5 for carbon tetrachloride, chloroform and tetrachloroethylene (as extraction solvents), respectively. For carbon tetrachloride and chloroform, their enrichment factor values were not significantly different. After the comparison of the results of these two solvents, carbon tetrachloride was preferred to chloroform. In detail, carbon tetrachloride formed a well stable cloudy solution and demanded a smaller volume consumption to obtain the 25 μL sedimented phase. Also, the sedimented phase could be easily removed by micropipette to be introduced into the graphite furnace.

3.3. Effect of the extraction solvent volume

In order to evaluate the effect of the extraction solvent volume, the solutions containing different volumes of carbon tetrachloride were subjected to the same DLLME procedures. The experimental conditions were fixed and included the use of 0.50 mL acetone, containing 5 μL DDTP and different carbon tetrachloride volumes (35–85 μL at 10 μL intervals). With the

volume increase of the carbon tetrachloride from 35 to 85 μL, the volume of the sedimented phase increased from 25 to 65 μL. Subsequently, the enrichment factor reduced from 155 to 60 with the volume increase of carbon tetrachloride. As a result, at a low volume of the extraction solvent, a high enrichment factor was attained. Thereby, in the following studies, the optimum volume of 35 μL was selected for the extraction solvent, consisting of the CCl$_4$ minimum required volume to reach 25 μL of the sedimented phase.

3.4. Selection of the disperser solvent

The main criterion for the selection of the disperser solvent is its miscibility in the organic phase (extraction solvent) and the sample. Acetone, acetonitrile, methanol and ethanol were tested for this purpose. A series of sample solutions were studied using 0.50 mL from each disperser solvent, containing 35 μL of carbon tetrachloride (extraction solvent) and 5 μL DDTP (chelating agent). The enrichment factors obtained for acetonitrile, acetone, methanol and ethanol were 145.5 ± 2.1, 146.3 ± 3.4, 151.1 ± 4.2 and 134.8 ± 3.6, respectively. The resulting data illustrated no significant statistical differences among the disperser solvents, apart from ethanol that presented the lowest enrichment factor. Thus, acetone was selected because of its low toxicity and cost.

3.5. Effect of the disperser solvent volume

After choosing acetone as the disperser solvent, it was necessary to optimize its volume. For defining the optimal acetone volume, various experiments were performed with different acetone volumes (0.25, 0.50, 0.75, 1.0, 1.25 and 1.50 mL), containing 34.0, 35.0, 36.0, 37.0, 38.5 and 40.0 μL of carbon tetrachloride, respectively. It was required to change the CCl$_4$ volume by changing the acetone volume in order to obtain a constant volume of the sedimented phase (25 ± 1 μL) in all experiments. Under these conditions, the volume of the sedimented phase remained constant (25 ± 1 μL). The results showed that there was no considerable variation on the enrichment factor using 0.25 and 0.50 mL of acetone as disperser solvent. The enrichment factor slightly decreased, when the acetone volume exceeded 0.50 mL. It was clear that with the increase of the acetone volume, the complex solubility in water increased. Therefore, the extraction recovery diminished. Accordingly, the acetone volume of 0.50 mL was chosen as the optimum one for the achievement of a better and more stable cloudy solution.

3.6. pH effect

Because pH plays a unique role in the metal-chelate formation and the subsequent extraction, the pH of the sample solution was the next critical factor evaluated for its effect on the DLLME preconcentration of Pb (II). In this work, diethyldithiophosphoric acid (DDTP) was used instead of the DDTP ammonium salt. The pH adjustment was carried out in the presence of HCl and CH$_3$COONa. At first, diethyldithiophosphoric acid was totally

transformed to the DDTP ammonium salt with the NH_3 (sura-pure) addition. An appropriate amount of this mixture was added to the 5.00 mL sample. A series of experiments was performed with the pH adjustment from 0.5 to 7.5 with hydrochloric acid and sodium acetate. The enrichment factor remained nearly constant (approximately 150) in the pH range of 1–4 and it reduced on the higher pH value. On the other hand, because the aqueous solution of diethyldithiophosphoric acid was almost acidic (pH 2.5 in 5.00 mL aqueous solution), in this study, the use of an acidic (or buffer) solution for the pH adjustment, being the contamination sources, was not necessary. For that reason, all experiments were conducted without the acid (or buffer) addition with the aid of diethyldithiophosphoric acid (chelating agent).

3.7. Effect of the DDTP concentration

The next influential factor, whose effect on the enrichment factor was studied, was the DDTP amount. This study was conducted in the DDTP concentration range of 0.01–0.5% (v/v). In this case, the enrichment factor increased with the increase of the DDTP amount up to 0.05% (v/v), reaching a plateau. A concentration of 0.1% (v/v) in 5.00 mL of the aqueous solution was chosen as the optimum amount for the lead determination to prevent any interference.

3.8. Effect of the extraction time

The influence of the extraction time was examined in the range of 0–60 min with the experimental conditions remaining constant. The results displayed that the extraction time had no notable effect on the enrichment factor. It was revealed that after the formation of the cloudy solution, the surface area among the extraction solvent and the aqueous phase was essentially large. As a consequence, the lead complex formation and its transfer from the aqueous phase to the extraction solvent were fast. This fact was one of the advantages of the DLLME technique.

3.9. Salt effect

For investigating the influence of the ionic strength on the DLLME performance, several experiments were performed by adding varying NaCl amount from 0% to 5% (w/v). The rest of the experimental conditions were kept constant. The resulting data disclosed that the salt addition from 0% to 5% had no significant impact on the enrichment factor. These observations offered the possibility of utilizing this method for the lead separation from saline solutions up to 5%.

3.10. Interference studies

The diethyldithiophosphate (DDTP) chelating agent complexes react with several transition metals and semi-metals in acidic media, but they do not react with alkali and alkaline earth metals and other elements [42,43]. The influence of the other metals that might replace lead in the original DDTP chelate was investigated with the purpose of identifying the potential

Table 2
Effect of interferents on the recovery of $0.50 \mu g L^{-1}$ Pb(II) in water sample using DLLME-ET AAS

Interferent	Concentration ($\mu g L^{-1}$)	Interferent/Pb(II) ratio	Recovery (%)
Na^+	1,000,000	2,000,000	101.0
Li^+	5,000	10,000	101.4
K^+	5,000	10,000	105.8
Ca(II)	5,000	10,000	100.3
Mg(II)	5,000	10,000	95.2
Ba(II)	5,000	10,000	102.0
Bi(III)	500	1,000	94.6
Mn(II)	500	1,000	97.1
Co(II)	500	1,000	101.4
Al(III)	500	1,000	100.0
Fe(II)	500	1,000	100.0
Ni(II)	500	1,000	94.0
Sn(IV)	500	1,000	96.3
Zn(II)	500	1,000	100.0
Cr(III)	500	1,000	96.7
Ag(I)	500	1,000	96.9
Cd(II)	500	1,000	94.6
Cu(II)	500	1,000	96.6
Si(II)	500	1,000	97.8
Se(II)	500	1,000	97.9
Hg(II)	500	1,000	104.4
Cl^-	1,000,000	2,000,000	94.2
NO_3^-	5,000	10,000	105.8
CH_3COO^-	50,000	100,000	94.8
SCN^-	5,000	10,000	94.5
$Cr_2O_7^{-2}$	5,000	10,000	97.6
SO_4^{-2}	5,000	10,000	100.0

interferents. The 5.00 mL recovery from solutions, containing $0.50 \mu g L^{-1}$ of Pb and various amounts of the interfering ions, was tested according to the recommended procedure. The tolerance level was defined as the maximum concentration of the foreign ion causing a change in the analytical signal no higher than 5%, when compared with the signal of $0.50 \mu g L^{-1}$ lead alone. The corresponding results are listed in Table 2, confirming that the lead recoveries were almost quantitative in the presence of the excessive amounts of the possible interfering cations and anions.

3.11. Analytical figures of merit

Table 3 summarizes the analytical characteristics of the optimized method, including the linear range, the limit of

Table 3
Analytical characteristics of DLLME-ET AAS for determination of Pb

Parameter	Analytical feature
Linear range ($\mu g L^{-1}$)	0.05–1
r^2	0.9994
Limit of detection ($\mu g L^{-1}$) (3σ, $n=7$)	0.02
Repeatability (R.S.D.[a], %) ($n=7$)	2.5
Enrichment factor	150
Sample volume (mL)	5.00
Sample preparation time (min)	<3

[a] Pb (II) concentration was $0.50 \mu g L^{-1}$ for which R.S.D. was obtained.

Table 4
Characteristic performance data obtained by using DLLME and other preconcentration techniques for determination of lead in water samples

Method	LOD[a] ($\mu g\,L^{-1}$)	R.S.D.[b] (%)	Enrichment factor (or enhancement factor)	Sample volume (mL)	Time (min)	Linear range ($\mu g\,L^{-1}$)	References
Liquid–liquid extraction GF AAS	1	2.7	5	5	20	2–30	[44]
Co-precipitation –GF AAS	0.5	4.6	20	200	>20	–	[45]
Off-line-SPE–GF AAS	0.039	–	100	200	20	–	[46]
On-line-SPE–GF AAS	0.012	3.2	20.5	>3.3	2	0.1–10	[47]
CPE–GF AAS	0.08	2.8	50	10.0	30	1–30	[2]
DLLME–GF AAS	0.02	2.5	150	5.00	<3	0.05–1	(Represented method)

[a] Limit of detection.
[b] Relative standard deviation.

detection, the reproducibility and the enrichment factor. The calibration graph was linear in the lead concentration range of 0.05–1 $\mu g\,L^{-1}$. The detection limit (calculated as three times the standard deviation of 7 blank measurements, divided by the slope of the calibration curve) for the lead cations was found to be 0.02 $\mu g\,L^{-1}$.

Concerning the reproducibility of the method, it was evaluated with 5.00 mL from the solution, containing the analyte ions in the Pb(II) concentration of 0.50 $\mu g\,L^{-1}$. The relative standard deviation (R.S.D.) for 7 replicate measurements was 2.5%. Finally, the high-enrichment factor of 150 was obtained for only a 5.00 mL water sample.

3.12. Application to real samples

The efficiency of the represented method was validated with the monitoring of the lead concentration in mineral, tap, well and sea water samples. The lead concentration in the tap, well and sea water samples was out of the calibration range. Therefore, a typical 1 + 4, 1 + 9, 1 + 2 dilution of the tap, well, sea water samples, respectively, was necessary before the separation and the preconcentration step. For this purpose, 5.00 mL of each sample (final volume after dilution at the mentioned ratio by ultra pure water) were preconcentrated with the optimized proposed method. The lead concentration in the mineral, tap, well and sea water samples was found to be smaller than the values of the detection limit (not detected), 0.104 ± 0.010 $\mu g\,L^{-1}$, 0.236 ± 0.011 $\mu g\,L^{-1}$, 0.256 ± 0.013 $\mu g\,L^{-1}$, respectively. The Pb amount in the tap, river and sea water samples (without dilution) was calculated to be 0.520 ± 0.050, 2.36 ± 0.11 and 0.768 ± 0.039 $\mu g\,L^{-1}$, respectively. The accuracy of the method was verified with the analysis of the samples, spiked with known lead amounts. The relative lead recoveries from the mineral, tap, well, river and sea water samples at the spiking level of 0.20 and 0.40 $\mu g\,L^{-1}$ were in the range of 93.3–105%. These results demonstrated that the tap, well, river and sea water sample matrices had little effect on the lead DLLME.

In order to establish the validity of the recommended procedure, the method was applied to the lead determination in a TM-23.3 certified reference water sample (certified lead value of 3.2 ± 0.06 $\mu g\,L^{-1}$) after the appropriate dilution. The lead concentration in this water sample was found 3.07 ± 0.15 $\mu g\,L^{-1}$ with the developed method. The result obtained was in agreement with the certified value.

3.13. Comparison of DLLME with the other sample preparation techniques

A comparison of the represented method with the other reported preconcentration methods for the lead extraction and determination from water samples is given in Table 4. Some of the preconcentration methods of this Table are the liquid–liquid extraction [44], the coprecipitation [45], the off-line-solid phase extraction [46], the on-line-solid phase extraction [47], the cloud point extraction [2]. Apparently, DLLME presented a low LOD (0.02 $\mu g\,L^{-1}$), a high-enrichment factor (150), a short extraction procedure (less than 3 min) and a low sample consumption (5 mL). These characteristics are of great interest for the routine laboratories in the trace analysis of metal ions.

4. Conclusions

DLLME combined with the electrothermal atomic absorption spectrometry (ET AAS) was evaluated for the separation, the preconcentration and the determination of the ultratrace amounts of lead (at sub-$\mu g\,L^{-1}$ level) from water samples. DLLME proved to be a fast simple, inexpensive and reproducible technique for the determination of trace metals with the use of low sample volumes. The high-preconcentration factor and the low sample volume requirements were the major advantages of the technique. An enrichment factor of about 150 times was attained with only a 5.00 mL from the sample. In this method, the sample preparation time (less than 3 min) as well as the consumption of the toxic organic solvents (at microlitre level) were minimized without affecting the method sensitivity. Although the obtained results of this research were related to the lead determination, the system could be readily applied to the determination of other metals with the help of various chelating agents, extractable by other organic solvents.

References

[1] J.F. van Staden, A. Botha, Talanta 49 (1999) 1099.
[2] J. Chena, S. Xiao, X. Wu, K. Fang, W. Liu, Talanta 67 (2005) 992.
[3] A.L.D. Comitrea, B.F. Reis, Talanta 65 (2005) 846.

[4] H.P. Wagner, J. Am. Soc. Brew. Chem. 53 (1995) 141.
[5] M.S.D. Nezio, M.E. Palomeque, B.S.F. Band, Talanta 63 (2004) 405.
[6] World Health Organization, Health Criteria and Other Supporting Information, vol. 2, 2nd ed., WHO, Geneva, 1996, p. 973.
[7] W.L. dos Santos, C.M.M. dos Santos, J.L.O. Costa, H.M.C. Andrade, S.L.C. Ferreira, Microchem. J. 77 (2004) 123.
[8] G.A. Zachariadis, A.N. Anthemidis, P.G. Bettas, J.A. Stratis, Talanta 57 (2002) 919.
[9] R.C. de Campos, H.R. dos Santos, P. Grinberg, Spectrochim. Acta Part B 57 (2002) 15.
[10] J.C.P. de Mattos, A.M. Nunes, A.F. Martins, V.L. Dressler, E.M. de Moraes Flores, Spectrochim. Acta Part B 60 (2005) 687.
[11] J.Y. Cabon, Spectrochim. Acta Part B 57 (2002) 513.
[12] J. Koksal, V. Synek, P. Janos, Talanta 58 (2002) 325.
[13] K.A. Wagner, J.D. Batchelor, B.T. Jones, Spectrochim. Acta Part B 53 (1998) 1805.
[14] K. Ndungu, S. Hibdon, A.R. Flegal, Talanta 64 (2004) 258.
[15] J.C.R. Garcia, J.B. Garcia, C.H. Latorre, S.G. Martian, R.M.P. Crecente, J. Agric. Food Chem. 53 (2005) 6616.
[16] E. Carasek, J.W. Tonjes, M. Scharf, Talanta 56 (2002) 185.
[17] K. Ndungu, R.P. Franks, K.W. Bruland, A.R. Flegal, Anal. Chim. Acta 481 (2003) 127.
[18] R.B.R. Mesquita, S.M.V. Fernandes, A.O.S.S. Rangel, Talanta 62 (2004) 395.
[19] G. Doner, A. Ege, Anal. Chim. Acta 547 (2005) 14.
[20] M.R. Jamali, Y. Assadi, F. Shemirani, M.R. Milani Hosseini, R. Rahnama Kozani, M. Masteri-Farahani, M. Salavati-Niasari, Anal. Chim. Acta 579 (2006) 68.
[21] M.R. Jamali, Y. Assadi, F. Shemirani, M. Salavati-Niasari, Talanta 71 (2007) 1524.
[22] M.D.G.A. Korna, J.B.D. Andrade, D.S.D. Jesus, V.A. Lemosc, M.L.S.F. Bandeira, W.N.L.D. Santos, M.A. Bezerra, F.A.C. Amorima, A.S. Souza, S.L.C. Ferreira, Talanta 69 (2006) 16.
[23] T.A. Maranhao, D.L.G. Borges, M.S. da Veigab, A.J. Curtius, Spectrochim. Acta Part B 60 (2005) 667.
[24] H. Ebrahimzadeh, Y. Yamini, F. Kamare, S. Shariati, Anal. Chim. Acta 549 (2007) 93.
[25] A.R. Ghiasvand, S. Shadabi, E. Mohagheghzadeh, P. Hashemi, Talanta 66 (2005) 912.
[26] F. Ahmadi, Y. Assadi, M.R. Milani Hosseini, M. Rezaee, J. Chromatogr. A 1101 (2006) 307.
[27] M.R. Khalili Zanjani, Y. Yamini, S. Shariati, J.A. Jonsson, Anal. Chim. Acta 585 (2007) 286.
[28] D. Djozan, Y. Assadi, S. Hosseinzadeh Haddadi, Anal. Chem. 73 (2001) 4054.
[29] D. Djozan, Y. Assadi, Chromatographia 60 (2004) 313.
[30] M. Rezaee, Y. Assadi, M.R. Milani Hosseini, E. Aghaee, F. Ahmadi, S. Berijani, J. Chromatogr. A 1116 (2006) 1.
[31] S. Berijani, Y. Assadi, M. Anbia, M.R. Milani Hosseini, E. Aghaee, J. Chromatogr. A 1123 (2006) 1.
[32] R. Rahnama Kozani, Y. Assadi, F. Shemirani, M.R. Milani Hosseini, M.R. Jamali, Talanta 72 (2007) 387.
[33] N. Fattahi, Y. Assadi, M.R. Milani Hosseini, E. Zeini Jahromi, J. Chromatogr. A 1157 (2007) 23.
[34] R. Rahnama Kozani, Y. Assadi, F. Shemirani, M.R. Milani Hosseini, M.R. Jamali, Chromatographia 66 (2007) 81.
[35] E. Zeini Jahromi, A. Bidari, Y. Assadi, M.R. Milani Hosseini, M.R. Jamali, Anal. Chim. Acta 585 (2007) 305.
[36] A. Bidari, E. Zeini Jahromi, Y. Assadi, M.R. Milani Hosseini, Microchem. J. 87 (2007) 6.
[37] M.A. Farajzadeh, M. Bahram, J.A. Jonsson, Anal. Chim. Acta 591 (2007) 69.
[38] L. Farina, E. Boido, F. Carrau, E. Dellacassa, J. Chromatogr. A 1157 (2007) 46.
[39] D. Nagaraju, S.D. Huang, J. Chromatogr. A 1161 (2007) 89.
[40] K. Demeestere, J. Dewulf, B.D. Witte, H.V. Langenhove, J. Chromatogr. A 1153 (2007) 130.
[41] A.B. Volynsky, B.Y. Spivakov, Y.A. Zolotov, Talanta 31 (1984) 449.
[42] M.A.M.D. Silva, V.L.A. Frescura, A.J. Curtius, Spectrochim. Acta Part B 55 (2000) 803.
[43] M.A.M.D. Silva, V.L.A. Frescura, F.J.N. Aguilera, A.J. Curtius, J. Anal. At. Spectrom. 13 (1998) 1369.
[44] T. kumamaru, Y. Okamaoto, S. Hara, H. Matsuo, M. Kiboku, Anal. Chim. Acta 218 (1989) 173.
[45] T. Minami, Y. Sohrin, J. Ueda, Anal. Sci. 21 (2005) 1519.
[46] Y. Cai, G. Jiang, J. Liu, X. Liang, At. Spectrosc. 23 (2002) 52.
[47] E.V. Alonso, M.T.S. Cordero, A.G.d. Torres, J.M.C. Pavón, Anal. Bioanal. Chem. 385 (2006) 1178.

Optimization of a FIA system with amperometric detection by means of a desirability function
Determination of sulfadiazine, sulfamethazine and sulfamerazine in milk

Celia Reguera [a], M. Cruz Ortiz [a,*], Ana Herrero [a], Luis A. Sarabia [b]

[a] *Department of Chemistry, University of Burgos, Pza. Misael Bañuelos s/n, 09001 Burgos, Spain*
[b] *Department of Mathematics and Computation, University of Burgos, Pza. Misael Bañuelos s/n, 09001 Burgos, Spain*

Abstract

A sensitive and cheap FIA, with amperometric detection, analytical procedure is developed in this paper to determine sulfadiazine, sulfamethazine and sulfamerazine in milk. A multicriteria optimization based on the use of a desirability function is used for optimizing two analytical responses (peak height and its variability) since single-objective optimizations lead to conflicting experimental conditions. In the optimum conditions, the determination of the three sulfonamides in milk samples is carried out, the analytical procedure being validated according to Commission Decision 2002/657/EC. The decision limit at 0 and 100 μg L^{-1} (which is the maximum residue limit in milk) are 13.9 and 110.2, 9.5 and 107.1 and 9.1 and 107.1 μg L^{-1} for sulfadiazine, sulfamethazine and sulfamerazine, respectively. Whereas the values of capability of detection, CCβ, obtained at 0 and 100 μg L^{-1} were 26.9 and 119.8, 18.2 and 113.6, and 17.5 and 113.7 μg L^{-1} for sulfadiazine, sulfamethazine and sulfamerazine, respectively. Recovery values between 67.4% and 119.1% are found for milk test samples of two brands of milk. The accuracy of the method is confirmed. The ruggedness of the procedure is evaluated by means of a Plackett–Burman design. The relative errors were lower than 2.5% ($n = 7$).
© 2007 Elsevier B.V. All rights reserved.

Keywords: Desirability function; Optimization; FIA; Amperometric detection; Sulfonamides; Milk; Decision limit; Capability of detection

1. Introduction

Sulfadiazine, sulfamerazine and sulfamethazine are synthetic agents classified as antibacterial compounds, rather than as antibiotics that act as bacteriostatic by competing with *p*-aminobenzoic acid in the enzymatic synthesis of dihydrofolic acid. They belong to the sulfonamides group, which are among the most used antibacterials in the veterinary practice as active disease treatment agents or growth promoters. Their widespread use has resulted in the risk that residues of these compounds or their metabolites are present in foodstuffs obtained from treated animals, which may result in the emergence of antibiotic resistance in both human and veterinary bacterial populations, having an impact on human health [1]. Subsequently, the European

Union establishes some maximum residue limits (MRLs) for all substances belonging to sulfonamide group in foodstuffs of animal origin in the Commission Regulation (EC) No 281/96 [2] amending Annexes I and III to Council Regulation (EEC) No 2377/90 [3]. The combined total residues of all substances within the sulfonamide group should not exceed 100 μg kg^{-1} for target tissues (muscle, liver or kidney) and for milk from all food-producing species.

Several analytical procedures are currently available for the determination of sulfonamides residues in foodstuffs. Lots of them are based on LC/MS determinations [4–6] and more recently on LC/MS/MS [7], others in HPLC with diode-array [8–10] or fluorescence [11,12] detection, fluorescence spectroscopy [13], capillary electrophoresis [14], etc. However, in routine analysis, flow injection systems are interesting because of their fast response, low-cost instrumentation, repeatability and accuracy, in addition to the large number of samples which can be analysed in very little time [15]. The combination of flow

---

* Corresponding author. Fax: +34 947 258 831.
  E-mail address: mcortiz@ubu.es (M.C. Ortiz).

injection analysis with electrochemical detection provides systems that in addition are highly selective and sensitive, providing low detection limits [16].

In this work, the response surface analysis methodology [17] has been used to find those experimental conditions which give a higher signal with lower variability. However, it is usual that the experimental conditions that optimize one aspect of the analytical signal (e.g. signal size) do not optimize another (e.g. its variability), so a conflict between objectives is evidenced.

To solve this conflict there are different possible approaches such as to optimize the signal–noise [18], the correlation coefficient or other more complex functions [19], which indirectly evaluate the sensitivity, precision, sample throughput or cost in a flow injection system. Also the vectorial optimization or Pareto optimality was applied to make a compromise between residence time and the peak height [20], a linear combination of them [21] or the peak height and coefficient of variation in a FIA system [22]. However, in chemical analysis the analyst usually knows the values in which the variability of the signal has to be maintained. In order to explicitly using this information, in this paper we propose the use of the Derringer desirability function [23,24] that in addition has been successfully applied in different analytical optimizations [16,25,26] when conflicting responses are found. In this work, the desirability function is used as multicriteria tool in the optimization stage of the analytical procedure proposed.

In the optimum reached, the analytical determination of sulfadiazine, sulfamethazine and sulfamerazine in milk by means of a FIA system with amperometric detection is carried out. The analytical procedure is validated according to ISO norm and Commission Decision 2002/657/EC [27]. In this paper, decision limit (CCα), detection capability (CCβ), trueness/recovery, precision and ruggedness have been estimated. The method is especially suitable for screening purposes since it has values in low cost and high throughput.

2. Theory

2.1. Desirability function

When optimizing k experimental responses, $y_1, \ldots, y_k$, it occurs that the point of the experimental domain (values of the experimental factors) at which each one of them reach the optimum is not the same, it is necessary to carry a multiresponse analysis. In this work, an overall desirability function [23,24] has been used. This multicriteria methodology is based on constructing an individual desirability function, d_i, for each response y_i. Each one of these desirability functions is a continuous and monotonous (increasing or decreasing) function which varies from zero (undesirable response) to 1 (optimal response). Through the individual functions, d_i, the analyst introduces the specifications that each response must fulfil in the analytical procedure and based on these individual desirability functions, d_i, the Derringer desirability function [23] is the weighted geometric average of them:

$$D = \sqrt[s]{d_1^{p_1} \times d_2^{p_2} \times \ldots \times d_k^{p_k}} \tag{1}$$

where p_i is the weight corresponding to each individual function and $s = 1/\sum_{i=1}^{k} p_i$.

In general, d_i functions are not derivable and so algorithms based on gradient cannot be used to obtain the maximum of D function. NemrodW [31] uses a simulated annealing algorithm for this task.

2.2. Detection capability (CCβ) and decision limit (CCα)

The capability of detection for a given probability of false positive, α, as defined by the International Organization for Standardization (ISO 11843) [28,29], is "the true net concentration of the analyte in the material to be analysed which will lead, with probability $1 - \beta$, to the correct conclusion that the concentration in the analysed material is larger than that in the blank material".

For a concentration x_0, the capability of detection, named CCβ in the European Decision [27] and x_d in ISO 11843-1, can be estimated [30] through a calibration model "signal *vs.* concentration" through Eq. (2):

$$CC\beta = \frac{\Delta(\alpha, \beta) w_{x_0} \hat{\sigma}}{\hat{b}} \tag{2}$$

where $\Delta(\alpha, \beta)$ is a non-centrality parameter of a noncentral t-distribution related to the probabilities α and β. $\hat{\sigma}$ is the residual standard deviation of the regression and $\hat{b}$ the slope. w_{x_0}, which is defined by Eq. (3), depends on the position of the standards in the calibration line (x_i) and is inversely proportional to the number of replicates (K) of the sample and to the number of standards (I) in the regression model:

$$w_{x_0}^2 = \frac{1}{K} + \frac{1}{I} + \frac{(x_0 - \bar{x})^2}{\sum_{i=1}^{I} (x_i - \bar{x})^2} \tag{3}$$

If the capability of detection is estimated with $x_0 = 0$ in Eqs. (2) and (3), α and β are the probabilities of false positive and false negative, respectively. But when the analyte has an established maximum residue limit, MRL, as is the case of total content of sulfadiazine in milk, the capability of detection must also be evaluated at those levels of concentration. In this case, the capability of detection is estimated as in Eqs. (2) and (3) with $x_0 = MRL$, so α and β are then the probabilities of false noncompliance and of false compliance, respectively.

On the other hand, the critical value (at zero) of the net concentration (Eq. (4)) has been defined in ISO 11843-2 as "the value of the net concentration the exceeding of which leads, for a given error probability α, to the decision that the concentration of the analyte in the analysed material is larger than that in the blank material". This definition has been adopted by European Decision [27] as decision limit or CCα:

$$CC\alpha = \frac{t_{1-\alpha}(\gamma) w_{x_0} \hat{\sigma}}{\hat{b}} \tag{4}$$

In Eq. (4), $t_{1-\alpha}(\gamma)$ is the 100 $(1 - \alpha)$%-quartile of the t-distribution with $\gamma = I - 2$ degrees of freedom.

For substances with a maximum residue limit, as is the case of sulfonamides in milk, the decision limit must also be estimated

at those levels of concentration with x_0 = MRL by Eqs. (3) and (4).

3. Experimental

3.1. Instrumentation

The flow injection system used was analogous to that described earlier [16] that consisted of a solvent system with helium sparge, a Perkin Elmer 200 LC Pump Isocratic version, a Rheodyne syringe loading sample injector model 7725i with a 20 μL loop and an ESA Coulochem II 5200A electrochemical detector with a 5011 high analytical cell and a conditioning cell 5021. The efficient coulometric electrode has been used in the amperometric mode operation as working electrode, the reference electrode being a hydrogen/palladium electrode. In addition, to reduce the possibility of particulates entering the analytical cell an ESA in-line carbon filter was fitted prior to the cell. To centrifuge the samples, a refrigerated tabletop centrifuge Sigma 2-16K was used. A Crison micro pH-2002 pH-meter was used for pH measurements.

Data were analysed using NEMRODW [31], STATGRAPHICS [32] and PROGRESS [33]. A home-made program, N_WAY_DET, was used to estimate the capability of detection.

3.2. Reagents and sample preparation

Sulfadiazine, sulfamerazine and sulfamethazine of analytical grade were purchased from Sigma (Steinheim, Germany). The stock solutions (9 mg L^{-1}) were prepared in methanol HPLC grade and stored at low temperature (close to 4 °C), and the aqueous calibration solutions were obtained by diluting the stock solutions with carrier. The carrier solutions were prepared by mixing acetic/acetate buffer and methanol HPLC grade as organic solvent. The water used was purified with a Milli-Q water purification system (Millipore).

The milk samples were deproteinized with tungsten reagent. This reagent contains sodium tungsten (F.E.R.O.S.A, Barcelona, Spain), *ortho*-phosphoric acid solution (88%, w/w) and 1 M sulfuric acid (Merck, Darmstadt, Germany). The pretreatment consisted of adding 10 mL of the tungsten reagent and the corresponding amount of the sulfonamide to 2.5 mL of milk, diluting with water to 25 mL and waiting a few minutes until a precipitate is formed. Then the sample was centrifuged, at 8000 rpm and 10 °C during 10 min, and filtered. The milk calibration solutions were obtained by dilution of appropriate amounts of filtrate with carrier solution.

3.3. Experimental procedure

Carrier was degassed by sparging with helium for 10 min. Then a sufficient quantity was passed through the system to displace the remains of the other samples. The detector was programmed for an amperometric mode operation defined by the following parameters: analytical cell potential, 0.9 V; conditioning cell potential, 0.2 V; sensitivity of the detector, 100 μA; signal output, 10 V. The characteristics of the carrier solution

are obtained in the optimization step: 19.88% of methanol, pH 5.56 and flow rate equal to 2.5 mL min^{-1}.

Afterwards, the electrode equilibration was allowed for a few minutes and the stability of the baseline evaluated. Then the sample (20 μL) was injected and the peaks in the obtained fiagram were quantified, the peak height being the analytical response.

4. Results and discussion

4.1. Optimization

The aims of this optimization were to maximize the peak height, estimated from the average of three fiagrams obtained under the same experimental conditions, and to minimize the variability of these signals estimated from the standard deviation of the *n* replicates. It can be debatable if is more suitable using the standard deviation, S.D., or the relative standard deviation, R.S.D., as response to optimize. However, simultaneous high or low values of peak height or of its standard deviation can lead to the same values of R.S.D., masking the true behaviour of standard deviation as a function of experimental factors. In addition, the use of desirability functions allows one to add constrains to S.D. taking into account the peak size as can be see further on. The choice of the experimental conditions that allows one to reach these goals was carried out with the help of the experimental design methodology.

A Doehlert design with two replicates at the central point was used to determine the effect of three experimental factors on two responses. The experimental factors studied were: the percentage of methanol, the pH and the flow rate of the carrier solution. The percentage of methanol (%methanol) and pH of the carrier solution influence both the analyte signal and the signal of the possible interferents that may be present in the sample and in the carrier solutions. The flow rate of the carrier solution (ϕ) is a hydrodynamic factor which influences the dispersion of the injected sample. The experimental domain is: % of methanol from 17.5% to 22.5%, flow rate from 0.5 to 2.5 mL min^{-1} and pH from 4 to 6.

Values of other experimental parameters not subjected to this optimization, such analytical or conditioning cell potentials and sensitivity of detector were chosen according to previous studies. For example, the conditioning cell potential was chosen to avoid possible chemical interferences but without reducing the analytical signal of the three sulfonamides; the analytical cell potential was in the plateau of the hydrodynamic voltammograms of each sulfonamide (see Fig. 1), etc.

In the experimental design, the values of %methanol and flow rate factors were maintained always at the theoretical values of the Doehlert design, whereas the true values of pH of each analysed sample were slightly different from the theoretical ones due to the presence of the organic solvent. Table 1 shows the true experimental pH values. One of the experiments, with coordinates in coded variables (0, −0.58, 0.82), was lost due an unfinished degasification of carrier solution, so the initial design (14 runs) results in the design shown in Table 1. The characteristics of the final experimental matrix, i.e. *G*-efficiency, variance inflation factors and maximum of variance function, were com-

Table 1
Doehlert matrix design (in coded and natural variables) and experimental responses

Run	Experimental matrix (coded variables)			Experimental plan (natural variables)			Experimental responses	
	x_1	x_2	x_3	u_1 = %methanol	$u_2 = \phi$ (mL min^{-1})	u_3 = pH	Peak height[a] (μA)	ln(s)
1	1	0	0	25.00	1.50	5.35	1.021	−1.75
2	−1	0	0	15.00	1.50	5.21	0.724	−3.06
3	0.5	0.87	0	22.50	2.50	5.31	1.351	−1.98
4	−0.5	−0.87	0	17.50	0.50	5.23	0.517	−2.51
5	0.5	−0.87	0	22.50	0.50	5.31	0.553	−3.57
6	−0.5	0.87	0	17.50	2.50	5.23	1.411	−3.51
7	0.5	0.29	0.82	22.50	1.83	6.20	1.080	−1.58
8	−0.5	−0.29	−0.82	17.50	1.17	4.24	0.899	−2.42
9	0.5	−0.29	−0.82	22.50	1.17	4.33	0.812	−1.67
10	0	0.58	−0.82	20.00	2.16	4.30	1.049	−1.62
11	−0.5	0.29	0.82	17.50	1.83	6.12	1.056	−1.94
12	0	0	0	20.00	1.50	5.29	1.058	−2.37
13	0	0	0	20.00	1.50	5.29	1.034	−1.84

ϕ: flow rate, ln(s): natural logarithm of standard deviation.

[a] Peak height means the average of three replicates.

parable to those of the initial design (e.g. the VIFs in the original design were lower than 1.4 and in the final design lower than 1.9, which is so lower than the threshold value 4 established by some authors [24]).

The two responses considered, the peak height and its variability, were studied independently to analyse if the experimental conditions of the optima reached individually for each one coincided in both cases. So a mathematical model was fitted for each response.

Since the three sulfonamides under study present hydrodynamic voltammograms which have similar oxidation potentials (see Fig. 1), one of them, sulfadiazine, has been chosen to perform the optimization. To carry out the study, a constant amount of $100\,\mu g\,L^{-1}$ of sulfadiazine in water, which corresponds to the MRL in milk [3], was injected and replicated three times in each experimental condition of the design.

4.1.1. Optimization of peak height (maximization)

Firstly, a second-order model (Eq. (1)) has been fitted for the peak height (mean of three replicates). In Eq. (1) variables are codified as in Table 1.
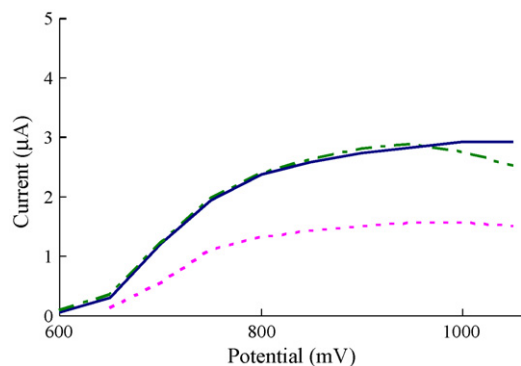

Fig. 1. Hydrodynamic voltammograms of sulfadiazine $1.8\,mg\,L^{-1}$ (solid line), sulfamethazine $1.8\,mg\,L^{-1}$ (dotted line), and sulfamerazine $1.8\,mg\,L^{-1}$ (dash–dot line).

The analysis of the variance (ANOVA) [31] allows one to affirm that the fitted model (Eq. (5)) explains significantly, at a 5%, the experimental peak height (p-value = 0.045). Also there is not evidence of lack of fit (p-value = 0.11) at a significance level of 5%. The coefficient of determination is $R^2 = 0.97$:

$$y = 1.05 + 0.04x_1 + 0.40x_2 + 0.03x_3 - 0.18x_1^2 - 0.06x_2^2$$
$$- 0.21x_3^2 - 0.08x_1x_2 + 0.13x_1x_3 + 0.38x_2x_3 \qquad (5)$$

In order to study this surface response fitted, a study of the optimum path of the response surface fitted was carried out. The optimum path of the response surface is determined by tracing spherical surfaces, centred on the center point of the experimental domain with growing radius, R, and calculating on each of these the maximum, $\hat{y}_{max}(R)$, and the minimum, $\hat{y}_{min}(R)$, of the response surface fitted [17,23]. The representation of the optimum path of the response surface fitted for the peak height (Eq. (5)) is shown in Fig. 2a.

The radius R is indicated in abscissas. In ordinates, the $\hat{y}_{max}(R)$ value is shown in the right side of the graph and the $\hat{y}_{min}(R)$ value is shown in the left part of the graph. Note that both sides of the abscissas axis have the same sign, since they represent positive distances from the center of the design.

It is clear that in the optimum path of the response shown in Fig. 2a, the maximum peak height, $1.44\,\mu$A, is reached at the boundary of the experimental domain, at distances $R = 1$ from the center of the experimental domain.

Ordinate axis in Fig. 2b has the values x_1, x_2 and x_3 of factors, in coded variables, that define each point of the experimental domain where maximum can be reached $\hat{y}_{max}(R)$ (on the right of the plot) or the minimum $\hat{y}_{min}(R)$ (on the left). In Fig. 2b, the dotted line shows the values of the maximum for $R = 1$, $x_1 = 0.042$, $x_2 = 0.875$ and $x_3 = 0.396$, which is where the global maximum of the fitted surface for peak height is found. That is, to reach a maximum value of the response, the flow rate has to take the highest value analysed, pH an intermediate value between the corresponding to the centre point and the highest value analysed in the experimental domain, and %methanol a

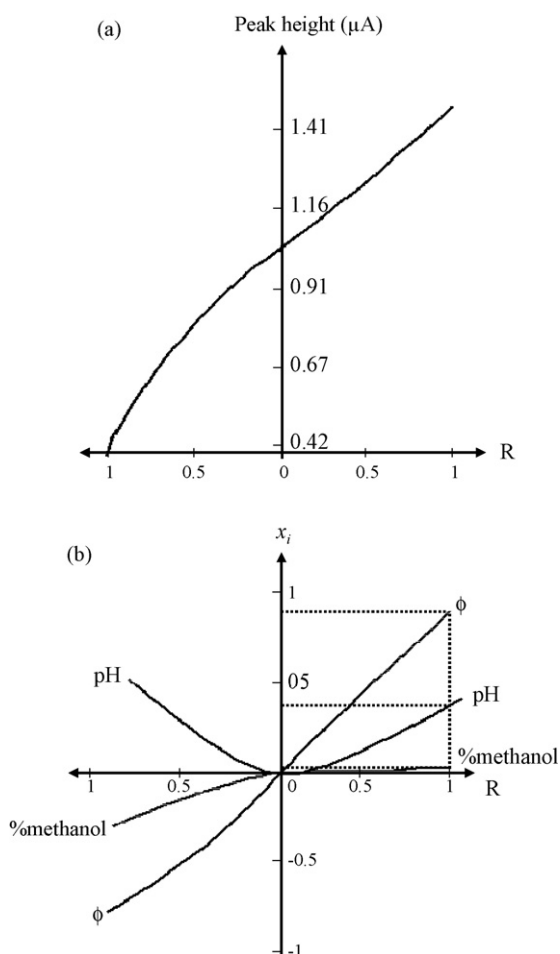(a)

Peak height (µA)

(b)

Fig. 2. (a) Optimum path of the response surface fitted to the peak height where ordinates represent the response reached on the built spheres for radius R indicated in abscissas; (b) coordinates of the points of plot (a) for each factor in coded variables. The right part of both plots refers to the maximization of the response; the left part of the plots refers to the minimization of the response.

value corresponding to the centre of the experimental domain. The coordinates for the maximum, Fig. 2b, transformed into real variables correspond to %methanol, flow rate and pH of 20%, 2.5 mL min^{-1} and 5.6, respectively.

Fig. 2b has also information about how peak height varies as a function of changes in pH, % of methanol and flow rate. As can be seen near to the maximum, the peak height is more sensitive to variations on flow rate and pH whereas it is insensitive to changes of %methanol.

4.1.2. Optimization of the standard deviation (minimization)

A second analysis, analogous to the previous one, was carried out for the standard deviation, but now a minimisation is wanted. In this case, the quadratic model fitted for the standard deviation of the peak height was not suitable. Therefore, a Box–Cox transformation [17] of the standard deviation is used with the objective of making the residuals of the regression more homoscedastic and closer to a normal distribution. A Box–Cox power transformation on the dependent variable is a useful method to alleviate heteroscedasticity when the distribu-
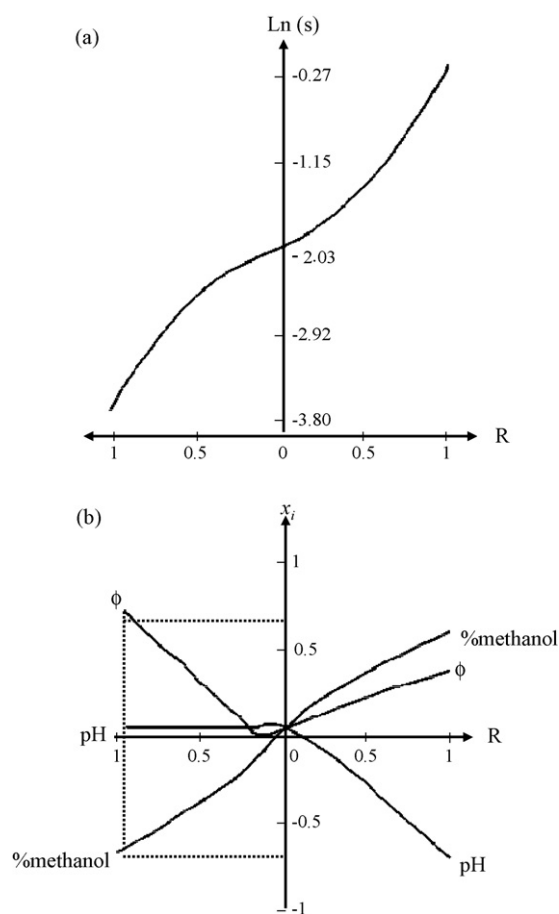
(a)

Ln (s)

(b)

Fig. 3. (a) Representation of the optimum path of the response surface fitted for the natural logarithm of standard deviation; (b) coordinates of the points of plot (a) for each factor in coded variables. The right part of both plots refers to the maximization of the response; the left part of the plots refers to the minimization of the response.

tion of the dependent variable is not known. The minimum of the graph ln(sum of squares of error) vs. λ is found for $\lambda = 0$, that means that a transformation that can be used is $\ln(y_i)$.

The model fitted (Eq. (6)) was adequate to describe the natural logarithm of the standard deviation of the peak height, $\ln(s)$, in the experimental domain at a significance level of 7%. The coefficient of determination was $R^2 = 0.95$:

$$y = -2.11 + 0.71x_1 + 0.31x_2 - 0.21x_3 - 0.24x_1^2 - 0.94x_2^2$$
$$+ 0.87x_3^2 + 1.53x_1x_2 - 0.93x_1x_3 - 0.65x_2x_3 \qquad (6)$$

The study of the optimal path of this response surface is shown in Fig. 3a, the minimum is also reached at the boundary of the experimental domain. In Fig. 3b, the dotted line shows the values of the minimum for $R = 1$, $x_1 = 0.717$, $x_2 = 0.696$ and $x_3 = 0.000$, which is where the global minimum of the fitted surface for natural logarithm of standard deviation. The analysis of Fig. 3b for values of R close to 1 shows that it is highly sensitive to the variation of %methanol and flow rate and practically insensitive to variations in pH. The minimum, transformed into real variables, is reached at (Fig. 3b) 16.5% methanol, 2.3 mL min^{-1} for flow rate and pH 5.
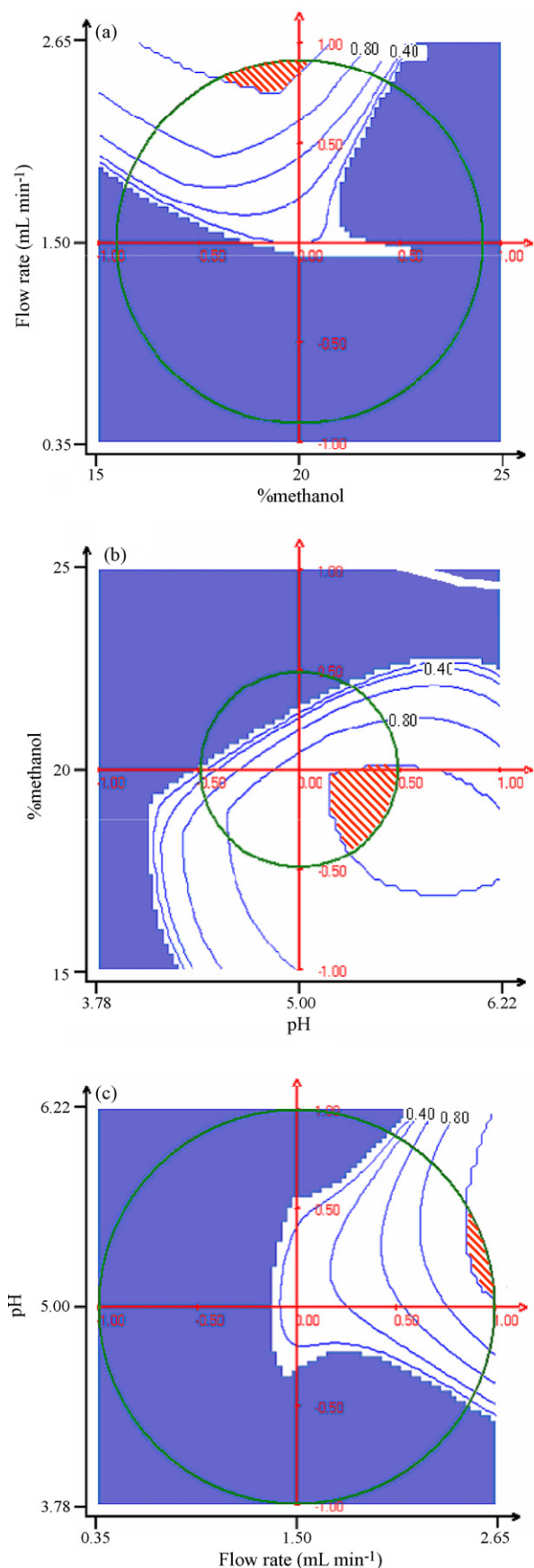
Comparing these values to those which lead to the optimum for the peak height, it is clear that these experimental conditions are different in the case of %methanol and, to a lesser extent, of pH. To obtain higher peak heights, the %methanol has to be 20%, around the central point of the domain, but it has to be maintained at low values, 16.5% methanol, to reach a minimum of natural logarithm of the standard deviation. pH has to be maintained at the central value (pH 5) of the design to minimize the variability and has to take higher values (pH 5.6) for maximizing the peak height. In the case of the flow rate, the value that maximizes the peak height (2.5 mL min^{-1}) is almost equal to that which minimizes the natural logarithm of standard deviation (2.3 mL min^{-1}). It is therefore necessary to reach a compromise solution between the two responses.

4.1.3. Multicriteria optimization: desirability function

The individual desirability function, d_1, for peak height has been defined in such a way that values higher or equal to 97% of the maximum experimental value are acceptable (desirability 1), whereas values lower than 70% of the maximum found are unacceptable (desirability 0). In this way, the threshold values of peak height were 1.40 and 1.00 μA, respectively. For values of peak height between 1.00 and 1.40 μA, d_1 varies linearly between 0 and 1.

On the other hand, in the case of the natural logarithm of the standard deviation, acceptable values (desirability $d_2 = 1$) were defined as those corresponding to a value of standard deviation lower than or equal to 5% of 1.4 μA (which is the minimum value considered with desirability 1 for peak height), whereas values of standard deviation higher than or equal to 10% of this peak height were considered unacceptable (desirability $d_2 = 0$). Thus, the threshold values for the natural logarithm of standard deviation were -2.66 and -1.97. Function d_2 also varies linearly between 1 and 0 when the natural logarithm of standard deviation varies between -2.66 and -1.97.

To obtain the overall desirability (Eq. (1)) $p_1 = p_2 = 1$ have been set, which means that the two desirability functions are equally weighted.

The maximum of the overall desirability function is found for 19.88% methanol, $\phi = 2.5$ mL min^{-1} and pH 5.56, the estimated values of peak height and standard deviation being 1.49 and 0.06 μA, respectively. Under these experimental conditions all the constraints imposed on the individual functions are fulfilled and overall and individual desirabilities of 1 are reached. A study of the stability of the desirability function shows that variations of a 10% of codified variables around the optimum leads to desirabilities between 1 and 0.8, which points out the stability of the optimum found.

Fig. 4 shows the contour lines of the overall desirability function in the experimental domain, the variable not represented in

Fig. 4. Contour plot of the global desirability function in the space of the variables %methanol vs. flow rate (a), pH vs. %methanol (b) and flow rate vs. pH (c). In each case, the variable not represented remains constant with the value corresponding to the optimum of the global function, i.e. pH 5.5 (a), flow rate = 2.5 mL min^{-1} (b) and %methanol = 20% (c); circles show the experimental domain in each case.

Table 2
Calibration curve for each sulfonamide

Parameters	Sulfadiazine	Sulfamethazine	Sulfamerazine
b_0	0.717	0.237	0.080
b_1	0.011	0.009	0.017
s_{yx}	0.042	0.043	0.074
ρ	0.997	0.995	0.996
$x_0 = 100\,\mu\text{g L}^{-1}$			
CCα	105.50	107.30	110.70
CCβ	110.70	114.00	120.20

b_0: intercept, b_1: slope, s_{yx}: residual standard deviation, ρ: correlation coefficient, CCα: limit of decision, and CCβ: capability of detection at the maximum residue limit ($x_0 = 100\,\mu\text{g L}^{-1}$) for pure standards.

each case remaining constant at the value corresponding to the optimum of the global function. Circles mean the size of the experimental domain obtained when fixing one of the variables in each plot. Grey zones means desirability 0, whereas contour lines ranges from 0 to 1.0. Lined zones are those of desirability 1, being the flow rate the experimental factor with smaller variability range for maintaining the desirability equal to 1, as can be seen in Fig. 4a and c.

Two complete designs (with two replicates) were repeated with 14 days between them including a change of filters. The peak height change, but the position of the optimum obtained for the global desirability is similar that obtained in the previous analysis: 18.7% methanol, $\phi = 2.49\,\text{mL min}^{-1}$, pH 5.53 and 18.1%, 2.37 and 5.64 mL min^{-1}, respectively.

4.2. Determination of sulfonamides in milk

The determination of the three sulfonamides independently was carried out in the optima conditions found in the previous stage. The calibration lines have been built with aqueous calibration solutions prepared as stated in Section 3. The concentrations of the calibrations ranged from 20.0 to 154.7 μg L^{-1} for sulfadiazine, from 39.2 to 169.1 μg L^{-1} for sulfamethazine, and from 39.6 to 171.0 μg L^{-1} for sulfamerazine. The mean of three replicates has been considered as analytical response. The parameters of the regression models fitted once outliers were removed using the least median of squares (LMS) regression [34] are shown in Table 2. As the maximum residue limit for sulfonamides in milk has been fixed at 100 μg L^{-1} [2,3], Table 2 contains also the values of CCα (Eq. (4)) and CCβ (Eq. (2)) for $x_0 = 100\,\mu$g L^{-1}.

The parameters of the three calibration lines have not a systematic behaviour and have to be analysed jointly for each line. For example, the higher slope corresponds to sulfamerazine but also the higher residual standard deviation. Since always exists a negative correlation between intercept and slope of calibration line, it occurs that different values of both of them can lead to analytical determinations of the same quality. So to comparatively study how the method worked it is more suitable using the capability of detection, since in CCβ estimation slope and standard deviation of calibration line take part (see Eq. (2)). To obtain the CCβ values shown in Table 2, probabilities α and β have been fixed at 0.05.

It can be seen that for equal s_{yx} values (sulfadiazine and sulfamethazine), higher values of slope b_1 correspond better CCα and CCβ, whereas if s_{yx} is higher, CCα and CCβ make worse (sulfamerazine). In any case, limit of decision and capability of detection at 100 μg L^{-1} are very similar for the three sulfonamides.

For each sulfonamide, the corresponding calibration line in Table 2 has been used to determine its concentration in spiked test samples of two different brands of milk pretreated as it has been indicated in Section 3.2. Both full-cream and skimmed milk samples were analysed. The recoveries of the analytical procedures estimated according to the procedure described in Section 3.1.2.1 of Ref. [27] with three replicates (% recovery = 100 × measured content/fortified level), were taken into account in the estimation of the concentration of the test samples shown in Table 3. The relative errors in percentage, column sixth of Table 3, are always inside the range fixed by the European Decision 2002/657/EC, that ranges from −20% to +10% at these levels of concentration.

4.3. Validation of the experimental procedure according to Commission Decision 2002/657/EC

Commission Decision 2002/657/EC [27] establish the performance criteria and procedures for validation of screening and confirmatory methods. In this paper, decision limit (CCα), detection capability (CCβ), trueness, precision and ruggedness of the used analytical procedure have being estimated.

4.3.1. Detection capability (CCβ) and decision limit (CCα)
The capability of detection, CCβ, and the decision limit, CCα, of the analytical procedure under study have been determined both at $x_0 = 0$ and at $x_0 = 100\,\mu$g L^{-1}, as normative establishes.

Table 3
True and calculated concentrations, recoveries and relative errors in prediction for milk test samples of two brands of milk (A and B)

Analyte	Milk	Test sample	c_{true} (μg L^{-1})	c_{calc} (μg L^{-1})	Recovery (%)	Relative error (%)
Sulfadiazine	Skimmed A	1	109.20	111.92	87.78	2.49
Sulfamethazine	Skimmed A	2	106.80	105.06	98.38	−1.63
	Skimmed B	3	106.80	106.30	89.75	−0.47
	Full-cream A	4	106.80	114.19	76.86	6.92
Sulfamerazine	Skimmed B	5	108.00	107.89	67.35	−0.10
	Full-cream A	6	108.00	109.63	119.08	1.51
	Full-cream B	7	108.00	104.48	84.06	−3.26

Table 4
Calibration curve for each sulfonamide and for a ternary mixture

Parameters	Sulfadiazine	Sulfamethazine	Sulfamerazine	Ternary mixture
b_0	0.585	0.628	0.573	0.475
b_1	0.011	0.007	0.014	0.012
s_{yx}	0.086	0.034	0.071	0.069
ρ	0.991	0.996	0.995	0.995
$x_0 = 0 \, \mu g \, L^{-1}$				
CCα	13.92	9.46	9.05	9.27
CCβ	26.87	18.16	17.47	17.97
$x_0 = 100 \, \mu g \, L^{-1}$				
CCα	110.20	107.10	107.10	107.20
CCβ	119.80	113.60	113.70	113.90

b_0: intercept, b_1: slope, s_{yx}: residual standard deviation, ρ: correlation coefficient, CCα: limit of decision, and CCβ: capability of detection at 0 ($x_0 = 0 \, \mu g \, L^{-1}$) at the maximum residue limit ($x_0 = 100 \, \mu g \, L^{-1}$) for milk samples.

CCα and CCβ values have been calculated with regression models signal *vs.* concentration using calibration milk samples prepared as stated in Section 3. The study has been carried out in two ways: (i) with each sulfonamide separately and (ii) with a ternary mixture of the three sulfonamides. As milk samples are used, the performance characteristics are more realistic than if they are determined by means of calibrations of aqueous samples.

The mean of three replicates has been considered as analytical response. The parameters of the regression models and the corresponding CCα and CCβ values are shown in Table 4. The probability of false positive or false non-compliance is fixed at 5%, and also the probability of false negative or false compliance. In all cases three replicates, $K = 3$ in Eq. (2), have been considered.

Fig. 1 indicates that the three analytes respond to the detector in a similar fashion and so each one of them would interfere in the determination of the others if it is present in the sample. However, the normative establishes the MRL for the total content of sulfonamides, so a calibration has been carried out with spiked samples with ternary mixtures of the three sulfonamides, results are shown in Table 4. In this case, the proportions of each of them have been equal and the total amount is set at nine levels equally spaced from 10.8 to 156.6 $\mu g \, L^{-1}$.

When comparing the results obtained for the calibration with ternary mixtures (fifth column) and the results obtained for each sulfonamide independently (columns two to four) it is clear that the interference caused by the presence of the other two sulfonamides does not modifies the capability of detection for the total sulfonamide amount.

At the MRL, the decision limit varies between 107.10 and 110.20 $\mu g \, L^{-1}$, and the capability of detection between 113.60 and 119.80 $\mu g \, L^{-1}$, which are very similar values to those obtained in aqueous calibrations, Table 2. This means that the determination in milk samples does not modify the capability of detection of the method. The same occurs at $x_0 = 0 \, \mu g \, L^{-1}$, where CC$\alpha$ varies from 9.05 to 13.92 $\mu g \, L^{-1}$ and CCβ from 17.47 to 26.87 $\mu g \, L^{-1}$. Similarly to the case of aqueous calibration, residual standard deviation, s_{yx}, is the parameter of the calibration that has a higher influence on capability of detection and limit of decision, both at zero concentration as at the MRL.

The difference between CCβ values, both at 100 $\mu g \, L^{-1}$ as at zero concentration, is due to the fact that the standard deviation of the response in all linear calibration is higher at the concentration range edges than in the centre. For example, at the MRL, 19.80 $\mu g \, L^{-1}$ of sulfadiazine can be detected, but only 26.87 $\mu g \, L^{-1}$ at zero concentration, in both cases with false non-compliant probability (false positive) and false compliant probability (false negative) equal to 0.05.

4.3.2. Accuracy (trueness and precision)

One way to estimate the accuracy of the analytical procedures is based on building regression lines between calculated, c_{calc}, and true, c_{true}, concentrations [35]. To determine trueness, it has been checked that the corresponding regression models ($y = 0.0053 + 0.9999x$ for sulfadiazine, $y = -0.0002 + 1.0000x$ for sulfamethazine, and $y = 0.0001 + 1.0000x$ for sulfamerazine) had slope and intercept statistically equal to 1 and 0, respectively; so the analytical procedures fulfil the property of trueness at significance level of 5%.

With regard to precision, this performance characteristic can be estimated for a range of concentrations from the uncertainty of the regression c_{calc} *vs.* c_{true}. The residual standard deviation of the regression model (s_{yx}) can be assimilated to the repeatability of the analytical procedure. The values obtained for precision, estimated through this approach, were 3.89 $\mu g \, L^{-1}$ for sulfadiazine, 4.77 $\mu g \, L^{-1}$ for sulfamethazine, and 4.42 $\mu g \, L^{-1}$ for sulfamerazine.

4.3.3. Ruggedness

Ruggedness is defined [27] as "the susceptibility of an analytical method to changes in experimental conditions which can be expressed as a list of the sample materials, analytes, storage conditions, environmental and/or sample preparation conditions under which the method can be applied as presented or with specified minor modifications". In this study, since the analytical signals of the three sulfonamides are very similar, only the signal of sulfadiazine has been taken into account.

As Commission Decision 2002/657/EC suggests, the Youden approach is used to evaluate the relevance of the possible changes in the results of the analytical procedure in the ruggedness study. The Youden approach consists simply of carrying out a Plackett–Burman experimental design [36]. In this case, a two-level design has been completed for seven experimental factors: %methanol, flow rate and pH of carrier solution, analytical and conditioning cell potentials, concentration of sulfadiazine and moment of measurement. The level (+1) of factors corresponds to 21.2%, 2.5 mL min⁻¹, 5.7 pH, 0.945 V, 0.210 V, 105 $\mu g \, L^{-1}$ and in the evening, respectively. Whereas the level (−1) corresponds to 18.8%, 2.4 mL min⁻¹, 5.2 pH, 0.855 V, 0.190 V, 95 $\mu g \, L^{-1}$ and in the morning, respectively. The values correspond to a variation of 5% with respect to the nominal conditions stated above.
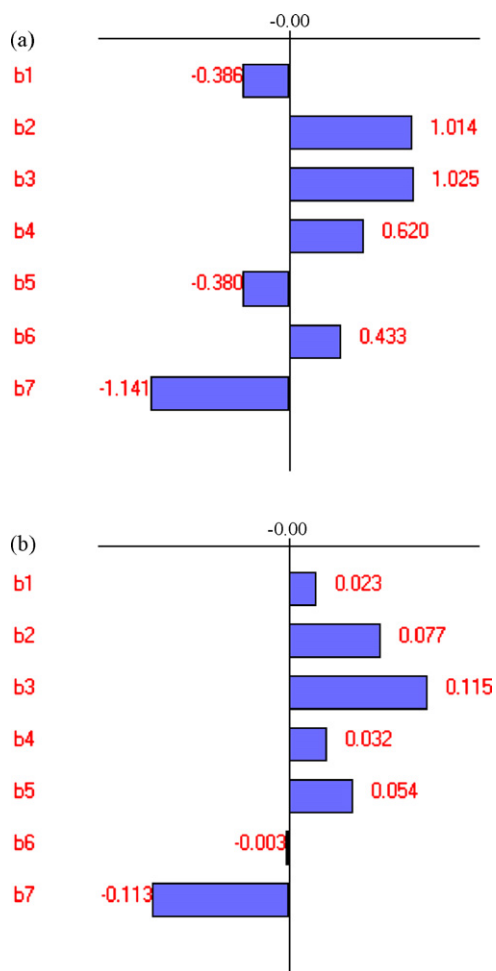
Fig. 5. Ruggedness analysis by means of Plackett–Burman designs: (a) peak height, (b) standard deviation of peak height. Coefficients estimated for the seven factors: %methanol (b_1), flow rate (b_2), pH (b_3) of carrier solution, analytical (b_4) and conditioning (b_5) cell potentials, concentration of sulfadiazine (b_6) and moment of measurement (b_7).

Two responses have been considered in this analysis since it is useful to know the ruggedness of the procedure carried out with respect to peak height and its variability. So two analyses have been performed taking as response either the mean or the standard deviation of three replicates of peak height.

The analysis was performed using the Lenth's approximation [24], since it does not need replicates to evaluate the significance of the coefficients. The Lenth's method estimates a robust value of the standard deviation (S.D.), from which the active effects can be identified. The coefficients higher than a critical value (set at 2.5 S.D.) are considered significant and are removed. The procedure is repeated until there are no significant effects.

In the case of peak height, the estimated coefficients are shown in Fig. 5a. Since no coefficient is greater than the corresponding critical value (±2.33) the conclusion is that variations in the factors do not affect the peak height. The same occurs in the case of the standard deviation of peak height, the corresponding coefficients are shown in Fig. 5b. In this case,

the critical value was ±0.20, which is not exceeded by any coefficient.

Acknowledgements

References

[1] M.E. Doyle, Veterinary Drug Residues in Processed Meats. Potential Health Risk, Food Research Institute, University of Wisconsin–Madison, FRI Briefings, 2006, http://www.wisc.edu/fri/briefs.htm (accessed March, 2007).
[2] Off. J. L 37 (15 February) (1996) 9–11.
[3] Off. J. L 224 (18 August) (1990) 1–8.
[4] A. Gentili, D. Perret, S. Marchese, TrAC Trends Anal. Chem. 24 (2005) 704.
[5] D.G. Kennedy, R.J. McCracken, A. Cannavan, S.A. Hewitt, J. Chromatogr. A 812 (1998) 77.
[6] T.A.M. Msagati, M.M. Hindi, Talanta 64 (2004) 87.
[7] K. Granelli, C. Branzell, Anal. Chim. Acta 586 (2007) 289.
[8] I. Pecorelli, R. Bibi, L. Fioroni, R. Galarini, J. Chromatogr. A 1032 (2004) 23.
[9] T.C.C. Yang, I.L. Yang, L.J. Liao, J. Liq. Chromatogr. Relat. Technol. 27 (2005) 501.
[10] I. García, M.C. Ortiz, L. Sarabia, J.M. Aldama, Anal. Chim. Acta 587 (2007) 222.
[11] K.E. Maudens, G.F. Zhang, W.E. Lambert, J. Chromatogr. A 1047 (2004) 85.
[12] A. Posyniak, J. Zmudzki, K. Mitrowska, J. Chromatogr. A 1087 (2005) 259.
[13] R. Díez, L. Sarabia, M.C. Ortiz, Anal. Chim. Acta 585 (2007) 350.
[14] M.R.S. Fuh, S.Y. Chu, Anal. Chim. Acta 499 (2003) 215.
[15] M. Catalá Icardo, J.V. García Mateo, M. Fernández Lozano, J. Martínez Calatayud, Anal. Chim. Acta 499 (2003) 57.
[16] M.E. Rueda, L.A. Sarabia, A. Herrero, M.C. Ortiz, Anal. Chim. Acta 479 (2003) 173.
[17] R.H. Myers, D.C. Montgomery, Response Surface Methodology, John Wiley & Sons, New York, 2002.
[18] T.A.H.M. Janse, P.F.A. Van der Wiel, G. Kateman, Anal. Chim. Acta 155 (1983) 89.
[19] E. Vereda, A. Rios, M. Valcarcel, Anal. Chim. Acta 348 (1997) 129.
[20] C. Vannecke, M.S. Bloomfield, Y. Vander Heyden, D.L. Massart, Anal. Chim. Acta 455 (2002) 117.
[21] S. Gang, Z. Yongyao, W. Huaiwen, C. Hongli, C. Xingguo, H. Zhide, Analyst 125 (2000) 921.
[22] M.C. Ortiz, L. Sarabia, A. Herrero, M.S. Sánchez, Chemometr. Intell. Lab. 83 (2006) 157.
[23] G. Derringer, R. Suich, J. Qual. Technol. 12 (1980) 214.
[24] G.A. Lewis, D. Mathieu, R. Phan-Tan-Luu, Pharmaceutical Experimental Design, Marcel Dekker, New York, 1999.
[25] M.E. Rueda, M.C. Ortiz, L.A. Sarabia, A. Herrero, Anal. Chim. Acta 498 (2003) 119.
[26] M.C. Ortiz, A. Herrero, S. Sanllorente, C. Reguera, Talanta 65 (2005) 246.
[27] Off. J. L 221 (17 August) (2002) 8–36.
[28] ISO 11843-1, Capability of Detection: Terms and Definitions, ISO, Geneva, 1997.
[29] ISO 11843-2, Capability of Detection: Methodology in the Linear Calibration Case, ISO, Geneva, 2000.
[30] M.C. Ortiz, L.A. Sarabia, Trends Anal. Chem. 13 (1994) 1.
[31] D. Mathieu, J. Nony, R. Phan-Tan-Luu, NEMRODW Ver. 2000, LPRAI, Marseille, 2000.

[32] STATGRAPHICS Plus 5.1 for Windows Ver. 4.0, Statistical Graphics Corp., Herndon, VA, 2001.

[33] P.J. Rousseeuw, A.M. Leroy, Robust Regression and Outlier Detection, John Wiley & Sons, Hoboken, NJ, 2001.

[34] M.C. Ortiz, L.A. Sarabia, A. Herrero, Talanta 70 (2006) 499.

[35] K. Danzer, M. Otto, L. Currie, Pure Appl. Chem. 76 (2004) 1215.

[36] D.L. Massart, B.G. Vandeginste, L.M.C. Buydens, S. De Jong, P.J. Lewi, J. Smeyers-Verbeke, Handbook of Chemometrics and Qualimetrics. Part A, Elsevier, Amsterdam, 1997.

Determination of iodine and molybdenum in milk by quadrupole ICP-MS

Helen J. Reid [a],*, Abdul A. Bashammakh [b], Phillip S. Goodall [c],
Mark R. Landon [a], Ciaran O'Connor [a], Barry L. Sharp [a]

[a] Department of Chemistry, Loughborough University, Loughborough, Leics, LE11 3TU, UK
[b] Department of Chemistry, Faculty of Science, King Abdulaziz University, P.O. Box 80203, Jeddah 21589, Saudi Arabia
[c] Nexia Solutions, Sellafield, Seascale, Cumbria, CA20 1PG, UK

Abstract

A reliable method for the determination of iodine and molybdenum in milk samples, using alkaline digestion with tetramethylammonium hydroxide and hydrogen peroxide, followed by quadrupole ICP-MS analysis, has been developed and tested using certified reference materials. The use of $He + O_2$ ($1.0\,ml\,min^{-1}$ and $0.6\,ml\,min^{-1}$) in the collision-reaction cell of the mass spectrometer to remove $^{129}Xe^+$ – initially to enable the determination of low levels of ^{129}I – also resulted in the quantitative conversion of Mo^+ to MoO_2^+ which enabled the molybdenum in the milk to be determined at similar mass to the iodine with the use of Sb as a common internal standard. In order to separate and pre-concentrate iodine at sub $\mu g\,l^{-1}$ concentrations, a novel method was developed using a cation-exchange column loaded with Pd^{2+} and Ca^{2+} ions to selectively retain iodide followed by elution with a small volume of ammonium thiosulfate. This method showed excellent results for aqueous iodide solutions, although the complex milk digest matrix made the method unsuitable for such samples. An investigation of the iodine species formed during oxidation and extraction of milk sample digests was carried out with a view to controlling the iodine chemistry.
© 2007 Elsevier B.V. All rights reserved.

Keywords: Iodine; Collision-reaction cell; Molybdenum; Milk; Sample preparation; ICP-MS

1. Introduction

Milk is recognized as the most complete food in the human diet because it contains all the macronutrients such as proteins, lipids and carbohydrates and all the essential micronutrients such as elements, vitamins and enzymes. A lot of information has been accumulated concerning the composition of milk in terms of fat, protein and vitamins [1]; however, less attention has been paid to the elemental composition of milk in spite of the great importance of essential elements in nutrition [2,3].

Iodine is one of the most important trace elements in human nutrition; its physiological function as a constituent of thyroxine, the hormone secreted by the thyroid gland, necessitates the control of intake levels, as deficiency or excessive exposure both have a detrimental affect on thyroid function [1,4]. Concentrations of iodine in cow's milk, which is a major contributor to

dietary exposure, are naturally influenced by the levels of iodine in feedstuffs, which vary seasonally [5]. It has been reported that iodine in milk is present mostly as free iodide [6] with relatively small amounts of organic iodine. Whilst ^{127}I is the only stable isotope, the most hazardous iodine species are the radioactive isotopes such as ^{129}I and ^{131}I which may enter the food chain via the air–grass–cow–milk pathway as a result of aerial emissions from nuclear reprocessing plants [7]. The long-lived radionuclide ^{129}I is monitored by regular measurement of ^{129}I content of liquid milk from cows in the potentially affected areas [8,9], typically by radiometric analysis after appropriate separation techniques [10].

Inductively coupled plasma mass spectrometry (ICP-MS) potentially offers a quick, simple method of monitoring iodine isotopes in milk; however there are a number of problems associated with the use of ICP-MS for this assay. Firstly, iodine has a relatively high detection limit in ICP-MS in comparison to other elements due to its high ionisation potential (10.45 eV). Also, signal memory effects can be a problem, due to evaporation of iodine as HI or I_2 from aerosol droplets in the spray chamber

---

* Corresponding author. Tel.: +44 1509 222593; fax: +44 1509 223925.
E-mail address: h.j.reid@lboro.ac.uk (H.J. Reid).

[11]. Furthermore, interference on the [129]I[+] signal arises from [129]Xe[+] and possibly also [127]IH$_2$[+] ions [12,13], making the use of oxygen as a collision/reaction gas an attractive option for this analysis.

Before considering instrumental conditions, however, it is necessary to carefully consider sample preparation, to avoid losses due to iodine's volatility and complex redox chemistry. At low pH iodide is easily oxidised to volatile molecular iodine by dissolved oxygen (or other dissolved oxidants):

$$4I^- + O_{2(g)} + 4H^+ \rightarrow 2H_2O + 2I_{2(aq)} \qquad E^0 = 0.61\,V \quad (1)$$

At high pH, the oxidation of iodide to iodine is avoided, and it is therefore usual to prepare samples in alkaline media to prevent the oxidation of I[-] to I$_2$ or the formation of HI. With milk samples, it is also important to destroy the organic matrix to reduce the spectral interferences from carbon species and the possibility of cone blockage in the ICP-MS interface. Thus decomposition with strong alkali, such as ammonia, potassium hydroxide or tetramethylammonium hydroxide (TMAH), alone or in combination, has been used to prepare milk samples for iodine determination [4,11,14,15]. These procedures lead to the conservation of the iodine as iodide or iodate, which is then determined by ICP-MS regardless of the iodine species present in the original sample. The use of alkaline conditions also potentially enables the simultaneous determination of other important anion-forming elements such as selenium, arsenic, sulfur and molybdenum, though this aspect appears to have received little attention in the literature, iodine usually being determined separately from other trace elements. The flexibility of this sample preparation technique is illustrated in the present study by the successful determination of molybdenum, an essential nutrient required for the function of molybdoenzymes, such as milk xanthine oxidase which catalyses the oxidation of xanthine to uric acid [16].

For iodine determination alone, an alternative approach is to deliberately convert iodine in the sample to elemental iodine vapour for analysis, and total iodine has been determined in milk by vapour generation ICP-optical emission spectrometry [17], though an alkaline digestion was still required to destroy the organic matrix prior to generating the iodine vapour. Iodine has been determined directly in milk powder by electrothermal vaporization-ICP, but again interference from the organic matrix was a problem, necessitating the use of pre-reduced Pd as a chemical modifier and internal standard [18].

The work reported here describes the preparation of milk samples for the determination of iodine and molybdenum by ICP-MS using sample pre-concentration and hexapole collision-reaction cell technology. The first aim was to develop a straightforward digestion method to break down the organic matrix of the milk, without loss of analyte, yielding a clear solution suitable for continuous nebulisation and analysis by ICP-MS. Once this was achieved, attention turned to pre-concentration of the digest before introduction to the ICP-MS to improve detection limits. To determine [129]I, the use of oxygen in the hexapole collision-reaction cell of the instrument removes [129]Xe[+] ions by a rapid charge-transfer mechanism (Eq. (2)) [19], thus preventing them interfering with [129]I determination.

$$Xe^+ + O_2 \rightarrow Xe + O_2{}^+$$
$$\Delta H = -0.06\,eV; k = 1.10 \times 10^{-10}\,cm^3\,s^{-1} \qquad (2)$$
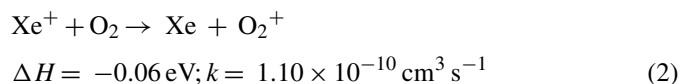
It has been reported that [129]Xe[+] reacts 10^4 times faster with O$_2$ than [129]I[+] does [20] and thus use of oxygen can selectively remove [129]Xe[+]. This may also be of importance in facilitating the use of low level [129]I spikes for isotope dilution determination of [127]I [21].

2. Experimental

2.1. Instrumentation

A VG PQ ExCell with Collision Cell Technology (CCT) (Thermo Elemental, Winsford, Cheshire, UK), was employed for ICP-MS analysis. The instrument, located in a general-purpose laboratory without air filtration or conditioning equipment, was used with a polyamide or glass nebuliser, a silica impact bead spray chamber, cooled to 5 °C by a Peltier cooler, and standard silica torch. Standard nickel sample and skimmer cones were used.

The ion optics were tuned to optimise the sensitivity of the signal at m/z 115 for a $1\,\mu g\,l^{-1}$ indium solution, which was typically 60,000–120,000 counts s[-1] in standard (non-CCT) mode. The relative standard deviation of $1\,\mu g\,l^{-1}$ [115]In signals was less than 1.5% and the oxide levels were monitored to ensure the [140]Ce^{+}/[140]Ce[16]O[+] ratio did not exceed 0.02. Typical operational conditions for the ICP-MS are given in Table 1.

Sb ($200\,ng\,g^{-1}$) was used as the internal standard and dilute tetramethylammonium hydroxide (TMAH, 0.5% in water) was

Table 1
Typical operating parameters for the VG PQ ExCell

RF power (W)	1350
Gases (l min^{-1})	
Plasma	12.60
Auxiliary	0.80
Nebuliser	1.03
Lenses	Tuned for optimum (In) signal
Hexapole pole bias (V)	−1.96
L3 (V)	−119.4
Focus (V)	+20.9
Deflector lens (V)	−35.8
Quadrupole pole bias (V)	+1 or −10[a]
Torch position	Tuned for optimum (In) signal
Acquisition parameters	
No of scans	100
Channels per mass	1
Dwell time (ms)	10
No of replicates	5
Scanning mode	Peak jump
m/z measured	92, 95, 96, 97, 98, 121, 123, 124, 127, 128, 129, 130, 131, 132
Delay time (s)	90
Wash time (s)	90

[a] Denotes quadrupole bias when collision cell mode enabled.

used as the wash solution, with a 4 min washout time between samples (extended from the normal 90 s to prevent carryover of iodine).

For removal of ^{129}Xe, helium and oxygen were introduced into the collision cell while aspirating a 5 ng g^{-1} iodide solution. With the He flow rate set to 1 ml min^{-1}, the O$_2$ flow was varied to maximise the 127/129 signal ratio whilst retaining sufficient sensitivity for iodine determination. Similarly pole bias settings of both the hexapole and quadrupole analyzer were adjusted to produce a high 127/129 ratio. Optimal conditions established this way were O$_2$ flow 0.6 ml min^{-1} with a hexapole bias of -2 V and quadrupole bias of -10 V. The slight negative bias on the hexapole is expected because the charge transfer reaction of Xe with O$_2$ is slightly endothermic ($+0.06$ eV) and is therefore favoured by more energetic ions [22].

Unicam 8700 series and Shimadzu UV-1601PC UV-Visible spectrophotometers were employed to monitor the presence of I$_2$, I$^-$ and I$_3^-$ in oxidation experiments.

A 757 VA Computrace (Metrohm, Herisau, Switzerland) was used for the electrochemical oxidation of potassium iodide in 0.1 M KCl using a platinum electrode with a potential sweep of -1.2 to 1.2 V.

2.2. Materials and reagents

Certified reference materials (CRMs) produced by the National Institute of Standards and Technology (Dried Whole Milk, NIST 8435) and the European Community Bureau of Reference (Dried Skimmed Milk, BCR 063R) were purchased from LGC, Teddington. A further sample of the NIST 8435 reference material was obtained from the Central Science Laboratory (CSL), York. Several liquid and dried milk samples were obtained from local Tesco and Safeway stores.

Two dried milk samples were supplied by British Nuclear Fuels Ltd. (BNFL): a sample of unknown ^{129}I content but believed to be below 0.01 ng g^{-1} in the liquid milk, and a further sample which had been spiked with 1 µg l^{-1} of ^{129}I, then freeze-dried to give a ^{129}I concentration of 8 ng g^{-1}.

Reagents for the digestion of the milk powder samples were purchased as follows: tetramethylammonium hydroxide (TMAH) from Apollo (Stockport, UK); hydrogen peroxide (20 vol) and Triton-X from Romil Pure Chemistry Ltd. (Cambridge, UK). Further treatment of the digests utilised Oxone® (potassium hydrogen peroxymonosulfate sulfate) and methyl-iso-butylketone, both from Aldrich Chemicals (Gillingham, Dorset, UK); methanol, ammonium thiosulfate, sodium chloride, potassium iodide and nitric acid (trace analysis grade) from Fisher Scientific (Loughborough, UK); and toluene and from Lancaster (Morecambe, Lancs, UK).

OnGuard-H^{TM} ion exchange cartridges (Dionex, Camberley, UK) were used for iodine pre-concentration, along with palladium nitrate (Avocado, Heysham, UK) and calcium standard solution (1000 µg ml^{-1}) (Fisher Scientific, Loughborough, UK). All solutions were made up using deionised water (18.2 MΩ) (Elga Maxima, Prima Systems, UK).

The ICP-MS instrument was set up using a multi-element tune solution supplied by SPEX Chemicals (Metuchen, NJ,

USA). Calibration standards were freshly prepared from purchased 1000 µg ml^{-1} standard solutions: iodide from SPEX Certiprep (Metuchen, NJ, USA), and molybdenum and antimony (internal standard) from Fisher Scientific (Loughborough, UK).

2.3. Digestion procedure

Five hundred milligram dried milk (or 3 g liquid milk) was weighed into a centrifuge tube. To the dried sample, 3 ml water was added and mixed well by shaking. Four millilitre each of tetramethylammonium hydroxide (TMAH, 25%), Triton X-100 (surfactant, 5% w/v) and H$_2$O$_2$ (20 vol) were then added. The tube was placed in a water bath at 70 °C for 2 h, agitating on a vortex mixer every 10–15 min. Following this, the digest was made up to 20 ml with water, including the addition of 1 ml of 400 µg l^{-1} Sb solution as internal standard, shaking to mix. The tube was placed in a centrifuge and spun at ∼5000 rpm for 5 min. This procedure was found to give a clear, stable solution that could be nebulised continuously and stored for several days in a refrigerator without degradation. Procedural blanks were prepared alongside each batch of samples.

2.4. Calibration procedure

Calibration standards were made up in the ranges 1–100 µg l^{-1} of iodide, and 1–20 µg l^{-1} of molybdenum, each standard solution containing the same concentrations of TMAH, Triton X-100 and Sb as the digests. A calibration curve of ^{127}I/^{121}Sb signal ratio versus iodine concentration was then used for quantification of ^{127}I in the digests. Molybdenum was quantified in the digests via calibration curves of ^{98}Mo/^{121}Sb (standard mode) or ^{128}MoO$_2$/^{121}Sb (collision-reaction cell mode) versus molybdenum concentration.

2.5. Pre-concentration procedures

2.5.1. Using oxidation/solvent extraction

The milk powder was digested as above, but excluding the addition of internal standard. The digest (20 ml) was then taken down to pH 2 via drop-wise addition of conc. HNO$_3$. Oxone® (0.2 g) and toluene (5 ml) were added simultaneously as soon as pH 2 was reached, and the vessel stirred using a vortex mixer for around 5 min. The mixture was spun on a centrifuge for a further 3 min to separate the layers; the organic layer was collected and the aqueous layer discarded.

Aqueous ammonium thiosulfate, 0.1 M (2 ml) was added to the organic layer and the mixture stirred on a vortex mixer for 5 min. Finally, the mixture was spun on a centrifuge (∼5000 rpm) and the aqueous layer removed for analysis.

In establishing the above procedure, the effect of using Oxone® as an oxidising agent for iodide was studied. UV–vis spectra of solutions of potassium iodide (0.3 mM), acidified to pH 2 with sulfuric acid, were recorded at measured time intervals after addition of Oxone® (40 µl of 1% or 2% solution), to monitor the presence of iodine species via the characteristic

Table 2
Determination of ^{127}I in milk powder samples

Reference material	Found value[a] ($\mu g\,g^{-1}$)	Certified value ($\mu g\,g^{-1}$)
BCR063R ($n=6$)	0.75 ± 0.12	0.81 ± 0.05
NIST8435 ($n=4$)	2.64 ± 0.40	2.3 ± 0.4

[a] Found values are expressed as mean $\pm 3\times$ standard deviation.

absorbance wavelengths of I_2 (460 nm), I_3^- (290 and 350 nm) and I^- (226 nm).

2.5.2. Using a cation-exchange column

An OnGuard-H^{TM} cartridge was loaded with Pd^{2+} by passing palladium nitrate solution (100 $\mu g\,ml^{-1}$, 8 ml) through the cartridge. Following this, 13 ml of an aqueous solution containing 500 $\mu g\,l^{-1}$ iodide and 50 $\mu g\,ml^{-1}$ Ca^{2+} was passed thorough the cartridge. The percentage of applied palladium and iodide retained on the cartridge was monitored by ICP-MS determination of these elements in the eluent. The cartridge was washed with methanol, before applying a solution of ammonium thiosulfate (0.01 M, 0.5 ml) to the cartridge to elute the iodide (as palladium iodide). This procedure was tried using the milk digest solution in place of the aqueous iodide/calcium solution.

3. Results and discussion

3.1. Determination of ^{127}I in milk powder

The basic digestion procedure, using TMAH, Triton-X and hydrogen peroxide as described above, was found to successfully digest the milk samples with the quantification of ^{127}I in the CRMs being in close agreement with certified values, as shown in Table 2. The limit of detection was blank-limited at about 0.1 $\mu g\,g^{-1}$ in the milk powder.

This sample preparation procedure could have wider application, including the determination of metals in oxy-anions (e.g. Cr(VI), As, Se, Mo), and other trace metals by addition of EDTA to maintain them in solution at the alkaline pH used [23]. Molybdenum was quantified in the milk digests, as described in the next section, but other elements were not determined in this work.

3.2. Removal of Xe^+ interference

In order to measure ^{129}I by ICP-MS it was necessary to remove Xe^+ interference and this was successfully carried out for aqueous samples, where the background m/z 129 signal was effectively eliminated with He (1.0 ml min^{-1}) and O_2 (0.6 ml min^{-1}) in the collision/reaction cell, due to the charge transfer reaction noted previously (Eq. (2)).

The milk digests, however, produced a sizeable signal at m/z 129. This was not due to residual Xe^+ (as the signal for ^{131}Xe was virtually zero), but was found to be due to the almost quantitative conversion of Mo^+ to MoO_2^+ in milk powder digests with O_2 in the cell. This was confirmed by running a standard (20 $\mu g\,l^{-1}$) Mo solution in standard and CCT modes. Standard mode signals for Mo isotopes at m/z 92, 94, 95, 96, 97, 98 and 100 disappeared in CCT mode to be replaced by signals (in the same isotopic proportions) at m/z 124, 126, 127, 128, 129, 130 and 132, as shown in Fig. 1.

This formation of MoO_2^+ is consistent with the findings of Koyanagi et al. [24] who showed that Mo^+ ions produced in an ICP source and thermalised by collision with Ar or He atoms react with O_2 at room temperature in a two stage reaction:

$$Mo^+ + O_2 \rightarrow MO^+ + O$$

$$MoO^+ + O_2 \rightarrow MoO_2^+ + O$$
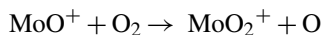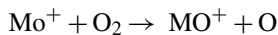
The signal at m/z 128 was used to quantify Mo in the two milk CRMs, the unspiked BNFL sample and a Safeways dried milk sample (selected at random), and the results compared with values obtained by measuring ^{98}Mo (and ^{97}Mo) in the same digests in standard (non-CCT) mode. In all cases ^{121}Sb was used as the internal standard for the determinations. The results are summarized in Table 3 and it can be seen that there is good agreement between the Mo values recorded in the two instrumental modes and also that the results for the CRMs are in acceptable agree-
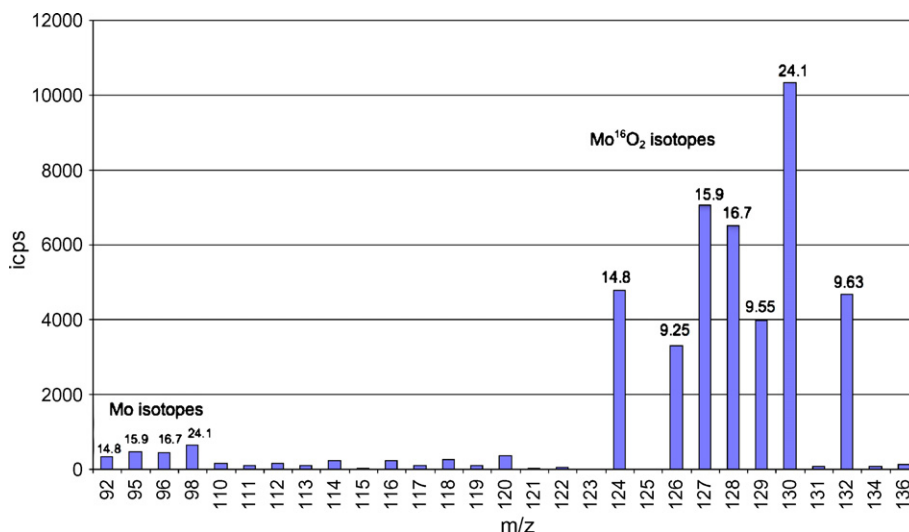

Fig. 1. 20 $\mu g\,l^{-1}$ Mo standard in water: ICP-MS with CCT using He + O_2 optimised for Xe removal; labels are natural abundances of Mo isotopes.

Table 3
Determination of molybdenum in milk powder samples in standard and CCT modes

Sample	Mo content ($\mu g\, g^{-1}$) from ^{98}Mo/^{121}Sb (standard mode)[a]	Mo content ($\mu g\, g^{-1}$) from ^{128}MoO$_2$/^{121}Sb (CCT mode)[a]	Certified (c) values ($\mu g\, g^{-1}$)
BCR063R	0.23 ± 0.03	0.23 ± 0.08	n/a
NIST8435	0.22 ± 0.04	0.24 ± 0.03	0.29 ± 0.13 (c)
BNFL (unspiked)	0.40 ± 0.10	0.37 ± 0.11	n/a
Safeways dried milk	0.31 ± 0.13	0.27 ± 0.16	n/a

[a] Experimental values are expressed as mean ± 3× standard deviation of results from three separate digests of each sample. Quantitation using ^{97}Mo/^{121}Sb gave the same results as ^{98}Mo/^{121}Sb.

ment with the certified value for NIST8435. The detection limit for Mo was 0.01 $\mu g\, g^{-1}$ in the milk powder in both standard and CCT modes.

As can be seen from Table 3, Mo concentrations in the milk samples were all similar and in the range 0.2–0.4 $\mu g\, l^{-1}$ (5–10 $\mu g\, l^{-1}$ in the digest solution). This is not high enough to cause noticeable interference with the measurement of ^{127}I in milk, though may be significant (5–10% increase in m/z 127 signal) for iodine levels less than 1 mg kg^{-1} in milk powder. However, interference on ^{129}I at low levels would clearly be severe, as can be seen in Table 4 which shows typical signal levels obtained for standards and digest solutions, with and without the use of gas in the collision cell.

Attempts were made to adjust conditions in the cell to try to remove as much Xe as possible whilst minimising production of MoO$_2^+$ and maintaining a strong iodine signal at m/z 127. A mixed standard solution containing 10 $\mu g\, l^{-1}$ molybdenum and 20 $\mu g\, l^{-1}$ iodine was investigated using CCT, varying gas and pole bias conditions. Xe$^+$ was tracked by monitoring the signal at m/z 131 and the 126/97 signal ratio monitored conversion of Mo$^+$ to MoO$_2^+$. Very little improvement was found by varying the pole bias conditions using He and O$_2$ gases, and the use of He + H$_2$ over a wide range of flow rates in the cell failed to provide any effective reduction in Xe interference (in contrast to results reported by Becker [25]), as the 127/131 signal ratio remained the same as with no gas in the cell. It was concluded that separation and pre-concentration of iodine in the digests would be needed to determine low levels (<0.01 ng g^{-1}) of ^{129}I.

3.3. Pre-concentration of iodine by trapping on a column

Initial attempts were made to concentrate and separate the iodide by addition of silver nitrate to precipitate silver halides, followed by filtration, dissolution of silver chloride with ammonium hydroxide and extraction of iodide from the filter with ammonium thiosulfate, but this approach met with little success. It was felt a column technique would be preferable, whereby sil-

ver ions on a cation exchange column (OnGuard-H^{TM}) could be used to retain the halides. However, the large excess of chloride in the digests made this problematical due to column overload. It was clear that a column method was needed that would trap iodide but not chloride.

To this end, the use of a Pd^{2+}-loaded column was investigated, to make use of the insolubility of PdI$_2$ compared to the solubility of PdCl$_2$. Passing Pd(NO$_3$)$_2$ solution (100 $\mu g\, ml^{-1}$, 8 ml) through an OnGuard-H^{TM} cartridge resulted in effective saturation of available sites with Pd^{2+}. However, on passing through aqueous solutions of potassium iodide, it was found that iodide was poorly retained on the cartridge, indicating that little PdI$_2$ was being formed. This problem was alleviated by the addition of Ca^{2+} which by competing for binding sites appeared to mobilise the Pd^{2+} making it available for PdI$_2$ formation. On passing 13 ml of an aqueous solution of 500 $\mu g\, l^{-1}$ I$^-$ plus 50 $\mu g\, ml^{-1}$ Ca^{2+} through the Pd^{2+}-loaded cartridge it was found that >97% of the iodide was retained on the cartridge; for lower levels of iodide (100 $\mu g\, l^{-1}$ I$^-$) the retention was a little less efficient, but still >80%.

It was found that a 0.01 M solution of ammonium thiosulfate was very efficient at eluting the PdI$_2$ from the cartridge in a small volume (the characteristic brown colour was seen within the first 0.5 ml of eluent, whereafter the eluent ran clear) whilst avoiding the column degradation observed with higher thiosulfate concentrations. Thus a high pre-concentration factor could be achieved. It was further found that methanol did not elute any of the iodide; thus methanol could be used as a wash step between loading and eluting the column, to remove any unwanted organic matter.

It was hoped that this success at pre-concentrating iodine (as iodide) in aqueous samples using a Pd^{2+}-loaded cartridge could be translated to the milk digest samples. This optimism was fuelled by the fact that the milk samples already contained sufficient calcium to facilitate retention on the cartridge, and the cartridges have a quoted pH working range of 0–14 and hence would not be adversely affected by the strongly alkaline digests.

Table 4
Typical signals (counts per second) for standards and digest solutions. Standard conditions employed no gas in cell; CCT used He + O$_2$ at 1.0 + 0.6 ml min^{-1}

	m/z 127		m/z 129		m/z 131	
	Standard	CCT	Standard	CCT	Standard	CCT
1 $\mu g\, l^{-1}$ Iodine solution	12,000	3000	3000	50	2800	10
Milk powder digest solution	12,000 per $\mu g\, l^{-1}$ iodine	3000 per $\mu g\, l^{-1}$ iodine	2000	1600	1700	20
10 $\mu g\, l^{-1}$ Mo solution	Blank level	3000	2400	2400	1900	30

However, the method did not work with the milk digests. The palladium was stripped from the cartridge on application of the digest solution and consequently iodide was not retained; it is likely that the Pd^{2+} was displaced by the tetramethylammonium ion present in large excess from the digestion reagent.

It was thought that it might be possible to form PdI_2 within the digest solution simply on addition of a large molar excess of $Pd(NO_3)_2$. However, experiments such as a Bjerrom plot and speciation simulations using CHESS (Chemical Equilibrium of Species and Surface environmental speciation modelling software, ARMINES, Fontainebleu, France) showed that, at the strongly alkaline pH of the digest solution, Pd^{2+} does not exist and that the dominant species will in fact be PdO (aq) and $Pd(OH)_2$. The Pd^{2+} ion will only exist in the solution if the pH < 2. This is important since it would suggest that the formation of PdI_2 would not be ionic and would not occur rapidly; instead the reaction would have to proceed by a ligand substitution reaction and could potentially be very slow.

3.4. Pre-concentration of iodine by oxidation/solvent extraction

As an alternative to a column separation, solvent extraction was tried, extracting the analyte as molecular iodine from an acidified digest (HNO_3 added to pH 2), using toluene as the solvent. The non-polar, but highly polarisable, molecular iodine should be extracted into the toluene layer. Ammonium thiosulfate or TMAH could then be used to back-extract the iodine as iodide into a small volume of aqueous solution. However, very low and variable amounts of iodine were extracted from digests (as measured by ICP-MS), despite various modifications to the conditions (e.g. pH adjustments, omission of Triton-X, addition of NaCl) to try to improve the separation and extraction process.

The I_2 may well have been lost through one or more of a variety of other reactions which may have been favoured under the conditions used, such as:

- Formation of I_2–Cl^- (due to high Cl^- in digests)
- Interaction of I_2 with H_2O, e.g.

$$I_2 + H_2O \rightleftharpoons HOI + I^- + H^+ \qquad (3)$$
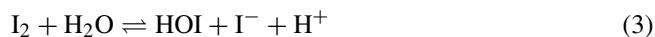
- Loss of I_2 via disproportionation to I^- and IO_3^-
- Formation of I_3^-:

$$I_2 + I^- \rightleftharpoons I_3^- \qquad (4)$$
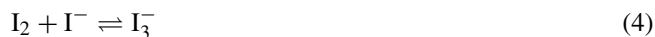
Spiking the digests with potassium iodide (ca. 0.1 mM or $20\,\mu g\,ml^{-1}$) appeared to enable the formation of molecular iodine and its subsequent reduction to iodide to be visibly tracked although later studies showed that the visible species was almost certainly I_3^-. In addition, the H_2O_2/HNO_3 in the digest may have provided insufficient oxidation potential to form I_2 reliably.

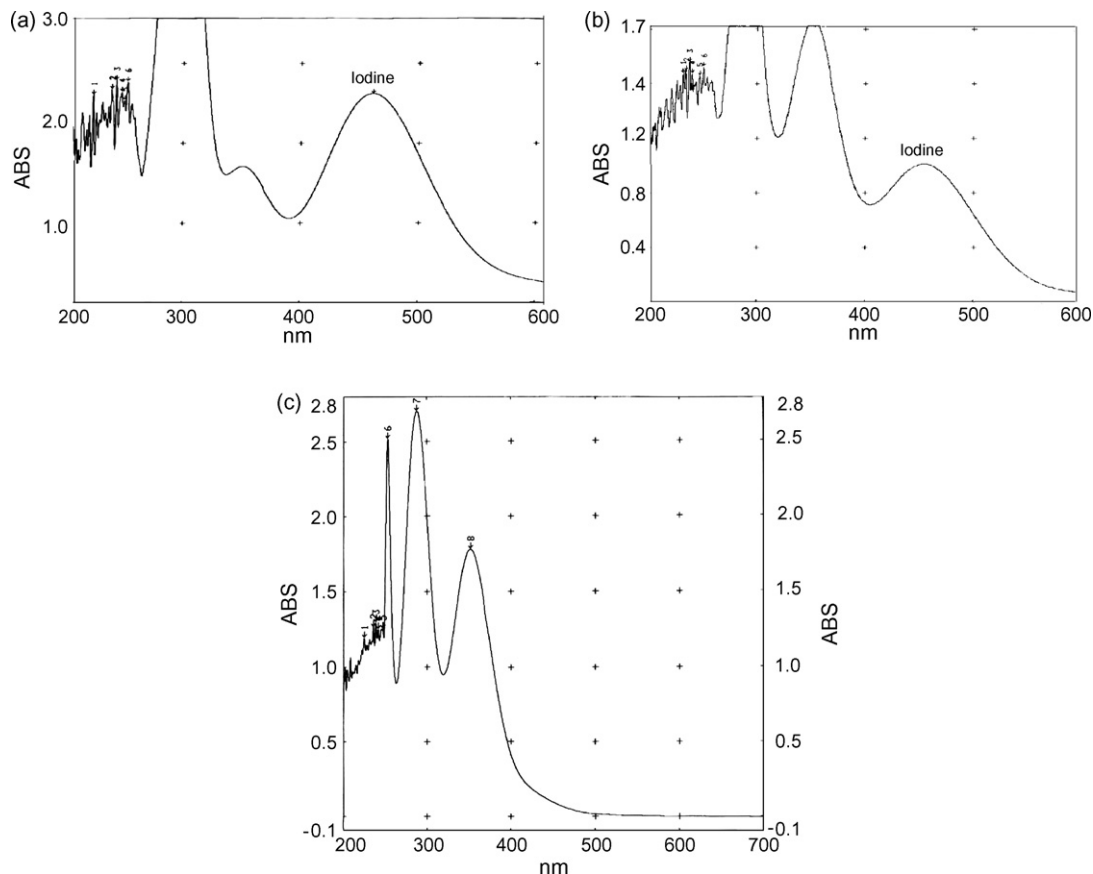Fig. 2. UV–vis absorbance spectra of potassium iodide solution after oxidation (a) with H_2O_2 at pH 1, (b) with H_2O_2 at pH 2.2 and (c) electrochemically in water + 0.1 M KCl. Peaks indicate the presence of I_3^- (290 and 350 nm) in (a–c) and I_2 (460 nm) in (a and b).

The formation of I_3^- (Eq. (4)) was clearly shown by measuring UV–vis spectra of acidified solutions (pH 1–2) containing potassium iodide (2–10 mM) and hydrogen peroxide (20 vol, 4 ml) in 20 ml water, which showed sizeable peaks at 350 nm and 460 nm (Fig. 2(a) and (b)) indicating the presence of I_3^- and I_2, thus showing oxidation of the iodide to iodine, with significant I_3^- also produced.

The size of the I_2 peak (460 nm) decreased at pH > 1 and at pH 3 and higher the I_2 peak disappeared, though the I_3^- peak could be seen up to pH 6, indicating that any I_2 produced under these less acidic conditions appeared to be complexed with the large excess of I^-. (Note that the large peak at ca. 300 nm is due to the nitrate ion of the nitric acid used to acidify the solution). Further evidence for the formation of I_3^- in oxidised iodide solutions was found during studies into a possible method for removing trace iodine contamination from the TMAH reagent by a polarographic method. Electrochemical oxidation of potassium iodide (in deionised water with 0.1 M KCl electrolyte) produced a straw-coloured liquid with a UV–vis spectrum having characteristic I_3^- peaks (290 nm and 350 nm) but no I_2 peak at 460 nm (Fig. 2(c)).

3.5. Use of Oxone® as oxidising agent

As oxidation to I_2 may not have been taking place reliably in the acidified digest, it was felt that a more powerful oxidising agent than $H_2O_2 + HNO_3$ in the digest was required. Oxone® (Dupont Chemicals) has as its active ingredient potassium monopersulfate ($KHSO_5$) which is present in the triple salt potassium hydrogen peroxymonosulfate sulfate ($2KHSO_5 \cdot KHSO_4 \cdot K_2SO_4$, molecular weight 614.7) [26]. Oxone® dissolved in water is naturally acidic (pH 2.3 for 1% solution, pH 2.0 for 3% solution), and undergoes reduction as shown in the following half reaction:

$$HSO_5^- + 2H^+ + 2e^- \rightarrow HSO_4^- + H_2O \qquad E^0 = +1.44\,V$$

and thus the reduction potential is sufficiently positive to enable Oxone® to reliably and completely oxidise I^- to I_2 at room temperature in acid solution, via the reaction:

$$HSO_5^- + 2H^+ + 2I^- \rightarrow HSO_4^- + I_2 + H_2O \qquad (5)$$
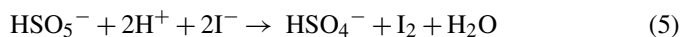
By monitoring the characteristic UV–vis absorbance wavelengths of I_2 (460 nm), I_3^- (290 and 350 nm) and I^- (226 nm) in test solutions, Gazda et al. [27] showed that Oxone® treatment was capable of converting not only I^- but also I_3^- to I_2, probably as a result of oxidation of all available I^- causing a shift in the equilibrium of Eq. (4).

To investigate the effect of using Oxone® instead of H_2O_2 as an oxidising agent for iodide, Oxone® (1.25 mM) was added to 20 ml of potassium iodide solution (5 mM). The UV–vis spectrum of the solution was measured at 10 min intervals. The spectra were very different from those observed using H_2O_2 at the same pH (pH 2). Only the I_2 peak (460 nm) was evident; the I_3^- peaks were entirely absent, and the I_2 peak gradually decreased over time, disappearing completely an hour after the Oxone® was first added (Fig. 3).
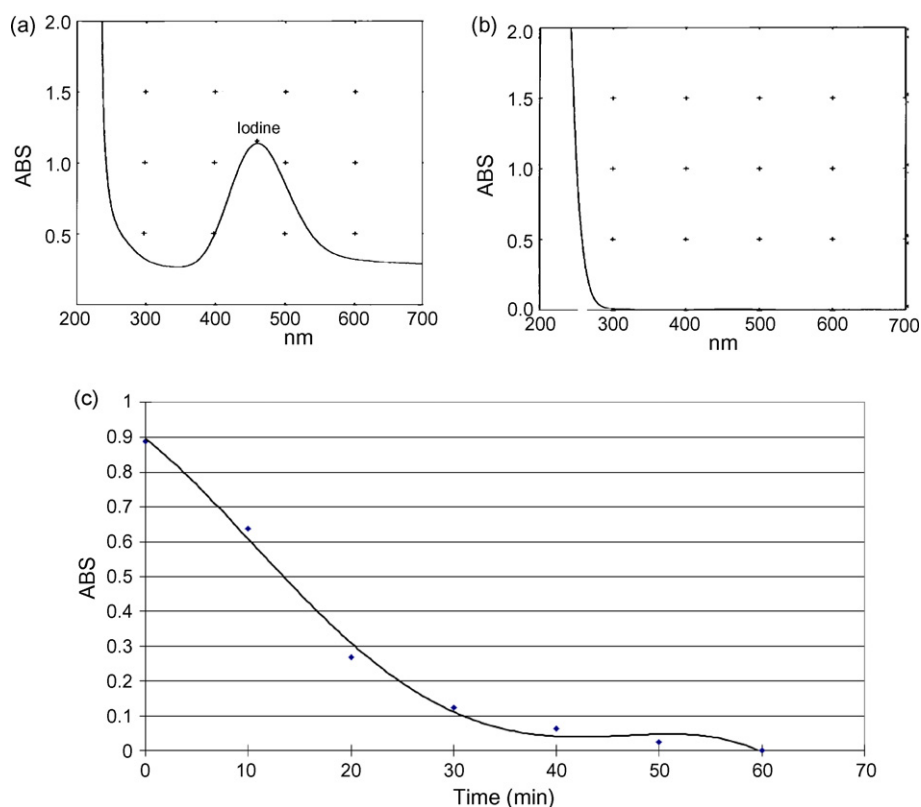

Fig. 3. UV–vis spectra showing the gradual disappearance of I_2 produced in acidified potassium iodide solution (a) immediately after adding Oxone® and (b) 1 h later; (c) shows the decline in absorbance at 460 nm (I_2 peak) over the 1-h period.

A possible reason for this decline in I_2 could be due to the formation of volatile HI in acidic solution, or reaction with water to produce HOI and I^- (Eq. (3)). Although Oxone® has sufficient oxidation potential in principle to convert I_2 to IO_3^- ($E^0 = +1.21$ V), in practice this reaction is not favoured at low pH.

Acidic conditions are necessary for the Oxone® to work (Eq. (5)) and this was confirmed in practice. A 1% aqueous solution of Oxone® had a natural pH of 2 and adjusting to alkaline pH meant that the iodide was not oxidised.

Subsequent experiments with varying concentrations of potassium iodide showed that a concentration of 50 µg ml^{-1} (0.3 mM), acidified to pH 2 with sulfuric acid (to avoid interfering nitrate peaks) produced a very large but on-scale iodide peak and such a solution was used to follow the oxidation process, by adding Oxone® directly into the quartz cuvette and observing the change in the spectrum over time. The UV–vis spectrum of Oxone® solution alone showed only one peak at 202 nm; thus any un-reacted Oxone® would not mask the peaks due to iodine species.

After measuring the spectrum of the 50 µg ml^{-1} acidified potassium iodide solution, 40 µl of Oxone® solution (1%) was added and the spectrum recorded immediately, then again after 5 min and 10 min. On addition of Oxone®, the iodide peak (226 nm) reduced in size and small peaks at 290 nm, 350 nm and 460 nm appeared. However, after 5 min, the peaks at 290 and 350 nm (I_3^-) had more than doubled in size, whilst that at 460 nm (I_2) remained very small. The spectrum after 10 min remained virtually the same with a very slight further reduction in the iodide peak at 226 nm (see Fig. 4a).

The above experiment was repeated, but this time doubling the amount of Oxone® added. This time the iodide peak essentially disappeared on addition of Oxone®, and three small peaks at 290, 350 and 460 nm appeared, but after 5 min the first two of these had gone, leaving a single peak at 460 nm, which almost

doubled in size from 0 to 5 min before gradually decreasing but remaining at about two-thirds of its maximum height after an hour (see Fig. 4b). This indicated that the higher level of Oxone® had successfully oxidised the I^- to I_2, and the I_3^- formed (according to Eq. (4)) had also been quantitatively converted to I_2, as previously reported [27].

The above experiments showed that if insufficient Oxone® were added, such that un-oxidised iodide remained, any I_2 formed would complex with the remaining I^- to leave I_3^- as the dominant oxidised species. Therefore Oxone® should be added in excess to a solution at pH 2 to ensure quantitative conversion to I_2.

Whilst the iodine species formed in aqueous iodide solutions treated with Oxone® could usefully be monitored via their UV–vis absorbance profiles, it was not possible to monitor the iodine species in the digest solutions directly by UV–vis spectroscopy, due to large absorbances of other components in the digest matrix masking the iodine peaks.

3.6. Solvent extraction following Oxone® oxidation

Digests of the milk sample spiked with ^{129}I were prepared for analysis using the Oxone oxidation/extraction scheme as detailed in Section 2. These, along with procedural blanks and un-extracted digests for comparison, were introduced to the ICP-MS, with the collision cell employed as described earlier. The signals at m/z 95, 97, 126, 127, 128, 129, 130 and 131 were measured. By monitoring m/z 131, it was seen that Xe$^+$ had been successfully removed. Monitoring m/z 126–130 showed clearly the characteristic pattern of MoO_2^+ for the un-extracted digest, except that the signal at m/z 129 was higher than would be expected from the Mo isotope ratios, indicating that ^{129}I was being detected, albeit largely masked by the MoO_2^+ signal. In principle, the pre-concentration procedure should remove the molybdenum and lead to a 10-fold increase
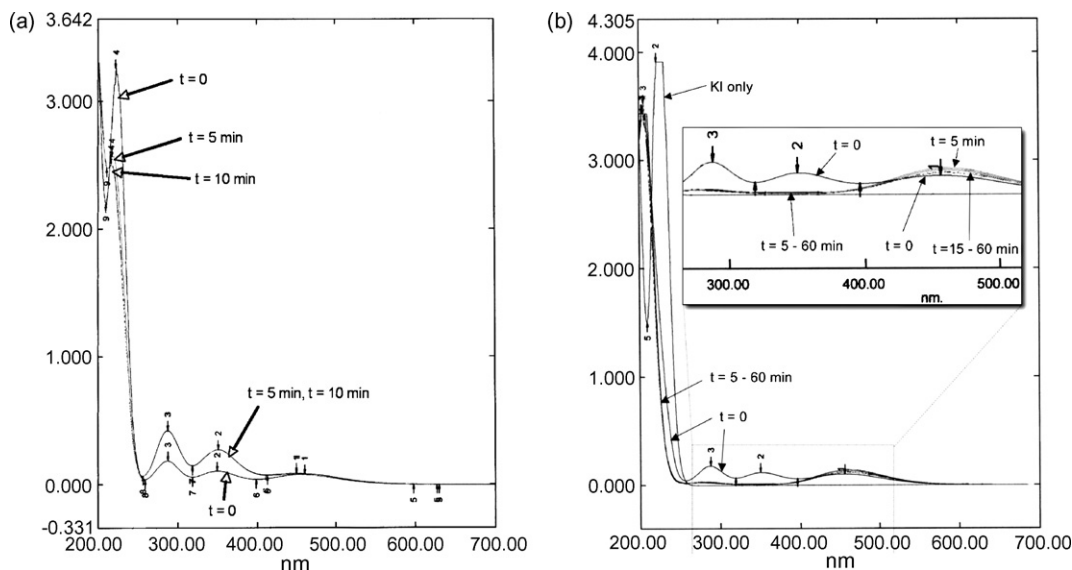

Fig. 4. UV-vis spectra showing the effect of treating a 50 µg ml^{-1} solution of acidified potassium iodide (pH 2) in a standard UV cuvette with (a) 40 µl of 1% Oxone® solution and (b) 40 µl of 2% Oxone® solution, where t is the time period between the addition of Oxone and recording the spectrum (the peak at ∼200 nm is probably due to residual Oxone®).

in iodine signals at m/z 127 and 129 (20 ml digest solution to 2 ml ammonium thiosulfate extract). Whilst analysis of the pre-concentrated digest showed that the MoO_2^+ interference had been essentially removed, the signal at m/z 129 was much lower than would be expected for the [129]I (assuming a concentration factor of 10). Moreover the [127]I signal had only increased by a factor of 3.

Possible reasons for the poor extraction efficiency can be suggested by considering the stages in the extraction and the possible iodine species formed. In the initial digest, it is assumed that the iodine is present mostly as free iodide [6] and some organic iodine which is released according to:

$$R\text{--}I + OH^- \rightleftharpoons R\text{--}OH + I^-$$
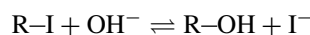
which is heavily biased towards the right hand side of the equilibrium when TMAH is present.

Once the iodide is oxidised to iodine on addition of Oxone® (Eq. (5)), there is the possibility that it may be complexed by residual organic matter in solution. The addition of a strong complexing agent with a high affinity for iodine might mitigate this effect and aid the extraction of iodine. Polyvinylpyrrolidone (PVP) should fulfil this function, and the yellow colour of the iodine–PVP complex (used as a colorimetric reagent for iodine determination [27]) could aid visual tracking of the extraction.

Alternatively, it has been shown that iodine readily complexes with iodide ions to form I_3^-. In the presence of a large excess of chloride ions in the digest (of the order of 250 μg ml^{-1}), I_2Cl^- may be formed, thus hampering extraction of I_2 into toluene. One solution to this would be to add silver nitrate after the I_2 has been formed, to precipitate out the chloride as AgCl and thus avoid the formation of I_2Cl^-.

Addition of either PVP or silver nitrate to the digests yielded no improvement in extraction efficiency, although the work was hampered by high blanks at m/z 127 and m/z 129 from the addition of the reagents, as seen in the procedural blanks.

4. Conclusion

The complex redox chemistry of iodine makes this a difficult element to extract from complex biological matrices and determine at low (sub μg l^{-1}) concentrations, as encountered when monitoring low levels of [129]I in milk. This work has yielded a reliable method for the determination of [127]I in milk samples (verified with certified reference materials), using alkaline digestion with TMAH and hydrogen peroxide, followed by quadrupole ICP-MS analysis. The digestion method has been successfully applied to the determination of molybdenum in milk and could also be used to prepare biological materials for determination of other anions, e.g. of Se and As and, with the addition of EDTA, trace metals analysis.

Investigation of pre-concentration/extraction techniques to remove the matrix interferences, as well as raising the [129]I concentration to measurable levels, has resulted in a new method for the separation and pre-concentration of iodide, using a Pd^{2+}-loaded cation-exchange column followed by elution with ammonium thiosulfate, which although unsuitable for the milk digests, is applicable to aqueous samples.

A new method for the pre-concentration of iodide and removal of interferences in the milk digest solutions, via oxidation with Oxone®, extraction into toluene and back-extraction into ammonium thiosulfate, has shown some promise, although the extraction efficiency was low. Further measures to control the iodine chemistry during the extraction would need to be developed before this can be considered a viable method for this application.

Acknowledgements

References

[1] R.G. Jensen (Ed.), Handbook of Milk Composition, Academic Press, USA, 1995.
[2] F.A.R. Martino, M.L.F. Sanchez, A.S. Medel, J. Anal. At. Spectrom. 15 (2000) 163.
[3] P. Bratter, I.N. Blasco, V.E.N. de Bratter, A. Raab, Analyst 123 (1998)821.
[4] P.A. Fecher, I. Goldmann, A. Nagengast, J. Anal. At. Spectrom. 13 (1998) 977.
[5] E.H. Larsen, P. Knuthsen, M. Hansen, J. Anal. At. Spectrom. 14 (1999) 41.
[6] L.F. Sanchez, J. Szpunar, J. Anal. At. Spectrom. 14 (1999) 1697.
[7] O.T. Farmer, C.J. Barinaga, D.W. Koppenaal, J. Radioanal. Nucl. Chem. 234 (1998) 153.
[8] B.G. Fritz, G.W. Patton, J. Environ. Radioact. 86 (2006) 64.
[9] K. Simpson, S.J. Parry, M.J. Fulker, J. Radioanal. Nucl. Chem. 249 (2001) 89.
[10] S.J. Parry, B.A. Bennett, R. Benzing, A.E. Lally, C.P. Birch, M.J. Fulker, Sci. Total Environ. 173 (1995) 351.
[11] H. Vanhoe, F.V. Allemeersch, J. Versiek, R. Dams, Analyst 118 (1993) 1015.
[12] A.V. Izmer, S.F. Bouliger, J.S. Becker, J. Anal. At. Spectrom. 18 (2003) 1339.
[13] P. Bienvenu, E. Brochard, E. Excoffier, M. Piccione, Can. J. Anal. Sci. Spect. 49 (2004) 423.
[14] H. Baumann, Fresenius' J. Anal. Chem. 338 (1990) 809.
[15] S. Sturup, A. Buchert, Fresenius' J. Anal. Chem. 354 (1996) 323.
[16] R. Hille, Arch. Biochem. Biophys. 433 (2005) 107.
[17] E. Niedobova, J. Machat, V. Otruba, V. Kanicky, J. Anal. At. Spectrom. 20 (2005) 945.
[18] M. Resano, E. Garcia-Ruiz, L. Moens, V. Vanhaecke, J. Anal. At. Spectrom. 20 (2005) 81.
[19] M.A. Dexter, Ph.D. thesis, Loughborough University, 2003.
[20] G.C. Eiden, C.J. Barinaga, D.W. Koppenaal, Rapid Commun. Mass Spectrom. 11 (1997) 37.
[21] R. Santamaria-Fernandez, P. Evans, C.S.J. Wolff-Briche, R. Hearn, J. Anal. At. Spectrom. 21 (2006) 413.
[22] M.A. Dexter, H.J. Reid, B.L. Sharp, J. Anal. At. Spectrom. 17 (2002) 676.
[23] A.A. Bashammakh, Ph.D. thesis, Loughborough University, 2003.
[24] G.K. Koyanagi, D. Caraiman, V. Blagojevic, D.K. Bohme, J. Phys. Chem. A 106 (2002) 4581.
[25] J.S. Becker, J. Anal. At. Spectrom. 17 (2002) 1172.
[26] DuPont Oxone® Monopersulfate Compound Technical Information, http://www.dupont.com/oxone/techinfo/index.html. (accessed 7 June 2007).
[27] D.B. Gazda, R.J. Lipert, J.S. Fritz, M.D. Porter, Anal. Chim. Acta 510 (2004) 241.

ELSEVIER

Talanta

Amperometric and voltammetric detection of hydrazine using glassy carbon electrodes modified with carbon nanotubes and catechol derivatives

Abdollah Salimi [a,b,*], Layla Miranzadeh [a], Rahman Hallaj [a]

[a] *Department of Chemistry, University of Kurdistan, P.O. Box 416, Sanandaj, Iran*
[b] *Research Center for Nanotechnology, University of Kurdistan, P.O. Box 416, Sanandaj, Iran*

Abstract

A simple procedure was developed to prepare a glassy carbon (GC) electrode modified with carbon nanotubes (CNTs) and catechol compounds. First, 25 μL of DMSO–CNTs solutions (0.4 mg/mL) was cast on the surface of GC electrode and dried in air to form a CNTs film. Then the GC/CNTs modified electrode immersed into a chlorogenic acid, catechine hydrate and caffeic acid solution (electroless deposition) for a short period of time (2–80 s). The cyclic voltammogram of the modified electrode in aqueous solution shows a pair of well-defined, stable and nearly reversible redox couple (quinone/hydroquinone) with surface confined characteristics. The combination of unique electronic and electrocatalytic properties of CNTs and catechol compounds results in a remarkable synergistic augmentation on the response. The electrochemical reversibility and stability of modified electrode prepared with incorporation of catechol compound into CNTs film was evaluated and compared with usual methods for attachment of catechols to electrode surfaces. The transfer coefficient (α), heterogeneous electron transfer rate constants (k_s) and surface concentrations (Γ) for GC/CNTs/catechol compound modified electrodes were calculated through the cyclic voltammetry technique. The modified electrodes showed excellent catalytic activity, fast response time and high sensitivity toward oxidation of hydrazine in phosphate buffer solutions at pH range 4–8. The modified electrode retains its initial response for at least 2 months if stored in dry ambient condition. The properties of modified electrodes as an amperometric sensor for micromolar or lower concentration detection of hydrazine have been characterized.
© 2007 Elsevier B.V. All rights reserved.

Keywords: SWCNTs; MWCNTs; Chlorogenic acid; Caffeic acid; Catechine hydrate; Glassy carbon; Modified electrode; Electrocatalysis; Hydrazine

1. Introduction

Catechol compounds including quinizarine, caffeic acid, chlorogenic acid, catechine hydrate, pyrocatechol, hematoxylin, rutin, coumestan, 3,4-dihydroxybenzaldehyde and other derivatives, have been used as electron transfer mediators in electrochemical processes due to their high electron transfer efficiency, excellent redox reversibility and low cost [1–10]. The catechol derivative mediators were immobilized on the electrodes surfaces by methods such as adsorption [10], mixing into carbon paste [1], direct electropolymerization [11] and sol–gel techniques [2]. Although different modified elec-

trodes have been prepared via several catechol derivatives, most of these electrodes present quasi-reversible electrochemical behavior and even ill defined cyclic voltammograms with large background currents. They also have some disadvantages, such as considerable leaching of electron transfer mediator, poor long term stability, complex preparation procedure and time consuming for fabrication as well as renewing. Therefore, the immobilization of different electron transfer reagents on the surface of various electrode materials is receiving increasing interest in the field of chemically modified electrodes, electrocatalysis and electroanalysis. For heterogeneous catalysis, different supporting carbon materials have been used to disperse and stabilize electron transfer mediators due to their low background currents, wide potential windows, chemical inertness and low cost [12].

Carbon nanotubes (CNTs) are new kinds of carbon nanostructure materials possessing properties such as high electrical

* Corresponding author at: Department of Chemistry, University of Kurdistan, P.O. Box 416, Sanandaj, Iran. Tel.: +98 871 6624001; fax: +98 871 6624008.
 E-mail addresses: absalimi@yahoo.com, absalimi@uok.ac.ir (A. Salimi).

conductivity, high surface area, chemical stability and significant mechanical strength [13]. They can be used to promote electron transfer reactions when applied as electrode materials in electrochemical devices [14]. The electronics properties of these nanomaterials have been exploited as a means to promote the electron transfer reaction for a wide range of molecules and biological species including: insulin [15], thiols [16], carbohydrates [17], hydrogen peroxide [18], trinitrotoluene [19], nucleic acids [20], dopamine, ascorbic and uric acids [21], norepinephrine [22], aminophenol [23], 6-mercuptopurine [24], nitric oxide [25], cytochrome *C* [26], myoglobine [27], thymine [28], morphine [29], metronidazole and ranitidine [30] epinephrine [31] and glucose [32].

Furthermore, CNTs are novel and interesting members of nanostructure materials that can be used as support for immobilization different electron transfer mediators onto electrode surfaces and making ideal miniaturized sensors. Recently covalent and non-covalent approaches have been used for fictionalizations of carbon nanotubes with various molecules and biomolecules [33–35]. Among these approaches, non-covalent method is an effective way to preserve the sp^2 structures of carbon nanotube. In addition, strong interaction of aromatic groups with π-staking of carbon nanotubes is a manner to achieve desired purpose similarly. Immobilization of molecules and biomolecules on CNTs has been pursued in the past and motivated by the prospects of using nanotubes as new types of sensors and biosensors. The compatibility and electrochemical applications of carbon nanotubes for immobilization a variety of species on the external and internal surfaces of MWCNTs have been reported [33–37].

We have recently used MWCNTs and SWCNTs modified electrodes for immobilization of different electron transfer mediators and their applications for sensor fabrication and analytical purposes [38–40]. In the current study a simple one-step procedure was used for modification of glassy carbon electrode with MWCNTs, SWCNTs and three catechol derivatives: catechine hydrate, chlorogenic acid and caffeic acid.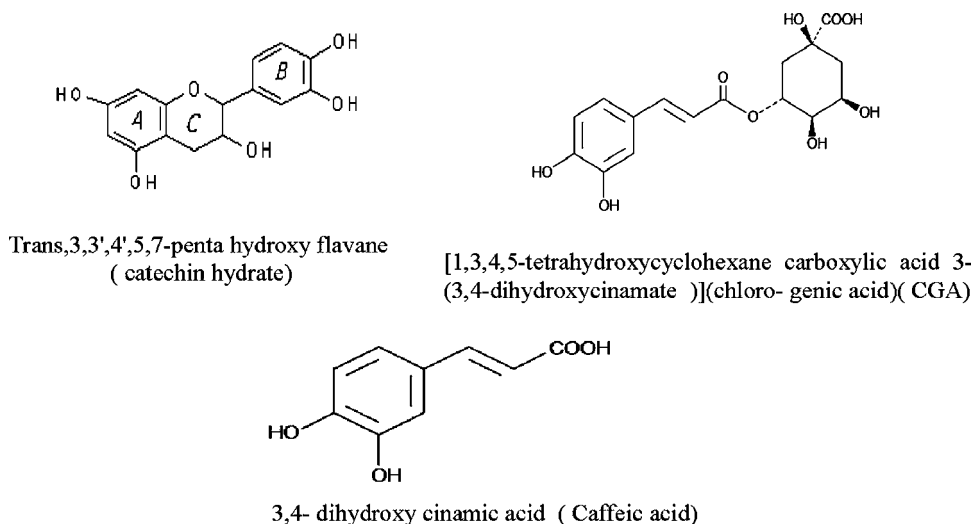 The modified electrode was used for electrocatalytic oxidation of hydrazine, an important compound used in rocket fuels, missile systems, and weapons of mass destruction, fuel cells and corrosive inhibitors [41] and DNA damage [42]. Stability, electrocatalytic activities and electroanalytical applications of modified electrodes toward electrooxidation and detection of hydrazine were evaluated by different electrochemical techniques [1–8,43,44]. Due to the excellent electrocatalytic ability of selected catechol used and the unique physicochemical properties of CNTs and especially the synergy of CNTs and catechol compounds, the sensor exhibits a remarkable and stable current response. Finally, the catechol base-CNTs modified glassy carbon electrodes have been used for amperometric detection of hydrazine in micromolar or lower concentration range at reduced over potential in wide pH range.

2. Experimentals

2.1. Chemicals and reagents

The catechine hydrate (*trans*,3,3′,4′,5,7-penta hydroxy flavane) (catechin hydrate), chlorogenic acid [1,3,4,5-tetrahydroxycyclohexane carboxylic acid 3-(3,4-dihydroxy-cinnamate)] (CGA) and 3,4-dihydroxy cinnamic acid (caffeic acid) (Scheme 1) were from Aldrich and used as received.

Multiwall carbon nanotubes with purity 95% (10–20 nm diameter) and 1 μm length were obtained from Nanolab (Brighton, MA). Single wall carbon nanotubes with purity 95% (2–5 nm diameters) and 1 μm length were manufactured by CNI (USA). Double distillate water was used to prepare all solutions and buffer solutions (0.1 mol L^{-1}) were prepared from sulfuric acid (H$_2$SO$_4$), phosphoric acid (H$_3$PO$_4$), sodium acetate (CH$_3$COONa) and di-sodium hydrogen phosphate (Na$_2$HPO$_4$). Hydrogen chloride (HCl) and sodium hydroxide (NaOH) were used for pH adjustment. Solutions were deaerated by bubbling high purity (99.99%) argon gas for 5 min through them prior to the experiments. All electrochemical experiments were carried out at room temperature 25 ± 0.1 °C.

Trans,3,3',4',5,7-penta hydroxy flavane
(catechin hydrate)

[1,3,4,5-tetrahydroxycyclohexane carboxylic acid 3-(3,4-dihydroxycinamate)](chloro- genic acid)(CGA)

3,4- dihydroxy cinamic acid (Caffeic acid)
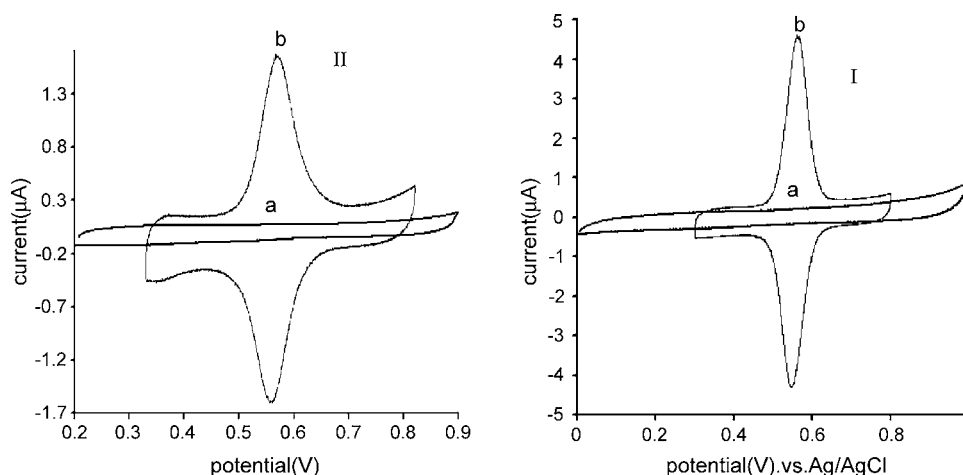
Scheme 1. The structure of used catechol derivatives.

Fig. 1. (I) Cyclic voltamograms of a MWCNTs/GC modified electrode (a) in buffer solution (pH 1), (b) as (a) for MWCNTs/CGA modified electrode, the immersing time for electrode modification is 60 s, scan rate 100 mV s^{-1}. (II) as (I) For SWCNTs modified electrodes, the immersing time for electrode modification is 20 s.

2.2. Instrumentation

Electrochemical experiments were performed with a computer controlled μ-Autolab modular electrochemical system (Eco Chemie Ultecht, The Netherlands) driven with GPES software (Eco Chemie). A conventional three-electrode cell was used with a Ag/AgCl/(sat KCl) as reference electrode, a Pt wire as counter electrode and a glassy carbon disk (modified and unmodified) as working electrode. Voltammetry on electrodes coated with catechol–CNTs was done in buffers containing no catechol. All electrodes were from Metrohm and data storage and processing were done by a personal computer.

2.3. Preparation of catechol–CNTs–GC modified electrodes

The glassy carbon electrode was first carefully polished with alumina on polishing cloth and the electrode was placed in ethanol and was subject to ultrasonic radiation to remove adsorbed particles. Then 25 μL of DMSO–CNTs solutions (0.4 mg/mL) was dropped on the surface of GC electrode and dried in air to form a CNTs film. By immersing the CNTs–GC electrode in 0.1 mmol L^{-1} aqueous solution of catechol derivative for 2–80 s, a stable film of catechol adsorbed on the surface of the electrodes. After rinsing of the modified electrodes with water they could be used for electrochemical experiments immediately. The effective areas of the electrodes modified with immobilization of MWCNTs and SWCNTs were determined as 0.12 and 0.15 cm^2 from cyclic voltammograms of 1 mmol L^{-1} K$_3$[Fe(CN)$_6$] in buffer solution (pH 7). For adsorption of catechol on the surface of reactivate GC electrode, the process was carried out in two steps. First, the glassy carbon electrode was held under a constant potential of 1.8 V for 20 min in 1 M sulfuric acid solution. Second, the preanodized GC electrode was immersed in 0.1 mmol L^{-1} catechol solution for 10 min.

3. Results and discussions

3.1. Electrochemical properties of catechol modified electrodes

Fig. 1 shows the cyclic voltammograms of MWCNTs, SWCNTs, MWCNT/chlorogenic acid and SWCNTs/chlorogenic acid modified GC electrodes at (pH 1) buffer solution. According to the cyclic voltammogram of CNTs/GC electrode in buffer solution, we found no redox peak between 0.0 and 1.0 V and the background current was low; thus, this CNTs electrode provided a broad potential window to investigate the voltammetric behavior of chlorogenic acid. By immersing the electrode for 2–80 s, a stable thin layer of chlorogenic acid adsorbed on the surface of carbon nanotube modified glassy carbon electrode. A pair of well-defined redox waves of chlorogenic acid (Fig. 1b) was observed at the CNTs film modified electrode with low peak potential separation (5 mV for MWCTs and 10 mV for SWCNTs), suggesting that the reversibility of chlorogenic acid was significantly improving.

The porous interfacial layer of the CNT-modified electrode with a high specific surface area increases the conductive area and chlorogenic acid can penetrate through the conductive porous channels onto the electrode more easily. Therefore, CNTs can be used as new material for immobilization and electron transfer reactions of chlorogenic acid. The ability of CNTs for immobilization catechol compounds was compared with reported method. For the GC electrode modified with immersing the preanodized GC electrode in 0.1 mmol L^{-1} chlorogenic acid solution for 10 min a cyclic voltammogram with low peak currents (0.6 μA) and high peak potential separation (50 mV) was observed (not shown). As a result, the preparation of the GC electrode modified with catechol derivatives involves two different steps (electroactivation and electrodeposition) taking at least 30 min, and they cannot be renewed after contamination in short periods of time (1 min). Fig. 2 shows cyclic voltammograms of modified GC electrode that prepared with immersing
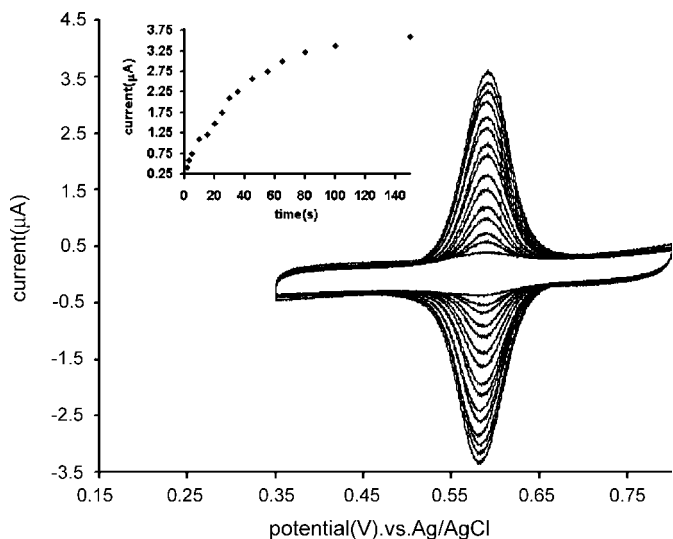
Fig. 2. Cyclic voltammetric responses of MWCNTs/CGA modified GC electrode in buffer solution (pH 1) at scan rate 50 mV s^{-1} modified with immersion in 0.1 mmol L^{-1} CGA for different time (from inner to outer) 2, 3, 5, 10, 15, 20, 30, 35, 45, 55, 65, 80, 100 and 150 s. Inset shows the variation of peak currents vs. immersing time.

of MWCNTs/GC electrode in chlorogenic acid solution for different times.

As shown in this figure, by immersing the electrode for 2 s a stable thin layer of CGA adsorbed at the electrode surface. By increasing the immersing time, the surface concentration of CGA is increased and starts to level off after 60 s. It was observed that by immersing the SWCNTs coated GC electrode for 5 s, a stable thin layer of CGA was adsorbed at the surface of electrode (not shown). In this case by increasing the time immersion, the surface concentration of CGA is increased, but in comparison to MWCNTs coated GC electrode peak cur-

rents start to level off after 80 s. This is due to the fact that the effective surface area of SWCNTs is higher, they are highly permeable porous films, electrolytes can penetrate through the film [45] and more catechol molecules are adsorbed. The same behavior was observed for catechine hydrate and caffeic acid immobilized onto GC electrodes modified with SWCNTs and MWCNTs.

Fig. 3 shows the cyclic voltammograms of the MWCNTs/GC electrode modified by immersing in 0.1 mM chlorogenic acid for 10 s at different scan rates in potential range 0.3–0.85 V in buffer solution (pH 1). As shown in inset of Fig. 3A, the peak currents increased linearly with increasing scan rate between 10 and 2000 mV s^{-1} as expected for a surface process. Moreover, the anodic peak currents were almost the same as the corresponding cathodic peak currents and the peak potential did not change by increasing the scan rate. The peak-to-peak potential separation is about 5 mV for sweep rates below 100 mV s^{-1}, suggesting facile charge transfer kinetics over this range of sweep rate. At higher sweep rates, the plot of peak currents vs. scan rate plot deviates from linearity and the peak current becomes proportional to the square root of the scan rate (Fig. 3B), indicating a diffusion controlled process, which is reflection of the relatively slow diffusion of counter ions (H^{+}) into the electrode surfaces.

At higher sweep rates ($v > 2000$ mV s^{-1}) peak separations begin to increase, indicating the limitation due to charge transfer kinetics. Based on Laviron theory [46], the electron transfer rate constant (k_s) and charge transfer coefficient (α) can be determined by measuring the variation of peak potential with scan rate. The values of peak potentials were proportional to the logarithm of the scan rate for scan rates higher than 2.0 V s^{-1} (Fig. 3C) and the slope of the E_p vs. log(v) was about 77.4 mV. Using the equation $E_p = K - 2.3030(RT/\alpha nF) \log(v)$ and 2 electrons transferred for chlorogenic acid a charge transfer coefficient, $\alpha = 0.38$ was obtained. Introducing this α value in the
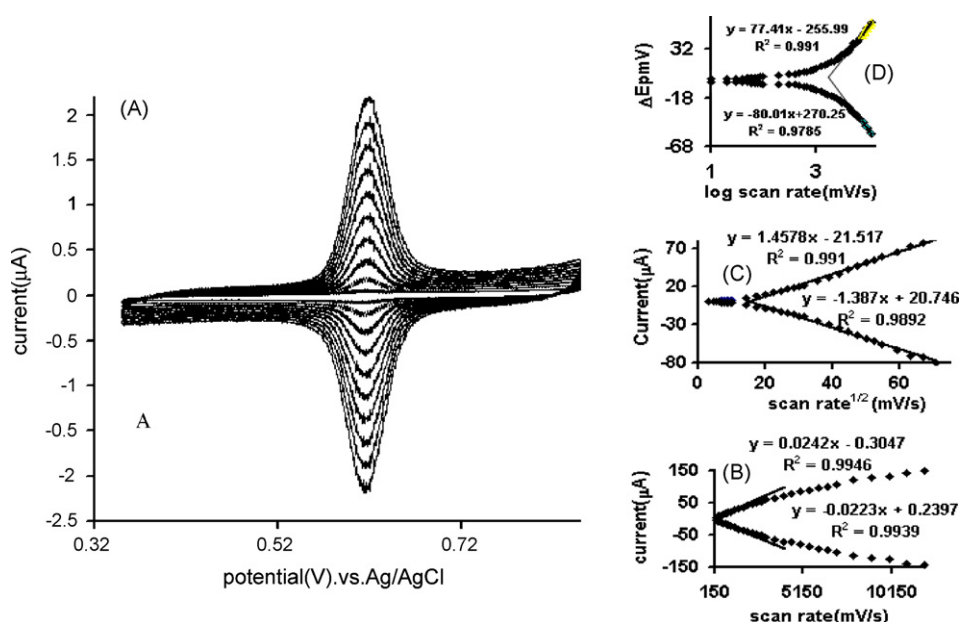

Fig. 3. (A) Cyclic voltammetric responses of MWCNTs/CGA modified GC electrode in buffer solution (pH 1) at scan rates; (inner to outer) 10, 20, 30, 40, 50, 60, 70, 80, 90, and 100 mV s^{-1}. (B and C) plot of peak currents vs. scan rate and square root of scan rate. (D) The variation of peak potential separation vs. log v.

Table 1
The calculated values of α, k_{cat}, k_s and Γ for CNTs/catechols modified glassy carbon electrodes

| Catechol compound | CNT | | | | | | | |
| | SWCNT | | | | MWCNT | | | |
	α	k_s (s^{-1})	Γ (mol cm^{-2})	k_{cat} ($\times 10^4$ M^{-1} s^{-1})	α	k_s (s^{-1})	Γ (mol cm^{-2})	k_{cat} ($\times 10^4$ M^{-1} s^{-1})
Catechin hydrate	0.37	3.9	2.7×10^{-11}	7.5	0.4	13.42	8.6×10^{-10}	0.13
Chlorogenic acid	0.41	18.8	3.7×10^{-11}	2.6	0.4	53	5.4×10^{-11}	1.42
Caffeic acid	0.41	44	$4.8 \times 10-$	–	0.31	50	4.2×10^{-11}	2.25

following equation:

$$\log k_s = \alpha \log(1 - \alpha) + (1 - \alpha) \log \alpha - \log\left(\frac{RT}{nFv}\right)$$
$$- \frac{\alpha(1 - \alpha)nFE}{2.3RT} \tag{1}$$

An apparent surface electron transfer rate constant, $k_s = 53.11(\pm 3)$ s^{-1}, was estimated. For CGA/SWCNTs/GC modified electrode these values are 0.41 and 18.8(± 2) s^{-1}, respectively. This value for electron transfer rate constant is larger than that obtained for self assembled monolayer of chlorogenic acid adsorbed onto carbon ceramic electrode (8.4 s^{-1}) [2] and CGA adsorbed onto preanodized GC electrode [6]. The large value of electron transfer rate constant indicates high ability of CNTs for electron promoting between CGA and electrode surface. The surfaces of MWCNTs contain a large number of defects and special nanostructure of CNT may act as molecular wires enhancing the direct electron transfer of CGA at CNT. The charge transfers and electron transfer rate constants are reported in Table 1. The surface concentration of electroactive species, Γ can be calculated from the slope of the plot of I_p versus scan rate ($v < 100$ mV s^{-1}) by the following equation [47].

$$I_p = \frac{n^2 F^2 v A \Gamma_c}{4RT} \tag{2}$$

where v is the sweep rate, A is the geometric surface area and the other symbols have their usual meaning. In the present case, the calculated values of Γ are 3.7×10^{-11} and 5.42×10^{-11} mol cm^{-2} for $n = 2$ for CGA/MWCNTs/GC and CGA/SWCNTs/GC modified electrodes, respectively. The calculated Γ values for other catechols have been reported in Table 1.

3.2. Stability and pH dependence of the CNTs/catechols modified GC electrodes

The stability of the GC/MWCNTs/catechin hydrate modified electrode and the reproducibility of the electrochemical behavior were investigated by cyclic voltammetry. Under continuous potential sweeping at 100 mV s^{-1} between 0.25 and 0.9 V in buffer solution (pH 1), an insignificant decay in the peak currents was observed during the initial cycles (3% for first 5 cycles and the rate of current decreased (6% after 150 cycles (not shown).

In addition, the current only decreased by 5% when the electrode was immersed in buffer solution (pH 1) for 30 h. The stability of the modified electrodes was evaluated by the same method in electrolyte solutions with pH 7 and 11. The results indicated that the modified electrode was stable in acidic solution, but at alkaline media (pH 11) decreasing of peak current was observed (20% after 100 cycles) due to solution of deprotonated form of catechols. These results suggest that the initial decay might be due to the material that is weakly bonded to the electrode surface. Since the method of the electrode preparation is simple and fast (less than 1 min), the current decay is not a serious limitation for this modified electrode. To study the reproducibility of the electrode preparation, the GC electrodes were modified with MWCNTs, and then immersed for 50 s in 1 mM chlorogenic acid. For five successive preparations the relative standard deviation of 4% is observed from measurement of anodic peak currents. The high stability of adsorbed chlorogenic acid against desorption in aqueous solution is related to the strong interaction of aromatic groups of the catechols with π-staking of carbon nanotubes and the possible interaction between the catechol molecules and carbon nanotubes. Our results indicate that by adding aromatic or hydrocarbon cycle groups on the catechol molecular structure the stability of the modified electrode increased. The stability of the modified electrodes is as the following order: catechin hydrate > chlorogenic acid > cafeic acid. Due to the chemical stability, electrochemical reversibility and high electron transfer rate constant of catechols, they can be widely used in electrocatalysis as electron transfer mediators to shuttle electrons between analytes and substrate electrodes.

The effect of pH on the electrochemical behavior of modified electrode was investigated by recording cyclic voltammograms of MWCNTs/catechin hydrate/GC electrode in buffer solution at various pH values from 1 to 12 (not shown). As results indicate, the formal potential of the surface redox couple was pH dependent. A plot of $E^{o'}$ vs. pH gives a straight line from pH 1 to 12 with a slope of 55 mV/pH, which is very close to the anticipated Nernstian value of 59 mV for a two electron–two proton process. The slope of $E^{o'}$ vs. pH plot for other catechols is about 60 mV/pH. As can be seen, there was a decrease in surface coverage as pH values increased. A fraction of catechine hydrate in its reduced form may be in its deprotonated form, which would be expected to be more soluble due to its higher charge.

3.3. Electrocatalytic oxidation of hydrazine at CNTs/catechols modified GC electrodes

The catalytic oxidation of hydrazine at the catechol/CNTs modified glassy carbon electrode has been examined to evalu-
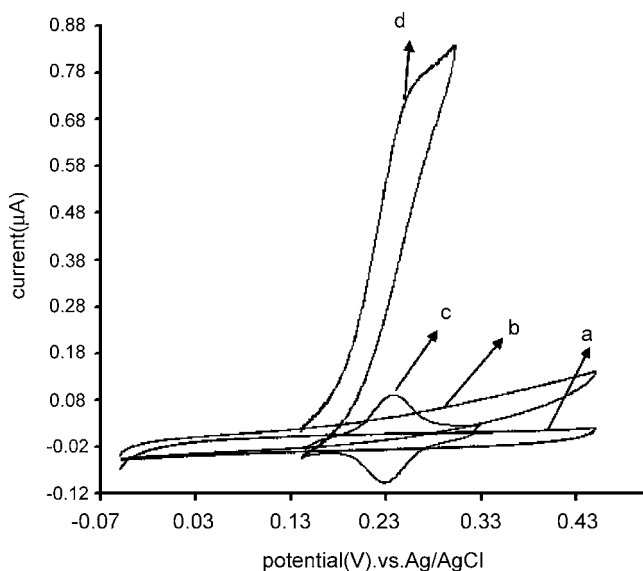
Fig. 4. Cyclic voltammograms of a CGA/MWCNTs modified GC electrode at 20 mV s^{-1} in 0.1 m phosphate buffer solution (pH 7), (c) in the absence and (d) in the presence 0.5 m mol L^{-1} of hydrazine. (a and b) as (c and d) for MWCNTs modified GC electrode.

ate the feasibility of the modified electrodes in electrocatalysis purposes and electroanalysis processes. One of the objectives of current study was to fabricate a modified electrode that was capable for the electrocatalytic oxidation of hydrazine at reduced overpotential. In order to test the electrocatalytic activity of the modified electrodes, the cyclic voltammograms were obtained in the absence and presence of hydrazine in buffer solution (pH 7). Fig. 4 shows cyclic voltammograms of glassy carbon electrodes modified with SWCNTs and chlorogenic acid + SWCNTs in buffer solution (pH 7) containing hydrazine. Upon the addi-

tion of 0.5 mmol L^{-1} analyte, there is a dramatic enhancement of the anodic peak current and the cathodic peak currents disappears (Fig. 4d), indicating a strong catalytic effect. No anodic peak was observed for hydrazine oxidation at SWCNTs modified glassy carbon electrode at potential range −0.07 to 0.45 V. The same electrochemical activity was observed for other selected catechols/CNTs modified GC electrodes toward hydrazine oxidation.

In order to optimize the electrocatalytic response of modified electrode toward hydrazine oxidation, the effect of pH on the catalytic behavior was investigated. The cyclic voltammograms of the modified electrode in 1 mmol L^{-1} hydrazine at different pH values 5–10 were recorded (not shown). At pH 5–10, the modified electrode shows electrocatalytic activity, but higher peak currents observed at pH 7 and this value was chosen as optimized. Additionally, peak potentials shifted to positive potentials with increasing pH values. Fig. 5 shows cyclic voltammograms of CGA/MWCNTs and catechin hydrate/MWCNTs modified glassy carbon electrode in solutions containing different concentrations of hydrazine and the inset shows that the catalytic current is proportional to hydrazine concentration.

The plot of catalytic current vs. hydrazine concentration in the concentration range of 0.05–0.5 mM fitted the equations; I_p (μA) = 1.775 μA × mol^{-1} L + 0.0502 μA and R^2 = 0.9945 and I_p (μA) = 7.16 μA × μmol^{-1} L + 0.3063 μA and R^2 = 0.9937 for CGA/MWCNTs and catechin hydrate/MWCNTs modified glassy carbon electrodes, respectively. The detection limit is 5 and 2 μmol L^{-1} for modified electrodes when signal to noise ratio is 3. The detection limit, linear concentration range and sensitivity of other modified electrodes for hydrazine detection have been reported in Table 2.
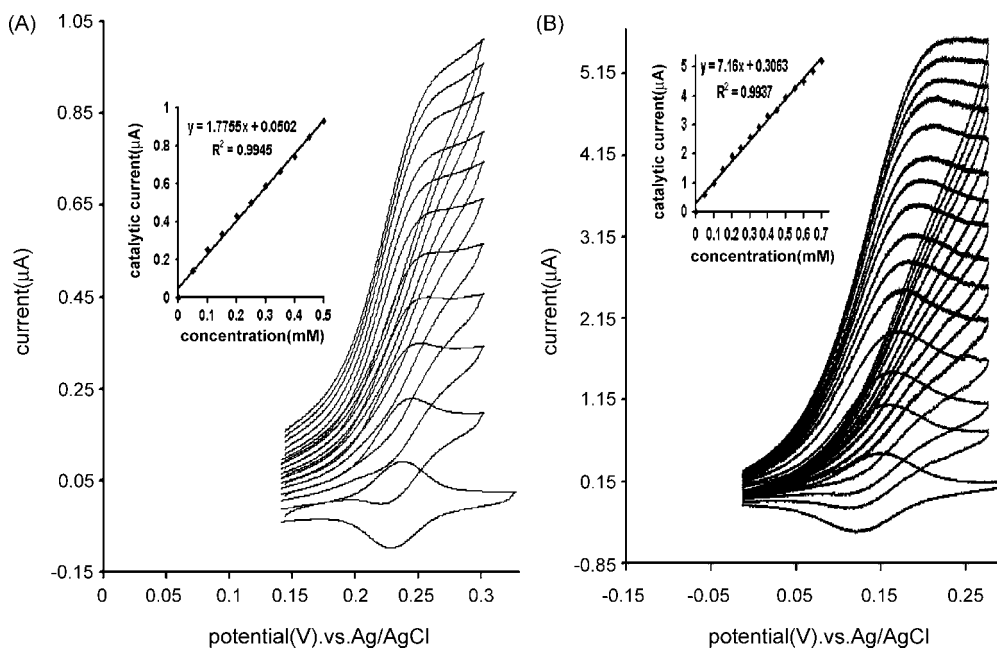

Fig. 5. (A) Cyclic voltammograms of CGA/MWCNTs modified GC electrode in (pH 7) buffer solution at different concentration of hydrazine from inner to outer, 0.0, 0.05, 0.1, 0.15, 0.2, 0.25, 0.3, 0.35, 0.4, 0.45, 0.5 and 0.55 mmol L^{-1}. Inset: Plot of the catalytic peak current vs. hydrazine concentrations. (B) as (A) for catechin hydrate/MWCNTs modified GC in different concentration of hydrazine, scan rate, 10 mV s^{-1}.

Table 2
Detection limit, linear concentration range and sensitivity for hydrazine detection at CNTs/ catechols modified glassy carbon electrodes

Catechols	CNT											
	SWCNT						MWCNT					
	Cyclic voltammetry				Amperometry		Cyclic voltammetry				Amperometry	
	DL[a] (μM)	LCR[b] (μM–mM)	Sensitivity (μA/mM)	DL (nM)	LCR (μM–mM)	Sensitivity (μA/μM)	DL (μM)	LCR (μM–mM)	Sensitivity (μA/mM)	DL (nM)	LCR[c] (μM–mM)	Sensitivity (μA/μM)
CAT[d]	2.0	50–2.0	7.16	40	0.5–1	0.183	2.5	25–1.0	3.05	50	0.5–2.5	0.0376
CGA[e]	3.0	25–1.5	1.77	80	0.5–3	0.0494	2.0	50–2.0	4.493	50	0.5–4	0.0251
CFA[f]	–	–	–	–	–	–	8	25–1.5	0.6768	200	2.5–5.0	0.0041

[a] Detection limit.
[b] Linear calibration range.
[c] $mmol\,L^{-1}$–$\mu mol\,L^{-1}$.
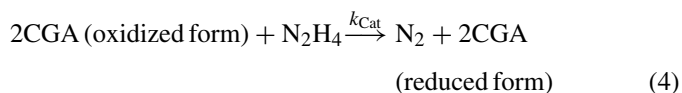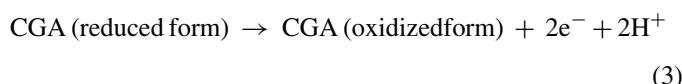[d] Catechin hydrate.
[e] Caffeic acid.
[f] Chlorogenic acid.

To verify further that the electrochemical oxidation of hydrazine is diffusion controlled a study of the effects of scan rate on the electrochemical signal was undertaken. Fig. 6A shows the cyclic voltammograms of 0.4 mM hydrazine solution at different scan rates.

The anodic peak current of hydrazine concentration is proportional to the square root of the scan rate (inset B of Fig. 6), suggesting that the process is controlled by diffusion of analyte as expected for a catalytic system. A plot of the scan rate-normalized current ($I_p/v^{1/2}$) vs. scan rate (inset C of Fig. 6) also exhibited the characteristic shape of a typical EC′ catalytic process [48]. The same results for oxidation of hydrazine at other

modified electrodes were observed. Based on the results, the following catalytic scheme (EC′ catalytic mechanism) describes the oxidation of hydrazine.

$$CGA\,(reduced\,form)\ \rightarrow\ CGA\,(oxidized form)\ +\ 2e^-\ +2H^+ \tag{3}$$

$$2CGA\,(oxidized\,form) + N_2H_4 \xrightarrow{k_{Cat}} N_2 + 2CGA$$
$$(reduced\,form) \tag{4}$$

In order to get the information about the rate determining step, a Tafel plot was drawn, using the data derived from the rising
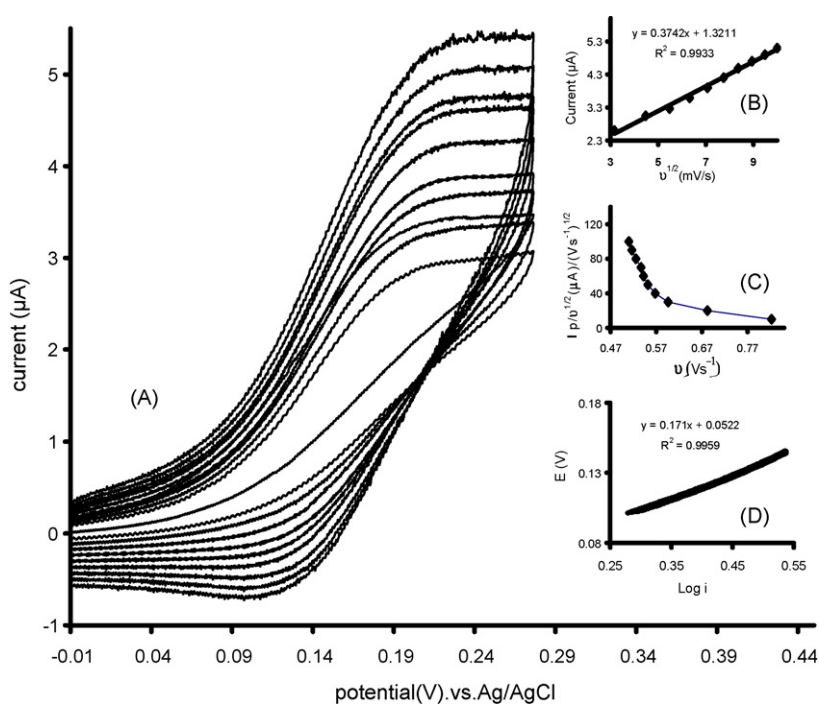

Fig. 6. (A) Cyclic voltammetry response of a catechin hydrate–MWCNTs modified GC electrode in pH 7 buffer solution containing 0.4 mM of hydrazine at scan rates (inner to outer) 10, 20, 30, 40, 50, 60, 70, 80, 90 and 100 mV s^{-1}. (B) Plot of I_p vs. $v^{1/2}$ (C) Plot of anodic current function $I_p/v^{1/2}$ vs. v. (D) The variation of potential vs. Log i (Tafel plot) for rising part of recorded cyclic voltammogram at 20 mV s^{-1}.

part of the current–voltage curve recorded at scan rate 20 mV s^{-1} (inset D of Fig. 6). The value of Tafel slope, 171 mV s^{-1}, indicates that a one-electron transfer process in the rate determining step assuming a transfer coefficient of α about 0.36. Under the above conditions for an EC′ mechanism, the Andrieux and Saveant theoretical model [49] can be used to calculate the catalytic rate constant. Based on this theory, a relation between the peak current and the concentration of substrate compound for the case of slow scan rates and large catalytic rate constant exists:

$$I_\mathrm{p} = 0.446 n F A D^{1/2} \left(\frac{\nu F}{RT} \right)^{1/2} C_\mathrm{s} \tag{5}$$

where D and C_s are the diffusion coefficient (cm^2 s^{-1}) and the bulk concentration (mol cm^{-3}) of substrate (hydrazine), respectively and other symbols have their usual meanings. Low values of k_cat result in values of the coefficient lower than 0.496. For low scan rate (5–20 mV s^{-1}), the average value of this coefficient was found to be 0.41 for a catechin–MWCNTs modified glassy carbon electrode with a coverage of 8.68×10^{-10} mol cm^{-2} and a geometric area (A) of 0.12 cm^2 in 0.4 mmol L^{-1} hydrazine at pH = 1. According to the approach of Andrieux and Saveant and using Fig. 1 ref. [49], the average value of k_cat calculated is $1.38(\pm0.2) \times 10^3$ M^{-1} s^{-1}. The catalytic rate constants for oxidation of hydrazine at other modified electrodes are reported in Table 1. Due to high catalytic rate constants, the catechol adsorbed onto CNTs can be used as an electron transfer mediator for electrocatalytic oxidation of hydrazine. The number of electrons in the overall reaction (n) can also be obtained from the slope of I_p vs. $\nu^{1/2}$ according to the following equation [50].

$$I_\mathrm{p} = 3.01 \times 10^5 n [n_\alpha(1 - \alpha)]^{1/2} A C_s^{1/2} \nu^{1/2} \tag{6}$$

where α is the charge transfer coefficient (calculated from the Tafel slope) and all other symbols have their usual meanings. For hydrazine oxidation the n is about 3.95–4.15 and the oxidation product is N$_2$. Repetitive scanning at scan rate 20 mV s^{-1} checked the stability of electrocatalytic activity of the modified electrode toward oxidation of hydrazine (not shown). In the first three scans, the electrocatalytic currents decreased with scan number, and then the current remained at 85% of its initial value after 50 cycles. For evaluation the repeatability of the sensor five repetitive measurements for hydrazine solution (0.3 mmol L^{-1}) was done. The relative standard deviation of 3% is observed from measurement of anodic peak currents. Furthermore, the reproducibility of modified electrode for oxidation of hydrazine was evaluated by 5 separate modification with chlorogenic acid and then recording the cyclic voltammograms in 0.3 mM of hydrazine solution (R.S.D. for measured anodic peak current was 4%).

3.4. Amperometric detection of hydrazine at CNT–catechol-modified GC electrode

Since amperometry under stirred conditions has a much higher current sensitivity than cyclic voltammetry, it was used to estimate the lower limit of detection. As discussed above, the carbon nanotube–catechol modified glassy carbon electrode has excellent and strong mediation properties and facilitates the low potential amperometric measurements of hydrazine. Fig. 7 displays the typical steady-state catalytic current time response of the rotated catechin/SWCNTs modified electrode (2000 rpm) with successive injection of hydrazine at an applied potential 0.18 V vs. reference electrode.

As shown, during the successive addition of 0.2 mmol L^{-1} and 0.5 μmol L^{-1} of hydrazine a well-defined response was

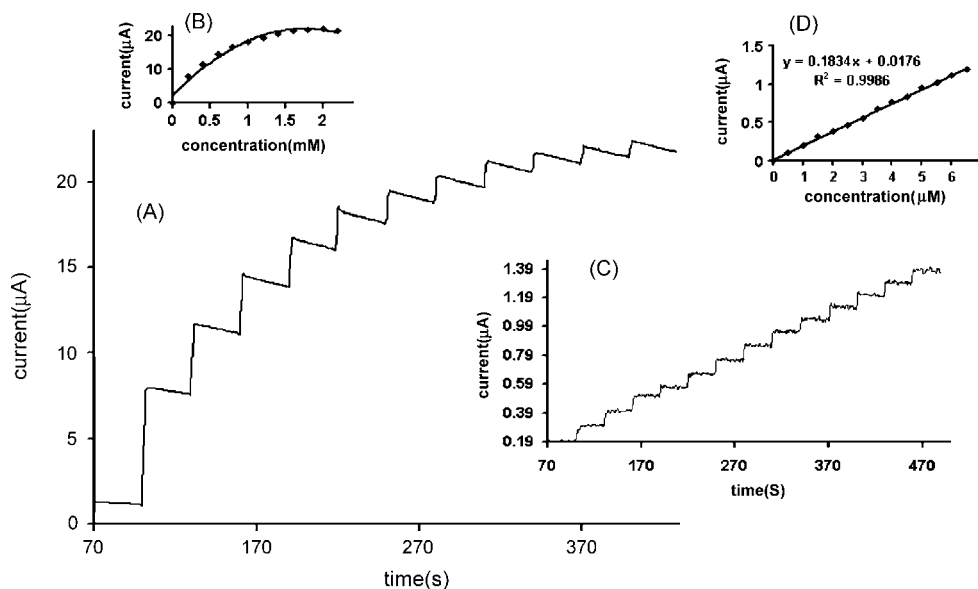Fig. 7. Amperometric response at rotating catechin hydrate–MWCNTs modified GC electrode in buffer solution (pH 7) (rotation speed 2000 rpm) held at 0.18 for successive addition of (A) 0.2 mM and (C) 0.50 μmol L^{-1} hydrazine (C and D) Plot of chronoamperometric currents vs. hydrazine concentrations.

observed, demonstrating stable and efficient catalytic ability of the electrocatalyst immobilized on the CNTs film. The response current is linear with the hydrazine concentration in the range $0.50\,\mu mol\,L^{-1}$ to $1\,mmol\,L^{-1}$, while for a higher concentration of hydrazine, the plot of current values vs. analyte concentration deviates from linearity (Fig. 7 plots c and d). The linear least squares calibration curve over the range of 0.50–$6.5\,\mu mol\,L^{-1}$ (13 points) is $I\,(\mu A) = 0.1834[hydrazine] + 0.0176\,\mu A$ with a correlation coefficient of 0.9986, indicating that the regression line is fitted very well with the experimental data and the regression equation can be applied in the unknown sample determination. The detection limit (signal to noise ratio of 3) and sensitivity were $50\,nmol\,L^{-1}$ and $183.4\,nA/\mu mol\,L^{-1}$, respectively. The detection limit, linear calibration range and sensitivity for hydrazine detection at other modified electrodes were reported in Table 2. The response time measured in amperometric determination is 2 s or less to 90% of the full signal. These analytical parameters are comparable or better than results reported for hydrazine determination at the surface recently fabricated modified electrodes [1–9,51–54]. An extremely attractive feature of the electrodes modified with CNTs and catechol derivatives is its highly stable amperometric response toward hydrazine. The amperometric response of $30\,\mu mol\,L^{-1}$ of hydrazine was recorded over a continuous 20 min period (not shown). The response of the modified electrode remains stable throughout the experiments (only 6% decrease in current is observed over 20 min) indicating no inhibition effect of hydrazine and its oxidation products for modified electrode surface. Also, the amperometric current of hydrazine remained unchanged after the modified electrode was stored for 3 weeks in air at room temperature, indicating that it can be used as stable sensor for hydrazine detection. For GC electrode modified with CNTs and caffeic acid the responses are unstable due to desorption of catechol.

4. Conclusions

A simple, fast, reproducible and direct procedure was used for adsorption of catechols as electron transfer mediator on glassy carbon electrode modified with CNTs. Catechol deposited onto CNTs films acts as an excellent electrocatalyst for hydrazine oxidation, due to the chemical stability, electrochemical reversibility and high electron transfer rate constant. The catalytic rate constants of the modified electrode for hydrazine oxidation are in order $10^4\,M^{-1}\,s^{-1}$, which are comparable or higher than previously reported about catechol derivatives modified electrodes. The modified electrode based on coupling CNTs with catechols has been shown to be promising for hydrazine detection at reduced overpotential with many desirable properties including low detection limit, high sensitivity, short response time, satisfactory linear concentration range and high reproducibility. The simple fabrication and extreme stability in storage of modified electrode are obvious advantages. The nanomolar concentration of hydrazine was determined amperometrically at the surface of this modified electrode.

References

[1] H.R. Zare, N. Nasirzadeh, Electroanalysis 18 (2006) 507.
[2] A. Salimi, R. Hallaj, Electroanalysis 16 (2004) 1964.
[3] P.V.A. Pamidi, J. Wang, Electroanalysis 8 (1996) 244.
[4] M.M. Ardakani, P.E. Karimi, P. Rahimi, H.R. Zare, H. Naeimi, Electrochim. Acta 52 (2007) 6118.
[5] H.R. Zare, N. Nasirzadeh, Electrochim. Acta 52 (2007) 4153.
[6] S.M. Golabi, H.R. Zare, J. Electroanal. Chem. 465 (1999) 168.
[7] H.R. Zare, Z. Sobhani, M.M. Ardakani, J. Solid State Electrochem. 11 (2007) 971.
[8] A. Salimi, K. Abdi, G.R. Khayatian, Microchim. Acta 144 (2004) 161.
[9] S.M. Golabi, H.R. Zare, Electroanalysis 11 (1999) 1293.
[10] F. Pariente, F. Tobalina, G. Moreno, L. Hemandez, E. Lorenzo, H.D. Abruna, Anal. Chem. 69 (1997) 4065.
[11] Z. Gao, K.S. Siow, A. Ng, Y. Zhang, Anal. Chim. Acta 343 (1997) 49.
[12] F. Valentini, A. Amines, S. Olanducci, M.L. Terranova, G. Pallesschi, Anal. Chem. 75 (2003) 5413.
[13] B.I. Yakobson, R.E. Smally, Flullerene nanotubes, Am. Sci. 85 (1997) 324.
[14] Y.Y. Yang, S.W. Chen, Q.B. Xue, A. Biris, W. Zhao, Electrochim. Acta 50 (2005) 3061.
[15] J. Wang, M. Mosameh, Anal. Chim. Acta 511 (2004) 33.
[16] A. Salimi, R. Hallaj, Talanta 66 (2004) 967.
[17] R.P. Deo, J. Wang, Electrochem. Commun. 6 (2004) 284.
[18] J. Wang, M. Mosameh, Y. Lin, J. Am. Chem. Soc. 125 (2003) 2408.
[19] J. Wang, S.B. hocevar, B. Ogorevc, Electrochem. Commun. 6 (2004) 176.
[20] M.L. Pedano, G.A. Rivas, Electrochem. Commun. 6 (2004) 10.
[21] M.D. Rubianes, G.A. Rivas, Electrochem. Commun. 5 (2003) 689.
[22] J. Wang, M. Li, Z. Shi, N. Li, Z. Gu, Electroanalysis 14 (2002) 225.
[23] W. Huang, W. Hu, J. Song, Talanta 61 (2003) 411.
[24] X.N. Cao, L. Lin, Y.Y. Zhou, G.Y. Shi, W. Zhang, K. Yamamoto, L.T. Jin, Talanta 60 (2003) 1063.
[25] F.H. Wu, G.C. Zhou, X.W. Wei, Electrochem. Commun. 4 (2002) 690.
[26] J. Wang, M. Li, Z. Shi, N. Li, Z. Gu, Anal. Chem. 74 (2002) 1993.
[27] G.C. Zhao, L. Zhang, X.W. Wei, Z.S. Yang, Electrochem. Commun. 5 (2003) 825.
[28] Z. Wang, Y. Wang, G. Luo, Electroanalysis 15 (2003) 1129.
[29] A. Salimi, R. Hallaj, G.R. Khayatian, Electroanalysis 17 (2005) 873.
[30] A. Salimi, M. Izadi, R. Hallaj, M. Rashidi, Electroanalysis 19 (2007) 1668.
[31] A. Salimi, C.E. Banks, R.G. Compton, Analyst 129 (2004) 225.
[32] A. Salimi, R.G. Compton, R. Hallaj, Anal. Biochem. 333 (2004) 49.
[33] N.S. Lawrence, J. Wang, Electrochem. Commun. 8 (2005) 71.
[34] K. Zhao, H. Song, S. Zhung, L. Dai, P. He, Y. Fang, Electrochem. Commun. 9 (2007) 65.
[35] Z. Li, J. Chen, D. Pan, W. Tao, L. Nie, S. Yao, Electrochim. Acta 51 (2006) 4255.
[36] F. Frehill, J.G. Vos, S. Benrezzak, A.A. Koos, Z. Konya, M.G. Ruther, W.J. Blau, A. Fonseca, J.B. Nagy, L.P. Biro, A.I. Minett, M. Panhuis, J. Am. Chem. Soc. 124 (2002) 13694.
[37] R.J. Chen, Y. Zhang, D. Wang, H. Dai, J. Am. Chem. Soc. 123 (2001) 3838.
[38] A. Salimi, A. Noorbakhash, M. Gadermazi, Sens. Actuators B 123 (2007) 530.
[39] A. Salimi, H. Mamkhezri, S. Mohebbi, Electrochem. Commun. 8 (2006) 688.
[40] A. Salimi, H. Mamkhezri, R. Hallaj, S. Zandi, Electrochim. Acta 52 (2007) 6097.
[41] C.B. McAuley, C.E. Banks, A.O. Simm, T.G.J. Jones, R.G. Compton, Analyst 131 (2006) 103.

[42] S. Garrod, M.E. Bollard, A.W. Nicollas, S.C. Connor, J. Connelly, J.K. Nicholson, E. Holmes, Chem. Res. Toxicol. 18 (2005) 115.

[43] M. Revenga-Parra, E. Lorenzo, F. Pariente, Sens. Actuators B 107 (2005) 678.

[44] J. Wang, M. Chicharro, G. Rivas, X. Cai, N. Dontha, D.A.M. Farias, H. Shiraishi, Anal. Chem. 68 (1996) 2251.

[45] J. Li, A. Cassell, L. Delzeit, J. Han, M. Meyyappan, J. Phys. Chem. B 106 (2002) 9299.

[46] E. Lavion, J. Electroanal. Chem. 101 (1979) 19.

[47] J. Wang, Analytical Electrochemistry, VCH, New York, 1994.

[48] F. Pariente, E. Lorenzo, F. Tobalina, H.D. Abruna, Anal. Chem. 67 (1995) 3936.

[49] C.P. Andriex, J.M. Saveant, J. Electroanal. Chem. 93 (1978) 163.

[50] S. Antoniadou, A.D. Jannakoudakis, E. Theodoridou, Synth. Met. 30 (1980) 295.

[51] J.M. Pingarron, I. Ortiz-Hernandez, A. Gonzales-Cortes, P. Yanez-Sendeno, Anal. Chim. Acta 439 (2001) 281.

[52] J.S. Pinter, K.L. Brown, P.A. DeYoung, G.F. Peaslee, Talanta 71 (2007) 1219.

[53] C.C. Yang, A.S. Kumar, M.C. Kuo, S.H. Chien, J.M. Zen, Anal. Chim. Acta 554 (2005) 66.

[54] C.B. McAuley, C.E. Banks, A.O. Simm, T.G.J. Jones, R.G. Compton, Analyst 131 (2006) 106.

Selective determination of ultra trace amounts of gold by graphite furnace atomic absorption spectrometry after dispersive liquid–liquid microextraction

Mojtaba Shamsipur [a,*], Majid Ramezani [a,b]

[a] Department of Chemistry, Faculty of Science, Razi University, Kermanshah, Iran
[b] Iranian Aluminum Company, Arak, Iran

Abstract

A simple, rapid and sensitive method is proposed for selective determination of ultra trace amounts of gold from different samples. The method is based on highly efficient separation and pre-concentration of gold by dispersive liquid–liquid microextraction of gold followed by its determination with graphite furnace atomic absorption spectrometry. The pre-concentration procedure results in quantitative extraction of gold by victoria blue R from a 10-mL sample into fine droplets of chlorobenzene, with a sedimented volume of 25 μL. Then, 20 μL of 0.04% Pd(NO$_3$)$_2$, as chemical modifier, followed by 10 μL of the sedimented phase were consecutively pipetted into the same auto-sampler device and the content is injected into the graphite tube and the gold content is determined by graphite furnace atomic absorption spectrometry. After optimizing the extraction conditions and instrumental parameters, a pre-concentration factor of about 388 is obtained for the system. The analytical curve is linear in a concentration range of 0.03–0.5 ng mL^{-1}. The detection limit and relative standard deviation are 0.005 ng mL^{-1} and 4.2%, respectively. The method was successfully applied to the extraction and determination of gold in tap water and silicate ore samples.
© 2007 Elsevier B.V. All rights reserved.

Keywords: Gold; Dispersive liquid–liquid microextraction; Graphite furnace atomic absorption spectrometry; Silica ore

1. Introduction

Gold is one of the most important noble metals due to its wide application in industry and economic activity. Several techniques, such as inductively coupled plasma atomic emission spectrometry (ICP-AES) [1], flame atomic absorption spectrometry (FAAS) [2], electrothermal atomic absorption spectrometry [3] electrochemical methods [4], neutron activation analysis [5], and spectrophotometry [6] have widely been applied to the determination of gold. In most of the methods used, the sample preparation steps typically consist of a pre-concentration procedure that results in isolation and enrichment of component of interest from a sample matrix [7–14].

A number of extraction-spectrophotometric methods for the determination of gold based on the extraction of AuCl$_4$$^-$ ion-association complexes in hydrochloric acid medium with various basic dyes including rhodamine B [15], victoria blue R [16], brilliant green [17] and methylene blue [18] are reported in the literature. However, liquid–liquid extraction (LLE), as the oldest pre-concentration and separation technique in analytical chemistry, is time-consuming and requires large amount of organic solvents [19]. Thus, single drop microextraction (SDME) was developed as an inexpensive alternative, in which sub-mL amounts of organic solvents are used so that there is minimal exposure to toxic organic solvents and has a good enrichment factor [20]. However, in order to break up the organic drop and air bubbled formation as the result of fast stirring, the method needs a long time to reach equilibrium and complete extraction. Flow injection analyses (FIA) analysis are also reported as a convenient methods for determination of gold [1,2,23]. Solid-phase extraction (SPE) and cloud point extraction (CPE) methods are very time-consuming and can be relatively expensive although they use much less organic solvent than LLE [6,21,22]. Therefore, the introduction of simple, rapid, clean and efficient pre-concentration techniques are of urgent need.

* Corresponding author. Tel.: +98 21 66908031; fax: +98 21 66908030.
  E-mail address: mshamsipur@yahoo.com (M. Shamsipur).

Recently, Assadi and co-workers introduced a novel microextraction method called dispersive liquid–liquid microextraction (DLLME) as a highly sensitive, efficient and powerful method for the pre-concentration and determination of traces of organic and inorganic compounds in water samples [24,25]. In this work we used this method for the selective extraction and pre-concentration of sub-nanogram amounts of Au(III) by victoria blue R (VBR), as a suitable reagent for gold [16], and subsequent determination using graphite furnace atomic absorption spectrometry (GFAAS). In this method, an appropriate mixture of extraction solvent and disperser solvent is injected rapidly into an aqueous sample containing gold(III) ions and VBR by a syringe. Then, the resulting cloudy solution is centrifuged and the fine droplets sedimented in a few-μL volume at the bottom of the conical test tube are finally introduced into the GFAAS for the determination of its gold content.

2. Experimental

2.1. Reagents and standards

Reagent grade chlorobenzene, carbon tetrachloride and chloroform, as extraction solvents, and acetone, acetonitrile, and methanol, as disperser solvents, and victoria blue R were purchased from Merck chemical company. Doubly distilled deionized water was used throughout. Analytical grade gold(III) chloride and nitrate salts of other cations (all from Merck) were of the highest purity available and used without any further purification except for vacuum drying.

2.2. Instrumentation

The experiments were performed using a Shimadzu atomic absorption spectrometer (AA 6800G), equipped with a graphite furnace atomizer GFA-6500 and an auto-sampler ASC-6100. Deuterium background correction was employed to correct non-specific absorbances. All measurements were performed using the peak height. A gold hollow cathode lamp (Hamamatsu Photonic Co. Ltd., L233-series) and a pyrolytic coated graphite tube (Shimadzu part no. 206-69984-02) were used. The sample injection volume was $10\,\mu L$ in all experiments. The instrumental parameters and temperature program for the graphite atomizer are listed in Table 1. Argon gas with 99.95% purity was

purchased from Roham Gas Co. (Tehran, Iran) was used as protected and purge gas. A Behdad Universal Centrifuge (Tehran, Iran) was used for centrifugation. All 10-mL screw cap falcon test tubes with conical bottom (extraction vessel) were maintained into $0.1\,mol\,L^{-1}$ HNO_3 for cleaning of any inorganic compounds and washed with doubly deionized water and then with acetone for proper sedimentation of fine droplets of the extraction solvent in the centrifuging step.

2.3. General procedure

In a calibrated 10-mL volumetric flask was added $2\,mL$ of $2.5\,mol\,L^{-1}$ HCl, $1\,mL$ of $4.0\times10^{-5}\,mol\,L^{-1}$ victoria blue R (VBR) and a spiked level of $2\,\mu g\,L^{-1}$ of $AuCl_4^-$ solution and diluted to the mark with deionized water and mixed well. The solution was then completely removed into a 15-mL falcon conical test tube. One microlitre acetone, as disperser solvent, containing $40\,\mu L$ chlorobenzene, as extraction solvent, was injected rapidly into the sample solution by using a proper Hamilton syringe and the mixture was gently shaken. A cloudy solution (water/acetone/chlorobenzene) was formed in the test tube, where the $AuCl_4$–VBR adducts is extracted into the fine droplets of chlorobenzene. The mixture was then centrifuged for 2 min at 4000 rpm. After this process, the dispersed fine droplets of chlorobenzene were sedimented at the bottom of test tube ($25\pm1\,\mu L$). Finally, $20\,\mu L$ of 0.04% $Pd(NO_3)_2$, as chemical modifier, followed by $10\,\mu L$ of the sedimented phase were consecutively pipetted into the same auto-sampler device and the content was injected into the graphite tube and the gold content is determined by graphite furnace atomic absorption spectrometry.

3. Results and discussion

In order to reach the optimized experimental conditions for high enrichment factor and quantitative extraction of gold ions by VBR via DLLME method, the influence of different parameters including nature and concentration of the chelating agent, concentration of HCl, nature and volume of both extraction and disperser solvents and extraction time were investigated. The enrichment factor (EF) was defined as the ratio of the curve slope of pre-concentration sample to that obtained form extraction with the proposed method [26,27]. The extraction recovery was defined as the percentage of the total amount of analyte (m),

Table 1
GF-AAS instrumental parameters for gold determination[a]

Stage	Temperature (°C)	Heat mode	Time (s)	Argon gas flow (mL min^{-1})
Drying	150	Ramp	60	200
Drying	250	Ramp	20	200
Pyrolysis	1000	Ramp	15	1000
Pyrolysis	1000	Step	10	1000
Pyrolysis	1000	Step	3	0
Atomizaition	2100	Step	4	0
Cleaning	2500	Step	2	1000

[a] Spectrometer parameters: wavelength, 242.8 nm; slit width, 0.5 mm; lamp current, 12 mA. Absorbance measurements were made by peak height, using $Pd(NO_3)_2$ as a modifier.

which was extracted into the sedimented phase

$$R(\%) = \left(\frac{m_{sed}}{m_o}\right) \times 100 = \left(\frac{C_{sed}}{C_o}\right)\left(\frac{V_{sed}}{V_{aq}}\right) \times 100$$

where V_{sed}, V_{aq}, C_o and C_{sed} are the volume of sedimented phase, volume of sample solution, initial concentration of analyte in aqueous sample and concentration of analyte in sedimented phase, respectively. The C_{sed} was calculated from the calibration graph obtained by conventional LLE–GFAAS method (in the presence of Pd^{2+} modifier), after centrifuging of a solution containing 3.50 mL standard aqueous sample of Au(III), in the concentration range of 25–175 $\mu g\,L^{-1}$, 1 mL HCl (0.5 mol L^{-1}), 0.5 mL VBR (4×10^{-5} mol L^{-1}) and 5.00 mL C_6H_5Cl.

3.1. Nature and volume of extraction solvent

The selection of an appropriate solvent as a key parameter is very important for the DLLME process. Organic solvents are selected based on their higher densities than water and their extraction efficiencies for the $AuCl_4$–VBR adduct. The ability of carbon tetrachloride, chloroform, and chlorobenzene with respective densities of 1.590, 1.492 and 1.107 $g\,mL^{-3}$ for the extraction of $AuCl_4$–VBR by the proposed method were compared. A series of sample solutions was studied by using 1 mL of acetone, as dispersing solvent, containing different volumes of the extraction solvent to achieve a final 25 μL volume of sedimented phase (i.e., 35 μL CCl$_4$, 40 μL CHCl$_3$ and 65 μL C$_6$H$_5$Cl). The results revealed that C_6H_5Cl (101.4 ± 2.1%) and CHCl$_3$ (100.6 ± 2.5%) have the highest extraction efficiency in comparison with CCl$_4$ (70.6 ± 2.8%) for a 0.2 $\mu g\,L^{-1}$ of Au(III). However, since chlorobenzene possesses a closer density to that of water and forms a very stable fine cloudy solution, it was selected as the best extraction solvent for the system.

In order to evaluate the effect of extraction solvent volume, solutions containing different volumes of chlorobenzene were examined with the same DLLME procedures. The experimental conditions are fixed and include the use of 1.00 mL acetone containing different volumes of chlorobenzene (i.e., 25.0, 40.0, 70.0, 100 and 150 μL). The results are illustrated in Fig. 1. According to Fig. 1, by increasing the volume of chlorobenzene, the volume
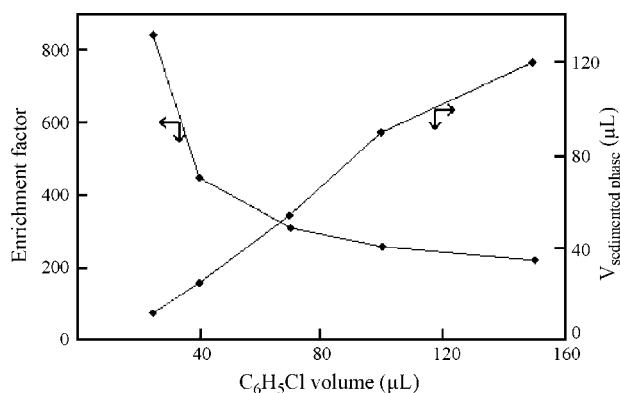

Fig. 1. Effect of volume of chlorobenzene on the volume of sedimented phase and on the enrichment factor of Au(III) in DLLME. Extraction conditions: sample volume, 10.00 mL; concentration of Au(III), 0.2 $\mu g\,L^{-1}$, disperser solvent (acetone), 1.00 mL; room temperature.

of sedimented phase increases from 10.0 to 123 μL. The result showed that the extraction recovery is almost quantitative in the case of all solvent volumes examined, which emphasizes the high distribution coefficient of $AuCl_4$–VBR in chlorobenzene under the experimental conditions used. However, as expected, the enrichment factor decreased significantly with increasing volume of the sediment phase, as also shown in Fig. 1. Subsequently, at low volume of the extraction solvent, high enrichment factor and quantitative recovery are reachable. However, our experience revealed that, in chlorobenzene volumes lower than 40 μL, picking up of 10 μL of the resulting sedimented phase was practically difficult. Thus, 40 μL of chlorobenzene was selected as the optimum volume of extraction solvent.

3.2. Nature and volume of disperser solvent

The mutual miscibility of disperser solvent in organic phase (extraction solvent) and aqueous phase (sample solution) is the most important point for the selection of a disperser solvent. Thereby, acetone, methanol and acetonitrile, which possess these abilities, were tested as potential disperser solvents. Thus, under the same experimental conditions, a series of sample solutions were studied by using 1 mL of each disperser solvent containing 40 μL of chlorobenzene and following the recommended procedure. The results showed that the variations in gold recovery by using acetone (101.9 ± 2.2), acetonitrile (99.86 ± 1.8) and methanol (100.6 ± 1.3) are not remarkable; thus, acetone was selected as disperser solvent due to its lower toxicity and cost.

Since the variation in volume of acetone (as disperser solvent) caused a change in the volume of sedimented phase, it was necessary to optimize the volume of disperser solvent. It was found that, at low volumes of acetone, the cloudy solution was not formed completely while, at high acetone volume, the solubility of chlorobenzene in aqueous solution was increased. Therefore, it was important to consider the influence of the volume of acetone on the extraction efficiency.

In order to achieve a constant volume of sedimented phase, the volumes of acetone and chlorobenzene were changed simultaneously so that the volume of the sedimented phase remained more or less constant at 25 ± 1 μL. Thus, the DLLME of a constant concentration of gold(III) (0.2 $\mu g\,L^{-1}$) with a sample volume of 10.00 mL with varying volumes of acetone (mL)/chlorobenzene (μL) ratios of 0.5/37, 0.75/38, 1.0/40, 1.5/41.5 and 2.0/43 were performed and the results are shown in Fig. 2. As seen, the extraction efficiency increases with increasing volume of acetone until a volume of 1.0 mL is reached; a further increase in volume of acetone will result in decreased efficiency of the extraction process. The observed decrease in the extraction efficiency at lower acetone volumes than 1 mL seems to be due to incomplete formation of cloudy state. While at higher acetone volumes, the decreased extraction efficiency is due to the increased solubility of $AuCl_4$–VBR adduct in water, which results in diminished distribution coefficient and extraction recovery of gold. According to the results thus obtained, a volume of 1 mL acetone was chosen as the optimum disperser volume.
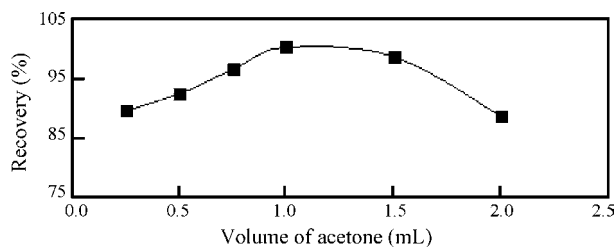
Fig. 2. Effect of the volume of acetone on the recovery of Au(III) in DLLME. Extraction conditions: sample volume, 10.00 mL; concentration of Au(III), $0.2 \mu g L^{-1}$; sedimented phase volume, $25 \pm 1 \mu L$.

3.3. Effect of extraction time

In DLLME, the extraction time is considered as the time interval between the injection moment of the disperser/extraction solvent mixture and the moment of starting the centrifugation process. In order to reach the optimum extraction time, under the same experimental conditions, the extraction procedure was carried out at different time intervals in the range of 0–5 min. The results clearly revealed that the proposed extraction method is very fast so that the extraction time has no measurable effect on the extraction efficiency. This is mainly due to an infinitely large surface area between extraction solvent and aqueous phase. Such a short extraction time can be considered as one of the main advantages of the DLLME method, as reported before [24,25].

3.4. Effect of HCl concentration

The concentration of HCl is one of the most important variables influencing the formation of $AuCl_4$–VBR complex and its subsequent extraction. Thus, the influence of the HCl concentration (in the rang of $0.0–1.5 \, mol \, L^{-1}$) in test solutions on the extraction of $0.25 \, ng \, mL^{-1}$ of Au(III) from 10 mL aqueous solution by the proposed method was studied. According to the results, the absorbance signal was increased by increasing concentration of HCl up to $0.125 \, mol \, L^{-1}$, and remained more or less constant upon further increase in acid concentration (up to $1.5 \, mol \, L^{-1}$). Thereby, a $0.5 \, mol \, L^{-1}$ concentration of HCl for quantitative extraction of $AuCl_4$–VBR was selected for further studies.

3.5. Effect of nature and concentration of complexing agent

In a hydrochloric acid medium, four different basic dyes, namely, rhodamine B [15], victoria Blue R [16], brilliant green [17] and methylene blue [18] were tested as potential candidates for the formation of ion-association complexes with gold, existing as $AuCl_4^-$ in solution, extractable into chlorobenzene as extraction solvent. The results clearly demonstrated that, under the same experimental conditions, quantitative extraction of Au(III) is achieved using rhodamine B (96%) and, especially, victoria blue (100%) as complexing agents. While, in the cases of methylene blue (47%) and brilliant green (44%), the gold extraction is quite low. Therefore, victoria blue R was selected as a proper basic dye for the formation of ion-association complex with Au(III) [16].
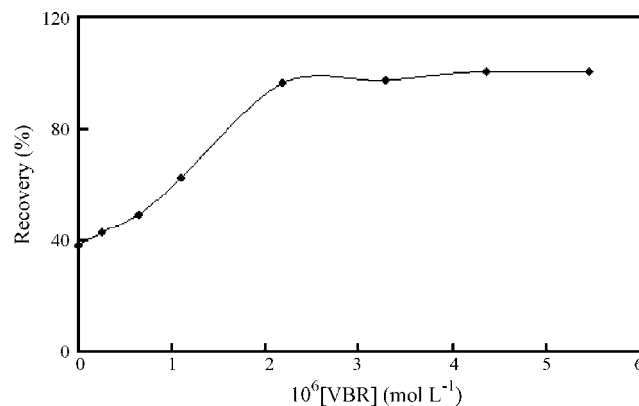

Fig. 3. Effect of VBR concentration on the recovery of Au (III) in DLLME. Extraction conditions: same as Fig. 1.

In the next step, the influence of the concentration of VBR on the efficiency of DLLME of gold was investigated and the results are shown in Fig. 3. As seen, the extraction efficiency increased with increasing concentration of the reagent until a reagent concentration of about $2.0 \times 10^{-6} \, mol \, L^{-1}$ is reached, where the gold extraction is almost quantitative. Further increase in concentration of the reagent showed no significant change in extraction efficiency. Thus, a VBR concentration of $4.0 \times 10^{-6} \, mol \, L^{-1}$ was chosen for subsequent experiments.

3.6. Optimization of the furnace conditions

In order to reduce interfering effects and increase the accuracy of determinations in GFAAS, the use of a chemical modifier has become indispensable for stabilization of elements during the pretreatment step [27–29]. By using higher pyrolysis temperatures, less interference is encountered in the atomization step [30]. Thus, in these experiments, we used aqueous solutions of Pd^{2+} as a suitable modifier. It should be noted that the organic solvents are compatible with ETAAS. Since the contact angle of sediment phase with carbon surface of the graphite used in ETAAS is between $0°$ and $10°$, the sedimented organic phase can easily spread into the graphite tube, and the modifier (aqueous Pd^{2+} solution) is simply injected on it [30]. The influence of palladium ion on background level and absorbance signal was of utmost importance. Addition of a 0.04% (w/v) solution of $Pd(NO_3)_2$, allowed increasing the pyrolysis temperature to $1000 °C$ and atomization temperature to $2100 °C$ with considerable background reduction without losing the atomic signal (Fig. 4). The absorbance signals were enhanced by 30% when the injected volume of the palladium solution was increased from 10 to $20 \mu L$. For aliquots larger than $20 \mu L$, the signal was not further improved. The modifier volume was thus chosen as $20 \mu L$ of a 0.04% (w/v) solution of $Pd(NO_3)_2$.

3.7. Effect of diverse ions

In order to study the effect of various cations and anions on the determination of Au(III), a fixed amount of gold ($0.2 \mu g L^{-1}$) was taken with different amounts of those foreign ions, which are reported to be usually present in different gold real samples
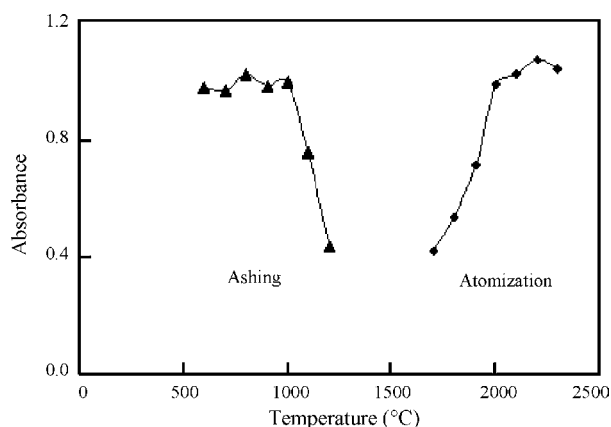
Fig. 4. Pyrolysis and atomization temperature curves after pre-concentration. Initial gold concentration is 0.4 ng mL^{-1}.

[1–18,21,23,32,33], and the recommended procedure was followed. A relative error of 3% was considered tolerable. The results are summarized in Table 2. The results showed that none of the ions examined interfere in extraction and determination of gold, even at an interfering ion-to-gold ratio of 1000 and higher.

3.8. Figures of merit

In Table 3 are compared the figures of merit of the proposed DLLME–GFAAS method with those of conventional GFAAS method. Table 3 clearly demonstrates a distinct improvement in the figures of merit of GFASS brought about upon its combination with DLLME technique.

A calibration curve was constructed by pre-concentrating 10 mL of sample standard solution. Under the optimum experimental condition, the calibration curve for Au(III) was linear form 0.03 to 0.5 μg L^{-1} with a regression coefficient of 0.994. The enrichment factors for the proposed method is 388, as obtained from the ratio of slope of the pre-concentrated sam-

Table 2
Effect of foreign ions on the pre-concentration and determination of gold (0.2 ng mL^{-1})

Ion	Ion/Au ratio	Extraction recovery (%)
Co^{2+}	2000	101.4
Tl^{3+}	1000	99.8
Ni^{2+}	2000	100.8
Cd^{2+}	2000	100.5
Pd^{2+}	2000	100.6
Ag$^+$	2000	100.1
Hg^{2+}	2000	99.7
Cu^{2+}	2000	100.3
Sn^{2+}	2000	100.4
Zn^{2+}	2000	100.1
Pb^{2+}	2000	100.0
Fe^{3+}	1000	99.6
Ga^{3+}	1000	99.7
Sb^{5+}	1000	99.3
Cr^{3+}	2000	100.4
Mn^{2+}	1000	101.1
NO$_3$$^-$	2000	100.1
Br$^-$	2000	100.2

Table 3
Analytical characteristics of the method

Element condition	DLLME–GFAAS	GFAAS
Linear range (ng mL^{-1})	0.03–0.5	10–175
Correlation coefficient (r)	0.994	0.997
Slope	2.655	0.006
Intercept	0.12	0.027
Enrichment factor[a]	388	–
RDS (%, $n=8$)[b]	4.2	4.7
LOD (ng mL^{-1})[c]	0.005	2.5

[a] Calculated as the ratio of slop of pre-concentrated samples to that obtained without pre-concentration.
[b] At a gold concentration of 0.2 ng mL^{-1}.
[c] Determined as three times of the standard deviation of the blank signal, and slop of calibration curve after pre-concentration.

ple (2.328) to that obtained without pre-concentration (0.006). It should be noted, in both cases, 20 μL of a 0.04% (w/v) solution of Pd(NO$_3$)$_2$ was used as chemical modifier. The limit of detection (LOD) was calculated as the ratio of three times of standard deviation of the blank signal and the slop of calibration curve after pre-concentration (LOD = 0.005 ng mL^{-1}). The high sensitivity presented by GFAAS is a decisive factor when analytes have to be determined at very low concentration [31]. The relative standard deviation for the eight replicate recoveries of 0.2 μg mL^{-1} Au(III) from 10 mL of aqueous solutions was found to be ±4.2%.

3.9. Comparison of DLLME–GFAAS with other methods

In Table 4 are compared the main analytical characteristics (i.e., LR, LOD and RSD) of the proposed DLLME–GFAAS method for the determination of Au(III) with those of some of the best previously reported methods for this purpose including spectrophotometry, using 2-carboxyl-1-naphthalthiorhodanine as reagent [32], SPE-spectrophotometry, using 5-(2-hydroxy-5-nitrophenylazo)thiorhodanine on C18 cartridge [6], FIA–FAAS, where Au is adsorbed on a 2-mercaptopyrimidine chemically modified silicagel packed microcolumn and eluted with thiourea solution [2], ETAAS-anion exchange separation, using Amberlite IRA-35 as anion-exchange resin for separation of AuCl$_4$$^-$ [3], kinetic-spectrophotometry, based on catalytic effect of gold on oxidation of methylene blue B by ammonium peroxo-disulfate [33], cathodic stripping voltametry, with an epoxy-impregnated graphite tube composite electrode modified with 2-mercaptobenzoxazole [4], neutron activation analysis incorporating substoichiometric solvent extraction of Au^{3+} with 1,2,3-benzotriazole into n-butanol [5], FI-ICP-AES, using microcolumns of Amberlyst A-26 and sulfhydryl cotton [1], CPE–FAAS, using ammonium O,O-diethyldithiophosphate and Triton X-114 as reagent and surfactant [22] and FI-CVG-AAS, based on reduction of Au^{3+} by NaBH$_4$ and flow injection into AAS in the presence of DDTC [23].

As can be seen from Table 4, LODs of the proposed DLLME–GFAAS method, with a sample volume of only 10.00 mL, is significantly improved over all the previously proposed methods. In addition, the extraction time is very short,

Table 4
Comparison of DLLME–GFAAS with previously reported methods for determination of Au(III)

Method	LOD ($\mu g\,L^{-1}$)[a]	LR ($\mu g\,L^{-1}$)[b]	RSD (%)[c]	References
Kinetic-spectrophotometric	5.5	90–2,900	2.5	[33]
Anion exchange-ETAAS	0.27	–	5.6	[3]
CPE–FAAS	0.53	0–15	2.5	[23]
Spectrophotometry	0.02	10–2,000	2.05	[32]
SPE-spectrophotometry	0.02	100–3,000	2.18	[6]
Anion exchange-NAA	0.01–0.02	–	–	[5]
FIA-FAAS	3.1	–	≤2.5	[2]
Cathodic stripping voltammetry	0.4	200–20,000	6.33	[4]
FI-CVG-AAS[d]	24	200–2,000	2	[21]
FI-ICP-AES	0.8–1.7	–	1.2–3.5	[1]
DLLME–GFAAS	0.005	0.03–0.5	4.2	This work

[a] Limit of detection.
[b] Linear range.
[c] Relative standard deviation.
[d] Flow injection-chemical vapor generation-atomic absorption spectrometry.

which indicates the fact that DLLME is a very sensitive and rapid technique that can be used for the pre-concentration and determination of Au(III) from real samples.

3.10. Analytical application

The proposed method was applied to the extraction and determination of gold in silica ore (prepared from Muteh gold mine, Isfahan, Iran), tap water and two different synthetic samples, and the results are summarized in Table 5. An accurately measured sample (0.2000 g) of the silica ore sample was dissolved in aqua regia. The solution was evaporated to near dryness, to remove the nitrogen oxides. Then, 15 mL distilled water and a few drops of concentrated hydrochloric acid were added. The solution was filtered, and the filtrate was transferred completely

Table 5
Determination of Au(III) in real samples

Sample	Added ($ng\,mL^{-1}$)	Found ($ng\,mL^{-1}$)[a]	Recovery (%)
Silica ore[b]	–	0.188 ± 0.02	
	0.1	0.283 ± 0.03	98.3
	0.2	0.380 ± 0.03	97.9
Tap water	–	–	
	0.05	0.049 ± 0.01	98.0
	0.2	0.203 ± 0.02	101.5
	0.4	0.397 ± 0.02	99.2
Synthetic sample 1[c]	0.1	0.097 ± 0.02	97.0
	0.2	0.196 ± 0.02	98.0
	0.3	0.292 ± 0.03	97.3
Synthetic sample 2[d]	0.1	0.098 ± 0.01	98.0
	0.2	0.190 ± 0.02	95.0
	0.3	0.289 ± 0.02	96.3

[a] Mean of three experiments ± standard deviation.
[b] The quantitative analysis of gold content in the silica ore sample by XRF (Geological Survey of Iran (Tehran, Iran)) and the proposed method was found to be $1.80 \pm 0.02\,\mu g\,g^{-1}$ and $1.83 \pm 0.03\,\mu g\,g^{-1}$, respectively.
[c] Synthetic sample 1 contained $200\,ng\,mL^{-1}$ of Hg^{2+}, Pd^{2+}, Ni^{2+}, Co^{2+}, Ag^+, and $100\,ng\,mL^{-1}$ of Ga^{3+}, Sb(V).
[d] Synthetic sample 2 contained $200\,ng\,mL^{-1}$ of Cu^{2+}, Zn^{2+}, Cd^{2+}, Pb^{2+}, and Cr^{3+}, $500\,ng\,mL^{-1}$ of Mg^{2+} and Ca^{2+} and $100\,ng\,mL^{-1}$ of Fe^{3+} and Mn^{2+}.

into a calibrated 200-mL volumetric flask and diluted to the mark with water. The extraction and determination of gold content was carried out following the general procedure described, and the results are given in Table 5. The gold content of the silica ore sample was also determined by XRF. As it is obvious from Table 5, there is a satisfactory agreement between the results obtained by XRF ($1.80 \pm 0.02\,\mu g\,g^{-1}$) and the proposed method ($1.83 \pm 0.03\,\mu g\,g^{-1}$).

In addition, the proposed method was also validated by the recovery studies of Au(III) from a tap water sample and two different synthetic samples and the results are also included in Table 5. As is obvious, the extraction efficiency was excellent and showed no serious matrix effects.

4. Conclusions

In this paper we introduced a DLLME–GFAAS method for the analysis of ultra trace amounts of Au(III) in real samples such as silicate ore, tap water and two different synthetic samples. The important features of DLLME method are low cost, use of minimized toxic organic solvents, simplicity of operation, rapidity, high enrichment factor and high sensitivity and selectivity. The limit of detection of the proposed DLLME–GFAAS method ($0.005\,ng\,mL^{-1}$) is significantly improved over that of some of the best previously methods for gold determination, including spectrophotometry, SPE-spectrophotometry, FIA–FAAS, ETAAS-anion exchange separation, kinetic-spectrophtometry, cathodic stripping voltametry, neutron activation analysis, FI-ICP-AES, CPE–FAAS and FI-CVG-AAS.

References

[1] M.M. Gomez, C.W. McLeod, J. Anal. At. Spectrom. 8 (1993) 461.
[2] P. Liu, Q. Pu, Q. Sun, Z. Su, J. AOAC Int. 86 (2003) 839.
[3] I. Matsubara, Y. Takeda, K. Ishida, Anal. Sci. 19 (2003) 1427.
[4] R. Ye, S. Beng Khoo, Analyst 124 (1999) 353.
[5] S. Kumar, R. Verma, S. Gangadharan, Analyst 118 (1993) 1085.
[6] Q. Hu, X. Chen, X. Yang, Z. Huang, J. Chen, G. Yang, Anal. Sci. 22 (2006) 627.
[7] X.-P. Luo, Q. Yan, H.-Q. Peng, Hydrometallurgy 82 (2006) 144.

[8] G.E.M. Hall, J.C. Pelchat, D.W. Boomer, M. Powell, J. Anal. At. Spectrom. 3 (1988) 791.

[9] M. Dominguez, E. Antico, L. Beyer, A. Aguirre, S.G. Granda, V. Salvado, Polyhedron 21 (2002) 1429.

[10] S. Martinez, A.M. Sastre, F.J. Alguacil, Hydrometallurgy 52 (1999) 63.

[11] Z. Marczenko, Separation and Spectrophotometric Determination of Elements, Ellis Hardwood, London, 1986.

[12] S. Akita, L. Yang, H. Takenchi, Hydrometallurgy 43 (1996) 37.

[13] H. Yang, Z. Zhou, M. Zhang, X. Zhang, B. Ruan, Polyhedron 10 (1991) 1025.

[14] N.R. Das, S.N. Bhattacharya, Talanta 23 (1976) 535.

[15] B.J. MacNulty, L.D. Woollard, Anal. Chim. Acta 13 (1955) 154.

[16] P.P. Kish, N.L. Shestidesyatnaya, F.F. Pitsur, Zh. Anal. Khim. 24 (1969) 1501.

[17] A.G. Fogg, C. Burgess, D.T. Burns, Analyst 95 (1970) 1012.

[18] N. Ganchev, A. Dimitrova, Mikrochim. Acta (1969) 1257.

[19] H. Liu, P.K. Dasgupta, Anal. Chem. 68 (1996) 1817.

[20] M.A. Jeannot, F.F. Cantwell, Anal. Chem. 69 (1997) 235.

[21] X. Du, S. Xu, Fresenius J. Anal. Chem. 370 (2001) 1065.

[22] M. Bagheri, M.H. Mashadizadeh, S. Razee, Talanta 60 (2003) 839.

[23] M.A.M. da Silva, V.L.A. Frescura, F.J.N. Aguilera, A.J. Curtius, J. Anal. At. Spectrom. 13 (1998) 1369.

[24] M. Rezaee, Y. Assadi, M.R. Milani Hosseini, E. Aghaee, F. Ahmadi, S. Berijani, J. Chromatogr. A 1116 (2006) 1.

[25] E. Zeini Jahromi, A. Bidari, Y. Assadi, M.R. Milani Hosseini, M.R. Jamali, Anal. Chim. Acta 585 (2007) 305.

[26] C.G. Pinto, J.L.P. Pavon, B.M. Cordero, E.R. Beato, S.S. Sanchez, J. Anal. At. Spectrom. 11 (1996) 37.

[27] W.-M. Yang, Z.-M. Ni, Spectrochim. Acta B 52 (1997) 241.

[28] O. Acar, A.R. Türker, Z. Kilic, Fresenius J. Anal. Chem. 357 (1997) 656.

[29] S. Imai, N. Hssegawe, Y. Nishiyama, Y. Hayashi, K. Satio, J. Anal. At. Spectrom. 11 (1996) 601.

[30] B. He, Z.-M. Ni, J. Anal. At. Spectrom. 11 (1996) 165.

[31] C.D. Stalikas, Trends Anal. Chem. 21 (2002) 343.

[32] Z. Chen, Z. Huang, J. Chen, J. Yin, Q. Su, G. Yang, Anal. Lett. 39 (2006) 579.

[33] S.M. Rancic, S.D. Nikolic-Mandic, L.M. Mandic, Anal. Chim. Acta 547 (2005) 144.

Determination of aflatoxins B1 and B2 using ion mobility spectrometry

Ali Sheibani, Mahmoud Tabrizchi [*,1], Hassan S. Ghaziaskar

Department of Chemistry, Isfahan University of Technology, Isfahan 84156-83111, Iran

Abstract

This paper describes total determination of aflatoxins B1 and B2 in pistachio samples using corona discharge ion mobility spectrometry (IMS). A new injection port was designed to introduce liquid samples into the IMS. Using this port, the liquid solvent (methanol) containing standard aflatoxins or an extracted sample was directly introduced into the injection port. Calibration curves resulting from experimental analyses were linear within two orders of magnitude and relative standard deviations (R.S.D.) were less than 10%. The limit of detection (LOD) was found to be 0.25 ng for both aflatoxins. Addition of ammonia as the dopant to the carrier gas improved the LOD by a factor of 2.5. Pistachio samples were analyzed to demonstrate the capability of the proposed method in detecting aflatoxins in real samples.
© 2007 Elsevier B.V. All rights reserved.

Keywords: Aflatoxin B1; Aflatoxin B2; Ion mobility spectrometry; Pistachio

1. Introduction

Aflatoxins are a family of mycotoxins produced as secondary metabolites by food spoilage fungi, particularly *Aspergillus flavus* and *A. parasiticus* growing on a variety of food products such as nuts, grains, dried fruits, and spices [1–3]. Aflatoxins (Fig. 1) are highly toxic and carcinogenic compounds that cause disease in livestock and humans. Among these, aflatoxin B1 (AFB1) is one of the most potential environmental carcinogenics [4,5].

Determination of aflatoxins in food and feed typically involves two major steps: (a) extraction or recovery of aflatoxins from the sample matrix and (b) quantitative determination of the extracted aflatoxins by various methods. The more common methods include thin-layer chromatography (TLC), high performance liquid chromatography (HPLC) with UV-absorption, fluorescence, mass spectrometry (MS), or amperometric detection systems [6–10]. Other methods used include gas chromatography (GC) with MS or electron capture detector (ECD) [11], enzyme-linked immunosorbent assay (ELISA) [12], and supercritical fluid chromatography (SFC)

with flame ionization or MS detector [13]. In addition to these, there is nowadays an increasing demand for rapid and reliable methods to determine mycotoxins in food and feed. The objective of the present study was to investigate the capability of ion mobility spectrometry (IMS) in quantitative determination of trace levels of aflatoxins in pistachio.

Ion mobility spectrometry is basically a gas-phase ion separation technique which has gained widespread acceptance in many applications for detecting contaminants thanks to its excellent sensitivity and fast operation. A full description of the method is given in several books and review articles [14–18]. Its main advantages include low detection limit, fast response, simplicity, portability, and relatively low cost. The technique is similar to time of flight mass spectrometry except that it operates under atmospheric pressure. A broad range of compounds such as explosives [19], narcotics [20], herbicides [21], pesticides [22], and drugs of abuse [23] have been detected by IMS. Various atmospheric pressure ionization sources including ^{63}Ni radioactive source [14], UV ionization [24], and corona discharge (CD) [25–28] have been used for ionization in IMS. Corona discharge has proved to be a reliable ionization source in IMS and is currently used in detecting many compounds. The main advantages of the corona discharge ionization source are simplicity and increased signal-to-noise ratio, which results in a higher sensitivity and a longer dynamic range. In the present study, corona discharge is used for ionization of aflatoxins in

---

* Corresponding author. Tel.: +98 311 3913272; fax: +98 311 3912350.
E-mail address: m-tabriz@cc.iut.ac.ir (M. Tabrizchi).

[1] Regular Associate of the Abdus Salam ICTP.

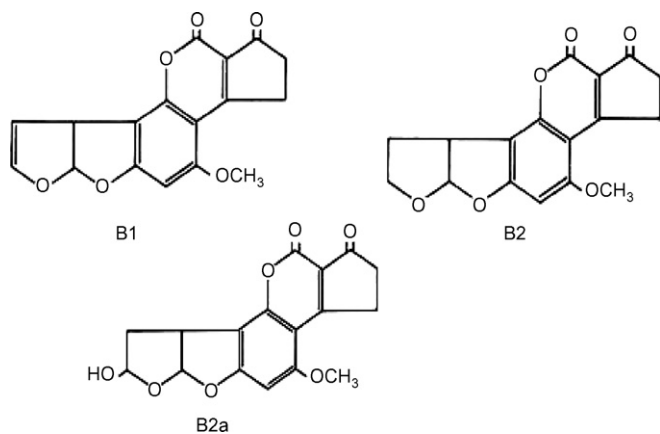Fig. 1. Chemical structures of aflatoxin B1, B2 and B2a.

Table 1
The optimized experimental conditions for aflatoxins

Parameter	Setting
Length of drift tube	11 (cm)
Drift field	500 (V cm^{-1})
Corona voltage	2000 (V)
Flow of drift gas (N$_2$)	600 (mL min^{-1})
Flow of carrier gas (N$_2$)	300 (mL min^{-1})
Doping gas	NH$_3$
Flow rate of doping gas	20 (mL h^{-1})
Injection port temperature	230 (°C)
IMS cell temperature	170 (°C)
Pressure	630 (Torr)
Typical shutter grid pulse width	100 (µs)

IMS. Furthermore, the sample introduction system is improved to allow for direct injection of liquid samples into IMS.

2. Experimental

2.1. Instrumentation

The IMS used in this study was constructed in our laboratory at Isfahan University of Technology. An IMS cell (installed in an oven), a needle for producing the corona, two high voltage power supplies, a pulse generator, an analog to digital converter, and a computer to record spectra comprised the main components of the instrument. A detailed description of the instrument and its corona discharge ionization source can be found in Ref. [26].

A new injection port was designed to allow for introduction of liquid samples into the IMS. This injection port consisted of an aluminum tube connected to a T-shape swagelock fitting heated up to 250 °C. The carrier gas flowed through the port at a flow rate of 300 mL min^{-1}. The tube was filled with steel wool to facilitate the evaporation of the liquid. This design prevents the sample from reaching the IMS cell in liquid form. Meanwhile, the evaporation process is fast enough to create a short and intense plume of the analyte vapor entering into the IMS cell, resulting in higher sensitivity levels. This new injection port is capable of introducing up to 20 µL of liquid solvent such as methanol in each run.

Ammonia was doped into the carrier gas in order to evaluate the effect of ammonia on the determination of aflatoxins. A small cap vessel filled with ammonium carbonate was connected to the carrier gas via a capillary tube while a syringe pump (Genie-Kent Scientific Corporation, USA) was used to pump air into the vessel at a flow rate ranging between 1 and 30 mL h^{-1} (Fig. 2). Solid ammonium carbonate is in equilibrium with the gaseous ammonia with a vapor pressure of 188 hPa at 20 °C [29]. This method ensures continuous introduction of a constant amount of ammonia into the carrier gas. The drift and the carrier gases were both filtered with a 13× molecular sieve trap. A unidirectional gas flow system was used in this experiment. Table 1 presents the optimized experimental conditions for obtaining ion mobility spectra of aflatoxins. A UV–vis spectrophotometer (Jasco, Model V-570, Japan) was used to verify the concentration of aflatoxin standard solutions.

2.2. Materials and chemicals

Pistachio samples (*Pistachia Vera* L.) were obtained from Institute of Standards and Industrial Research of Iran Rafsanjan Branch. The samples were ground, passed through a mesh 16 sieve, and stored in sealed bags in the refrigerator. Methanol, chloroform, acetone, and *n*-hexane were used as solvents in HPLC grade quality (Merck, Darmstadt, Germany). Aflatoxin standards (AFB1, AFB2, and AFB2a) were purchased from Sigma (St. Louis, MO, USA). Stock standard solutions of
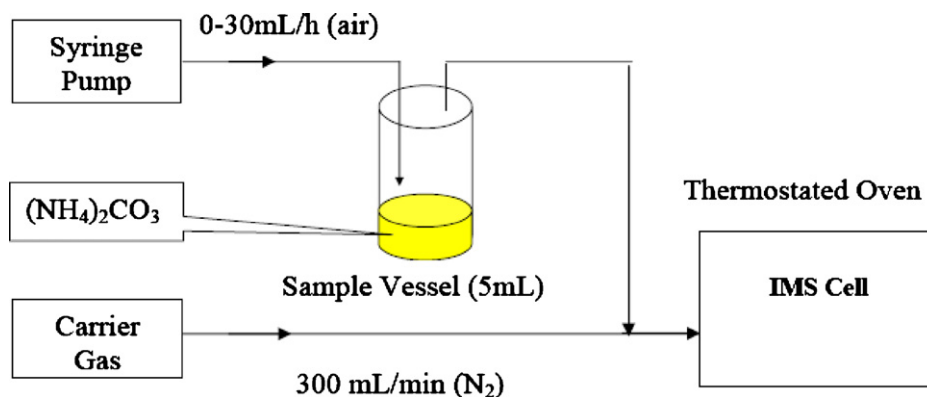

Fig. 2. Schematic diagram of the ammonia doping system.

aflatoxins were prepared at concentrations of 8–10 ($\mu g\,mL^{-1}$) by dissolving solid standards in methanol. The concentrations of aflatoxin standard solutions were verified using a UV–vis absorption spectrophotometer as recommended by AOAC [30]. Working standard solutions of AFB1 and AFB2 were prepared by diluting the stock standard solutions and stored at temperatures below 5 °C for the experiments. Pre-coated silica gel 60 TLC aluminum plates with the dimensions 5 cm × 10 cm, were obtained from Merck (Darmstadt, Germany). Immunoaffinity columns (IAC AflaTest), used for cleanup of the sample in some experiments was purchased from Vicam (USA).

2.3. The extraction procedure of aflatoxins

Extraction of aflatoxins from pistachio and the cleanup procedures were performed according to the AOAC method [31]. Ground pistachio samples (50 g) were mixed with 2.5 g NaCl, 200 mL of 80% (v/v) solution of methanol in water, 100 mL of *n*-hexane and blended in a blender for 5 min. 100 mL of the slurry solution was then centrifuged to remove the fat content extracted into the upper phase. After filtration, 25 mL of the lower phase was shaken for 1 min in 25 mL of chloroform in a separatory funnel. Finally, the chloroform phase was separated and evaporated to dryness at 50 °C. The extracted aflatoxins were then redissolved in 200 μL of methanol. Finally, 5 μL of this solution was introduced into the injection port of the IMS.

2.4. Identification and detection by UV-lamp

In order to verify the presence of aflatoxins in the real sample by a method other than the IMS, 5 μL of the final solution, described in Section 2.3, was spotted on a TLC plate with the dimensions 5 cm × 10 cm, together with the prepared standards. The aflatoxins were separated on the plate using chloroform–acetone (90:10) as the development solvent. The identification and detection of the separated aflatoxins were performed by comparing their R_f values with those of the standard aflatoxins using a UV-lamp at 366 nm. At this wavelength, AFB1 and AFB2 show a blue fluorescence light [32].

3. Results and discussion

3.1. Improvement of the sample introduction system

A reliable and replicable quantitative determination by IMS relies on using a proper sample introduction technique. Gas samples as well as the headspace of the liquid samples can be introduced directly into the IMS after proper dilution of the samples. These techniques are usually precise and repeatable since a specified small amount of the sample can be introduced in each run. For solid samples with low vapor pressure, however, it is not possible to introduce a known small amount of the solid directly into the IMS. The procedure commonly used in these cases involves dissolving the solid in a solvent followed by introducing a fraction of the solution on a probe, and then allowing the solvent to evaporate. Using this procedure, a small amount of the

solid sample is deposited on the probe, which is later inserted into the IMS injection port. The deposited material is then evaporated by heating the probe. There are a number of drawbacks associated with this method. One such problem is that a portion of the material in the solvent is lost in the solvent evaporation stage. This will increase the detection limit and decrease the potential for repeating the measurement. Another issue of concern is that complete solvent evaporation can be time-consuming. Furthermore, the initial temperature of the solid probe affects the evaporation rate of the deposited sample. This seems to be the main cause for the poor repeatability of the method.

For the purposes of our study, we improved the sample introduction system in a manner that the sample solutions could be introduced in the liquid form using a micro syringe directly into the injection port, as described in the experimental section. This technique does not require a solvent evaporation step prior to injection; hence, no material losses during the preparation step. Moreover, the initial temperature of the liquid is always the same for each injection. These provisions lead to improved measurement repeatability, enhanced sensitivity, and increased speed of analysis.

The operating temperature of the injection port must, obviously, be higher than the solvent boiling point. The solvent must also possess a lower proton affinity than the analyte (in the positive mode of operation) to allow ionization of the analyte in the presence of large amounts of the solvent. Additionally, the solvent must be pure enough to show a clean spectrum for the blank. Methanol (i.e., HPLC grade) and distilled water proved satisfactory solvents in meeting all these requirements. Additionally, the temperature of the IMS cell needs to be high enough to avoid solvent condensation inside the cell. This high temperature also helps ions and solvent molecules decluster, resulting in a better resolution [33]. The appropriate operating temperature for aflatoxins was found to be above 160 °C. In practice, when 10 μL of methanol was injected into the port, the corona discharge was shortly disturbed. This was monitored through a quick change in the baseline of the spectrum that was then quickly stabilized after injection.

3.2. Ion mobility spectra

The ion mobility spectrum of AFB1, shown in Fig. 3, was obtained under optimized experimental conditions, as given in Table 1. The spectrum shows only one peak at 13.17 ms which is much longer than that of reactant ion peaks within the range 4–5.2 ms. The reactant ions consist of water clusters of NH_4^+, NO^+, and H_3O^+. The chemical formula of the product ions originating from AFB1 cannot be fully characterized without mass spectrometer coupled to the IMS. However, due to its structure (Fig. 1), aflatoxin is expected to be easily protonated. Since no other peaks were observed at shorter drift times, no fragmentation was assumed to have taken place. The drift time of the peak is long enough (~3 times that of the reactant ion) to attribute the peak to a heavy ion such as protonated aflatoxin ($M = 313$).

AFB2 also gave the same spectrum as AFB1, i.e., a single peak at a drift time identical to that for AFB1. This was expected because of their similar chemical structures (Fig. 1) and their
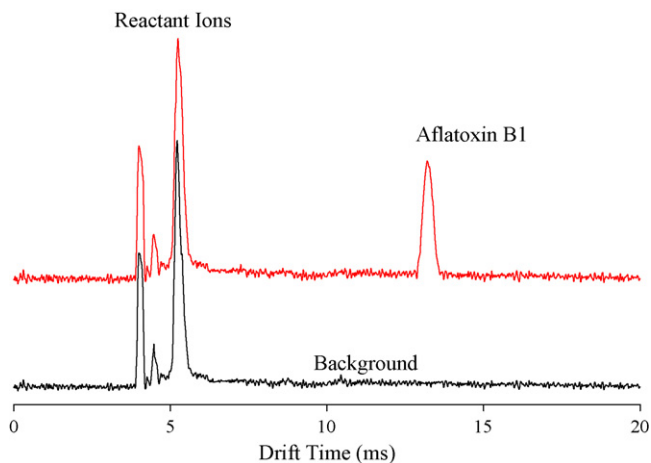
Fig. 3. An example of ion mobility spectrum obtained for AFB1 (4 ng) as well as the background spectrum. AFB2 also gave the same spectrum.

very close molecular weights (312 and 314). Moreover, AFB2a (Fig. 1), that is a hemiacetal form of AFB1 with a molecular weight of 330, gave a similar spectrum. In conclusion, IMS does not distinguish between AFB1 and AFB2 or AFB2a. Therefore, a separation step prior to IMS is required if AFB1 and AFB2 need to be determined individually. In our experiments, we measured the total AFBs due to their identical response factors in the IMS as described below.

3.3. The effect of NH_3 as dopant

Dominant reactant ions produced in the corona discharge are hydrated protons, $H^+(H_2O)_n$. However, other ions including $NH_4^+(H_2O)_n$ and $NO^+(H_2O)_2$, where n takes values from 1 to 10, are also observed [14]. A doping material is usually added to the carrier or to the drift gas to enhance selectivity and sensitivity in the IMS. For example, by doping the system with ammonia, $NH_4^+(H_2O)_n$, reactant ions are formed that selectively ionize the compound with a higher proton affinity than ammonia [18]. It was observed that NH_4^+ not only ionized the aflatoxins but also enhanced the sensitivity level. This is shown
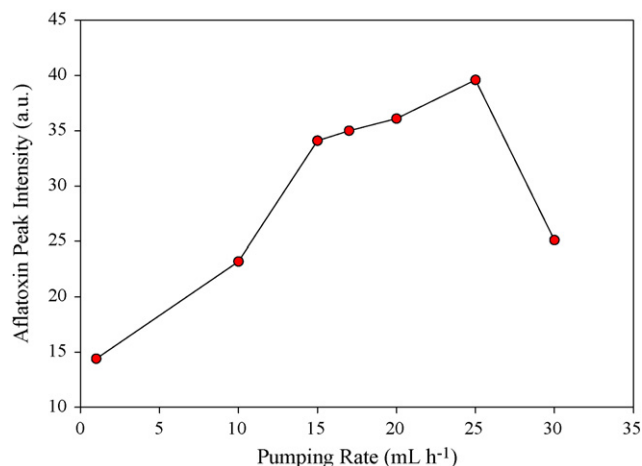

Fig. 4. The response of the corona discharge IMS for AFB1 versus the pumping rate of NH_3 vapor, introduced into the carrier gas.
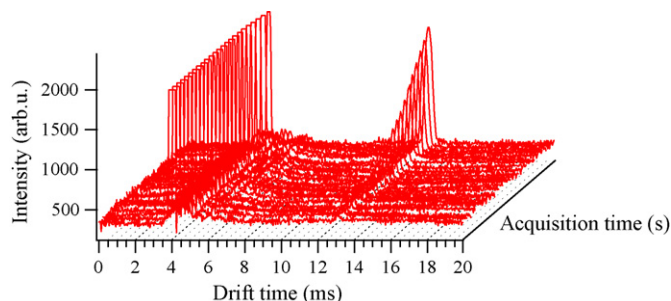

Fig. 5. A 3D plot of the ion mobility spectra of AFB1.

in Fig. 4 where the intensity of AFB1 peak is plotted versus pumping rate of ammonia. The signal intensity increases in the presence of ammonia and exhibits its maximum level within the $15–25\,\mathrm{mL\,h^{-1}}$ range corresponding to ~50–80 ppm of ammonia in the ionization region. At higher concentrations, the intensity decreases probably due to the competition between ammonia and the analyte for proton attachment.

3.4. Calibration curves for AFB1 and AFB2

Different volumes of the standard solutions (described in Section 2.2) were injected into the IMS port. The aflatoxin peak appeared after a short time, reached its maximum level, and decayed exponentially, as shown by the 3D plot in Fig. 5. The height of the analyte peak was integrated over the acquisition time and taken as the response of the IMS to the analyte. The calibration curve for the analyte was then obtained by plotting the response against analyte quantity.

The calibration curves for AFB1 and AFB2 were obtained under two different conditions: with and without NH_3 as a dopant gas. As seen in Fig. 6, different calibration curves obtained for AFB1 with and without the dopant.

The linear dynamic ranges (LDR) for the analyte are 1.0–10 and 2.0–70 ng, with and without dopant, respectively. Clearly, the sensitivity has increased in the presence of the dopant (Fig. 6). The relative standard deviation (R.S.D.) for 5 times measurement of a 4 ng solution of aflatoxin was found to be below 10%.
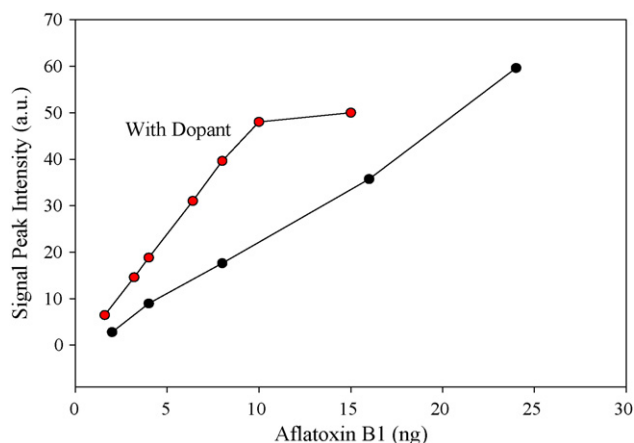

Fig. 6. Calibration curve for AFB1, with and without ammonia as a dopant gas.

Table 2
The analytical parameters for the determination of AFB1

Parameters	With NH$_3$	Without NH$_3$
Formula	$Y = -2 + 5.18X$	$Y = 1.71 + 2.16X$
R^2	0.9942	0.9998
LDR (ng)	1–10	2–70
LOD (ng)	0.1	0.25
R.S.D. (%)	10	

Table 3
Statistical results for the slope comparison of the calibration curves

Curve	Slope ± S.D.	F_{exp}	F_{table}	±ts
AFB1	2.16 ± 0.07	1.66	7.14	±0.18
AFB2	2.18 ± 0.09	1.66	7.14	±0.24

The LOD was obtained using the equation LOD = $3S_b/m$, where S_b is the standard deviation of the height of the blank spectrum at the drift time similar to that of the analyte, and m is the slope of the calibration curve. LODs were 0.1, and 0.25 ng for aflatoxin under the above-mentioned two conditions, respectively.

The calibration curve for AFB2 was obtained in a manner similar to that for AFB1. The results were almost similar to those of AFB1 curves. The analytical parameters of the corona discharge IMS method for the determination of AFB1 are presented in Table 2.

As mentioned above, the product ions of AFB1 and AFB2 appear at identical drift time so that their peaks completely overlap. The slopes on their calibration curves are also very close to each other. Statistical calculations, given in Table 3, show that the slight difference in the slopes is due to the experimental random error (with a confidence limit of 95%). This means that IMS yields identical response factors to both AFB1 and AFB2. It is, therefore, possible to determine AFB1 and AFB2 as total AFB.
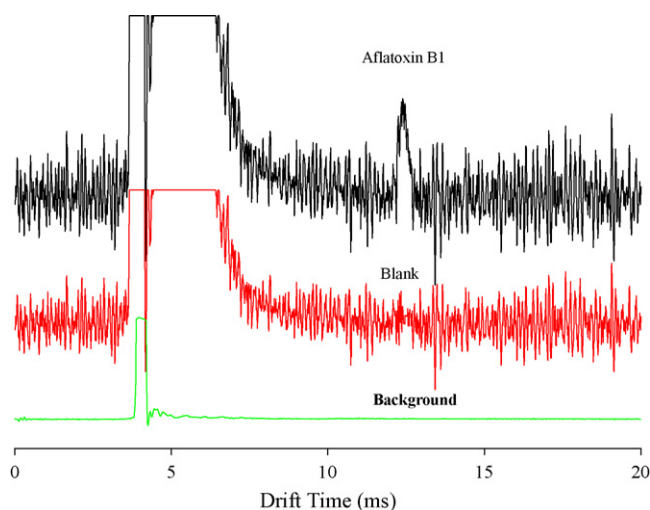

Fig. 7. The ion mobility spectra of background with ammonia dopant, blank (the extracted stuff from non-contaminated pistachio sample), and after addition of 1.0 ng of AFB1 to the blank. The sensitivity for the blank and aflatoxin was enhanced.
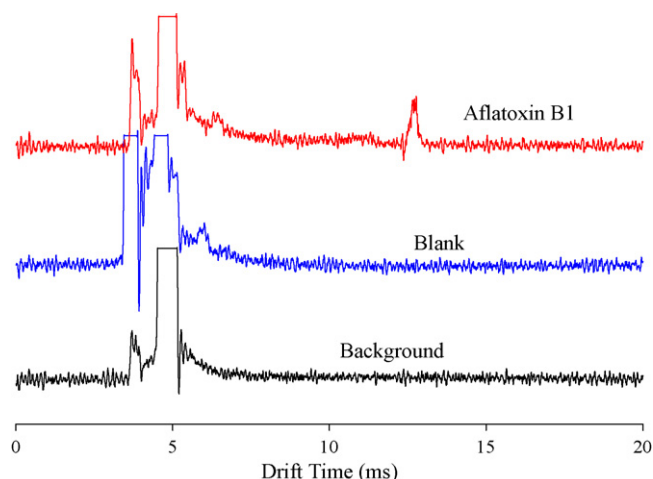

Fig. 8. The ion mobility spectra of background, blank, and after addition of 0.5 ng of AFB1 to the blank using an immunoaffinity column in cleanup step.

3.5. Analysis of real samples

Aflatoxins were extracted from pistachio samples using the AOAC method (Section 2.3). 5 µl of the extracted aflatoxins (redissolved in 200 µl methanol) was injected into the IMS. The blank spectrum obtained for the pistachio sample is shown in Fig. 7, where it is compared with the background spectrum. Clearly, the blank spectrum shows additional intense peaks of around 5–8 ms due to unidentified substances surviving through the extraction and the cleanup steps. However, spiking aflatoxin to the extracted sample caused the aflatoxin peak to appear well-separated from the unwanted peaks, as depicted in Fig. 7. This means that the aflatoxins are detectable in pistachio in spite of their complicated matrix. The limit of quantification (LOQ) was determined by successive standard additions until the analyte

Table 4
Comparison of the limit of detection (LOD), limit of quantification (LOQ), and linear dynamic range (LDR) for different methods as well as IMS for analysis of aflatoxins

Method	LOD (ng)	LOQ (ng)	LDR (ng)
Liquid chromatography–tandem mass spectrometry [35]	10	25	10–600
Atmospheric pressure photo-ionization liquid chromatography–mass spectrometric [36]	0.11–0.5 (ng g^{-1})	–	–
MALDI-TOF mass spectrometry [37]	~0.5 (pg)	–	–
HPLC with fluorescence detection [38]	3.5 (ng g^{-1})	4 (ng g^{-1})	4–20 (ng g^{-1})
HPLC with amperometric detection [39]	7–10		
Densitometric scanning of the developed TLC plate [40]	1.2–1.7	1.9–2.8	1–9[a]
Overpressure—Layer chromatography [41]	0.018–0.15	0.27–0.36	1–10
This work (IMS)	0.1	0.5	1–10

[a] Aflatoxin B1 concentrations per spot on TLC plate.

peak was measurable. The LOQ was found to be about 1.0 ng as injected into IMS.

The detection limit is further lowered if the matrix effect is eliminated. One way to achieve this is to use immunoaffinity columns in the cleanup step in order to eliminate unwanted substances from the extracted aflatoxin. This results in more efficient ionization of aflatoxin and enhanced the sensitivity. Clean up with immunoaffinity columns was performed according to the procedure described in Ref. [34]. The results are demonstrated in Fig. 8. Comparison of Figs. 7 and 8 shows that the unwanted substances, co-extracted with aflatoxins, have been efficiently removed by the use of immunoaffinity column. Furthermore, the LOQ was reduced to 0.5 ng which is half of the value obtained without immunoaffinity column.

The LOD, LOQ and LDR obtained in this work lies within the range of those reported in the literature, given in Table 4 [35–41].

4. Conclusion

The present work demonstrates the capability of positive corona discharge ion mobility spectrometry for determination of total AFB1 and AFB2 in real samples at an acceptable detection limit. Although other methods possibly yield lower detection limits, they can generally be time-consuming due to such factors as the requirement to convert aflatoxins to more intense fluorescent derivatives [39]. Fast response, low cost, and portability of the IMS make it competitive with other low detection limit techniques.

Another facet of our study involves direct introduction of the liquid solution into the corona discharge ionization region of an IMS. This is a promising practice for future projects such as coupling HPLC or LC to an IMS without using electrospray ionization. The combination of the separation power of HPLC with the detection capability of IMS can be an excellent tool for many analytical purposes.

References

[1] J. Stroka, R.V. Otterdijk, E. Anklam, J. Chromatogr. A 904 (2000) 251.
[2] M.J. Sweeney, A.D.W. Dobson, Int. J. Food Microbiol. 43 (1998) 141.
[3] I.Y.S. Rustom, Food Chem. 59 (1997) 57.
[4] H.S. Hussein, J.M. Brasel, Toxicology 167 (2001) 101.
[5] M. Peraica, B. Radić, A. Lucić, M. Pavlovic, B. World Health Organ. 77 (1999) 754.
[6] S. Taguchi, S. Fukushima, T. Summoto, S. Yoshida, T. Nishmune, J. AOAC Int. 78 (1995) 325.
[7] T. Panalaks, P.M. Scott, J. AOAC 60 (1976) 583.
[8] W.T. Kok, T.C.H. Van Neer, W.A. Traag, L.G.M.T. Tunistra, J. Chromatogr. 363 (1998) 23.
[9] J. Gilbert, E.A. Vargas, J. Toxicol. 22 (2003) 381.
[10] M. Aghamohammadi, J. Hashemi, G. Asadi Kram, N. Alizadeh, Anal. Chim. Acta 582 (2007) 288.
[11] P.M. Scott, Trends Anal. Chem. 12 (1993) 373.
[12] S. Li, R.R. Marquardt, D. Abramson, J. Food Protect. 63 (2000) 281.
[13] H.T. Kalinosk, H.R. Udseth, B.W. Wright, R.D. Smith, Anal. Chem. 58 (1986) 2421.
[14] G.A. Eiceman, Z. Karpas, Ion Mobility Spectrometry, CRC Press, Boca Raton, FL, 2005.
[15] F.W. Karasek, Res. Dev. 21 (1970) 34.
[16] T.W. Carr, Plasma Chromatography, Plenum Press, New York, 1984.
[17] G.A. Eiceman, Crit. Rev. Anal. Chem. 22 (1991) 17.
[18] C.S. Creaser, J.R. Griffiths, C.J. Bramwell, S. Noreen, C.A. Hill, C.L.P. Thomas, Analyst 129 (2004) 984.
[19] T. Khayamian, M. Tabrizchi, M.T. Jafari, Talanta 59 (2003) 327.
[20] T. Khyamian, M. Tabrizchi, M.T. Jafari, Talanta 69 (2006) 795.
[21] B.H. Clowers, W.E. Steiner, H.M. Dion, L.M. Matz, M. Tam, E.E. Tarver, H.H. Hill, Field Anal. Chem. Technol. 6 (2002) 302.
[22] K. Tuovinen, H. Paakkanen, O. Hänninen, Anal. Chim. Acta 404 (2000) 7.
[23] T. Keller, A. Miki, P. Regenscheit, R. Dirnhofer, A. Schneider, H. Tsuchi-hashi, Forensic Sci. Int. 94 (1998) 55.
[24] J.I. Baumbach, S. Sielemann, Z. Xie, H. Schmidt, Anal. Chem. 75 (2003) 1483.
[25] J. Stach, J. Adler, M. Brodacki, H.R. Döring, Proceedings of the Third International Workshop on Ion Mobility Spectrometry, vol. 71, 1995.
[26] M. Tabrizchi, T. Khayamian, N. Taj, Rev. Sci. Instrum. 71 (2000) 2321.
[27] H. Borsdorf, H. Schelhorn, J. Flachowsky, H.R. DÖring, J. Stach, Anal. Chim. Acta 403 (2000) 235.
[28] H. Borsdorf, A. Rämmler, J. Chromatogr. A 1072 (2005) 45.
[29] Chemicals Reagents, Merck, 2002, p. 65.
[30] AOAC Official Method 970.44, 1995.
[31] AOAC Official Method 968.22, 1988.
[32] L.D. Castro, E.A. Vargas, Ciênc. Technol. Aliment. 21 (2001) 115.
[33] M. Tabrizchi, Talanta 62 (2004) 65.
[34] S.M. Pearson, A.A.G. Candlish, K.E. Aidoo, J.E. Smith, Biotech. Tech. 13 (1999) 97.
[35] M. Ventura, A. Gómez, I. Anaya, J. Díaz, F. Broto, M. Agut, L. Comellas, J. Chromatogr. A 1048 (2004) 25.
[36] M. Takino, T. Tanaka, K. Yamaguchi, T. Nakahara, Food Addit. Contam. 21 (2004) 76.
[37] R.R. Catharino, L.D.A. Marques, L.S. Santos, A.S. Baptista, E.M. Gloria, M.A. Calori-Domingues, E.M.P. Facco, M.N. Eberlin, Anal. Chem. 77 (2005) 8155.
[38] S.M. Braga, F.D. Medeiros, E.J. Oliveira, R.O. Macedo, Phytochem. Anal. 16 (2005) 267.
[39] M.P. Elizalde-González, J. Mattusch, R. Wennrich, J. Chromatogr. A 828 (1998) 436.
[40] J. Stroka, E. Anklam, J. Chromatogr. A 904 (2000) 263.
[41] E. Papp, K. H-Otta, G. Záray, E. Mincsovics, Microchem. J. 73 (2002) 39.

Talanta

Review

Antimony in the environment as a global pollutant: A review on analytical methodologies for its determination in atmospheric aerosols

Patricia Smichowski [a,b,*]

[a] *Comisión Nacional de Energía Atómica, Gerencia Química, Av. Gral. Paz 1499, B1650KNA-San Martín, Pcia de Buenos Aires, Argentina*
[b] *Consejo Nacional de Investigaciones Científicas y Técnicas (CONICET), Argentina*

Abstract

This review summarizes and discusses the research carried out on the determination of antimony and its predominant chemical species in atmospheric aerosols. Environmental matrices such as airborne particulate matter, fly ash and volcanic ash present a number of complex analytical challenges as very sensitive analytical techniques and highly selective separation methodologies for speciation studies. Given the diversity of instrumental approaches and methodologies employed for the determination of antimony and its species in environmental matrices, the objective of this review is to briefly discuss the most relevant findings reported in the last years for this remarkable element and to identify the future needs and trends. The survey includes 92 references and covers principally the literature published over the last decade.
© 2007 Elsevier B.V. All rights reserved.

Keywords: Antimony; Analytical techniques; Speciation; Airborne particulate matter; Ashes

Contents

1. Introduction

Antimony is a fascinating element that has been used by human cultures since the Early Bronze Age. Excavations at Tello in Ancient Chaldea found fragments of an antimony base that dates back to 4000 B.C. Different documents testify that alchemists and quacks have used antimony compounds in medicine, veterinary and cosmetics. It is impressive that this metalloid was prescribed in the past as the universal remedy for syphilis, chest pains, the plague, melancholy and especially for fever [1]. Antimony, together with lead, was used in the Roman Period producing a long history of contamination of waters, sediments and soils. Around 1990 the uses and applications of Sb expanded in scope and it was mainly used for making alloys, pigment, paints, pharmaceutical preparations (tartar emetic, quinine antimonite), as opacifying agent for enamels (antimony oxide and sodium antimonite), glazing for pottery and tiles (Naples yellow), colouring matter for paper and cloth and for vulcanizing rubber (antimony pentasulfide) [1]. Modern uses of Sb include: catalyst in the manufacture of PET (polyethylene terephthalate), component of brake linings (as S_3Sb_2), cable covering, ammunitions and bearings as well as flame retardant in adhesives, papers, rubber and textiles. Natural sources are also responsible for Sb emissions into the environment. Hinkley et al. [2] reported that about 5 tonnes year^{-1} are released to the atmosphere by volcanoes. According to Shotyk et al. [3] volcanic emission appears to account for only 3–5% of Sb global emission. Rock weathering and soil runoff have been identified as other natural sources. For these reasons, a large amount of Sb-containing compounds is released annually into the environment where a considerable interconversion of Sb compounds by chemical and biological action can occur.

Antimony is potentially toxic at very low concentrations and has no known biological functions. Elemental Sb is more toxic than its salts and inorganic species of Sb are more toxic than the organic ones. Sb(III) compounds are about 10 times more toxic than Sb(V) species. The International Agency for Research on Cancer (IARC) has reported that there is sufficient evidence for the carcinogenicity of antimony trioxide in experimental animals [4]. On the other hand, the U.S. Environmental Protection Agency and the German Research Community have listed Sb as a prioritary pollutant but it has not been classified for carcinogenicity [5,6]. In contrast to As, there is evidence that Sb is not detoxified via methylation in mammals, but the mechanism responsible for the antimony's genotoxicity is not clearly known.

Daily intake of inhaled Sb from ambient air is approximately 0.6 µg assuming a volume of 20 m^3 of air to be inhaled daily on average [7]. The absorption from lungs is in average ∼15% depending on the size of the particles and the solubility of the specific Sb compounds. Children bellow 5 years of age have a higher air intake per unit and may absorb a higher percentage of inhaled metals [7].

At present, many research groups invest time and resources to study Sb under different aspects including its determination in environmental matrices. The state-of-the art of analytical methods for Sb speciation in waters at trace and ultratrace levels was reported by Smichowski et al. [8]. A critical review of the various techniques and methodologies employed for the determination of Sb in terrestrial environment samples was presented by Nash et al. [9]. Burguera and his group have developed different analytical techniques for the determination and speciation analysis of Sb in biological fluids, tissues and pharmaceuticals [10–12]. Shotyk et al. [13] presented a comprehensive review covering different aspects of the anthropogenic impacts on the biogeochemistry and cycling of antimony. Special attention was paid to atmospheric emissions of Sb to the environment and its occurrence in the atmosphere, soils, sediments, plants and waters. The solution chemistry of this element was thoroughly reviewed by Filella et al. [14,15]. Recently, the role of atomic spectrometry techniques applied to the determination of chemical elements in atmospheric aerosols was reviewed by Smichowski et al. [16]. This landscape evidences that atmospheric emissions of Sb to the environment require more attention.

In spite of all above described, exists a gap in our knowledge of some aspects of antimony such as its direct input and subsequent integration into the environment's biogeochemical cycle. These aspects have been far less studied in comparison with other elements such as As, Cr, Hg and Pb and only few groups have focused to study aspects related to Sb in atmospheric aerosols.

What I did perceive today is that the scientific community has put more attention on this metalloid in recent years and that many chemical disciplines have been inter-worked to deeply study different methodologies for Sb determination. It is not by chance that in 2005 the Institute of Environment Geochemistry at the University of Heidelberg has organized and hosted the First International Workshop on Antimony in the Environment, attended by participants from 20 countries [17].

The atmosphere is an important vector of global element transport between regions and as a consequence population

is exposed to metals and metalloids in airborne particles that often are well above natural background levels. Antimony is part of the atmospheric pollutants and its determination in the total air particulate as well as in the corresponding inhalable fractions represents an important parameter in evaluating the possible implications onto the public health. One of the most crucial properties of metals, which differentiate them from other pollutants with a certain degree of toxicity, is that they are not biodegradable in the environment [18].

The purpose of this review is to summarize the research done in the last decade as regards the quantification of Sb in atmospheric aerosols by means of different analytical techniques, their environmental implications, the progress made so far in this field and the problems met. As a consequence of the low concentrations (μg m^{-3} down to ng m^{-3}) of Sb in airborne particulate matter (APM) and related matrices, analytical approaches fit for their reliable determination are mandatory.

The growth in the number of sophisticated techniques and experimental approaches and the mounting awareness that Sb determination in atmospheric aerosols is contributing significantly to environmental sciences is well reflected by the papers and chapter of books that have become available in recent years. For this reason, it is obviously impracticable to cite even briefly all the contributions on Sb determination in atmospheric aerosols that enriched the relevant literature to date. Hence, only a few selected representative contributions published mainly over the last decade in this field are reported.

2. Antimony in environmental matrices: general considerations

The problematic of total Sb determination and its speciation analysis in environmental matrices can be summarized as follows:

(i) Low concentrations: in unpolluted environments Sb was detected at trace and ultratrace levels ranging from $0.2 \,\mu$g L^{-1} (natural waters) to $1.0 \,\mu$g g^{-1} (soils) [19]. In atmospheric aerosols, from natural and anthropogenic emission, Sb is found at ng m^{-3} levels.

(ii) The extraction efficiencies of inorganic and organic Sb compounds from environmental and biological matrices is low.

(iii) Lack of stability of Sb compounds during the overall analytical process (sampling, extraction, separation, determination).

(iv) Lack of appropriate Sb standards to identify individual species that have been separated and measured in extracts of soils, APM and sewage sludges.

(v) Necessity of more adequate matrix-matched reference materials with certified concentrations for total Sb determination.

(vi) No certified reference materials are available for species.

3. Analytical methods for antimony determination

3.1. Total antimony determination

Numerous analytical techniques and experimental approaches have been proposed in the last two decades to identify and measure Sb aimed at obtaining reliable results and correct evaluations in the field of environmental chemistry. Environment assessment is benefiting from developments of innovative analytical methodologies where atomic spectrometric techniques are important tools for element determination. The outstanding developments undergone by these techniques over the last years have marked a parallel and irreversible progress in the exploitation of such techniques for environmental purposes from the viewpoint of research activities, routine analysis and regulatory tasks.

Atomic spectrometric methods based on flame atomic absorption spectrometry (FAAS), electrothermal atomic absorption spectrometry (ETAAS), atomic fluorescence spectrometry (AFS) and plasma-based techniques, namely inductively coupled plasma optical emission spectrometry (ICP OES) and inductively coupled plasma-mass spectrometry (ICP-MS) have been extensively used to determine Sb in different kind of samples. Notwithstanding an impressive number of analytical advantages of plasma-based techniques, their detection power is sometimes inadequate to comply with the requirements posed by the determination of very low levels of Sb in environmental samples. This fact is more severe for ICP OES. In this context, on-line preconcentration methods using specific sorbents and biosorbents have been extensively used for Sb determination [20–25]. Difficulties may also result from high matrix ion concentrations and subsequent analytical interferences. In these cases, preconcentration and/or separation of Sb from the matrix results mandatory. These methods also include solvent extraction [26] and selective adsorption [27].

The introduction of Sb as a gas into a spectroscopic source has converted in a useful tool to minimize considerably the extent of problems associated to matrix interferences and has considerably improved the sensitivity of measurements. In addition and when plasma-based techniques are used for detection, gaseous sample introduction promotes more efficient atomization, excitation and ionization of the analyte. For this reason, hydride generation combined with a diversity of atomic and plasma-based techniques has become a method of choice for the determination of Sb at trace and ultra-trace levels. In spite of the known advantages, HG is affected by different kind of interferences in the liquid and gaseous phase. To alleviate or solve this drawback, the physical and chemical generation conditions have to be carefully optimized or the use of complexing or masking agents has to be considered.

With the aid of trapping systems (e.g., cold traps) in conjunction with hydride generation of Sb, as stibine, is separated from the matrix and preconcentrated with a significant improvement of the detection limit. In a comprehensive study, Andreae et al. [28] determined Sb(III), Sb(V) and methylantimony species namely, methylstibonic and dimethylstibinic acids in aqueous solutions by HG-AAS. The gaseous forms of Sb were

collected on a liquid nitrogen-cooled trap and separated chromatographically after heating the trap. Detection limits from 0.3 to 0.6 ng L^{-1} were achieved for 100 mL of sample in a batch system. This was the first report on the presence of methylantimony compounds in nature.

More recently, Kratzer and Dědina studied a simple and very sensitive method for Sb preconcentration and determination based on the in situ trapping of stibine in an externally heated quartz tube atomizer [29]. Using a collection time of 300 s and a sample volume of 20 mL a detection limit as low as 2.8 pg mL^{-1} was reached.

Atomic fluorescence spectroscopy coupled to HG has received increasing attention because its suitability for Sb determination at trace levels due to its high sensitivity, wide dynamic range (4–6 orders of magnitude), simplicity and very low instrumental cost [30–32]. The limits of detection achieved for Sb are comparable to those reported for ICP-MS. The main advantage of fluorescence detection compared to adsorption measurements is the greater sensitivity achievable because the fluorescence signal has a very low background.

Less common techniques, used along or combined with preconcentration or hydride generation steps, for total Sb determination in different kind of matrices include: microwave induced plasma-atomic emission spectrometry (MIP-AES) [33], neutron activation analysis (NAA) [34], X-ray fluorescence spectrometry (XRF) [35], laser induced fluorescence [36] and electroanalytical techniques such as anodic stripping voltammetry (ASV), cathodic stripping voltammetry (CSV), differential pulse polarography (DPP) [37–39].

Important progress in atomic spectrometric techniques has been achieved owing to improvements in instrumentation as well as to the use of new methodologies for sample preparation. The widespread use of flow injection facilities, slurry sampling, miniaturization and automation of procedures has played an important role to increase sensitivity, selectivity, improve performance, facilitate contamination control and reduce analysis time.

3.2. Determination of antimony species

It has been recognized that the determination of total Sb in environmental samples is useful to have information on levels of contamination but does not give an accurate estimation of its potential environmental impact. Speciation analysis has become an indispensable tool for studying the biogeochemistry and potential toxic aspects of this metalloid as well as for regulatory purposes. All these issues have led to the development of hyphenated techniques that involves the coupling of a selective separation with sensitive and precise elemental specific detection.

Numerous analytical methods of separation and detection have been proposed to identify and measure individual species of Sb. Traditional methods were based on the determination of Sb(III) being Sb(V) calculated as the difference between total Sb and Sb(III). At present, these techniques are inadequate because the expected levels of Sb(III) and Sb(V) in matrices of environmental interest are far below those achieved using

these procedures. In addition, for most speciation studies, more detailed chemical speciation data are required. Solvent extraction, precipitation and coprecipitation were more attractive in the past to analysts seeking to achieve speciation analysis [40–42]. Selective hydride generation using different reaction media was attempted as a mean of determining Sb species [28,43–45]. Even when far less used, electroanalytical techniques based on the different electroactivities of Sb species, have been used with speciation purposes [46,47].

Gas chromatography (GC) and high-performance liquid chromatography (HPLC) are especially attractive techniques for speciation analysis. Particularly HPLC displays great flexibility and can be used to separate nonvolatile and thermally labile compounds. GC coupled to mass spectrometry (GC–MS) provides useful molecular information about volatile Sb species. GC was coupled to ICP-MS to increase sensitivity in the study of volatile Sb compounds and fermentation gases in landfill [48]. Low temperature GC coupled on-line with ICP-MS was used to identify volatile Sb compounds in gases and condensates from a domestic waste deposit [49].

Among the most promising combined approaches, the direct coupling of HPLC to ICP OES or ICP-MS has been the hyphenated techniques more used for speciation studies as they offer the advantage of a powerful fractionation technique characterized by a high degree of selectivity together with the simultaneous multielemental detection ability, relative freedom of matrix interference, element specificity and wide dynamic range of plasma-based techniques [50–53]. Krachler et al. [54] discussed the limitations and problems such as the preservation of species, the extractability of Sb and the availability of Sb standard compounds related to the speciation analysis of Sb and mainly focused on hyphenated instrumental techniques.

Several authors have reviewed different aspects of Sb speciation in environmental matrices and for this reason; this survey only reports the more recent research carried out in the field of atmospheric chemistry.

4. Determination of antimony in airborne atmospheric aerosols

The information on Sb content in atmospheric aerosols is scarce and fragmentary. In a pioneer study, Rubens reported that levels of Sb in air were between <1 g m^{-3} (in Antarctica) to >50 ng m^{-3} (in Paris) [55]. Natural and anthropogenic sources are responsible for Sb input into the environment. Coal combustion has been recognized as one of the major anthropogenic sources of many metals and metalloids into the atmosphere. The amount and nature of elements released are related to the composition of the coal burned and the technology employed in the power station. Antimony is enriched in coal and for this reason the emission of this element to the environment is strongly linked to the combustion of fossil fuels. Other important sources are non-ferrous metals refining and incineration of waste and sewage sludge.

Little is known about the chemical forms and physicochemical transformations of Sb in the atmosphere. It is believed that Sb is oxidized to Sb_2O_3 in the atmosphere by reaction with

atmospheric oxidants. Many studies evidenced that Sb is highly enriched in aerosols from urban and rural areas in comparison with background levels [56,57].

4.1. Antimony determination in atmospheric aerosols: general consideration

  (i) Antimony in ambient air is transferred by wet or dry deposition to soils and water where it can enter the food chain.
 (ii) Extended occupational exposure to Sb and its compounds causes irritation to the respiratory tract and may be responsible of pneumoconiosis.
(iii) Dusts and ashes containing Sb or Sb compounds can induce keratitis, dermatitis, conjunctivitis and gastritis.
 (iv) Sb(III) oxide by inhalation has shown to cause lung cancer in rats [58].
  (v) Aerosol samples are normally collected on different kind of filters. Filters are not free of trace metals and high background levels due to the filter material are expected. This is an important issue to take into account especially for elements such as Sb that are normally determined at trace or ultra-trace levels in atmospheric aerosols.
 (vi) Rapid, robust, reliable, efficient and, if possible, low cost methods are necessary for sample treatment.
(vii) Lack of appropriate Sb standards to identify individual species that have been separated and measured in extracts of APM.

4.2. Sample preparation for elemental analysis

Sample treatment is a key step in the overall analytical process and decomposition is crucial to obtaining reliable results. In general terms, the goal of sample treatment is the quantitative release of the element under study from the matrix, providing it in an aqueous inorganic solution. In order to make the best use of the power of the instrumental analytical techniques it is necessary that dissolved samples be free from contamination. Losses of the analyte by volatilization should also be avoided.

Two general approaches have been applied to airborne particulate matter, dusts and ashes: leaching (partial dissolution) and total dissolution. In the first case, a selective dissolution of elements is performed. For APM deposited on filters, the filter is not dissolved and it is the method of choice in studies of fractionation of metals and metalloids [59]. In total dissolution procedures, the complete sample and the filter (total or a portion) are dissolved [60]. The complete digestion of APM sample presents advantages that can be summarized as follows:

  (i) A complete digestion of the filter will be more representative of the sample in comparison with a direct solid sampling technique that only uses a small portion of the filter (e.g., X-ray fluorescence).
 (ii) Microwave digestion procedures avoid losses of more volatile elements such as antimony.
(iii) Less possibility of interferences is expected in diluted samples.

Methods of wet sample digestion using microwave (MW) ovens have been very used during the last few decades because they are more efficient than conventional procedures. Optimal conditions for closed systems decomposition such as sample weight, nature and volume of reagents, temperature and reaction time will depend on the characteristics of the sample and on the decomposition device available. The main advantages of these methods are summarized as follows:

  (i) Complete isolation of the operation from the laboratory atmosphere.
 (ii) Faster digestion process by using high pressures and temperatures.
(iii) Reduced quantity of acids.
 (iv) Commercial apparatus enhance operator safety.

Atmospheric aerosols are difficult to digest samples, which contain a variety of components including oxides, carbonates, silicates and organic compounds. Strong acid oxidizing mixtures in combination with high pressure and temperature conditions have been used for sample digestion for subsequent elemental determination.

Many methods have been proposed for the dissolution of APM due to the difficulties caused by the extremely low levels of certain elements (e.g., Pd, Pt, Rh) and by the diversity and complexity of the matrices involved. The critical factor for the decomposition of inorganic and organic compounds present in atmospheric aerosols is the choice of the acid or mixture of acids to be used. It is necessary to use high quality acids with appropriate specifications. Laboratory water is an important reagent and it is necessary to ensure that the water employed is of the desired quality.

In trace and ultratrace analysis of Sb in atmospheric aerosols the size and fluctuation of the blank must be minimized and special procedures must be employed for the purification and storage of analytical reagents. In addition, a strict control of the amount of reagents used and the contact time of samples with containers at high temperatures is necessary because these parameters contribute to the size and variability of the blanks.

Different oxidizing acids with high degree of purity such as HNO_3, $HClO_4$, H_2SO_4 and non-oxidizing acids such as HCl and HF are used to digest atmospheric aerosols deposited on filters and fly ashes and their uses, pros and cons are briefly described below.

• Nitric acid is an almost universal digestion reagent and it is intended to destroy organic compounds breaking down the complex hydrocarbons into H_2O and CO_2 and to oxidize metals. In addition, nitric acid forms water-soluble salts with most elements and consequently precipitation is not expected. Most nitrates are less volatile than the corresponding chlorides, preventing losses due to volatilization but nitric acid can form insoluble oxides of Sb. When ICP-MS is used for Sb quantification, nitric acid is recommended because H, N and O are present in the plasma. Nitric acid can also be used together with H_2O_2 and HCl to improve the performance of the digestion.

- Hydrochloric acid is non-oxidizing and chlorides are in general terms soluble, except for Ag, Hg, Pb and Tl. This acid is widely used for the dissolution of inorganic matrices even when hydrochloric acid can form volatile compounds with several elements (e.g., As, Ge, Hg and Se) including Sb. Hydrochloric and sulphuric acids are avoided when digested aerosols are analyzed by ICP-MS because they introduce additional possible interfering elements such as Cl and S. In addition, sulphuric acid cannot be used with ICP-MS instruments employing Ni cones.
- Perchloric acid has the advantages of forming very soluble perchlorates (except KClO), to attack organic matter and the inability to form complexes with metals and metalloids. It presents oxidizing properties when heated and special attention has to be paid when organic matter is present to avoid explosions. For this reason, it is recommended to remove the organic matter first, then cool the solution and then add perchloric acid for the total digestion of the sample.
- Sulphuric acid is less used than other acids because many metal sulfates are insoluble. It can be used for the digestion of airborne particulate matter when organic compounds are expected. The main characteristic of this acid is the combination of acidic, oxidative and dehydrating properties.
- When different acids are combined, powerful conditions can be obtained that will help to breakdown the sample matrix. Aqua regia is a 3:1 mixture (v/v) of concentrated hydrochloric and nitric acids that has much more oxidizing power and complexing properties than the acids alone due to the formation of chlorine and nitrosyl chloride (NOCl). Aqua regia was extensively used to digest airborne particulate matter containing different trace elements including Sb [59,61]. It is a useful reagent to attack different minerals present in airborne particulate matter (no silicates) and noble metals.
- Hydrofluoric acid is mandatory when silicates are present in APM to break up the silica matrix and to dissolve mineral constituents. Bettinelli et al. [62] reported that the addition of HF substantially improved the recovery of Cr and did not influence the recovery of As and Sb. Mixing HF with an oxidizing acid can been used to combine in a mixture acid, oxidant and complexation properties. Due to the corrosive characteristics of this acid and to avoid damages, it has to be handled with especial care and an evaporation step is normally included after digestion. Even with this additional step increasing pretreatment time and the risks of losses and chemical contamination, it has the advantage to decrease possible spectral interferences from acidic ions. When ICP-MS is used for Sb measurements, an excessive amount of HF may cause damages to the torch and corrosion of the Ni cones, causing signal drift. The addition of H_3BO_3 to the final solution is beneficial to neutralize the excess of HF. In spite of the advantages of using this acid, it is important to remark that solids in solution will be increased and spectral interferences by B species can be expected. Other alternative, when possible because Sb is normally found at very low levels, is the dilution of the samples after digestion to reduce acid concentration.
- Hydrogen peroxide has been less used in aerosols digestion even when it is a very efficient oxidizing agent. Hydrogen peroxide has a strong oxidation power and is safer in comparison with aggressive acids. Other remarkable advantages of H_2O_2 are: (i) it is converted to water and oxygen during the dissolution of organic matter, (ii) it is available at high purity, (iii) no corrosion on the materials used for the attack takes place, (iv) no insoluble salts are formed and (v) no change of the sample matrix occurs. When Sb is determined in digested solutions by ICP-MS, the presence of H_2O_2 does not introduce extra spectral interferences to the mass spectrum since H and O already exist in the solutions introduced into ICP. It is recommended to avoid the use H_2O_2 in excess to prevent explosion. Hydrogen peroxide is often a good alternative to perchloric acid.

Wet digestion has been very used in the past and thanks to the introduction of new developments it is still the most frequent methodology for sample decomposition for Sb determination in APM and fly ashes. There is no universal sample preparation system and it has to be carefully evaluated for each specific case.

In conclusion and as a final remark, all the acids mentioned above are corrosive and have to be handled with care, especially when hot and concentrated. Since APM contains silicates, HF has been extensively used for sample digestion but it is a particularly hazardous acid and should be handled with care. Also special attention has to be paid when perchloric acid is used hot and organic matter is present in the aerosol samples. Besides it must never be taken to dryness directly.

4.3. Other approaches

Even when far much less used, the slurry sampling method has been employed for the analysis of different kinds of environmental samples by atomic spectrometric techniques in order to simplify sample preparation procedures and to avoid some inconveniences related to wet decomposition and dry ashing procedures. Introduction of slurry samples combines the advantages of reducing sample preparation time, contamination and possible analyte losses due to volatilization and/or retention by insoluble residues. In addition, slurry sampling avoids the use of hazardous and concentrated acids such as $HClO_4$ and HF. However, slurry sampling could involve some drawbacks such as loss of precision and possibility of high background levels, among others. The combination of slurry sampling and electrothermal vaporization (ETV) has been used for the determination of Sb in fly ashes [63].

5. Analytical methods for antimony determination in atmospheric aerosols

Expected concentrations of Sb in APM are at $ng\,m^{-3}$ level or lower. The inadequate detection power of many instrumental techniques to reach such low levels puts severe constraints on the determination of Sb in atmospheric aerosols. The approaches quite often used are based on plasma-based techniques namely,

inductively coupled plasma optical emission spectrometry and inductively coupled plasma-mass spectrometry and neutron activation analysis.

5.1. Antimony determination in airborne particulate matter

5.1.1. Total antimony determination

In a comprehensive study on the chemical composition of atmospheric aerosols, Rahn [64] compiled data on Sb and many other elements for more than 20 cities around the world and showed that Sb exhibits one of the greatest ranges in enrichment factors (EF) in APM. The enrichment factor is the ratio between the concentration of an element in APM respect to Earth's crust. During the last two decades a substantial increase of metal emission from traffic (gasoline, additives, vehicle and vehicle parts wear) has occurred and it is known that vehicular traffic is one of the main sources of Sb in highly populated urban areas. Since Sb level in airborne particulate matter is low, ICP-MS has become the technique of choice for its determination in this kind of matrices.

Many studies evidenced that Sb is a traffic related element (TRE) by the use of Sb_2S_3 in brake pads. The environmental interest in Sb in APM arises mainly from the potential toxicity of compounds such as Sb_2S_3 and Sb_2O_3. A considerable Sb concentration has been found in brake pads and dust probably partly present as Sb_2O_3 [65]. Antimony trisulfide (Sb_2S_3) is used as a lubricant in friction material and Sb-containing additives are employed during vulcanization. A study related to brake wear particulate matter emissions on new vehicles evidenced that on average, 35% of the brake pad mass loss was emitted as airborne particulate matter [66].

Recently, Iijima et al. [67] studied the particle size and composition distribution of dusts from brake abrasion for the evaluation of Sb sources in APM. From the results obtained the authors concluded that automotive brake abrasion dusts, containing Sb at percentage level, would be one of the predominant sources of fine APM enriched in antimony.

The association of Sb with traffic, its occurrence in airborne dust, deposition and accumulation in standardized grass cultures was studied in Munich (Germany) [68]. Filters loaded with airborne particles were digested in open PTEF vessels with a mixture of HNO_3, H_2O_2 and HF. The membrane filters were dissolved in HNO_3 and heated to 130 °C for 1 h with a PTFE (polytetrafluoroethylene) cover on the vessel. Then, the other reagents were added carefully and the solution heated for another 2 h. In a last step, the solution was slowly evaporated nearly to dryness and the residue dissolved in HNO_3. The analytical determinations of Sb were accomplished by ICP-MS using the mass 121. For quality control purposes mass 123 was also monitored. Airborne Sb was predominantly found on particle <10 μm (PM-10). Antimony levels varied from 1.26 to 13.6 ng m^{-3}. In heavy traffic impacted areas, mean Sb levels were 2.4 and 11.1 ng m^{-3}. The detection limit of Sb in airborne particles was 0.01 ng m^{-3}. The authors observed a preferential Sb enrichment in coarse particles, which are not characteristic of exhaust emission. They suggested that Sb impacts were partially due to abrasion of tyres and brake pads. To corroborate this, brake linings were analyzed

by X-ray spectrometry indicating Sb concentrations from 1 to 4%. Even when open systems in wet digestion procedures are very cheap, well documented in the literature and available in all laboratories devoted to routine analysis or research, they present some drawbacks. It is important to remark that digestion methods using open PTEF vessels are limited by a low maximum temperature that for many samples is not enough to obtain a complete dissolution of the matrix, require the use of large amounts of reagents and the danger of losses of elements present at trace levels.

In a comprehensive study, Weckwerth [69] demonstrated that in ambient air of Cologne (Germany), Sb, Cu and Mo are traffic-related elements emitted by abrasion of brake linings. To separate the fine-grained condensation components from coarse-grained aerosols of mechanical origin; a two-stage impactor with a separation point at 2.5 μm was used to collect the APM. Particles <2 μm; 2.5–10 μm and <10 μm were analyzed. Following sampling, filters loaded with APM were enclosed in cylindrical polyethylene cylinder and irradiated for 6 h in the central core of a reactor. All analyses were performed by instrumental neutron activation analysis (INAA) and to obtain representative values, 4–8 different samples were measured. Levels of Sb from ~15 to 90 μg g^{-1} were reported. From all the elements that exhibited enrichment in the APM, Sb remained the highest, indicating the presence of at least one significant component of mechanical origin (particle size > 2.5 μm) with high Sb-content. Using the correlation Cu/Sb it was demonstrated that both elements had the same origin.

Smichowski et al. [59] assessed the content of 13 elements, including Sb, in airborne particulate matter of Buenos Aires (Argentina). Samples were collected in ash-free-glass fibre filters using high volume samplers with PM-10 sampling heads. The authors selected a combination of aqua regia and perchloric acid for leaching metals from filters and Sb was quantified in the extracts by ICP-MS. Antimony concentrations (all in ng m^{-3}) ranged from 0.9 to 15.3 with a mean concentration of 4.7 ng m^{-3}. A limit of detection of 3.3 ng mL^{-1} (equivalent to 0.06 ng m^{-3} in air) was reported. To further support the view that brake lining contributes significantly to Sb content in PM-10 in a megalopolis such as Buenos Aires (Argentina) with an overall traffic density of 1,5000,000 vehicles per day, the ratios of Cu and Mo with respect to Sb were calculated [70]. The trend observed was supportive of the correlation between the three elements that are brake lining components. The highest concentrations of Sb were detected in streets showing a "stop-and-go" pattern during peak hours.

In a comprehensive study on size-classified airborne particulate matter collected in Tokyo (Japan) between 1995 and 2004, concentrations, enrichment and predominant sources of Sb and other elements were assessed [60]. Particles of APM <2 μm, 2–11 μm and >11 μm were collected. Filters loaded with APM were subjected to MW-assisted digestion using a mixture of HNO_3, H_2O_2 and HF. Plasma-based techniques were used for elemental analysis. ICP-MS was used to quantify Sb and other trace elements in the digests while ICP OES was used to determine major elements. To confirm that the analytical procedures were correct, a standard reference material (SRM) of

airborne particulate matter from NIST SRM 1648 (Urban particulate matter) was analyzed. The reference value (non-certified) for Sb was $45 \, \mu g \, g^{-1}$ and the authors found a concentration of $46.84 \pm 0.6 \, \mu g \, Sb \, g^{-1}$. Concentrations reported for Sb (in $\mu g \, g^{-1}$) were: 199 (APM $< 2 \, \mu m$), 188 (APM 2–11 μm) and 53.0 (APM $> 11 \, \mu m$). Surprisingly, high EFs were obtained for Sb as follows: 20,9000 (APM $< 2 \, \mu m$), 4330 (APM 2–11 μm) and 634 (APM $> 11 \, \mu m$). The shape of single particles was examined by SEM-EDX (scanning electron microscopy) and the study revealed that fine particles were rich in S and Sb, which are two components of brake pads.

In other approach, ICP-MS combined with laser ablation (LA–ICP-MS) was used for direct sample introduction. Fifteen elements in atmospheric particulate matter collected in Tokyo (Japan) were determined [71]. Analysis of APM using this micro-analytical technique has the advantage that no lengthy dissolution processing is required which has the risk to be incomplete and can also introduce contamination to the sample. In addition, a dry sample is introduced to the plasma with a resulting lack of polyatomic interferent species produced by the interaction of water and acids with the Ar plasma. The need for well-characterized, homogeneous standards is a drawback to face. In this case, analyte element calibration was easily performed using a standard filter sample prepared by dropping an aqueous standard solution on the surface of the same type of membrane filter as those used for collecting atmospheric particles. Antimony levels found in the atmosphere of Tokyo depended on the sampling period and ranged from 5.7 to 16 ng m^{-3}. A relative detection limit (calculated by dividing the absolute detection limit by 1.44) of 6.94×10^{-3} ng m^{-3} was achieved. In general terms, Sb results were in good agreement with those obtained by INAA. Considering the technique used, the precision of the method was good as reflected by the RSD reached (<10% for Sb).

In situ trapping procedures utilizing the graphite furnace as the concentration and the atomization cell (HG-ETAAS) have demonstrated to be useful to increase the detection power of atomic spectrometric methods available for the hydride forming elements. Recently, Moreda-Piñeiro et al. [72] reported a simple and rapid method for the direct determination of As, Bi, Sb and Sn by HG-ETAAS in filters loaded with APM (PM-10 and PM-2.5) without any pre-treatment of the samples. A $2^8 \times 3/64$ Placket-Burman design was used as a multivariate method for evaluating the effect of the different variables affecting the hydride generation, trapping and atomization efficiencies. In the six samples analyzed Sb concentrations ranged from 0.54 ± 0.04 to 2.23 ± 0.2 ng m^{-3} for PM-10 and <0.150 to 0.69 ± 0.05 ng m^{-3} for PM-2.5. An absolute detection limit of 30 ng Sb L^{-1} (equivalent to 0.045 ng m^{-3} in air) was reached. The advantage of this method is that the time required for sample pre-treatment is significantly reduced with respect to acid digestion or slurry preparation methodologies.

5.1.2. Speciation studies

Little is known about the distribution of Sb species in APM and only few studies have been conducted to this end. For the efficient separation achieved by HPLC it resulted particularly

suited in conjunction with plasma-based techniques for speciation studies. A number of the studies identified Sb(III) and Sb(V) using an anionic polymer-based column (PRP-X100). Aside from this popular column, size-exclusion, cationic and reversed-phase columns have also been used for Sb speciation studies in APM.

Furuta and his group have carried out a series of comprehensive research studies on the determination and identification of Sb species in APM [50,60,73–76]. Total and water-soluble Sb compounds were determined in a Japanese quality control APM sample, a standard reference material (NIST 1648-urban particulate matter) and an APM sample collected in Tokyo (Japan) [73]. Antimony speciation was performed using HPLC coupled to ICP-MS. To shorten the retention time of Sb(III) and peak tailing in the chromatographic column, the authors found that a shorter silica-based anion-exchange column namely, Synchropak Q300 was more adequate than the extensively used PRP-X100 to achieve the separation of Sb(III) and Sb(V) using 2 mmol L^{-1} phthalic acid as a mobile phase in a pH range between 4.3 and 5.0 According to their findings, the addition of 5 mmol L^{-1} EDTA improved the separation of the inorganic species. In spite of their efforts, a broad peak for Sb(III) was still observed and no significant improvements in the separation of inorganic species of Sb was obtained in comparison with previous reported studies [50]. The total reported concentrations of Sb in APM and in the aqueous extract were 195 ± 13 and $37.9 \pm 0.8 \, \mu g \, g^{-1}$, respectively. A low recovery of Sb (19.4%) was obtained in the water-soluble fraction. Detection limits were found to be 0.1 μg L^{-1} for Sb(V) and 0.3 1 μg L^{-1} for Sb(III). The application of the developed method to the speciation analysis of Sb evidenced the presence of organic Sb species in APM.

In an attempt to shed light to the identification of the unknown Sb species detected, a new HPLC–ICP-MS procedure for the speciation analysis of Sb in APM was devised by the same group [74]. Samples were subjected to MW-assisted acid digestion and a total concentration of $56.0 \pm 4.1 \, \mu g \, g^{-1}$ of Sb was quantified by ICP-MS in the solution. For extracting Sb species from the filters loaded with APM, three solvents were tested. Each solvent (Milli-Q water, phosphate and EDTA) was selected according to a different affinity for trace metals. Milli-Q water was used to extract water-soluble Sb compounds, phosphate to remove metal fraction which is adsorbed by ion exchange mechanism and EDTA to put in solution carbonate-bound and organically-bound fractions of Sb. Anion-exchange and size-exclusion HPLC-ICP-MS were tested for speciation studies. The aqueous extract of APM was first injected in the HPLC-ICP-MS system and Sb(V) was detected as the predominant species. Three non-identified Sb species were detected. Further experiments using hydride generation showed that these species were active Sb species with different efficiency of generation. The aqueous extracts were injected in a size-exclusion chromatography–ICP-MS (SEC–ICP-MS) system that evidenced the presence of TMSb. Sb(V) was the predominant species (~80%). The presence of TMSb and hydride active species in APM corroborates the existence of organic species and indicates that special attention should be paid when using hydride generation for the selective determination of Sb(III) and Sb(V) in this kind of

samples. The authors proposed electrospray-mass spectrometry (ES-MS) as a possible alternative to identify the unknown species.

Another study carried out by the same group was based on the complexation of Sb compounds with citric acid and its application to the speciation analysis of Sb(III) and Sb(V) using HPLC–ICP-MS [75]. The complexation of both Sb compounds with citric acid was examined by ES-MS. They found that both species of Sb could form very stable complexes with citric acid in aqueous extracts of APM. This allowed the separation of Sb(III) and Sb(V) on a PRP X-100 anion exchange column with 10 mmol L^{-1} EDTA to 1.0 mmol L^{-1} phthalic acid at pH 4.5 as mobile phase with the advantage that both complexes were retained and no elution of any of them was observed in the solvent front. The stabilizing effect of the complexing agent allowed a significant improvement of the limits of detection. Detection limits for Sb(III) and Sb(V) were improved in one order of magnitude in comparison with those previously reported [50,73]. The detection limits reached for Sb(III) and Sb(V) were 0.005 μg L^{-1} and 0.07 μg L^{-1}, respectively. The author analyzed an APM sample containing 104 ± 3 μg g^{-1} of Sb and both inorganic species of Sb were detected and the ratio Sb(V) to Sb(III) was found to be ∼4.6:1.

In other study, the same group used ES time-of-flight mass spectrometry (ES-TOF-MS) to investigate positive and negative ion electrospray mass spectra of commonly encountered organic Sb compounds namely, trimethlantimony dichloride (TMSbCl$_2$) and trimethylantimony dihydroxide (TMSb(OH)$_2$) and inorganic Sb compounds, potassium hexahydroxyantimoniate (Sb(V)) and potassium antimonyl tartrate (Sb(III)) [76]. Samples were dissolved in a mixture of methanol-water (v/v, 50:50) and introduced into the ion source. Based on their findings, the authors proposed a mechanism for the solution chemistry of TMSb(OH)$_2$. With respect to TMSbCl$_2$, they speculated that in aqueous solution it might be hydrolyzed to form (CH$_3$)Sb(OH)(Cl). According to Furuta and co-workers [73,74], they detected for the first time the presence of Sb(III), TMSb and several hydride active unknown Sb species in aqueous extracts of APM collected in Tokyo (Japan).

An important point to remark is that the complexation of inorganic Sb species prevented the oxidation of Sb(III) to Sb(V) during the ultrasonic-assisted and MW-assisted extraction of APM samples. Recently, Hansen and Pegartis further investigated the formation of an Sb(V)-citrate complex by HPLC–ICP-MS and HPLC–ES-MS/MS due to their relevance in food chemistry [77].

5.2. Antimony determination in fly ashes

Fly ashes generated in combustion processes are important carriers of hazardous substances into the environment such as toxic metals. For this reason, the determination of toxic and potentially toxic elements in this matrix is an issue of permanent research.

Fly ash is a complex heterogeneous material; highly diverse that is present in a wide range of sizes. They are composed by fine particles of aluminosilicate glass, quartz, mullite, hematite, ferrite and anhydrite or lime in different stages of transformation depending on their origin [78]. The chemical composition of fly ashes varies depending on the type of carbon used but in general terms are enriched in many elements including toxic elements. As a chalcophilic element, Sb is enriched in coal to such an extent that up to 3000 μg Sb g^{-1} has been detected in the ash of some German coals. Valkovik [79] reported a worldwide average concentration of Sb in coals of 3 μg g^{-1}, which is an evidence of its enrichment with respect to its abundance in the Earth's crust. Antimony vaporizes during combustion, resulting in the largest single source of anthropogenic Sb to the global atmosphere [80].

5.2.1. Total antimony determination in fly ashes

Most analytical techniques have an intrinsic requirement for liquid sample introduction. In the case of fly ashes, sample digestion is not an easy task. Methods based on fusion may increase blank values due to contamination of the reagents normally used and/or to losses due to volatilization. Volatilization is also a problem to tackle when open systems are employed for fly ash dissolution and consequently the use of closed pressurized systems is recommended. Fast and efficient acid decomposition procedures have been reported using microwave ovens (MW) [81–83].

Lachas et al. [84] evaluated two digestion procedures namely, wet ashing digestion with open vessel and microwave extraction to put in solution 17 elements present in coal fly ash reference materials. In spite of the problems related to the use of open systems above described the authors reported that open vessel acid digestion was far superior to the efficient MW procedure. In both cases, Sb was determined by ICP-MS with a limit of quantification of 0.1 μg g^{-1} (dilution factor: 1000). Four reference materials were used for the validation of both sample preparation procedures and ICP-MS determination.

The combination of slurry sampling and electrothermal vaporization (ETV) has been proposed for the analysis of environmental samples. To avoid possible errors arising from spectral and non-spectral interferences, residue accumulation in furnace, possible analyte loss during transportation and poor reproducibility problems, ultrasonic slurry sampling (USS) ETV-ICP-MS was proposed as a valid alternative. Several elements including Sb were determined in a power plant fly ash and in the standard reference materials NIST 1633a and 1633b (coal fly ash) by USS-ETV-ICP-MS using Pd as chemical modifier [65]. Since Sb was no certified, results obtained by USS-ETV-ICP-MS were compared with those obtained by digesting the samples and analyzing the solutions by pneumatic nebulization dynamic reaction cell (DRC) ICP-MS. A good agreement was found between both techniques. A concentration of Sb in a power plant fly ash of 4.7 ± 0.5 μg g^{-1} was reported and the detection limit estimated from the standard addition method was about 0.11 μg g^{-1}.

Arsenic, Sb and Se were quantified in acid extract from fly ashes, coal and slag samples [85]. Firstly, samples were subjected to a MW-aqua regia extraction procedure and then analytes were converted into their respective hydrides. The volatile species were "in situ" preconcentrated in a treated graphite tube (coated with Zr) and atomized. A collection time of 30 s and

a trapping temperature of $600\,^\circ$C were used for Sb retention. The combination of HG and trapping of the hydrides in the graphite tubes allowed reaching a LOD in fly ash as low as $0.35\,\mu g\,Sb\,kg^{-1}$.

5.2.2. Speciation studies

One area of particular interest in environmental chemistry is the impact of fine particles containing toxic or potentially toxic inorganic compounds when released from power stations and deposited downwind of the emission source. Hence, to investigate the leachability of elements from coal fly ashes is an issue of prime importance in the assessment of the environmental and health risks of coal uses. In extraction studies, special attention has to be paid in selecting the appropriate extraction conditions to avoid changes in the original form of Sb in the fly ash by means of hydrolysis or complexed species formation, even when no oxidation/reduction reaction takes place.

Only few studies regarding the identification and quantification of Sb species from fly ash using chemical extraction are available in the literature. The presence of chemical species of As, Se and Sb in fly ash from six coal fuel thermal power stations from different countries was investigated by Narukawa et al. [86]. Total Sb in the fly ash samples was measured by ICP-MS following MW-assisted digestion using HCl, HF and HNO$_3$. The detection limit for Sb under the measurement conditions adopted was $0.01\,\mu g\,g^{-1}$. In fly ash Sb concentrations ranged from 1.0 to $3.9\,\mu g\,g^{-1}$. To determine the mode of occurrence of this metalloid a five-step chemical fractionation scheme was applied. In the most bioavailable fraction, Sb concentrations varied from 0.05 to $1.14\,\mu g\,g^{-1}$ and it appeared that almost of Sb was present in the residual fraction. Inorganic Sb species were determined by HPLC–ICP-MS in aqueous extracts. Less than 3% of total Sb was as Sb(V) while Sb(III) was the dominant species.

Seames et al. [87] assessed the solubility of inorganic compounds from five different size-segregated coal fly ash samples. Antimony concentration in coal varied from 0.3 to $2.3\,\mu g\,g^{-1}$. As expected, Sb leachability was highly influenced by pH, being Sb partially soluble at pH 5 and exhibiting higher solubility at lower pHs. In general terms, Sb resulted fairly soluble at pH 5.0 and very soluble at pH 2.9. The authors reported that the results obtained were consistent with the following compounds: Sb, Sb$_2$O$_4$ and Sb$_2$O$_5$, but inconsistent with the existence of Sb$_2$O$_3$. The pH 5 leachability data constitutes useful information to assess the potential of Sb contained in small particles to migrate into the water supply after ground deposition downwind of the power plant.

An investigation on the species of As, Se and Sb in samples of fly ash obtained from six coal-fired power stations in various countries was undertaken [87]. Water-soluble Sb species in the fly ashes were extracted and determined by HPLC–ICP-MS. The concentrations of Sb ranged from 1.0–$3.9\,\mu g\,g^{-1}$ and the dominant chemical form of Sb was as extractable Sb(III), the most toxic species.

To obtain information on the distribution of Sb species in coal fly ash Miravet et al. [88] evaluated extraction procedures and analytical techniques. Two extractant solutions were tested: (i) an aqueous solutions at a pH range from 1 to 12, and (ii)

$1\,mol\,L^{-1}$ citrate at pH 5. Regarding the solubility of Sb species in water, a poor leachability was observed at basic pHs while the highest yield was obtained at pH ≤ 2. In all cases the best efficiency of extraction (22–36% of soluble Sb) was reached when a chelating solution of citrate at pH 5 was tested. These values suggested that most Sb was bound to the residual and no soluble fraction. For the speciation analysis, the extracts were analyzed by HPLC–ICP-MS and HPLC-HG-AFS and the performance of both couplings was compared. The hydride generation technique was selected to improve sensitivity and selectivity in Sb determination. However, it was severely hampered when high levels of Ca, Fe and Pb were present in the leachates and the authors recommended using HPLC-ICP-MS for the determination of Sb species. For validation purposes, the SRM 1633b (coal fly ash) from NIST was subject to the same analytical process that the samples. The study evidenced that Sb(V) was the predominant species in the leachates ($1.63\,\mu g\,g^{-1}$) although minor amounts of Sb(III) ($0.36\,\mu g\,g^{-1}$) were detected.

Studies based on the use of chemical sequential schemes report a wide variability of results since different experimental extraction conditions are used. The amount of metal released at each step of the leaching procedure depends both on the type of reagents selected and the sequence in which they are used. In this kind of studies it will be recommendable to harmonize the different procedures proposed in order to facilitate comparability of data as well as to optimize the operating conditions. In a spite of this, in all cases there is an agreement in that both inorganic Sb species were present in the fly ash but with different levels of concentration. This fact is also related to the different characteristics and origin of coal of the fly ash analyzed.

5.3. Antimony determination in volcanic ashes

Studies on volcanic ashes have been mainly focused to investigate environmental, geological and geophysical aspects and transport effects. In spite of this, the emission of toxic elements during eruptions is important for studying the cycle of trace elements in the environment and for assessing the extent of regional and global pollution. Only few papers report the determination of Sb in volcanic ashes. This matrix is a complex physical mixture of crystals of different minerals, silicates, rocks and non-silicate particles. Analysis of the chemical species in the individual particles and the bulk samples performed by SEM and energy dispersive X-ray analysis (EDAX) revealed that individual particles contained a variety of chemical compounds that only occasionally were particles of a pure chemical species [89]. From the analytical chemistry point of view volcanic ash is a challenging matrix for its complexity and diversity of elements and compounds present.

The state of the art as regards speciation is also traced back to other categories based on, as example, physical separations. In this connection, Gómez et al. [90] performed a fractionation study on size-classified volcanic ashes for the determination of chemical elements and compounds. Samples of deposited ashes ejected from Copahue volcano (Argentina) were collected 1 day after the first eruption and characterized using different ana-

Table 1
Concentrations data of Sb and Sb species in APM, fly ash and volcanic ash from different cities

Matrix	Location	Analytical technique	Antimony concentration	Refs.	Year
Size-classified APM	Munich, Germany	ICP-MS	$1.26–13.6\,\text{ng m}^{-3}$	[68]	1997
Size-classified APM	Tokyo, Japan	LA–ICP-MS	$5.7–16\,\text{ng m}^{-3}$	[71]	1998
Fly ash		ICP-MS		[84]	1999
APM	Tokyo, Japan	HPLC–ICP-MS	Total Sb: $195 \pm 13\,\mu\text{g g}^{-1}$ Sb(V): $255 \pm 11\,\mu\text{g g}^{-1}$ NIS-1[a]: $14.0 \pm 3.0\,\mu\text{g L}^{-1}$ NIS-2: $26.6 \pm 1.6\,\mu\text{g L}^{-1}$ NIS-3: $14.7 \pm 1.6\,\mu\text{g L}^{-1}$ NIS-4: $4.94 \pm 0.08\,\mu\text{g L}^{-1}$	[73]	2000
APM and water soluble extracts	Tokyo, Japan	HPLC–ICP-MS	Total Sb: $56.0 \pm 4.1\,\mu\text{g g}^{-1}$ Aqueous extracts: Sb(V) ($\sim$80%), TMSb, three hydride active unknown Sb species $\sim$15–90 $\mu\text{g g}^{-1}$	[74]	2000
Size-classified APM	Cologne, Germany	INAA	Total Sb: $104 \pm 3\,\mu\text{g g}^{-1}$	[69]	2001
APM and water soluble extracts	Tokyo, Japan	ICP-MS	Sb(V), Sb(III) ratio: $\sim$4.6:1.	[75]	2001
Size-classified volcanic ashes	Neuquén, Argentina	ICP-MS	$0.39–1.07\,\mu\text{g g}^{-1}$ Mean concentration in each fraction: $1.03 \pm 0.02\,\mu\text{g g}^{-1}$; $0.56 \pm 0.02\,\mu\text{g g}^{-1}$; $0.44 \pm 0.02\,\mu\text{g g}^{-1} \pm 0.590.02\,\mu\text{g g}^{-1}$	[90,92]	2002, 2003
PM-10	Buenos Aires, Argentina	ICP-MS	$0.9–15.3\,\mu\text{g m}^{-3}$ Mean: $4.7\,\mu\text{g m}^{-3}$	[59,70]	2004, 2005
Size-classified APM	Tokyo, Japan	ICP-MS	APM < 2 μm $199\,\mu\text{g g}^{-1}$; APM 2–11 μm: $188\,\mu\text{g g}^{-1}$; APM > 11 μm: $53.0\,\mu\text{g g}^{-1}$	[60]	2005
Fly ash	Taipei, Taiwan	USS-ETV–ICP-MS	Total Sb: $4.7 \pm 0.5\,\mu\text{g g}^{-1}$	[65]	2005
Fly ash	Various countries	HPLC–ICP-MS	$1.0–3.9\,\mu\text{g g}^{-1}$ Sb(III) predominant species in aqueous extracts	[86]	2005
Fly ash	Barcelona, Spain	HPLC–ICP-MS and HPLC–HG-AFS	Sb(III): $0.36\,\mu\text{g g}^{-1}$ Sb(V): $1.63\,\mu\text{g g}^{-1}$	[88]	2006
Size-classified volcanic ashes	Neuquén, Argentina	HPLC–ICP-MS	Sb(III): $0.07–0.36\,\mu\text{g g}^{-1}$ Sb(V): $0.88–1.63\,\mu\text{g g}^{-1}$	[89]	2007
PM-10 and PM-2.5	A Coruña, Spain	Direct sampling HG-ETAAS	PM-2.5: <0.150 to $0.69 \pm 0.05\,\text{ng m}^{-3}$ PM-10: 0.54 ± 0.04 to $2.23 \pm 0.2\,\text{ng m}^{-3}$	[72]	2007

[a] NIS: non-identified species.

lytical techniques. Ash samples were collected, dried at room temperature and sieved obtaining four fractions with the following particle diameter: $A < 36\,\mu m$, $B = 35–45\,\mu m$, $C = 45–150\,\mu m$ and $D = 150–300\,\mu m$. Major and minor elements (Al, Ca, Cl, Fe, K, Mg, Mn, Na, S, Si and Ti) were detected by energy dispersive X-ray analysis (EDAX). Trace elements (As, Cd, Cr, Cu, Hg, Ni, Pb, Sb, U, V and Zn) content was quantified by ICP-MS. Nuclear activation analysis (NAA) was employed for the determination of Ce, Co, Cs, Eu, Hf, La, Lu, Rb, Sc, Sm, Ta and Yb. For elemental determination by ICP-MS each fraction was digested using a mixture of HNO_3, HF and H_2O_2. Antimony was the element that exhibited the highest EF in the four fractions. Furthermore, Sb was more enriched in the smallest size fraction that can be considered as a surrogate for inhalable particulate matter. The enrichment factors reported for each fraction are: *A*, 6.26; *B*, 2.51; *C*, 2.34 and *D*, 2.44. The highest emission factor of Sb agrees with the well-known fact that volcanoes constitute the most important natural input of this element to the environment [91].

In other study, concentrations of Sb in volcanic ashes measured by ICP-MS varied between 0.39 and $1.07\,\mu g\,g^{-1}$ [92]. The isotope ^{121}Sb was affected by mass interferences that were easily corrected by means of appropriate mathematical equations. A satisfactory correction was supported by results obtained in the CRM (GBW 07105-Rocks from the NRCCRM, China) analysis (certified value: $0.008 \pm 0.05\,\mu g\,g^{-1}$; found value $0.008 \pm 0.01\,\mu g\,g^{-1}$)

In an effort to get information on the speciation of Sb in the size-classified four fractions, each fraction was subjected to an extraction procedure by using $1\,mol\,L^{-1}$ citrate buffer at pH 5 [89]. Antimony(III) and (V) in the extracts were separated by HPLC and quantified on-line by ICP-MS (HPLC–ICP-MS). Antimony species concentrations $(\mu g\,g^{-1})$ in the four fractions varied from 0.07 to 0.36 for Sb(III) and from 0.88 to 1.63 for Sb(V). The study showed, for the first time, the occurrence of both inorganic Sb species in the extractable portion of volcanic ash. Sb(III) was always the predominant species.

Table 1 summarizes concentrations data of Sb and Sb species in APM, fly ash and volcanic ash from different cities reported by the above-cited studies.

6. Conclusions

The scenario depicted in the previous pages is probative of the interest raised by Sb determination and speciation in atmospheric aerosols in the last decade. In spite of this, all this information clearly testifies that a gap exists with respect to other much more studied elements and that more systematic studies on total Sb determination and its speciation in atmospheric aerosols are necessary.

Total antimony determination in atmospheric aerosols is readily achievable as a result of many atomic spectroscopic and well-consolidated plasma-based techniques available. For its intrinsic characteristics, ICP-MS is to date the more used technique. In addition, a significant reduction of spectral interferences in these complex matrices can be achieved thanks to the MS detection. Microwave assisted digestion has consolidated

as the best alternative for dissolution of solid samples avoiding loss of Sb due volatilization. However, the selection of acid and reagents requires special attention because Sb may be bound to silicates in APM and fly or volcanic ashes.

In speciation studies, the coupling of HPLC with ICP-MS has consolidated but the lack of standards for species makes more difficult the identification of unknown species in the chromatograms as it was stated before. Other drawback to tackle is the low extraction efficiency of Sb compounds in solid environmental matrices and this issue needs to be improved for a reliable assessment of the occurrence of Sb species in airborne particulate matter and fly ashes.

Considering fractionation studies, it will be recommendable to harmonize the different chemical sequential procedures reported in order to facilitate comparability of data as well as to optimize the operating conditions, and to introduce on-line procedures aimed at reducing reagents consumption and the time demand of the different steps. For validation purposes, there is both a need and a demand for more airborne particulate matter reference materials and especially certified reference materials whose extractable contents were certified.

References

[1] J. Nriagu, Keynote lecture at the 1st International Workshop on Antimony in the Environment, Heidelberg, Germany, 2005.

[2] T.K. Hinkley, P.J. Lamothe, S.A. Wilson, D.L. Finnegan, T.M. Gerlach, Earth Planet Sci. Lett. 170 (1999) 315.

[3] W. Shotyk, M. Krachler, M. Chen, Global Biogeochem. Cycle 18 (2004) 1016.

[4] International Agency for Research on cancer, Summary & Evaluations, http://www.inchem.org/documents/iarc/vol47/47-11.html.

[5] U.S. Environmental Protection Agency, Integrated Risk Information System (IRIS) on Antimony, National Center for Environmental Assessment, Office of Research and Development, Washington, DC, 1999.

[6] Deutsche Forschungsgemeinschaft (DFG) Analysis of Hazardous Substances in Biological Materials, VCH, Weinheim, 1994, p. 51.

[7] M. Patriarca, A. Menditto, B. Rossi, T.D.B. Lyon, G.S. Fell, Microchem. J. 67 (2000) 351.

[8] P. Smichowski, Y. Madrid, C. Cámara, Fresenius J. Anal. Chem. 360 (1998) 623.

[9] M.J. Nash, J.E. Maskall, S.J. Hill, J. Environ. Monit. 2 (2000) 97.

[10] Y. Petit de Peña, O. Vielma, J.L. Burguera, M. Burguera, C. Rondon, P. Carrero, Talanta 55 (2001) 743.

[11] C. Rondón, J.L. Burguera, M. Burguera, M.R. Brunetto, M. Gallignani, Y. Petit de Peña, Fresenius J. Anal. Chem. 353 (2006) 133.

[12] E.C. Figuereido, P.O. Luccas, M.A.Z. Arruda, Anal. Lett. 39 (2006) 543.

[13] W. Shotyk, M. Krachler, B. Chen, in: A. Siegel, H. Siegel, R.K.O. Siegel (Eds.), Anthropogenic Impacts on the Biogeochemistry and Cycling of Antimony in Metal Ions in Biological Systems, vol. 44, M. Dekker, New York, 2005.

[14] M. Filella, N. Belzile, Y.W. Chen, Earth Sci. Rev. 57 (2002) 125.

[15] M. Filella, N. Belzile, Y.W. Chen, Earth Sci. Rev. 59 (2002) 265.

[16] P. Smichowski, G. Gómez, G. Polla, Curr. Anal. Chem. 1 (2005) 373.

[17] W. Shotyk, M. Krachler, B. Chen, J. Environ. Monit. 7 (2005) 1135.

[18] Y. Thomassen, E. Nieboer, D. Ellingsen, S. Hetland, T. Norseth, J.O. Odland, N. Romanova, N. Chemova, V.P. Tchachtchine, J. Environ. Monit. 1 (1999) 15.

[19] H.J.M. Bowen, Environmental Chemistry of the Elements, Academic Press, London, 1979.

[20] S. Garbos, E. Bulska, A. Hulaniki, N.I. Shcherbinina, E.M. Sedykh, Anal. Chim. Acta 342 (1997) 167.

[21] X.-P. Yan, W. Van Mol, F. Adams, Analyst 121 (1996) 1061.

[22] P. Smichowski, M.B. de la Calle, C. Cámara, Fresenius J. Anal. Chem. 348 (1994) 380.

[23] A. Menegario, A.J. Silva, E. Pozzi, S.F. Durrant, C.H. Abreu, Spectrochim. Acta Part B 61 (2006) 1074.

[24] Z. Fang, Microchim. Acta 152 (2005) 29.

[25] Erdem, A.E. Eroğlu, Talanta 68 (2005) 86.

[26] E.M. Donaldson, Talanta 37 (1990) 955.

[27] H. Narakasi, Anal. Sci. 2 (1986) 371.

[28] M.O. Andreae, J.-F. Asmodé, P. Foster, L. Van't dack, Anal. Chem. 53 (1981) 1766.

[29] J. Kratzer, J. Dědina, Spectrochim. Acta Part B 60 (2005) 859.

[30] B. Chen, M. Krachler, W. Shotyk, J. Anal. At. Spectrom. 18 (2003) 1256.

[31] R. Miravet, E. Bonilla, J.F. López-Sánchez, R. Rubio, J. Environ. Monit. 7 (2005) 1207.

[32] W.-B. Zhang, W.-E. Gan, X.-Q. Lin, Anal. Chim. Acta 539 (2005) 335.

[33] C. Dietz, Y. Madrid, C. Cámara, P. Quevauviller, J. Anal. At. Spectrom. 14 (1999) 1349.

[34] J.G. Dorea, E. Merchan-Hamann, D.E. Ryan, J. Holzbecher, Clin. Chem. 36 (1990) 680.

[35] E. Haffer, D. Schmidt, P. Freimann, W. Gerwinski, Spectrochim. Acta Part B 52 (1997) 935.

[36] H.L. Pacquette, S.A. Elwood, M. Ezer, J.B. Simeonsson, J. Anal. At. Spectrom. 16 (2001) 152.

[37] L.K. Shpigun, V.K. Lunina, J. Anal. Chem. 58 (2003) 983.

[38] S.B. Koo, J. Zhu, Analyst 121 (1996) 1983.

[39] W. Wagner, S. Sander, G. Henze, Fresenius J. Anal. Chem. 354 (1996) 11.

[40] W.M. Mok, C.M. Wai, Anal. Chem. 59 (1987) 233.

[41] Y.C. Sun, J.Y. Yang, Y.F. Lin, M.H. Yang, Z.B. Alfassi, Anal. Chim. Acta 276 (1993) 33.

[42] O. Kujirai, M. Kobri, K. Yamada, H. Okochi, Anal. Sci. 6 (1990) 379.

[43] S.C. Apte, A.G. Howard, J. Anal. At. Spectrom. 1 (1986) 221.

[44] L.S. Cutter, G.A. Cutter, M.C. San Diego-McGlone, Anal. Chem. 63 (1991) 1138.

[45] M.B. de la Calle-Guntiñas, Y. Madrid, C. Cámara, Fresenius J. Anal. Chem. 343 (1992) 597.

[46] M. Bond, S. Kratsis, O.M.G. Newman, Anal. Chim. Acta 372 (1998) 307.

[47] N. Belzile, Y.W. Chen, J. Can, J. Anal. Sci. Spectrosc. 44 (1999) 85.

[48] J. Feldman, I. Koch, W.R. Cullen, Analyst 123 (1998) 815.

[49] J. Feldmann, R. Grümping, A.V. Hirner, Fresenius J. Anal. Chem. 350 (1994) 228.

[50] P. Smichowski, Y. Madrid, M.B. de la Calle-Guntiñas, C. Cámara, J. Anal. At. Spectrom. 10 (1995) 815.

[51] T. Lindemann, A. Prange, E. Dannecker, B. Neidhart, Fresenius J. Anal. Chem. 346 (1999) 462.

[52] M. Krachler, H. Emons, J. Anal. At. Spectrom. 15 (2000) 281.

[53] M. Krachler, H. Emons, Anal. Chim. Acta 429 (2001) 125.

[54] M. Krachler, H. Emons, Z. Zheng, Trends Anal. Chem. 20 (2001) 79.

[55] S. Rubens, Handbook of Elements, Howard W. Sams, Indianapolis, USA, 1968.

[56] J. Bogen, Atmos. Environ. 7 (1973) 1117.

[57] W. Maenhaut, P. Cornille, J.M. Pacyna, V. Vitols, Atmos. Environ. 23 (1989) 2551.

[58] T. Gebel, Chem. Biol. Interact. 107 (1997) 131.

[59] P. Smichowski, D.R. Gómez, L.E. Dawidowski, M.F. Giné, A.C. Sánchez Bellato, S.L. Reich, J. Environ. Monit. 6 (2004) 286.

[60] N. Furuta, A. Iijima, A. Kambe, K. Sakai, K. Sato, J. Environ. Monit. 7 (2005) 1155.

[61] F. Petrucci, B. Bocca, A. Alimonti, S. Caroli, J. Anal. At. Spectrom. 15 (2000) 525.

[62] M. Bettinelli, S. Spezia, U. Baroni, G. Bizarri, Microchem. J. 59 (1998) 203.

[63] J.-L. Ni, Ch.-C. Liu, S.-J. Jiang, Anal. Chim. Acta 550 (2005) 144.

[64] K.A. Rahn, The chemical composition of atmospheric aerosols, Technical Report, Graduate School of Oceanography, University of Rhode Island, Kingston, USA, 1976, p. 265.

[65] O. von Uexküll, S. Skerfving, R. Doyle, M. Braungart, J. Cleaner Prod. 13 (2005) 19.

[66] B.D. Garg, S.H. Cadle, P.A. Mulawa, P.J. Groblicki, C. Laroo, G.A. Parr, Environ. Sci. Technol. 34 (2000) 4463.

[67] A. Ijima, K. Sato, K. Yano, H. Tago, M. Kato, H. Kimura, N. Furuta, Atmos. Environ. 41 (2007) 4908.

[68] Dietl, W. Reifenhäuser, L. Peichl, Sci. Total Environ. 205 (1997) 235.

[69] G. Weckwerth, Atmos. Environ. 35 (2001) 5525.

[70] D.R. Gómez, M.F. Giné, A.C. Sánchez Bellato, P. Smichowski, J. Environ. Monit. 7 (2005) 1162.

[71] S. Tanaka, N. Yasuhi, N. Sato, T. Fukasawa, S. Juari, K. Yamanaka, T. Ootoshi, J. Anal. At. Spectrom. 13 (1998) 135.

[72] J. Moreda-Piñeiro, C. Moscoso-Pérez, M. Piñeiro-Igleasias, P. López-Mahía, S. Muniategui-Lorenzo, E. Fernández-Fernández, D. Prada-Rodríguez, Talanta 71 (2007) 1834.

[73] J. Zhen, M. Ohata, N. Furuta, Anal. Sci. 16 (2000) 75.

[74] J. Zheng, M. Ohata, N. Furuta, Analyst 125 (2000) 1025.

[75] J. Zheng, A. Akihiro, N. Furuta, J. Anal. At. Spectrom. 16 (2001) 812.

[76] J. Zheng, A. Ijima, N. Furuta, J. Anal. At. Spectrom. 16 (2001) 62.

[77] H.R. Hansen, S.A. Pergantis, J. Anal. At. Spectrom. 21 (2006) 1240.

[78] M.A. López-Antón, M. Díaz-Somoano, D.Al. Spears, M.R. Marínez-Tarazon, Environ. Sci. Technol. 40 (2006) 3947.

[79] V. Valkovic, Trace Elements in Coal, CRC Press, 1983.

[80] J.M. Pacyna, E.G. Pacyna, Environ. Rev. 9 (2001) 269.

[81] Z. Mester, M. Angelote, C. Brunonri, C. Cremisini, H. Munteau, R. Morabito, Anal. Chim. Acta 395 (1999) 157.

[82] K. Das, R. Chakraborty, M. de la Guardia, M.L. Cervera, D. Goswami, Talanta 54 (2001) 975.

[83] P. Smichowski, G. Polla, A.J. Fernández Espinosa, A. Calleja López, Fuel 87 (2008) 1249.

[84] H. Lachas, R. Richard, K.E. Jarvis, A.A. Herod, D.R. Dugwell, R. Kandiyoti, Analyst 124 (1999) 177.

[85] J. Moreda-Piñeiro, C. Moscoso-Pérez, P. López-Mahía, S. Muniategui-Lorenzo, E. Fernández-Fernández, D. Prada-Rodriguez, At. Spectrosc. 22 (2001) 386.

[86] T. Narukawa, A. Takatsu, K. Chiba, K.W. Riley, D.H. French, J. Environ. Monit. 7 (2005) 1342.

[87] W.S. Seames, J. Sorooshian, J.O.L. Wendt, J. Aerosol. Sci. 33 (2002) 77.

[88] R. Miravet, E. Bonilla, J.F. López-Sánchez, R. Rubio, Anal. Chim. Acta 576 (2006) 200.

[89] R. Miravet, J.F. López-Sánchez, R. Rubio, P. Smichowski, G. Polla, Anal. Bioanal. Chem. 387 (2007) 1949.

[90] D. Gómez, P. Smichowski, G. Polla, A. Ledesma, S. Resnizky, S. Rosa, J. Environ. Monit. 4 (2002) 972.

[91] R.J. Lanzy, F.T. MacKenzi, Cosmochim. Acta 43 (1979) 511.

[92] P. Smichowski, D. Gómez, S. Rosa, G. Polla, Microchem. J. 75 (2003) 109.

Microchip gel electrophoresis with programmed field strength gradients for ultra-fast detection of canine T-cell lymphoma in dogs

Kumar K. Suresh [a], Mi-Jin Lee [b], Jinho Park [b], Seong Ho Kang [a],*

[a] *Department of Chemistry and Basic Science Research Institute, Chonbuk National University, Jeonju 561-756, South Korea*
[b] *College of Veterinary Medicine and Bio-Safety Institute, Chonbuk National University, Jeonju 561-756, South Korea*

Abstract

This paper describes the applicability of microchip gel electrophoresis using a programmed field strength gradients (MGE-PFSG) method coupled with a polymerase chain reaction (PCR) for the ultra-fast diagnosis of canine T-cell lymphoma. The variable region in the T-cell receptor γ (TCRγ) gene from a T-cell lymphoma was used in PCR amplification. The contributions of the various parameters, including the effects of the molecular weight, concentration of the sieving matrix and field strength in MGE, were examined. 0.5% poly (ethyleneoxide) (PEO, M_r 8 000 000) was used as the sieving matrix for the ultra-rapid separation of the amplified-PCR products (90 and 130-bp DNA fragments) from the PFSG at an effective length of 20 mm in a glass microchip. The PCR products (90 and 130-bp DNA) of the T-cell lymphoma were analyzed within 41.7 ± 0.1 s, 15.5 ± 0.2 s and only 7.0 ± 0.1 s using a low-constant field strength, high-constant field strength and the PFSG, respectively. When 11 clinical samples were analyzed using the MGE-PFSG method, there was a 100% correlation with those obtained using conventional slab gel electrophoresis. The ultra-fast detection and rapid separation capabilities of MGE-PFSG make it an efficient tool for diagnosing T-cell lymphoma in clinical samples with high sensitivity.
© 2007 Elsevier B.V. All rights reserved.

Keywords: Microchip electrophoresis; Canine T-cell lymphoma; Ultra-fast detection; Diagnosis

1. Introduction

Canine lymphoma is a common, spontaneously occurring hematopoietic tumor in dogs [1], and is defined as a monoclonal lymphoproliferative disease. The clinical presentation and biological behavior of this disease in dogs closely resembles their human counterparts. Consequently, dogs with lymphoma and leukemia have been considered suitable models for human cancer [2]. The availability of molecular genetic methods has further enhanced our ability to diagnose and classify lymphoid malignancies [3]. The major application of molecular genetic methods to an evaluation of a lymphoid neoplasm involves the determination of the B- and T-cell receptors. T-cell lymphocytes have a surface membrane protein complex, which is known as the T-cell receptor (TCR). TCR is structurally similar to the immunoglobulin receptor [3,4]. Recent advances

in immunology require an improvement in the methodology used in various clinical and experimental systems. Therefore, considerable effort has been devoted to the development of new methods for diagnosing and detecting lymphoma in blood samples, including flow cytometry [5] and southern blotting [3,6]. However, these methods are expensive, laborious and time consuming when applied to the detection of lymphoma in veterinary medicine [7]. Hence, a high speed and high throughput technique is needed for the rapid, sensitive and inexpensive assay and detection of canine lymphoma in the clinical field.

The polymerase chain reaction (PCR) is playing important role in modern biological research, and has greatly aided and gained widespread use in the rapid and sensitive measurement of DNA information in molecular biology with direct applications to a medical diagnosis [8]. In addition, PCR is the most popular method for assaying and evaluating a lymphoma. PCR has distinct advantages over southern blotting and flow cytometry. It is inexpensive and requires only 1 day to produce results [3]. Many different molecular markers have been evaluated to increase the

---

* Corresponding author. Tel.: +82 63 270 3421; fax: +82 63 270 3408.
 E-mail address: shkang@chonbuk.ac.kr (S.H. Kang).

sensitivity of these diagnostic tools. Among these, the clonal rearrangements of immunoglobulin (variable (V), diversity (D) and joining (J) segments) and TCR receptor (TCRγ V and J segments) genes have attracted considerable attention [9,10]. A PCR assay for identifying the TCRγ gene has recently been validated in veterinary medicine for the diagnosis of canine lymphoma.

Microchip gel electrophoresis (MGE) is a highly promising technique for rapid and sensitive analysis, and has potential in clinical diagnosis. This is despite the fact that traditional slab gel electrophoresis is a clearly established method for examining PCR-amplified DNA fragments [11–15]. MGE has attracted increasing attention as an alternative system since its introduction at the beginning of this decade [16]. The clonality in the lymphoid processes in humans has been examined using capillary electrophoresis [17,18]. The molecular diagnostics of T-cell lymphoma in dogs using PCR with capillary electrophoresis was recently reported [19]. In addition, the PCR products from T-cell lymphoma were electrophoresed under the agarose gel for slab gel electrophoresis. PEO for capillary electrophoresis and the PCR products were identified in 1 h by slab gel electrophoresis and 4 min by capillary electrophoresis. However, the current reviews on microchips stated that the MGE system has distinct advantages over the traditional capillary and slab gel electrophoresis with respect to time, resolution and sensitivity, particularly for PCR analysis in molecular biology [20]. At the same time, traditional systems cannot detect the PCR products in a single run. This paper reports the development of a novel microchip-based capillary gel electrophoresis with programmed field strength gradients (MGE-PFSG) in order to obtain more rapid separation and improved reproducibility for the ultra-fast diagnosis of canine T-cell lymphoma using the PCR-amplified products of the V and J regions in the TCRγ genes in a clonal lymphocyte population of dogs.

2. Experimental

2.1. Chemical and reagents

The $10\times$ PCR buffer (w/20 mM MgCl$_2$), 2.5 mM dNTPs and 5 U *Taq* DNA polymerase were purchased from iNtRon Biotechnology (Daejeon, Korea). The $1\times$ TBE buffer (0.089 M Tris, 0.089 M borate and 0.002 M EDTA, pH 8.31) was prepared by dissolving a pre-mixed powder (Amerosco, Solon, OH, USA) in deionized water. A dynamic coating matrix of the microchip was made by dissolving 0.5% (w/v) of polyvinylpyrrolidone (PVP, M_r 1 000 000) (Polyscience, Warrington, England) in the $1\times$ TBE buffer together along with 0.5 μg/mL ethidium bromide (EtBr, Sigma, St. Louis, MO, USA). The mixture was shaken for 2 min and left to stand for 2 h to remove all the air bubbles. The sieving matrices were made by dissolving 0.5% (w/v) of poly (ethyleneoxide) (PEO, M_r 8 000 000) and 1.5% (PEO, M_r 600 000) (Sigma, St. Louis, MO, USA) in a $1\times$ TBE buffer together with 0.5 μg/mL EtBr. The resulting mixture was then stirring slowly overnight. A 50-bp DNA ladder (25 ng/μL) (Invitrogen, Carlsbad, CA, USA) was used in slab gel electrophoresis and MGE.

2.2. Clinical sample preparation

The canine T-cell lymphoma samples were acquired from the Department of Veterinary Internal Medicine, Chonbuk National University. A 6-year-old neutered male Chihuahua had a history of an enlarged sub maxilla lymph node. The dog was diagnosed with a multicentric lymphoma (grade IV) according to the WHO standard, the physical examinations and cytology assessment of the fine needle aspirations. In addition, 2 mL of peripheral blood was obtained by venipuncture and collected into an ethylenediaminetetraacetic acid (EDTA) anticoagulant tube for a diagnosis of T-cell lymphoma by PCR.

2.3. PCR sample preparation

The genomic DNA was extracted from the peripheral blood using a GENE ALL^{TM} total DNA extraction kit for blood (Generalbiosystem, Seoul, Korea), according to the manufacturer's instructions. Sigmf1 (5′-TTC CCC CTC ATC ACC TGT GA-3′) and Srμ3 (5′-GGT TGT TGA TTG CAC TGA GG-3′) were used as the positive control primers to amplify the Cμ gene. These PCR primers were designed using Primer Express software v 2.0 (Applied Biosystems, Foster, CA, USA). The total volume of the PCR reaction was 50 μL. The compositions of the PCR are described elsewhere [18]. Briefly, the TCRγ1 (5′-ACC CTG AGA ATT GTG CCA GG-3′), TCRγ2 (5′-GTT ACT ATA AAC CTG GTA AC-3′) and TCRγ3 (5′-TCT GGG A/GTG TAC/T TAC TGT GCT GTC TGG-3′) primers were used to amplify the TCRγ gene. These PCR primers were designed using Primer Express software v 2.0 (Applied Biosystems, Foster, CA, USA). PCR was performed in a thermal cycler, MJ Research PTC-200 (Waltham, MA, USA) using the following temperature protocol: initial denaturation at 95 °C for 15 min followed by 35 cycles of denaturation at 94 °C for 8 s, annealing at 60 °C for 10 s, and extension at 72 °C for 15 s.

2.4. Slab gel electrophoresis

The amplified DNA fragments were identified by slab gel electrophoresis in 2% agarose gel (Sigma, St. Louis, MO, USA) using a $1\times$ TAE buffer. The gel loading, conditions and slab gel electropherograms are reported elsewhere [19]. The presence of a 90-bp DNA band was recorded as a positive result. The sizes of the DNA product were determined relative to those of the size marker, i.e. the 50-bp DNA ladder.

2.5. Microchip-based capillary gel electrophoresis

MCGE was performed on a DBCE-100 Microchip CE system (Digital Bio Technology Co., Korea) equipped with a diode-pumped solid-state laser (excitation at 532 nm and fluorescence at 605 nm; Power Technology Inc., Little Rock, AZ, USA) and a high-voltage device (DBHV-100, Digital Bio Technology Co., Korea). The microchip and schott borofloat glass were purchased from Micralyne (MCBF4-TT100, Micralyne, Canada). The injection design was a double-T channel with a 100-μm offset. The design of the chip channels and filling

of the buffer, coating matrix and sieving matrix are described elsewhere [14,15].

3. Result and discussion

3.1. Identification of the amplified-PCR products by slab gel electrophoresis

The sizes of the amplified-PCR products of the variable region in the TCRγ genes of the T-cell lymphoma were identified in the clonal lymphocyte population using slab gel electrophoresis. The amplified-PCR DNA fragments of the TCRγ gene were electrophoresed with 2.0% agarose gel, and stained with EtBr. Three different primers were used to amplify the TCRγ gene, TCRγ1, TCRγ2 and TCRγ3. The electropherograms of slab gel electrophoresis are reported elsewhere [19]. According to the reported data, the amplified-PCR products was identified and confirmed to be 130-bp for the positive DNA control of Cμ, 90-bp for the amplified product of TCRγ, the PCR product of normal cattle blood and the water control for the primers of the Cμ and TCRγ genes.

3.2. Optimum MGE conditions for the amplified-PCR products of TCRγ gene

The development of MGE with programmed field strength gradients for DNA separation allows an evaluation of the size of the PCR product, which is an indication of PCR amplification in a simple manner. This study examined the effectiveness of MCGE for the rapid analysis of the amplified-PCR products of a T-cell lymphoma between 50 and 150 bp in size. The standard 50-bp DNA ladder, varying in size from 50 to 2652-bp, was used as a model to optimize the separation of the DNA fragments. The important operating parameters such as the effect of the sieving gel matrix concentration and the effect of the electric field strength were investigated.

3.2.1. Effect of PEO molecular weights and concentration

A wide survey of the literature reveals that PEO, PVP, poly(dimethylacrylamide), poly (N-hydroxyethylacerylamide), hydroxypropylcellulose and some other polymers are dynamic polymers for the electrophoretic separation of DNA. Considerable effort has also been made on selecting the appropriate dynamic sieving matrix for DNA separation. In this study, PEO was selected as a sieving matrix, and the effects of the molecular weight and concentration of PEO on DNA separation were examined. Initially, the effect of the molecular weights of the sieving gel PEO (M_r 600 000 and 8 000 000) for the best separation of the 50-bp DNA ladder fragments in the MCGE system was examined by applying an electric field strength of 117.6 V/cm. This is because the molecular weights of PEO play an important role in separating the DNA fragments [21]. In addition, the applicable concentration of each PEO gel was examined by comparing the electropherograms of each PEO gel (data was not shown). The applicable concentrations of these PEO gels are as follows: 1.5% for PEO (M_r 600 000) and 0.5% for PEO (M_r 8 000 000). Among them, the PEO (M_r 8 000 000) sieving matrix was found to be more suitable for the effective separation of DNA fragments in a 50-bp DNA ladder with respect to the migration time, resolution and shorter overall analysis time. The overall analysis was complete within 90 s because the 50-bp fragment migrated at 38.28 s using PEO with $M_r = 8 000 000$. Moreover, the 50-bp fragment migrated at 60.18 s and all the DNA base pairs migrated within 150.6 s. This means that 0.5% PEO with $M_r = 8 000 000$ is better than 1.5% PEO with $M_r = 600 000$. Therefore, PEO with $M_r = 8 000 000$ was used for further experiments.

Selection of the sieving matrix concentration is the most important factor in separating DNA fragments by MGE. Electrophoresis theory suggests that the DNA molecule travels along its axis through the sieving medium with large interfiber spacing in the channel under the influence of an electric field [22]. Therefore, the effect of the sieving matrix (M_r 8 000 000) on the migration characteristics of the DNA fragments was investigated. The separation of a known 50-bp DNA ladder was performed using various PEO concentrations ranging from 0.1 to 1.1%. The migration time and resolution of the selected DNA fragments (50/100 and 100/150-bp, in the 50-bp DNA ladder by applying electric field at 117.6 V/cm) (Table 1) were examined because the amplified-PCR fragments of a T-cell lymphoma are 90 and 130-bp. The above table shows that 0.5% PEO is more suitable for separating the DNA fragments in the MGE system in terms of the migration time of the DNA base pairs. This is because the viscosity of the liner sieving matrices increases with increasing concentration [23], which would make separation more difficult and increase the time needed to fill or clean

Table 1
Migration time and resolution (R_s) of the 50, 100 and 150-bp DNA fragments at various PEO (M_r 8 000 000) gel concentrations under LCFS

PEO (%)	Migration time (s)[b]		(R_s)[a,b]	Migration time (s)[b]		(R_s)[a,b]
	50-bp	100-bp		100-bp	150-bp	
0.1	18.2 ± 0.1	18.7 ± 0.1	–	18.7 ± 0.1	19.0 ± 0.01	–
0.3	32.5 ± 0.1	33.3 ± 0.1	1.0 ± 0.1	33.3 ± 0.1	35.0 ± 0.1	1.2 ± 0.1
0.5	38.3 ± 0.1	40.0 ± 0.1	4.2 ± 0.1	40.0 ± 0.1	42.1 ± 0.1	4.8 ± 0.1
0.7	52.4 ± 0.1	60.2 ± 0.1	6.0 ± 0.1	60.2 ± 0.1	75.5 ± 0.1	6.9 ± 0.1
0.9	95.2 ± 0.1	110.3 ± 0.1	7.9 ± 0.1	110.2 ± 0.1	121.3 ± 0.1	8.7 ± 0.1
1.1	120.4 ± 0.2	135.3 ± 0.2	9.1 ± 0.2	135.3 ± 0.2	150.6 ± 0.2	10.2 ± 0.2

[a] $R_s = \Delta t/W_{ave}$ (Δt is the difference in the migration time of two adjacent peaks and W_{ave} is the average peak width of the baseline).
[b] Mean ± standard deviation ($n = 5$).

the sieving matrix with a higher concentration in the microchip channel. It was found that 0.5% PEO provides a shorter analysis time with the best resolution (4.2 ± 0.1 for 50/100-bp and 4.8 ± 0.1 for 100/150-bp, $n = 5$) with an adequate viscosity than the other PEO concentrations.

3.2.2. Effect of electric field on the ultra-fast DNA separation

Initially, a low-constant field strength (LCFS), 117.6 V/cm, was used to separate all the DNA base pairs in the 50-bp DNA ladder. At this strength, all the DNA base pairs were separated within 90 s (data was not shown). Furthermore, the application of a high-electric field strength in capillary electrophoresis leads to a shorter analysis time and a decrease in the above 800-bp separation efficiency [24]. This rapid decrease in the total migration time at high-electric field strength might be due to the increase in the electrophoretic velocity (V_{EP}) of DNA molecules: under the influence of an electric field (E), negatively charged DNA molecules will migrate through a buffer with an electrophoretic velocity (V_{EP}), which can be expressed as the product of the electric field and electrophoretic mobility (μ_{EP}) at a given field strength ($V_{EP} = \mu_{EP} \times E$) [25]. Since E is the voltage/length, changing the voltage is an easy way of controlling the velocity of DNA molecules because it produces a variation in electric field [14]. However, a high-electric field strength can also have deleterious effects on the DNA fragments and PCR products due to microchip heating and other effects. Moreover, a high-electric field strength can increase in the microchip temperature due to Joule heating caused by Ohm's law [26], which contributes significantly to zone spreading of the DNA peaks in the electropherograms. Therefore, it is important to determine the optimum electric field strength for the rapid diagnosis of T-cell lymphoma in dogs. The migration time and resolution of the 50, 100, 150-bp DNA were examined at various electric fields ranging from 29.40 to 499.80 V/cm at a 20 mm effective length in the microchip. Fig. 1 shows the migration time and resolution of the selected 50/100 and 100/150-bp as a function of the electric field strength. The results show that the migration time and resolution of the DNA fragments was inversely proportional to the applied field strength. It was found that all the DNA fragments were separated within 90 s at the low-constant electric field strength (LCFS) of 117.6 V/cm. The electric field strength was increased gradually up to 499.8 V/cm, and the separation efficiency and resolution of the selected base pairs was examined. A high-constant electric field strength (HCFS) of 294.0 V/cm was selected as the optimum high-constant field strength with respect to the migration time and resolution of the selected DNA fragments (50, 100 and 150-bp; Fig. 2). However, although increasing the electric field to 294.0 V/cm reduced the migration time of the DNA base pairs, the DNA base pairs migrated more rapidly with adequate resolution by applying a non-uniform electric field strength.

Table 2 shows the advantages of the MGE-PFSG method over the LCFS and HCFS with respect to the migration time and resolution of the selected DNA base pairs. The velocity of the DNA molecule is increased by increasing the electric field. In
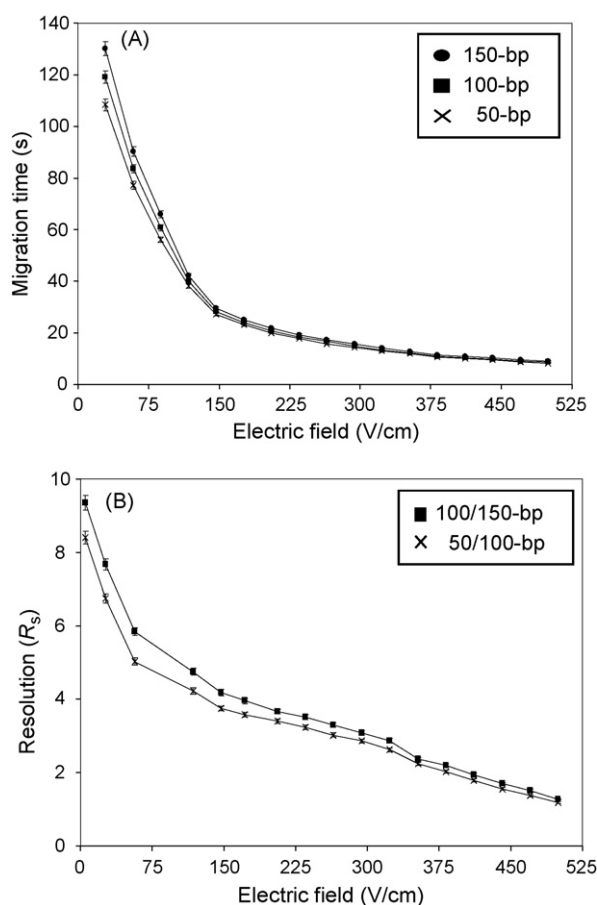

Fig. 1. (A) Migration time and (B) resolution of the 50–150-bp DNA fragments as a function of the applied electric field. MGE voltage conditions; applied separation voltage, from 29.4 to 499.8 V/cm; sample, 50-bp DNA ladder fragment (50-, 100- and 150-bp); the running buffer, 1× TBE buffer (pH 8.31) with 0.5 ppm EtBr; coating matrix, 0.5% PVP (M_r 1 000 000); sieving matrix, 0.5% PEO (M_r 8 000 000).

this PFSG, the migration time of the 50-bp DNA was reduced to 6 s by applying an electric field of 470.4 V/cm. After the migration of the 50-bp DNA, the electric field was decreased to 205.8 V/cm for 2 s to obtain the appropriate resolution between

Table 2
Comparison of the PFSG method over the MGE for the ultra-fast separation of the 100 and 150-bp DNA fragments in a 50-bp DNA ladder

Applied MGE methods	Migration time (s)		$R_s{}^a$
	100-bp	150-bp	
LCFS	40.0 ± 0.1	42.1 ± 0.1	4.8 ± 0.1
HCFS	15.1 ± 0.2	16.0 ± 0.2	2.8 ± 0.2
PFSG	6.6 ± 0.1	7.5 ± 0.1	2.7 ± 0.1

Applied separation voltage: 117.6 V/cm for LCFS, 294.0 V/cm for HCFS; applied PFSG: 470.4 V/cm for 6 s, 205.8 V/cm for 2 s, 470.6 V/cm for 20 s; run buffer: 1× TBE buffer (pH 8.31) with 0.5 ppm of EtBr; coating matrix: 0.5% PVP (M_r 1 000 000); sieving matrix: 0.5% PEO (M_r 8 000 000) at effective length 20 mm.
[a] R_s (resolution between 100 and 150-bp DNA fragments) = $\Delta t / W_{ave}$ (Δt is the difference of migration time of two adjacent peaks and W_{ave} is the average peak width of baseline).
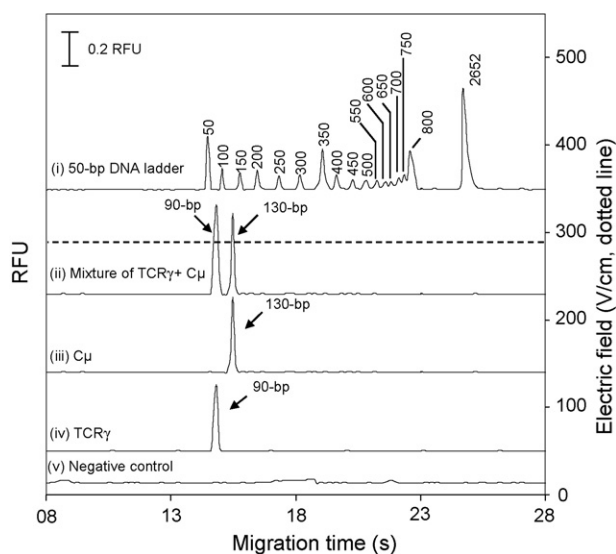
Fig. 2. MGE separation of the amplified-PCR products of T-cell lymphoma. (i) 50-bp DNA ladder; (ii) mixture of TCRγ and Cμ; (iii) positive control Cμ (130-bp); (iv) TCRγ (90-bp); and (v) negative control. ME condition: running buffer 1× TBE buffer (pH 8.31) with 0.5 ppm EtBr; coating matrix, 0.5% PVP (M_r 1 000 000); sieving matrix, 0.5% PEO (M_r 8 000 000); electrokinetic injection 56.50 V/cm for 60 s, applied separation voltage, 294.0 V/cm; effective length, 20 mm; RFU, relative fluorescence unit. The dotted lines represent the applied electric field.
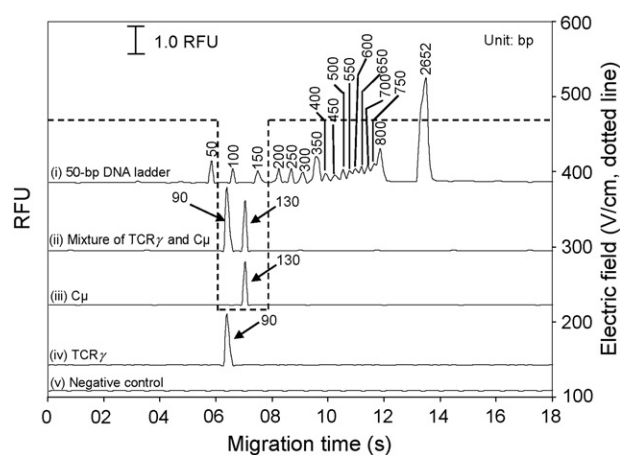

Fig. 3. Electropherograms of the amplified-PCR products of a T-cell lymphoma in dogs along with the 50-bp DNA ladder by MGE-PFSG. (i) 50-bp DNA ladder; (ii) mixture of TCRγ and Cμ; (iii) positive control Cμ (130-bp); (iv) TCRγ (90-bp); and (v) negative control. MGE-PFSG condition: running buffer 1× TBE buffer (pH 8.31) with 0.5 ppm EtBr; coating matrix, 0.5% PVP (M_r 1 000 000); sieving matrix, 0.5% PEO (M_r 8 000 000); electrokinetic injection 56.50 V/cm for 60 s, applied PFSG, 470.4 V/cm for 6 s, 205.8 V/cm for 2 s and 470.4 for 20 s; effective length, 20 mm; RFU, relative fluorescence unit. The dotted lines represent the applied electric field.

the 50/100 and 100/150-bp DNA. After the migration of the 150-bp DNA, the electric field was increased to 470.4 V/cm for 20 s to allow the rapid migration of the DNA fragments above 150-bp (Fig. 3). In this interval all the DNA fragments had migrated within 13.90 s with poor resolution. However, the resolution of the above 150-bp fragments is not important to this study because the PCR products of the T-cell lymphoma are <150-bp. Fig. 2 (HCFS) and Fig. 3 (PFSG) show the electropherograms of T-cell lymphoma PCR products obtained under different electric fields. The resolution did not change significantly by applying non-uniform electric filed strengths in the microchip. It should be noted that the MGE-PFSG system electrophoresed the PCR products within 7.0 ± 0.1 s by applying non-uniform electric field strength. The reproducibility of the present method was examined and the results are shown in Table 2. The table confirms the accuracy of PFSG for the ultra-fast detection of selected DNA fragments with a migration time for the 100 and 150-bp of 6.6 ± 0.1 and 7.5 ± 0.1 s,

respectively, and a resolution of 2.5 ± 0.1 and 2.7 ± 0.1, respectively.

3.3. Application of clinical samples

In addition, clinical samples from three dogs with a suspected lymphoma and normal seven dogs were measured to compare MGE with slab gel electrophoresis (Table 4). Three different field strengths, LCFS, HCFS and PFSG, were applied. Among them, the PFSG method was found to more rapidly detect the target DNA base pairs than the other methods with adequate resolution. This highlights the precision and accuracy of the present method. The present method was applied to the rapid diagnosis of the amplified-PCR products of T-cell lymphoma in dogs. Good reproducibility and accuracy of the amplified-PCR products of T-cell lymphoma was obtained with a migration time of 39.1 ± 0.1 and 41.3 ± 0.2 s for TCRγ (90-bp) and the positive control Cμ (130-bp) by LCFS, respectively (data not shown). The resolution of the 90/130-bp products and the migration times of TCRγ (90-bp) and positive control Cμ (130-bp) by HCFS were 2.6 ± 0.1, 14.8 ± 0.1 and 15.5 ± 0.2 s, respectively (Fig. 2 and Table 3).

Table 3
Comparison of the migration time, peak area and resolution of mixtures of TCRγ (90-bp) and Cμ (130-bp) fragments at a sieving gel containing 0.5% PEO (M_r 8 000 000), high-electric field strength and programmed field strength gradients at an effective length 20 mm

MGE methods	Migration time (s)[a]		R_s[b]	Peak area[a]	
	TCRγ (90-bp)	Cμ (130-bp)		TCRγ (90-bp)	Cμ (130-bp)
HCFS	14.8 ± 0.1	15.5 ± 0.2	2.6 ± 0.1	43.5 ± 0.1	30.7 ± 0.2
PFSG	6.4 ± 0.1	7.0 ± 0.1	2.6 ± 0.1	41.2 ± 0.2	28.2 ± 0.2

[a] Mean ± standard deviation ($n = 5$).
[b] $R_s = \Delta t / W_{ave}$ (Δt is the difference in the migration time between two adjacent peaks and W_{ave} is the average peak width of the baseline).

Table 4
Comparison of the MGE technique with the conventional slab gel electrophoresis for the detection of the amplified-PCR products of T-cell lymphoma in clinical samples

Case number	Kinds of canine blood	MGE	Slab gel electrophoresis
1	T-cell lymphoma[a]	+	+
2	Normal[b]	−	−
3	T-cell lymphoma[a]	+	+
4	Normal[b]	−	−
5	Normal[b]	−	−
6	T-cell lymphoma[a]	+	+
7	Normal[b]	−	−
8	Normal[b]	−	−
9	T-cell lymphoma[a]	+	+
10	Normal[b]	−	−
11	Normal[b]	−	−

[a] Positive for T-cell lymphoma.
[b] Negative for T-cell lymphoma.

MGE-PFSG was used to analyze the amplicons from the clinical samples. The performance of the MGE-PFSG was compared with that of slab gel electrophoresis. Eleven samples were amplified and analyzed using the MGE method. All real clinical samples had previously been analyzed in PCR/slab gel electrophoresis. The results of the two methods were compared with those from slab gel electrophoresis, and there was a 100% correlation between the negative and positive control of the clinical samples (Table 4). Among them, four samples tested positive to the TCRγ gene (90-bp) and seven samples tested negative. In HCFS, 16, 14.81 and 15.46 s was required to obtain these results for the 90/130-bp PCR products, TCRγ (90-bp) and for Cμ (130-bp), respectively. At the same time, MGE-PFSG analyzed the 90/130-bp products, TCRγ (90-bp) and positive control Cμ (130-bp) in 8, 6.48 and 7.03 s, respectively (Fig. 3). Although a high-electric field was used non-uniformly, there was no major difference in the resolution of the target base pairs compared with the HCFS and PFSG. However, the migration time of the target base pairs was reduced greatly by applying a non-uniform electric field strength. It should be noted that all the amplified-PCR products were quite visible with a high sensitivity, and the procedure was much faster than conventional slab gel electrophoresis. Furthermore, only several hundred nL ($\times10^{-9}$ L) of the introduced-sample was required for microchip analysis. In the case of slab gel electrophoresis, a sample volume of 10–12 μL and 1 h was needed for amplified-PCR analysis. These results clearly show the superiority of the MGE-PFSG method over slab gel electrophoresis.

This method has considerable advantages over slab gel electrophoresis such as an accurate evaluation of the DNA size, high efficiency, easy operation as well as low-sample consumption. Overall, MGE-PFSG is useful for analyzing the PCR products <150-bp. In clinical applications, this method will be a powerful tool in clinical diagnoses e.g. analysis of the amplified-PCR products of the T-cell lymphoma (90-bp DNA fragment) within 8 s.

4. Conclusions

The MGE-PFSG system can separate the DNA amplification products in an automated fashion with an adequate resolution in molecular biology, particularly to the analysis of amplified-PCR products. The capability of MGE-PFSG for the ultra-fast diagnosis of canine lymphoma in dogs was highlighted using the amplified-PCR products. In this method, the TCRγ gene (90-bp DNA) and positive control Cμ (130-bp DNA) were used to diagnose T-cell lymphoma in dogs. To the best of our knowledge, this is the first report of a diagnosis of canine lymphoma in dogs using a MCGE technique. This method provided good accuracy and reproducibility for the analysis of the DNA fragments and PCR products. Furthermore, the potential of MGE for the analysis of amplified-PCR products was also demonstrated. As a result, with a PFSG, MGE showed improved speed, simplicity and resolution as well as improved throughput. This method is simple, less time consuming and inexpensive compared with conventional slab gel electrophoresis, and will greatly reduce the level of sample and chemical consumption. Overall, accurate DNA sizing with MGE-PFSG makes it suitable for making a rapid diagnosis of canine lymphoma in dogs and is expected to have other clinical applications.

References

[1] E. Teske, Vet. Quart. 16 (1994) 209.
[2] E.B. Dickerson, S. Fosmire, M.L. Padilla, J.F. Modiano, S.C. Helfand, J. Immunother. 25 (2002) 36.
[3] W.N. Rezuke, E.C. Abernathy, G.J. Tsongalis, Clin. Chem. 43 (1997) 1814.
[4] D.G. Schatz, M.A. Oettinger, M.S. Schlissel, Annu. Rev. Immunol. 10 (1992) 359.
[5] A. Beineke, U. Siebert, N. van Elk, W. Baumgartner, Vet. Immunol. Immnopathol. 98 (2004) 59.
[6] D. Xu, J. Du, H. Kamino, H. Ratech, Am. J. Dermatopathol. 26 (2004) 385.
[7] K.A. Hodges, C.M. Kosciol, W.N. Rezuke, E.C. Abernathy, W.T. Pastuszak, G.J. Tsongalis, Ann. Clin. Lab. Sci. 26 (1996) 114.
[8] R.K. Saiki, S. Scharf, F. Faloona, K.B. Mullis, G.T. Horn, H.A. Erlich, N. Arnheim, Science 230 (1985) 1350.
[9] K. Tamura, H. Yagihara, M. Isotani, K. Ono, T. Washizu, M. Bonkobara, Vet. Immunol. Immnopathol. 110 (2006) 163.
[10] W. Vernau, P.F. Moore, Vet. Immunol. Immnopathol. 69 (1999) 145.
[11] M.A. Burns, B.N. Johnson, S.N. Brahmasandra, K. Handique, J.R. Webster, M. Krishnan, T.S. Sammarco, P.M. Man, D. Jones, D. Heldsinger, C.H. Mastrangelo, D.T. Burke, Science 282 (1998) 484.
[12] Y. Kim, J.-S. Chae, S.H. Kang, J. Korean Chem. Soc. 48 (2004) 483.
[13] D.K. Kim, S.H. Kang, J. Chromatogr. A 1064 (2005) 121.
[14] S.H. Kang, M. Park, K. Cho, Electrophoresis 26 (2005) 3179.
[15] Y.-J. Kim, J.-S. Chae, J.K. Chang, S.H. Kang, J. Chromatogr. A 1083 (2005) 179.
[16] C.S. Effenhauser, G.J. Bruin, A. Paulus, Electrophoresis 18 (1997) 2203.
[17] T.L. Chang, M. Salto-Tellez, P.T. Thamboo, Y.S. Lee, E.S. Koay, Clin. Chem. 49 (2003) 513.

[18] V. Luo, S.R. Lessin, R.B. Wilson, H. Rennert, C. Tozer, B. Benoit, D.G. Leonard, Mol. Diagn. 6 (2001) 169.
[19] S.S. Jeon, M.J. Lee, J. Park, S.H. Kang, J. Chromatogr. B 854 (2007) 268.
[20] S.F. Li, L.J. Kricka, Clin. Chem. 52 (2006) 37.
[21] R. Sonoda, H. Nishi, K. Noda, Chromatographia 48 (1998) 569.
[22] O.J. Lumpkin, P. Dejardin, B.H. Zimm, Biopolymers 24 (1985) 1573.
[23] M.N. Albarghouthi, A.B. Barron, Electrophoresis 21 (2000) 4096.
[24] A. Guttman, B. Wanders, N. Cooke, Anal. Chem. 64 (1992) 2344.
[25] D.R. Baker, Capillary Electrophoresis, John Wiley & Sons, New York, 1995, pp. 5–143.
[26] A.S. Rathore, K.J. Reynolds, L.A. Colon, Electrophoresis 23 (2002) 2918.

Short communication

Micelle mediated extraction of titanium and its ultra-trace determination in silicate rocks

Pranab K. Tarafder *, Raghbendra Thakur

*Regional Centre for Exploration & Research, Atomic Minerals Directorate, Department of Atomic Energy, Khasmahal,
P.O. Tatanagar, Jamshedpur 831002, India*

Abstract

A highly sensitive method for extractive spectrophotometric determination of titanium in silicate rocks is described. Titanium in the range 0–10 μg as TiO_2 is extracted into benzene or toluene by the formation of a ternary complex of the metal with thiocyanate (SCN^-) and cetyltrimethylammonium bromide (CTA) in the ratio 1:2:2. A deep yellowish-orange ternary complex thus formed is suitable for the determination of titanium at wavelength 421 nm. The optimum colour intensity of this ternary complex was attained when the complex was extracted from an aqueous solution having concentrations of thiocyanate and HCl, in the range, 1.5–2.5 and 1–5 mol L^{-1}, respectively. The molar absorptivity and Sandell's sensitivity of the extracted species were found to be 1.1–1.0 $\times 10^5$ L mol^{-1} cm^{-1} and 0.47 ng cm^{-2} (referred to titanium), respectively, at λ_{max} of 421 nm. Except Fe^{3+}, Nb^{5+} and V^{5+}, no interference was encountered in the estimation of titanium. While up to 10 mg L^{-1} Nb and V did not interfere in the determination of titanium, the interference of Fe^{3+} was eliminated by reducing it to Fe^{2+} using $SnCl_2$ solution. The method is highly sensitive and selective. The results obtained for titanium estimation in a host of silicate rock samples have been found to be highly reproducible, accurate and favourably comparable with certified values of reference materials and those obtained from standard methods.
© 2007 Elsevier B.V. All rights reserved.

Keywords: Extraction; Titanium; Spectrophotometry; Silicate rocks

1. Introduction

There are many spectrophotometric methods [1–4] for the estimation of titanium in silicate rocks. Mention may be made of a few such methods using well-known reagents like H_2O_2 [5], tiron [6], chromotropic acid [7], gallic acid [8], di-antipyrilmethane [9], chloro-salicylic acid [10], 2,3-dihydroxynaphthalene [11,12], etc. The sensitivity of most of these methods is not sufficient (ε in the range 1.5–3.2 $\times 10^4$ L mol^{-1} cm^{-1}) for trace determination of titanium in silicate rocks of diverse matrices.

Besides, there are a few highly sensitive methods such as those using bromo-pyrogallol red [13] and phenylflourones [14] and its derivatives. Although the cited methods are sensitive, these are not practically suitable for applications to silicate rock samples of diverse matrices owing to their poor selectivity. The flame atomic absorption spectrophotometry is insensitive for

titanium determination [15]. Though the determination of titanium in silicate rocks by ICP-AES is quite satisfactory, but spectral interferences can cause problem and cost the analyst a good deal of time in their elimination [16].

Therefore, the spectrophotometry is the mainstay for titanium determination, and accordingly, it was incumbent on us to devise a suitable spectrophotometric method for application to such samples where titanium is present in traces.

Unlike iron (Fe^{3+}), thiocyanate does not form colour complexes with titanium in aqueous solution. However, under suitable experimental conditions, i.e., at high concentration of thiocyanate (5.85 mol L^{-1} NaSCN) and requisite amount of acidity, the yellowish-orange binary complex of titanium with thiocyanate can be extracted into acetone–water mixture or in MIBK without any counter cation [1]. The poor selectivity and incomplete extraction of the complex in these solvents discouraged us to use such method, although sensitivity was found reasonably high ($\acute{\varepsilon} = 7.8 \times 10^4$ L mol^{-1} cm^{-1}).

Ternary complex formation often facilitates extraction of metals with concomitant increase in the colour intensity of the extracted species. Sometimes, it also enhances the stability of

---

* Corresponding author. Tel.: +91 657 2297689; fax: +91 657 2297689.
E-mail address: ptarafder@sify.com (P.K. Tarafder).

the complex formed to a great extent [17,18]. Keeping this in mind, many workers in the past extracted titanium as its ternary or mixed ligand complexes with thiocyanate and a host of other hetero-ligands.

Besides, some other hetero-ligands like monooctyl-α-anilinobenzyl-phosphonate [19], 1-phenyl-2-methyl-3-hydroxy-4-pyridone [20], *N*-hydroxy-*N*-*N*′-diphenyl benzamidine [21] are also reported to form mixed ligand complexes of titanium with thiocyanate having very poor sensitivities, i.e., the molar absorptivities (ε) ranging from 1.1×10^4 to 2.65×10^4 L mol^{-1} cm^{-1}

In most of the above-mentioned ternary systems, the hetero-ligands are attached to the metal either as solvated species or as an adductant.

Though the above-mentioned methods were separately applied to steel and aluminium alloys, fused silica, platinum chloride and sea waters by different workers, most of these could not be satisfactorily applied to complex matrices of silicate rocks owing to poor selectivity, lack of reproducibility and difficulty in extraction.

While carrying out investigations on the micelle mediated extraction of metals for last few years in our laboratory, we found that the binary thiocyanate complexes of iron(III) and titanium, which are extremely insensitive in aqueous solution, could be promptly extracted into suitable organic solvent in the presence of CTA. On extraction in the presence of CTA, the intensity of the colour increased manifold. Although Fe^{3+}–thiocyanate system could be extracted into ethyl acetate without the use of CTA, no apparent increase in the colour intensity was noticed. However, on extraction in the presence of CTA, the sensitivity increased at least four-fold and, at the same time, the very limited range of Beer's law adherence broadened appreciably. Besides, the highly unstable binary Fe^{3+}–thiocyanate complex got stabilized for many hours on the formation of ternary complex with CTA [22].

The striking features of the present system are that, compared with other reported ternary systems already discussed, the selectivity and sensitivity are much better. Moreover, the extraction was also found to be facile. Only Nb and V interfered, that too, if present in at least 10-fold excess concentration to titanium. Besides, the stability of the colour and reproducibility of the results are excellent.

In this context, it is pertinent to mention here that during the course of our investigation on this project, a report on the spectrophotometric determination of Ti(IV) by extraction of its thiocyanate complex into chloroform or CH$_2$Cl$_2$ in the presence of cetyltrimethylammonium (CTA), cetylpyridinium (CP) and tetradecyldimethylbenzylammonium (TDMA) cations appeared in literature [23]. However, the sensitivity of the above system is reported to be much less ($\varepsilon = 6.1$, 6.3 and 7.0×10^4 L mol^{-1} cm^{-1} for CTA, CP and TDMA systems, respectively) compared to 1.1×10^5 L mol^{-1} cm^{-1} for the present system. Besides, the validity of the reported method was tested on the simple matrices of bauxite and aluminium alloys.

In view of the above, and in continuation of our on-going independent project work on the micelle mediated extraction of metals with thiocyanate and CTA [22,24,25], we present here the results of a detailed and systematic study on the micelle medi-

ated extraction of titanium in toluene (although in the present system, benzene as a solvent was found marginally better than toluene and xylene, it is, however, not prescribed for further use because of its reported carcinogenic nature) and its extraction spectrophotometric determination in silicate rocks.

2. Experimental

2.1. Apparatus

A double beam spectrophotometer (Model-Chemito 2500) equipped with 1 cm quartz cells was used for the absorbance measurements.

2.2. Reagents

All the reagents used were of Analytical Reagent grade.

Stock Ti solution (400 µg mL^{-1}): A 0.1 g TiO$_2$ was weighed into a silica crucible and fused with 4 g potassium bisulfate. The fused mass was dissolved in 250 mL distilled water containing about 40 mL concentrated H$_2$SO$_4$. A working standard solution (40 µg mL^{-1}) was made by transferring 10 mL of the stock solution into a 100 mL volumetric flask followed by the addition of 5 mL concentrated sulfuric acid and then diluting the solution to 100 mL with distilled water. Reagents used were potassium thiocyanate (5.15 mol L^{-1}), stannous chloride (4.43×10^{-1} mol L^{-1}) in 1.1 mol L^{-1} HCl, hydrochloric acid (11 mol L^{-1}), hydrofluoric acid (22.6 mol L^{-1}), cetyltrimethylammonium bromide (2.74×10^{-1} mol L^{-1}) and solvents like benzene, toluene, xylene, etc.

2.3. Procedure

2.3.1. Dissolution of silicate rock samples

The rock sample solutions were prepared by following the recommended procedure [3].

2.3.2. Extraction and spectrophotometric measurements

A 2 mL sample aliquot containing Ti up to 6 µg (10 µg TiO$_2$) was taken in a 100 mL separating funnel. To it was added 5 mL of 5.15 mol L^{-1} KSCN and mixed well. To this solution were added 1 mL of 4.43×10^{-1} mol L^{-1} SnCl$_2$ and 2 mL of 11 mol L^{-1} HCl. Mixed well and allowed to stand for 2 min. Then added 10 mL of benzene or toluene and 1 mL of 2.74×10^{-1} mol L^{-1} aqueous solution of CTA. Shaken vigorously for 3 min and set aside for 5 min to allow for phase separation. A yellowish-orange ternary complex of Ti–SCN–CTA was formed which was readily extracted into benzene or toluene. The aqueous portion was carefully drained out and the organic portion was filtered into a dry and clean quartz cell through Whatman filter-paper 540 for spectrophotometric measurements at λ_{max} (421 nm). The measurements were made against a process blank.

3. Results and discussion

For subsequent experiments 10 µg TiO$_2$ was taken in about 11 mL aqueous solution and extracted into 10 mL organic solvent for absorbance measurements.
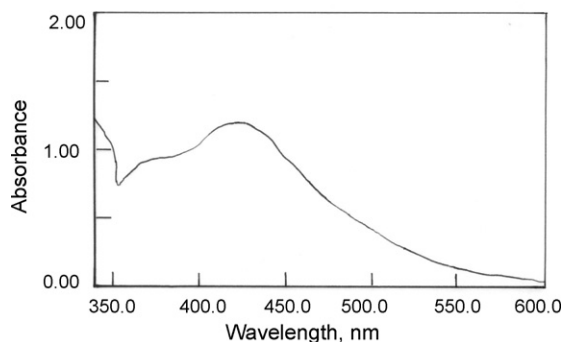
Fig. 1. Absorption spectrum of the complex against reagent blank. *Conditions*: $[TiO_2] = 1.0\,mg\,L^{-1}$; $[HCl] = 2.0\,mol\,L^{-1}$; $[SCN] = 2.34\,mol\,L^{-1}$ and $[CTA] = 2.49 \times 10^{-2}\,mol\,L^{-1}$.

3.1. Absorption spectra

The absorption spectrum was scanned over a wavelength range, 300–600 nm against benzene/toluene. The λ_{max} was found at 421 nm. Similarly, the absorption of reagent blank against benzene/toluene was also scanned and it was found that the reagent blank had got a negligible absorbance, i.e., <0.001. But for experimental purposes, measurements of absorbance were always made against a reagent blank. The absorption spectrum of complex is shown in Fig. 1.

3.2. Effect of KSCN and CTA concentrations

The concentration of thiocyanate was varied from 0.1 to 3.5 mol L^{-1}. Under the optimized conditions of hydrochloric acid and cetyltrimethylammonium bromide, thiocyanate in the range, 1.5–2.5 mol L^{-1} was found to have given maximum absorbance for 1.0 mg L^{-1} TiO$_2$, i.e., 1.35, 1.30 and 1.25 absorbance units for benzene, toluene and xylene, respectively. For this purpose, a 5 mL of 5.15 mol L^{-1} potassium thiocyanate was fixed for colour development and extractive recovery of titanium. At this optimized concentration of thiocyanate, the effect of cetyltrimethylammonium bromide was studied by varying its concentration over a wide range. It was found that in the presence of SnCl$_2$ which was required for reducing Fe^{3+} into Fe^{2+} in order to avoid interference of ferric ion, a 1 mL of 2.74×10^{-1} CTA was required to attain highest sensitivity for titanium. In this context, it is pertinent to mention here that in the absence of SnCl$_2$, a less amount of CTA (5 mL of 2.74×10^{-2} mol L^{-1}) was sufficient to attain the sensitivity of the order of $\varepsilon = 1.00 \times 10^5$ L mol^{-1} cm^{-1}. Fig. 2 shows the effect of thiocyanate and CTA in the extraction of titanium.

3.3. Effect of acidity

The effect of acidity in the development of the colour of the complex as well as maximum extraction of titanium was studied by using different mineral acids such as nitric, sulfuric and hydrochloric acids. The use of nitric acid was avoided because of its decomposition in the reaction medium as well as due to its possible redox-reaction with thiocyanate. Similarly, sulfu-
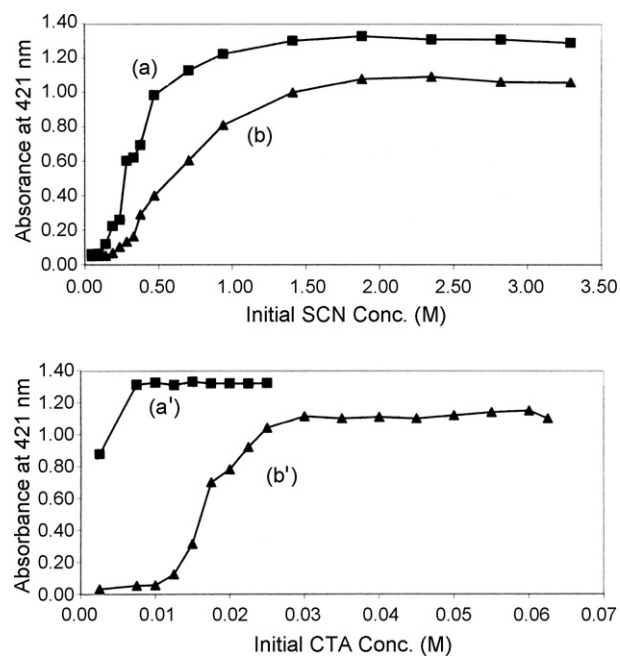

Fig. 2. Dependence of the absorbance of extracted titanium(IV)–thiocyanate complex on the initial molar concentration of SCN /CTA. *Conditions*: $[TiO_2] = 1.0\,mg\,L^{-1}$; $[HCl] = 2.0\,mol\,L^{-1}$; (1) absorbance vs. molar concentration of SCN; curve (a) $[CTA] = 2.49 \times 10^{-2}\,mol\,L^{-1}$ and $[SnCl_2] = nil$. Curve (b) $[CTA] = 2.49 \times 10^{-2}\,mol\,L^{-1}$ and $[SnCl_2] = 4.03 \times 10^{-2}\,mol\,L^{-1}$. (2) Absorbance vs. molar concentration of CTA; curve (a′), $[SCN] = 2.34\,mol\,L^{-1}$ and $[SnCl_2] = nil$. Curve (b′), $[SCN] = 2.34\,mol\,L^{-1}$ and $[SnCl_2] = 4.03 \times 10^{-2}\,mol\,L^{-1}$.

ric acid was also avoided because of its exothermic reaction with water leading to the possible decomposition of the complex as well as solvent. Therefore, hydrochloric acid was tried and found to be suitable for this purpose in order to achieve maximum sensitivity and recovery of titanium. The concentration of this acid was varied over a wide range, i.e., from 0.1 to 5.0 mol L^{-1}. A 2 mL of 11 mol L^{-1} HCl (total molarity of acid being 2.0 mol L^{-1}) was fixed, although its concentration in the range 1–5 mol L^{-1} did not affect the percentage extraction and intensity of the complex (Fig. 3).

3.4. Effect of volume ratio of the solvents, electrolyte concentration and equilibrium time

Under the optimized condition of reagents such as KSCN and CTA as well as that of hydrochloric acid, the ratio of volume of the aqueous phase to that of organic phase was varied over a wide range, i.e., from 1:5 [aqueous:organic] to 5:1 [aqueous:organic]. It was found that 1:1 ratio of the volume of aqueous to organic phase yielded the most satisfactory results, i.e., highest sensitivity coupled with maximum recovery of Ti. However, a variation of volume ratio of aqueous to organic phase between 1:1.5 and 1.5:1 had not affected the recovery of Ti and the sensitivity of the reaction. The effect of electrolytes like NaCl, KCl and ammonium chloride up to 1 mol L^{-1} was also studied. None had any effect on the intensity of the colour and recovery of Ti. An equilibrium time of 2 min was sufficient for maximum recovery of Ti, however for safer sides, extraction for 3 min was employed
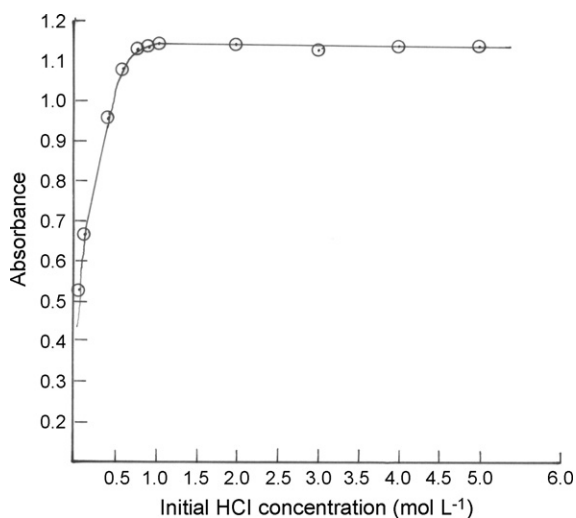
Fig. 3. Effect of HCl concentration on the extraction of titanium (plot of absorbance vs. HCl concentration). *Conditions*: $[TiO_2] = 1.0\,mg\,L^{-1}$; $[HCl] = 2.0\,mol\,L^{-1}$; $[SCN] = 2.34\,mol\,L^{-1}$; $[CTA] = 2.49 \times 10^{-2}\,mol\,L^{-1}$ and $[SnCl_2] = 4.03 \times 10^{-2}\,mol\,L^{-1}$.

for all the experiments carried out. Extraction even up to 15 min did not change the intensity of the colour.

3.5. Effect of reducing agent

The effect of reducing agents like ascorbic acid, hydroxylamine–hydrogen chloride, and tin(II) chloride were tested separately. It was found that tin(II) chloride was more effective in reducing Fe^{3+}, which otherwise seriously interfered in the estimation of Ti. Contrary to what has been reported in literature and experienced elsewhere in the estimation of Nb, Mo, etc. tin(II) chloride did not enhance the distribution ratio of titanium in benzene or toluene in the present study. However, it adversely affected the sensitivity, i.e., sensitivity was gradually decreased with the increase in $SnCl_2$ concentration. But in real samples, where iron is invariably present, the use of tin(II) chloride could not be avoided. Hence, a reduced sensitivity ($\varepsilon = 8.0 \times 10^4\,L\,mol^{-1}\,cm^{-1}$) was compromised with 1 mL of $4.43 \times 10^{-1}\,mol\,L^{-1}$ $SnCl_2$ in $1.1\,mol\,L^{-1}$ HCl.

3.6. Effect of solvents

Various polar and non-polar solvents like benzene (C_6H_6), toluene, xylene, chloroform, carbon tetrachloride, MIBK, ethyl acetate, butanol, *n*-butyl acetate, etc. were tried in our laboratory but in most cases, the sensitivity was not high enough (less than 50% compared to benzene or toluene or xylene as solvent) and the complex formed was not very stable. Besides, extraction was also found to be tedious and incomplete. On the contrary, when C_6H_6 or toluene was used as a solvent, the extraction was found to be facile and the equilibrium period for the complete distribution of Ti from aqueous to organic phase was less than 2 min. Besides, high distribution ratio (recovery of Ti was more than 99% in a single extraction) coupled with maximum sensitivity

and excellent stability of the colour formed (the complex is stable for more than 24 h) was achieved when benzene or toluene was used as solvent.

3.7. Optimum concentration range, sensitivity and precision

The Beer's law is obeyed over a range, $0–1\,mg\,L^{-1}$ TiO_2. The detection limit is 0.4 ng of $Ti\,mL^{-1}$. The limit of detection was defined as $C_L = 3S_B/m$, where C_L, S_B and m are the limit of detection, standard deviation of the blank and the slope of the calibration graph, respectively. The molar absorptivities of the complex in the absence and in the presence of tin(II) chloride are $(1.1 \pm 0.05) \times 10^5\,L\,mol^{-1}\,cm^{-1}$ and $(8.00 \pm 0.05) \times 10^4\,L\,mol^{-1}\,cm^{-1}$, respectively. Similarly, the Sandell's sensitivities of the complex in the absence and presence of tin(II) chloride are 0.47 and $0.50\,ng\,cm^{-2}$, respectively. The standard deviation (σ) and relative standard deviation (R.S.D.) of $1\,\mu g\,mL^{-1}$ TiO_2 over a period of nine consecutive days were found to be 0.032 and 2.73%, respectively.

3.8. Composition of the complex

The stoichiometry of the complex was investigated by plotting $\log D$ vs. $\log[Reagent]$ (curve fitting method [26]). In the plotting (Fig. 4), curves 'a' and 'b' show a slope of 1.98 and 1.97, respectively, both close to the integer 2. Therefore, the ratio of Ti(IV):SCN:CTA in the extracted complex should be 1:2:2, respectively. Accordingly, it may be presumed that 2 mol of thiocyanate are coordinated to Ti(IV) as ligands while 2 mol of CTA are attached as adductants. The overall reaction can be written as,

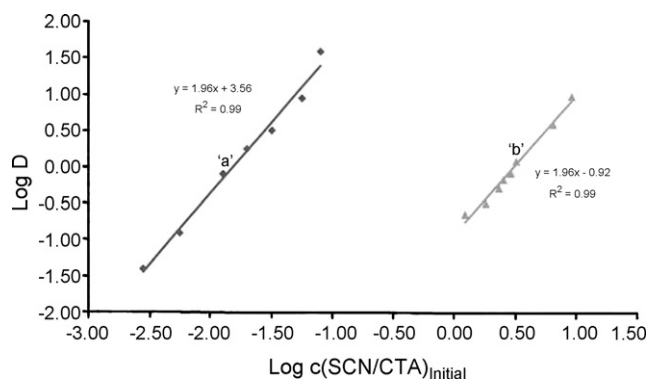$$TiO^{2+} + 2SCN^- + 2CTA = [TiO(SCN)_2]\cdot 2CTA_O$$

The subscript "O" denotes the organic phase.

Fig. 4. Determination of ratio of the variables in $[TiO(SCN)_X]$ $yCTA$ by curve fitting method (plot of $\log D$ vs. log of initial molar concentration of SCN/CTA). *Conditions*: $[TiO_2] = 1.0\,mg\,L^{-1}$; $[HCl] = 2.0\,mol\,L^{-1}$; $[SnCl_2] = 4.03 \times 10^{-2}\,mol\,L^{-1}$; ('a') $\log D$ vs. $\log c(SCN)_{Initial}$, $[CTA] = 2.49 \times 10^{-2}\,mol\,L^{-1}$; ('b') $\log D$ vs. $\log c(CTA)_{Initial}$, $[SCN] = 2.34\,mol\,L^{-1}$. *Note*: The percentage extraction and distribution ratio (D) were calculated by determining TiO_2 in the organic phase by tiron method (spectrophotometry) after stripping off the metal ion into water.

Table 1
Effect of foreign ions on the determination of titanium

Ions	Tolerance limits (mg L^{-1})
Al, Be, Na, K, Sn, Rb, Cl$^-$, Br$^-$ and SO$_4{}^{2-}$	>2000
Ca, Mg, Ba, Sr, NO$_3{}^-$, ascorbate, borate, tartarate, citrate	500
Be, La, Y, Hg, Pb, Bi, PO$_4{}^{3-}$	200
As, Sb, Ni, Zn, Fe	100
Cu, Co, Mn	50
Ta, Zn, Cr, Ce, W, U, Mo,	20
Nb, V	10

Conditions: [TiO$_2$] = 1.0 mg L^{-1}; [HCl] = 2.0 mol L^{-1}; [SCN] = 2.34 mol L^{-1}; [CTA] = 2.49 × 10^{-2} mol L^{-1} and [SnCl$_2$] = 4.03 × 10^{-2} mol L^{-1}.

Unlike the findings reported in the paper [23], the colour intensity of the extracted species was found to be independent of chloride ion concentration. Hence, the possibility of chloride ion being coordinated as a hetero-ligand with titanium metal, leading to the formation of an anionic complex requiring CTA$^+$ as a counter cation for its extraction is thus ruled out. The formation of similar complex adducts, as tentatively shown above, is, however, not un-precedented [19–22]. In this context, it is pertinent to mention here that the reported neutral complex [Ti(OH)(SCN)$_3$] is extractable into MIBK, and as such, does not require any counter-cation for its extraction [1]. However, in the present system, the surfactant, CTA enhances the sensitivity of the [TiO(SCN)$_2$] complex by providing micelle medium to the reacting species.

3.9. Interference studies

The effect of diverse ions on the estimation of 1.0 mg L^{-1} of TiO$_2$ was studied separately. Nb and V interfered when present at 10 mg L^{-1} level or above. However, the abundance of these elements in silicate rocks is usually lower than that of Ti, hence their interference is ruled out. The tolerance limits for other elements commonly present in silicate rocks (Table 1) were quite high. The interference of iron(III) was suppressed by the addition of SnCl$_2$ which reduced Fe^{3+} into Fe^{2+} ion. Ferrous ion

did not interfere. As SnCl$_2$ reduces the intensity of the colour, a minimum amount (1 mL) of 4.43 × 10^{-1} mol L^{-1} was recommended. At this concentration level of SnCl$_2$, 100 mg L^{-1} Fe^{3+} did not pose any problem in the determination of titanium in the prescribed concentration range. Usually in other ternary systems of titanium with thiocyanate and a hetero-ligand, the coloured thiocyanato complexes of the elements like Fe^{3+}, Cu^{2+}, W(IV), Mo(VI) and Nb(V), if present in the samples, also get extracted along with titanium, thereby causing serious interference. However, in the present system, except V and Nb, no element formed extractable coloured complexes. Hence, most elements did not interfere in this method. It is pertinent to mention here that in silicate rocks, the effects of major elements such as Al, Ti, Fe, Mn and alkali metals, were studied in milligram level and those of minor as well as trace elements were studied in microgram level, i.e., mg/µg quantity of the diverse ions were added to 11 mL of aqueous test solution containing 10 µg TiO$_2$, and the recovery of titanium was studied on its extraction into 10 mL of organic solvent. In both the cases, the concentration of diverse ions under study was expressed in mg L^{-1}. Similarly, anions such as F$^-$, PO$_4{}^{3-}$, Cl$^-$, NO$_3{}^-$, SO$_4{}^{2-}$, tetra-borate, citrate, acetate and ascorbate did not interfere in the estimation of titanium. Based upon the studies of interference due to commonly associated elements cited in Table 1, it appears that the proposed method is quite selective for the estimation of titanium in silicate rocks.

4. Application of the method

A number of silicate rock samples were opened by the procedure described in literature [3]. The method was thoroughly applied to a host of silicate rocks and international geo-standard samples of diverse matrices containing TiO$_2$ in the range, 0.002–0.142%. The results obtained, as shown in Table 2, were found to be in good agreement with certified values and those obtained by standard methods [1,3]. The results show that the method is highly reliable for the determination of TiO$_2$ in silicate rocks of diverse matrices and can be used for routine analysis of samples.

Table 2
Results of the estimation of TiO$_2$ in rock samples

Sl. no.	Sample no.	TiO$_2$, % found		Tiron method	Certified value (%)
		Proposed method[a]	R.S.D. (%)		
1.	RT-1	0.045 ± 0.001	2.2	0.039	
2.	RT-2	0.086 ± 0.002	2.3	0.081	
3.	RT-3	0.142 ± 0.002	1.4	0.139	
4.	RT-4	0.046 ± 0.001	2.1	0.042	
5.	RT-5	0.140 ± 0.002	1.4	0.136	
6.	RT-6	0.046 ± 0.001	2.2	0.047	
7.	SY-3[b]	0.140 ± 0.002	1.4	0.150	0.130
8.	CRM 782-1[b]	0.0023 ± 0.0001	4.3	[c]	0.0025

RT-(1–6) are silicate rock samples.

[a] ±Standard deviation.

[b] Geo-standard reference materials.

[c] Not detected.

5. Conclusions

A highly sensitive and reasonably selective method for trace and ultra-trace determination of titanium in silicate rocks has been developed. This method is suitable for application to silicate rock samples containing titanium in traces.

Acknowledgement

References

[1] Z. Markzenko, Separation and Spectrophotometric Determination of Elements, Horwood, Chichester, 1986, pp. 590–601.
[2] L. Sommer, Analytical Absorption Spectrophotometry in the Visible and Ultraviolet, Elsevier, Budapest, 1989, p. 237.
[3] A. Maxwell, Rock and Minerals Analysis, Wiley, New York, 1968, p. 382.
[4] E.B. Sandell, H. Onishi, Photometric Determination of Traces of Metals, Wiley, New York, 1978, p. 297.
[5] V.T. Athavale, M.N. Nadkarni, C. Venkateswarlu, Anal. Chim. Acta 23 (1960) 438.
[6] L. Sommer, Collect. Czech. Chem. Commun. 28 (1963) 2102.
[7] L. Sommer, Talanta 9 (1962) 439.
[8] V.T. Athavale, K.R. Krishnamurthy, C. Venkateswarulu, Talanta 15 (1968) 315.
[9] P.C. Jeffery, G.R.E.C. Gregory, Analyst 90 (1965) 177.
[10] H. Sedaira, K.A. Idriss, M.S. Abel-Aziz, Analyst 121 (1996) 1079.
[11] P.K. Tarafder, S. Durani, R. Saran, G.V. Ramanaiah, Talanta 41 (1994) 1345.
[12] R.K. Mandal, P.K. Tarafder, Microchim. Acta 148 (2004) 327.
[13] S. Koch, G. Ackermann, H. Mosler, Talanta 31 (1984) 667.
[14] H.D. Gunawardhana, Analyst 108 (1983) 952.
[15] J.E. Cantle (Ed.), Atomic Absorption Spectrometry-Technique and Instrumentation in Analytical Chemistry, vol. 5, Elsevier, Amsterdam, 1986, p. 48.
[16] B. Weltz, Atomic Absorption Spectrophotometry, second ed., VCH Publisher, New York, 1985, p. 260.
[17] K.L. Cheng, K. Ueno, T. Imamura (Eds.), CRC Hand book of Organic Analytical reagents, Boca Raton, Florida, 1982.
[18] D. Attwood, A.T. Florence, Surfactant Systems, Chapman and Hall, London, 1985, p. 689.
[19] B. Tamhina, M.J. Herak, V. Jagodic, Anal. Chim. Acta 86 (1976) 223.
[20] B. Tamhina, V. Vojkovic, M.J. Herak, Croat. Chem. Acta 49 (1977) 533.
[21] C.P. Savariar, K. Vijayan, Talanta 36 (1989) 1047.
[22] P.K. Tarafder, R. Thakur, Microchem. J. 80 (2005) 39.
[23] V. Vojkovic, V.A. Zivcic, V. Druskovic, Spectrosc. Lett. 37 (2004) 401.
[24] P.K. Tarafder, P. Murugan, L. Kunkal, D.P.S. Rathore, J. Radioanal. Nucl. Chem. 253 (2002) 135.
[25] P.K. Tarafder, R.K. Mondal, L. Kunkal, P. Murugan, D.P.S. Rathore, Chem. Anal. (Warsaw) 49 (2004) 251.
[26] L.G. Sillen, Acta Chem. Scand. 10 (1956) 185.

Development and validation of HPLC method for the resolution of drug intermediates: DL-3-Phenyllactic acid, DL-O-acetyl-3-phenyllactic acid and (±)-mexiletine acetamide enantiomers

Alemu Tekewe, Sawraj Singh, Manpreet Singh, Utpal Mohan, U.C. Banerjee*

Biocatalysis Laboratory, Department of Pharmaceutical Technology (Biotechnology), National Institute of Pharmaceutical Education and Research (NIPER), Sector 67, S.A.S. Nagar 160062, India

Abstract

Sensitive and specific, high-performance liquid chromatography (HPLC) methods have been developed and validated for linearity, accuracy and precision for the quantification of DL-3-phenyllactic acid, DL-O-acetyl-3-phenyllactic acid and (±)-mexiletine acetamide enantiomers. Chromatographic separations were performed on a Chiralcel OJ-H column (0.46 mm × 250 mm, 5 μm, Daicel Chemical Industries, Japan) based on cellulose tris-(4-methyl benzoate) chiral stationary phase. The mobile phase consists of hexane and isopropanol (IPA) in the ratio of 90:10 containing 0.1% trifluoroacetic acid (in case of DL-3-phenyllactic acid and DL-O-acetyl-3-phenyllactic acid) and hexane and IPA (95:5) containing 0.1% triethylamine (in case of (±)-mexiletine acetamide) and the flow rate was set at 0.5 ml/min at 25 °C. The detection was carried out at 261 nm for DL-3-phenyllactic acid and DL-O-acetyl-3-phenyllactic acid and at 254 nm for (±)-mexiletine acetamide. The developed methods were utilized for monitoring the progress of lipase catalyzed enantioselective synthesis of O-acetyl-3-phenyllactic acid and mexiletine acetamide from DL-3-phenyllactic acid and (±)-mexiletine, respectively.
© 2007 Elsevier B.V. All rights reserved.

Keywords: DL-3-Phenyllactic acid; DL-O-Acetyl-3-phenyllactic acid; (±)-Mexiletine acetamide; (±)-Mexiletine; Chiral HPLC

1. Introduction

DL-3-phenyllactic acid and its derivative, DL-O-acetyl-3-phenyllactic acid, in non-racemic form are frequently used as components of pharmaceuticals and natural antibiotic agents [1]. Pure enantiomers of 3-phenyllactic acid represent an integral part of bioactive peptides, such as aeruginosins [2] and microcin [3] which were shown to be potent protease inhibitors. The *p*-fluoro-analog of enantiopure 3-phenyllactic acid is a key building block for the synthesis of AG7088 (Ruprintrivir), a potent rhinovirus inhibitor currently in clinical trials to treat the common cold [4]. D-(+)-3-Phenyllactic acid is an integral part of a cyclic depsipeptide, YM-254890, which is a novel $G_{q/11}$ protein inhibitor [5]. L-(−)-3-Phenyllactic acid and L-(−)-O-acetyl-3-phenyllactic acid are used for the synthesis of chiral intermediates-which are used for the synthesis of antiviral and antitumour compounds: mycalamides, pederin, onnamides and theopederins [6].

Mexiletine [1-(2,6-dimethylphenoxy)-2-amino-propane], which is classified as a class Ib antiarrhythmic drug [7], is a therapeutically relevant chiral compound, clinically used as antiarrhythmic, antimyotonic, and analgesic agent, in its racemic form. Ates et al. [8] compared the neuroprotective effect of mexiletine and its superiority over phenytoin and riluzole as sodium channel blocker. However, several lines of evidences have shown that mexiletine enantiomers differ both in their pharmacodynamics and pharmacokinetics properties [9]. Based on the *in vitro* experiments, Vandamme et al. [10] suggested that in human microsomes, the aliphatic and aromatic hydroxylation of mexiletine is stereoselective. Aliphatic hydroxylation seems to be predominant for the *R*-(−) enantiomer, while aromatic hydroxylation is favored for the *S*-(+) enantiomer [11]. It had been suggested that the antiarrhythmic effect of mexiletine is stereoselective, with the *R*-(−) enantiomer showing higher activity than the corresponding *S*-(+) enantiomer as well as the racemic form.

* Corresponding author. Tel.: +91 172 2214682 87x2142;
fax: +91 172 2214692.

E-mail address: ucbanerjee@niper.ac.in (U.C. Banerjee).

Owing to the existence of pharmacological and toxicological differences between enantiomers of drugs/drug intermediates, the regulatory bodies demand the development of many new chiral chemical entities as single enantiomers, rather than racemic mixture. Several approaches such as synthesis from a homochiral starting material(s) or resolution of (±)-racemates and/or distillation of the diastereomeric salts have been reported to obtain DL-3-phenyllactic acid [12] and mexiletine [9] in non-racemic form. Various analytical methods can be used to monitor the progress of such type of synthesis. Li et al. [13] have developed a selective LC–MS/MS method for the determination of mexiletine in human plasma. However, high-performance liquid chromatography (HPLC) methods are one of the most useful techniques for the determination and quantification of compounds from chemical or biological samples. For example, Tatar Ulu et al. [14] have reported a high-performance liquid chromatographic method based on reversed-phase HPLC with UV–vis absorbance detection for the determination of mexiletine and its enantiomers in biological fluids. Strom et al. [1] have developed preparative HPLC method using C18 column for separation, purification and characterization of DL-3-phenyllactic acid and its enantiomers from biological samples. But to the best of our knowledge no direct HPLC method based on Chiralcel column is available to determine enantiomers of both mexiletine and DL-3-phenyllactic acid from biological samples or to monitor the conversion, enantiomeric ratio and enantiomeric excess of resolution of these racemic chiral drugs or drug intermediates.

In the present study, (±)-mexiletine acetamide and DL-O-acetyl-3-phenyllactic acid were synthesized chemically from (±)-mexiletine and DL-3-phenyllactic acid, respectively and a high-performance liquid chromatography (HPLC) methods were developed and validated using Chiralcel OJ-H column for the resolution of the synthesized compounds [(±)-mexiletine acetamide and DL-O-acetyl-phenyllactic acid] and DL-3-phenyllactic acid. The chemical structures of all the compounds used in this study are given in Fig. 1.

2. Experimental

2.1. Chemicals

(±)-Mexiletine, D-(+)-3-phenyllactic acid, L-(−)-3-phenyllactic acid and DL-3-phenyllactic acid were purchased from Sigma–Aldrich Co. (±)-Mexiletine acetamide and DL-O-acetyl-3-phenyllactic acid were synthesized chemically from (±)-mexiletine and DL-3-phenyllactic acid, respectively. Solvents required for synthesis and extraction were acquired from commercial sources and they were either of analytical or commercial grades. Solvents used for HPLC analyses were obtained from J.T. Baker, Rankem, Merck Ltd. and were of HPLC grade.

2.2. Synthesis of (±)-mexiletine acetamide and DL-O-acetyl-3-phenyllactic acid

2.2.1. Synthesis of (±)-mexiletine acetamide

To a solution of (±)-mexiletine (1.11 mmol) in dichloromethane as a solvent (5 ml), acetyl chloride (95 μl)

and triethylamine (135 μl) were added. The reaction mixture was stirred at room temperature until disappearance of (±)-mexiletine [TLC control, hexane:ethyl acetate 7:3 (v/v)]. Then, the reaction mixture was washed with brine solution and the amide was isolated by extraction with dichloromethane. The organic layer was dried by anhydrous sodium sulphate and then evaporated under reduced pressure. The amide was purified by recrystallization using hexane as solvent and the pure white crystals were characterized by NMR spectroscopy, FTIR and LC–MS.

2.2.2. Synthesis of DL-O-acetyl-3-phenyllactic acid

DL-O-Acetyl-3-phenyllactic acid was synthesized chemically through the treatment of the corresponding DL-3-phenyllactic acid (0.25 g, 1.5 mmol) in acetic anhydride (4 ml) and pyridine (0.3 ml) [6] .The reaction mixture was stirred at 4 °C until the disappearance of DL-3-phenyllactic acid, which was monitored by TLC using dichloromethane:methanol; 20:1(v/v) as mobile phase. After the completion of reaction, the solution was poured into ice-water (50 ml), which was acidified with HCl (3.0 M) to pH 1–2 and extracted three times with ethyl acetate. The combined organic layers were washed with water and brine, dried with anhydrous sodium sulphate and evaporated to yield DL-O-acetyl-3-phenyllactic acid.

2.3. Analytical methods

2.3.1. Spectral analysis

^{1}H NMR and ^{13}C NMR were obtained with Bruker DPX 300 (1H 300 MHz and ^{13}C 75.5 MHz) spectrometers, using CDCl$_3$ as solvent. Chemical shifts were expressed in parts per million (ppm), with tetramethylsilane as an internal standard. IR spectra (wave number, in cm^{-1}) were recorded on Nicolet FT-IR impact 400 instruments as either neat for liquid or KBr pellets for solid samples. LC–MS analysis was done on a Finninganmat LCQ instrument (USA) using a C-18 Hypersil ODS (4.6 mm × 15 mm, 5 μm) column. Optical rotations were measured on a Rudolph Polarimeter (Rudolph Research Autopol IV) for identification of the enantiomers.

2.3.2. Chromatographic systems and conditions

The HPLC system comprising of a dual piston reciprocating pump (LC-10ATVP), UV–vis dual wavelength detector (SPD-10AVP), an auto injector (SIL-10ADVP), and in-line degasser (DGU-14AM). The data was acquired using CLASS-VP software (all from Shimadzu, Kyoto, Japan). Direct separation of enantiomers was performed using a Chiralcel OJ-H and OD-H column (0.46 mm × 250 mm, 5 μm, Daicel Chemical Industries, Japan) under the following conditions: mobile phase, hexane:2-propanol:triethylamine (95:5:0.1, v/v); detection, UV at 254 nm (in case of (±)-mexiletine acetamide) and hexane:2-propanol:trifluoroacetic acid (90:10:0.1, v/v) and detection, UV at 261 nm (in case of DL-3-phenyllactic acid and DL-O-acetyl-3-phenyllactic acid). The mobile phase was run at a flow rate of 0.5 ml/min and separations were performed at ambient temperature (25 °C). The order of elution was determined by injecting standards of individual enantiomers of DL-3-phenyllactic acid
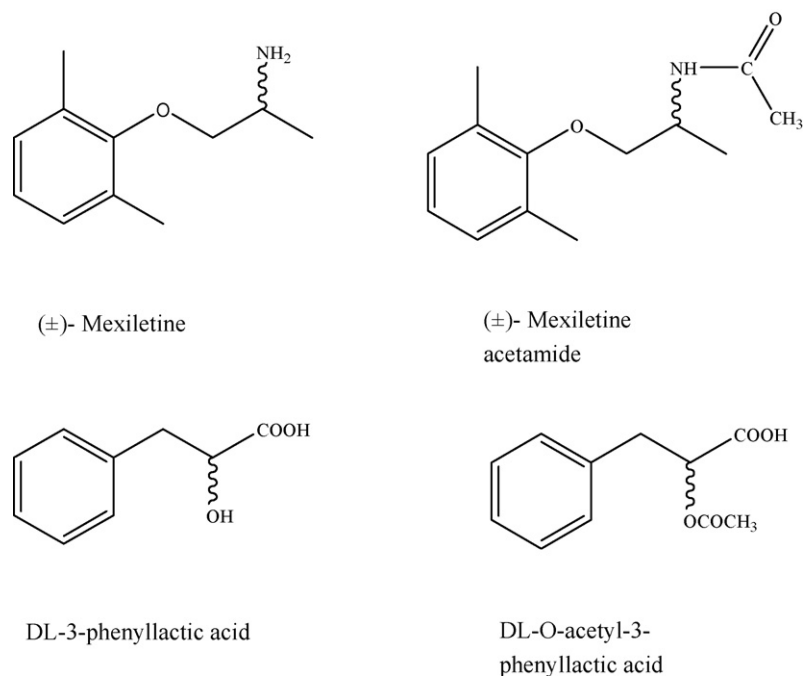
Fig. 1. Chemical structure of (±)-mexiletine, (±)-mexiletine acetamide, DL-3-phenyllactic acid and DL-*O*-acetyl-3-phenyllactic acid.

which were purchased from SIGMA. In case of (±)-mexiletine acetamide and DL-*O*-acetyl-3-phenyllactic acid, the separated optical isomers were identified by using polarimeter.

2.4. Method development and validation

2.4.1. Development of method

The compounds were completely separated using different mobile-phase composition comprising of hexane and 2-propanol. Triethylamine and trifluoroacetic acid was added to get sharp peaks and to achieve better resolution of enantiomers of the racemic compounds. In all cases, the mobile phase was filtered through a 0.45 μm nylon membrane and degassed before use.

2.4.2. Validation

Linearity was established by injecting the samples in triplicate, containing (±)-mexiletine acetamide in the concentration range of 80–960 μg/ml, DL-3-phenyllactic acid and DL-*O*-acetyl-3-phenyllactic acid in the concentration range of 5–80 μg/ml on the same day for each particular compound. Limits of detection and quantification were determined by calculation of signal-to-noise ratio. Signal-to-noise ratio of approximately 3:1 and

10:1 were used for estimating the detection and quantification limit, respectively. Intra-day precision was established by making six injections of lowest, middle and highest concentration in the above range (240, 560 and 880 μg/ml in case of (±)-mexiletine acetamide) and (15, 45 and 75 μg/ml in case of DL-3-phenyllactic acid and DL-*O*-acetyl-3-phenyllactic acid). These studies were also repeated on different days to determine inter-day precision. Accuracy was evaluated by fortifying reaction mixture with three known concentrations of the compound. The recovery of the added compound was determined.

3. Results and discussion

3.1. Synthesis of (±)-mexiletine acetamide and DL-*O*-acetyl-3-phenyllactic acid

The compounds used for the method development, were chemically synthesized. (±)-Mexiletine acetamide was synthesized in one step acetylation of racemic mexiletine (Fig. 2) by using acetylchloride as the acyl donor and triethylamine and dichloromethane as a basic catalyst and solvent, respectively. The synthesized product was purified by solvent-solvent extraction followed by recrystallization from hexane. The yield of
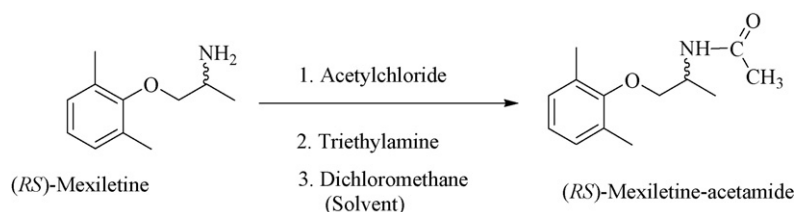

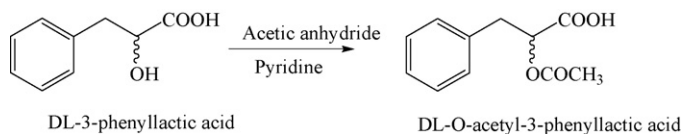
Fig. 2. Synthesis of (±)-mexiletine acetamide.

Fig. 3. Acetylation of DL-3-phenyllactic acid.

(±)-mexiletine acetamide obtained was more than 80%. The pure crystalline amide was characterized by different spectroscopy techniques. The data obtained was in agreement with the literature [15].

(±)-Mexiletine acetamide: white crystals (yield = >80% after recrystallization from hexane), IR (KBr): 3278 (–NH–) and 1648 (C=O) cm^{-1}. ^{1}H NMR (300 MHz, CDCl$_3$): δ 7.02–6.90 (m, 3H, Ar–H), 5.96 (s, 1H, NH), 4.35 (m, 1H, CH), 3.82–3.69 (dd, 2H, J_1 = 3.97 Hz, J_2 = 5.06 Hz, CH$_2$), 2.25 (s, 6H, Ar–CH$_3$), 2.02 (s, 3H, COCH$_3$), 1.38 (d, 3H, J = 6.84 Hz, CH$_3$). ^{13}C NMR (75.5 MHz, CDCl$_3$): ppm 170 (C=0), 155.4 (C), 131.3 (C), 129.6 (CH), 124.7 (CH), 74.4 (CH$_2$), 45.9 (CH), 24 (CH$_3$), 18.3 (CH$_3$), 15.9 (CH$_3$). LC–MS m/z (relative intensity): 221.9 (M + H).

DL-O-Acetyl-3-phenyllactic acid was synthesized by one step acetylation of DL-3-phenyllactic acid (Fig. 3) using acetic anhydride as the acyl donor and pyridine as a basic catalyst. The reaction was carried out at 4 °C and the progress was monitored by thin layer chromatography (TLC). After the completion of the reaction the reaction mixture was poured in ice-water (50 ml), which was acidified with HCl (3 M) to pH 1–2 and the resultant solution obtained was extracted three times with ethyl acetate. The organic layer was washed with water and brine, dried with anhydrous sodium sulphate and evaporated to yield DL-O-acetyl-3-phenyllactic acid.

DL-O-Acetyl-3-phenyllactic acid: Oily liquid (yield = 86.2%); FTIR (neat): 2926 (CH), 1739 (COOH), 1732 (COO–); ^{1}H NMR (CDCl$_3$): δ 2.07 (s, 3H, CH$_3$), 3.06–3.26 (m, 2H, CH$_2$), 5.23 (dd, 1H, J_1 = 3.68 Hz, J_2 = 5.21 Hz, CH), 7.23–7.33 (m, 5H, Ar–H), 12.36 (s, 1H, COOH); ^{13}C (CDCl$_3$) ppm 178.9 (COOH), 171.3 (OCO–), 136.6 (C), 129.6 (CH), 127.6 (CH), 78.1 (CH), 32.5 (CH$_2$), 21.1 (OCH$_3$).

3.2. Separation of (±)-mexiletine acetamide, DL-3-phenyllactic acid and DL-O-acetyl-3-phenyllactic acid enantiomers by Chiral HPLC

Two different columns, viz., Chiralcel OD-H [cellulose tris-(3,5-dimethyl phenyl carbamate)] and Chiralcel OJ-H [cellulose
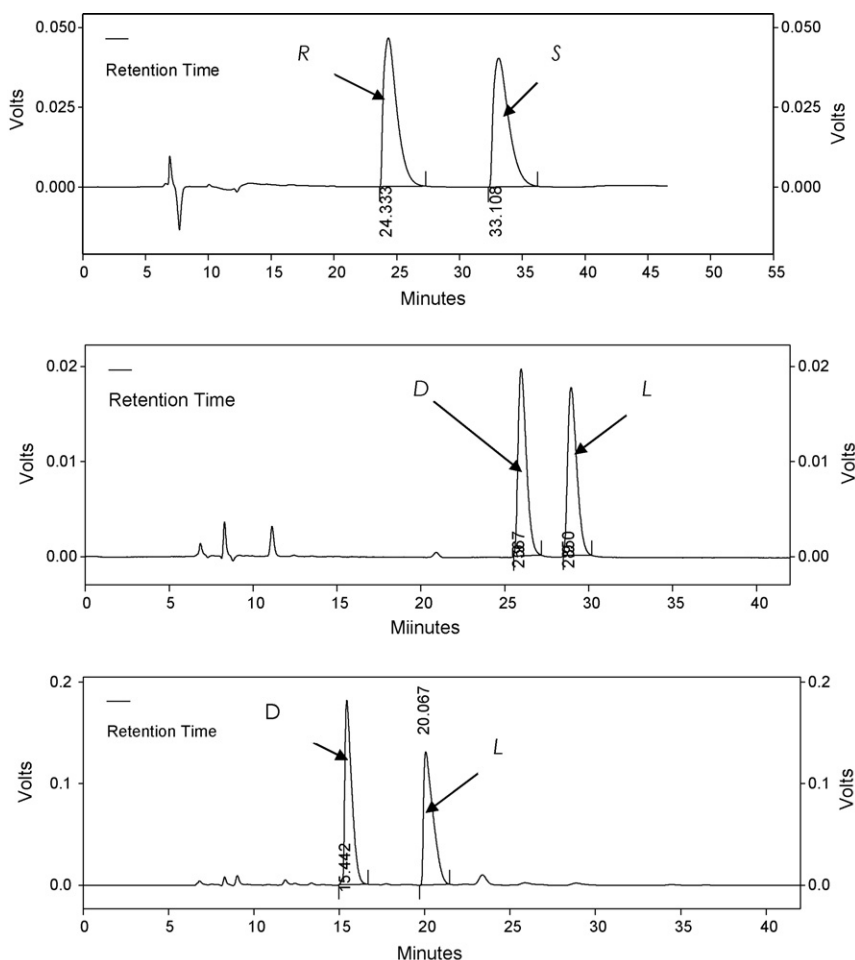

Fig. 4. Chromatograms showing the direct separation of the enantiomers of: (a) (±)-mexiletine acetamide; (b) DL-3-phenyllactic acid and (c) DL-O-acetyl-3-phenyllactic acid.

Table 1
Regression parameters of the standard plots of the enantiomers of (±)-mexiletine acetamide, DL-3-phenyllactic acid and DL-O-acetyl-3-phenyllactic acid

Compounds	Range (µg/ml)	Enantiomers	Slope[a]	Intercept[a]	Correlation coefficient[a]
(±)-Mexiletine acetamide	80–960	R	1151 ± 2.100, 0.182	−9414 ± 117.0, 1.240	0.9962 ± 0.0003, 0.03
		S	1157 ± 4.800, 0.420	−13050 ± 414.0, 3.200	0.9964 ± 0.0002, 0.02
DL-3-Phenyllactic acid	5–80	D	82662 ± 1204, 1.470	−142162 ± 252.0, 0.177	0.9974 ± 0.0020, 0.14
		L	83285 ± 853.0, 1.020	−157535 ± 1799, 1.140	0.9983 ± 0.0010, 0.10
DL-O-Acetyl-3-phenyllactic acid	5–80	D	35609 ± 525.0, 1.470	−54213 ± 598.0, 1.100	0.9988 ± 0.0020, 0.20
		L	33611 ± 221.0, 0.007	−28391 ± 459.0, 1.620	0.9987 ± 0.0030, 0.30

[a] Values are mean ± S.D., R.S.D. (%).

tris-(4-methyl benzoate)] were evaluated for the direct separation of (±)-mexiletine acetamide, DL-3-phenyllactic acid and DL-O-acetyl-3-phenyllactic acid enantiomers by using different compositions of *n*-hexane and 2-propanol alcohol as mobile phase. Chiralcel OD-H column could not resolve the enantiomers of the three compounds where as Chiralcel OJ-H column recognized the enantiomers of all the three compounds. But, baseline separation of the enantiomers was not achieved and the enantiomers of all the three compounds eluted as a non-separated peaks in different compositions of *n*-hexane and isopropanol alcohol as mobile phase. Finally, this problem was overcome by the addition of small amounts of triethylamine in mobile phase for resolution of (±)-mexiletine acetamide and trifluoroacetic acid for the resolution of DL-3-phenyllactic acid and DL-O-acetyl-3-phenyllactic acid.

Thus, the direct separation of the enantiomers of the three compounds was achieved on a Chiralcel OJ-H column (Fig. 4) by employing a simple isocratic system using isopropanol alcohol and *n*-hexane containing 0.1% (v/v) triethylamine (in case of (±)-mexiletine acetamide) and 0.1% (v/v) trifluoroacetic acid (in case of DL-3-phenyllactic acid and DL-O-acetyl-3-phenyllactic acid). Elution was carried out with a mixture of isopropanol alcohol and *n*-hexane in the ratio of 5:95 (in

case of (±)-mexiletine acetamide) and 10:90 (in case of DL-3-phenyllactic acid and DL-O-acetyl-3-phenyllactic acid) at a constant flow rate of 0.5 ml/min at 25 °C. The analytical wavelength was 254 nm for (±)-mexiletine acetamide and 261 nm for DL-3-phenyllactic acid and DL-O-acetyl-3-phenyllactic acid. The two enantiomers of mexiletine acetamide were eluted at 24.3 and 33.1 min. The enantiomers of DL-3-phenyllactic acid had a retention time of 25.5 and 28.4 min and the enantiomers of DL-O-acetyl-3-phenyllactic acid were eluted at 16 and 20 min.

3.3. Validation of the method

3.3.1. Linearity, limits of detection and quantification

Table 1 shows the regression parameters of the standard plots of the enantiomers of the three compounds. It is evident that the responses for the enantiomers of the three compounds were strictly linear in the studied concentration range, which is evident from the relative standard deviation (R.S.D.) values of slope, intercept and correlation coefficient (less than 2%). Limits of detection (LOD) and quantification (LOQ) were calculated using signal/noise (*S*/*N*) ratio method. LOD was taken as a concentration of the analyte where *S*/*N* was 3 and found to be (9.69 and 6.66) $\times 10^{-9}$ g/ml for *R*- and *S*-mexiletine

Table 2
Intra- and inter-day precision data[a]

Compounds	Actual concentration (µg/ml)	Enantiomers	Intra-day precision[a]	Interday precision[a]
(±)-Mexiletine acetamide	240	R	122.303 ± 1.240, 1.010	122.596 ± 0.889, 0.730
		S	119.092 ± 0.471, 0.004	120.652 ± 1.090, 0.009
	560	R	278.905 ± 1.420, 0.510	281.023 ± 1.590, 0.570
		S	279.888 ± 1.150, 0.004	279.588 ± 1.370, 0.005
	880	R	439.004 ± 0.537, 0.120	439.657 ± 0.904, 0.210
		S	439.718 ± 1.080, 0.002	441.079 ± 1.640, 0.004
DL-3-Phenyllactic acid	15	D	7.663 ± 0.100, 0.013	7.660 ± 0.095, 0.012
		L	7.503 ± 0.047, 0.006	7.557 ± 0.063, 0.008
	45	L	22.620 ± 0.052, 0.002	22.683 ± 0.068, 0.003
		L	22.510 ± 0.062, 0.003	22.680 ± 0.069, 0.003
	75	D	37.570 ± 0.061, 0.002	37.580 ± 0.044, 0.001
		L	37.470 ± 0.036, 0.001	37.547 ± 0.060, 0.002
DL-O-Acetyl-3-PLA	15	D	7.501 ± 0.079, 0.011	7.523 ± 0.172, 0.023
		L	7.847 ± 0.021, 0.003	7.700 ± 0.087, 0.011
	45	D	22.857 ± 0.095, 0.004	22.967 ± 0.065, 0.003
		L	22.803 ± 0.250, 0.011	22.867 ± 0.045, 0.002
	75	D	39.697 ± 0.491, 0.012	39.893 ± 0.601, 0.015
		L	37.690 ± 0.231, 0.006	37.727 ± 0.133, 0.004

[a] Values are observed concentration (µg/ml) ± S.D., R.S.D. The determinations were made three times in a same day for intra-day precision and the same experiment was repeated for three consecutive days for inter-day precision.

Table 3
Recovery studies

Compounds	Actual concentration (µg/ml)	Enantiomers	Observed concentration[a] (µg/ml)	Recovery (%)
(±)-Mexiletine acetamide	240	R	118.722 ± 0.594	98.93
		S	120.623 ± 0.781	100.52
	560	R	280.896 ± 1.740	100.32
		S	279.941 ± 1.400	99.98
	880	R	440.120 ± 0.206	100.03
		S	439.955 ± 1.370	99.99
DL-3-Phenyllactic acid	15	D	7.543 ± 0.071	100.58
		L	7.540 ± 0.060	100.53
	45	D	22.577 ± 0.072	100.34
		L	22.657 ± 0.021	100.70
	75	D	37.490 ± 0.053	99.97
		L	37.470 ± 0.082	99.92
DL-O-Acetyl-3-PLA	15	D	7.560 ± 0.070	100.80
		L	7.793 ± 0.055	103.91
	45	D	22.773 ± 0.080	101.21
		L	22.770 ± 0.165	101.20
	75	D	38.260 ± 0.591	102.03
		L	37.810 ± 0.182	100.82

[a] Values are mean ± S.D. of three determinations.

acetamide, $(1.67$ and $2.72) \times 10^{-10}$ g/ml for D- and L-O-acetyl-3-phenyllactic acid, and $(6.81$ and $6.45) \times 10^{-10}$ g/ml for D- and L-3-phenyllactic acid, respectively. LOQ was taken as a concentration of the analyte where S/N was 10. It was found to be $(3.23$ and $2.22) \times 10^{-8}$ g/ml for R- and S-mexiletine acetamide, $(5.56$ and $9.06) \times 10^{-10}$ g/ml for D- and L-O-acetyl-3-phenyllactic acid and $(2.27$ and $2.15) \times 10^{-9}$ g/ml for D- and L-3-phenyllactic acid, respectively.

3.3.2. Precision

Table 2 provides data obtained from the precision experiments. The R.S.D. values for intra- and inter-day precision were <1.02 and <0.74%, respectively, there by indicating that the method was sufficiently precise. A similar qualitative separation of the enantiomers of these compounds was obtained even on analysis on a different chromatographic system on a different day, indicating that the method has good enantiomer precision.

3.3.3. Accuracy

Percentage recovery was calculated from differences between the peak areas obtained for fortified and unfortified solutions. As shown in the data in Table 3, excellent recoveries were made at each added concentration. The percentage recovery were between 98.93 and 103.91% with <1.75% R.S.D.

3.4. Method application

The method was applied for monitoring the resolution of DL-3-phenyllactic acid via lipase catalyzed transesterification using vinyl acetate as acyl donor in different organic solvents. Under these conditions, lipase catalyzed the enantioselective conversion of one of enantiomer of DL-3-phenyllactic acid to its corresponding enantiomer of DL-O-acetyl-3-phenyllactic acid. Thus, the method was used to monitor the conversion, enan-

tiomeric excess of both the product formed and the remaining enantiomer of the substrate and the enantiomeric ratio of the reaction. Different lipases were also used for the enantioselective resolution of (±)-mexiletine using ethyl acetate as acyl donor and solvent. In this case, some lipases catalyzed the enantioselective conversion one of the enantiomers of (±)-mexiletine to the corresponding enantiomers of (±)-mexiletine acetamide. Thus, the developed method was used to monitor the rate of conversion, the enantiomeric excess of the acetamide formed and the enantiomeric ratio of the reaction. The enantiomeric excess of the unreacting mexiletine was determined indirectly by using the developed method after derivatization of mexiletine to mexiletine acetamide as described above in Section 2.2.1. This is because (±)-mexiletine could not be resolved directly by the developed method.

4. Conclusions

(±)-Mexiletine acetamide and DL-O-acetyl-3-phenyllactic acid were chemically synthesized and the separation and determination of the enantiomers of the synthesized compounds and DL-3-phenyllactic acid on two different polysaccharide-based chiral stationary phases, viz., Chiralcel OD-H and Chiralcel OJ-H columns were studied. Chiralcel OJ-H column showed excellent resolution of the enantiomers of the three compounds while no resolution was found in Chiral OD-H column. The method was validated with respect to accuracy, precision, linearity, limit of detection (LOD) and limit of quantification (LOQ). The developed method is simple, reproducible and sensitive. This method can be successfully used for determining the conversion, enantiomeric excess and enantiomeric ratio of enzyme mediated resolution of these drugs and drug intermediates.

Acknowledgements

References

[1] K. Strom, J. Sjogren, A. Broberg, J. Schnurer, Appl. Environ. Microbiol. 68 (2002) 4322.
[2] K. Ishida, Y. Okita, H. Matsuda, T. Okino, M. Murakami, Tetrahedron 55 (1999) 10971.
[3] N. Valls, M. Vallribera, M. López-Canet, J. Bonjoch, J. Org. Chem. 67 (2002) 4945.
[4] J. Tao, K. McGee, Org. Process Res. Dev. 6 (2002) 520.
[5] M. Taniguchi, K. Suzumura, K. Nagai, T. Kawasaki, T. Saito, J. Takasaki, K. Suzuki, S. Fujita, S.I. Tsukamoto, Tetrahedron 59 (2003) 4533.
[6] A.D. Abell, J.W. Blunt, G.J. Foulds, M.H.G. Munro, J. Chem. Soc., Perkin Trans. 1 (1997) 1647.
[7] A. Kohjitania, T. Miyawakia, M. Funahashib, Y. Mitohb, R. Matsuob, M. Shimadaa, Eur. J. Pharmacol. 465 (2003) 145.
[8] O. Ates, S.R. Cayli, I. Gurses, Y. Turkoz, O. Tarim, C.O. Cakir, A. Kocak, J. Clin. Neurosci. 14 (2007) 658.
[9] A. Carocci, A. Catalano, F. Corbo, A. Duranti, R. Amoroso, C. Franchini, G. Lentinia, V. Tortorellaa, Tetrahedron Asymmetry 11 (2000) 3619.
[10] N. Vandamme, F. Broly, C. Libersa, C. Courseau, M. Lhermitte, J. Card. Pharmacol. 21 (1993) 77.
[11] V.L. Lanchote, P.S. Bonato, S.A.C. Dreossl, P.V.B. Gonqalves, E.J. Cesarino, C. Bertucci, J. Chromatogr. B 685 (1996) 281.
[12] T. Storz, P. Dittmar, P.F. Fauquex, P. Marschal, W.U. Lottenbach, H. Steiner, Org. Process Res. Dev. 7 (2003) 559.
[13] S. Lia, G. Liua, J. Jiaa, Y. Liua, C. Panb, C. Yua, Y. Caia, J. Ren, J. Chromatogr. B 847 (2007) 174.
[14] S. Tatar Ulu, Talanta 72 (2007) 1172.
[15] A. Carocci, C. Franchini, G. Lentini, F. Loiodice, V. Tortorella, Chirality 12 (2000) 103.

Topical isotopic exchange and compartmental analysis approach for probing solute behaviour at the soil/arsenate solution interface

J.T. van Elteren [a],[*], K.J. Kroon [b], Z. Šlejkovec [c], T.G. Verburg [b], Z.I. Kolar [b]

[a] *Analytical Chemistry Laboratory, National Institute of Chemistry, Hajdrihova 19, 1001 Ljubljana, Slovenia*
[b] *Department of Radiation, Radionuclides & Reactors, Faculty of Applied Sciences, Delft University of Technology,*
Mekelweg 15, 2629 JB Delft, The Netherlands
[c] *Jožef Stefan Institute, Jamova 39, 1111 Ljubljana, Slovenia*

Abstract

Isotopic exchange based approaches have for many years been applied in soil and solute research. However, acquiring and elaboration of experimental data were not always straightforward and complete. A strict and correct use of combined isotopic exchange-compartmental analysis may widen the knowledge database and provide information not available as yet. The experiments were carried out with arsenic (arsenate) from IAEA-SOIL-5 in contact with water or phosphate solution in dynamic equilibrium. After contacting the soil suspension for 28 days, the amount of arsenate released is 2.8 and 6.3 % of arsenic (solutes) in the soil, respectively. Addition of a radioactive arsenate ^{73}As(V)-spike and following the distribution of this radiotracer from the aqueous to the solid phase in time shows that the accessible fraction, i.e. available for exchange, is in both cases 12%. This implies that the remainder of the arsenic is enclosed in the lattice of minerals and for that reason unavailable for exchange, at least on the time scale of the experiment (weeks). From deconvolution of compartmental analysis results the distribution of accessible arsenate in the soil could be attributed to sorption onto external surfaces (2.6 and 2.0% of total arsenic present for the water and phosphate system, respectively) and sorption onto internal surfaces after diffusion through soil particle pores (6.5 and 4.2% of total arsenic present for the water and phosphate system, respectively). The mean residence time in two out of three compartments was in the order of minutes for the external surfaces and in the order of days for the diffusion-controlled internal surfaces.
© 2007 Elsevier B.V. All rights reserved.

Keywords: Soil; Arsenate; Radiotracer; Isotopic exchange; Compartmental analysis; Speciation; Kinetics

1. Introduction

Solute (dissolved arsenate) behaviour at the soil/aqueous solution interface has been the subject of scientific studies for more then a century [1,2]. Both the mentioned soils and solutions usually contain one or more metal ions (e.g. [3–6] or oxy anions (e.g. [7–9]). The abovementioned and many other authors developed various specific experimental and mathematical working methods aimed at elucidation of soil–solute relations and their kinetics. The use of radionuclides, i.e. radioisotopes (such as ^{32}P [9], ^{63}Ni [3], ^{65}Zn [6], ^{73}As [7], ^{109}Cd [5]) as labels in radiotracers became indispensible for soil studies. Most of these studies are based on the so-called "isotopic exchange method"

[10]. Isotopic exchange under equilibrium conditions can be described as homomolecular exchange of ions or molecules between so-called "compartments". Addition of an adequate radiotracer to one of the compartment and subsequent measuring of the decrease of the radiotracer concentration as a function of time in a compartment enables calculation of the number of compartments and exchange rates. The use of the "isotopic exchange method" requires accompanying measurements, specific modelling, occasionally elaborate calculations and necessary reasoning [3,11,12].

A tool not frequently used in evaluation of radiotracer data obtained in isotopic exchange experiments in soil research was applied in this study, viz. compartmental analysis [13–15]. This is an attempt to probe the utility of the compartmental analysis approach for soil research and to provide novel information pertaining to solute behaviour at the soil/aqueous solute interface including pores in the soil particles.

In compartmental analysis one defines a system consisting of compartments interconnected with matter transport channels. One also assumes the system to be in a state of dynamic equilibrium, i.e. there is no net mass transport between the compartments. The transfer of matter (trace) in the system is made "visible" by monitoring a radiotracer of the same chemical composition as the trace, added to one compartment and measured in the same or other compartments.

All the experiments were carried out with IAEA-SOIL-5 – which was easily available – and containing a known content of arsenate but it was not a subject of the investigation as such.

Arsenic in its various forms is a known environmental pollutant [16]. The predominant arsenic species is arsenate, originating from both natural (geologic formations, geothermal activity and vulcanic activity) and anthropogenic (wood preservatives, agricultural uses, industrial uses, mining and smelting) sources. To understand the fate of arsenate in soil systems, i.e. mobility and bioavailability, it is essential to have insight into sorption mechanisms [1].

The arsenate concentration in soil solution is especially governed by adsorption onto surfaces of iron oxides [17]. Goethite (α-FeOOH) is ubiquitous and the most stable iron oxide in soil environments [18]. Kinetics of arsenate sorption onto goethite has been studied using pressure-jump relaxation techniques [19]. These techniques use pressure perturbation as a means of shifting equilibrium states which are monitored by conductivity measurements. Conventional batch and flow methods are said to be too slow to follow sorption kinetics. It was proven that arsenate forms inner-sphere surface complexes with goethite, both mono- and bidentate, with a fast initial ligand exchange reaction in the first-step and a slower second ligand exchange reaction in the second-step. This sequence of steps is completed within seconds but sorption increases further over days/months. Extended X-ray absorption fine structure (EXAFS) spectroscopy has shown that no other chemical reactions are responsible for this slows sorption process so that a surface diffusion into goethite pore particles was suggested (Fendorf et al. [20]).

In this work a radioactive ^{73}As(V) tracer was used to follow transfer, i.e. exchange of arsenate between different physical or chemical states, in a system comprising water or 10 mmol l^{-1} phosphate solution (pH 6.0) and SOIL-5 from the International Atomic Energy Agency (IAEA). A phosphate solution was used, as phosphate is an analogon of arsenate which may compete with arsenate for binding to sorption sites. Isotopic exchange methods have been applied in all kind of studies, also, e.g. to get insight into the phosphate behaviour in soil systems [9,21].

2. Experimental

2.1. Samples and reagents

A certified reference material for trace element determination (IAEA-SOIL-5) with a certified As concentration of 93.9 ± 7.5 mg kg^{-1} was used in the isotopic exchange experiments. This soil originates from the Agricultural Experimental Station La Molina, Lima, Peru (20 cm topsoil depth). A ^{73}As(V)

radiotracer ($T_{1/2} = 80.3$ days, γ photons/disintegration and γ energy, $E_{\gamma} = 0.10$ and 53.4 keV) was purchased from Los Alamos National Laboratory, USA with the following specifications: 95.8 MBq ml^{-1} with an arsenic concentration of ca. 20 μg ml^{-1} as As(V) in 0.1 mol l^{-1} HCl. This radiotracer stock solution was diluted with water to a ^{73}As(V)-working solution with an activity concentration of 0.48 MBq ml^{-1}. The specific activity of ca. 4.8×10^{12} Bq g^{-1} is sufficiently high to prevent equilibrium shifts in the isotopic exchange experiments as a result of addition of mass via the radiotracer. All chemicals were at least of analytical reagent grade. Milli-Q-Plus water (Millipore-waters, Milford, MA, USA) was used for all solution preparations.

2.2. Exchange experiments

Soil samples of 250 mg (based on dry weight) were placed in 50 ml polypropylene centrifuge tubes with screw cap (Nalge Nunc International, Rochester, NY, USA) and either 10 ml water or 10 mmol l^{-1} phosphate solution (pH 6.0) was added, followed by shaking of the suspensions in a temperature-controlled reciprocal water bath (model R76 from New Brunswick Scientific) for ca. 26 days at a temperature of 25 °C. After this contacting period the 10 ml samples were centrifuged for 30 min at 3000 rpm (ca. 1800 g). Then 200 μl supernatant aliquots were taken for determination of the As concentrations (see below), followed by resuspending the pellet and addition of 100 μl of the ^{73}As(V)-working solution. This gave an initial activity concentration in the contacting solutions of 4.9 kBq ml^{-1} ($t = 0$) with an arsenic concentration increase due to the spike of ca. 1 ng ml^{-1}. As above the samples were shaken and at strategic time intervals filtered (up to 1 day exchange) or centrifuged (after 1 day exchange) and 5 ml filtrate or supernatant aliquots taken for immediate counting (see below). For the filtration (0.4 μm polycarbonate filter, Nucleopore) whole sample tubes were sacrificed whereas for the centrifugation (30 min at 3000 rpm) counted supernatant aliquots were joined with their respective pellet-liquid mixtures, resuspended and shaking resumed. The very small error introduced via transfer losses at centrifugation was corrected for by weighing and the time needed for centrifugation and counting was negligible in comparison with the length of the experiment.

2.3. As and ^{73}As determination

Arsenic in the water and phosphate supernatants was determined by FI-HGAFS [22]. Since it was established by HPLC-HGAFS [23] that only As(V) is desorbed from IAEA-SOIL-5, and no reduction to arsenite occurs in the course of the experiment, it was sufficient to measure total As by FI-HGAFS to generate As(V) concentrations. The 200 μl aliquots were 1 + 10 diluted with water and As measured with the method of standard additions. ^{73}As in the 5 ml aliquots was counted for 10 min using an automatic γ-counter (NaI(Tl) scintillation detector; Wallac 1480 Wizard); the counting error was ≤5%. Corrections were made for background radioactivity and ^{73}As decay.
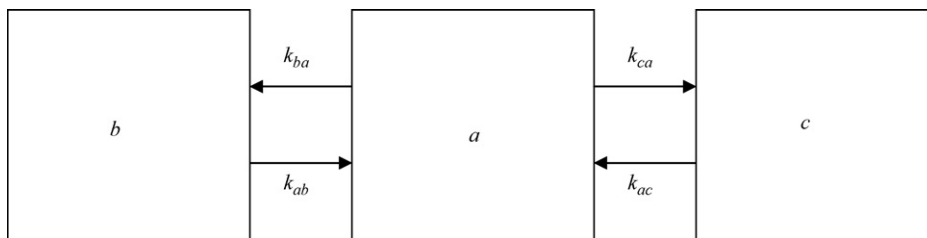
Fig. 1. Proposed 3-compartmental parallel model: (a) As(V) in the bulk solution, (b) As(V) adsorbed onto external surfaces and (c) As(V) adsorbed onto internal surfaces. The arrows depict the rate constants for transport of As(V) from and to the compartments.

3. Results and discussion

With reference to what is known about sorption of arsenic onto goethite [19,20]) and the fact that IAEA-SOIL-5 contains a significant amount of iron (4.45 wt.%), we propose a parallel three-compartmental model to explain transfer of arsenate in a system comprising water or 10 mmol l^{-1} phosphate solution (pH 6.0) and IAEA-SOIL-5. We tentatively define the compartments in a 10 ml system as follows: (a) As(V) in the bulk solution, (b) As(V) adsorbed onto external surfaces and (c) As(V) adsorbed onto internal surfaces after diffusion through soil particle pores (see Fig. 1). The quantity of trace in a compartment is denoted as Q, e.g. Q_a is the quantity in compartment a (in mol); the rate of transfer (flow) of trace as F, e.g. F_{ba} is the rate of transfer to compartment b from compartment a (in mol s^{-1}); the rate constant of transfer of trace including radiotracer as k, e.g. $k_{ba} = F_{ba}/Q_a$ (in s^{-1}); the quantity of radiotracer in a compartment at time t and zero, respectively as $q(t)$ and $q(0)$, e.g. $q_a(0)$ is the quantity of radiotracer at $t = 0$ in compartment a, the compartment to which the radiotracer was added at $t = 0$ (in Bq). General equations which describe the tracer quantities q_a, q_b and q_c in compartments a, b and c in time, for any three-compartmental model, are given by

$$\frac{q_a(t)}{q_a(0)} = H_1 \exp(-g_1 t) + H_2 \exp(-g_2 t) + H_3 \tag{1}$$

$$\frac{q_b(t)}{q_a(0)} = K_1 \exp(-g_1 t) + K_2 \exp(-g_2 t) + K_3 \tag{2}$$

$$\frac{q_c(t)}{q_a(0)} = L_1 \exp(-g_1 t) + L_2 \exp(-g_2 t) + L_3 \tag{3}$$

As the result of integration of the differential equations leading to above equations (for three compartments) the coefficients H_i will emerge as equivalents of complex expressions involving rate constants, k, and the exponents, g, and other expressions for rate constants in terms of exponents also will evolve [24–26]. The forms of these expressions depend on the number of compartments and the (tentative) structure of the compartmental model delineating the system under investigation. The results of the exchange experiments for the water and phosphate system, expressed as $q_a(t)/q_a(0)$ versus time, t, are given in Fig. 2. Non-linear curve fitting of the experimental data in Eq. (1) using Microcal$^{\text{TM}}$ Origin$^{\circledR}$ version 6.0 (Microcal Software Inc., Northampton, USA) yields H's and g's as given in the insert of Fig. 2. It should be noted that the curves are forced through the point ($t = 0$, $q_a(t)/q_a(0) = 1$) to allow $H_1 + H_2 + H_3 = 1$ for all
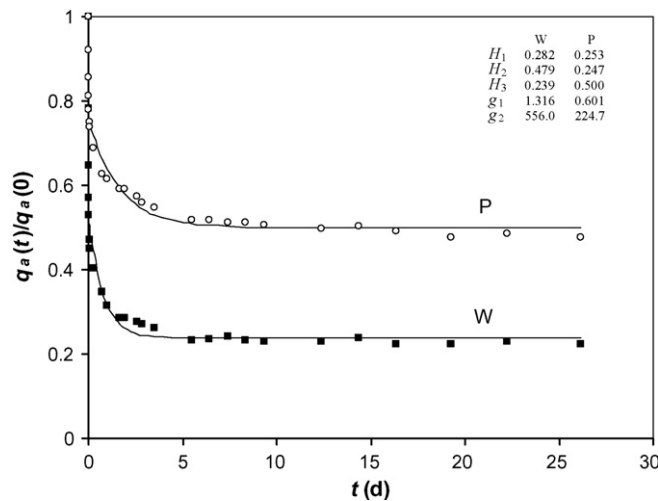

Fig. 2. Time course of As(V) in the bulk solution ($q_a(t)$) given as a fraction of the initially added radiotracer dose ($q_a(0)$) for both the water (W) and phosphate (P) system; the lines represent the best fits according to Eq. (1) and the insert gives the fit parameters. Note that for W: $R^2 = 0.9958$, P-value (at $\alpha = 0.05$) < 0.0001 and for P: $R^2 = 0.9991$, P-value (at $\alpha = 0.05$) < 0.0001.

t's. The relative residual distribution curves for the water and phosphate system are given in Fig. 3 and show a maximum deviation of about 10% (absolute) with a random distribution around zero. This is an indication for a proper fit; modelling with two compartments gave an inadequate fit and although with
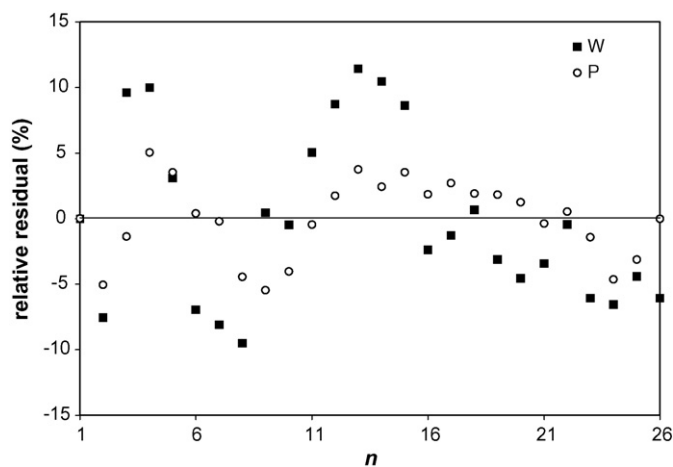

Fig. 3. Relative residual distribution curves for each of the 26 data points n given as $100 \times$ (observed − fitted)/fitted (%) for both the water (W) and phosphate (P) system.

Table 1
Rate constants and standard deviations (in day^{-1}) for the three-compartmental parallel model pertaining to the water (W) and phosphate (P) system

	W	P
k_{ab}	289.99 ± 50.81	169.24 ± 26.66
k_{ba}	265.39 ± 41.29	55.44 ± 8.35
k_{ac}	0.60 ± 0.12	0.40 ± 0.05
k_{ca}	1.37 ± 0.26	0.27 ± 0.03

four compartments the fit was somewhat better no strong physical and/or chemical evidence could be found to choose such a model. H_3 represents the value of $q_a(t)/q_a(0)$ for $t = \infty$ which should be equal to the fraction of arsenate in the bulk solution (compartment a):

$$H_3 = \frac{Q_a}{Q_a + Q_b + Q_c} \tag{4}$$

The Q_a's measured are 8.88 and 19.3 nmol for the water and phosphate system, respectively. The total quantities ($Q_T = Q_a + Q_b + Q_c$) calculated from these values and H_3's derived are 37.2 and 38.6 nmol for the water and phosphate system, respectively. Since the total quantity of As in soil is 313 nmol this implies that only 11.9 and 12.3% is accessible (available for exchange) for the water and phosphate system, respectively.

The rate constants, k, for a three-compartmental parallel model (b ↔ a ↔ c) may be calculated from H's and g's derived from fitting. This yields rate constants as given in Table 1. The mean residence times in compartment b and c are defined as $\tau_b = 1/k_{ab}$ and $\tau_c = 1/k_{ac}$, respectively. For compartment b, τ_b is 5.0 min (water system) and 8.5 min (phosphate system); for compartment c, τ_c is 1.7 days (water system) and 2.5 days (phosphate system). We ascribe the short residence times to external adsorption and the long residence times to diffusion-limited internal adsorption. It should be noted that no a priori choice can be made which of the compartments b or c is related to the fast or slow process. In this case it is obvious that our choice in Fig. 1 was a proper one; otherwise we should have changed the compartment labels. The compartment size Q_a (for the water and phosphate systems) has been calculated above; the compartment sizes Q_b and Q_c may be calculated from the following equations knowing that there is no net mass transport:

$$F_{ab} = k_{ab}Q_b = F_{ba} = k_{ab}Q_a \tag{5}$$

and

$$F_{ac} = k_{ac}Q_c = F_{ca} = k_{ca}Q_a \tag{6}$$

The calculated compartment sizes are given in Table 2. If we assume that compartment c is merely determined by diffusion this implies that the arsenate concentration in the pores is identical to the arsenate concentration in the bulk solution (compartment a), viz. 0.888 nmol ml^{-1} (water system) and 1.93 nmol ml^{-1} (phosphate system). Knowing the arsenate quantity in the pores (compartment c), viz. 20.2 nmol (water system) and 13.0 nmol (phosphate system), it follows that the

Table 2
Compartment sizes and standard deviations (in nmol) for the three-compartmental parallel model pertaining to the water (W) and phosphate (P) system

	W	P
Q_a	8.88	19.30
Q_b	8.13 ± 1.91	6.32 ± 1.82
Q_c	20.17 ± 5.61	13.00 ± 2.07
Q_T	37.20	38.60

pore volumes are 22.7 ml (water system) and 6.7 ml (phosphate system). Relating this to a soil quantity of 0.25 g in the system this is an impossibility, proving that arsenate in these pores is not "freely" present in pore water but bound (possibly similar to arsenate onto the external surfaces).

In spite of the fact that more arsenate is released from soil (Q_a) in the phosphate than in the water system, probably due to competitive ion exchange, the amount of accessible arsenate (Q_T) is the same in both systems. Although this competition leads to a lower amount of arsenate in the available bound fraction ($Q_b + Q_c$), the ion exchange process should be the same for externally (Q_b) and internally (Q_c) bound arsenate under dynamic equilibrium conditions. Thus, the Q_b/Q_c ratios have to be equal for both systems in case we accept that a competitive ion-exchange mechanism controls the sorption of arsenate. On average we find a Q_b/Q_c ratio of 0.44 ± 0.06 what is an indication of similar ion exchange processes occurring on the internal and external surfaces.

In Fig. 4 graphs are given which relate all measured and deduced data, i.e. the distribution kinetics of the arsenate
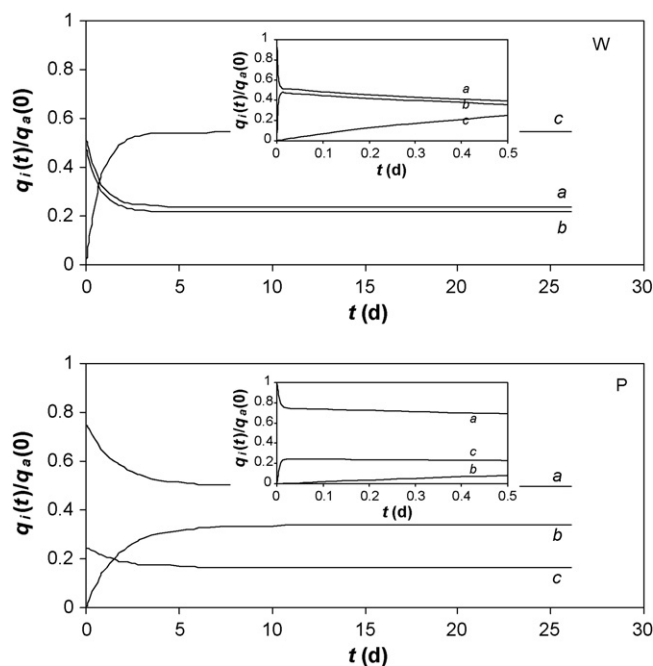

Fig. 4. Distribution kinetics of ^{73}As(V) from compartment a over all compartments i (a–c) for the water (W) and phosphate (P) system, assuming a three-compartmental parallel model; inserts give a zoomed version of the kinetics during the first 0.5 day.

radiotracer from compartment a over all compartments for the water and phosphate system.

4. Conclusions

The isotopic exchange approach combined with compartmental analysis for data evaluation is a powerful tool to derive soil sorption site characteristics. In case a radiotracer with a sufficiently high specific activity is used non-intrusive measurements can be made, i.e. without changing the properties of the system in dynamic equilibrium.

The accessible arsenic (arsenate) fraction for IAEA-SOIL-5 was ca. 12% of the arsenic present in the soil, independent of medium (water or phosphate system). This implies that the remainder of the arsenic is enclosed in the lattice of minerals and for that reason unavailable for exchange, at least on the time scale of this experiment (weeks). We deduced that in IAEA-SOIL-5 at least two sorption sites are responsible for the exchange behaviour of arsenate and that phosphate behaves as a competitive anion for sorption.

References

[1] D.L. sparks, J. Plant Nutr. Sci. 163 (2000) 563.
[2] R.E. Homan, I. Bertrand, M.J. McLaughin, Aust. J. Soil Res. 40 (2002) 1371.
[3] G. Echevarria, J.L. Morel, J.C. Fardesau, E. Leclerc-Cessac, J. Environ. Qual. 27 (1998) 1064.
[4] S. Sinaj, F. Mächer, E. Frossard, Soil Sci. Soc. Am. J. 63 (1999) 1618.
[5] E. Gérard, G. Echevarria, T. Sterckeman, J.L. Morel, J. Environ. Qual. 29 (2000) 1117.
[6] H. Zhang, W. Davison, A.M. Tye, N.M.J. Crout, S.D. Young, Environ. Toxicol. Chem. 25 (2006) 664.
[7] A.M. Tye, S.D. Young, N.M.J. Crout, H. Zhang, S. Preston, E.H. Bailey, W. Davison, S.P. Mcgrath, G.I. Paton, K. Kilman, Environ. Sci. Technol. 36 (2002) 982.
[8] K.A. Mir, A. Rutter, I. Koch, P. Smith, K.J. Reimer, J.S. Poland, Talanta 72 (2000) 1507.
[9] R. McDowell, S. Sinaj, A. Sharpleva, E. Frossard, Soil Sci. 166 (2001) 365.
[10] H. McKay, Nature 142 (1938) 997.
[11] N.M.J. Crout, A.M. Tye, H. Zhang, S.P. McGrath, S.D. Young, Environ. Toxicol. Chem. 25 (2006) 659.
[12] I.A.M. Ahmed, S.D. Young, N.M.J. Crout, Geochim. Cosmochim. Acta 70 (2006) 4850.
[13] J.J.M. Binsma, Z. Kolar, Solid State Ionics 16 (1985) 225.
[14] E.P. Achterberg, J.T. van Elteren, Z.I. Kolar, Environ. Sci. Technol. 36 (2002) 914.
[15] Z.I. Kolar, T.G. Verburg, H.J.M. van Dijk, J. Inorg. Biochem. 90 (2002) 61.
[16] J.O. Nriagu (Ed.), Arsenic in the Environment. Part 2. Cycling and Characterization, John Wiley & Sons Inc., London, 1994.
[17] M. Sadiq, Mar. Chem. 31 (1990) 285.
[18] J.L. Jambor, J.E. Dutrizac, Chem. Rev. 98 (1998) 1998.
[19] P.R. Grossl, M. Eick, D.L. Sparks, S. Goldberg, C.A. Ainsworth, Environ. Sci. Technol. 31 (1997) 313.
[20] S. Fendorf, M.J. Eick, P.R. Grossl, D.L. Sparks, Environ. Sci. Technol. 31 (1997) 315.
[21] S. Sinaj, E. Frossard, J.C. Fardeau, Soil Sci. Soc. Am. J. 61 (1997) 1413.
[22] J.T. van Elteren, Z. Šljekovec, H.A. Das, Spectrochim. Acta B 54 (1992) 311.
[23] Z. Šlejkovec, J.T. van Elteren, A.R. Byrne, Talanta 49 (1999) 619.
[24] C.W. Sheppard, Introduction to Mathematical Tracer kinetics, John Wiley & Sons Inc., New York, 1962.
[25] R.A. Shipley, R.E. Clark, Tracer Methods for In Vivo Kinetics, Academic Press, New York, 1972.
[26] J.S. Robertson, L.G. Colombetti (Editor & Editor-in-Chief), Compartmental Distribution of Radiotracers, CRC Press Inc., Boca Raton, Florida, USA.

On-line micellar-enhanced spectrofluorimetric determination of rhodamine dye in cosmetics

Chien Chun Wang [c], Adriana N. Masi [b,c], Liliana Fernández [a,c,*]

[a] *Área de Química Analítica, Facultad de Química, Bioquímica y Farmacia,*
Universidad Nacional de San Luis, Argentina
[b] *Área de Bromatología, Ensayo y Valoración de Medicamentos,*
Facultad de Química, Bioquímica y Farmacia,
Universidad Nacional de San Luis, Argentina
[c] *CONICET, Chacabuco y Pedernera, 5700 San Luis, Argentina*

Abstract

A simple FI-fluorimetric analytical methodology for the continuous and sequential determination of rhodamine B (RhB) in cosmetic products has been developed and evaluated in terms of sensibility and selectivity. The influence of several surfactant solutions on RhB fluorescence signal has been studied; particular attention was paid in the aggregation behavior of RhB–SDS system. Linear response has been obtained in the range of 1.6×10^{-9} and 1×10^{-6} mol L^{-1}, with a detection limit of 5×10^{-10} mol L^{-1}. The novel technique provides a simple dissolution of sample, on-line filtration with sampling rate higher than 100 samples h^{-1} and has been satisfactorily applied to the RhB determination in commercial lipsticks.
© 2007 Elsevier B.V. All rights reserved.

Keywords: Flow injection spectrofluorimetry; Rhodamine B; Cosmetics; Micelles

1. Introduction

Cosmetic products cover a wide range of preparations that are used for cleansing, beautifying or promoting attractiveness. The economic impact of these products cannot be underestimated, worth possibly billions of dollars per year to the cosmetic industries [1].

As cosmetic products are applied on the skin, direct contact with harmful substance could cause skin disease such as irritation, allergic reactions and could be absorbed and be stored in different organs, manifesting at short or long time their toxicity, reason by which governmental entities have listed prohibit substances for cosmetic use.

Among the list, the Food and Drug Administration (FDA) has now regulated the use of Rhodamine B (RhB, $C_{28}H_{31}N_2O_3Cl$) in the cosmetic industries, because of its carcinogenesis.

RhB is a fluorescent dye derivative of the xanthene dyes class, synthesized from condensation of phthalic anhydride with *m*-dialkylaminophenols; it is between the oldest and most commonly used synthetic dyes applied in cloth and food coloring [2]. As fluorescent dye, it is noted due to its special photochemical and photophysical properties [3,4] being very efficient sensitizer in photography [4–8], bioanalytical chemistry [9,10], laser dyes [11–13] and fluorescence probes [14–16] causing a vast and increasing up applications in chemistry, biochemistry and physics probes. In pharmaceutical industries, it has been used as a drug and cosmetic color additive in aqueous drug solutions, tablets, capsules, toothpaste, soap, hair-waving fluids, bath salts, lipsticks [17], eyes shadows and rouges [18].

It has been demonstrated that the acute exposure to RhB results in mucous membrane and skin irritation [19] and its carcinogenesis has been probed injecting RhB subcutaneously in

---

* Corresponding author at: Área de Química Analítica, Facultad de Química, Bioquímica y Farmacia, Universidad Nacional de San Luis, Argentina. Fax: +54 2652 430224.

E-mail address: lfernand@unsl.edu.ar (L. Fernández).

rats, producing local sarcomas [20–21]. Applied on lips, it has the capacity of decreasing the collagen content of the fibroblast cell layer of the human lips, which may result from a non-specific inhibition of protein synthesis without non-specific cell damage [22].

Customary standard methods for cosmetic analysis involve an assessment by microscopy and/or microspectrophotometry [23,24], separation techniques such as electrokinetic capillary chromatography [25], thin layer and high-pressure liquid chromatography [24,26]. Most of techniques are not entirely satisfactory since they have inadequate sensitivity, either involve a subjective opinion, or require a complicated pretreatment to isolate the dyes and pigments from the waxy matrix.

In this paper, a direct quantitative determination method of RhB in real cosmetic samples based on its native fluorescence without extraction or pretreatment step has been developed. Enhancement of sensitivity was attempted employing an anionic surfactant SDS (sodium laurylsulfate); likewise the effect of RhB on the aggregation processes of SDS at the experimental conditions was investigated, which suggests that the formation of micelles involving RhB and SDS occurs at concentrations below the critical micelle concentration (cmc). Under established optimal conditions, the system was adapted to flow injection analysis (FIA), showing a very short sampling time, potentially useful to control in routine analysis.

2. Experimental

2.1. Apparatus

A Shimadzu RF-5301PC spectrofluorimeter (Shimadzu Corporation, Analytical Instrument Division, Kyoto, Japan), equipped with a Xenon discharge lamp and 1 cm quartz cells were used for the fluorescent measurements.

Solutions were propelled by Gilson Minipuls 3 peristaltic pumps with PVC pumping tubes. All tubing connecting the different components of the flow system was PVC, 0.8 mm i.d. and a homemade valve was used for FIA configuration.

A pH meter (Orion Expandable Ion Analyzer, Orion Research, Cambridge, MA, USA) Model EA 940 with combined glass electrode was used for monitoring pH adjustment.

2.2. Reagents

Stock standard solution of $50 \mu g mL^{-1}$ was prepared by dissolving RhB (Fluka AG, Chemische Fabrik, Buchs SG, Switzerland) in ultra pure water and stored in a dark bottle at room temperature. In these conditions, RhB was stable at least for 4 weeks. A working standard of $5 \mu g mL^{-1}$ was prepared by adequate dilution of the stock standard solution with ultra pure water. Sodium dodecylsulfate (SDS), Triton® X-100 and hexadecyltrimethyl-ammonium bromide (HTAB) were purchased from Tokyo Kasei Industries (Chuo-Ku, Tokyo, Japan). Sodium tetraborate were purchased from Mallinckrodt Chemical Works (New York, Los Angeles, St. Louis, USA), concentrated chlorhydric acid, sodium hydroxide, sodium chloride and potassium chloride were purchased from Merck (Darmstadt, Germany). Lipstick samples were obtained from several commercial available trademarks.

2.3. Sample preparation

A fraction of 5.0 mg of lipstick sample was accurately weighted and transferred to 50 mL beaker. 20 mL of ultra pure water were added and dissolved by mechanical stirring during 15 min at 333 K before being introduced in the FIA system for its determination.
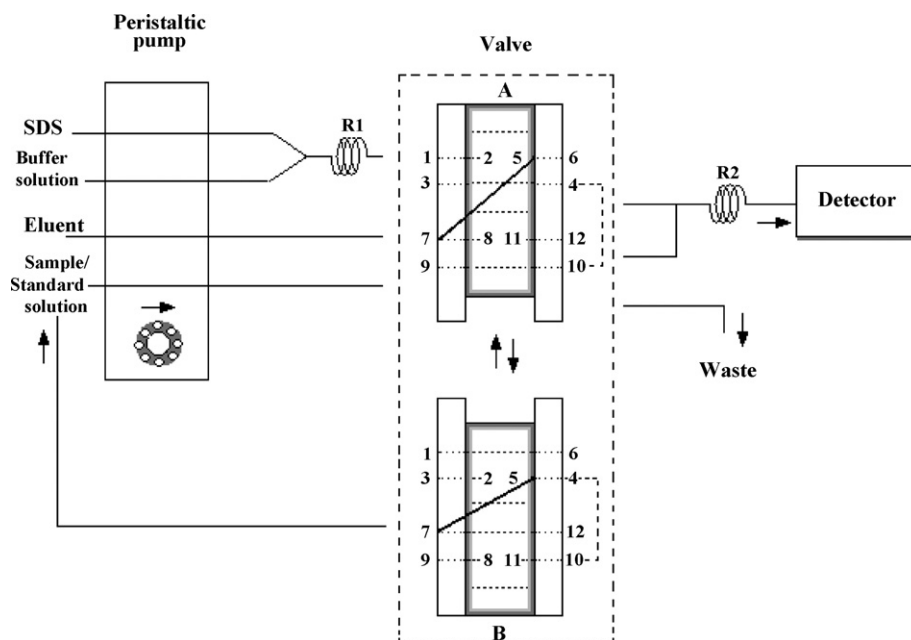

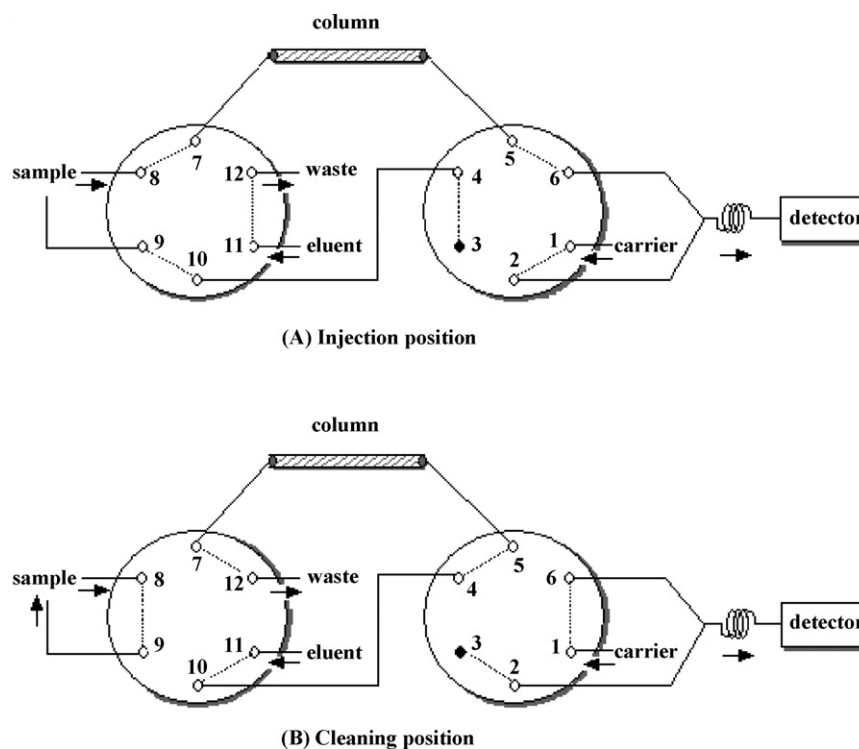Fig. 1. FIA manifold RhB determination.

Fig. 2. Detail valve position. Schematic representation of the manifold where the valve could be fit at two positions: (A) at the injection position, the sample or standard solutions are injected to the detector after going through the column and being mixed with carrier solution; (B) at cleaning position, the eluent is washing the mini-column in back-stream, while sample or standard solutions are recycled.

2.4. Experimental procedure

A stream of SDS (2.1×10^{-3} mol L^{-1}) solution was combined with borax (0.1 mol L^{-1}) into reactor R$_1$, forming the carrier stream (Fig. 1). The sample/standard solution went through to a homemade mini-column packed with cotton wool (CC) to collect the waxy component of the sample solution, and then injected for 15 s into the carrier stream. RhB contained in the sample/standard is interacted with the carrier stream into reactor R$_2$, and then flowed to the fluorescence detector, measured at λ_{ex} 560 nm and λ_{em} 577 nm. The whole of linearity range was obtained varying the slit widths of 1.5–1.5 nm to 5–5 nm. After injecting, the valve was switched allowing the eluent stream (ultra pure water at 338 K) go through the CC column in the contra-stream, cleaning the retained waxy components and conducting to waste (Fig. 2).

3. Results and discussion

3.1. Spectrum properties of RhB

The RhB exists in solution as ionized species, neutral form, lactone and/or molecular aggregates, depending on pH, solvent, temperature and concentration. Each form of RhB is characterized by typical absorption and emission spectra which are further influenced by specific medium effect, i.e. ionic strength, additive presences, etc. Therefore, spectroscopic properties of RhB are still the subject of numerous research studies and controversies [27–29].

Traditionally Rhs have large molar absorptivity in the visible region of the electromagnetic spectrum, which is attributed to a $\pi \rightarrow \pi^*$ transition [27]. The absorption and fluorescent emission are influenced by the substituents on the nitrogen atom of the amino groups of the xanthene base.

3.2. Influence of surfactant's nature

In order to perform the luminescent emission, the fluorescence properties of RhB in various surfactant media were studied: anionic surfactant (SDS, $0–9 \times 10^{-3}$ mol L^{-1}), cationic surfactant (HTAB, $0–5 \times 10^{-2}$ mol L^{-1}) and non-ionic surfactant (TX-100, $0–1 \times 10^{-3}$ mol L^{-1}). Experimental data showed that the enhancement factor for RhB–SDS system (2.5 folds respect to RhB fluorescence in water medium) was higher than RhB–HTAB (2.0 folds) (Fig. 3). For RhB–TX-100, an important spectrum interference was observed; thus, the anionic surfactant SDS was chosen for further work. At SDS concentration above 1×10^{-2} mol L^{-1}, solubility problems appeared causing errors in the measurement of fluorescence.

The SDS aggregation equilibrium in presence of RhB in our optimal experimental conditions showed a quite different behavior than pure SDS aqueous solution. For RhB–SDS system, the fluorescent response showed an inflection point at [SDS] = 3.1×10^{-4} mol L^{-1} (Fig. 4). The change in the SDS cmc suggests the formation of mixed aggregates at concentrations below the cmc reported (8.1×10^{-3} mol L^{-1}) [30]; in concordance to obtained results, other authors have reported similar behavior for SDS systems [31–34].

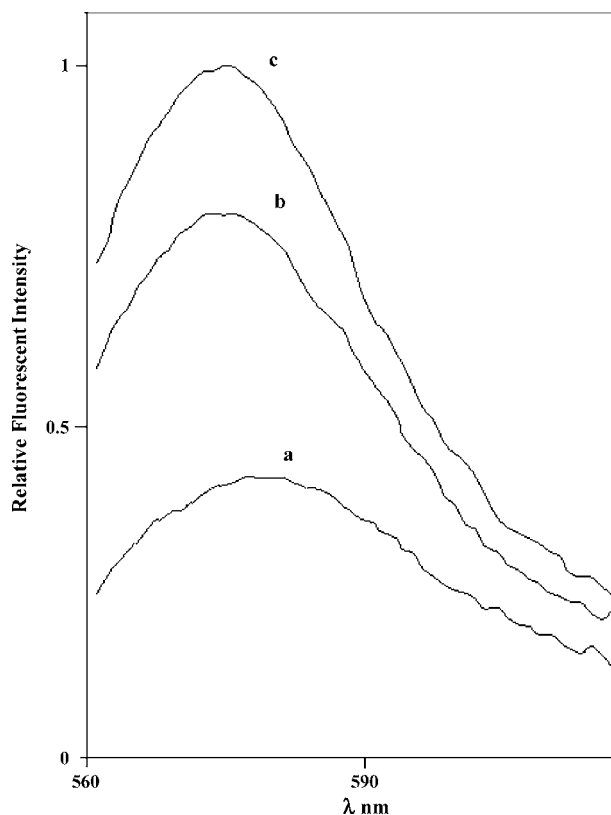Fig. 3. Emission spectra of RhB in micellar media. $\lambda_{ex} = 560$ nm and $\lambda_{em} = 577$ nm. (a) aqueous solution; (b) $C_{HTAB} = 4 \times 10^{-2}$ M; (c) $C_{SDS} = 2 \times 10^{-3}$ M.

The enhancement of RhB fluorescent intensity by addition of SDS was associated to a slight hypsochromic shift of the maximum λ_{em} (Fig. 3); it reflects that the microenvironment around the dye is quite different from that in aqueous solution. It can be attributed to restrictions imposed on the free rotational motions which are competitive with luminescent emission [35]. In addition, the RhB equilibrium of molecular aggregate forma-
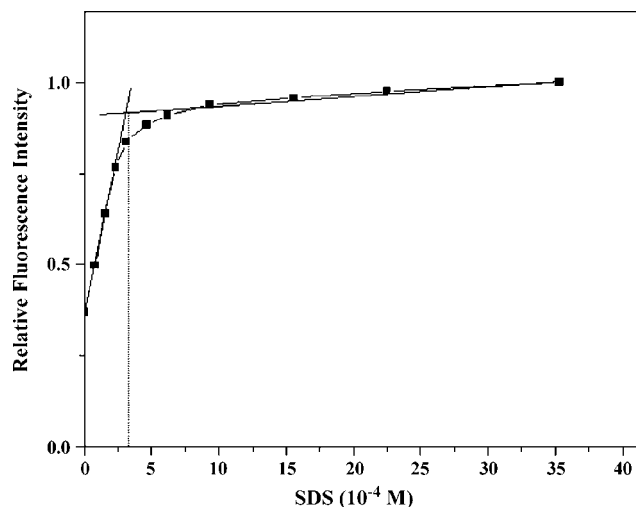
Fig. 4. RhB emission at different SDS concentration levels. $\lambda_{ex} = 560$ nm and $\lambda_{em} = 577$ nm. $C_{RhB} = 1 \times 10^{-7}$ M.
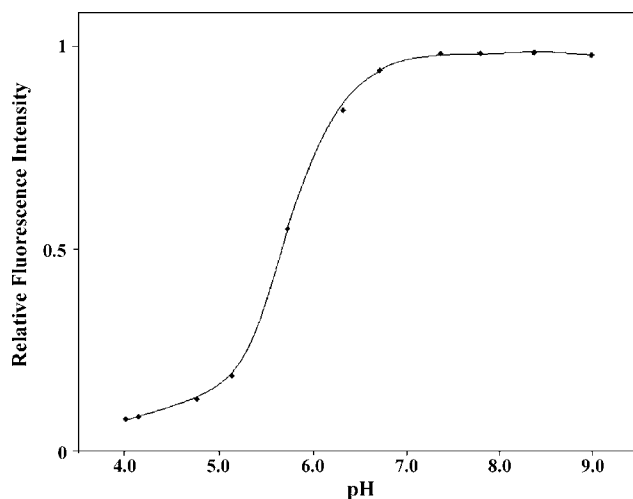

Fig. 5. Luminescent emission of RhB at different pH in SDS micelles. $\lambda_{ex} = 560$ nm and $\lambda_{em} = 577$ nm. $C_{RhB} = 1 \times 10^{-7}$ M; $C_{SDS} = 2 \times 10^{-3}$ M.

tion could be displaced to the monomer species, taking place the disaggregation of the dye.

3.3. Influence of pH and ionic strength

Fluorescent intensity of RhB in SDS solution reached a maximum value between pH 7.0 and 8.5 (Fig. 5); hence, pH 8.0 was selected as optimum acquired with sodium tetraborate for further assays.

In order to study the effect of the addition of inert salts on micellar solutions of RhB, NaCl and KCl solutions were tested. In all studied cases, an increase of concentration above 6×10^{-2} mol L^{-1} provoked a clouding phenomenon to the system, and below these values no significant effect was observed.

3.4. Sample dissolution parameters

In polar solvents as water, RhB is widely soluble and is found as ionic species. Therefore, ultra pure water was chosen as an adequate solvent for sample dissolution.

The complex matrix of cosmetic products complicates their routine analysis, not only due to the presence of potential dyes interfering, but also for the diverse matrix compounds and additives in such products. A lipstick typically consists of high percents of castor oil, a variable percent of beeswax, carnauba wax, and lanolin, a variable number of soluble and insoluble dyes, pigments and perfume [36].

The waxy composition of lipstick makes difficult its complete dissolution at room temperature; therefore, a heat applied to help this process was necessary during 15 min with mechanic stirring. The influence of temperature for sample dissolution was studied in the range of 298–363 K, being melting range for the waxy component next to 333 K. At these conditions, non-decomposition was observed for the dye.

Although the presence of ethanol accelerates the dissolution process helping the partial dissolution of the waxy components, when the proportion of ethanol is raised, increase of turbidity

Table 1
Optimization of FIA variables for RhB–SDS system

Variables	Studied ranges	Optimum values
SDS 2.0×10^{-3} mol L^{-1} flow rate (ml min^{-1})	0.50–5.00	4.00
Buffer borax 1×10^{-2} mol L^{-1} flow rate (ml min^{-1})	0.50–5.00	4.00
Sample solution flow rate (ml min^{-1})	0.50–5.00	4.20
Eluent flow rate (ml min^{-1})	1.00–8.00	6.00
Loading time (s)	5–30	15
Reactor R$_1$ length (mm)	100–300	200
Reactor R$_2$ length (mm)	100–300	200
Cotton wool weight (mg)	10–40	25

of final filtrate was observed due to the emulsification of the system.

3.5. Optimization of the FIA variables

The variables influencing the performance of the method were studied and optimized in order to obtain a high signal and good reproducibility, using univariated method. The studied range of the FIA variables and their optimum values are listed in Table 1.

In order to achieve on-line waxy and/or particulate components retention, a homemade mini-column using a 100 μL conical polypropylene tube packed with different filtering materials was tested (as natural and synthetic fiber). For this hitch, the commercial cotton wool was found to provide satisfactory waxy retention, holding a good reproducibility.

To remove the retained material in the CC and prepare the FIA system for the next assay, ultra pure water at different temperatures was tested (298–353 K) as washing solution being efficient at 338 K.

3.6. Analytical performance

Calibration curves of RhB were realized under optimal working conditions according to the procedure described above. It was obtained linearity in the range of 1.6×10^{-9} to 1×10^{-6} mol L^{-1} (concentration before dilution on-line), varying the excitation and emission slit widths of 1.5–1.5 nm to 5.0–5.0 nm.

Fig. 6 shows the fiagram obtained with its corresponding calibration graph for excitation and emission slit widths of 3 and 5 nm, respectively. Data were fitted by standard least-squares treatment giving the regression equations for calibration graphs of $F = 11.867 + 9 \times 10^9\, C$ ($r^2 = 0.9995$), where F is the fluorescence intensity (average of three measurement for each) and C is the concentration of RhB expressed in mol L^{-1}. The slope of the calibration graph is the calibration sensitivity according to IUPAC definition which supported the validation of the proposed procedure for quantification of RhB.

The detection limit [37] employing excitation and emission slit width of 5.0–5.0 nm, was estimated as the concentration of
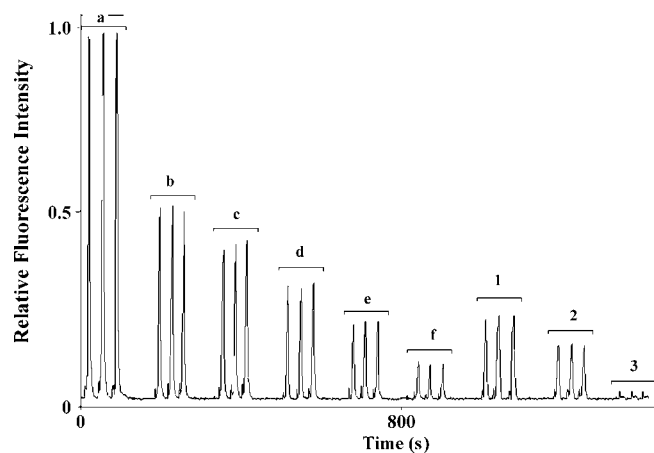

Fig. 6. Calibration curve and sample signals. Standard solution of RhB (a) 1×10^{-7} M; (b) 5.2×10^{-8} M; (c) 4.1×10^{-8} M; (d) 3.1×10^{-8} M; (e) 2.1×10^{-8} M; (f) 1×10^{-8} M. $C_{SDS} = 6.6 \times 10^{-4}$ M. Real lipstick samples of different trademark (1) 2.52×10^{-8} M; (2) 1.74×10^{-8} M; (3) not detectable. $\lambda_{ex} = 560$ nm and $\lambda_{em} = 577$ nm. Slit width exc = 3 nm and em = 5 nm. Injection time: 15 s.

analyte which produces an analytical signal equal to three times the standard deviation (SD = 1.456) of the background fluorescence giving a value of 5×10^{-10} mol L^{-1} and the quantification limit equal to 10 times SD of the background fluorescence (1.6×10^{-9} mol L^{-1}). These values were 2 orders magnitude lower than others reported [25].

3.7. Application and validation

In order to check the applicability of the proposed methodology for quantitative determination of RhB in cosmetic products, it was successfully applied to different trademark lipsticks. Since there does not exist official or standard methods to this determination, to validate the developed methodology recovery studies were carried out on these samples and the obtained results are shown in Table 2.

Table 2
Determination of RhB in real lipsticks samples

Samples	Base value (mol L^{-1})	RhB added (mol L^{-1})	RhB found[a] (mol L^{-1})	Recovery ± RSD (%)[b]
1	–	–	2.52×10^{-8}	–
	2.52×10^{-8}	1×10^{-8}	3.54×10^{-8}	102.4 ± 1.0
	2.52×10^{-8}	2×10^{-8}	4.45×10^{-8}	98.5 ± 2.1
	2.52×10^{-8}	3×10^{-8}	5.52×10^{-8}	100 ± 1.5
2	–	–	1.74×10^{-8}	–
	1.74×10^{-8}	1×10^{-8}	2.75×10^{-8}	101.2 ± 1.8
	1.74×10^{-8}	2×10^{-8}	3.67×10^{-8}	98.2 ± 1.9
	1.74×10^{-8}	3×10^{-8}	4.64×10^{-8}	98 ± 2.2
3	–	–	Not detectable	–
		1×10^{-8}	9.92×10^{-9}	99.2 ± 2.5
		2×10^{-8}	1.96×10^{-8}	98 ± 1.8
		3×10^{-8}	2.98×10^{-8}	99.5 ± 1.6

$\lambda_{ex} = 560$ nm and $\lambda_{em} = 577$ nm.
[a] Mean value, $n = 6$.
[b] $100 \times [(\text{found} - \text{base})/\text{added}]$.

The preliminary selection of the sample was made choosing the colors palettes which possibly contained the studied dye; they included the group of strong pink, fuchsia and red lipsticks. The applications were performed taking by triplicate 5 mg of 10 real samples, and after suitable dilution, they were injected by triplicate in the FIA system. In Fig. 6 the results of three samples are presented in which two of them present a significant level of RhB (12.0 and 8.3 μg L^{-1}, respectively), and the third represents the rest of samples with no detectable levels of RhB.

The RhB levels found in our samples could vary greatly with other reported, due to the multiplicity of samples, as well as different dye proportion. Other consideration to be take into account is the politics of the place where lipsticks are made or commercialized. In our sample, the detected levels were similar than others [24–26,38].

The obtained results showed good reproducibility, low dispersion and adequate sensibility for each peak series of the assayed samples. Additionally, high sampling rate was obtained (more than 100 samples h^{-1}) comparing other reported methodologies which involve time-consuming pretreatment sample, indicating the utility of the proposed method for routine analytical control.

4. Conclusions

The FIA spectrofluorimetric method proposed for the determination of RhB in real samples of lipsticks has the advantages of simplicity, speed, accuracy, low detection limit and the use of inexpensive equipment. The use of SDS micellar system provides a simple means to enhance the fluorescence from RhB giving about 2.5-fold increase in sensitivity and improves the limit of detection without further sample manipulation. The recommended procedure was found to be selective enough to tolerate the common additive present in commercial cosmetic forms. Additionally, it can be remarked the wide range linearity obtained in the calibration curve, with high sensitivity resulting adequate for the quality control and routine analysis of lipsticks.

This methodology has demonstrated potentiality in its applications; it could be applied to the determination of RhB present in other cosmetics products as eye shadows, rouge and other types of samples. Likewise, we are working in the development of a new application for the determination of RhB in foods and beverages.

Acknowledgements

References

[1] http://clearlyexplained.com/culture/fashion/lipstick.html.
[2] D.C. Neckers, O.M. Valdes-Aguilera, in: D. Volman, G.S. Hammond, D.C. Neckers (Eds.), Advances in Photochemistry, vol. 18, Wiley, New York, 1993.
[3] M.J. Snare, F.E. Treloar, K.P. Ghiggino, P.J. Thistlethwaite, J. Photochem. 18 (1982) 335.
[4] K.H. Drexhage, in: F.P. Schafer (Ed.), Dye Laser, Springer, Berlin, 1973.
[5] S.A. Al-Tamrah, A. Townshend, Anal. Chim. Acta 202 (1987) 247.
[6] A. Townshend, R.A. Wheatley, Analyst 123 (1998) 267.
[7] A. Townshend, R.A. Wheatley, Analyst 123 (1998) 1041.
[8] R.W. Ramette, E.B. Sandell, J. Am. Chem. Soc. 78 (1956) 4872.
[9] Y.J. Ma, M. Zhou, X.Y. Jin, B.Z. Zhang, H. Chen, N.Y. Guo, Anal. Chim. Acta 464 (2002) 289.
[10] H. Chen, M. Zhou, X.Y. Jin, Y.M. Song, Z.Y. Zhang, Y.J. Ma, Anal. Chim. Acta 478 (2003) 31.
[11] J.E. Selwyn, J.I. Steinfeld, J. Phys. Chem. 76 (1972) 762.
[12] P. Vrábel, P. Táborský, M. Ryvolová, J. Havel, J. Preisler, J. Lumin. 118 (2006) 283.
[13] T.Y. Tou, S.S. Yap, O.H. Chin, S.W. Ng, Opt. Mater. 29 (2007) 963.
[14] P. Ilich, P.K. Nisra, S. Macura, T.P. Burghardt, Spectrochim. Acta A 2 (1996) 1332.
[15] Q. Meng, M. Yu, H. Zhang, J. Ren, D. Huang, Dyes Pigments 73 (2007) 254.
[16] Z. Lacza, E.M. Horváth, E. Pankotai, A. Csordás, M. Kollai, C. Szabó, D.W. Busija, J. Pharmacol. Toxicol. Methods 52 (2005) 335.
[17] A. Varvaresou, E. Tsirivas, E. Tsaoula, E. Protopapa, Rev. Clin. Pharmacol. Pharmacokin. Int. Ed. 19 (2005) 11.
[18] http://www.osha.gov/dts/sltc/methods/partial/pv2072/pv2072.html.
[19] D.J. Dire, J.A. Wilkinson, J. Toxicol. Clin. Toxicol. 25 (1987) 603.
[20] IARC Monographs on the Evaluation of the Carcinogenic Risk of Chemicals to Man, International Agency for Research on Cancer: Lyon, 1978, vol. 16, pp. 221–243.
[21] J.H. Zar, Biostatistical Analysis, 2nd ed., Prentice Hall, Englewood Cliffs, NJ, 1984, p. 120.
[22] T. Kaji, T. Kawashima, Ch. Yamamoto, M. Sakamoto, Toxicol. Lett. 61 (1992) 81.
[23] D.J. Reuland, A.E. Welch, J. Forensic Sci. Soc. 20 (1980) 111.
[24] M.Y. Choudhry, J. Forensic Sci. 36 (1991) 366.
[25] C. Desiderio, C. Marra, S. Fanali, Electrophoresis 19 (1998) 1478.
[26] D.J. Reuland, W.A. Trinler, J. Forensic Sci. Soc. 24 (1984) 509.
[27] S. Miljanic, Z. Cimerman, L. Frkanec, M. Zinic, Anal. Chim. Acta 468 (2002) 13.
[28] N.O. Mchedlov-Petrossyan, Y.V. Kholin, Russ. J. Appl. Chem. 77 (2004) 414.
[29] J.C. Micheau, G.V. Zakharova, A.K. Chibisov, Phys. Chem. Chem. Phys. 6 (2004) 2420.
[30] E. Pramauro, E. pelizzetti, Surfactants in analytical chemistry, in: Applications of Organized Amphiphilic Media, vol. 31, Elsevier, Amsterdam, The Netherlands, 1996, p. 12.
[31] A.C.S. Neves, et al., Effect of terbium(III) chloride on the micellization properties of sodium decyl- and dodecyl-sulfate solutions, J. Colloid Interf. Sci. 306 (2007) 166–174.
[32] A.J.M. Valente, H.D. Burrows, R.F. Pereira, A.C.F. Ribeiro, J.L.G.C. Pereira, V.M.M. Lobo, Langmuir 22 (2006) 5625.
[33] F.I. Talens, P. Patón, S. Gaya, Langmuir 14 (1998) 5046.
[34] P. Paton-Morales, F.I. Talens-Alesson, Langmuir 17 (2001) 6059.
[35] T.A. Fayed, S. El-Din, H. Etaiw, N.Z. Saleh, J. Lumin. 21 (2006) 431.
[36] A.M.L. Barker, P.D.B. Clarke, J Forensic Sci. 12 (1972) 449.
[37] Pure Appl. Chem. 45 (1976) 99.
[38] L. Gagliardi, D. de Orsi, G. Cavazzutti, G. Multari, D. Tonelli, Chromatographia 43 (1996) 76–78.

Obituary

Professor Zhao-Lun Fang

It is our great sorrow to announce the death of Professor Zhao-Lun Fang on 12 November 2007 at the age of 73. Professor Fang was well known internationally for his contributions in atomic spectrometry, flow injection analysis and microfluidics.

Zhao-Lun Fang was born in 16 August 1934, Tianjin, China. He graduated from the Department of Chemistry, Peking University in 1957, afterwards he started working as Research Assistant in the Institute of Forestry and Soil Science in Shenyang, Chinese Academy of Sciences, until 1965 when he was to promoted Research Associate. He was promoted to Associate Professor in 1977 and to full Professor in 1986 in the Institute, which was then renamed the Institute of Applied Ecology, where he founded the Flow Injection Analysis Research Center in 1989. In 1996 he joined the Department of Chemistry, Northeastern University, and founded the Research Center for Analytical Sciences in 1998. In 2000, he founded another institute, i.e., the Institute of Microanalytical Systems in the Department of Chemistry, Zhejiang University, Hangzhou, China.

Professor Fang was elected as a Member of the Chinese Academy of Sciences (Academician) in 1997. He was also a Member of the Standing Committee of the Chemistry Division of CAS and a Fellow of the Royal Society of Chemistry. He served as Editorial Board or Editorial Advisory Board Member for various international journals, including Analytica Chimica Acta, Talanta, Journal of Analytical Atomic Spectrometry, International Journal of Environmental Analytical Chemistry, Spectrochimica Acta Part B, Lab-on-a-Chip, Analytical and Bio-analytical Chemistry, Chinese Journal of Analytical Chemistry, Spectroscopy and Spectral Analysis. He received various scientific awards, including Natural Science Award from the Chinese Academy of Sciences for two times in 1990 and 1993, the first Hai-Guang Award for Analytical Chemistry in 1994, a State Natural Science Award in 1995, a Natural Science Award of Liaoning Province in 2001, and a Natural Science Award from the Ministry of Education in 2007.

His major research areas included: flow injection and sequential injection methods and techniques for on-line separation and preconcentration and their applications in environmental, biological and pharmaceutical analysis; atomic spectrometry; capillary electrophoresis; microfluidic analytical systems. He is the author or co-author of more than 300 scientific papers and 6 monographs, including 2 monographs on flow injection analysis in English, these are "Flow Injection Separation and Preconcentration" published by VCH, 1993, and "Flow Injection Atomic Absorption Spectrometry" published by John Wiley & Sons, 1995. Both monographs have been widely cited by the international researchers. The monograph "Design and Application of Microchip Systems (in Chinese)" was probably the first in the field.

Professor Fang was the major promoter for the research of microfluidics in China since 1990s. In 2001, he organized the 165th Xiang-Shan science conference in Beijing with the topic of Microfluidics, and based on this conference, quite a few most important proposals and suggestions on this field were submitted to the Chinese government. Afterwards, from 2002 to 2006, Professor Fang presided over the first major program project on Microfluidics supported by the National Natural Science Foundation of China. Ten top Chinese universities and research institutes were involved in this project. The achievements of this project greatly promoted the development of microfluidics in China. While professor Fang was in the hospital, he initiated and organized the First Shenyang International Colloquium on Microfluidics (October 2007), which had been proved to be a great success in promoting microfluidic research in the world.

Professor Zhao-Lun Fang is survived by his wife Shu-rong Yue, daughter Jin Fang, son Qun Fang and grandchildren Fangjing Zou and Xiaoqing Fang, and also his colleagues and friends.

Jianhua Wang
Research Center of Analytical Sciences, Northeastern University, Box 332, Shenyang 110004, China
E-mail address: jianhuajrz@mail.neu.edu.cn

Available online 23 December 2007

Use of surface-modified CdTe quantum dots as fluorescent probes in sensing mercury (II)

Yun-Sheng Xia*, Chang-Qing Zhu*

*Anhui Key Laboratory of Chemo-Biosensing, College of Chemistry and Materials Science,
Anhui Normal University, Wuhu, 241000, PR China*

Abstract

Thioglycolic acid (TGA)-capped CdTe quantum dots (QDs) were synthesized in aqueous medium, and their interaction with metal cations was studied with UV–vis absorption, steady-state and time-resolved fluorescence spectra. The results demonstrated that Hg(II), Cu(II) and Ag(I) could effectively quench the QD emission based on different action mechanisms: Cu(II) and Ag(I) quenched CdTe QDs because they bound onto particle surface and facilitated non-radiative electron/hole recombination annihilation of QDs; electron transfer process between the capping ligands and Hg(II) was mainly responsible for the remarkable quenching effect of Hg(II). To prevent the approach of metal cations to QD core, the original TGA-capped CdTe QDs were further coated by denatured bovine serum albumin (dBSA). It was found that the dBSA-coated CdTe QDs could be quenched effectively by Hg(II), but Cu(II) and Ag(I) could hardly quench the QDs even at fairly higher concentration levels because the dBSA shell layer effectively prevented the binding of metal cations onto the QD core. On the basis of this fact, a simple, rapid and specific method for Hg(II) determination was proposed. Under optimal conditions, the quenched fluorescence intensity increased linearly with the concentration of Hg(II) ranging from 0.012×10^{-6} to 1.5×10^{-6} mol L^{-1}. The limit of detection for Hg(II) was 4.0×10^{-9} mol L^{-1}. The developed method was successfully applied to the detection of trace Hg(II) in real samples.
© 2007 Elsevier B.V. All rights reserved.

Keywords: Quantum dots; Surface modification; Fluorescence; Quenching mechanism; Hg(II)

1. Introduction

Much attention has been focused on the development of chemical sensors for the selective and efficient of chemically and biologically important ionic species [1]. The toxic effect of Hg(II) in the microorganism and environment has been well known. A variety of optical methods have been developed for the detection of Hg(II), however, most fluorescent sensors for Hg(II) are based on small organic molecules [2,3] that usually work in organic media [4,5]. Many of these small synthetic molecules lack water solubility, and although metal ions are relatively easy to chelate in organic solvents it is rather difficult to directly recognize them in aqueous solutions because of their strong hydration. Furthermore, these conventional organic fluorescent dyes usually suffer from some limitations such as low

signal intensities and photobleaching, and most of them tend to have narrow excitation spectra and often exhibit broad emission band with red tailing [6,7].

Colloidal semiconductor nanoparticles, often referred to as "quantum dots" (QDs), can overcome problems encountered by organic dye molecules. Since the first reports using modified CdSe/ZnS core/shell QDs as fluorescence labels to stain biological samples [6,7], QDs have attracted considerable attention as novel fluorescence indicators of different biological process and bioanalysis in recently years. Meanwhile, considerable efforts have also been focus on the development of a general sensing means, with QDs via analyte-induced fluorescence changes, for small molecules and ions [8]. Such as, Chen and Rosenzweig [9] demonstrated that the capping ligands have a profound effect on the fluorescence response of CdS QDs to different metal cations. On the basis of this finding, they first realized the selective detection of Cu(II) and Zn(II) using CdS QDs capped by thioglycerol and cysteine as fluorescent probes, respectively. Then, peptide-coated CdS QDs

* Corresponding authors. Tel.: +86 553 3869303; fax: +86 553 3869303.
  E-mail addresses: xiayunsheng2005@yahoo.com.cn (Y.-S. Xia),
zhucq625@163.com (C.-Q. Zhu).

have been synthesized for the fluorescent detection of Ag(I) and Cu(II) in water solution [10]. Also, Jin et al. [11] reported surface-modified CdSe quantum dots as luminescent probes for CN⁻. Up to now, other groups and we have developed some QDs-based sensing systems for the detection of Hg(II) [12–14], Cu(II) [9,10,15–17] and Ag(I) [18–20], based on the quenching of QDs by analytes. However, lack of selectivity is the major problem reported for some of the procedures proposed.

Although some previous reports showed that Hg(II), Cu(II) and Ag(I) can quench Cd-chalcogenide QDs, different mechanisms have been proposed to explain the quenching effect. Isarov and Chrysochoos [21] demonstrated that Cu(II) quenches the fluorescence of CdS QDs by forming either Cu_xS ($x = 1, 2$) precipitate or isolated Cu(I) on the surface of CdS QDs, Chen and Zhong [15] studied the quenching effect of thiol-capped CdTe QDs in the presence of Cu(II) and also proposed the interaction of QDs with Cu(II) should be of the ion-binding type. Ag(I) changes CdTe QD emission due to the fact that the free Ag(I) binds with bare Te atoms and forms the AgTe structure on the particle surface, as proposed by Ren's group [22] and us [20]. Two different mechanisms were proposed for explaining the quenching effect of Hg(II): Chen et al. [12,14] thought that Hg(II) quenches the fluorescence of QDs due to facilitating non-radiative electron/hole recombination anniliation through an effective electron transfer process between capping ligands and Hg(II); Cai et al. [13] demonstrated that CdS QDs are quenched by Hg(II) because of forming size-quantized HgS particle at the particle surface, similar to that of Cu(II) binding on the surface of CdS QDs [21]. However, these investigations are independent of each other. Herein, we systematically studied the quenching effect of Hg(II), Cu(II) and Ag(I) on thioglycolic acid (TGA)-capped CdTe QDs with UV–vis absorption, steady-state and time-resolved fluorescence spectra. The experimental results demonstrated that Cu(II) and Ag(I) ions quench the QDs because they bind to the QD surface and facilitate non-radiative electron/hole recombination annihilation; the quenching mechanism of Hg(II) ions may be complex: both electron transfer and ion-binding can lead to the decrease of QD emission, but the former effect may play a leading role. According to above, an obvious conclusion can be drawn: Cu(II) and Ag(I) ions do not quench the QDs until they bind onto the QD core, but Hg(II) ions needn't. So, we thought whether selective detection of Hg(II) and elimination the interference of Cu(II) and Ag(I) could be achieved by means of taking proper steps to prevent the contact between metal cations and QD core. With this thought, we coated the original TGA-capped CdTe QDs with an additional biomacromolecule, namely, denatured bovine serum albumin (dBSA) [23]. As expected, the dBSA-coated CdTe QDs could be quenched by Hg(II) with high sensitivity and selectivity, other metal cations, including Cu(II) and Ag(I), could hardly quench the QDs even at fairly higher concentration levels because the dBSA shell layer effectively prevented the binding of cations onto the QD core. On the basis of this fact, a fluorescent method for the selective and sensitive detection of Hg(II) using dBSA-coated CdTe QDs as probes was presented.

2. Experimental

2.1. Apparatus and reagents

UV–vis absorption spectra were recorded with a Hitachi U-3010 spectrophotometer (Tokyo, Japan). Fluorescence measurements were performed using a Hitachi F-4500 spectrofluorimeter equipped with a 1cm quartz cell. pH values were measured with a Model pHs-3c meter (Shanghai, China). Fluorescence decay curves were performed with the time correlated single photo counting technique on the combined steady-state and lifetime spectrometer (Edinburgh Analytical Instruments, FLS920). All optical measurements were performed at room temperature under ambient conditions.

All chemicals used were of analytical grade or of the highest purity available. All solutions were prepared with double deionized water (DDW). Te powder (−60 mesh, 99.999 %) and TGA (97 +%) were purchased from Alfa Aesar (Karlsruhe, Germany), BSA was obtained from Sino-American Biotechnology Co., $NaBH_4$ (96 %), $CdCl_2·2.5H_2O$, $HgCl_2$, $AgNO_3$, $CuCl_2·2H_2O$ and other routine chemicals were acquired from Guoyao Chemical Reagent Company (Shanghai, China) and used as received without further purification. A $0.02 \, mol \, L^{-1}$ of pH 7.4 phosphate buffer solution (PBS) was used in the experiments.

2.2. Preparation of CdTe QDs

The colloidal CdTe QDs were prepared based on the method described elsewhere [24]. Briefly, 1.25×10^{-3} mol of $CdCl_2·2.5H_2O$ was dissolved in 100 mL of DDW, and 3.0×10^{-3} mol of TGA was added under stirring, followed by adjusting the pH to 11.2 by dropwising $1 \, mol \, L^{-1}$ NaOH. The solution was deaerated by N_2 bubbling for 40 min. Under vigorous stirring, 0.5×10^{-3} mol freshly prepared oxygen-free NaHTe was injected to the above solution. Afterward, the resulting solution mixture was heated to 100 °C and refluxed 1.5 h. QD solution concentration was estimated from the absorption spectra using molar absorptivity at first maximum for QDs of this size reported by Peng's group [25].

2.3. Preparation of dBSA

dBSA was prepared by chemically treating BSA with $NaBH_4$, based on a previous literature report [23]. First, 0.2358 g of BSA was dissolved in 50 mL of DDW, and second 0.012 g of $NaBH_4$ was added as a reductant into solution under stirring. The reaction proceeded at room temperature for 1 h and then at 75 °C until no more H_2 was generated. Under these conditions, BSA was denatured and most of its disulfide bonds were converted to sulfhydryl groups. The final concentration of dBSA aqueous solution was $7.15 \times 10^{-5} \, mol \, L^{-1}$.

2.4. Preparation of dBSA-coated CdTe QDs

The crude TGA-capped CdTe QDs solution was concentrated about five times using a rotary evaporator. Then, the QDs were precipitated with acetone and then isolated by centrifugation and
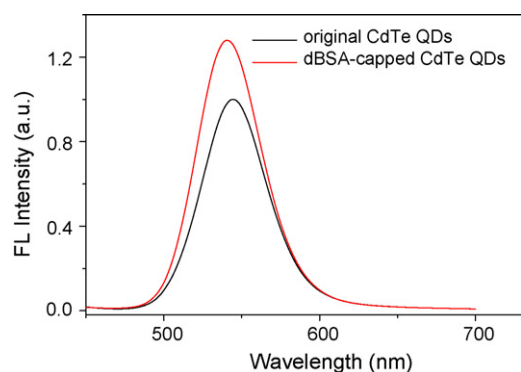
Fig. 1. Fluorescence spectra of original TGA-coated QDs and dBSA-coated QDs incubated for 3 days.

decantation to remove free TGA molecules. The purified QDs were redissolved into a measured amount of dBSA solution. The resulting solutions were incubated at 75 °C for 30 min before PBS buffer solution (pH 7.4) was added to reach the desired concentration, and then stored in dark at room temperature.

2.5. Procedure for spectrofluorometric detection of Hg(II)

To a 10 mL calibrated test tube 1 mL 2.2×10^{-6} mol L^{-1} the dBSA-capped CdTe QD solution ($C_{dBSA}/C_{QDs} = 6$), 0.5 mL of PBS (pH 7.4) and certain amounts of Hg(II) were sequentially added. The mixture was then diluted to volume with DDW and mixed thoroughly. The fluorescence intensity of the solution was recorded at 541 nm with the excitation wavelength of 380 nm. Both slit widths of excitation and emission were 5 nm.

3. Results and discussion

3.1. Fluorescent feature of dBSA-coated CdTe QDs

Due to its cooperative and amplifying effects of the multiple binding sites, dBSA provides enhanced coordinated interactions between CdTe surface and sulfur atoms through the formation of shell-like CdTe$_x$(dBSA)$_{1-x}$ complex [23]. Such a shell structure can efficiently remove the dangling bonds and surface defects, resulting in higher fluorescence quantum yield compared with the original TGA-capped CdTe QDs (Fig. 1). In addition, it is
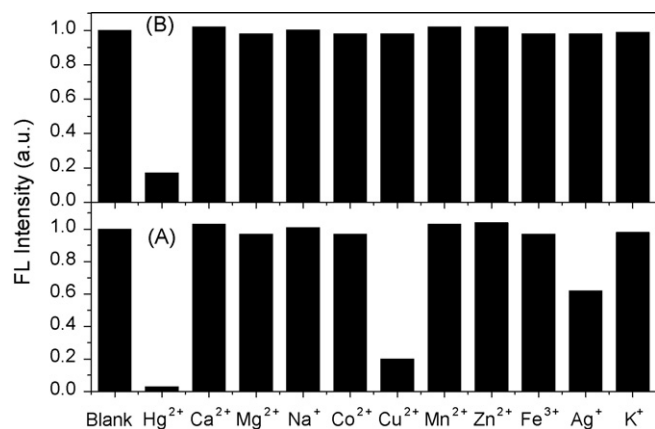

Fig. 2. Effect of cations on the fluorescence of (A) original TGA-capped QDs, (B) dBSA-coated QDs (K$^+$, Na$^+$, Mg^{2+} and Ca^{2+}: 4.5×10^{-5} mol L^{-1}; Fe^{3+}, Mn^{2+}, Co^{2+}, and Zn^{2+}: 4.5×10^{-6} mol L^{-1}; Hg^{2+}, Cu^{2+} and Ag$^+$: 1.5×10^{-6} mol L^{-1}).

found that the emission peak position of dBSA-capped CdTe QDs shift to blue about 3 nm incubated at room temperature for 3 days, due to the formation of the complex shell CdTe$_x$(dBSA)$_{1-x}$ and a decrease in the size of the inner CdTe "core" [23,26].

3.2. Interaction of CdTe QDs with Hg(II), Cu(II) and Ag(I) ions

Fig. 2A shows that the fluorescence intensity of original TGA-capped CdTe QDs decreases by 97, 80 and 38% in solutions containing 1.5×10^{-6} mol L^{-1} of Hg(II), Cu(II) and Ag(I) ions, respectively, as compared to the emission of these QDs in an ion-free solutions, which is agreement with the previous reports [12,15,20,22]. Fig. 3B displays the typical fluorescence spectra as functions of the concentration of Cu(II). It is observed that the emission intensity reduces successively with the increasing of Cu(II) ion concentration. Meanwhile, the spectral wavelength maximum is red-shifted about 19 nm with an obvious change of fluorescence spectrum profiles, which indicates the change of surface states of QDs [21,22]. As shown in Fig. 3C, addition of Ag(I) to TGA-capped CdTe QD solution leads to a similar spectral change to that of Cu(II), except for a little fluorescence enhancement of QDs in the presence of
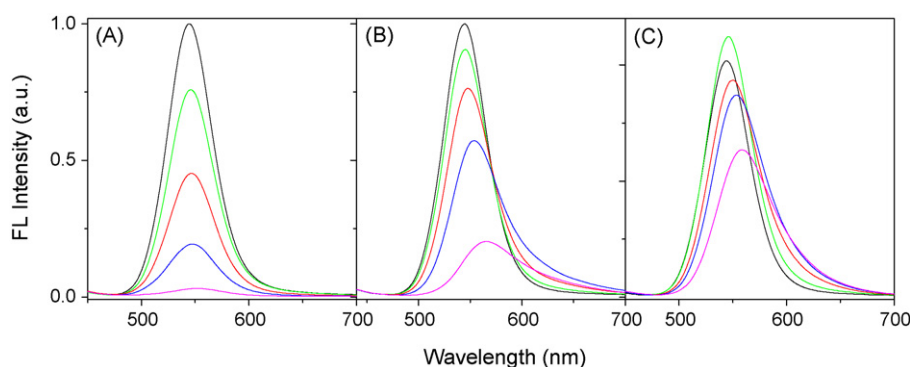

Fig. 3. Fluorescence response of original TGA-capped CdTe QDs to addition of Hg(II), Cu(II) and Ag(I) in PBS (pH 7.4). Final cation concentrations (10^{-6} mol L^{-1}): 0 (black lines), 0.08 (green lines), 0.2 (red lines), 0.5 (blue lines), 1.5 (purple lines).

very low concentration of Ag(I), which has been investigated in our lab [20]. Different from Cu(II) and Ag(I), Hg(II) does not lead to an obvious change of spectral widths and the emission maximum of the QDs (Fig. 3A). Herein, the difference of the fluorescence spectrum changes induced by different metal cations may indicate the different quenching mechanisms. In the following experiments, we studied the fluorescence response of dBSA-coated CdTe QDs ($C_{dBSA}/C_{QDs} = 6$) to the three cations. As shown in Fig. 2B, the dBSA layer can effectively eliminate the quenching of Cu(II) and Ag(I), but Hg(II) can still effectively quench the dBSA-coated QDs, though the quenching degree (83%) is a little lower than that of original TGA-capped QDs (97%). One possible explanation for Figs. 2 and 3 is due to different quenching mechanisms of the three cations: Cu(II) and Ag(I) ions quench the QDs because they bind to the QD core and facilitate non-radiative electron/hole recombination annihilation [20–22], after the original QDs are coated by dBSA, the quenchers cannot approach to the QD core, so the quenching is eliminated; the quenching mechanism of Hg(II) may be complex: both electron transfer and ion-binding can lead to the decrease of QD emission, but the former effect may play a leading role. The QD-cation systems were further studied by UV–vis absorption spectra for validating the action mechanisms. As depicted in Fig. 4A, the absorption threshold of original TGA-capped CdTe QDs shifts to longer wavelength to some extent in the presence of 1.5×10^{-6} mol L^{-1} metal cations.
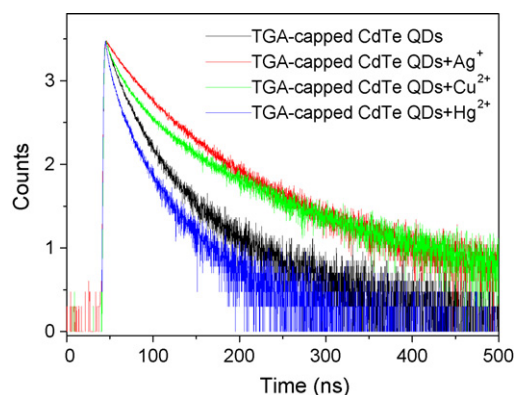
Fig. 5. Fluorescence decay curves ($\lambda_{ex} = 380$ nm, measured at the maximum of the fluorescence) of TGA-capped QDs in the absence and presence of metal cations.

This absorption behavior is attributed to the change of surface states of QDs because metal ions bind onto the particle surface [20,21,27]. In contrast, the absorption threshold of dBSA-coated QDs has almost no any shift at the same experimental conditions (Fig. 4B), indicating the effective barrier effect of dBSA layer shell for metal cations. Although the above results provide strong proof for the proposed quenching mechanisms of the three metal cations, to further verify them, the fluorescence decays were examined. The intensity decays of original TGA-capped CdTe QDs are shown in Fig. 5, measured at the maximum of the fluorescence for both before and after addition of 1.0×10^{-6} mol L^{-1} quenchers. The decays of all the samples were multiexponential and fitted using the third-order equation, as shown in Table 1. The fluorescence lifetime of TGA-capped CdTe QDs was quenched by Hg(II) ions, which may result from the ultrafast electron transfer from QDs to Hg(II) [28]. In contrast, when Cu(II) or Ag(I) ions were added to TGA-capped CdTe QD solutions, the fluorescence lifetimes were increased, as shown in Fig. 5 and Table 1. The enhanced decay times may arise from the trap-state emission of the QDs, since some surface defects formed because of ion-binding effect [21,29].

3.3. Factors affecting the fluorescence detection for Hg(II) with dBSA-coated CdTe QDs

To investigate the effect of the concentration of the dBSA-coated CdTe QDs, a series of calibration functions (the quenched fluorescence intensity against the concentration of Hg(II)) were obtained with various concentrations of the dBSA-coated CdTe QDs. The optimal concentration of the dBSA-coated CdTe QDs should give the highest sensitivity
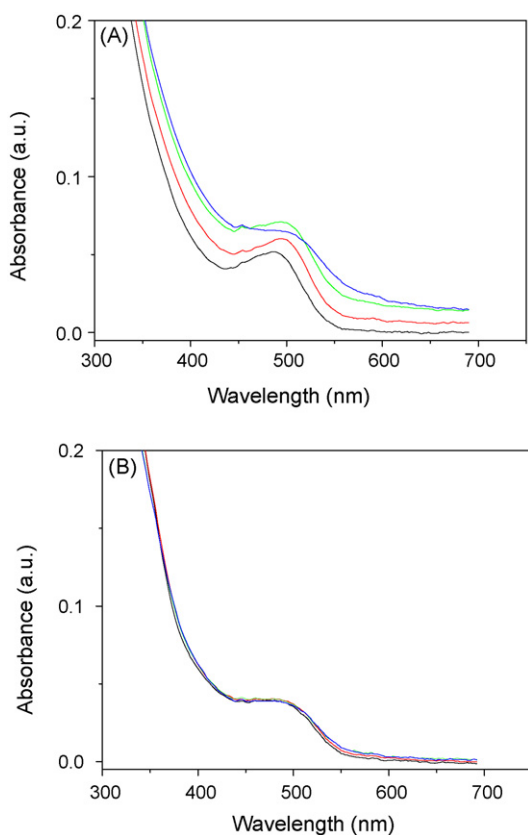

Fig. 4. UV–vis absorption spectra of original TGA-capped (A) and dBSA-coated (B) CdTe QDs in the presence of 1.5×10^{-6} mol L^{-1} metal cations (blank: black lines, Hg(II): red lines, Cu(II): green lines, Ag(I): blue lines).

Table 1
The fit results of fluorescence lifetimes before and after quenching of TGA-capped CdTe QDs

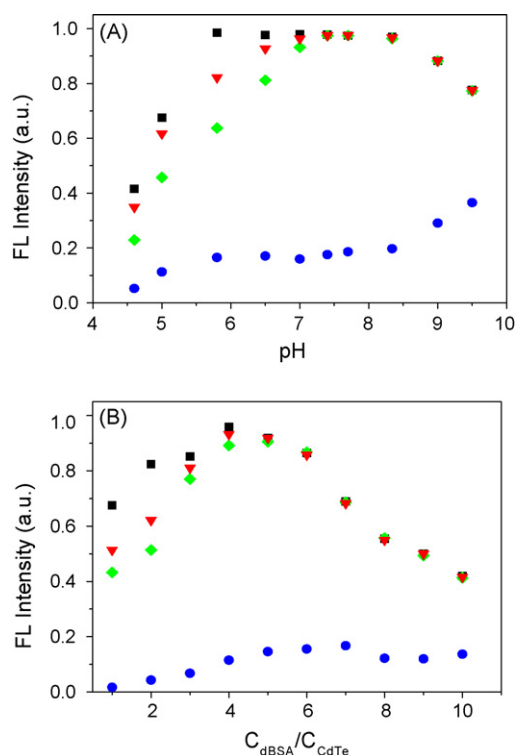|	τ_1/ns	τ_2/ns	τ_3/ns	α_1	α_2	α_3	χ^2
Before quenching	7.03	18.79	58.16	960	1621	152	1.119
Quenched by Hg(II)	3.39	12.03	33.35	1112	1309	284	1.084
Quenched by Cu(II)	8.26	27.54	92.66	1168	1338	294	1.097
Quenched by Ag(I)	17.99	38.51	105.54	1075	1609	217	1.046

Fig. 6. (A) Effect of pH on reaction between cations and dBSA-coated CdTe QDs. (B) Effect of molar rations of dBSA/CdTe on reaction between cations and dBSA-coated CdTe QDs at pH 7.4. The concentration of cations: 1.5×10^{-6} mol L^{-1}, blank: black squares, Ag (I): red triangles, Cu (II): green diamonds, Hg (II): blue dots.

(i.e. the slope of calibration function) and the widest linear range of the calibration function. As the concentration of the dBSA-coated CdTe QDs increased, the linear range of calibration function became wider whereas the sensitivity decreased. For a compromise between the sensitivity and the linear range of calibration function, 2.2×10^{-7} mol L^{-1} the dBSA-capped CdTe QD solution was employed for further experiments.

The effect of pH in a range between 4.6 and 9.5 was studied in order to select the optimum conditions for the determination of Hg(II) with dBSA-coated CdTe QDs. As shown in Fig. 6A, the fluorescence intensity has negligible change in the pH range between 5.8 and 8.4, and the optimal pH ranged from 5.8 to 7.8. However, Cu(II) and Ag(I) ions quench the fluorescence of dBSA-coated CdTe QD at pH < 7.0. The reason may be that electrostatic repulsion effect of protonated amino group at pH < 7 causes some opening of the dBSA capping layer and favors the approach of quenchers to QD core. So, 0.5 mL of PBS (pH 7.4) was recommended for used in this work.

In order to study the effect of dBSA/CdTe molar ration on the determination of Hg(II), the molar rations of dBSA/CdTe were varied from 1 to 10. The experimental results indicate that the optimal molar ratio for the determination of Hg(II) is 1–6, and for effective elimination the interferences of Cu(II) and Ag(I) is 4–10 (Fig. 6B). So, in this work, a molar ration of dBSA/CdTe = 6 was chosen to run the assay. Very recently, Wang et al. [19] reported that the dBSA-coated CdTe QDs purified by column chromatogram could be effectively quenched by Ag(I)

and Cu(II), this is possible because the purification process lead to the partial dissociation of dBSA from the QD surface, and quenchers can bind onto the exposed part of the core. So, some excessive dBSA molecules may be essential for eliminating the interferences of Ag(I) and Cu(II) ions.

Fig. 2B indicates the dBSA-coated CdTe QDs have good selectivity for Hg(II). Following the experiments, the fluorescence titration of dBSA-coated CdTe QDs with various coexistence ions was conducted to further evaluate the detection selectivity. As shown in Table 2, high concentrations of Na(I), K(I), Mg(II), Ca(II), Zn(II), Mn(II), Co(II), Fe(III) and common anions do not produce any noticeable effect on the emission signals of the dBSA-coated CdTe QDs. In the Table 2 it is shown the results for the colourless complex FeF$_6^{3-}$ instead of Fe(III) because Fe(III) produced an obvious quenching effect at 1.0×10^{-5} mol L^{-1} concentration level attributed to an inner filter resulting from its strong absorption at the excitation wavelength [9]. This interference can be eliminated by adding fluoride ions to the solution. Both previous reports [9,10,15–20] and our experimental results (Figs. 2A and 3) showed Ag(I) and Cu(II) ions have strong quenching effect on the Cd-based QDs. After the CdTe QDs coated by dBSA, this quenching effect can be effectively eliminated, as described in Fig. 2B and Table 2. The experimental results showed that Cu(II) at a concentration of 3.0×10^{-6} mol L^{-1} and Ag(I) at a concentration of 4.5×10^{-6} mol L^{-1} had no measurable effect on 5.0×10^{-8} mol L^{-1} Hg(II) measurement using dBSA-coated CdTe QDs as probes. Namely, at least 60 times higher coexisted Cu(II) and 90 times higher coexisted Ag(I) amounts do not interfere with the detection of Hg(II). Using dBSA-coated CdTe QDs as probes for Hg(II) detection, the tolerated amounts of Cu(II) and Ag(I) ions enhance 100- and 120-fold, respectively, as compared to those using original TGA-capped CdTe QDs.

Table 2
Test of the interference of different ions on the fluorescence of original TGA-capped QDs and dBSA-coated QDs, respectively

Coexisting substance	TGA-capped QDs		dBSA-coated QDs	
	CC[a]	CFI[b]	CC	CFI
K$^+$	400	−2.1	400	−1.7
FeF$_6^{3-}$	45	−3.7	45	−3.4
Na$^+$	500	−1.8	500	−1.2
Cu^{2+}	0.3	−4.8	30	−3.0
Co^{2+}	40	−3.6	60	−2.8
Mg^{2+}	250	−2.8	250	−1.8
Mn^{2+}	45	+4.0	60	+2.7
Ag$^+$	0.4	+5.3	45	−2.6
Ca^{2+}	200	+3.8	200	+2.8
Zn^{2+}	40	+4.0	60	+3.4
SO$_4^{2-}$	120	+3.6	120	+2.0
CO$_3^{2-}$	50	+2.8	80	+2.6
F$^-$	150	−1.8	150	−1.8
Br$^-$	120	−2.0	120	−1.6
I$^-$	120	−2.8	120	−1.5

Concentration of Hg^{2+}: 8.0×10^{-8} mol L^{-1}. Other conditions are the same as those described in the procedure.
[a] CC: coexisting concentration (10^{-7} mol L^{-1}).
[b] CFI: Change of fluorescence intensity (%).

Table 3
Comparison of the linear range and detection limit of QDs-based sensing systems for determination of Hg(II)

Probes	$\lambda_{ex}/\lambda_{em}$	Linear range (10^{-7} mol L^{-1})	LOD (10^{-9} mol L^{-1})	Reference
L-Cysteine-capped CdS QDs	360/495	0.16–1.12	2.4	[13]
L-Cysteine-capped CdSe QDs	430/530	0.00–20	6.0	[14]
TGA-capped InP QDs	750/826	25–398	997	[30]
MPA-capped CdTe QDs	365/535	0–1.28	0.5	[12]
dBSA-coated CdTe QDs	380/541	0.12–15	4.0	This work

Table 4
Determination of Hg(II) in natural water samples

Samples	Hg(II) added (10^{-9} mol L^{-1})	Hg(II) founded (10^{-9} mol L^{-1})[a]		Recovery (%)
		This method	AAS	
Fountain water	75	82	77	109
	300	313	305	104
Pond water	75	80	78	107
	300	309	307	103

[a] The average of five replicate determinations.

3.4. Analytical performance of dBSA-coated CdTe QDs

The fluorescence spectra of dBSA-coated CdTe QDs and its fluorescence titration with Hg(II) were recorded at optimum experimental conditions. The fluorescence of dBSA-coated CdTe QDs is significantly decreased with increasing the concentration of Hg(II). A very good linear relationship ($R = 0.9995$) was observed up to Hg(II) concentration ranging from 1.2×10^{-8} to 1.5×10^{-6} mol L^{-1} when using the well-known Stern-Volmer equation. And the detection limit, calculated following the 3α IUPAC criteria, was 4.0×10^{-9} mol L^{-1}. The standard deviation for six replicate measurements of a solution containing 1.0×10^{-7} mol L^{-1} Hg(II) was 1.6%. The calibration equation obtained in our experiments was

$$\frac{I_0}{I} = 1 + K_{SV}C$$

where I_0 and I are the intensity in the absence and presence of the quencher (Hg(II)), K_{SV} is the Stern-Volmer quenching constant, and C is the concentration of the quencher, K_{SV} is found to be 2.78×10^6 mol^{-1}. It is interesting to note that the selectivity and sensitivity of the dBSA-coated CdTe QDs to Hg(II) detection was unaltered after more than 2 months storage of the luminescent probe in the dark, under ambient conditions, although the emission peak shifted to blue about 15 nm (results not shown). For comparative purpose, the analytical performance of several selected fluorimetric methods for Hg(II) detection using QDs-based sensing systems is summarized in Table 3. In comparison with previous results, the proposed methodology possesses comparable or superior detection limit and linear range. However, it must be emphasized that dBSA-coated CdTe QDs provide much better selectivity towards Hg(II) than that of original thiol-capped QDs.

The proposed method was then applied for the determination of Hg(II) in pond water and fountain water samples, which were filtered three times through qualitative filter paper before use.

The real samples showed that Hg(II) was not present in them, so they were spiked with standard Hg(II) solution and then the samples were analyzed by standard addition method. The determination results were presented in Table 4. From Table 4 it can be seen that the results of recovery for the two samples were satisfied, and the proposed method determination results were in a good agreement with the results obtained by atomic absorption spectroscopy (AAS) suggesting that the method is reliable and practical.

4. Conclusions

A simple dBSA-QDs system was successfully constructed for selective and sensitive detection of Hg(II) in aqueous solution, based on the strong specific quenching effect of analytes. The strong interferences of Cu(II) and Ag(I) could be eliminated by forming a dBSA shell layer surrounding the original QDs, which effectively prevented the binding of the cations onto QD core. In comparison with original thiol-capped QDs, dBSA-coated nanoparticles were brighter, more stable against pH, and showed higher selectivity.

References

[1] A.P. de Silva, H.Q.N. Gunaratne, T. Gunnlaugsson, A.J.M. Huxley, C.P. McCoy, J.T. Rademacher, T.E. Rice, Chem. Rev. 97 (1997) 1515.
[2] G. Hennrich, H. Sonnenschein, U. Resch-Genger, J. Am. Chem. Soc. 121 (1999) 5073.
[3] E.M. Nolan, S.J. Lippard, J. Am. Chem. Soc. 125 (2003) 14270.

[4] K. Rurack, U. Resch-Genger, J.L. Bricks, M. Spieles, Chem. Commun. (2000) 2103.
[5] D.S. McClure, J. Chem. Phys. 20 (1952) 682.
[6] M. Bruchez Jr., M. Moronne, P. Gin, S. Weiss, A.P. Alivisatos, Science 281 (1998) 2013.
[7] W.C.W. Chan, S. Nie, Science 281 (1998) 2016.
[8] J.M. Costa-Fernández, R. Pereiro, A. Sanz-Medel, TrAC Trends Anal. Chem. 25 (2006) 207.
[9] Y.F. Chen, Z. Rosenzweig, Anal. Chem. 74 (2002) 5132.
[10] K.M. Gattás-Asfura, R.M. Leblanc, Chem. Commun. (2003) 2684.
[11] W.J. Jin, M.T. Fernandez-Argüelles, J.M. Costa-Ferándz, R. Pereiro, A. Sanz-Medel, Chem. Commun. (2005) 883.
[12] B. Chen, Y. Yu, Z. Zhou, P. Zhong, Chem. Lett. 33 (2004) 1608.
[13] Z.X. Cai, H. Yang, Y. Zhang, X.P. Yan, Anal. Chim. Acta 559 (2006) 234.
[14] J.L. Chen, Y.C. Gao, Z.B. Xu, G.H. Wu, Y.C. Chen, C.Q. Zhu, Anal. Chim. Acta 577 (2006) 77.
[15] B. Chen, P. Zhong, Anal. Bioanal. Chem. 381 (2005) 986.
[16] M.T. Fernández-Argüelles, W.J. Jin, J.M. Costa-Fernández, R. Pereiro, A. Sanz-Medel, Anal. Chim. Acta 549 (2005) 20.
[17] H.Y. Xie, J.G. Liang, Z.L. Zhang, Y. Liu, Z.K. He, D.W. Pang, Spectrochim. Acta Part A 60 (2004) 2527.
[18] J.G. Liang, X.P. Ai, Z.K. He, D.W. Pang, Analyst 129 (2004) 619.
[19] J.H. Wang, H.Q. Wang, H.L. Zhang, X.Q. Li, X.F. Hua, Y.C. Cao, Z.L. Huang, Y.D. Zhao, Anal. Bioanal. Chem. 388 (2007) 969.
[20] Y.S. Xia, C. Cao, C.Q. Zhu, J. Lumin. 128 (2008) 166.
[21] A.V. Isarov, J. Chrysochoos, Langmuir 13 (1997) 3142.
[22] C. Dong, H. Qian, N. Fang, J. Ren, J. Phys. Chem. B 110 (2006) 11069.
[23] Q. Wang, Y. Kuo, Y. Wang, G. Shin, C. Ruengruglikit, Q. Huang, J. Phys. Chem. B 110 (2006) 16860.
[24] Y. Xia, T. Zhang, X. Diao, C. Zhu, Chem. Lett. 36 (2007) 242.
[25] W.W. Yu, L. Qu, W. Guo, X. Peng, Chem. Mater. 15 (2003) 2854.
[26] K. Akamatsu, T. Tsuruoka, H. Nawafune, H. Kobe, J. Am. Chem. Soc. 127 (2005) 1634.
[27] A. Eychmüller, A. Hässelbarth, H. Weller, J. Lumin. 53 (1992) 113.
[28] R. van Beek, A.P. Zoombelt, L.W. Jenneskens, C.A. vanWalree, C. de Mello Donegá, D. Veldman, R.A.J. Janssen, Chem. Eur. J. 12 (2006) 8075.
[29] C.W. Wang, M.G. Moffitt, Langmuir 20 (2004) 11784.
[30] C.Q. Zhu, L. Li, F. Fang, J.L. Chen, Y.Q. Wu, Chem. Lett. 34 (2005) 898.

Water-compatible molecularly imprinted polymers for selective extraction of ciprofloxacin from human urine

Hongyuan Yan [a], Kyung Ho Row [a,*], Gengliang Yang [b]

[a] *Department of Chemical Engineering, Inha University, Incheon 402-751, Republic of Korea*
[b] *College of Pharmacy, Hebei University, Baoding 071002, China*

Abstract

Water-compatible molecularly imprinted polymers (MIPs) were prepared in water–methanol systems for selective extraction and separation of ciprofloxacin from human urine samples. Molecular recognition properties, binding capability, and chromatographic applications of the MIPs were evaluated and the results revealed the obtained MIPs have high affinity for ciprofloxacin in aqueous environment and the selectivity can be easily controlled by adjusting the pH of mobile phase. After centrifugation, the urine samples were directly injected into the MIPs column and ciprofloxacin could be selectively retained on the column while other biological matrixes were quickly washed out. Good linearity was obtained from 0.1 to 100 mg L^{-1} ($r = 0.999$) with the relative standard deviations less than 3.6%. The limit of detection of the method was 0.03 μg/mL and the recoveries were more than 94.5% at three different concentrations. Moreover, by increasing the injection volume, the detection limits of the method could be improved more than 100-folds.
© 2007 Elsevier B.V. All rights reserved.

Keywords: Molecularly imprinted polymer; Selective extraction; Ciprofloxacin; Urine

1. Introduction

Molecular imprinting is a rapidly developing technique for the preparation of polymers having specific molecular recognition properties for a given compound, its analogues or for a single enantiomer [1–5]. Molecularly imprinted polymers (MIPs) are prepared by mixing the template molecule with functional monomers, cross-linking monomers and a radical initiator in a proper solvent, most often an aprotic and non-polar solvent. After polymerization, extraction of the template molecule reveals recognition cavities complementary to the template molecule in shape, size and chemical functionality, which enable the resultant polymers selectively to rebind the template molecule from a mixture of closely related compounds [6,7]. As a technique for the creation of artificial receptor-like binding sites with a 'memory' for the shape and functional group positions of the template molecule, molecular imprinting has become increasingly attractive in many fields of chem-

istry and biology, particularly as chromatography [8], artificial antibodies [9], chemical sensors [10,11], and selective adsorbents for solid phase extraction (SPE) [12,13]. However, in the majority of MIPs applications, optimum synthesis and molecular recognition occurs in non-polar or low polar system, often the one used in the polymerization process. The presence of polar solvents, especially water, can disturb the formation of the prepolymerization complex during imprinting procedure, and interactions between monomers and the template are disrupted easily [14–16]. Although some MIPs synthesized by the use of specifically designed monomer–solvent combinations or hydrophilic comonomers exhibit recognition properties under aqueous conditions [17–19], the use of additional sample pretreatment procedures were required to remove harmful matrix components and suppress the non-specific binding.

Ciprofloxacin (1-cyclopropyl-6-fluoro-1,4-dihydro-4-oxo-7-(1-piperazinyl) quinoline-3-carboxylic acid) is the most potent fluoroquinolone antibiotic against Gram-positive and Gram-negative bacteria through inhibition of their DNA gyrase, a critical enzyme to bacterial chromosome replication [20,21]. It is used in a wide range of gastrointestinal urinary and respiratory tract as well as ocular and skin infections.

* Corresponding author. Tel.: +82 32 860 7470; fax: +82 32 872 0959.
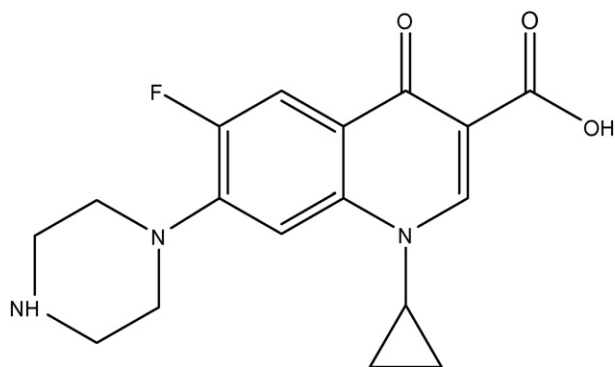*E-mail address:* rowkho@inha.ac.kr (K.H. Row).

Fig. 1. Molecular structure of ciprofloxacin.

Monitoring the concentration and residues of such antibiotics is suggested not only in the investigation of pharmacokinetics of ciprofloxacin but also in design and development of new antibiotics pharmaceutics. Although a large number of analytical methods have been proposed for the analysis of ciprofloxacin in urine [22–25], the sample preparing process was considered very complicating and time-consuming due to biological fluids are very complex and contain large amounts of proteins. Protein precipitation, liquid–liquid extraction and SPE were used routinely in pharmaceutical laboratories. In order to improve the substantial drawback of conventional SPE, Caro et al. [26,27] prepared ciprofloxacin and enrofloxacin MIPs by bulk polymerization using dichloromethane as porogenic solvent and applied it as a selective sorbent in a two-step SPE (a commercial Oasis cartridge and a molecularly imprinted SPE cartridge were combined) to extract quinolones from urine samples. It is necessary to include a clean-up in the SPE protocol to enhance the selectivity of the MIP and the urine extracts obtained after this two-step SPE procedure were relatively clean compared to the original samples for HPLC/MS determination. However, these procedures are complicate, time-consuming, and drugs may be partly lost in sample preparation steps.

In this work, ciprofloxacin imprinted polymers were prepared in water-containing system using methacryclic acid as monomer and ethylene glycol dimethacrylate as cross-linker for the selective separation of ciprofloxacin from human urine sample. The obtained imprinted polymers show high affinity to ciprofloxacin in aqueous media and were successfully applied as special chromatographic stationary phase to selective separation of ciprofloxacin from human urine samples. The present method is simple, rapid, and the sensitivity could be greatly improved by increasing the injection volume.

2. Experimental

2.1. Materials

Ciprofloxacin was obtained from Sigma (St. Louis, MO, USA) and its molecule structure was shown in Fig. 1. Methacrylic acid (MAA) was purchased from Kanto Chemical Co., Inc. (Tokyo, Japan) and purified by distillation. Acrylamide (AM) was from Duksan Pure Chemical Co., Inc. (Korea) and

recrystallized prior to use. Ethylene glycol dimethacrylate (EDMA) was from Tokyo Kasei Kogyo Co., Ltd. (Tokyo, Japan) and was extracted with $2.0 \, mol \, L^{-1}$ NaOH solution and dried over anhydroxide magnesium sulfate. α,α′-Azobis (isobutyronitrile) (AIBN) was the product of Junsei Chemical Co., Ltd. (Tokyo, Japan) and was recrystallized prior to use. Trifluoroacetic acid (TFA) was from Acros Organics (Geel, Belgium). Acetonitrile, chloroform and methanol are all of HPLC grade and from Duksan Pure Chemical Co., Ltd. (Ansan, Korea). All the other reagents used in the experiment were of the highest grade commercially available. Double deionized water was filtered with 0.45 μm filter membrane before use.

2.2. HPLC analysis

HPLC analysis was performed using a liquid chromatography system containing a Waters 600s Multisolvent Delivery System and a Waters 616 pump (Milford, MA, USA), a Waters 486 Tunable Absorbance UV detector (Milford), and a Rheodyne injection valve (5.0 mL sample loop). Autochro 2000 data software (Younglin, Anyang, Korea) was used as the data acquisition system. Chromatographic assay was carried out at ambient temperature. UV wavelength was set at 280 nm.

2.3. Preparation of the imprinted polymers

The ciprofloxacin imprinted polymers were prepared by thermal-initiated polymerization within a 25 mL thick-walled glass tube. The polymerization mixture composed of 1.0 mmol ciprofloxacin, 6 mmol MAA, 30 mmol EDMA, and 0.08 g AIBN was dissolved in appropriate porogenic solvents (methanol:water = 7:3, v/v). The solution was sonicated for 10 min and purged with helium gas for 10 min before being sealed under helium. Polymerization was performed under 58 °C in water bath for 24 h. After the polymerization, the polymers were grinded and sieved through 32 μm sieve, and then suspended by acetone until the upper solution was clearly. Finally, the particles were dried under vacuum and put into a column and washed with methanol:acetic acid (4:1, v/v) to remove the templates. After washing with methanol and drying in a drying oven (50 °C), the particles were stored at ambient temperature until use. The non-imprinted blank polymers (in the absence of template) were prepared and treated in an identical manner.

2.4. Binding property of the imprinted polymers

In order to investigate the binding property of the imprinted polymers, static absorption experiment and Scatchard analysis were employed in this work. 20 mg imprinted particles, 3.0 mL standard solution with different concentrations of ciprofloxacin were putted into 5.0 mL flasks and oscillated in dark at room temperature for 24 h. These solutions were centrifuged and filtered then examined for the free concentrations analysis by HPLC. The absorption quantity (Q) was calculated by subtracting the free concentrations from the initial concentrations.

2.5. Determination of ciprofloxacin in human urine

Human urine samples were obtained from fasting healthy volunteer. The samples were centrifuged for 20 min at 10,000 rpm and then filtered through a cellulose acetate filter (0.20 μm pore size, Advantec MFS Inc., CA, USA). The filtrate were collected in glass containers and stored at −20 °C until analysis was performed, with the minimum possible delay.

Stock standard solutions of ciprofloxacin were prepared in water. Further dilution steps were made by human urine. Working standard solutions were prepared by adding appropriate volumes of ciprofloxacin solution and the volume added was always less than 2% of the final urine volume to preserve the integrity of the samples. After aliquoting, the urine samples were stored at −20 °C until analysis.

3. Results and discussion

3.1. Optimum of polymerized components and polymerization conditions

In order to obtain MIPs which demonstrate specific recognition ability to target molecule in water environment, MIPs using methacrylic acid/acrylamide as monomers and EDMA as cross-linker were synthesized in non-polar solvent and polar porogenic solvents especially water-containing system. The results revealed that the imprinted polymers prepared in methanol–water system show better molecular recognition ability in aqueous environment than MIPs prepared in organic solvent such as chloroform and acetonitrile. Moreover, the proportion of water in the polymerization mixtures is a critical effect for the pore properties and surface area of the resulted polymers, which is due to water as porogenic solvent not only bring all the components (template, functional monomers, cross-linker and initiator) into one phase but also creating macropore structures in the imprinted polymers. The MIPs using methacrylic acid as monomer show higher recognition ability to target molecule than the MIPs prepared using acrylamide due to methacrylic acid have stronger electrostatic and hydrophobic interactions with target in polar environment. Additional, due to ciprofloxacin suffer degradation processes under UV irradiation, so thermal-initiated polymerization was chosen in this work.

3.2. Binding capacity of the imprinted polymers

The maximum binding capacity and dissociation constant were employed to evaluate the binding properties of the MIP. The data of static absorption experiment were further processed with Scatchard equation:

$$\frac{Q}{C_{\text{free}}} = \frac{Q_{\text{max}} - Q}{K_{\text{D}}}$$

where Q is the amount of ciprofloxacin bounded to MIP at equilibrium, Q_{max} is the maximum binding capacity, C_{free} is the free analyte concentration at equilibrium and K_{D} is the dissociation constant. As shown in Fig. 2, the Scatchard plot was not a single straight line, suggesting that the binding sites in
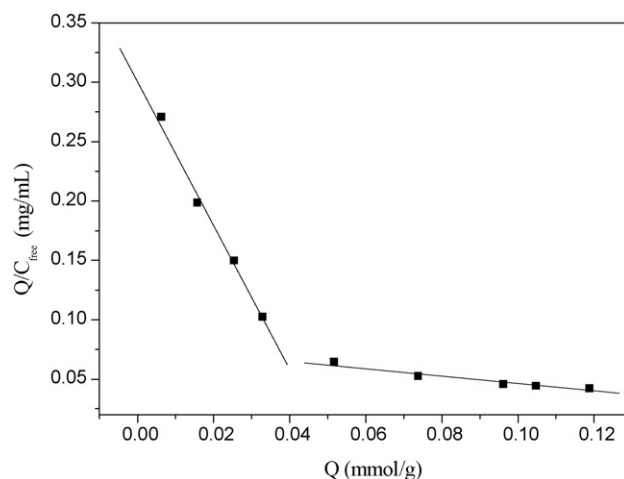

Fig. 2. Scatchard analysis of ciprofloxacin MIPs.

imprinted polymers are heterogeneous in respect to the affinity for ciprofloxacin. There are two distinct sections within the plot which can be regarded as straight lines, so it would be reasonable to assume that the binding sites can be classified into two distinct groups with specific binding properties. The respective K_{D} and Q_{max} values were shown in Table 1.

3.3. Chromatographic evaluation of the imprinted polymers

To evaluate the imprinting effect of the obtained MIPs, the imprinted particles were packed into a chromatographic column (100 mm × 4.6 mm I.D.) for further chromatographic evaluation. Several different kinds of mobile phases were investigated and the results show that ciprofloxacin can not be eluted out the MIP column within 60 min and unrelated molecules with template such as caffeine and catechin were eluted out less than 15 min when acetonitrile, methanol, and water were used as mobile phase. To probe the selectivity of the MIP for other structurally related analytes, enrofloxacin was also injected at same condition and a very broad chromatographic peak was observed together with a longer retention time, which presumably was related to strong contact ion pairs forming between MAA and the piperazine ring of enrofloxacin. At the same time, ciprofloxacin and enrofloxacin was quickly washed out the blank column (<10 min) under the same condition, which indicated that the affinity of the MIP column to ciprofloxacin was due to special imprinted recognition, mainly dependent on the stereo structures and arrangement of functional groups of the cavities in MIP. With the increasing of acetic acid or trifluoracetic acid in mobile phase, the elution ability of mobile phase increasing and ciprofloxacin begin to be eluted out, which was due to the electrostatic and hydrophobic interactions destroyed with

Table 1
The results of Scatchard analysis

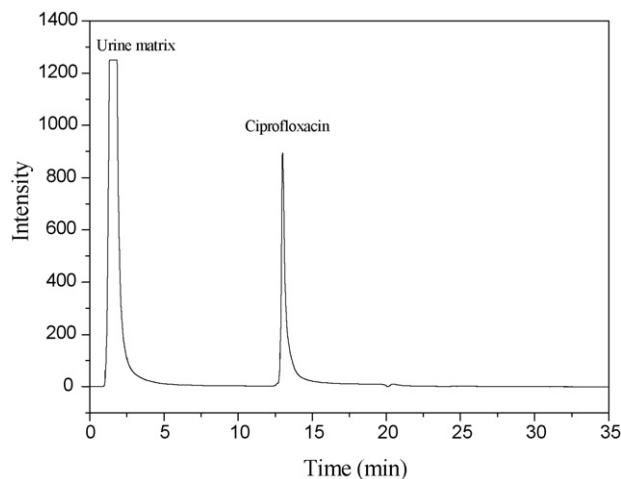| Binding sites	Linearity	K_{D}	Q_{max} (mmol g^{-1})
Higher affinity site	$Q/C_{\text{free}} = 0.305 - 6.198Q$	0.162	0.049
Lower affinity site	$Q/C_{\text{free}} = 0.0794 - 0.330Q$	3.028	0.241

Fig. 3. Chromatographam of spiked urine sample.

Fig. 4. Chromatographam of human urine samples after oral administration.

the increasing of polarity modifiers. When the content of tri-fluoracetic acid increased to 0.5% (v/v), ciprofloxacin could be eluted out within 5 min. These values, taken together with the elution profiles demonstrated that the MIP column has higher affinity to ciprofloxacin in polar environment and the retention ability can be easily adjusted by changing the pH of mobile phase. These characteristics give the MIP the potential as selective adsorbent used in the enrichment, separation and detection of ciprofloxacin in biological and environmental samples.

In order to optimize the process of selectively extract and separate ciprofloxacin from human urine, gradient elution were investigated with different proportions of water and methanol-trifluoracetic acid as mobile phase. According to the above results, water was selected as mobile phase firstly due to it is similar to urine matrix and no toxicity. Fig. 3 shows that using water as mobile phase, proteins and other biological matrix could be quickly washed out and ciprofloxacin was selectively retained and enriched on the MIP column. Then methanol-trifluoracetic acid was applied as mobile phase and ciprofloxacin could be quickly washed out. Moreover, by changing the time of gradient elution, the retention factor of ciprofloxacin could be adjusted freely. No interferences from the urine matrixes were observed, which demonstrates the special selectivity of the synthesized MIP in water environment.

3.4. Pretreatment of human urine samples

The complex matrices of biological fluids make the determination of ciprofloxacin difficult at low concentration, especially when the analytes have to be extracted and quantified under maximum residue limit levels. We investigated several previous methods to pretreatment human urine samples, such as protein precipitation with trichloroacetic acid, methanol and acetonitrile, then centrifuged and analyzed by using C_{18} column. Due to ciprofloxacin have low solubility in both organic and water solution, the recoveries was not sufficient (<80%).

In order to completely eliminate matrix interferences and concentrate the analyte, MIPs synthesized in water-containing environments were employed as selective chromatographic sta-
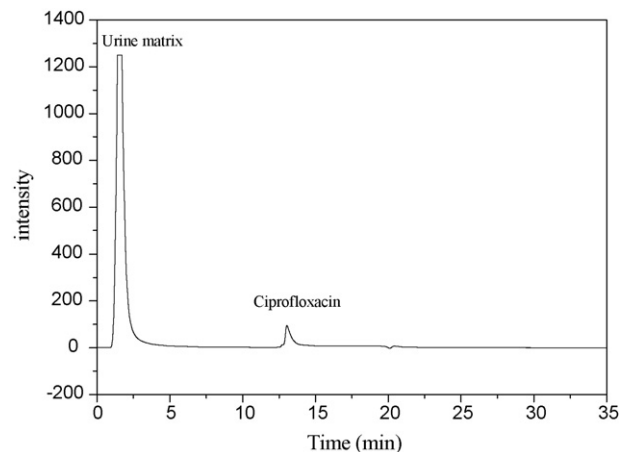
tionary phase to process for human urine samples. Human urine samples were pretreated only by centrifuged 20 min at 10,000 rpm then injected into HPLC directly and analysis under gradient elution. Five randomly selected control drug-free human urine samples were processed directly into chromatographic system and analyzed to determine the extent to which endogenous components may contribute to interfere with the retention time of the drug. No peak was observed in the chromatogram at the same retention time with ciprofloxacin, which indicated all templates was already removed from polymer matrix and no interferences for endogenous compounds were found in the physiological matrices.

3.5. Calibration curves, accuracy, and precision

Calibration curves were constructed using the areas of the chromatographic peaks measured at nine increasing concentrations, in a range from 0.1 to 100 mg L^{-1} of ciprofloxacin. The results showed good linearity throughout the concentration and the linear correlation equations was: $y = 1.15 \times 10^5 x + 1.81 \times 10^3$ ($r = 0.9993$). According to the
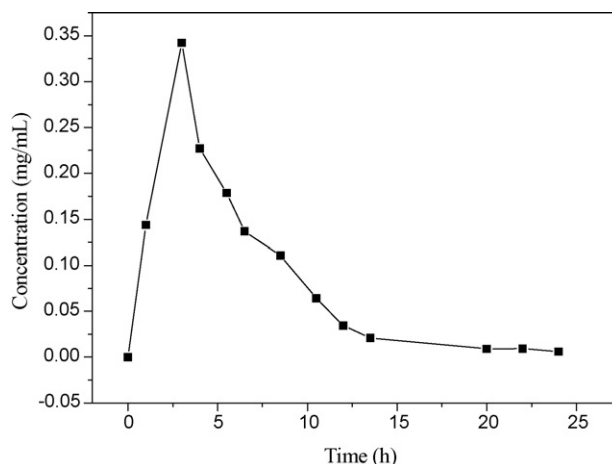

Fig. 5. Urine concentration–time curve of ciprofloxacin.

Table 2
The recoveries of ciprofloxacin in three spiked urine samples ($n = 5$)

	Spiked level					
	0. 8 mg L^{-1}		4.0 mg L^{-1}		20 m g L^{-1}	
	Recoveries	R.S.D.	Recoveries	R.S.D.	Recoveries	R.S.D.
Ciprofloxacin	94.5%	5.60%	95.8%	3.15%	99.1%	2.68%

signal-to-noise relation rule equal to 3.0, the limit of detection for ciprofloxacin was 0.03 µg/mL. The standard curves were used to calculate concentrations of ciprofloxacin in urine sample from the measured peak area.

The accuracy and precision of the method were assessed by performing replicate analyses of quality control samples at three different concentrations of ciprofloxacin in five replicates in the same day and consecutive days. The results showed that the intra- and inter-assay relative standard deviations and inter-assay relative standard deviations of the proposed method were lower than 2.9% and 3.6%.

3.6. Analysis of ciprofloxacin in human urine samples

Human urine samples were collected from healthy volunteer before (blank) administration and during the 24 h following oral administration of a pharmaceutical compound containing 300 mg of ciprofloxacin. The urine samples were centrifuged at 10,000 rpm for 20 min and then injected directly into the chromatograph without any other pretreatment. Fig. 4 shows no interferences from endogenous of human urines compounds were observed. The variety of ciprofloxacin concentration in human urine within 24 h was shown in Fig. 5. To investigate the recovery of this method, urine samples were spiked with ciprofloxacin at three different concentrations. The chromatographic peak areas of analyte were compared to those of standards at the same concentration to provide the recovery values and the results were shown in Table 2.
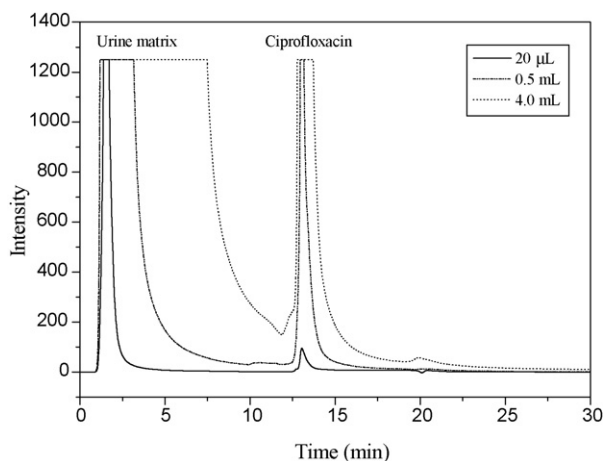

Fig. 6. Chromatographam of urine samples with different injection volumes.

3.7. Improve the detection limit by increasing injection volume

Due to ciprofloxacin could be selectively retained on the MIPs column when water was used as mobile phase, so the retention factor of ciprofloxacin could be adjusted freely by changing the start time of methanol-trifluoracetic acid in grade elution. Moreover, the peak height of ciprofloxacin could be greatly improved by increasing the injection volume. This procedure likes an on-line solid phase microextraction of using water as washing solution and methanol-trifluoracetic acid as eluting solution. Fig. 6 shows that the peak height of ciprofloxacin greatly enhanced with the injection volume increasing, proteins and other biological matrixes were also quickly washed out and no interferences were observed. When the injection volume increased to 2.0 mL, the detection limit of ciprofloxacin could be improved 100-folds according to the peak height of ciprofloxacin at small injection volume (5.0 µL). So the trace analysis of ciprofloxacin in biological sample could be easy achieved.

4. Conclusion

Ciprofloxacin imprinted polymers were prepared in water-containing system for selective extraction and separation of ciprofloxacin from human urine followed by high performance liquid chromatography with UV detection. The imprinted polymers show high affinity and selectivity to ciprofloxacin in aqueous environment and the affinity can be easily adjusted by control the acidity of the mobile phase. Using the MIPs as selective chromatographic stationary phase, proteins and other biological matrix could be quickly washed out and ciprofloxacin was selectively retained and enriched. Moreover, by increasing injection volume, the sensitivity and detection limit could be greatly improved. This expedient greatly simplified the overall procedure, resulting in a rapid and efficient sample analysis while maintaining precision and accuracy.

Acknowledgement

References

[1] M.J. Whitcombe, L. Martin, E.N. Vulfson, Chromatographia 47 (1998) 457.

[2] M. Kempe, K. Mosbach, J. Chromatogr. A 694 (1995) 3.

[3] H. Yan, K.H. Row, Int. J. Mol. Sci. 7 (2006) 155.

[4] H. Sun, F. Qiao, G. Liu, J. Chromatogr. A 1134 (2006) 194.

[5] H. Yan, K.H. Row, Biotechnol. Bioprocess. Eng. 11 (2006) 357.

[6] N. Lavignac, C.J. Allender, K.R. Brain, Anal. Chim. Acta 510 (2004) 139.

[7] G. Vlatakis, L.I. Andersson, R. Miller, K. Mosbach, Nature 361 (1993) 645.

[8] K. Hosoya, Y. Shirasu, K. Kimata, N. Tanaka, Anal. Chem. 70 (1998) 943.

[9] L. Ye, K. Mosbach, React. Funct. Polym. 48 (2001) 149.

[10] F. Breton, P. Euzet, S.A. Piletsky, M.T. Giardi, R. Rouillon, Anal. Chim. Acta 569 (2006) 50.

[11] S. Marx, A. Zaltsman, I. Turyan, D. Mandler, Anal. Chem. 76 (2004) 120.

[12] N. Masqueè, R.M. Marceè, F. Borrull, Trends Anal. Chem. 20 (2001) 477.

[13] E. Caro, R.M. Marce, F. Borrull, P.A.G. Cormack, D.C. Sherrington, Trends Anal. Chem. 25 (2006) 143.

[14] P.A.G. Cormack, A.Z. Elorza, J. Chromatogr. B 804 (2004) 173.

[15] F. Qiao, H. Sun, H. Yan, K.H. Row, Chromatographia 64 (2006) 625.

[16] S.A. Piletsky, H.S. Andersson, I.A. Nicholls, J. Mol. Recog. 11 (1998) 94.

[17] B.R. Hart, K.J. Shea, J. Am. Chem. Soc. 123 (2001) 2072.

[18] B. Sellergren, Anal. Chem. 66 (1994) 1678.

[19] J.L. Urraca, A.J. Hall, M.C. Moreno-Bondi, B. Sellergren, Angew. Chem. Int. Ed. 45 (2006) 5158.

[20] D.M. Campoli Richards, P.J. Monk, A. Price, P. Benfield, P. Todd, A. Ward, Drugs 35 (1988) 373.

[21] A.A. Firsov, S.N. Vostrov, A.A. Shevchenko, S.H. Zinner, G. Cornaglia, Y.A. Portnoy, Antimicrob. Agent Chemother. 42 (1998) 2841.

[22] M. Kamberi, N. Hajime, P. Kamberi, N. Uemura, K. Nakamura, S. Nakano, Ther. Drug Monit. 21 (1999) 335.

[23] S. Wei, J. Lin, H. Li, J.M. Lin, J. Chromatogr. A 1163 (2007) 333.

[24] A. Espinosa-Mansilla, A.M. Peña, D. González Gómez, F. Salinas, J. Chromatogr. B 822 (2005) 193.

[25] A. Navalón, O. Ballesteros, R. Blanc, J.L. Vílchez, Talanta 52 (2000) 845.

[26] E. Caro, R.M. Marce, P.A.G. Cormack, D.C. Sherrington, F. Borrull, J. Sep. Sci. 29 (2006) 1230.

[27] E. Caro, R.M. Marce, P.A.G. Cormack, D.C. Sherrington, F. Borrull, Anal. Chim. Acta 562 (2006) 145.

Study on chiral resolution of three beta-blockers by affinity electrokinetic chromatography

Guoqiang Yang, Yifang Zhao, Meixian Li, Zhiwei Zhu [*], Qiankun Zhuang

Institute of Analytical Chemistry, College of Chemistry and Molecular Engineering, Peking University, Beijing 100871, PR China

Abstract

The chiral resolution of three beta-blockers including propranolol, pindolol and oxprenolol, was studied by affinity electrokinetic chromatography. The effect of various chiral selectors and some key parameters including buffer pH, buffer concentration, capillary temperature and applied voltage were carefully studied, respectively. At optimum condition, based on the signal-to-noise ratio of 3, the detection limits for the simple resolution and chiral resolution were found to be 1.0×10^{-5} and 4.0×10^{-5} M, respectively. In addition, the interactions of these beta-blockers with bovine serum albumin (BSA) were studied and the binding constant (K_a) between BSA and each of beta-blockers were calculated. Based on linear correlation coefficient, it can be concluded that the binding ratio of pindolol (oxprenolol) combining with BSA is 1:1, and that the binding number of propranolol interacting with BSA deviates one.
© 2007 Elsevier B.V. All rights reserved.

Keywords: beta-Blockers; Chiral resolution; Bovine serum albumin; Affinity electrokinetic chromatography

1. Introduction

The resolution of chiral drugs continues to be an important area in pharmaceutical analysis. There are a number of analytical techniques such as high-performance liquid chromatography (HPLC) which give reliable and stable assays for chiral drugs as racemic mixtures or when single enantiomers are manufactured [1,2]. Nowadays, compared with HPLC, capillary electrophoresis (CE) has been shown to be particularly successful in this area due to its several competitive advantages including higher separation efficiency, shorter analysis time, low cost, small volumes of sample and reagents, easy changes of separation media, etc. [3,4]. However, the usage of HPLC and CE for a particular application is very dependent upon the relative merits of each technique to the individual assay [5].

The beta-blockers comprise a group of drugs used to treat various disorders associated with the circulatory system [6]. Each of these drugs possesses at least one chiral center and an inherent high degree of enantio-selectivity in binding to the beta-adrenergic receptor. The enantiomers of beta-blockers have

markedly different pharmacodynamics and pharmacokinetics in some cases. Numerous approaches to their chiral separations in CE have been described in recent years, primarily due to the demand for enantiomeric purity in drug products [7–9]. The most commonly used chiral selectors are cyclodextrin compounds [10,11], although there is interest in a variety of other types of selectors as well, such as chiral surfactants and micelles, antibiotics, crown ethers, and polymeric phases. Meanwhile, another type of selector, i.e. protein, has received increased attention for use as stereoselective binding agents in CE [12,13]. These proteins interact with beta-blockers besides having the possibility of discriminating a chiral molecule due to the chirality of themselves and this kind of interactions are similar to the process drugs work in human body in a way. Consequently, using CE to study the interactions between proteins and beta-blockers has its specific meanings.

There are two modes when proteins are chosen as chiral selectors in CE: one is called affinity electrokinetic chromatography (AEKC), corresponding to the case of proteins being used as additives into the running buffer; and the other is called affinity capillary electrochromatography (ACEC), corresponding to the case of proteins as immobilized selectors. AEKC has indeed several advantages over ACEC. Methodological developments in AEKC are easily carried out since this technique does not require

---

[*] Corresponding author. Tel.: +86 10 62757953; fax: +86 10 62751708.
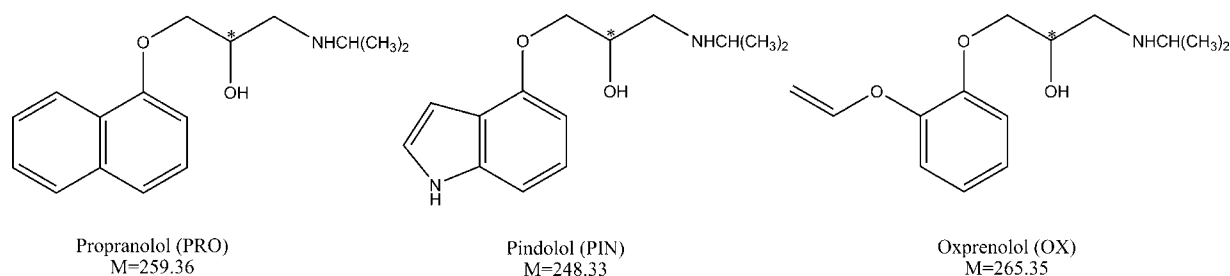*E-mail address:* zwzhu@pku.edu.cn (Z. Zhu).

Fig. 1. Chemical structures of propranolol (PRO), pindolol (PIN) and oxprenolol (OX) (the asterisk (*) denotes chiral center).

protein immobilization [14,15]. Furthermore, AEKC is a simple and feasible method for studying the interactions between drugs and proteins, which can be used in determining the drug–protein binding constant [16]. Meanwhile, the use of soluble proteins eliminates the possibility of altering both structure and binding properties of proteins, which makes this investigation, is closer to a real living system.

The aim of this work was to study the chiral separation of three beta-blockers taking advantage of the different affinities of their enantiomers for BSA as well as their interactions each other by means of AEKC. The molecular structures of these three beta-blockers in this paper are shown in Fig. 1.

2. Experimental

2.1. Apparatus

All experiments were performed with a CAPEL105 CE system with water-cooling and a UV detector (Lumex, Russia). Separations were performed in 58.5 cm (50.0 cm to detector) × 50 μm i.d. uncoated fused-silica capillaries (Yongnian Optical Fiber Factory, China). UV detection was carried out at 220 nm. Prior to separation, the new capillary was flushed with 1.0 M sodium hydroxide for 10 min, then with deionized water for 10 min, and finally with running buffer for 15 min. Between consecutive analysis, the capillary was flushed with 1.0 M sodium hydroxide for 1 min, then with deionized water for 2 min, and finally running buffer for 2 min in order to improve the reproducibility.

2.2. Reagents and solutions

Propranolol (PRO), pindolol (PIN), and oxprenolol (OX) were purchased from Acros or Sigma. Bovine serum albumin (BSA) and hemoglobin (HB) were obtained from Sigma. All the other chemicals used were of analytical-reagent grade. Deionized water was used to prepare the buffer and sample solutions.

2.3. Procedure

The mixed solution that containing PRO, PIN and OX (0.1 mM each) was prepared with deionized water. Phosphoric acid buffer solution (PBS) was selected as the running buffer. Prior to separation, all electrolyte solutions were filtered through a 0.45 μm polytetrafluoroethylene membrane filter. All measurements were carried out at least three times.

3. Results and discussion

3.1. Separations of three beta-blockers in capillary zone electrophoresis (CZE) mode

First of all, normal CZE mode was used to separate these three beta-blockers. Each of the beta-blockers was injected singly to the capillary with the running buffer of 100 mM pH 6.9 PBS in order to determine the order of the peaks in their mixture. As shown in Fig. 2, there is little difference among the retention time of the three beta-blockers owing to their similar structure and molecular weight. Actually, the amino group in blockers can be protonated to a certain extent, which causes blockers to carry some positive charge under this experimental condition. For their mixture, the order of the peaks has no much relation with their molecular weight, but depends on their structures more closely. In addition, from the figure, it can be found that the absorptions of PRO and PIN are obviously stronger than OX. It is because they have more conjugated ring structures in comparison to OX.

The parameters in CZE mode were optimized carefully. When the temperature in the capillary increased, the viscosity of the solution reduced, and the increasing electroosmotic flow (EOF) significantly shortened their retention time at a descending rate of about −0.14 min/°C (from 15 to 30 °C). So the higher the temperature is, the faster the separation goes, as shown in Fig. 3. However, a higher temperature may lead to a more obvi-
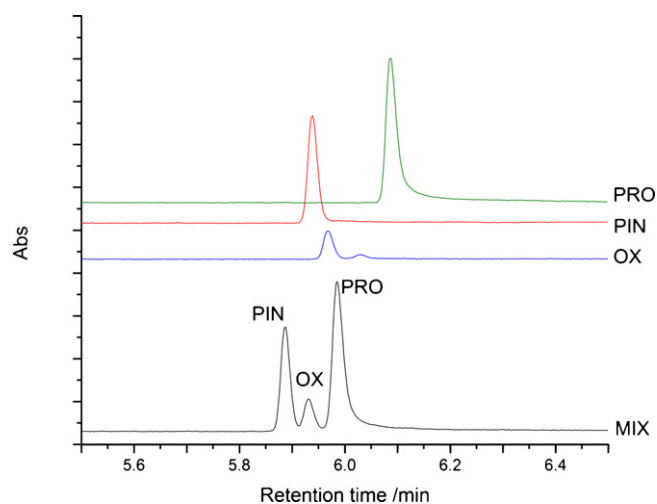

Fig. 2. The separation of PRO, PIN and OX (0.1 mM each) in 100 mM pH 6.9 PBS by normal CZE. Separation conditions: injection at 30 mbar for 5 s, 20 kV applied voltage, 25 °C capillary temperature.
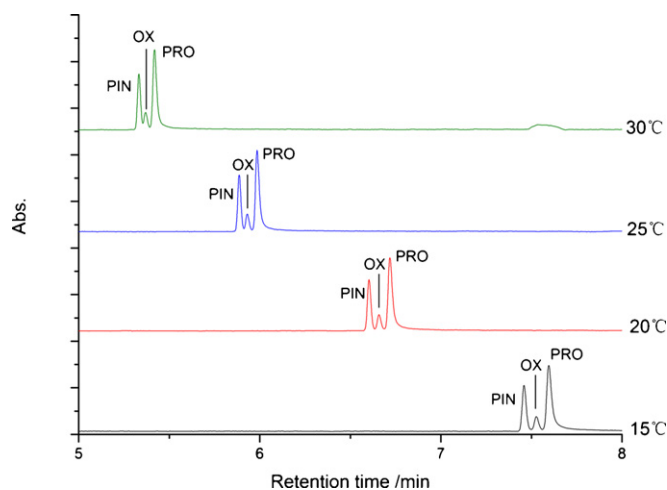
Fig. 3. Effect of capillary temperature on the separation of PRO, PIN and OX (0.1 mM each) by normal CZE. Separation conditions: 100 mM pH 6.9 PBS, 20 kV applied voltage, injection at 30 mbar for 5 s.

ous diffusion and a lower resolution besides a shorter retention time. From Fig. 3, it can be observed that the peaks of PIN and OX have overlapped considerably at 30 °C. That is much worse than the case at a lower temperature. Consequently, taking account of all related factors above, we choose 25 °C as our operating temperature in the experiment. But for a better resolution, we can also choose 15 °C if a prolonged retention time is acceptable.

Running buffer affects the separation remarkably, as shown in Fig. 4. When the PBS concentration increased continually, the retention time became longer and longer, and the resolution also became better and better. In this system, 100 mM PBS was chosen as optimal running buffer.

The separation results are affected obviously by buffer pH value because of different protonization extent of amino group in beta-blockers at different pH values. This effect should be considered from two aspects: on one hand, at a lower pH, the higher
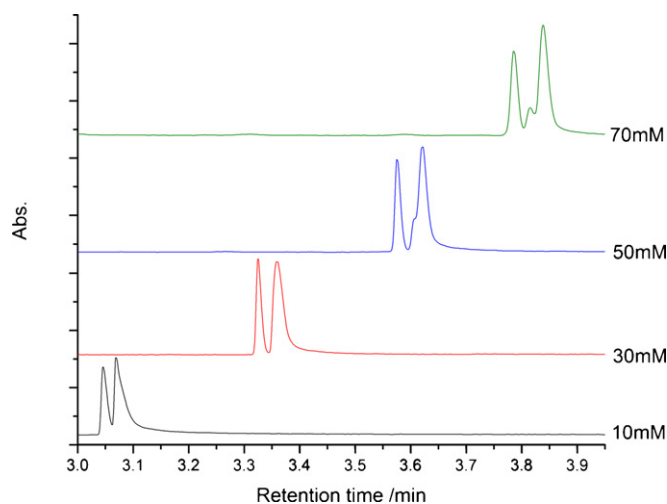

Fig. 4. Effect of PBS concentration on the separation of PRO, PIN and OX (0.1 mM each) by normal CZE. Separation conditions: pH 6.9 PBS, 25 kV applied voltage, 25 °C capillary temperature, injection at 30 mbar for 5 s.
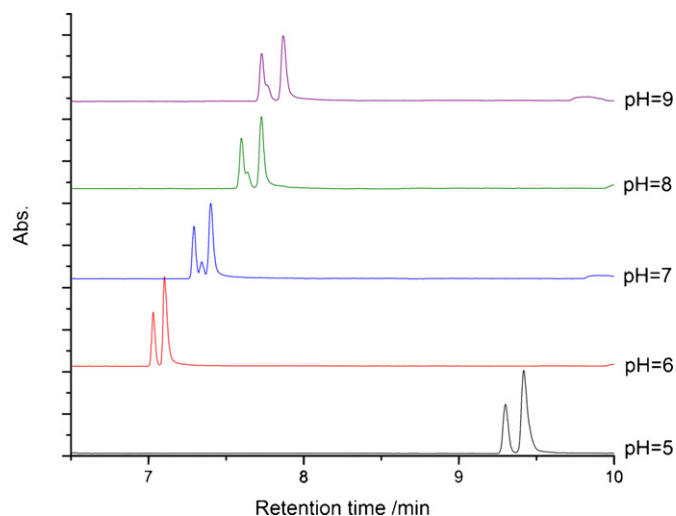

Fig. 5. Effect of buffer pH on the separation of PRO, PIN and OX (0.1 mM each) by normal CZE. Separation conditions: 100 mM PBS, 15 kV applied voltage, 25 °C capillary temperature, injection at 30 mbar for 5 s.

protonization grade of amino group gives samples a higher electrophoresis velocity in the positive electric field; on the other hand, at a lower pH, a higher concentration of hydrogen ion may have a stronger interaction with silicon-hydroxy at the inner wall of the capillary, which makes the net negative charge decrease remarkably, and largely reduces EOF and prolongs the retention time. As shown in Fig. 5, pH 7 is obviously the optimal condition for the separation of these blockers. In particular, it is notable that the separation result at pH 5 is a bit abnormal comparing with the case at other pH values. We suppose that EOF should be affected by buffer pH more than the protonization extent of amino group in beta-blockers when the pH value is lower than 6.

Methanol has been used as the additive to improve the separation in this system. It can be found that methanol affects EOF to a certain extent. The more methanol is added, the more obviously EOF decreases, and the more retention time is prolonged. Meanwhile, the difference of the retention time between PRO and OX is also getting greater with that between PIN and OX being reduced. Actually, methanol has no remarkable advantage for improving the separation effect. Considering the next investigation being focused on the interaction with BSA, a little even no methanol should be added.

In a word, considering all those factors above, the optimal conditions for baseline separation of the three beta-blockers in normal CZE mode are as follows: 30 mbar injection for 5 s, 15 kV applied voltage, 15 °C capillary temperature, 100 mM PBS (pH 6.9), as shown in Fig. 6. Under these conditions, the determination limit was 1.0×10^{-5} M based on the signal-to-noise ratio of 3.

3.2. Chiral separations of three beta-blockers in AEKC mode

We have tried G1 dendrimers and some biomoleculars including L-tyrosine, cytochrome c, hemoglobin, fish sperm DNA as chiral selective reagents in order to resolve these three beta-blockers. And also, we attempted to reverse the voltage with
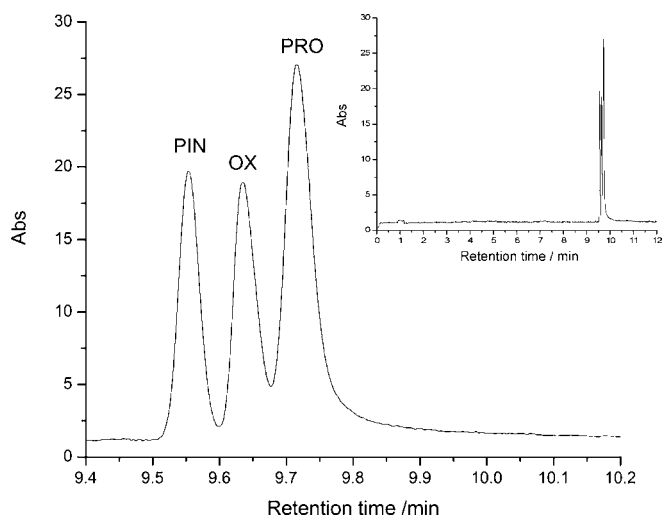
Fig. 6. The separation of 0.1 mM PRO, 0.1 mM PIN and 0.3 mM OX in 100 mM PBS (pH 6.9) by normal CZE. Separation conditions: injection at 30 mbar for 5 s, 15 kV applied voltage, 15 °C capillary temperature.

Fig. 8. Effect of BSA concentration on the separation of 0.1 mM (±)-PRO, 0.1 mM PIN and 0.3 mM (±)-OX in 100 mM PBS (pH 6.9) in AEKC mode. Separation conditions: injection at 30 mbar for 5 s, 20 kV applied voltage, 25 °C capillary temperature.

beta-CD in micellar electrokinetic chromatography (MEKC) mode, but all the above methods did not bring about perfect resolution effects. Only if bovine serum albumin (BSA) was added, the enantiomers of PRO and OX were discriminated from each other, as shown in Fig. 7. Unfortunately, PIN still could not be resolved by BSA due to minor difference between its enantiomers when interacting with BSA. Obviously, because of the interaction between BSA and the chiral drugs, the retention time of the three beta-blockers were prolonged, and the peaks had a little tailing, comparing with the case of absence of BSA in running buffer.

As shown in Fig. 8, the separation results were improved when increasing the BSA concentration. When it reached 0.10 mM, (±)-PRO and (±)-OX could be baseline separated. However, when the sample concentration was fixed, BSA at a too high concentration did not result in a higher resolution, but

a more background noise and more serious tailing peaks. So the BSA concentration of 0.1 mM is appropriate for separation. Meanwhile, buffer pH was still fixed to 6.9 based on the following reasons: (1) pH 6.9 is close to physiological condition and that is helpful for us to investigate BSA interacting with blockers; (2) CZE experiments confirmed that good separating results could be got at this pH.

Similarly, the concentration of PBS in the running buffer also has great effect on the separation under a fixed concentration of BSA and a fixed buffer pH. In this system, 70 mM PBS (pH 6.9) containing 0.1 mM BSA can resolve (±)-PRO and (±)-OX with a better resolution than other concentrations. The detail resolution data are summarized in Table 1.

Considering all those factors above including instrumental parameters, we found the optimal conditions for the resolution of the three beta-blockers in AEKC mode as follows: 30 mbar injection for 5 s, 20 kV applied voltage, 25 °C capillary temperature, 70 mM PBS (pH 6.9) containing 0.1 mM BSA. Under these conditions, the determination limit was 4.0×10^{-5} M based on the signal-to-noise ratio of 3.

3.3. Calculation of binding constants K_a between BSA and enantiomers of the three beta-blockers

Drug–protein interactions are determining factors in the therapeutic, pharmacodynamic, toxicology and so on. Obviously,
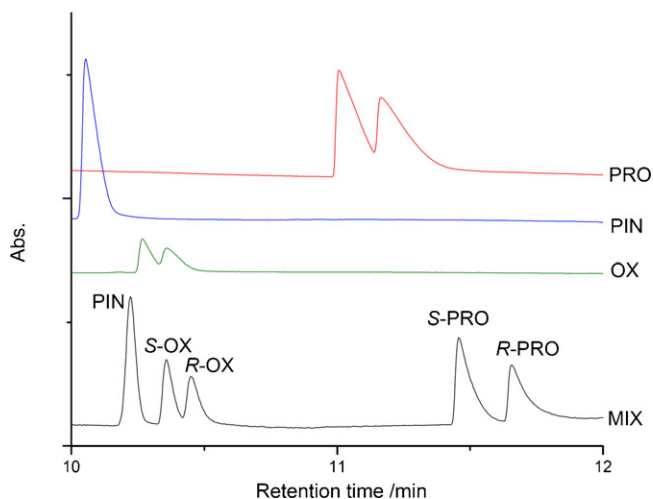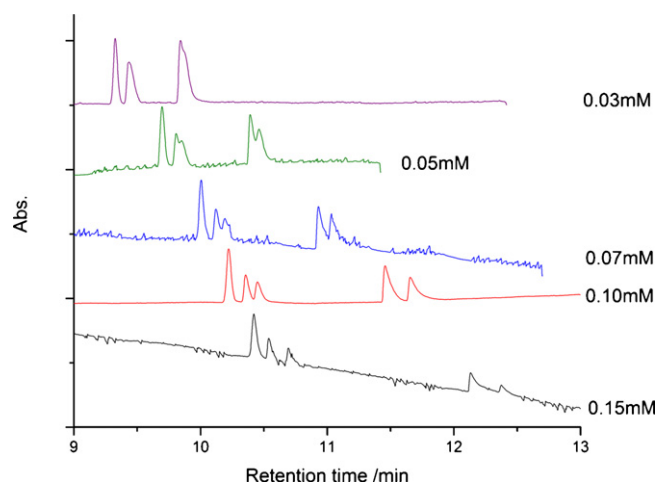

Fig. 7. The separation of 0.1 mM (±)-PRO, 0.1 mM PIN and 0.3 mM (±)-OX in 100 mM PBS (pH 6.9) containing 0.1 mM BSA in AEKC mode. Separation conditions: injection at 30 mbar for 5 s, 20 kV applied voltage, 25 °C capillary temperature.

Table 1
Resolution of (±)-PRO and (±)-OX in different concentration of PBS containing 0.1 mM BSA in AEKC mode

C_{PBS} (mM)	$R_{(\pm)\text{-OX}}$	$R_{(\pm)\text{-PRO}}$
100	0.7	1.0
70	1.1	1.1
50	0.7	1.0
30	0.4	1.0
10	Unseparated	Unseparated

Table 2
Experimental results for the K_a of beta-blockers and BSA

beta-Blocker	K_a (L/mol)	r
PIN	1.8×10^5	0.9895
S-OX	1.8×10^5	0.9890
R-OX	1.7×10^5	0.9879
S-PRO	1.3×10^5	0.9655
R-PRO	1.2×10^5	0.9648

drugs as the sample can combine with proteins as a buffer additive in the capillary, thus it is possible that the change of the moving velocity of drugs can be used to calculate the binding constant between drugs and proteins in AEKC. It is assumed that drugs (D) and proteins (P) only produce a simple complex:

$$D + P = DP \tag{1}$$

And f is defined as the ratio of DP in total D:

$$f = \frac{c_{DP}}{c_D + c_{DP}} \tag{2}$$

As DP has different moving velocity from D, it means different electrophoresis mobility,

$$\mu_D^P = (1 - f)\mu_D + f\mu_{DP} \tag{3}$$

where μ_D^P is the electrophoresis mobility of D at a certain protein concentration (C_P), μ_D is the mobility of D without protein, and μ_{DP} is the mobility of DP. From Eq. (3), the following equation can be deduced:

$$f = \frac{\mu_D^P - \mu_D}{\mu_{DP} - \mu_D} \tag{4}$$

Additionally, the binding constant (K_a) between D and P is:

$$K_a = \frac{c_{DP}}{c_D c_P} \tag{5}$$

Introducing Eq. (5) into (2) leads to:

$$\frac{1}{f} = \frac{1}{K_a c_P} + 1 \tag{6}$$

Combining Eqs. (4) and (6), the following equation can be obtained:

$$\frac{1}{\Delta\mu_D^P} = \frac{1}{K_a \Delta\mu_{max}} \frac{1}{c_P} + \frac{1}{\Delta\mu_{max}} \tag{7}$$

where $\Delta\mu_D^P = \mu_D^P - \mu_D$, $\Delta\mu_{max} = \mu_{DP} - \mu_D$.

Based on Eq. (7), the experiments can be designed that a series of D mobility (μ_D^P) are determined when P concentration is changed and D concentration is fixed. After the linear regression of $1/\Delta\mu_D^P$ to $1/C_P$, the resulting intercept and slope of the regression line are $1/\Delta\mu_{max}$ and $1/K_a\Delta\mu_{max}$, respectively. Obviously, their ratio is K_a.

Table 2 shows the binding constants (K_a) between BSA and unseparated PIN, enantiomers of ($\pm$)-PRO and ($\pm$)-OX, which are calculated according to Eq. (7). Based on linear correlation coefficient, it can be concluded that the suppose of PIN (OX) and BSA combining with the binding ratio of 1:1 is reasonable, but the binding number of PRO interacting with BSA deviates one. It still needs further careful investigation.

4. Conclusions

Propranolol, pindolol and oxprenolol can be determined with a high speed and efficiency by CE, and baseline separation can be achieved in normal CZE mode. When bovine serum albumin (BSA) is used as a buffer additive, the enantiomers of propranolol and oxprenolol can be chirally separated by AEKC, and the binding constants (K_a) between BSA and the three beta-blockers are calculated. Use of AEKC to studying the interaction of blockers enantiomers with protein confirmed a good and unique approach.

References

[1] C.G. Lv, G.F. Jia, W.T. Zhu, J. Qiu, X.Q. Wang, Z.Q. Zhou, J. Sep. Sci. 30 (2007) 344.
[2] G.W. Ponder, S.L. Butram, A.G. Adams, C.S. Ramanathan, J.T. Stewart, J. Chromatogr. A 692 (1995) 173.
[3] S. Fanali, J. Chromatogr. A 875 (2000) 89.
[4] B.K. Patel, M. Hanna-Brown, M.R. Hadley, A.J. Hutt, Electrophoresis 25 (2004) 2625.
[5] S.L. He, Y.F. Zhao, Z. Zhu, H.W. Liu, M.X. Li, Y.H. Shao, Q.K. Zhuang, Talanta 69 (2006) 166.
[6] Microsoft Corporation, Microsoft Encarta 2006.
[7] P. Ptacek, J. Macek, J. Klima, J. Chromatogr. B 789 (2003) 405.
[8] H. Kataoka, S. Narimatsu, H.L. Lord, J. Pawliszyn, Anal. Chem. 71 (1999) 4237.
[9] H.H. Maurer, O. Tenberken, C. Kratzsch, A.A. Weber, F.T. Peters, J. Chromatogr. A 1058 (2004) 169.
[10] M. Hammitzsch, R.N. Rao, G.K.E. Scriba, Electrophoresis 27 (2006) 4334.
[11] E. Szoko, K. Magyar, J. Chromatogr. A 709 (1995) 157.
[12] Y. Tanaka, S. Terabe, J. Chromatogr. A 694 (1995) 277.
[13] C. Millot, J. Chromatogr. B 797 (2003) 131.
[14] J.J. Martinez-Pla, Y. Martin-Biosca, S. Sagrado, R.M. Villanueva-Camanas, M.J. Medina-Hernandez, Anal. Chim. Acta 507 (2004) 171.
[15] M.A. Martinez-Gomez, R.M. Villanueva-Camanas, S. Sagrado, M.J. Medina-Hernández, Electrophoresis 26 (2005) 4116.
[16] N. Na, Y. Hua, J. Ouyang, W.R.G. Baeyens, J.R. Delanghe, T.D. Beer, Anal. Chim. Acta 527 (2004) 139.

Analysis of quinolizidine alkaloids in *Sophora flavescens* Ait. by capillary electrophoresis with tris(2,2′-bipyridyl) ruthenium (II)-based electrochemiluminescence detection

Jianyuan Yin [a,b], Yuanhong Xu [a], Jing Li [a], Erkang Wang [a,*]

[a] *State Key Laboratory of Electroanalytical Chemistry, Changchun Institute of Applied Chemistry, Chinese Academy of Sciences, Changchun, Jilin 130022, China*
[b] *Department of Traditional Chinese Medicinal Chemistry, Pharmacy College, Jilin University, Changchun 130021, China*

Abstract

A capillary electrophoresis method coupled with electrochemiluminescence detection for the analysis of quinolizidine alkaloids was established, especially, oxymatrine (OMT) which could not be measured by previous electrochemiluminescence methods was detected sensitively herein. Complete separation of sophoridine (SR), matrine (MT) and OMT was achieved within 13 min using a background electrolyte of 50mM phosphate buffer at pH 8.4 and a separation voltage of 15 kV. The calibration curves showed a linear range from 2.8×10^{-8} to 4.4×10^{-7} M for SR, 2.7×10^{-8} to 4.4×10^{-7} M for MT, and 2.5×10^{-7} to 4.0×10^{-6} M for OMT, respectively. The relative standard derivations for all analytes were below 3.1%. Good linear relationships were showed with correlation coefficients for all analytes exceeded 0.987. The detection limits were 1.0 nM for SR and MT, and 40 nM for OMT under the optimal conditions, respectively. The developed method was nearly harmless to the human and environment.
© 2007 Elsevier B.V. All rights reserved.

Keywords: Capillary electrophoresis; Electrochemiluminescence; Matrine; Oxymatrine; Sophoridine

1. Introduction

Sophora flavescens Ait., a typical traditional Chinese medicinal herb, has been used for treatment of various diseases in China as antifebrile, diuretic, anthelmintic and antidote [1]. The roots of *S. flavescens* Ait. are known to contain quinolizidine alkaloids as bioactive constituents [2]. A simple and efficient method for determination of these components is prerequisite to effectively utilize the plant. Up to now, a number of methods have been developed, including thin-layer chromatography (TLC) [3], high performance liquid chromatography (HPLC) [4–6], capillary electrophoresis (CE) [7,8], gas chromatography–mass spectrometry (GC–MS) [9], etc. In recent years, the electrochemiluminescence (ECL) method using $Ru(bpy)_3^{2+}$ has become an attractive detection means for alkaloids [10,11]. The method of HPLC coupled with ECL to examine quinolizidine

alkaloids was adopted by Yi et al. [12], because quinolizidine alkaloids contain tertiary amine functional groups that could react with $Ru(bpy)_3^{2+}$ to produce ECL.

Knight and Greenway [13] reviewed the effect of substituent attached to the nitrogen atom in amines. Generally, electron-withdrawing substituent, e.g. oxygen group, attached to the nitrogen atom caused its carrying charge from negative to positive, which destabilize electro-oxidation product, positive nitrogen radical ion, reduces the ECL activity of the compound. The bright light emission could be obtained for MT in the experimental condition. However, the emission of OMT could not be measured due to an oxygen group attached to the nitrogen atom in the molecular structure of OMT [14].

According to Chinese Pharmacopoeia [15], the total content of MT and OMT is a quality control of evaluating *S. flavescens*. Thus, a method detecting MT and OMT together is required. Previously the authors developed a HPLC method with $Ru(bpy)_3^{2+}$ ECL detection for quinolizidine alkaloids of MT, SR, and sophocarpine, but OMT was not detected [12]. Unlike the HPLC coupling with ECL detection, the

* Corresponding author. Tel.: +86 431 8526 2003; fax: +86 431 8568 9711.
E-mail address: ekwang@ciac.jl.cn (E. Wang).

CE–ECL is an attractive approach for the analysis of alkaloids with low detection limit and wide linear working range [10,16].

The present study is intended to develop a CE–ECL assay for determination of SR, MT, and OMT simultaneously. In addition, we investigated the influence of the detection potential, buffer pH in detection reservoir and separation buffer pH on migration time and separation resolution between analytes. Using this method, we successfully determined the above three alkaloid components in *S. flavescens* Ait.

2. Experimental

2.1. Materials and reagents

The standard samples of SR, MT, and OMT (Fig. 1) were supplied by the National Institute for the Control of Pharmaceutical and Biological Products of China (Beijing, PR China). Ru(bpy)$_3$Cl$_2$·6H$_2$O was obtained from Sigma–Aldrich (St. Louis, MO, USA). All other reagents were of analytical grade. Water ($\geq$18.2 MΩ) used throughout the experiments was generated by a Milli-Q water purification system (Millipore, Bedford, MA, USA). All solutions for CE were stored in the refrigerator at 4 °C prior to use. The solutions were made up to volume with appropriate buffer.

2.2. Apparatus

A CE–ECL detection system (Xi'an Remex Electronics Co. Ltd., Xi'an, China) was used [10]. Data acquisition and recording of electropherograms were accomplished with a MPI-A software. Fused-silica capillaries (25 μm i.d., 360 μm o.d.) were the products of Yongnian Photoconductive Fibre Factory, Hebei Province, China. The construction of the ECL detection cell has been presented in a previously published work [17], in which a 500 μm diameter Pt disc electrode, a Pt wire counter electrode, and an Ag/AgCl reference electrode were situated. A high-voltage power supply (Shanghai Nucleus Institute, Shanghai, China) was used to supply high voltage for the injection and separation of samples. The capillary was rinsed with 0.1 M NaOH for 20 min, followed by water and running buffer for 2 min each. The running electrolyte was refreshed after every 10 runs.
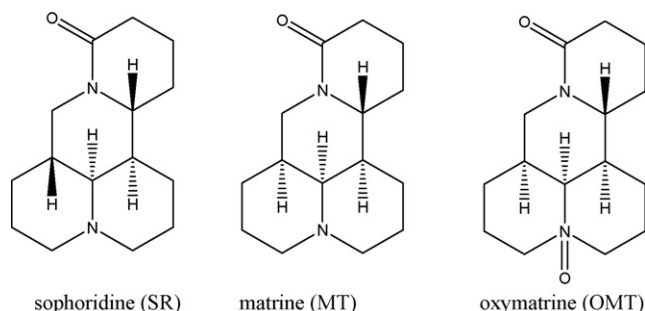

Fig. 1. Molecular structures of three quinolizidine alkaloids.

sophoridine (SR)   matrine (MT)   oxymatrine (OMT)

2.3. Preparation of standard solutions

Stock standard solutions of three quinolizidine alkaloids were prepared by dissolving each in methanol to concentration of 100 μg/ml. All solutions were stored in the refrigerator at 4 °C for 1 month, and the working solutions were diluted by running buffer and filter through 0.22 μm membrane before use.

2.4. Preparation of herbal drug extract

A 20 mg amount of pulverized *S. flavescens* Ait. was weighted accurately in a 50-ml flask. Forty millilitres chloroform and 0.5 ml of ammonia water were exactly added and then weighted again correctly. After staying overnight, it was subjected to ultrasonication at room temperature for 30 min. The solution was cooled down to ambient temperature and then made up to the weight with chloroform and mixed up. Accurately 20 ml of the successive filtrate was evaporated to dryness *in vacuum*, the residue was dissolved with methanol into a volumetric flask and adjusted to the volume of 10 ml. This solution was passed through a 0.22 μm membrane filter prior to use.

3. Result and discussion

3.1. Voltammetric analysis

To our Knowledge, MT and SR produce strong luminescence in the presence of Ru(bpy)$_3$$^{2+}$ in an aqueous alkaline buffer solution, while OMT trends to reduce the ECL activity as stated due to the oxygen atom bonded to the nitrogen atom [12,14]. When Ru(bpy)$_3$$^{2+}$ was oxidized to Ru(bpy)$_3$$^{3+}$ at a glassy carbon electrode, the strong reducing intermediate (radical ions) resulting from MT or SR produces the excited state, Ru(bpy)$_3$$^{2+*}$, by an electron transfer reaction with trivalent ruthenium species. Cyclic voltammetry (CV) was performed in 0.1 M phosphate buffer (pH 8.0). The anodic current intensity of Ru(bpy)$_3$$^{2+}$ was increased in the presence of MT or SR. The evidences showed that oxidized Ru(bpy)$_3$$^{2+}$ reacted with MT or SR, which obviously increased the oxidation rate of Ru(bpy)$_3$$^{2+}$ on the Pt electrode, in alkaline solution.

The N-oxide of OMT without a tertiary amine functional group in the molecule, however, could not be measured by Ru(bpy)$_3$$^{2+}$ ECL condition from the point of view of some authors [14]. While in the cyclic voltammograms in this experiment, an electrochemical catalytic wave could be obtained in the presence of OMT, though there was a relatively minor anodic current increase by OMT compared with those by SR or MT (Fig. 2). Thus, Ru(bpy)$_3$$^{2+}$ ECL was supposed to detect OMT. This phenomenon was further confirmed by electropherograms as shown in Fig. 5.

The problem with the weak of luminescence for OMT can be solved by optimal selection for the type, concentration and pH of the buffer in detection reservoir, and detection potential. Finally, analytical conditions such as separation buffer concentration and pH were optimized for achieving most favorable separation efficiency, peak shape, sensitivity, and duration of the CE–ECL analysis.
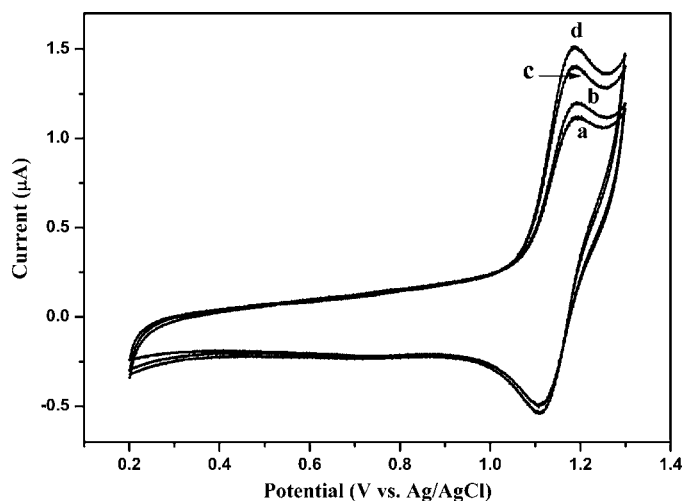
Fig. 2. Cyclic voltammograms of $Ru(bpy)_3^{2+}$, SR, MT and OMT on a platinum disc electrode (500 μm diameter). Potential sweep rate was 100 mV/s. Voltammogram (a) 5 mM $Ru(bpy)_3^{2+}$ + 50 mM phosphate buffer (pH 8.4); (b) 4.0×10^{-5} M OMT + 5 mM $Ru(bpy)_3^{2+}$ + 50 mM phosphate buffer (pH 8.4); (c) 4.4×10^{-6} M MT + 5 mM $Ru(bpy)_3^{2+}$ + 50 mM phosphate buffer (pH 8.4); (d) 4.4×10^{-6} M SR + 5 mM $Ru(bpy)_3^{2+}$ + 50 mM phosphate buffer (pH 8.4).

In the cyclic voltammograms, the $Ru(bpy)_3^{2+}/Ru(bpy)_3^{3+}$ couple displayed electrochemical catalytic CV wave on the Pt disc electrode, whereas SR, MT, or OMT did not show an obvious electrochemical response in the potential range from 0 to +1.35 V. When CV of $Ru(bpy)_3^{2+}$ was repeated in the presence of SR, MT or OMT, electrochemical catalytic waves produced by the reduction of $Ru(bpy)_3^{3+}$ by SR, MT or OMT were observed (Fig. 2, voltammograms d, c and b). These evidences suggest that the addition of quinolizidine alkaloids in $Ru(bpy)_3^{2+}$ solution obviously increased the oxidation rate of $Ru(bpy)_3^{2+}$ on the glassy carbon. The cyclic voltammograms compared, a lesser anodic current increase (from 1.11 to 1.18 μA) was produced resulting from the reduction of $Ru(bpy)_3^{3+}$ by OMT (Fig. 2a), whereas the anodic current increases were from 1.10 to 1.20 μA for SR (Fig. 2d) and from 1.11 to 1.20 μA for MT (Fig. 2c), respectively.

3.2. Selection of detection potential

Since the electrochemiluminescence reaction is voltage dependent, so we measured the ECL intensity at a various applied potentials to determine the optimum potential for the ECL of SR, MT and OMT. The highest ECL intensity obtained was at 1.2 V as shown in Fig. 3, so the most sensitive detection potential for SR, MT and OMT should be maintained at 1.2 V.

3.3. Selection of optimum pH in the detection reservoir

In order to obtain the optimal sensitivity of the analytes in CE–ECL system, the buffer pH value in the detection reservoir is a crucial factor. The effect of buffer pH in the detection reservoir was studied in a pH range from 6.0 to 10.0 in 0.4 pH units. As shown in Fig. 4, the highest ECL intensity of SR, MT was at pH 9.2, whereas the ECL intensity of OMT reached a peak value
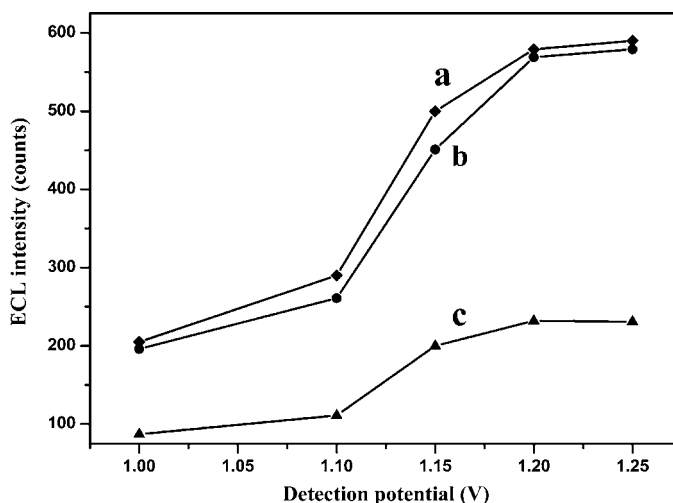

Fig. 3. Effect of detection potential on ECL intensity of the analytes. (a) ECL intensity of 4.4×10^{-6} M SR; (b) ECL intensity of 4.4×10^{-6} M MT; (c) ECL intensity of 4.0×10^{-5} M OMT. Conditions: Electrokinetic injection: 10 s at 10 kV. 5 mM $Ru(bpy)_3^{2+}$ and 50 mM phosphate buffer at pH 8.4 in the detection reservoir. Separation voltage: 15 kV. Each point in the line of (a–c) is the average of at least three scans with error bars at 2.5%, 3.1% and 3.1%, respectively.

at pH 8.4. To obtain good sensitivity for OMT, the appropriate phosphate buffer of pH 8.4 in the detection reservoir was used for the whole experiments.

3.4. Selection of separation buffer pH

The separation buffer pH influences not only the net charge of the analytes, but also the electroosmotic flow (EOF) inside the capillary, which results in different migration times for analytes. The separation resolution (R_s) between SR and MT is calculated with the following equation: $R_s = 2(t_2 - t_1)/(W_{b1} + W_{b2})$, where
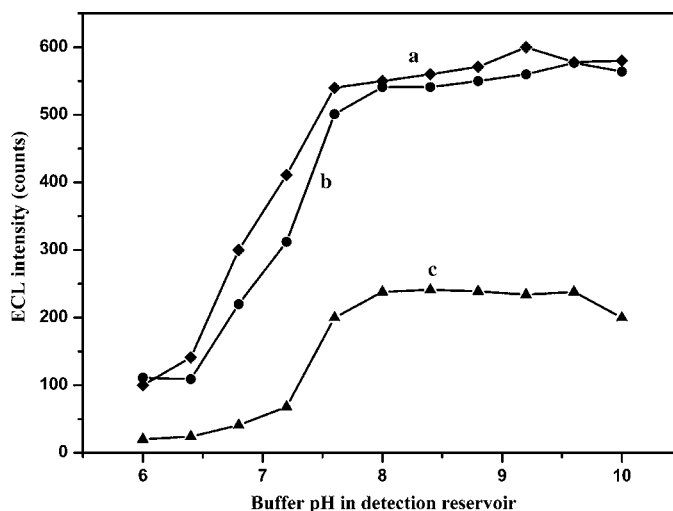

Fig. 4. Effect of buffer pH in detection reservoir on ECL intensity of the analytes. (a) ECL intensity of 4.4×10^{-6} M SR; (b) ECL intensity of 4.4×10^{-6} M MT; (c) ECL intensity of 4.0×10^{-5} M OMT. Conditions: 50 mM phosphate buffer containing 5 mM $Ru(bpy)_3^{2+}$ in the detection reservoir. Detection voltage: 1.2 V. Electrokinetic injection: 10 s at 10 kV. Separation voltage: 15 kV. Each point in the line of (a–c) is the average of at least three scans with error bars at 4.1%, 3.5% and 4.0%, respectively.

t_1 and t_2 are the migration times of SR and MT, respectively, W_{b1} and W_{b2} are the peak widths of SR and MT measured at the baseline. When the buffer pH from 6.0 to 8.0 was used, the peaks of SR and MT overlapped partially. The buffer pH increased, the two peaks separated partially. When the pH reached over 8.4, the three peaks of SR, MT and OMT got baseline separation ($R_{s(SR/MT)}$ 1.08). In order to meet the optimum pH 8.4 in the detection reservoir, the separation phosphate buffer pH was selected at 8.4 in further experiments.

3.5. Reproducibility, linearity, detection limits of SR, MT and OMT

Under the optimal conditions, namely ECL detection at 1.2 V, separation voltage at 15 kV, 50 mM phosphate buffer at pH 8.4, electrokinetic injection for 10 s at 10 kV, 5 mM Ru(bpy)$_3^{2+}$ and 50 mM phosphate buffer at pH 8.4 in the detection reservoir, a standard mixture solution containing SR (4.4×10^{-6} M), MT (4.4×10^{-6} M) and OMT (4.0×10^{-5} M) was electrokinetic injection consecutively six times to determine the reproducibility of ECL intensity based on peak height and migration time for the alkaloids. Relative standard derivations (R.S.D.) of the migration time (s) and the ECL intensity (counts) were 1.17% and 2.68% for SR, 1.08% and 3.06% for MT, 1.71% and 5.70% for OMT, respectively. The high reproducibility indicates that this method is accurate for detection of quinolizidine alkaloids. To investigate the detection linearity of the alkaloids by CE–ECL, a series of standard mixture solutions containing three alkaloids were tested. The relationships between ECL intensity and the concentration of SR, MT and OMT are shown in Fig. 5. With the increase in SR concentration, the ECL intensity increases dramatically within 2.8×10^{-8} to 4.4×10^{-7} M, then the intensity increase becomes smaller within 8.8×10^{-7} to 3.6×10^{-6} M, which indicates that the 4.4×10^{-7} M of SR reacting with Ru(bpy)$_3^{3+}$ was close to the maximum. The similar phenomena were obtained for MT and OMT. The maximum ECL intensities were at 4.4×10^{-7} M for MT, 4.0×10^{-6} M for OMT, respectively. The calibration equations and regression coefficients were: $y = 8.23x + 122.30$ and $R = 0.987$ for SR, $y = 8.65x + 111.85$ and $R = 0.991$ for MT, $y = 0.98x + 29.45$ and $R = 0.993$ for OMT in terms of peak height response as a function of analyte concentration. Detection limits of 1.0 nM for SR and MT, and 40 nM for OMT were obtained (S/N = 3). Comparison of the proposed method with other methods is listed in Table 1. Hence, CE–ECL is a sensitive method for determination of SR, MT, and OMT.
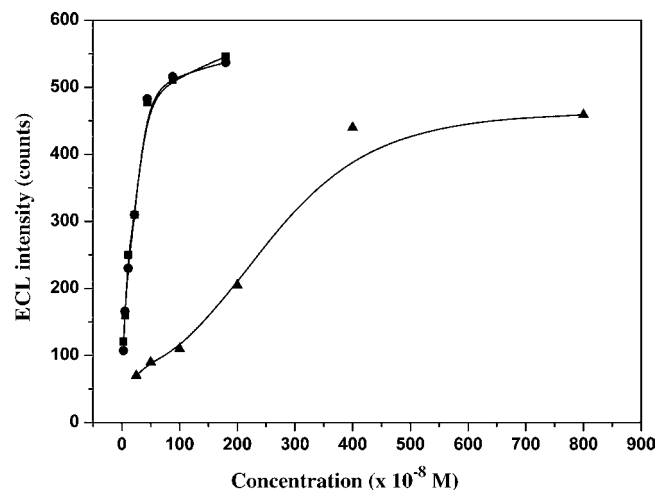

Fig. 5. The influences of the concentration of SR, MT and OMT on ECL intensities. (■) SR; (●) MT; (▲) OMT. Conditions: Electrokinetic injection: 10 s at 10 kV. 5 mM Ru(bpy)$_3^{2+}$ and 50 mM phosphate buffer at pH 8.4 in the detection reservoir. Running buffer: 50 mM phosphate buffer (pH 8.4). Detection voltage: 1.2 V. Separation voltage: 15 kV.

3.6. Analytical application

The developed CE–ECL method was employed for the determination of SR, MT and OMT in the extract of *S. flavescens* under the optimized conditions. Identification of the three analytes in herbal extracts was confirmed by comparing the electropherograms of the extracts with that of the extracts spiked with SR, MT, or (and) OMT, where the increase of peak height at certain migration time was directly proportional to the amount spiked with SR, MT, or OMT. Fig. 6 shows a typical electropherogram of the herbal extract described in Section 2.4 with the optimized conditions. The three alkaloids were identified matching their normalized migration times with those of a standard solution. As the figures show, the analytes are visible as neat electrophoretic peaks without interference.

The content of three alkaloids in the herbal extract was determined by the developed CE–ECL method with the condition as follows: electrokinetic injection: 10 s at 10 kV; running buffer: 50 mM phosphate buffer (pH 8.4); 5 mM Ru(bpy)$_3^{2+}$ and 50 mM phosphate buffer at pH 8.4 in the detection reservoir; detection voltage: 1.2 V; separation voltage: 15 kV.

The contents of SR, MT, and OMT were (mean ± R.S.D., $n = 3$) at 0.38 ± 0.03 mg/g, 0.49 ± 0.02 mg/g and 7.49 ± 0.10 mg/g, respectively.

Table 1
Comparison of various methods for determination of SR, MT and OMT

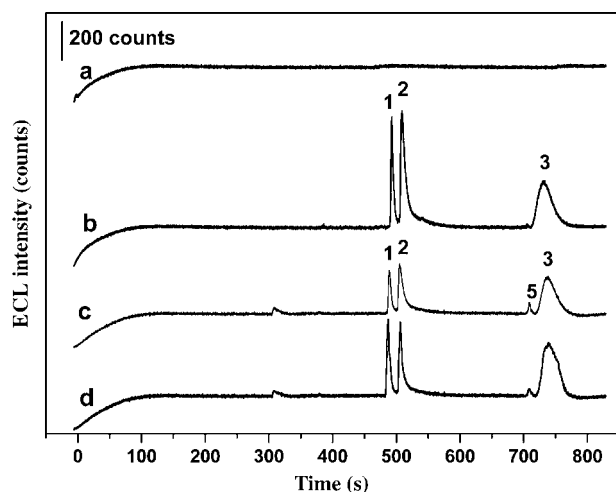| Method	Detection limit (M)			R.S.D. (%)			Reference
	SR	MT	OMT	SR	MT	OMT	
HPLC-FD	–	3.2×10^{-6}	–	–	1.0	–	[4]
HPLC-UV	–	8.0×10^{-9}	–	–	<4.0	–	[5]
HPLC-UV	3×10^{-6}	4×10^{-6}	3×10^{-6}	4.6	1.8	4.9	[18]
HPLC–ECL	4.0×10^{-9}	1.2×10^{-8}	–	3.2	2.5	–	[12]
CE–ECL	1.0×10^{-9}	1.0×10^{-9}	4×10^{-8}	2.5	3.1	3.1	This paper

Fig. 6. Electropherograms of standard mixture and the extracted sample. (a) Methanol; (b) the standard mixture: SR (4.4×10^{-6} M), MT (4.4×10^{-6} M) and OMT (4.0×10^{-5}M) dissolved in methanol; (c) the extracted sample; (d) the extracted sample spiked with SR (2.2×10^{-6} M), MT (2.2×10^{-6} M) and OMT (2.0×10^{-5} M). (1) SR; (2) MT; (3) OMT; (4 and 5) unknown compounds in the extract. Conditions: Electrokinetic injection: 10 s at 10 kV. 5mM Ru(bpy)$_3$$^{2+}$ and 50 mM phosphate buffer at pH 8.4 in the detection reservoir. Running buffer: 50 mM phosphate buffer (pH 8.4). Detection voltage: 1.2 V. Separation voltage: 15 kV.

4. Conclusion

This is the first report to describe the determination of OMT by CE–ECL. All relevant operational parameters have been optimized for the adopted experiment described in this paper. The assay is proved simple, sensitive and practicable, which may be used for the quantitative determination of quinolizidine alkaloids in some natural product samples.

References

[1] D.C. Cai, M.J. Gu, J.D. Zhang, G.P. Zhu, T.Y. Zhang, Ni. Li, Y. Ito, J. Liq. Chromatogr. 13 (1990) 2399.
[2] K.L. Miao, J.Z. Zhang, Y.Y. Dong, Y.F. Xi, Nat. Prod. Res. Dev. 13 (2001) 69.
[3] L.X. Jin, Y.Y. Cui, G.D. Zhang, Acta Pharm. Sinica 28 (1993) 136.
[4] K. Li, Y.S. Yuan, X.B. Jia, Chin. Pharm. J. 30 (1995) 302.
[5] W.Y. Yang, N.L. Yang, T.Y. Wang, Chin. J. Chin. Mater. Med. 22 (1997) 732.
[6] F.L. Deng, B.M. Chen, S.X. Liang, G.H. Chen, L.W. Xia, Chin. Tradit. Patent Med. 23 (2001) 670.
[7] Y.R. Ku, L.Y. Chang, J.H. Lin, L.K. Ho, J. Pharm. Biomed. Anal. 28 (2002) 1005.
[8] Y.Q. Yu, P.L. Ding, D.F. Chen, Anal. Chim. Acta 523 (2004) 15.
[9] D.S.T. Sit, G.H. Gao, F.C.P. Law, P.C.H. Li, J. Chromatogr. B 808 (2004) 209.
[10] Y. Gao, Y.L. Tian, E.K. Wang, Anal. Chim. Acta 545 (2005) 137.
[11] J.Y. Yin, W.W. Guo, Y. Du, E.K. Wang, Electrophoresis 27 (2006) 4836.
[12] C.Q. Yi, P.W. Li, Y. Tao, X. Chen, Microchim. Acta 147 (2004) 237.
[13] A.W. Knight, G.M. Greenway, Analyst 121 (1996) 101R.
[14] X. Chen, C.Q. Yi, M.J. Li, X. Lu, Z. Li, P.W. Li, X.R. Wang, Anal. Chim. Acta 466 (2002) 79.
[15] National pharmacopoeia committee (Ed.), Chinese Pharmacopoeia 2005, vol.1, Chemical Industry, Beijing, 2005, p. 141.
[16] X.B. Yin, H.B. Qiu, X.H. Sun, J.L. Yan, J.F. Liu, E.K. Wang, Anal. Chem. 76 (2004) 3846.
[17] X.P. Sun, J.F. Liu, W.D. Cao, X.R. Yang, E.K. Wang, Y.S. Fung, Anal. Chim. Acta 470 (2002) 137.
[18] S.H. Liu, Q.F. Li, X.G. Chen, Z.D. Hu, Electrophoresis 23 (2002) 3392.

Improved separation efficiency of neurotransmitters on a native printed capillary electrophoresis microchip simply by manipulating electroosmotic flow

Hui Yu [a], Feng-Yun He [b], Yu Lu [a], Yu-Lin Hu [a], Hai-Yan Zhong [a], Xing-Hua Xia [a],*

[a] *Key Lab of Analytical Chemistry for Life Science, School of Chemistry and Chemical Engineering, Nanjing University, Nanjing 210093, China*
[b] *Department of Chemistry, Nanjing Xiaozhuang University, Nanjing 210017, China*

Abstract

Separation and determination of dopamine and epinephrine with end-channel electrochemical (EC) detection integrated on a native printed microchip capillary electrophoresis (CE) system was investigated. Factors influencing the separation and detection were investigated and optimized. Results show manipulating EOF, which can be easily achieved by adjusting buffer pH, is a simple and effective way to achieve the baseline separation of dopamine and epinephrine in native polymeric microchips. Without surface modification of microchannel, printed microchips with advantages of low cost and easy preparation can achieve high performance like other microfluidic devices.
© 2008 Published by Elsevier B.V.

1. Introduction

Since 1990s, microfluidics has become an important field of analytical chemistry due to its advantages over conventional analysis methods, such as rapid speed, low reagent consumption, more environmentally appealing, and its potential portability and disposability [1–3]. The microfluidic devices developed in the early years were mostly fabricated from silicon and glass using photolithography and etching techniques [4,5]. However, these fabrication processes are costly (ca. $200 for a research chip), time-consuming and labor intensive. In most of the cases, clean-room conditions are usually required. The fabricated microfluidic devices are also fragile and mass production is not easy to be achieved. Recently, these materials have been mainly displaced by plastics [6]. Polymeric microchips are of increasing interest because they offer attractive mechanical and chemical properties, low cost (ca. $2 for a research chip), ease of fabrication, biocompatibility, and higher flexibility [7,8]. Such polymeric chips have been fabricated using laser ablation [9,10],

plasma etching [10], imprinting [11], hot embossing [12], injection molding [13], and compression molding [14] techniques. However, special fabrication instruments are still required for most polymeric microchips, which restricts their application in common laboratories. Lago et al. further simplified microfabrication procedures [15,16] and proposed a very simple and convenient microfabrication process based on direct printing for mass production of microfluidic devices at very low cost (ca. 4 cents for a research chip). Since dozens of devices can be printed on a transparent film sized A4, average fabrication of one device is less than half an hour which dramatically shortens the fabrication time. We have improved this fabrication method and investigated the electroosmotic flow (EOF) characteristics on such chips [17]. Besides, we have also extended this simple method to fabricate micromixer [18], enzyme microreactor [19], and electrophoresis microchip for the analysis of acetaminophenol and its hydrolysate [20].

Dopamine and epinephrine have been widely investigated on microchip capillary electrophoresis of different substrates, such as glass [21–23], PDMS [24], PDMS/glass [25]. They can be well separated on a glass chip but failed on other type chips. To improve separation efficiency, the most adopted methods are to modify channel surface. Chen et al. modified the PDMS

---

* Corresponding author. Tel.: +86 25 83597436; fax: +86 25 83597436.
E-mail address: xhxia@nju.edu.cn (X.-H. Xia).

surface with gold nanoparticles [26] and proteins [27,28] for reducing the adsorption of analytes on the channel surface, and thus satisfactory separation of the two analytes was obtained. Similar results were achieved by modifying the PDMS surface with silica nanoparticles [29]. These modification procedures are somewhat inconvenient for chip preparation. Adjustment of pHs of running buffer is a simple and effective method in common capillary electrophoresis. However, such a simple way was seldom adopted in microchip electrophoresis [17,20,22]. In this paper, pH of running buffer was optimized to obtain effective separation of the two analytes on an integrated printed microchip. Other factors of separation voltage, detection potential and injection time influencing the separation and detection were also investigated for achieving optimal separation and detection of the analytes. Results showed the pH is a dominant factor in separation on unmodified polymeric electrophoresis chips, which is consistent with our previous studies [20,30]. Under optimum conditions, dopamine and epinephrine could be effectively separated and detected within 180 s. Compared with other unmodified chips in literatures, the resolution is better than that of other unmodified polymeric chips [26,28] and similar to those of glass chip [22] and modified polymeric chips [26,28,29]. Though the separation time is somewhat longer than the above mentioned methods, it is a practical alternative with very low cost of chip materials, ease of preparation.

2. Experimental

2.1. Materials and reagents

Transparency films, poly(ethylene terephthalate) (PET, 100 μm thick) were used as the base material of electrophoresis microchips (STD Printing Materials Limited Company, Suzhou, China). Another PET sheet of 80-μm thick covered with a 5-μm thick adhesive polyethylene adhesive on one side was used for final plastification of the PET-toner chips. All solvents and reagents were of analytical grade. The stock solutions of dopamine (Sigma, USA) and epinephrine (Sigma, USA) were prepared by dissolving the reagents in a 1 mM HClO$_4$ aqueous solution to reach the final concentration of 10 mM. Both stock solutions of dopamine and epinephrine were kept at 4 °C. Sample solutions were prepared by diluting the stock solution with running buffer prior to use. 50 mM phosphate buffer solutions (PBS) with different pH served as running buffer. All aqueous solutions were prepared from deionized water (18 MΩ, PURE-LAB Classic, PALL, USA). All solutions were passed through a 0.22 μm cellulose acetate filter (Xinya Purification Factory, Shanghai, China) before electrophoresis measurements.

2.2. Fabrication of microchips

The basic procedures used to fabricate microchips have been described previously in detail [17–20,30]. In brief, the layout of the microchip capillary electrophoresis was designed using the computer software Adobe Illustrator 10.0 and was printed on a transparency film with blank region as the channels. Then, two printed films with mirrored images were laminated together by
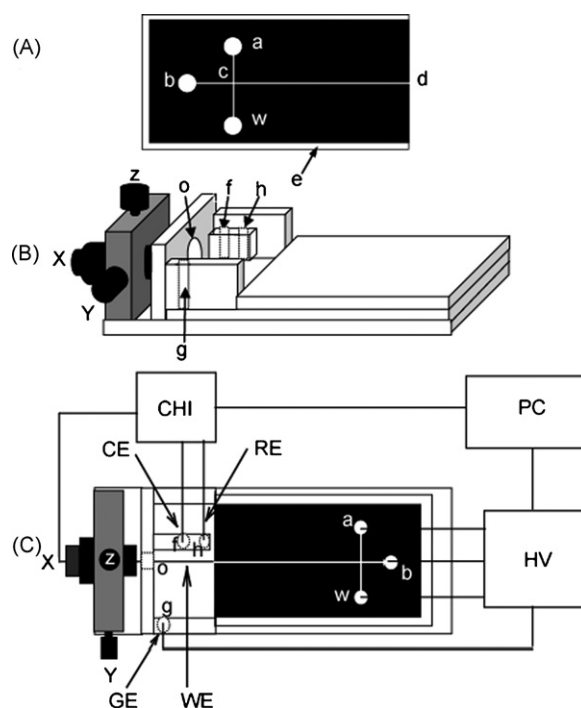

Fig. 1. Schematic layout of a printed microchip and home-made plexiglass holder integrated with a three-dimensional micromanipulator. (A) Plastified printed microchip: (a) sample reservoir; (b) buffer reservoir; (w) sample waste reservoir; (c) injection crossing; (d) end-channel detection point and (e) plastification film. Separation channel, total length bd = 6 cm; effective length, cd = 5 cm; injection channel, aw = 2 cm (not to scale). (B) Side three-dimensional view of the home-made plexiglass holder integrated with a three-dimensional micromanipulator: X-, Y-, Z-direction adjustor; (o) working electrode hole; (f) auxiliary electrode hole; (h) reference electrode hole and (g) CE ground electrode hole. (C) Top view of the holder and printed microchip. WE: working electrode; CE: counter electrode; RE: reference electrode; GE: ground electrode; HV: high voltage; PC: personal computer.

a heating laminator, producing the channels with access holes. Another two adhesive sheets of PET with access holes at the corresponding places were finally laminated over the PET toner microchip for increasing the performance stability. The layout was printed out on an EPL 5800 Laser Printer (Epson, Japan) with the toner cartridge S050010 at 1200 dots per inch (dpi). The geometry of microchip is shown in Fig. 1A. Its total separation channel length is 6 cm with an efficient length 5 cm and an injection channel length 2 cm.

2.3. Electrophoresis procedures

Fig. 1 shows the schematic representation of the setup for microchip electrophoresis integrated with electrochemical detection. For each new microchip, the channels were washed in sequence with deionized water, 50% (v:v) ethanol, 1.0 M NaOH and deionized water each for 2 min. Then, they were rinsed with buffer solution for several minutes. Electrophoresis experiments were carried out by a laboratory-made voltage power supplier with a voltage range between 0 and +5000 V. The applied voltage could be automatically controlled by a personal computer via an AD/DA converter. The separation current could be real time monitored and the corresponding data could be saved in

text files. The running buffer was introduced directly into the reservoirs and flushed through the channels under vacuum for several minutes. Then, voltages were applied to the separation (between b and d) and injection channels (between a and w), respectively, for several minutes until the separation and injection currents leveled off. The electrochemical detection reservoir was also restocked with fresh buffer. The buffer reservoirs (b and w) and the sample reservoir (a) were restocked with fresh buffer and fresh sample, respectively. The injection was carried out by applying a high voltage (HV) to the sample reservoir for a given time via the Pt electrodes (dia. 0.3 mm) connected to a HV power supplier, with the sample waste reservoir (w) grounded and the other reservoirs floating. Once sample injection was completed, separation voltage was applied to the buffer reservoirs (b and d) with the detection reservoir (d) grounded and the other reservoirs floating.

2.4. EOF measurements

The current monitoring method was used to measure the EOF in a 5-cm long PET channel (200 μm wide and 10 μm deep) under electric field strength of 120 V/cm. All reservoirs were filled with buffer. Voltage was applied to the separation channel for several minutes until the separation currents leveled off. The buffer was then changed with dilute buffer (buffer:water (v:v) = 9:1), and the potential was reapplied. The time required for the appearance of new leveled off electrophoresis current was measured for each run, which indicated that the diluted buffer filled the separation channel. The running electrolyte for electrophoresis experiments was phosphate buffer (pH 2.5–6.5).

2.5. Electrochemical detection

A 10 μm Pt microelectrode sealed in a Pyrex tube (Shanghai Chenhua Instrument Company, Shanghai, China) was used as the working electrode for detection. Before use, the electrode was polished with 0.05 μm alumina powder, rinsed with deionized water. Then, the electrode was cleaned by potential scanning between −0.2 and 1.2 V against the Ag/AgCl (3.0 M KCl) reference electrode in a 0.5 M H_2SO_4 until a stable current–potential profile was obtained.

A home-made plexiglass holder integrated with a three-dimensional micromanipulator was fabricated for fixing the microchip and housing the detector and reservoirs (Fig. 1B and C). Proper seal of the solution reservoir at the end of microchannel was achieved by using silicone grease. This reservoir served as both the cathodic buffer reservoir for the CE system and the electrochemical detection reservoir. A three-dimensional micromanipulator (Shanghai Lianyi Instrument Factory of Optical Fiber and Laser, Shanghai, China) was fixed on the plexiglass holder for precise positioning of the working electrode. Alignment of the working electrode to the microchannel was performed under a microscope (Jiangnan Optical Instrument Factory, Nanjing, China). A home-made saturation Ag/AgCl reference electrode, an 2 cm^2 platinum sheet counter electrode, and a ground Pt electrode for CE were also placed in the reservoir along with the working electrode. Amperometric detection

was carried out in a three-electrode configuration. Linear sweep voltammetry and amperometric detection were carried out on an Electrochemical Workstation CHI 630 (Shanghai Chenhua Instrument Company, Shanghai, China).

3. Results and discussion

3.1. Effect of running buffer pH

The solution pH directly alters the charges of the channel surfaces and therefore changes the resulting EOF as described previously for a fused silica capillary [31]. The native EOF properties of the present device fabricated according to our improved method were firstly evaluated using the modified current monitoring technique of Huang et al. [32]. The relationship between the pH and EOF is shown in Table 1. Obviously, the resulting EOF depended considerably on the solution pH. It changed from 0 to $2.20 \times 10^{-4} \, cm^2 \, V^{-1} \, s^{-1}$ over a pH range of 2.5–6.5 in a 50 mM phosphate buffer solution, which is consistent with our previous report [17].

The difference of effective mobility ($\Delta\mu_{ef} = \mu_{ef(2)} - \mu_{ef(1)}$) of two analytes is the base of electrophoresis separation. The resolution (R_s) of the two analytes can be described as equation (1) [33]:

$$R_s = \frac{1}{4\sqrt{2}} \Delta\mu_{ef} \left[\frac{Vl}{DL(\mu_{ef} + \mu_{eo})} \right]^{1/2} \tag{1}$$

where, V is the separation voltage, L and l are the effective separation length and total length, respectively; D is the diffusion coefficient of the analytes; μ_{ef} and μ_{eo} are the effective electrophoretic and electroosmotic mobility, respectively.

For a given microchip, the total and effective lengths of the separation channel are fixed. The separation voltage is kept constant, and the diffusion coefficient of the analytes can be considered as constant. Therefore, R_s is determined by $\Delta\mu_{ef}$, μ_{ef} and μ_{eo}. We can modify R_s by manipulating the μ_{eo} if μ_{ef} is constant or with minute fluctuation. The pK_a of dopamine and epinephrine is 8.87 and 8.55, respectively. They should exist as protonated cations in solutions with pH ranging from 2.5 to 6.5. And their ionic radius and the solvent viscous coefficient can also be considered as constants in our experimental conditions. So according to the Eq. (2), $\Delta\mu_{ef}$ and μ_{ef} are all constant.

$$\mu_{ef} = \frac{q}{6\pi\eta r} \tag{2}$$

On the other hand, EOF can be dramatically decreased in solutions with pH ranging from 6.5 to 2.5, which can be seen in Table 1. The remarkable decrease of μ_{ef} results in the improvement of R_s (according to equation (1)). Fig. 2 shows the effect of buffer pH on the separation efficiency of dopamine and epinephrine. The electropherograms obtained from dopamine

Table 1
The EOF value of different PBS pH

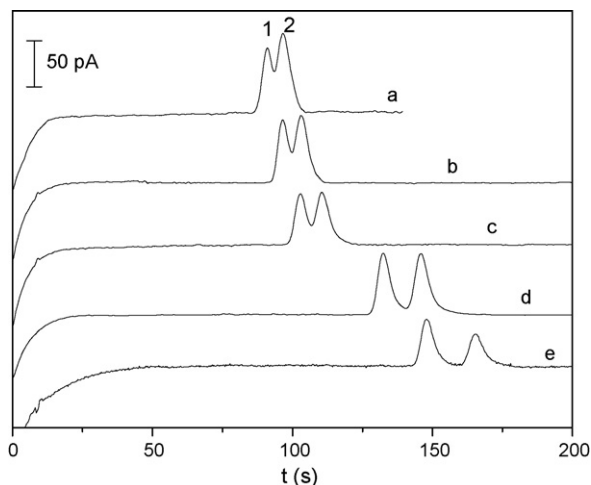| pH	2.5	3.5	4.5	5.6	6.5
EOF ($10^{-4} \, cm^2 \, V^{-1} \, s^{-1}$)	0	1.00	1.24	1.97	2.20

Fig. 2. The influence of running buffer pH on the electropherograms of 100 μM dopamine and 100 μM epinephrine. Separation voltage: 1200 V; sample injection: at 400 V for 10 s; running buffer: 50 mM phosphate buffer; detection potential: +1.2 V (vs. Ag/AgCl). pH: (a) 6.5, (b) 5.6, (c) 4.5, (d) 3.5 and (e) 2.5. Peak 1: dopamine; Peak 2: epinephrine.

and epinephrine in 50 mmol L^{-1} PBS at pH 2.5, 3.5, 4.5, 5.6 and 6.5. It is clear that the resolution of the two analytes was poor when running buffer pH was larger than 3.5. However, this resolution could be considerably improved as the running buffer pH decreased. When the pH decreased, the migration velocities of both analytes were decreased due to the decrease of EOF, and thus the separation time increased. This could result in widen separation band. However, the buffer pH has negligible effect on the peak width at half height ($W_{1/2}$) for both analytes (Table 2). As a result, the resolution of the analytes increased as the buffer pH decreased (Table 2). At buffer pH 2.5, dopamine and epinephrine could be well separated. Therefore, running buffer pH 2.5 was chosen for further experiments.

3.2. Influence of separation voltage

Fig. 3 shows the effect of separation voltage on the amperometric response and separation efficiency. As expected, with the decrease of separation voltage from 1400 to 600 V (in 200 V increments, curves a–e), the migration time increased significantly from 110.8 to 289.9 s and from 125.7 to 327.9 s for dopamine and epinephrine, respectively. The half-height peak width also decreased from 19.8 s at 600 V to 7.2 s at

Table 2
The half-height peak width and resolution of separation at different PBS pH

	pH				
	2.5	3.5	4.5	5.6	6.5
Half-height peak width ($W_{1/2}$)					
Dopamine	5.1	5.1	4.8	5.1	–
Epinephrine	5.4	5.4	5.4	5.4	6.0
Resolution	1.44	0.87	0.61	0.58	–

The electrophoresis and electrochemical detection conditions were the same as in Fig. 2.
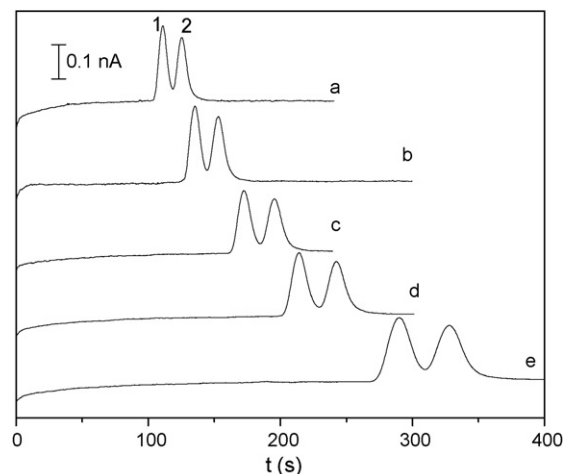

Fig. 3. Influence of separation voltage on the electropherograms of 100 μM dopamine and 100 μM epinephrine at pH 2.5. Separation performed at high voltage, V: (a) 1400; (b) 1200; (c) 1000; (d) 800; (e) 600. Injection time: 20 s. Other conditions were the same as in Fig. 2. Peak 1: dopamine; Peak 2: epinephrine.

1400 V for dopamine and 21.6 s at 600 V to 8.1 s at 1400 V for epinephrine. Taking consideration of the separation speed, separation efficiency, signal/noise ratio and baseline, a separation voltage of 1200 V (Fig. 3, curve b) was employed for further experiments. Theoretical plate number of 25040 and 26567 m^{-1} was calculated at separation voltage of 1200 V for dopamine and epinephrine, respectively. At separation voltage of 1200 V, dopamine and epinephrine on native printed-CE microchip integrated EC detection could be effectively separated (with resolution of 1.0) and sensitively detected electrochemically as shown in Fig. 3, curve b.

3.3. Influence of detection potential

The detection potential plays an important role in the separation and electrochemical detection system. Fig. 4 shows the
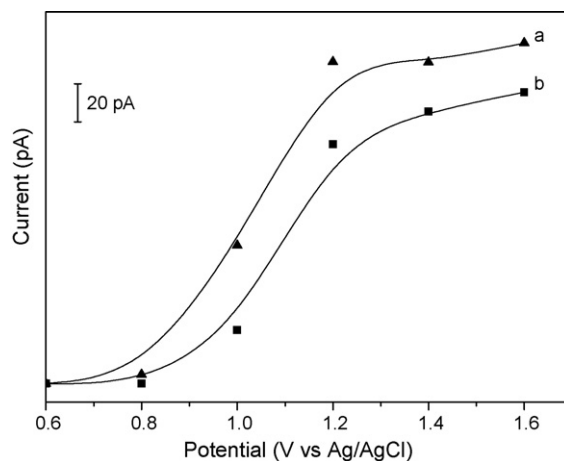

Fig. 4. Hydrodynamic voltammograms at a Pt ultramicroelectrode in a solution of PBS containing 100 μM dopamine (a) and 100 μM epinephrine (b). Running buffer: 50 mM phosphate buffer (pH2.5). Other conditions were the same as in Fig. 2.

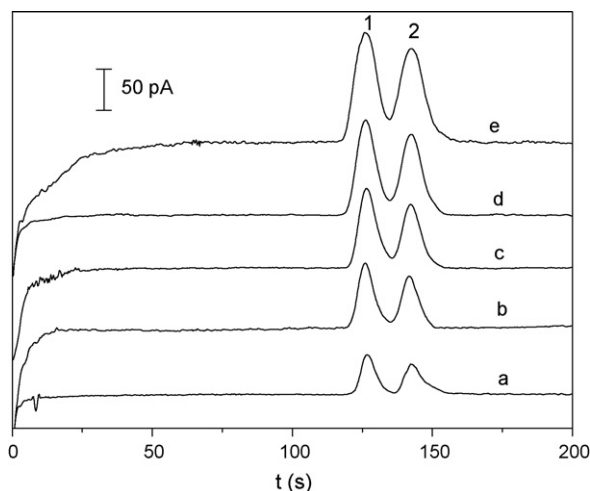Fig. 5. Influence of injection time on electropherograms at pH 2.5. Injection time (s): (a)10 (b) 20 (c) 30 (d) 40 (e) 50. Other conditions were the same as in Fig. 2. Peak 1: dopamine; Peak 2: epinephrine.

hydrodynamic voltammograms of dopamine and epinephrine on a 10 μm platinum ultramicroelectrode. The oxidation peak currents for both analytes started at 0.70 V and increased rapidly with the increase of detection potential up to 1.20 V. When the potentials exceeded 1.20 V, the peak currents for both analytes increased slowly. Since too higher anodic detection potential will result in higher background current, the detection potential in microchip system was set at 1.2 V.

3.4. Effect of injection time

Injection time can control the volume of sample plug, which also greatly affects separation efficiency and detection limit. The influence of injection time on the responses of both analytes was also investigated from 10 to 50 s. As expected, the peak currents of both analytes increased with increasing injection time from 10 to 50 s. However, prolonged injection time also resulted in broader peaks. Twenty seconds was chosen as injection time for its comparatively high efficiency and proper detection sensitivity (Fig. 5).

3.5. Linearity, detection limit and reproducibility

The oxidation peak currents for dopamine and epinephrine on a Pt ultramicroelectrode at 1.2 V showed a linear relationship in the concentration range from 5 to 400 μM with sensitivities of 1.49 and 1.43 pA/μM and intercepts of 1.47 and −0.32 pA (correlation coefficients 0.9997 and 0.9995 for dopamine and epinephrine, respectively). Detection limits for both analytes were 1.0 μM (at S/N = 3). Five repetitive injections of a mixture containing 100 μM dopamine and epinephrine resulted in a RSD of 2.1% and 4.2% for the current response and of 1.4% and 1.5% for the migration times for dopamine and epinephrine, respectively, showing good reproducibility. The linearity and the detection limit are similar to those of the literatures [24–27].

4. Conclusion

In this paper, we proposed a simple method for separation and detection of dopamine and epinephrine in a printed chip with end-channel electrochemical detection using a Pt ultramicroelectrode. Neither by the surface modification of microchannels nor by the additives in the running buffer adopted, dopamine and epinephrine were effectively separated simply by adjusting running buffer pH. The running buffer pH can remarkably influence EOF of chips, which is the main factor of separation in this system. This strategy can be applied to separate analytes with similar pK_a and molecular structures. The simple and fast fabrication procedures, low cost and mass production of the printed-CE microchip device offer a great promise for bioanalysis, clinical analysis and medicine quality control.

References

[1] A. Manz, D.J. Harrison, E.M.J. Verpoorte, J.C. Fettinger, A. Paulus, H. Lüdi, H.M. Widmer, J. Chromatogr. A 593 (1992) 253.
[2] D.R. Reyes, D. Iossifidis, P. Auroux, A. Manz, Anal. Chem. 74 (2002) 2623.
[3] P. Auroux, D. Iossifidis, D.R. Reyes, A. Manz, Anal. Chem. 74 (2002) 2637.
[4] Q.F. Xue, F. Foret, Y.M. Dunayevskiy, P.M. Zavracky, N.E. McGruer, B.L. Karger, Anal. Chem. 69 (1997) 426.
[5] A. Scherer, S.R. Quake, Science 290 (2000) 1536.
[6] G.M. Whitesides, Nature 442 (2006) 368.
[7] H. Becker, L.E. Locascio, Talanta 56 (2002) 267.
[8] H. Becker, C. Gartner, Electrophoresis 21 (2000) 12.
[9] M.A. Roberts, J.S. Rossier, P. Bercier, H. Girault, Anal. Chem. 69 (1997) 2035.
[10] J. Rossier, F. Reymond, P.E. Michel, Electrophoresis 23 (2002) 858.
[11] C.H. Yuan, J. Shiea, Anal. Chem. 73 (2001) 1080.
[12] J. Narasimhan, I. Papautsky, J. Micromech. Microeng. 14 (2004) 96.
[13] T.L. Edwards, S.K. Mohanty, R.K. Edwards, C.L. Thomas, A.B. Frazier, Sensor. Mater. 14 (2002) 167.
[14] Y. Liu, D. Ganser, A. Schneider, R. Liu, P. Grodzinski, N. Kroutchinina, Anal. Chem. 73 (2001) 4196.
[15] C.L. Lago, H.D.T. Silva, C.A. Neves, J.G.A. Brito-Neto, J.A.F. Silva, Anal. Chem. 75 (2003) 3853.
[16] W.K.T. Coltro, J.A.F. Silva, H.D.T. Silva, E.M.R. Richter, L. Angnes, C.L. Lago, L.H. Mazo, E. Carrilho, Electrophoresis 25 (2004) 3832.
[17] F.Y. He, A.L. Liu, J.H. Yuan, W.K.T. Coltro, E. Carrilho, X.H. Xia, Anal. Bioanal. Chem. 382 (2005) 192.
[18] A.L. Liu, F.Y. He, K. Wang, T. Zhou, Y. Lu, X.H. Xia, Lab Chip 5 (2005) 974.
[19] A.L. Liu, T. Zhou, F.Y. He, J.J. Xu, Y. Lu, H.Y. Chen, X.H. Xia, Lab Chip 6 (2006) 811.
[20] A.L. Liu, F.Y. He, Y.L. Hu, X.H. Xia, Talanta 68 (2006) 1303.
[21] H.M. Sorouraddin, A. Hibara, T. Kitamori, Fresen. J. Anal. Chem. 371 (2001) 91.
[22] Y.Y. Wu, J.M. Lin, R.G. Su, F. Qu, Z.W. Cai, Talanta 64 (2004) 338.
[23] J.J. Xu, N. Bao, X.H. Xia, Y. Peng, H.Y. Chen, Anal. Chem. 76 (2004) 6902.

[24] Y. Zeng, H. Chen, D.W. Pang, Z.L. Wang, J.K. Cheng, Anal. Chem. 74 (2002) 2441.
[25] N.A. Lacher, S.M. Lunte, R.S. Martin, Anal. Chem. 76 (2004) 2482.
[26] A.J. Wang, J.J. Xu, H.Y. Chen, Electroanalysis 19 (2007) 674.
[27] A.J. Wang, J.J. Xu, Q. Zhang, H.Y. Chen, Talanta 69 (2006) 210.
[28] A.J. Wang, J.J. Xu, H.Y. Chen, J. Chromatogr. A 1107 (2006) 257.
[29] W. Wang, L. Zhao, J.R. Zhang, X.M. Wang, J.J. Zhu, H.Y. Chen, J. Chromatogr. A 1136 (2006) 111.
[30] F.Y. He, A.L. Liu, X.H. Xia, Anal. Bioanal. Chem. 379 (2004) 1062.
[31] M.F.M. Tavares, V.L. McGuffin, Anal. Chem. 67 (1995) 3687.
[32] X.H. Huang, M.J. Gordon, R.N. Zare, Anal. Chem. 60 (1988) 1837.
[33] Y.Z. Deng, J.L. He, High Performance Capillary Electrophoresis, Science Press, Perking, 1996, p. 35.